ELSEVIER DEVELOPMENTS IN SEDIMENTOLOGY 54

GEOLOGY AND HYDROGEOLOGY OF CARBONATE ISLANDS

EDITED BY
H. LEONARD VACHER AND TERRENCE M. QUINN



DEVELOPMENTS IN SEDIMENTOLOGY 54

GEOLOGY AND HYDROGEOLOGY OF CARBONATE ISLANDS

LIST OF CASE STUDIES

2 (Bermuda): Hermeneutics and the Pleistocene sea-level history of Bermuda.
4 (Bahamian archipelago): Blue holes of the Bahamas.
5 (Florida Keys): Interplay of carbonate islands, coral reefs and sea level.
6 (Florida Bay): Hydrogeochemical evidence of diagenesis.
7 (n.e. Yucatan): Influence of climate on early diagenesis of carbonate eolianites.
8 (Cayman Islands): The Cayman Island karst.
9 (Isla de Mona): Evolution of the Mona Reef complex.
10 (St Croix): Dolomitization on St. Croix.
11 (Barbados): Early near-surface diagenesis
12 (Pitcairns): Geological evolution of Henderson Island, an emergent limestone island.
14 (Makatea): Volcanic-isostatic polyphase motion and uplifted atolls.
15 (Fr. Polynesia): Interstitial waters of reefs and endo-upwelling.
16 (Cooks): Subsurface geology beneath the lagoons as revealed by drilling.
17 (Niue): Dolomitization at Niue.
18 (Tonga): Freshwater lens at Tongatapu.
19 (Kiribati): 1, Mid-Holocene highstand; 2, Calculating the water balance for Tarawa.
20 (Marshall Islands): Modeling development alternatives in dual-aquifer atoll islands.
21 (Anewetak): Use of Sr isotopes to determine accommodation, subsidence and sea-level change.
22 (Enewetak): Numerical modeling of Enjebi Island groundwater.
23 (Federated States of Micronesia): Hydrogeologic reconnaissance on remote atoll islands by electromagnetic surveying.
26 (Fiji): Reconnaissance investigations of groundwater lenses in limestone on Vatoa and Oneata.
28 (Houtman Abrolhos): Chronology and sea-level history of the Abrolhos reefs in the Late Quaternary.
29 (Great Barrier Reef): Status of coral cays of the GBR during a period of global climatic change.
30 (Heron): Nutrient dynamics in a vulnerable ecosystem.
31 (Cocos [Keeling]): Development of surface morphology of Cocos Atoll.
32 (Diego Garcia): Effects of climatic variation on groundwater supply.

DEVELOPMENTS IN **SEDIMENTOLOGY 54**

GEOLOGY AND HYDROGEOLOGY OF CARBONATE ISLANDS

H. LEONARD VACHER AND TERRENCE M. QUINN
UNIVERSITY OF SOUTH FLORIDA, TAMPA, FLORIDA, USA

2004



ELSEVIER

Amsterdam – Boston – Heidelberg – London – New York – Oxford
Paris – San Diego – San Francisco – Singapore – Sydney – Tokyo

ELSEVIER B.V.	ELSEVIER Inc.	ELSEVIER Ltd	ELSEVIER Ltd
Sara Burgerhartstraat 25	525 B Street, Suite 1900	The Boulevard, Langford Lane	84 Theobalds Road
P.O. Box 211, 1000 AE	San Diego, CA 92101-4495	Kidlington, Oxford OX5 1GB	London WC1X 8RR
Amsterdam, The Netherlands	USA	UK	UK

© 1997 Elsevier Science B.V. All rights reserved.

This work is protected under copyright by Elsevier B.V., and the following terms and conditions apply to its use:

Photocopying
Single photocopies of single chapters may be made for personal use as allowed by national copyright laws. Permission of the Publisher and payment of a fee is required for all other photocopying, including multiple or systematic copying, copying for advertising or promotional purposes, resale, and all forms of document delivery. Special rates are available for educational institutions that wish to make photocopies for non-profit educational classroom use.

Permissions may be sought directly from Elsevier's Rights Department in Oxford, UK: phone (+44) 1865 843830, fax (+44) 1865 853333, e-mail: permissions@elsevier.com. Requests may also be completed on-line via the Elsevier homepage (http://www.elsevier.com/locate/permissions).

In the USA, users may clear permissions and make payments through the Copyright Clearance Center, Inc., 222 Rosewood Drive, Danvers, MA 01923, USA; phone: (+1) (978) 7508400, fax: (+1) (978) 7504744, and in the UK through the Copyright Licensing Agency Rapid Clearance Service (CLARCS), 90 Tottenham Court Road, London W1P 0LP, UK; phone: (+44) 20 7631 5555; fax: (+44) 20 7631 5500. Other countries may have a local reprographic rights agency for payments.

Derivative Works
Tables of contents may be reproduced for internal circulation, but permission of the Publisher is required for external resale or distribution of such material. Permission of the Publisher is required for all other derivative works, including compilations and translations.

Electronic Storage or Usage
Permission of the Publisher is required to store or use electronically any material contained in this work, including any chapter or part of a chapter.

Except as outlined above, no part of this work may be reproduced, stored in a retrieval system or transmitted in any form or by any means, electronic, mechanical, photocopying, recording or otherwise, without prior written permission of the Publisher.
Address permissions requests to: Elsevier's Rights Department, at the fax and e-mail addresses noted above.

Notice
No responsibility is assumed by the Publisher for any injury and/or damage to persons or property as a matter of products liability, negligence or otherwise, or from any use or operation of any methods, products, instructions or ideas contained in the material herein. Because of rapid advances in the medical sciences, in particular, independent verification of diagnoses and drug dosages should be made.

First edition (hardbound) 1997
First edition (paperback) 2004

Library of Congress Cataloging in Publication Data
A catalog record is available from the Library of Congress.

ISBN: 0-444-81520-1 (hardbound)
0-444-51644-1 (paperback)

♾ The paper used in this publication meets the requirements of ANSI/NISO Z39.48-1992 (Permanence of Paper).
Printed in The Netherlands.

PREFACE

About a hundred years ago, Alexander Agassiz, after making a fortune from Michigan copper and becoming the world authority on sea urchins [*Revision of the Echini* (1873)], undertook to investigate coral reefs and limestone islands. Agassiz's coral reef expeditions, which he financed largely himself, lasted about a decade (1893-1902) and took him to the Bahamas, Bermuda, the Florida Keys, the Great Barrier Reef, the Fijis, Tongatapu, the Society islands, the Cook islands, the Carolines, the Marshalls, Guam, and Niue — to name only carbonate islands that are examined in this book. Intellectually, the driving force behind those studies was Darwin's theory of coral reefs [*Structure and Distribution of Coral Reefs* (1842)]. Now, studies of carbonate-island geology are energized by concepts and data of plate tectonics; deep-sea and on-island drilling; isotope geochemistry and geochronology; facies models and diagenetic pathways; sea-level curves and Milankovitch cycles.

At roughly the same time, W. Badon Ghyben in the Netherlands (1888) and A. Herzberg in Germany (1901) independently published analyses of the hydrostatics whereby fresh groundwater floats on ocean-derived saline groundwater in coastal settings. Now, in addition to the Ghyben-Herzberg principle and Ghyben-Herzberg lenses of island settings, we have brackish-water mixing zones, dual-aquifer conceptualizations, hydrologic budgets, and variable-density flow and transport modeling. We now know of the temperature-driven flow of Kohout convection and endoupwelling at greater depths, beneath the meteoric realm. There have been feedback studies relating the rocks to the flows, and the flows to the rocks, and these studies shed light on old questions such as dolomitization. According to one of our chapters, the deep flows explain Darwin's paradox – how the oligotrophic reefs of carbonate islands can exist in the first place, in such vast nutrient deserts.

The purpose of this book is to sample the geological and hydrogeological knowledge of particular islands now, some hundred years after Agassiz and Ghyben and Herzberg. We have enlisted authors who, between them, cover twenty-nine major islands or island groups. They range from islands where geological studies go back to the time of Lyell (Bermuda, Bahamas) and those visited by Darwin on the HMS *Beagle* (Society islands, Cocos [Keeling] islands), to ones that are just becoming known to the geological community (Isla de Mona) and ones where the first geological studies are just beginning (Henderson Island in the Pitcairns). They include popular holiday islands (e.g., Bermuda, the Keys, Bahamas, Barbados, n.e. Mexico, Caymans, Rottnest, Guam, Fiji), phosphate islands (Nauru, Makatea), nuclear islands (Enewetak, Mururoa), a military outpost (Diego Garcia), many other

remote atolls, and uninhabited islands in a variety of settings (islands of the Great Barrier Reef, the Houtman Abrolhos, mud islands of Florida Bay). Geologically, they include well-known locales where Holocene depositional processes are the dominant story (e.g., islands of the GBR), others where Pleistocene history is classic (e.g., Barbados), and others where the Tertiary geology is preeminent (e.g., Eniewetak, Niue). Tectonic settings include shelf margins, mid-plate dipsticks, and uplifted islands of convergent boundaries.

The chapters are of three types: those focusing on geology, those focusing on hydrogeology, and those covering both. Although the geology chapters do not all have the same format, they are all intended to include a mix about the tectonic and climatic setting, depositional facies, diagenesis, stratigraphy, and geologic history, albeit weighted according to the proclivities of the particular island and authors. Similarly, the hydrogeology chapters are intended to include information on the geologic setting, geologic framework, permeability distribution, groundwater occurrence and flow, water budget and recharge, and water resources. In addition, many chapters include information about the human side of the island so that readers might begin to get a feel for these fascinating places, which so few of us — unlike Agassiz — will get to visit in great numbers.

In addition to these subjects that the chapters have in common, many of the chapters have an appended Case Study, where the author goes into more detail about an aspect of the island that is of particular interest to the author and/or is particularly well displayed by the island. These Case Studies, which are listed in a separate Contents page, constitute something of a symposium volume of specialized topics, interleaved with the survey material that makes up the main part of the chapters. Chapters 3B and 3C, on aspects of the geology of the Bahamas, serve the role of Case Studies accompanying the main, broad-scope review of Bahamian geology in Chapter 3A; the organization here is like that of the various classic post-War U.S. Geological Survey Professional Papers on Pacific islands.

Assembling this information has taken more than four years, and in this time we have been helped by many people. We especially thank Bob Buddemeier, David Budd, Tony Falkland, John Mylroie, and Colin Woodroffe for their support, encouragement and advice; Chris Reich for redrawing many of the figures; Nancy Mole for reformatting many tables. We also want to thank our authors for their patience and perseverance through the long process. We acknowledge a still unpaid debt to Dan Muhs, Fred Hochstaedter, Terry Scoffin, David Budd, June Oberdorfer and Bob Buddemeier, John Mylroie, and Rob Ross and Warren Allmon for their chapters in a once-anticipated, but unrealized, concepts volume.

As we dug more deeply into the subject, we have come to appreciate the "Giants of Geology" who left their mark on carbonate island studies – e.g., Charles Darwin, James Dwight Dana, Alexander Agassiz, T.W. Edgeworth David, Reginald Daly, A.E. Verrill, Wayland Vaughan, Henry Menard, Charles K. Wentworth, Joshua Tracey, Harold Stearns, Preston Cloud, Ed Hoffmeister, J Harlan Bretz and, more in our time, David Stoddart, Rhodes Fairbridge, and Robert Ginsburg. We have also been struck with how great ideas on the subject have come and gone, waxed and waned, with only some surviving, and then only with caveats or, at least, more

precisely defined premises and conditions. In this context, we note one of these island giants, Professor Edgeworth David, who, at the time of Agassiz's expeditions, put down the famous core to 1,114 ft (340 m) on Funafuti atoll (1897). Later, he accompanied Shackleton to Antarctica to study an "ice age in being" and published (posthumously) a three-volume set on the geology of Australia [David and Brown, *Geology of the Commonwealth of Australia* (1950)] following a monumental geological map of Australia. The accompanying notes to that map close with a thought which, according to Charles Schuchert in his obituary to David [Am. J. Sci, 28: 399 (1934)], sums up the philosophy of this great field geologist: "To attain to absolute truth, we neither aspire nor desire, content, however faint and weary, to be still pursuing, for in the pursuit we find an exceeding great reward." Carbonate islands will always invite study, and we can only wonder what a sampling might contain two hundred years after Agassiz, and Ghyben and Herzberg, and the Funafuti drillcore.

H. LEONARD VACHER
TERRENCE M. QUINN
Tampa, Florida
December, 1996

This Page Intentionally Left Blank

LIST OF CONTRIBUTORS

Paul Aharon [17, Niue]. Department of Geology and Geophysics, Louisiana State University, Baton Rouge, Louisiana 70803, USA.

Stephen S. Anthony [23, FSM]. U.S. Geological Survey, Water Resources Division, 667 Alamona Blvd, Suite 415, Honolulu, Hawaii 96813, USA.

S.G. Blake [12, Pitcairns]. Environmental Resources Information Network, Department of Environment, Sport and Territories, GPO Box 787, Canberra, A.C.T., 2601, Australia.

Jan Bronders [26, Fiji]. Mineral Resources Department, Suva, Fiji. [now: Vrouwvlietstraat 59, 2800 Mechelen, Belgium.]

Ann F. Budd [9, Mona]. Department of Geology, The University of Iowa, Iowa City, Iowa 52242-1379, USA.

Robert W. Buddemeier [22, Enewetak]. Kansas Geological Survey, 1930 Constant Ave, The University of Kansas, Lawrence, Kansas 66047-3720, USA.

Danièle C. Buigues [13, Mururoa]. CEA/LDG/BP12, 91680 Bruyres le Chatel, France.

Gilbert F. Camoin [14, Makatea]. CNRS, Universite de Provence, Centre de Sedimentologie, 3 Place V. Hugo, 13331 Marseille, Cedex 3 France.

James L. Carew [3A, Bahamas]. Department of Geology, University of Charleston, Charleston South Carolina 29424, USA.

Delton Chen [30, Heron]. Department of Chemical Engineering, University of Queensland, St. Lucia, Queensland 4072, Australia.

Lindsay B. Collins [28, Houtman Abrolhos]. School of Applied Geology, Curtin University of Technology, Perth, Western Australia 6102, Australia.

Pascale Déjardin [15, Fr. Polynesia]. ORSTOM - Reef Oceanography Laboratory, B.P. 529, Papeete, Tahiti (French Polynesia).

A.C. Falkland [19, Kiribati; 31, Cocos]. Hydrology and Water Resources Branch, ACT Electricity and Water, GPO Box 366, Canberra, A.C.T., 2601, Australia.

John Ferry [26, Fiji]. Mineral Resources Department, Suva, Fiji. [now: Geraghty and Miller International, Inc., Conqueror House, Vision Park, Histon, Cambridge CB4 1AH, England.]

Renaud Fichez [15, Fr. Polynesia]. ORSTOM - Reef Oceanography Laboratory, B.P. 529, Papeete, Tahiti (French Polynesia).

Lindsay Furness [18, Tonga]. Douglas Partners Pty Ltd, 27 Jeays Street, Bowen Hills, Queensland 4006, Australia.

Fereidoun Ghassemi (Nauru). Australian National University, Canberra, A.C.T., 0200, Australia.

Ivan P. Gill [10, St. Croix]. Dept. of Geology, University of Puerto Rico, Mayaguez, Puerto Rico 00681.

Luis A. González [9, Mona]. Department of Geology, The University of Iowa, Iowa City, Iowa 52242-1379, USA.

Sarah C. Gray [16, Cooks]. Marine and Environmental Studies, University of San Diego, 5998 Alcala Park, San Diego, California 92110, USA.

Robert B. Halley [5, Fla Keys]. U.S. Geological Survey, Center for Coastal and Regional Marine Geology, 600 4th St. South, St. Petersburg, Florida 33701, USA.

Paul J. Hearty [3B, Bahamas]. Chertsey #112, P.O. Box N-337, Nassau, Bahamas.

James R. Hein [16, Cooks]. U.S. Geological Survey, 345 Middlefield Rd., MS 999, Menlo Park, California, USA.

Peter J. Hill [24, Nauru]. Australian Geological Survey Organisation, Box 378, Canberra, A.C.T., 2601, Australia.

David Hopley [29, GBR]. Director, Sir George Fisher Centre, James Cook University of North Queensland, Townsville, Qld 4811, Australia. [now: Director, Coastal and Marine Consultancies Pty, Ltd, Townsville, Australia.]

Dennis K. Hubbard [10, St. Croix]. Virgin Islands Marine Advisors, 5046 Cotton Valley Rd, Christiansted, St. Croix, 00820.

John D. Humphrey [11, Barbados]. Department of Geology and Geological Engineering, Colorado School of Mines, Golden, Colorado 80401, USA.

Charles D. Hunt [32, Diego Garcia]. U.S. Geological Survey, Water Resources Division, 667 Alamona Blvd, Suite 415, Honolulu, Hawaii 96813, USA.

I.G. Hunter [8, Caymans]. Department of Geology, University of Alberta, Edmonton, Alberta T6G 2E3, Canada.

Gerry Jacobson [24, Nauru]. Australian Geological Survey Organisation, Box 378, Canberra, A.C.T., 2601, Australia.

Brian Jones [8, Caymans]. Department of Geology, University of Alberta, Edmonton, Alberta T6G 2E3, Canada.

Pascal Kindler [3B, Bahamas], Department of Geology and Paleontology, University of Geneva, Maranchers 13, 1211 Geneva 4, Switzerland.

Philip A. Kramer [6, Fla Bay]. Rosenstiel School of Marine and Atmospheric Sciences, University of Miami, 4600 Rickenbacker Causeway, Miami, Florida 33149, USA.

André Krol [30, Heron]. Hamersley Iron Pty Ltd, GPO Box A42, Perth, WA 6001, Australia.

Prem B. Kumar [26, Fiji]. Mineral Resources Department, Private Bag, GPO, Suva, Fiji.

John Lewis [26, Fiji]. Mineral Resources Department, Private Bag, GPO, Suva, Fiji.

Jose Luis Masaferro [3C, Bahamas]. Rosenstiel School of Marine and Atmospheric Sciences, University of Miami, 4600 Rickenbacker Causeway, Miami, Florida 33149, USA.

Peter P. McLaughlin [10, St. Croix]. Exxon Exploration Co., P.O. Box 4778, Houston Texas 77210-4778, USA.

Leslie A. Melim [3C, Bahamas]. Department of Geology, Western Illinois University, 1 University Circle, Macomb, Illinois 61455, USA.

John F. Mink [25, Guam]. Vice President, Mink and Yuen, Inc., 100 North Beretania St. 303, Honolulu, Hawaii 96817, USA.

Vanessa Monell [9, Mona]. Department of Geology, Queens College, CUNY, Flushing, New York 11367, USA.

Lucien F. Montaggioni [14, Makatea]. CNRS, Universite de Provence, Centre de Sedimentologie, 3 Place V. Hugo, 13331 Marseille, Cedex 3 France.

Clyde H. Moore, Jr. [10, St. Croix]. Department of Geology and Geophysics, Louisiana State University, Baton Rouge LA 70803, USA.

John E. Mylroie [3A, Bahamas]. Department of Geosciences, Mississippi State University, P.O. Box 2194, Mississippi State, Mississippi 39762, USA.

K.-C. Ng [8, Caymans]. The Water Authority, Box 1104, George Town, Grand Cayman, British West Indies.

June A. Oberdorfer [22, Enewetak]. Department of Geology, San Jose State University, One Washington Square, San Jose, California 95192-0102, USA.

J.M. Pandolfi [12, Pitcairns]. Center for Tropical Paleoecology and Archaeology, Smithsonian Tropical Research Institute, Apartado 2072, Balboa, Republica de Panama.

Frank L. Peterson [20, Marshalls]. Department of Geology and Geophysics, University of Hawaii, Honolulu, Hawaii 96822, USA.

Phillip E. Playford [27, Rottnest]. Geological Survey of Western Australia, 100 Plain Street, East Perth, Western Australia 6004, Australia.

Terrence M. Quinn [21, Anewetak]. Department of Geology, University of South Florida, 4202 E. Fowler Ave., Tampa, Florida 33620, USA.

Bruce M. Richmond [16, Cooks]. U.S. Geological Survey, MS 999, 345 Middlefield Road, Menlo Park, California 94025, USA.

Francis Rougerie [15, Fr. Polynesia]. Centre Scientifique de Monaco, Observatoire Océanologique Européan, Avenue St. Martin, MC 98000, Monaco.

Mark P. Rowe [2, Bermuda]. Ministry of Works and Engineering, P.O. Box HM 525, Hamilton HM CS, Bermuda.

Héctor Ruiz [9, Mona]. Department of Geology, The University of Iowa, Iowa City, Iowa 52242-1379, USA.

Saller, Arthur [21, Anewetak]. UNOCAL, 14141 Southwest Freeway, Sugarland, Texas 77478, USA.

Eugene A. Shinn [5, Fla Keys]. U.S. Geological Survey, Center for Coastal and Regional Marine Geology, 600 4th St. South, St. Petersburg Florida 33701, USA.

Peter L. Smart [4, Bahamas]. Department of Geography, University of Bristol, University Road, Bristol BS8 1SS, England UK.

Peter K. Swart [5, Fla Bay], Rosenstiel School of Marine and Atmospheric Sciences, University of Miami, 4600 Rickenbacker Causeway, Miami, Florida 33149, USA.

Bruce E. Taggart [9, Mona]. U.S. Geological Survey, Caribbean District Office, P.O. Box 364424, San Juan, Puerto Rico 00936-4424.

H. Leonard Vacher [1, Introduction; 2, Bermuda; 5, Fla Keys; 25, Guam]. Dept of Geology, University of South Florida, 4202 E. Fowler Ave., Tampa, Florida 33620, USA.

William C. Ward [7, Yucatan]. Department of Geology and Geophysics, University of New Orleans, New Orleans, Louisiana 70148, USA. [now: 26328 Autumn Glen, Boerne Texas 78006, USA.]

Christopher Wheeler [17, Niue]. Department of Geology and Geophysics, Louisiana State University, Baton Rouge, Louisiana 70803, USA.

Fiona Whitaker [4, Bahamas]. Department of Geology, Wills Memorial Building, Queens Road, Bristol BS8 1RJ, England, UK.

Colin D. Woodroffe [19, Kiribati; 31, Cocos]. School of Geosciences, University of Wollongong, Wollongong, New South Wales 2522, Australia.

Karl-Heinz Wyrwoll [28, Houtman Abrolhos]. Department of Geography, University of Western Australia, Nedlands, Western Australia 6009, Australia.

Zhong Rong Zhu [28, Houtman Abrolhos]. School of Applied Geology, Curtin University of Technology, Perth, Western Australia 6102, Australia.

This Page Intentionally Left Blank

CONTENTS

List of Case Studies ii

Preface v

List of Contributors ix

1. INTRODUCTION: VARIETIES OF CARBONATE ISLANDS AND HISTORICAL PERSPECTIVE
H.L. Vacher 1

2. GEOLOGY AND HYDROGEOLOGY OF BERMUDA
H.L. Vacher and Mark P. Rowe 35

3A. GEOLOGY OF THE BAHAMAS
James L. Carew and John E. Mylroie 91

3B. GEOLOGY OF THE BAHAMAS: ARCHITECTURE OF BAHAMIAN ISLANDS
Pascal Kindler and Paul J. Hearty 141

3C. GEOLOGY OF THE BAHAMAS: SUBSURFACE GEOLOGY OF THE BAHAMAS BANKS
Leslie A. Melium and Jose Luis Masaferro 161

4. HYDROGEOLOGY OF THE BAHAMIAN ARCHIPELAGO
Fiona F. Whitaker and Peter L. Smart 183

5. GEOLOGY AND HYDROGEOLOGY OF THE FLORIDA KEYS
Robert B. Halley, H.L. Vacher and Eugene A. Shinn 217

6. GEOLOGY OF MUD ISLANDS IN FLORIDA BAY
Peter K. Swart and Philip A. Kramer 249

7. GEOLOGY OF COASTAL ISLANDS, NORTHEASTERN YUCATAN PENINSULA
William C. Ward 275

8. GEOLOGY AND HYDROGEOLOGY OF THE CAYMAN ISLANDS
Brian Jones, K.-C. Ng and I.G. Hunter 299

9. GEOLOGY OF ISLA DE MONA, PUERTO RICO
Luis A. González, Héctor M. Ruiz, Bruce E. Taggart, Ann F. Budd and Vanessa Monell 327

10. GEOLOGY AND HYDROGEOLOGY OF ST. CROIX, VIRGIN ISLANDS
Ivan P. Gill, Dennis K. Hubbard, Peter P. McLaughlin and Clyde H. Moore, Jr.. 359

11. GEOLOGY AND HYDROGEOLOGY OF BARBADOS
John D. Humphrey 381

12. GEOLOGY OF SELECTED ISLANDS OF THE PITCAIRN GROUP, SOUTHERN POLYNESIA
S.G. Blake and J.M. Pandolfi 407

13. GEOLOGY AND HYDROGEOLOGY OF MURUROA AND FANGATAUFA, FRENCH POLYNESIA
Danièle C. Buigues 433

14. GEOLOGY OF MAKATEA ISLAND, TUAMOTU ARCHIPELAGO, FRENCH POLYNESIA
Lucien F. Montaggioni and Gilbert F. Camoin 453

15. GEOMORPHOLOGY AND HYDROGEOLOGY OF SELECTED ISLANDS OF FRENCH POLYNESIA: TIKEHAU (ATOLL) AND TAHITI (BARRIER REEF)
Francis Rougerie, Renaud Fichez and Pascale Déjardin. 475

16. GEOLOGY AND HYDROGEOLOGY OF THE COOK ISLANDS
James R. Hein, Sarah C. Gray and Bruce M. Richmond 503

17. GEOLOGY AND HYDROGEOLOGY OF NIUE
Christopher Wheeler and Paul Aharon. 537

18. HYDROGEOLOGY OF CARBONATE ISLANDS OF THE KINGDOM OF TONGA
Lindsay J. Furness 565

19. GEOLOGY AND HYDROGEOLOGY OF TARAWA AND CHRISTMAS ISLAND, KIRIBATI
A.C. Falkland and C.D. Woodroffe. 577

20. HYDROGEOLOGY OF THE MARSHALL ISLANDS
Frank L. Peterson 611

21. GEOLOGY OF ANEWETAK ATOLL, REPUBLIC OF THE MARSHALL ISLANDS
Terrence M. Quinn and Arthur H. Saller 637

22. HYDROGEOLOGY OF ENEWETAK ATOLL
Robert W. Buddemeier and June A. Oberdorfer 667

23. HYDROGEOLOGY OF SELECTED ISLANDS OF THE FEDERATED STATES OF MICRONESIA
Stephen S. Anthony 693

24. GEOLOGY AND HYDROGEOLOGY OF NAURU ISLAND
Gerry Jacobson, Peter J. Hill and Fereidoun Ghassemi 707

25. HYDROGEOLOGY OF NORTHERN GUAM
John F. Mink and H.L. Vacher 743

26. HYDROGEOLOGY OF SELECTED ISLANDS OF FIJI
J. Ferry, P.B. Kumar, J. Bronders and J. Lewis 763

27. GEOLOGY AND HYDROGEOLOGY OF ROTTNEST ISLAND, WESTERN AUSTRALIA
Phillip E. Playford 783

28. GEOLOGY OF THE HOUTMAN ABROLHOS ISLANDS
Lindsay B. Collins, Zhong Rong Zhu and Karl-Heinz Wyrwoll 811

29. GEOLOGY OF REEF ISLANDS OF THE GREAT BARRIER REEF, AUSTRALIA
David Hopley 835

30. HYDROGEOLOGY OF HERON ISLAND, GREAT BARRIER REEF, AUSTRALIA
Delton Chen and André Krol 867

31. GEOLOGY AND HYDROGEOLOGY OF THE COCOS (KEELING) ISLANDS
C.D. Woodroffe and A.C. Falkland 885

32. HYDROGEOLOGY OF DIEGO GARCIA
Charles D. Hunt 909

Subject Index 933

This Page Intentionally Left Blank

Geology and Hydrogeology of Carbonate Islands. Developments in Sedimentology 54
edited by H.L. Vacher and T. Quinn
© 1997 Elsevier Science B.V. All rights reserved.

Chapter 1

INTRODUCTION: VARIETIES OF CARBONATE ISLANDS AND A HISTORICAL PERSPECTIVE

H.L. VACHER

INTRODUCTION

The purpose of this book is to provide a sampling of the geology and hydrogeology of carbonate islands. As discussed in this chapter, there are several different kinds of islands included in the survey. Among these are islands of atolls and other modern reefs, islands composed of uplifted reef deposits, islands composed of reefs stranded by earlier highstands of sea level, and islands composed of Quaternary eolianites. Also included are "composite islands" — islands of "mixed geology" — where underlying noncarbonate rocks are also exposed. Overall, the chapters cover about thirty islands and island groups in some detail (see Table 1-1).

The carbonates of the islands included in this book are Cenozoic in age. In a general way, the islands either formed as part of the present depositional environment or are, at least, still part of a modern carbonate setting; in general, the fact that the carbonate deposits are on islands is reflected in the formative geology. Islands composed of "ancient carbonates" that are more appropriately considered in conjunction with their neighboring continents are not included — islands such as Silba, which lies off the coast of Croatia and is composed of the upper Chalk (Bonacci and Margeta, 1991), and Gotland, which is in the Baltic Sea and is composed largely of Paleozoic limestones (Manten, 1971). Also excluded are large islands such as Puerto Rico and Jamaica.

Although this book provides a sampling of many islands with Cenozoic carbonates in present-day carbonate settings, there are, of course, many such islands where important geological work has been done that are not included. In other words, there is no claim that the sampling in this book is exhaustive — even in the types of carbonate islands that are present in carbonate areas.

The organization of chapters is, in a general way, east to west: Atlantic and Gulf of Mexico (Bermuda, Bahamas, Florida); Caribbean (coastal Yucatan, Cayman Islands, Isla de Mona, St. Croix, Barbados); Polynesia (Pitcairns, Mururoa and Fangataufa, Makatea, Tikehau and Tahiti, Tonga); Micronesia (Enewetak, the Marshalls, Nauru, Guam); Melanesia (Fiji); coastal Australia (Great Barrier Reef, Rottnest, the Houtman Abrolhos); and the Indian Ocean (Cocos [Keeling], Diego Garcia). This chapter attempts to organize the material conceptually and give a sense of the history.

Table 1-1

Varieties of carbonate islands in this book

Kind	Examples	Chap
I.	Reef islands and reef composite islands	
	Atolls	
	Mururoa, Fangataufa (Fr. Polynesia)	13
	Tikehau (Fr. Polynesia)	15
	Rakahanga, Manuihiki, Pukapuka (Cook Islands)	16
	Tarawa, Christmas Island (Kiribati)	19
	Majuro, Kwajalein, Bikini (Republic of Marshall Islands)	20
	Enewetak (Republic of Marshall Islands)	21, 22
	Mwoakiloa, Pingelap, Sapwuahfik (Fed. St. Micronesia)	23
	Cocos (Keeling) Islands (Indian Ocean, near Indonesia)	31
	Diego Garcia (Chagos Archipelago, central Indian Ocean)	32
	Modern reefs	
	Great Barrier Reef	29
	Heron Island (Great Barrier Reef)	30
	Low, Quaternary reef islands	
	Upper Keys (Florida)	5
	Cozumel (northeastern Yucatan)	7
	Houtman Abrolhos Islands (Western Australia)	28
	Uplifted atolls, other elevated reef islands	
	Makatea (Fr. Polynesia)	14
	Niue (South Pacific)	17
	Nauru (central Pacific)	24
	Isla de Mona (Puerto Rico)	9
	Henderson Island (Pitcairn Islands)	12
	Tongatapu (Tonga)	18
	Almost-atoll	
	Aitutaki (Cook Islands)	16
	Composite islands with elevated reef limestone	
	Barbados (Lesser Antilles)	11
	Atiu, Mitiaro, Mauke, Mangaia (Cook Islands)	16
	Guam (Mariana Islands)	25
II.	Eolianite islands	
	Bermuda	2
	Bahamian islands	3
	Cancun (northeastern Yucatan Peninsula, Mexico)	7
	Rottnest Island (Western Australia)	27
III.	Other carbonate islands	
	Lower Keys (Florida): Pleistocene oolitic shoals	5
	Islands of Florida Bay: Holocene mud islands	6
	Grand Cayman Island: Low island with varied Sangamonian shallow-water deposits against Tertiary platform carbonates	8
	St. Croix: Composite island with Tertiary pelagic to shallow-water carbonates	10
	Lau Group (Fiji): Composite and solely carbonate islands with carbonates of various facies built up on submerged volcanic cones	26

HISTORICAL PERSPECTIVE

Perspective on the history of carbonate-island geology can be gained by looking at the subject and its context two hundred years ago, at the birth of modern geology, and then one hundred years ago. Two hundred years ago, Sir Joseph Banks — "the most prominent English patron of natural sciences" (Boorstin, 1985, p. 282), and a man whom Linnaeus referred to as "the immortal Banks" (Watkins, 1996, p. 52) — had returned from the South Seas and was President of the Royal Society. One hundred years ago, Alexander Agassiz was visiting all the carbonate islands he could, and there was the Funafuti Expedition of the Royal Society to test Darwin's coral-reef theory.

Two hundred years ago

Banks. Sir Joseph Banks (1743–1820) had accompanied Captain James Cook (Table 1-2) on the *Endeavour* (1768–1771) and brought back an estimated 30,000 specimens of plants and animals. His collection from the South Seas trip would enhance "the list of plant species published in the *Species plantarum 1762–63* of Linnaeus by about one-fifth" (Carter, 1994, p. 5), and his expedition to Iceland (1772; see Agnarsdóttir, 1994) was a factor in the Neptunist vs. Vulcanist debate of the origin of basalt (Torrens, 1994). But more than his own scientific achievements, Banks from the age of 35 was President of the Royal Society and one of the history of science's "influentials" (Stanton, 1994, p. 149). According to Watkins (1996, p.36), "Few men were as famous in his own time or more important to the history of the natural sciences. Few saw more of the world; few did more to change it. And few enjoyed life quite so much as Banks, sitting at the center of the web." Also, his self-financed participation in Cook's voyage was seminal. According to Stanton (1994, p.149), with this trip "Banks launched the modern age of discovery. Thereafter no national exploring expedition worthy of the name failed to find a place for a naturalist." Thus started the tradition that included Darwin on the *Beagle* and Dana on the U.S. Exploring Expedition (Table 1-2).

Cook. If Banks' trip with Captain Cook marked the launching of the "modern age of discovery" from the perspective of natural history, then Cook's voyages marked the climax of the "Era of Discovery" of Pacific islands (Oliver, 1961, p. 84) from the perspective of a western geographer. To be sure, this era of discovery by Europeans during the sixteenth, seventeenth and eighteenth centuries was not the first for the islands. Menard (1989, p. 3), for example, wrote

> "... almost every island was successively found and populated by plants, animals, non-Europeans, and Europeans"

and he discussed each wave of discovery. Oliver (1961, p. 84) put the point colorfully:

> "To hail westerners as discoverers of the Pacific Islands is inaccurate as well as ungracious. While Europeans were still paddling around in their small landlocked Mediterranean Sea or timidly venturing a few miles past the Pillars of Hercules, the Oceania "primitives" were moving about the wide Pacific in their fragile canoes and populating all its far-flung islands."

Table 1-2

Time line for the history of reef-island geology

1768–1779	The three voyages of Captain James Cook.
1831–1836	Voyage of the *Beagle*, Captain Robert Fitzroy. Charles Darwin, unpaid naturalist.
1838–1842	U.S. Exploring Expedition, Captain Charles Wilkes. James Dwight Dana, member of the scientific staff.
1842	*The Structure and Distribution of Coral Reefs*, by Charles Darwin.
1849	*Geology of the U.S. Exploring Expedition*, by James Dwight Dana.
1859	Last European discovery of an atoll, Midway.
1872	*Corals and Coral Islands*, by James Dwight Dana.
1872–1876	Voyage of HMS *Challenger*. C. Wyville Thompson, chief of scientific staff. John Murray, a junior scientist.
1880–1895	Publication of the final report of the Challenger expedition, edited by John Murray.
1888	"A criticism of the theory of subsidence as affecting coral reefs" by H.B. Guppy.
1892–1902	Expeditions of Alexander Agassiz to coral reefs and islands. Published in several Bulletins and Memoirs of the Mus. Comp. Zool., Harvard.
1896–1898	Deep drilling at Funafuti; limestone to 1,114 ft. Coral Reef Committee of the Royal Society. Drilling results: "The geology of Funafuti" by T.W. Edgeworth David and G. Sweet (1904).
1897–1908	Discovery and initiation of mining of phosphate on elevated carbonate islands: Christmas I. (Indian Ocean), Nauru, Ocean Island, Makatea.
1910–1934	"Pleistocene glaciation and the coral reef problem" by Reginald A. Daly (1910); "The glacial-control theory of coral reefs" by Daly (1915); *The Changing World of the Ice Age* by Daly (1934).
1913–1928	"Dana's confirmation of Darwin's theory of coral reefs by William Morris Davis (1913); *The Coral Reef Problem* by Davis (1928).
1930–1954	"Erosion of elevated fringing reefs" by J. Edward Hoffmeister (1930); "Foundations of atolls: a discussion" by Hoffmeister and Harry S. Ladd (1935); "The antecedent platform theory" by Hoffmeister and Ladd (1944); "Solution effects on elevated limestone terraces" by Hoffmeister and Ladd (1945); "The shape of atolls: an inheritance from subaerial erosion forms" by F.S. MacNeil (1954).
1947–1950	"Contributions to the geology of the Houtman's Abrolhos, Western Australia" by Curt Teichert (1947); "Recent and Pleistocene coral reefs of Australia" by Rhodes W. Fairbridge (1950); "Late Quaternary sea-level changes at Rottnest Island, Western Australia" by Teichert (1950).
1947–1952	Deep drilling at Bikini and Enewetak, Marshall Islands. Deepest drill hole (2,556 ft) at Bikini did not reach volcanics (1947). Two drill holes (4,158 and 4,610 ft) reached volcanics at Enewetak (1952). Many reports as separately published chapters in U.S. Geol. Surv. Prof. Pap. 280. Summary results in Emery et al. (1954) and Schlanger (1963).
1961	"Eustatic changes in sea level" by Fairbridge.
1962–1990	Numerous reports of expeditions and summary papers by David R. Stoddart and associates about Caribbean atolls; atolls and islands in the Indian Ocean; islands of the Great Barrier Reef; uplifted islands of the Cook and Austral Islands.
1968	"Geology and origin of the Florida Keys" by Hoffmeister.
1968–1974	"Th230/U238 and U234/U238 ages of Pleistocene high sea level stand" by Veeh (1966); "Milankovitch hypothesis supported by precise dating of coral reefs and deep-sea sediments" by Broecker et al. (1968); "Quaternary sea level fluctuations on a tectonic coast: new 230Th/234U dates from the Huon Peninsula, New Guinea" by Bloom et al. (1974).
1973–1977	*Biology and Geology of Coral Reefs* (4 vols), edited by O.A. Jones and R. Endean.
1974	"Reef configurations, cause and effect" by Edward G. Purdy.
1982	*The Geomorphology of the Great Barrier Reef: Quaternary Development of Coral Reefs* by David Hopley.
1988	*Coral Reef Geomorphology* by A. Guilcher

From the perspective of carbonate-island geology, it is no doubt safe to say that Captain Cook was the premier discoverer of carbonate islands. Referring to Cook and the Era of Discovery, Oliver (1961, p. 84) wrote:

> "The era was brought to a close by the voyages of Captain James Cook, who did such a thorough job of it that in the words of a Frenchman, "he left his successors with little to do but admire."

As illustration, the following excerpt from Oliver (1961, p. 95–96) gives a taste of Cook's vast range amongst the carbonate islands of the Pacific:

> "At the age of forty, (Cook) was commissioned by the Admiralty and the Royal Society to lead an expedition to Tahiti in order to observe from that point the forthcoming transit of Venus.... In addition, Cook received secret instructions to search for the south continent and to stake out English claims to any lands he might discover.
>
> The log of Cook's first voyage, extending from 1768 to 1771, has now become such a classic that it is almost impertinent to attempt a summary. Nevertheless, for the continuity of this chronicle it will be useful to repeat once more his list of discoveries, after he had successfully completed his mission at Tahiti; they included the Leeward Islands, Rurutu, and a survey of the coasts of New Zealand and of almost the entire eastern coast of Australia.
>
> During his second voyage (1772–1775) Cook circumnavigated the globe, going close to the Antarctic in a vain search for the fabled southern continent that continued to engage imaginations. On the same voyage he revisited many islands seen during his first expedition and made many new Oceanic discoveries, including islands in the Tuamotus, the Southern Cooks, Fatu-huku (Marquesas), Palmerston, Niue, New Caledonia, and Norfolk. During his third voyage (1776–1779), undertaken partly to seek a northern passage from the Pacific to the Atlantic, Cook discovered Mangaia, Atiu, Tubuai, and Christmas Island; he is also credited with the discovery of the Hawaiian Islands, although some historians ascribe that feat to Juan Gaetana, in 1555. In any event, it was the hospitable Hawaiians who finally put an end to his fabulous career by cutting him to pieces in one of the most beautiful settings in the South Seas."

The impact of Cook on the discovery of islands is illustrated in a compilation by Menard (1986), who plotted the European discoveries of Pacific islands in fifty-year periods. Menard's study area was the main Pacific Basin east of the island arcs. Within this area, there were 113 islands discovered in the half-century before 1800 (i.e., time interval including Cook) in comparison to 12 in 1700–1750, 64 in 1800–1850, and two in 1850–1900. Menard specifically addressed Cook's effect on these numbers (Menard, 1986, p. 11):

> "In the central Pacific basin, Cook found and surveyed 30 islands. Through his unique influence and training, his lieutenants and their lieutenants, seemingly everyone associated with him, continued to explore. His lieutenant Clerke found the last two high Hawaiian Islands. A decade later, his former navigator, Captain Bligh, discovered two islands with HMS *Bounty*. When the mutiny occurred, Bligh and the loyal sailors were placed in an open boat. They then made the longest recorded voyage in such a boat, all the way to Batavia, seldom touching land for fear of the Melanesian cannibals, who even paddled out from shore to intercept them. In the midst of all these hardships and perils, Bligh discovered — and surveyed one side of — eleven islands in the Fiji and Banks groups.... His chief mutineer, Lieutenant Fletcher Christian, discovered the fertile Raratonga (and the Raratongans) with *Bounty* before reversing course and eventually burning the ship off the landing on isolated uninhabited Pitcairn."

Not only oceanic carbonate islands and reefs of the Pacific, but also the Great Barrier Reef of the Australian shelf was introduced to European science by Cook and Banks. For example, Hopley (1982, p. 1), in his definitive book on this great, island-studded, carbonate province, gave the following account:

> "The first contact of science with the Great Barrier Reef of Australia was far from auspicious. H.M.S. *Endeavour*, under the command of Capt. James Cook and carrying a party of scientists led by Joseph Banks, sailed 1400 km inside the Great Barrier Reef northward up the Queensland coast. Having spotted reefal shoals only on the previous day, at about 11 PM on 11 June 1770, they struck hard upon what is now known as Endeavour Reef. Joseph Banks' own comments on the event are typical of the attitude of scientists of the day towards coral reefs: "We were little less than certain that we were upon sunken coral rocks, the most dreadful of all others on account of their sharp points and grinding quality which cut through a ships bottom almost immediately" (Beaglehole, 1962, vol. 2)....
>
> Coral reefs were regarded first and foremost as navigational hazards. Indeed, it had been only 43 years previously that Andre de Peysonnel [in a note in the Histoire de l'Académie Royale des Sciences in 1727] had indicated to the scientific world that coral polyps were animal, not plant, organisms, a fact that took the Royal Society of London a further 24 years to accept.
>
> ....Banks, who was to become president of the Royal Society for 41 years, although showing the seaman's dread of coral reefs, also recognized them as significant areas of research. After passing through the outer barrier into deep water on 14 August he commented: "A Reef such as one as I now speak of is a thing scarcely known in Europe or indeed anywhere but in these seas: it is a wall of Coral rock rising almost perpendicularly out of the unfathomable ocean, always overflown at high water commonly 7 or 8 feet and generally bare at low water; the large waves of the vast ocean meeting with so sudden a resistance make here a most terrible surf Breaking mountain high, especialy when, as in our case, the general trade wind blows directly upon it." (Beaglehole, 1962, vol. 2)."

Banks and Hutton. Publication of *The Theory of the Earth* by James Hutton two hundred years ago (in 1795) is generally taken to mark the beginning of modern geology. Hutton lived in the "Edinburgh of David Hume, Adam Smith, and James Watt" (Gould, 1987, p. 17). Eleven letters between Hutton and Watt have recently been published by Jones et al. (1994, 1995), who noted a connection between Banks and Hutton through Letter V (from Hutton in Edinburgh to Watt in Birmingham, 1774):

> "Hutton describes his erratic progress home.... After roistering in Warwickshire he went through Derbyshire.... His friends at Buxton were "with Omai" and must have included Sir Joseph Banks who took Omai on a tour of the Midlands in September 1774, using the Banks' family seat at Overton as a base. Hutton had been in touch with Banks two years earlier and subsequently met him in Edinburgh on Banks' return from Iceland."

Omei was a young Polynesian who had taken refuge in Tahiti during Cook's second voyage and had asked to be taken to England in the *Adventure* when she returned early. Omei was placed in the care of Banks and "took polite society by storm" (Jones et al., 1995, p. 358). Letter V was four years after Banks' encounter with the Great Barrier Reef.

Banks' role in the early days of modern geology is discussed in detail by Torrens (1994). He was instrumental, for example, in having William Smith's map published. The relevant point here is the connection in time between the beginning of carbonate-island science and the modern science of geology itself. The two are the same age.

One hundred years ago

Agassiz. At the end of the nineteenth century, the big issue concerning reefs and carbonate islands was the argument for and against Darwin's coral-reef theory. A major player was Alexander Agassiz. The following excerpt from the book on Agassiz by his son (G.R. Agassiz, 1913, p. 273–280) captures the scene, illustrates the allure of the subject, and defines the problem on Agassiz's terms.

> "The year 1892 marks the close of a distinct period in Agassiz's life. Until then he had devoted himself chiefly to marine zoölogy. The main scientific interest of his later life was, however, the study of coral islands and reefs, and the method of their formation....
>
> Many of us remember, in the physical geographies of our youth, an illustration of a coral atoll. It captivated our fancy, being so different from anything that had come within our own personal experience .... The picture, to which we loved to return from the perusal of more trying subjects, showed a low, rakish-looking schooner lying peacefully at anchor in a quiet lagoon surrounded by a circle, deceptively perfect, formed of a narrow strip of land studded with cocoanut palms, under which nestled a few native huts, whose primitive outlines appealed to our imagination. On the outside rim huge rollers, heaped up by the trade winds, beat with savage force....
>
> It is impossible to suppose that these curious coral formations have grown up from the depths of the ocean, since twenty fathoms appears to be about the limit at which reef-building corals usually flourish abundantly....
>
> The beauty and simplicity of (Darwin's theory) appealed to the layman as well as to the man of science; it was strengthened by the investigations of Dana, published in 1840, who as naturalist accompanied Captain Wilkes on his memorable voyage.... For many years it remained unquestioned as the true explanation of the causes that had led to the creation of these curious formations. But this theory does not rest on the patient investigations that characterized Darwin's other work; he himself says in his autobiography that it was formed before he even saw a coral reef.... Dana's observations, although more extensive, appear to have been much curtailed by Wilkes' fear that his distinguished companion would be eaten by savages.
>
> Both Darwin and Dana, it may be noted, have assumed a possibility as a fact.... Indeed, the advocates of Darwin's view have assumed a subsidence from the existence of atolls in regions where there are innumerable proofs of elevation....
>
> During his cruise on the Blake, Agassiz satisfied himself that Darwin's theory could not account either for the formation of the Florida Reefs, or the Alacran Reef, an atoll-shaped coral growth to the north of Yucatan. For it seemed evident to him that subsidence could not offer a correct explanation for events that had taken place in regions of elevation, or districts that had long remained stationary. He reached the conclusion that the coral reefs of these localities had begun their growths on banks which had been built up by various agencies until they had reached a point where the depth was suitable for the growth of corals, and that in this region the coral reefs were a comparatively thin crust resting on such foundations....
>
> It is worth emphasizing that the strongest opponents of the new theories were men who had never seen a coral reef, and may possibly have been in somewhat the same attitude of mind as a frank layman of Agassiz's acquaintance, who confessed that, having acquired Darwin's theory in his youth at the cost of much pain and labor, he could not possibly assimilate another."

In 1893–1894, Agassiz studied the Bahamas, the coast of Cuba, Bermuda, and the Florida Keys. In 1896 was his expedition to the Great Barrier Reef. On the recommendation of Dana, among others, Agassiz next studied the Fijis, in 1897–1898. After a winter trip to South African gold and diamond mines in 1898–1899, he returned to the subject during the winter of 1899–1900, "for an extended voyage through the islands of the South Seas, to include practically all the coral-reef regions of the Pacific which he had not yet visited" (G. Agassiz, p. 347). These included the

Marquesas, the Society Islands, the Cook Islands, Niue, Tonga, Funafuti and others of the Ellice Islands, the Gilbert Islands, the Marshall Islands, and the Caroline Islands. Then in the winter of 1901–1902, he wrapped up his study with an expedition to the Maldives in the Indian Ocean.

Murray. Agassiz carried on a prodigious correspondence. Among the scientists with whom he exchanged letters about coral reefs and islands were Darwin, Huxley, T.W.E. David, and particularly his great ally, Sir John Murray. At the time of Agassiz's voyages in the 1890s, Murray was completing the report on the *Challenger* expedition (Table 1-2). One of the geological breakthroughs of that expedition was a realization of the significance of pelagic sediments on the ocean floor, and Murray believed that oceanic accumulation could raise antecedent platforms to the level of reef productivity. But it is also of interest that the completion of the *Challenger* report was funded by carbonate islands. As told by Menard (1986, p. 162–163):

> "It was Sir John Murray who first realized the potential of the high islands that have been major world sources of phosphate for the past eighty years.... (Murray) never obtained a degree, but at age 31 he sufficiently impressed Sir Wyville Thomson, the organizer of the *Challenger* Expedition, to obtain a position as junior scientist. He spent much of the time from late 1872 to 1876 at sea, and by default he was made responsible for the collection and analysis of deep sea sediments. Allowing for inflation, the *Challenger* was probably the most expensive oceanographic expedition that ever sailed. After its return, the British Treasury allotted funds for analysis and publication of results, and Murray was part of the small permanent staff. He became leader of the project when Thomson died. Volume after volume of great grey-green monographs poured out, but the Treasury stopped its funding in 1889, even though much remained to be done. At age 48, John Murray was unemployed.
>
> In that year, Murray married Isabel Henderson, the only daughter of the owner of the Anchor Line, operating steamships out of Glasgow.... One of Murray's shipmates from the *Challenger* happened to be on H.M.S. *Egeria* in 1887 and was a member of the shore party that landed on uninhabited Christmas Island in the Indian Ocean [see Fig. 31-1; this is not the Pacific Ocean Christmas Island of Chap. 19] .... He sent a small rock sample from the island to Murray, who did a chemical analysis. It was a very rich ore of phosphate.
>
> Murray immediately realized the implications of his find, and, in the same year, he persuaded the British Government to annex the island. It was 300 kilometers southwest of Java, isolated, and not of the slightest interest to anyone else. Four years later, Murray and a Mr. Koss of the Cocos Islands obtained a lease of the island. At his own expense, Murray sent C.W. Andrews, of the British Museum, to survey the island in 1897–1898. Construction of a railroad and docks followed, and exploitation began in earnest about 1900. The results of this investment were dazzling. When Sir John Murray, K.C.B., was killed in an automobile accident, in 1914, the rents royalties, and taxes from Christmas Island had long since completely repaid the British Government for the *Challenger* Expedition. Indeed, Murray had maintained that one was the direct consequence of the other. Disdaining further government help, he moved the Challenger Society office to his country mansion, and, like his old friend Alexander Agassiz, he undertook private oceanographic research."

Funafuti. This was also the time (1896–1898) of the great expeditions to Funafuti under the auspices of the Royal Society to investigate the depth and structure of an atoll. On the third expedition, led by the Australian geologist Professor (later Sir) T.W. Edgeworth David, the atoll was drilled to 1,114 ft (340 m), where "the work was stopped as the party had exhausted its supply of diamonds" (G. Agassiz, 1913,

p. 343). Although limestone was encountered through the entire thickness of the deep drill, Murray and Agassiz were not convinced; they thought the great thickness of limestone represented reef talus. As noted by Menard (1986, p. 135), "a basement platform under the lagoon might be quite shallow and composed of any material."

In a letter to Murray, Agassiz wrote (G. Agassiz, 1913), "I have been looking over again the Funafuti book.... The boring should be done in a region where volcanic beds are underlying the coral reefs." Of course, it would be another half-century before sub-atoll volcanics would be drilled in the nuclear test islands of Enewetak (Chap. 21) and Mururoa (Chap. 13) and close this chapter of the coral-reef debate. Ironically, magnetic surveys from the first Funafuti expedition showed the presence of a volcanic high beneath the limestones (Menard, 1986, p. 134). Davis (1928, p. 514, in Wiens, 1962, p. 86) argued that proof of subsidence was in hand from the Funafuti core:

> "The most significant result gained from the boring was that the fossils found in the core were characteristic of shallow water only; while the living organisms dredged from the external slope of the atoll at depths similar to those reached by the boring were in part such as lived at those depths and in part such as, living at lesser depths, sank to deeper water when dead."

The Funafuti Expedition did much more, of course, than further the debate over Darwin's subsidence theory. The study of mineralogy of the Funafuti core by Cullis (1904) was a harbinger of numerous issues that lace through carbonate-island studies of the latter part of our century and constitute major themes in this book. Almost 70 years after Cullis' great work, Bathurst, in his book on carbonate sedimentology, wrote (Bathurst, 1975, p. 350): "Of all the researches into the early stages of near-surface diagenesis, none rivals, in variety, in detail, or in the clarity of its illustrations, the description by Cullis (1904)." Among the issues opened by Cullis was that of mineralogic change and cementation of carbonates as a function of time (depth), and the whole monstrous subject of dolomites and dolomitization within the carbonate caps of ocean islands. There would be a period of dormancy of more than 60 years before the subdiscipline of carbonate diagenesis would burst onto the scene with the carbonate-island work of S.O. Schlanger in Guam and Enewetak, R.K. Matthews in Barbados, and L.S. Land in Bermuda and Jamaica, and their concepts and models of mineralogic stabilization, solution unconformities, vadose vs. phreatic diagenesis, and mixing-zone dolomitization.

Also from the Funafuti Expedition, the interpretation by David and Sweet (1904) of higher sea levels from fossil corals was one of the opening shots of what eventually would become a controversy concerning postglacial highstands of sea level (e.g., McLean and Woodroffe, 1994; see also Chap. 19 of this book). R.A. Daly included Funafuti in his list of places that caused him to hypothesize a "general sinking of sea level in recent time" (Daly, 1920, p. 246). At the height of the controversy during the 1960s and 1970s, there was a battle of Holocene sea-level curves, and islands figured prominently in it. Rottnest Island (Chap. 25) and the Houtman Abrolhos (Chap. 26) were type localities for separate highstands on the well-known Fairbridge curve (Fairbridge, 1961). The equally well-known Shepard-Curray curve (Shepard, 1963; Shepard and Curray, 1967) had large support from highly regarded studies of marsh

cores by Redfield (1967) and Neumann (1969) in Bermuda (Chap. 2). Shepard and Curray put together the *Carmasel* expedition to examine reported evidence of higher Holocene sea levels at, for example, Guam (Stearns, 1941) and Micronesian atolls (e.g., Wiens, 1962) and "... found no direct evidence of postglacial high stands of sea level" (Shepard et al., 1967, p. 542; see also Curray et al., 1970). Within a decade, however, there was reported new evidence of postglacial highstand(s) at Enewetak (Tracey and Ladd, 1974; Buddemeier et al., 1975; see also Chap. 22) and Tarawa (Schofield, 1977; see also Chap. 19).

Now, thanks to an appreciation of hydro-isostasy (e.g., Daly, 1925; Bloom, 1967; Walcott, 1972) and the results of modeling the response of the earth to changes in the shifting of load from ice sheets to global ocean (e.g., Clark et al., 1978; Nakada, 1986; Lambeck, 1990), a "Caribbean sea-level curve" without a highstand and "Pacific sea-level curve" with Holocene emergence can peacefully coexist (McLean and Woodroffe, 1994, p. 278) as manifestations of "intermediate-field" and "far-field" locations relative to the ice sheets (e.g., Lambeck, 1990). Thus the post-Funafuti history illustrates a comment by Matthews (1990, p. 88): "Attempting to understand Quaternary sea-level history provides a vigorous intellectual workout." That subject is one of the attractions and challenges of carbonate islands, and understandably, it is still a subject with some dispute (e.g., Chaps. 2, 3A, 3B).

GEOLOGICAL VARIETIES OF CARBONATE ISLANDS

One way of organizing the material in this book conceptually is to group the island chapters according to type of island. Variables that can be used for classification include size ("small" vs. "very small"), height ("high" vs. "low"), amount of carbonate (composite vs. solely carbonate), sedimentary facies (reef vs. eolianite vs. other), age of the dominant carbonates (Tertiary vs. Quaternary), and tectonic setting (intraplate islands vs. plate-boundary islands). Although probably little would be gained by developing a rigorous and quantitative taxonomy for carbonate islands — and certainly none is intended here — Table 1-1 is organized to show the variety of carbonate islands included in this book. The variables that were most useful in organizing Table 1-1 are the amount of carbonate, the depositional facies of the carbonate, and island height (more precisely, "Why are reef deposits exposed?"). The hierarchical scheme behind the categories is shown in Figure 1-1. The purpose of this section is to illustrate the diversity of carbonate islands in this book in terms of variables by which the islands can be classified and the thinking that leads to Figure 1-1.

Small and very small islands

"Small islands" present an obvious challenge for water supply, and this fact is of great interest to UNESCO. Thus one of the themes of UNESCO's International Hydrological Program (IHP) was the Hydrology of Small Islands (IHP-III, Theme 4.6). A product of that group effort was a major technical report prepared mainly by

A. Falkland and E. Custodio (Falkland, 1991, Editor) that collected information from various IHP national committees and international organizations interested in the hydrology and water resources of small islands. According to Falkland (1991), one of the first questions was, "What is a small island?" Perhaps it is not a surprise that there was not an easy answer (Falkland, 1991, p. 1):

> "Hydrologists from countries at different latitudes and with a range of water resources problems and skills agreed that the hydrology of small islands was dictated by specific hydrological features. Although many limiting areas for small islands were proposed, it was not possible to reach a consensus. After discussions with many specialists, intergovernmental agencies and international scientists' associations with experience in the hydrology of islands, it was decided that the term "small island" should apply to islands with areas less than approximately 1,000 km^2 and to larger, elongated, islands where the maximum width of the island does not exceed 10 km..."

At a subsequent meeting, the limit was revised upward (2,000 km^2, Falkland, 1991, p. 1). In any event, the objective of the definition was clear: to separate out islands where "methods, techniques and approaches to hydrology and water resources issues cannot be directly applied from continental situations" (Falkland, 1991, p. 1).

The UNESCO guide recognized a subclass, very small islands. Although it did not mean the definition to be rigid, the guide followed Dijon (1984) in adopting limits of 100 km^2 or a width no greater than 3 km. Again quoting Falkland (1991, p. 1),

> "These physical limits generally mean that very limited surface or groundwater resources will be present. In very small islands, approaches to the assessment, development and management of water resources is normally required on an island specific basis, whereas there may be some scope for a slightly more generalized approach with groups or archipelagos of larger-size small islands."

By these definitions, the carbonate islands detailed in this book are small or very small islands. Guam (549 km^2), Barbados (430 km^2), Niue (259 km^2), Tongatapu (257 km^2) and Grand Cayman Island (196 km^2), for example, are small islands; Bermuda (50 km^2), Nauru (22 km^2), Rottnest Island (19 km^2) and countless atoll and reef islands are very small islands. For size comparison, Puerto Rico and Jamaica — composite islands with well-known carbonate terranes — are 9,104 and 10,991 km^2 in area, respectively.

High and low islands

If area is the relevant size parameter for island hydrology, the height of the island has been historically important as the relevant dimension for the island's visibility. The point is made by Menard (1986) in his discussion of the European exploration of the Pacific:

> "The oceanic islands of the main Pacific Basin east of the island arcs comprise 184 atolls or rocks barely above sea level and 83 high islands, including elevated atolls. The distinction is made between high islands and low because height is what determines how far an island can be seen — its "size," for the purpose of discovery. (Menard, 1986, p. 11).
>
> The high islands were found generally before the low ones. This is best seen in the last century of discovery. All but two of the high islands were found by 1800 and the last,

> Rimatara, by 1811. In contrast, more low islands were found in the 1820s than in any other decade.... Atolls continued to be found for 48 years after the last high island....
>
> The first high island to be discovered in the Pacific region of interest here was Ponape, 786 m high, in 1529. Ponape is one of three widely separated high islands among the abundant atolls and drowned atolls of the Caroline group. The atolls surrounding Ponape were discovered in 1529, 1568, 1773, and 1824. It is evident that atolls can easily escape notice. (Menard, 1986, p. 14.)"

Menard's discussion illustrates a common distinction: volcanic islands fringed or bordered by reefs are "high islands," and atolls are "low islands." Uplifted atolls also may be considered "high," but as the excerpt suggests, they lie somewhere in between "high" and "low," so that labeling them as "high" requires explicit mention.

Amount of carbonates: Volcanic, composite, and purely carbonate islands

Ever since Darwin, it has been standard and useful to classify oceanic islands of the "coral seas" into three basic categories (Menard, 1986; Nunn, 1994): islands composed of volcanic rocks (volcanic islands); islands in which the volcanic rocks are draped with younger limestones (composite islands); and islands in which the volcanic rocks are completely buried ("carbonate islands" of many authors). This subdivision of islands obviously parallels Darwin's evolutionary sequence of reefs forming on a subsiding volcanic edifice: first, a volcanic island with no reef; then, a volcanic island bordered by a "fringing reef" (implying a separation from the island by at most a boat channel; e.g., Guilcher, 1988, Chap. 4); then, remnants of a volcanic island bordered by a "barrier reef" (implying a separation from the volcanic island remnant by a relatively wide and deep lagoon); and finally, a reef encircling a lagoon with no remnant volcanic islands (atoll). As an intermediate step between the barrier-reef island and atoll, Davis (1928) and Tayama (1952) introduced the term "almost-atoll" for cases where the area of volcanic island remnants is small relative to that of the lagoon (Stoddart, 1975).

Just as there are "low" atoll islands and "high" uplifted atolls, there are composite islands on subsiding foundations and composite islands where the carbonates have been uplifted. In the first category are barrier-reef islands and almost-atolls such as Bora-Bora in French Polynesia and Aitutaki in the Cooks Islands (Chap. 16). In the second category are islands such as Barbados (Chap. 11) in the West Indies and Mitiaro, Atiu, Mauke, and Mangaia in the southern Cooks (Chap. 16). This second category can be further subdivided into islands where the carbonates formed during progressive uplift (e.g., Barbados) and those where the uplift followed subsidence (e.g., southern Cooks). Although such distinctions are not troubling now, it is worth noting that the identification of uplifted atolls and high volcanic islands draped with elevated reef deposits vigorously fueled the debate over Darwin's theory of coral reefs that formed on subsiding volcanic edifices. To Agassiz, evidence of uplift directly contradicted Darwin's postulated subsidence. As pointed out by Menard (1986), Agassiz was impressed with the carbonate islands of plate boundaries, whereas Darwin's theory pertains mainly to midplate oceanic settings. For a plate-tectonic view of the evolution of carbonate islands, see Scott and Rotundo (1983a, b) and Guilcher (1988, Chap. 3).

Nonvolcanic basement. Characterizing composite islands as carbonates with an exposed volcanic foundation is an obvious oversimplification: the basement beneath the carbonate rocks of interest can be nonvolcanic. A well-known example is Barbados where Pleistocene fringing reefs offlap a basement composed of uplifted oceanic sedimentary rocks (Chap. 11). The basement rocks of Saint Croix consist of intrusives and deep-water sedimentary rocks (Chap. 10). The Great Barrier Reef system includes 617 composite islands where continental rocks are fringed with modern reef (Chap. 29).

Facies of carbonates: reef, eolianite, other

Carbonate islands of this book — both those consisting solely of carbonate rocks, and composite islands — divide lithologically into three main categories (Table 1-1). The first category comprises islands where the carbonates are either modern reef-derived sediments or Pleistocene or Tertiary reef and reef-associated deposits ("reef islands"). The second category comprises islands where the carbonates consist largely of Quaternary eolianites ("eolianite islands"). These two categories appear to be somewhat antithetical: carbonate eolianite islands occur on the higher-latitude margins of the carbonate belt, and reef islands define its core, within the "coral seas." The third category consists of islands where the carbonate sediments or rocks are of some other depositional facies.

Reef islands. Reef islands are part of the classic debate (Table 1-2) involving Darwin and Dana (subsidence and the evolution from fringing, to barrier, then atoll reefs); Guppy, Murray, and Agassiz (upbuilding from antecedent platforms, subsidence not necessary); Daly (the "glacial control theory" — glacioeustasy); and Hoffmeister and Ladd, MacNeil, Purdy, and Bourrouilh (the "karst saucer theory;" Guilcher, 1988, p. 75). The story of this great debate has been told many times (e.g., Davis, 1928; Wiens, 1962; Stoddart, 1973; Steers and Stoddart, 1977), and excellent recent accounts are provided in books by Hopley (1982, Chap. 1), Menard (1986, Chap. 7), Guilcher (1988, Chap. 3), and Nunn (1994, Chap. 7). Today, there is no question that many reefs and atolls — in midplate, oceanic settings — formed on subsiding volcanic foundations; that some reef islands formed in areas of uplift and progressive emergence, whereas others have been uplifted after a history of subsidence; that glacial/interglacial cycles led to alternate emergence and submergence of reefs, produced succeeding generations of reefs on top of earlier generations, and resulted in reef islands above present sea level even in the absence of uplift; and that karst features, formed when the reef complex was emergent, are now submerged in many reef systems.

The main remaining geomorphological question of reef islands now seems to be the relative importance of depositional vs. erosional relief. In this regard, it is useful to keep in mind the distinction made by Stoddart (1973) and Steers and Stoddart (1977) between the explanation of the structure of the atoll edifice (i.e., subsidence and the great depth to volcanic basement predicted by Darwin) and that of its

surface morphology (i.e., the interplay of depositional and erosional processes in a time frame of sea-level changes) (McLean and Woodroffe, 1994). It is also useful to appreciate that the occurrence of reef limestone in the rim of an "uplifted atoll," for example, does not preclude karst erosion of the interior as an important process. For a range of views on the subject of depositional vs. erosional relief for particular uplifted limestone islands, see the chapters in this book on Isla de Mona in the Caribbean (Chap. 9), Henderson Island in the Pitcairns (Chap. 12), Makatea in French Polynesia (Chap. 14) and the Fijis in the southwest Pacific (Chap. 26).

In the context of modern reef islands, it is worthwhile also to distinguish between processes resulting in the surface configuration of the major edifice (the reef and lagoon) and those producing and shaping the islands themselves, on top of the edifice. McLean and Woodroffe (1994) have recently discussed island formation in coral-reef settings. For particular examples, see the chapters in this book on the islands of the Great Barrier Reef (Chap. 29) and the atoll islands of the Cocos Islands (Chap. 32).

"High" and "low" reef islands. Reef islands that consist solely of carbonate rocks can be subdivided into three main types:

1. Islands consisting of modern sediments associated with modern reefs; examples include the atolls of Table 1-1 and islands of the Great Barrier Reef (Chap. 29), including Heron Island (Chap. 30).
2. Islands where the reefs are emergent because they record one or more Quaternary sea-level highstands above present sea level. Examples include Key Largo of Florida (Chap. 5) and the Houtman Abrolhos Islands (Chap. 28).
3. Islands where Cenozoic reefs are emergent because of uplift. These islands include uplifted atolls such as Nauru (Chap. 24), Niue (Chap. 17), and Makatea (Chap. 14), and elevated limestone islands such as Isla de Mona (Chap. 9), Henderson Island (Chap. 12), and Tongatapu (Chap. 18).

Islands of atolls and other modern reefs (the first category) are unequivocally "low islands." Maximum elevations may range up to several meters in storm ridges. Islands consisting of reefs stranded from Quaternary sea-level highstands (second category) are within the height of storm ridges of modern Pacific atolls, and so these islands, too, can reasonably be considered as "low islands." As already noted, there is some precedent for regarding uplifted atolls and other elevated limestone islands (the third category) as "high islands," a label that also applies to reef-fringed volcanic islands such as Tahiti (2,241 m) and Raratonga (653 m). Sample elevations of the high points of these uplifted limestone islands are: Isla de Mona, 90 m; Nauru, 71 m; Niue, 66 m; Tongatapu, 65 m.

Atolls. Atolls occupy a special place in the subject of coral reefs and carbonate islands. Bryan (1953) lists 425 atolls (Stoddart, 1965), including some 285 in the Pacific (Falkland, 1991, p. 2). In this book, there are ten chapters dealing with atolls and groups of atolls (Table 1-1). These chapters give a rather extensive survey of issues involved in the study of atoll geology and hydrogeology today (Table 1-3).

Table 1-3

Geology and hydrogeology of atolls and atolls islands

Subject	Chapters
Geomorphology	
Reef geomorphology	15, Polynesian atolls
Surface morphology and Holocene history	19, Tarawa and Christmas I. 22, Enewetak 31, Cocos (Keeling)
Subsurface Geology	
Below carbonate cap: the volcanic basement and transitional interval of volcanic rocks, volcaniclastics, and carbonates.	13, Mururoa and Fangataufa
Stratigraphy, sedimentary facies and diagenetic history of Tertiary limestones and dolomites.	13, Mururoa and Fanataufa 21, Enewetak
Quaternary reef growth, sea-level history and diagenesis	16, Cook Islands 21, Enewetak
Shallow, meteoric groundwater	
Shallow stratigraphy, dual-aquifer permeability distribution, and relation to occurrence of fresh and brackish groundwater	19, Tarawa and Christmas I. 20, Marshall Islands 22, Enewetak 23, Fed. States Micronesia 32, Diego Garcia
Mapping freshwater lenses on remote islands	23, Fed. States Micronesia
Recharge and temporal variability of freshwater lenses	19, Tarawa and Christmas I.
Modeling flow and salinity distribution of a brackish system	22, Enewetak
Modeling development alternatives	20, Marshall Islands
Climatic variations and groundwater supply	32, Diego Garcia
Deep, thermal circulation	
General character and temperature distribution	13, Mururoa and Fangataufa
Permeability data	13, Mururoa and Fangataufa
Endo-upwelling and relation to nutrient budget of interstitial waters of reefs	15, Tikehau

The compilation of Table 1-3 follows the American Geological Institute's *Glossary of Geology* (Gary et al., 1972) in that an atoll is considered to be a low-lying reef surrounding a central lagoon. Islands listed as atoll islands in Table 1-1 are low islands composed of modern reef debris. There is some variation in the set, as illustrated by Christmas Island (Chap. 19) where the lagoon is largely filled in and some Pleistocene limestone is exposed, and the Cocos Islands (Chap. 31), where eolian dunes are present. The variation, however, is limited. Table 1-3 does not include Bermuda, for example, despite the fact that the main carbonate structure of Bermuda (the Bermuda Platform) comprises a rim of reefy shoals and (eolianite) islands surrounding an interior lagoon (for another view see Garrett and Scoffin, 1977, and Meischner and Meischner, 1977). The Bermuda Platform, which at 32°20′ latitude includes the northernmost reefs in the Atlantic (see Guilcher, 1988, Chap. 1), can be considered a variety of eolianite-reef complex bordering on — perhaps even

transitional with — the distinctly different lagoon-enclosing reef structures that one normally associates with the word "atoll."

Makatea islands. Mitiaro, Atiu, Mauke, and Mangaia in the southern Cooks (Chap. 16) are well-known "makatea islands," a term that is widely used in the geomorphologic literature of Pacific islands. Makatea islands are characterized by: an exposed volcanic core; a prominent rim composed of reef limestone; and distinct, commonly swampy lowlands between the volcanics and the limestone rim. This type of island is so common in the Pacific that Nunn (1994) uses the term "makatea island" as a synonym for "composite island." From the accounts of makatea islands and makatea topography (e.g., Stoddart and Spencer, 1980; Stoddart et al., 1990), the lowlands between the volcanic core and the elevated reef limestone are an essential feature. One can picture that this topography is the kind that would be produced by uplift of a reef rim surrounding a volcanic remnant (i.e., fringing reefs with significant boat channels, or barrier-reef island, or almost-atoll).

The detailed work by Stoddart and colleagues in the makatea islands of the southern Cook Islands (Chap. 16) led them to conclude that the lowlands in those islands are due largely to solution and retreat of the landward edge of the bordering, Tertiary-age reef limestone (see also Nunn, 1994). The interpretation of erosional vs. depositional origin of the lowlands of these makatea islands is analogous to the competing interpretations of erosional vs. depositional origin of the interior basin of uplifted atolls (e.g., "karst saucer theory").

Unfortunately for the terminology, as Nunn (1994) has pointed out, the Polynesian island of Makatea (Chap. 14) is *not* a makatea island, or a composite island of any kind; it is an uplifted atoll. The word "makatea," derived from the Polynesian, refers to limestone of the elevated rim (Gary et al., 1972) and, as such, has been used for the limestone on both uplifted atolls and makatea islands. One can say that a makatea island is characterized by makatea limestone separated by lowlands from the core volcanics. Detailed accounts by Stoddart and Spencer (1980) and Stoddart et al. (1990) describe the makatea as consisting of Tertiary reef limestones; Pleistocene reef limestones are second-order features around the periphery. The same is true in the uplifted atolls: the Pleistocene deposits are second-order peripheral features against the limestones comprising the main elevated rim that generates the name "uplifted atoll" (e.g., Figs. 14-5, 24-9). Thus overall, and from the interior to the coastline of the island, the makatea island consists of: exposed basement rocks, lowlands, makatea limestone, and peripheral fringe of Quaternary features (see Fig. 16-3).

The foregoing characterization does not describe the geomorphology or architecture of the composite island of Barbados, where the exposed basement rocks are offlapped by a succession of Pleistocene reef terraces. In Barbados, the rising accretionary complex on which the island occurs did not reach the level where reefs would develop until the Pleistocene (Chap. 11).

Eolianite islands. Recognition that some islands are composed of cemented, windblown, "coral sand" dates back to the time of Lyell in Bermuda (Chap. 2) and the Bahamas (Chap. 3) (see also Fairbridge, 1995, for discussion of Darwin's rec-

ognition of eolian carbonates on his voyage on the *Beagle*). The eolian character of eolianite was (and is) evident from the rolling topography of dune-shaped hills of the islands, and large-amplitude, high-angle cross-bedding exposed in the coastal cliffs. Associated red paleosols (terra rossa) and fossiliferous marine units gave early testimony (late nineteenth century) to a history of the changing vertical position of land and sea. Although now those changes are known to have resulted from glacioeustasy, there are different views on how glacial-interglacial cycles correlate with deposition of the eolianite: during interglacials in Bermuda, Bahamas, and coastal Yucatan (Chap. 7); during glacial lowstands in Australia, including Rottnest Island (Chap. 27).

Many eolianite islands reach elevations comparable to those of "high" reef islands such as uplifted atolls. Sample high points of eolianite islands are: 79 m in Bermuda; 63 m at Cat Island in the Bahamas; 45 m at Rottnest Island. Eolianite islands, therefore, might be considered "high islands," even though they owe their elevation to depositional processes rather than uplift.

Eolianite composite islands. Just as purely carbonate islands are more often composed of reef and reef-associated facies than eolianites, composite islands consisting of reef carbonates on older basement are more numerous than composite islands consisting of eolianites and related deposits on older basement. One example of the latter is San Clemente Island off southern California, where an uplifted structural block composed mostly of Miocene andesite supports Quaternary terrace deposits and carbonate eolianites (Muhs, 1983). An intraplate oceanic example is Lord Howe Island, where the carbonate eolianite facies has begun to develop on the remnants of a hotspot-related, shield volcano in the Tasman Sea (Woodroffe et al., 1994). Lord Howe Island, at 31°33′ S, is the site of the world's southernmost coral reefs (Guilcher, 1988, Chap. 1). Thus Lord Howe Island plays the same role for oceanic composite islands as Bermuda plays for purely carbonate islands that cover an oceanic, volcanic edifice; in both cases, the carbonate rocks are mainly Quaternary eolianite, in keeping with their setting at the margins of the world's carbonate belt.

Preliminary classification. From these considerations of "high" vs. "low" and the facies and age of the carbonate deposits, one can easily discern four main classes of carbonate islands where the noncarbonate basement is not exposed. These are: (1) islands on modern atolls and other reefs; (2) "low" islands consisting of reef deposits from Quaternary sea-level highstands; (3) "high" islands consisting of uplifted reefs; and (4) "high" islands consisting of Quaternary eolianites. In addition, one can easily add: (5) "low" islands consisting of other types of carbonate deposits stranded from Quaternary highstands (e.g., the oolitic islands of the southern Florida Keys, Chap. 5), and (6) "low" islands consisting of other types of modern carbonate deposits (e.g., the mud islands of Florida Bay, Chap. 6). Number 5 is a variant of 2, and number 6 is a variant of 1. As shown in Figure 1-1, one can also recognize parallel classes in a branch of carbonate islands where underlying noncarbonate basement is exposed (i.e., composite islands). This crude classification is sufficient to organize the chapters (Table 1-1).

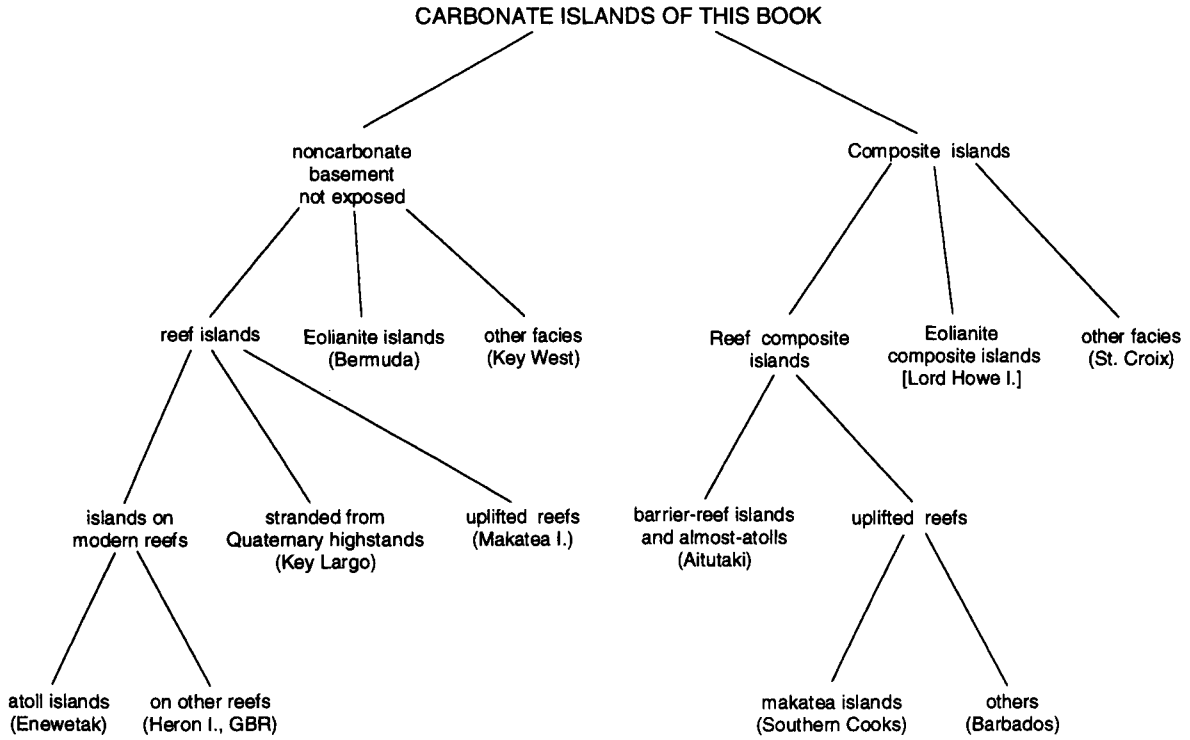


Fig. 1-1. Preliminary classification of carbonate islands. The figure is intended to explain the groupings in Table 1.1. Islands in parentheses are examples that are covered in this book. Islands in brackets are not covered in this book.

Tectonic setting

Nunn (1994) subdivided oceanic islands into two main categories on the basis of tectonic setting: islands occurring within oceanic plates ("intraplate islands" of Nunn, 1994, p. 10), and islands along plate margins ("plate-boundary islands"). This book includes a third category (outside the scope of Nunn's book on oceanic islands): carbonate islands along passive continental margins.

The diversity and tectonic complexity of composite and carbonate islands of oceanic intraplate settings are illustrated by the summary comments on tectonics in the chapters on French Polynesia (Chaps. 13–15), the Cook Islands (Chap. 16) and Enewetak (Chap. 21). French Polynesia, a region of 2,700 km by 2,300 km, contains five NW-SE archipelagoes (the Tuamotu Archipelago and the Society, Australes, Gambier, and Marquesas Islands; see Chap. 13) that are related to four identified hotspots. The well-known Society Islands — including the Darwinian succession of Tahiti, Bora-Bora and atolls — is the most like a classic hotspot trace with its progression of ages and elevations. The Australes Islands and their extension, the southern Cook Islands, are thought to be related to the volcanically active MacDonald Seamount, but the volcanic ages in these archipelagoes are inconsistent with a simple hotspot theory. Included in the southern Cook Islands are the uplifted makatea islands (e.g., Mauke); these are the islands that spawned the explanation (McNutt and Menard, 1978) of uplift from flexure due to loading from a nearby volcano; the volcano in question is Rarotonga, which is to the side of the line of makatea islands (see Fig. 16-1). In contrast, the Tuamotu Archipelago of atolls occurs on a broad volcanic plateau (at −2,000 m). Mururoa and Fangataufa (Chap. 13), located at the southeastern end of the Tuamotus, were built when the plate moved over the hotspot zone that is associated with the Pitcairn Islands (Chap. 12) and the Gambier Islands. Near the northwestern end of the Tuamotos is the older, uplifted atoll of Makatea, where Montaggioni and Camoin (Case Study of Chap. 14) recognize three distinct episodes of uplift in the past 18. m.y. — the first two due to thermal rejuvenation (Detrick and Crough, 1978) as the island passed near two different hotspots, and the most recent due to flexure and loading (McNutt and Menard, 1978) from nearby Tahiti and Moorea. Much farther away — and with many islands in between — are the Marshall Islands (Chap. 20), including Enewetak (Chaps. 21, 22); formation of these islands is now thought to have involved multiple episodes of volcanism, uplift, reef-building and subsidence during the Cretaceous as they interacted with hotspots that have more recently formed and interacted with islands of the Australes-Cooks region (Chap. 21).

Numerous composite and purely carbonate islands occur in association with convergent boundaries in the Pacific Ocean. Guam (Chap. 25), a composite island, lies along a frontal arc of the Mariana system between the Pacific and Philippine Plates. Other islands discussed in this book lie in the vicinity of the Tonga Trench, the boundary between the Pacific and Indo-Australian Plates. The composite and purely carbonate islands of Tonga (Chap. 18) lie along a frontal arc between the trench and the volcanic arc. The composite and purely carbonate islands of the Lau Group, Fiji (Chap. 26), lie on a remnant arc which separated from the zone of

convergence by relatively recent back-arc spreading. The uplifted atoll of Niue (Chap. 17) is on the Pacific Plate that is being subducted and is elevated as it rides over the bulge in front of the Tonga Trench before descending into it.

In the Caribbean, the Limestone Caribbes consisting of both purely carbonate islands (e.g., Barbuda) and composite islands (e.g., Antigua) form a frontal arc in the northern half of the Lesser Antilles, which mark the eastern convergent boundary of the Caribbean Plate. Barbados (Chap. 11) is along the same convergent margin, but in the southern half of the Lesser Antilles and further in front of the volcanic islands (e.g., St. Vincent with its famous volcano Soufrière). St. Croix (Chap. 10), Isla de Mona (Chap. 9) and the Cayman Islands (Chap. 8) are on the complex northern boundary zone of the Caribbean Plate (with the Greater Antilles of Cuba, Hispaniola, Puerto Rico, and Jamaica), a transform boundary with a long history including earlier convergence. Composite islands of the Netherlands Antilles (Aruba, Curaçao, Bonaire) lie along the southern boundary zone of the Caribbean Plate, another transform boundary with a long and complex history (including the mountain system of northern Venezuela).

Islands of passive, intraplate continental margins are represented in this book by islands of two main areas. The first is associated with the broad carbonate province running from the Yucatan Peninsula through Florida to the Bahamas. Islands of this province include eolianite islands that are emergent because of their depositional topography (e.g., Cancun, Chap. 7; Bahamian islands, Chap. 3); reef and other shoal-water deposits that formed during Pleistocene sea-level highstands (Florida Keys, Chap. 5; Cozumel, Chap. 7); and modern sediments deposited slightly above present sea level (mangrove islands of Florida Bay, Chap. 6). The second area is the Australian shelves. The western shelf includes Rottnest Island (Chap. 27) and the Houtman Abrolhos Islands (Chap. 28) consisting largely of Quaternary eolianites and Quaternary reef deposits, respectively. The eastern shelf is the site of the vast Great Barrier Reef (Chaps. 29, 30), which includes a variety of low islands (e.g., unstable cays, vegetated sand or shingle cays, low wooded islands) as well as higher, composite islands where continental rocks are fringed by deposits of the modern reefs.

HYDROGEOLOGICAL VARIETIES OF CARBONATE ISLANDS

Islands, in general, are hydrologically circumscribed units. Inflows and outflows are local, except in cases where deep, confined units cross relatively narrow, relatively shallow channels bordering the islands (e.g., barrier islands off Long Island, New York; Perlmutter et al., 1959). Recharge, for example, can be viewed as autochthonous with respect to the island unit.

Four facts characterize carbonate islands in particular:

1. They involve fresh groundwater of meteoric derivation, salty groundwater of marine derivation, and mixtures of the two. The density differences and resultant stratification of fresh, brackish and salty groundwater are always critically relevant to the hydrogeology.

2. Heads in carbonate islands are intimately related to sea level. Because the islands are small and the carbonates have a very high hydraulic conductivity, the water table is inevitably very close to sea level in the carbonates that are hydraulically connected to the sea. Moreover, the large hydraulic conductivities mean that changes in water level are strongly affected by sea-level variations — not only the familiar tides, but also meteorologic and steric changes, which are disproportionately more important because their lower frequency results in less dampening.

3. The carbonates typically are much more permeable than the underlying basement.

4. Within the carbonates, hydraulic conductivity varies step-wise by orders of magnitude. In at least the young parts of the carbonate section exposed to the circulation of meteoric waters, the general pattern is that hydraulic conductivity increases with age. This correlation between stratigraphy and hydraulic conductivity reflects the progressive development of karst-related porosity.

The first two facts — the critical importance of the underlying saltwater and the intimate connection to sea level apply to islands in general, but there is an important case where they do not. In volcanic islands, and the volcanic part of composite islands, "dike water" (Meinzer, 1930; Stearns, 1942) is commonly impounded behind impermeable dikes of the rift zone of the shield volcanoes (e.g., see Hunt et al., 1988). This dike water is compartmentalized, effectively isolated from the sea, and characterized by step-changes in water levels when dikes are crossed. In carbonate islands, on the other hand, the water table of the carbonate rocks forms a low, smooth, continuous surface.

The last two facts — the large hydraulic conductivity of the carbonates, and the stepwise increases in hydraulic conductivity — lead to hydrogeological distinctions between carbonate islands.

Composite islands

In composite islands, permeable carbonates form coastal, wedge-like bodies that overlie and pinch out against relatively impermeable, outcropping noncarbonate rocks. Where the base of these coastal wedges dips below sea level, there is a layer of fresh groundwater floating on salty groundwater with an intervening transition zone. This coastal layer of fresh groundwater, which is characterized by a water table at about sea level, was named "basal water" in Hawaii (Meinzer, 1930) to distinguish it from perched water and dike water characterized by the higher, disconnected water levels. The term "basal water" is widely used in Pacific islands where hydrogeological studies have been influenced by the U.S. Geological Survey.

In Guam (Chap. 25), a further distinction has been made between basal water, which is the part of the freshwater wedge that is underlain by an interface or transition zone, and "parabasal water" (Mink, 1976), which is the part of the freshwater wedge that rests directly on impermeable basement (see Fig 25-7). Basal and parabasal water are hydraulically continuous, underlying a single water table; the parabasal part of the freshwater wedge is landward of the termination of the

freshwater-saltwater interface against the sloping basement. Parabasal water constitutes the premier water resource in Guam because of its immunity to upconing.

In Barbados (Chap. 11), a distinction is made between "sheet water," which is underlain by the coastal water table, and "stream water," which lies updip along the limestone-basement contact, landward of the coastal water table. The zone of sheet water is analogous to the basal and parabasal water of Guam. The zone of stream water refers to streams in connected caverns, and the layer of water between them, perched on the contact. Groundwater development is important in both the stream and sheet water zones of Barbados.

Combining Guam and Barbados, it is evident that the sloping limestone-basement contact produces three hydrogeological zones in the limestones of these composite islands. From the coast landward, these are (1) basal water, (2) parabasal water, and (3) stream water. In some islands, drainage in the latter would connect to surface-water streams in the high noncarbonate areas upslope from the coastal limestones. In the makatea islands of the Cook Islands, the radial streams of these highlands enter the surrounding makatea, "proceed to the coast via underground tunnels and passageways.... and surface at the outer reef as fresh- or brackish-water springs" (Chap. 16). In composite islands of Fiji, springs are common at the base of the limestones in contact with underlying volcanics, and at places freshwater ponds occur along the contact (Chap. 26). In Barbados and Guam, where the downstream contact between limestone and basement is buried, it is nevertheless of paramount interest because it defines drainage basins in the zone of sheet water (Barbados) and flow basins in the zone of parabasal water (Guam, Fig. 25-13).

Dual-aquifer carbonate islands

The breakthrough concept in the comparative hydrogeology of purely carbonate islands is the "dual-aquifer model" that has come out of study of atoll islands (e.g., Buddemeier and Holladay, 1977; Wheatcraft and Buddemeier, 1981). In islands of atolls (see Table 1-3) and other reefs (e.g., Heron Island, Chap. 30), Holocene sands with relatively low hydraulic conductivity overlie Pleistocene reef deposits with relatively high hydraulic conductivity. The difference in hydraulic conductivity is one or two orders of magnitude — from the order of 10^0–10^1 m day^{-1} for the medium sand of the upper layer, to the order of 10^2–10^3 m day^{-1} for somewhat karsted, young limestone of the lower layer (e.g., Chaps. 19, 20, 22).

The two-layer arrangement of atoll and reef islands has at least two major consequences: (1) a refraction of flowlines as the meteoric water, flowing from the interior of the island to the shoreline, enters and leaves the more-conductive Pleistocene layer; and (2) the easier passage of tidal fluctuations to the interior of the island through the buried Pleistocene limestone. The identifying feature of a dual-aquifer island is that tidal efficiency (well-to-ocean amplitude ratio) in piezometers increases with depth in the Holocene sands (see Fig. 20-4, Fig. 30-5) — in contrast to the hypothetical unlayered case where tidal efficiency decreases simply inland from the shoreline (e.g., Fig. 2-18). As a result of the refraction, and the enhanced interior

mixing due to the further penetration of the tides, freshwater lenses of dual-aquifer atoll and reef islands tend to be truncated at the unconformity (the "Thurber Discontinuity" of some authors in this book). Such is the case described by Falkland at Tarawa (Chap. 19), Peterson at Laura on Majuro Atoll in the Marshalls (Chap. 20), Falkland at Cocos (Chap. 31), and Hunt at Diego Garcia (Chap. 32). In some cases, such as that described by Buddemeier and Oberdorfer at Enewetak Atoll (Chap. 22), the mixing is so extensive that the lens in the Holocene sediments is entirely brackish (Fig. 22-5).

Dual-aquifer relationships and truncated lenses are not limited to islands of atolls and reefs where Holocene reef sediments overlie Pleistocene reef limestone. In the Lower Keys of Florida, where relatively low-conductivity oolitic limestone of substage 5e makes up an upper layer, and relatively high-conductivity reef limestone of older interglacials makes up a lower layer, the base of the freshwater lens is limited by the base of the younger oolitic unit (see Fig. 5-9); here, as in the dual-aquifer layers of atolls and reefs, there is an order-of-magnitude contrast in hydraulic conductivity between the two layers, but the individual hydraulic conductivities are each about an order of magnitude higher than in the atoll and reef cases involving the "Thurber Discontinuity." Similarly in the Bahamas, the base of the freshwater lens is limited by the base of the Pleistocene Lucayan Formation (see Chap. 4) in islands that are sufficiently large and sufficiently recharged that the freshwater lens can reach the discontinuity (Cant and Weech, 1986). Vacher and Wallis (1992) used "Bahama-type islands" as a label for such islands where the thickness of the freshwater lens is limited by the occurrence of units with higher hydraulic conductivity at depth (see Fig. 4-8). These Bahama-type islands (in the Bahamas and Lower Keys) are simply older, more conductive versions of the dual-aquifer systems of modern atolls and reefs that involve the "Thurber Discontinuity."

Islands with cross-island variations in hydraulic conductivity

In Bermuda, the sediment bodies of successive interglacials occur more alongside each other than in vertical succession because of the lateral accretion of younger, thick coastal-dune units against older ones. As a result, the upper part of the saturated zone consists of lateral sectors, rather than major horizontal layers, with order-of-magnitude stepwise contrasts in hydraulic conductivity. Accordingly, the freshwater lens is preferentially developed (thicker and less mixed) in the sectors of lower hydraulic conductivity. Vacher and Wallis (1992) called this type of island, where the shape of the lens is controlled by lateral variations in hydraulic conductivity, a "Bermuda-type island."

Whereas in Bermuda the lateral contrasts involve upper Pleistocene units with a hydraulic conductivity on the order of 10^2 m day^{-1} and middle Pleistocene units with a hydraulic conductivity on the order of 10^3 m day^{-1}, cross-island variations in Bahamian islands involve contrasts between Pleistocene units with hydraulic conductivity on the order of 10^2 m day^{-1} and Holocene strandplains with a hydraulic conductivity on the order of 10^1 m day^{-1}. These values and ages are comparable to

those of dual-aquifer layers of atoll and reef islands, but the geometry is rotated 90°. In the Bahamas, freshwater lenses occur in both the Pleistocene bedrock of the island and the reentrants ("bights") filled with Holocene strandplain deposits. Island areas and widths required to support a lens are much larger for the bedrock limestone than for the strandplains.

Uplifted reef islands with Quaternary fringes are another example of cross-island variations in hydraulic conductivity. A particularly comprehensive account is given in this book for Nauru (Chap. 24), where the Miocene limestones of the interior plateau are fractured and host to a lens that is mostly mixing zone, and the groundwater of the coastal terrace aquifer would be a resource, but is polluted. In Isla de Mona, geophysical reconnaissance studies have revealed two freshwater lenses, one beneath the interior plateau, and the other under the coastal fringe (Chap. 9).

Cross-island asymmetry is common in the lenses of atoll islands: the freshwater lens is commonly thicker on the lagoon side than on the reef side of the island. A cross-island variation in hydraulic conductivity is the usual explanation. For example, in the Marshall Islands, "... on the two islands for which detailed subsurface geologic data are available — Kwajalein Island in Kwajalein Atoll and the Laura area of Majuro Atoll — the freshwater lens is thicker on the lagoon side of the islands because the Holocene deposits there generally are fine-grained and hence less permeable than on the ocean side of the islands" (Peterson in Chap. 20).

Other explanations, however, are also possible for cross-island asymmetry of atoll-island lenses. For example, Falkland (Chap. 19) found no systematic areal variation in hydraulic conductivity from 180 in situ permeability tests on Tarawa, and attributed the asymmetry to greater recharge on the lagoon side of the island due to the removal of the water-demanding coconuts there. Similarly, Peterson (Chap. 20), noted that the greatest thickness of the freshwater lens on Kwajalein occurs directly beneath an area receiving recharge from a runway; also (Chap. 20), a small island on Bikini Atoll (Eneu Island) contains a freshwater lens, whereas a larger island on the atoll (Bikini Island) does not — Eneu has a runway, less vegetation and poorly permeable beachrock at the coastline. Recharge can also be greater on the lagoon side of some islands because the occurrence of the cemented reef plate beneath the reef side of the island can act as a confining bed limiting recharge (Fig. 23-3). Cross-island asymmetry can be further complicated by the effects of higher sea level on one side of the island than on the other, and this is a distinct possibility in atolls with restricted lagoons. Buddemeier and Oberdorfer (Chap. 22), for example, note the possibility at Enewetak Atoll of cross-island marine head gradients from wave set-up on the windward reefs and consequent cross-reef transport and lagoon ponding.

Islands with areal variations reflected by saline lakes

In topographically low areas of carbonate islands, the groundwater is effectively exposed in lakes if the topographic lows dip below the water table. In dry regions

where potential evapotranspiration exceeds rainfall, there is an actual deficit that applies directly to the lens at those lakes, as if there was a large extraction network there. The lens is thinned as a result, and, in extreme cases, the underlying seawater can be upconed to the extent that the lake is brackish or even saline. Groundwater drains toward the lakes. Saline lakes thus become like internal boundary conditions for the areal geometry of the freshwater lens: the freshwater lenses wrap around the saline lakes.

The pattern of freshwater lenses nestled amongst saline lakes is common in the southeastern, dry islands of the Bahamian archipelago (Chap. 4), and Vacher and Wallis (1992) termed such islands "Exuma-type" islands after one of them. Rottnest Island of Western Australia (Chap. 27) is a similar eolianite island with saline lakes. Christmas Island of Kiribati (Chap. 19), another dry island, is a variation on the theme — a largely filled-in atoll with saline lakes in the topographically low interior and freshwater lenses in the peripheral "ridges."

Ghyben-Herzberg lenses

Like the word "atoll" used to discuss the geomorphology of carbonate islands, the term "Ghyben-Herzberg lens" holds a special place in the vocabulary used to discuss the hydrogeology of carbonate islands. The word derives from the Ghyben-Herzberg Principle (Ghyben, 1888; Herzberg, 1901), which says: where fresh groundwater floats on seawater, there are 40 ft (or m) of freshwater below sea level for every foot (or meter) above sea level. This principle treats the fresh groundwater and underlying seawater as hydrostatic, immiscible fluids. The picture is like that of an iceberg (the Ghyben-Herzberg lens) with the root 40 times the sliver above sea level. The number 40 is the density-difference ratio between seawater and freshwater: $\rho_f/(\rho_s-\rho_f)$, where ρ is density and the subscripts refer to freshwater (f) and seawater (s).

Obviously, the assumptions behind the Ghyben-Herzberg Principle are problematic, and the picture of an iceberg is inappropriate. Neither the recharge-derived fresh groundwater of the lens nor the sea-level-driven saltwater beneath it are static. The fluids are certainly miscible; there is a transition zone of brackish groundwater between them, not a sharp freshwater-saltwater interface. There is a circulation of saltwater below the transition zone that provides the salt to balance the shoreline exit of salt carried by the brackish transition zone (Cooper, 1959). Thus saltwater heads are not zero, and so the ratio of the height of the water table to the base of the freshwater is not given by the density-difference ratio — or any other simple ratio — even in the hypothetical case where one assumes a sharp interface (Hubbert, 1940). Further, even in the hypothetical case, the Ghyben-Herzberg Principle applies to the water-table end and the interface end of a line of equal potential (Hubbert, 1940); if this equipotential is curved (rather than vertical and straight), the relationship cannot be applied to give the depth of the interface directly below the place where the water-table elevation is known.

The problematic assumptions mean that the Ghyben-Herzberg Principle must be applied with care. It is only an idealized model. Certainly, the presence of a tran-

sition zone implies that the depth to the base of the freshwater is less — sometimes much less — than 40 times the elevation of the water table. It may be more useful to reword the Ghyben-Herzberg Principle as a relationship that *attempts to find the depth of the sharp freshwater-saltwater interface that would be present if there were no mixing*. Buddemeier and Oberdorfer (see Chap. 22) refer to this depth, and the volume bounded by it, as the "freshwater inventory," meaning the amount of meteoric water present in the lens. They distinguish between this recharge-derived freshwater inventory and the "inventory of water that is fresh (e.g., potable) as opposed to brackish or saline." In the island they describe (Enjebi Island, Enewetak Atoll), the freshwater lens is so highly mixed that it is inappropriate to speak of a freshwater lens in the normal way (Fig. 22-5). A somewhat similar, scaled-up version occurs in the uplifted atoll Nauru (Fig. 24-15), where the freshwater lens (<7 m thick) is very much smaller than the freshwater inventory, because the transition zone is some 60 m thick. With areal variations in the thickness of the transition zone, it is understandable that the elevation of the water table is a poor guide to the thickness of the freshwater lens at some islands. Falkland (Chap. 19) makes the case for that conclusion at Christmas Island, and he underscores "the need for salinity-monitoring boreholes, as opposed to simple water-table monitoring, as the main means of tracking the behaviour of the freshwater lens."

There are islands, however, where the freshwater lens is more nearly the same volume as the freshwater inventory. One example is Guam (Chap. 25), where, for most of the Northern Guam Lens, the transition zone is relatively small in comparison to the thickness of fresh groundwater (Fig. 25-10, right panel). Bermuda (Chap. 2) is an intermediate case, where the transition zone is less than half (though still a significant fraction) of the freshwater inventory (Fig. 2-17). Although the depth of the base of fresh groundwater in Bermuda is clearly not a constant multiple (40 or any other single number) of the water-table elevation, Rowe (1984) has shown that, over a period of years, the depth of the midline of the transition zone averages about 40 times the water-table elevation.

Diagrams showing island lenses as icebergs are misleading. They are typically shown as icebergs — i.e., with thickness of the same order as width — in order for the diagrams to have the space to label the "h" and "40h" of the portions above and below sea level, respectively. Because of the large hydraulic conductivities, island lenses of carbonate islands typically have thickness-to-width ratios around 10^{-2}. Drawing such islands to scale on a normal page would mean practically losing the thickness of freshwater to the width of lines delimiting it. Therefore, freshwater lenses are drawn with large vertical exaggeration, and the figures in this book are no exception. Readers should not, however, get the impression that these are iceberg-like lenses; they are more like thin slabs or plates.

Because of the slab-like geometry of island lenses, the shoreward flow of recharge-derived fresh groundwater is nearly horizontal, except very close to the shoreline. Diagrams that vertically exaggerate the outline of the lens also overstate the vertical component of flow relative to the horizontal. If one assumes the shoreward drift of fresh groundwater in the freshwater inventory is driven by vertical equipotentials and that there is a sharp freshwater-saltwater interface, then that

flow can be modeled relatively simply. The vertical equipotentials imply that a relationship between the water-table elevation and interface depth can be applied along a straight vertical line. If one further assumes zero salt-water heads, the relationship between water-table elevation and interface depth reduces to that of the standard Ghyben-Herzberg Principle, and so, with these assumptions, the thickness of flow is a multiple (41) of the head. Combining this with Darcy's Law and the well-known Dupuit assumptions (e.g., Bear, 1972), which apply when equipotentials are vertical, leads to Dupuit-Ghyben-Herzberg (DGH) analysis (Bear, 1972; Fetter, 1972; Vacher, 1988).

Modeling. Various techniques have been used to treat the freshwater-saltwater interface or mixing zone in carbonate islands. The DGH approach has been used to model the steady-state configuration of carbonate-island lenses (i.e., the freshwater inventories of such lenses). Examples include Tongatapu (Chap. 18), Bermuda (Chap. 2), Tarawa (Volker et al., 1985), Great Exuma Island, Bahamas (Wallis et al., 1991), and Big Pine Key, Florida (Chap. 5). DGH analysis has also been used to treat unsteady behavior of lenses at, for example, Grand Cayman Island (Chidley and Lloyd, 1977), Tarawa (Lloyd et al., 1980) and Bermuda (Ayers and Vacher, 1983). The sluggish behavior of the interface relative to changes in the water-table elevation due to variations in recharge (e.g., Contractor, 1983; Rowe, 1984) argues against use of DGH analysis for transient problems, because the ratio between water-table elevation and interface is not fixed.

DGH models are one-fluid models in that the saltwater is assumed to be static so that flow in only the freshwater layer is considered. The next level of modeling involves two-fluid models (e.g., Bear and Verruijt, 1987) where a flow equation is applied to each of two fluid regions that share a common boundary, a sharp interface. These models, which are used for transient problems, find the location of the interface at each time step by assuming that pressure is continuous across the interface, and so the relation between water-table elevation and depth to interface (a Ghyben-Herzberg ratio) is found rather than assumed. Typically such models assume horizontal flow in each layer so that the flow equations can be simplified by the Dupuit assumptions. Contractor (1983) and Contractor and Srivastava (1990) applied a two-fluid model to the Northern Guam Lens (Chap. 25).

The restrictions of a sharp interface and horizontal flow are removed by using powerful models coupling variable-density flow with solute-transport. One such model, SUTRA, a two-dimensional, vertical cross-sectional model, has been applied to a generic dual-aquifer atoll island by Underwood et al. (1992) and to some specific atoll islands: Enjebi (Enewetak Atoll) by Oberdorfer et al. (1990); Laura (Majuro Atoll) by Griggs and Peterson (1993) and Roi-Namur (Kwajalein Atoll) by Gingerich and Peterson (see Chaps. 20 and 21 for some details). Both HST3D, a three-dimensional model, and SUTRA have been applied to Nauru (Chap. 24) by Ghassemi et al. (1996).

Analytical models for the transition zone were developed for Tongatapu by Hunt (1979), using a solution to a one-dimensional dispersion equation, and for Tarawa by Volker et al. (1985), using equations of a boundary layer between fluids moving at

different velocities (fluid jet situations). In both cases, these transition-zone models were appended to results of DGH analysis.

CONCLUDING REMARKS

The science of carbonate islands is about the same age as the science of geology. The two hundred years of study of carbonate islands have made important contributions to geology in such areas as the deposition and diagenesis of carbonate rocks, the history and tectonics of ocean basins, the history of Cenozoic sea level, and the occurrence and behavior of island groundwater.

The two hundred years of carbonate-island geology includes one of the history of geology's great controversies. In looking back at the debate over Darwin's theory, it appears that much of the disagreement occurred when a deductive model for one type of island was countered by observations at another type of island, and, reciprocally, when empirical, inductive conclusions from some islands were applied as premisses for deductions about islands of different settings. In other words, there was overgeneralization and an insufficient appreciation of the diversity of carbonate islands. The debate was resolved when (1) Darwin's hypothesis stood up to tests of drilling (i.e., Funafuti and, later, the nuclear islands), and (2) insight was gained from new paradigms (sea-level changes, subaerial karst, and most importantly, plate tectonics). What remains of greatest value from the days of the old debate are (1) the observations, where they were recorded, and (2) the interpretations in the context of their now-constrained areas of applicability — to the extent that the observations or interpretations were not too much influenced by the sweeping generalizations from other areas. The same general comments can be made, of course, about various other disputes involving carbonate islands, such as sea-level curves and dolomitization.

In view of this history, it does not seem appropriate to make sweeping generalizations in this book, the intention of which is to collect information about carbonate islands (aside from the generalizations of an organizational nature pertaining to Table 1-1). Regarding the "staying power" of the following chapters, it is important to note that the authors have specific interest in the islands they cover. The chapters are typically based on long involvement in the islands, rather than brief visits as was the norm in the time of Agassiz. The amount of experience on these islands by these authors sums to quite a few hundreds of years. By design, the views are locally, rather than globally, biased, and that can be viewed as an asset. Taking the references cited into consideration, the amount of observation is enormous.

ACKNOWLEDGMENTS

I thank Bob Buddemeier and Colin Woodroffe who helped me get started on this review some years ago; Terry Quinn who encouraged me throughout the effort and commented on early drafts; Bob Ginsburg, whose column "Rock Stars" in *GSA Today* inspired a historical, snapshot-in-time approach; Hugh Torrens who advised

me about Sir Joseph Banks; and Peter Harries for a helpful review of the manuscript.

REFERENCES

Agassiz, G.R., 1913. Letters and Recollections of Alexander Agassiz with a Sketch of his Life and Work. Houghton Mifflin, Boston, 454 pp.

Agnarsdóttir, A., 1994. Sir Joseph Banks and the exploration of Iceland. In: R.E.R. Banks, B. Elliot, J.G. Hawkes, D. King-Hele, and G. Ll. Lucas (Editors), Sir Joseph Banks: A Global Perspective. Royal Botanic Gardens, Kew, pp. 31–48.

Ayers, J.F. and Vacher, H.L., 1983. A numerical model describing unsteady flow in a fresh water lens. Water Resour. Bull., 19: 785–792.

Bathurst, R.G.C., 1975. Carbonate Sediments and their Diagenesis. 2nd ed. Elsevier, Amsterdam, 658 pp.

Beaglehole, J.C., 1962. The Endeavor Journal of Joseph Banks 1768–1771. Angus and Robertson, Sydney, 2 vols.

Bear, J., 1972. Dynamics of Fluids in Porous Media. Elsevier, Amsterdam, 764 pp.

Bear, J. and Verruijt, A., 1987. Modeling Groundwater Flow and Pollution. Reidel, Dordrecht, 414 pp.

Bloom, A.L., 1967. Pleistocene shorelines: A new text of isostasy. Geol. Soc. Am. Bull., 78: 1477–1494.

Bloom, A.L., Broecker, W.S., Chappell, J.M.A., Matthews, R.K. and Mesolella, K.J., 1974. Quaternary sea-level fluctuations on a tectonic coast: New $^{230}Th/^{234}U$ dates from the Huon Peninsula, New Guinea. Quat. Res., 4: 185–205.

Bonacci, O. and Margeta, J., 1991. Case Study No. 12, Silba. In: A. Falkland (Editor), Hydrology and Water Resources of Small Islands: A Practical Guide. Unesco, Paris, pp. 394–400.

Boorstin, D.J., 1985. The Discoverers. Random House (Vantage Books), New York, 745 pp.

Broecker, W.S., Thurber, D.L., Goddard, J., Ku, T.-L., Matthews, R.K. and Mesolella, K.J., 1968. Milankovitch hypothesis supported by precise dating of coral reefs and deep-sea sediments. Science, 159: 297–300.

Bryan, E.H., Jr., 1953. Check list of atolls. Atoll Res. Bull., 19: 1–38.

Buddemeier, R.W. and Holladay, G.L., 1977. Atoll hydrology: island groundwater characteristics and their relationship to diagenesis. Proc. Third Int. Coral Reef Symp. (Miami), 2: 167–174.

Buddemeier, R.W., Smith, S.V. and Kinzie, R.A., III, 1975. Holocene windward reef-flat history, Enewetak atoll. Geol. Soc. Am. Bull., 86: 1581–1584.

Cant, R.V. and Weech, P.S., 1986. A review of the factors affecting the development of Ghyben-Hertzberg lenses in the Bahamas. J. Hydrol., 84: 333–343.

Carter, H.B., 1994. Sir Joseph Banks and the Royal Society. In: R.E.R. Banks, B. Elliott, J.G. Hawkes, D. King-Hele and G. Ll. Lucas (Editors), Sir Joseph Banks: A Global Perspective. Royal Botanic Gardens, Kew, pp. 1–12.

Chidley, T.R.E. and Lloyd, J.W., 1977. A mathematical model study of fresh-water lenses. Ground Water, 15: 215–222.

Clark, J.A., Farrell, W.E. and Peltier, W.R., 1978. Global changes in postglacial sea level: A numerical calculation. Quat. Res., 9: 265–287.

Contractor, D.N., 1983. Numerical modeling of saltwater intrusion in the Northern Guam Lens. Water Resour. Bull., 19: 745–751.

Contractor, D.N. and Srivastava, R., 1990. Simulation of saltwater intrusion in the Northern Guam Lens using a microcomputer. J. Hydrol., 118: 87–106.

Cooper, H.H., 1959. A hypothesis concerning the dynamic balance of fresh water and salt water in a coastal aquifer. J. Geophys. Res., 64: 461–467.

Cullis, 1904. The mineralogical changes observed in the cores of the Funafuti borings. In: Coral Reef Committee of the Royal Society of London, The Atoll of Funafuti: borings into a coral reef and the results. The Royal Society, London, pp. 392–420.

Curray, J.R., Shepard, F.P. and Veeh, H.H., 1970. Late Quaternary sea-level studies in Micronesia: CARMASEL Expedition. Geol. Soc. Am. Bull., 81: 1865–1880.
Daly, R.A., 1910. Pleistocene glaciation and the coral reef problem. Am. J. Sci., Ser. 4, 30: 297–308.
Daly, R.A., 1915. The glacial-control theory of coral reefs. Proc. Am. Acad. Arts and Sci., 51: 155–251.
Daly, R.A., 1920. A general sinking of sea-level in recent time. Nat. Acad. Sci. Proc., 6: 246–250.
Daly, R.A., 1925. Pleistocene changes of level. Am. J. Sci, 5th ser., 10: 281–313.
Daly, R.A., 1934. The Changing World of the Ice Age. Yale Univ. Press, New Haven, 271 pp.
Dana, J.D., 1849. Geology of the U.S. Exploring Expedition. Philadelphia.
Dana, J.D., 1872. Corals and Coral Islands. Dodd, Mead and Co., New York, 440 pp.
Darwin, C., 1842. Structure and Distribution of Coral Reefs. Being the first part of the Geology of the voyage of the Beagle under the command of Capt. Fitzroy, RN, during the years 1832 to 1836. Smith, Elder and Co., London, 214 pp.
David, T.W.E. and Sweet, G., 1904. The geology of Funafuti. In: Coral Reef Committee of the Royal Society of London, The Atoll of Funafuti: borings into a coral reef and the results. The Royal Society, London, pp. 61–124.
Davis, W.M., 1913. Dana's confirmation of Darwin's theory of coral reefs. Am. J. Sci., Ser. 4, 35: 173–188.
Davis, W.M., 1928. The Coral Reef Problem. Am. Geogr. Soc, Spec. Publ. 9, 596 pp.
Detrick, R.S. and Crough, S.T., 1978. Island subsidence, hot spots and lithospheric thinning. J. Geophys. Res., 83: 1236–1244.
Dijon, R., 1984. General review of water resources development in the region with emphasis on small islands. Proc. Regional Workshop on water Resources of Small Islands. Commonwealth Sci. Counc., Suva, Fiji, Tech Publ. 154, Part 2: 25–44.
Emery, K.O., Tracey, J.I., Jr., and Ladd, H.S., 1954. Geology of Bikini and nearby atolls. Part 1: Geology. U.S. Geol. Surv. Prof. Pap. 260-A.
Fairbridge, R.W., 1950. Recent and Pleistocene coral reefs of Australia. J. Geol., 58: 330–401.
Fairbridge, R.W., 1961. Eustatic changes in sea level. Phys. Chem. Earth, 4: 99–185.
Fairbridge, R.W., 1995. Eolianites and eustasy: Early concepts on Darwin's voyage of HMS Beagle. Carbonates and Evaporites, 10: 92–101.
Falkland, A. (Editor), 1991. Hydrology and Water Resources of Small Islands: A Practical Guide. Unesco, Paris, 317 pp.
Fetter, C.W., Jr., 1972. Position of the saline water interface beneath oceanic islands. Water Resour. Res., 8: 1307–1315.
Garrett, P. and Scoffin, T.P., 1977. Sedimentation on Bermuda's atoll rim. Proc. Third Int. Coral Reef Symp. (Miami), 87–95.
Gary, M., McAffee, R., Jr., and Wolf, C.L. (Editors), 1972. Glossary of Geology. Am Geol. Inst., Washington DC, 805 pp.
Ghassemi, F., Jakeman, A.J., Jacobson, G. and Howard, K.W.F., 1996. Simulation of seawater intrusion with 2D and 3D models: Nauru Island case study. Hydrogeol. J., 4: 4–22.
Ghyben, W.B., 1888. Nota in verband met de voorgenomen putboring nabij Amsterdam. Tijdschrift van Let Koninklijk Instituut van Ingenieurs, The Hague, Netherlands, pp. 8–22.
Gould, S.J., 1987. Time's Arrow, Time's Cycle. Harvard Univ. Press, Cambridge, 222 pp.
Griggs, J.E. and Peterson, F.L., 1993. Ground-water flow dynamics and development strategies at the atoll scale. Ground Water, 31: 209–220.
Guilcher, A., 1988. Coral Reef Geomorphology. Wiley, New York, 228 pp.
Guppy, H.B., 1888. A criticism of the theory of subsidence as affecting coral reefs. Scott. Geogr. Mag., 4: 121–137.
Herzberg, A., 1901. Die Wasserversorgung einiger Nordseebader. Wasserversorgung, 44: 815–819 and 842–844.
Hoffmeister, J.E., 1930. Erosion of elevated fringing reefs. Geol. Mag., 57: 549–554.
Hoffmeister, J.E. and Ladd, H.S., 1935. The foundation of atolls. J. Geol., 653–665.
Hoffmeister, J.E. and Ladd, H.S., 1944. The antecedent platform theory. J. Geol., 52: 388–401.

Hoffmeister, J.E. and Ladd, H.S., 1945. Solution effects on elevated limestone terraces. Geol Soc. Am. Bull., 56: 809–818.
Hoffmeister, J.E. and Multer, H.G., 1968. Geology and origin of the Florida Keys. Geol. Soc. Am. Bull., 79: 1487–1502.
Hopley, D., 1982. The Geomorphology of the Great Barrier Reef: Quaternary Development of Coral Reefs. Wiley, New York, 453 pp.
Hubbert, M.K., 1940. The theory of groundwater motion. J. Geol., 48: 785–944.
Hunt, B., 1979. An analysis of the groundwater resources of Tongatapu Island, Kingdom of Tonga. J. Hydrol., 40: 185–196.
Hunt, C.D., Jr., Ewart, C.J. and Voss, C.I., 1988. Region 27, Hawaiian Islands. In: W. Back, J.S. Rosenshein and P.R. Seaber (Editors), Hydrogeology. Geol. Soc. Am., The Geology of North America, O-2: 255–262.
Jones, J., Torrens, H.S. and Robinson, 1994. The correspondence between James Hutton (1726–1797) and James Watt (1736–1819) with two letters from Hutton to George Clerk-Maxwell (1715–1784): Part I. Ann. Sci., 51: 637–653.
Jones, J., Torrens, H.S. and Robinson, 1994. The correspondence between James Hutton (1726–1797) and James Watt (1736–1819) with two letters from Hutton to George Clerk-Maxwell (1715–1784): Part II. Ann. Sci., 52: 357–382.
Jones, O.A. and Endean, R. (Editors), 1973–1977. Biology and Geology of Coral Reefs. Academic Press, New York (1973, Volume I, Geology 1, 410 pp.; 1973, Volume II, Biology I, 480 pp.; 1976, Volume III, Biology 2, 435 pp.; 1977, Volume IV, Geology 2, 337 pp.
Lambeck, K., 1990. Glacial rebound, sea-level change and mantle viscosity. Q. J. R. Astr. Soc., 31: 1–30.
Lloyd, J.W., Miles, J.C., Chessman, G.R. and Bugg, S.F., 1980. A ground-water resources study of a Pacific Ocean atoll — Tarawa, Gilbert Islands. Water Res. Bull., 16: 646–653.
MacNeil, F.S., 1954. The shape of atolls: an inheritance from subaerial erosion forms. Am. J. Sci., 252: 402–427.
Manten, A.A., 1971. Silurian Reefs of Gotland. Elsevier, Amsterdam, 539 pp.
Matthews, R.K., 1990. Quaternary sea-level change. In: Geophysics Study Committee (National Research Council), Sea Level Change. National Academy Press, Washington DC., pp. 88–103.
McLean, R.F. and Woodroffe, C.D., 1994. Coral atolls. In: R.W.G. Carter and C.D. Woodroffe (Editors), Coastal Evolution. Cambridge Univ. Press, Cambridge, pp. 267–302.
McNutt, M. and Menard, H.W., 1978. Lithospheric flexure and uplifted atolls. J. Geophys. Res., 83: 1206–1212.
Meinzer, O.E., 1930. Ground water in the Hawaiian Islands. U.S. Geol. Surv. Water-Supply Pap, 616: 1–28.
Meischner, D. and Meischner, U., 1977. Bermuda South Shore reef morphology. Proc. Third Int. Coral Reef Symp. (Miami), 243–250.
Menard, H.W., 1986. Islands. Freeman, New York, 230 pp.
Mink, J.F., 1976. Groundwater resources of Guam: Occurrence and development. Univ. Guam, Water and Energy Resour. Inst. Tech. Rep. 1.
Muhs, D.R., 1983. Quaternary sea-level events on northern San Clemente Island, California. Quat. Res., 20: 322–341.
Nakada, M., 1986. Holocene sea levels in oceanic islands: Implications for the rheological structure of the Earth's mantle. Tectonophys., 121: 263–276.
Neumann, A.C., 1969. Quaternary sea-level data from Bermuda. In: Resumes des Communications, VIIIe Congres INQUA, Paris, p. 228–229.
Nunn, P.D., 1994. Oceanic Islands. Blackwell, Oxford, 413 pp.
Oberdorfer, J.A., Hogan, P.J. and Buddemeier, R.W., 1990. Atoll island hydrogeology: flow and fresh water occurrence in a tidally dominated system. J. Hydrol., 120: 327–340.
Oliver, D.L., 1961. The Pacific Islands. Rev. ed. Univ. Press of Hawaii, Honolulu, 456 pp.
Perlmutter, N.M., Geraghty, J.J. and Upson, J.E., 1959. The relation between fresh and salty ground water in southern Nassau and southeastern Queens Counties, Long Island, New York. Econ. Geol., 54: 416–435.

Purdy, E.G., 1974. Reef configurations: Cause and effect. In: L.F. Laporte (Editor), Reefs in Time and Space. Soc. Econ. Paleontol. Mineral. Spec. Publ. 18: 9–76.
Redfield, A.C., 1967. Postglacial change in sea level in the western North Atlantic Ocean. Science, 157: 687–692.
Rowe, M.P. 1984. The freshwater "Central Lens" of Bermuda. J. Hydrol., 73: 165–176.
Schlanger, S.O., 1963. Subsurface geology of Eniwetok Atoll. U.S. Geol. Surv. Prof. Pap. 260-BB: 991–1066.
Schofield, J.C., 1977. Late Holocene sea level, Gilbert and Ellice Islands, west central Pacific Ocean. N.Z. J. Geol. Geophys., 20: 503–529.
Scott, G.A.J. and Rotundo, G., 1983a. A model to explain the differences between Pacific Plate island-atoll types. Coral Reefs, 1: 139–149.
Scott, G.A.J. and Rotundo, G., 1983b. A model for the development of types of atolls and volcanic islands on the Pacific lithospheric plate. Atoll Res. Bull. 260, 33 pp.
Shepard, F.P., 1963. Thirty-five thousand years of sea level. In: T. Clements (Editor), Essays in Marine Geology in Honor of K.O. Emery. Univ. Southern Calif. Press, Los Angeles, pp. 1–10.
Shepard, F.P. and Curray, J.R., 1967. Carbon-14 determination of sea level changes in stable areas. In: Mary Sears (Editor), Progress in Oceanography. Pergamon Press, London, pp. 283–291.
Shepard, F.P., Curray, J.R., Newman, W.A., Bloom, A.L., Newell, N.D., Tracey, J.I., Jr., and Veeh, H.H., 1970. Science, 157: 542–544.
Stanton, W., 1994. Banks and New World Science. In: R.E.R. Banks, B. Elliott, J.G. Hawkes, D. King-Hele, and G. Ll. Lucas (Editors), Sir Joseph Banks: A Global Perspective. Royal Botanic Gardens, Kew, pp. 149–156.
Stearns, H.T., 1941. Shore benches on North Pacific islands. Geol. Soc. Am. Bull., 52: 773–380.
Stearns, H.T., 1942. Hydrology of volcanic terranes. In: O.E. Meinzer (Editor), Hydrology. McGraw Hill, New York, pp. 678–703.
Steers, J.A. and Stoddart, D.R., 1977. The origin of fringing reefs, barrier reefs and atolls. In: O.A. Jones and R. Endean (Editors), Biology and Geology of Coral Reefs, 4. Academic Press, New York, pp. 21–57.
Stoddart, D.R., 1965. The shape of atolls. Marine Geol., 3: 369–383.
Stoddart, D.R., 1973. Coral reefs: the last two million years. Geography, 58: 313–323.
Stoddart, D.R., 1975. Almost-atoll of Aitutaki: geomorphology of reefs and islands. In: D.R. Stoddart and P.E. Gibbs (Editors), Almost-atoll of Aitutaki: Reef studies in the Cook Islands, South Pacific. Atoll Res. Bull. 190: 31–57.
Stoddart, D.R. and Spencer, T., 1987. Rurutu reconsidered: The development of makatea topography in the Austral Islands. Atoll Res. Bull. 297, 19 pp.
Stoddart, D.R., Woodroffe, C.D. and Spencer, T., 1990. Mauke, Mitiaro and Atiu: Geomorphology of makatea islands in the southern Cooks. Atoll Res. Bull. 341, 65 pp.
Tayama, R. 1952. Coral reefs in the South Seas. Bull. Hydrograph. Office (Japan), 11: 1–292.
Teichert, C., 1947. Contributions to the geology of Houtman's Abrolhos, Western Australia. Proc. Linn. Soc. N.S.W., 71: 145–196.
Teichert, C., 1950. Late Quaternary changes of sea level at Rottnest Island, Western Australia. Proc. Roy. Soc. Victoria, 59: 63–79.
Torrens, H.S., 1994. Patronage and problems: Banks and the earth sciences. In: R.E.R. Banks, B. Elliott, J.G. Hawkes, D. King-Hele and G. Ll. Lucas (Editors), Sir Joseph Banks: A Global Perspective. Royal Botanic Gardens, Kew, pp. 49–75.
Tracey, J.I., Jr. and Ladd, H.S., 1974. Quaternary history of Enewetak and Bikini atolls, Marshall Islands. Proc. Second Int. Coral Reef Symp. (Brisbane), 2: 537–550.
Underwood, M.R., Peterson, F.L. and Voss, C.I., 1992. Groundwater lens dynamics of atoll islands. Water Resour. Res., 28: 2889–2902.
Vacher, H.L., 1988. Dupuit-Ghyben-Herzberg analysis of strip-island lenses. Geol. Soc. Am. Bull., 100: 580–591.
Vacher, H.L. and Wallis, T.N., 1992. Comparative hydrogeology of freshwater lenses of Bermuda and Great Exuma Island, Bahamas. Ground Water, 30: 15–20.

Veeh, H.H., 1966. Th^{230}/U^{238} and U^{234}/U^{238}ages of Pleistocene high sea level stand. J. Geophys. Res., 71: 3379–3386.
Volker, R.E., Mariño, M.A. and Rolston, D.E., 1985. Transition zone width in groundwater on ocean atolls. Am. Soc. Civil Eng. J. Hyd. Eng., 111: 659–675.
Walcott, R.I., 1972. Past sea levels, eustasy and deformation of the Earth. Quat. Res., 2: 1–14.
Wallis, T.N., Vacher, H.L. and Stewart, M.T., 1991. Hydrogeology of the freshwater lens beneath a Holocene strandplain, Great Exuma, Bahamas. J. Hydrol., 125: 93–100.
Watkins, T.H., 1996. Sir Joseph Banks: The greening of the Empire. Nat. Geogr., 190 (5): 28–52.
Wheatcraft, S.W. and Buddemeier, R.W., 1981. Atoll island hydrology. Ground Water, 19: 311–320.
Wiens, H.J., 1962. Atoll Environment and Ecology. Yale University Press, New Haven, 532 pp.
Woodroffe, C.D., Murray-Wallace, C.V., Bryant, E.A., Brooke, B., Heijnis, H. and Price, D.M., 1995. Late Quaternary sea-level highstands in the Tasman Sea: evidence from Lord Howe Island. Marine Geol., 125: 61–72.

This Page Intentionally Left Blank

Geology and Hydrogeology of Carbonate Islands. Developments in Sedimentology 54
edited by H.L. Vacher and T. Quinn
© 1997 Elsevier Science B.V. All rights reserved.

Chapter 2

GEOLOGY AND HYDROGEOLOGY OF BERMUDA

H.L. VACHER and MARK P. ROWE

INTRODUCTION

Bermuda is an isolated group of limestone islands in the western North Atlantic Ocean (Fig. 2-1). The nearest land is Cape Hatteras, North Carolina, USA, about 1,000 km to the WNW. The island group consists of more than 150 islands that lie together in an elongate cluster near the southern margin of the shallow, 650 km^2 Bermuda Platform. Nearly all of the 50 km^2 of Bermuda's land area is in five main islands that are connected by short bridges or causeways (Fig. 2-2).

Bermuda was uninhabited when Spanish explorers visited the islands in 1503. The British established a colony for the Virginia Company in 1612, and the British Crown assumed responsibility in 1684. African slaves were brought in for plantation labor; slavery was abolished in 1834, and universal suffrage was introduced in 1962. Today, Bermuda is a self-governing Crown colony with a Constitution dating from 1968. The population is about 60,000, about 60% of whom are of African descent. With an economy now based on tourism and financial services, Bermuda has one of the highest per capita incomes in the world. The Government and business center is the capital city of Hamilton (Fig. 2-2). Nearly all the rest of the connected five islands have a suburban character, with winding roadways and pastel-colored white-roofed houses recessed into eolianite hills (Fig. 2-3A). The islands are visited by some 600,000 tourists per year who come to enjoy the many hotels and cottage colonies, the taxi tours and motorbikes, the friendly environment, and world-famous carbonate beaches (Fig. 2-3B).

SETTING

Tectonic setting

Bermuda Pedestal. The elongated Bermuda Pedestal (Heezen et al., 1959) includes three topographic highs, the largest of which is the Bermuda Platform containing Bermuda (Fig. 2-1). The other two highspots are the submerged Plantagenet (Argus) and Challenger Banks, which rise to depths of about −50 m and lie within 50 km of Bermuda. Pirsson (1914) referred to these topographic highs as "aligned volcanoes". According to Pirsson (1914), the Bermuda Platform is about 50 km by 25 km at −185 m (the 100-fathom line) and elongated NE-SW like the pedestal. The two submerged banks are roughly circular, a few kilometers in diameter, and separated by water depths on the order of 1,000–1,200 m (Pirsson, 1914). The relatively gentle

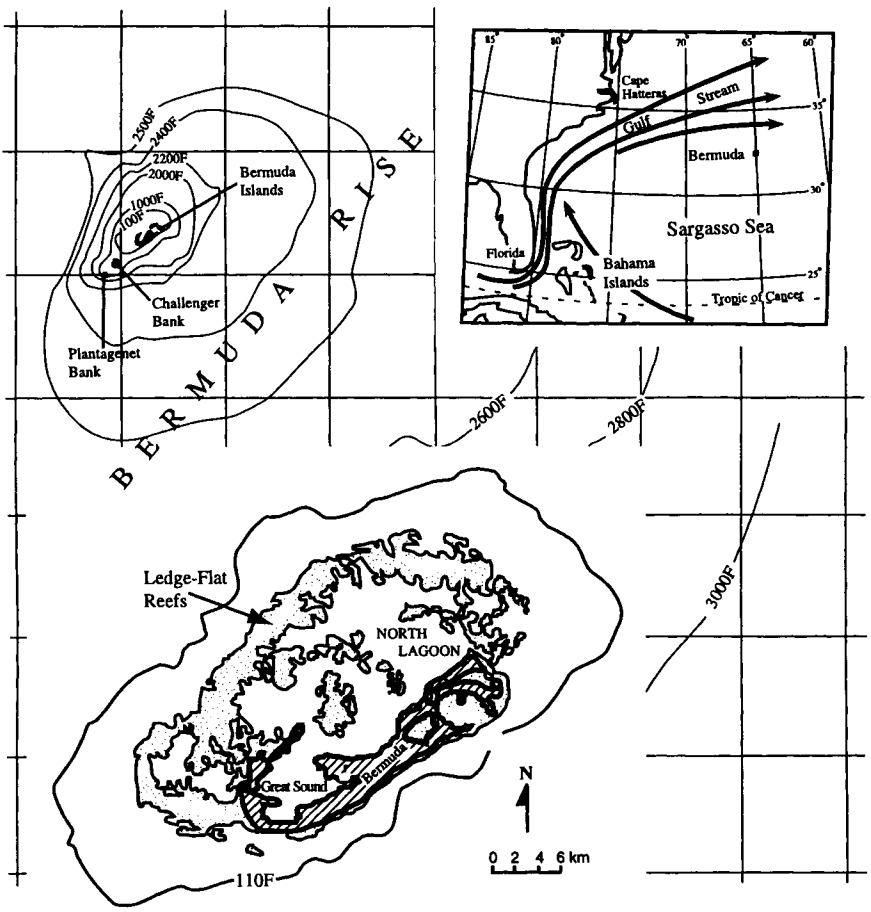


Fig. 2-1. Location of Bermuda. Small-scale map (upper right) shows Bermuda relative to the Gulf Stream and the Florida-Bahamas carbonate province. (Modified after Garrett et al., 1971, Fig. 1.) Intermediate-scale map shows Bermuda Platform and the two nearby culminations, on the top of the Bermuda Pedestal, which crowns the Bermuda Rise. Grid indicates degrees of latitude and longitude. (Modified after Officer et al., 1952, Plate 2.) Large-scale map shows location of Bermuda on the southeastern margin of the Bermuda Platform. (modified after Garrett et al., 1971, Fig. 3.)

southeast slope of the pedestal drops from −185 m to −4,200 m, the pedestal's base, in a distance of about 37 km (Officer et al., 1952). The base of the pedestal is 130 km by 80 km (Heezen et al., 1959), and its volume — effectively all of which is the igneous edifice — is estimated to be 10^4 km^3 (Pirsson, 1914).

The volcanic basement lies at shallow depths: at about −75 m (relative to present sea level) across the Bermuda Platform (Officer et al., 1952), and commonly at about −50 m on the island (from deep disposal boreholes; Rowe, unpub. data). It reaches a high point of about −15 m in the vicinity of Castle Harbour. A deep-drilling project



Fig. 2-2. Index map showing the nine parishes making up Bermuda and localities mentioned in text.

(Reynolds and Aumento, 1974) at the Bermuda Biological Station for Research (BBSR) near Castle Harbour reached volcanics at −26 m and continued through 700 m of tholeiitic lavas and intrusive lamprophyric sheets. As reported by Reynolds and Aumento (1974), the intrusive rocks were dated at about 33 Ma; results of 48 and 91 Ma for the lavas were more tentative because of difficulties due to hydrothermal alteration. According to Vogt (1991, p. 41), these "possibly unreliable ... dates ... hint at earlier volcanism."

Bermuda Rise. Surrounding the Bermuda Pedestal is the Bermuda Rise (Heezen et al., 1959), a broad, mid-basin swell which trends NE-SW and is surrounded by abyssal plains. According to Detrick et al. (1986), the Bermuda Rise is approximately delineated by the 5,000-m depth contour and measures about 900 km by 600 km. The pedestal lies astride the M-0 magnetic anomaly (Tucholke, Vogt, et al.,

1979), which dates the crust around Bermuda as about 120 Ma (Kent and Gradstein, 1986). The spreading rate is about 15 mm y^{-1} (Liu and Chase, 1989).

The history of the Bermuda Rise and the Bermuda Pedestal is known from seismic-reflection studies and deep drilling of the Bermuda Rise (Tucholke, Vogt et al., 1979; Tucholke and Mountain, 1986). The occurrence on the western Bermuda Rise of an abrupt change from deposition of turbidites from the U.S. continental margin to deposition of pelagic sediments dates the initial uplift of the rise as middle to late-middle Eocene (45–50 Ma). The occurrence of volcaniclastic turbidites at a DSDP drill site 140 km southeast of Bermuda indicates that the Bermuda volcanoes built up to sea level and were being actively eroded during the late-middle Eocene to early Oligocene (43–35 Ma). The end of deposition of the volcaniclastics and, by inference, the end of subaerial erosion and the time that the Bermuda volcanic rocks subsided below sea level, was in the late Oligocene (25 Ma).

Bermuda hotspot. By several accounts (e.g., Crough, 1983; Morgan, 1983; Detrick et al., 1986; Liu and Chase, 1989), the Bermuda Rise is a midplate hotspot swell. The residual depth anomaly (the depth relative to that predicted by age and cooling history of the crust) of the Bermuda Rise is about 800–1,000 m (Sclater and Wixon, 1986). The geoid anomaly is about 6–8 m and roughly coincides with the residual depth anomaly (Detrick et al., 1986). These anomalies over the Bermuda Rise are similar in magnitude to those at other swells surrounding recent volcanic islands such as Hawaii (Detrick et al., 1986) and, therefore, suggest a similar origin (Detrick et al., 1986). The present location of the "Bermuda hotspot," which is interpreted to have been responsible for a variety of tectonic events in North America (Morgan, 1983; deBoer et al., 1988), is 500–1,000 km southeast of Bermuda.

The hotspot interpretation has some difficulties in the details. Detrick et al. (1986) found a relatively small heat-flux anomaly: 8–10 mW m^{-2} (relative to the heat flux off the swell), which is comparable to that along the older portion of the Hawaiian Swell near Midway (Detrick et al., 1986). Another problem is the small amount of subsidence, which Liu and Chase (1989) estimated to be less than 100 to 200 m in the past 25 m.y. Those authors pointed out that a simple cooling model produces more than 500-m subsidence in 25 m.y. and a heat-flux anomaly of more than 20 Mw m^{-2}. Also, "curiously" (Detrick et al., 1986, p. 3702) the elongation of the Bermuda Rise and the Bermuda Pedestal is normal to the spreading direction (see also Vogt, 1991). According to numerical heat-flow modeling by Detrick et al. (1986), the differences between Bermuda and Hawaii can be explained by the North American plate moving more slowly over a distributed heat source. Numerical modeling by Liu and Chase (1989) showed that the Bermuda anomalies can be simulated by assuming a weak plume that is insufficient to thin the overriding plate, which would then act as a conductive lid. Vogt (1991), on the other hand, suggested that non-hotspot mantle processes must be considered because, among other reasons, the present location of the putative hotspot is within a geoidal low and is devoid of volcanism. Vogt (1991) proposed two alternatives: midplate magmatism stimulated by stress intensification preceding global plate reorganization (the 42–37 Ma bend in the Hawaii-Emperor chain), and asthenospheric upwelling traveling with the North American plate.

Climatic and oceanographic setting

The Bermuda Platform, which is 1,400 km from the nearest hermatypic coral reefs in the Florida-Bahamas region (Fig. 2-1), is the site of the northernmost coral reefs in the Atlantic. The subtropical climate, which is rather out of place at such a latitude (32°20′N), is due to the Gulf Stream which lies to the west and north of the island. Ocean temperatures off Bermuda vary between a February-March minimum of 19.3°C and an August-September maximum of 27.3°C (Garrett et al., 1971). The reef fauna and flora are considerably less diverse than in the Caribbean. Of the 72 coral species known from the Caribbean, for example, only 22 are known in Bermuda (Garrett et al., 1971); the most notable absence is the genus *Acropora*. "Nevertheless, the reefs are well developed" (Garrett et al., 1971, p. 645). Their geology has been described by Garrett et al. (1971), Ginsburg and Schroeder (1973), Schroeder and Zankl (1974), Garrett and Scoffin (1977), Meischner and Meischner (1977), and Logan (1988), and environmental impacts from human activities have been described recently by Cook et al. (1994). The geology of the platform sediments was described by Upchurch (1970) and Vollbrecht (1990). A wealth of data about Bermuda's marine environment is in the compilation by Morris et al. (1977).

The main weather determinant is the Bermuda-Azores high-pressure cell which controls the southwesterly airflow across the central part of the North Atlantic. The location of this subtropical anticyclone varies from 28°N in March to 36°N in August-September (Tucker and Berry, 1984), and it intensifies during the summer. During summer months, therefore, the fronts of the westerlies are deflected to the north of Bermuda; during the winter months, they cross Bermuda.

Rainfall frequency and amounts (Vacher, 1974) are obviously important controls on the hydrology of the groundwater lenses, but they are critical for household water supply, which is predominantly from rooftop catchments (Fig. 2-3A). Such supply is made possible because the rainfall (146 cm y^{-1}) is fairly evenly distributed through the year: 10–12 cm mo^{-1} in December through July, and 13–17 cm mo^{-1} during August through November. According to the compilation by Rudloffe (1981), each month has an average of 11–17 raindays (>0.2 mm) per month, with a total of 168 raindays per year (nearly 46% of the days).

The winter rainfall is associated with the passage of fronts; the summer rainfall is from thunderstorms and hurricanes. Accordingly, there is an uneven distribution of "sunniness" and windiness. During June through September, there is sunshine during 60–70% of the daylight period, but only 49–50% during December through February (Rudloffe, 1981). So, although rainfall is evenly distributed through the year, its character varies; the winter is considered to be the rainy season. According to water-budget studies (Vacher, 1974; Rowe, 1984) this is the time of natural recharge to the lens.

Bermuda is not only a rainy place, but a windy one — which is relevant to deposition of Bermuda's principal rock type, carbonate eolianite. From a year-round perspective, there is no single dominant wind direction (Mackenzie, 1964a; Garrett et al., 1971). Southeasterlies predominate in the summer, and southwesterlies predominate in the winter. Gales are common during the winter and blow mainly from

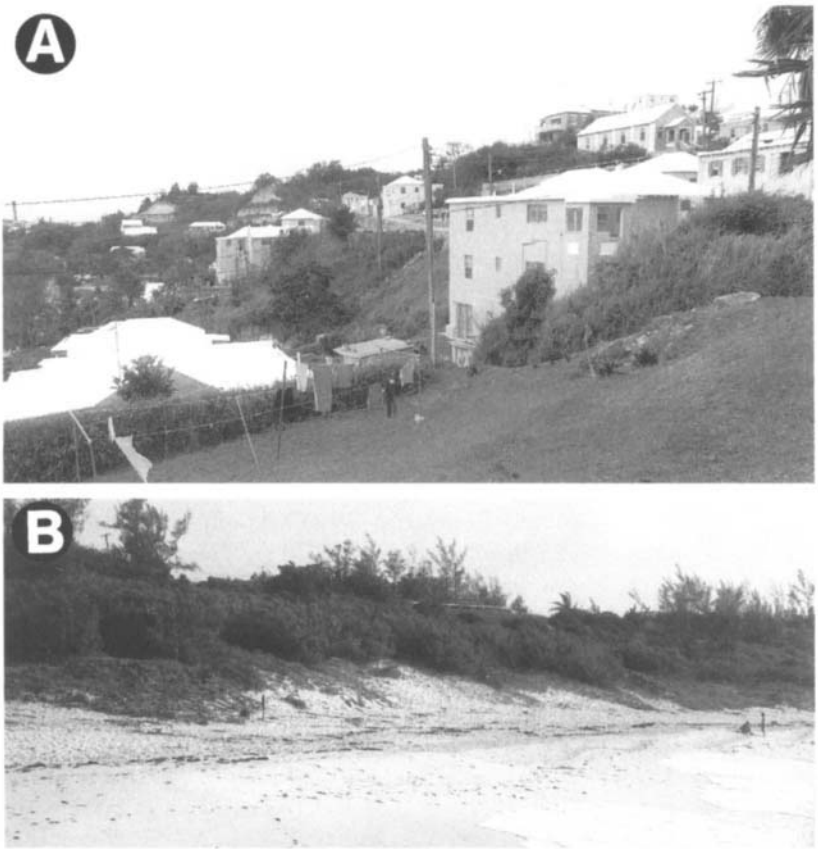


Fig. 2-3. Pleistocene vs. modern dunes. (A) View looking west along complex eolian ridge that forms barrier between Pembroke Marsh (on extreme left side of photo) and the north shore (over the hill to the right). This is the ridge that is cut through by Blackwatch Pass (Fig. 2-21), which is about 1 km west of the photographer. (B) Modern dunes along one of the longest beaches in Bermuda: Warwick Long Bay. The ridge in the background (with railing along South Road seen at skyline) is eolianite of the Southampton Formation.

the west and northwest. Overall, the average windspeed is about 22 km h^{-1} (14 mi h^{-1}), and gales occur on average 36 days a year (Vacher, 1973).

The spring tidal range is 1.3 m, and the neap range is 0.6 m (Garrett et al., 1971). The overall tide spectrum has been studied in detail (Shaw and Donn, 1964; Wunsch, 1972). Of special interest to the hydrogeology of the island is the information on meteorological and steric components of the sea-level variation, because these are the dominant controls on the day-to-day and seasonal water-table variations (Vacher, 1974, 1978a; Rowe, 1984). Atmospheric pressure variations and winds account for 14% of the total sea-level variance (Wunsch, 1972); the barometric fluctuation, in which the ocean level rises about 1 cm for a drop in atmospheric pressure of 1 mb, is

associated with the passage of fronts during winter months and involves many sea-level changes of 10–20 cm (Vacher, 1978a). In addition, the steric fluctuation affects monthly mean sea level and has a range of 20–30 cm with highest levels typically in October and November (Shaw and Donn, 1964; Rowe, 1984). This fluctuation results from density changes in the upper layers of the ocean due to the annual cycle of heating and cooling (the principal factor), evaporation and precipitation.

GEOLOGIC OVERVIEW

One's first impression of Bermuda's geology derives from its striking geomorphology: rolling hills, dramatic coastal cliffs, picturesque pocket beaches, and a complex interior shoreline wrapping around numerous inshore sounds and reaches (Fig. 2-2). Equally striking is the ubiquitous eolian cross-bedding (Fig. 2-4). Rock cuts seem to be everywhere in Bermuda because there are almost no naturally level surfaces. Roadways and houselots require that recesses be cut into these eolianite hills, which are thus opened up for observation. People familiar with carbonate eolianites elsewhere in the world are invariably impressed with the abundance of exposure in Bermuda.

The eolian origin of Bermuda's limestone has been clear since the beginning of geological observations in Bermuda. Lieutenant (later Captain) Richard J. Nelson,

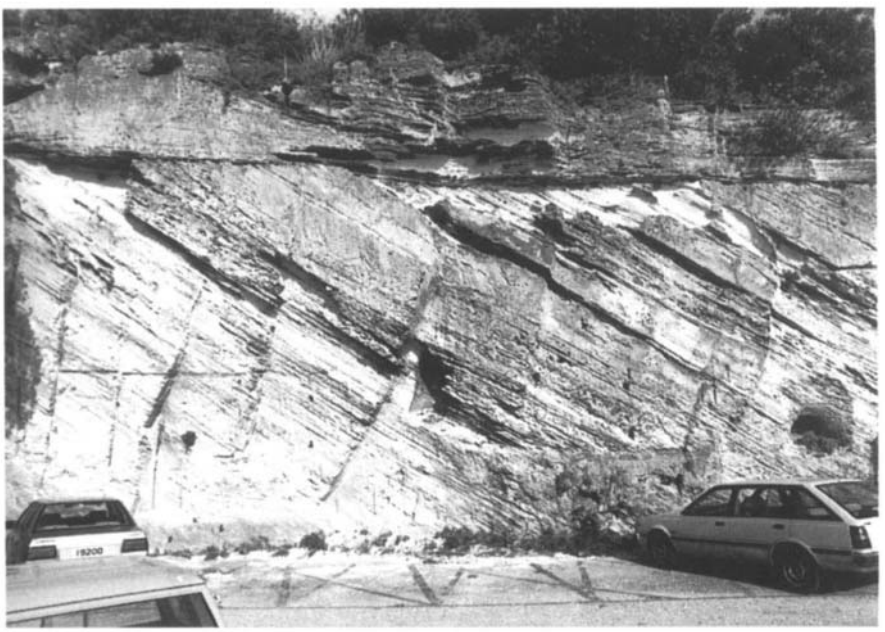


Fig. 2-4. Foresets and overlying topsets of eolianite. Lower member of Town Hill Formation. Near Bacardi Building (Front Street), just west of city limits, City of Hamilton.

who was stationed in Bermuda from 1827 to 1833, is credited with first recognizing the rocks as eolian deposits (Nelson, 1837). Sir C. Wyville Thomson, who visited Bermuda in 1873 as the Director of Civilian Scientific Staff on the HMS *Challenger*, referred to "... a bank of blown sand in various stages of consolidation" (Thomson, 1873, p. 266; Land et al., 1967, p. 993). The following from Alexander Agassiz (1895) is still appropriate:

> "Captain Nelson was the first to call attention to the aeolian character of the rocks of the Bahamas and Bermudas. This character *saute aux yeux* in every direction. In the Bahamas the vertical cliffs of the weather side of the islands show this to perfection, and here and there a quarry or a cut leaves no doubt that the substructure as well as the superstructure of the island is all of the same character. On the Bermudas one comes upon quarries of all sizes at all points, close to the sea level or near the highest summits, and at all possible intermediate elevations. The rock everywhere presents the same structure. There are also endless rock cuts for the passage of roads, giving excellent exposures of the aeolian strata...."

Probably the most influential — and still instructive — discussion of Bermuda's eolianites is that of Sayles (1931). In this paper, Sayles coined the word "eolianite" for the bioclastic grainstones that make up Bermuda's dune-shaped hills (Fairbridge, 1995). Accordingly, Bermuda has been heralded (Vacher et al., 1995) as the type locality for the carbonate eolianite facies. This facies is widespread along the margins of the world's carbonate belt (Johnson and Fairbridge, 1968; Fairbridge, 1995) and is prominent in several carbonate islands (Bahamas, q.v., Chap. 3; islands along coast of northeastern Yucatan, q.v., Chap. 7; Rottnest Island, Australia, q.v., Chap. 27).

The eolian limestone is laced through by paleosols (Fig. 2-5A), indicating that eolian buildup of Bermuda was episodic. Sayles (1931) provided their explanation by introducing to Bermuda the concept of glacioeustatic control (see Case Study). By current interpretation, the eolianites formed during interglaciations (Bretz, 1960; Land et al., 1967), mostly when sea level was below its present position (Sayles, 1931), in many cases shortly after it had peaked at a higher level (Vacher and Hearty, 1989; Vacher et al., 1995). Thus, by this latter interpretation, the largely erosional coastline represented by today's cliffs and pocket beaches is only an introduction to interglacial sedimentation; the main eolian deposition will come later.

The hilly topography obviously reflects the eolian depositional origin of the rocks making up Bermuda, but closer observation reveals that the morphology also evolved post-depositionally. Again, it was Sayles (1931, p. 445) who made the critical observation: the rounded, subdued mounds of the older eolianite ridges ("Older Bermuda") are in "striking contrast" to the highstanding dune-shaped ridges of the outer coastline ("Younger Bermuda"). The fact that Bermuda's interior shoreline of sounds and reaches occurs within Older Bermuda led Bretz (1960) to a somewhat obvious conclusion: much of Bermuda is a partially drowned, Pleistocene karst. Although the concept was probably overstated in Bretz's classic paper (Land et al., 1967), geologic mapping and hydrogeologic studies have clarified the significance and role of chemical erosion in the post-depositional modification of the initial dune landscape, particularly in the development of the inshore water bodies that dominate the island outline (Vacher, 1978b; Mylroie et al., 1995).

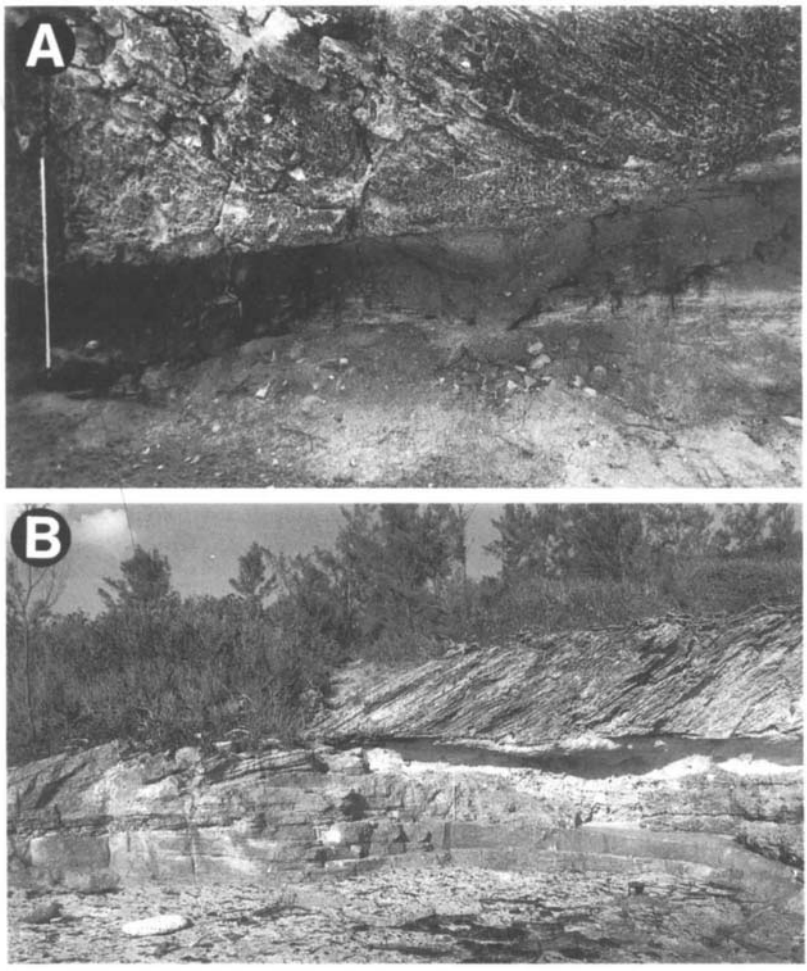


Fig. 2-5. Exposures at Old Fort (Devonshire Bay locality of Land et al., 1967; Rocky Bay locality of Vacher et al., 1989). (A) Terra rossa paleosol (Shore Hills Geosol) between two eolianites (Rocky Bay Formation above, Belmont Formation below) in pathway to battery at top of knoll headland between Devonshire and Rocky Bays. Meter rule for scale. (B) At the shoreline on the Rocky Bay side of the headland. Meter rule rests on unconformity between conglomeratic coastal marine deposits of the Rocky Bay Formation and underlying thick-bedded beach deposits of the Belmont Formation. Rocky Bay marine deposits are overlain by a protosol (the white, unstratified layer) and eolianite (with conspicuous foresets), which is also the upper eolianite in A. Note the vertical contact between the Rocky Bay marine unit and the Belmont Formation, and that Belmont beach deposits grade upward and landward into eolian cross-bedding at left of the vertical contact.

STRATIGRAPHY

Depositional facies

The limestones of Bermuda are an assemblage of five marginal-marine facies. Two of them are coastal-terrestrial facies, and three are coastal-marine facies. The entire assemblage consists of biocalcarenites and volumetrically minor conglomerate. The preponderant component of the assemblage is a voluminous eolian facies within which the other facies are tongues or layers at a multitude of stratigraphic positions (Fig. 2-6).

The eolian facies occurs in hillocky mounds and roughly shore-parallel ridges. Deposition was as retention ridges (Vacher, 1973; Vacher et al., 1995) formed by lateral coalescence of lobate, coastal dunes (Bretz, 1960; Mackenzie, 1964b) that typically stood a few tens of meters above the source beaches. The ridges did not advance inland more than some 0.5–1 km (Vacher, 1973). Detailed analysis of the foreset orientation indicates that gale-force winds were more important than the prevailing winds in the piling up of these large dunes (Vacher, 1973). The common occurrence of enormous sets of conformable foresets that remain unbroken or uninterrupted by soils or bioturbation for several tens of meters suggests that the ridges were built mostly during a small number of major storms when conditions of sediment supply were optimal. In places they can be seen to have engulfed trees (Fig. 2-7). Between storms, the carbonate sand mostly accumulated as temporary storage on seaward-prograding beaches.

The second terrestrial limestone facies consists of "calcarenite protosols" (Vacher and Hearty, 1989, p. 160) that occur as layers and lenses within the eolian facies or between the marine facies and overlying eolian deposits (Fig. 2-5B, 2-8A). These paleosols are typically unconsolidated, 0.3–1 m thick, and slightly colored in shades of buff, tan or brown. They have been described as "regosols ... in which few or no

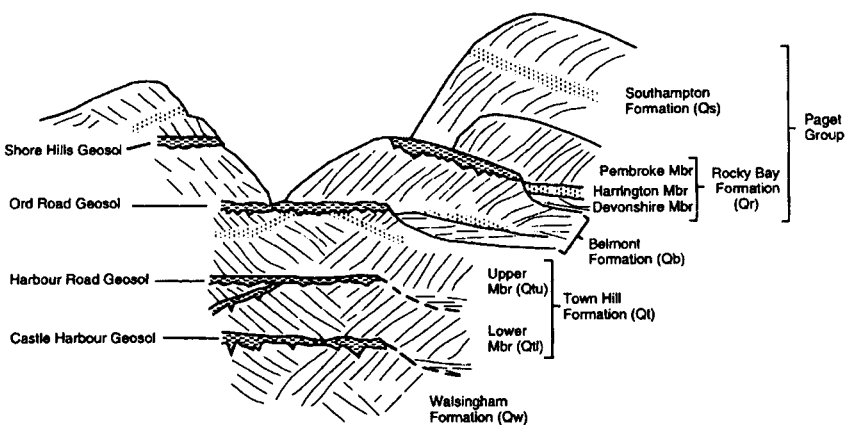


Fig. 2-6. Stratigraphic column of Bermuda. (From Vacher et al., 1995.)

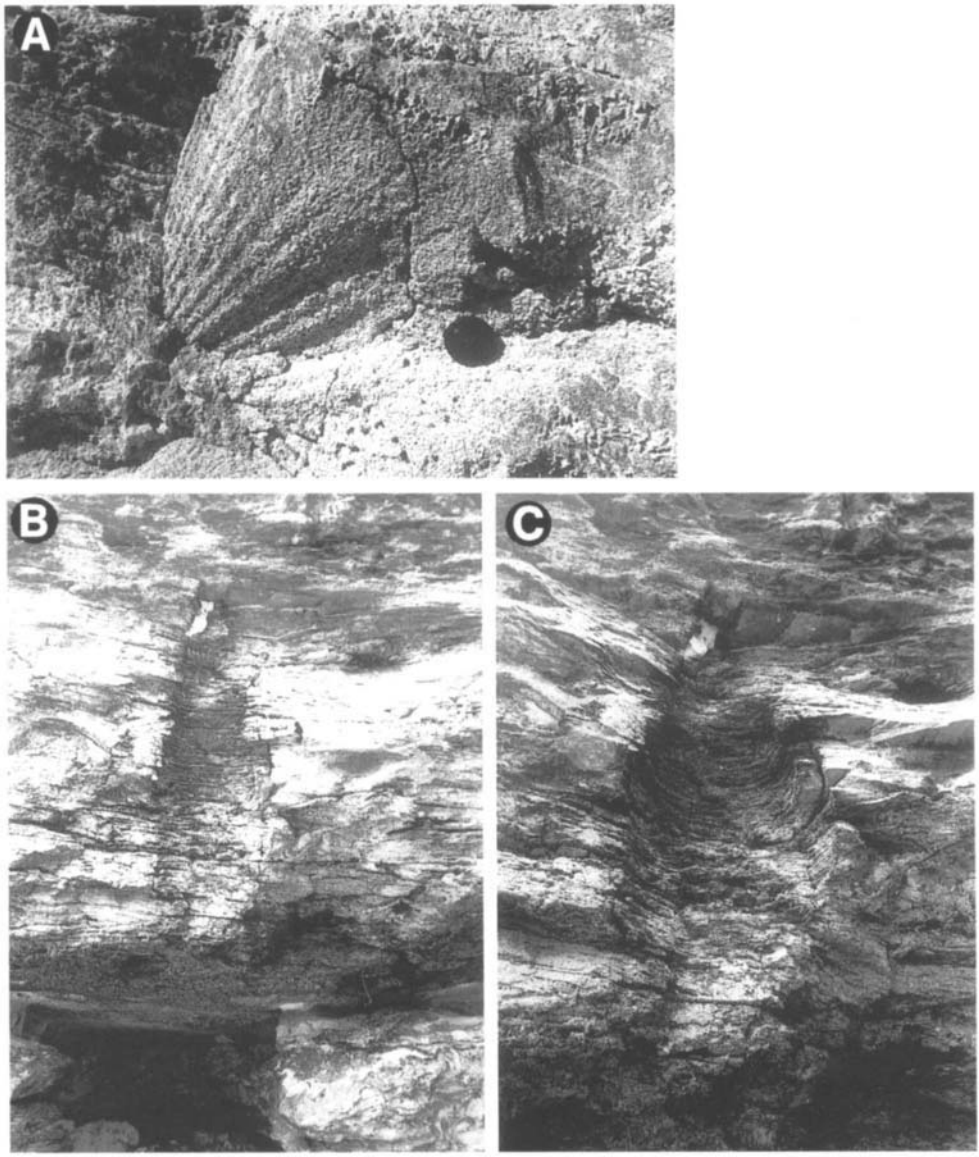


Fig. 2-7. Mold of palmetto tree in eolianite of Rocky Bay Formation at Hungry Bay. (A) A frond. (B) Trunk rising from protosol at base of the eolianite. (C) View looking up the trunk mold. In other exposures, the fossil trunks are preserved as an unstratified, friable sand that makes a striking contrast with the surrounding foresets (see Kindler and Hearty, 1996, Fig. 11, for a Bahamian example). The sand has been washed away in this exposed, sea-cliff setting.

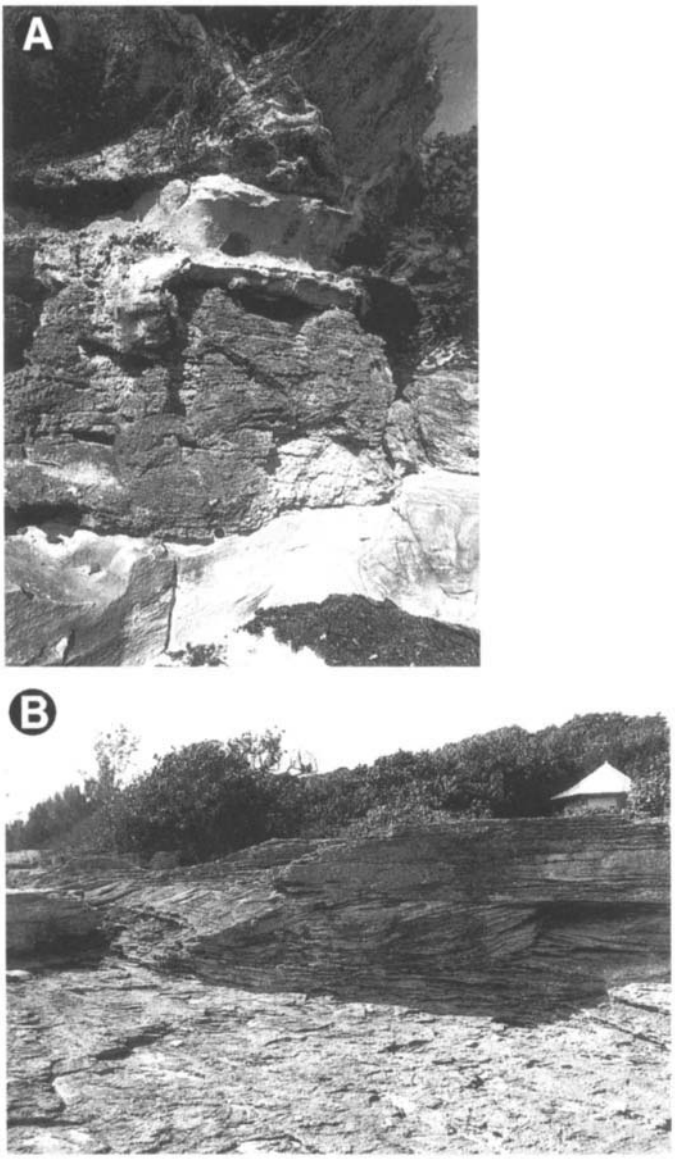


Fig. 2-8. Stratigraphy at Grape Bay. (A) Typical three-part succession of the Rocky Bay Formation resting unconformably on Belmont Formation (lens cap at contact). The Rocky Bay Formation consists of: well-stratified coastal-marine sediments (Devonshire Member); white, unstratified protosol (Harrington Member); foresets of an eolianite (Pembroke Member). (B) Intertidal and subtidal cross-beds in the beach deposits of the Belmont Formation. See Meischner et al. (1995) for thorough description and more illustrations.

clearly expressed soil characteristics have developed" (Ruhe et al., 1961, p. 1138). According to D.R. Muhs (pers. comm., in Vacher et al., 1995), these weakly developed paleosols are probably equivalent to Entisols, Inceptisols, and minimally developed Alfisols in the U.S. Soil Taxonomy. Protosols typically contain abundant well-preserved fossils of *Poecilozonites*, the land snail whose phylogeny (Gould, 1969) provided one of the type examples of evolution by punctuated equilibrium (Gould, 1969; Eldridge and Gould, 1972). These paleosols reflect relatively brief interruptions and inactive areas in the accumulation of carbonate sand.

The three types of coastal-marine deposits are: erosional-coastline marine facies representing rocky shorelines and small pocket embayments comparable to those of the present coastline; depositional-coastline marine facies representing long beaches that supplied dune ridges; and protected-coastline marine facies representing shorelines of inshore sounds and reaches. The erosional-coastline facies consists of discontinuous lenses and pods of marine-fossiliferous calcarenite and conglomerate resting on erosional benches (Fig. 2-5B), against paleo-seacliffs, and within coastal notches; the fossil corals that have provided the U-series geochronology for Bermuda (Harmon et al., 1978, 1981, 1983) are mainly from these deposits. The depositional-coastline marine facies consists of long, shore-parallel wedges consisting of skeletal grainstones that typically contain no whole shells (Fig. 2-8B); in some cases, it is difficult to distinguish them from the deposits of the windward part of eolianites where low-angle, conformable cross-beds are common (Vacher, 1973). Deposits of the protected-coastline facies contain many marine fossils, but these deposits are rare, probably because of erosion accompanying lateral expansion of the inshore water bodies (Neumann, 1965; Vacher, 1978b; Mylroie et al., 1995).

Perhaps the best single locality to compare and contrast the erosional- and depositional-coastline marine facies in Bermuda is at Grape Bay (Fig. 2-8), along the southern, margin-facing shoreline. This magnificent outcrop has been described in detail by Meischner et al. (1995). In reference to that paper, the beach deposits of the Rocky Bay Formation are erosional-coastline deposits (Fig. 2-7A), and the beach deposits of the Belmont Formation are depositional-coastline deposits (Fig. 2-8B). A comparably instructive outcrop is at Rocky Bay (Old Fort, Devonshire Parish) (Fig. 2-5). At both localities, one has no difficulty distinguishing the depositional-coastline beach deposits of the Belmont Formation from the eolian facies with which they intergrade.

Dividing up the assemblage of marginal-marine carbonate facies are islandwide, reddish to reddish-brown paleosols (terra rossas; see Herwitz et al., 1996, for color photographs) that represent relatively long interruptions in calcarenite accumulation. Sayles (1931) called these red paleosols "soils of weathering" and thought they were the insoluble residue of large amounts of eolianite. It is now recognized that the noncarbonate fraction of these paleosols was derived largely from fallout of atmospheric dust (Bricker and Mackenzie, 1978), most likely from the Sahara judging from trace-element indicators (Herwitz et al., 1996). The terra rossas are thickest and best developed in paleo-topographic lows, and *Poecilozonites*, though present, is typically poorly preserved. Commonly where the terra rossa layer has been eroded, there are remnants of it in the form of cylindrical bodies of soil protruding down-



Fig. 2-9. Truncated soil pipe at Grape Bay. The Shore Hills terra rossa has been stripped away leaving truncated soil pipes in the Belmont Formation as remnants. Soil in the pipe in the foreground has been removed leaving a mold; pipe in the background is still filled. Lens cap is 5 cm in diameter.

ward into the underlying limestone (Fig. 2-9; see also Herwitz et al., 1996, plate 4). Herwitz (1993) explained these structures (called "palmetto stumps" by Sayles, 1931; "roots" by Bretz, 1960; "solution pipes" by Land et al., 1967, and "soil pipes" by Vacher et al., 1995) as having been formed from dissolution promoted by acidic tree-trunk-guided water (a variety of stemflow) which is, then, followed by soil and roots.

Facies model

The two most common vertical facies successions are shown in Fig. 2-10A. In one (labelled I in Fig. 2-10A), the upward succession consists of an erosional-coastline marine unit, protosol, and eolianite: the marine unit overlies a coastal-erosion surface that truncates the terra rossa paleosol which, in turn, overlies older limestone; the eolianite oversteps the coastal erosion surface and lies directly on the older limestone and terra rossa. In the other mosaic (II, in Fig. 2-10A), eolianite overlies a depositional-coastline deposit with an apparently gradational contact. At a few localities (Fig. 2-11; see also Meischner et al., 1995), it can be shown that these two common successions are different parts of a single facies mosaic as shown in

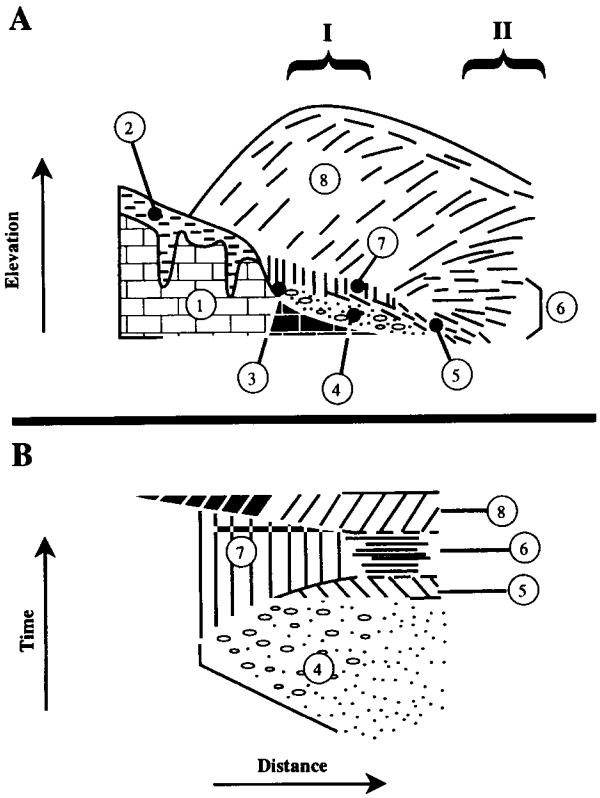


Fig. 2-10. (A) Facies mosaic showing relation of coastal-marine and coastal-terrestrial deposits (Key: 1, older limestone; 2, terra rossa; 3, coastal erosional unconformity; 4, erosional-coastline marine deposit; 5, depositional-coastline marine deposit; 6, beach ridge; 7, protosol; 8, eolianite of the dune ridge. Location I is the distal part of the mosaic (Figs. 2-5B, 2-8A), and Location II is the proximal part (Fig. 2-11). Units 1, 2, and 8 are shown in Fig. 2-5A; units 1, 3, 4, 7, 8 are in Fig. 2-5B; units 5, 7, 8 are in Fig. 2-11A; units 5, 6, 7 are in Fig. 2-11B. (B) Time-stratigraphic interpretation of the units comprising the facies mosaic. The vertical dimension is time, rather than elevation. (From Vacher et al., 1995)

Fig. 2-10. The succession with the erosional-coastline deposit and protosol is in the distal (landward part) of the mosaic; the succession with the vertical intergradation between beach and dune deposits is in the proximal (seaward) part of the mosaic.

The history recorded by the facies mosaic of Fig. 2-10A is illustrated by the time-distance cross section (Wheeler diagram, Vacher et al., 1995) shown in Figure 2.10B. The first deposits are those of an erosional coastline (unit 4). As sediment is delivered to the shoreline, the pocket beaches prograde seaward; the back part of the beach develops as a grassed-over supratidal accumulation of sand (unit 7, the protosol) washed and blown in from the beach. As delivery of offshore sediment increases, long beaches (unit 5) develop and prograde seaward. Beach ridges (unit 6) and, finally, large landward-prograding dune ridges (unit 8) develop with the continued

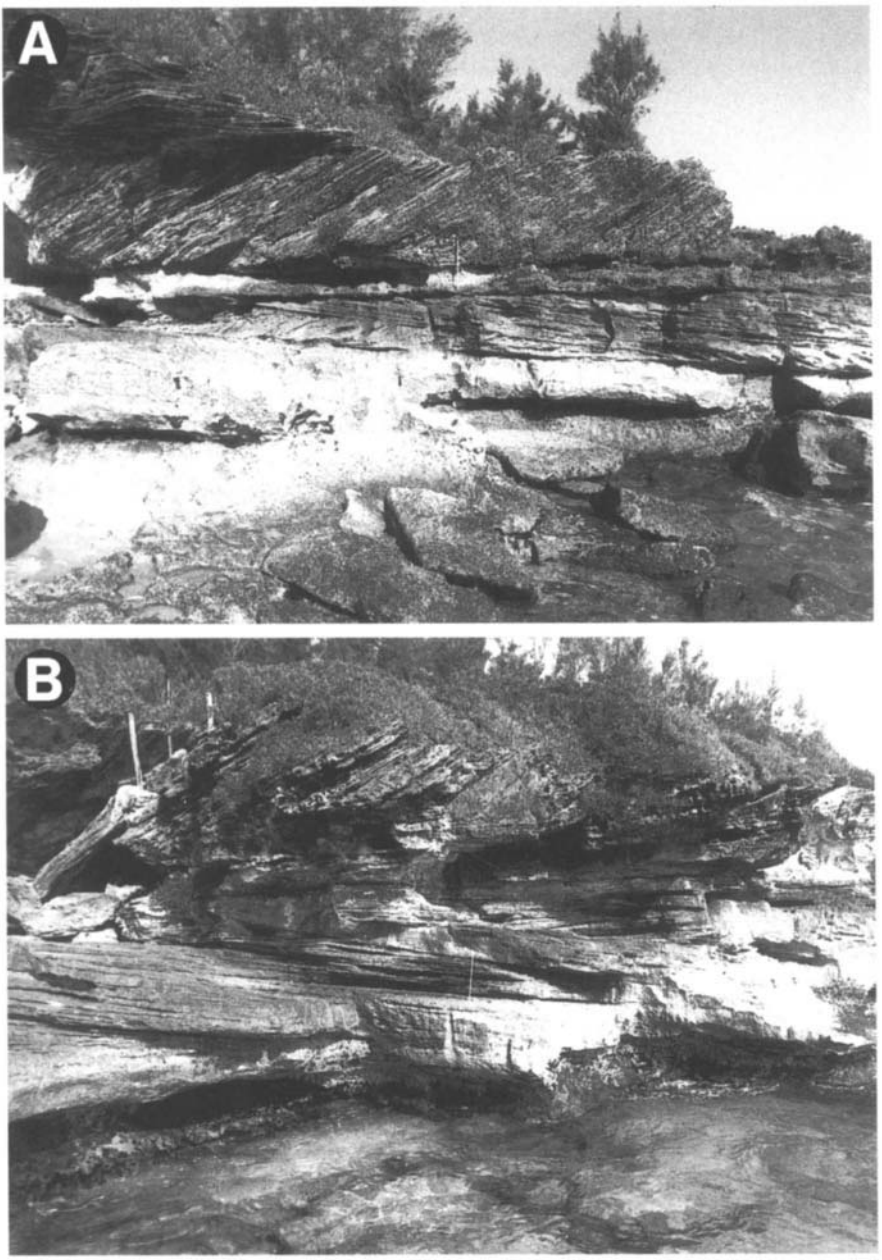


Fig. 2-11. Facies mosaic in the Belmont Formation at Spittal Pond as seen in two headlands, 700 m apart. (A) Exposure in the headland at the west end of the park (near Spencer's Point). Meter rule rests on the sharp break between coastal-marine deposits below and eolianite above. Discontinuity traces into a protosol to left. (B) Exposure in the headland at the east end of the park (near North's Point). Gradual, upward transition between coastal-marine deposits below and eolianite above.

delivery of offshore sediment. The dunes are then the main repository for the offshore sediments delivered to the shoreline.

At many places, the protosol (unit 7) and eolianite (unit 8) can be traced down to present water level. It is clear in these cases that the transition from an erosional coastline to a depositional coastline with dunes occurred as sea level was falling below its present position (Vacher et al., 1995). This observation, however, does not mean that a drop in sea level is a necessary condition for the deposition of eolianite. According to Vacher et al. (1995), the critical factor may be, simply, time: with sufficient time, sediment sources build up, and transport routes to the shoreline develop; a few thousand years after the initial submergence of the Bermuda Platform may have been required for development of the store of offshore sediments that was tapped and eventually delivered to the shoreline in quantities to build dunes the size of those of the Pleistocene record. Such deposition has not happened yet during the Holocene submergence (Fig. 2-3).

Not all beach and dune transitions in Bermuda fit the facies model of Fig. 2-10, and probably not all eolianites in Bermuda were formed while sea level fell. Particularly noteworthy is a prominent eolianite and associated beach deposit along the north shore of the central parishes (near Blackwatch Pass; see Case Study). As pointed out by Vacher et al. (1995. p. 283), the "data admit to a variety of interpretations regarding sea-level history and its relation to eolianite deposition. It is entirely possible that the timing of deposition of eolian sediment derived from the heart of the North Lagoon is different from that derived from the platform margin." One of the possibilities is that the store of sediment in the North Lagoon may have been tapped and transported to the island late in a period of platform submergence during a short, rapid rise in sea level that nullified the wave-barrier effects of the northern reef tract (Vacher, 1973; Hearty and Kindler, 1995; see Case Study).

Discussion. The presence of beach-to-dune transitions above present sea level (Figs. 2.5B, 2.11B) was the principal observation that led Bretz (1960) to conclude that Bermuda's eolianites were deposited during interglacial highstands. This idea replaced the earlier interpretation of Sayles (1931) that the dunes formed during glaciations when the platform was fully exposed and previously deposited sand was blown onto Bermuda. Bretz's idea of interglacial eolianites, however, does not seem to accord with the observation that originally led Sayles (1931) to his idea of glacial-age eolianites: the widespread and striking occurrence of foresets at the present water line — a fact that clearly indicates that much eolianite deposition occurred when sea level was below its present position. These two, apparently contradictory observations — beach-dune transitions above sea level, and eolian foresets prominent at the water line — are reconciled by consideration of the facies mosaic (Fig. 2-10): eolianite deposition occurred late in the interglacial as sea level was falling (probably coincidentally). As noted, there is also the possibility that, in some cases, eolianite deposition was brought about by a rapid rise in sea level, late in the interglacial (Hearty and Kindler, 1995). In each scenario, the eolianite deposition was an interglacial phenomenon; each involved the accumulation of carbonate sand on the platform during the early part of the interglacial, and, in

each, the transport of that sand to the present island was by marine, rather than subaerial, processes.

Around the world, there is a variety of interpretations of the timing of eolianite deposition. Most notably, the usual interpretation in Australia is that the eolianite formed during glacial lowstands (e.g., Fairbridge, 1995); the best-known island example is Rottnest Island [q.v., Chap. 27]. A comparable interpretation is held for the islands off southern California (Muhs, 1983). In the Bahamas [Chap. 3A, 3B], the interpretation is that the eolianites record interglacials, and that transgressive, as well as regressive, eolianites are significant (e.g., Carew and Mylroie, 1995a; see Chapter 3A of this book). It is not unreasonable to expect differences between different eolianite areas. Consider, for example, Bermuda vs. the Bahamas. A major contrast is that Holocene eolianites are large and widespread in the Bahamas (thus transgressive eolianites, early in the interval of submergence); no Holocene eolianites are recognized in Bermuda (consistent with no eolianites during the early part of a submergence). But Bermuda, the site of the northernmost coralgal reefs in the Atlantic, is on the very fringe of the carbonate belt. Corals, for example, are at the limit of their range and likely temperature tolerances (Cook et al., 1994). One can expect slower rates of sediment production, hence longer times for the source of the eolian sediment to develop in Bermuda.

Stratigraphic classification

Vacher et al. (1995) discussed the history and philosophy of stratigraphic classification and nomenclature in Bermuda. The present column (Fig. 2-6; Table 2-1; Vacher et al., 1989; Rowe, 1990; Hearty et al., 1992) is based on geologic mapping (Fig. 2-12; Vacher et al., 1989) that accompanied a groundwater exploration program carried out by the Bermuda Government. Although it is clear that glacioeustasy is the ultimate control for the cyclic alternation of limestones and terra rossas in Bermuda (Land et al., 1967), the main issue for the formulation of the column was mappability, not geologic history. The present stratigraphy uses multiple systems of classification (see Vacher et al., 1995, for details).

Lithostratigraphy. The lithostratigraphic column (Table 2-1) consists of five multi-facies formations. Each formation is preponderantly eolianite, and each includes one or more coastal-marine tongues. In addition, there are four soil-stratigraphic units, or geosols ("geosol" is a term stipulated by the NACSN, 1983, to serve for soil stratigraphy in the same way that "formation" is the fundamental unit in lithostratigraphy). These geosols correspond to terra rossa paleosols. Calcarenite protosols occur within each formation and are not geosols.

The portion of Bermuda that is above sea level and exposed in cliffs and rock cuts was nearly entirely deposited in the eolian depositional environment and altered in the vadose-meteoric diagenetic environment. Lithostratigraphic subdivision of this body of rock — the vadose-altered eolianite facies — ultimately depends on lithologic variables that change with time: amount of high-Mg calcite and aragonite relative to

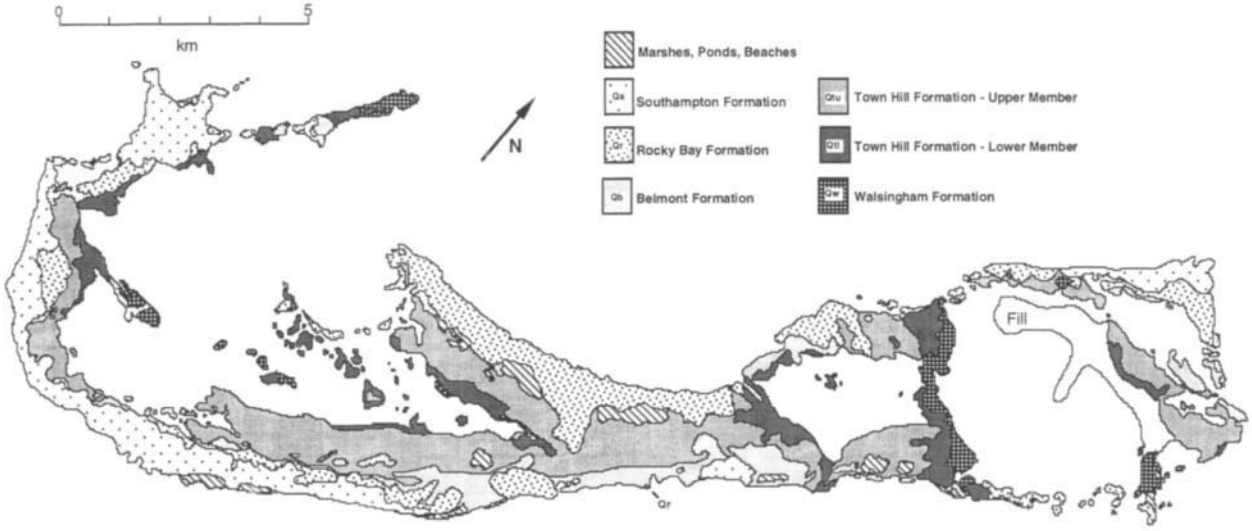


Fig. 2-12. Geologic map of Bermuda. (Generalized after Vacher et al., 1989; from Vacher et al., 1995)

Table 2.1

Stratigraphic Column of Bermuda

Lithostratigraphic unit *Pedostratigraphic unit*	Comments
Southampton Fm	Large eolianites including numerous protosols in n. St. George's Island, at Saucos Hill, along South Shore w. of Elbow Beach, and much of w. Southampton Parish and Somerset Island. Eolianites include some of the highest hills in Bermuda (e.g., Gibbs Hill Lighthouse). Isolated marine deposits at Fort St. Catherine and Conyers Bay.
Rocky Bay Formation	Most places (e.g., Rocky Bay, Grape Bay, Hungry Bay, Whalebone Bay): vertical section as in Figures 2.5B and 2.8A. North Shore of Pembroke and Devonshire Parishes: Succession of two or three eolianites with intervening protosols, and beach(?) deposits at shoreline.
Shore Hills Geosol (e.g., Rocky Bay; Grape Bay; upper of two terra rossas in hills between South and Middle South Rds, Paget and Warwick Parishes).	
Belmont Formation	Prominent coastal-marine deposits grading landward and/or upward to relatively small eolianites (Spittal Pond, Rocky Bay, Hungry Bay). Vertical succession includes prominent protosol between underlying coastal marine deposits and overlying eolianite at Saucos Hill and Spencers Point. Eolianite well displayed along North Rd s. of Shelly Bay.
Ord Road Geosol (e.g., lower of two terra rossas in hills between South and Middle Rds, Paget and Warwick Parishes).	
Town Hill Formation	
Upper member	Large complex of eolianites and protosols forming the core of the Main Island and highest and most prominent hills in Bermuda, including Town Hill, Knapton Hill, St. David's Lighthouse, and hills along Ferry Reach. Intergrades with coastal marine deposits at Whalebone Bay (see Vollbrecht and Meischner, 1993). Includes prominent protosol that extends for several km near Middle Rd (Paget and Warwick Parishes).
Harbour Road Geosol (e.g., along Harbour Rd, Paget and Warwick Parishes; city of Hamilton, along Cavendish Rd; Bierman Quarry; Shark Hole).	
Lower member	Poorly known complex of eolianites and protosols exposed in windows such as deep quarries (e.g., Bierman Quarry) and shores of inshore water bodies. Coastal marine(?) deposits at Belmont Wharf and Devils Hole. Conglomerate at Stokes Point and Government Quarry. Includes another terra rossa in Naval Air Station (St. Davids Island).
Castle Harbour Geosol (e.g., entrance to Castle Harbour Hotel; in Shore Hills Quarry; Casemates Prison; in back of the Swizzle Inn).	
Walsingham Formation	Eolianites in the cave district around Castle Harbour (e.g., Government Quarry) and Ireland Island. Includes shelly marine rocks at Shore Hills Quarry (adjacent to BBSR).

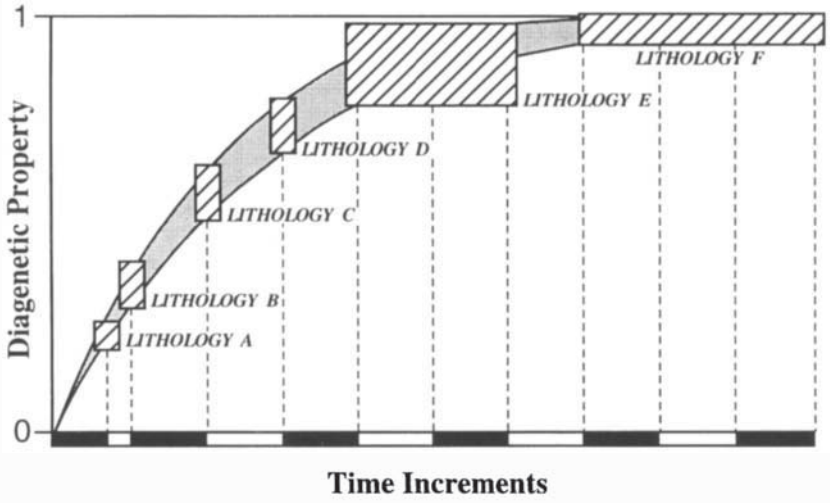


Fig. 2-13. Conceptualization of how lithology would vary as a function of time if one looked at a single depositional site (that of eolian ridges) and a single diagenetic environment (that of the intermediate vadose zone), assuming that the starting material was the same for each ridge (see Vacher et al., 1995, for discussion). Model illustrates how resolution breaks down in older units. (From Vacher et al., 1995.)

low-Mg calcite; distribution and amount of cement. Because of the uniform starting material and the single "ultimate fate" — a cemented bioclastic grainstone consisting of low-Mg calcite — lithologic differences between limestones of successive interglacials diminish as that ultimate fate is approached (Fig. 2-13). It is for this reason that there are multiple interglacial-glacial cycles represented in the formations low in the column, whereas two formations (Southampton and Rocky Bay) represent one interglacial (deep-sea, oxygen isotope stage 5) at the top of the column.

In our mapping we consciously tried to separate the "signal" from the "noise." We focused on the in-the-field appearance of large exposures (cliffs, roadcuts, backyard rock faces) of the vadose-altered eolianite facies of the formations (specifically the region of vadose seepage in the intermediate vadose zone, between the soil-affected uppermost vadose zone and the capillary fringe). Numerous other diagenetic environments are certainly present: phreatic, perched phreatic, upper vadose (within the zone of influence of the soil), and areas of vadose flow (preferred pathways between the areas of the more usual vadose seepage). The different overprint from these other environments (e.g., Land et al., 1967; Land, 1970; Vollbrecht and Meischner, 1993) results in a large lithologic variation within formations and, as emphasized by Land et al. (1967), considerable blurring of stratigraphic differences.

Aminostratigraphy. The geologic map (Vacher et al., 1989) and, hence, the stratigraphic column of Table 2-1, were in press before an extensive campaign was begun by Paul Hearty to determine the amino acid racemization (AAR) history of Bermuda's limestones. The aminostratigraphy developed by Hearty (Hearty and

Hollin, 1986; Vacher and Hearty, 1989; Hearty et al., 1992; Hearty and Vacher, 1994; Vacher et al., 1995) was based on D-alloisoleucine/L-isoleucine (A/I) ratios in pelecypods from coastal-marine deposits; *Poecilozonites* from protosols, terra rossas and eolianites; and whole-rock samples of eolianite. The ratios were internally consistent and, with only 7 exceptions out of 257, they agreed with the independently mapped lithostratigraphy. Thus the aminostratigraphy supported the definition and mapping of lithostratigraphic units. When coupled to U-series dates on corals from the marine deposits (Harmon et al., 1981; 1983) and a kinetic model for racemization (Mitterer and Kriasaukal, 1989), the A/I ratios also provided a means of correlating Bermuda's stratigraphy with global time-stratigraphic units (Hearty et al., 1992; Vacher et al., 1995; Hearty and Kindler, 1995).

Time stratigraphy. From the A/I ratios and U-series data on corals, it is clear that the Rocky Bay Formation correlates with substage 5e of the oxygen-isotope time stratigraphy; that the Southampton Formation correlates with later substages of stage 5; and that the Belmont Formation correlates with stage 7. From the A/I ratios, the upper and lower members of the Town Hill Formation are middle Pleistocene; the upper member is probably stage 9, and the lower member is at least stage 11. The Walsingham is early Pleistocene.

Diagenesis

Some of the classic early work on carbonate diagenesis was done on the skeletal grainstones of Bermuda. For example, Gross (1964) recognized variations in stable isotopes; Friedman (1964) documented the mineralogical stabilization from high-Mg calcite and aragonite to low-Mg calcite; Land et al. (1967) developed the concept of diagenetic grade; and Land (1970) identified a fossil water table from the contrast of vadose and phreatic diagenesis. In addition, Ginsburg and Schroeder (1973) documented the character of marine cementation in the modern reefs, and Schroeder (1973) described its counterpart in a Pleistocene (substage 5e) block. More recently, Vollbrecht and Meischner (1993, 1996) have provided detailed descriptions and careful analyses showing how petrography records the history of alternating meteoric and marine porewater conditions at selected coastal exposures.

GEOMORPHIC EVOLUTION OF BERMUDA

Buildup of Bermuda

The cardinal feature of Bermuda's stratigraphic mosaic is that successive beach-dune complexes are arranged in a pattern of lateral accretion (Sayles, 1931; Vacher, 1973; Vacher et al., 1995). As a result of the large depositional relief of the eolian facies, coastal-dune complexes of later interglacials accumulated on the outside margin of the deposits of earlier interglacials. The geologic map (Fig. 2-12; Vacher et al., 1989) documents the relation in detail; in general, the section gets younger

toward the external shorelines. The Walsingham and Town Hill Formations occur in the interior of the island next to the inshore water bodies, and the Belmont, Rocky Bay and Southampton Formations successively offlap this core.

Not all constructional episodes in the buildup of Bermuda were equal; neither, apparently, were all the hiatuses. In terms of volume of accumulated eolian sediment, stages 5 and 9 were the most important (Hearty and Vacher, 1994). The terra rossa of the Castle Harbour Geosol is, by far, the best developed and thickest paleosol, and the Ord Road terra rossa is generally better developed than the Shore Hills Geosol. According to Hearty and Kindler (1995), the time interval represented by the Castle Harbour Geosol is as long or longer than the time interval represented by the rest of the column above it.

Because of the pattern of lateral accretion, the water table in Bermuda cuts across formations. This is an important factor in Bermuda's hydrogeology because it is at the top of the saturated zone, just below the water table, that the freshwater lenses develop, given favorable geological conditions. The distribution of fresh groundwater in Bermuda can be attributed to the pattern of offlapping geological formations, with older limestones rimming the inshore water bodies and younger ones bordering the external coastlines (Fig. 2-12).

Evolution of inshore basins

Bretz (1960, p. 1729) called attention to Bermuda's many inshore water bodies: "The curvilinear fingers constituting the Bermuda Islands enclose or nearly enclose almost 60 square miles of sounds, reaches and bays, approximately three times the total land area." Vacher (1978b) proposed a conceptual model that explains how these inshore basins of Bermuda evolved from initial, depositional, interdune lows over a time period of alternating submergences and emergences. In brief, the model holds that marshes become the nucleus of inshore reaches and sounds of future interglacial highstands (Vacher, 1978b; Mylroie et al., 1995). As Bermuda expands outward with the accretion of new eolian ridges along the exterior shoreline, the interior shoreline advances inland, amoeba-like, as expanded marsh basins become incorporated into the coalesced aggregate of inshore karst basins.

The elements of the conceptual model are (1) landlocked (i.e., eolianite-enclosed) marshes within an area of freshwater lenses, (2) a positive water budget (i.e., rainfall > evapotranspiration), and (3) a succession of glacioeustatic cycles. During interglacial stages, inter-eolianite topographic lows are partially submerged. During the sea-level rise to the interglacial submergence, the landlocked lows become marshes and peat accumulates. While the topographic low is a marsh, CO_2-enriched calcite-unsaturated waters radiate outward and dissolve the neighboring saturated zone (Plummer et al., 1976). As sea-level falls, the peat is exposed in the vadose zone and is leached by descending waters that deepen the basin. Meanwhile, the general landscape is lowered by chemical denudation resulting from the soil-water excess associated with the positive water budget (Vacher, 1978b). Upon a later sea-level rise, one or more low passes in the hillocky ridge are reached by sea level and the former marsh basin begins to be incorporated into a inshore marine water body. The

limestones that are thus brought next to an inshore water body become the site of dissolution accompanying freshwater-saltwater mixing. This, coupled with marine processes of bioerosion that characterize the shores of inshore water bodies in Bermuda (e.g., Neumann, 1965), leads to further expansion of the basin and the eventual formation of a sound.

Evidence. The model of marsh-to-sound evolution of topographic basins in Bermuda explains a number of observed relationships:

1. Older Bermuda of Sayles (1931) borders the inshore water bodies (Fig. 2-12). Older Bermuda, composed largely of the Town Hill Formation (Vacher et al., 1989), presents a lowered, subdued eolian landscape (Bretz, 1960) with reentrants of the inshore sounds and reaches. Geologic mapping (Vacher et al., 1989) suggests that once-continuous eolian ridges within the Town Hill are now segmented. Remnants occur within the sounds and reaches (Fig. 2-12).
2. The setting of interdune lows occupied by present-day marshes is geometrically similar to that of the interdune lows occupied by sounds and reaches, with the significant exception of the age of the bordering eolianites. The marshes are bordered on the outside (i.e., toward the external shoreline) by an eolianite complex consisting of one or more of the Southampton, Rocky Bay, or Belmont Formations; on the inside, the marshes are bordered by Upper Town Hill. The basins of the sounds, on the other hand, are between Town Hill eolianites, or between Town Hill and Walsingham eolianites.
3. The peat that is presently in the marsh basins and within deeper closed contours within the reaches and sounds is Holocene in age. This is known from the studies by Neumann (1971) of the history of Holocene sea level in Bermuda. Neumann's data consisted of radiocarbon dates from peat resting on bedrock in such basins as Devonshire Marsh, Pembroke Marsh, and Harrington Sound. By implication, pre-Holocene peat is absent, even though the basins themselves are older, as indicated by the age of the eolianites that close them off. The peat of earlier, pre-Holocene submergences apparently did not survive exposure during lowstands.

The conceptual model also explains a geomorphic contrast between Bermuda and depositionally similar islands in the Bahamas [q.v., Chaps. 3A, 3B]. In Bermuda, the island-interior inter-eolianite topographic lows are marshes, and groundwater radiates out ("centrifugally") from them because of the island's positive water budget. In the southeastern Bahamas, island-interior inter-eolianite topographic lows are occupied by saline ponds, and groundwater flows ("centripetally") toward them. This hydrogeologic contrast prompted Vacher and Wallis (1992) to distinguish between Bermuda-type islands and Exuma-type islands [see Fig. 4.8]. The inter-eolianite lows of Exuma-type islands (with the saline ponds) retain their depositional morphology, and, in general, these islands do not have the vast network of inland sounds, reaches and bays that characterize Bermuda. As argued by Mylroie et al. (1995, p. 265), "the positive water budget of Bermuda promotes interdune enlargement, whereas the negative water budgets of the southeast Bahamas lead to preservation of the original depositional topography."

The conceptual model of how depositional lows expand and coalesce into karst basins may provide an explanation for post-depositional morphology of the type that Purdy (1974) argues characterizes the Bermuda Platform and many other carbonate island platforms.

QUATERNARY SEA LEVEL

Assuming that subsidence due to cooling is proportional to the square root of time (Turcotte and Schubert, 1982, Eq. 4-202) and that the total subsidence of the Bermuda Pedestal during the past 25 Ma is less than 100–200 m (Liu and Chase, 1989), then the present subsidence rate of Bermuda due to this process is less than 0.6–1.2 cm ky^{-1}. According to this figure, Bermuda has probably subsided no more than a few centimeters in the past few thousand years, and no more than about a meter since the last interglacial (ca. 100 ky). Bermuda has been likened to a "tide gauge" (Land et al., 1967, p. 993) for reading the history of Pleistocene sea level, by which it is meant that there is effectively no need to correct for tectonics.

The literature concerning Bermuda's "Pleistocene tide gauge" is extensive (Land et al., 1967; Vacher, 1973; Harmon et al., 1978, 1981, 1983; Vacher and Hearty, 1989; Hearty and Vacher, 1994; Meischner et al., 1995; Hearty and Kindler, 1995) and, unfortunately, contradictory. Problems have arisen because of changing nomenclature, changing techniques, changing correlations within Bermuda, a tendency to interpret rock relations from geochronology or evidence from outside Bermuda (which also changes), and, more than anything, the fact that the record within these eolianites and intercalated shoreline deposits is difficult to read. We believe that the Pleistocene sea-level curves that have been published (Land et al., 1967; Vacher, 1973; Harmon et al., 1983; Hearty and Kindler, 1995) give a false impression of the uncertainties with which the history of sea level in Bermuda is actually known (see Case Study of this chapter).

Unlike the Pleistocene sea-level curve, the Holocene sea-level curve for Bermuda (Redfield, 1967; Neumann, 1971) is not disputed. Bermuda is in the part of the world (Clark et al., 1978; Lambeck, 1990) where the postglacial rise of relative sea level is characterized by a smooth, rising curve that slows in the last 5 ky and reaches present datum in the past 0.5–2 ky with no highstand above present sea level. According to Neumann (1971), the rise was 3.7 m ky^{-1} from 9200 to 4000 y B.P., after which, at about −4 m, it rose at about 1 m ky^{-1} to its present position. The evidence for the curve is radiocarbon dates on basal peat deposits from several marshes, ponds, and inshore basins. There are no Holocene beach deposits above sea level and, unlike in the Bahamas, no Holocene eolianites.

The latest Holocene sea-level history has been interpreted by Ellison (1993) from a transgressive stratigraphy of subtidal sand over intertidal mangrove peat at Hungry Bay. According to this study, the mangrove swamp kept up with the slowly rising sea level for over a thousand years. It then retreated because its accretion rate (8.5–10.6 cm per century) was exceeded by a faster sea-level rise (14.3 cm per century) in the last few centuries. As noted by Ellison (1993), records of the tide gauge at BBS

indicate an even more rapid rise: 24 cm per century (Barnett, 1984) and 28 cm per century (Pirazzoli, 1987). These rates are of the same magnitude as the Holocene rise before 4000 y B.P.

HYDROGEOLOGY

Distribution of fresh groundwater and hydrostratigraphy

The hydrogeology of Bermuda's groundwater lenses is known from an extensive and on-going program carried out by the Department of Works and Engineering of the Bermuda Government. As the first step of that program (Vacher, 1974), the distribution of fresh and brackish groundwater was mapped (Fig. 2-14) by Vacher and Rowe from the conductivity of household wells and discussions with local well drillers. Now, after the drilling of hundreds of wells and monitoring boreholes by the Government, the occurrence and behavior of the freshwater lenses (Fig. 2-15) is known in detail. As shown in Figures 2-14 and 2-15, there is one main lens (the Central Lens; Rowe, 1984) in the heart of the Main Island and three minor lenses at the western and eastern extremities of Bermuda. There is also a constellation of small, thin discontinuous lenses near the south shore beaches of Warwick and Southampton Parishes (Rowe, 1991).

The key fact of the hydrogeology is that the location of the lenses is controlled by the distribution of hydraulic conductivity in the uppermost part of the saturated zone (Vacher, 1974, 1978b; Rowe, 1984). Because of the lateral accretion in the

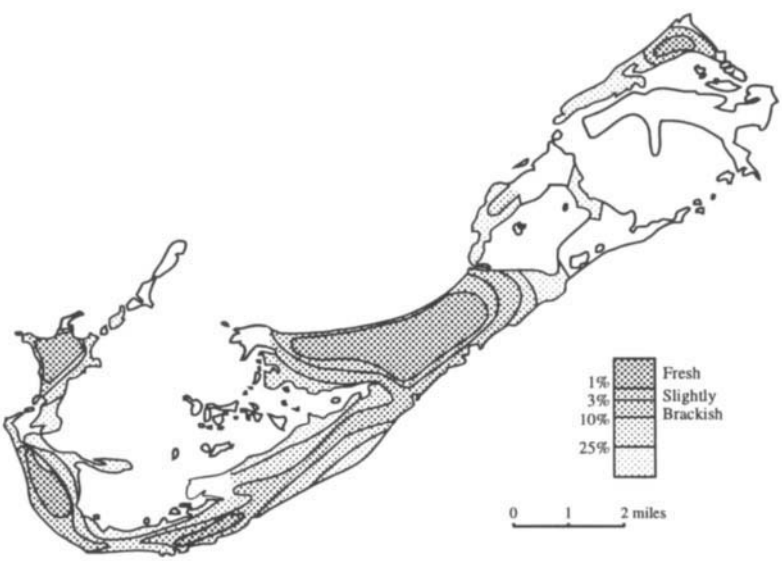


Fig. 2-14. Location of freshwater lenses in Bermuda. Map shows contours of percent seawater in household wells, 1972–1974. (From Vacher, 1974.)

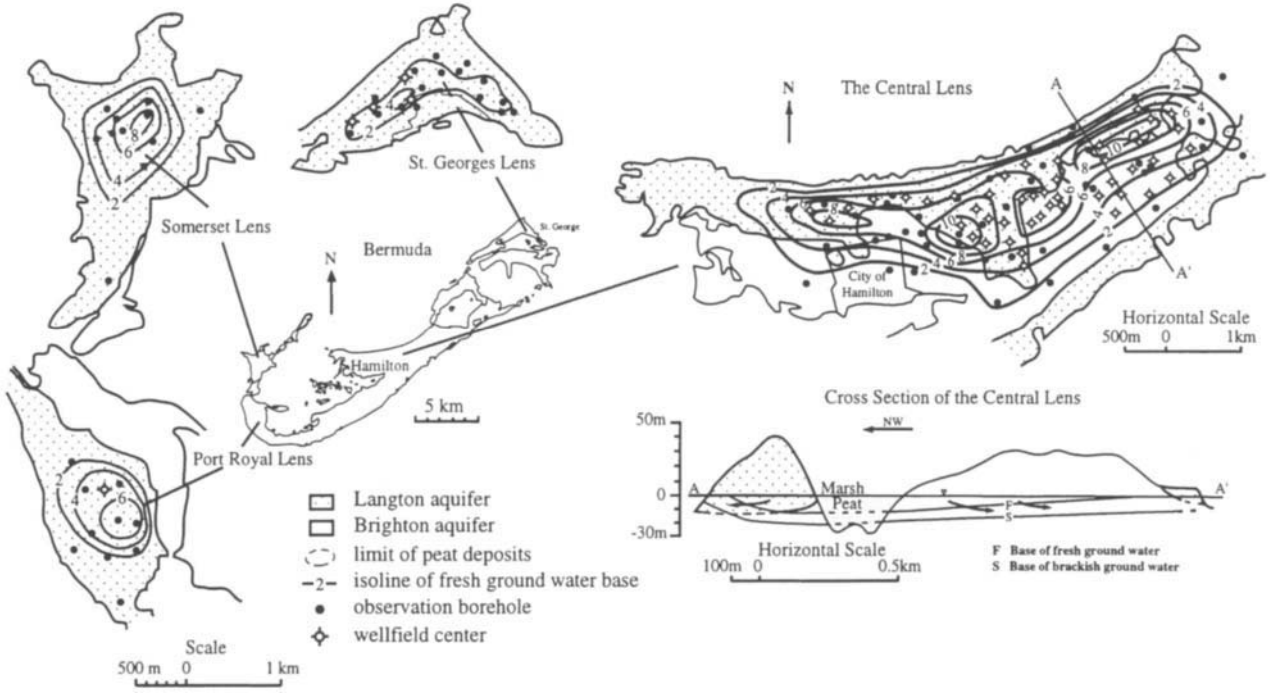


Fig. 2-15. Freshwater lenses of Bermuda. Map shows thickness of the freshwater lenses, distribution of Langton and Brighton Aquifers, and location of observation boreholes and extraction centres. (From Rowe, 1991)

buildup of Bermuda, there is a stratigraphic partitioning of the upper saturated zone. According to current nomenclature (Rowe, 1991; Vacher et al., 1995), the partitioning involves two hydrostratigraphic units (Fig. 2-15): the Langton Aquifer and the Brighton Aquifer. The Langton Aquifer consists of the Southampton, Rocky Bay and Belmont Formations of the lithostratigraphic classification and, therefore, is the younger body of rock. The Brighton Aquifer consists of the Town Hill Formation.

The hydraulic conductivity of the Langton Aquifer is some 30–120 m day^{-1}. The hydraulic conductivity of the Brighton Aquifer is on the order of 1,000 m day^{-1}, a number that clearly reflects increased secondary porosity. In addition to these two aquifers, there is a hydrostratigraphic unit corresponding to the Walsingham Formation. This unit does not usually figure in discussions of Bermuda hydrogeology because it is highly cavernous and, therefore, occupied by salty groundwater.

The freshwater lenses are localized in the Langton Aquifer (Fig. 2-15). Groundwater in the Brighton Aquifer is generally brackish at the water table. Where fresh groundwater does occur in the Brighton Aquifer, it is usually an extension of a lens centered in the Langton Aquifer (Fig. 2-15).

There is an extensive literature on the hydrogeology of Bermuda (e.g., Vacher et al., 1974, 1978a,b; Plummer et al., 1976; Rowe, 1984; Thomson 1989; Morse and Mackenzie, 1990) that uses an earlier hydrostratigraphic nomenclature that may lead to confusion if used in conjunction with the more recent geologic map and lithostratigraphic column (Vacher et al., 1989, 1995). Earlier, the stratigraphic control was described in terms of two units: the Paget Formation and the Belmont Formation. The Paget Formation of those papers corresponds to the Langton Aquifer of the current nomenclature, and the Belmont Formation of those papers parallels the Brighton Aquifer now. Confusing the synonymy is the fact that "Belmont" during the early stages of the geologic mapping (1970s) was used for the vast body of rocks between the Walsingham Formation and what is now known as the Rocky Bay Formation. Now, the Belmont is restricted to the definition of Land et al. (1967), and nearly all of the volume of rock between Walsingham and Rocky Bay is identified as Town Hill Formation. It is this volume that, in the saturated zone, constitutes the Brighton Aquifer.

The freshwater lenses

The groundwater monitoring program carried out by the Hydrogeology Section of the Department of Works and Engineering now includes a network of more than a hundred drilled boreholes (Rowe, 1991). In most cases, the boreholes penetrate into the seawater beneath the freshwater lenses and underlying transition zone. Salinity profiles in all monitoring boreholes are measured quarterly with a conductivity probe. The thickness of the four main freshwater lenses (1993) is shown in Fig. 2-15. The Central Lens covers an area of approximately 7.2 km^2 and reaches maximum thicknesses exceeding 10 m. The Port Royal, Somerset, and St. Georges Lenses are all in the range of 0.5–0.7 km^2 in area. The thin lenses in Warwick and Southampton Parishes are not routinely monitored.

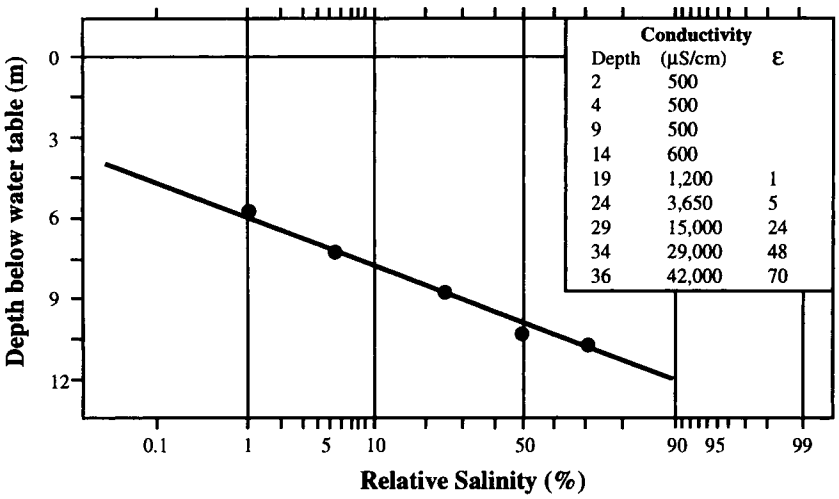


Fig. 2-16. Plot of percent seawater against depth in freshwater-saltwater transition zone. Relative salinity, which is plotted on probability scale, is calculated as the difference in salinity between the sample and unmixed fresh groundwater divided by the difference in salinity between the seawater endmember and the unmixed fresh groundwater. (From Vacher, 1974.)

The salinity profiles give information on the structure of the transition zone and the quantity of recharge-derived water in the lens. The salinity data generally produce straight lines when relative salinity is plotted on a probability scale vs. depth on an arithmetic scale (e.g., Fig. 2-16). These probability-paper plots indicate a simple error-function variation of relative salinity vs. depth, which is consistent with one-dimensional dispersion models. The error-function variation also means that the depth of particular percentiles of relative salinity can be read easily from the graphs. One of these, where the relative salinity is 50%, is taken as the position of the "interface", that is, where the base of the freshwater lens would be if there were no mixing. The thickness between the water table and this 50% datum provides a measure of the "meteoric water inventory" [see Chaps. 1, 22]; the (smaller) thickness of freshwater from a water-resources standpoint, of course, is given by the break in slope at the top of the transition zone.

Across the island (Fig. 2-17), the depth of the interface (50% relative salinity), the thickness of the transition zone (1% to 99%), and the thickness of the freshwater lens (depth to 1% relative salinity) all vary with the hydrostratigraphy and illustrate the geologic control on the distribution of fresh and brackish groundwater (Fig. 2-15). Clearly, compared to the Brighton Aquifer, the lower-permeability Langton Aquifer impedes the escape of recharge-derived fresh groundwater. Also, tides and other sea-level variations are less effective in mixing the freshwater and saltwater in the Langton Aquifer than in the Brighton Aquifer. The transition zone decreases in thickness inland in both units but more rapidly per unit distance in the Langton Aquifer than in the Brighton Aquifer.

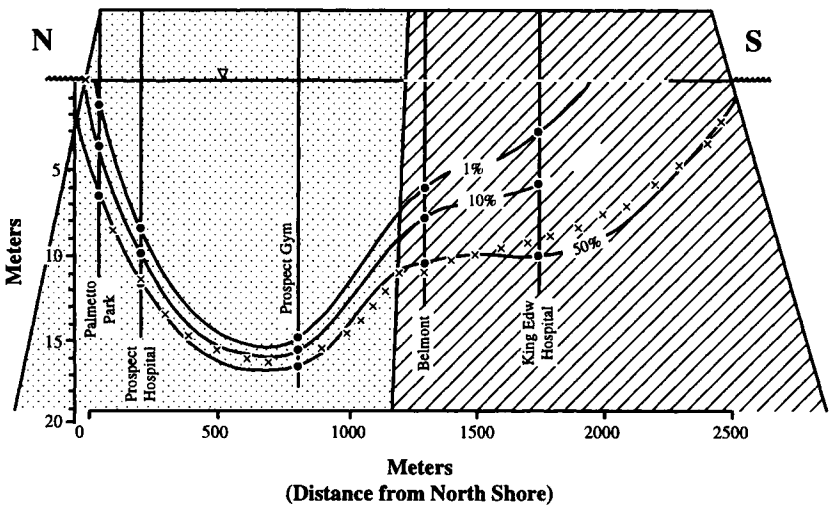


Fig. 2-17. Cross section of Central Lens according to Vacher (1974) showing across-island variation in thickness of fresh groundwater, thickness of transition zone, and depth to the "interface" (50% relative salinity). Evident correlation with the stratigraphy (Langton Aquifer on the left, Brighton Aquifer on the right). (From Vacher, 1974; also discussed in Plummer et al., 1976, and Vacher, 1978b.)

Vacher (1974, 1978b) has shown that simple analytical steady-state models can be used to explain the across-island variation in the depth of the "interface" (50% relative salinity). These models — Dupuit-Ghyben-Herzberg (DGH) models [see Chap. 1] — assume a sharp interface, a Ghyben-Herzberg relation between the elevation of the water table and the depth to the interface, the Dupuit assumptions of vertical equipotentials, and negligible outflow face (Vacher, 1988; Vacher et al., 1990). For example, the x's in Fig. 2-17 are for a DGH model assuming a strip island consisting of two sectors meeting at a vertical contact. In one sector (corresponding to the Langton Aquifer), the hydraulic conductivity is 80 m day^{-1}; in the other sector (Brighton Aquifer), the hydraulic conductivity is 1,000 m day^{-1}. In both, the assumed recharge is 0.35 m y^{-1}.

A long time series of water-table data is available at several monitoring boreholes in the Central Lens. To remove the effect of semidiurnal tides on a given measurement day, the water level is measured twice, six hours apart, and averaged. All monitoring boreholes in a particular lens are measured in one, or at most two, days. Over the years, with increasing sites in the monitoring network and changing priorities toward the direction of identifying long-term trends in lens thicknesses, the frequency of measurements has been reduced to once monthly. Levels are reduced to sea level as measured by the Hydrogeology Section at a tide recorder station on the north shore. The average height of the water table above sea level over an 8-year period (1975–1982) in the Central Lens (Rowe, 1984, Fig. 4) was about 1/40 the depth below sea level of the surface of 50% relative salinity for the same period

(Rowe, 1984). Thus, for long-term averages, the Central Lens can achieve Ghyben-Herzberg equilibrium (Rowe, 1984).

Recharge

Recharge has been evaluated in a variety of ways and, over the years, has been repeatedly revised upwards. In the early study, Vacher (1974; Plummer et al., 1976) used a water-budget accounting method to estimate recharge and actual evapotranspiration from monthly averages of rainfall and potential evapotranspiration and ignored the unnatural contributions; the result was about 18 cm y^{-1} (12% of the annual rainfall of 150-cm y^{-1}). Rowe (1981) applied a conceptually similar scheme but coupled it to a land zonation based on percentage coverage by housing, roads and marshlands; by including such processes as road runoff and recharge through cesspits, the recharge result increased to about 30 cm y^{-1}. Vacher and Ayers (1980) obtained values of 35–45 cm y^{-1} from three independent methods: evaluation of outflows and change in storage (hence inflows, by difference) in an area of diversion around a major development area; fitting of the lens geometry by DGH equations with independently inferred values of K; and the ratio of the Cl^- concentration in rainfall to that in the freshest part of the lenses. In his summary paper on the Central Lens, Rowe (1984) indicated that the earlier values from the water-budget accounting for natural surfaces were too low, because they were derived from monthly rather than daily values. Rowe (1984) suggested that the actual value for recharge, including the unnatural contributions, may range up to 55–65 cm y^{-1} in some places.

The most recent estimate of recharge is in connection with a steady-state model of the Central Lens (Thomson, 1989) developed as part of a U.N. study. In that model, the recharge is a distributed parameter which varies according to percentage of rooftop coverage. In Bermuda, most households capture water from their roofs and then dispose of it in soakaways. Thomson (1989) calculated cell-by-cell recharge as a weighted average of 90% of the rainfall that falls on impervious surfaces (roofs and roads) and the somewhat high figure of 25% of the annual rainfall that falls on natural surfaces. With these assumptions, combined with the percentage coverage by paved surfaces (5–40%), Thompson obtained recharge rates of 40–75 cm y^{-1} (Thomson, 1989). The same assumptions, of course, imply that in areas where the percentage coverage by pavement exceeds 22%, more than half of the recharge is obtained by recycling from these paved surfaces (with the total recharge being about 39% of the rainfall). This includes a significant fraction of the area of the Central Lens (Thomson, 1989).

Transient Behavior

Effects of sea level. With the exception of dug wells in some of the marshes, all the dug wells and boreholes in Bermuda are tidal, and most are strongly tidal. For a given distance inland of the shoreline, the tidal fluctuation is markedly larger in the Brighton Aquifer than in the Langton aquifer (Fig. 2-18), indicating greater dam-

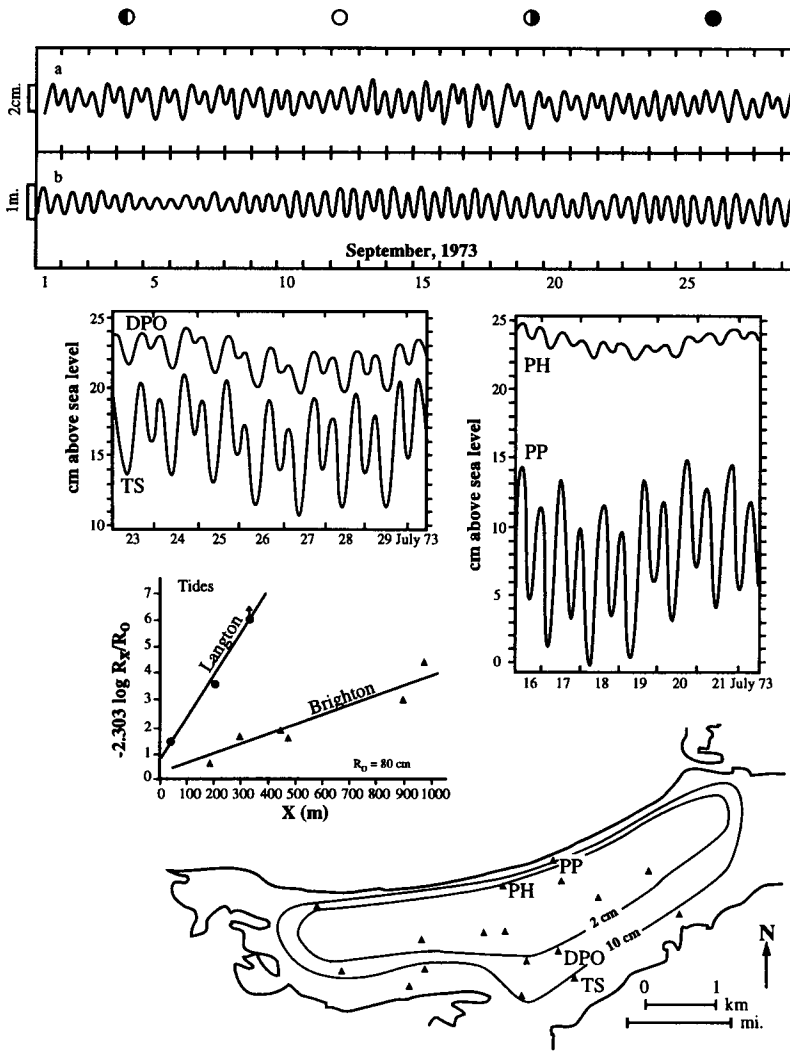


Fig. 2-18. Tidal fluctuations in the Central Lens. DPO and TS are observation boreholes in the Brighton Aquifer, and PH and PP are in the Langton Aquifer. The upper pair of curves compares the record at DPO to the tide gauge at BBSR. The various graphs show a greater dampening of the semidiurnal component relative to the diurnal component, and a greater dampening in the Langton Aquifer than in the Brighton Aquifer. (From Vacher, 1974.)

pening in the latter unit. The water-table fluctuation is not a simple scaled-down version of ocean tide (Fig. 2-18): the semidiurnal inequality is significantly enhanced in the water-table fluctuation, indicating that the diurnal component passes through more easily than the semidiurnal component.

The simplest model treating the dampening of tides is that of Ferris (1951), which treats a single confined layer and a horizontally propagated signal. According to that model, the tidal amplitude decreases exponentially inland such that a semilog plot of

tidal efficiency (well-to-ocean amplitude ratio) vs. distance would produce a straight line with slope proportional to the ratio of storativity to transmissivity and inversely proportional to the tidal period. Using such plots (Fig. 2-18), Vacher (1974, 1978b) found that the implied contrast in hydraulic conductivity between the Brighton and Langton sectors to be a factor of about 14. For comparison, the fit of the DGH lens of Fig. 2-17 assumes a Brighton-to-Langton hydraulic-conductivity ratio of 18. It should be noted that the straight-line plots of Fig. 2-18 do not go through the origin, and more data from more recent boreholes (Rowe unpub. data) suggest that the "lines" are curves that slightly decrease in slope inland.

If the diurnal component of the tide is dampened significantly less than the semidiurnal component, it should be no surprise that low-frequency behavior of sea level would have a large effect on the position of the water table in Bermuda. Thus, day-to-day variations in the water table reflect the barometric fluctuation of sea level (Vacher, 1978a; Rowe, 1984). As shown in Fig. 2-19, the day-to-day variations in the water table behave like tides in that they diminish inland exponentially, and at a greater rate in the Langton Aquifer than in the Brighton Aquifer. In addition, the year run of monthly or semimonthly averages tracks the seasonal, steric variation in sea level (Rowe, 1984).

Effects of recharge variations. Hydrographs in the marshes show a nontidal water-level variation related to changes in freshwater storage (Vacher, 1974). The marsh levels rise rapidly in response to rainfall, decay exponentially after the rainfall, and fluctuate with a diurnal periodicity in response to evapotranspiration-driven with-

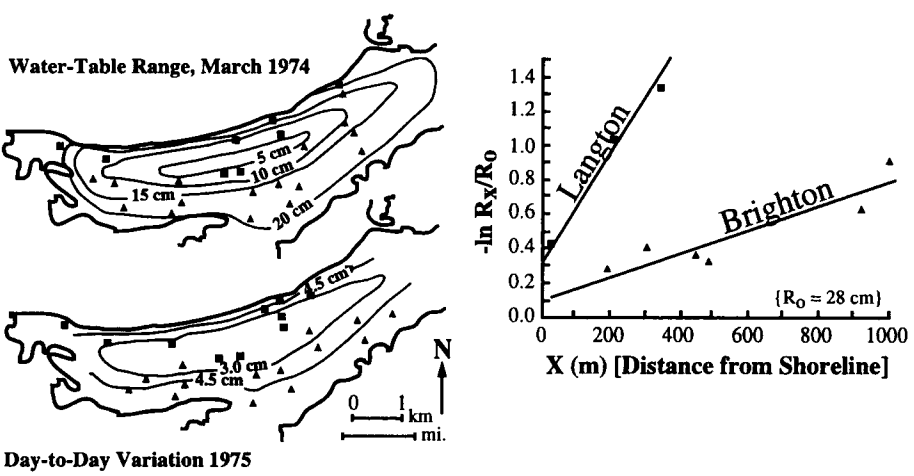


Fig. 2-19. Water-table fluctuations related to changes in atmospheric pressure, Central Lens. The water-table range for 1974 was from a single rise of the water table over a 10-day period when pressure dropped 28 cm. The "day-to-day variation for 1975" is the average of 12 monthly standard deviations of water-table elevation determined on 5–9 measurement days per month. The figures show that these statistics decrease inland from the shoreline in the same manner that the tidal amplitude does. (From Vacher, 1978a.)

drawals. In contrast, recharge events due to rainfall are not at all evident in hydrographs from boreholes in the limestone. As already noted, the dominant water-table fluctuations correlate with changes in sea level, not with volumetric changes in the lens. Attempts to subtract out the sea-level variation in order to look at volume-related residuals have been frustrated by the uniqueness of the sea-level influence at each borehole (Rowe, 1984).

Comparison of yearly averages do reveal variations due to recharge (Rowe, 1984). Maps of the annual average water table in the Central Lens are now available for some 20 years. During wet years, the reduced water levels can be 50% higher than those of dry years. The interface (50% relative salinity), however, is not in Ghyben-Herzberg equilibrium with this interannual variation. In a single borehole, the ratio of water-table elevation to depth of interface can vary from 1:25 in wet years to 1:58 in dry years. Thus the interface lags in its response to these water-table changes (Rowe, 1984). These results argue against the use of DGH models to simulate transient variation of the meteoric water inventory stored in the lens.

Groundwater chemistry

Plummer et al. (1967) examined the major-ion chemistry of the meteoric lenses and mapped the saturation state of aragonite and calcite in a study addressing rock-water interactions in phreatic diagenesis. Simmons et al. (1985) and Simmons and Lyons (1994) investigated the distribution of nitrogen and phosphorus in groundwaters of the Central Lens in a study addressing nutrient cycling. This cycling includes large inputs from the many cesspits and subsequent outflow to the nearshore marine waters. The outflow may sustain higher than normal algal growth in some areas, particularly the inshore water bodies (Morris et al., 1977; Lapointe and O'Connell, 1989; Simmons and Lyons, 1994).

WATER RESOURCES AND WATER SUPPLY

For the private household in Bermuda, the principal water supply is rainwater. Planning Department regulations require that each household have its own rainwater roof catchment (Fig. 2-3A) and subsurface tank. When the rainfall is average and is evenly distributed throughout the year, this supply is adequate.

The household rainwater catch is augmented by about 3,000 household wells. Drinking of water from these wells requires approval of the Health Department and is generally discouraged. The well water is used largely for flushing toilets.

According to Hayward et al. (1981), the usage of freshwater has increased from about 30 L day^{-1} $person^{-1}$ since the mid-1940s to about 100 L day^{-1} $person^{-1}$, and typical figures for tourists can run up to 450 L day^{-1} $person^{-1}$.

The main groundwater extractors are the Government and a private water company which, together, operate a limited mains distribution network. The primary purpose of this distribution system is to deliver treated groundwater to offices and hotels. More recently, the Government has allowed the construction of cluster

developments, which are properties with roof areas that are too small to catch sufficient rain to meet the demand of the residents; these cluster developments are supplied by the mains distribution system. Hotels that are outside the reach of the mains system or need supplemental supply use seawater desalination systems. Households that need to supplement their catch typically buy water from truckers, who, in turn, are supplied from licensed wells, typically Government's.

Total groundwater abstraction by major commercial and Government operations in Bermuda amounts to an average of 5,900 m^3 day^{-1}, some 90% of which is from the Central Lens. This development is managed by the Department of Works and Engineering and overseen by a statutory body of citizens, the Water Authority. The development plan makes use of a safe-yield concept (Rowe, 1984, 1991), where the lens is allowed to be thinned to about 1/2 of its pre-development thickness while maintaining certain standards with respect to salinity. These are that traditionally fresh areas of the Langton Aquifer must remain fresh (less than 700 mg L^{-1} TDS) and that parts of the Brighton Aquifer and coastal locations in the Langton Aquifer used as source water for RO and electrodialysis plants must remain only slightly brackish (less than 1,200 mg L^{-1} TDS). The provision that the lens can be thinned to half of its predevelopment thickness means that total extractions are 3/4 of the recharge (Rowe, 1984), because the development philosophy is to spread extractions and use a large number of small-yield wells; thus extractions are designed to resemble negative recharge. As yet, there has been no case where a groundwater resource in Bermuda has had to be abandoned because of saline intrusion or upconing. One or two areas that were overpumped did experience upconing prior to imposition of localized controls which, concurrently, protected groundwater quality and forced the spread of abstractions. Currently, the Central Lens is developed to about 80% of its estimated safe yield (Rowe, 1991).

CASE STUDY: HERMENEUTICS AND THE PLEISTOCENE SEA-LEVEL HISTORY OF BERMUDA

In a recent analysis of geologic reasoning, Frodeman (1995) introduced the term *hermeneutics* to the geologic community. He argued, "Geologic understanding is best understood as a hermeneutic process" (Frodeman, 1995, p. 963). He explained: "The term *hermeneutics* means theory of interpretation; hermeneutics is the art or science of interpreting texts.... Hermeneutics has claimed that the deciphering of meaning always involves the subtle interplay of what is 'objectively' there in the text with what the reader brings to the text in terms of presuppositions and expectations. In effect, hermeneutics rejects the claim that facts can ever be completely independent of theory" (Frodeman, 1995, p. 962).

It has been said that Bermuda offers a "tide gauge" for reading Pleistocene sea levels. The record of that tide gauge has been read and reread, and those readings have been drawn up in a number of sea-level curves. Reading a "Pleistocene tide gauge," however, is not like reading an oceanographic tide gauge. The Pleistocene curves depict subjective interpretations of rock exposures and necessarily reflect —

to varying degrees — presuppositions and expectations of the geologists who have completed the studies. According to Frodeman (1995, p. 963), "Examining an outcrop is not simply a matter of 'taking a good look.'" If so, then what can we know for sure about Bermuda's Pleistocene sea-level history?

The purpose of this Case Study is to examine that question. First, we will discuss how Frodeman's perspective on geological reasoning applies to studies of Bermuda's Pleistocene sea-level history. Second, we will break down the understanding of Bermuda's sea-level history into six constituent issues and list them according to certainty of their central conclusions. And finally, we will argue that Bermuda's Pleistocene sea-level history needs to be examined without applying foreknowledge of how high sea level must have been from coeval deposits at other places, and other extra-Bermuda considerations.

Part 1: Hermeneutics

Hermeneutics and Bermuda forestructures: preconceptions

In the language of hermeneutics, prejudgments that we bring to our work are *forestructures*. Foremost among them are "our preconceptions, the ideas and theories that we rely on when thinking about an object" (Frodeman, 1995, p. 964). Three such preconceptions or background notions have played a significant — perhaps determinative — role in studies of Bermuda's Pleistocene record: glacioeustatic control, Milankovitch cycles, and Antarctic surges.

Glacioeustatic control. The premier forestructure for approaching Bermuda's rocks today is the concept that the eolianites formed during interglacials and that terra rossas mark glacial stages. As noted in the main text of this chapter, the current notion (Bretz, 1960; Land et al., 1967; Vacher et al., 1995) is the reverse of the original glacioeustatic control scheme of Sayles (1931), where the dunes were thought to have formed during glacial lowstands. The relevant point now is that Sayles (1931) was led to this concept by two, more-antecedent ideas:

1. The presupposition that the platform needed to be exposed to generate the eolianites. This idea was consistent with the interpretation argued in the substantial and authoritative reports on Bermuda by Agassiz (1895) and Verrill (1907) that the Bermuda dunes were partially submerged due to subsidence of a larger Bermuda; Verrill (1907) called it "Greater Bermuda."
2. Daly's idea of glacial control for coral reefs.

It should be noted that neither of these antecedent notions has survived — and neither has Sayles' particular notion of glacioeustatic control of eolianites in Bermuda. The important point, however, is that the conjunction of the two prior ideas led Sayles to notice and appreciate the presence of terra rossa paleosols at different stratigraphic horizons. This observation has formed the basis of all subsequent work on Quaternary stratigraphy and sea-level history in Bermuda.

The history and logic of Sayles' thinking is clearly stated near the beginning of his paper:

> "A subsidence of sixty feet would change the area from about two hundred square miles to the present size of about twenty square miles. As I was very familiar with the glacial control theory of coral reefs advanced by Daly, it was most logical to explain a (rising) water-level by deglaciation of the Pleistocene ice caps. It was at this point in the reasoning that it occurred to me that the buried soil I had seen and puzzled over might mean an interglacial episode of the Pleistocene.... On the other hand, while the northern continents were buried under ice, ... Bermuda should be larger ... and a larger Bermuda would explain the great dune formations....
>
> If the fossil soil found really meant an interglacial interval, there should be more than one...."

Milankovitch cycles. The correspondence between Milankovitch cycles, deep-sea isotope stages and Pleistocene sea-level history became well known in the late 1960s and early 1970s (e.g., Broecker et al., 1968; Bloom et al., 1974). The curve of Land et al. (1967) is the one and only sea-level curve from Bermuda that preceded and was not influenced by the Milankovitch-Barbados-New Guinea forestructure.

A signal feature of the Land et al. (1967) curve was its two distinct highstands (Devonshire and Spencer's Point Formations of Land et al., 1967) in the interval between the Belmont and Southampton Formations. These highstands were associated with early U-series coral ages of ~125–135 ka. The overlying Southampton Formation (thought to be exclusively an eolian unit) was attributed to a sea-level rise (above the platform edge but not as high as present sea level). The age of the Southampton (~35 ka) was from radiocarbon and was known to represent a minimum age.

When Vacher (1973) mapped rocks of this interval (now classified as Rocky Bay and Southampton Formations), he found (1) no consistent red soil (i.e., no glacial stage) within the succession and (2) a small marine unit (at Fort St. Catherine) associated with the youngest eolianites. The deposits at Fort St. Catherine suggested a highstand at about present sea level very late in the history. With no new dates, Vacher (1973) used the Milankovitch-Barbados forestructure to reason that the post-Belmont succession represents the entire stage-5 interglacial interval, that the Southampton represents the later substages, and that the marine deposit at Fort St. Catherine formed late in substage 5a.

The geochronological studies of Harmon et al. (1978, 1981, 1983), which established the time frame for Bermuda's late Pleistocene history, were directed at Bermuda's sea-level curve as a nontectonic-island reference. The curve followed from U-series dates on corals and submerged speleothems, elevations of the marine deposits, depths of the speleothems, a re-examination of old outcrops, and geological reasoning to correlate where geochronological evidence could not. In the process, the double peak of the Land et al. (1967) curve was abandoned; relatively high elevation deposits at Blackwatch Pass (BWP) were reinterpreted to be eolian rather than marine (see below); and all evidence (including some U-series dates on corals) suggesting highstands above present sea level during late stage 5 was attributed to storms that emplaced the deposits far above "proper" sea level. For more detailed discussion, see Vacher and Hearty (1989). The point here is that, in full force, the Milankovitch forestructure gave rise to expectations not only to the timing, but also to the elevation, of Pleistocene sea-level events.

Antarctic surges. The Antarctic surge hypothesis (Wilson, 1964; Hollin, 1965) asserts that a large portion of the Antarctic ice sheet becomes unstable late in an interglacial and surges into the ocean, thus causing a rapid rise in global sea level. According to proponents of this hypothesis, the rapid rise of sea level can be as large as 10 m.

Vacher (1973), following Land et al. (1967), was one who had thought the "relatively high elevation deposits" at BWP were marine. Land et al. (1967) had correlated these deposits (~17 m) with some high conglomerates (~10 m) at Spencer's Point; both these deposits, which led to the second peak of the double peak of Land et al. (1967), are significantly higher than those of the first peak (Devonshire deposits, typically at ≤6 m). Vacher (1973), however, made a case for one highstand: he interpreted the "marine-eolian" relations at and near BWP (Fig. 2-20) to be transgressive and thought, overall, that the field relations could be explained if the BWP deposits were deposited soon after the typical Devonshire deposits in a quick rise (from "Devonshire level") that allowed sediment to be swept from the North Lagoon to the north shore. Vacher (1973) noted that this interpretation would be consistent with the Antarctic surge hypothesis. To the point of this discussion, Vacher had met Hollin at the 1968 INQUA meeting and had been impressed with his story of surges, and so was not averse to "seeing" geological features that could be explained by rapid sea-level rises during interglacials.



Fig. 2-20. Low-angle cross-beds along the north shore, 2.8 km east along shore from Blackwatch Pass. Are these beach or eolian deposits? If the exposure shows an upward transition between the two, where is paleosea level? The base of the meter stick is ~6 m above present sea level.

Hollin (1980) later included BWP in his paper using evidence from localities around the world to argue for Antarctic surges and consequent rapid rises in sea level. From the first available dates from the south shore conglomerates (Harmon et al., 1978), Hollin (1980) argued that the BWP deposits fit well with a surge at about 95 ka, but his idea was vigorously opposed by Harmon et al. (1981, 1983) on the basis of their speleothem data. Of perhaps more lasting consequence, Hollin's interest in BWP led to Hearty's involvement in Bermuda's stratigraphy and geochronology (e.g., Hearty and Hollin, 1986).

The curve by Hearty and Kindler (1995) is the most recent sea-level curve for Bermuda (actually a composite for Bermuda and the Bahamas). The curve includes a double peak within substage 5e, and a rapid rise to about 10 m at the end of the second peak [see also Fig. 3B.8]. As Bermuda evidence, Hearty and Kindler (1995) cite the 10-m "high conglomerate" at Spencer's Point. Ironically, the deposits at BWP do not figure into the rapid rise interpreted by Hearty and Kindler (1995), who state that the low-angle cross-beds are marine to an elevation of only a few meters above present sea level. Thus use of the Antarctic-surge forestructure in Bermuda may have outlived the field interpretation that first brought it to Bermuda.

Hermeneutics and Bermuda forestructures: goals

The second type of forestructure is "our idea of the presumed goal of our inquiry and our sense of what will count as an answer" (Frodeman, 1995, p. 964). Since Sayles (1931) introduced the concept of glacioeustatic control, there has been a tradition that the goal of stratigraphic inquiry in Bermuda would be an understanding of the controlling variable, sea level (Land et al., 1967; Vacher, 1973; Harmon et al., 1978, 1981, 1983; Hearty and Kindler, 1985). What "would count as an answer" would be the sea-level curve. Obviously relevant to such studies are the many coastal sections where both marine and eolian units are exposed and superposition is clear.

Our stratigraphic studies were directed at a different goal: the production of a geologic map (Vacher et al., 1989; Rowe, 1990). For us, the important question was, "How do these puzzle pieces of eolianites, marine units, and paleosols fit together geometrically?" and the answer would be the map. The inquiry started as part of Vacher's dissertation (Vacher, 1971) with Fred Mackenzie, one of the authors of Land et al. (1967). The question later proved crucially relevant to the Bermuda Government's groundwater program, which began in the early 1970s; Rowe became its first permanent hydrogeologist soon after. Our mapping focused on the alternation of eolianites and soils as seen in the inland roadcuts, quarries, and household exposures. By heading inland from the coastline, we encountered the older part of the section that, as it turned out, was only incompletely or ambiguously represented in coastal exposures (Hearty et al., 1992; Vacher et al., 1995).

Hermeneutics and Bermuda forestructures: tools

The third type of forestructure comprises "the implements, skills, and institutions that one brings to the object of study.... The nature of these tools shape the type of

information collected." Clearly, the outstanding example of this type of forestructure is U-series dating of corals, which provided a breakthrough in Bermuda (Harmon et al., 1978, 1981, 1983) by providing a time scale. It also drew attention to the previously neglected speleothems. But corals are rare in Bermuda, and U-series geochronology cannot reach into the lower part of the stratigraphic record that is exposed over much of Bermuda.

The use of AAR data for initially intra-Bermuda correlation and later for age estimation produced a relative, and then numerical, time scale between and beyond the time markers provided by U-series dates. The AAR work also drew attention to protosols for they contain *Poecilozonites*, the first object to which AAR geochronology was applied. These white paleosols had been recognized in the stratigraphic nomenclature of Sayles (1931), but Land et al. (1967) drew a distinction between them and the terra rossa paleosols — as a distinction between stratigraphically insignificant and stratigraphically significant disconformities. Land et al. (1967) retained only one of Sayles' (1931) white paleosols as a named stratigraphic unit — the Harrington Soil between the underlying Devonshire marine unit and the overlying Pembroke eolianite.

In the first application of AAR geochronology in Bermuda, Mitterer and Kriausakul (in Harmon et al., 1983) found that *Poecilozonites* from the Harrington Formation at classic localities (e.g., at Rocky Bay of the "south shore section" of the central parishes) gave a larger ratio (greater relative age) than *Poecilozonites* from demonstrably younger deposits (Southampton). They also found that *Poecilozonites* from some other protosols gave distinctly larger ratios. Then, Hollin and Hearty (1986) found that ratios from marine shells in what is now recognized as the upper part of the column cluster into three groups and proposed three aminostages for the marine units. The uppermost aminozone represented the marine deposit at Fort St. Catherine, and the other two were the well-known Devonshire and Belmont units. The two studies, together, showed that (using present terminology) the Southampton, Rocky Bay, and older units could be distinguished on the basis of A/I ratios in both the marine facies and in protosols.

Hearty and Mitterer joined forces (Hearty et al., 1992) and coordinated their geochronological work to the geologic map of Vacher et al. (1989). Results of this collaboration showed that, although the protosols may be "stratigraphically insignificant," they are stratigraphically valuable. Two results stand out:

1. There are numerous temporally disjunct protosols below the Belmont of the "south shore section" (Hearty et al., 1992; Hearty and Vacher, 1994), as had been indicated independently by field relations (Vacher et al., 1989). A relatively long section is exposed in Bermuda.

2. There are two "Harrington" soils in the "south shore section" (Vacher and Hearty, 1989; Hearty et al., 1992) — one within the Belmont and one within the Rocky Bay. This result was anticipated by Gould (1969; and pers. comm., in Vacher, 1973) on the basis of the shell morphology of *Poecilozonites*. The result indicates that the original argument for the double peak (Land et al., 1967) is not compelling (Vacher and Hearty, 1989). Another implication is that the three-part succession of

marine unit, protosol, and eolianite (Fig. 2-10) is a recurring facies motif, not a fingerprint of a particular interglacial.

The hermeneutic circle and Blackwatch Pass

According to Frodeman (1995), the hermeneutic circle is the founding concept of hermeneutics. He explained the concept as follows (Frodeman, 1995, p. 963):

> "When we strive to comprehend something, the meaning of its parts is understood from its relationship to the whole, while our conception of the whole is constructed from an understanding of its parts.... Thus our understanding of a region is based on our interpretation of the individual outcrops in that region, and vice versa."

The concept is well illustrated by the evolving understanding of the exposure at BWP. Examining that exposure has not been simply a matter of "taking a good look."

BWP is a cut some 30 m deep through the eolianite ridge between Hamilton and the north shore (2-21A), and, as is illustrated in the foregoing discussion, the locality has figured prominently in interpretations of Bermuda's late Pleistocene sea-level history. The spectacular cut, which was hand dug as part of a marsh reclamation project that provided public assistance during the Depression, was opened by the Governor on 2 June, 1934, and now lies along one of the two main routes out of Hamilton to the east end of the Island. BWP exposes the anatomy of an eolian ridge (Fig. 2-3A) that grades into the problematic low-angle cross-beds at the shoreline a few tens of meters north of the cut (Fig. 2-21). These low-angle cross-beds extend along strike for several kilometers in the low (~10 m) cliffs of the north shore (Fig. 2-20).

Beach or eolian? Bretz (1960), who introduced the locality to the geological literature, thought that low-angle cross-beds that extend up to some 30 m (100 ft) in the cut are beach deposits. Land et al. (1967) considered Bretz's high-elevation wedge of low-angle cross-beds to be eolian, and identified a lower-elevation wedge at the northernmost part of the cut to be beach; this gave an elevation of some 17 m (60 ft) for their Spencer's Point highstand. Vacher (1973) accepted the elevation and thought the successive onlap of wedges and the large aggregate thickness meant the unit formed during a rising sea level. Harmon et al. (1981, 1983) concluded that all the deposits in the cut and above a few meters in the coastal cliffs are eolian — i.e., that nothing in these deposits contradicted their speleothem dates indicating a single highstand in stage 5 that reached no higher than a few meters above present sea level. Hearty and Kindler (1995) also took the position that beach deposits are limited to low elevations in the cliffs (but were deposited during a second substage-5e highstand).

We prefer to be noncommittal on the location of sea level in these deposits except to suggest that they warrant study by specialists in beach and paleobeach sedimentology who have no particular foreknowledge of Pleistocene sea-level history.

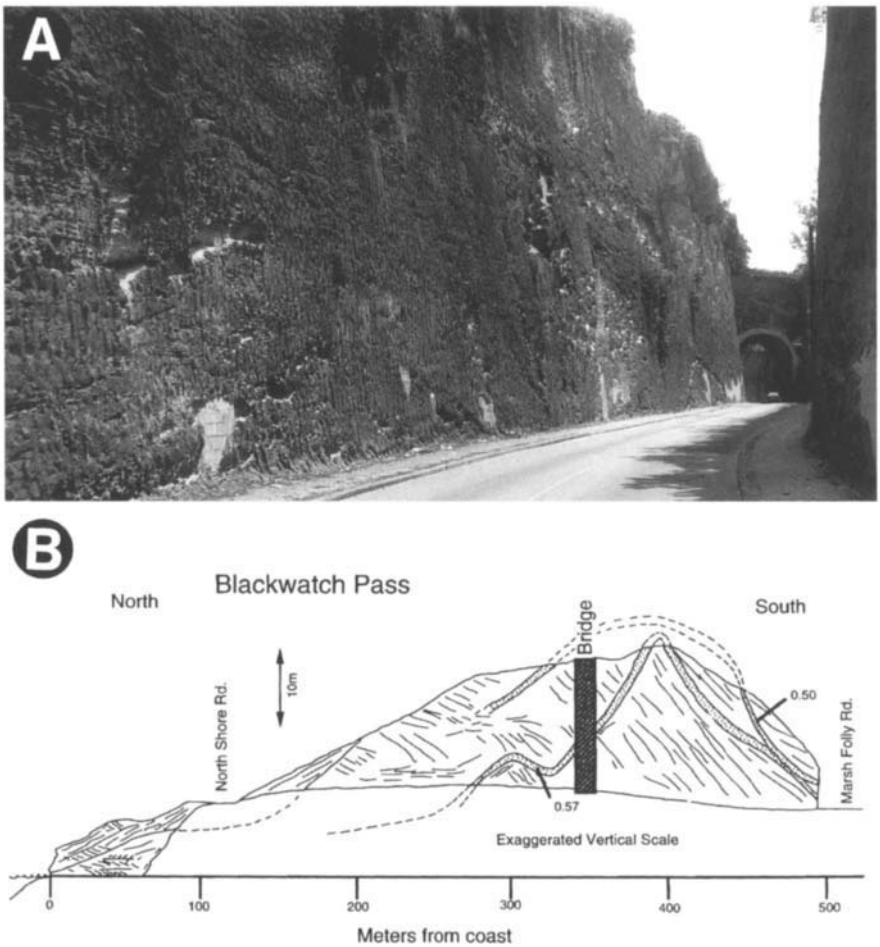


Fig. 2-21. Blackwatch Pass, Pembroke Parish. (A, upper panel) Looking southward, into the pass. (B, lower panel) Cross section as interpreted and drawn by Paul Hearty (in Vacher et al., 1995). Numbers on the two protosols refer to A/I ratios on *Poecilozonites*.

Protosols. The road cut exposes a prominent, *Poecilozonites*-rich protosol along the road level. The stratigraphy in BWP (Fig. 2-21B) is: (1) an older eolianite along the south end of the road, (2) a prominent snail-rich protosol, and (3) a large complex that defines the topography of the ridge and merges with the problematic low-angle cross-beds of the shoreline. As shown in Fig. 2-21B, there is a second protosol in the cut, within the upper eolian complex. This paleosol is high in the cut, difficult to see and, for many years, either unseen or dismissed as insignificant.

In contrast to the section at BWP, the typical succession for this part of the column in the classic localities of the "south shore section" consists of the Devonshire (marine unit), Harrington (protosol) and Pembroke (eolianite) units of Land

et al. (1967). It is impossible to correlate these two sections without more information. The additional information for Land et al. (1967) and Vacher (1973) was Bermuda's sea-level history inferred from all the localities they knew. The U-series coral dates of Harmon et al. (1978, 1981, 1983) did not address the correlation directly, because corals (and megafossils, in general) are absent from the low-angle beach(?) deposits.

The first tie between the two sections that did not depend on sea-level reasoning was from AAR data (Mitterer and Kriasaukal, in Harmon et al., 1983). A/I ratios on *Poecilozonites* from the prominent protosol in BWP fell between the "two Harringtons." When Mitterer and Hearty pooled their data, they realized that *Poecilozonites* from a protosol at Marsh Folly Road (around the corner at the south end of BWP) gave the same ratio as the "younger" Harrington of the south shore. Reexamination of BWP led to the new understanding that there are actually two important snail-bearing protosols in the BWP-Marsh Folly area (Hearty and Kindler, 1995; Vacher et al., 1995): the lower one is the prominent soil in the cut; the upper one is well exposed along Marsh Folly and occurs as an inconspicuous lens within the large eolian complex of the cut (Fig. 2-21B). In other words, lab ratios clarified field relations, which are geometrically complex and obscured by some maddening gaps in the exposure.

One hypothesis that would explain the correlations implied by the AAR data is that there were two sea-level highstands during substage 5e (before and after the lower of the two protosols in BWP). This is the position taken by Hearty and Kindler (1995).

Part 2: Pleistocene Sea Level in Bermuda

By the nature of the subject, the study of Bermuda's Pleistocene sea level appears to be a tangle of forestructures and observations. It seems appropriate, therefore, to take stock of the accumulating interpretations and parse what we think we know for sure from what is less certain.

Following are six issues that we believe constitute much of the published understanding of Bermuda's Pleistocene sea-level history. The list is arranged in order of decreasing certainty of the core conclusion. In terms of certainty, the six issues divide into three categories. For the first category (issues 1–3), a conclusion can be drawn that is not contradicted by other available evidence in Bermuda. For the second (issue 4), there are mutually exclusive alternative hypotheses that are each refuted by evidence in Bermuda that supports the alternative; i.e., there is an unresolved dilemma. In the third category (issues 5–6), available information, we believe, is insufficient to draw a conclusion.

1. The yo-yo of sea level

Meischner et al. (1995) have likened the ups and downs of Bermuda sea level to those of a yo-yo. By this they mean simply that sea level rose repeatedly to *about* the same level.

The stratigraphic column (Fig. 2-6, Table 2-1) consists of six named units, the bottom five of which are separated from each other by terra rossa paleosols. Each unit consists largely of eolianites, which, it has been concluded, represent the eolian, close-to-the-beach component of a marginal-marine complex of facies (Fig. 2-10). The occurrence of these eolianites on the present island indicates sea levels close to the present position. As the uppermost two (Rocky Bay and Southampton Formations) represent stage 5, it can be concluded that sea level came at least close to its present position during at least five separate odd-numbered stages of the deep-sea chronology.

More difficult are questions relating to how high sea level actually got, and the number of times it rose above its present position during any given odd-numbered stage (see below). But indisputably, the overwhelming preponderance of *unequivocal* marine deposits on the island is no more than a few meters above present sea level. The two exceptions we know are the conglomerate at Spencer's Point (10 m) and a now-removed conglomerate at and near Government Quarry (18–22 m, Land et al., 1967). The Spencer's Point conglomerate is an unusually high 5e deposit, and the Government Quarry conglomerate is very old (Hearty et al., 1992) on the Bermuda time scale. Thus the *main* message of Bermuda's exposed marine deposits is a sea-level position only slightly higher than present sea level.

In combination, the eolianites and unequivocal marine deposits indicate that the main pattern for the "yo-yo" of sea level is that it returned repeatedly to positions somewhere between "close to" but below present sea level, and "slightly higher" than present sea level. It is clear also that there is a more detailed story, possibly including minor signals, that is not covered by these statements.

2. The main 5e signal

There is no question that substage 5e of the deep-sea record is represented in Bermuda by the Rocky Bay Formation, and that this formation includes extensive marine deposits (Devonshire member) at ≤ 6 m elevation. Elevations vary in part because the position of the erosion surface on which these deposits are draped is affected by diagenetic features affecting the induration of the underlying Belmont (Land et al., 1967; Land, 1970). The highest measured Devonshire at Hungry Bay is 5 m (Land and Mackenzie, 1970); 5.6 m at Grape Bay (Meischner et al., 1995); and 6 m in an extensive set of deposits in the islands of Great Sound (Peter Garrett, unpub. data). Alpha-count, U-series dates on corals from typical Devonshire deposits are in the range of 118 ± 11 ka to 134 ± 8 ka (Harmon et al., 1983).

The preceding statement leaves out information that can be interpreted in a variety of ways. Specifically, it is uncertain how the 10-m-elevation conglomerate at Spencer's Point and the problematic low-angle beds near Blackwatch Pass fit in (e.g., one highstand or two).

3. One or more stage-7 highstands above present sea level

The Belmont beach deposits along the south shore clearly underlie deposits correlating with substage 5e. Progradation of these beach deposits and the presence of a

fossil water table in penecontemporaneous eolianite indicate that sea level was ~1–2 m above its present position when these south shore deposits were formed (Land et al., 1967; Land, 1970). Geochronological interpretation of A/I ratios from both marine mollusks and *Poecilozonites* from the Belmont Formation in the same outcrop belt indicates a stage-7 correlation. U-series dates on corals from isolated deposits outside the classic localities, but at the same elevation and stratigraphic position, give 200-ka results indicative of stage 7 (Harmon et al., 1983). Thus it is clear that the Bermuda record includes at least one stage-7 highstand a couple of meters above present sea level. Recently, Meischner et al. (1995) concluded that two distinct highstands are recorded in the Belmont beach deposits at Grape Bay and correlated them with individual substages of stage 7.

According to isotope-derived ice-volume curves (Imbrie et al., 1984; Shackleton, 1986), there was a smaller volume of ocean water during stage 7 than there is now, and so the occurrence of any stage-7 highstand in Bermuda may seem surprising.

4. Substage-5a highstand 0–1 m above present sea level

The interpretation (Vacher, 1973; Vacher and Hearty, 1989; Hearty et al., 1992; Ludwig et al., 1996) that sea level in Bermuda rose as high as 0–1 m during Substage 5a is controversial. We believe there is evidence that compels it; on the other hand, there is published evidence that contradicts it.

The case for the 5a event in Bermuda was argued by Vacher and Hearty (1989). The hypothesis explains deposits that are present (as opposed to predicting the absence of data). In order of discovery, the first deposit is at Fort St. Catherine and was discussed above in the section on hermeneutics; *Oculina* from this deposit were dated at ~80 ka by Harmon et al. (1981, 1983) using alpha-count methods, and more recently the same age was obtained by Ludwig et al. (1996) using TIMS. Although direct superposition is not demonstrable at Fort St. Catherine, the geometric arrangement of the eolianite bodies in the area suggests that the marine deposits are younger than the main mass of Southampton (Vacher, 1973), which contains *Poecilozonites* yielding A/I ratios distinctly less than those from 5e deposits (Hearty et al., 1992). The second deposit — found and mapped by Peter Garrett (in Vacher et al., 1989) — is more convincing in the field because superposition is clear. This deposit, which is on the opposite side of the island and at the same elevation as the Fort St. Catherine deposit, is a discontinuous shelly deposit that laps up against a paleocliff cut in a huge mass of eolianite that was previously mapped as Southampton (and the source of the name "Southampton" used by Sayles, 1931, and redefined by Land et al., 1967). These Southampton eolianites contain a succession of protosols with *Poecilozonites*, the A/I ratios of which, again, fall into the cluster with distinctly smaller values than those of *Poecilozonites* from 5e deposits.

The argument (in Bermuda) against the notion that sea level reached its present level during substage 5a rests on Harmon's U-series dates on two submerged stalagmites (Harmon et al., 1983, Table V). One, at −6 m, has: a date of 97 ± 9 ka at a height of 2 cm above the base; a second date of 68 ± 6 ka, 20 cm above the base; and

no internal discontinuity in the calcite deposition between the dated horizons. The other, at −15 m, has dates of 111 ± 9 ka, 39 ± 7 ka, and 10 ± 2 ka at 1 cm, 14 cm, and 23 cm respectively, and no internal discontinuity. The implication is that there was continuous vadose deposition of calcite from 111 ka to 10 ka at a depth of −15 m.

The resolution advanced by Harmon et al. (1981, 1983) for the conflict between corals and speleothems — storms that emplaced the corals some 15–25 m above the level constrained by the stalagmites — grew out of coral dates (mostly around 100 ka) from south shore conglomerates (i.e., near Spencer's Point), where the deposits are patchy and occur along an exposed, high-energy coastline. The storm notion, however, seems incapable for resolving the conflict for the 5a deposits. First, there is nothing in the deposits at either Fort St. Catherine (Vacher and Hearty, 1989; Ludwig et al., 1996) or in the Conyer's Bay area (Vacher and Hearty, 1989) that would suggest storm deposition so high above "ambient" sea level. Moreover, the coastlines are more protected, and the deposits occur at the same level at opposite ends of the island.

In conclusion, there appears to be an unresolved contradiction between the marine deposits that say sea level was at about its present position late in substage 5a, and speleothem dates that say it could not have been. The occurrence of any substage-5a marine deposits above sea level in Bermuda conflicts with normal expectations derived from isotope-derived ice-volume curves and projections from Barbados and New Guinea. Moreover, correlative marine deposits have not been found at other places with a reputation for tectonic stability, including the Bahamas (Carew and Mylroie, 1995b; Kindler and Hearty, 1996) [see Chaps. 3A, 3B].

5. *Highstand above present sea level during the time interval represented by each of the named lithostratigraphic units*

Interpretation of pre-stage-7 sea level in Bermuda is difficult. There are very few deposits which unequivocally show that sea level was above its present position. On the other hand, there are many exposures of low-angle, beach-like planar cross-bedding; mostly these occur at the water line along the inshore water bodies. These deposits present two types of problems. First, do they represent a beach or only an eolian flat presumably close to the beach? The question is the same for these deposits as for the younger, problematic, and much better exposed low-angle cross-beds near Blackwatch Pass. Second, how do these deposits relate to the succession of eolianites on which the stratigraphic column is mainly based? For Sayles (1931), who was aware of many of these exposures, the classification was not difficult. He fit them all into his Belmont Formation, a marine unit that was the only unit between the overlying marine Devonshire Formation (now known to correlate with 5e) and the underlying eolianites of the Walsingham Formation. That part of the stratigraphic column now is known to include a large succession of eolianites, and so there are many more options for classification of the marine deposits.

Vacher et al. (1989) had to answer these questions in order to include known marine deposits on their geologic map. According to that map, marine deposits

occur in each of the named stratigraphic units below the Belmont Formation: upper Town Hill, lower Town Hill, and Walsingham. As the Belmont correlates with stage 7, and there is a terra rossa between each of these lower named units, the map implies that sea level rose above its present position in at least five separate odd-numbered stages of the deep-sea chronology (5, 7, and three more). From subsequent A/I ratios on *Poecilozonites* and whole-rock samples, and ages calculated from those ratios, it appears that interglacials represented by stages 9, 11, probably 13, and at least two significantly older ones all produced at least one highstand in Bermuda (Hearty et al., 1992; Hearty and Vacher, 1994). Although we are not aware of any Bermudian data that contradict either these statements or the identification and stratigraphic classification of pre-Belmont marine deposits of Vacher et al. (1989), we need to say that these interpretive conclusions are not as certain as similar ones higher in the column — such as for the 5a deposits, for example.

In conclusion, there is strong evidence that there is a significant pre-stage-7 history of sea-level excursions to above present sea level in Bermuda. Our knowledge of that history is not sufficiently clear and quantitative for us to draw a sea-level curve showing elevations and ages, without applying external forestructures and accepting local stratigraphic correlations and identifications that are less than certain. The curves of Hearty and Vacher (1994) and Hearty and Kindler (1995), we believe, are best considered as attempts to fit interpretations and hypotheses together graphically.

6. Double peak in substage 5e

As has been discussed, the double peak in the Land et al. (1967) sea-level curve — based on 5-m Devonshire deposits for the first peak, and the 10-m conglomerate at Spencer's Point and 17-m beach-like deposits at BWP — was abandoned on the basis of mapping along the south shore of the central parishes (Vacher, 1973; Vacher and Hearty, 1989), ages of submerged speleothems (Harmon et al., 1981, 1983), and reevaluation of the deposits at Blackwatch Pass (Garrett and Vacher, unpub.; Harmon et al., 1981, 1983). Recently, the double peak has been brought back to Bermuda by Hearty and Kindler (1995) in their correlation of BWP and south shore sections. In the meantime, study of the now-famous succession of uplifted reefs in New Guinea revealed the presence of two 5e reefs, indicating two highstands, the second higher than the first (Bloom et al., 1974), and Aharon and Chappell (1980) attributed the second highstand to an Antarctic surge. More recently, a 5e double peak has been used to explain deposits in Hawaii (Sherman et al., 1993), and Hearty and Kindler (1995) recognize it in the Bahamas [q.v., Chap. 3B].

It is striking how like the 5e double peak is to the original Devonshire-Spencer's Point doublet of Land et al. (1967), whose work, as we have noted, preceded expectations concerning Milankovitch cycles and Antarctic surges. Although Land et al. (1967) may have been right all along, we believe the evidence in Bermuda, so far, is best considered as neutral on the subject of a 5e double peak above present sea level. The trans-Bermuda correlation by Hearty and Kindler (1995) is consistent with

both the available data and the notion of a 5e double peak, but it is also possible to correlate the sections without assuming more than a single highstand, especially given the latitude provided by the sedimentologic uncertainties concerning the deposits near BWP. On the other hand, it would be a mistake to conclude from what has been published that available evidence precludes a 5e double peak. The argument of Vacher and Hearty (1989) is simply that the eolianite on which the conglomerates at Spencer's Point rest is pre-Devonshire, not post-Devonshire, and so that argument negates only the inference that a second highstand is required. Similarly, the speleothem ages do not rule out the possibility that there may have been two closely spaced peaks within the intra-speleothem hiatus that Harmon et al. (1981, 1983) correlated with the Devonshire highstand.

Part 3: Bermuda and the Concept of Eustasy

Arguably the most tenacious forestructure in determining Pleistocene sea-level history in Bermuda is the concept of eustasy itself. It is time to put aside the notion that an interpreted elevation of a sea-level highstand at one island should be the same as that of a coeval sea-level highstand at another island, even though both islands could be considered to qualify as "nontectonic references."

Eustasy

The word "eustatic" was coined in 1888 by Suess for changes in sea level that were of the same amount over the whole globe (Dott, 1992). Eustatic changes came to refer to the "ocean's own changes" (Morner, 1976, p. 125) as opposed to crustal and glacial isostatic movements. This idea gave rise to the supposition that, if one puts aside changes due to tectonics and glacial isostasy, then the world's history of Pleistocene sea-level changes should have produced the same history of sea-level changes at different places around the world. The result was that an elevation (e.g., tectonically corrected, in places like New Guinea and Barbados; observed, in places like Bermuda) from previously investigated islands would be a forestructure for subsequent investigations of other islands.

The concept of glacioeustatic elevations, however, has become more complex, for two reasons. The first is recognition that hydro-isostasy is widely relevant (Bloom, 1967; Walcott, 1972). Not only did continental areas rise and subside in response to the changing ice load, but so did the ocean floor in response to the changing water load. Now there are computer models that treat the phenomenon as a global rheological problem (e.g., Walcott, 1972; Clark et al., 1978; Lambeck, 1990). These models show that one can expect a variety of differences, including: (1) between locations in the near field (affected by post-glacial isostatic rising of the ice-loaded surface), the intermediate field (post-glacial subsidence of the forebulge), and the far field (beyond the forebulge); (2) between oceanic islands and continental shorelines because of tilting associated with the subocean-to-subcontinent flow of mantle material; (3) between such far-field islands as Fiji and Niue because of their different

sizes (Lambeck, 1990, Fig. 6); and (4) between localities as close as 100 km along far-field continental shorelines (e.g., Clark et al., 1978, p. 284) because of variations in shoreline configuration.

The second complicating factor is an appreciation that the surface of gravitational equipotential that defines sea level (i.e., the geoid) would change in response to changes in the Earth's rotation or redistributions of mass having nothing to do with ice volumes (e.g., Morner, 1976). The benchmark islands, New Guinea and Barbados, for example, are located at a major geoidal hump and a major geoidal depression, respectively (Morner, 1976; Nunn, 1986, 1994). Vertical or horizontal shifts of such extrema (Morner, 1976; Nunn, 1986, 1994) would confuse the interpretation of uplift (Nunn, 1986), which has been used to interpret the elevation of former sea levels.

Bermuda in global models

Bermuda has been specifically considered in some global, geophysical analyses (e.g., Clark et al., 1978; Lambeck, 1990; Lambeck and Nakada, 1992). According to these studies, Bermuda is positioned in the intermediate field relative to Northern Hemisphere ice centers. Accordingly, one can expect for Holocene curves to show progressive submergence due to (1) addition of melt water and (2) subsidence of the forebulge. Therefore, excluding vertical tectonics and geoidal effects that were not taken into account, the Holocene history of relative sea level in Bermuda should be different from that in such farfield places as Niue, Fiji, the Cook Islands, Brazil, and coastal Australia, where the models predict a Holocene highstand with an elevation and timing that depends on location. [See Case Study in Chap. 28, on the Houtman-Abrolhos islands, Western Australia.]

Similarly, the models of Lambeck and Nakada (1992) show a striking difference between the predicted relative sea-level history in western Australia (relatively early highstand) and that of Bermuda, the Bahamas, and Barbados (relatively late highstand), for the Last Interglacial (substage 5e). One of the models of the same study also predicts that the relative sea level of the Last Interglacial highstand would be 5 m higher in Bermuda than in Barbados (ignoring uplift and geoidal shifts), and that the elevation of the same event in the Bahamas would be intermediate between that of Bermuda and Barbados.

Bermuda elevations

Of all the statements that can be made about Bermuda's Pleistocene sea-level history, the ones with the greatest uncertainty pertain to elevations of particular highstands. Because of the difficulty of recognizing sea-level and stratigraphic position in these deposits, there has been a tendency in Bermuda to fall back on forestructures from other areas.

The concept of eustasy that underlies the geophysical modeling of, for example, Clark et al. (1978) and Lambeck and Nakada (1992) now liberates observations of

sea-level elevations in Bermuda from expectations derived from other localities and isotope-derived ice-volume curves. Suppose we abandon this foreknowledge of elevations: What can we say for sure?

We can make three statements regarding Bermuda's late Pleistocene history:

1. There is a body of evidence that says that sea level reached an elevation of 0–1 m during substage 5a (although there is countervailing evidence also).

2. There is a large conglomerate at Spencer's Point that suggests sea level reached an elevation of some 10 m during substage 5e (and there are widespread marine deposits at ≤ 6 m).

3. There is widespread evidence that sea level stood at about 1–2 m during stage 7 (and higher according to Meischner et al., 1995).

These three statements *are consistent in that they involve elevations that are higher than those expected from conventional outside considerations* (e.g., isotope-derived ice-volume curves).

The modeling by Lambeck and Nakada (1992) predicts that the Bermuda "tide gauge" would register high relative to equivalent sea levels computed directly from ice-volume data, because Bermuda is in the intermediate field of Northern Hemisphere ice centers. In other words, there may be good reason why some highstands (e.g., 5a) are found above sea level in Bermuda but not, for example, in Florida and the Bahamas.

The inverse problem

According to the new views of eustasy, "observed" sea-level histories reflect not only ice-volume changes and vertical tectonics unrelated to sea level, but also the viscoelastic behavior of the Earth in its response to the changing loads and, possibly, other phenomena affecting the Earth's distribution of mass and rotation. Thus interpreting the "ocean's own changes" at an island like Bermuda calls for the solution of an inverse problem.

There is an analogy with groundwater modeling, where, in one type of problem, observed data consist of a hydrograph of water-level variations, and the goal is to "back out" the history of recharge using forward, groundwater-flow models. For the sea-level problem, the observed data similarly consist of elevations and times (i.e., ages), and the goal is to "back out" the eustatic component (i.e., ice-volume changes) from forward, earth-response models. In both cases, the models are calibrated by adjusting various parameters (e.g., hydraulic conductivity and its distribution for one, mantle viscosity and its distribution for the other) until the observed data are duplicated. It obviously would be inappropriate for a field hydrogeologist to be swayed by the elevation of water level in one well while measuring the elevation of water level in a second well. In the same way, it ultimately would be self-defeating if elevation data from one island were allowed to prejudice determination of the elevation of a coeval sea level at another island.

CONCLUDING REMARKS

Bermuda has a long history and rich tradition of geological investigation. Reasons that Bermuda has attracted so much interest include its proximity to North American and European educational institutions; the logistic convenience of the BBSR, a modern research laboratory from which much of the geological and oceanographic studies has been based; the well-educated, interested and sophisticated people; and the environmental awareness of the Bermuda Government. It is understandable, therefore, that Bermuda has contributed over the years to carbonate-island geology and hydrogeology. We have included a sampling of ideas that are of particular interest to us: relation of carbonate eolianites to glacioeustasy; strastigraphic reasoning and the role of geological mapping, A/I ratios, geochronology and sea-level interpretations; evolution and expansion of depositional topographic lows to karstic inshore water bodies; geologic control of freshwater lenses due to increase in permeability accompanying diagenesis; control of water-table fluctuations by oceanographic phenomena.

Bermuda has to be high on the list of areas in the world in terms of total number of words in geological articles per km^2 of area. Our Case Study addresses one of the long-standing topics of geologic inquiry in Bermuda — the history of late Pleistocene sea level — and illustrates why we can expect many more words per km^2 to come, even on such much-studied problems. Our recommendation for this particular topic is that there be more descriptions and analysis of actual exposures (e.g., such as that of Vollbrecht and Meischner, 1993, and Meischner et al., 1995) than continued argumentation about how Bermuda proves out one or another geological world view. In general, there have been very few detailed descriptions in Bermuda.

ACKNOWLEDGMENTS

After twenty-some years the list of people who have benefitted us in our studies of Bermuda is so long that we can acknowledge only a small fraction. HLV greatly appreciates the initial guidance and continuing encouragement of Fred Mackenzie, the early support by the BBSR, and the stimulating collaboration of Jerry Ayers, Peter Garrett, Russ Harmon, Dick Mitterer, Paul Hearty and John Mylroie. We both acknowledge the Bermuda Government for their support of hydrogeologic studies since 1972, and particularly James Smith and Norman Thomas (Directors of Public Works) for their roles in getting the hydrogeology program underway. We thank J. Mylroie and P. Playford for helpful reviews of an earlier draft of the chapter, and A. Curran, R. Frodeman, P. Harries, and T. Quinn for help with a later version.

REFERENCES

Agassiz, A., 1895. A visit to the Bermudas in March, 1894. Bull. Mus. Comp. Zool., Harvard, 26: 209–281.

Aharon, P., Chappell, J. and Compston, W., 1980. Stable isotope and sea-level data from New Guinea supports Antarctic ice-surge theory of ice ages. Nature, 283: 649–651.

Barnett, T.P., 1984. The estimation of global sea level change: a problem of uniqueness. J. Geophys. Res., 89: 7980–7988.

Bloom, A.L., 1967. Pleistocene shorelines: A new test of isostasy. Geol. Soc. Am. Bull., 78: 1477–1494.

Bloom, A.L., Broecker, W.S., Chappell, J.M.A., Matthews, R.K. and Mesolella, K.J., 1974. Quaternary sea-level fluctuations on a tectonic coast: New $^{230}Th/^{234}U$ dates from the Huon Peninsula, New Guinea. Quat. Res., 4: 185–205.

Bretz, J.H., 1960. Bermuda: A partially drowned late mature Pleistocene karst. Geol. Soc. Am. Bull., 71: 1729–1754.

Bricker, O.P. and Mackenzie F.T., 1970. Limestones and red soils of Bermuda, discussion. Geol. Soc. Am. Bull., 81: 2523–2524.

Broecker, W.S., Thurber, D.L., Goddard, J., Ku, T.-L., Matthews, R.K. and Mesolella, K.J., 1968. Milankovitch hypothesis supported by precise dating of coral reefs and deep-sea sediments. Science, 159: 297–300.

Carew, J.L. and Mylroie, J.E., 1995a. Depositional model and stratigraphy for the Quaternary geology of the Bahama Islands. In: Curran, H.A. and White, B. (Editors), Terrestrial and Shallow Marine Geology of the Bahamas and Bermuda. Geol. Soc. Am. Spec. Pap., 300: 5–32.

Carew, J.L. and Mylroie, J.E., 1995b. Quaternary tectonic stability of the Bahamian Archipelago: Evidence from fossil coral reefs and flank margin caves. Quat. Sci. Rev., 14: 145–153.

Clark, J.A., Farrell, W.E. and Peltier, W.R., 1978. Global changes in post-glacial sea level: a numerical calculation. Quat. Res., 9: 265–287.

Cook, C.B., Dodge, R.E. and Smith, S.R., 1994. Fifty years of impacts on coral reefs in Bermuda. In: R.N. Ginsburg (Editor), Proceedings of the Colloquium Global Aspects of Coral Reefs, Health Hazards and History, University of Miami, Coral Gables FL, pp. 160–166.

Crough, S.T., 1983. Hotspot swells. Annu. Rev. Earth Planet. Sci., 11: 165–193.

deBoer, J.Z., McHone, J.G., Puffer, J.H., Ragland, P.C. and Whittington, D., 1988. Mesozoic and Cenozoic magmatism. In: R.E. Sheridan and J.A. Grow. (Editors), The Atlantic Continental Margin, U.S. Geol. Soc. Am., The Geology of North America, I-2: 217–241.

Detrick, R.S., Von Herzen, R.P., Parsons, B., Sandwell, D. and Dougherty, M., 1986. Heat flow observations on the Bermuda Rise and thermal models of midplate swells. J. Geophys. Res, 91: 3701–3723.

Dott, R.H., Jr., 1992. An introduction to the ups and downs of eustasy. In Dott, R.H., Jr. (Editor), Eustasy: The Historical Ups and Downs of a Major Geological Concept. Geol. Soc. Am. Mem. 180: 1–16.

Eldridge N. and Gould, S.J., 1972. Punctuated equilibria: an alternative to phyletic gradualism. In: T.J.M. Schopf (Editor), Models in Paleobiology. Freeman, San Francisco, pp. 82–115.

Ellison, J.C., 1993. Mangrove retreat with rising sea-level, Bermuda. Estuarine, Coastal Shelf Sci., 37: 75–87.

Fairbridge, R.W., 1995. Eolianites and eustasy: Early concepts on Darwin's voyage of HMS Beagle. Carbonates and Evaporites, 10: 92–101.

Ferris, J.G., 1951. Cyclic fluctuations of water level as a basis for determining aquifer transmissibility. Assem. Gen. Bruxelles, Assoc. Int. Hydrol. Sci., 2: 149–155.

Friedman, G.M., 1964. Early diagenesis and lithification in carbonate sediments. J. Sediment. Petrol., 29: 87–97.

Frodeman, R., 1995. Geological reasoning: Geology as an interpretive and historical science. Geol. Soc. Am. Bull., 107: 960–968.

Garrett, P. and Scoffin, T.P., 1977. Sedimentation on Bermuda's atoll rim. Proc. Third Int. Coral Reef Symp. (Miami), 87–95.

Garrett, P., Smith D.K., Wilson, A.O. and Patriquin, D., 1971. Physiography, ecology, and sediments of two Bermuda patch reefs. J. Geol., 79: 647–668.

Ginsburg, R.N. and Schroeder, J.H., 1973. Growth and submarine fossilization of algal cup reefs, Bermuda. Sedimentol., 20: 575–614

Gould, S.J., 1969. An evolutionary microcosm: Pleistocene and Recent history of the land snail *P.* (*Poecilozonites*) in Bermuda. Bull. Mus. Comp. Zool., Harvard, 138: 407–532.

Gross, M.G., 1964. Variations in the O^{18}/O^{16} and C^{13}/C^{12} ratios of diagenetically altered limestones in the Bermuda Islands. J. Geol., 72: 170–194.

Harmon, R.S., Schwarcz, H.P. and Ford, D.C., 1978. Late Pleistocene sea level history of Bermuda. Quat. Res. 9: 205–218.

Harmon, R.S., Land, L.S., Mitterer, R.M., Garrett, P., Schwarcz, H.P. and Larson, G.J., 1981. Bermuda sea level during the last interglacial. Nature, 289: 481–483.

Harmon, R.S., Mitterer, R.M., Kriausakul, N., Land, L.S., Schwarcz, H.P., Garrett, P., Larson, G.J., Vacher, H.L. and Rowe, M., 1983. U-series and amino-acid racemization geochronology of Bermuda: Implications for eustatic sea-level fluctuation over the past 250,000 years. Palaeogeogr., Palaeoclimatol., Palaeoecol., 44: 41–70.

Hayward, S.J., Gomez, V.H. and Sterrer, W., 1981. Bermuda's Delicate Balance: People and the Environment. Bermuda Biological Station for Research (St. Georges West), Spec. Pub. 20.

Hearty, P.J. and Hollin, J.T., 1986. Aminostratigraphy of Quaternary shorelines in Bermuda. Geol. Soc. Am. Abstr. Programs, 18: 663.

Hearty, P.J. and Kindler, P., 1995. Sea-level highstand chronology from stable carbonate platforms (Bermuda and The Bahamas). J. Coastal Res., 11: 675–689.

Hearty, P.J. and Vacher, H.L., 1994. Quaternary stratigraphy of Bermuda: A high-resolution pre-Sangamonian rock record. Quat. Sci. Rev., 13: 685–697.

Hearty, P.J., Vacher, H.L. and Mitterer, R.M., 1992. Aminostratigraphy and ages of Pleistocene limestones of Bermuda. Geol. Soc. Am. Bull., 104: 471–480.

Heezen, B.C., Tharp, M. and Ewing, M. 1959. The Floors of the Oceans I. The North Atlantic. Geol. Soc. Am. Spec. Pap. 65, 122 pp.

Herwitz, S.R., 1993. Stemflow influences on the formation of solution pipes in Bermuda eolianite. Geomorphol., 6: 253–271.

Herwitz, S.R., Muhs, D.R., Prospero, J.M., Mahan, S. and Vaughn, B., 1996. Origin of Bermuda's clay-rich Quaternary paleosols and their paleoclimatic significance. J. Geophys. Res., 101: 23,389–23,400.

Hollin, J.T., 1965. Wilson's theory of ice ages. Nature, 208: 12–16.

Hollin, J.T., 1980. Climate and sea level in isotope stage 5: an East Antarctic ice surge at ~95,000 BP? Nature, 283: 629–633.

Imbrie, J., Hays, J.D., Martinson, D.G., McIntyre, A., Mix, A.C., Morley, J.J., Pisias, N.G., Prell, W.C. and Shackleton, N.J., 1984. The orbital theory of Pleistocene climate: Support from a revised chronology of the marine $\delta^{18}O$ record. In: A.L. Berger et al. (Editors), Milankovitch and Climate, Part 1. Reidel, Dordrecht, pp. 269–305.

Johnson, D.L. and Fairbridge, R.W., 1968. Eolianite. In: R.W. Fairbridge, Encyclopedia of Geomorphology. Dowden, Hutchinson, and Ross, Stroudsburg, pp. 279–282.

Kent, D.V. and Gradstein, F.M., 1986. A Jurassic to recent chronology. In: P.R. Vogt and B.E. Tucholke (Editors), The Western North Atlantic Region. Geol. Soc. Am., The Geology of North America, M: 45–50.

Kindler, P. and Hearty, P.J., 1996. Carbonate petrography as an indicator of climate and sea-level changes: New data from Bahamian Quaternary units. Sedimentol., 43: 381–399.

Lambeck, K., 1990. Glacial rebound, sea-level change and mantle viscosity. Q. J. R. Astron. Soc., 31: 1–30.

Lambeck, K. and Nakada, M., 1992. Constraints on the age and duration of the last interglacial period and on sea-level variations. Nature, 357: 125–128.

Land, L.S., 1970. Phreatic versus vadose meteoric diagenesis of limestones: Evidence from a fossil water table. Sedimentol., 14: 175–185.

Land, L.S. and Mackenzie, F.T., 1970. Field Guide to Bermuda Geology. Bermuda Biological Station (St. Georges West, Bermuda) Spec. Publ. 4, 14 p.

Land, L.S., Mackenzie, F.T. and Gould, S.J., 1967. The Pleistocene history of Bermuda. Geol. Soc. Am. Bull., 78: 993–1006.

Lapointe, B.E. and O'Connell, J., 1989. Nutrient-enhanced growth of *Cladophora prolifera* in Harrington Sound, Bermuda: Eutrophication of a confined, phosphorus-limited marine ecosystem. Estuarine, Coastal Shelf Sci., 28: 347–360.

Liu M. and Chase, C.G., 1989. Evolution of midplate hotspot swells: Numerical solutions. J. Geophys. Res., 94: 5571–5584.

Logan, A., 1988. Holocene reefs of Bermuda. Sedimenta IX. Univ. Miami, Coral Gables FL, 63 pp.

Ludwig, K.R., Muhs, D.R., Simmons, K.R., Halley, R.B. and Shinn, E.A., 1996. Sea-level records at ~80 ka from tectonically stable platforms: Florida and Bermuda. Geology, 24: 211–214.

Mackenzie, F.T., 1964a. Bermuda Pleistocene eolianites and paleowinds. Sedimentol., 3: 52–64.

Mackenzie, F.T., 1964b. Geometry of Bermuda calcareous dune cross-bedding. Science, 144, 1449–1450.

Meischner, D. and Meischner, U., 1977. Bermuda South Shore reef morphology. Proc. Third Int.. Coral Reef Symp. (Miami), 243–250.

Meischner, D., Vollbrecht, R. and Wehmeyer, D., 1995. Pleistocene sea-level yo-yo recorded in stacked beaches, Bermuda South Shore. In: H.A. Curran and B. White (Editors), Terrestrial and Shallow Marine Geology of the Bahamas and Bermuda. Geol. Soc. Am. Spec. Pap., 300: 295–310.

Mitterer, R.M. and Kriausakul, N., 1989. Calculation of amino acid racemization ages based on apparent parabolic kinetics. Quat. Sci. Reviews, 8: 353–357.

Morgan, W.J., 1983. Hotspot tracks and the early rifting of the Atlantic. Tectonophys., 94: 123–139.

Morner, N.A., 1976. Eustasy and geoid changes. J. Geol., 84: 123–151.

Morris, B., Barnes, J., Brown, F. and Markham, J., 1977. The Bermuda Marine Environment, v. 1. Bermuda Biological Station (St. Georges West, Bermuda) Spec. Publ. 15, 120 pp.

Morse, J.W. and Mackenzie, F.T., 1990. Geochemistry of Sedimentary Carbonates. Elsevier, New York, 707 pp.

Muhs, D.R., 1983. Quaternary sea-level events on northern San Clemente Island, California. Quat. Res., 20: 322–341.

Mylroie, J.E., Carew, J.L. and Vacher, H.L., 1995. Karst development in the Bahamas and Bermuda. In: H.A. Curran and B. White (Editors), Terrestrial and Shallow Marine Geology of the Bahamas and Bermuda. Geol. Soc. Am. Spec. Pap., 300: 251–267.

NACSN [North American Commission on Stratigraphic Nomenclature], 1983, North American Stratigraphic Code. Am. Assoc. Petrol. Geol. Bull., 67: 841–875.

Nelson, R.J., 1837. On the geology of the Bermudas. Geol. Soc. London Trans., 5: 103–123.

Neumann, A.C., 1965. Processes of recent carbonate sedimentation in Harrington Sound, Bermuda. Bull. Mar. Sci., 15: 987–1035.

Neumann, A.C., 1971. Quaternary sea level data from Bermuda. Quaternaria, 14: 41–43.

Nunn, P.D., 1986. Implications of migrating geoid anomalies for the interpretation of high-level fossil coral reefs. Geol. Soc. Am. Bull., 97: 946–952.

Nunn, P.D., 1994. Oceanic Islands. Blackwell, Oxford, 413 pp.

Officer, C.B., Ewing, M. and Wuenschel, P.C., 1952. Seismic refraction measurement in the Atlantic Ocean basin — IV. Bermuda, Bermuda Rise and Nares Basin. Geol. Soc. Am. Bull,, 63: 777–809.

Pirazzoli, P.A., 1987. Recent sea-level changes in the North Atlantic. In: D.B. Scott, P.A. Pirazzoli and C.A. Honig, (Editors), Later Quarternary Sea-Level Correlation and Applications. Kluwer, Boston, pp. 153–167.

Pirsson, L.V., 1914. Geology of Bermuda Island: The igneous platform. Am. J. Sci., 36: 189–106.

Plummer, L.N., Vacher, H.L., Mackenzie, F.T., Bricker, O.P. and Land, L.S., 1976. Hydrogeochemistry of Bermuda: A case history of ground-water diagenesis of biocalcarenites. Geol. Soc. Am. Bull., 87: 1301–1316.

Purdy, E.G., 1974. Reef configurations: Cause and effect. In: L.F. Laporte (Editor), Reefs in Time and Space. Soc. Econ. Paleontol. Mineral. Spec. Publ. 18: 9–76.

Redfield, A.C., 1967. Postglacial change in sea-level in the western North Atlantic Ocean. Science 157: 687–692.

Reynolds, P.R. and Aumento, F.A., 1974. Deep Drill 1972: Potassium-argon dating of the Bermuda drill core. Can. J. Earth Sci., 11: 1269–1273.

Rowe, M.P., 1981. The Central Lens of Bermuda: A Ghyben-Herzberg lens in disequilibrium. M.Sc. Project, Univ. Coll. London, London, 108 pp.

Rowe, M.P., 1984. The freshwater "Central Lens" of Bermuda. J. Hydrol., 73: 165–176.

Rowe, M.P., 1990. An explanation of the geology of Bermuda, with reference to the Geological Map of Bermuda (1989). Bermuda Gov., Ministry of Works and Engineering, Hamilton, Bermuda, 28 pp.

Rowe, M.P., 1991. Bermuda. In: Falkland, A. (Editor), Hydrology and Water Resources of Small Islands: A Practical Guide. UNESCO, Paris, pp. 333–338.

Rudloff, W., 1981. World-Climates. Wissenschaftliche Verlagsgesellschaft, Stuttgart, 632 pp.

Ruhe, R.V., Cady, J.G. and Gomez, R.S., 1961. Paleosols of Bermuda. Geol. Soc. Am. Bull., 72: 1121–1142.

Sayles, R.W., 1931. Bermuda during the Ice Age. Am. Acad. Arts and Sci., 66: 381–468.

Schroeder, J.H., 1973. Submarine and vadose cements in Pleistocene Bermuda reef rock. Sediment. Geol., 10: 179–204.

Schroeder, J.H. and Zankl, H., 1974. Dynamic reef formation: A sedimentological concept based on studies of Recent Bermuda and Bahama reefs. Proc. Second Coral Reef Symp. (Brisbane), 2: 413–428.

Sclater, J.G. and Wixon, L. 1986. The relationship between depth and age and heat flow and age in the western North Atlantic. In: P.R. Vogt and B.E. Tucholke (Editors), The Western North Atlantic Region. Geol. Soc. Am., The Geology of North America, M: 257–270.

Shackleton, N.J., 1987. Oxygen isotopes, ice volumes and sea level. Quat. Sci. Rev., 6: 183–190.

Shaw, D.N. and Donn, W.L., 1964. Sea level variations at Iceland and Bermuda. J. Mar. Res., 22: 111–122.

Sherman, C.E., Glenn, C.R., Jones, A.T., Burnett, W.C. and Schwarcz, H.P., 1993. New evidence for two highstands of the sea during the last interglacial, oxygen isotope substage 5e. Geology, 21: 1079–1082.

Simmons, J.A.K. and Lyons, B.W., 1994. The ground water flux of nitrogen and phosphorus to Bermuda's coastal waters. Water Resour. Bull., 30: 983–991.

Simmons, J.A.K., Jickells, T., Knap, A. and Lyons, W.B., 1985. Nutrient concentrations in ground waters from Bermuda: Anthropogenic effects. In: D.E. Caldwell, J.A. Brierley and C.L. Brierly (Editors), Planetary Ecology. Van Nostrand Reinhold, New York, pp. 383–398.

Thomson, C.W., 1873. Geological peculiarities of the Bermudas. Nature, 13: 266–267.

Thomson, J.A.M., 1989. Modeling ground-water management options for small limestone islands: The Bermuda example. Ground Water, 27: 147–154.

Tucholke, B.E. and Mountain, G.S., 1986. Seismic stratigraphy, lithostratigraphy, and paleosedimentation patterns in the North American basin. In: M. Talwani, W. Hay and W.B.F. Ryan (Editors), Deep Drilling Results in the Atlantic Ocean: Continental Margins and Paleoenvironments, Maurice Ewing Ser., 3: 58–86.

Tucholke, B.E., Vogt, P.R. et al., 1979. Initial Reports of the Deep Sea Drilling Project, 43. U.S. Gov. Printing Office, Washington D.C., 1114 pp.

Tucker, G.B. and Barry, R.G., 1984. Climate of the North Atlantic Ocean. In: H. Van Loon (Editor), Climates of the Oceans. World Survey of Climatology, 15: 193–262.

Turcotte, D.L. and Schubert, G., 1982. Geodynamics. Wiley, New York, 450 pp.

Upchurch, S.B., 1970. Sedimentation on the Bermuda Platform. Ph.D. Dissertation, Northwestern Univ., Evanston IL, 206 pp.

Vacher, H.L., 1971. Late Pleistocene sea-level history: Bermuda evidence. Ph.D. Dissertation, Northwestern Univ., Evanston IL, 153 pp.

Vacher, H.L., 1973. Coastal dunes of Younger Bermuda. In: Coates D.R. (Editor), Coastal Geomorphology. State Univ. New York, Binghamton N.Y., pp. 355–391.
Vacher, H.L., 1974. Ground Water Hydrology of Bermuda. Bermuda Public Works Department, Hamilton, Bermuda, 85 pp.
Vacher, H.L., 1978a. Hydrology of small oceanic islands — Influence of atmospheric pressure on the water table. Ground Water, 16: 417–423.
Vacher, H.L., 1978b. Hydrogeology of Bermuda — Significance of an across-the-island variation in permeability. J. Hydrol. 39: 207–226.
Vacher, H.L., 1988. Dupuit-Ghyben-Herzberg analysis of strip-island lenses. Geol Soc. Am. Bull., 100: 580–591.
Vacher, H.L. and Ayers, J.F., 1980. Hydrology of small oceanic islands — Utility of an estimate of recharge inferred from the chloride concentration of the freshwater lenses. J. Hydrol., 45: 21–37.
Vacher, H.L. and Hearty, P.J., 1989. History of stage 5 sea level in Bermuda: Review with new evidence of a brief rise to present sea level during substage 5a. Quat. Sci. Rev., 8: 159–168.
Vacher, H.L. and Mylroie, J.E., 1991. Geomorphic evolution of topographic lows in Bermudian and Bahamian islands: Effect of climate. In: R.J. Bain (Editor), Proc. Fifth Symp. Geol. Bahamas, pp. 221–234.
Vacher, H.L. and Wallis, T.N., 1992. Comparative hydrogeology of fresh-water lenses of Bermuda and Great Exuma Island, Bahamas. Ground Water, 30: 15–20.
Vacher, H.L., Rowe, M.P. and Garrett, P., 1989. The Geologic Map of Bermuda. Scale 1:25,000. Oxford Cartographers, London. Bermuda Gov., Ministry of Works and Engineering.
Vacher, H.L., Bengtsson, T.O. and Plummer, L.N., 1990. Hydrology of meteoric diagenesis: Residence time of meteoric ground water in island fresh-water lenses with application to aragonite-calcite stabilization rate in Bermuda. Geol. Soc. Am. Bull., 102: 223–232.
Vacher, H.L., Hearty, P.J. and Rowe, M.P., 1995. Stratigraphy of Bermuda: Nomenclature, concepts, and status of multiple systems of classifications. In: Curran, H.A. and White, B. (Editors), Terrestrial and Shallow Marine Geology of the Bahamas and Bermuda. Geol. Soc. Am. Spec. Pap., 300: 271–294.
Verrill, A.E., 1907. The Bermuda Islands. Part IV, Geology and paleontology, and Part V, An account of the coral reefs. Conn. Acad. Arts & Sci. Trans., 12: 45–348.
Vogt, P.R., 1991. Bermuda and Appalachian-Labrador rises: Common non-hotspot processes? Geology, 19: 41–44.
Vollbrecht, R., 1990. Marine and meteoric diagenesis of submarine Pleistocene carbonates from the Bermuda carbonate platform. Carbonates and Evaporites, 5: 13–96.
Vollbrecht, R. and Meischner, D., 1993. Sea level and diagenesis — A case study of Pleistocene beaches, Whalebone Bay, Bermuda. Geol. Rundschau, 82: 148–162.
Vollbrecht, R. and Meischner, D., 1996. Diagenesis in coastal carbonates related to Pleistocene sea level, Bermuda Platform. J. Sediment. Res., 66: 243–258.
Walcott, R.I., 1972. Past sea levels, eustasy and deformation of the Earth. Quat. Res., 2: 1–14.
Wilson, A.T., 1964. Origin of Ice Ages: an ice shelf theory for Pleistocene glaciation. Nature, 201: 147–149.
Wunsch, C., 1972. Bermuda sea level in relation to tides, weather, and baroclinic fluctuations. Rev. Geophys. Space Phys., 10: 1–49.

Geology and Hydrogeology of Carbonate Islands. Developments in Sedimentology 54
edited by H.L. Vacher and T. Quinn
© 1997 Elsevier Science B.V. All rights reserved.

Chapter 3A

GEOLOGY OF THE BAHAMAS

JAMES L. CAREW and JOHN E. MYLROIE

INTRODUCTION

Geographical background

The Commonwealth of The Bahamas comprises the majority of an extensive archipelago of carbonate islands and shallow banks in the western North Atlantic Ocean (21° to 27°30′ N and 69° to 80°30′W) (Fig. 3A-1). The southeastern portion of the same archipelago consists of the Turks and Caicos Islands (British West Indies), and the submerged Mouchoir, Silver, and Navidad banks. This chapter concerns the Bahamas, but the geology of the Turks and Caicos is similar (Wanless et al., 1989). The Bahamian archipelago covers 300,000 km^2, of which 136,000 km^2 is shallow bank, and 11,400 km^2 is subaerial land (Meyerhoff and Hatten, 1974). The banks are generally less than 10 m deep and are bounded by near-vertical declivities into very deep water. The Bahamas consists of 29 land masses referred to as islands, 661 cays (pronounced "keys", generally minor islands), and 2,387 rocks (Albury, 1975). [The term "island" is used in this chapter to refer to both formal islands and cays.] The islands are predominantly low lying, and the topography is dominated by eolianite (dune) ridges that extend up to 30 m on most, but not all, major islands. The highest elevation (63 m) occurs on Cat Island (Fig. 3A-1).

In the northwest, the archipelago consists of scattered islands on two large banks, Great Bahama Bank and Little Bahama Bank. Great Bahama Bank is embayed by two deep troughs: Tongue of the Ocean (TOTO) in the center (1400–2000 m), and Exuma Sound to the east (1700–2000 m). Little Bahama Bank is separated from Great Bahama Bank by Northwest and Northeast Providence Channels. To the southeast, the islands are on small banks that are separated by deep water (2000 m to >4800 m). In many cases, the islands that occupy these banks encompass most of the bank area (e.g., Great Inagua Island, Figure 3A-1). In the Bahamas, only Cay Sal Bank (Fig. 3A-1) lacks significant islands.

Climatically, the Bahamas range from subtropical temperate in the north to semiarid in the south. For example, on Grand Bahama Island the average temperature is 18°C (January) to 28°C (July), and average annual rainfall is 1355 mm, whereas on Great Inagua Island average temperature is 23.5°C (January) to 28.5°C (July), and annual rainfall averages only 700 mm (Sealey, 1990). Historical accounts indicate that Bahamian islands were once heavily vegetated with mixed tropical broadleaf coppice including mahogany. Today, the northern islands are largely covered by pine barrens with palmetto, but there are regions of limited broadleaf coppice. South of New Providence Island, the coppice becomes less dense, and tree

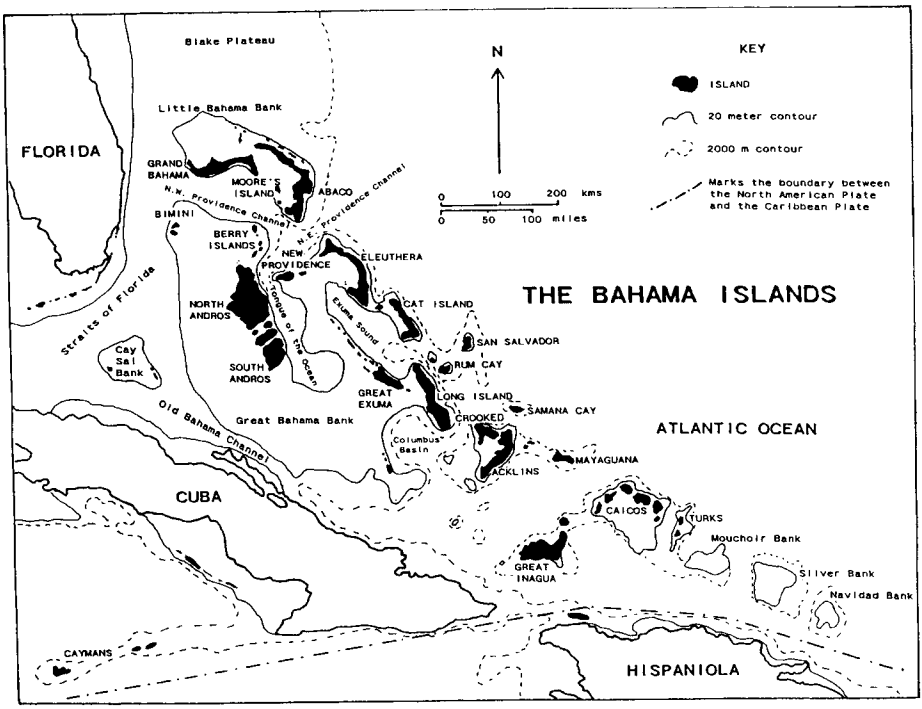


Fig. 3A-1. Map of the Bahamas and adjacent region showing the bank margins and most of the locations mentioned in the text. Locations not labeled on the map include: Conception Island located northwest of Rum Cay; Lee Stocking Island in the Exuma chain slightly north of Great Exuma; Joulter Cays just north of North Andros Island; Little San Salvador Island between the north end of Cat Island and the south end of Eleuthera; Schooner Cays slightly north of the northwestern projection at the south end of Eleuthera; and West Plana Cay between Mayaguana and Acklins islands.

size declines as the climate becomes drier; on many islands, xeric vegetation and scrub dominate (Sealey, 1990).

The Bahamas lie within the zone of the northeast trade winds, and that has resulted in the preferential occurrence of islands on the eastern (windward) side of most banks. Trade winds have influenced the position and shape of many of the topographic ridges, but some eolianite ridges are aligned with other wind directions, especially that of the seasonal westerlies associated with fronts from the North American continent. Some islands have high ridges largely limited to the windward side (e.g., Andros Island), but most do not show such pronounced asymmetry.

Marine waters of the Bahamas average 18°C (winter) to 28°C (summer). The north equatorial current (Antilles Current) delivers water to the banks from the southeast. The current diverges and flows northwestward along the eastern margin of the archipelago at 0.6–0.8 kn, and northwestward through Old Bahama Channel south of Great Bahama Bank at 0.9 kn. The Bahamas are bounded on the west by

the Florida Strait and Gulf Stream which flows at ~2.5–2.8 kn. (Data from the Hydrographic Chart of The Commonwealth of The Bahamas, first edition, 1977.) The Bahamas are a wholly carbonate province because these currents effectively isolate them from terrigenous sediment from the Greater Antilles and North America (Fig. 3A-1).

Historical background

The Bahamas are known as the site of Christopher Columbus' first landfall in the "New World", in 1492. Today, it is generally agreed that San Salvador Island (formerly known as Watling's Island, and called Guanahani by the native Lucayans) was most likely that landfall. According to Columbus' log, when he sailed from the island of his first landfall, many islands could be seen to the southwest. Interestingly, one can see many "islands" from San Salvador when atmospheric conditions are favorable. These "islands" are in fact the refracted images of hills on Rum Cay and Conception Island that lie 35 km and 54 km respectively to the southwest of San Salvador (Fig. 3A-1) (see Carew et al., 1995).

Following Columbus' voyage, exploitation and disease brought by the Spanish resulted in the rapid extinction of the native Lucayan and Arawak peoples, probably within just 25 years. The Bahama islands remained largely uninhabited for the following century and a half, until British adventurers began sparse settlement of the area in the mid-1600s. Much piracy occurred in the Bahamas, and that provoked Spanish raids in the area until the early 1700s, when the British began to exert some control on the governance of the archipelago.

When the American colonies won their independence, some British loyalists from the southeastern United States chose to leave and settle in the British-held Bahamas. Because the size of the land grant from the Crown depended on family size, including slaves, plantation owners moved their families and slaves to the Bahamas with the intention of re-establishing their plantations there. During this time of British influence, additional African slaves were brought in to work the plantations. Unfortunately, the soils of the Bahamas could not support long-term production of cotton or other large-scale farming, and the plantations soon began to fail. The Bahamas languished under British inattention, and most of the plantation owners ultimately left the Bahamas. The former slaves, freed by British government decree in 1834, were left behind, and the current population is composed largely of their descendants.

In the late eighteenth and early nineteenth centuries, the economy of these islands was based on agriculture, privateering, and wrecking. Following that, the Bahamas went through modest boom times and intervening relatively hard times. As examples, significant boom times resulted from gun-running to the Confederacy during the U. S. Civil War, and rum-running during Prohibition. Tourism began to flourish when wealthy Americans vacationed in the Bahamas during Prohibition, and it has grown into the dominant industry of the Bahamas today. In 1973, the Bahamas gained independence from Great Britain, but remained a British Commonwealth nation.

GEOLOGIC OVERVIEW

The geologic literature on the Bahamas is voluminous, and because of space limitations no attempt is being made herein to cover all of the relevant issues or references. We draw attention to many papers that contain extensive bibliographies, and we encourage any reader that wishes to become fully cognizant of the relevant literature on the Bahamas to consult those works. Recently, the Geological Society of America published Special Paper 300 (Curran and White, 1995, editors) on the geology of the Bahamas and Bermuda, and the references contained in the papers in that volume constitute an extensive bibliography. In addition, there is a large body of important work that documents the development of recent ideas concerning the geology of Bahamian islands, which is published in the Geology of the Bahamas Symposium Proceedings volumes and field trip guidebooks, as well as other publications, of the Bahamian Field Station on San Salvador Island, Bahamas.

Geologic research in the Bahamas dates back to the mid-nineteenth century (see summaries by Meyerhoff and Hatten, 1974, and Sealey, 1991). Amongst the earliest work is that of Captain Nelson who worked on Bermuda in the early 1830s, and was later assigned to the Bahamas. It was Nelson who first recognized the similarities between Bermuda (q.v., Ch. 2) and the Bahamas, and he recognized that eolian deposits dominate both island groups. It is particularly interesting that Nelson's 1853 paper on the geology of the Bahamas was read to the Geological Society of London by none other than Sir Charles Lyell.

Other early views of the Bahamas held that they were the coral and carbonate-mantled northern portion of a mountain range that once stretched from Central America through the Greater Antilles to Florida; another interpretation suggested that the Bahamas were the result of delta-like deposition of the Gulf Stream that buried the northern extension of the eastern Caribbean mountain range mentioned above. Still other workers saw the Bahamas as entirely derived from corals, and that many of the islands were uplifted coral atolls (Sealey, 1991).

There is also lively discussion in the early literature about the apparent relative changes in sea level that can be discerned from the geological record of the Bahamas. Nelson contended that there was no evidence for either elevation or subsidence of the Bahamas. However, somewhat later views required no less than $\sim$100 m of subsidence to account for the depths of ocean blue holes, and Shattuck and Miller (1905) called for repeated relatively rapid elevation and subsidence of the Bahamas. Field et al. (1931) appear to have been the first to make a connection between the seemingly disparate data and the changes in sea level associated with Pleistocene glaciation. In that sense, Field's work was the start of the modern view of the geological development of the Bahamas.

Much of the post-1930s geologic research in the Bahamas has focused on tectonic evolution, modern carbonate depositional environments, and subsurface stratigraphy and bank evolution. Recently the terrestrial geology of some Bahamian islands has received considerable attention, and that is the primary focus of this chapter.

Tectonic evolution

There was much debate in the 1970s and 1980s about the early geologic evolution of the Bahamas. A major question concerned the nature of the crust that underlies the 5–10 km of predominantly shallow-water carbonates of the Bahamas (i.e., continental vs. volcanic vs. oceanic; e.g., Dietz et al., 1970; Lynts, 1970; Uchupi et al., 1971; Meyerhoff and Hatten, 1974; Mullins and Lynts, 1977; Sheridan et al., 1988; and references therein). Another question concerned the origin of the deep channels and the segmentation of the Bahamas into separate isolated banks. One school of thought held that the deep channels and banks began as grabens and horsts respectively, reflecting direct structural control (e.g., Ball, 1967a; Mullins and Lynts, 1977; Sheridan et al., 1988, and references therein). A second school of thought (e.g., Dietz et al., 1970) held that the channels and banks reflect a long-term dynamic equilibrium between normal depositional (i.e., shallow-water carbonate accumulation that keeps pace with subsidence) and erosional processes (i.e., turbidity currents that deepen and carve channels). A third school of thought held that the present channel and bank configuration evolved since the Late Cretaceous, and that formerly there was one large unsegmented bank, or "megabank" (e.g., Meyerhoff and Hatten, 1974; Schlager and Ginsburg, 1981; Sheridan et al., 1988, and references therein). Sheridan et al. (1988) summarize the diverse results of previous geologic and geophysical research concerning the tectonic evolution of the Bahamas, and they present a revised geologic history for this area, a brief synopsis of which follows.

The crust underlying the carbonates of the Bahamas was a product of the processes associated with rifting of Pangea and the opening of the North Atlantic basin in the late Middle Jurassic. The basement rocks in the northwestern Bahamas, under the Florida Straits, the Northwest Providence Channel, and the northernmost Tongue of the Ocean (TOTO) is "intermediate" or "transitional" rift crust, composed of tilted fault blocks of Jurassic volcaniclastics. Southeast of that region, the Bahamas are underlain by oceanic crust. The nature of the crust in the transition area between the Bahamas and Cuba remains poorly defined.

Development of the thick carbonate banks began in the Late Jurassic, and those carbonates formed a "megabank" that included the west Florida shelf, the Florida Platform, the Bahama Platform, and the Blake Plateau (Emery and Uchupi, 1972; Meyerhoff and Hatten, 1974). Although there is some evidence that deep-water reentrants penetrated the "megabank" in the Early Cretaceous, in most places that have been studied, the present channels and basins appear to be underlain by Lower Cretaceous shallow-water carbonates, which implies the absence of these deep areas at that time. The current deep-water channels and basins of the Bahamas appear to have existed in approximately their present positions since at least the Late Cretaceous (see Sheridan et al., 1988, and references therein).

Post-Cretaceous faulting that resulted in > 500 m displacement and tilting of blocks on the otherwise passive Atlantic margin has been attributed to interaction between the Caribbean and North American plates during the Late Cretaceous/Tertiary Cuban and Antillan orogenies. The orientations of the margins of the Bahama Banks are consistent with left-lateral wrench faulting caused by the oblique

subduction of the North American plate under the Caribbean plate near Cuba (Sheridan et al., 1988, and references therein).

Subsurface stratigraphy

The Tertiary history of the Bahama Banks is dominated by intervals of aggradation and progradation in response to sea-level change and variations in banktop sediment production (e.g., Eberli and Ginsburg, 1987; Wilber et al., 1990; Hine et al., 1981a; Wilson and Roberts, 1992; Milliman et al., 1993). The Tertiary evolution of the Bahamas is discussed in greater detail by Melim and Masaferro in Chapter 3C. A brief discussion follows.

The subsurface stratigraphy of the Bahamas has been studied using seismic refraction, seismic reflection, magnetics, and gravity (see review by Sheridan et al., 1988); more recently, the geology and geophysics of Great Bahama Bank has been the subject of intensive seismic investigation (e.g., Eberli and Ginsburg, 1987, 1989).

In addition, the subsurface stratigraphy of the Bahamas has been studied via deep and shallow drilling. Prior to the recent University of Miami Bahamas Drilling Project, some results of which are summarized by Melim and Masaferro in Chapter 3C, the lithology of the deep subsurface of the Bahamas was known from four deep wells drilled on Andros Island, Cay Sal, Long Island, and Great Isaac. Limestone, dolostone, and evaporites were recovered in those wells. The Cay Sal and Great Isaac wells penetrated Upper Jurassic carbonates at slightly greater than 5 km depth, and the Andros Island and Long Island wells ended in Lower Cretaceous dolostone (Meyerhoff and Hatten, 1974; Sheridan et al., 1988; and references therein).

Numerous shallow boreholes also have been drilled at a variety of locations in the Bahamas, including: Crooked Island, Mayaguana Island, Great Inagua Island, Hogsty Reef, Grand Bahama Island, Great Abaco Island; Andros Island, Eleuthera Island, San Salvador Island, and New Providence Island (e.g., Meyerhoff and Hatten, 1974; Supko, 1977; Beach and Ginsburg, 1980; Pierson and Shinn, 1985; Aurell et al., 1995). An apparently important stratigraphic conclusion reached by study of such shallow subsurface rocks was the recognition that, at the margins of Great Bahama Bank, there is a transition from Pliocene skeletal and reefal facies to Quaternary oolites and eolianites (Beach and Ginsburg, 1980). It has been suggested that this transition may be related to the onset of northern hemisphere glaciation and more frequent glacioeustatic changes (Schlager and Ginsburg, 1981).

Some shallow coring has indicated that Pleistocene-Holocene sediments are about 24 m thick on Little Bahama Bank and as much as 40 m thick on Great Bahama Bank (Beach and Ginsburg, 1980). It has been suggested that such data may reflect differential subsidence among the individual banks of the Bahamas (Schlager and Ginsburg, 1981), and Sheridan et al. (1988) argue that it is plausible that differential subsidence has continued into the Holocene; however, recent study of exposed coral reefs and flank margin caves in the Bahamas indicates that the entire archipelago appears to have behaved similarly (no more than 1–2 m subsidence per 100 ky) for at least the last 300 ky (Carew and Mylroie, 1995a,b). Also, the thickness of the

Quaternary sediment package does not vary systematically across the Bahamas (e.g., Cant and Weech, 1986).

Modern depositional systems

The lithofacies of the modern Bahama banks have been used as models for the interpretation of ancient carbonates (e.g., Bathurst, 1975). Classic work on the sediments of the Bahama banks includes that of Illing (1954), Purdy (1963), Ball (1967b), Enos (1974), Gebelein (1976), Hine et al. (1981b), among many others. At the large scale, four major shallow-marine lithofacies (coralgal, ooid, grapestone, and lime mud) have been recognized in the Bahamas (see Milliman, 1974; Bathurst, 1975; Tucker and Wright, 1990; and references therein). Intertidal and supratidal lithofacies of the Bahamas have also been intensively studied. In particular, western Andros Island has provided much information on the dynamics of micritic tidal flat deposition (see Shinn et al., 1969; Bathurst, 1975; Hardie and Shinn, 1986; Tucker and Wright, 1990; and references therein). While those studies have yielded a general understanding of the large-scale facies mosaic, such as that of the Great Bahama Bank (Fig. 3A-2), the reader should be cognizant of the fact that there is much

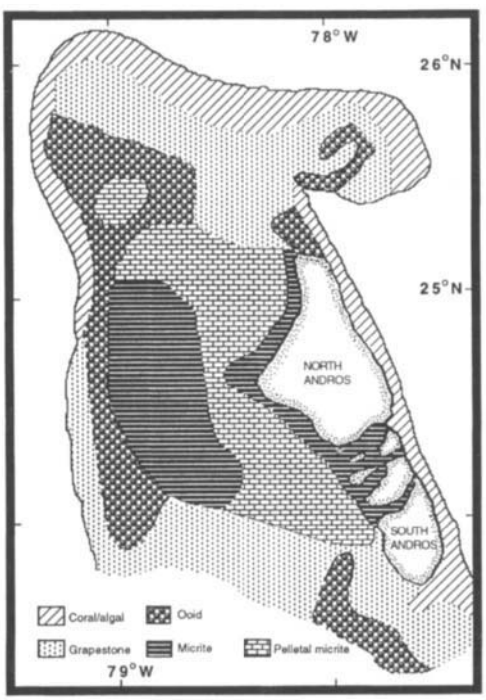


Fig. 3A-2. Map of western Great Bahama Bank showing the large-scale distribution of sediment facies. (Modified from Purdy, 1963.)

greater variability in sediment type and facies distribution than is suggested by such generalizations. Wide variability in accumulation, depositional style, and sediment type on the Bahama banks results from differences in orientation to currents and winds that influence the physical energy of various areas.

A wide variety of stromatolite development has been reported from the Bahamas. Forms include very large (> 2 m) subtidal stromatolites (Dravis, 1983; Dill et al., 1986; Shapiro et al., 1995, and references therein), small coastal and subtidal stromatolites (Pentecost, 1989), intertidal stromatolites (Reid and Browne, 1991), and stromatolites in hypersaline lakes (Neumann et al., 1989). Bahamian stromatolites generally occur where rapid currents (Dill, et al., 1986; Shapiro et al., 1995) or hypersalinity (Neumann et al., 1989) prevent grazing by macrofauna. Rapid cementation has also been invoked as an important factor in stromatolite development (Reid and Browne, 1991).

Surficial geology

The surficial geology of Bahamian islands has recently been studied with increasing detail (e.g., Titus, 1980; Garrett and Gould, 1984; Carew and Mylroie, 1985, 1995a; Hearty and Kindler, 1993; Kindler and Hearty, 1995, 1996). A striking feature of the surficial geology of most Bahamian islands is the occurrence of large eolianite ridges. The original interpretation of the origin of these deposits held that exposed banktop sediments were reworked into regressive sequences during sea-level fall (e.g., Titus, 1980), or during stillstand and regression (Garrett and Gould, 1984). Detailed work on San Salvador Island led to the realization that eolianite ridges form during all phases of a sea-level highstand, and that those deposited during the transgressive phase are often the most substantial accumulations (Carew and Mylroie, 1985, 1995a, and references therein). The detailed discussion of this depositional model presented in Carew and Mylroie (1995a) is summarized in this chapter, and is extensively cited as a source for additional citations to the relevant literature. [Kindler and Hearty give an account of the constructional architecture of Bahamian islands in Chapter 3B of this book. — Eds.]

GEOMORPHOLOGY OF BAHAMIAN ISLANDS

Landscapes

The Bahama islands exhibit a largely constructional landscape; that is, the landforms have been created by accumulation of biogenic and authigenic carbonate sediment deposited by currents, waves, and winds. All major islands in the Bahamas are dominated by two landforms: eolianite ridges that commonly rise up to 30 m above sea level (Fig. 3A-3), and lowlands composed of marine and terrestrial deposits. Most Bahamian islands are dominated by Pleistocene rocks, with a lesser amount of Holocene rocks, generally on island fringes. Analysis of the landforms on San Salvador Island has shown that the island comprises 2.6% beach, 4.5% Ho-

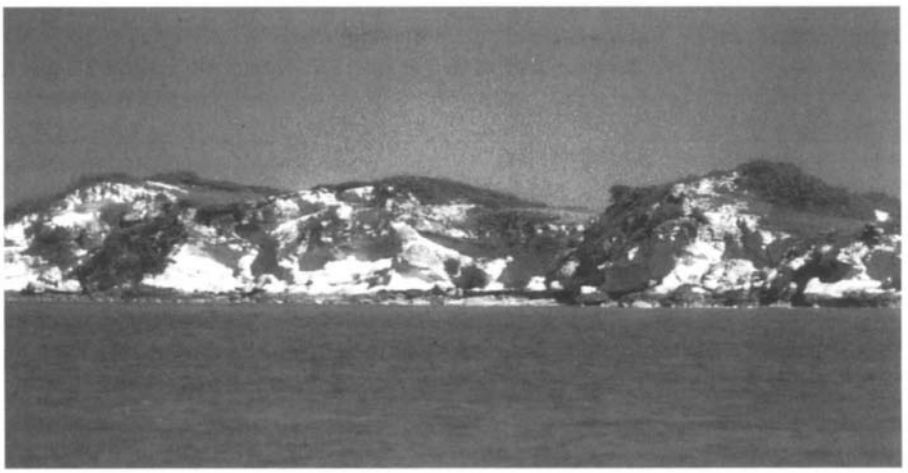


Fig. 3A-3. Photograph showing the dune form of an early Holocene eolianite ridge at North Point, San Salvador Island.

locene rocks, 22% lakes and tidal creeks, 21% eolianite ridges, and 49% lowlands (Wilson et al., 1995). Because the lowlands consist primarily of intertidal and subtidal deposits including fossil reefs that have radiometric ages that indicate formation during the last interglacial (oxygen isotope substage 5e, ~125 ka), Wilson et al. (1995) referred to them as the Sangamon Terrace.

In the interior of Bahamian islands, topographic lows that extend below sea level, especially inter-dune swales, commonly contain lakes that are usually marine to hypersaline. Surface streams are absent. All land above 7 m elevation consists of eolian deposits, but land below 7 m elevation is a mixture of marine and terrestrial (incl. lacustrine) lithofacies. Pleistocene rocks are covered with a red micritic calcrete or terra rossa paleosol (Carew and Mylroie, 1991) unless it has subsequently been removed by erosion. On the other hand, Holocene rocks lack a well-developed calcrete or terra rossa paleosol, but a thin micritized crust sometimes occurs.

Although most of the landscapes in the Bahamas are largely of Pleistocene origin, a few Bahamian islands such as Joulter Cays and Schooner Cays are entirely Holocene. These Holocene islands are hardly more than exposed shoals, and they are only 100's of m long and wide, only 1.5–2.5 m high, and consist of intertidal and back-beach dune facies that are at the same elevations as sediments being currently laid down in similar depositional environments (e.g., Budd, 1988; Budd and Land, 1989; Halley and Harris, 1979; Harris, 1983; Strasser and Davaud, 1986). These Holocene deposits are up to 10.7 m thick (Budd, 1988). Cementation is vertically and laterally variable, but where it occurs, it is minimal and dominated by vadose freshwater meniscus cements, with occasional marine cements (e.g., Strasser and Davaud, 1986; Budd, 1988). The greatest degree of cementation in these islands is usually found beneath the water table (e.g., Budd, 1988), as is also true of the Holocene deposits on larger islands (e.g., McClain et al., 1992). While many of these

Holocene islands are primarily oolitic, subaerially exposed Holocene stillstand-phase deposits on Bahamian islands are usually peloidal and bioclastic.

Karst processes

The subsurface hydrology of the Bahamian Archipelago is complex. In Chapter 4, Whitaker and Smart describe in detail the complexities of the freshwater lens, its flow dynamics, and its chemistry in Bahamian islands, and their Case Study concerns the Bahamian blue holes. The discussion presented herein focuses on karst that is observable in the subaerial environment.

Dissolution of the carbonates of the Bahama islands has produced a karst landscape that is superimposed on the overall constructional landscape (Mylroie and Carew, 1995; Mylroie, et al., 1995a,b; and references therein). The four major categories of karst features of the Bahamas are: karren, depressions, caves, and blue holes. Karren are centimeter- to meter-scale features of dissolutional sculpturing of carbonate bedrock. Karren tends to be jagged on exposed rock surfaces, but smooth and curvilinear on soil-mantled surfaces. Small dissolution tubes carry water away from the karren. This entire zone of karren, small tubes, and soil is called the epikarst, which usually extends downward from the surface for tens of centimeters to a meter or more. A special type of karren, often called coastal phytokarst, but more properly termed biokarst (Viles, 1988), commonly occurs on coastal rocks affected by sea spray.

The large closed-contour depressions seen on Bahamian topographic maps typically are depositional lows, rather than the product of dissolution. Many extend below sea level, and they are commonly occupied by lakes of varying salinities (typically normal marine to hypersaline), depending on climate, season, lake size, and whether there are cave conduits or blue holes that connect them to the sea.

There are four common types of caves developed in Pleistocene rocks in the Bahamas: pit caves, flank margin caves, banana holes, and lake drains. Pit caves are vertical shafts that conduct water from the epikarst through the vadose zone to the water table (Mylroie and Carew, 1995; Mylroie et al., 1995b). Flank margin caves are subhorizontal voids produced in the discharging margin of a freshwater lens (Mylroie and Carew, 1995; Mylroie et al., 1995b). During the last interglacial sea-level highstand (~125 ka), the Bahama islands consisted only of eolian ridges, each of which had its own small freshwater lens. The zone of vadose/phreatic freshwater mixing at the top of the lens, and the freshwater/marine phreatic mixing zone at the base of the lens are known to be environments where enhanced dissolution is likely to occur (James and Choquette, 1984; Mylroie and Carew, 1995; and references therein); so, at the lens margin where those two zones are superimposed, there is even greater potential for dissolution (Mylroie and Carew, 1995, and references therein). At the end of the last interglacial, these caves were abandoned as sea level and the freshwater lens fell. These caves commonly can be entered today through erosionally produced entrances along the flanks of many eolianite ridges.

Banana holes are ovoid depressions found in the Sangamon Terrace terrain of the Bahamas (Harris et al., 1995; Wilson et al., 1995). They are commonly a few meters

deep and up to 10 m wide. The walls vary from sloping sides, to near vertical or overhung. Some banana holes are connected to adjacent roofed chambers. Like flank margin caves, these voids developed during the last interglacial, but they formed just beneath the surface of a shallow freshwater lens rather than at the lens margin. At the end of the last interglacial, these caves were drained. Subsequent roof collapse coupled with karren development on the exposed walls accounts for the variety of wall morphologies that are seen.

Lake drains are conduits that transmit tidally influenced water into and out of some lakes in the Bahamas (Mylroie et al., 1995b). The presence of these drains allows sufficient seawater to enter the lakes so that they maintain normal marine salinity where hypersaline conditions would otherwise develop. As these conduits are below present sea level, and are commonly too small for divers to enter, their morphology and origins are poorly understood.

Blue holes have been defined as, "...subsurface voids that are developed in carbonate banks and islands; are open to the earth's surface; contain tidally influenced waters of fresh, marine, or mixed chemistry; extend below sea level for a majority of their depth; and may provide access to submerged cave passages" (Mylroie et al., 1995a, p. 231). Blue holes are further subdivided into ocean holes which open directly into the present marine environment, and inland blue holes that contain water of a variety of salinities (Mylroie et al., 1995a, and references therein; see also the Case Study of Chapter 4.).

Flank margin caves and banana holes are good indicators of past sea-level position because they form at the margin, or at the top, of a freshwater lens, respectively. They also developed very rapidly, in the 10–15 ky duration of the substage 5e sea-level highstand (Mylroie and Carew, 1995; Mylroie, et al., 1995b). Although the majority of the flank margin caves are developed in eolianites deposited prior to the interglacial associated with substage 5e (which formed the host islands in which these caves developed), banana holes and some flank margin caves are developed in carbonates deposited during substage 5e. These latter caves must have developed in transgressive or stillstand-phase deposits, during the regression from the acme of the last interglacial sea-level highstand (substage 5e). Flank margin caves and banana holes that are accessible today in the subaerial environment developed during the substage 5e highstand. Any flank margin caves or banana holes that formed during earlier highstands (pre-5e) are now below present sea level as a result of either a lower highstand position (relative to present) at the time of their formation, or subsequent isostatic subsidence of the Bahamas (Carew and Mylroie, 1995b).

Coastal processes

The coasts of Bahamian islands consist largely of rocky cliffs and sand beaches (Fig. 3A-4; see also 3A.12), but in some locales (such as the west coast of Andros Island) the lee sides may be flanked by tidal flats (Fig. 3A-5). Where coastal dynamics favor erosional processes, there are eroding Pleistocene and Holocene rocky cliffs, some of which have bioerosion notches (e.g., Salt Pond, Long Island)



Fig. 3A-4. Photograph of Grotto Beach on San Salvador Island illustrating the typical Bahamian island coastline consisting of rocky cliffs and sand beaches.

(Fig. 3A-6A). Throughout the Bahamas, there are numerous reentrants in the sides of Pleistocene eolianite ridges that have been considered to be fossil bioerosion notches formed during substage 5e. These reentrants are now recognized to be the eroded remnants of flank margin caves that have been largely removed by erosional retreat of the hillside that once contained them (Mylroie and Carew, 1991) (Fig. 3A-6B). The implications of this new interpretation are important because surface lowering of a few meters per 100 ky, which is in agreement with reported modern carbonate denudation rates (e.g., Ford and Williams, 1989, Tables 4-3 and 4-6), is sufficient to account for the several meters of hillside erosion necessary to reduce some flank margin caves to just the curving back wall. Such erosion would completely remove any bioerosion notches that had been on a hillside. Interpretation of these reentrants as "pristine" fossil bioerosion notches, which has been used to support a scenario that postulates extremely rapid sea-level fall at the end of the last interglacial (Neumann and Hearty, 1996), is incompatible with the interpretation that these reentrants are the eroded remnants of flank margin caves.

Tidal channels and creeks penetrate the shorelines of many islands, and there, tidal delta deposits may occur (e.g., Pigeon Creek, San Salvador Island; Deep Creek, South Andros Island). [The term "creek" in the Bahamas is derived from the British



Fig. 3A-5. Photograph showing an aerial view of a portion of the micritic tidal flats and creeks, western North Andros Island.

usage, and it refers to estuaries and restricted marine embayments, not surface streams.] Progradational strandplains have developed where there has been substantial deposition during the Holocene (Fig. 3A-7) (Garrett and Gould, 1984; Strasser and Davaud, 1986; Andersen and Boardman, 1989; Mitchell et al., 1989; Wallis et al., 1991; Carney et al., 1993, and references therein). An ever-changing distribution of depositional and erosional effects on the shorelines of Bahamian islands is the result of changes in offshore features such as reefs and shoals. Both depositional and erosional coastal features in the Bahamas show evidence of changing conditions that have occurred in a short time ($<10^2$ y), and with a nearly static sea-level position.

Particularly in the southeastern Bahamas, there is little evidence of cliffing of outcrops on the margins of lakes. Unlike the hillslopes above lake level, the original constructional slopes of dune swales that are the sites of the lakes are only slightly modified by coastal processes active at lake margins. This is because of the generally arid conditions that create hypersaline lakes wherein virtually no dissolution or bioerosion occurs (Mylroie et al., 1995b, and references therein).

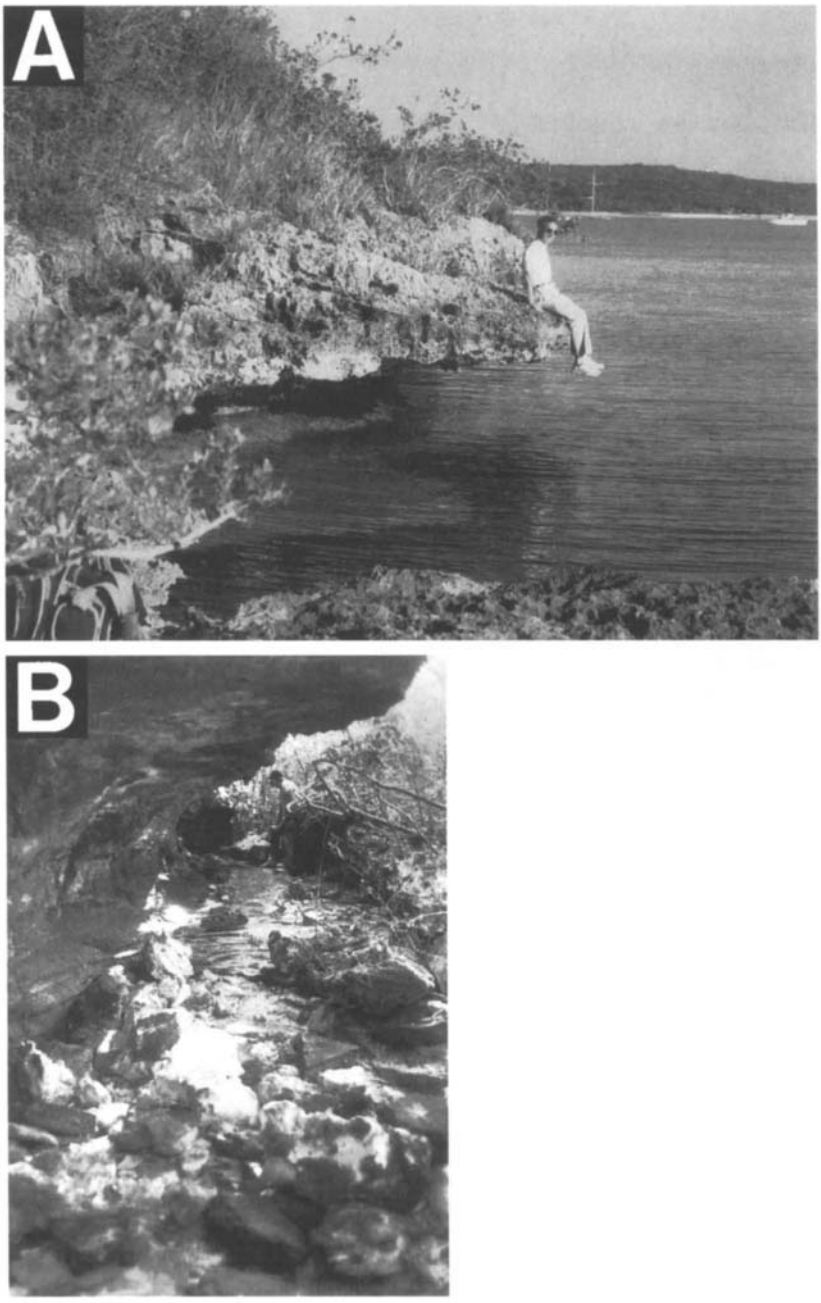


Fig. 3A-6. Photographs of modern and Pleistocene cliff-line notches. (A) A modern coastal bioerosion notch at Salt Pond, Long Island. (B) A notch in an inland cliff, San Salvador Island. Although the notch has the appearance of a coastal bioerosion notch, it is actually the remnant of the interior wall of a highly eroded flank margin cave. Note person in the center background for scale.



Fig. 3A-7. Aerial photograph of a Holocene strandplain with prominent accretionary beach ridges at Sandy Hook, southeastern San Salvador Island. North is at the top of the photograph.

QUATERNARY EVOLUTION OF BAHAMIAN ISLANDS

Overview

The Quaternary evolution of the Bahamian islands has been controlled largely by glacioeustatic sea-level fluctuations that affected both the deposition and subsequent alteration of the carbonate sediments. The quantitative record of Quaternary glacioeustasy is inferred largely from the deep-sea oxygen isotope record (e.g., Shackleton and Opdyke, 1973; Imbrie et al., 1984; Chappell and Shackleton, 1986; Shackleton, 1987) which is calibrated, in part, by the raised coral-reef terraces of Barbados and New Guinea. The shallow depth of the Bahamian bank margins (generally ~10 m) and the slow subsidence of the Bahamas during the Quaternary

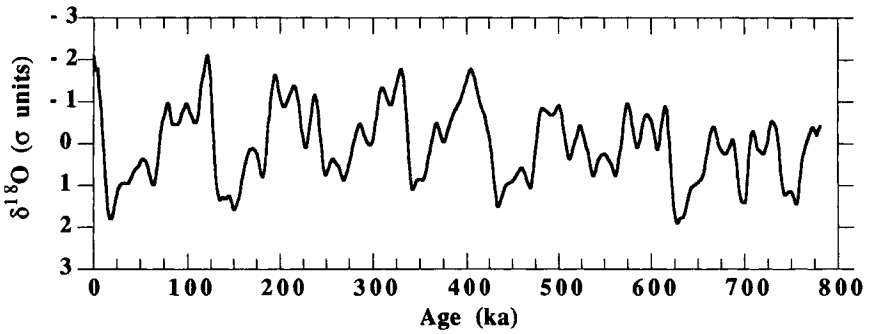


Fig. 3A-8. Variations in δ^{18} O from five deep-sea cores that were normalized, averaged, smoothed, and plotted on the SPECMAP time scale (Imbrie et al., 1984). The present high value of δ^{18}O represents the present highstand (stage 1); the earlier extreme low (~15 ka) is stage 2, the Wisconsinan lowstand, estimated to have been at −125 m; the peak at ~125 ka is the acme of the stage 5 (substage 5e) sea-level highstand which is commonly estimated to have been at about +6 m. The two lesser peaks younger than 5e are 5c and 5a. (From Imbrie et al., 1984.)

dictate that sea level must be within ~10 m of its present position before the banktops begin to flood and the subtidal "carbonate factory" produces abundant sediment. The isotope-derived sea-level curve (Fig. 3A-8) indicates that, for most of the Quaternary, sea level was at least 10 m below present datum (0.1 per mil change in δ^{18}O is equivalent to a 10 m change in sea level, Fairbanks and Matthews, 1978). In terms of Bahamian island evolution, therefore, the Quaternary has consisted primarily of long periods (10^5 years) of island emergence and subaerial diagenesis punctuated by short intervals (10^4 years) of submergence and substantial carbonate sediment production. Some carbonate sediment produced during banktop flooding remains in the shallow-marine environment, but much is exported off the banktops into deeper water (e.g., Droxler et al., 1988; Boardman and Neumann, 1984; Boardman et al., 1986; and references therein), or is reworked into beach sediment and subaerial dunes (Carew and Mylroie, 1995a). Terra rossa paleosols and erosion (karst) surfaces are formed largely during lowstands, but they develop at all times on exposed surfaces (Carew and Mylroie, 1985; 1995a).

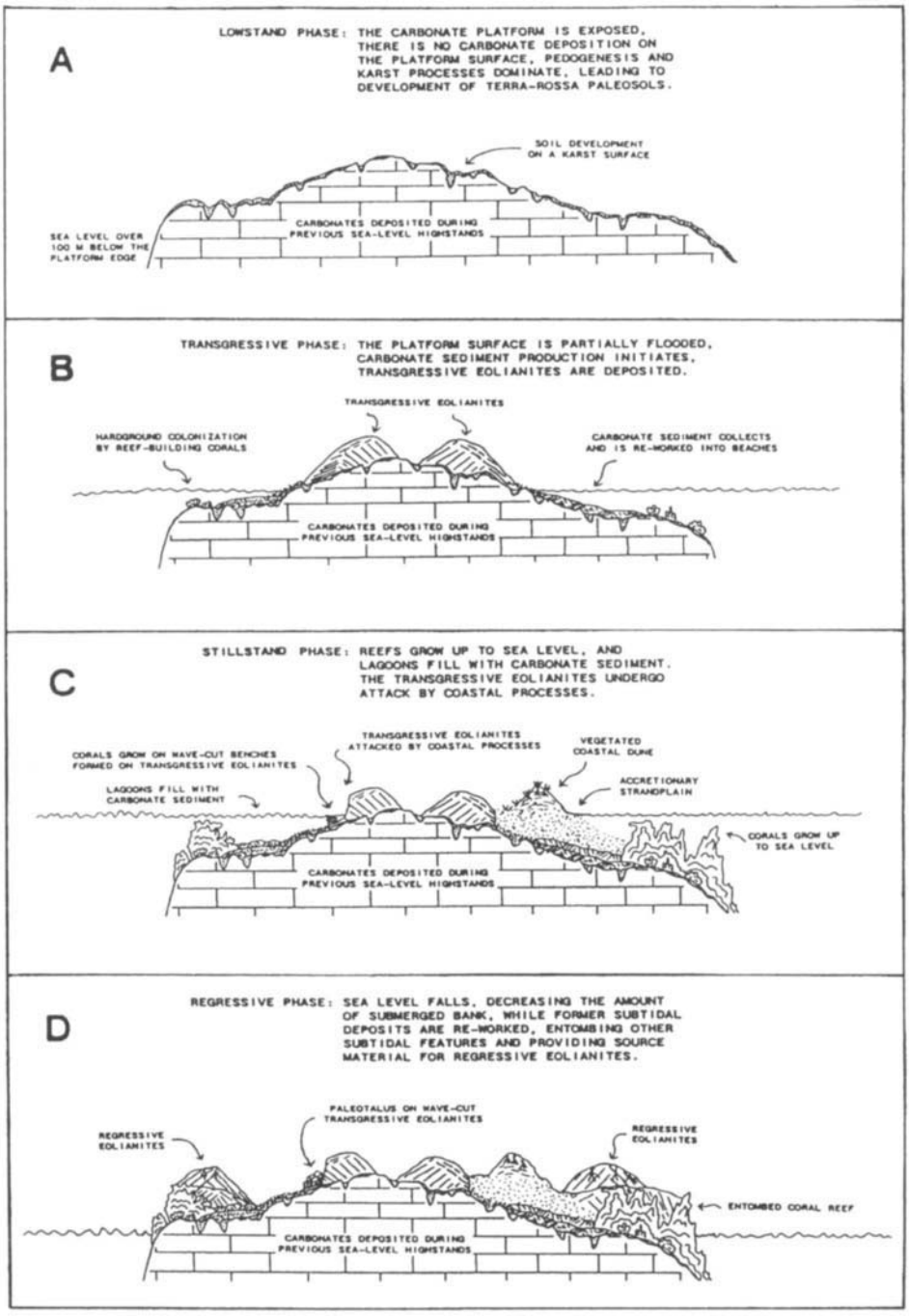
Prior to the present sea-level highstand (stage 1), the most recent previous highstand occurred during the last interglacial (Sangamon interglacial; substage 5e; ~125 ka). Numerous lines of evidence indicate that at that time sea level surpassed its present elevation by up to 6 m. During that highstand, significant deposits accumulated on Bahamian islands, including terrestrial (eolianites and lacustrine deposits) and marine beachface through subtidal deposits. Bahamian islands at that time consisted only of some of the existing eolianite ridges (e.g., Fig. 3A-9).

There are no known marine deposits that correlate with substages 5a or 5c. Elevations of sea-level highstands prior to the stage 5 interglacial (e.g., stages 7, 9, or 11) are less well known relative to stage 5 elevations, but the oxygen isotope record indicates that during the Pleistocene, sea level elevation was unlikely to have been higher than it was during stage 5 (Shackleton, 1987). The slow subsidence of the



Fig. 3A-9. Diagram showing San Salvador Island as it is today versus during the +6 m highstand of sea level, substage 5e ~125 ka. The black areas represent the 5e-highstand land masses. At that time all current Bahamian islands consisted of numerous small strip-islands composed of exposed eolianite ridges deposited during earlier highstands or during the transgressive phase of the 5e highstand. (Modified from Mylroie and Carew, 1990.)

Bahamas and inferred sea-level history of the Quaternary suggest that pre-5e marine deposits are unlikely to be exposed on Bahamian islands today (Carew and Mylroie, 1995b). It is possible, however, for pre-stage 5 eolianites to be exposed on Bahamian islands today because eolian sediments may be deposited more than 30 m above sea level at the time of deposition. These eolianites, however, have been subject to continuous erosion since their deposition unless they are buried and protected by deposits of younger highstands (Figs. 3A-10, 3A-11). Correlation of such deposits with a particular highstand (isotope stage) is difficult because of the spatially patchy nature of their accumulation. Moreover, sequential eolian deposits are often situated


A
LOWSTAND PHASE: THE CARBONATE PLATFORM IS EXPOSED, THERE IS NO CARBONATE DEPOSITION ON THE PLATFORM SURFACE, PEDOGENESIS AND KARST PROCESSES DOMINATE, LEADING TO DEVELOPMENT OF TERRA-ROSSA PALEOSOLS.
SOIL DEVELOPMENT ON A KARST SURFACE
CARBONATES DEPOSITED DURING PREVIOUS SEA-LEVEL HIGHSTANDS
SEA LEVEL OVER 100 M BELOW THE PLATFORM EDGE
B
TRANSGRESSIVE PHASE: THE PLATFORM SURFACE IS PARTIALLY FLOODED, CARBONATE SEDIMENT PRODUCTION INITIATES, TRANSGRESSIVE EOLIANITES ARE DEPOSITED.
TRANSGRESSIVE EOLIANITES
HARDGROUND COLONIZATION BY REEF-BUILDING CORALS
CARBONATE SEDIMENT COLLECTS AND IS RE-WORKED INTO BEACHES
CARBONATES DEPOSITED DURING PREVIOUS SEA-LEVEL HIGHSTANDS
C
STILLSTAND PHASE: REEFS GROW UP TO SEA LEVEL, AND LAGOONS FILL WITH CARBONATE SEDIMENT. THE TRANSGRESSIVE EOLIANITES UNDERGO ATTACK BY COASTAL PROCESSES.
TRANSGRESSIVE EOLIANITES ATTACKED BY COASTAL PROCESSES
VEGETATED COASTAL DUNE
CORALS GROW ON WAVE-CUT BENCHES FORMED ON TRANSGRESSIVE EOLIANITES
LAGOONS FILL WITH CARBONATE SEDIMENT
ACCRETIONARY STRANDPLAIN
CORALS GROW UP TO SEA LEVEL
CARBONATES DEPOSITED DURING PREVIOUS SEA-LEVEL HIGHSTANDS
D
REGRESSIVE PHASE: SEA LEVEL FALLS, DECREASING THE AMOUNT OF SUBMERGED BANK, WHILE FORMER SUBTIDAL DEPOSITS ARE RE-WORKED, ENTOMBING OTHER SUBTIDAL FEATURES AND PROVIDING SOURCE MATERIAL FOR REGRESSIVE EOLIANITES.
PALEOTALUS ON WAVE-CUT TRANSGRESSIVE EOLIANITES
REGRESSIVE EOLIANITES
REGRESSIVE EOLIANITES
ENTOMBED CORAL REEF
CARBONATES DEPOSITED DURING PREVIOUS SEA-LEVEL HIGHSTANDS

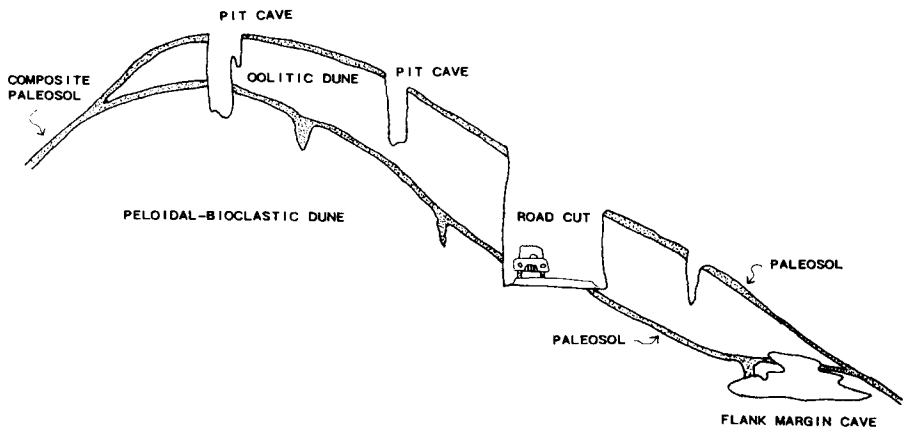


Fig. 3A-11. Potential onlap/overlap between eolianites deposited during separate sea-level highstands (e.g., substage 5e and earlier) and intervening terra rossa paleosols that accumulate largely when sea level is below the banktops. Note the various views of these relationships afforded by flank margin caves, pit caves, and road cuts or cliff exposures. (From Carew and Mylroie, 1995a.)

lateral to one another — not necessarily atop one another, as is the more common situation among other sediment facies.

Depositional model

Unraveling the geologic history of surficial deposits in the Bahamas is made difficult by the discontinuous nature of surficial sedimentation, the variable geometry of eolian deposits, the relatively sparse exposures, and the lack of material suitable for high-precision age determinations. Despite these difficulties, the surficial geology of Bahamian islands can be placed into a conceptual framework when the products and processes of subsidence, sea-level change, subaerial diagenesis, and carbonate sedimentation are integrated. Detailed studies of the surficial geology over many

Fig. 3A-10. Four stages of development of Bahamian islands during a glacial/interglacial sea-level cycle. During highstands the islands are the highest portions of steep-walled banks with quasi-flat tops that are not inundated. During lowstands (below −10 m) the entire banks are the islands. (A) Lowstand phase: sea level is > 10 m below present sea level; only dissolution and pedogenesis are significant geologic processes. (B) Transgressive phase: sea level rises above −10 m; platform tops are inundated by the sea, the "carbonate factory" produces abundant sediment, and relatively unvegetated dunes form and prograde landward as sea level continues to rise to its acme. (C) Stillstand phase: sea level hovers around its maximum elevation (usually for ~10 ky to 15 ky); reefs catch-up and lagoons fill; some heavily vegetated dunes form. (D) Regressive phase: sea level falls; lagoonal sediments are remobilized and eroded, and heavily vegetated dunes form and commonly prograde over subtidal deposits. The regressive phase ends when sea level descends below the platform top (about −10 m). (From Carew and Mylroie, 1995a.)

years permits us to delineate four stages, or phases, of island development in the Bahamas: transgressive phase, stillstand phase, regressive phase, and a lowstand phase (Fig. 3A-10) (see Carew and Mylroie, 1995a for a more thorough discussion).

Transgressive phase. In the early stages of banktop flooding by rising sea level, substantial subtidal sediment is produced, transported by waves to beaches, and then into dunes (Boardman et al., 1987). Formation of ooids and coated-grains is common during this phase (Carew and Mylroie, 1985, 1995a, and references therein; Hearty and Kindler, 1993); and ooid production must have occurred largely along the shoreface, such as reported by Lloyd et al. (1987) at the Turks and Caicos Islands and Ward and Brady (1973) along the Yucatan coastline.

Carbonate dunes do not develop far from, or migrate away from, their beach sources (Bretz, 1960; Carew and Mylroie, 1985, 1995a); so, as shoreline processes are driven inland by rising sea level, they "bulldoze" large amounts of sediment into high arcuate dune ridges that are commonly nucleated on and extend laterally (catenary) from high grounds remaining from previous highstand deposits (Carew, 1983; Garrett and Gould, 1984) (Fig. 3A-12). The beaches and dunes are composed of new allochems plus reworked allochems (particularly from eolianites) formed earlier in the same highstand (Andersen and Boardman, 1989), but it is rare to

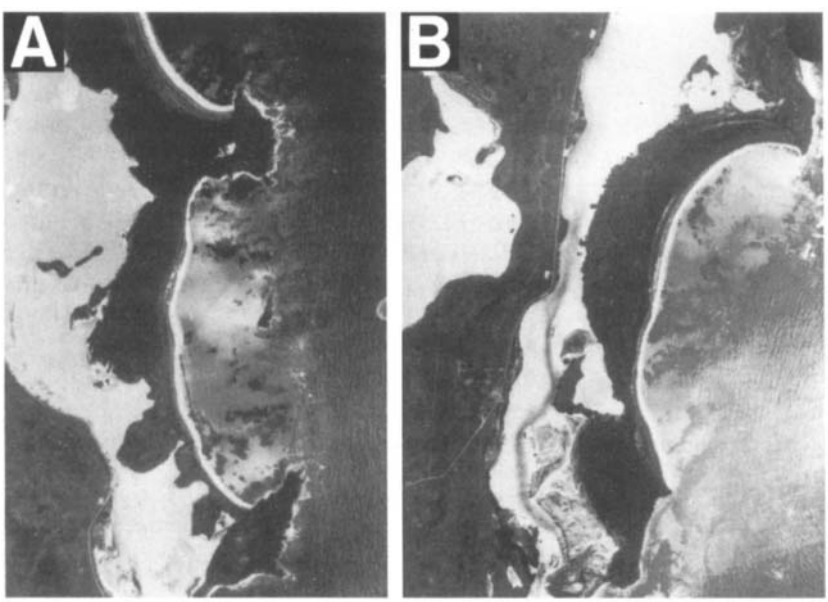


Fig. 3A-12. (A) Aerial photograph of a catenary eolianite ridge developed between two preexisting high grounds that acted as nucleation points, San Salvador Island. The ridge, bordered by a sand beach, extends southward from the rocky headland of Crab Cay to Almgreen Cay. (B) Aerial photograph of a comma-shaped eolianite ridge that is catenary on a rocky headland (The Bluff, San Salvador Island) at the north. This ridge is the same one seen in Fig. 3A-14.

encounter clearly identifiable reworked allochems from earlier highstands (Carew and Mylroie, 1995a). Because transgressive-phase dunes lie close to the shoreline for the duration of the highstand, they are subjected to the combined effects of sea spray and meteoric precipitation that promote rapid freshwater vadose (meniscus style) cementation, with occasional traces of marine cement (e.g., Halley and Harris, 1979; Strasser and Davaud, 1986; White, 1995).

Today on numerous Bahamian islands, because of continued rise of sea level since their emplacement, transgressive-phase Holocene eolianites have been subjected to marine erosion that has formed sea cliffs up to 20 m high (some of which contain sea caves) and subaerial and subtidal wave-cut benches, some of which are now colonized by corals and other taxa (Fig. 3A-13) (Carew and Mylroie, 1995a). In some places, beach progradation seaward of these eroded Holocene eolianites has produced inland cliffs (Fig. 3A-14). Eolianite deposition and marine erosion during a single highstand can be detected by the lack of a terra rossa paleosol between the transgressive-phase eolianite and later features (e.g., corals on a wave-cut bench, boulder rubble in a sea cave, regressive-phase eolianite). Truncated eolianite bedding covered by a terra rossa paleosol or calcrete indicates either: (1)



Fig. 3A-13. Photograph showing corals growing on a wave-cut platform carved into a Holocene transgressive-phase eolianite of the North Point Member on High Cay, San Salvador Island. In the background and right is the highly eroded transgressive-phase eolianite. Circular colonies of *Acropora palmata* in the foreground and center are nearly 4 m in diameter.



Fig. 3A-14. Photograph showing view to the northwest of an eroded transgressive-phase Holocene eolianite ridge of the North Point Member, and talus that has accumulated at the base of the cliff-line at Snow Bay, San Salvador Island. The windward half of the dune was eroded away by wave activity, and then apparent changes in coastal dynamics have led to accumulation of a sand beach seaward of the eroded eolianite ridge.

deposition and wave erosion during a single highstand, thus, a transgressive-phase eolianite (e.g., Fig. 3A-15A); or (2) deposition during one highstand, erosion on a subsequent highstand, and paleosol development during an ensuing lowstand (e.g., Fig. 3A-15B) (Carew and Mylroie, 1995a).

Holocene transgressive-phase eolianites have relatively few plant trace fossils, termed vegemorphs (Carew and Mylroie, 1995a), but they exhibit spectacular fine-scale (<1 mm) bedding such as sandflow, grainfall, and climbing wind-ripple cross laminae (e.g., White and Curran, 1988; Caputo, 1995) (Fig. 3A-16). Development of such laminae requires unobstructed windward slopes and lee slip faces, so they are not seen in the well-vegetated modern (stillstand phase) dunes in the Bahamas. Similar sedimentary architecture is also found among Pleistocene eolianites, especially those identified as transgressive phase (Caputo, 1993, 1995; and references therein). The transgressive-phase eolianites of the Bahama islands were probably sparsely vegetated because plant taxa adapted to mobile sand would have largely disappeared throughout the Bahamas during the preceding 100+ ky lowstand; hence, colonization would require recruitment from the North American mainland or Caribbean islands that do not have steep bank margins (Godfrey, pers. comm. 1994; Carew and Mylroie, 1995a). Direct analogs to these Holocene rocks and sediments can be seen in Pleistocene rocks (see Table 3A-1).

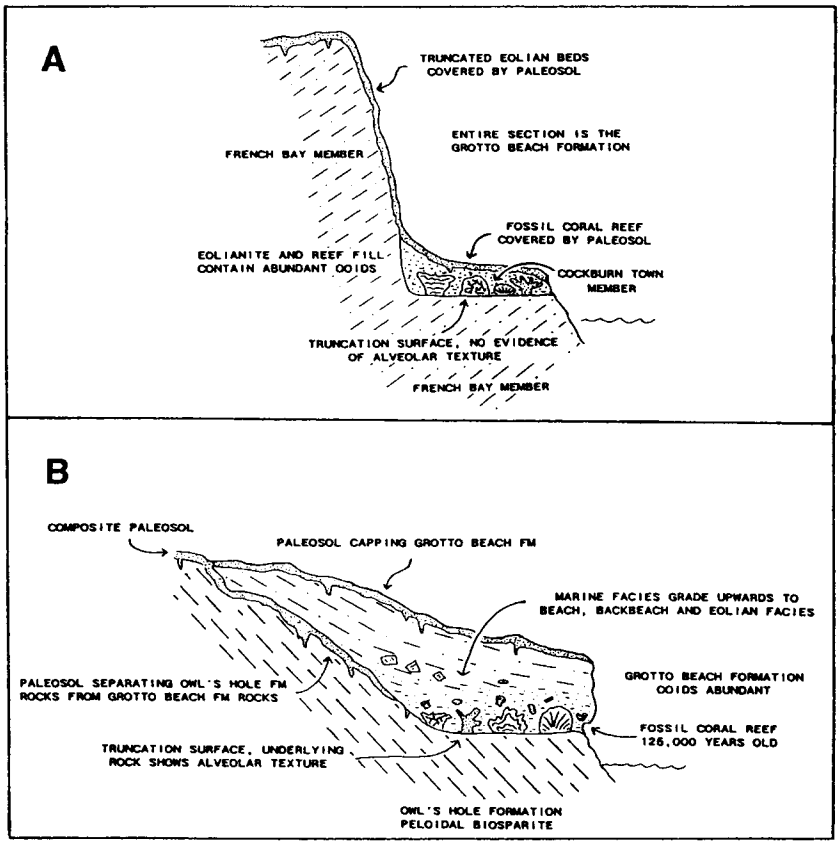


Fig. 3A-15. Diagrams illustrating the different temporal relationships that may occur where fossil reef deposits are seen to overlie a truncated eolianite. (A) Stratigraphic relationships at High Cay, South Andros Island, where corals are situated upon a wave-cut bench that was carved into the transgressive-phase French Bay Member later in the same highstand; this relationship is the same as that shown in Fig. 3A-13. (B) Stratigraphic relationships at Grotto Beach, San Salvador Island, where reefal deposits of the Grotto Beach Formation (substage 5e) are on an erosion surface developed on an eolianite of the pre-5e Owl's Hole Formation. (From Carew and Mylroie, 1995a.)

Stillstand phase. Using modern geological conditions as a guide, the scenario for the stillstand phase is as follows. During the acme of the highstand, when sea level remains relatively stable (e.g., the last 2–3 ky of the Holocene), carbonate sediment production remains high, reef growth catches up, and lagoons fill because of the quieter conditions behind reefs and transgressive-phase eolianite ridges (Carew and Mylroie, 1995a, and references therein). Much of the marine record on the islands is probably deposited during the stillstand phase. This is probably also a time of significant off-bank transport of bank-derived sediment, particularly early in the stillstand, before reefs become barriers to off-bank transport, and lagoons are filling. On the islands, strandplains and beaches develop, prograde into the subtidal, and

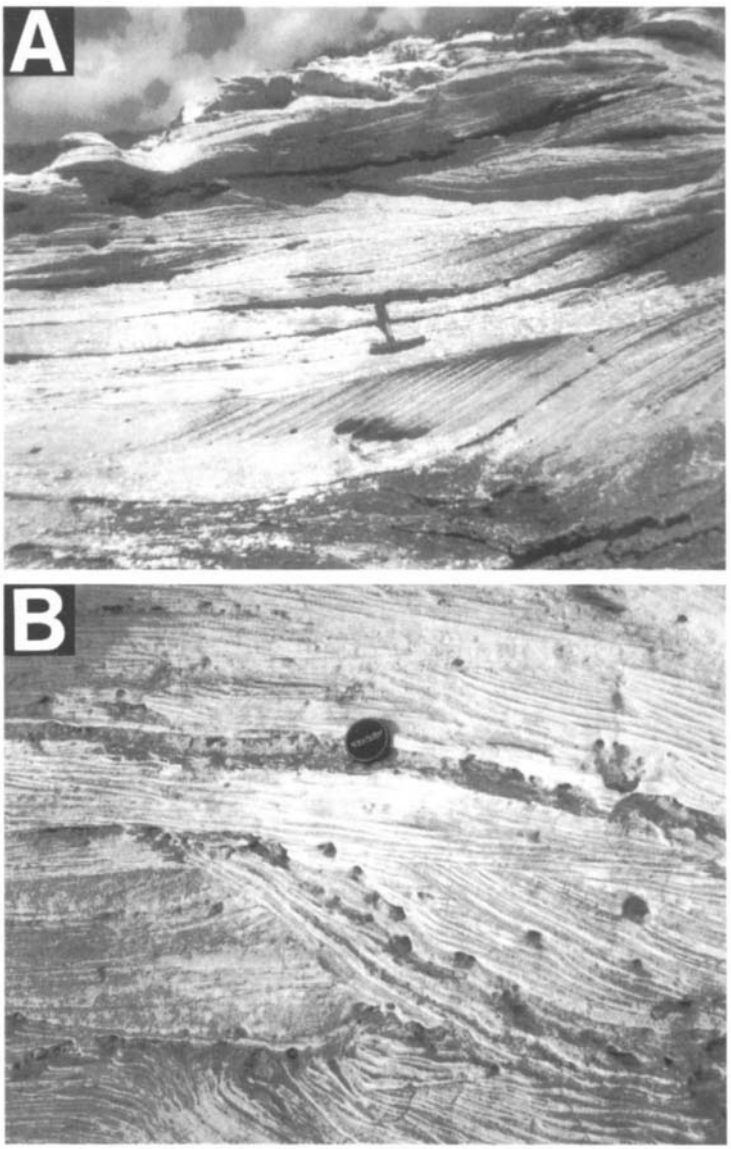


Fig. 3A-16. (A) Photograph of well-preserved fine-scale laminations in a Holocene transgressive-phase eolianite (North Point Member of the Rice Bay Formation, on Long Island). (B) Close-up view of the fine-scale laminations.

entomb subtidal deposits. Many stillstand-phase progradational deposits may be indistinguishable from regressive-phase deposits. Today in the Bahamas, shoreline deposits composed of lithified Holocene calcarenite blocks entombed in penecontemporaneous sand are common (Fig. 3A-17A). These facies indicate shoreline

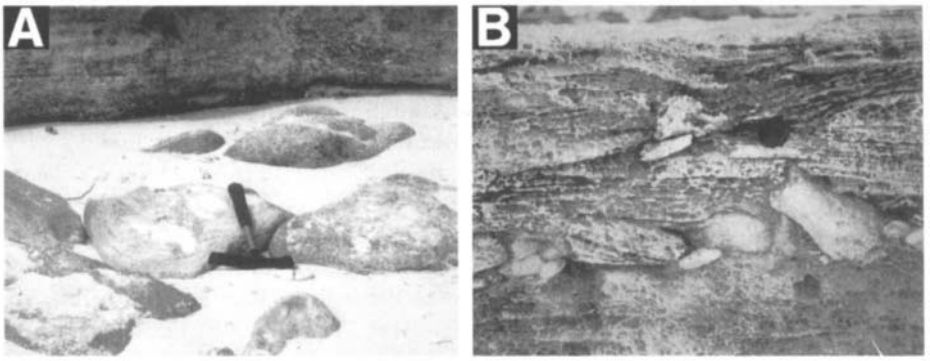


Fig. 3A-17. Photographs of shoreline breccia-block facies. (A) Blocks of lithified Holocene sediment (Hanna Bay Member of the Rice Bay Formation) partially entombed in modern sediment on Great Inagua Island. The allochems in the blocks and the enclosing sediment are indistinguishable from one another. (B) A shoreline breccia-block facies in the Pleistocene Cockburn Town Member (Grotto Beach Formation) at Sue Point, San Salvador Island. Again, the allochems of the blocks and entombing sediment are indistinguishable.

progradation and lithification followed by erosion to generate the blocks, and subsequent progradation that entombs the blocks. Similar deposits also occur in Pleistocene rocks (Fig. 3A-17B) (Carew and Mylroie, 1995a).

Table 3A-1

Characteristics associated with the transgressive (T), stillstand (S), and regressive (R) phases of the Quaternary depositional cycle

Characteristic	T	S	R
Eolian bedding preservation	fine scale	partially to highly disrupted	highly disrupted (esp. upper part)
Vegemorphs	few	abundant	extensive
Sea caves	penecontemporary	rare	none penecontemporary
Cliffing and boulder talus deposits	penecontemporary in beach and eolian facies	penecontemporary in back-beach to intertidal	no penecontemporary cliffing
Protosols	uncommon	common	common
Corals	on penecontemporary wave-eroded benches	not found on penecontemporary benches	no penecontemporary benches
Facies relationships	eolian facies dominant, onlapped by S and R deposits	marine facies abundant, shallowing-upward sequences	eolian facies dominant, often overstepping marine facies
Environments represented in exposed rocks	predominantly eolian, occasional beach facies	eolian, marine, strandplain, lacustrine, tidal deltas	predominantly eolian

During the stillstand phase, heavily vegetated coastal dunes develop (as they have in the Holocene), and protosols accumulate on transgressive-phase eolianites and in other locales (Carew and Mylroie, 1995a). Flood- and ebb-tidal delta deposits develop at passes between islands, and prograde at the mouths of some tidal creeks (e.g., Pigeon Creek, San Salvador Island). Inter-dune swales may contain lakes with ostracod and molluscan assemblages (Hagey and Mylroie, 1995; Noble et al., 1995; Teeter and Quick, 1990).

Regressive phase. Although we have no modern analog for the regressive phase, the following scenario can be inferred from the Pleistocene record. When sea level falls in response to renewed continental glaciation, beaches and their associated facies retreat toward the bank margin, and regressive-phase beach and dune deposits bury portions of the stillstand-phase marine deposits. As the shallow subtidal area is lessened, sediment production is reduced, but previously deposited subtidal sediment (including reefs) may be remobilized as the zone of shoreline processes retreats through them and removes some, or all, of the subtidal record. As the shorelines approach the bank margins, there may be a large pulse of bank-derived sediment



Fig. 3A-18. Photograph showing a calcarenite protosol that forms a horizontal protrusion in the center of this outcrop of regressive-phase eolianite of the Cockburn Town Member (Grotto Beach Formation) at The Bluff, San Salvador Island. (Photo previously published in Carew and Mylroie, 1995a.)

delivered to the deep environments off bank. Peloidal and bioclastic allochems will be important constituents of regressive-phase deposits where shoreline processes "chew-up" reefs and other subtidal deposits. Some of that sediment is reworked into regressive-phase dunes that may bury subtidal deposits that survive the passage through the retreating coastal zone (Carew and Mylroie, 1995a). Protosols commonly develop between times of major dune-building events during the stillstand and regressive phases (Fig. 3A-18; Table 3A-1). Regressive-phase dunes are likely to be well vegetated, and to bury vegetation, so regressive-phase eolianites commonly contain abundant vegemorphs and typically lack fine-scale bedding. Spectacular vegemorphs, often with abundant fossil pulmonate snails, are especially noted in the upper several meters of Pleistocene regressive-phase eolianites, where buried vegetation and roots provided preferred pathways for descending meteoric water (Fig. 3A-19) (Table 3A-1). Regressive-phase eolianites are occasionally seen to overlie fossil reefs (Fig. 3A-20). These regressive-phase eolianites generally should not be subjected to substantial wave erosion, as transgressive-phase eolianites are, but they may experience wave erosion during succeeding sea-level highstands.

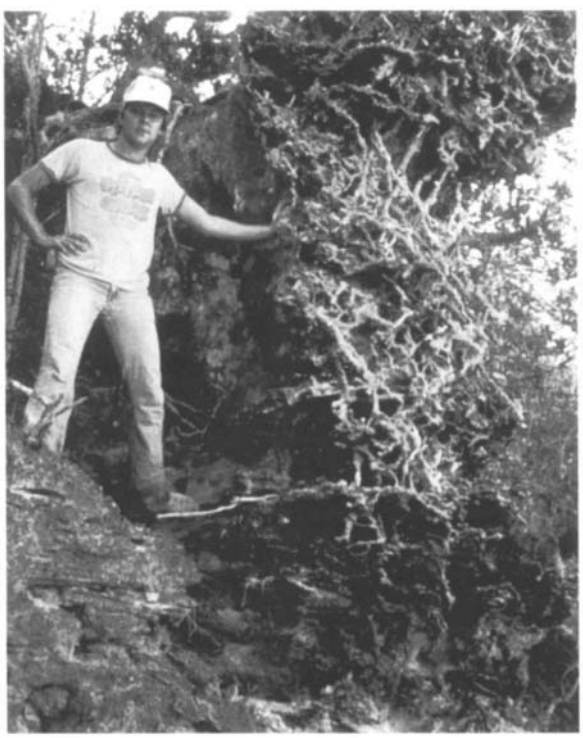


Fig. 3A-19. Photograph showing spectacular development of vegemorphs below the terra rossa paleosol that caps an exposure of regressive-phase eolianite of the Cockburn Town Member (Grotto Beach Formation) at Crab Cay, San Salvador Island. Such spectacular vegemorphs are usually associated with regressive-phase eolianites. (Photo courtesy of Jim Teeter.)

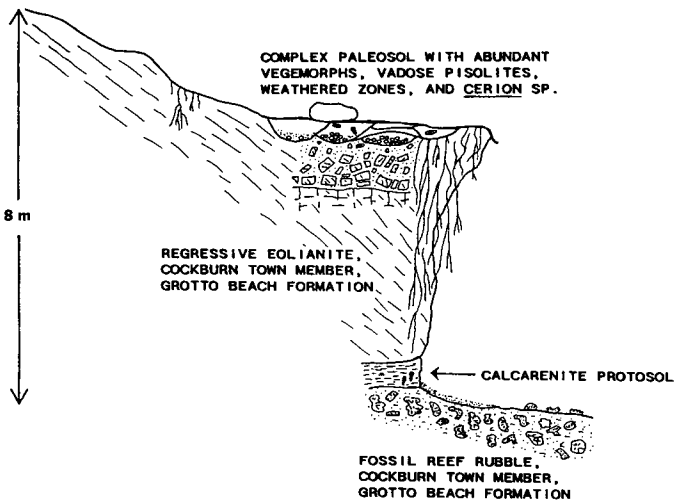


Fig. 3A-20. Facies of the Cockburn Town Member seen at The Gulf, San Salvador Island, where a regressive-phase eolianite and a calcarenite protosol overlie a substage 5e reef-rubble deposit that was probably torn up by wave action when sea level fell past an unprotected (not buried) reef during the regression from the stillstand of the 5e sea-level highstand. (From Carew and Mylroie, 1995a.)

Lowstand phase. Once sea level falls more than 10 m below its present position, the Bahama banks are largely subaerially exposed. From then until sea level again rises above −10 m, only subaerial diagenetic processes and products (e.g., terra rossa paleosol development, pedogenesis; dissolution, karstification; and cementation) occur on the banks/islands. As previously discussed, such exposure has been about an order of magnitude longer than the time that the banks have been flooded. For further details about Bahamian paleosols and karst see the discussion elsewhere in this chapter, and in Carew and Mylroie (1991, 1995a), Boardman et al. (1995), Foos and Bain (1995), Mylroie and Carew (1995), Mylroie et al. (1995b).

STRATIGRAPHY OF BAHAMIAN ISLANDS

Overview

Stratigraphic studies of the surficial deposits of the Bahamas have used a variety of geologic evidence to support various stratigraphic interpretations. The major types of evidence commonly used include products of depositional processes (e.g., sedimentary structures, landforms, facies distribution), products of subaerial diagenesis (e.g., soil formation, dissolution-precipitation of limestone), fossil content, geochronologic determinations, and predictions made from modern analogs. Each technique has strengths and weaknesses (Table 3A-2). Detailed interpretations of the depositional/erosional history of a Bahamian island may be attempted through the integration of as many of these lines of evidence as possible (e.g., Garrett and Gould,

Table 3A-2

Utility of various analytical methods and geologic evidence for interpretation of rocks exposed on Bahamian islands

Method	Utility	Difficulties	Relevant references
Paleosols	May mark stratigraphic boundaries.	May be misinterpreted.	20, 5, 7
Terra rossa	May separate deposits from different highstands.	Cave fills.	5
		Composite paleosols that represent more than one highstand/lowstand.	5
		Penetrative calcrete.	29
Calcarenite protosol	Identify pauses in deposition during highstand.	May be misinterpreted as surfaces that separate different highstands.	5, 10, 11
Petrology			
Allochems	May aid in identifying depositional environment or stratigraphic unit.	Extreme lateral variability; lack of time dependency.	30, 7, 21, 22
Cements and diagenesis	May be clues to depositional and post-depositional environment.	Extreme lateral variability and complex overprinting	28, 35, 7
Sedimentary structures	May aid in identifying depositional environment.		
Herringbone cross-bedding	Indicates subtidal deposits.		7
Fenestral porosity	May indicate intertidal deposits.	Also known from eolianites and other locales.	31, 32, 2
Paleontology			
Fossil coral	May indicate subtidal deposits.	Valid only in situ.	37, 7, 8
		Pristine reefs indicate rapid burial, not regression per se.	37, 16. 7

Table 3A-2

Contd

Method	Utility	Difficulties	Relevant References
Trace fossils	Can identify terrestrial, intertidal, and subtidal facies.	Must be congnizant of appropriate traces.	13, 14, 36, 11
Cerion	May be useful to identify stratigraphic units.	Common lack of morphologic distinction between units; individual islands differ.	15, 19, 23
Marine, lake, or terrestrial shells	May indicate marine, lake, or terrestrial deposits.	Hermit crabs and birds may dislocate shells.	17
Geochronology	May identify times of deposition.	Variable reliability among methods.	7
Carbon-14	Reliable for Holocene.	Yields allochem ages, not time of deposition.	1, 3, 7
Uranium-series	Useful for fossil coral and speleothems.	Alpha-count vs TIMS. Need unaltered material.	12, 7 12, 7
Paleomagnetics	May be useful to distinguish between terra rossa paleosols.	Young rock precludes reversals, so record of secular variation only, so resolution is difficult.	27, 7
Amino acid racemization	May help distinguish among units.	Correlation with other data is often poor.	
Cerion	Could be useful for deposits and paleosols.	Data is commonly unreliable.	24, 6, 7, 9
Whole-rock	May help distinguish among deposits.	Correlation with other data is often poor; yields composite allochem ages.	4, 18, 7

Table 3A-2

Contd

Geomorphology			
Karst	Older landforms may exhibit greater karst development.	Correlation of age and degree of karst development is not substantiated.	25, 26
Morphostratigraphy	May indicate sequence of development of landforms.	Field evidence is commonly contrary to hypothesis. Variable elevation of Quaternary sea levels scrambles relationships.	33, 15, 34, 18, 7, 9
Holocene Comparisons	Holocene deposits and relationships may provide a model for the Pleistocene.	Holocene not a complete cycle; regressive phase has not yet occurred.	7

References: 1, Andersen and Boardman (1989); 2, Bain and Kindler (1994); 3, Boardman et al. (1989); 4, Carew and Mylroie (1987); 5, Carew and Mylroie (1991); 6, Carew and Mylroie (1994b); 7, Carew and Mylroie (1995a); 8, Carew and Mylroie (1995b); 9, Carew and Mylroie (1995c); 10, Carew et al. (1992); 11, Carew et al. (1996); 12, Chen et al. (1991); 13, Curran (1984); 14, Curran and White (1991); 15, Garrett and Gould (1984); 16, Greenstein and Moffat (1996); 17, Hagey and Mylroie (1995); 18, Hearty and Kindler (1993); 19, Hearty et al. (1993); 20, James (1972); 21, Kindler and Hearty (1995); 22, Kindler and Hearty (1996); 23, Marcy et al. (1993); 24, Mirecki et al. (1993); 25, Mylroie and Carew (1995); 26, Mylroie et al. (1995b); 27, Panuska et al. (1995); 28, Pelle and Boardman (1989); 29, Rossinsky et al. (1992); 30, Schwabe et al. (1993); 31, Shinn (1967); 32, Shinn (1983); 33, Titus (1980); 34, Titus (1987); 35, White (1995); 36, White and Curran (1993); 37, White and Curran (1995).

Table 3A-3

Comparison of stratigraphies proposed for Bahamian islands

EPOCH	STAGE	Beach and Ginsburg 1980	Titus 1980[1]	Carew and Mylroie 1985	Titus 1987	Hearty and Kindler 1993	Carew and Mylroie 1995a	Kindler and Hearty 1996
HOLO-CENE	1	L	Recent sand	R.B. Fm	Unnamed Holocene	R.B. Fm E.B. Mbr	R.B. Fm	
		U		H.B. Mbr		H.B. Mbr	H.B. Mbr	Unit VIII
		C		N.P. Mbr		N.P. Mbr	N.P. Mbr	Unit VII
P	3	A		n.r.	G.L. Oolite	n.r.	**	n.r.
L	5a	Y	G.H. Ls	G.B. Fm	D.H. Ls	A.C. Fm[2]	**	Unit VI
E		A				Upper Mbr		
I		N		D.H. Mbr		Lower Mbr		
S						G.B. Fm	G.B. Fm	
T	5e	L			G.B.Ls	Fe.B.Mbr		Unit V
O		I		C.T.Mbr		C.T.Mbr	C.T.Mbr	
C		M	G.B. Ls	Fr.B. Mbr		Fr.B. Mbr	Fr.B. Mbr	Unit IV
E	7?	E				F.H. Fm		Unit III (Stage 7)
N	9?	S		O.H. Fm	Unnamed		O.H. Fm	
E	11?	T			Pre-Sangamonian	O.H. Fm n.r.		Unit II (Stage 7) Unit I (Stage 9?)

Abbrev: A.C., Almgreen Cay; C.T., Cockburn Town; D.H., Dixon Hill; E.B., East Bay; Fe.B., Fernandez Bay; Fr.B., French Bay; F.H., Fortune Hill; G.B. Grotto Beach; G.H., Grahams Harbour; G.L., Granny Lake; H.B., Hanna Bay; N.P. North Point; O.H., Owl's Hole; R.B., Rice Bay. n.r., no unit recognized in this position.

[1]Titus denoted his G.H. Ls and G.B. Ls only as Pleistocene, and made no correlation with oxygen isotope stages or absolute ages.

[2]Rocks assigned to the Almgreen Cay Formation by Hearty and Kindler (1993) are interpreted as regressive-phase deposits of the Grotto Beach Formation by Carew and Mylroie (1995a).

** No positively identifiable deposits at this position.

1984; Hearty and Kindler, 1993; Kindler and Hearty, 1996). However, because of the complexities created by the spatially patchy nature of deposition during highstands, differential erosion during lowstands, variability of amount and location of pre-existing high ground, and differences in sea level within and among highstands, such reconstructions are inherently interpretive — and possibly debatable (although provocative), or even wrong. On the other hand, our goal has been to develop a lithostratigraphic column for the Quaternary limestones of Bahamian islands (e.g., Carew and Mylroie, 1985, 1995a) that conforms to the Code of Stratigraphic Nomenclature (NACSN, 1983) and is based on criteria that can be utilized in the field, not only by ourselves but by others.

Beach and Ginsburg (1980) assigned all late Pliocene through Quaternary rocks in the Bahamas to the Lucayan Limestone (see Table 3A-3). The base of the Lucayan Limestone was defined biostratigraphically as coincident with the upper limit of the coral *Stylophora affinis* and a diagnostic molluscan assemblage equivalent to the Bowden Formation in Jamaica (Beach and Ginsburg, 1980; McNeill et al., 1988). The top of the Lucayan was defined as the present-day discontinuity surface, which is the land surface on Bahamian islands, and is recognized seismically beneath Holocene subtidal deposits on the submerged banks (Beach and Ginsburg, 1980). The thickness of the Lucayan Limestone is known to vary from about 43 m on Andros Island to as little as 10.5 m on Mayaguana Island (e.g., Cant and Weech, 1986). Magnetostratigraphic study of a core from San Salvador Island has suggested an age of 2.6–2.7 Ma (late Pliocene) for the base of the Lucayan Limestone (McNeill et al., 1988).

Studies of the surface geology of San Salvador Island led to abandonment of the term Lucayan Limestone for surficial rocks, because it was possible to recognize a more detailed stratigraphy. Moreover, the Lucayan as defined, mistakenly placed Holocene transgressive- and stillstand-phase rocks exposed on Bahamian islands within the Lucayan Limestone, while assigning currently-subtidal Holocene deposits to the post-Lucayan.

The first proposed stratigraphic column for the exposed rocks of a Bahamian island was that of Titus (1980) (see Table 3A-3). He interpreted the rocks of San Salvador Island as Pleistocene deposits that were laid down during sea-level regression from highstands. He made no suggestion concerning when in the Pleistocene they were deposited, and he indicated only that those units rested on pre-Pleistocene biomicrite.

In 1984, Garrett and Gould proposed phases of deposition for New Providence Island, but they did not tie the phases to a precise chronology or stratigraphy. The following year, we (Carew and Mylroie, 1985) proposed a revision to the stratigraphy of San Salvador (see Table 3A-3) because we recognized that: (1) much of the rock that Titus assigned to the Grahams Harbour Limestone, defined by Titus (1980), is Holocene rather than Pleistocene; (2) the rock cited as the type section for the Grahams Harbour Limestone does not correlate with the majority of rock assigned to that unit; (3) there is an older eolianite beneath Titus's Grotto Beach Limestone at its type locality and elsewhere; and (4) substantial portions of the rock record on San Salvador were deposited during the transgressive and stillstand phases of sea-level highstands, rather than only during the regression.

Later, Titus (1987) revised his stratigraphy to accommodate then-current information (see Table 3A-3), and later we revised our stratigraphy because amino acid racemization (AAR) data had been utilized (inappropriately) to define parts of our previous stratigraphic column (see Carew et al., 1992). Using morphostratigraphy and whole-rock AAR data, Hearty and Kindler (1993) proposed two additional formation-rank stratigraphic units and several members; more recently Kindler and Hearty (1996) proposed a total of eight units based on AAR data and petrology (see Table 3A-3). The units proposed by Hearty and Kindler (1993) were time-stratigraphic (hence interpretive) units, not lithostratigraphic units, despite their use of formal stratigraphic terminology (see discussion in Carew and Mylroie, 1994b, 1995a,c and Hearty and Kindler, 1994). More recently, Kindler and Hearty (1996) substituted a number designation for the proposed units of their interpretive history of Bahamian islands. [In Chap. 3B, Kindler and Hearty explicitly use a time-stratigraphic scheme. — Eds.]

Recently, it has been suggested (Kindler and Hearty, 1996) that it is possible to identify deposits formed during separate highstands of sea level, and derive the position of sea level at the time of deposition (relative to present sea level) based upon allochem composition of the rocks. Although there are some generalities that seem to apply to some of the surficial rocks of Bahamian islands, reliance on such criteria as grain composition is, we believe, inappropriately simplistic. Differences in allochem character are likely to represent differences, or changes, in source area during a single highstand, rather than deposition during different highstands and sea-level positions. On San Salvador Island, for example, the Holocene transgressive-phase eolianites (deposited when sea level was at least several meters below its present position) often contain abundant superficial ooids and coated grains, but they become progressively more peloidal/bioclastic up-section (Carney et al., 1993; White, 1995). This change may be related to the growth of reefs up to wave base, and subsequent change in lagoon dynamics.

Our stratigraphic column of the Bahamian islands consists of three major lithostratigraphic units (Carew and Mylroie, 1995a) (see Fig. 3A-21). As each of these units is a depositional package that is (or will be) bounded by unconformities, that largely represent times of low sea level, they are also allostratigraphic units (NACSN, 1983). As this stratigraphy was initially developed on San Salvador Island, the nomenclature refers to locales there, and all type locations are on San Salvador; however, the stratigraphy is applicable throughout the Bahamas, and has been used by us and other geologists on many other Bahamian islands (e.g., Andersen and Boardman, 1989; Curran and White, 1991; White and Curran, 1993, 1995; Carew and Mylroie, 1995a, and references therein; Kindler, 1995). A brief discussion of Bahamian stratigraphy follows; for a more thorough treatment see Carew and Mylroie (1995a).

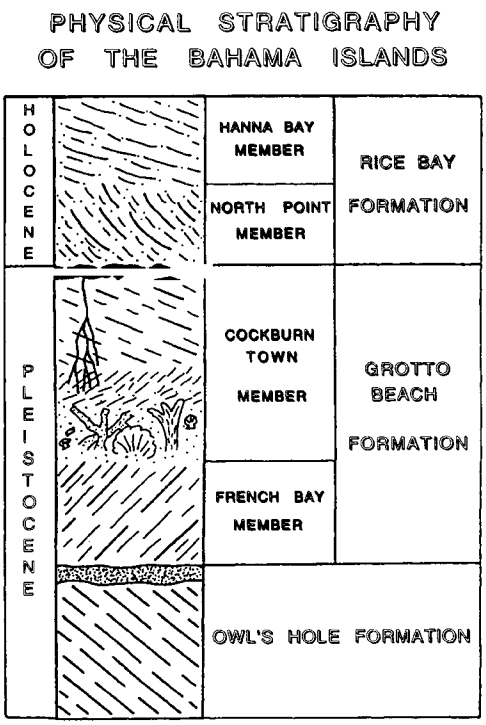


Fig. 3A-21. Lithostratigraphic column for the Bahama islands. In the field, individual units are not necessarily seen stacked atop one another, but are often found lateral to one another. The thin stippled and black layers are terra rossa paleosols, and they separate deposits formed during separate sea-level highstands. Where there are no intervening deposits such terra rossa paleosols represent the total time of one or more complete glacioeustatic sea-level cycles. (From Carew and Mylroie, 1995a.)

Nomenclature

Owl's Hole Formation. The oldest rocks exposed on Bahamian islands are assigned to the Owl's Hole Formation. By definition, the Owl's Hole Formation consists of eolianite that is capped by a terra rossa paleosol that can be shown to be overlain by either a highly oolitic eolianite that is itself capped by a second terra rossa paleosol, or by subtidal deposits (Carew and Mylroie, 1995a). The age of the interglacial sea-level highstand(s) during which these eolianites were deposited has not been conclusively established, but based on plausible isostatic subsidence rates, and the late Quaternary glacioeustatic history (Fig. 3A-8), they most likely represent one or more of the interglacial highstands associated with oxygen isotope stages 7 (~220 ka), 9 (~320 ka), or 11 (~410 ka) (Carew and Mylroie, 1995a). According to Kindler and Hearty (1995), eolianite deposits from two separate pre-5e interglacial highstands can be identified in exposures at the Cliffs section on Eleuthera Island.

In nearly all cases, Owl's Hole eolianites consist of fossiliferous pelsparites and peloidal biosparites (fossiliferous and peloidal grainstones) (Carew and Mylroie, 1995a; Kindler and Hearty, 1995), but oolitic rocks are also known from this unit, for example, on New Providence Island (Schwabe et al., 1993; Hearty and Kindler, 1995). Owl's Hole rocks are often extensively micritized at the exposed surface, but portions remain relatively weakly cemented. From detailed study of the wall rock of many caves in the eolianite ridges of several Bahamian islands, and the outcrop exposures of the ridges themselves, it has recently been shown that Owl's Hole rocks underlie many of the large Pleistocene eolianite ridges, and form more of the landscape of Bahamian islands than was previously thought (Schwabe et al., 1993; Carew and Mylroie, 1995a; Kindler and Hearty, 1995; and references therein).

Grotto Beach Formation. The most widespread depositional package exposed on Bahamian islands is the Grotto Beach Formation (Fig. 3A-21). It comprises eolianites and beach-face to subtidal marine limestones that, at places, can be subdivided into two members. The formation is capped by a terra rossa paleosol, except where it has been removed by later erosion. The Grotto Beach Formation contains exposed subtidal facies that are up to 5 m above modern sea level on numerous Bahamian islands, which is consistent with deposition during the substage-5e sea-level highstand (~132–119 ka, Chen et al., 1991; ~131–114 ka, Szabo et al., 1994; Carew and Mylroie, 1995b). Throughout the Bahamas, the transgressive-phase and some still-stand-phase eolianites of the Grotto Beach Formation are characterized by their abundant (up to 90% of the allochems) well-developed ooids that are similar to those seen at Joulter Cays today (Fig. 3A-22) (Carew and Mylroie, 1995a; Kindler and Hearty, 1995). Most of the subtidal facies and the regressive-phase eolianites of the Grotto Beach Formation are dominantly peloidal or bioclastic, but they com-

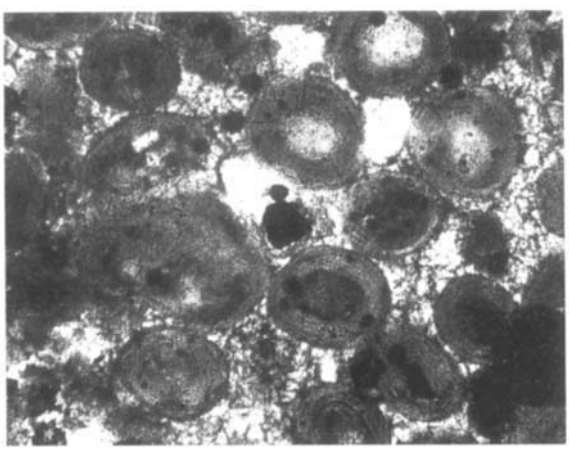


Fig. 3A-22. Photograph of thin section showing typical ooids from an eolianite of the Grotto Beach Formation on South Andros Island. Field of view is ~1.8 mm. (Photo previously published in Carew and Mylroie, 1995a.)

monly contain ooids, except where they are close to a source of bioclastic debris (Carew and Mylroie, 1995a). Also, in some localities, such as on North and South Andros, there are abundant late Pleistocene oolitic subtidal shoal/beach deposits. Kindler and Hearty (1996) have suggested that oolitic deposits on the present major islands imply that sea level was above the current datum at the time of deposition. If one projects such an interpretation to a future sea-level highstand that is a few meters lower than present, then the Holocene Joulter Cays oolitic deposits would be a part of the Andros Island geology, and they would be incorrectly interpreted to represent sea-level conditions higher than present. Furthermore, in our experience, ooids seem to be more common in transgressive-phase deposits, which are typically developed at a sea-level position below the acme of a highstand (see discussion of the French Bay and North Point members). Perhaps ooids are so abundant in rocks of the Grotto Beach Formation because that highstand (substage 5e) submerged the platform for a longer time and reached a higher elevation than stage 1 sea level; as a result, those deposits are disproportionately represented in the rocks exposed above sea level today.

French Bay Member. The French Bay Member comprises the transgressive-phase eolianites through beach facies of the Grotto Beach Formation (Carew and Mylroie, 1995a). These rocks are predominantly fine to medium oosparites (oolitic grainstones) that exhibit grain fall, grain flow, and climbing wind-ripple laminae, and limited vegemorph development (Table 3A-1). Additional evidence that these rocks were deposited during the transgressive phase include outcrops containing: (1) a fossil sea cave containing boulder rubble, (2) cliff-line paleotalus deposits, and (3) outcrops of overlying regressive-phase eolianites (Carew and Mylroie, 1985, 1995a). The French Bay Member can be recognized on many Bahamian islands (e.g., High Cay off South Andros Island; West Plana Cay; the Exuma islands; San Salvador Island). At all these places, fossil corals lie on a wave-cut surface carved into French Bay eolianites with no intervening paleosol, or evidence of an eroded paleosol (Fig. 3A-5A). Identical relationships can be seen today on some Holocene transgressive-phase eolianites (e.g., Fig. 3A-13).

Cockburn Town Member. The Cockburn Town Member comprises the subtidal and stillstand- through regressive-phase beach and eolian deposits of the Grotto Beach Formation (Carew and Mylroie, 1995a). Subtidal deposits extend up to ~5 m above current sea level, and commonly grade upward into, or are entombed by, stillstand- and regressive-phase beach and dune deposits (Carew and Mylroie, 1985, 1995a, b; White and Curran, 1995; Carew et al., 1996). The marine subtidal deposits of the Cockburn Town Member are recognized in the field by features such as herring-bone cross bedding, asymmetrical ripples (Fig. 3A-23), abundant fossil marine molluscs, corals and marine trace fossils (e.g., *Ophiomorpha*, see Fig. 3A-24), and by coral reefs. Curran and White (1985) provided a detailed map and cross section illustrating facies changes at Cockburn Town fossil reef on San Salvador Island, and White (1989) described and illustrated the Sue Point fossil reef (see Fig. 3A-25). The near pristine preservation of many fossil reefs in the Bahamas

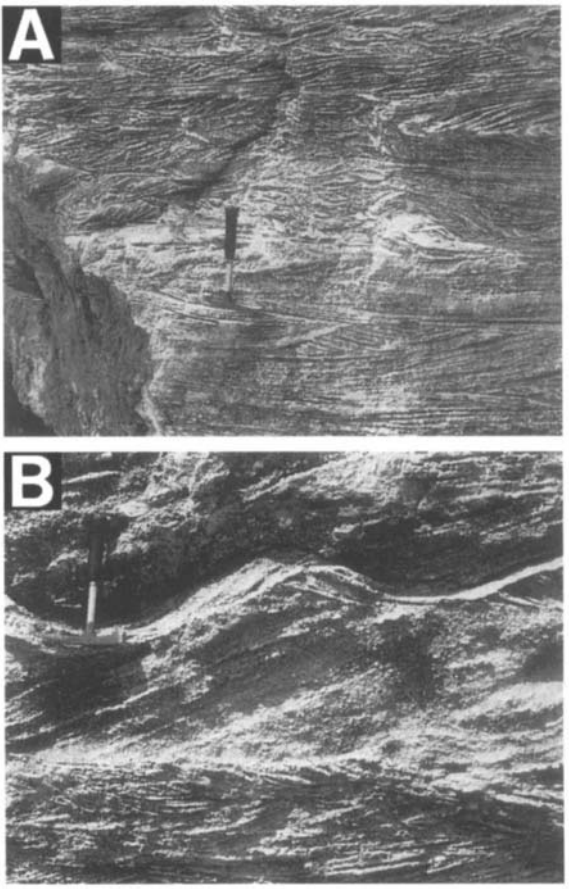


Fig. 3A-23. Photographs of outcrops showing cross bedding and ripples in subtidal facies of the Cockburn Town Member of the Grotto Beach Formation at Clifton Point, New Providence Island. (A) General view showing complex subtidal cross bedding. (B) Close-up view showing preserved ripple surface. (Photos previously published in Carew and Mylroie, 1995a.)

(Fig. 3A-25) indicates that they were catastrophically buried before the regression at the termination of the 5e highstand (Carew and Mylroie, 1995a, and references therein; Greenstein and Moffat, 1996). At the shoreline cliffs at Clifton on New Providence Island, subtidal shoal deposits can be seen to grade upward to beach facies (Garrett and Gould, 1984; Carew et al., 1992; Carew and Mylroie, 1995a; Carew et al., 1996). Precise mass-spectrometric $^{234}U/^{230}Th$ ages from fossil coral reefs on San Salvador and Great Inagua islands indicate that the substage-5e highstand lasted from about 132 to 119 ka (Chen et al., 1991). Data from in situ fossil coral reefs throughout the Bahamas are consistent with deposition during only that highstand (Carew and Mylroie, 1995b). White and Curran (1995) have suggested that there may have been a minor short-lived depression of sea level to at least

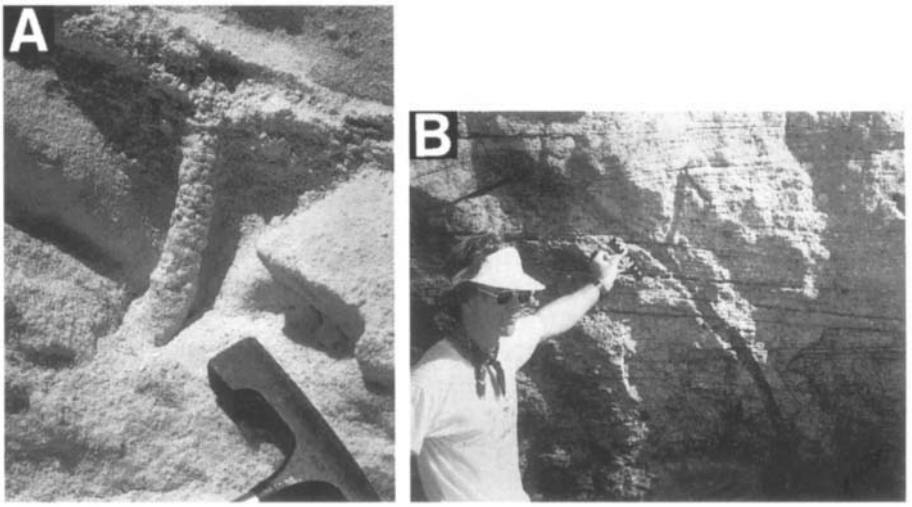


Fig. 3A-24. Photographs of ichnofossils seen in rocks of Bahamian islands. (A) An *Ophiomorpha* burrow (made by *Callianassa* sp., mud shrimp) in an ebb-tidal delta deposit of the Cockburn Town Member (Grotto Beach Formation) that crops out in North Pigeon Creek Quarry, San Salvador Island. This trace fossil is indicative of the shallow subtidal environment. A Y-shaped *Psilonichnus upsilon* burrow (made by *Ocypode quadrata*, ghost crab) in rocks of the Hanna Bay Member (Rice Bay Formation), at Hanna Bay, San Salvador Island. This trace fossil is indicative of the shoreface to backbeach environment.

the position of current sea level during the 5e highstand, and TIMS $^{234}U/^{230}Th$ dates from corals above and below the purported erosion surface indicate that the low may have lasted no more than 10^3 years centered at about 125 ka.

The stillstand through regressive-phase beach facies and eolianites are also assigned to the Cockburn Town Member because there is an unbroken gradation from marine to eolian rocks at many outcrops, and no terra rossa paleosol separates the marine and eolian facies (see Carew and Mylroie, 1995a). Eolianites of the Cockburn Town Member exhibit some, or all, of the following (Table 3A-1): disrupted internal bedding, calcarenite protosols, abundant vegemorphs, beach-face breccia facies, and eolianites overstepping fossil reefs; for examples, see Carew and Mylroie (1995a). Cockburn Town eolianites are commonly capped by elaborate paleosols with vadose pisolites, complex caliche/calcrete crusts, and abundant fossil pulmonate snails (mostly *Cerion*); unlike eolianites of the French Bay Member, eolianites of the Cockburn Town Member lack evidence of wave attack coeval with the highstand during which the dunes formed (Carew and Mylroie, 1995a). Subtidal shoal, lagoonal, and ebb-tidal delta deposits of the Cockburn Town Member occur up to ~5 m above present sea level on many Bahamian islands (e.g., Garrett and Gould, 1984; Titus, 1987; Carew et al., 1992, 1996; Carew and Mylroie, 1995a; Hagey and Mylroie, 1995; Noble et al., 1995; White and Curran, 1995; and references therein).

Formerly, we assigned some of the Grotto Beach Formation to a separate member (Dixon Hill Member) that was erroneously thought to have been deposited



Fig. 3A-25. Photograph of in situ *Acropora palmata* at Sue Point fossil reef, San Salvador Island. This superb preservation of elk horn coral in current-oriented growth position (inclined seaward) in the Cockburn Town Member of the Grotto Beach Formation indicates that it was protected by rapid burial before sea-level regression. (Photo previously published in Carew and Mylroie, 1995a.)

in association with substage 5a (Carew and Mylroie, 1985). We eliminated that member from our stratigraphy in 1992. For a more detailed discussion of this issue see Hearty and Kindler (1993, 1994) and Carew and Mylroie (1985, 1994a,b, 1995a,c).

Rice Bay Formation. The Holocene Rice Bay Formation comprises all rocks above the paleosol that caps the Grotto Beach Formation (Fig. 3A-21) (Carew and Mylroie, 1985, 1995a). Throughout the Bahamas, the Rice Bay Formation consists of eolianites and beach facies rocks that have been deposited during the transgressive and stillstand phases of the current sea-level highstand (stage 1). In places, two members can be recognized by differences in bedding character, allochem composition, and their position relative to current sea level (Carew and Mylroie, 1985, 1995a). Although there is some incipient development of thin calcretes (< 1 mm) on some transgressive-phase eolianites of the Rice Bay Formation, terra rossa paleosols are absent on Rice Bay rocks. However, calcarenite protosols are currently forming in coastal areas and in swales between and on transgressive-phase eolianites.

Unlike the commonly oolitic beach and dune facies of the Grotto Beach Formation, rocks of the Rice Bay Formation are characterized by: (1) a generally low abundance of ooids (usually less than 25%, rarely up to 50%), especially high in the section; (2) the superficial nature and small size of those ooids (i.e., only a few laminae); (3) dominance of peloids and bioclasts, especially in the Hanna Bay Member; (4) limited diagenetic micritization; and (5) generally weak, meniscus, low-Mg calcite cements (Carew and Mylroie, 1985, 1995a). Superficial-ooid production occurred during the early phase of the Holocene transgression of the San Salvador platform, but in most places ooid production seems to have ceased by ~3 ky B.P. At Joulter Cays, Schooner Cays, and elsewhere, there are abundant well-developed Holocene ooids, but more generally, the Rice Bay Formation lacks such ooids, even where ooid shoals are present offshore (e.g., east coast of South Andros Island).

North Point Member. The North Point Member comprises the transgressive-phase eolianites (Table 3A-1; Figs. 3A-3, 3A-13) of the Rice Bay Formation. These rocks are commonly peloidal, but superficial ooids are common low in the section. Most rocks of the North Point Member have meniscus calcite cement, but in coastal outcrops there is occasional marine cement (Carew and Mylroie, 1995a, and references therein ; White, 1995). At depth, these deposits are commonly uncemented. These eolianites were deposited when sea level was lower than at present, as indicated by steeply dipping foreset beds that continue at least 2 m below current sea level (Carew and Mylroie, 1985, 1995a). They are known on many Bahamian islands, but the most extensive deposits of this member that we have seen are found on Long Island.

Based solely on stratigraphic relationships, it was suggested that the North Point Member is <10 ky old (Carew and Mylroie, 1985). Radiocarbon ages obtained from whole-rock samples of North Point Member rocks range from 6.1 to 3.7 ky B.P., and average about 5 ky B.P. (Carew and Mylroie, 1995a; Boardman et al., 1987; Boardman et al., 1989). Apparently, significant sand was produced and incorporated into the North Point Member at a time that corresponds to the inflection on the Bahamian sea-level curve (see Boardman et al., 1989, Fig. 1; or Carew and Mylroie, 1995a, Fig. 17) that indicates the change to a slower rate of sea-level rise during the past ~4 ky.

Hanna Bay Member. The Hanna Bay Member comprises the stillstand-phase beach and eolian facies of the Rice Bay Formation. This member was initially limited to currently lithified rocks (Carew and Mylroie, 1985), but currently unlithified Holocene sediments and future regressive-phase deposits are now also considered to be part of the Hanna Bay Member, in similar fashion to the Cockburn Town Member of the Grotto Beach Formation (Carew and Mylroie, 1995a). This member consists largely of peloidal/bioclastic grainstones (except in ooid areas such as Joulter Cays) with predominantly meniscus low-Mg calcite cements. These rocks were deposited in equilibrium with current sea level; that is, lithified intertidal and beach facies of this member occur at the same elevation as corresponding facies of the modern beaches (Carew and Mylroie, 1985, 1995a). Radiocarbon ages of whole-

rock samples of the Hanna Bay Member range from ~0.3 to 3.2 ky B.P., and generally they are less than 2.5 ky B.P. (Boardman et al., 1987; Carew and Mylroie, 1995a). Rocks of the Hanna Bay Member are known on nearly all Bahamian islands and cays.

CONCLUDING REMARKS

The Quaternary depositional history of the shallow banks and islands of the Bahamas has been controlled principally by the glacioeustatic sea-level changes associated with glaciation and deglaciation of the continents. Significant production of carbonate allochems and mud occurred only when highstands of sea level flooded the bank tops (above −10 m). As a result, the sedimentary record on Bahamian islands consists of packages of transgressive-phase, stillstand-phase, and regressive-phase deposits that were produced during the highest (interglacial) stands of Quaternary sea level. Between those relatively short depositional intervals, only subaerial erosion and fallout of atmospheric dust occurred on the platforms. Soils that would become terra rossa paleosols thus developed on the exposed surfaces, and now usually intervene between deposits of successive interglacials.

As a result of the glacioeustatic control of limestone deposition in the Bahamas, the lithostratigraphic units of Bahamian islands are also allostratigraphic units that are usually bounded by terra rossa paleosols. Because of the current high elevation of sea level, and the slow isostatic subsidence (1–2 m per 100 ky), the only marine subtidal deposits exposed on Bahamian islands are those deposited during oxygen isotope Substage 5e (~125 ka). Besides those subtidal rocks, eolianites possibly deposited during oxygen isotope stages 11 (~410 ka), 9 (~320 ka), 7 (~220 ka), and beach facies through eolianites of stages 5 (~125 ka), and 1 (present) comprise the surficial rocks of the islands of the Bahamas. Based upon physical stratigraphy, the rocks of the Bahamian islands can be divided into three major units: the middle Pleistocene Owl's Hole Formation, the overlying late Pleistocene Grotto Beach Formation, and the Holocene Rice Bay Formation. The formal stratigraphy that was first developed on San Salvador Island (Carew and Mylroie, 1985, 1995a) is applicable to all other Bahamian islands known to us.

ACKNOWLEDGMENTS

We thank Dr. Donald T. Gerace (C.E.O.), Kathy Gerace, Dr. Dan Suchy (Executive Director), and the staff of the Bahamian Field Station for their logistical and financial support during the many years that we have worked in the Bahamas. Additional financial support has been provided by the University of Charleston, Mississippi State University, the Southern Regional Education Board, and the International Blue Holes Research Project. Bahamian government permission to conduct research in the Bahamas is greatly appreciated. Discussions with many colleagues have added to our understanding of, and led to clarification of our ideas

about the geology of the Bahamas, but only we are responsible for the ideas expressed herein. Over the years, John Goddard, Richard Lively, June Mirecki, Bruce Panuska, Sam Valastro, and John Wehmiller have provided us with geochronological data. We thank all our fellow carbonate enthusiasts with whom we have shared ideas, and we especially thank Roger Bain, Mark Boardman, Al Curran, Conrad Neumann, Neil Sealey, Peter Smart, Jim Teeter, Bob Titus, Len Vacher, Brian White, and Jude Wilber. We have also had the benefit of help from the many graduate and undergraduate students who have worked with us in the Bahamas. Reviews of earlier versions of this manuscript by Len Vacher, Terry Quinn, Pete Smart, David Budd, and three anonymous reviewers are appreciated. We thank Joan Newell for help with drafting and word processing.

REFERENCES

Albury, P., 1975. The story of the Bahamas. St. Martin's Press, New York, 294 pp.

Andersen, C.B. and Boardman, M.R., 1989. The depositional evolution of Snow Bay, San Salvador. In: J.E. Mylroie (Editor), Proc. 4th Symp. Geol. Bahamas (1988). Bahamian Field Station, San Salvador, p. 7–22.

Aurell, M., McNeill, D.F., Guyomard, T. and Kindler, P., 1995. Pleistocene shallowing-upward sequences in New Providence, Bahamas: Signature of high-frequency fluctuations in shallow carbonate platforms. J. Sed. Res., B65: 170–182.

Bain, R.J. and Kindler, P., 1994. Irregular fenestrae in Bahamian eolianites: a rainstorm-induced origin. J. Sed. Res., A64: 140–146.

Ball, M.M., 1967a. Tectonic control of the configuration of the Florida-Bahama Platform. Trans. Gulf Coast Assoc. Geol. Soc., 17: 265–267.

Ball, M.M., 1967b. Carbonate sand bodies of Florida and the Bahamas. J. Sediment. Petrol., 37: 556–591.

Bathurst, R.C.G., 1975. Carbonate Sediments and Their Diagenesis. Elsevier, Amsterdam, 658 pp.

Beach, D.K. and Ginsburg, R.N., 1980. Facies succession of Pliocene-Pleistocene carbonates, northwestern Great Bahama Bank. Am. Assoc. Petrol. Geol. Bull., 64: 1634–1642.

Boardman, M.R. and Neumann, A.C., 1984. Sources of periplatform carbonates: Northwest Providence Channel, Bahamas. J. Sediment. Petrol., 54: 1110–1123.

Boardman, M.R., Neumann, A.C., Baker, P.A., Dulin, L.A., Kenter, R.J., Hunter, G.E. and Kiefer, K.B., 1986. Banktop responses to Quaternary fluctuations in sea level recorded in periplatform sediments. Geology, 14: 28–31.

Boardman, M.R., Carew, J.L. and Mylroie, J.E., 1987. Holocene deposition of transgressive sand on San Salvador, Bahamas (abstr.). Geol. Soc. Am., Abstr. with Prog., 19(7): 593.

Boardman, M.R., Neumann, A.C. and Rasmussen, K.A., 1989. Holocene sea level in the Bahamas. In: J.E. Mylroie (Editor), Proc. 4th Symp. Geol. Bahamas (1988). Bahamian Field Station, San Salvador, pp. 45–52.

Boardman, M.R., McCartney, R.F. and Eaton, M.R., 1995. Bahamian paleosols: Origin, relation to paleoclimate, and stratigraphic significance. In: H.A. Curran and B. White (Editors), Terrestrial and Shallow Marine Geology of the Bahamas and Bermuda. Geol. Soc. Am. Spec. Pap., 300: 33–49.

Bretz, J H., 1960. Bermuda: A partially drowned, late mature, Pleistocene karst. Geol. Soc. Am. Bull., 71: 1729–1754.

Budd, D.A., 1988. Aragonite-to-calcite transformation during freshwater diagenesis of carbonates: insights from pore-water chemistry. Geol. Soc. Am. Bull., 100: 1260–1270.

Budd, D.A. and Land, L.S., 1989. Geochemical imprint of meteoric diagenesis in Holocene ooid sands, Schooner Cays, Bahamas: correlation of calcite cement geochemistry with extant groundwaters. J. Sediment. Petrol., 60: 361–378.

Cant, R.V. and Weech, P.S., 1986. A review of the factors affecting the development of Ghyben-Hertzberg lenses in the Bahamas. J. Hydrol., 84: 333–343.

Caputo, M.V., 1993. Eolian structures and textures in oolitic-skeletal calcarenites from the Quaternary of San Salvador Island, Bahamas: A new perspective on eolian limestones. In: B.D. Keith and C.W. Zuppann (Editors), Mississippian Oolites and Modern Analogs. Am. Assoc. Petrol. Geol. Studies Geol., 35: 243–259.

Caputo, M.V., 1995. Sedimentary architecture of Pleistocene eolian calcarenites, San Salvador Island, Bahamas. In: H.A. Curran and B. White (Editors), Terrestrial and Shallow Marine Geology of the Bahamas and Bermuda. Geol. Soc. Am. Spec. Pap., 300: 63–76.

Carew, J.L., 1983. Geochronology of San Salvador. In: D.T. Gerace (Editor), Field Guide to the Geology of San Salvador, 3rd Ed. Bahamian Field Station, San Salvador, pp. 160–172.

Carew, J.L. and Mylroie, J.E., 1985. The Pleistocene and Holocene stratigraphy of San Salvador Island, Bahamas, with reference to marine and terrestrial lithofacies at French Bay. In: H.A. Curran (Editor), Pleistocene and Holocene Carbonate Environments on San Salvador Island, Bahamas. Geol. Soc. Am. Annu. Meet. Field Trip Guideb., Field Trip 2. CCFL Bahamian Field Station, Fort Lauderdale, pp. 11–61.

Carew, J.L. and Mylroie, J.E., 1991. Some pitfalls in paleosol interpretation in carbonate sequences. Carbonates and Evaporites, 6: 69–74.

Carew, J.L. and Mylroie, J.E., 1994a. Geology and Karst of San Salvador Island, Bahamas: a field trip guidebook. Bahamian Field Station, San Salvador, 32 pp.

Carew, J.L. and Mylroie, J.E., 1994b. Discussion of: Hearty, P.J. and Kindler, P. 1993. New Perspectives on Bahamian Geology: San Salvador Island, Bahamas. Journal of Coastal Research, 9: 577–594. J. Coastal Res., 10: 1087–1094.

Carew, J.L. and Mylroie, J.E., 1995a. Depositional model and stratigraphy for the Quaternary geology of the Bahama islands. In: H.A. Curran and B. White (Editors), Terrestrial and Shallow Marine Geology of the Bahamas and Bermuda. Geol. Soc. Am. Spec. Pap., 300: 5–32.

Carew, J.L. and Mylroie, J.E., 1995b. Bahamian archipelago tectonic stability: evidence from fossil coral reefs and flank margin caves. Quat. Sci. Rev., 14: 145–153.

Carew, J.L and Mylroie, J.E., 1995c. Rejoinder to Hearty, P.J. and Kindler, P., 1994, Straw men, glass houses, apples and oranges: a response to Carew and Mylroie's comment on Hearty and Kindler (1993), Journal of Coastal Research, 10(4), 1095–1105. J. Coastal Res., 11: 256–260.

Carew, J.L., Mylroie, J.E. and Sealey, N.E., 1992. Field guide to sites of geological interest, western New Providence Island, Bahamas; Field Trip Guidebook, 6th Symp. Geol. Bahamas. Bahamian Field Station, San Salvador, pp. 1–23.

Carew, J.L., Drost, D.M., Sealey, N.E. and Mylroie, J.E., 1995. Refracted images of Bahamian islands, and possible implications regarding the first landfall of Christopher Columbus. Bahamas J. Sci., 2: 29–33.

Carew, J.L., Curran, H.A., Mylroie, J.E., Sealey, N.E. and White, B., 1996. Field Guide to sites of geological interest, western New Providence Island, Bahamas. Bahamian Field Station, San Salvador, Bahamas, 36 pp.

Carney, C., Stoyka, G.S., Boardman, M.R. and Kim, N., 1993. Depositional history and diagenesis of a Holocene strand plain, Sandy Hook, San Salvador, Bahamas. In: B. White (Editor), Proc. 6th Symp. Geol. Bahamas (1992). Bahamian Field Station, San Salvador, pp. 35–45.

Chappell, J. and Shackleton, N.J., 1986. Oxygen isotopes and sea level. Nature, 324: 137–140.

Chen, J.H., Curran, H.A., White, B. and Wasserburg, G.J., 1991. Precise chronology of the last interglacial period: ^{234}U-^{230}Th data from fossil coral reefs in the Bahamas. Geol. Soc. Am. Bull., 103: 82–97.

Curran, H.A., 1984. Ichnology of Pleistocene carbonates on San Salvador, Bahamas. J. Paleont., 59: 312–321.

Curran, H.A. and White, B., 1985. The Cockburn Town fossil coral reef. In: H.A. Curran (Editor), Pleistocene and Holocene carbonate environments on San Salvador Island, Bahamas. Geol. Soc. Am. Annu. Meet. Field Trip Guideb., Field Trip 2. CCFL Bahamian Field Station, Fort Lauderdale, pp. 95–120.

Curran, H.A. and White, B., 1991. Trace fossils of shallow subtidal to dunal ichnofacies in Bahamian Quaternary carbonates. Palaios, 6: 498–510.

Curran, H.A. and White, B. (Editors), 1995. Terrestrial and Shallow Marine Geology of the Bahamas and Bermuda. Geol. Soc. Am. Spec. Pap. 300, 344 pp.

Dietz, R.S., Holden, J.C. and Sproll, W.P., 1970. Geotectonic evolution and subsidence of the Bahama platform. Geol. Soc. Am. Bull., 81: 1915–1928.

Dill, R.F., Shinn, E.A., Jones, A.T., Kelly, K. and Steinen, R.P., 1986. Giant subtidal stromatolites forming in normal salinity water. Nature, 324: 55–58.

Dravis, J., 1983. Hardened subtidal stromatolites, Bahamas. Science, 219: 385–386.

Droxler, A.W., Morse, J.W. and Kornicker, W.A., 1988. Controls on carbonate mineral accumulation in Bahamian basins and adjacent Atlantic Ocean sediments. J. Sediment. Petrol., 58: 120–130.

Eberli, G.P. and Ginsburg, R.N., 1987. Segmentation and coalescence of Cenozoic carbonate platforms, northwestern Great Bahama Bank. Geology, 15: 75–79.

Eberli, G.P. and Ginsburg, R.N., 1989. Cenozoic progradation of NW Great Bahama Bank – a record of lateral platform growth and sea level fluctuations. In: P.D. Crevello, J.L. Wilson, J.F. Sarg and J.F. Reed (Editors), Controls on Carbonate Platform and Basin Development. Soc. Econ. Paleontol. Mineral., Spec. Publ., 44: 339–355.

Emery, K.O. and Uchupi, E., 1972. Western North Atlantic Ocean: Topography, rocks, structure, water, life, and sediments. Am. Assoc. Petrol. Geol. Mem. 17, 532 pp.

Enos, P., 1974. Surface sediment facies map of the Florida-Bahamas plateau. Geol. Soc. Am., Map Ser., MC–5, 4 pp.

Fairbanks, R.G. and Matthews, R.K., 1978. The marine oxygen isotope record in Pleistocene corals, Barbados, West Indies. Quat. Res., 10: 181–196.

Field, R.M. and collaborators, 1931. Geology of the Bahamas. Geol. Soc. Amer. Bull., 42: 759–784.

Foos, A. and Bain, R.J., 1995. Mineralogy, chemistry, and petrography of soils, surface crusts, and soil stones, San Salvador and Eleuthera, Bahamas. In: H.A. Curran and B. White (Editors), Terrestrial and Shallow Marine Geology of the Bahamas and Bermuda. Geol. Soc. Am. Spec. Pap., 300: 223–232.

Ford, D., and Williams, P., 1989. Karst Geomorphology and Hydrology. Chapman and Hall, New York, 601 pp.

Garrett, P. and Gould, S.J., 1984. Geology of New Providence Island, Bahamas. Geol. Soc. Am. Bull., 95: 209–220.

Gebelein, C.D., 1976. Modern Bahamian platform environments. Geol. Soc. Am. Annu. Meet. Field Trip Guideb., 96 pp.

Greenstein, B.J. and Moffat, H.A., 1996. Comparative taphonomy of Modern and Pleistocene corals, San Salvador, Bahamas. Palaios, 11: 57–63.

Hagey, D. and Mylroie, J.E., 1995. Pleistocene lake and lagoon deposits, San Salvador Island, Bahamas. In: H.A. Curran and B. White (Editors), Terrestrial and Shallow Marine Geology of the Bahamas and Bermuda. Geol. Soc. Am. Spec. Pap., 300: 77–90.

Halley, R.B. and Harris, P.M., 1979. Fresh-water cementation of a 1,000 year old oolite. J. Sediment. Petrol., 49: 969–988.

Hardie, L.A. and Shinn, E.A., 1986. Carbonate depositional environments, modern and ancient, part 3: tidal flats. Colo. Sch. Mines Quart., 81: 1–74.

Harris, J.G., Mylroie, J.E. and Carew, J.L., 1995. Banana holes: Unique karst features of the Bahamas. Carbonates and Evaporites, 10: 215–224.

Harris, P.M., 1983. The Joulters ooid shoal, Great Bahama Bank. In: T.M. Peryt (Editor), Coated Grains. Springer-Verlag, Berlin, pp. 132–141.

Hearty, P.J. and Kindler, P., 1993. New perspectives on Bahamian geology: San Salvador Island, Bahamas. J. Coastal Res., 9: 577–594.

Hearty, P.J. and Kindler, P., 1994. Straw men, glass houses, apples and oranges: a response to Carew and Mylroie's comment on Hearty and Kindler (1993). J. Coastal Res., 10: 1095–1105.

Hearty, P.J. and Kindler, P., 1995. Sea-level highstand chronology from stable carbonate platforms (Bermuda and The Bahamas). J. Coastal Res., 11: 675-689.

Hearty, P.J., Kindler, P. and Schellenberg, S.A., 1993. The late Quaternary evolution of surface rocks on San Salvador Island, Bahamas. In: B. White (Editor), Proc. 6th Symp. Geol. Bahamas (1992). Bahamian Field Station, San Salvador, pp. 205–222.

Hine, A.C., Wilber, R.J., Bane, J.M., Neumann, A.C. and Lorenson, K.R., 1981a. Offbank transport of carbonate sands along open, leeward bank margins: northern Bahamas. Mar. Geol., 42: 327–348.

Hine, A.C., Wilber, R.J. and Neumann, A.C., 1981b. Carbonate sand bodies along contrasting shallow bank margins facing open seaways in northern Bahamas. Am. Assoc. Petrol. Geol. Bull., 65: 261–290.

Illing, L.V., 1954. Bahamian calcareous sands. Am. Assoc. Petrol. Geol. Bull., 38: 1–95.

Imbrie, J., Hays, J.D., Martinson, D.G., McIntyre, A., Mix, A.C., Morley, J.J., Pisias, N.G., Prell, W.L. and Shackleton, N.J., 1984. The orbital theory of Pleistocene climate: support from a revised chronology of the marine ^{18}O record. In: A.I. Berger et al. (Editors), Milankovitch and Climate, Part 1. Reidel, Dordrecht, pp. 269–305.

James, N.P., 1972. Holocene and Pleistocene calcareous crust (caliche) profiles: criteria for subaerial exposure. J. Sediment. Petrol., 42: 817–836.

James, N.P. and Choquette, P.W., 1984. Diagenesis 9: limestones - the meteoric diagenetic environment. Geosci. Canada, 11: 161–194.

Kindler, P., 1995. New data on the Holocene stratigraphy of Lee Stocking Island (Bahamas) and its relation to sea level history. In: H.A. Curran and B. White (Editors), Terrestrial and Shallow Marine Geology of the Bahamas and Bermuda. Geol. Soc. Am. Spec. Pap., 300: 105–116.

Kindler, P. and Hearty, P.J., 1995. Pre-Sangamonian eolianites in the Bahamas? New evidence from Eleuthera Island. Mar. Geol., 127: 73–86.

Kindler, P. and Hearty, P.J., 1996. Carbonate petrography as an indicator of climate and sea-level changes: new data from Bahamian Quaternary units. Sedimentol., 43: 381-399.

Lloyd, R.M., Perkins, R.D. and Kerr, S.D., 1987. Beach and shoreface deposition on shallow interior banks, Turks and Caicos Islands, British West Indies. J. Sediment. Petrol., 57: 976–982.

Lynts, G.W., 1970. Conceptual model of the Bahamian platform for the last 135 million years. Nature, 225: 1226–1228.

Marcy, D., Carew, J.L., Colgan, M.W. and Katuna, M.P., 1993. Biometrics of *Cerion* shells using a new computer method (abstr.). Bull. S.C. Acad. Sci., 55: 97.

McClain, M.E., Swart, P.K. and Vacher, H.L., 1992. The hydrogeochemistry of early meteoric diagenesis in a Holocene deposit of biogenic carbonates. J. Sediment. Petrol., 62: 1008–1022.

McNeill, D.F., Ginsburg, R.N., Shih-Bin, R.C. and Kirschvink, J.L., 1988. Magnetostratigraphic dating of shallow-water carbonates from San Salvador, Bahamas. Geology, 16: 8–12.

Meyerhoff, A.A. and Hatten, C.W., 1974. Bahamas salient of North America: Tectonic framework, stratigraphy, and petroleum potential. Am. Assoc. Petrol. Geol. Bull., 58: 1201–1239.

Milliman, J.D., 1974. Marine carbonates. Springer-Verlag, Berlin, 375 pp.

Milliman, J.D., Freile, D., Steinen, R.P. and Wilber, R.J., 1993. Great Bahama Bank aragonite muds: mostly inorganically precipitated, mostly exported. J. Sediment. Petrol., 63: 589–595.

Mirecki, J.E., Carew, J.L. and Mylroie, J.E., 1993. Precision of amino acid enantiomeric data from fossiliferous late Quaternary units, San Salvador Island, The Bahamas. In: B. White (Editor), Proc. 6th Symp. Geol. Bahamas (1992). Bahamian Field Station, San Salvador, pp. 95–101.

Mitchell, S.W., Baldwin, J.N., Buening, N. and Westell, B., 1989. Holocene depositional history of Conception Island, Bahamas. In: J.E. Mylroie (Editor), Proc. 4th Symp. Geol. Bahamas (1988). Bahamian Field Station, San Salvador, pp. 209–220.

Mullins, H.T. and Lynts, G.W., 1977. Origin of the northwestern Bahama Platform: Review and reinterpretation. Geol. Soc. Am. Bull., 88: 1447–1461.

Mylroie, J.E. and Carew, J.L., 1990. The flank margin model for dissolution cave development in carbonate platforms. Earth Surf. Processes and Landf., 15: 413–424.

Mylroie, J.E. and Carew, J.L., 1991. Erosional notches in Bahamian carbonates: bioerosion or ground water dissolution? In: R.J. Bain (Editor), Proc. 5th Symp. Geol. Bahamas (1990). Bahamian Field Station, San Salvador, pp. 185–191.

Mylroie, J.E. and Carew, J.L., 1995. Karst development on carbonate islands. In: D.A. Budd, A.H. Saller and P.M. Harris (Editors), Unconformities and Porosity in Carbonate Strata. Am. Assoc. Petrol. Geol. Mem. 63, pp. 55–76.

Mylroie, J.E., Carew, J.L. and Moore, A.I., 1995a. Blue holes: Definition and genesis. Carbonates and Evaporites, 10: 225–233.

Mylroie, J.E., Carew, J.L. and Vacher, H.L., 1995b. Karst development in the Bahamas and Bermuda. In: H.A. Curran and B. White (Editors), Terrestrial and Shallow Marine Geology of the Bahamas and Bermuda. Geol. Soc. Am. Spec. Pap., 300: 251–267.

Nelson, R.J., 1853. On the geology of the Bahamas and on coral formation generally. Q. J. Geol. Soc. London, 9: 200–215.

Neumann, A.C. and Hearty, P.J., 1996. Rapid sea-level changes at the close of the last interglacial (substage 5e) recorded in Bahamian island geology. Geology, 24: 775–778.

Neumann, A.C., Bebout, B.M., McNeese, L.R., Paull, C.K. and Paerl, H., 1989. Modern stromatolites and associated mats: San Salvador, Bahamas. In: J.E. Mylroie (Editor), Proc. 4th Symp. Geol. Bahamas (1988). Bahamian Field Station, San Salvador, pp. 235–251.

Noble, R.S., Curran, H.A. and Wilson, M.A., 1995. Paleoenvironmental and paleoecologic analyses of a Pleistocene mollusc-rich lagoonal facies, San Salvador Island, Bahamas. In: H.A. Curran and B. White (Editors), Terrestrial and Shallow Marine Geology of the Bahamas and Bermuda. Geol. Soc. Am. Spec. Pap., 300: 91–103.

NACSN [North American Commission on Stratigraphic Nomenclature], 1983. North American Stratigraphic Code. Am. Assoc. Petrol. Geol. Bull., 67: 841–875.

Panuska, B.C., Mylroie, J.E., Kirkova, J.T. and Carew, J.L., 1995. Correlation of paleosols on San Salvador Island using paleomagnetic directions. In: M.R. Boardman (Editor), Proc. 7th Symp. Geol. Bahamas (1994). Bahamian Field Station, San Salvador, pp. 82–88.

Pelle, R.C. and Boardman, M.R., 1989. Stratigraphic distribution and associations of trace elements in vadose-altered multicomponent carbonate assemblages. In: J.E. Mylroie (Editor), Proc. 4th Symp. Geol. Bahamas (1988). Bahamian Field Station, San Salvador, pp. 275-294.

Pentecost, A., 1989. Discovery of *Phormidium* stromatolites in Grahams Harbour, San Salvador, Bahamas. In: J.E. Mylroie (Editor), Proc. 4th Symp. Geol. Bahamas (1988). Bahamian Field Station, San Salvador, pp. 303–304.

Pierson, B.J. and Shinn, E.A., 1985. Cement distribution and carbonate mineral stabilization in Pleistocene limestones of Hogsty Reef, Bahamas. In: N. Schneidermann and P.M. Harris (Editors), Carbonate Cements. Soc. Econ. Paleont. Min. Spec. Publ., 36: 153–168.

Purdy, E.G., 1963. Recent calcium carbonate facies of the Great Bahama Bank: 1) Petrography and reaction groups; 2) Sedimentary facies. J. Geol., 71: 334–355, 472–497.

Reid, R.P. and Browne, K.M., 1991. Intertidal stromatolites in a fringing Holocene reef complex, Bahamas. Geology, 19: 15–18.

Rossinsky, V. Jr., Wanless, H.R. and Swart, P.K., 1992. Penetrative calcretes and their stratigraphic implications. Geology, 20: 331–334.

Schlager, W. and Ginsburg, R.N., 1981. Bahama carbonate platform - the deep and the past. Mar. Geol., 44: 1–24.

Schwabe, S.J., Carew, J.L. and Mylroie, J.E., 1993. Petrology of Bahamian Pleistocene eolianites and flank margin caves: Implications for late Quaternary island development. In: B. White (Editor), Proc. 6th Symp. Geol. Bahamas (1992). Bahamian Field Station, San Salvador, pp. 149–164.

Sealey, N.E., 1990. The Bahamas Today. MacMillan Education Ltd., London, 120 pp.

Sealey, N.E., 1991, Early views on the geology of the Bahamas: 1837-1931. In: R.J. Bain (Editor), Proc. 5th Symp. Geol. Bahamas (1990). Bahamian Field Station, San Salvador, pp. 203–207.
Shackleton, N.J., 1987. Oxygen isotopes, ice volume, and sea level. Quat. Sci. Rev., 6: 183–190.
Shackleton, N.J. and Opdyke, N.D., 1973. Oxygen isotope and paleomagnetic stratigraphy of equatorial Pacific core V28-238: Oxygen isotope temperatures and ice volumes on a 10^5 to 10^6 year scale. Quat. Res., 3: 39–55.
Shapiro, R.S., Aalto, K.R., Dill, R.F. and Kenny, R., 1995. Stratigraphic setting of a subtidal stromatolite field, Iguana Cay, Exumas, Bahamas. In: H.A. Curran and B. White (Editors), Terrestrial and Shallow Marine Geology of the Bahamas and Bermuda. Geol. Soc. Am. Spec. Pap., 300: 139–155.
Shattuck, G.B. and Miller, B.L., 1905. Physiography and geology of the Bahama islands. In: G.B. Shattuck (Editor), The Bahama Islands. Macmillan, New York, pp. 3–20.
Sheridan, R.E., Mullins, H.T., Austin, J.A., Jr., Ball, M.M. and Ladd, J.W., 1988. Geology and geophysics of the Bahamas. In: R.E. Sheridan and J.A. Grow (Editors), The Atlantic Coastal Margin, U.S. Geol. Soc. Am., The Geology of North America, I-2: 329–364.
Shinn, E.A., 1967. Practical significance of birdseye structures in carbonate rocks. J. Sediment. Petrol., 38: 215–223.
Shinn, E.A., 1983. Birdseyes, fenestrae, shrinkage pores, and loferites: a reevaluation. J. Sediment. Petrol., 53: 619–628.
Shinn, E.A., Lloyd, R.M. and Ginsburg, R.N., 1969. Anatomy of a modern carbonate tidal-flat, Andros Island, Bahamas. J. Sediment. Petrol., 39: 1202–1228.
Strasser, A. and Davaud, E., 1986. Formation of Holocene limestone sequences by progradation, cementation, and erosion: two examples from the Bahamas. J. Sediment. Petrol., 56: 422–428.
Supko, P.R., 1977. Subsurface dolomites, San Salvador, Bahamas. J. Sediment. Petrol., 47: 213–220.
Szabo, B.J., Ludwig, K.R., Muhs, D.R. and Simmons, K.R., 1994. Thorium-230 ages of corals and duration of the last interglacial sea-level high stand on Oahu, Hawaii. Science, 266: 93–96.
Teeter, J.W. and Quick, T.J., 1990. Magnesium-salinity relation in the saline lake ostracode *Cyprideis americana*. Geology, 18: 220–222.
Titus, R., 1980. Emergent facies patterns on San Salvador Island, Bahamas. In: D.T. Gerace (Editor), Field Guide to the Geology of San Salvador. CCFL Bahamian Field Station, Miami, pp. 92–105.
Titus, R., 1987. Geomorphology, stratigraphy, and the Quaternary history of San Salvador. In: H.A. Curran (Editor), Proc. 3rd Symp. Geol. Bahamas (1986). CCFL Bahamian Field Station, Fort Lauderdale, pp. 155–164.
Tucker, M.E. and Wright, V.P., 1990. Carbonate Sedimentology. Blackwell, Oxford, U.K., 482 pp.
Uchupi, E., Milliman, J.D., Luyendyk, B.P., Brown, C.O. and Emery, K.O., 1971. Structure and origin of the southeastern Bahamas. Am. Assoc. Petrol. Geol. Bull., 55: 687–704.
Viles, H.A., 1988. Organisms and karst geomorphology. In: H.A. Viles (Editor), Biogeomorphology. Basil Blackwell, New York, pp. 319–350.
Wallis, T.N., Vacher, H.L. and Stewart, M.T., 1991. Hydrogeology of a freshwater lens beneath a Holocene strandplain, Great Exuma, Bahamas. J. Hydrol., 125: 93–109.
Wanless, H.R., Tedesco, L.P., Rossinsky, V., Jr. and Dravis, J.J., 1989. Carbonate environments and sequences of Caicos platform. 28th Int. Geol. Cong., IGC Field Trip Guideb. T374. Am. Geophys. Union, Washington D.C., 75 pp.
Ward, W.C. and Brady, M.J., 1973. High-energy carbonates in the inner shelf, northeastern Yucatan peninsula. Trans. Gulf Coast Assoc. Geol. Soc., 23: 226–238.
White, B., 1989. Field guide to the Sue Point fossil coral reef San Salvador Island, Bahamas. In: J.E. Mylroie (Editor), Proc. 4th Symp. Geol. Bahamas (1988). Bahamian Field Station, San Salvador, pp. 353–365.
White, B. and Curran, H.A., 1988. Mesoscale physical sedimentary structures and trace fossils in Holocene carbonate eolianites from San Salvador Island, Bahamas. Sediment. Geol., 55: 163–184.

White, B. and Curran, H.A., 1993. Sedimentology and ichnology of Holocene dune and backshore deposits, Lee Stocking Island, Bahamas. In: B. White (Editor), Proc. 6th Symp. Geol. Bahamas (1992). Bahamian Field Station, San Salvador, pp. 181–191.

White, B. and Curran, H.A., 1995. Entombment and preservation of Sangamon coral reefs during glacioeustatic sea-level fall, Great Inagua Island, Bahamas. In: H.A. Curran and B. White (Editors), Terrestrial and Shallow Marine Geology of the Bahamas and Bermuda. Geol. Soc. Am. Spec. Pap., 300: 51–61.

White, K.S., 1995. An imprint of Holocene transgression in Quaternary carbonate eolianites on San Salvador Island, Bahamas. In: H.A. Curran and B. White (Editors), Terrestrial and Shallow Marine Geology of the Bahamas and Bermuda. Geol. Soc. Am. Spec. Pap., 300: 125–138.

Wilber, R.J., Milliman, J.D. and Halley, R.B., 1990. Accumulation of Holocene banktop sediment on the western margin of Great Bahama Bank: modern progradation of a carbonate megabank. Geology, 18: 970–975.

Wilson, P.A. and Roberts, H.H., 1992. Carbonate-periplatform sedimentation by density flows: a mechanism for rapid off-bank and vertical transport of shallow-water fines. Geology, 20: 713–716.

Wilson, W.L., Mylroie, J.E. and Carew, J.L., 1995. Caves as a geologic hazard: A quantitative analysis from San Salvador Island, Bahamas. In: B.F. Beck (Editor), Karst Geohazards: Engineering and Environmental Problems in Karst Terrane. Balkema, Brookfield IL, pp. 487–495.

This Page Intentionally Left Blank

Geology and Hydrogeology of Carbonate Islands. Developments in Sedimentology 54
edited by H.L. Vacher and T. Quinn
© 1997 Elsevier Science B.V. All rights reserved.

Chapter 3B

GEOLOGY OF THE BAHAMAS: ARCHITECTURE OF BAHAMIAN ISLANDS

PASCAL KINDLER and PAUL J. HEARTY

INTRODUCTION

For many years, studies on the makeup and stratigraphy of the Bahama islands were few compared to the vast literature dealing with modern geological processes and products in the region. Bahamian islands were generally considered simply as late Pleistocene oolitic buildups (e.g., Newell and Rigby, 1957; Bathurst, 1975), which were formally named the "upper interval of the Lucayan Limestone" by Beach and Ginsburg (1980). The covering of most land surface by thriving vegetation, the rarity of vertical succession of rock units, and the poor lateral continuity of deposits all probably contributed to the relative lack of interest in the geology of the islands. Beginning in the 1980s, and largely with work facilitated by the Bahamian Field Station on San Salvador Island, there has been an outpouring of papers on the Pleistocene and Holocene deposits of the islands. Part of this work is represented by papers in the recent Geological Society of America Special Paper on the Bahamas and Bermuda (Curran and White, 1995, editors). Carew and Mylroie provide a general review in Chapter 3A of this book.

In this chapter, we will focus on the three-dimensional mosaic making up the islands. We will use our stratigraphic scheme (Hearty and Kindler, 1993a; Kindler and Hearty, 1995, 1996), which differs from the formal lithostratigraphic column developed by Carew and Mylroie (1985, 1991a, 1995a). [See Chap. 3A, by Carew and Mylroie, for review of their column and their perspective on stratigraphic classification in the Bahamas. — Eds.]

It has become clear to us that there is variability amongst Bahamian islands with respect to their stratigraphic architecture, and that there are patterns to this variability. We see a more complete record, for example, on some types of islands than on others. Such observations lead us to present in this chapter a tentative classification of islands where we have found or expect to find different types of stratigraphic architecture. Although the classification is still a hypothesis, which we will be testing by studying more Bahamian islands, we include it here as an organizer and because we believe it provides a potential framework for (1) understanding Bahamian islands more fully, and (2) comparing Bahamian islands to other kinds of carbonate islands.

STRATIGRAPHIC BACKGROUND

During the 1980s, pioneer work on New Providence (Garrett and Gould, 1984) and San Salvador Islands (Titus, 1980, 1987; Carew and Mylroie, 1985, 1987) led to recognition of three limestone units separated by terra rossa paleosols. Carew and Mylroie (1985, 1987, 1995a) developed a lithostratigraphic column and nomenclature that they and others have applied widely. They interpret their three formations (descending order: Rice Bay, Grotto Beach, Owl's Hole) as Holocene, Sangamonian (oxygen isotope substage 5e), and pre-Sangamonian, respectively.

We have developed a stratigraphic scheme (Table 3B-1) that greatly expands on the column of Carew and Mylroie. As shown in Table 3B-1, we use an informal chronostratigraphic classification where unit names are derived from grain composition and interpreted age, and are expressed in terms of oxygen isotope stages and substages. We now recognize nine units, ranging in age from middle Pleistocene to late Holocene, and representing five (possibly six) separate interglacials, with multiple depositional events within interglacials. We first developed our scheme on San Salvador Island (Hearty and Kindler, 1993a) and have now expanded and extended it to several island groups (Hearty and Kindler, 1993b, 1997; Kindler and Hearty, 1995, 1996).

Our stratigraphy is based on integration of a variety of field and laboratory data. We have found that approaches to Bahamian stratigraphy based on a single kind of data are insufficient to resolve the complex succession that is present on the islands. We have used a multi-method approach including morphostratigraphy, geomorphology, sedimentology, petrography, paleopedology, and radiocarbon and amino-acid racemization (AAR) dating. Morphostratigraphic analysis using the principles of lateral accretion (Vacher, 1973) and headland anchoring of catenary ridges (Garrett and Gould, 1984) (see Hearty and Kindler, 1993a; Kindler and Hearty, 1996) was performed on aerial photos and topographic maps to establish a preliminary chronology of landforms and determine field sites. In the field, additional age information was given by the color and maturity of capping paleosols, the thickness of associated calcretes, and the development of karst features. Large- and small-scale sedimentary structures (e.g., beach cross-bedding; fenestrae) were used to reconstruct depositional settings and sea-level elevations. The constituent-particle composition of the limestone was used as an additional tool for correlating stratigraphic units within and between islands (Kindler and Hearty, 1996), and diagenetic features (cement fabrics and mineralogy, secondary porosity) gave information on early diagenetic environments (e.g., meteoric vs marine) and the possible age of the deposits (e.g., Friedman, 1964; Land et al., 1967). D-alloisoleucine/L-isoleucine (or A/I) ratios were measured on both whole-rock and terrestrial snail samples to further refine unit correlation and determine their relative age. Whole-rock radiocarbon dating was performed on a few Holocene samples (see Kindler and Bain, 1993, for discussion). The paper by Kindler and Hearty (1995) on northern Eleuthera illustrates how we piece outcrops together to interpret a composite succession of units (Fig. 3B-1).

The main geomorphic, petrographic, sedimentological, and geochemical features of all but the lowest of these units are in Kindler and Hearty (1996). The reader is referred there for details, especially Table 2 of that paper for island-by-island

Table 3B-1

Stratigraphy of Bahamian islands (modified from Kindler and Hearty, 1996)

Name (Unit of Kindler and Hearty, 1996)/Descriptive notes
Stage-1 bioclastic calcarenite (Unit VIII). Multiple generations of beach and eol. deposits. Usually rests on Pleist. limestones; locally overlies stage-1 oolite. Eol. ridges (>40 m elev. on Lee Stocking I.) capped by sandy brown soil and thick vegetation. Grains preponderantly bioclasts; some peloids and ooids, probably reworked. A/I[1] ~0.09.
Stage-1 oolite (Unit VII). Small unit, along island strandlines; partly submerged, low-elev. eolianite remnants. Predominantly superficial ooids and peloids. DG[2], I–II. Youthful morphology of landforms. A/I[1], ~0.1.
Substage-5a bioclastic calcarenites (Unit VI). Well-preserved eol. ridges on windward islands bordering shelf margin. Except for some basal samples that may contain reworked ooids, grains are pristine bioclasts, largely made of coral and red algae. Barely altered; DG[2], II; Mg-calcite retained in some samples; sparry cement rare. A/I[1], 0.29–0.31.
Early and late substage-5e oolites (Units IV and V). Occur throughout Bahamas, including the highest hill (63 m, Cat I.). Include two sets of fossil shoreline deposits, both with various features indicating reef, shoreface, foreshore and backshore (incl. eolian and washover) environments. Grains preponderantly thickly coated, tangential ooids and peloids, still aragonite; bioclasts rare, esp. in older unit. DG[2], III–IV. Associated karst features include vert. dissolution pits, but not the horiz. conduits and phreatic caves common in stage 9/11 limestones. A/I[1], 0.35–0.43.
Stage-7 bioclastic calcarenites (Units II and III). Seen in vert. superposition between 5e and 9/11 and older units in Eleuthera, where it consists of two bioclastic deposits separated by a sandy, orange protosol. Consists of altered bioclastic frags, mostly benthic forams and red algal debris. DG[2], IV; meteoric cements <10%; metastable minerals present in some samples; micrite envelopes rarely filled. A/I[1], 0.53–0.58.
Stage-9/11 oolitic-peloidal limestones (included in Unit I). Usually occur inside islands or at base of retreating seacliffs. On Eleuthera, constitute bulk of some high cliffs. Incl. two similar units showing marine and eolian facies, separated from each other by terra rossa or deeply karsted surface. Separated from younger rocks by mature paleosol. Oolitic-peloidal grainstones; typically <15% bioclasts. DG[2], IV; constituents commonly leached; several generations of meteoric and marine cements; some remaining aragonite. A/I[1], 0.64–0.68.
Stage-13(?) bioclastic calcarenites (not identified; Unit 0). Recently identified on n. Eleuthera where it occurs at base of seacliffs composed of stage-9/11 limestones. Consists of altered bioclastic fragments, mostly benthic forams and algal debris. Highly altered; DG[2], V; little primary porosity; several generations of meteoric cement; spar-filled micrite envelopes; no metastable minerals remain. Occurs below dark red, clay-rich soil.

1. Whole-rock AAR ratios, from Table 2 in Kindler and Hearty (1996).
2. Diagenetic grade, concept developed by Land et al. (1967).

summaries of the AAR data and Tables 3–10 for island-by-island and unit-by-unit petrographic data.

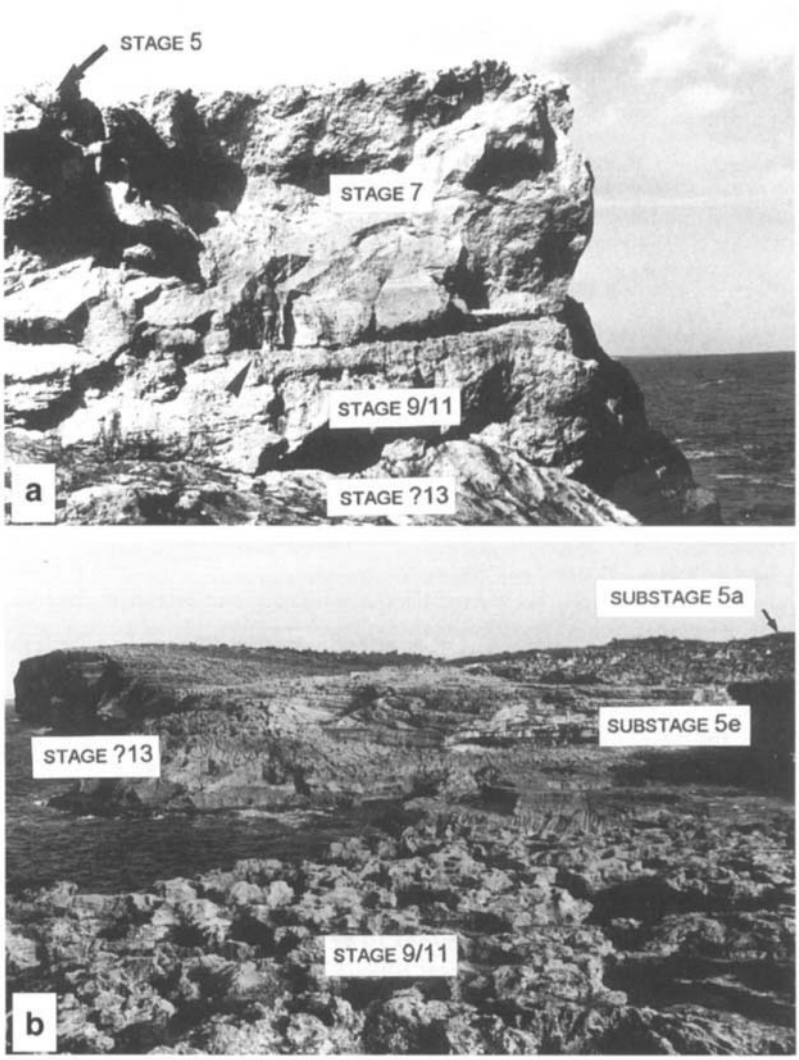
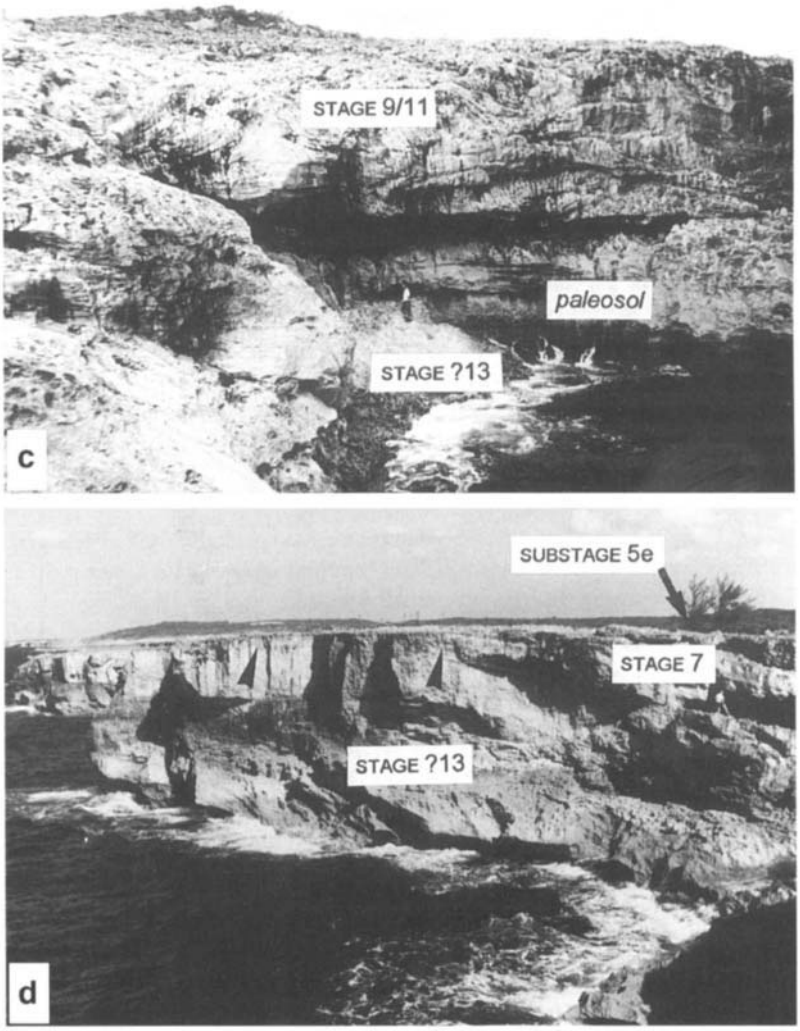


Fig. 3B-1. Outcrops in northern and central Eleuthera consist predominantly of vertically stacked middle and late Pleistocene limestone units separated by paleosols. Outcrop locations are shown on Fig. 3B-3; standing geologists are ~1.80 m tall. (a) Glass Window. Dark triangle points to well-developed paleosol between stage-7 and stage-9/11 units; cliff top is at 20 m. (b) Boiling Hole. Sangamonian deposits occur in a depression between middle Pleistocene units; background cliff height is 20 m. (Modified from Kindler and Hearty, 1995). (c) Goulding Cay. Heavily karstified stage-9/11 oolites overlie stage-?13 bioclastic calcarenites. A deep red, clayey, breccia-rich paleosol occurs at the contact. (d) The Cliffs. The entire cliff section consists of bioclastic calcarenites. Dark triangles point to major paleosol between stage-7 and stage-?13 units. (See Kindler and Hearty, 1995, for more detail).



BAHAMIAN ISLANDS

Geologists have long observed that Bahamian islands are mostly located close to the platform margins (e.g., Field et al., 1931; Newell and Rigby, 1957) and that oceanic setting (i.e., bottom topography, current regime) controlled the geometry of Holocene and Pleistocene sand bodies (Ball et al., 1967; Hine et al., 1981). We recognize also that islands and cays usually occur near the bank edges; however, they differ by their extension on the platforms, the width of the outer shelf, and, as stated

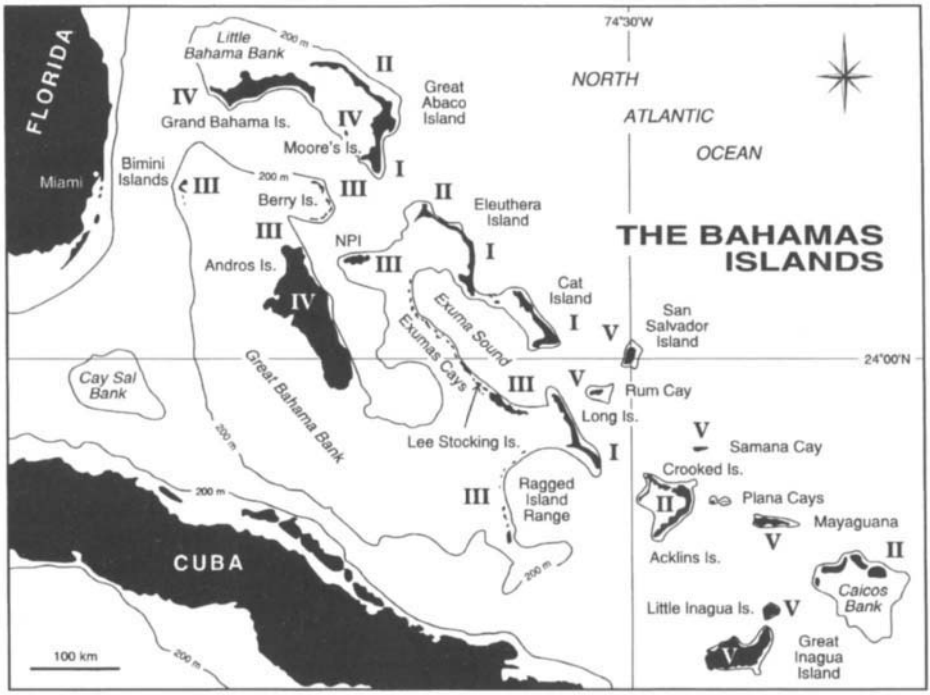


Fig. 3B-2. Preliminary classification of the Bahamas islands based on exposure to wind and wave energy, position and extension on the platforms. Six types (I-VI) have so far been recognized. Islands of the same type tend to show similar sedimentary architecture and stratigraphic successions. See text for explanation.

by Ball (1967), their exposure to open-ocean energy. We hypothesize that these variables can be used to construct an island classification scheme that will help to understand and forecast the surficial geology of Bahamian islands, because islands situated in a similar setting will likely show similar geologic features. On the basis of work we have done to date, we differentiate six categories (Fig. 3B-2). We summarize them here together with some examples from our experience.

This classification pertains to islands that consist largely of Pleistocene limestone. We are not considering Holocene cays, which, for our purposes, are "proto-islands."

Class I islands (e.g., Eleuthera, s. Abaco, Cat, Long Islands)

Class I islands (*windward islands — narrow, steep shelf*) are located on the windward margins of large platforms and are separated from the bank edge by narrow, steep, outer shelves. These islands are fully exposed to the high waves and winds of the open Atlantic Ocean. Class I islands are long, narrow and high, and are not fronted by offshore cays because of the steep gradient of the outer shelf. These islands usually display a complex record of vertically stacked deposits encompassing multiple interglacial periods.

Example: Northern Eleuthera Island. Figure 3B-3 shows the distribution of our stratigraphic units in a small part of northern Eleuthera. This map includes the area discussed by Kindler and Hearty (1995) and all but one of the outcrops shown in Figure 3B-1. Vertical stacking of stratigraphic units is typical in this region, so units that in other islands are found alongside of each other (lateral accretion) are seen in this area in vertical succession (vertical accretion). All the middle and late Pleistocene units we have identified so far in the Bahamas can be observed in the shoreline cliffs of this map area.

The vertical stacking is presumably due to increasing energy conditions since the middle Pleistocene. The pre-Sangamonian record is essentially made up of large eolianites that probably accumulated behind extensive beaches, when the outer platform was wider. Substage-5e oolites form washovers and small pocket beaches, which formed in the depressions between older dunes, but do not seem to have prograded seaward indicating a higher energy level than before. Such fair-weather beaches do not occur in this area today. Subrecent and Holocene sedimentation is limited to thick lobes of washover sands that were transported during storms over the seacliffs, which stand some 15 m high.

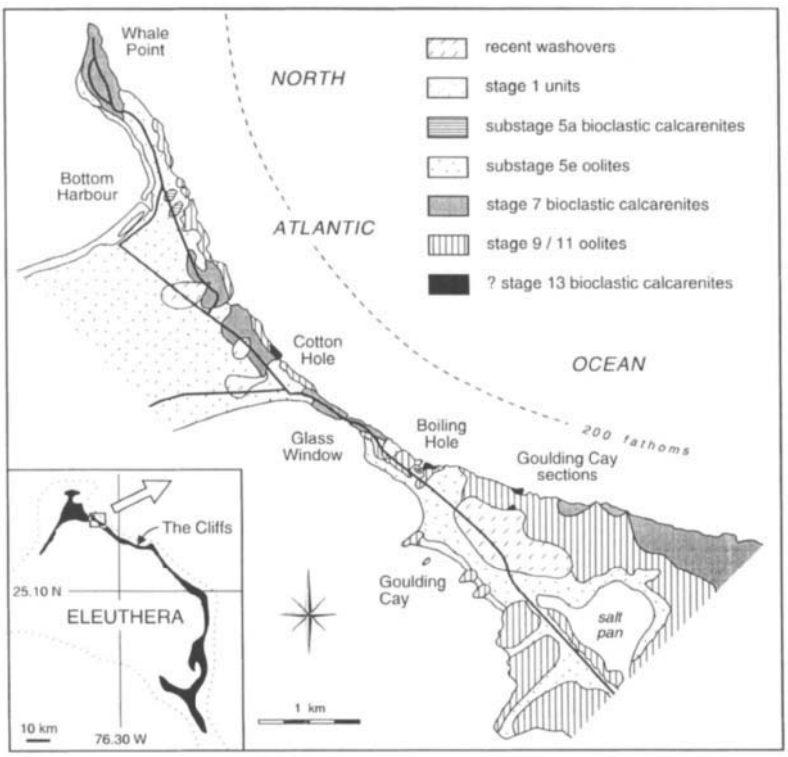


Fig. 3B-3. Geologic map of the Glass Window area in northern Eleuthera.

Class II islands (e.g., North and Central Abaco, northernmost Eleuthera, Crooked, Acklins, Caicos and Turks Islands)

Class II islands (*windward islands — broad, shallow shelf*) are like Class I islands, except that they are separated from the bank edge by a broad, gently sloping shelf. They are usually long, usually broader than Class I islands, and are commonly fronted by offshore cays. These islands typically display numerous offlapping or separate ridges.

Example: Great Abaco Island. Located on the eastern portion of the Little Bahama Bank, Abaco is characteristically flanked by a wide shelf from the northern tip down to Cherokee (Fig. 3B-4A), and by a much narrower shelf from there to the southern end. Deposits occur in lateral juxtaposition in the northern and central reaches of the island (e.g., Fire Road Village, Fig. 3B-4B), whereas they tend to form vertical successions in the southern part of the island (e.g., Hole in the Wall, which we believe is the most instructive vertical section exposed in the Bahamas, Fig. 3B-4C). Very clear anchor-catenary relationships between middle Pleistocene and late Pleistocene oolitic units occur in the Wilson City area (Fig. 3B-4A).

Class III islands (e.g., Bimini and Berry Islands, most of the Exuma Islands, Ragged and New Providence Islands)

Class III islands (*semi-protected, deep-water margin islands*) are located close to deep oceanic channels, such as the Florida Straits, Providence Channel and Exuma Sound. They are exposed to moderate waves and winds. Channel-facing shorelines characteristically have rather high deposits, whereas the platform sides of the islands are low, with occasional small beach ridges.

Example: New Providence Island. The map of New Providence Island by Garrett and Gould (1984) was one of the first geologic maps of a Bahamian island, and it has recently been updated by Hearty and Kindler (1997). Garrett and Gould (1984) clearly recognized the contrasting morphology of the exposed north shore and the protected south shore. The north shore is characterized by numerous high eolian ridges; lowlands, from former marine flats, predominate in the south. With respect to the northern part of the island (Fig. 3B-5), we find successive stratigraphic units forming distinctive offlapping sequences. The units are more closely spaced on the western side (narrow shelf) than on the eastern side (wider shelf).

New Providence Island includes many sites of geological interest such as Clifton Pier (Ball, 1967; Strasser and Davaud, 1986; Aurell et al., 1995; Carew et al., 1996), Hunt's Cave Quarry (Fig. 3B-9a), where stage-9/11 foreshore deposits were identified for the first time in the Bahamas (Hearty and Kindler, 1993b; 1995a), and Lyford Cay.

The western road cut exposure on Lyford Cay has figured prominently in the geological literature about Bahamian stratigraphy. Garrett and Gould (1984)

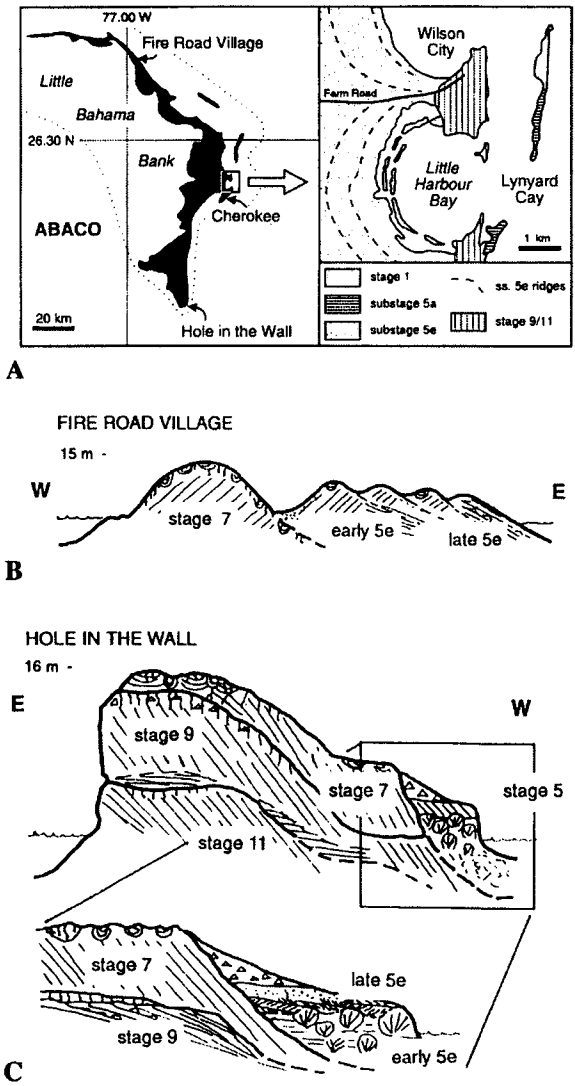


Fig. 3B-4. Geological features in Abaco. (A) Geologic map in central Abaco. Note the anchor-catenary relationship between middle Pleistocene and Sangamonian units. (B) Lateral juxtaposition of stratigraphic units at Fire Road Village, northern Abaco. (C) Vertical stacking of stratigraphic units at Hole in the Wall, southern Abaco. Due to a narrower outer platform, this site is more exposed to wave energy than that at Fire Road Village.

identified six oolitic units separated by paleosols at this locality. Four of these units are eolianites, but the other two represent beach-dune complexes with evidence for paleosea levels at 9.7 and 10 m respectively (Garrett and Gould, 1984). On the basis of *Cerion* assemblages, Garrett and Gould (1984) placed all six units in the same biostratigraphic zone which they correlated with isotopic stage 5. $^{230}Th/^{234}U$ dating

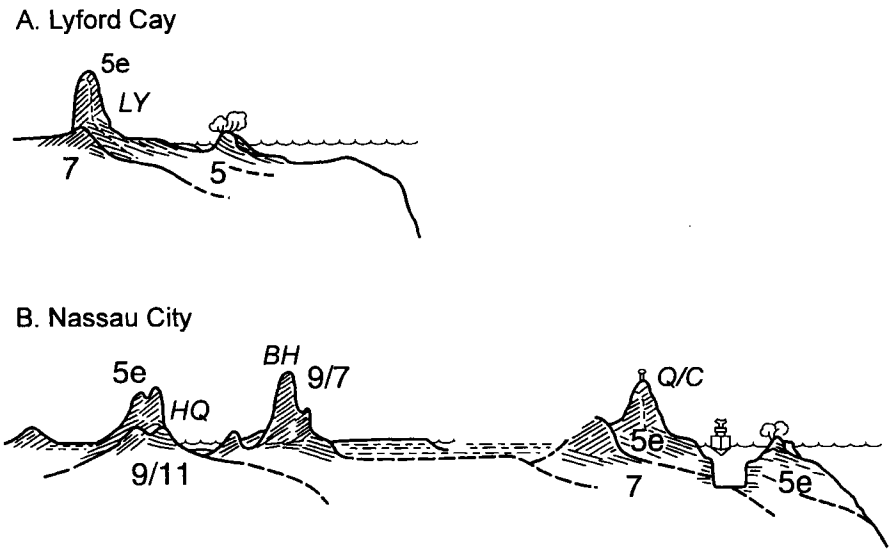


Fig. 3B-5. Cross sections across the northern part of New Providence Island. The outer platform gets wider eastward (towards Nassau), resulting in increased spacing of stratigraphic units. Key: LY, Lyford Cay; HQ, Hunt's Cave Quarry; BH, Blue Hill; Q/C, Queen's Staircase/Collins Avenue. (For more details on the geology of New Providence, refer to Carew et al., 1996, and Hearty and Kindler, 1997).

of whole-rock samples by Muhs and Bush (1987) and Muhs et al. (1990) confirmed the Sangomonian age of the uppermost five units, but yielded ages between 197 and 212 ka (isotopic stage 7) for the lowest one. These geochronological results are consistent with the field interpretation by Carew and Mylroie (1991b), who distinguished the paleosol overlying the lowest unit (a terra rossa) from those higher in the section (calcarenite protosols). The two Sangamonian beach-dune complexes at Lyford Cay were dated by Muhs et al. (1990) at ~128 and ~117 ka, respectively; the ages agree very well with more recent TIMS U-series ages on aragonitic corals from Inagua Island (Chen et al., 1991). The latest piece of information on the Lyford Cay outcrop — but certainly not the last one — was brought by Hearty and Kindler (1993b; 1997) who recognized the pre-Sangamonian unit as a bioclastic calcarenite in agreement with their general petrostratigraphic scheme for the Bahamas (Kindler and Hearty, 1996).

New Providence Island includes Nassau, the capital and largest city in the Bahamas.

Example: Lee Stocking Island. Although nearly all island types can be found within the 220-km-long Exuma chain, many are like Lee Stocking Island, lying close to the bank edge and bearing high deposits on the shorelines facing Exuma Sound. The Holocene record is particularly noteworthy on Lee Stocking, where stage-1 units occur both in lateral juxtaposition and vertical succession (Fig. 3B-6). The occur-

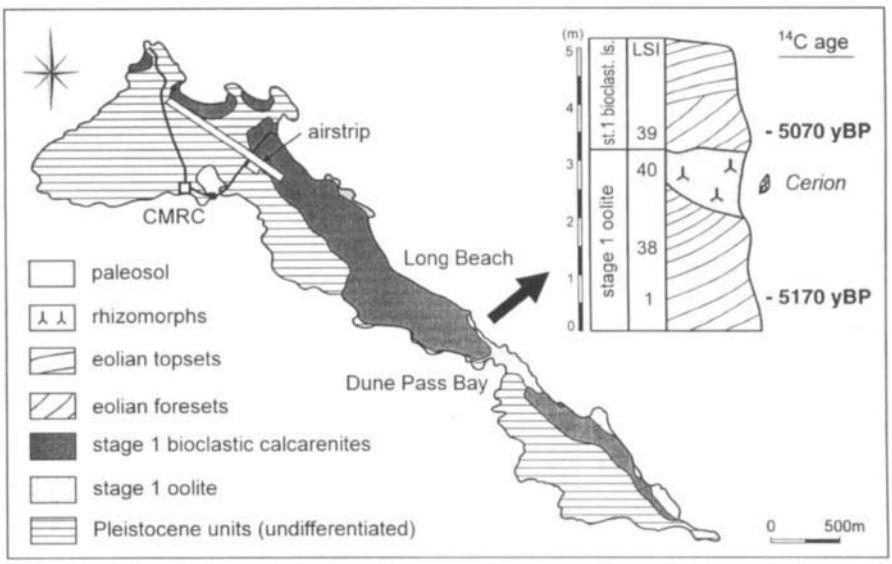


Fig. 3B-6. Geologic map of Lee Stocking Island, Exumas. Note the voluminous Holocene record. Section shows the vertical succession of both stage-1 units. Minor ^{14}C-age difference is presumably due to reworking of the middle Holocene oolite in the upper skeletal unit. Key: CMRC, Caribbean Marine Research Center. (Modified from Kindler, 1995).

rence of a protosol between these units indicates that eolianite sedimentation was episodic during the continuous Holocene sea-level rise (Kindler, 1992; 1995). The substage-5e record is represented by numerous patch reefs (e.g., Halley et al., 1991, Aalto and Dill, 1996), and cliffing and notching of middle Pleistocene units.

Lee Stocking Island is well known in the world of sedimentary geologists and biologists because of the recent discovery of giant subtidal stromatolites in nearby tidal channels (Dill et al., 1986).

Class IV islands (e.g., Andros and Grand Bahama Islands)

Class IV islands (*protected leeward islands*) are exposed to relatively low waves and winds because of their position away from the windward margin of a bank, or because they are protected by another island. These islands are usually large, broad, and low. They show numerous, laterally accreted beach ridges dating principally from the last interglacial. Bank-facing coastlines are dominated by mangrove accretion and accumulation of lime mud up to sea level.

Example: Grand Bahama Island. Lacking open-ocean exposure because of its position on the lee side of Abaco, Grand Bahama Island is generally low in elevation (mostly below 5 m) with extensive flatlands across the northern part. The highest point on the island is only 20 m. Much of Grand Bahama Island consists of fossil

ooid shoals and low ridges deposited mainly during substage 5e when sea level was falling from a ~+8 m datum (Gerhardt, 1983). Middle Pleistocene, late Sangamonian (substage 5a) and Holocene deposits also occur on Grand Bahama Island, but they are not large.

Grand Bahama Island includes Freeport, one of the Bahamas' best-known tourist destinations and the country's second largest city.

Class V islands (e.g., San Salvador, Mayaguana and Inagua Islands, and Samana, Rum and Plana Cays)

Class V islands (*isolated islands*) are located on small platforms and usually occupy a significant portion of them. On windward shorelines, the high energy favors vertical buildup of deposits, whereas the lower energy on the leeward sides leads to lateral accretion.

Example: San Salvador Island. Occupying much of its isolated platform, San Salvador Island is exposed to the open ocean and the trade winds. According to our morphostratigraphic map (Hearty and Kindler, 1993a), most of the material forming the island is derived from the east side. The eastern shelf, however, is fairly wide, more like that off northern Abaco (Class II) than Eleuthera (Class I), and so the high cliffs and vertically stacked successions typical of Eleuthera are lacking in San Salvador. Instead, the units generally tend to occur in offlapping or laterally juxtaposed sequences, the older ones being located in a more landward position. High oolitic ridges in the south-central portion of the island probably date from the middle Pleistocene (isotopic stage 9 or 11). On the western side, there is a similar pattern of lateral accretion, but with smaller units.

San Salvador, which is the site of the popular Bahamian Field Station where the biannual Symposium on Bahamian Geology is held, was the birthplace of the stratigraphy of Carew and Mylroie (1985, 1991a), the location of our first study of a Bahamian island (Hearty and Kindler, 1993a), and the subject of a vigorous debate (Carew and Mylroie, 1994; Hearty and Kindler, 1994; Carew and Mylroie, 1995b).

Class VI islands (Moore's Island on Little Bahama Bank; Rocky Dundas and other cays in the Exumas)

Class VI islands (isolated mid-bank island remnants) are located well inside the platform margin, away from high-energy sources, and are in the process of being destroyed by dissolution and wave- and bioerosion. These islands and rocks are typically small, isolated, vertically sided, and represent the remnants of larger islands of middle Pleistocene age. They usually consist of very indurated, red-stained, cavernous eolianites deeply notched at multiple levels. Figure 3B-7 shows an example: Rocky Dundas (in the Exumas), which consists largely of a middle Pleistocene eolianite that is riddled with caves and onlapped with a substage-5e reef.

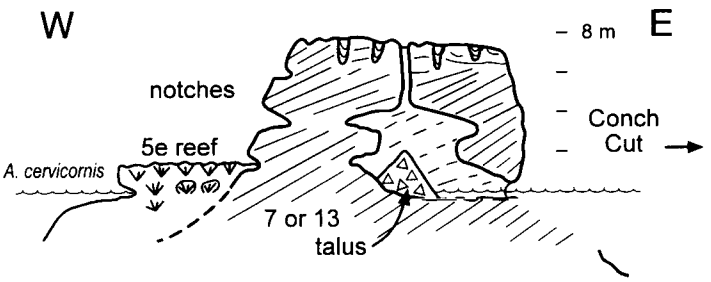


Fig. 3B-7. Cross section of Rocky Dundas, Exumas, a typical class VI island, dominated by erosional processes.

Discussion: Island evolution

Once an island core has been initiated — by emergence of a shoal (e.g., Joulters or Schooner Cays) or by incomplete flooding of an area — the island grows by a variety of processes controlled by sediment availability, energy setting, and pre-existing topography. In very quiet environments, on the lee side of the newly formed island cores, mud flats may build up to sea level and thus contribute to island expansion (e.g., w. Andros). In quiet settings, distant or protected from the high-energy platform margin, growth occurs by lateral accretion or catenary development of beach ridges between older headlands (e.g., New Providence). In exposed environments, islands have built up by vertical stacking of deposits (e.g., n. Eleuthera). In such settings, washover processes can transport large masses of sediment onto the back side of high (15 m) seacliffs.

SEA-LEVEL HISTORY

Our view of Bahamian stratigraphy and the style of construction of Bahamian islands has evolved as we have studied more and more examples. At the same time, our view of the Quaternary sea-level history recorded on these islands has also grown (Hearty and Kindler, 1995a).

Figure 3B-8 shows our interpretation of sea-level history in the Bahamas and how it relates to the relevant part of the deep-sea $\delta^{18}O$ curve of Imbrie et al. (1984), a proxy record of continental ice volume and thus sea level. It is clear that our stratigraphic scheme and the sea-level history we infer correspond in a general way with the deep-sea $\delta^{18}O$ record, but there are some important differences. Among them are:

- We infer a double highstand during substage 5e. The two highstands are represented by two oolitic substage-5e units (Table 3B-1; units IV and V of Kindler and Hearty, 1996). The boundary between the two units may be a simple discontinuity (e.g., within the reef facies, Hattin and Warren, 1989; Chen et al., 1991; Hearty and Kindler, 1993a) or a dm-thick, tan, sandy, *Cerion*-rich paleosol, where fossil standing trees locally may be found (e.g., Kindler and Hearty, 1996, Fig. 11). The two oolites

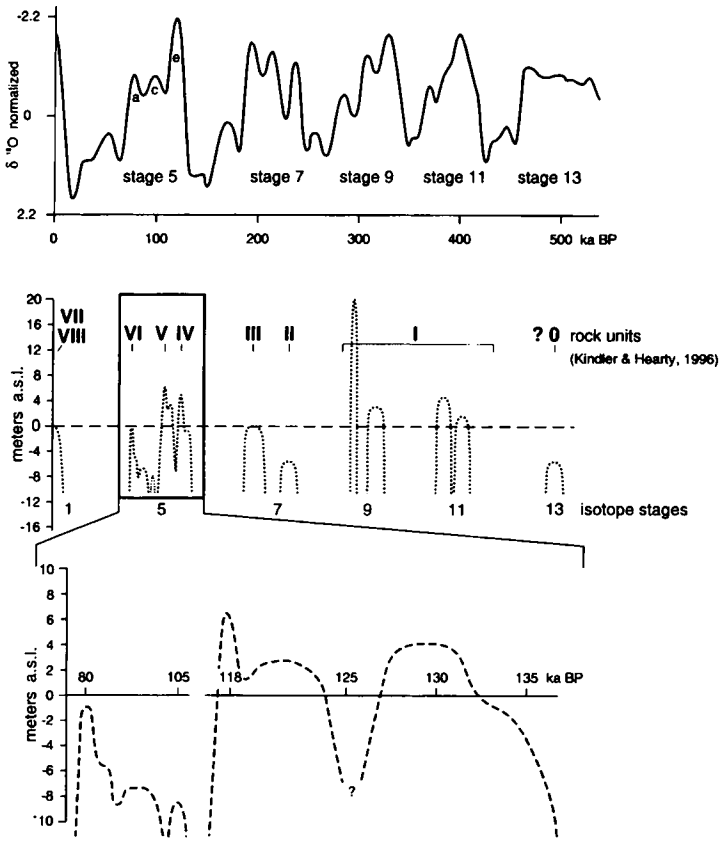


Fig. 3B-8. Top diagram is a $\delta^{18}O$ curve for the late Quaternary from Imbrie et al. (1984). Bottom diagram is a late Quaternary sea-level curve based on geologic evidence from the Bahamas from this and earlier studies (Hearty and Kindler, 1993a; Hearty and Kindler, 1995a; Kindler and Hearty, 1996; Neumann and Hearty, 1996). The Sangamonian sea-level record is detailed in the lowermost part of the figure. Roman numbers placed on the middle curve correspond to the lithostratigraphic units described in Kindler and Hearty (1996). Unit 0 (stage-?13 bioclastic calcarenite) is a new unit; Unit I includes several oolitic rock bodies corresponding to distinct sea-level events during stages 9 and 11. Note that Sangamonian units (IV, V and VI) reflect different sea-level highstands.

are displayed at Collins Avenue, New Providence, where a sandy paleosol occurs between them (Fig. 3B-9b); the intricacies of sea-level history during substage 5e can be worked out at the western cut, Lyford Cay, on New Providence (Garrett and Gould, 1984; Hearty and Kindler, 1995a). The double peak in isotope substage 5e is consistent with findings in New Guinea (Aharon et al., 1980), Mediterranean coastlines (Hearty, 1986; Miller et al., 1986), Red Sea shorelines (Plaziat et al., 1995) and Hawaii (Sherman et al., 1993).

- We infer a rapid rise in sea level at the close of substage 5e. One of the lines of evidence is the occurrence in unit V (Table 3B.1) of "chevron ridges" (Hearty and Neumann, 1994) that can be likened to giant overwash deposits (Fig. 3B-9c). These

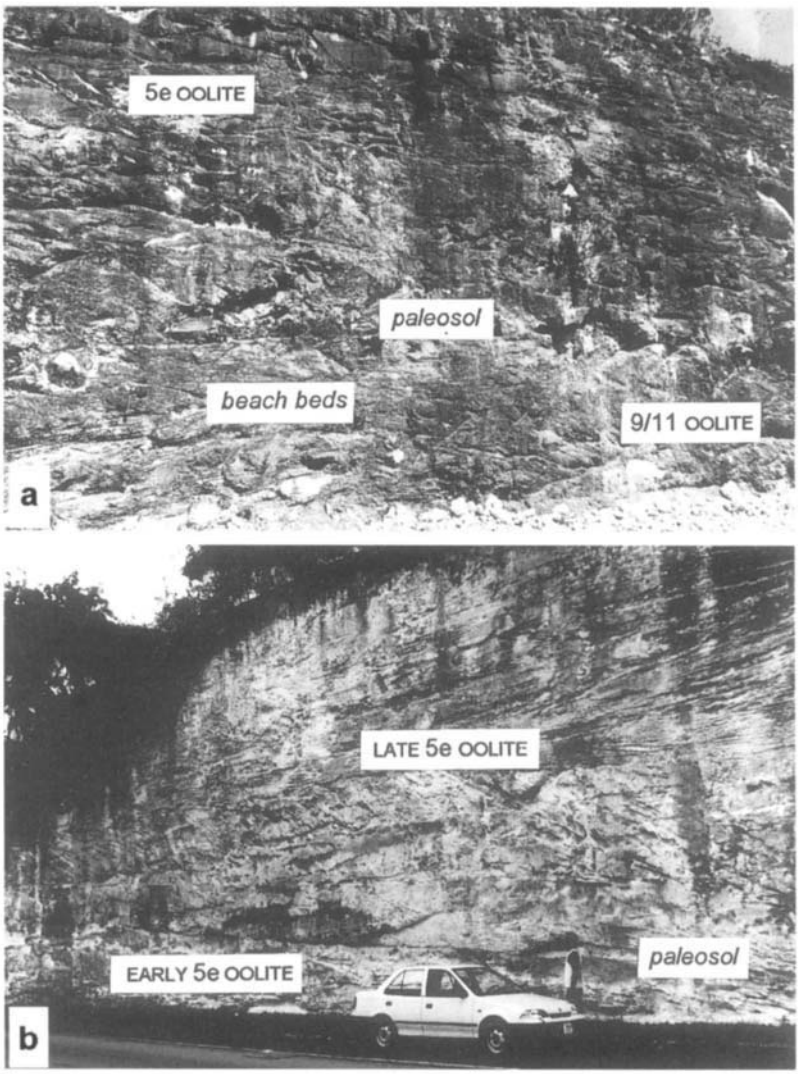


Fig. 3B-9a,b. Geologic evidence of high sea levels in the Bahamas. (a) Hunt's Cave Quarry, New Providence. Stage-9/11 foreshore deposits (beach beds, with shell hash and fenestrae) underlie stage-5 eolianites. Base of outcrop is at +5 m; outcrop height is 9 m. We have more about this section in Kindler and Hearty (1996) and Hearty and Kindler (1995a, 1997). (b) Collins Avenue section, Nassau, New Providence Island. The early and late substage-5e oolites are separated by a paleosol including some breccia horizons and standing trees. Both units, which yield distinctive A/I ratios, were deposited during separate sea-level highstands during substage 5e. (c) Aerial view of Harvey Cays, central Exumas, showing typical chevron ridge probably formed by large waves at the end of substage 5e (Hearty and Neumann, 1994). Bank edge visible in the upper part of the photo. Scale is given by airport strip on Staniel Cay. (d) Road cut near Whale Point, northern Eleuthera. Substage-5a bioclastic eolianites occur between two paleosols, one capping substage-5e oolites and the other underlying Holocene units. These rocks demonstrate the occurrence of a late Sangamonian high-stand of sea level.

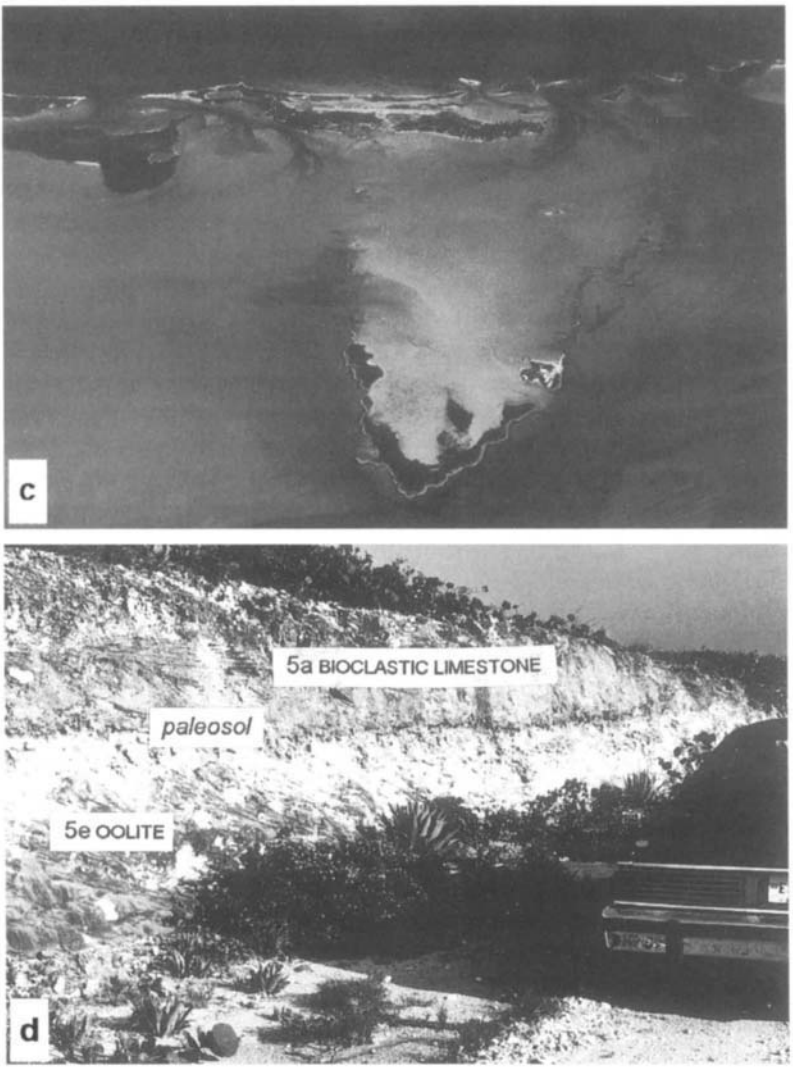


Fig. 3B-9c,9d.

landforms, which are 3–6 km long and 0.5–2 km wide, are shaped like V's opening toward the bank margin and are composed mainly of low-angle, planar cross-beds containing numerous fenestrae. These chevron ridges, together with contemporaneous stranded corals and high notches, suggest that, at the close of 5e, there may have been sudden sea-level fluctuations possibly linked to Antarctic ice collapse (Neumann and Hearty, 1996).

- We infer that, during substage 5a, sea level rose much higher than the values of < -15 m obtained from isotopic data (Imbrie et al., 1984) and indicated by Bahamian speleothem data (Li et al., 1989). We base this inference on the recognition of

bioclastic substage-5a eolianites (Almgreen Cay Formation of Hearty and Kindler, 1993a; unit VI of Kindler and Hearty, 1996) along many windward shorelines. One of the best exposures, where the bioclastic substage-5a and oolitie substage-5e units are directly superimposed with a terra rossa between them, is at Whale Point, northern Eleuthera (Fig. 3B-9d). We have found no marine deposits above sea level in the substage 5a in the Bahamas. Our interpretation of substage-5a eolianites is consistent with the Southampton Formation in Bermuda (Vacher and Hearty, 1989) [q.v., Chap. 2] and a substage-5a reef offshore the modern reef tract of the Florida Keys (Ludwig et al., 1996) [q.v., Chap. 4].

- We infer the occurrence of relatively high-frequency, low-amplitude fluctuations superimposed on the later part of the Holocene sea level rise. Evidence includes the presence of fenestrae and meniscus vadose cements within a $\sim$1,000-year-old submerged beachrock off the southern shoreline of San Salvador (Kindler and Bain, 1993). Such fluctuations, which could possibly be related to sunspot cycles, are consistent with findings in south Florida (Gelsanliter and Wanless, 1995).
- The deep-sea $\delta^{18}O$ curve of Imbrie et al. (1984) suggests that sea level was below its present position during stage 7, and that it may have been as high or higher than its present position during stages 9 and 11. We have recently found fenestrae-rich, planar cross-beds that may be interpreted as beach facies at up to 2 m, grading up to an eolianite of our bioclastic stage-7 unit on New Providence (Hearty and Kindler, 1997). At several outcrops on New Providence (Hearty and Kindler, 1995a) and Eleuthera (Hearty and Kindler, 1995b), we have found stage-9/11 oolites with shoreface and foreshore sediments at elevations exceeding those of the substage-5e marine facies. Although we have not yet published complete descriptions of these deposits, we believe it is probably incorrect to say that no pre-stage-5 marine deposits are preserved above present sea level in the Bahamas (Carew and Mylroie, 1995c).

In Kindler and Hearty (1996), we point out that the general correlation between our stratigraphic units and grain composition is paralleled by a correspondence with sea-level elevation. Thus, with the exception of the relatively small oolitic stage-1 unit, which we consider an anomaly, the bioclastic units (from stage 1, substage 5a, 7, and ?13) are those in which sea level was equivalent to, or lower than, its modern position, and the oolitic units (from substage 5e and stages 9 and 11) are those in which sea level was significantly higher than its present position. We explain this correspondence with the hypothesis (Kindler and Hearty, 1996) that bioclastic sands reflect times of partial or modest platform flooding when the bulk of the sediment brought to islands originates from bank-margin reefs, whereas oolitic-peloidal units reflect major flooding events and active water circulation on the bank top.

CONCLUDING REMARKS

The architecture of Bahamian islands shows that they grow by lateral accretion or vertical stacking depending on their exposure to the open ocean and the width of the outer platform. The islands increase in size during sea-level highstands, and they are eroded during both highstands and lowstands by a variety of biological, chemical

and physical processes. The resulting complex record emphasizes the need for equally complex interpretations, including stratigraphic ones, to adequately represent our understanding of the geology of these islands.

ACKNOWLEDGEMENTS

This work was supported by a grant from the National Science Fund of Switzerland (#20-40638.94). Reviews of an earlier draft by Len Vacher, Terry Quinn and three anonymous reviewers greatly improved the final version of this paper. This paper is dedicated to Kindler's mother who passed away during the reviewing process.

REFERENCES

Aalto, K.R. and Dill, R.F., 1996. Late Pleistocene stratigraphy of a carbonate platform margin, Exumas, Bahamas. Sediment. Geol., 103: 129–143.

Aharon, P., Chappell, J. and Compston, W., 1980. Stable isotope and sea-level data from New Guinea supports Antarctic ice-surge theory of ice ages. Nature, 283: 649–651.

Aurell, M., McNeill, D.F., Guyomard, T. and Kindler, P., 1995. Pleistocene shallowing-upward sequences in New Providence, Bahamas: signature of high-frequency sea-level fluctuations in shallow carbonate platforms. J. Sediment. Res., B65: 170–182.

Ball, M.M., 1967. Carbonate sand bodies of Florida and the Bahamas. J. Sediment. Petrol., 37: 556–591.

Bathurst, R.B.G., 1975. Carbonate sedimentology and diagenesis. Elsevier, Amsterdam, 658 pp.

Beach, D.K. and Ginsburg, R.N., 1980. Facies succession of Pliocene-Pleistocene carbonates, Northwestern Great Bahama Bank. Am. Assoc. Pet. Geol. Bull., 64: 1634–1642.

Carew, J.L. and Mylroie, J.E., 1985. The Pleistocene and Holocene stratigraphy of San Salvador Island, Bahamas, with reference to marine and terrestrial lithofacies at French Bay. In: H.A. Curran (Editor), Pleistocene and Holocene carbonate environments on San Salvador Island, Bahamas. Geol. Soc. Am. Annu. Meet. Field Trip Guideb., Field Trip 2. CCFL Bahamian Field Station, Fort Lauderdale, pp. 11–61.

Carew, J.L. and Mylroie, J.E., 1987. A refined geochronology for San Salvador Island, Bahamas. In: H.A. Curran (Editor), Proc. 3rd Symp. Geol. Bahamas. CCFL Bahamian Field Station, For Lauderdale, pp. 35–44.

Carew, J.L. and Mylroie, J.E., 1991a. A stratigraphic and depositional model for the Bahama Islands (abstr.). Geol. Soc. Am. Abstr. Programs, 23/1: 14.

Carew, J.L. and Mylroie, J.E., 1991b. Some pitfalls in paleosol interpretation in carbonate sequences. Carbonates and Evaporites, 6: 69–74.

Carew, J.L. and Mylroie, J.E., 1994. Discussion of: Hearty, P.J., and Kindler, P., 1993. New perspectives on Bahamian Geology: San Salvador, Bahamas. Journal of Coastal Research, 9, 577–594. J. Coastal Res., 10: 1087–1094.

Carew, J.L. and Mylroie, J.E., 1995a. Depositional model and stratigraphy for the Quaternary geology of the Bahama Islands. In: H.A. Curran and B. White (Editors), Terrestrial and Shallow Marine Geology of the Bahamas and Bermuda. Geol. Soc. Am. Spec. Pap., 300: 5–32.

Carew, J.L. and Mylroie, J.E., 1995b. Rejoinder to Hearty, P.J., and Kindler, P., 1994, Straw men, glass houses, apples and oranges: a response to Carew and Mylroie's comment on Hearty and Kindler, 1993. Journal of Coastal Research, 10(4), 1095–1105. J. Coastal Res., 11: 256–260.

Carew, J.L. and Mylroie, J.E., 1995c. Fossil reefs and flank margin caves: indicators of late Quaternary sea level and tectonic stability of the Bahamas. Quat. Sci. Rev., 14: 145–153.

Carew J.L., Curran, H.A., Mylroie, J.E., Sealy, N.E. and White B., 1996. Field guide to sites of geological interest, western New Providence, Bahamas. Bahamian Field Station, San Salvador, 36 pp.

Chen, J.H., Curran, H.A., White, B. and Wasserburg, G.J., 1991. Precise chronology of the last interglacial period: ^{234}U-^{230}Th data from fossil coral reefs in the Bahamas. Geol. Soc. Am. Bull., 103: 82–97.

Curran, H.A. and White, B. (Editors), 1995. Terrestrial and Shallow Marine Geology of the Bahamas and Bermuda. Geol. Soc. Am. Spec. Pap. 300, 344 pp.

Dill, R.F., Shinn, E.A., Jones, A.T., Kelly, K. and Steinen, R.P., 1986. Giant subtidal stromatolites forming in normal salinity waters. Nature, 324: 55–58.

Field, R.M. and collaborators, 1931. Geology of The Bahamas. Geol. Soc. Am. Bull., 42: 759–784.

Friedman, G.M., 1964. Early diagenesis and lithification in carbonate sediments. J. Sediment. Petrol., 34: 777–813.

Garrett, P. and Gould, S.J., 1984. Geology of New Providence Island, Bahamas. Geol. Soc. Am. Bull., 95: 209–220.

Gelsanliter, S. and Wanless, H.R., 1995. High-frequency sea-level oscillations in the late Holocene of South Florida: a dominating control on facies initiation and dynamics (abstr.). First SEPM Congr. on Sediment. Geol. (St Pete Beach FL), Progr. Abstr.: 58.

Gerhardt, D.J., 1983. The anatomy and history of a Pleistocene strand plain deposit, Grand Bahama Island, Bahamas. M.S. Thesis, Univ. Miami, Coral Gables FL, 131 pp.

Halley, R.B., Muhs, D.R., Shinn, E.A., Dill, R.F. and Kindinger, J.L., 1991. A +1.5-m reef terrace in the southern Exuma Islands, Bahamas (abstr.). Geol. Soc. Am. Abstr. Programs, 23/1: 40.

Hattin, D.E. and Warren, V.L., 1989. Stratigraphic analysis of a fossil *Neogoniolithon*-capped patch reef and associated facies, San Salvador, Bahamas. Coral Reefs, 8: 19–30.

Hearty, P.J., 1986. An inventory of last interglacial (sensu lato) age deposits from the Mediterranean basin. Z. Geomorph. N.F., 62: 51–69.

Hearty, P.J. and Kindler, P., 1993a. New perspectives on Bahamian geology: San Salvador Island, Bahamas. J. Coastal Res., 9: 577–594.

Hearty, P.J. and Kindler, P., 1993b. An illustrated stratigraphy of the Bahama Islands: in search of a common origin. Bahamas J. Sci., 1: 28–45.

Hearty, P.J. and Kindler, P., 1994. Straw men, glass houses, apples and oranges: a response to Carew and Mylroie's comment on Hearty and Kindler, 1993. J. Coastal Res., 10: 1095–1106.

Hearty, P.J. and Kindler, P., 1995a. Sea-level highstand chronology from stable carbonate platforms (Bermuda and the Bahamas). J. Coastal Res., 11: 675–689.

Hearty, P.J. and Kindler, P., 1995b. The geology of North Eleuthera, Bahamas: a "rosetta stone" of Quaternary stratigraphy and sea levels. First SEPM Congr. Sediment. Geol. (St. Pete Beach FL) Field Trip Guideb, Field Trip 3, 23 pp.

Hearty, P.J. and Kindler, P, 1997. The stratigraphy and surficial geology of New Providence and surrounding islands. J. Coastal Res., 13, in press.

Hearty, P.J. and Neumann, A.C., 1994. Parabolic beach/dune ridge system marks catastrophic end of Substage 5e in the Bahamas (abstr.). Geol. Soc. Am. Abstr. Progams, 26/7: 515.

Hine, A.C., Wilber, R.J. and Neumann, A.C., 1981. Carbonate sandbodies along contrasting shallow bank margins facing open seaways in Northern Bahamas. Am. Assoc. Pet. Geol. Bull., 65: 261–290.

Imbrie, J., Hays, J.D., Martinson, D.G., McIntyre, A., Mix, A.C., Morley, J.J., Pisias, N.G., Prell, W.L. and Shackleton, N.J., 1984. The orbital theory of Pleistocene climate: support from a revised chronology of the marine δ^{18} O record. In: A.L. Berger et al. (Editors), Milankovitch and Climate, Part I. Reidel, Dordrecht, pp. 269–305.

Kindler, P., 1992. Coastal response to the Holocene transgression in the Bahamas: episodic sedimentation versus continuous sea-level rise. Sediment. Geol., 80: 319–329.

Kindler, P., 1995. New data on the Holocene stratigraphy of Lee Stocking Island (Bahamas) and its relation to sea-level history. In: H.A. Curran and B. White (Editors), Terrestrial and Shallow-Marine Geology of the Bahamas and Bermuda, Geol. Soc. Am. Spec. Pap., 300: 105–116.

Kindler, P. and Bain, R.J., 1993. Submerged Upper Holocene beachrock on San Salvador Island, Bahamas: implications for recent sea-level history. Geol. Rundschau, 82: 241–247.

Kindler, P. and Hearty, P.J., 1995. Pre-Sangamonian eolianites in the Bahamas? New evidence from Eleuthera Island. Mar. Geol., 127: 73–86.

Kindler, P. and Hearty, P.J., 1996. Carbonate petrography as an indicator of climate and sea-level changes: new data from Bahamian Quaternary units. Sedimentol., 43: 381–399.

Land, L.S., MacKenzie, F.T. and Gould, S.J., 1967. Pleistocene history of Bermuda. Geol. Soc. Am. Bull., 78: 993–1006.

Li, W.-X., Lundberg, J., Dickin, A.P., Ford, D.C., Schwarcz, H.P., McNutt, R. and Williams, D., 1989. High-precision mass-spectrometric uranium-series dating of cave deposits and implications for paleoclimate studies. Nature, 339: 534–536.

Ludwig, K.R., Muhs, D.R., Simmons, K.R., Halley, R.B. and Shinn, E.A., 1996. Sea-level records at ~80 ka from tectonically stable platforms: Florida and Bermuda. Geology, 24: 211–214.

Miller, G.H., Paskoff, R. and Stearns, C.E., 1986. Amino acid geochronology of Pleistocene littoral deposits in Tunisia. Z. Geomorph. N.F., 62: 197–207.

Muhs, D.R. and Bush, C.A., 1987. Uranium-series age determinations of Quaternary eolianites and implications for sea-level history, New Providence Islands, Bahamas (abstr.). Geol. Soc. Am. Abstr. Programs, 19: 780.

Muhs, D.R., Bush, C.A., Stewart, K.C., Rowland, T.R. and Crittenden, R.C., 1990. Geochemical evidence of Saharan dust parent material for soils developed on Quaternary limestones of Caribbean and western Atlantic islands. Quat. Res, 33: 157–177.

Neumann, A.C. and Hearty, P.J., 1996. Rapid sea-level changes at the close of the last interglacial (substage 5e) recorded in Bahamian island geology. Geology, 24: 775–778.

Newell, N.D. and Rigby, J.K., 1957. Geological studies on the Great Bahama Bank. In: R.J. Le Blanc and J.G. Breeding (Editors), Regional aspects of carbonate deposition. Soc. Econ. Paleontol. Mineral. Spec. Publ., 5: 15–72.

Plaziat, J.-C., Baltzer, F., Choukri, A., Conchon, O., Freytet, P., Orszag-Sperber, F., Purser, B., Raguideau, A. and Reyss, J.-L., 1995. Quaternary changes in the Egyptian shoreline of the Northwestern Red Sea and Gulf of Suez. Quat. Int., 29/30: 11–22.

Sherman, C.E., Glenn, C.R., Jones, A.T., Burnett, W.C. and Schwarcz, H.P., 1993. New evidence for two highstands of the sea during the last interglacial, oxygen isotope substage 5e. Geology, 21: 1079–1082.

Strasser, A. and Davaud, E., 1986. Formation of Holocene limestone sequences by progradation, cementation, and erosion: two examples from the Bahamas. J. Sediment. Petrol., 56: 422–428.

Titus, R., 1980. Quaternary emergent facies patterns of San Salvador, Bahamas. In: D.T. Gerace (Editor), Field Guide to the Geology of San Salvador. CCFL Bahamian Field Station, Fort Lauderdale, pp. 97–116.

Titus, R., 1987. Geomorphology, stratigraphy, and the Quaternary history of San Salvador. In: H.A. Curran (Editor), Proc. 3rd Symp. Geology of the Bahamas. CCFL Bahamian Field Station, Fort Lauderdale, pp. 155–164.

Vacher, H.L., 1973. Coastal dunes of Younger Bermuda. In: D.R. Coates (Editor), Coastal Geomorphology. Publications in Geomorphology, State University of New York, Binghamton, pp. 355–391.

Vacher, H.L. and Hearty, P.J., 1989. History of stage 5 sea level in Bermuda: review with new evidence of a rise to present sea level during substage 5a. Quat. Sci. Rev., 8: 159–168.

Geology and Hydrogeology of Carbonate Islands. Developments in Sedimentology 54
edited by H.L. Vacher and T. Quinn
© 1997 Elsevier Science B.V. All rights reserved.

Chapter 3C

GEOLOGY OF THE BAHAMAS: SUBSURFACE GEOLOGY OF THE BAHAMAS BANKS

LESLIE A. MELIM and JOSE LUIS MASAFERRO

INTRODUCTION

The Bahamian archipelago consists of a series of shallow-water banks (<10 m deep) separated by deep basins (>800 m deep) (Fig. 3C-1). As a result of their isolation from the North American landmass, the Bahamas have been an exclusively carbonate province throughout the Tertiary, and the surface geology of the Bahamas has long been used to develop models for the deposition and diagenesis of carbonate sediments (e.g., Newell et al., 1959; Bathurst, 1975). Chapters 3A and 3B have addressed the surface geology of the Bahamian islands. This chapter is concerned with the underlying platforms, particularly the subsurface of Great Bahama Bank.

We will focus here on three aspects of the subsurface geology: (1) the structure, particularly of Great Bahama Bank, as it relates to the evolution of the banks; (2) the sedimentology based on seismic facies and available core data; and (3) the diagenesis in shallow cores from various Bahamian banks and from two deep cores (Clino and Unda) in Great Bahama Bank with an emphasis on the role of marine pore fluids.

The Bahamas Drilling Project

This chapter draws heavily on some results of the Bahamas Drilling Project (BDP) carried out by the Rosenstiel School of Marine and Atmospheric Science (RSMAS), University of Miami, under the support of the U.S. National Science Foundation and the Industrial Associates Program of the T. Wayland Vaughan Comparative Sedimentology Laboratory (R.N. Ginsburg's research group), and on related seismic work conducted at RSMAS. A full presentation of the findings of the BDP is being prepared as an SEPM (Society for Sedimentary Geology) Contributions in Sedimentology volume (Ginsburg, in press). The BDP drilled two cores (Clino and Unda) in 1990 into the western margin of Great Bahama Bank using a wire-line diamond drilling rig with overall recovery in both holes of 80% (Fig. 3C-1). There were three principal goals for the BDP: (1) to calibrate prograding seismic sequences identified in an earlier seismic stratigraphic analysis (Eberli and Ginsburg, 1987, 1989); (2) to retrieve and analyze formation fluids from a cemented carbonate platform and to investigate mechanisms of fluid circulation (Swart et al., in press); and (3) to investigate styles of diagenesis in sediments which were altered primarily in sea water or evolved sea water (Melim et al., 1995; in press).

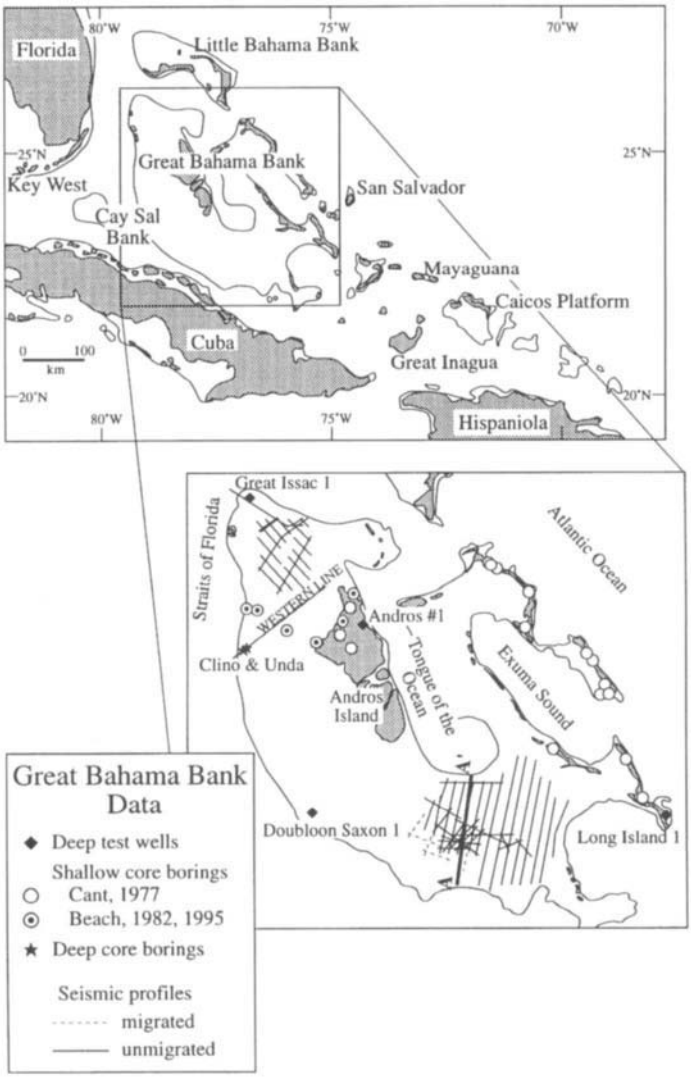


Fig. 3C-1. Bahamas regional map with detail showing location of deep test wells, deep and shallow core borings, and seismic profiles from Great Bahama Bank. See Table 3C-1 for list. Seismic line labeled WESTERN LINE is line of Fig. 3C-2. A-A′ is approximate line of section for Fig. 3C-4. Bank outlines follow 100-m contour.

DATA

The location and source of data used here are shown in Fig. 3C-1, Table 3C-1. There are four deep wells that have been drilled on Great Bahama Bank by the oil industry (Table 3C-1, Fig. 3C-1). Andros #1, Long Island-1, and Doubloon Saxon-1

Table 3C-1

Available data on the subsurface geology of Great Bahama Bank[1]

	Depth (m)	Date	References
Deep test wells			
Andros #1	4,448	1947	Spencer, 1967
Long Island-1	5,355	1970	Meyerhoff and Hatten, 1974
Great Issac-1	5,433	1971	Schlager et al., 1988
Doubloon Saxon 1	6,631	1986	Walles, 1993
Shallow core borings			
17 core borings	17–51	pre-1975?	Cant, 1977
6 core borings	42–75	1977	Beach, 1977, 1995
Deep core borings			
Clino	677	1990	Papers in Ginsburg, in press
Unda	454	1990	Papers in Ginsburg, in press
	Length (km)	**Date**	**References**
Seismic data			
Northwestern GBB	~700	1983	Eberli and Ginsburg, 1987, 1989
Southern GBB	~1,800	1984–85	Masaferro and Eberli, 1994

[1]See Figure 3C-1 for locations.

penetrated Pleistocene to Lower Cretaceous shallow-water limestones, dolomites, and minor evaporites (Spencer, 1967; Meyerhoff and Hatten, 1974; Walles, 1993). Great Issac-1 recovered a somewhat different sequence: mid-Cretaceous shallow-water carbonates and evaporites at the bottom, followed by, first, mid-Cretaceous through Miocene deep-water carbonates and, then, Miocene and younger shallow-water carbonates (Schlager et al., 1988); the uppermost 200 m of the section was not sampled. An additional deep core, Cay Sal IV-1, was drilled by Standard Oil Company in 1958–1959 on Cay Sal Bank (Fig. 3C-1). The section recovered was very similar to that of Andros #1 with a total depth of 5,766 m bottoming out in shallow-water carbonates and anhydrites of Late Jurassic to Early Cretaceous age (Meyerhoff and Hatten, 1974).

The shallow subsurface of Great Bahama Bank has been sampled by a series of core borings (17–75 m), mainly on the islands, but also in a transect extending across the bank west of Andros Island (Cant, 1977; Beach and Ginsburg, 1980; Beach, 1982) (Fig. 3C-1). These core borings, which were drilled by the Commonwealth of the Bahamas, Union Oil Research and the University of Miami, recovered highly porous, shallow-water limestones with dolomite in the lower portion of one core (Cant, 1977; Beach and Ginsburg, 1980; Beach, 1982). Shallow cores have also been drilled on San Salvador (Supko, 1970), Little Bahama Bank (Williams, 1985) and several southeastern Bahamian banks (Pierson, 1982).

Cores Unda (454 m) and Clino (677 m) of the BDP were drilled on the western margin of Great Bahama Bank along a seismic line previously studied by Eberli and

Ginsburg (1987, 1989) (Figs. 3C-1, 2). Depths for the BDP cores are reported throughout this summary as meters below mud pit (driller's convention). For core Clino, sea level was 7.3 m below the mud pit, and the seafloor was 14.9 m; for Unda, sea level was 5.2 m below the mud pit, and the seafloor was 11.9 m. The section from Unda consists of three intervals of Miocene to Pleistocene shallow-water platform and reef deposits, alternating with intervals of coarse sand to silt-sized deeper-margin deposits. In contrast, the sediments from core Clino consist of a single shallowing-upward succession of Miocene to Pliocene lower-to-upper-slope facies that is overlain by Pliocene to Pleistocene forereef, reef, and platform facies (Kievman and Ginsburg, in press; Kenter et al., in press).

Two large grids of multichannel seismic data exist from the top of Great Bahama Bank. One on northwest Great Bahama Bank is approximately 700 km in length and connected to the Great Issac-1 well. In the initial studies, only the top 1.1 s (two-way travel time) of the section was available, except for an isolated cross-bank profile where the profile extended down to 1.7 s (Eberli and Ginsburg, 1987, 1989) (Figs. 3C-1, 2). A second data set (~1,800 km) from southern Great Bahama Bank, with data down to 5 s (Fig. 3C-1), displays the internal architecture of the bank in the vicinity of the Cuban collision zone (Masaferro and Eberli, 1994).

STRUCTURE

Great Bahama Bank

Seismic data on Great Bahama Bank have provided insight into the origin of one of the most striking features of the Bahamas: the bank-and-trough configuration of the structure. There have been three main explanations of this geometry. The first, emphasizing the role of tectonism, argues that the modern configuration is inherited from the horsts and grabens of Early Jurassic rifting (Mullins and Lynts, 1977). Others have proposed that the configuration is the result of a mid-Cretaceous drowning event caused by a worldwide crisis in carbonate and reef growth, in which only isolated platforms survived (Bryant et al., 1969; Paulus, 1972; Meyerhoff and Hatten, 1974; Sheridan, 1974; Hooke and Schlager, 1980; Schlager and Ginsburg, 1981). According to this idea, the present bank-and-trough topography is constructional and reflects more rapid sedimentation on the bank top than in the deep troughs (Hooke and Schlager, 1980). On the basis of seismic data from the deep water troughs, a hybrid model has been proposed with a regional platform of Jurassic-Early Cretaceous age faulted during the Late Cretaceous by wrench faulting associated with Cuban-North American tectonics (Sheridan et al., 1988). According to this model, the Late Cretaceous faulting produced small-scale relief that controlled the position of the present-day platforms (Sheridan et al., 1988). Additional post-Cretaceous faulting or tilting may have played a role (Austin et al., 1988), but sedimentologic processes are believed to account for most of the current relief (Sheridan et al., 1988).

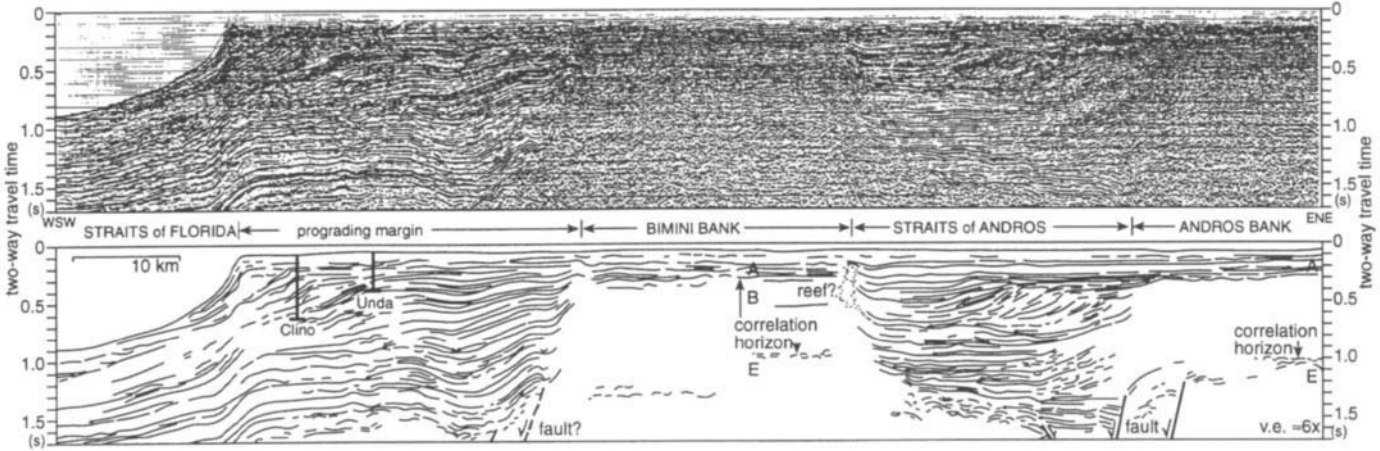


Fig. 3C-2. Western Geophysical seismic line showing complex fill in Straits of Andros separating Andros Bank from Bimini Bank and westward-prograding margin of Bimini Bank. Note location of cores Clino and Unda, which are discussed in text. See Fig. 3C-1 for location of seismic line. (After Eberli and Ginsburg, 1987.)

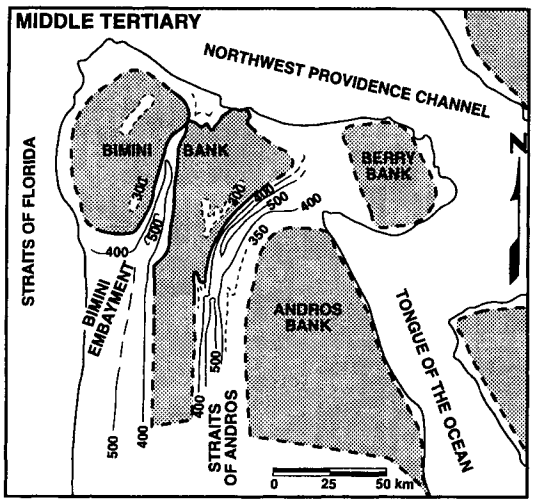


Fig. 3C-3. Paleogeographic map of northwestern Great Bahama Bank in the middle Tertiary. Berry Bank cannot be documented with the existing dataset, but, assuming that the Straits of Andros formed an open seaway, it can be postulated. In the middle Tertiary(?), the newly formed Bimini embayment subdivides Bimini Bank, and the Straits of Andros are partially filled with the basin axis west of center due to progradation of the eastern margin. Stipple = 250–300 m. (From Eberli and Ginsburg, 1987.)

The work of Eberli and Ginsburg (1987, 1989) showed that the modern configuration of Great Bahama Bank is best explained by repeated tectonic segmentation in the mid-Cretaceous and mid-Miocene, followed by coalescence of the banks during their growth (Figs. 3C-2, 3). The seismic data clearly reveal that Great Bahama Bank is not a single bank but is composed of several nuclear banks that welded together by basin infilling and platform progradation (Eberli and Ginsburg, 1987, 1989) (Figs. 3C-2, 3).

The deep seismic data of Masaferro and Eberli (1994) from the southern Great Bahama Bank also reveal a complicated internal structure of the bank. Like the shallow seismic data from northern Great Bahama Bank, these data show a pattern of buried banks and troughs, but they also reveal deep basement faults that control the bank-and-trough configuration. It is now clear that a Lower Cretaceous passive-margin platform of evaporites to carbonates developed following Triassic-Jurassic (?) rifting (Fig. 3C-4, F1). During the mid-Cretaceous, faulting dissected the Lower Cretaceous platform along its northern edge (Fig. 3C-4, F2) and created a northeastward-prograding margin. A Late Cretaceous/early Tertiary event of transtensional faulting (strike-slip faulting with extension, Fig. 3C-4, F3) was triggered by the collision of Cuba and the Bahamas Platform and led to the formation of symmetric intraplatform depressions. Tectonic quiescence since the early Tertiary has allowed infilling of these depressions and the development of the broad Great Bahama Bank seen today (Fig. 3C-4) (Masaferro and Eberli, 1994).

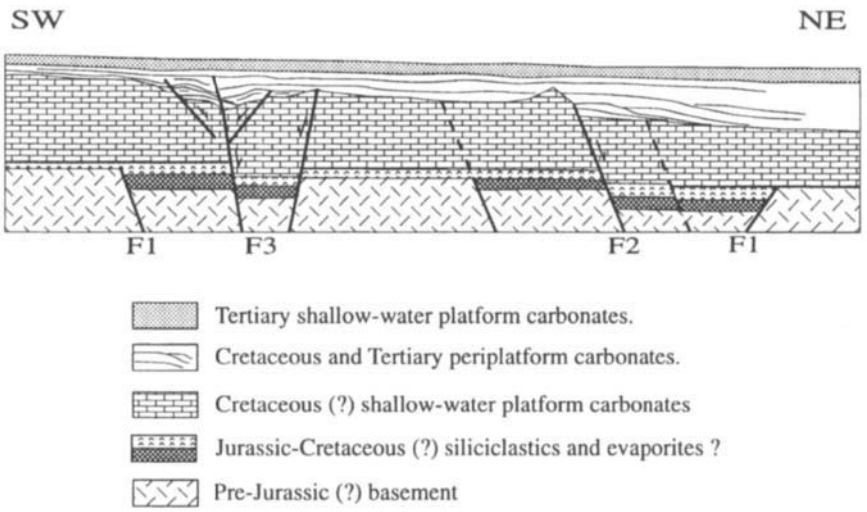


Fig. 3C-4. Schematic NNE-SSW cross section A-A′ displaying the major structural (F1, F2, F3) and stratigraphic elements of southern Great Bahama Bank. Siliciclastics and evaporites were deposited during Triassic-Jurassic(?) rifting (F1) followed by development of a Cretaceous carbonate platform. Mid-Cretaceous fault reactivation (F2) caused the first segmentation of the bank and led to a northward-prograding margin. Transtensional faulting (F3) during the Late Cretaceous-early Tertiary Cuban/Bahamian collision formed symmetric intraplatform depressions. Tectonic quiescence since the early Tertiary has allowed infilling of these depressions and the development of the broad Great Bahama Bank seen today. Lithologies are based on seismic facies interpretation (Masaferro and Eberli, 1994) and limited core data (Walles, 1993). See Fig. 3C-1 for location of cross section.

The evolution of Great Bahama Bank, therefore, is the result of a dynamic interaction between opposing processes of tectonic fragmentation and subsequent infilling of the resulting basins in a highly productive carbonate environment. The modern deep troughs are likely deep-seated, fault-controlled features that carbonate sedimentation has been unable to fill. The present platform is the result of the coalescence of numerous smaller platforms (Figs. 3C-3, 4) (Eberli and Ginsburg, 1987, 1989; Masaferro and Eberli, 1994), not the remains of a single, partially drowned platform.

Other Bahamian banks

The Bahamas show a dramatic change in character from the large banks of the northern Bahamas to smaller, more isolated banks to the southeast (Fig. 3C-1). Although the underlying basement changes from transitional, rift-related crust in the north to oceanic crust to the south (Sheridan et al., 1981; Sheridan et al., 1988), the differences between the two regions are the result of increasing tectonic activity to the south (Mullins et al., 1992). The Late Cretaceous/early Tertiary Cuban and Antillian orogenies affected a wide area including Great Bahama Bank (Eberli and Ginsburg,

1987, 1989; Sheridan et al., 1988; Masaferro and Eberli, 1994), Cay Sal Bank (Ball et al., 1985), and the southeastern Bahamas (Sheridan et al., 1988). During the late Tertiary, while the northern Bahamas were tectonically quiescent, the collision of Hispaniola with the southeastern Bahamas led to renewed fragmentation and tectonism (Mullins et al., 1992). Bank segmentation is continuing in the vicinity of the active subduction zone, while the northern banks – Little Bahama Bank and Great Bahama Bank – are large coalesced edifices in a tectonically quiet area.

SEISMIC FACIES AND SEDIMENTOLOGY

Introduction

The subsurface of Great Bahama Bank shows three distinct seismic facies (Fig. 3C-5). The upper facies consists of high-amplitude horizontal reflections. One lower facies consists of high-amplitude inclined reflections, and the other lower facies generally consists of chaotic reflections (Fig. 3C-5). The inclined reflections indicate prograding deposits that infill structural basins, and the chaotic facies makes up the buried platforms. These seismic facies, combined with the available well data, form the basis for the following interpretation.

Seismic Facies 1: High-amplitude horizontal reflections on platform top

The uppermost seismic facies of continuous horizontal reflections occupies the top 0.1 to 0.2 s (~100–300 m) of Great Bahama Bank. This interval is latest Pleistocene at the top, but the base varies in age from east to west. On the western margin, a Pliocene age has been obtained from cores Clino and Unda that completely pene-

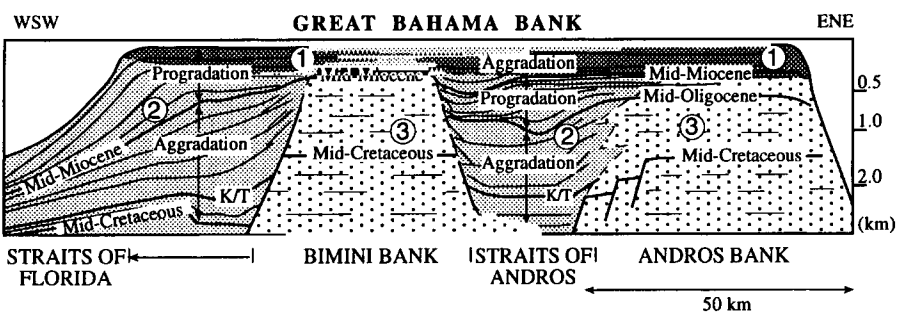


Fig. 3C-5. Schematic cross section over northwestern Great Bahama Bank showing evolution of the bank and the approximate distribution of the seismic facies. Seismic facies 1 is the modern surface of the bank and the underlying high-amplitude horizontal reflections. Seismic facies 2 includes the Straits of Andros and the prograding western margin, both with high-amplitude inclined reflections. Seismic facies 3 includes the chaotic reflections of the buried Bimini and Andros banks. (After Gregor P. Eberli, Christopher G. St. C. Kendall, Phil Moore, Gregory L. Whittle, and Robert Cannon, 1994; reprinted by permission of the American Association of Petroleum Geologists.)

trated this interval (Budd and Kievman, in press; McNeill et al., in press). On the eastern margin, only the poorly dated deep test wells extend through seismic facies 1. Shallower wells that did not sample the base of this interval give Miocene ages (Beach, 1982; McNeill, 1989).

Seismic facies 1 includes both platform-margin and platform-interior facies. The modern bank margins are dominated by ooid shoals, with limited reef facies found along portions of the windward (eastern) margin (e.g., Newell et al., 1959). In the shallow subsurface, however, ooids are generally replaced by reef facies on both the windward and leeward margins below ~10 m (Cant, 1977; Beach and Ginsburg, 1980; Beach, 1982). Beach and Ginsburg (1980) interpreted these data to support the model of Newell (1955) that considered Great Bahama Bank a steep-sided reef-rimmed atoll until Pleistocene sea-level fluctuations led to the development of the modern ooid-dominated system. More recently, however, seismic data have shown that the leeward margin had a gentle ramp morphology until the late Pleistocene, giving the bank a strongly asymmetric profile (Eberli and Ginsburg, 1987, 1989).

The bank-interior portion of seismic facies 1 shows two distinct sedimentary packages (Beach and Ginsburg, 1980; Beach, 1982): an upper package (~40–50 m thick) of nonskeletal packstones and wackestones (the Lucayan Formation), and a lower package consisting of skeletal-rich packstones to grainstones. The Lucayan Formation also contains more subaerial exposure horizons (1 per 3 m of core) than the sub-Lucayan interval (1 per 5 m of core), a difference that Beach and Ginsburg (1980) and Beach (1982) attributed to the higher frequency of sea-level fluctuations during the Pleistocene. According to Beach and Ginsburg (1980) and Beach (1982, 1995), the sub-Lucayan unit (pre-late Pliocene) is an open-marine facies deposited in >10 m of water, and the Lucayan Formation (late Pliocene to Pleistocene) was deposited in shallower, more-restricted environments similar to the modern bank. The boundary between these two units represents a change in the character of the western margin of Great Bahama Bank from an open-marine ramp to a flat-topped, steep-edged margin that restricted circulation.

The Lucayan Formation has also been recognized on other Bahamian banks on the basis of a similar lithology change in the platform facies (Pierson, 1982; Williams, 1985). The thickness, however, varies: 15–30 m on Little Bahama Bank and the southeastern banks; 40–50 m on Great Bahama Bank (Beach, 1982; Pierson, 1982; Williams, 1985). Superimposed on this regional variation, there are also local variations; for example, Pierson (1982) found the thickness of the Lucayan Formation to be approximately twice as large on Great Inagua as on Mayaguana (15–30 m vs. 0–15 m, respectively). Pierson (1982) interpreted this variation to indicate structural independence of the small banks of the southeastern Bahamas. This interpretation is consistent with the increased tectonism to the south in the late Tertiary (Mullins et al., 1992).

Seismic Facies 2: High-amplitude prograding reflections infilling basins

Seismic facies 2 is defined by high-amplitude inclined reflections that make up the fill in the buried channels (e.g., the Straits of Andros) as well as the prograding

margin of Great Bahama Bank into the Straits of Florida (Fig. 3C-2) (Eberli and Ginsburg, 1987, 1989) and Tongue of the Ocean (Fig. 3C-4) (Masaferro and Eberli, 1994). Progradation in northwestern Great Bahama Bank was consistently to the west (Eberli and Ginsburg, 1987), probably due to leeward transport by the regional wind pattern (Hine and Neumann, 1977; Eberli and Ginsburg, 1987), but buried platform margins in southern Great Bahama Bank prograded to the northeast (Fig. 3C-4) (Masaferro and Eberli, 1994).

The sediments that make up seismic facies 2 have been sampled by Great Issac-1 well and by cores Clino and Unda. Where completely penetrated by the Great Issac-1 well, this facies ranges from mid-Cretaceous to Miocene age (Schlager et al., 1988). In cores Clino and Unda, only the Miocene to Pliocene upper portion was penetrated (Eberli et al., in press; McNeill et al., in press). The sediments are mainly deep-water slope deposits but also include some margin facies (Schlager et al., 1988; Kenter et al., in press). In Great Issac-1, the slope sediments are pelagic chalks in which constituent particles derived from shallow water increase upsection (Schlager et al., 1988).

In core Clino, seismic facies 2 consists of a mixture of pelagic foraminifera with skeletal and peloidal grains derived from shallow water. Kenter et al. (in press) distinguished between thin lowstand deposits consisting of reworked coralgal sediment and thicker highstand deposits consisting of fine sand to silt-sized mixed-skeletal and/or peloidal packstones to grainstones. In Unda, the more proximal of the two Bahamas Drilling Project cores, seismic facies 2 includes both deeper-margin skeletal deposits and a lowstand reef to platform interval (Kenter et al., in press). In both cores Clino and Unda, the transition to the overlying seismic facies 1 is picked where flat-bedded reef to backreef facies take over from inclined forereef to slope facies. At this time (Miocene to Pliocene), the western margin of Great Bahama Bank had a ramp profile rather than the steep margin seen today where the upper slope is a bypass zone (Grammer and Ginsburg, 1992).

Seismic Facies 3: Chaotic platform facies

Chaotic reflections with rare low-amplitude horizontal reflections characterize much of Great Bahama Bank (Fig. 3C-3). Of all the seismic facies, this is the least understood as only the deep test wells (Fig. 3C-1, Table 3C-1) have penetrated it and many details are lacking. The chaotic facies ranges from Jurassic to Miocene(?) (Spencer, 1967; Meyerhoff and Hatten, 1974; Schlager et al., 1988; Walles, 1993). Well descriptions do not indicate any facies or lithology change to explain the transition from chaotic to horizontal reflections (Spencer, 1967; Meyerhoff and Hatten, 1974; Walles, 1993).

Seismic facies 3 consists of shallow-water carbonates underlain by mixed carbonates and evaporites below 5,000 m in the south (Spencer, 1967; Meyerhoff and Hatten, 1974; Walles, 1993) and below 2,000 m in the north (Schlager et al., 1988). Cretaceous to Eocene volcaniclastics are found below 1,500 m in Great Issac-1 but are not known from elsewhere in the Bahamas (Schlager et al., 1988). Goodell and Garman (1969) documented extensive dolomitization in Andros #1, and Walles (1993) showed similar composition for Doubloon Saxon-1. Cavernous porosity is

common to great depth in these platform carbonates and even caused the loss of most of the drill string (~ 2,400 m of pipe) into a cavern below 3,200 m in Andros #1 (Spencer, 1967; Meyerhoff and Hatten, 1974; Walles, 1993).

Evolution of Great Bahama Bank

The modern Great Bahama Bank can be characterized as a large, flat-topped bank with steep margins dropping rapidly off into very deep water. It is clear that this characterization applies to only the later history of the bank (Figs. 3C-2, 3) (Eberli and Ginsburg, 1987). Following the Late Cretaceous/early Tertiary fragmentation, the development of the profile of the modern Great Bahama Bank involved two phases: (1) the coalescence of smaller banks into one large bank; and (2) the evolution of a steep, aggrading western margin from an earlier, more gentle, prograding margin. The first phase, coalescence, was completed by the middle Eocene in the south (Masaferro and Eberli, 1994) but not until the middle Miocene in the north (Eberli and Ginsburg, 1989). Once a single bank was formed, progradation greatly expanded the dimensions of the bank (Eberli and Ginsburg, 1987, 1989; Eberli et al., 1994), contrary to the earlier view of mainly vertical growth on carbonate platforms (Schlager and Ginsburg, 1981).

Even after coalescence of a single Great Bahama Bank, its profile was significantly different than that of today (Eberli and Ginsburg, 1987). Although the eastern margin appears to have always been steep, the western margin remained a low-angle ramp until the late Pleistocene (Fig. 3C-2) (Eberli and Ginsburg, 1987, 1989). This finding has important implications, because carbonate ramps, unlike flat-topped platforms, tend to maintain productivity during sea-level lowstands as facies shift laterally downslope (Sarg, 1988; Schlager, 1992). The lowstand reef in Unda is an example of such a system (Eberli et al., in press).

The transition of the western margin from a ramp to a steep edge appears to have been gradual (Fig. 3C-2). Neither reef growth (Beach and Ginsburg, 1980) nor submarine/meteoric cementation (Hine and Neumann, 1977; Mullins and Lynts, 1977) seem adequate to explain this change. Eberli and Ginsburg (1989) showed that basin-platform relief of <500 m is necessary for progradation, and the present relief across the western margin is >800 m. In addition, the Florida Current is actively eroding the margin and carrying sediment northward (Mullins, 1983). The combination of increased relief and erosion by the Florida Current likely forced a change to a steep margin as they prevented further progradation.

DIAGENESIS

Lower limit of meteoric diagenesis

The upper part of both cores Clino and Unda has been heavily altered by meteoric fluids. Evidence of meteoric diagenesis includes (Melim et al., in press): well-devel-

oped subaerial exposure horizons; moldic, vuggy, and cavernous porosity; blocky phreatic and vadose calcite cements; and consistently depleted stable isotopic values ($\delta^{18}O = -3.0 \pm 0.7‰$; $\delta^{13}C = -1.6 \pm 1.7‰$). These features are essentially identical to those described by Supko (1970), Beach (1982, 1995), Pierson (1982) and Williams (1985) for shallow cores drilled in the Bahamas. Cores Clino and Unda, however, extend through the zone of meteoric diagenesis and into an underlying interval where only marine to marine-burial diagenesis is evident (Melim et al., 1995, in press; Melim, 1996).

The transition from meteoric to marine-burial diagenesis is best documented in the bulk-rock stable isotope data (Fig. 3C-6), particularly the oxygen data (Fig. 3C-7). Looking first at core Clino, the bulk-rock oxygen isotopic values are $-2‰$ to $-3‰$ from the top of the core down to 110 m, where they begin a shift to more positive values with increasing depth; they reach a purely marine value of $+1\%$ at 152 m (Fig. 3C-7), which is taken as the lower limit of meteoric diagenesis in core Clino. In core Unda, the bulk-rock oxygen isotopic values begin a similar shift higher in the core (at ~85 m), but the depth of the final marine value is obscured by earlier seafloor dolomitization (with $\delta^{18}O = +4‰$, Melim et al., in press) (Figs. 3C-6, 7). The best estimate for a lower limit of meteoric diagenesis in Unda is 130 m, but it may be 5–10 m higher (Fig. 3C-7) (Melim, 1996).

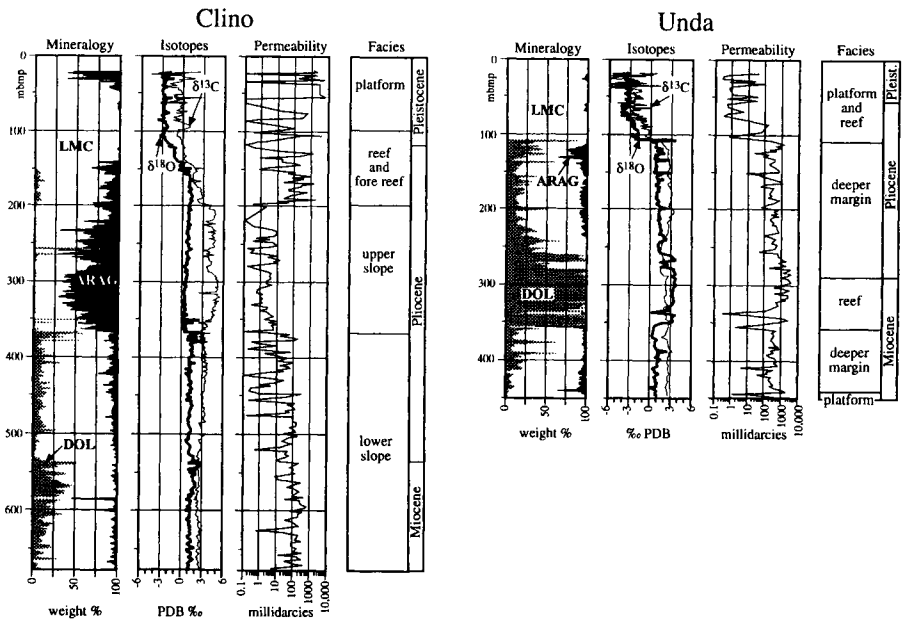


Fig. 3C-6. X-ray diffraction mineralogy, bulk-rock stable isotopic data, permeability, facies, and ages for cores Clino and Unda. Key: LMC, low-Mg calcite; ARAG, aragonite; DOL, dolomite. Ages from McNeill et al. (in press). Facies from Kenter et al. (in press) and Kievman and Ginsburg (in press). Depths are meters below mud pit (mbmp); for Unda, sea level was 5.2 mbmp; for Clino, sea level was 7.3 mbmp. (From Melim et al., 1995.)

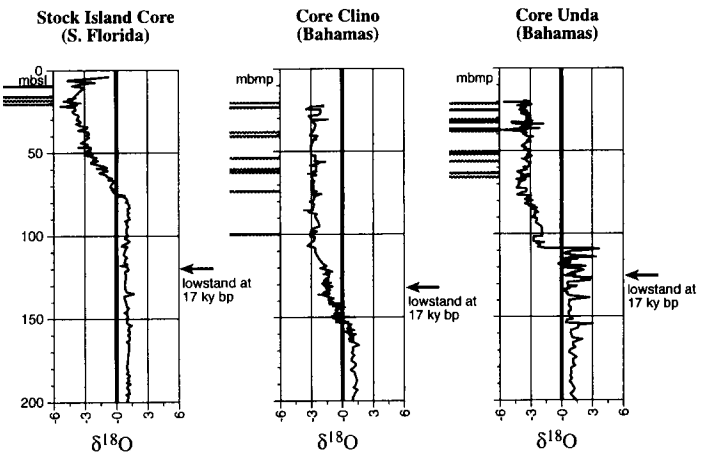


Fig. 3C-7. Bulk-rock oxygen isotopic data for the upper 200 m of Bahamian cores Clino and Unda as well as from the Stock Island core (located near Key West, Florida). Also shown are the positions of subaerial exposure surfaces (line to the left of each plot; Clino and Unda surfaces from Kievman and Ginsburg, in press, and Stock Island surfaces from K. Cunningham, pers. comm., 1995), and the elevation in each core of the latest Pleistocene sea-level lowstand (Fairbanks, 1989). Depths in core Stock Island are meters below sea level (mbsl) but cores Clino and Unda are meters below mud pit (mbmp). See text for discussion.

Also shown in Fig. 3C-7 is the upper 200 m of bulk-rock oxygen isotopic data for a core at Stock Island, near Key West, Florida (Fig. 3C-1). The facies in the Stock Island core are similar to those at core Unda except that the first occurrence of shallow-water reef facies is much higher in the core (45 m vs. 105 m) (K. Cunningham, pers. comm. 1995). The bulk-rock oxygen isotopic values in the Stock Island core follow exactly the same pattern as for cores Clino and Unda: negative values near the top, shifting to more positive values with depth. The marine value of +1‰ is reached at 78 m (Fig. 3C-7).

As shown in Fig. 3C-7, the thickness of the zone of transition between meteoric and marine-burial diagenesis is remarkably similar in the three cores (42–48 m). But, significantly, the position in the three cores is different: 110–152 m in core Clino, 85–130 m in core Unda, and 30–78 m at Stock Island. Also, the top of the zone of transition occurs within 10–15 m of the lowest subaerial exposure horizon in each core (Fig. 3C-7). It appears, therefore, that the zone of transitional isotopic ratios is tied to the *first* sea-level fall that exposed the particular site to fresh groundwater rather than to the later, perhaps larger-amplitude, lowstands of sea level (Melim, 1996). For example (Fig. 3C-7), the position of the latest Pleistocene sea-level lowstand (−120 m; Fairbanks, 1989) is located within the zone of transition for cores Clino and Unda, but about 40 m below the apparent base of meteoric diagenesis in the Stock Island core (Fig. 3C-7). Melim (1996) proposed that there is a maximum depth of 50–80 m below ground level that a meteoric groundwater lens can drive diagenesis in the climatic conditions of southern Florida and Great Bahama Bank. If some or all of the ~40-m-thick zone of transitional isotopic data represents dia-

genesis in a freshwater-saltwater mixing zone, then this depth of 50–80 m must be considered more than the associated sea-level fall, because the mixing zone extends some depth below sea level. Therefore, greater drops in sea level must lead to chemically inactive lenses. Two factors could lead to such chemically inactive lenses during large-scale sea-level lowstands: (1) a greater percolation distance leading to chemical saturation of meteoric water before it enters the lens; and (2) a greater distance from a source of soil-derived organic matter, which is known to drive diagenesis within meteoric lenses (Smart et al., 1988; McClain et al., 1992).

Marine-burial diagenesis in cores Clino and Unda

Most of the deeper-water facies in cores Clino and Unda were altered exclusively in the marine-burial environment (Fig. 3C-8, Melim et al., 1995; in press). Petrographic fabrics are similar to those found after meteoric diagenesis but stable isotopic values ($\delta^{18}O$, $+0.9 \pm 0.3‰$; $\delta^{13}C$, $+3.0 \pm 0.9‰$) identify marine porewater as the diagenetic fluid (Fig. 3C-6, Melim et al., 1995; in press). Petrographic fabrics fall into two contrasting groups, apparently controlled by the sediment permeability (Fig. 3C-8, Melim et al., 1995; in press). The most common fabric formed in permeable grainstones (permeability >100 md) and includes minor preserved aragonite, minor secondary dolomite, abundant moldic porosity, and trace amounts of dogtooth and overgrowth calcite cements (Fig. 3C-8). A thick peloid-rich interval with low permeability (<10 md) shows minimal diagenesis with up to 70% preserved detrital aragonite. Skeletal grainstones in the this peloid-rich interval, however, are characterized by aragonite neomorphism and near-complete blocky calcite cementation just like classic fabrics from areas of meteoric diagenesis (Fig. 3C-8). Apparently low permeability allows a more closed-system style of marine-burial diagenesis with dissolution and precipitation occurring simultaneously. The high-permeability intervals, in contrast, show extensive dissolution but most of the dissolved material is completely removed from the system without forming significant amounts of cement.

Dolomitization

Although abundant dolomite occurs in the deeply buried Cretaceous and older strata (Spencer, 1967; Meyerhoff and Hatten, 1974), the only detailed studies concern Miocene to Pliocene dolomite, particularly on San Salvador (Supko, 1970; Dawans and Swart, 1988; Vahrenkamp et al., 1991) and Little Bahama Bank (Fig. 3C-1) (Vahrenkamp, 1988; Vahrenkamp et al., 1991; Vahrenkamp and Swart, 1994). Dolomite is found also on Great Bahama Bank (Beach, 1982; Melim et al., in press) and in the southeast Bahamas (Fig. 3C-1) (Pierson, 1982). The amount and spatial distribution of the dolomite are highly variable between the different Bahamian banks. On Little Bahama Bank, dolomite is found in Miocene to Pleistocene sediments below 20–50 m in seven shallow cores (Williams, 1985; Vahrenkamp et al., 1991) and occurs at similar depths on San Salvador (Supko, 1970; Dawans and Swart, 1988) and

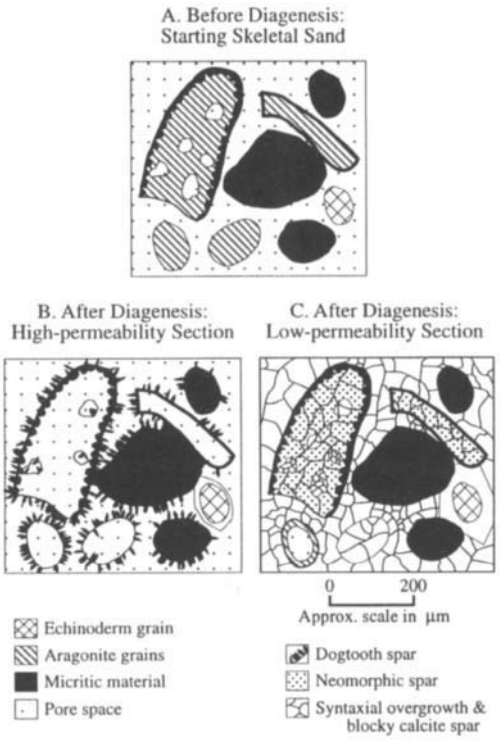


Fig. 3C-8. Characteristics of marine burial diagenesis. (A) Starting sediment. (B) End product, high-permeability section. Note minor overgrowth and dogtooth spar cementation and abundant moldic porosity. (C) End product, low-permeability section. Note nearly complete overgrowth and blocky spar cementation coeval with aragonite neomorphism and minor dissolution. (From Melim et al., 1995.)

Mayaguana and Great Inagua in the southeast Bahamas (Fig. 3C-1) (Pierson, 1982). On Great Bahama Bank, however, the shallowest dolomite is below 50 m and occurs only in one of the many shallow cores drilled (Beach, 1982). Dolomite occurs also in Miocene and Pliocene rocks below 250 m in core Unda, but this dolomite is much deeper than most of the Miocene-Pliocene dolomite in the Bahamas (Fig. 3C-6, Melim et al., in press). Melim et al. (in press) also identified significant seafloor dolomite in the deeper-water facies of cores Clino and Unda (Fig. 3C-6).

Dolomite fabrics are remarkably consistent throughout the Bahamas. Dawans and Swart (1988) identified four dolomite types in a core from San Salvador: (1) crystalline mimetic (CM) dolomite, a dense replacement dolomite that preserves the depositional fabric; (2) crystalline non-mimetic (CNM) dolomite, a dense mosaic of subhedral to anhedral crystals with no preserved precursor fabric; (3) microsucrosic (MS) dolomite, an open mosaic of euhedral 10–50-μm dolomite rhombs; and (4) a fabric transitional between MS and CM (CMS). Vahrenkamp and Swart (1994) modified this classification for Little Bahama Bank by the addition of sucrosic (S) for

MS dolomites with larger (>50 μm) crystals. Pierson (1982), working in the southeast Bahamas, and Beach (1982) and Melim et al. (in press), working on Great Bahama Bank, have documented similar textures to those identified by Dawans and Swart (1988) and Vahrenkamp and Swart (1994).

Vahrenkamp et al. (1991) used strontium isotope data to differentiate five post-early Miocene dolomitization phases with the two most important occurring during the late Miocene and the late Pliocene. Stable isotope and trace element data indicate dolomitization from a fluid near seawater in composition (Dawans and Swart, 1988; Vahrenkamp et al., 1991; Vahrenkamp and Swart, 1994; Whitaker et al., 1994; Melim et al., in press). Hydrologic models proposed to circulate seawater through Bahamian platforms include thermal (Kohout) convection (Dawans and Swart, 1988; Whitaker et al., 1994), lateral flow due to an across-the-bank head difference (Whitaker and Smart, 1993; Whitaker et al., 1994), reflux of mesosaline (salinity of 40–45‰) brines (Simms, 1984; Whitaker et al., 1994), and seawater circulation beneath a meteoric lens (Vahrenkamp and Swart, 1994). With so many independent dolomitization events, different circulation models may have operated at different times.

Implications for Fluid Flow

The predominant role that has been assigned to meteoric diagenesis of carbonate sediments is based largely on observations from modern meteoric lenses and from presently exposed carbonate rocks altered during earlier highstands (e.g., James and Choquette, 1984; Moore, 1989). Although it was reasonable to expect that this style of alteration continued during large-scale lowstands (e.g., Beach, 1995), the results from cores Clino, Unda, and Stock Island indicate that active meteoric diagenesis, in fact, may be restricted to depths less than 50–80 m below the ground surface (Melim, 1996). Because vuggy to cavernous porosity forms generally within a chemically active meteoric lens, it should only be expected in relatively shallow-water facies that are within the reach of such a lens during subsequent sea-level lowstands. Seismic facies 3, for example, is known from the deep test wells to be shallow-water facies and has vuggy to cavernous porosity to great depth (e.g., Spencer, 1967). Seismic facies 2, on the other hand, is predominantly deeper-water facies and generally lacks vuggy to cavernous porosity (Melim et al., in press). Also, there is no requirement that shallow-water facies be exposed to meteoric diagenesis. For example, the lower-platform facies in core Unda (below 430 m, Fig. 3C-6) was buried by deeper-water facies during a relative sea-level rise (Kenter et al., in press). As a result, this interval was altered only by marine pore fluids despite the fact that it was deposited in shallow waters (Melim et al., in press).

Indirect evidence of active flow of saline fluids though the subsurface of the Bahamian banks includes: (1) the amount of dolomite present requires a flow system capable of providing the Mg^{2+}; and (2) the aragonite dissolved during marine-burial diagenesis requires sufficient fluid migration to transport the $CaCO_3$ away without cementation. The first direct evidence of active flow of saline fluids was provided by Whitaker and Smart [see Chap. 4]. They showed that slightly increased salinity water,

derived from the shallow bank to the west of Andros Island, migrates easterly under Andros Island and discharges through blue holes on the eastern margin of Great Bahama Bank (Whitaker and Smart, 1990, 1993). This flow is believed to be driven by a combination of reflux and either thermal convection or lateral flow related to trans-bank differences in sea-level elevation (Whitaker and Smart, 1990, 1993). On the basis of Mg^{2+} depletion in the refluxing fluids, Whitaker et al. (1994) proposed that these fluids are actively forming trace amounts of dolomite. Whitaker and Smart (1993) estimated a maximum depth of reflux-driven circulation to be 168 m from the density of the refluxing fluids relative to the underlying saline groundwater. Swart et al. (in press) sampled fluids down to 600 m in cores Clino and Unda and also found evidence of significant fluid flow. Unlike Whitaker and Smart (1990, 1993), however, they did not find water with an elevated salinity, possibly because the far western location of the cores places them up-gradient from the source of refluxing fluids immediately west of Andros Island (Fig. 3C-1). Rather, Swart et al. (in press) found well-mixed fluids in the upper 200 m of the platform, with compositions near surface seawater. At greater depths, they found chemical gradients that they interpreted as indicating active carbonate diagenesis, particularly in core Clino.

Although many early studies emphasized the importance of meteoric fluids in the transformation of aragonite-rich sediments into calcitic limestones (e.g., James and Choquette, 1984), there is an increasing awareness that similar processes occur in marine pore fluids (e.g., Saller, 1984; Freeman-Lynde et al., 1986; Enos et al., 1995; Melim et al., 1995). Because surface seawater is saturated with respect to aragonite, many workers have restricted marine aragonite dissolution to below 300 m, where seawater becomes undersaturated (Saller, 1984; Freeman-Lynde et al., 1986; Enos et al., 1995). Marine-burial diagenesis, however, occurs as shallow as 130 m in core Unda (and 78 m in the Stock Island core), and seawater entering the platform should be saturated at this depth. The seawater, therefore, must become undersaturated within the burial environment. The most likely drive for this undersaturation is oxidation of organic matter leading to sulfate reduction and dissolution of aragonite by H_2S (Melim et al., in press). Although Swart et al. (in press) found evidence of continuing diagenesis in modern deep subsurface fluids, the majority of marine-burial diagenesis likely occurs before a 100-m burial, because marine-burial fabrics are fully developed in the Stock Island core at 78 m.

CONCLUDING REMARKS

The surface geology of the Bahamas has played a pivotal role in the development of carbonate depositional and diagenetic models (e.g., Newell et al., 1959; Bathurst, 1975). The surface geology largely reflects the role of Pleistocene sea-level fluctuations [Chap. 3A, 3B)]. Core and seismic data go below the surface veneer, revealing the long-term evolution of this classic carbonate system.

Facies models for isolated carbonate platforms tend to emphasize flat-topped banks with steep margins because this is the modern profile of Great Bahama Bank. This thinking leads to models where sediment production during sea-level highstands

is contrasted with exposure and meteoric diagenesis during sea-level lowstands (e.g., Sarg, 1988; Tucker and Wright, 1990). During most of its history, however, Great Bahama Bank had an asymmetric profile with a steep eastern margin and a gentle ramp profile to the west. This difference is important in that carbonate ramps, unlike platforms with rimmed margins, can continue sediment production during sea-level lowstands (e.g., Sarg, 1988; Schlager, 1992). For example, lowstand reefs recovered in both cores Unda (Miocene) and Clino (Pliocene-Pleistocene) attest to active carbonate sedimentation while the majority of Great Bahama Bank was exposed (Eberli et al., in press). During the late Pleistocene, on the other hand, lowstand sediment production was minimal as the steep margins provided little area for carbonate production (Droxler and Schlager, 1985; Grammer and Ginsburg, 1992).

In addition to a different bank profile, the sedimentation patterns of subsurface Great Bahama Bank differs from that of the modern. The modern bank is primarily a nonskeletal environment characterized by large areas of peloid- and/or ooid-rich sediments (Newell et al., 1959). Skeletal sediment is restricted to relatively narrow bands along the margins (Newell et al., 1959). Prior to the late Pliocene, however, open-marine skeletal facies were common across Great Bahama Bank (Beach and Ginsburg, 1980), as well as Little Bahama Bank (Williams, 1985) and the southeastern Bahamian banks (Pierson, 1982). This dramatic change needs to be remembered when using the Bahamas as an analog for ancient isolated platforms.

As noted by Tucker and Wright (1990), the extensive near-surface meteoric diagenesis caused by exposure during Pleistocene glacioeustatic sea-level fluctuations has biased diagenetic models towards alteration by meteoric fluids. The data from research cores Clino, Unda, and Stock Island, however, have provided new insight into the limitations of meteoric diagenesis. For example, rather than the extensive diagenesis predicted for large-scale lowstands (e.g., Beach, 1995), meteoric diagenesis in the Bahamas and Florida appears to be restricted to depths above 50–80 m below the land surface (Melim, 1996).

The depth limit for meteoric diagenesis in the Bahamas is consistent with data from the Yucatan Peninsula where the water table is ~30 m below the land surface and the fresh groundwater is near saturation to slightly supersaturated with respect to calcite, and only becomes chemically active during coastal mixing with seawater (Back and Hanshaw, 1970; Back et al., 1986). However, Nauru [q.v., Chap. 24] and Niue [q.v., Chap. 17], two raised atolls in the Pacific, have chemically active lenses beneath water tables located ~30–70 m below the land surface. These active lenses are at, or extend below, the predicted limit for the Bahamas. The most likely reason for this difference is the much higher rainfall and recharge rates for the Pacific raised atolls than for the Bahamas [Chap. 24 and Chap. 17 vs. Chap. 4]. At Nauru, the presence of abundant phosphate in the vadose zone may also contribute to more aggressive groundwaters (Jankowski and Jacobson, 1991).

Not only is meteoric diagenesis more limited than asserted in some conceptual models, but diagenesis in marine pore fluids is much greater. The Bahamas data extend the alteration by deep, cold, undersaturated seawater noted by previous workers (e.g., Saller, 1984; Freeman-Lynde et al., 1986; Enos et al., 1995) to the

shallow depths where seawater is supersaturated with respect to both calcite and aragonite (Melim et al., 1995). The study also shows that marine-burial diagenesis produces a limestone with fabrics essentially identical to those of meteoric diagenesis, thus making petrographic determination of diagenetic environment more difficult (Melim et al., 1995).

Differences between the surface and subsurface geology of Great Bahama Bank provide a cautionary note to models based on near-surface geology alone. Care is needed to separate factors that are unique to the modern interglacial period from those that are of more general applicability.

ACKNOWLEDGMENTS

The manuscript was improved by early reviews by G.P. Eberli and P.K. Swart and by later reviews by H.L. Vacher and three anonymous reviewers. We thank Texaco Inc. for providing us with the seismic data, and Pecten International for additional migrated seismic profiles. Numerous discussions with Chris Avenius, Tim Dixon and John Hurst were of great benefit to some of the ideas presented in the paper. The diagenetic study presented in this paper was supported by DOE grant DE-FG05-92ER14253 to G.P. Eberli and P.K. Swart. Support for coring of Clino and Unda, which led to the calibration of the seismic data, was provided by NSF grants OCE-8917295 and 9204294 to R.N. Ginsburg and P.K. Swart and the Industrial Associates Program of the Comparative Laboratory for Sedimentology. The Stock Island core was drilled by the Florida Geological Survey; analysis of the core was supported by the South Florida Water Management District. Core descriptions of the Stock Island core by K. Cunningham and E.R. Warzeski were very useful for the study. The Stable Isotope Laboratory was supported by NSF grants EAR-8417424, 8618727, and 9018882 to P.K. Swart.

REFERENCES

Austin, J.A., Jr., Ewing, J.I., Ladd, J.W., Mullins, H.T. and Sheridan, R.E., 1988. Seismic stratigraphic implications of ODP Leg 101 site surveys. In: J.A. Austin, W. Schlager et al., Proc. ODP, Sci. Results, 101. Ocean Drilling Program, College Station, pp. 391–424.

Back, W. and Hanshaw, B.B., 1970. Comparison of chemical hydrogeology of the carbonate peninsulas of Florida and Yucatan. J. Hydrol., 10: 330–368.

Back, W., Hanshaw, B.B., Herman, J.S. and Van Driel, J.N., 1986. Differential dissolution of a Pleistocene reef in the ground-water mixing zone of coastal Yucatan, Mexico. Geology, 14: 137–140.

Ball, M.M., Martin, R.G., Bock, R.G., Sylvester, R.E., Bowles, R.M., Taylor, D., Coward, E.L., Dodd, J.E. and Gilbert, L., 1985. Seismic structure and stratigraphy of northern edge of Bahaman-Cuban collision zone. Am. Assoc. Petrol. Geol. Bull., 69: 1275–1294.

Bathurst, R.G.C., 1975. Carbonate Sediments and Their Diagenesis. Elsevier, Amsterdam, 658 pp.

Beach, D.K., 1982. Depositional and diagenetic history of Pliocene-Pleistocene carbonates of northwestern Great Bahama Bank: Evolution of a carbonate platform. Ph.D. Dissertation, Univ. Miami, Coral Gables FL, 600 pp.

Beach, D.K., 1995. Controls and effects of subaerial exposure on cementation and development of secondary porosity in the subsurface of Great Bahama Bank. In: D.A. Budd, A.H. Saller and P.M. Harris (Editors), Unconformities and Porosity in Carbonate Strata. Am. Assoc. Petrol. Geol. Mem., 63: 1–33.

Beach, D.K. and Ginsburg, R.N., 1980. Facies succession of Pliocene-Pleistocene carbonates, northwestern Great Bahama Bank. Am. Assoc. Petrol. Geol. Bull., 94: 1634–1642.

Bryant, W.R., Meyerhoff, A.A., Brown, N.K., Furrer, M.A., Dyle, T.E. and Antoine, J.W., 1969. Escarpments, reef trends and diapiric structures, eastern Gulf of Mexico. Am. Assoc. Petrol. Geol. Bull., 53: 2506–2542.

Budd, A.F. and Kievman, C.M., in press. Coral assemblages and reef environments in the Bahamas Drilling Project cores. In: R.N. Ginsburg (Editor), The Bahamas Drilling Project, SEPM Concepts in Sedimentol.

Cant, R.V., 1977. Role of coral deposits in building the margins of the Bahama Banks. Proc. Third Int. Coral Reef Symp. (Miami), 2: 9–13.

Dawans, J.M. and Swart, P.K., 1988. Textural and geochemical alterations in Late Cenozoic Bahamian dolomites. Sedimentol., 35: 385–403.

Droxler, A.W. and Schlager, W., 1985. Glacial versus interglacial sedimentation rates and turbidite frequency in the Bahamas. Geology, 13: 799–802.

Eberli, G.P. and Ginsburg, R.N., 1987. Segmentation and coalescence of Cenozoic carbonate platforms, northwestern Great Bahama Bank. Geology, 15: 75–79.

Eberli, G.P. and Ginsburg, R.N., 1989. Cenozoic progradation of NW Great Bahama Bank—A record of lateral platform growth and sea-level fluctuations. In: P.D. Crevello, J.L. Wilson, J.F. Sarg and J.F. Read (Editors), Controls on Carbonate Platform and Basin Development. Soc. Econ. Paleontol. Mineral. Spec. Publ., 44: 339–355.

Eberli, G.P., Kendall, C.G.St.C., Moore, P., Whittle, G.L. and Cannon, R., 1994. Testing a seismic interpretation of Great Bahama Bank with a computer simulation. Am. Assoc. Petrol. Geol. Bull., 78: 981–1004.

Eberli, G.P., Kenter, J.A.M., McNeill, D.F., Ginsburg, R.N., Swart, P.K., and Melim, L.A., in press. Facies, diagenesis, and timing of prograding sequences on western Great Bahama Bank. In R.N. Ginsburg (Editor), The Bahamas Drilling Project. SEPM Concepts in Sedimentol.

Enos, P., Camoin, G.F. and Ebren, P., 1995. Sedimentary sequence from sites 875 and 876, outer perimeter ridge, Wodejebato Guyot. In: J.A. Haggerty, I. Premoli Silva, F. Rack and M.K. McNutt (Editors), Proc. ODP, Sci. Results, 144. Ocean Drilling Program, College Station, pp. 295–310.

Fairbanks, R.G., 1989. A 17,000-year glacio-eustatic sea level record: influence of glacial melting rates on the Younger Dryas event and deep-ocean circulation. Nature, 342: 637–642.

Freeman-Lynde, R.P., Whitley, K.F. and Lohmann, K.C., 1986. Deep-marine origin of equant spar cements in Bahama escarpment limestones. J. Sediment. Petrol., 56: 799–811.

Ginsburg, R.N. (Editor), in press. The Bahamas Drilling Project. SEPM Concepts in Sedimentology.

Goodell, H.G. and Garman, R.K., 1969. Carbonate geochemistry of Superior deep test well, Andros Island, Bahamas. Am. Assoc. Petrol. Geol. Bull., 53: 513–536.

Grammer, G.M. and Ginsburg, R.N., 1992. Highstand versus lowstand deposition on carbonate platform margins: insight from Quaternary foreslopes in the Bahamas. Mar. Geol., 103: 125–136.

Hine, A.C. and Neumann, A.C., 1977. Shallow carbonate-bank-margin growth and structure, Little Bahama Bank, Bahamas. Am. Assoc. Petrol. Geol. Bull., 61: 376–406.

Hooke, R.L. and Schlager, W., 1980. Geomorphic evolution of the Tongue of the Ocean and Providence channels, Bahamas. Mar. Geol., 35: 343–366.

James, N.P. and Choquette, P.W., 1984. Diagenesis 9: Limestones: The meteoric diagenetic environment. Geosci. Can., 11: 161–194.

Jankowski, J. and Jacobson, G., 1991. Hydrochemistry of a groundwater-seawater mixing zone, Nauru Island, central Pacific Ocean. BMR J. Aust. Geol. Geophys., 12: 51–64.

Kenter, J.A.M., Ginsburg, R.N., and Troelstra, S.R., in press. Western Great Bahama Bank: Sea level-driven sedimentation patterns on the slope and margin. In: R.N. Ginsburg (Editor), The Bahamas Drilling Project. SEPM Concepts in Sedimentol.

Kievman, C.M. and Ginsburg, R.N., in press. Pliocene to Pleistocene depositional history of the upper platform margin, northwest Great Bahama Bank. In: R.N. Ginsburg (Editor), The Bahamas Drilling Project. SEPM Concepts in Sedimentol.

Masaferro, J.L. and Eberli, G.P., 1994. Structural control of the evolution of a carbonate platform along a compressional plate boundary, southern Great Bahama Bank (abstr.). Geol. Soc. Am. Abstr. Programs, 26: A364–A365

McClain, M.E., Swart, P.K. and Vacher, H.L., 1992. The hydrogeochemistry of early meteoric diagenesis in a Holocene deposit of biogenic carbonates. J. Sediment. Petrol., 62: 1008–1022.

McNeill, D.F., 1989. Magnetostratigraphic dating and magnetization of Cenozoic platform carbonates from the Bahamas. Ph.D. Dissertation, Univ. Miami, Coral Gables FL, 210 pp.

McNeill, D.F., Eberli, G.P., Lidz, B.H., Swart, P.K., and Kenter, J.A.M., in press. Chronostratigraphy of prograding carbonate platform margins: A record of sea-level changes and dynamic slope sedimentation. In: R.N. Ginsburg (Editor), The Bahamas Drilling Project. SEPM Concepts in Sedimentol.

Melim, L.A., 1996. Limitations on lowstand meteoric diagenesis in the Pliocene-Pleistocene of Florida and Great Bahama Bank: Implications for eustatic sea-level models. Geology, 24: 893–896.

Melim, L.A., Swart, P.K. and Maliva, R.G., 1995. Meteoric-like fabrics forming in marine waters: Implications for the use of petrography to identify diagenetic environments. Geology, 23: 755–758.

Melim, L.A., Swart, P.K., and Maliva, R.G., in press. Meteoric and marine burial diagenesis in the subsurface of Great Bahama Bank. In: R.N. Ginsburg (Editor), The Bahamas Drilling Project. SEPM Concepts in Sedimentol.

Meyerhoff, A.A. and Hatten, C.W., 1974. Bahamas salient of North America: Tectonic framework, stratigraphy, and petroleum potential. Am. Assoc. Petrol. Geol. Bull., 58: 1201–1239.

Moore, C.H., 1989, Carbonate Diagenesis and Porosity. Elsevier, Amsterdam, 338 pp.

Mullins, H.T., 1983. Modern carbonate slopes and basins of the Bahamas. In: H.E. Cook, A.C. Hine and H.T. Mullins (Editors), Platform Margin and Deep Water Carbonates. Soc. Econ. Paleontol. Mineral. Short Course 12: 4/1–4/138.

Mullins, H.T., Breen, N., Dolan, J., Wellner, R.W., Petruccione, J.L., Gaylord, M., Andersen, B., Melillo, A.J., Jurgens, A.D. and Orange, D., 1992. Carbonate platforms along the southeast Bahamas-Hispaniola collision zone. Mar. Geol., 105: 169–209.

Mullins, H.T. and Lynts, G.W., 1977. Origin of the northwestern Bahama Platform: Review and reinterpretation. Geol. Soc. Am. Bull. 88: 1447–1461.

Newell, N.D., 1955. Bahamian platforms. In: A. Poldervaart (Editor), The Crust of the Earth, a Symposium. Geol. Soc. Am. Spec. Pap. 62: 303–315.

Newell, N.D., Imbrie, J., Purdy, E.G. and Thurber, D.L., 1959. Organism communities and bottom facies, Great Bahama Bank. Am. Mus. Nat. History Bull., 117: 177–228.

Paulus, F.J., 1972. The geology of site 98 and the Bahamas platform. In: C.D. Hollister, J.T. Ewing, et al., Initial Reports of the Deep Sea Drilling Project, 11. U.S. Gov. Printing Office, Washington D.C., pp. 877–897.

Pierson, B.J., 1982. Cyclic sedimentation, limestone diagenesis and dolomitization in upper Cenozoic carbonates of the southeastern Bahamas. Ph.D. Dissertation, University of Miami, Coral Gables, 312 pp.

Saller, A.H., 1984. Petrologic and geochemical constraints on the origin of subsurface dolomite, Enewetak Atoll: an example of dolomitization by normal sea water. Geology, 12: 217–220.

Sarg, J.F., 1988. Carbonate sequence stratigraphy. In: C.K. Wilgus, B.S. Hastings, H. Posamentier, J. Van Wagoner, C.A. Ross, and C.G. St. Kendall, Sea-level Changes: An Integrated Approach. Soc. Econ. Paleontol. Mineral. Spec. Publ., 42: 155–182.

Schlager, W., 1992. Sedimentology and Sequence Stratigraphy of Reefs and Carbonate Platforms. Am. Assoc. Petrol. Geol., Cont. Edu. Course Note Ser., 34, 71 pp.

Schlager, W., Bourgeois, F., Mackenzie, G. and Smit, J., 1988. Boreholes at Great Issac and site 626 and the history of the Florida Straits. In: J.A. Austin, W. Schlager et al. (Editors), Proc. ODP, Sci. Results, 101. Ocean Drilling Program, College Station, pp. 425–437.

Schlager, W. and Ginsburg, R.N., 1981. Bahama carbonate platforms-the deep and the past. Mar. Geol., 44: 1–24.

Sheridan, R.E., 1974. Atlantic continental margin of North America. In: C.A. Burk and C.L. Drake (Editors), Geology of Continental Margins, Springer-Verlag, New York, pp. 391–407.

Sheridan, R.E., Crosby, J.T., Bryan, G.M. and Stoffa, P.L., 1981. Stratigraphy and structure of southern Blake Plateau, northern Florida Straits, and northern Bahamas from multichannel seismic reflection data. Am. Assoc. Petrol. Geol. Bull., 65: 2571–2593.

Sheridan, R.E., Mullins, H.T., Austin, J.A., Jr., Ball, M.M. and Ladd, J.W., 1988. Geology and geophysics of the Bahamas. In: R.E. Sheridan and J.A. Grow (Editors), The Atlantic Continental Margin, U.S. Geol. Soc. Am., The Geology of North America, I-2: 329–364.

Simms, M.A., 1984. Dolomitization by groundwater-flow systems in carbonate platforms. Trans. Gulf Coast Assoc. Geol. Soc., 34: 411–420.

Smart, P.L., Dawans, J.M. and Whitaker, F., 1988. Carbonate dissolution in a modern mixing zone. Nature, 337: 811–813.

Spencer, M., 1967. Bahamas deep test. Am. Assoc. Petrol. Geol. Bull., 51: 263–268.

Supko, P.R., 1970. Depositional and diagenetic patterns in subsurface Bahamian rocks. Ph.D. Dissertation, Univ. Miami, Coral Gables FL, 168 pp.

Swart, P.K., Elderfield, H. and Ostlund, G., in press. The geochemistry of pore fluids from the Great Bahama Bank. In: R.N. Ginsburg (Editor), The Bahamas Drilling Project. SEPM Concepts in Sedimentol.

Tucker, M.E. and Wright, V.P., 1990. Carbonate Sedimentology. Blackwell, Oxford U.K., 482 pp.

Vahrenkamp, V.C., 1988. Constraints on the formation of platform dolomite: A geochemical study of late Tertiary dolomite from Little Bahama Bank, Bahamas. Ph.D. Dissertation, Univ. Miami, Coral Gables FL, 434 pp.

Vahrenkamp, V.C. and Swart, P.K., 1994. Late Cenozoic sea-water generated dolomites of the Bahamas: Metastable analogues for the genesis of ancient platform dolomites. In: B.H. Purser, M. Tucker and D.H. Zenger (Editors), Dolomites, A Volume in Honour of Dolomieu. Int. Assoc. Sedimentol. Spec. Publ., 21: 133–153.

Vahrenkamp, V.C., Swart, P.K. and Ruiz, J., 1991. Episodic dolomitization of late Cenozoic carbonates in the Bahamas: evidence from strontium isotopes. J. Sediment. Petrol., 61: 1002–1014.

Walles, F.E., 1993. Tectonic and diagenetically induced seal failure within the south-western Great Bahamas Bank. Mar. Petrol. Geol., 10: 14–28

Whitaker, F.F. and Smart, P.L., 1990. Active circulation of saline ground waters in carbonate platforms: Evidence from the Great Bahama Bank. Geology, 18: 200–203.

Whitaker, F.F. and Smart, P.L., 1993. Circulation of saline groundwaters in carbonate platforms: a review and case study from the Bahamas. In: A.D. Horbury and A.G. Robinson (Editors), Diagenesis and Basin Development. Am. Assoc. Petrol. Geol. Studies Geol., 36: 113–132.

Whitaker, F.F., Smart, P.L., Vahrenkamp, V.C., Nicholson, H. and Wogelius, R.A., 1994. Dolomitization by near-normal seawater? Field evidence from the Bahamas. In: B.H. Purser, M. Tucker and D.H. Zenger (Editors), Dolomites, A Volume in Honour of Dolomieu. Int. Assoc. Sedimentol. Spec. Publ., 21: 111–132.

Williams, S.C., 1985. Stratigraphy, facies evolution, and diagenesis of late Cenozoic limestones and dolomites, Little Bahama Bank, Bahamas. Ph.D. Dissertation, Univ. Miami, Coral Gables FL, 217 pp.

Geology and Hydrogeology of Carbonate Islands. Developments in Sedimentology 54
edited by H.L. Vacher and T. Quinn
© 1997 Elsevier Science B.V. All rights reserved.

Chapter 4

HYDROGEOLOGY OF THE BAHAMIAN ARCHIPELAGO

FIONA F. WHITAKER and PETER L. SMART

INTRODUCTION

The Bahamian archipelago, which includes the separate political units of the Bahamas and the Turks and Caicos Islands, stretches some 1,000 km from southern Florida to Haiti and covers a total area of 260,000 km^2. Approximately half of this area comprises extensive shallow carbonate banks less than 20 m deep, but only 5.5% of the total area is emergent islands. Many of these islands are long and narrow and lie along the eastern (windward) edges of the banks. The islands comprise predominantly Pleistocene marine limestones and aeolianites, the latter forming ridges up to 63 m high. Extensive low-lying areas of Holocene lime muds occur along many leeward shores.

The Bahamas has a tropical marine climate. Winters are mostly dry, with occasional cold fronts that bring rain to the northern islands. Persistent trade winds with convective rainfall characterise the summer (Sealey, 1985). There is a marked climatic gradient from the cooler wetter northwest to the warmer drier southeast (Fig. 4-1). The whole of the archipelago lies within the North Atlantic hurricane belt.

The vegetation of the four northern islands (Grand Bahama, the Abacos, New Providence and North Andros) consists largely of forests of Caribbean Pine and Palmetto Palm. Farther south, the drier conditions give rise to relatively dense, mixed tropical broad-leaf coppice of high diversity. At the southern extreme, vegetation degenerates to low scrub (Campbell, 1978). At all latitudes mangrove swamps are developed along low-lying coastal areas. Much of the vegetation has been affected by man and is secondary. An extreme example is the almost complete denudation of the salt islands of Grand Turk, Salt Cay and South Caicos, which were cleared by early settlers in an attempt to enhance evaporation from salt pans.

BAHAMIAN AQUIFERS

Hydraulic conductivity of Bahamian limestones

Two carbonate aquifers with very different permeability characteristics are used for water supply in the Bahamas and the Turks and Caicos Islands. Local strand and beach sands form the unconsolidated to partially consolidated Holocene aquifer [the Rice Bay Formation; see Chap. 3A], which is characterised by high primary porosity and relatively low hydraulic conductivity. The principal aquifer on most islands is

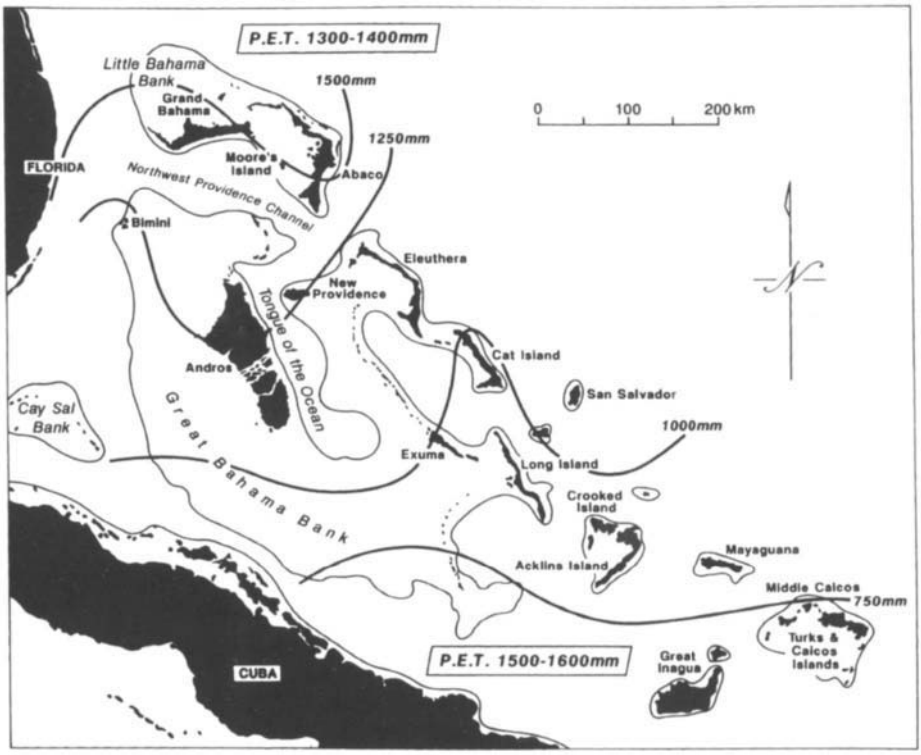


Fig. 4-1. Map of the Bahamian archipelago showing location of named islands and regional variation of rainfall. (After Sealey, 1985.).

the Pleistocene Lucayan Limestone [which includes the Owl's Howl and Grotto Beach Formations; see Chap. 3A], which has very high hydraulic conductivities due to development of dissolutional secondary porosity. Much less is known about the hydrogeology of the older, pre-Lucayan limestones and dolomites, which contain saline groundwater and are utilized on more-developed islands for cooling and waste disposal.

The transmission properties of the Holocene sands and the Lucayan Limestone are presented here (Table 4-1, Fig. 4-2) at a range of scales of investigation: laboratory permeameter data (10^{-1} m); estimates of hydraulic conductivity at the local scale from packer tests (10^{0} m), slug and bailer tests (10^{0}–10^{1} m) and pumping tests (10^{2} m); and at the regional scale (10^{4} m) based on lags in the response of water levels to semidiurnal ocean tides. All the theoretical solutions applied here assume laminar flow, and the saturated aquifer thickness has been assumed to be equivalent to the saturated depth of the borehole. At all scales of investigation the distribution of hydraulic conductivity is lognormal and, consequently, all values of the mean and coefficient of variation (CV = standard deviation/mean) given here are calculated from log values. The use of hydraulic conductivity here implies prevailing kinematic

Table 4-1

Scale-dependent nature of hydraulic conductivity of Holocene Sands and Pleistocene Limestone Aquifers

Aquifer Tests	Site (Source)	Mean K (m day^{-1})	CV (%)	n
A. Holocene Sands Aquifer				
Permeameter				
Submarine Grainstones	Great Bahama Bank (1)	25	10	12
Vadose	Joulter Cays (2)	0.15	39	14
Phreatic	Joulter Cays (2)	0.50	19	15
Vadose	Ocean Bight, Exuma (3)	10	–	–
Vadose	Gold Rock, Grand Bahama (4)	11	23	18
Slug & Bailer	Wood Cay, Eleuthera (5)	22	32	17
	Water Cay, Eleuthera (5)	79	15	9
Pumping Tests*	Ocean Bight, Exuma (6)	200	–	–
	Mid Eleuthera (7)	220	–	–
	Providenciales (8)	50–1500†	–	–
B. The Pleistocene Aquifer, Northern Bahamas				
Permeameter	North Andros (9)	0.039	100	81
Packer Tests	New Providence (10)	0.15	7.5	21
Slug Tests	Grand Bahama (11)	97	28	44
Pumping Tests	North Andros (12)	470	25	31
	Grand Bahama (13)	1200	25	74
Tidal Lags	North Andros (12)	6.6×10^6	4.0	8

* May be underestimates because of the (undocumented) use of a cementing compound to prevent collapse (R.V. Cant pers. comm.).

† Maximum and minimum values quoted.

Sources: (1) Enos & Sawatsky, 1981; (2) Halley & Harris, 1979; (3) Wallis et al., 1991; (4) Brooks and Whitaker, 1997; (5) Budd, 1984; (6) Cant, 1979; (7) Little et al., 1977; (8) United Nations, 1976; (9) Beach, 1982; (10) Peach, 1991; (11) Smart et al., 1992; (12) Little et al., 1973; (13) Little et al., 1976.

viscosity and relates to intrinsic permeability such that K = 1 m day^{-1} here converts to about $k = 1.2 \times 10^{-8}$ cm^2.

The Holocene aquifer

The Holocene aquifer comprises unconsolidated or partially consolidated calcareous sands occurring in two settings: beach-ridge complexes and spits onlapping Pleistocene limestones, and emergent shoal complexes that form small, bank-margin islands such as the oolitic Joulter Cays north of Andros Island. On some islands, including Grand Bahama and Andros Islands, subaerial Holocene deposits are volumetrically insignificant and locally distributed. However, many windward islands, such as Eleuthera and Cat Island, have an almost continuous coastal fringe of Holocene sands, and relatively extensive and thick deposits may accumulate within coastal embayments as at Ocean Bight on Great Exuma Island. The sands are

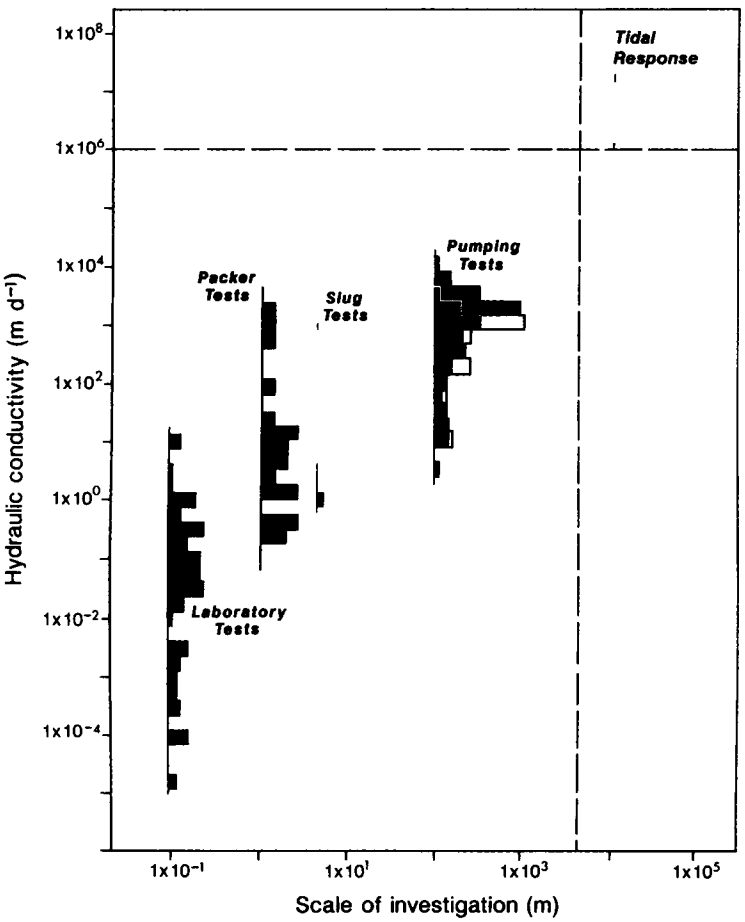


Fig. 4-2. Relationship between aquifer hydraulic conductivity and scale of investigation for Andros (laboratory, tidal and shadow histogram for pumping tests), New Providence (packer tests) and Grand Bahama (slug and pumping tests). Data are in Table 4.2. The inverse log-log relationship between the mean hydraulic conductivity and the coefficient of variation is significant at 99.9% for the 5 scales of investigation, and at 97.5% if the tidal-lag data are excluded. Note the extremely high values from calculations based on tidal lags.

generally bioclastic, and ooids are locally abundant where an offshore source is present. The typical sand is moderately well to well sorted, with grain sizes of 0.1–0.7 mm and some fragments up to 2 mm. In addition, poorly sorted fine-grained marls of Holocene age have been reported to occur locally on a few islands (Little et al., 1977).

Although the Holocene sands have a high total porosity (typically 40–50%; e.g., Halley and Harris, 1979), the small amplitude of groundwater tides indicates the relatively low transmissivity of the sands. Permeameter values for hydraulic conductivity are somewhat lower than those of the modern bank-top grainstones which

constitute the source sediments (Table 4.1). The difference suggests that the interparticle pore system is partially occluded by cementation during meteoric diagenesis. The reduction in hydraulic conductivity appears to be greater at Joulter Cays than at Ocean Bight, possibly because of enhanced diagenesis associated with the greater freshwater flux in the wetter climate of the northern Bahamas.

Cementation varies vertically and spatially. A partially cemented to well-cemented zone at and below the water table results from degassing of CO_2 from phreatic waters (Halley and Harris, 1979; Budd, 1988a; McClain et al., 1992). Thus, on Wood and Water Cays, there is a logarithmic increase in hydraulic conductivity with depth in the upper 1–1.5 m of the phreatic zone, and higher values are found towards the island periphery where cementation is significantly less (Budd, 1984). Although flow within the Holocene aquifer is predominantly intergranular, Budd (1988a,b) report development and coalescence of mouldic porosity at Wood and Water Cays, and at Joulter Cays, Halley and Harris (1979) observed root holes and vesicular voids suggesting early channelling of flow. Such occurrences may explain why, at Joulter Cays, permeabilities observed in the vadose zone are higher and more variable than in the freshwater phreatic zone. The secondary porosity may also provide the increased integration of flow evident from the higher hydraulic conductivities measured at larger scales of investigation (Table 4.1).

Despite these heterogeneities, the Holocene aquifer in general has a moderate and relatively uniform hydraulic conductivity. The moderate hydraulic conductivity results both in potential for retention of a thick freshwater lens and suppression of tide-driven mixing. Despite difficulties in abstraction, the sands form a locally important aquifer, particularly in the more arid southern Bahamas (Cant and Weech, 1986; Wallis et al., 1991).

The Pleistocene aquifer

The Lucayan Limestone (Beach and Ginsburg, 1980) is the major freshwater aquifer on most Bahamian islands. In most places on land, the upper boundary of the unit is the present-day subaerial discontinuity surface, but locally on the islands, and over most of the submerged banks, the Lucayan is overlain by Holocene sediments. The Lucayan is predominantly calcitic and comprises irregularly cemented, poorly stratified packstones and wackestones in which peloids and ooids are the predominant grains. This lithology contrasts markedly with the stratified skeletal limestones of the underlying unnamed unit, the transition with which is dated as late Pliocene (McNeill et al., 1988).

The thickness of the Lucayan Limestone varies for individual banks. According to Pierson (1982), this variation is controlled by regional flexure, which determines the areal variation of subsidence rate. The Lucayan reaches a maximum thickness of 43 m on Andros Island and the Great Bahama Bank, and a minimum on Mayaguana of 10.5 m (Cant and Weech, 1986). Laterally continuous disconformity surfaces formed by subaerial exposure of the marine deposits during sea-level lowstands are present throughout the unit (Beach, 1982). The frequency of these

surfaces (on average 1 per 3 m) is twice that in the underlying unit and reflects the considerable eustatic sea-level fluctuations of the Pleistocene. These sea-level variations and the associated meteoric diagenesis were responsible for the extensive development of secondary, fissure and cavernous porosity in the Lucayan Limestone and underlying Pliocene units.

At all scales of investigation, the transmission properties of the Lucayan Limestone are governed by dissolutional secondary porosity. Macroscopic porosity seen in core is almost exclusively secondary and includes vuggy and channel porosity (<1 mm to 10 cm, Beach, 1982). Permeameter data indicate a low average core permeability but very high heterogeneity, with values ranging over 6 orders of magnitude. Vertical channels, probably of vadose origin, are numerous and frequently follow burrow mottling. Horizontally oriented channels and cavernous zones (indicated by low core recovery) appear to be controlled by subaerial discontinuity surfaces and/or paleo-water tables. The latter have a high lateral continuity and, at the scale of slug and pump tests, seem to be the predominant control on hydraulic conductivity, giving higher and less variable values (Table 4.1).

Both the number and size of secondary openings are reflected by the fissuration index, defined as the percentage of the saturated thickness over which the diameter of a borehole is larger than the nominal diameter. The average fissuration index determined from caliper logs of boreholes on Grand Bahama is 82 ± 6.2% (n = 14); all boreholes show enlargement for more than 67% of their length (Smart et al., 1992). As shown in Figure 4-3A, there is a remarkably good relationship between the fissuration index and the measured hydraulic conductivity. This relation confirms that the fissure voids integrate laterally and are responsible for the large aquifer transmissivity.

Although the minimum hydraulic conductivities from slug and pumping tests are comparable and equal to the maximum core permeabilities, more than 60% of the values from pumping tests exceed the maximum derived from slug tests. This distribution indicates that the relatively large cone of depression created by pumping intersects dissolution conduits, which are sufficiently widely spaced that the probability of direct penetration by randomly placed boreholes is low. The overlap between the range of hydraulic conductivities derived from core, slug and pumping tests suggests good links between fissure and cavernous porosity.

On a regional scale, tidal lags yield extremely high average hydraulic conductivities, suggesting problems applying the theoretical solution of Ferris (1951) to the heterogeneous karstified aquifers of the Bahamas. However, Little et al. (1976) report that the tidal fluctuation in deep boreholes in Long Island is larger than that of the sea surface on the west coast of the island. This observation suggests that the tidal signal can pass beneath the island more effectively than across the shallow bank. This evidence, together with the inverted subsurface geothermal gradients (Whitaker and Smart, 1993; Walles, 1993), does indicate a high degree of exchange with the surrounding ocean water and very high hydraulic conductivities at the regional scale.

In contrast to core and slug-test hydraulic conductivities which appear essentially independent of depth, pumping tests for Grand Bahama Island reveal an increase of

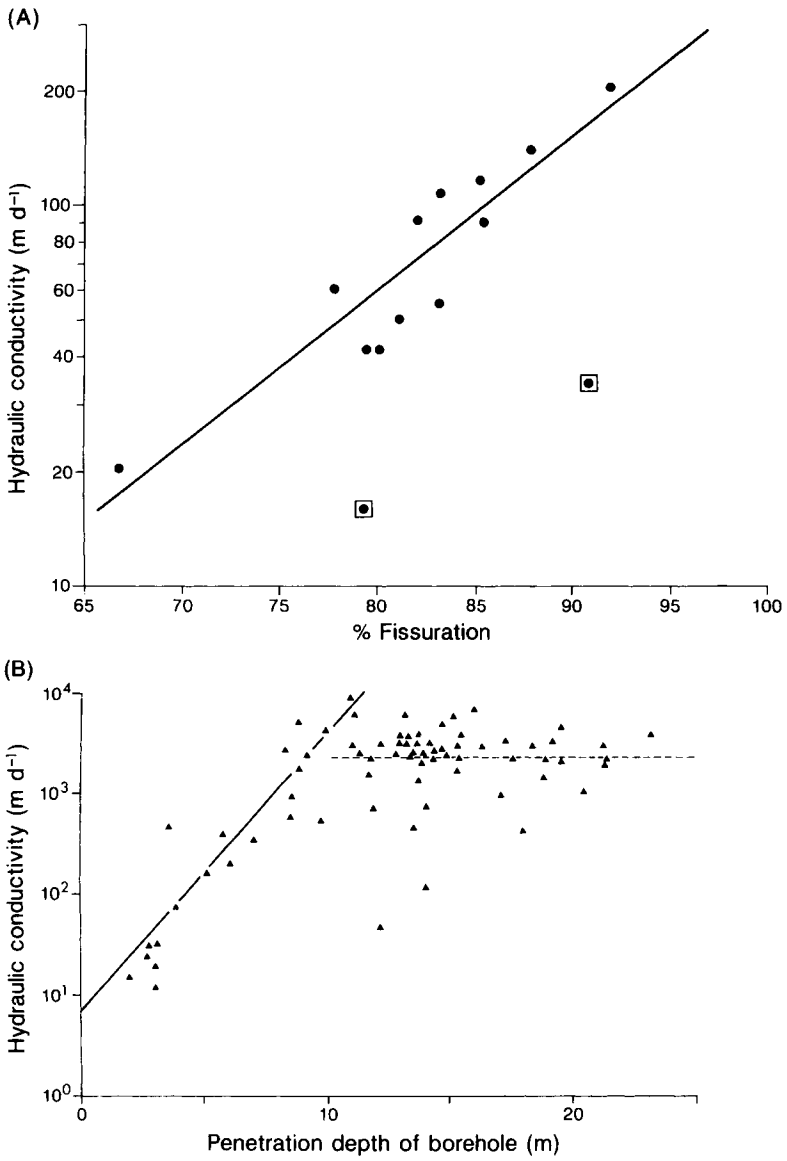


Fig. 4-3. Variation of hydraulic conductivity of the Pleistocene Lucayan Limestone: local scale, from pumping tests. (A) Hydraulic conductivity vs. degree of fissuration. Positive correlation is significant at 99%, excluding the two boxed outliers. (After Smart et al., 1992.) (B) Hydraulic conductivity vs. depth of borehole penetration. Solid line is best fit regression for boreholes < 10 m saturated thickness (significant at >99.9%, n = 21); dashed line is average for boreholes < 10 m saturated thickness. (After Whitaker and Smart, 1997a).

one order of magnitude per 3.2-m saturated thickness to a maximum depth of 10 m (Fig. 4-3B), below which the values are randomly distributed around a mean of 2,100 m day^{-1} (12% CV). This depth corresponds both to the base of the upper subunit of the Lucayan Limestone, differentiated by a larger number of exposure surfaces compared to underlying subunits (Beach and Ginsburg 1980), and to the "Hard Brown Crust", a major discontinuity surface that occurs throughout the northern islands and locally generates confining conditions (Cant and Weech, 1986). On Grand Bahama Island, Smart et al. (1992) found an increase in the fissuration index with depth to a maximum sampled depth of 33 m. Also, tidal efficiency (well-to-ocean amplitude ratio) increases as borehole depths increase, and decreases on backfilling (Mather and Buckley, 1973). Overall, the increase in hydraulic conductivity with depth reflects progressive diagenetic evolution with time. The increase is most marked for the more transmissive components of the flow system (fissure and cavernous porosity) that are apparent at a larger scale of investigation.

Regional variations in hydraulic conductivity have been examined by Whitaker and Smart (1997a) using pumping test data for 244 boreholes from 13 islands distributed through the archipelago (Fig. 4-4). Despite the small sample size and large intraisland variation, there appears to be a systematic variation in hydraulic conductivity, with a reduction of 2–3 orders of magnitude from Grand Bahama and Abaco Islands in the north to Middle Caicos Island in the south. This reduction parallels the strong climatic gradient from the wetter northwestern islands to the dryer southeastern islands. The relationship may reflect differences in the rates of diagenetic processes that are strongly dependent upon the net groundwater flux, such as the rate of carbonate dissolution (Smart and Whitaker, 1988) and the rate of initial mineralogical stabilisation (Halley and Harris, 1979, cf. Pierson and Shinn, 1985). Secondary cementation at and below exposure surfaces (e.g., calcrete deposition) is probably also of importance, as is illustrated by the reduction of porosity by 60–75% at subsurface exposure horizons on North Andros Island (Beach, 1995). Calcrete development appears to be more extensive in the arid southern islands (Wanless et al., 1989). The implication of these findings is that the climatic gradient which occurs at present through the Bahamas is a long-standing feature of the region and has played a fundamental role in the diagenetic evolution of the aquifer during the Pleistocene.

Throughout the Bahamian archipelago the transmission properties of the Lucayan Limestone aquifer are controlled by development of dissolutional secondary porosity at a range of scales from mouldic, through channelised, to large-scale karstic cavernous porosity. Hydraulic conductivity thus increases both with the rate of diagenetic processes, as controlled by interisland differences in rainfall, and with time, which gives an increase in permeability with depth. The latter is important in controlling the extent of development of the freshwater lens. The high permeabilities at depth also mean that relatively small differences in hydraulic potential can generate large-scale circulation of saline groundwater deep within the platform.

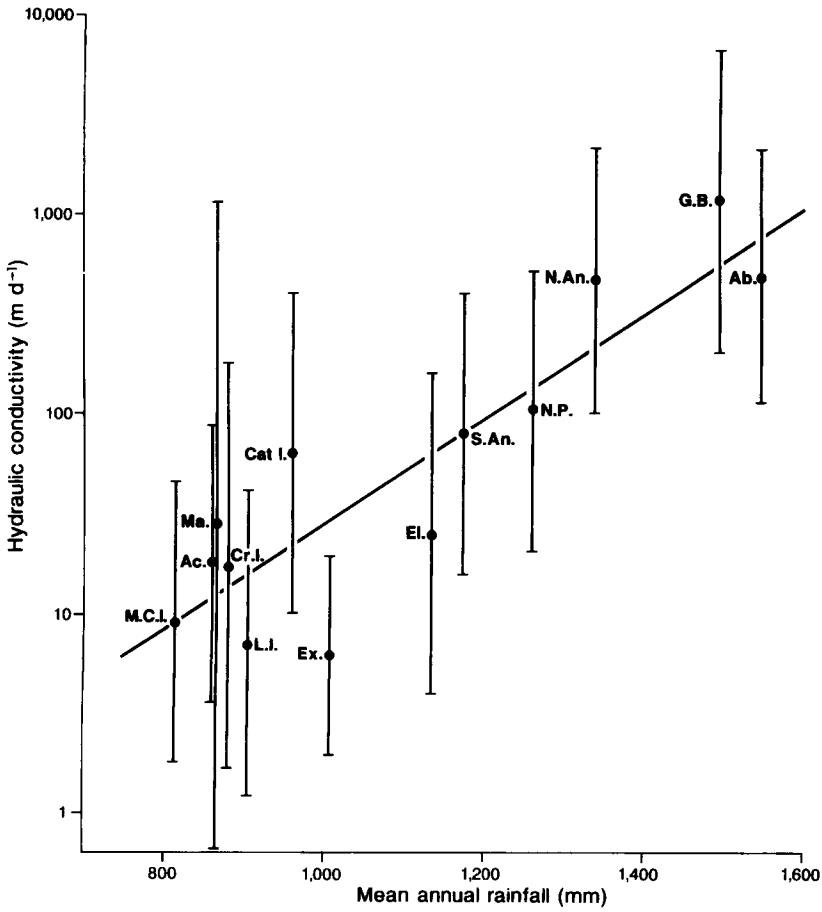


Fig. 4-4. Pumping test hydraulic conductivity vs. MAR across the archipelago. The bar represents $\pm 1\sigma$ from the island mean. Correlation is significant at >99.9%, n = 13. Abbreviations: see Figure 4.6. (After Whitaker and Smart, 1997a).

HYDROLOGY OF THE BAHAMAS

Rainfall and evapotranspiration

The temporal and spatial distribution of rainfall is highly variable (Fig. 4-1). There is a general climatic gradient from a mean annual temperature (MAT) of 24°C and a mean annual rainfall (MAR) of 1,550 mm in the northwest to a MAT of 27°C and MAR of 690 mm in the southeast. More westerly parts of larger islands tend to receive more convective rainfall than easterly parts of smaller islands as clouds developed over the land are displaced by the trade winds.

Estimates of potential evapotranspiration (PET) from New Providence are 1,610 ± 34 mm y^{-1} (Penman) and 1,581 ± 52 mm y^{-1} (open-pan). PET is likely to

be considerably higher in the hotter southern islands, but no estimates are available. However, evapotranspiration can occur at the potential rate only where recharge waters remain at the surface or the vadose zone is thin so that the land surface is within the capillary fringe. Accordingly, Cant and Weech (1986) estimate the actual evapotranspiration (AET) to be 1,150 mm y^{-1}, based on the rainfall total above which surface freshwater bodies can be maintained by recharge from the lens. This estimate of AET for the whole archipelago approximates that of Little et al. (1973, 1975) for the northern Bahamas but is substantially higher than estimates from the southern islands. These estimates range from 830 mm y^{-1} for Great Exuma (Wallis et al., 1991) to as low as 540 mm y^{-1} for Great Inagua (R.V. Cant, pers. comm., 1994). The general rule used for water-resources planning in the Bahamas is that effective recharge is 25% of MAR.

Vadose zone hydrology and aquifer recharge

Over large areas of most islands, the land surface is very close to sea level and the vadose zone is generally less than 1 m thick. Locally beneath aeolian dune ridges the vadose zone is up to 30 m thick, with the maximum, 63 m, at Mount Alvernia on Cat Island. The partially lithified Holocene sands have a high infiltration capacity, and no surface runoff occurs. In his study of Wood and Water Cays, Budd (1984) suggests that more than 70 mm of rainfall are required to bring the sands from wilting point to field capacity and permit recharge to groundwater and, therefore, that recharge on these cays occurs only in October. This interpretation, however, probably underestimates total recharge because field capacity will be reached after several consecutive days of heavy rainfall, and some short-circuiting of the vadose zone by flow through macropores may also occur. Over large areas of many islands the rooting depth reaches the water table, and evapotranspirative losses from the freshwater lens are considerable, an estimated 30% of rainfall at Abaco (Little et al., 1973). The fraction of rainfall that discharges via groundwater flow is estimated to be 20% at Abaco (Little et al., 1973) and 26% at North Andros (Whitaker, 1992).

Most exposed Pleistocene limestone surfaces in the archipelago are cemented. Dense laminated micritic crusts are common, and they guide the surficial flow locally into shallow surface depressions. Bacterial decomposition of accumulating plant litter may accentuate this relief and lead eventually to small depressions locally termed "banana holes" (Smart and Whitaker, 1988; Whitaker and Smart, 1997b; Mylroie et al., 1995a; Harris et al., 1995). Root channels and karstic fissures often form the outlets for micro-catchments, permitting rapid concentrated recharge to occur. Even on aeolian ridges, many woody roots penetrate the full thickness of the vadose zone in order to draw water from the freshwater lens. Through time, these root-guided fissures enlarge preferentially as a result of both flow concentration and enhanced rates of dissolution due to acid root exudates and CO_2 generated by root respiration leading to the eventual formation of open potholes or shafts. Wedging by tree roots (Rossinsky et al., 1992), the action of fire, and wind heave of larger trees such as the pines of the northern islands, all act to break up the surface crust and

result in a shallow brecciated zone. Lateral channelling of flow may occur in this zone (Mylroie et al., 1995a). This flow may be important in preferentially shedding water from aeolian ridges towards the interdune swales, thus giving locally enhanced recharge. Cave development with respect to the vadose zone and the freshwater lens is reviewed in Mylroie and Carew (1995).

The highly dynamic nature of the Bahamian freshwater lenses is seen in their response to temporally variable recharge. Water-level records for two boreholes and an adjacent cenote blue hole on North Andros (Little et al., 1973) show a very rapid rise in response to rainfall, a peak within 2 h, and a recession to 30–40% of the peak value within 8 h. Assuming an aquifer porosity of 30%, the ratio of water-level responses of blue hole and borehole of 1.8 suggests that at least 60% of the rainfall passes through the 1.4-m-thick vadose zone within 2 h. Borehole records from Grand Bahama Island show a similarly rapid water-table response, with transmission of 90–100% of the rainfall within a few hours of the storm event. This response seems to be independent of wet or dry antecedent conditions, suggesting that storage within the vadose zone is minimal (Whitaker, 1992).

The rapid water-table response to individual storm events is superimposed on a longer-term seasonal rise in the water table during the wet summer months and slow decline during the dry season. This longer-term variation is accompanied by a downward shift in the position of the base of the freshwater lens and an associated thickening of the upper part of the mixing zone. On North Andros Island, expansion of the lens thickness by approximately 1 m from April to June is followed by a return to its dry-season position in August and then a further 1-m expansion in October (data from Johnson and McWhorter, 1977). On smaller islands, the thickness of the lens also expands significantly during the wet season; for example, the area of the lens increases on average by a factor of 4.7 in the Holocene ooid sands of Schooner Cays (Budd, 1988; Budd and Land, 1989). Seasonality is also apparent in the salinity of waters extracted from the upper part of the freshwater lens. As shown in Figure 4-5, the freshwater system responds rapidly to individual rainfall events with dilution and expansion of the lens. These individual events are superimposed on a seasonal increase in chloride concentration that reflects evapotranspirative losses and contraction of the lens due to discharge and abstraction over the dry season (Whitaker, 1992).

Spatial variation in salinity of the lens is a function of differences in the amount of mixing with saline waters. This mixing is controlled largely by tide-driven fluctuations in groundwater levels, which decrease linearly with distance from the coast. On North Andros Island, for example, there is a reduction in tidal efficiency of 3% km^{-1} and a parallel reduction in the salinity of the upper part of the lens of 20 mg L^{-1} km^{-1} (Whitaker, 1992). A similar pattern is apparent in the vicinity of tidal creeks due to both tidal mixing and lateral encroachment by brackish and saline creek waters at high tides. Mixing is also the primary control on the vertical distribution of salinity through the lens. Superimposed on the gradual increase in salinity with depth are a number of salinity steps which frequently correspond to paleoexposure surfaces. On Grand Bahama Island, 42% of the boreholes show such a step at 11 m which correlates with a change in lithology from "soft" to "hard" limestones (Little et al., 1975).

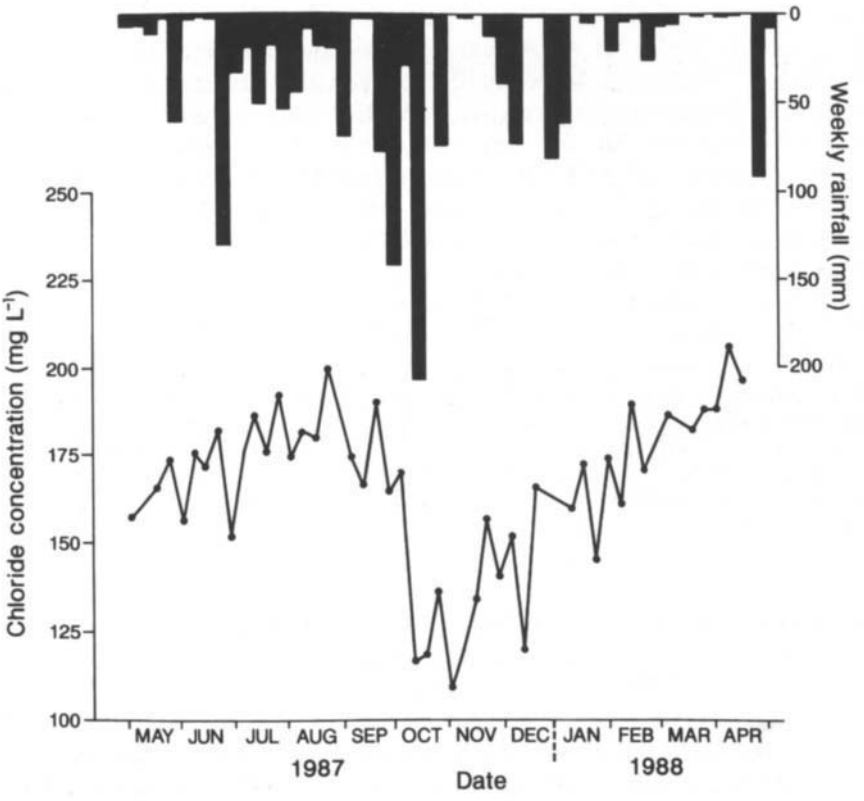


Fig. 4-5. Time series of weekly rainfall at Fresh Creek, North Andros, and Cl^- of bulked waters from an abstraction wellfield, AUTEC Naval Base. (From Whitaker, 1992.).

Geometry of the freshwater lens

The islands of the Bahamian archipelago offer a unique opportunity to investigate the role of island size, topography, effective rainfall and aquifer properties on the volume and geometry of the freshwater lens, both empirically (Cant and Weech, 1986) and by modelling (Vacher, 1988; Wallis et al., 1991; Vacher and Wallis, 1992). Extending the empirical analysis of Cant and Weech (1986) by application of stepwise multiple regression, we have found that the best predictor of lens volume is island area (Table 4-2), with the larger northern islands providing the major water resource in the archipelago. Surprisingly, there is only a poor direct correlation between lens volume and mean annual recharge (estimated to be 25% of MAR). This variable, however, provides a significant explanation of the residuals of the relationship between island area and lens volume; wetter northern islands have larger lenses than the drier southern islands of the same size (Fig. 4-6). Both area and recharge contribute significantly ($>98\%$) to the multiple regression equation,

Table 4-2

Correlation matrix for predictive model of lens volume

	Log Lens Volume (m^3)	Effective Precipitation (m y^{-1})	Log Hydraulic Conductivity (m y^{-1})	Log Island Area (m^2)	Lens/Island Area (%)
Effective Precipitation	0.15				
Log Hydraulic Conductivity	0.82	0.88			
Log Island Area	0.85	−0.20	0.72		
Lens/Island Area	0.78	0.42	0.78	0.68	
Maximum Island Width (m)	0.77	0.17	0.71	0.74	0.78

Note: For lens volume, aquifer hydraulic conductivity (K) and island area, a log 10 transformation is employed to linearise relationships. For all variables except, K, n = 22; correlation coefficient (r) for >99.9% confidence interval (C.I.) is 0.65, and r for >95% C.I. is 0.42. K data are available for n = 13 islands; r for >99.9% C.I. is 0.80 and for >95% C.I. is 0.55. Great Inagua, where the many inland lakes result in the lens occupying <1% of the island area, is a consistent outlier in the relationships and is omitted.

$$\text{Log}_{10}\text{Lens Volume } (m^3) = -6.4 + 1.52\ \text{Log}_{10}\text{Island Area } (m^2) + 4.65\ \text{Recharge (m y}^{-1}),$$

which explains 87% of the observed variance (n = 22). There is, however, also a high degree of multicollinearity between independent variables; for example, hydraulic conductivity correlates with both island area and effective precipitation. This correlation may explain why, contrary to expectations, lens volume seems to vary directly with hydraulic conductivity.

In low-lying islands such as the majority of the Bahamas, the role of topography is critical in controlling the continuity and distribution of the freshwater lens. On the larger islands, the thickness of the lens is limited by the presence of tidal creeks such as Stafford and Fresh Creeks on North Andros Island (Fig. 4-7A). These creeks function as estuaries discharging fresh and brackish water to the adjacent ocean; this role is apparent from the contours of the freshwater lens (Fig. 4-7A) and long-term flow measurements (Whitaker and Smart, unpublished data). The salinity of creek waters varies both temporally and spatially, being greatest at high tide and nearer to the coast, and vertical density stratification is locally pronounced where wind-driven mixing is restricted (Smart, 1984; Fig. 4-7B). Cavernous porosity, both vertical fracture and horizontal cave systems, functions in a similar manner, providing routes for enhanced discharge of both fresh and brackish groundwaters (Whitaker, 1992).

Where the vadose zone is thin, or closed water bodies are exposed at the surface in topographic lows, evaporative loss of groundwater occurs at the potential rate. In the northern Bahamas, where annual PET is equal to or somewhat less than MAR, inland lakes have a net positive water balance and are fresh or only slightly brackish at the end of the dry season (Little et al., 1973). In the much drier southern islands, PET exceeds rainfall. Consequently, inland lakes have a negative water balance and

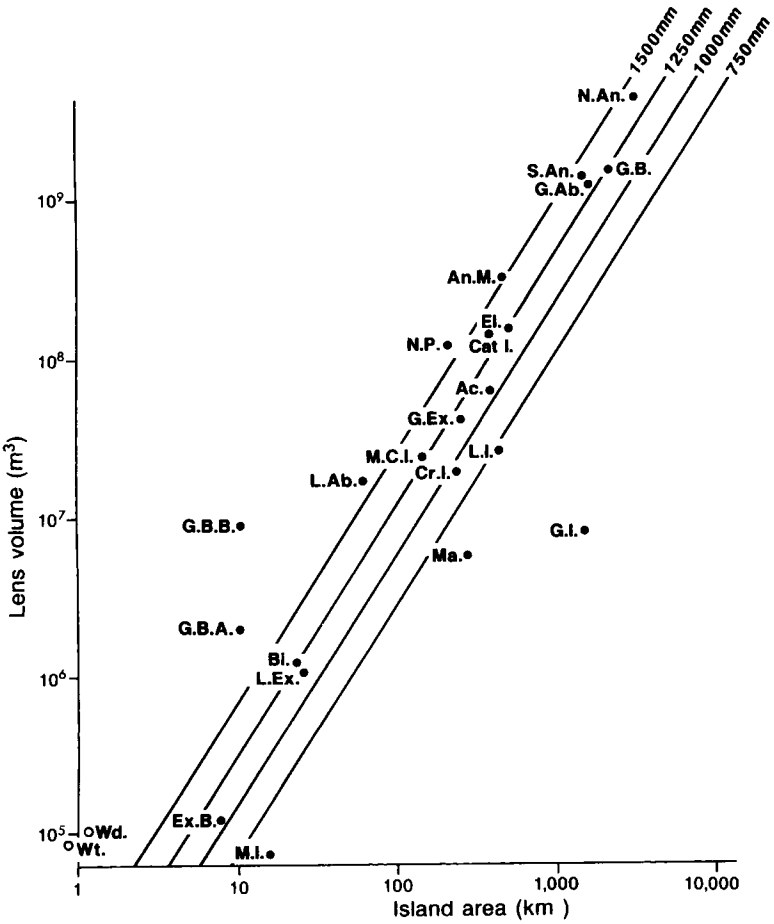


Fig. 4-6. Relationship between island area, volume of freshwater lens, and MAR. Open circles (lower left) are islands composed exclusively of Holocene sediments. Abbreviations: Abaco (Ab.) Great (G.Ab.) and Little (L.Ab.); Acklins (Ac.); Andros (An.), North (N.An.), South (S.An.) and Mangrove Cay (An.M.); Bimini (Bi); Cat Island (Ca.I.); Crooked Island (Cr.I.); Eleuthera (El.); Exuma (Ex.), Great (G.Ex.), Little (L.Ex.) and Barraterra (Ex.B.); Grand Bahama (G.B.), August Cay (G.B.A.) and Bush Cay (G.B.B.); Great Inagua (G.I); Long Island (L.I.); Mayaguana (Ma.); Middle Caicos Island (M.C.I.); Moore's Island (M.I.); and New Providence (N.P.); Wood Cay (Wd.) and Water Cay (Wt.), Schooners Cays. Data from Budd (1984), Cant and Weech (1986) and Sparkes (1985).

are commonly saline to hypersaline (Little et al., 1977; Wallis et al., 1991). Unless these lakes become isolated by a low-permeability mud or evaporitic seal, evaporation causes significant groundwater discharge, and fresh groundwater may become limited to beneath topographic highs (Davis and Johnson, 1989; Wanless et al., 1989; Vacher and Wallis, 1992). Using Dupuit-Ghyben-Herzberg modeling, Wallis et al. (1991) demonstrated that the measured net water deficit of 0.5 m y^{-1} from inland

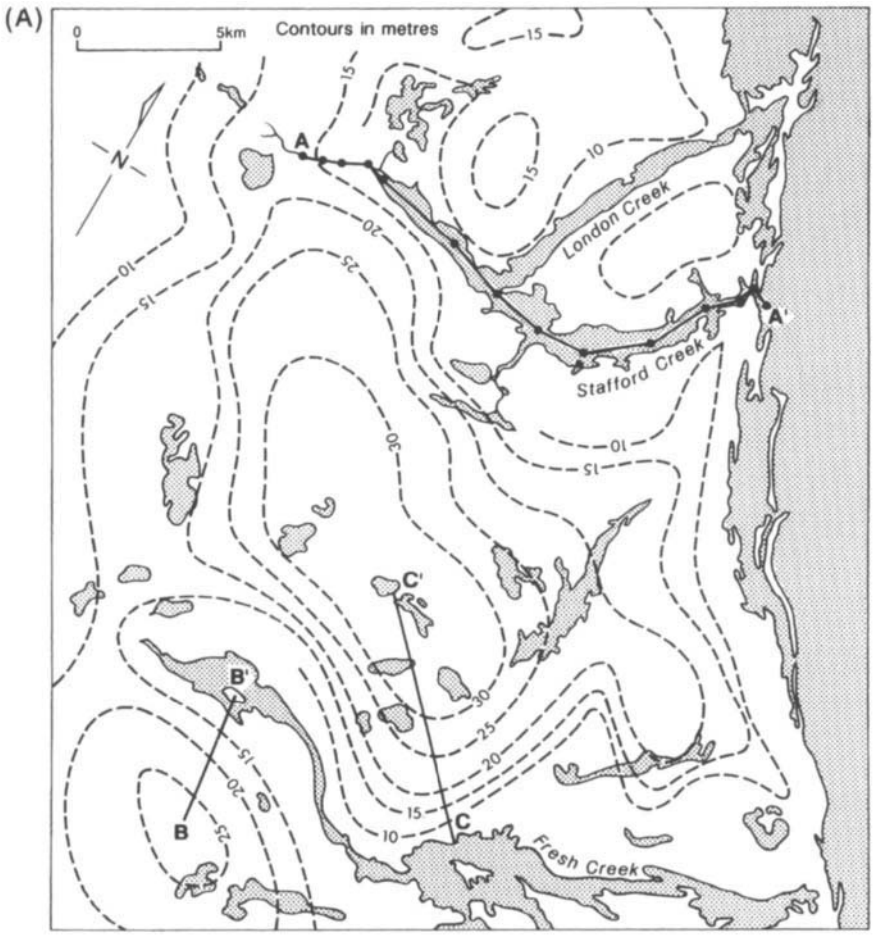


Fig. 4-7. Role of tidal creeks in controlling groundwater hydrology of North Andros. (A) Dissection of the freshwater lens. Contours are thickness of lens (m). (After Little et al., 1973.) (B) Salinity of waters in Stafford Creek. (After Smart, 1984.) (C) Composite section through the aquifer in the vicinity of Fresh Creek, North Andros. (After Whitaker, 1992.).

ponds can cause the isolation of the lens beneath the beach-ridge strandplain between the ponds and the shoreline. The modeling also demonstrates the importance of the much lower hydraulic conductivity of the Holocene aquifer in retaining water, the 1-km-wide Ocean Bight aquifer hosting a lens of greater depth than the 3.5-km-wide Forest Hill lens developed in the Pleistocene limestone. This contrast is also evident when comparing the minimum island diameter required to maintain a freshwater lens in Holocene sediments (approx. 200 m, Budd and Vacher, 1990) and Pleistocene limestones (2 km, Cant and Weech, 1986). Furthermore, the percentage area of Holocene islands underlain by freshwater is 4–6 times larger than that of Pleistocene islands receiving a comparable amount of rainfall.

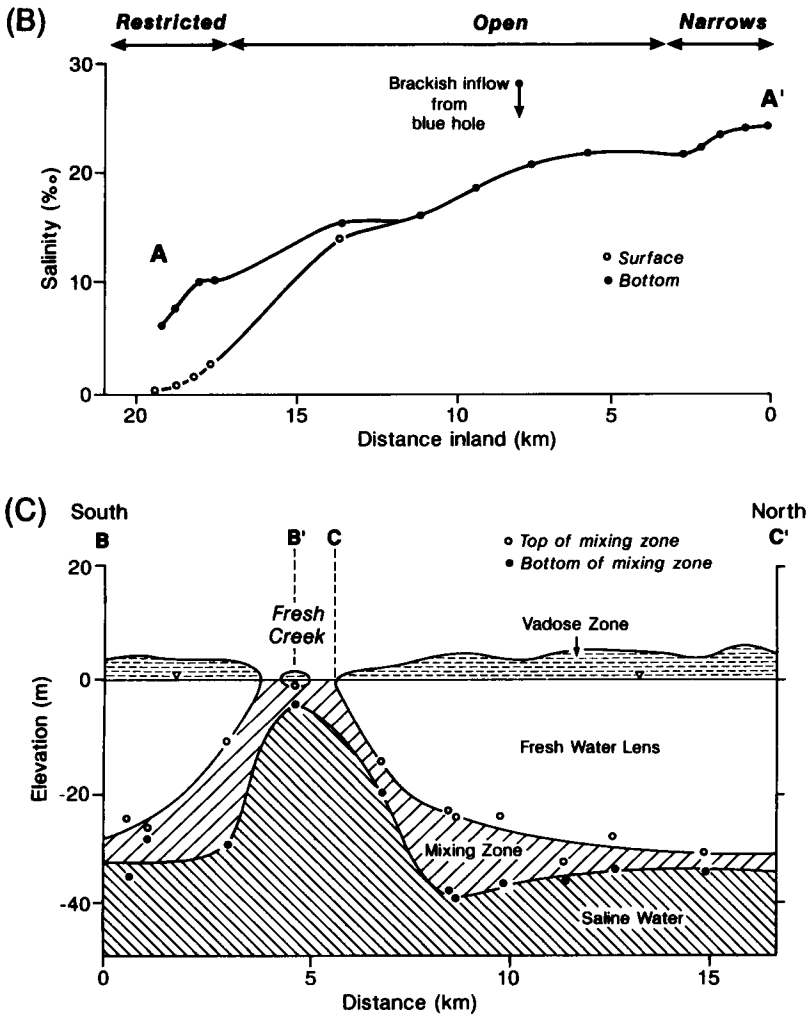


Fig. 4-7B,C.

Where Holocene sands mantle the coast, they create a barrier to both freshwater discharge and tide-driven mixing. This barrier maintains high hydraulic heads and, consequently, a relatively thick lens close to the coast. For example, on the southern coast of Grand Bahama Island, there is a narrow prograding Holocene dune/barrier-beach sequence overlying the Lucayan Limestone, and the freshwater lens obtains a thickness of 14 m only 200 m from the coast. Although there is no local comparable case where Holocene sands are absent, there is less than 4 m of freshwater 200 m inland from the saline waters of the Grand Lucayan Waterway, which bisects the freshwater lens and provides an artificial analogue (Smart and Whitaker, 1990).

The importance of contrasts in hydraulic conductivity of adjacent aquifers in controlling the geometry of the lens was first recognised on Bermuda [Chap. 2, Fig. 2-17], and Vacher and Wallis (1992) hence termed this a "Bermuda-type island" (Fig. 4-8A). Islands where the lens is bisected by evaporation are termed "Exuma-type" (Fig. 4-8B), although a similar distribution also results where tidal creeks penetrate inland. However, as recognised by Cant and Weech (1986), the effect of increasing permeability with depth (see above) is a more general control on lens geometry in the Bahamas [and in many atoll and reef islands; see "dual aquifer" carbonate islands, Chap. 1]. In the northern islands of Abaco and Grand Bahama, the limited thickness of the Lucayan Limestone restricts the depth of the freshwater lenses. Similarly, there is truncation of the base of the lens at the contact between the Holocene aquifer and the underlying Lucayan Limestone. At Ocean Bight, Great Exuma, for example, the depth of the lens beneath the permeability contact is < 50% that predicted for a homogeneous aquifer of Holocene sand permeability (Wallis et al., 1991). Islands which have a positive water balance and where permeability increases with depth are termed "Bahama-type" (Fig. 4.8C), after Grand Bahama Island, by Vacher and Wallis (1992).

Dupuit-Ghyben-Herzberg models (Vacher, 1988) have proved useful in demonstrating the importance of water budget and aquifer configuration in controlling

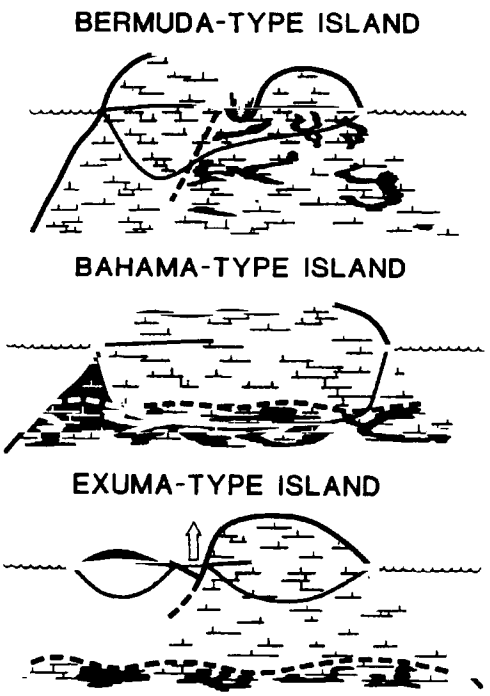


Fig. 4-8. Schematic diagram of three main types of freshwater lenses identified in the Bahamas. (From Vacher and Wallis, 1992.).

freshwater lens geometry in the Bahamas. However, application of these models without adequate consideration of the role of karstic circulation at depth in permitting substantial discharge of freshwater by enhanced mixing can lead to significant overestimation of freshwater lens thickness (Oberdorfer et al., 1990) [see Chap. 22]. The tidal amplitude in the Bahamas is about 0.4 m on broad banks and 0.8–1.0 m on open coasts, compared to 2 m in the Pacific atolls studied by Oberdorfer et al. (1990), and consequently, in the Bahamas, vertical groundwater flow and tide-induced mixing is much less. Nevertheless, there is evidence of discharge of brackish water from oceanic blue holes offshore (see below).

Freshwater-saltwater mixing zone

In comparison with the freshwater lens, relatively little is known about the hydrology of Bahamian mixing zones due largely to the limited borehole access. The only available data from Holocene sands is from Schooner Cays (Budd, 1988b), where the average thickness of the mixing zone appears to be independent of distance from the coast. On Water Cay, the average thickness is 2.1 m, and on Wood Cay, which is of similar width but is more elongate, the average thickness is 2.9 m. Volumetrically, the mixing zone on these islands is always more important than the overlying freshwater lens, which varies seasonally between 0 and almost 1.0 m thick.

Within the Pleistocene limestones of North Andros and Grand Bahama islands, the mixing zone is much thicker, ranging from 12 m to more than 20 m at a distance inland (50–100 m) comparable to that at the centre of Schooner Cays (Whitaker, 1992). The large thickness reflects the greater efficacy of tide-induced mixing in these more transmissive limestones, as well as greater freshwater discharge from the larger islands. The thickness of the mixing zone decreases exponentially with distance inland and away from the tidal creeks because of the reduced influence of tidal head fluctuations and decreasing groundwater flux. For example, the mixing-zone thickness measured in storm drainage boreholes in the Freeport area of Grand Bahama Island (Whitaker, 1992) decreases inland from a maximum of 17.5 m immediately adjacent to the south coast to a minimum of 1.5 m in the centre of the island, some 4 km from the coast (Fig. 4-9). Both the rate of decrease and the maximum thickness vary spatially, however, with the temporally variable upconing beneath the two major abstraction wellfields generating relatively thick mixing zones some distance inland.

The steepest rate of inland decrease of the thickness of the mixing zone at Grand Bahama Island occurs at the south coast to the west of the Grand Lucayan Waterway (Fig. 4.9). Along this stretch of coastline, the Pleistocene limestones are overlain by a Holocene transgressive beach barrier which, being of lower hydraulic conductivity, attenuates inland propagation of the tidal water-level fluctuations and maintains both a larger freshwater lens and thinner mixing zone adjacent to the coast. Along the Waterway, where this barrier complex has been breached by excavation of a canal network, the coastal mixing zone is displaced inland, and increased propagation of tidal fluctuations in the exposed Pleistocene limestones gives much less rapid reduction of the mixing zone inland.

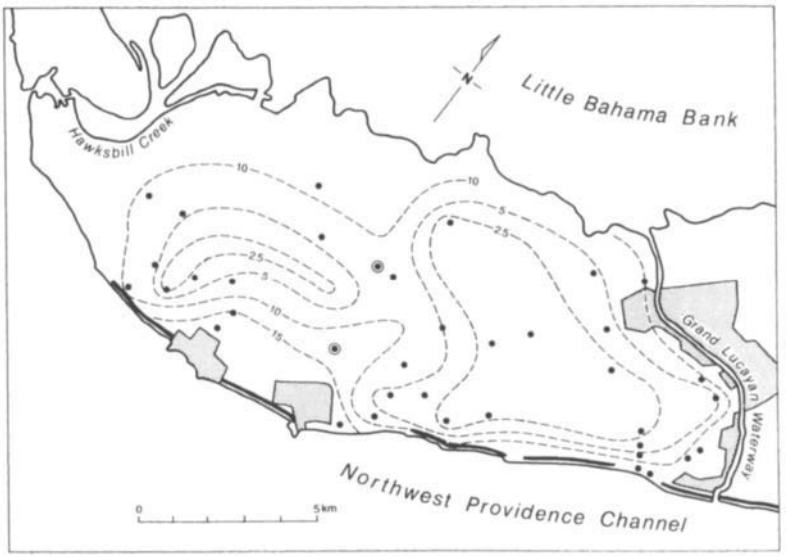


Fig. 4-9. Thickness of the mixing zone measured in boreholes in the Freeport area of Grand Bahama. Dashed lines are contours of mixing-zone thickness (m) derived from drainage boreholes (solid dots). Circled dots are major abstraction boreholes. Heavy lines are Holocene dune ridges, and areas of stipple are canal networks. (From Whitaker, 1992.).

On North Andros Island, the mixing zones observed in inland cenote blue holes range in thickness from 15–20 m adjacent to the coast to 3–6 m beneath the centre of the lens, at a distance of more than 10 km inland measured along the hydraulic gradient. The inland decrease, which appears to be similar to that for the exposed Pleistocene limestones of Grand Bahama Island, follows an exponential pattern described by

$$\text{MZ thickness (m)} = 12.3 - (8.80 \times \text{Log}_{10}\ \text{Distance Inland}),$$

which is significant at $>99.9\%$ ($n = 24$). Note that the thickness of the mixing zone declines exponentially inland, although the tidal efficiency decreases linearly, reflecting the influence of discharging freshwater in addition to simple tidal dispersion. This analysis excludes nine sites on islands in the tidal creeks or within 500 m of the creek margins. These sites appear to have anomalously thin mixing zones (3.1 ± 1.9 m; Fig. 4.8C), possibly due to upward movement of saline groundwaters in response to the low hydraulic head of the creeks (Smart, 1984; Whitaker and Smart, 1990). While at one-third of the sites the mixing zone discharges towards the coast in the generally recognised manner, flow at the others is rather towards tidal creeks, where discharge of brackish mixing-zone waters is evidenced by the vertical salinity stratification (Fig. 4.8B).

Within the mixing zone, there is a sigmoidal increase in salinity with depth which is linear when expressed on a probability scale, and is maintained irrespective of the salinity of the waters forming the overlying lens (which may be up to 10‰ in South

Andros fracture blue holes; Whitaker and Smart, 1997c). Superimposed on this general trend, however, are cm-scale steps in salinity which may be associated with vertical contrasts in hydraulic conductivity. A similar feature occurs within cave systems on Grand Bahama Island which lead inland from tidal ponds and creeks developed in dune swales on the south coast. A wedge of uniform-salinity creek water, characteristically 20–21‰ and 23–27°C, extends up to 750 m into the cave and thins exponentially with distance from the coast (Whitaker, 1992). Beyond the zone of influence of the creek wedge, the mixing zone is very sharp (< 0.3 m) relative to that in the surrounding aquifer.

Zone of saline groundwater

The majority of the carbonates of the Bahama Banks are, and for a large part of their history have been, submerged in groundwaters of near seawater composition. At the surface of the platform, local shuttling of seawater is driven both by high-frequency wave-generated variations in head and by semidiurnal reversals in tidal gradients, both between shallow bank and open ocean (Matthews, 1974) and between the water table beneath the island and surrounding sea (Whitaker and Smart, 1990). On the northwestern Great Bahama Bank, there is also evidence for a large-scale circulation of saline groundwater beneath Andros Island (Whitaker and Smart, 1990, 1993). This circulation has important implications for the formation of massive platform dolomites (Whitaker et al., 1994).

Ocean blue holes (see Case Study) along the eastern coast of Andros Island are characterised by strong, semidiurnally reversing currents developed in response to local tidal head. Volumetric measurements of groundwater discharge derived from oceanographic recording current meters deployed in two such sites indicate that the duration of outflow is longer than that of inflow and attains higher velocities. At both sites there is a considerable net groundwater discharge ranging from 2×10^4 to 2×10^5 m^3 per tidal cycle. This outflow is greater by a factor of 3–4 in the autumn and winter than in the summer, which suggests that the saline groundwater circulation is responding either to changing weather conditions (total rainfall, wind direction/strength or atmospheric pressure) affecting the surface of the bank, or to seasonal variations in the currents in the surrounding oceans. Assuming that discharge at these sites is representative of that from the ten known ocean holes along this 80-km stretch of coast, and ignoring any other discharges, it follows that the net outflow of saline groundwater is at least 4–49 $m^3\ d^{-1}\ m^{-1}$ of coastline.

The distribution of salinity and temperature within the saline groundwater body provides direct evidence of groundwater source and evolution and, therefore, the mechanism(s) driving the circulation. Groundwaters discharging from the oceanic blue holes during the summer have a salinity of 37.7 ± 1.7‰ at the termination of the outflow phase. This value is high relative to that of Tongue of the Ocean and Straits of Florida seawater (36.6 and 36.3‰ respectively, the former reflecting its relatively enclosed position). Elevated salinities (38.1 ± 2.4‰) are also measured at depths of 50–100 m in inland cenote blue holes distributed across North Andros Island, although three sites on the west coast of the island are significantly more

saline (44.0 ± 0.9‰). The high salinities can derive only from the shallow banks to the west of the island where seasonally high evaporation rates produce salinities >38‰ over large areas of the bank and >45‰ in the immediate lee of the island (Cloud, 1962). Thus, as predicted by Simms (1984), large-scale reflux of waters with only slightly elevated salinity apparently is occurring from the Great Bahama Bank. Saline groundwater flowing eastward beneath the island to discharge into the Tongue of the Ocean may be responsible for the plume of high-salinity water (up to 37‰) observed at 160–180 m depth in the Tongue of the Ocean adjacent to the eastern side of the island (Busby and Dick, 1964).

Static groundwater temperatures should increase with depth in response to geothermal heating (e.g., at 2.5°C per 100 m in nearby peninsular Florida), while reflux-derived waters could be expected to be similar to mean annual temperature on the bank surface (25.5°C). At inland cenotes, however, groundwaters, which are isothermal below the depth of surface warming because of in-hole convection, are relatively cold (24.4 ± 0.5°C) with temperatures varying inversely with the maximum depth of the hole (at −1.4°C per 100 m). Furthermore, the saline groundwaters appear to cool progressively from west to east beneath the island at a rate of 0.25°C km^{-1} from almost 26°C on the west coast to 24°C near the east coast (Whitaker and Smart, 1993). Groundwaters discharging from oceanic blue holes on the east coast are also relatively cold, reaching a minimum temperature of 21°C during the summer. The similarity between groundwater and oceanic temperature profiles indicates the operation of a second circulation system involving cold, normal-salinity seawater. Mixing calculations suggest this seawater is derived from depths in excess of 240 m in the adjacent oceans.

As reflux waters flow eastward to discharge into the Tongue of the Ocean, they mix with and become diluted by cold, normal-salinity ocean waters which actively circulate through the platform and reverse the normal geothermal gradient. This cold circulation system may be driven by geothermal convection (Fig. 4-10A) as argued in Florida by Kohout et al. (1977). Alternately, the west-to-east circulation pattern may better be explained by a sustained difference in sea-surface elevation across the platform (Fig. 4.10B), such as that generated across the Straits of Florida by the Gulf Stream (Maul, 1986). The maintenance of significant rates of groundwater flow, despite the relatively small hydraulic gradient generated by these drives, confirms the highly permeable and cavernous nature of the platform at depth as indicated by drillers' reports of bit drops and loss of circulation which occurs to depths in excess of 3,000 m (Walles, 1993).

Saline groundwaters sampled in inland blue holes and discharging ocean holes have an elevated PCO_2, a depressed calcite-saturation index, and are depleted in SO_4^{2-} by up to 5% compared to seawater (Whitaker et al., 1994). These waters are also depleted in Mg^{2+} and enriched in Ca^{2+} relative to open ocean and bank input waters, suggesting that replacement dolomitisation is occurring. Combining the estimated groundwater flux (calculated as $3–35 \times 10^{-2}$ m day^{-1}, Whitaker and Smart, 1993) with an average Mg^{2+} depletion of 67 mg L^{-1} indicates an approximate rate of dolomitisation of $2–22 \times 10^{-6}$% y^{-1}. Taking account of subsidence rates and sea-level history, these rates are sufficient to account for the sparse micro-dolomites and

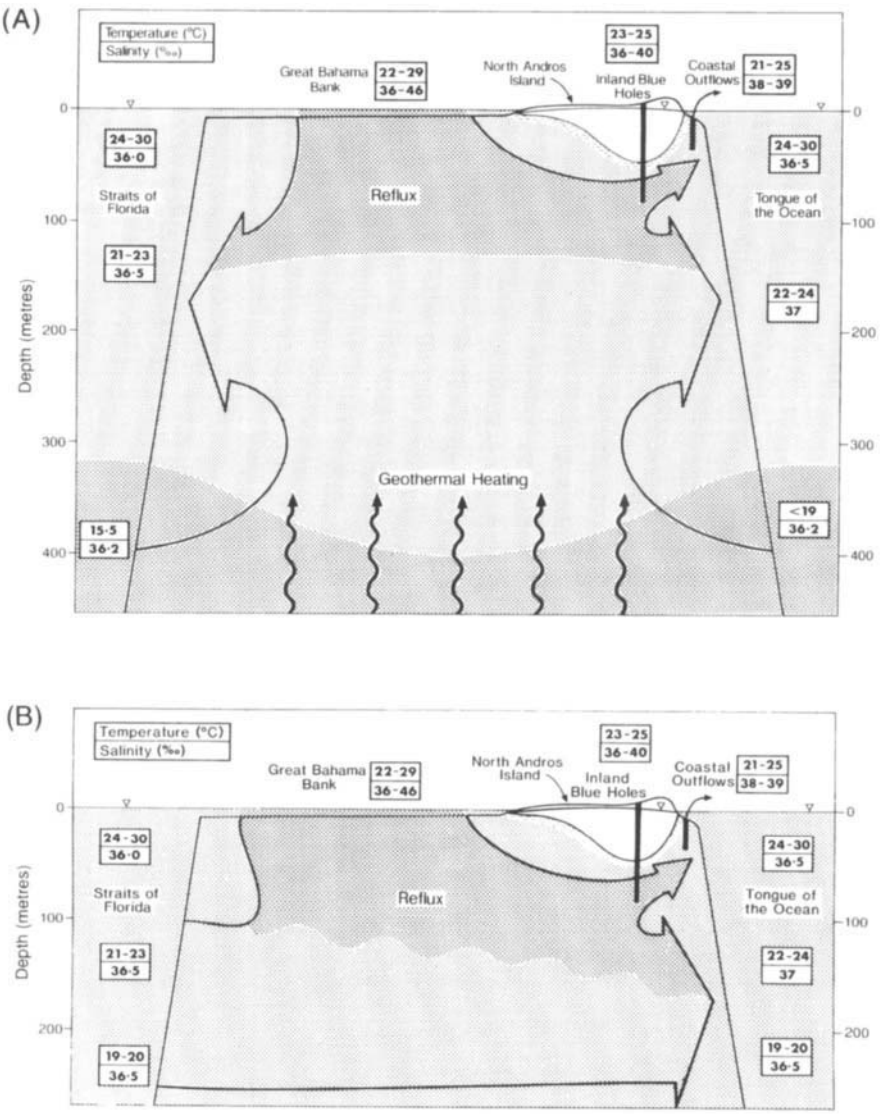


Fig. 4-10. Two alternative saline groundwater circulation systems postulated for the northwest Great Bahama Bank. (A) Thermal convection with reflux. (B) Reflux with trans-bank difference in sea-surface elevation. Weight of stipple is proportional to groundwater density. (From Whitaker and Smart, 1993; reprinted by permission of the American Association of Petroleum Geologists.).

dolomitic cements sampled from the walls of Stargate Blue Hole, South Andros, at depths of 30–40 m. This suggestion is supported by the trace-element and isotopic analyses of the dolomites which suggest precipitation from cold, nearly normal-salinity seawater (Whitaker et al., 1994).

WATER RESOURCES OF THE BAHAMAS

The population of the Bahamian archipelago is relatively small (< 250,000 in the Bahamas and < 9,000 in the Turks and Caicos) but occupies an area some 4,000 km^2. More than 35 of the hundreds of islands are inhabited permanently or seasonally. The majority of islands are thus sparsely populated (3.3 people km^{-2}, Sealey 1990), with settlements small and scattered, and per capita water consumption is relatively low. New Providence Island (density 5,554 people km^{-2}) and Grand Bahama Island (density 199 people km^{-2}) together host almost 75% of the population of the Bahamas and almost all major tourism and industrial development. Water demands are increasing rapidly on these islands; between 1985 and 1990, consumption rose by almost 15% to more than 30 megalitres (ML) day^{-1} on Grand Bahama, where per capita consumption is about twice that of New Providence. In the Turks and Caicos Islands, water consumption is generally low, but recently has been increasing with development of tourism on Providenciales.

Individual roof catchments and rainwater storage tanks are the traditional means of supply and are still important on smaller and more southerly islands. In the Turks and Caicos, roof catchments are mandatory for new houses, which must have a storage capacity of 500 L m^{-2} of roof area. Rainwater catchment systems are highly efficient, enabling utilisation of 85–90% of total rainfall compared with < 20% from groundwater abstraction. Their utility, however, is limited by available storage capacity and susceptibility to contamination.

An estimated 80–90% of the population of the Bahamas relies on groundwater supplies, traditionally via shallow dug wells, although public wellfields have now been developed on all Bahamian islands with freshwater lenses > 5 m thick. To prevent saline upconing in the very transmissive limestones, abstraction is distributed between multiple boreholes that are arranged in a linear or cruciform pattern and are pumped at relatively low rates (maximum 4,500 L day^{-1}) for 16 or 24 h day^{-1}; the maximum recommended drawdown for these wells is 3 cm. On some smaller and southerly islands, fresh groundwater is restricted to the lower-permeability Holocene sands, despite their common nearshore location. Pumping rates are generally very low in these deposits, or bucket abstraction is used; high concentrations of H_2S are common.

Where the vadose zone is thin, groundwater may also be abstracted via a parallel or cruciform system of shallow (< 1 m water depth), open trenches, 150–1,850 m long. These water-table trenches enable distributed abstraction from the top of the lens and thus minimise the risk of saline intrusion. Problems with this system include direct contamination and water loss by evaporation, which also causes local increases in salinity. Trench fields are operated on North Andros Islands, where the freshwater lens is large and local demand is relatively small, and also on New Providence Island. Water is barged from North Andros to the Bahamian capital, Nassau (New Providence Island), which is some 35 miles away. This system was established in 1978 as an emergency measure and now supplies an average of 11.4 ML day^{-1} (1988–1992), which is equivalent to 33.6% of the New Providence supply (Weech, 1993). With the high start-up and operational costs, this barged

water is more than three times the cost of the locally abstracted groundwater. Abstraction installations, particularly the trenches, occupy large areas of land – for example, 12% of the island of New Providence.

Both the volume and quality of fresh groundwaters are under threat from development, particularly on New Providence and Grand Bahama Islands, and to a lesser extent Providenciales. In order to limit evapotranspirative losses, infiltration of runoff is enhanced by a system of drainage ditches and boreholes in urban areas such as along the highways of Grand Bahama and around Nassau Airport. At the airport, this practice coupled with the absence of significant vegetation has increased the local recharge and produced a dome on the water table (Peach, 1991). Elsewhere, the salinity of parts of some of the freshwater lenses used for abstraction has increased due to periodic overpumping, particularly by unregulated private wells (estimated to number 12,000–20,000; Weech, 1993). Subsequent recovery of brackish wellfields has been very slow. At Blue Hills on New Providence Island, for example, despite a MAR of 1,260 mm, a 12-m-thick freshwater lens has taken some 30 years to re-establish after overpumping (Sealey, 1985).

Given the generally thin vadose zone and high transmissivity of the Lucayan Limestone, the limited fresh groundwater resources are particularly susceptible to contamination from human activity. Contamination by pesticides and other agricultural and industrial products is not widespread in the Bahamas. On the more developed islands, however, improper or accidental disposal of wastes or poor construction of disposal systems has been an occasional problem. Fuel and oil spills are a common feature of groundwater contamination; one reported spillage of 4 ML of diesel fuel over 10 years at a site on New Providence Island has necessitated long-term rehabilitation pumping.

Fewer than 10% of the residents of the Bahamas are served by a sewer system. In Nassau the 1928 sewage system has been recently modernised and extended, with disposal by injection into saline groundwaters at depths of 120–200 m. The nominated "disposal zone", which receives various types of liquid waste (Cant, 1988), has a high cavernous permeability and rapid flow rates that facilitate dispersion and dilution and reduce the risk of contamination of the overlying hydraulically connected lens.

A growing threat to freshwater resources has arisen from marine developments. These developments are particularly problematic where canals cut through coastal Holocene deposits that provide a barrier to fresh groundwater discharge, as on the south coast of Grand Bahama Island (Fig. 4.9). The most ambitious waterway project in the islands is the Grand Lucayan Waterway. A main channel up to 250 m wide and 3 m deep was cut through the middle of Grand Bahama Island. Since 1977, the waterway has connected the north and south coasts with an extensive branching network of secondary canals on either side. Construction methods involved dewatering isolated sections of the canal by using 90-cm-diameter pumps abstracting at rates of 2,000–3,000 L s^{-1}. This pumping generated significant upconing of saline water, which affected the adjacent lens. The Waterway has no lock gates or other flow-control mechanisms and, therefore, is completely saline, although some sections remain unconnected to the ocean to protect nearby wellfields. The construction of

the Grand Lucayan Waterway has turned the freshwater lens, which was originally 10–12 m thick, saline or brackish for a strip 1–1.5 km wide on either side of the canal zone, with loss of freshwater storage totalling 3,400 ML (Cant et al., 1990). Now, almost 30 years after construction began, there has been some recovery as local freshwater lenses have become established limited in depth to the base of the concrete facing walls of the canals (< 2 m depth).

CASE STUDY: BLUE HOLES OF THE BAHAMAS

"Blue holes", the most conspicuous feature of karstic dissolution in the Bahamian archipelago, are entrances to underwater caves. The local term is derived from the intense blue colour of the deep water found in the cave entrances (Agassiz, 1894) which may lead into extensive underwater cave systems at depth (see also Mylroie et al., 1995b). Blue holes open both from the subaerially exposed surface of the islands (inland blue holes) and the submerged shallow banks (ocean holes); both have been explored and surveyed using specialist cave diving techniques (Benjamin 1970; Palmer 1984, 1985, 1989). In addition to giving direct access to the interior of the banks, blue holes provide routes for enhanced groundwater circulation and locally modify the position and thickness of the mixing zone. The geochemistry of the cave waters in all hydrological zones is substantially altered by the enhanced mixing and particularly by the enhanced input of surface-derived organic matter (Whitaker, 1992).

Three main morphological types of blue holes can be recognised (Fig. 4-11): circular shafts or "cenotes" (after similar features in the Yucatan Peninsula of Mexico); laterally extensive, predominantly horizontal cave systems; and vertically extensive, linear caves developed on bank-margin fracture systems (see also Mylroie et al., 1995b).

Cenotes (Type I) are vertical shafts up to 200 m deep (Deans Hole, Long Island), but more generally 50–100 m deep. They have circular entrances typically 50–150 m in diameter and frequently bell out at depth. A small number have open horizontal passages leading off at depth, but more usually, these passages appear to have been blocked by breakdown material and/or surface-derived infill. The cenote walls in the upper 20–30 m are crumbly and rotten, indicating locally high rates of dissolution, while at depth the blocky overhanging cliffs are suggestive of collapse. In areas where sediment production is high, infill is almost complete, and cenotes are often no more than circular, shallow, sediment-floored ponds or depressions. Although cenotes are present on most Bahamian islands, they are a particular feature of Andros, with a very high density of holes (118 inland cenotes on North Andros alone), the distribution of which appears to be independent of dune ridges and other surficial topographic features. Several sets of cenotes appear to have developed along linear trends, possibly reflecting joint/fracture patterns or the lines of major conduits into which collapse has occurred.

The mode of formation of cenotes and associated hydrological and geochemical processes remains elusive (Mylroie et al., 1995b). Early workers attributed devel-

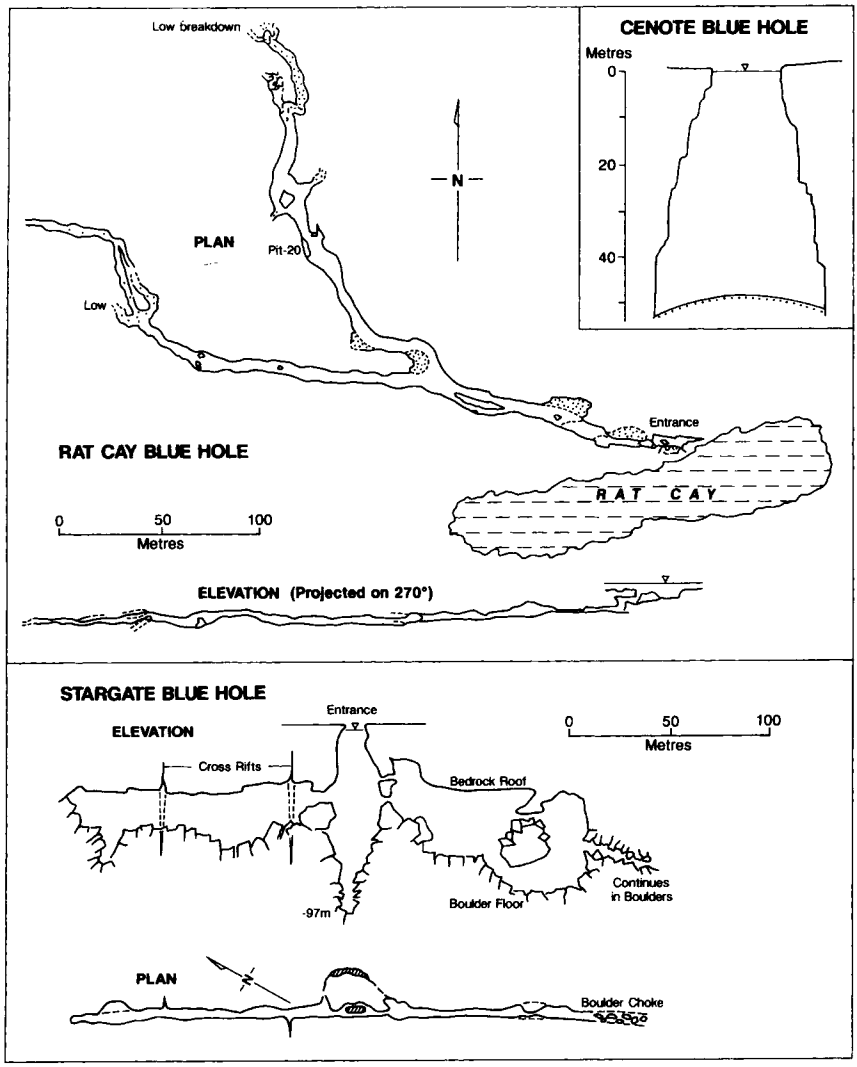


Fig. 4-11. Surveyed sections of representative examples of the three types of blue holes present in the Bahamas: North Andros Cenote (Type I); Rat Cay oceanic blue hole, a horizontal system on North Andros (Type II); and Stargate Blue Hole, developed on a major bank marginal fracture system on the east coast of North Andros (Type III). (From Whitaker, 1992.).

opment to meteoric dissolution within the vadose zone during Pleistocene sea-level lowstands when the whole platform surface was emergent (Agassiz, 1894; Vaughan, 1919). This mechanism would require relatively rapid rates of dissolution and the presence of a widespread, relatively impermeable seal such as a calcrete which would enable water to be shed laterally to points of concentrated recharge. Alternatively, development of the cenotes may have been in two stages: first, enlargement of a

water-filled cave void by phreatic dissolution that lengthened and weakened the roof span; then subsequent collapse when sea-level lowering decreased the buoyant support and increased the effective load on the span (Cole, 1910; termed "aston development" by Jimenez, 1984). A third alternative is that continued input of organic material into topographic lows may promote downward dissolution of the cenote from the surface; this process is described in the Yucatan by Socki et al. (1984) as the H_2S drill.

Roof collapses, such as those leading to the formation of cenotes, also provide access to laterally extensive, horizontal cave systems (Type II). An example is Lucayan Caverns, Grand Bahama Island, which has more than 14 km of surveyed passage and is one of the longest known underwater caves in the world. Such caves appear to develop preferentially around the island margin. They form a maze-like complex of passages adjacent to the coast, reducing inland to a smaller number of distinct subparallel passages. These passages tend to be relatively small (average 2–3 m in diameter), and their walls often show dissolutional "swiss-cheese" fretting. Although some passage cross sections are suggestive of modification by vadose entrenchment, most are circular or elliptical, pointing to a predominantly phreatic origin. The passages are developed at one or more horizontal levels. Active upward stoping may displace the open void upward, thus creating stepped passage ceilings with a planar bedrock surface and an accumulation of fretted breakdown covering the original floor.

Development of such horizontal systems is most likely related to dissolution at the water table and/or mixing zone during periods of enduring, sea-level highstands (e.g., during oxygen isotope substage 5e, as documented in the Bahamas by Chen et al., 1991). Above modern sea level, there are numerous subaerial caves, of which most are less than 100 m in length (Vogel et al., 1990; Mylroie et al., 1991), although the longest known subaerial cave, Conch Bar on Middle Caicos, exceeds 3 km. These subaerial caves characteristically comprise oval or linear chambers with a maze of smaller radiating passages either looping back on one another or terminating abruptly in blank walls [flank margin caves; see Chap. 3A]. Located within the Pleistocene dune ridges, these caves are interpreted to have formed during periods of sea-level highstands at the distal margins of the paleo-freshwater lens where vadose-phreatic and freshwater-saltwater mixing zones are superimposed (Mylroie and Carew, 1990). Many horizontal passages in the present phreatic zone are occupied by the freshwater-saltwater mixing zone where waters are undersaturated with respect to calcite and wallrock dissolution is active (Smart et al., 1988; Whitaker, 1992). However, because the existence of a cavernous void serves to localise the position of the mixing zone, the original void may considerably predate the modern groundwater system.

Fracture caves (Type III) comprise predominantly vertical linear systems developed on major fracture systems running subparallel (e.g., east coast South Andros; Palmer, 1986; Whitaker and Smart, 1997c) or perpendicular (e.g., East End, Grand Bahama; Palmer and Heath, 1985) to the coast. Fracture-guided passages are laterally continuous, average 2–5 m wide, and may reach depths in excess of 100 m. The vertical bedrock walls are rough but mostly planar and show evidence of both

dissolution and spalling. Upward passages terminate in bedding-plane ceilings or collapsed boulders jammed in narrow, but continuing, fissures. Fallen blocks of wallrock up to several metres in diameter form a jumbled mass on the floor and, in places, bridge across the passage. These voids are identical to some of the larger neptunian dykes and fissure fills noted in ancient limestones (Smart et al., 1987).

Although the controlling fractures are often multiple, complex and vertical, they show no evidence of vertical displacement. They may be surface representations of deep graben structures that control the deep-water channels such as the Tongue of the Ocean and Northwest Providence Channel (Mullins and Lynts, 1977). Alternatively, the fractures may result from basal undercutting and/or lateral unloading of the bank margins (Freeman-Lynde et al., 1981). Although the blue holes have formed as synsedimentary fractures, their present size and extent are due to dissolutional activity, predominantly in the freshwater-saltwater mixing zone (Smart et al., 1988, Whitaker, 1992). In this zone, the fractures are preferentially enlarged, and tubular elliptical passages are developed along bedding planes. Spalling of wallrock sheets parallel to the fracture walls occurs, particularly below the base of the present mixing zone, most likely in response to loss of buoyant support during sea-level lowstands.

Blue holes, which are an endmember of a continuum of secondary porosity, control the hydraulic conductivity of the Lucayan and pre-Lucayan limestones at the largest scale. The tide-driven semidiurnal water-table fluctuations in the cenotes increase with depth of the hole. This pattern is similar to that in boreholes (Mather and Buckley, 1973) and reflects an increasing aquifer permeability with depth. For example, at a 90-m-deep cenote in the centre of North Andros (some 18 km inland), the tidal efficiency is 6.3% and the lag is 216 min, whereas in an adjacent 34-m-deep borehole, the values are 3.7% and 277 min, respectively. Thus during high tide there is radial flow of water from the cenote into the aquifer, which is reversed at low tide. This back-and-forth exchange may explain the advanced state of dissolution affecting the bedrock surrounding many of the cenotes.

The fresh groundwater in the cenotes is generally more saline than that in adjacent boreholes. At the same North Andros site, the salinities are 870 and 300 mg L^{-1} at cenote and borehole, respectively. The enhanced mixing in the cenote eliminates minor salinity steps which are characteristic of salinity profiles in both the lens and mixing zone of boreholes, although the position of the base of the lens is maintained in the cenote. Where the vadose zone is very thin, the cenotes function as estavelles with a radiating system of small tidal creeks. Offshore, ocean blue holes have strong tidally reversing currents and are frequently surrounded by a halo of coral reef (Trott and Warner, 1986). Most of the ocean holes of both North Andros and Grand Bahama Islands discharge a significant component of either circulating saline groundwater or brackish groundwater from the mixing zone. Brackish discharge occurs from shallow and/or nearshore ocean holes, and appears to be more active during the rainy season.

On South Andros Island, where a major bank-marginal fracture runs onshore from the banks for some 9 km, tidal pumping along the fracture causes enhanced mixing both in the caves and the adjacent aquifer (Whitaker and Smart, 1997c).

Within the fracture caves, the lens is brackish rather than fresh, with a salinity of 3‰ increasing to 9‰ from north to south along the fracture. This observation, combined with the progressive thinning of the lens from 20 m to 11 m and considerable thickening of the mixing zone, suggests that there is a net north-to-south flow of saline water along the fracture. This flow, which is confirmed by dye tracing, is most readily explained by a difference in sea-surface elevation between the two ends of the onshore section of the fracture. The difference in elevation is caused by the tidal lags which exist from north to south in the Tongue of the Ocean and possibly amplified by the complex topography of the offshore reefs and cays. The fracture caves also intercept and integrate diffuse saline-groundwater circulation from beneath the platform, thereby directing the discharge to ocean blue holes (Whitaker et al., 1994). The active circulation along the fracture is accompanied by a tide-driven exchange of groundwater between the fracture blue holes and the adjacent aquifer. The displacement of the brackish lens water into the surrounding aquifer affects a zone up to 200 m wide on either side of the fracture.

Geochemically, waters of blue holes differ significantly from those in the adjacent aquifer. The differences reflect the high flow rates, enhanced mixing, the presence of open entrances which permit ingress of surface-derived organic material, and, in the immediate entrance area, sunlight (Whitaker, 1992). Near the water table, degassing of CO_2 generates carbonate supersaturation and cementation by low-Mg calcite. Photosynthesis may also be important, particularly in the many cenotes where entrances are large and surrounding cliffs are absent or low. Below this zone, however, waters are undersaturated with respect to aragonite and, in the freshwater-saltwater mixing zone, to calcite (Smart et al., 1988). Dissolution of the predominantly low-Mg calcite bedrock is very active, pervasively affecting both allochems and matrix, enhancing porosity and producing a characteristic, macro-scale "swiss cheese" fretting. Bacterially mediated processes are an important control on the geochemistry of the cave waters. The processes include aerobic oxidation of surface-derived organic matter in the freshwater lens and upper mixing zone, and sulphate reduction in the anoxic mixing and saline zones (Smart et al., 1988; Bottrell et al., 1991). The position of the redox interface is controlled by the rates of input and consumption of oxygen and organic matter, and is an important locus for dissolution driven by the re-oxidation of reduced sulphur species (Whitaker, 1992). Oxidation of organic matter by sulphate reduction also appears to be an important control on dolomitisation, both in the saline zone (Whitaker et al., 1994) and within specific subzones of the freshwater-saltwater mixing zone (Whitaker, 1992).

CONCLUDING REMARKS

Within the broadly tropical marine climate of the Bahamian archipelago, there is a marked gradient from the cooler, wetter, northern islands to the hotter and more arid islands up to 1,000 km farther south. This gradient is an important control on island hydrology and, via its effect on diagenesis, also on the hydraulic conductivity of the limestones. In the northern islands, the lenses are larger because of greater

rainfall, despite the fact that aquifer permeabilities are also larger because of more intense meteoric diagenesis.

There are significant contrasts in hydraulic conductivity between the partially consolidated Holocene sands and the underlying lithified Pleistocene limestones. Within the limestones, hydraulic conductivity increases with depth because of the greater extent of karstification in the older limestones. The most conspicuous features of this karstification are the blue holes – underwater caves which range from circular shafts to horizontal maze systems and vertically extensive linear fractures. The distinctive morphologies of the blue holes arise from strong structural control and the combination of phreatic dissolution and collapse during sea-level lowstands.

The increase in permeability with depth typically leads to truncation of the base of the freshwater lens. The lens is also limited by tidal creeks and ponds, which are developed in topographic lows and range from fresh in the northern islands to hypersaline in the south. Beneath the lens and associated freshwater-saltwater mixing zone there is active large-scale circulation of saline groundwater. The circulation is driven by lateral variations in sea-surface elevation, salinity gradients, and geothermal heating, causing dolomitisation of the platform carbonates.

The islands of the Bahamian archipelago and the surrounding banks have been a keystone in the development of depositional models of carbonate sedimentology. There is now increasing awareness of the pivotal role which the hydrology of fresh, mixed and saline groundwaters may play in controlling the distribution and extent of carbonate diagenesis. The wide range of environments across the archipelago allow examination of a range of extrinsic controls (e.g., climate and island physiography) and intrinsic controls (e.g., sedimentology and mineralogy of depositional facies) on the various groundwater flow systems and the associated diagenesis. Thus the islands of the Bahamian archipelago may prove also to be a keystone of models of carbonate diagenesis.

ACKNOWLEDGMENTS

We would like to thank Neil Sealey, Steve Hobbs, Alan Edwards, David Richards and Rob Palmer for assistance in the field, and Phillip Weech and Richard Cant (Bahamas Ministry of Works and Utilities) and Brian Riggs (Turks and Caicos National Museum) for supplying unpublished reports. Reviews by Bob Buddemeier, David Budd, and in particular Len Vacher substantially improved the manuscript.

REFERENCES

Agassiz, A., 1894. A reconnaissance of the Bahamas and of the elevated reefs of Cuba in the steam yacht "Wild Duck," January to April, 1893. Bull. Mus. Comp. Zool., Harvard, 26: 1–203.

Beach, D.K., 1982. Depositional and diagenetic history of Pliocene–Pleistocene carbonates of northwestern Great Bahama Bank: evolution of a carbonate platform. Ph.D Dissertation, Univ. Miami, Coral Gables FL, 600 pp.

Beach, D.K., 1995. Controls and effects of subaerial exposure on cementation and development of secondary porosity in the subsurface of Great Bahama Bank. In: D.A. Budd, A.H. Saller, and P.M. Harris (Editors), Unconformities in Carbonate Strata — Their Recognition and the Significance of Associated Porosity. Am. Assoc. Petrol. Mem., 63: 1–33.

Beach, D.K. and Ginsburg, R.N., 1980. Facies succession of Pliocene–Pleistocene carbonates, northwestern Great Bahama Bank. Am. Assoc. Petrol. Geol. Bull., 64: 1634–1642.

Benjamin, G.T., 1970. Blue holes of the Bahamas. Natl. Geogr. Mag., 138: 346–363.

Bottrell, S.H., Smart, P.L., Whitaker, F.F. and Raiswell, R., 1991. Geochemistry and isotope systematics of sulphur in the mixing zone of Bahamian Blue Holes. Appl. Geochem., 6: 97–103.

Brooks, S.M. and Whitaker, F.F., 1997. Geochemical and physical controls on vadose zone hydrology of Holocene carbonate sands, Grand Bahama Island. Earth Surf. Processes and Landf., 22: 48–58

Budd, D.A., 1984. Freshwater diagenesis of Holocene ooid sands, Schooner Cays, Bahamas. Ph.D. Dissertation, Univ. of Texas, Austin, 492 pp.

Budd, D.A., 1988a. Petrographic products of freshwater diagenesis in Holocene ooid sands, Schooner Cays, Bahamas. Carbonates and Evaporites, 3: 143–163.

Budd, D.A., 1988b. Aragonite to calcite transformation during fresh water diagenesis of carbonates: insights from porewater chemistry. Geol. Soc. Am. Bull., 100: 1260–1270.

Budd, D.A. and Land, L.S., 1989. Geochemical imprint of meteoric diagenesis in Holocene ooid sands, Schooner Cays, Bahamas: correlation of calcite cement geochemistry with extant groundwaters. J. Sediment. Petrol., 60: 361–378.

Budd, D.A. and Vacher H.L., 1990. Predicting freshwater lenses in carbonate paleo-islands. J. Sediment. Petrol., 61: 43–53.

Busby, R.F. and Dick, G.F., 1964. Oceanography of the Eastern Great Bahama Bank, Part I, Temperature and Salinity Distribution. U.S. Navy Oceanographic Office, 42 pp.

Campbell, D.G., 1978. The Ephemeral Isles. Macmillan, London, 151 pp.

Cant, R.V., 1988. Geological implications of deep well disposal in the Bahamas. In: J.E. Mylroie (Editor), Proc. 4th Symp. Geol. Bahamas. Bahamian Field Station, San Salvador, pp. 53–60.

Cant, R.V. and Weech, P.S., 1986. A review of the factors affecting the development of Ghyben–Hertzberg lenses in the Bahamas. J. Hydrol., 84: 333–343.

Cant, R.V., Weech, P.S. and Hall, E.E., 1990. Saltwater intrusion in the Bahamas; A case study of the Grand Lucayan Waterway, Grand Bahama, Commonwealth of the Bahamas, Int. Symp. on Tropical Hydrol. & Fourth Caribbean Islands Water Resour. Cong., 23–27 July, San Juan, Puerto Rico (Oral Presentation).

Carew, J.L. and Mylroie, J.E., 1995. Fossil reefs and flank margin caves: indicators of late Quaternary sea level and tectonic stability of the Bahamas. Quat. Sci. Rev., 14: 145–153.

Chen, J.H., Curran, H.A., White, B. and Wasserburg, G.J., 1991. Precise chronology of the last interglacial period: $^{234}U/^{230}Th$ data from fossil coral reefs in the Bahamas. Geol. Soc. Am. Bull., 103: 82–97.

Cloud, P.E., 1962. Environments of carbonate deposition west of Andros Island, Bahamas. U.S. Geol. Surv. Prof. Pap. 350, 138 pp.

Cole, L.J., 1910. The caverns and people of the Northern Yucatan. Bull. Am. Geogr. Soc., 42: 321–336.

Davis, R.L. and Johnson, C.R., Jr., 1989. Karst hydrology of San Salvador. In: J.E. Mylroie (Editor), Proc. 4th Symp. Geol. Bahamas. Bahamian Field Station, San Salvador, 118–135.

Enos, P. and Sawatsky, L.H., 1981. Pore networks in Holocene carbonate sediments. J. Sediment. Petrol., 31: 961–985.

Ferris, J.G., 1951. Cyclic fluctuations of water level as a basis for determining aquifer transmissibility. Assem. Gen. Bruxelles, Assoc. Int. Hydrol. Sci., 2: 149–155.

Freeman-Lynde, R.P., Cita, M.B., Jadoul, F., Miller, E.L. and Ryan, W.B.F., 1981. Marine geology of the Bahama Escarpment. Mar. Geol., 44: 119–156.

Halley, R.B. and Harris, P.M., 1979. Freshwater cementation of a 1000-year-old oolite. J. Sediment. Petrol., 49: 469–988.

Harris, J.G., Mylroie, J.E. and Carew, J.L., 1995. Banana holes: Unique karst features of the Bahamas. Carbonates and Evaporites, 10: 215–224.

Jimenez, A.N., 1984. Cuevas y Carsos. Editora Militar, Habana, Cuba, 431 pp.

Johnson, D.W. and McWhorter, D.B., 1977. Hydrological observations and water usage, BART-AD Project, North Andros Island. Consulting Report, Bahamas Agriculture Research, Training and Development Project, 23 pp.

Kohout, F.A., Henry, H.R. and Banks, J.E., 1977. Hydrogeology relating to geothermal conditions in the Floridan Plateau. In: D.I. Smith and G.M. Griffin (Editors), The Geothermal Nature of the Floridan Plateau. Fla. Bur. Geol. Spec. Publ., 21: 1–40.

Little, B.G., Buckley, D.K., Jefferiss, A., Stark, J. and Young, R.N., 1973. Land Resources of the Commonwealth of the Bahamas, 4, Andros Island. Unpubl. report for the Ministry of Overseas Development, Surbiton, England, 87 pp.

Little, B.G., Buckley, D.K., Cant, R.V., Jefferiss, A., Stark, J. and Young, R.N., 1975. Land Resources of the Commonwealth of the Bahamas, 5, Grand Bahama Island. Unpubl. report for the Ministry of Overseas Development, Surbiton, England, 198 pp.

Little, B.G., Cant, R.V., Buckley, D.K., Jefferiss, A., Stark, J. and Young, R.N., 1976. Land Resources of the Commonwealth of the Bahamas, 6A and 6B, Great Exuma, Little Exuma and Long Island. Unpubl. report for the Ministry of Overseas Development, Surbiton, England, 130 pp.

Little, B.G., Buckley, D.K., Cant, R.V., Henry, P.W.T., Jefferiss, A., Mather, J.D., Stark, J. and Young, R.N., 1977. Land Resources of the Commonwealth of the Bahamas. Land Resource Study 27, Ministry of Overseas Development, Surbiton, England, 133 pp.

Mather J.D. and Buckley, D.K., 1973. Tidal fluctuations and groundwater conditions in the Bahamian archipelago. Proc. Second Int. Conf. on Salt Groundwaters, May 1973, Palermo, Italy.

Matthews, R.K., 1974. A process approach to diagenesis of reefs and reef associated limestones. In: L.F. Laporte (Editor), Reefs in Time and Space. Soc. Econ. Palaeontol. Mineral. Spec. Publ., 18: 234–256.

Maul, G.A., 1986. Linear correlations between Florida current volume transport and surface speed with Miami sea-level and weather during 1964–1970. Geophys. J. R. Astronom. Soc., 87: 55–66.

McClain, M.E., Swart, P.K. and Vacher, H.L., 1992. The hydrogeochemistry of early meteoric diagenesis in a Holocene deposit of biogenic carbonates. J. Sediment. Petrol., 62: 1008–1022.

McNeill, D.F., Ginsburg, R.N., Chang, S-B.R. and Kirschvink, J.L., 1988. Magnetostratigraphic dating of shallow-water carbonates from San Salvador, Bahamas. Geology, 16: 8–12.

Mullins, H.T. and Lynts, G.W., 1977. Origin of the Northwest Bahama Platform: review and interpretation. Geol. Soc. Am. Bull., 88: 1447–1461.

Mylroie, J.E. and Carew, J.L., 1990. The flank margin model for dissolutional cave development in carbonate platforms. Earth Surf. Processes and Landf., 15: 413–424.

Mylroie, J.E. and Carew, J.L., 1995. Karst development on carbonate islands. In: D.A. Budd, A.H. Saller and P.M. Harris (Editors), Unconformities and Porosity in Carbonate Strata. Am. Assoc. Petrol. Geol. Mem. 63, pp. 55–76.

Mylroie, J.E., Carew, J.L., Sealey, N.E. and Mylroie J.R., 1991. Cave development on New Providence Island and Long Island, Bahamas. Cave Sci., 18(1): 39–151.

Mylroie, J.E., Carew, J.L. and Vacher H.L., 1995a. Karst development in the Bahamas and Bermuda. In: H.A. Curran and B. White (Editors), Terrestrial and Shallow Marine Geology of the Bahamas and Bermuda. Geol. Soc. Am. Spec. Pap., 300: 251–268.

Mylroie, J.E., Carew, J.L. and Moore, A.I., 1995b. Blue holes: Definition and genesis. Carbonates and Evaporites, 10: 225–233.

Oberdorfer, J.A., Hogan, P.J. and Buddemeier, R.W., 1990. Atoll island hydrogeology: flow and freshwater occurrence in a tidally dominated system. J. Hydrol., 120: 327–340.

Palmer, R.J. (Editor), 1984. Bahamas blue holes; collected papers from expeditions 1981–1982. Cave Sci., 11, 64 pp.

Palmer, R.J., 1985. The Blue Holes of the Bahamas. Johnathan Cape, London, 183 pp.

Palmer, R.J., 1986. Hydrology and speleogenesis beneath Andros Island. Cave Sci., 13: 7–12.

Palmer, R.J., 1989. Deep into the Blue Holes. Unwin Hyman, London, 164 pp.
Palmer R.J. and Heath L., 1985. Effect of anchihaline factors and fracture control on cave development below Eastern Grand Bahama. Cave Sci., 12: 93–101.
Peach, D.W., 1991. Hydrogeological investigations: New Providence and North Andros. Unpubl. report to the Bahamas Water and Sewerage Corporation and the U.N. Development Program, 81 pp.
Pierson, B.J., 1982. Cyclic sedimentation, limestone diagenesis and dolomitisation in the Upper Cenozoic carbonates of the Southeastern Bahamas. Ph.D. Dissertation, Univ. Miami, Coral Gables FL, 312 pp.
Pierson, B.J. and Shinn, E.A., 1985. Cement distribution and carbonate mineral stabilisation in Pleistocene limestones of Hogsty Reef, Bahamas. In: N. Schneidermann and P.M. Harris (Editors), Carbonate Cements. Soc. Econ. Palaeontol. Mineral. Spec. Publ., 36: 153–168.
Rossinsky, V. Jr., Wanless, H.R. and Swart, P.K., 1992. Penetrative calcretes and their stratigraphic implications. Geology, 20: 331–334.
Sealey, N.E., 1985. Bahamian Landscapes. Collins Caribbean, London, 96 pp.
Sealey, N.E., 1990. The Bahamas Today, An Introduction to the Human and Economic Geography of the Bahamas. Macmillan Caribbean, London, 120 pp.
Simms, M. 1984. Dolomitisation by groundwater flow systems in carbonate platforms. Trans. Gulf Coast Assoc. Geol. Soc., 24: 411–420.
Smart, C.C., 1984. The hydrology of inland blue holes. Cave Sci., 11: 23–29.
Smart P.L. and Whitaker, F.F., 1988. Controls on the rate and distribution of carbonate bedrock dissolution in the Bahamas. In: J.E. Mylroie (Editor), Proc. 4th Symp. Geol. Bahamas. Bahamian Field Station, San Salvador, pp. 313–322.
Smart, P.L. and Whitaker, F.F., 1990. Comment on "Geological and environmental aspects of surface cementation, north coast Yucatan, Mexico". Geology, 18: 802–804.
Smart, P.L., Palmer, R.J., Whitaker, F.F. and Wright, V.P., 1987. Neptunian dykes and fissure fills: an overview and account of some modern examples. In: N.P. James, and P.W. Choquette (Editors), Paleokarst. Springer-Verlag, New York, pp.149–163.
Smart, P.L., Dawans, J.M. and Whitaker, F.F., 1988. Carbonate dissolution in a modern mixing zone, South Andros, Bahamas. Nature, 335: 811–813.
Smart, P.L., Edwards, A.J. and Hobbs, S.L., 1992. Heterogeneity in carbonate aquifers; effects of scale, fissuration, lithology and karstification. Proc. Third Conf. Hydrology, Ecology, Monitoring and Management of Groundwater in Karst Terranes. Natl. Water Well Assoc., Dublin OH, pp. 373–387.
Socki, R., Gaona-Vizcayno, P., Perry, E. and Villasuso-Pino, M., 1984. A chemical drill: sulfur isotope evidence for the mechanism of formation of deep sinkholes in tropical karst, Yucatan, Mexico (abstr.). Geol. Soc. Am., Abstr. Programs, pp. 662.
Sparkes, K.F., 1985. Brief notes on water supplies in the Turks and Caicos Islands. Unpubl. report to the Turks and Caicos Ministry of Works and Utilities, 12 pp.
United Nations, 1976. Bahamas, Turks and Caicos. In: Groundwater in the Western Atmosphere, U.N. National Resources/Water Ser. 4, United Nations, New York, pp. 125–132.
Trott, R.J. and Warner, G.F., 1986. The biota in the marine blue holes of Andros Island. Cave Sci., 13: 13–19.
Vacher H.L., 1988. Dupuit–Ghyben–Herzberg analysis of strip island lenses. Geol. Soc. Am. Bull., 100: 580–591.
Vacher, H.L. and Wallis, T.N., 1992. Comparative hydrogeology of freshwater lenses of Bermuda and Great Exuma Island, Bahamas. Ground Water, 30: 15–20.
Vaughan, T.W., 1919. Coral and the formation of coral reefs. Report of Smithsonian Inst. for 1917, Washington D.C., pp. 189–276.
Vogel, P.N., Mylroie, J.E. and Carew J.L., 1990. Limestone petrology and cave geomorphology on San Salvador Island, Bahamas. Cave Sci., 17: 19–30.
Walles, F.E., 1993. Tectonic and diagenetically induced seal failure within the south-western Great Bahama Bank. Mar. Petrol. Geol., 10: 14–28.

Wallis, T.N., Vacher, H.L. and Stewart, M.T., 1991. Hydrogeology of the freshwater lens beneath a Holocene strandplain, Great Exuma, Bahamas. J. Hydrol., 125: 93–100.

Wanless, H.R., Tedesco, L.P., Rossinsky, V., Jr., and Dravis, J.J., 1989. Carbonate environments and sequences of Caicos platform. 28th Int. Geol. Cong., IGC Field Trip Guideb. T374. American Geophysical Union, Washington D.C., 75 pp.

Weech, P.S., 1993. Country Paper – Bahamas. Paper prepared for the regional workshop on Water Quality in the Caribbean, Port of Spain, Trinidad, July 1993, 18 pp.

Whitaker, F.F., 1992. Hydrology, geochemistry diagenesis of modern carbonate platforms in the Bahamas. Ph.D. Dissertation, Univ. Bristol, 347 pp.

Whitaker, F.F. and Smart, P.L., 1990. Circulation of saline groundwaters through carbonate platforms: evidence from the Great Bahama Bank. Geology, 18: 200–204.

Whitaker, F.F. and Smart, P.L., 1993. Circulation of saline groundwaters through carbonate build-ups: a review and case study from the Bahamas. In: H.A. Horbury, and A. Robinson, (Editors), Diagenesis and Basin Development. Am. Assoc. Petrol. Geol. Studies Geol., 36: 113–131.

Whitaker, F.F. and Smart, P.L., 1997a. Climatic control on hydraulic conductivity of Bahamian limestones. Ground water (in press). Queens University Belfast.

Whitaker, F.F. and Smart, P.L., 1997b. Geochemistry of meteoric waters and porosity generation in carbonate islands of the Bahamas. In: J. Hendry, P. Carey, J. Parnell, A. Ruffell and R. Worden (Editors) Geofluids II '97, 415–418.

Whitaker, F.F. and Smart, P.L., 1997c. Groundwater circulation and geochemistry of a karstified bank-marginal fracture system, South Andros Island, Bahamas. J. Hydrol. (in press).

Whitaker, F.F., Smart, P.L., Vahrenkamp, V.C., Nicholson, H. and Wogelius, R.A., 1994. Dolomitisation by near-normal sea water? Evidence from the Bahamas. In: B. Purser, M. Tucker, and D. Zenger (Editors), Dolomites, a Volume in Honour of Dolomieu. Int. Assoc. Sedimentol. Spec. Publ., 21: 111–132.

Geology and Hydrogeology of Carbonate Islands. Developments in Sedimentology 54
edited by H.L. Vacher and T. Quinn
© 1997 Elsevier Science B.V. All rights reserved.

Chapter 5

GEOLOGY AND HYDROGEOLOGY OF THE FLORIDA KEYS

ROBERT B. HALLEY, H.L. VACHER and EUGENE A. SHINN

INTRODUCTION

The Florida Keys, which border the southeastern tip of the Florida peninsula (Fig. 5-1), are low-lying islands composed of Pleistocene limestone. They form an arcuate chain extending from Soldier Key (15 km southeast of Miami) south and west to Key West, a distance of 240 km. The Keys are divided into the Upper Keys, from Bahia Honda northward, and the Lower Keys, from Big Pine Key to Key West. Technically, the Holocene mud islands of Florida Bay (Fig. 5-1), the sandy islands west of Key West (the Marquesas and Dry Tortugas), and ephemeral islands and rocks of the reef tract are all also Florida "keys". The mud islands of Florida Bay are discussed in the next chapter. This chapter concerns the islands formed of Pleistocene limestone. These islands, which are crossed when driving from Miami to Key West, are typically regarded as "the Florida Keys."

The Florida Keys were largely ignored during the sixteenth, seventeenth, and eighteenth centuries, although the waters just offshore provided a major shipping thoroughfare to and from the New World. For three centuries, the islands were notorious for their treacherous reefs, pirates and Caloosa Indians, and the scarcity of water and fertile soil. After Florida was ceded by Spain to the United States in 1821, Key West became an important military outpost guarding the entrance to the Gulf of Mexico. The island began to grow as a trading center between the Gulf and Atlantic coasts and between Cuba and the United States. Trading, fishing, and recovering goods from shipwrecks provided livelihood for Keys residents, and boosts to the economy were derived from the Civil, Spanish-American, and World Wars. The Overseas Railway and Overseas Highway, completed in 1912 and 1938, respectively, provided the backbone of transportation in the Keys.

Bridged transportation, together with a water pipeline from the mainland built to supply the military in Key West during World War II, set the stage for post-war development. With the advent of widespread air-conditioning and mosquito spraying, the Keys have developed into one of the most popular tourist destinations in North America. The beauty of the area's coral reefs and clear blue water, the excitement offered by sports fishing and diving, and the diversity of the region's wildlife, all combine to make the Florida Keys one of the premier natural wonders of the United States.

The outstanding and fragile character of ecosystems on and around the Florida Keys has prompted State and Federal efforts to protect and preserve the remaining public portions of the region. The northernmost Florida Keys lie within Biscayne National Park. Florida Bay, northwest of the Keys, lies almost entirely within

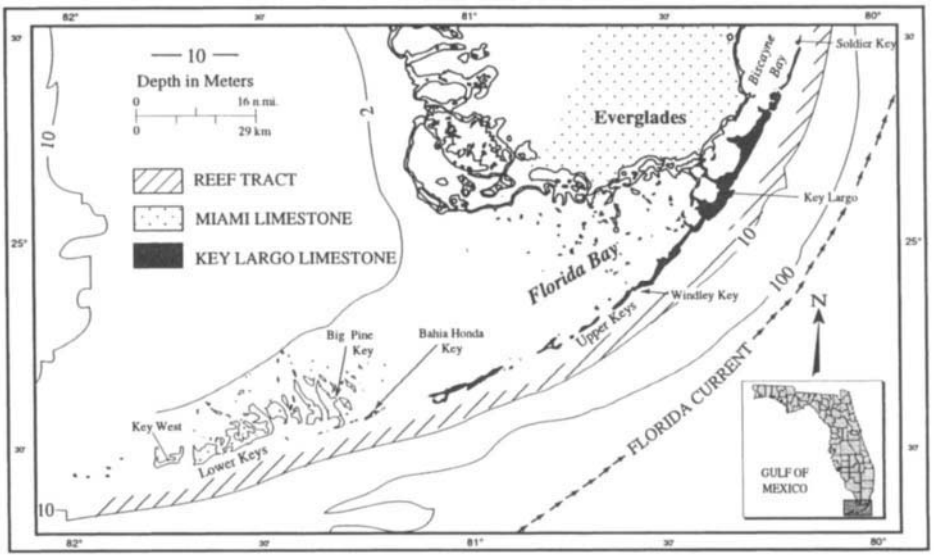


Fig. 5-1. Map showing the Florida Keys, their lithology, and location relative to mainland and reef tract.

Everglades National Park. The Dry Tortugas, 110 km west of Key West, lie in Fort Jefferson National Park. The remainder of the Keys are within the Florida Keys National Marine Sanctuary. Numerous smaller refuges and preserves are found throughout the islands.

During the last decade, there has been increasing concern for the environmental well-being of the region, including the Everglades and other South Florida terrestrial ecosystems. Large-scale declines in bird and fish populations, infestations of exotic biota, and mortality of seagrasses and corals have raised questions about the effects of agricultural and urban development on South Florida's native ecosystems. Changes brought about by water-management practices have received the most attention, particularly the draining of wetlands that began at the turn of the century. Currently, a massive Federal and State program is being developed to restore the water flow patterns and cycles of remaining natural areas to something comparable to their predevelopment condition (Holloway, 1994; Culotta, 1995).

A geological showcase

The pre-bridges geological literature of the Florida Keys and surrounding environments includes works by some of America's most celebrated and influential natural scientists. Louis Agassiz, whose Etudes sur les glaciers (1840) in Switzerland opened the concept of the Ice Ages, did a study of the reefs some five years after immigrating to the United States to become, in 1847, Professor of Zoology at Harvard College, where he established what grew to be the Museum of Comparative

Zoology. His son, Alexander Agassiz, wrote specifically of the Keys ("The elevated reef of Florida," Agassiz, 1894) from a visit in the winter of 1893; this visit was among the first of his expeditions specifically to study coral reefs [see Chap. 1], coming after expeditions to the Bahamas and the coast of Cuba in the winter of 1893 and Bermuda in the spring of 1894, and before the Great Barrier Reef in 1896.

From 1908 to 1915, T. Wayland Vaughan studied the corals, reefs, sediments, and organism-sediment relations while based at the Carnegie Institution's Marine Biological Laboratory in the Dry Tortugas. This work was part of a line of investigation that included one of the seminal papers in paleoecology (Vaughan, 1940; cf., Ladd, 1957), which he gave as his Presidential address to the Geological Society of America, after retiring as Director of Scripp's Institution of Oceanography. One of the concluding sentences of that paper — "There should be continuous shuttling from studies of the modern to studies of the ancient and back again from the ancient to the modern" (Vaughan, 1940, p. 466) — describes the comparative approach to carbonate geology that has been possible in the Keys and nearby Bahamas.

As the best known marine carbonate depositional setting in the continental United States, the Keys and surrounding environments became a showcase for geologic field trips for academic and industrial groups. Particularly noteworthy are the field trips led by Robert N. Ginsburg from his lab on Fisher Island. Ginsburg named this lab, which was part of the University of Miami (Rosenstiel School of Atmospheric and Marine Sciences), the T. Wayland Vaughan Laboratory of Comparative Sedimentology (see Ginsburg, 1995, for an account). A huge number of carbonate geologists in the U.S. petroleum industry in the 1970s and 1980s participated in these trips, and many, having later entered the academic ranks, are bringing subsequent generations to this geological showcase.

The classic field trip guide is Ginsburg (1964), and it is still instructive. The book by Multer (1977) compiles much of the literature of the 1960s and 1970s and is designed for students and visitors. The field guide to the reefs by Shinn et al. (1989) incorporates work done from the U.S. Geological Survey Fisher Island Station over the 15 years of its existence. Shinn (1988) and Randazzo and Halley (1997) give summaries specifically on the geology of the Keys.

SETTING

Climatic and oceanographic setting

The Florida Keys enjoy a subtropical climate with mean January temperatures of 21°C (69°F) and mean July temperatures of 28°C (83°F). Winter freezes occur rarely in the Upper Keys and have never been known to extend to the Lower Keys. A well-developed gradient in rainfall extends across the Keys, with the northern Keys receiving an average of 140 cm (55 in.) and Key West averaging slightly less than 100 cm (40 in.). Rainfall is also highly seasonal. Almost two-thirds of the annual rainfall occurs as wet-season thunderstorms between May and October. The predominant wind direction is from the east and characterizes the summer months;

however, this wind is a gentle summer breeze that rarely exceeds 10 km h^{-1} except during summer thunderstorms. The relative calm of the summer is occasionally punctuated by tropical storms and hurricanes that pass through the Keys with a recurrence interval of about 2 years. During the winter dry season, rain is associated with periodic, almost weekly, cold fronts sweeping through the Keys as they cross the eastern North American continent. These storms bring strong westerly and northerly winds between calmer periods of easterly and southeasterly breezes.

On the Atlantic Ocean side of the Keys, the Florida Current flows northward, parallel to the Keys and east of the 5–8-km wide shelf that supports the growth of modern coral reefs along its outer margin (Fig. 5-1). Pleistocene reefs form relict ridges along the margin a few hundred meters seaward of the modern reef tract (Fig. 5-2). The Florida Current varies from 22°C (71°F) in winter to 28°C (83°F) in summer and is a moderating influence on the climate of the Keys. Landward of the reef tract is White Bank, a shallow sand shoal studded with patch reefs, and Hawk Channel, an inner shelf lagoon 6–8 m deep. Just seaward of the Keys, bare limestone equivalent to that of the Keys is exposed for as much as a kilometer offshore (Fig. 5-2).

Florida Bay [q.v., Chap. 6] lies west of the Upper Keys (Fig. 5-1) and is a shallow lagoon (average depth, 1.3 m) characterized by mangrove-covered Holocene mud and peat islands, mudbanks, and shallow marine basins locally called "lakes." This shallow water typically remains close to atmospheric temperature and may be as warm as 35°C (95°F) in the summer and reach extremes of 13°C (55°F) during winter

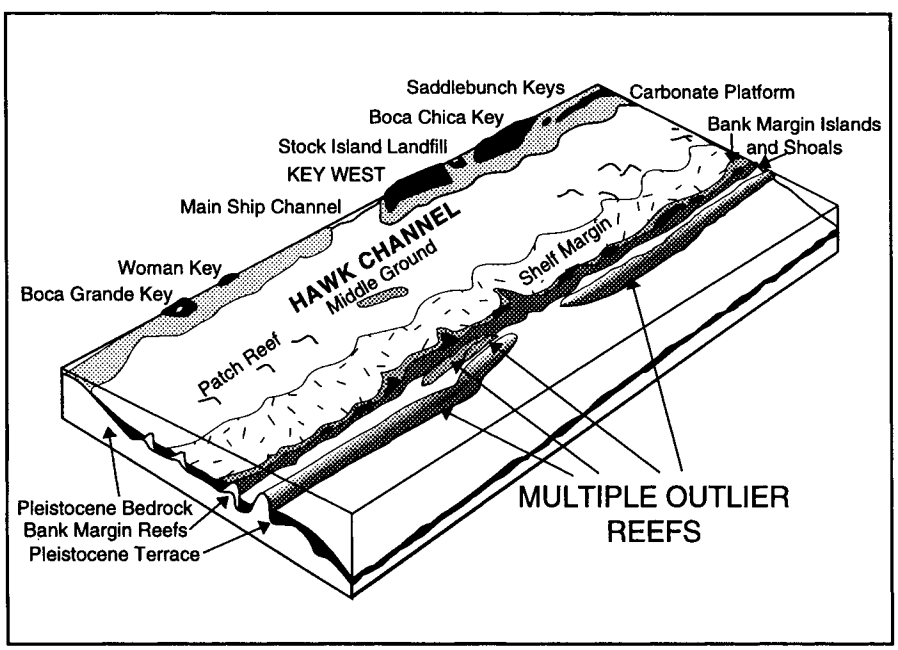


Fig. 5-2. Block diagram showing relations between major physiographic and bathymetric features of the Lower Keys. (Courtesy of Barbara Lidz, U.S. Geol. Surv.)

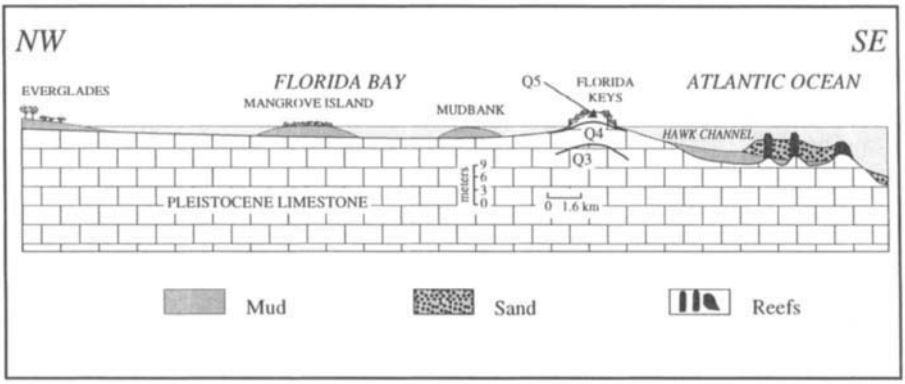


Fig. 5-3. Diagrammatic cross section showing relation of the Upper Florida Keys to reefs and Florida Bay. The eastern Everglades and Lower Keys are underlain by the Miami Limestone; the Upper Keys are underlain by the Key Largo Limestone. The facies transition between the two formations is hidden beneath Florida Bay and identified as (undifferentiated) Pleistocene limestone. The position of subaerial-exposure surfaces (bold lines) beneath the Upper Keys is modified from Perkins (1977), Harrison and Coniglio (1985), and unpublished data by the authors (EAS and RBH).

cold episodes. Lakes, mudbanks, and islands are underlain by Pleistocene limestone that is a facies variant of limestones forming the Florida Keys (Fig. 5-3).

Before the arrival of Europeans, vegetation of the Keys was of three kinds: (1) mangroves; (2) tropical and subtropical hardwoods; and (3) pines and palmettos. Typically the small and narrow islands support hardwoods. Larger, broad islands support pine-palmetto vegetation. The pine-palmetto ecotope, characteristic of much of South Florida, dominates where periodic fires sweep the larger Keys. All islands are fringed with mangroves; the lowest islands are typically entirely mangrove. Many of the islands were cleared for agriculture during the last century and early part of this century (Craighead, 1971), and much of the original vegetation has now given way to development on the islands.

Topographically, the Keys are low and flat. Hoffmeister and Multer (1968) estimated that about one-half of the area of the Keys is covered by mangrove swamps. The rest is mostly <1 m in elevation; the highest elevation is 5.5 m (18 ft) at Windley Key (Hoffmeister and Multer, 1968). There are only a few sand beaches in the Florida Keys. Most of the shoreline is characterized by rock or muddy intertidal flats that border mangrove shorelines (Hoffmeister and Multer, 1968).

Tectonic setting

The Florida Keys occupy the southern portion of the Florida Platform, a 5-km-thick sequence of shallow-water carbonates and evaporites with relatively minor components of terrigenous sediments. The platform represents continued sedimentation and subsidence on a passive continental margin that overlies transitional crust

formed during the initial opening of the Atlantic Ocean (Klitgord et al., 1984). The Florida Platform was part of a great Mesozoic carbonate bank or "gigaplatform" (Hine, 1997), which stretched from Mexico and the Bahamas to Canada along the Atlantic side of North America (Hine, 1997).

During the Cretaceous and Tertiary, deep troughs developed in the platform and formed basins such as the Straits of Florida and the Tongue of the Ocean. Development of these basins reflect complex interactions of sedimentation and erosion rates of carbonate sediments, involving such factors as changes in sea level, circulation patterns, nutrient supply, and climate change (Hine, 1997). During the Miocene, Pliocene and, most recently, Pleistocene, some terrigenous clastic deposits extended from North Florida to the southern tip of the platform (Enos and Perkins, 1977; Warzeski et al., 1996). During the late Pleistocene, carbonate sediments dominated the Keys region as they do today.

The continental margin has experienced about 200 m.y. of cooling and subsidence since the formation of the Atlantic (Steckler et al., 1988). This period of rapid cooling and subsidence ended at about 150 Ma, and now the Florida Platform is near the distal end of its cooling and subsidence curve. As noted by Steckler et al. (1988), various cooling models converge to very slow subsidence rates after 200 m.y. such that the Florida Keys can be considered to be located on a very stable, old margin at the present time. As described later, the age and elevation of the coralline Florida Keys, along with correlation to other reefal limestones in the western Atlantic, suggest that less than a few meters of subsidence has occurred in the last 100 ky.

It should also be noted, particularly with regard to sea-level estimates for the Pleistocene, that the Florida Keys are slightly influenced by isostatic motions associated with the shift in load back and forth from continental ice to the global ocean. Peltier (1986) calculated that deglaciation-induced downward vertical motions of the Atlantic margin should be expected for the entire east coast of the United States, and that this subsidence may amount to about 0.1 cm y^{-1} in Florida.

PLEISTOCENE GEOLOGY

The current understanding of the bedrock geology of the Florida Keys derives from a series of benchmark papers by Hoffmeister and Multer in the 1960s (Hoffmeister and Multer, 1964a,b, 1968; Hoffmeister et al., 1964, 1967; Hoffmeister, 1974), and subsequent work that has been built on that foundation. The key facts are: (1) the long linear islands of the Upper Keys represent a reef tract formed during high sea levels of the last interglacial, and (2) the larger Lower Keys are fossil oolitic shoals, also formed during high sea levels of the last interglacial.

Early workers were well aware of the two kinds of islands. For example, Sanford (in Matson and Sanford, 1913, p. 61–62) described the arrangement as follows:

> "The Florida Keys are separated by Bahia Honda Channel into two distinctly differentiated divisions. East of the channel the islands are narrow and lie along a sweeping arc curved toward the southeast. Outside this arc is the Florida Strait....

> West of Bahia Honda the keys form an archipelago roughly triangular in outline. In this group, the westward prolongation of the arc in which lie Bahia Honda and the keys to the east and northeast is found in the southern shoreline of the keys; but the keys themselves, instead of lying parallel to this arc, have a prevailing north-northwest, south-southeast arrangement, perpendicular to the arc....
>
> Bahia Honda and the keys east of it represent an uplifted coral reef more or less covered with sand and marl; hence their basement rock ridges have the trend of the coral patches of the old reef. The keys west of Bahia Honda consist of an oolitic limestone formed from deposits in a broad expanse of shallow water."

We should note that the early work in the Keys preceded knowledge of Pleistocene glacioeustasy and sea-level highstands. In particular, Alexander Agassiz considered the "elevated reef of Florida" (Agassiz, 1896) to be one of a number of examples posing problems for Darwin's subsidence theory for the origin of coral reefs.

Fresh from his visits to the Bahamas and Bermuda, Agassiz thought that the oolitic limestone, evident near Key West and near Miami, was formed as eolian dunes, capping the elevated reef throughout the higher keys. According to Agassiz (1896, p. 50),

> "The keys are all built upon this elevated coral reef foundation, which crops to the surface, as we have seen, at many points, and from the beaches on the sea face of this elevated reef has been obtained the oolitic material which as aeolian sand has raised the keys to a height of sometimes ten to eighteen feet. This sand has been blown to the northward ... to form low aeolian hills and bluffs between the patches and stretches of the old coral reef; or it has accumulated upon the top of patches and stretches of reef to form the higher keys...."

As it turns out, the highest elevation is at Windley Key, one of the Upper Keys, which now are known to be composed of the reefal unit. Sanford (in Matson and Sanford, 1913), who argued for the subaqueous rather than subaerial origin of the oolite, called attention to the difficulties of interpreting the geology of the islands without exposures and the benefits he had from the exposures opened up by railroad construction. Referring to the reefal unit in Key Largo, Sanford wrote (Matson and Sanford, 1913, p. 185),

> "Borrow pits expose the limestone, not only where it was lightly covered by leaf mold but where it was buried under several feet of marl and sand, and dredging has revealed its character where it lies, as in channels between the keys, 10 feet or more below sea level. Hence, the opportunities for observing the various phases of the rock and determining its origin are incomparably better than when A. Agassiz visited the keys in 1894."

The now-closed Windley Key quarry, which was first opened for railroad ballast, is the source of decorative coralline limestone used throughout South Florida.

Today, the reefal unit is known as the Key Largo Limestone; the oolitic rocks make up a facies of the Miami Limestone. The Upper Keys, which are elongated and oriented parallel to the shelf edge, consist of the Key Largo Formation; the Lower Keys, which are elongated perpendicular to the shelf edge, are composed of oolite of the Miami Limestone. Stratigraphic nomenclature and usage are summarized in Randazzo and Halley (1997). Unlike the Miami Limestone, which has direct modern analogs that aid in its interpretation, the Key Largo Limestone apparently does not have a modern counterpart. Its interpreted origin has evolved over the past two decades.

Miami Limestone

The oolite facies of the Miami Limestone in the Lower Keys consists of well-sorted ooids with varying amounts of skeletal material (corals, echinoids, mollusks, algae) and some quartz sand. Oolite in the Lower Keys has less quartz sand and fewer marine fossils than the Miami Limestone near Miami (Sanford, 1909; Hoffmeister and Multer, 1968; Weisbord, 1974) and was deposited as a marine oolitic bank or bar system (Hoffmeister et al., 1967; Halley and Evans, 1983). Thickness of the cross-bedded oolite facies is 3–5 m and is greatest along the seaward edge, both in Miami and in the Lower Keys.

Overall, the geometry of the Lower Keys has the configuration of a tidal-bar system (Fig. 5-4). The islands correspond to the bars; the paleo-tidal channels occur between the islands. A similar lithified tidal-bar system occurs in the Miami-Homestead region (Fig. 5-4) (Halley et al., 1977). The Miami system is higher, such that paleo-tidal channels are not submerged but now form part of the main peninsula of South Florida (Fig. 5-4).

Key Largo Limestone

The Key Largo Limestone in the Keys consists of hermatypic corals with intra- and interbedded calcarenites and thin beds of quartz sand. According to Hoffmeister and Multer (1968), the thickness of the Key Largo varies widely, but more than 60 m was identified from core borings at Big Pine Key. The upper part of the formation is visible in many cuts and quarries in the Upper Keys. In the terminology of Dunham (1962), the upper Key Largo consists of boundstones, grainstones, wackestones, and packstones (Harrison et al., 1984; Shinn et al., 1989). Coral geometries vary with phyletic groups and conditions of preservation, but, in general, the formation contains a surprising amount of coral in growth position (Hoffmeister et al., 1964). Coral boundstones are interbedded with and surrounded by grainstones and wackestones, with the highest concentrations of corals at the topographically higher positions beneath the islands. Seaward of the islands, grainstones are common in the Key Largo; in contrast, wackestones and packstones dominate on the Gulf of Mexico side of the Keys. Coral distribution appears to occur in large, elongate patches several hundred meters wide and several kilometers long, generally conforming to the geometry of the islands (Stanley, 1966; Hoffmeister and Multer, 1968).

Although there is general agreement that the Key Largo Limestone represents a Pleistocene reef tract, there are significant geometric and biologic differences between the Key Largo reef tract and the modern reefs. These differences gave rise to a small controversy in the 1960s about what kind of reef the Key Largo might have been. As shown on Fig. 5-1, the Key Largo trend is parallel to the present reef tract and set back from it by about 7 km. The Key Largo trend is wider than the present reef tract, which is simply a discontinuous line of linear shelf-margin reefs, none longer than a few kilometers. In contrast, the island of Key Largo itself is about 70 km long.

The differences between the Key Largo and the present reefs extend to faunal composition and implied wave energy. Most striking is the absence of *Acropora*

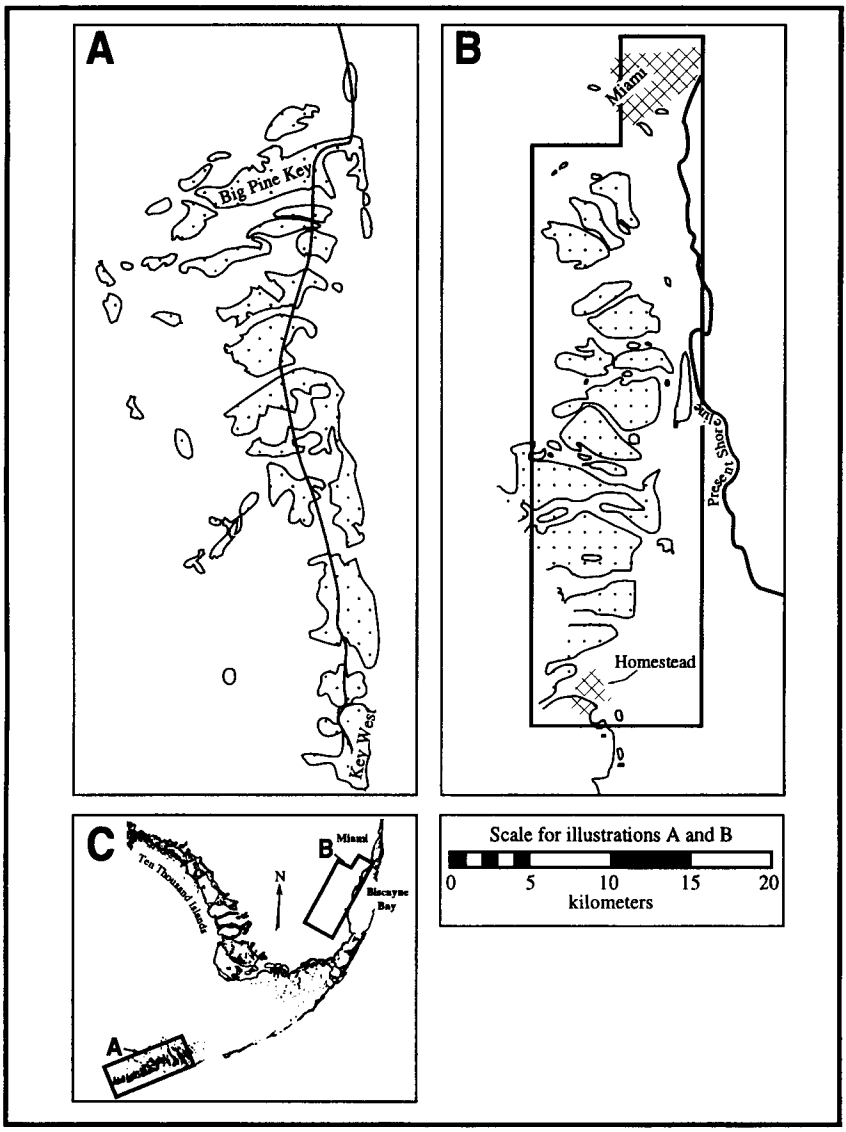


Fig. 5-4. Geometry of the Lower Keys compared with topography of the southeast Florida coast west of Biscayne Bay. (A) Generalized shoreline of the Lower Keys with the islands (stippled) showing broad topography with elongation parallel to tidal channels. (B) Topography in the Miami-Homestead area west of Biscayne Bay showing areas higher in elevation than 2.7 m (9 ft) for comparison with A. (C) Index showing relation of areas in A and B to the South Florida Peninsula. The similarity of geometry derives from the fact that both areas are underlain by Pleistocene oolite that retains the topography of ooid sand shoals.

palmata (Stanley, 1966; Hoffmeister and Multer, 1968), which is the principal reef-crest structural element of the modern outer reefs (Ginsburg, 1956; Shinn, 1963). The main framework element of the Key Largo is *Montastrea annularis*, implying lower wave energy (Stanley, 1966). In addition, *Millepora* and coralline algae are underrepresented in the Key Largo, and *Halimeda* is overrepresented in the Key Largo relative to the modern reef tract (Hoffmeister and Multer, 1968). Stanley (1966) proposed, therefore, that the Key Largo formed as a relatively deep water, outer reef tract, at water depths comparable to the modern *Montastrea* zone of West Indian reefs (6–15 m; Storr, 1964); he did not believe that the Key Largo formed as a line of coalesced patch reefs behind a now-absent outer reef tract, because he could not accept that any such outer reef tract could have been eroded in the time available post-depositionally while the Key Largo continued to be preserved.

Hoffmeister and Multer (1968) rejected the deep-water interpretation of Stanley (1966) on evidence of a strandline at an elevation of about 7.5 m (25 ft) in the Miami Limestone (in Miami) that was then (and now) thought to be contemporaneous with the Key Largo fossil reef tract. Hoffmeister and Multer (1968) argued strongly for a backreef interpretation, accepted the implied erosion, and added the possibility of structural tilting as a means of lowering the outer platform. Also, Hoffmeister and Multer (1968) encountered fragments of *Acropora palmata* at 17 m (58 ft) below sea level in a core near Looe Key Reef at the edge of the platform and considered them to be remnants of the missing outer reef tract contemporary with the Key Largo. Dodd et al. (1973) reviewed the arguments of Stanley (1966) and Hoffmeister and Multer (1968) and pointed out that reefs off Newfoundland Harbor Keys, although less extensive than the Key Largo Limestone, share many similarities with the Pleistocene reef.

The work of Perkins (1977) and Enos (1977) sharpened the dilemma. From considerations of regional relationships (South Florida) and what was known of late Pleistocene sea levels in general, the interpretation of shallow water for the Key Largo was acceptable (Perkins, 1977). On the other hand, the hypothesized coeval outer reef tract could not be accepted. According to Perkins (1977), regional isopachs, facies patterns, and shelf gradients also ruled out tectonic adjustments during the Pleistocene. According to Enos (1977), the highest culminations of the Pleistocene surface on the outer reef tract are 8–11 m below present sea level. Adding the ~7-m layer above present sea level, the implied erosion of the hypothetical outer reef and associated sediments would be 15–18 m — over an area 5 to 8 km wide and more than 100 km long (Harrison and Coniglio, 1985). In order to resolve the dilemma of shallow-water origin and absent outer barrier, Perkins (1977) proposed that the Key Largo is the leading edge of a complex of patch reefs and sand shoals that were initiated near the outer shelf edge and migrated laterally as sea level rose.

The presently accepted interpretation is that of Harrison and Coniglio (1985): the Key Largo Formation is a complex of shallow-water shelf-margin reefs and associated deposits along a topographic break; the absence of *Acropora palmata* and other biotic differences is due to environmental stress. The concept of environmental stress derives from observations of the modern depositional system (Ginsburg and Shinn, 1964; Marszalek et al., 1977). As discussed in the Case Study, modern reefs

are best developed seaward of protective islands; the reefs are not developed opposite intervening passes. The islands shield the reefs from injurious waters generated in the shallow lagoon behind them. At the time the Key Largo reef was alive, there were no insular shields and the shoreline was 160 km or more farther north (Perkins, 1977).

Stratigraphy

Hoffmeister et al. (1964) found that the oolite facies of the Miami Limestone passes laterally into the Key Largo Limestone at the southeastern point of Big Pine Key (Fig. 5-5). They also found that the oolite in the rest of the island is underlain by

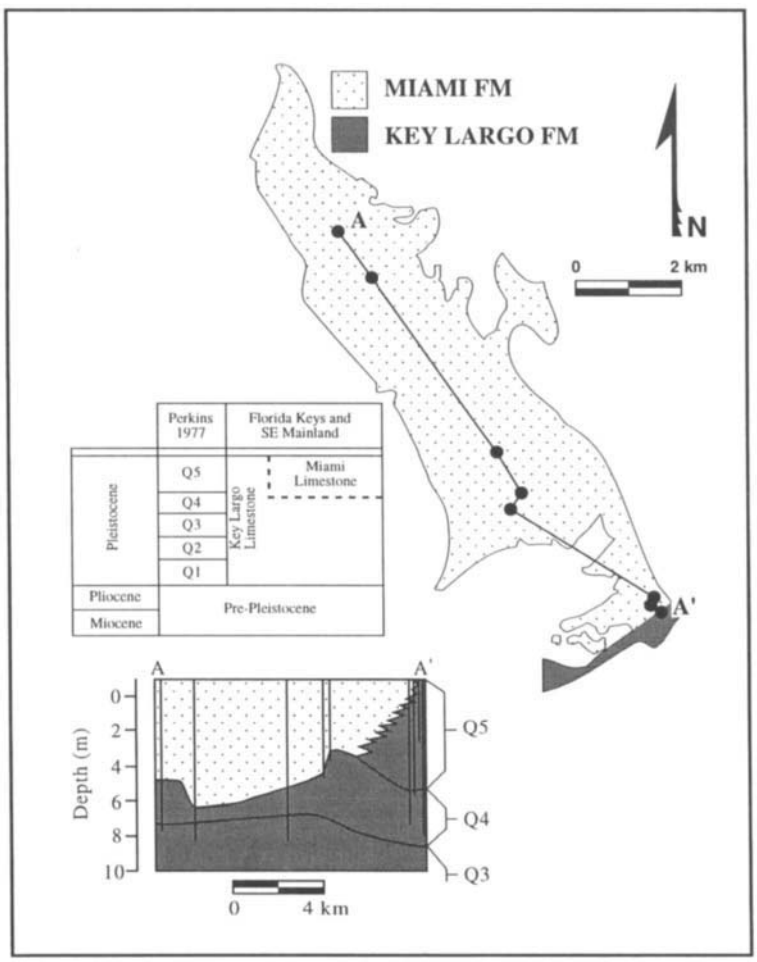


Fig. 5-5. Geologic map and cross section of Big Pine Key (adapted from Vacher et al., 1992, after Coniglio and Harrison, 1985). Inset shows relation of Key Largo and Miami Limestones to stratigraphic nomenclature of Perkins (1977).

the Key Largo Formation. The facies intergradation and superposition of the two units were mapped in detail by Coniglio and Harrison (1983a) using cores from nine shallow wells drilled by the U.S. Geological Survey (Fig. 5-5). As indicated by these cores, the contact between the Miami and Key Largo Limestones in most places in Big Pine Key lies at a depth of 4–6 meters (Hanson, 1980). The facies transition between the two units in southeastern Big Pine Key occurs laterally over a few hundred meters (Kindinger, 1986).

Perkins (1977) recognized and mapped regional subaerial discontinuity surfaces within the Quaternary of South Florida and used them to divide the section into five units, numbered Q1 (oldest) to Q5 (youngest). As mapped regionally by Perkins (1977), the Q4 and Q5 units include both the Key Largo and Miami Limestones, and the Q1, Q2, and Q3 units include only the Key Largo (Fig. 5-5, inset). Coniglio and Harrison (1983a) found that the facies transition between the Key Largo and Miami Limestone at Big Pine Key occurs within the Q5 unit, and that the superposition of the Miami Limestone on the Key Largo Limestone over the rest of the island coincides with the Q5-on-Q4 contact.

Harrison and Coniglio (1985) also studied the Key Largo Limestone on the island of Key Largo (Fig. 5-6), its type locality in the Upper Keys (Fig. 5-1). They confirmed the presence of subaerial discontinuity surfaces and traced Perkins' (1977) three shallowest units, Q5, Q4 and Q3, among ten shallow borings on the island. They noted the presence of a quartz sandstone layer about 10 m below the surface just above the boundary between Q3 and Q4. Harrison and Coniglio (1985) demonstrated that a topographic high beneath Key Largo persisted through several sea-level highstands. Recent drilling off both sides of Key Largo island suggests that the Q5 portion of the Key Largo Limestone is an isolated ridge, with Q4 exposed at the surface on either side of the Key. The underlying Q4 ridge served as a focus for reef growth and is a partial explanation for the location of the modern Florida Keys (Fig. 5-3). Antecedent topography is generally accepted as a fundamental control of reef position (Tucker and Wright, 1990, p. 204) and is likely to have influenced several episodes of reef growth in South Florida during various Pleistocene sea-level highstands.

Diagenesis

The Key Largo Limestone and Miami Limestone have experienced a variety of alteration processes that are typical during early freshwater diagenesis of shallow-water marine carbonate sediments. The Keys have been exposed to subaerial diagenesis since they emerged from the sea about 125 ka (Hoffmeister and Multer, 1964). The highest elevations in the Keys are close to the estimated maximum sea level at that time, so exposure was practically coincident with sea-level lowering. Such exposure of the marine carbonates to meteoric weathering has produced widespread minor karstification (Dodd and Siemers, 1971). A peculiar and spectacular exception is a recently identified sinkhole seaward of Key Largo, 600 m in diameter and as much as 100 m deep, now filled with Holocene sediments (Shinn et al., 1996).

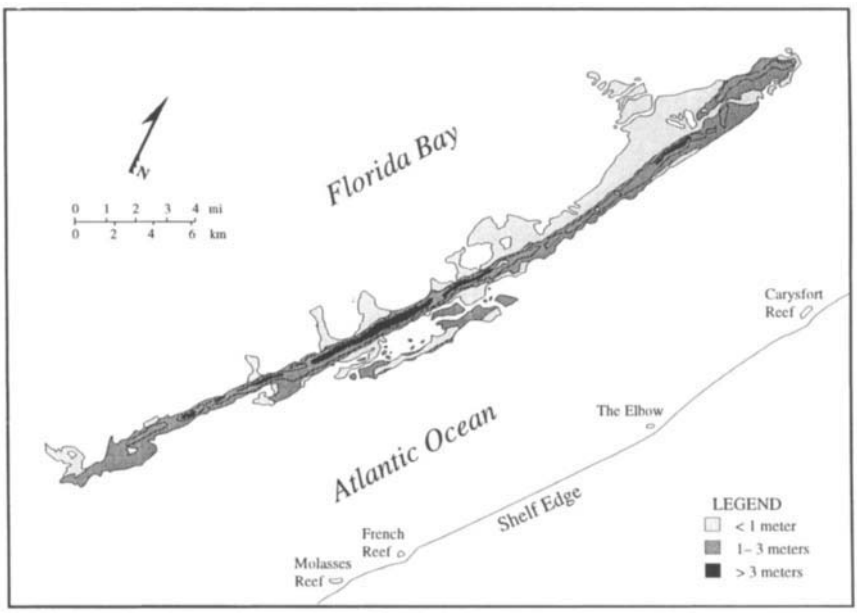


Fig. 5-6. Topographic map of Key Largo (after Harrison and Coniglio, 1985) showing positions of important coral reefs formed by living *Acropora palmata* at the shelf margin east of the island.

A more common weathering feature is a crust that coats the surface of much of the Keys and was established to have formed by subaerial exposure, as opposed to algal processes, by Multer and Hoffmeister (1968). These laminated crusts (calcretes) are typically reddish-brown and are best exposed along the margins of the islands, where they may be eroded and removed by marine bioerosional processes along the coast. Although originally described by Kornicker (1958) from the Bahamas, the crusts of the Keys are well known from the papers by Multer and Hoffmeister (1968), Kahle (1977), Perkins (1977), and Coniglio and Harrison (1983b) and have proved especially valuable in determining stratigraphy and past sea levels (Perkins, 1977). Robbin and Stipp (1979) and Robbin (1981) used ^{14}C ages of laminated crusts to calculate depositional rates of crusts and to infer sea-level change. By carefully sectioning and dating the tops of the crusts, they hoped to avoid contamination by old, radioactively dead carbon in the Key Largo Limestone. Interestingly, even though the Key Largo is believed to be more than 100 ky old, ^{14}C ages of the limestone generally fall between 20,000 and 30,000 y B.P. This indicates exchange or addition of some modern carbon with the original matrix of this rock.

Within the formations, diagenetic alteration is typical of what occurs when metastable marine carbonate minerals interact with meteoric pore fluids (Friedman, 1964; Land, 1967; Halley and Harris, 1979). Alteration processes include dissolution of aragonite, loss of magnesium from high-Mg calcite, precipitation of calcite cement, and the development of secondary porosity. In the upper portions of these formations, metastable minerals are still present (Q4 and Q5 units of Perkins, 1977).

In the older units, metastable minerals are absent, and diagenetic processes altering high-Mg calcite and aragonite to low-Mg calcite have gone to completion.

An important result of these diagenetic processes is that net porosity in these formations has changed little, although the mineralogy and permeability are radically altered compared to those of modern sedimentary analogs. Wholesale chemical and pore-distribution changes are affected during early freshwater diagenesis without massive pore-volume reduction (Halley and Schmoker, 1983; Halley and Evans, 1983). The result is a rock with high porosity and permeability — as is characteristic of most carbonate islands throughout Florida and the Bahamas.

Geochronology

Substage 5e. Radiometric age dating ($^{230}Th/^{234}U$) has been attempted several times using corals and oolite from the Q5 unit of Perkins (1977), and the results have been reviewed in detail by Muhs et al. (1992). The first attempts were by Broecker and Thurber (1965) and Osmond et al. (1965), early in the development of U-series methods. As noted by Muhs et al. (1992), the samples from those studies that were 95–100% aragonite gave ages of 90 ± 9 and 120 ± 10 ka for oolite from the Miami Limestone and a range of ages from 95 ± 9 to 145 ± 14 ka for coral from the Key Largo Limestone. The latter range is comparable to the spread of comparable-vintage (alpha-spectrometric) values from corals of the Rendezvous Hill Terrace of Barbados [q.v., Chap. 11] as reported by Ku et al. (1990) — the unit in the classic Barbados stratigraphy that is unarguably associated with isotope substage 5e.

Later, a coral from Windley Key quarry was used by Harmon et al. (1979) as part of the Uranium-Series Intercomparison Project. The mean age of the coral was 139 ka. As noted by Muhs et al. (1992), the sample contained only 90% aragonite; thus, the relatively large age might reflect some loss of U because of recrystallization. Finally, Muhs et al. (1992) added an alpha-spectrometric result of their own: 144 ± 8 ka for a coral taken from a drill core on Key Largo island. According to Muhs et al. (1992), this coral, like the others before it, did not meet all the criteria that assure a closed system.

Without question, the Q5 unit of the Florida Keys formed during the interval of high sea levels associated with the last interglacial. As Muhs et al. (1992) note, however, the uncertainty in the ages prevents precise correlation of the oolitic shoals of the Miami Limestone with the Key Largo reefs and determination of how, exactly, these deposits fit with the ~125-ka peak of the deep-sea oxygen-isotope curve (substage 5e). Muhs et al. (1992) list three alternatives: (1) the Key Largo reefs possibly formed in an early peak, and the Miami oolite in a slightly later one; (2) the two may be correlative over a relatively long interval of high sea level; (3) perhaps the whole question in the Keys should await re-examination using mass-spectrometric methods and better samples (if they can be found).

Younger rocks. Lidz et al. (1991) have identified a series of reef ridges a few hundred meters seaward of the modern, shelf-edge reefs in the Lower Keys. These

fossil features, termed outlier reefs, are 10–20 km long, up to 30 m high, and < 1 km wide. They crest at water depths of 12–30 m and are covered with thin Holocene coral rubble. Two cores from the ridges indicate that the veneer is less than 1 m thick and that it overlies a variety of massive corals in growth position, among which *Montastrea annularis* is the most common. Mass-spectrometric U-series dating of corals (Ludwig et al., 1996) indicate this reef grew at about 80 ka and is correlative with oxygen isotope stage 5a. These outlier reefs may be more similar to the Key Largo Limestone in composition and geometry than to any living reef.

Older rocks. Pre-stage-5 geochronology is more tenuous. A pre-stage-5 Quaternary section is certainly present in the subsurface, as indicated by the subaerial discontinuity surfaces and the stratigraphy proposed by Perkins (1977). There is a single radiometric date (Szabo and Halley, 1988; Muhs et al., 1992) from the core on Key Largo, where the 144-ka Q5 coral was obtained. According to Muhs et al. (1992), this older coral was the only aragonitic coral recovered from the Q4 unit in the drilling reported by Harrison and Coniglio (1985), and it gave an age of 361 + 120/−60 ka. Muhs et al. (1992) also noted that addition of ^{234}U was indicated, and thus the age must be considered a minimum. This result from the Keys, together with results from corals regionally distributed in southern peninsular Florida, led Muhs et al. (1992) to conclude that there was extensive deposition of marine sediment during the middle Pleistocene. They found no evidence, however, that any of their middle Pleistocene samples were as young as isotope stage 7 (ca. 200 ka).

The early work of Mitterer (1974, 1975), using amino-acid racemization (AAR) geochronology, is also relevant to the interpreted age of the Q units of Perkins (1977). D-alloisoleucine/L-isoleucine (or A/I) ratios on *Mercenaria* at a variety of South Florida localities defined three groups that Mitterer (1975) and Perkins (1977) correlated with the Q5, Q4, and Q3 units. Using the U-series age and A/I ratio for Q5 as a calibration point, Mitterer (1975) obtained the following ages: 170-191 ka for Q4, and 212–223 ka for the Q3. More recently, Mitterer has developed a new calculation technique for estimating ages from A/I ratios (parabolic kinetics; Mitterer and Kriausakul, 1989) and applied it to Bermuda (Hearty et al., 1989). Vacher used the new technique to recalculate ages from Mitterer's South Florida ratios and obtained the following results for units below the Q5 calibration horizon (Vacher et al., 1992): 184–216 ka for Q4, and 245 to >260 ka for Q3. These results are comparable to those in Bermuda [q.v., Chap. 2] for the Belmont Formation and the upper member of the Town Hill Formation, respectively, which are correlated by Hearty et al. (1992) with isotope stages 7 and 9, respectively.

The coral data, which do not reveal the presence of stage 7, and AAR data are not necessarily contradictory because these Pleistocene units can be extremely discontinuous. The stage-7 Belmont Formation in Bermuda is small and patchily distributed, in contrast to deposits in Bermuda of stage 5 and those interpreted as stage 9. In South Florida, Holocene carbonate deposits are not continuous, and large areas of Pleistocene "bedrock" are exposed offshore on both sides of the Keys (Enos, 1977). If stage-7 deposits are present in the Keys, they may well be missing in many drill cores. If five Q units occur in one drill core, and five Q units occur in another,

then it may be too much to expect that the two sets correlate unit-to-unit. The possibility that the older Pleistocene units of the Keys are discontinuous illustrates the difficulty of resolving the stratigraphy in detail.

HOLOCENE GEOLOGY

The many studies of carbonate depositional environments in the general vicinity of the Florida Keys are clearly beyond the scope of this chapter. Three aspects of the Holocene geology, however, form classic elements of the geologic story of the islands themselves: (1) Holocene sea-level history; (2) formation of modern dolomite at Sugarloaf Key; and (3) how the presence of the Keys has affected the Holocene buildup of reefs. The first two are discussed below and the third is the subject of the Case Study.

Florida Keys Sea-Level Curve

The Florida Keys are in the geographic region where curves of relative sea level during the late Holocene can be expected to show a history of continual submergence up to the present day (Zone III of Clark et al., 1978, and Peltier et al., 1978). The observed curve is that of Robbin (1984), and it is in general agreement with both the modeling by Clark et al. (1978) and the well-known curve of South Florida derived from the mangrove coast of southwestern Florida by Scholl and Stuiver (1968). Robbin's (1984) curve was based on ^{14}C dates from soilstones and mangrove peat obtained by underwater drilling at six localities in the Upper Keys. The peat samples were obtained mostly by horizontal "push coring" into "walls of peat" exposed along the edges of channels cut through mangrove islands. The resultant sea-level curve shows a rise of 0.12 cm y^{-1} from about 7.0 m at 7 ka to about 0.75 m at 2 ka, followed by a rise of 0.03 cm y^{-1} from 2 ka to the present. The curve plots slightly below the curve of Scholl and Stuiver (1968), in which sea level was at about 1.6 m at 3.5 ka and 0.5 m at 1.7 ka. In neither case is there any indication of an emergence during the Holocene history.

Wanless (1982) called attention to the fact that tidal records from 1932 indicate that relative sea level has been rising at Key West at a rate of 0.23 cm y^{-1}. Recently the Key West record has been examined in detail by Maul and Martin (1993). With newly discovered data going back to 1846, Maul and Martin (1993) report a 30-cm rise in the nearly 150-year period. For the period 1851 to 1987, the linear trend was 0.22 ± 0.05 cm y^{-1}. Breaking this submergence into its geodetic and oceanographic components, Maul and Martin (1993) used the model of Peltier (1986) to infer that about 1/3 of the rise (0.08 cm y^{-1}) was due to global isostatic adjustment to deglaciation. The remainder, they concluded, could be explained by a trend during the same period of dynamic height anomaly of the upper 1,000 m of the adjacent water column.

Lidz and Shinn (1991) reconstructed the paleogeography of the general vicinity of the Keys to illustrate how the platform was flooded, reef growth was displaced

shoreward, and the region of the Keys was progressively drowned and separated. According to those authors, if sea level continued to rise at its present rate (0.38 cm y^{-1}), most of the Keys would be flooded in 260 years (+1 m), and all but a few islands would disappear in 520 years (+2 m).

Holocene Dolomite

One particularly interesting aspect of diagenesis in the Florida Keys was the early identification of Holocene dolomite (Shinn, 1964). This mineral, common in ancient carbonate rocks, was known to be forming in only one other Holocene setting at the time of its identification in South Florida. Dolomite from Holocene mud in Florida Bay was initially thought to be authigenic (Taft, 1961), but the absence of ^{14}C activity and other characteristics demonstrated its detrital origin (Deffeyes and Martin, 1962). The dolomite identified by Shinn (1964) is lithologically distinct and demonstrably Holocene by ^{14}C dating. It occurs disseminated in cemented crusts of the supratidal zone of Sugarloaf Key, and its discovery became a key to recognizing analogous supratidal environments in ancient carbonate rocks. Carballo et al. (1987) have emphasized the importance of tidal pumping of sea water through these sediments to produce the dolomite.

HYDROGEOLOGY

Hydrogeologically, the Florida Keys fall into two natural groups defined by the distribution of their principal geologic units. The first group consists of the narrow and elongate Upper Keys comprised of the Key Largo Limestone. Groundwater is at best brackish in these islands and has not been studied. The second group consists of the Lower Keys, which are relatively large and comprised of the Miami Limestone. Small freshwater to slightly brackish lenses occur on the largest of these islands. Lenses on Key West and Big Pine Key have been the subject of published water-resources studies by the U.S. Geological Survey.

Key West

Key West, which includes the southernmost point of land in the continental United States, is a popular tourist destination. According to the report on the water resources of Key West by Mackenzie (1990), the permanent population is about 28,000 and there are an additional 1.5 million tourists per year on the island that now measures 6 km by 1.5 km. The size and shape of the island have been altered considerably (Fig. 5-7A,B). The western, unreclaimed part is completely urban; this is the famous "Old Town," which has been home to such personages as John James Audubon, Ernest Hemingway, Tennessee Williams, and Jimmy Buffett.

Mackenzie (1990) mapped the freshwater lens on Key West. The mapping was based on two techniques. The first was fluid-conductivity profiles at 12 wells that

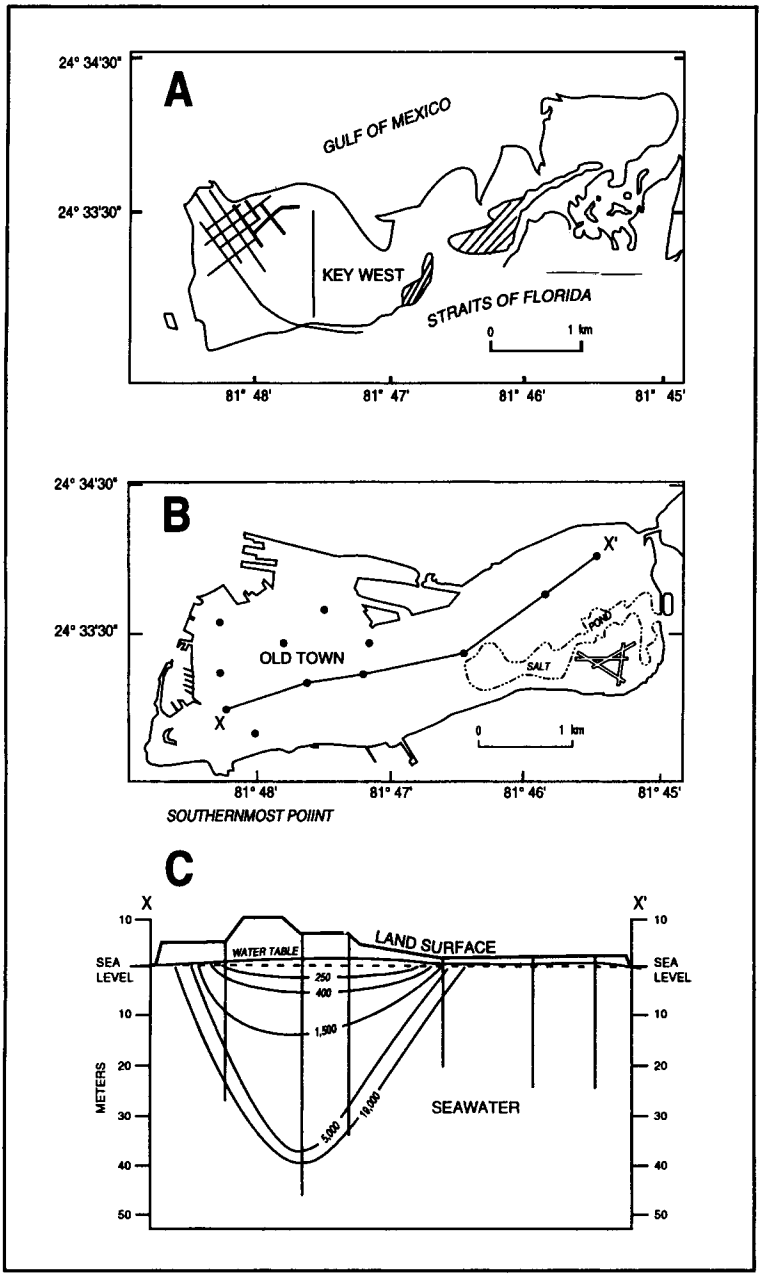


Fig. 5-7. Freshwater lens at Key West. (A) Map showing Key West in 1850. (B) Map showing Key West in 1988. Dots indicate observation wells of Mackenzie (1990). (C) Cross section showing Cl^- concentration (mg L^{-1}), October 1986, from well data. Line of cross section shown in B. (D) Map showing distribution of Cl^- concentration (mg L^{-1}), October 1986 (wet season), at depth of 1.3 m below water table. (E) Map showing distribution of Cl^- concentration (mg L^{-1}), April 1987 (dry season), at depth of 1.3 m below water table. (F) Map showing variation of resistivity (ohm-m), November 1986, from survey with EM-16R VLF meter. (Adapted from Mackenzie, 1990.)

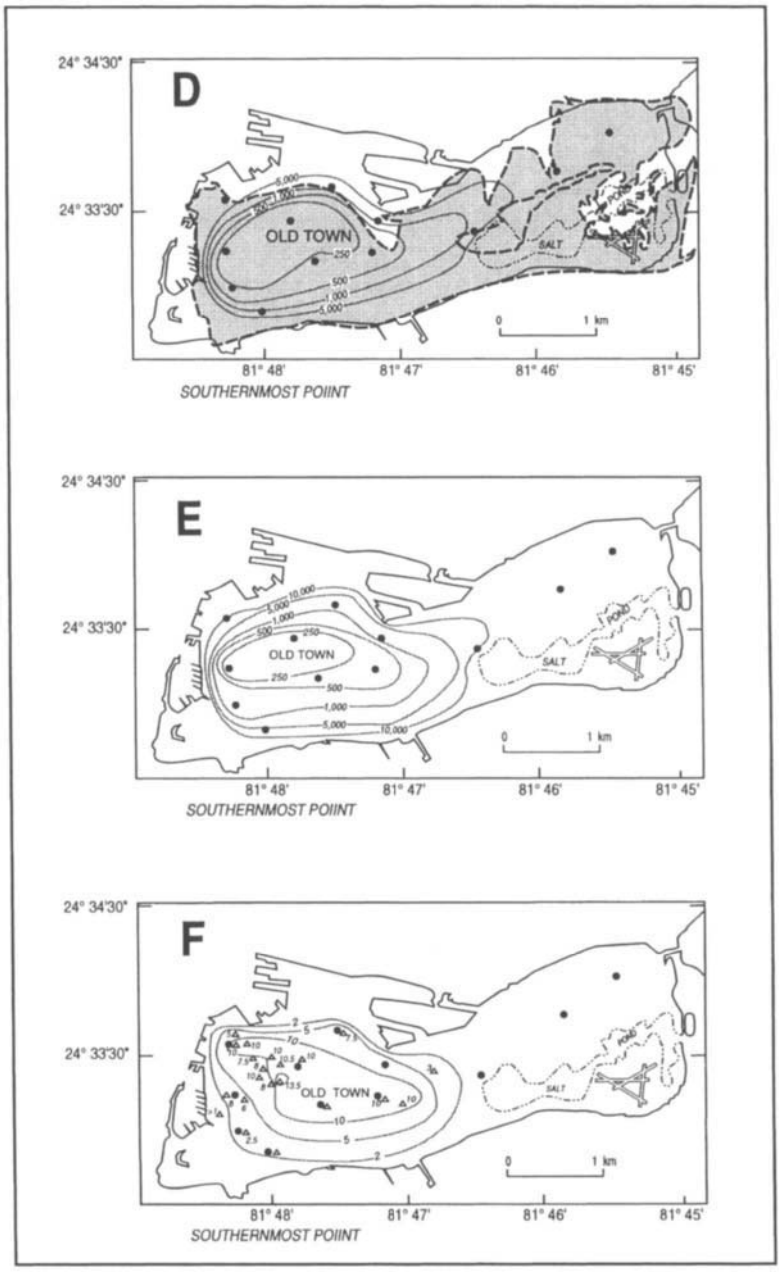

D
24° 34'30"
24° 33'30"
OLD TOWN
SALT
0
1 km
81° 48'
81° 47'
81° 46'
81° 45'
SOUTHERNMOST POIINT
E
24° 34'30"
24° 33'30"
OLD TOWN
SALT
0
1 km
81° 48'
81° 47'
81° 46'
81° 45'
SOUTHERNMOST POIINT
F
24° 34'30"
24° 33'30"
OLD TOWN
SALT
0
1 km
81° 48'
81° 47'
81° 46'
81° 45'
SOUTHERNMOST POIINT

Fig. 5-7D,E,F.

were drilled through the freshwater column and transition zone; the fluid conductivity was calibrated to Cl^- using local waters. The second was a surface geophysical survey using the EM-16R VLF, a resistivity instrument capable of operating in an area with electrical interferences such as magnetic fences and overhead electrical wires. As shown in Fig. 5-7, the mapping by the downhole conductivity probes (Fig. 5-7C,D,E) and the surface geophysics (Fig. 5-7F) agree: both locate the freshwater lens in Old Town.

According to the downhole conductivity profiles, the thickness of the freshwater lens (<250 mg L^{-1} Cl^-) is small, averaging little more than 1 m at its center, which is below Old Town (Mackenzie, 1990). The transition zone, which thickens inland, is large relative to the freshwater column (Fig. 5-7C); for example, the interval of very slightly saline water (250–400 mg L^{-1} Cl^-, classification of Mackenzie, 1990) is typically twice the thickness of freshwater. The depth to seawater Cl^- values is about 12 m (40 ft) in the center of the island (Mackenzie, 1990). According to the profiles in the report, the downhole variation in salinity is not that of a symmetric error function. As pointed out by Mackenzie (1990), the salinity profile is affected by tides, with the freshwater column in an observation well tending to be larger at low tide than at high tide. The vertical movement of isochlors in the well is larger in the upper part of the transition zone than in the lower part.

Mackenzie (1990) calculated the volume of freshwater in the lens from the conductivity profiles by producing slice maps of the lens at intervals of 0.6 m (2 ft) down to the base of the freshwater. Examples of slice maps (at depth 1.2 m) are shown in Figures 5.7D and E, for the end of the rainy season (October) and the end of the dry season (April), respectively. Mackenzie's result, which assumed a porosity of 0.2, was a volume of 110×10^3 m^3 (30 Mgal, U.S.) at the end of the rainy season and 75×10^3 m^3 (20 Mgal, U.S.) at the end of the dry season. From this result (10 Mgal y^{-1} recharge in a lens averaging 25 Mgal storage), it would appear that the residence time of freshwater in the freshwater lens is less than 2.5 years.

According to Mackenzie (1990), the water table fluctuates with the tide in all the observation wells, and the tidal range decreases inland. Recharge events could not be read from the hydrographs, except for the most extreme rainfalls. This is due partly to the extreme variability in rainfall over short distances in South Florida. For example, at a well near the center of the lens, the water table responded to rainfalls of 16.9 cm and 13.4 cm with rises of 17.8 and 21.6 cm, respectively. There was no noticeable effect of other major rainfalls that ranged from 3.7 to 8.8 cm. The rapid decay of the two rises (1 and 4 h, respectively) attests to the high permeability of the oolite. Coastal wells showed smaller or no response to the same rainfalls.

Big Pine Key

Big Pine Key, about 40 km east of Key West, is the largest and easternmost of the Lower Keys. The northern half of the island is located within the Key Deer National Wildlife Refuge and is uninhabited by people; the rest of the island is suburban residential zoning. According to the water-resources study of the island by Hanson

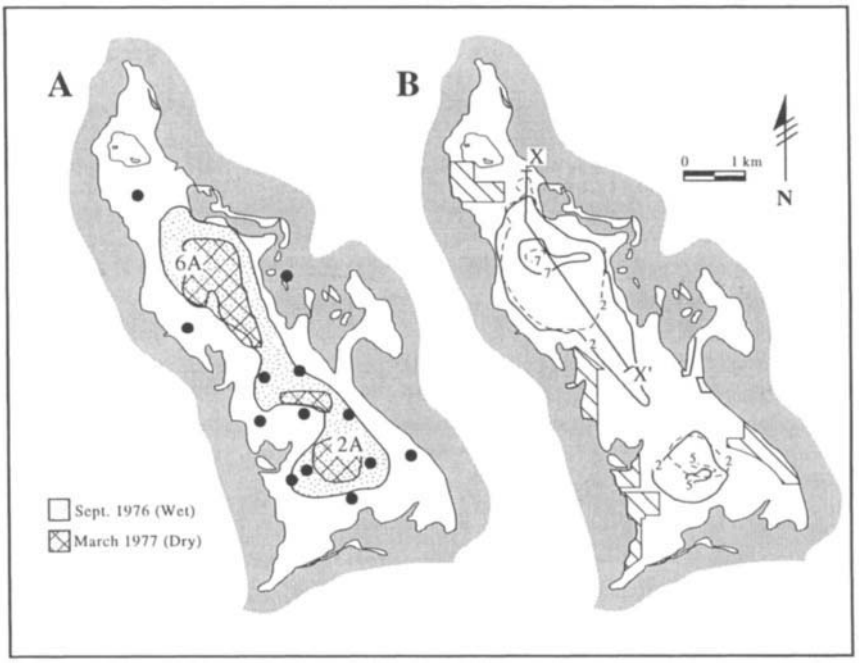


Fig. 5-8. Maps showing seasonal variation in freshwater lens at Big Pine Key. (A) Boundary of lens defined by the contour of 500 mg L^{-1} Cl^- at 1.5-m depth below water table as mapped by Hanson (1980) from wells (indicated as dots). Stippled area shows limit of freshwater lens in September 1976 (wet season); cross-hatched area shows limit of freshwater lens in March 1977 (dry season). (Adapted from Vacher et al., 1992, after Coniglio and Harrison, 1983.) (B) Location of freshwater-saltwater interface at selected depths (2, 5, and 7 m) below water table as defined by electromagnetic profiling (Wightman, 1990). Dashed line indicates limit in March 1987 (dry season); solid line indicates limit in August 1987 (wet season). Cross-hatching in B indicates areas of finger canals, which clearly limit lens area. (Adapted from Vacher et al., 1992.)

(1980), the permanent population is about 800; with the tourists, the population swells to about 2,000 during the winter, which is the dry season.

Hanson (1980) mapped the freshwater lenses in Big Pine Key (Fig. 5-8A) by monitoring the downhole variation in salinity at monthly intervals (6/76 to 4/77) at 22 shallow observation wells. These wells included the core holes of the stratigraphic study by Coniglio and Harrison (1983a). The results, which were presented in terms of slice maps of the same type as shown in Fig. 5-7 for Key West, indicated a considerable lateral expansion and contraction of the lens in response to the seasonal recharge. The maximum thickness of the freshwater column, however, remained fixed, at about 5 m.

Wightman (1990; Vacher et al., 1992) mapped the thickness of the freshwater column during March and August 1987 by electromagnetic profiling. The surveys measured ground conductivity at 20-m intervals along roadside transects. The ground-conductivity readings were converted to values of freshwater thickness by

use of a three-layer model with known (assumed) conductivity and thickness of the unsaturated zone (ground elevation), fluid conductivity of the freshwater, and fluid conductivity and thickness (infinite) of the saltwater (Stewart, 1988, 1990). The freshwater thickness thus calculated gives the depth to a freshwater-saltwater "interface" which empirically falls in the upper part of the transition zone, commonly in the range of 2,000–4,000 mg L^{-1}. The results (Fig. 5-8B) correlate well with those of Hanson (1980). They also confirm the considerable lateral, but limited vertical, expansion and contraction of the lens with the seasonal recharge.

As noted in the discussion of stratigraphy, Coniglio and Harrison (1983a) found that the Miami/Key Largo Limestone contact, which extends across Big Pine Key, corresponds to the contact between the Q5 and older Q units of the Perkins' (1977) classification. The mapping of lenses on Big Pine Key shows that this contact corresponds to a major boundary in hydraulic conductivity as well. According to the fluid-conductivity profiles of Hanson (1980), the top of the transition zone starts at or just below the geological contact (Fig. 5-9A). According to the electromagnetic profiling of Wightman (1990), the depth of the "EM interface" is limited by the location of the geological contact (Fig. 5-9B). In effect, Big Pine Key is a "dual-aquifer carbonate island" [see Chap. 1], a variation of a theme exemplified by many atoll islands, where the base of the lens is refracted or truncated at the Holocene/Pleistocene contact; in Big Pine Key, the truncation occurs at the contact between the late and middle Pleistocene limestones.

Wightman (1990) evaluated the contrast in hydraulic conductivity by fitting a two-layer analytical model using the assumptions of Dupuit-Ghyben-Herzberg

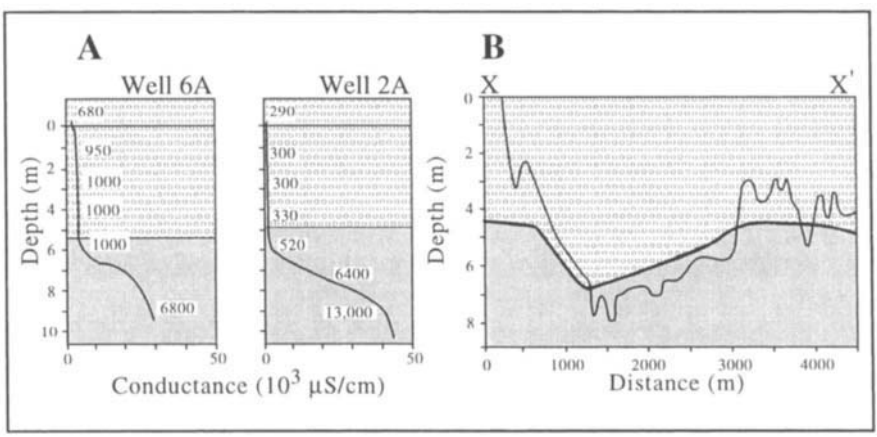


Fig. 5-9. Correlation of base of freshwater lens and the Miami/Key Largo contact. (A) Graphs of conductance vs. depth at two wells superimposed on stratigraphic section. Locations of wells shown in Fig. 5-8A. Numbers on curves indicate Cl^- in mg L^{-1}. Note how the sigmoid of the transition zone appears to be "hung" from the lithologic boundary. (B) Cross section showing position of freshwater-saltwater interface defined by electromagnetic profiling (irregular line). Depth to contact between the Miami and Key Largo Formations (stippled and shaded, respectively) is from Hanson (1980). Location of cross section is shown in Figure 5.8B. (From Vacher et al., 1992.)

(DGH) analysis (Vacher, 1988) [Chap. 1]. The model assumed a circular island and was fit to the observed configuration of the "EM interface" along a transect of the northern lens, where it is most like a circle. The result indicates a 12-fold contrast in hydraulic conductivity, with R/K1 and R/K2 being 2×10^{-3} and 1.7×10^{-4}, respectively (R is recharge, and K1 and K2 are hydraulic conductivity of the Miami and Key Largo Limestones, respectively). R was estimated at 0.24 m y^{-1} (20% of the rainfall) by the chloride-ratio technique (Vacher and Ayers, 1980) using the Cl^- of rainfall and freshest groundwater in the lens. Therefore, the hydraulic conductivities are estimated to be about 1,400 m day^{-1} for the underlying middle Pleistocene Key Largo Formation and 120 m day^{-1} for the late Pleistocene Miami Limestone. These values are very similar to those of the middle and late Pleistocene aquifers in Bermuda [q.v., Chap. 2].

Wightman (1990) went on to model the interface in a two-layer island shaped like Big Pine Key in order to assess the variation in freshwater residence time within the Key. The model was a steady-state, finite-difference DGH model like that of Fetter (1972) and used the values of R, K1, and K2 from the circle fit. The results for the depth to the interface are shown in Fig. 5-10. The interface contours were used to define streamlines (in map view; Fig. 5-10A) that divide the lens into curving wedges extending downward to the interface. These wedges were divided into streamtubes (in vertical section; Fig. 5-10C) by apportioning the discharge along vertical intercepts, while taking into account the changing widths and different hydraulic conductivities (Vacher et al., 1992). Incremental travel times along the streamlines then were calculated and summed to give the residence time of a parcel of water that entered at particular points as seen on the map. The result (Fig. 5-10B) shows how long (in years) it takes a parcel of water to flow out of the lens after entering at the water table in the interior of the island. The residence time of individual parcels varies up to 8 years. The streamtube construction also calls attention to the funneling of discharge through the upper part of the buried K2 layer (Vacher et al., 1992).

While Wightman (1990) mapped the regional configuration of the lens in Big Pine Key, Beaudoin (1990), using the same surface-geophysical instruments, focused on the periphery. The specific object of Beaudoin's study was on the finger canals, which are a common feature in the Keys. The purpose of the canals is to provide boat access for residences inland of the shoreline. According to Beaudoin (1990), approximately 10.5 km of canals are dredged to depths of 2.5–6 m into Big Pine Key. Most of the canals are in the northern half of the island. The effect on the lens is clearly shown in Fig. 5-11: the canals act as a lateral boundary for the lens and focus the discharge there.

WATER RESOURCES

In general, water resources in the Florida Keys are insufficient for the human population of the area. Studies by Parker et al. (1955) and Klein (1970) indicate that most Keys have only ephemeral freshwater lenses and cannot be relied on for perennial supplies of potable water. Only the largest of the Lower Keys, Big Pine and

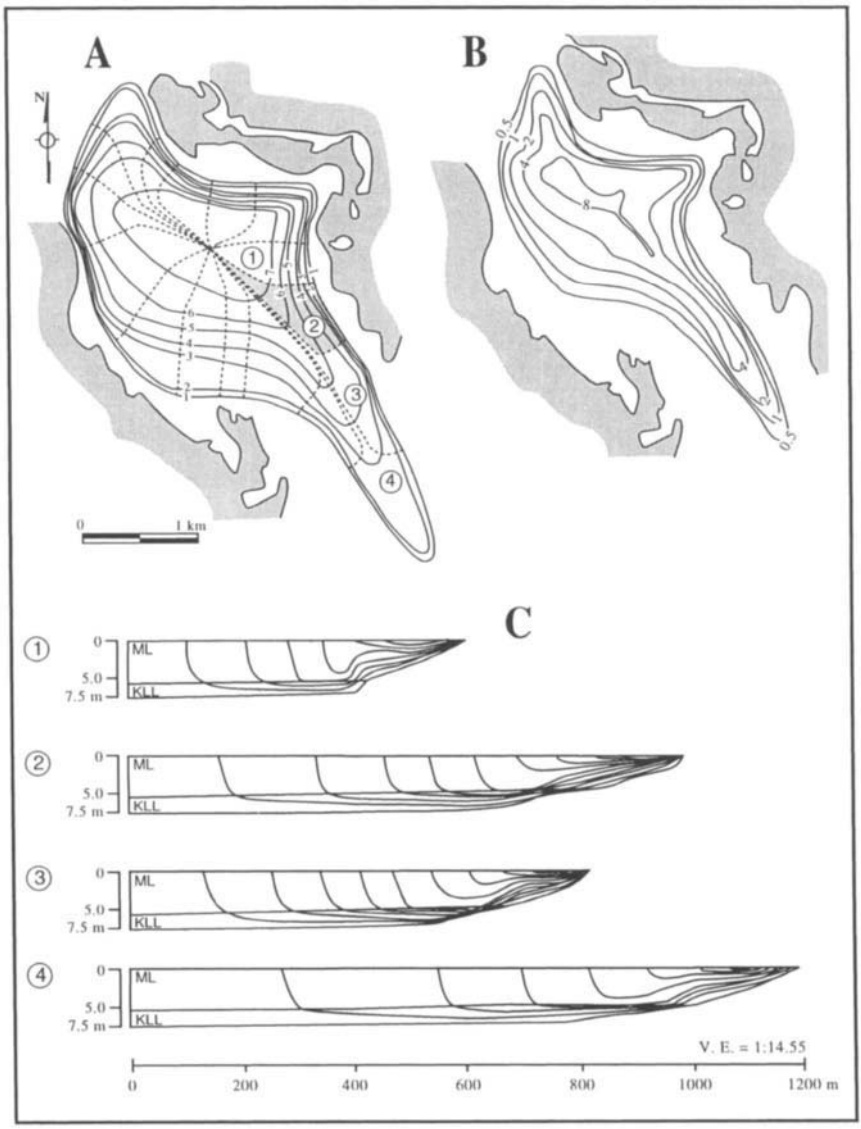


Fig. 5-10. DGH modeling of Big Pine Key (Wightman, 1990). (A) Map showing thickness of freshwater lens (in meters) as produced by finite-difference, two-layer model. Dotted transects are streamlines defined as normals to the thickness contours. These streamlines delimit 17 streamwedges. (B) Map showing contours of exit time in years (geometric scale), the time for groundwater to travel from a given point at the water table to the shoreline. Values were determined from streamlines of A and DGH potentials. (C) Cross sections of four of the 17 streamwedges (numbered in A). Each streamwedge is divided into ten equal-discharge streamtubes. Note the funneling of discharge in the upper Key Largo Limestone (KLL), below the Miami Limestone (ML).

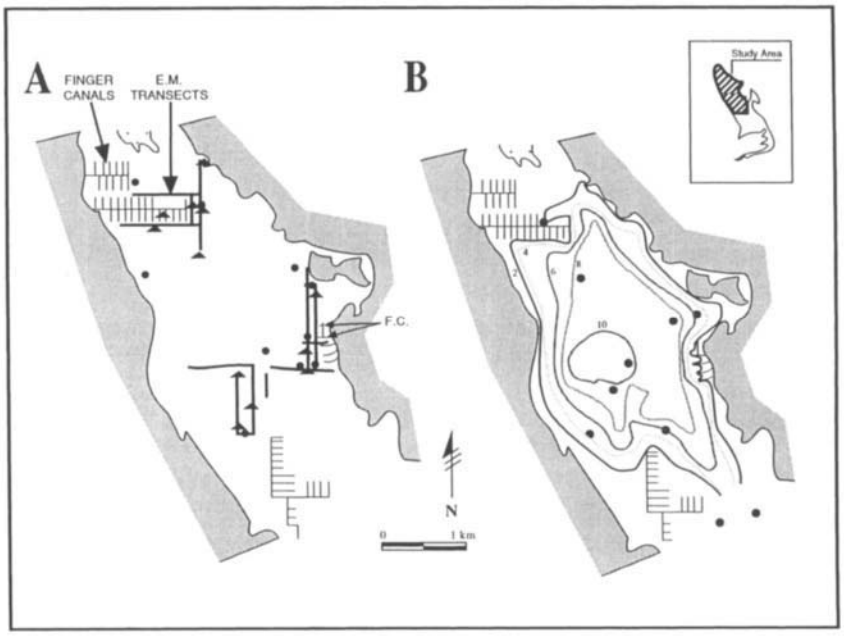


Fig. 5-11. Surface geophysical surveys of northern Big Pine Key (1988–1989). (A) Location of data control and network of finger canals (FC). Heavy lines indicate transects with EM-34; dots and triangles show location of vertical electrical soundings conducted with DC resistivity in May, 1988, and March, 1989, respectively. (B) Contours show interpreted depth (in meters) of freshwater-saltwater interface from the geophysical data. Dots show location of control wells from Hanson (1980). (Adapted from Beaudoin, 1990.)

Key West for example, have permanent freshwater lenses. Even the large Upper Keys, Elliott Key for example (Klein, 1970), do not have permanent lenses, even though rainfall increases northward. The Lower Keys are more likely to have lenses because of their geometry and geology. These Keys, in plan view (Fig. 5-4), retain the broad flat of an ooid shoal in contrast to the Upper Keys which are narrow and elongate parallel to the shelf. In addition, the surficial lithologic unit of the Lower Keys (oolite) is less transmissive than that of the Upper Keys (reef).

Although some groundwater is used for irrigation (on Big Pine Key), and some potable water is provided by cisterns and reverse-osmosis facilities, more than 95% of water for domestic use is now provided by the Florida Keys Aqueduct Authority via pipeline from a wellfield on the mainland. Currently about 57,000 m^3 day^{-1} (15 Mgal day^{-1}, U.S.) are pumped to the Florida Keys (NOAA, 1995). The volume of this flow for two days is comparable to the volume of the freshwater lens beneath Key West during the wet season, as estimated by Mackenzie (1990).

The majority of water pumped to the Keys is for domestic use. Key West and Key Colony Beach (Marathon) have sewage-treatment facilities and ocean outfalls. Much of the remaining freshwater is disposed of as sewage through septic tanks and shallow wells (10–30 m) beneath the islands. The sewage is rich in nutrients, pro-

viding a potential environmental problem in this region of oligotropic waters. The ultimate fate of the sewage beneath the islands is a topic of continuing study (Shinn et al., 1994). Based on water usage and disposal methods, it is clear that freshwater piped to the Florida Keys can be a significant contribution to small and ephemeral lenses of these islands.

CASE STUDY: INTERPLAY OF CARBONATE ISLANDS, CORAL REEFS, AND SEA LEVEL

The most significant reef growth along the Florida reef tract is seaward of the largest Keys. Reefs are generally absent opposite channels between islands. In an 1851 report to the Superintendent of the Coast Survey, Louis Agassiz described the relation between reefs and Keys as follows (Agassiz, 1880, p. 5):

> "Though continuous, the outer reef is, however, not so uniform as not to present many broad passages over its crest, dividing it, as it were, into many submarine elongated hillocks, similar in form to the main keys, but not rising above the water, and in which the depressions alluded to correspond to the channels intersecting the keys."

More than a century later, Newell and Rigby (1957) observed a similar relation between channels in Andros Island, Bahamas, and the barrier reef along that island's east side. Newell and Rigby (1957) surmised that the distribution of reefs east of Andros might be due, in part, to the eastward flow of bank water unfavorable to coral growth.

Ginsburg and Shinn (1964, 1994) noted that the relation between islands, channels and reefs in the Florida Keys and Bahamas suggests that reefs grow best where they are protected from extremely shallow bay waters. Reefs are absent in Florida Bay because the water is too cold in the winter, too hot in the summer, and too variable in salinity to support reef-building coral growth (Holmquist et al., 1989; Robblee et al., 1989). Similarly, reef growth is limited where bay water passes between the Keys to the shelf (Shinn et al., 1989; Ginsburg and Shinn, 1994).

During a rising sea level, circulation between shelves and coastal bays increases on low-relief carbonate platforms. As water depths increase and larger areas of the platforms are flooded, the volume of the tidal wedge increases. On platform tops, waters may become increasingly warm, saline, or, in the case of the Bahamian platforms, cold in the winter (Roberts et al., 1982). Reefs that become established along the margins of platforms may thrive for thousands of years until the platform is flooded. Healthy reefs may grow rapidly enough to keep up with all but the largest rates of sea-level rise (Schlager, 1981). Eventually, flooded lagoons or platforms develop water conditions that limit coral growth. After thousands of years of sea-level rise, shelf-margin reefs may be "shot in the back" (Neumann and McIntyre, 1985, p. 107) by their own bays and lagoons as circulation increases between the platform interior and shelf edge. Thus harmful platform and lagoon waters may be an important factor in terminating reef growth on time scales of thousands of years.

Today, sea level continues to rise in the Florida Keys. The measured rise at Key West has been almost 30 cm since 1850 (Maul and Martin, 1993). Although the

impact of this sea-level rise is not fully understood, it is thought that an increase of 30 cm would have been sufficient to change the circulation dynamics of Florida Bay significantly. Florida Bay, on average, is about 1.5 m deep now, so the historical rise represents a 25% increase in bay depth and, presumably, would have resulted in a significant increase in tidal exchange between the bay and reef tract. However, water depth is also affected by sedimentation rates in the bay. For much of the bay, sedimentation rates are undetermined. The detailed relation between the current sea-level rise and reef health will require more study before the concept that reefs are "shot in the back" by their own lagoons can be applied predictively to the Florida reef tract and Florida Bay.

Continued sea-level rise will diminish the size of the Keys and their freshwater to brackish lenses, eventually eliminating both. Lidz and Shinn (1991), projecting the rise of the recent geologic past, have forecast how rising sea level might flood the islands in the future. A rise of a little more than 5 m would completely drown the Keys. Other factors such as global temperature change and disease might affect reef health, but the long-term fate of Florida's *Acropora palmata* coral reefs is toward continued decline if sea level continues to rise and the protective islands are diminished.

The Florida Keys provide evidence that the long-term relation between sea-level rise and declining reef health is not continuous. When sea level is 5–6 m above its present position, reef growth will probably start anew on the hard surfaces of the drowned Keys, initiating the next episode of reef growth, such as that observed in the late Pleistocene sequence. At that time, as in the past, the Florida shoreline will have transgressed 200 km to the north, the Florida Current may meander much farther onto the shelf, and the passage of severe winter cold fronts may be less frequent. At this future time, reef growth may change style, but a healthy, if faunally distinct, reef may flourish again on the Florida Keys.

CONCLUDING REMARKS

The Florida Keys are now recognized as one of the great recreational and environmental resources of the United States. The islands are outposts of a laid-back, tropical resort culture that has as its foundation warmth and clear water. A significant part of the attraction is fishing, diving, and boating around the area's coral reefs, which the islands protect. But the reefs were not always so highly valued.

From the sixteenth to the early nineteenth century, the islands were a desolate place. Most of those who lived in the Florida Keys survived on the misfortune of others. The islands were home to pirates and "wreckers." The latter made their living from salvaging shipwrecks, and some islanders were not above moving lights to lure ships onto the reefs at night. The toll on shipping was so great that by the mid-1800s, Louis Agassiz was sent by the Coast Survey to determine "whether the growth of coral reefs can be prevented, or the result remedied, which are so unfavorable to the safety of navigation" (Agassiz, 1880, p. 39). If it had been possible, the U.S. Government might have terminated reef growth in the Keys during the last century!

After careful study, Agassiz replied that the reef would continue to grow and that "the sooner a system of lighthouses and signals is established along the whole reef, the better" (Agassiz, 1881, p. 40). Thus the Federal government began an ambitious period of lighthouse building in the Keys that lasted from 1852 until 1886. Ironically, a few years ago the major shipping lanes in the Straits of Florida were moved away (seaward) from the Florida Keys — not for the protection of shipping, but for the protection of the reefs.

It is now widely recognized that coral cover is decreasing on many reefs off the Florida Keys (NOAA, 1995). The cause is generally believed to be direct and indirect human impacts, particularly those associated with water quality. The great increase in development on the Florida Keys is most often cited as the source of decreased water quality in the region, although the detailed mechanisms for reef decline are not yet established. The Florida Keys that have protected the reefs for millennia, may now be the source of the agents which will accomplish what Agassiz thought was beyond man's power a century ago.

REFERENCES

Agassiz, A., 1896. The elevated reef of Florida. Bull. Mus. Comp. Zool., Harvard, 28 (2): 1–62.

Agassiz, Louis, 1880. Report on the Florida Reefs. Mem. Mus. Comp. Zool., Harvard, 7: 1–61.

Beaudoin, C.M., 1990. Effects of dredge and fill canals on fresh-water resources of a small oceanic island, Big Pine Key, Florida. M.S. Thesis, Univ. South Florida, Tampa FL, 97 pp.

Broecker, W.S. and Thurber, D.L., 1965. Uranium-series dating of corals and oolites from Bahaman and Florida Keys limestones. Science, 149: 58–60.

Carballo, J.D., Land, L.S. and Miser, D.E., 1987. Holocene dolomitization of supratidal sediments by active tidal pumping. J. Sediment. Petrol., 57: 153–165.

Clark, J.A., Farrell, W.E. and Peltier, W.R., 1978. Global changes and postglacial sea level: A numerical calculation. Quat. Res., 9: 265–287.

Coniglio, M. and Harrison, R.S., 1983a. Facies and diagenesis of Late Pleistocene carbonates from Big Pine Key, Florida. Bull. Can. Petrol. Geol., 31: 135–147.

Coniglio, M. and Harrison, R.S., 1983b. Holocene and Pleistocene caliche from Big Pine Key, Florida. Bull. Can. Petrol. Geol., 31: 3–13.

Craighead, F.C., Sr., 1971. The Trees of South Florida, v. 1, The natural environments and their succession. Univ. Miami Press, Coral Gables FL, 212 pp.

Culotta, Elizabeth, 1995. Bringing back the Everglades. Science, 268: 1688–1690.

Deffeyes, K.S. and Martin, E.L., 1962. Absence of carbon-14 activity in dolomite from Florida Bay. Science, 136: 782.

Dodd, J.R. and Siemers, C.T., 1971. Effect of Late Pleistocene karst topography on Holocene sedimentation and biota, Lower Florida Keys. Geol. Soc. Am. Bull., 82: 211–218.

Dodd, J.R., Hattin, D.E. and Leibe, R.M., 1973. Possible living analog of the Pleistocene Key Largo reefs of Florida. Geol. Soc. Am. Bull. 84: 3995–4000.

Dunham, R.J., 1962. Classification of carbonate rocks according to depositional texture. In: W.D. Ham (Editor), Classification of Carbonate Rocks, A Symposium. Am. Assoc. Petrol. Geol. Mem., 1: 108–121.

Enos, P., 1977. Quaternary sedimentation in south Florida. In: P. Enos and R.D. Perkins (Editors), Quaternary Sedimentation in South Florida. Geol. Soc. Am. Mem., 147: 1–130.

Enos, P. and Perkins, R.D., 1977. Quaternary Sedimentation in South Florida. Geol. Soc. Am. Mem. 147, 198 pp.

Fetter, C.W., Jr., 1972. Position of the saline water interface beneath oceanic islands. Water Resour. Res., 8: 1307–1314.
Friedman, G.M., 1964. Early diagenesis and lithification in carbonate sediments. J. Sediment. Petrol., 34: 777–813.
Ginsburg, R.N., 1956. Grain size of Florida carbonate sediments. Am. Assoc. Petrol. Geol. Bull., 40: 2384–2427.
Ginsburg, R.N., 1964. South Florida Carbonate Sediments. Geol. Soc. Am. Annu. Meet. Field Trip Guideb., Field Trip 1, 72 pp. (Reprinted as Ginsburg, 1972, Sedimenta II, University of Miami, Miami FL.)
Ginsburg, R.N., 1995. Formative years of the scientific career of T. Wayland Vaughan. GSA Today, 5: 233–234.
Ginsburg, R.N. and Shinn, E.A., 1964. Distribution of the reef-building community in Florida and the Bahamas (abstr.). Am. Assoc. Petrol. Geol. Bull., 48: 527.
Ginsburg, R.N. and Shinn, E.A., 1994. Preferential distribution of reefs in the Florida reef tract: the past is the key to the present: In: Global Aspects of Coral Reefs, Health Hazards and History, University of Miami, Coral Gables FL, pp. H21–H26.
Halley, R.B. and Evans, C.C., 1983. The Miami limestone: A guide to selected outcrops and their interpretation. Miami Geol. Soc., Coral Gables, 67 pp.
Halley, R.B. and Harris, P.M., 1979. Fresh-water cementation of a 1000-yr-old oolite. J. Sediment. Petrol., 49: 969–988.
Halley, R.B. and Schmoker, J.W., 1983. High-porosity Cenozoic carbonate rocks of South Florida: progressive loss of porosity with depth. Am. Assoc. Petrol. Geol. Bull., 67: 191–200.
Halley, R.B., Shinn, E.A., Hudson, J.H. and Lidz, B.H., 1977. Pleistocene barrier bar seaward of ooid shoal complex near Miami, Florida. Am. Assoc. Petrol. Geol. Bull., 61: 519–526.
Hanson, C.F., 1980. Water resources of Big Pine Key, Monroe County, Florida. U.S. Geol. Surv., Open-File Rep., 80–447, 36 pp.
Harmon, R.S., Ku, T.-L., Matthews, R.K. and Smart, P.L., 1979. Limits of U-series analysis: Phase 1 results of the Uranium-Series Intercomparison Project. Geology, 7: 405–409.
Harrison, R.S. and Coniglio, M., 1985. Origin of the Key Largo Limestone, Florida Keys. Bull. Can. Petrol. Geol., 33: 350–358.
Harrison, R.S., Cooper, L.D. and Coniglio, M., 1984. Late Pleistocene of the Florida Keys. Can. Soc. Petrol. Geol. Core Conf. (Calgary), pp. 291–306.
Hearty, P.J., Vacher, H.L. and Mitterer, R.M., 1992. Aminostratigraphy and ages of Pleistocene limestones of Bermuda. Geol. Soc. Am. Bull., 104: 471–480.
Hine, A.C., 1997. Structural, stratigraphic, paleoceanographic development of the margins of the Florida Platform. In: A.F. Randazzo and D.S. Jones (Editors), The Geology of Florida. Univ. Florida Press, Gainesville FL, pp. 169–194.
Hoffmeister, J.E., 1974. Land from the Sea, the Geological Story of South Florida. Univ. Miami Press, Coral Gables FL, 143 pp.
Hoffmeister, J.E. and Multer, H.G., 1964a. Pleistocene limestones of the Florida Keys. In: R.N. Ginsburg (Editor), Geol. Soc. Am. Annu. Meet. Field Trip Guideb., Field Trip 1, pp. 57–61.
Hoffmeister, J.E. and Multer, H.G., 1964b. Growth rate estimates of a Pleistocene coral reef of Florida. Geol. Soc. Am. Bull., 75: 353–358.
Hoffmeister, J.E. and Multer, H.G., 1968. Geology and origin of the Florida Keys. Geol. Soc. Am. Bull., 79: 1487–1502.
Hoffmeister, J.E., Jones, J.I., Milliman, J.D., Moore, D.R. and Multer, H.G., 1964. Living and fossil reef types of South Florida. Geol. Soc. Am. Annu. Meet. Field Trip Guideb., Field Trip 3, 28 pp.
Hoffmeister, J.E., Stockman, K.W. and Multer, H.G., 1967. Miami Limestone of Florida and its Recent Bahamian counterpart. Geol. Soc. Am. Bull., 78: 175–190.
Holloway, Marguerite, 1994. Nurturing Nature. Sci. Am., 270: 98–108.
Holmquist, J.G., Powell, G.V.N. and Sogard, S.M., 1989. Sediment, water level and water temperature characteristics of Florida Bay's grass covered mudbanks. Bull. Mar. Sci., 44: 348–364.
Kahle, C.F., 1977. Origin of subaerial Holocene calcareous crusts: role of algae, fungi and sparmicritization. Sedimentol., 24: 413–435.

Kindinger, J.L., 1986. Geomorphology and tidal-bar depositional model of Lower Florida Keys (abstr.). Am. Assoc. Petrol. Geol. Bull., 70: 607.

Klein, H., 1970. Preliminary evaluation of availability of potable water on Elliot Key, Dade County, Florida. U.S. Geol. Surv. Open File Rep. 70010, 15 pp.

Klitgord, K.D., Popenoe, P. and Schouten, H., 1984. Florida, a Jurassic transform plate boundary. J. Geophys. Res., 89: 7753–7721.

Kornicker, L.S., 1958. Bahamian limestone crusts. Trans. Gulf Coast Assoc. Geol. Soc., 8: 167–170.

Ku, T.-L., Ivanovich, M. and Luo, S., 1990. U-series dating of last interglacial high sea stands: Barbados revisited. Quat. Res., 33: 129–147.

Ladd, H.S. (Editor), 1957. Treatise on Marine Ecology and Paleoecology, v. 2, Paleoecology. Geol. Soc. Am. Mem. 67, 1077 pp.

Land, L.S., 1967. Diagenesis of skeletal carbonates. J. Sediment. Petrol., 37: 914–930.

Lidz, B.H., Hine, A.C., Shinn, E.A. and Kindinger, J.L., 1991. Multiple outer-reef tracts along the south Florida bank margin: Outlier reefs, a new windward-margin model. Geology, 19: 115–118.

Lidz, B.H. and Shinn, E.A., 1991. Paleoshorelines, reefs, and a rising sea: South Florida, USA. J. Coastal Res., 7: 203–229.

Ludwig, K.R., Muhs, D.R., Simmons, K.R., Halley, R.B. and Shinn, E.A., 1996. Sea-level records at ~80 ka from tectonically stable platforms: Florida and Bermuda. Geology, 24: 211–214.

Mackenzie, D.J., 1990. Water-resources potential of the freshwater lens at Key West, Florida. U.S. Geol. Surv. Water-Resour. Invest. Rep., 90–4115, 24 pp.

Marszalek, D.S., Babashoff, G., Jr., Noel, M.R. and Worley, D.R., 1977. Reef distribution in south Florida. Proc. Third Int. Coral Reef Symp. (Miami), pp. 223–229.

Matson, G.C. and Sanford, S., 1913. Geology and Ground Waters of Florida. U.S. Geol. Surv. Water-Supply Pap. 319, 445 pp.

Maul, G.A. and Martin, D.M., 1993. Sea level rise at Key West, Florida, 1846–1992: America's longest instrument record? Geophys. Res. Lett., 20: 1955–1958.

Mitterer, R.M., 1974. Pleistocene stratigraphy in southern Florida based on amino acid diagenesis in fossil *Mercenaria*. Geology, 2: 425–428.

Mitterer, R.M., 1975. Ages and diagenetic temperatures of Pleistocene deposits of Florida based on isoleucine epimerization in Mercenaria. Earth Planet. Sci. Lett., 28: 275–282.

Mitterer, R.M. and Kriausakul, 1989. Calculation of amino acid racemization ages based on apparent parabolic kinetics. Quat. Sci. Rev., 8: 353–357.

Multer, H.G., 1977. Field Guide to Some Carbonate Rock Environments, Florida Keys and Western Bahamas. Kendell Hunt Publ. Co., Dubuque, 415 pp.

Multer, H.G. and Hoffmeister, J.E., 1968. Subaerial laminated crusts of the Florida Keys. Geol. Soc. Am. Bull., 79: 183–192.

Muhs, D.R., Szabo, B.J., McCartan, L., Maat, P.B., Bush, C.A. and Halley, R.B., 1992. Uranium-Series estimates of corals from Quaternary marine sediments of southern Florida. In: T.M. Scott and W.D. Allmon (Editors), The Plio-Pleistocene Stratigraphy and Paleontology of Southern Florida. Fla. Geol. Surv. Spec. Publ. 36: 41–49.

Neumann, C.A. and McIntyre, I.G., 1985. Reef response to sea-level: catch up, keep up, or give up. Proc. Fifth Int. Coral Reef Cong. (Tahiti), 3: 105–110.

Newell, N.D. and Rigby, J.K., 1957. Geological studies on the Great Bahama Bank. In: R.J. Le Blanc and J.G. Breeding (Editors), Regional Aspects of Carbonate Deposition. Soc. Econ. Paleontol. Mineral. Spec. Publ., 5: 15–72.

NOAA (National Oceanic and Atmospheric Administration, U.S. Department of Commerce), 1995. Florida Keys National Marine Sanctuary: Draft Management Plan/Environmental Impact Statement, 3 vols.

Osmond, J.K., Carpenter, J.R. and Windom, H.L., 1965. $^{230}Th/^{234}U$ age of the Pleistocene corals and oolites of Florida. J. Geophys. Res. 70: 1843–1847.

Parker, G.G., Ferguson, G.E., Love, S.K., et al., 1955. Water resources of southeastern Florida, with special reference to the geology and ground water of the Miami area. U.S. Geol. Surv. Water-Supply Pap. 1255, 965 pp.

Peltier, W.R., 1986. Deglaciation-induced vertical motion of the North American continent. J. Geophys. Res., 91: 9099–9123.

Peltier, W.R., Farrell, W.E. and Clark, J.A., 1978. Glacial isostasy and relative sea level: a global finite element model. Tectonophys., 50: 81–110.

Perkins, R.D., 1977. Depositional framework of Pleistocene rocks in south Florida. In: P. Enos and R.D. Perkins (Editors), Quaternary Sedimentation in South Florida. Geol. Soc. Am. Mem., 147: 131–198.

Randazzo, A.F. and Halley, R.B., 1997. The geology of the Florida Keys region. In: A.F. Randazzo and D.S. Jones (Editors), The Geology of Florida. University of Florida Press, Gainesville FL, pp. 251–259.

Robbin, D.M., 1981. Subaerial $CaCO_3$ crust: a tool for timing reef initiation and defining sea level changes. Proc. Fourth Int. Coral Reef Symp. (Manila), 1: 575–579.

Robbin, D.M., 1984. A new Holocene sea level curve for the upper Florida Keys and Florida Reef Tract. In: P.J. Gleason (Editor), Environments of South Florida, Present and Past, II. Miami Geol. Soc., Coral Gables, pp. 437–4458.

Robbin, D.M. and Stipp, J.J., 1979. Depositional rate of laminated soilstone crust, Florida Keys. J. Sediment. Petrol., 49: 175–180.

Robblee, M.B., Tilmant, J.T. and Emerson, J., 1989. Quantitative observations on salinity in Florida Bay (abstr.). Bull. Mar. Sci., 44: 523.

Roberts, H.H., Rouse, L.J., Walker, N.D. and Hudson, J.D., 1982. Cold-water stress in Florida Bay and the northern Bahamas — a product of cold-air outbreaks. J. Sediment. Petrol., 52: 145–155.

Sanford, S., 1909. Topography and geology of southern Florida. Fla. Geol. Surv. Annu. Rep., 2: 175–231.

Schlager, W., 1981. The paradox of drowned reefs and carbonate platforms. Geol. Soc. Am., 92: 197–211.

Scholl, D.W. and Stuiver, M., 1967. Recent submergence of southern Florida: A comparison with adjacent coasts and other eustatic data. Geol. Soc. Am. Bull., 78: 437–454.

Shinn, E.A., 1963. Spur and groove formation on the Florida reef tract. J. Sediment. Petrol., 33: 291–303.

Shinn, E.A., 1964. Recent dolomite, Sugarloaf Key. In: R.N. Ginsburg (Editor), Geol. Soc. Am. Annu. Meet. Field Trip Guideb., Field Trip 1, 62–67.

Shinn, E.A., 1988. The Geology of the Florida Keys. Oceanus, 31 (1): 46–53.

Shinn, E.A., Lidz, B.H., Kindinger, J.L., Hudson, J.H. and Halley, R.B., 1989. Reefs of Florida and the Dry Tortugas, A Guide to the Modern Carbonate Environments of the Florida Keys and the Dry Tortugas. Int. Geol. Cong., IGC Field Trip T176. Am. Geophys. Union, Washington DC, 54 pp.

Shinn, E.A., Reese, R.S. and Reich, C.D., 1994. Fate and pathways of injection-well effluent in the Florida Keys. U.S. Geol. Surv. Open-File Rep., 4–276, 121 pp.

Shinn, E.A., Reich, C.D., Locker, S.D. and Hine, A.C., 1996. A giant sediment trap in the Florida Keys. J. Coastal Res., 12: 953–959.

Stanley, S.M., 1966. Paleoecology and diagenesis of Key Largo Limestone, Florida. Am. Assoc. Petrol. Geol. Bull., 50: 1927–1947.

Steckler, M.S., Watts, A.B. and Thorne, J.A., 1988. Subsidence and basin modeling at the U.S. Atlantic passive margin. In: R.E. Sheridan and J.A. Grow (Editors), The Atlantic Continental Margin, U.S. Geol. Soc. Am., The Geology of North America, I-2: 399–416.

Stewart, M.T., 1988. Electromagnetic mapping of fresh-water lenses on small oceanic islands. Ground Water, 26: 187–191.

Stewart, M.T., 1990. Rapid reconnaissance mapping of fresh-water lenses on small oceanic islands. Soc. Explor. Geophys. Invest. Geophys., 5: 57–66.

Storr, J.F., 1964. Ecology and oceanography of the coral-reef tract, Abaco Island, Bahamas. Geol. Soc. Am. Spec. Pap. 79, 98 pp.

Szabo, B.J. and Halley, R.B., 1988. $^{230}Th/^{234}U$ Ages of aragonitic corals from the Key Largo Limestone of South Florida (abstr.). Am. Quat. Assoc. Prog. and Abstr., Amherst, Mass., p. 154.

Taft, W.H., 1961. Authigenic dolomite in modern carbonate sediments along the southern coast of Florida. Science, 134: 561–562.

Tucker, M.E. and Wright, V.P., 1990. Carbonate Sedimentology. Blackwell, Oxford, 482 p.

Vacher, H.L., 1988. Dupuit-Ghyben-Herzberg analysis of strip-island lenses. Geol. Soc. Am. Bull., 100: 580–591.

Vacher, H.L. and Ayers J.F., 1980. Hydrology of small oceanic islands — Utility of an estimate of recharge inferred from the chloride concentration of the fresh-water lenses. J. Hydrol., 45: 21–37.

Vacher, H.L., Wightman, M.J. and Stewart, M.T., 1992. Hydrology of meteoric diagenesis: Effect of Pleistocene stratigraphy on freshwater lenses of Big Pine Key, Florida. In: C.H. Fletcher, III, and J.F. Wehmiller (Editors), Quaternary Coasts of the United States: Marine and Lacustrine Systems. SEPM (Soc. Sediment. Geol.) Spec. Publ., 48: 213–219.

Vaughan, T.W., 1940. Ecology of modern organisms with reference to paleogeography. Geol. Soc. Am. Bull., 51: 433–468.

Wanless, H.R., 1982. Sea level is rising. So what? J. Sediment. Petrol., 52: 1051–1054.

Warzeski, R.E., Cunningham, K.J., Ginsburg, R.N., Anderson, J.B. and Ding, Z.-D., 1996. A Neogene mixed siliciclastic and carbonate foundation for the Quaternary carbonate shelf, Florida Keys. J. Sediment. Res., 66: 788–800.

Weisbord, N.E., 1974. Late Cenozoic corals of South Florida. Bull. Am. Paleontol., 66: 259–511.

Wightman, M.J., 1990. Geophysical analysis and Dupuit-Ghyben-Herzberg modeling of fresh-water lenses on Big Pine Key, Florida. M.S. Thesis, Univ. South Florida, Tampa FL, 122 pp.

Geology and Hydrogeology of Carbonate Islands. Developments in Sedimentology 54
edited by H.L. Vacher and T. Quinn
© 1997 Elsevier Science B.V. All rights reserved.

Chapter 6

GEOLOGY OF MUD ISLANDS IN FLORIDA BAY

PETER K. SWART and PHILIP A. KRAMER

INTRODUCTION

Florida Bay is a large triangular body of water located to the south of peninsular Florida and to the north of the limestone keys discussed in Chapter 5. Some 237 Holocene carbonate mud islands occupy about 1.73% (1,500 km^2) of the total area of the bay (Enos, 1989). Despite having "Key" attached to their names, the mud islands of Florida Bay are composed of fine-grained, unconsolidated carbonate muds that have accumulated over the last 4,000 years as Florida Bay was flooded by rising sea level (Scholl, 1966; Davies, 1980). These islands, therefore, are distinct from the better-known Florida Keys to the south. Similar mud islands exist in other parts of the world, although they are not common and are limited to low-energy coastal areas lacking siliciclastic input. Examples occur along the west coast of Andros island (Bahamas), Belize, and on both the northern and southern coasts of Cuba (Bathurst, 1971; Ginsburg and James, 1974).

The mud islands were used by the Calusa Indians while fishing and hunting within Florida Bay (Tabeau, 1968). None of the islands appear to have been used as a permanent camp; there are no shell mounds that typically mark Indian establishments on islands further to the north and along the Florida Keys. Settlement of the area began during the early 1900s by plume hunters, fisherman, and loggers. On some of the higher islands, charcoal burners set up camps and cut down the larger hardwood trees (Craighead, 1964). Attempts to cultivate tomatoes and other vegetables were periodically made on islands in the northwest portion of the bay, but most of these tiny establishments were short-lived and swept away by hurricanes. Today, the islands serve as important nesting and foraging habitats for a variety of birds, reptiles, and aquatic invertebrates.

Several features of the Florida Bay mud islands stand out hydrochemically and separate them from other carbonate islands. Their extremely low elevation (less than 50 cm above MSL) and small size (generally about 0.5 km^2) allow seawater to flood over them during lunar tides and storms. As a result of this periodic flooding, shallow ponds collect on the interior of the islands and are subsequently evaporated. Consequently, both pond waters and groundwaters have salinities of 45–140 g kg^{-1} in spite of the large annual rainfall. In addition, some of the older islands have sediment layers composed of up to 30% authigenic dolomite. Diagenetic alteration, therefore, has occurred, and it appears to be related to an island-specific process (Videlock, 1983; Swart et al., 1989a).

In this chapter, we review the geology and hydrology of Florida Bay and the mud islands. We will focus on the geochemistry and diagenesis using data collected from

earlier (Swart et al., 1989a,b; Burns and Swart, 1992) and ongoing studies (Kramer et al., 1993, 1994; Juster, 1995; Juster et al., in press). These studies, which make use of groundwater chemistry and stable isotope data, indicate that significant recrystallization is taking place in these sediments, but the data do not conclusively prove that dolomite is forming at the present time. Either rates of dolomitization are too slow to be properly documented by groundwater chemistry, or the dolomite is a relict from an earlier time in the island's history.

REGIONAL SETTING

Geography of Florida Bay

Florida Bay is a shallow lagoon (depth < 4 m) located immediately below the southern tip of peninsular Florida (Fig. 6-1), approximately 80 km southwest of Miami. Bordered on the north by the Everglades and to the south and east by the Florida Keys, the majority of Florida Bay lies within the boundaries of Everglades National Park. The mud islands of Florida Bay are generally located atop or along the maze-like "mudbanks" which dissect Florida Bay into a series of "basins" (Fig. 6-1). "Mudbank" indicates a mound of unconsolidated carbonate mud that is exposed during low tides; "basin" refers to the large, relatively deeper water areas (> 2 meters) amongst the mudbanks and islands. "Groundwater" as used in this chapter refers to the water in the saturated zone of these exposed carbonate sediments; this water is generally called "porewater" in the literature of diagenesis of these islands, which reflects the sedimentological context and marine-geochemical approach of the studies.

The Holocene sediments of Florida Bay lie unconformably on limestone bedrock, the late Pleistocene Miami Limestone (Hoffmeister et al., 1967) (Fig. 6-2A, B). The gentle slope of the Miami Limestone from east to west has allowed for thinner, narrow mudbanks in the east and thicker, wider mudbanks in the west (Fig. 6-2B). Most of the mudbanks and mud islands in the bay are positioned over karstic depressions and irregularities (30–200 cm in relief) within the Miami Limestone (Wanless and Tagett, 1989).

Climate

The Florida Bay region has a tropical to subtropical climate. Air temperatures are 16–33°C, with an average of 28°C. Prevailing winds are southeasterly and easterly, but swing around to the north to northeast during the winter and spring. Winds are on average stronger during the winter (10–20 kn) than during the summer (5–10 kn). Precipitation in Florida Bay can exceed 150 cm y^{-1}, but it is often localized and associated with afternoon thunderstorms that form over the Everglades and move out over the bay. The pronounced wet season extends from June through October, accounting for over 70% of the yearly rainfall, and is characterized by slightly higher

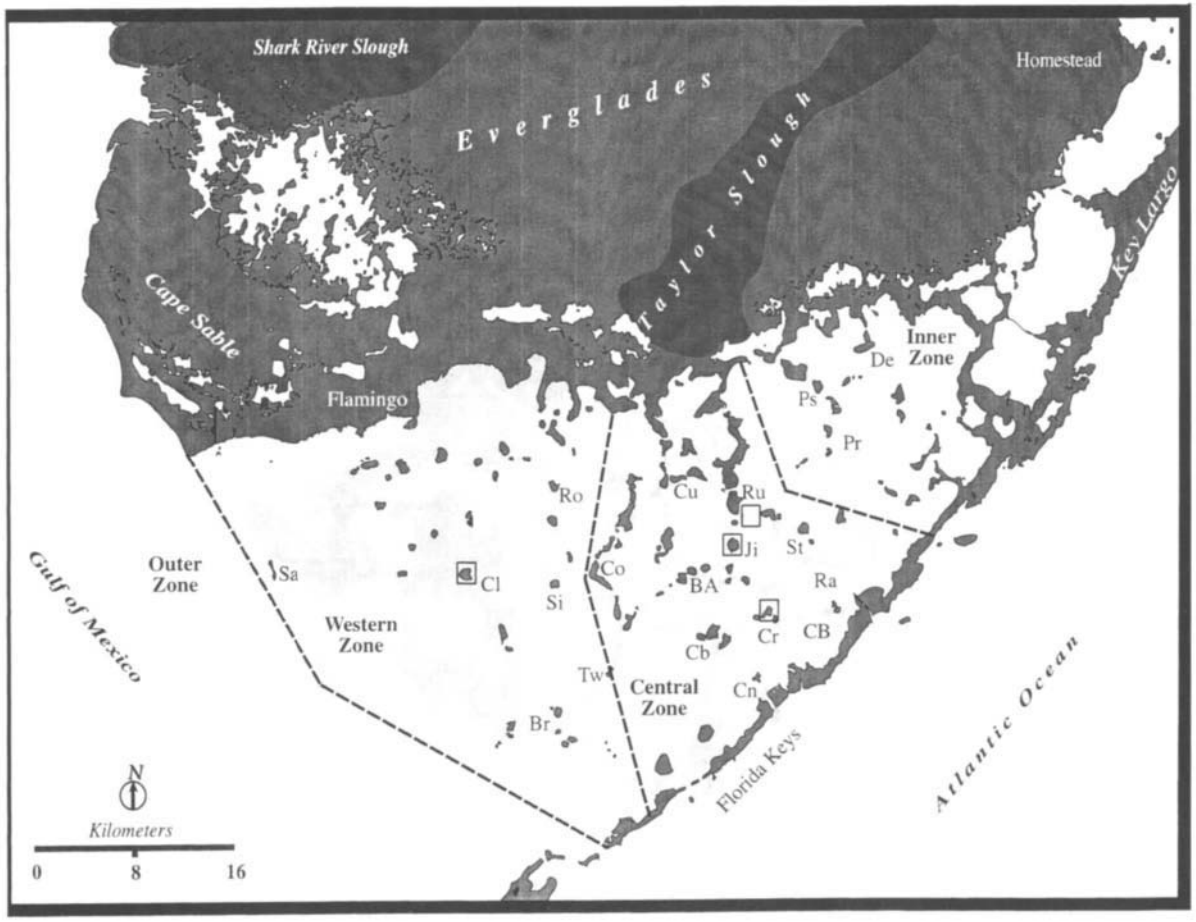


Fig. 6-1. Location map of Florida Bay showing position of major Holocene mudbanks (shaded regions), islands, and basins. The coastal Everglades swamp forms the northern boundary, and the Pleistocene-limestone Florida Keys define the southern boundary of the Bay. Four boxed areas are shown in detail in Fig. 6-4. Four zones of mudbank development have been added (dashed lines) from Wanless and Tagett (1989). Abbreviations of Keys in Florida Bay: Sa, Sandy; Cl, Cluett; Si, Sid; Ro, Roscoe; Br, Barnes; Co, Corinne; Tw, Twin; Ji, Jimmy; Cu, Club; BA, Bob Allen; Cb, Crab; Ru, Russel; Cr, Crane; St, Stake; Pr, Park; Ps, Pass; De, Deer; Cn, Cotton; Ra, Ramshorn shoal; CB, Cross Bank.

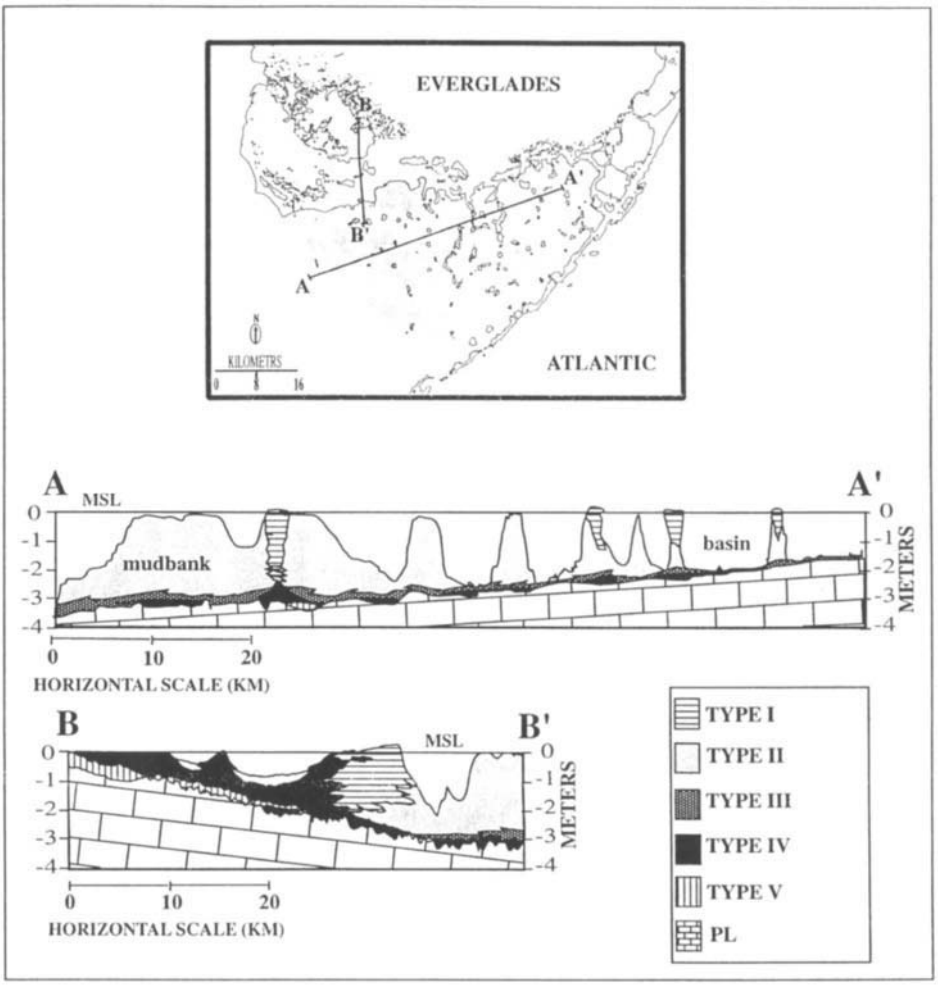


Fig. 6-2. (A) NE-SW cross section (A-A′) showing how mudbanks are wider and thicker in the west, changing to narrow, well-defined thin banks in the east. Also note the eastward-rising slope of the underlying Pleistocene limestone. (B) Cross section (B-B′) from northern bay into Everglades swamp showing transgressive/regressive sequences of the Holocene sediments (Modified from Roberts et al., 1977). Lithologies: Type I, supratidal mudstone (island); Type II, bioturbated wackestone (mudbank); Type III, mollusk packstone (basin); Type IV, peat (mainly mangrove); Type V, calcite mud (freshwater marsh, as in Everglades); PL, Pleistocene limestone.

afternoon relative humidity (77%). The dry season, which generally starts in January and extends through May, has lower afternoon relative humidity (64%) and strong afternoon winds. In general, evaporation exceeds rainfall except during the late summer and fall months.

Florida Bay experiences approximately 15 major storms a year; mainly they coincide with the passage of cold fronts during the winter (Roberts et al., 1982). In

addition, hurricanes (Ball et al., 1967) strike south Florida approximately every 5–7 years. Hurricanes occur between June and October and can have a tremendous effect on Florida Bay by altering circulation, redistributing sediment, and removing vegetation on the islands.

Hydrography of Florida Bay

Water levels. Water levels within Florida Bay are controlled by tides, winds, and seasonal changes in sea level. Tides in Florida Bay are mixed diurnal-semidiurnal along the Gulf of Mexico boundary, and semidiurnal along the Atlantic. Tidal range is greatest at the open, western and southern portions of the bay (up to 80 cm). In the interior and northeastern areas of the bay, the tide is essentially damped (< 3 cm) by the numerous shallow mudbanks. Winds are significant controls of water level in these interior regions. For example, the water level in northeastern Florida Bay can be increased by up to 40 cm above normal tide levels when the wind blows strongly for several days from the southwest, and lowered by as much as 40 cm when it blows strongly from the northeast. A seasonal steric effect in the Gulf of Mexico causes water levels within Florida Bay to change annually by as much as 20 cm (Kramer et al., 1994). Because of this effect, water levels reach their yearly maximum levels during the fall (September–November) and their lowest levels during the spring (March–May).

Salinity. The variation in salinity of Florida Bay waters reflects intra- and interannual patterns. In general, there is less variation along the more-open western and southern portions of the bay and increased variation in the interior portion. Salinities as high as 80 g kg^{-1} and as low as 15 g kg^{-1} have been reported in the central portion of the bay. These variations are related to (1) freshwater input and (2) seawater penetration from the Gulf of Mexico and through the Florida Keys. The freshwater input into the bay is derived principally from three sources: Shark River, Taylor Slough, and local rainfall. Approximately 90 km^3 y^{-1} of water is discharged through Shark River to the west of peninsular Florida (Fig. 6-1). A portion of this runoff is believed to find its way into the western portion of the bay although the precise amount is not known. The smaller discharge of Taylor Slough (9 km^3 y^{-1}) is perhaps volumetrically more important to Florida Bay as it enters directly into northeastern Florida Bay. Historically, the magnitude of the Taylor Slough runoff was probably larger, as it is now highly controlled by agricultural and urban interests in the south Miami area.

Stable isotope composition. Although there are slight differences in behavior between δD and $\delta^{18}O$ in Florida Bay, the behavior of the two isotopes can be considered identical for the purposes of this account, and so discussion here will be limited to $\delta^{18}O$ (Swart et al., 1989b). The $\delta^{18}O$ composition of Florida Bay waters is governed by a combination of four distinct influences (Fig. 6-3). First is input of isotopically heavy freshwater ($\delta^{18}O = +3‰$ SMOW) from the Everglades; these

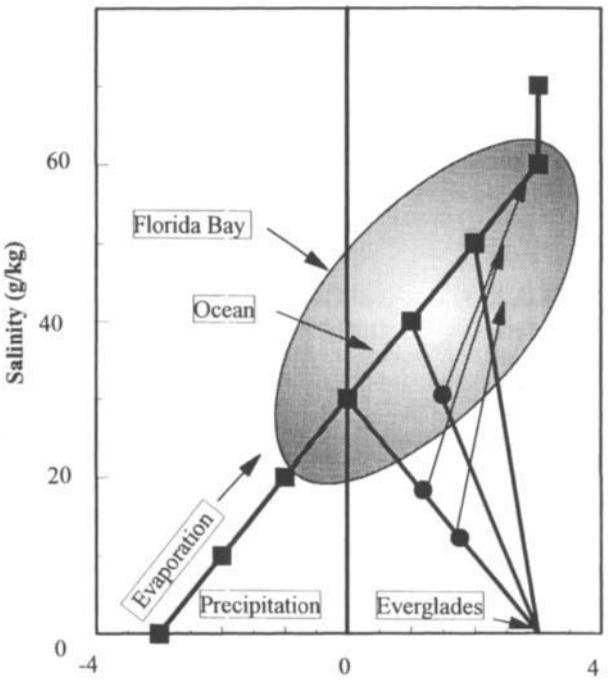


Fig. 6-3. Hypothetical model showing possible causes of the oxygen isotopic composition and salinity in Florida Bay. Sources of water are Everglades, ocean, and local precipitation. The mixing of waters from these sources combined with the evaporation effect leads to the large range in Florida Bay water (shaded).

waters are enriched as a result of extensive evaporation that occurs during their slow flow through the Everglades. Second, there is the isotopically normal marine water from the Florida Keys ($\delta^{18}O$ = 0‰ to +1‰ SMOW), and third, an input of isotopically depleted rainwater ($\delta^{18}O$ = −3.0 SMOW; Swart et al., 1989b). Finally, and perhaps the most important influence, is the evaporation of water in the bay itself. The maximum $\delta^{18}O$ isotopic composition that can be attained by the water within the bay is dictated by isotopic exchange between the atmosphere and the bay and, therefore, is related to the relative humidity and temperature. For conditions prevalent in south Florida, this maximum $\delta^{18}O$ value is approximately +3‰ SMOW. Therefore, inundation of Florida Bay by marine water, which can act to either lower or raise the salinity, will usually act to decrease $\delta^{18}O$. Increased discharge from the Everglades, on the other hand, will decrease the salinity but will not affect the oxygen isotopic composition of the water (Swart et al., 1989b).

Sediments

Unconsolidated carbonate sediments comprise nearly 95% of the sediments within Florida Bay; the remainder consists of silica and detrital clays. The majority

of these sediments is believed to be the result of biogenic precipitation of skeletal material, principally as organisms which encrust the *Thalassia* communities (Nelson and Ginsburg, 1986; Bosence, 1989). As the organic portion of the grass dies and decomposes, the small carbonate encrustations (red algae *Melobesia membranacea* and *Fosliella farinosa*; serpulid worm *Spirobis* spp.) are released to form part of the sediment. The production from these encrustations in eastern Florida Bay has been estimated to be 118 g m^{-2} y^{-1}, six times more than that derived from Penicillus in a similar area (Nelson and Ginsburg, 1986). Minor amounts of sediments are supplied by calcareous green algae such as *Halimeda* spp. and *Penicillus* spp., the small finger coral *Porites* spp., various species of mollusks, and foraminifera. Opaline silica (radiolaria, diatoms and sponge spicules) and organic matter are also found in the sediment.

The gentle east-to-west slope of the underlying Miami Limestone has led to marked differences between eastern and western Florida Bay. The eastern portions of Florida Bay, for example, generally have a sparse bottom fauna and lower carbonate production. Basins are characterized by smaller amounts of sediment; most of the finer material has been winnowed by wave action, leaving only a coarse lag deposit of molluscan shell fragments (Ginsburg, 1956; Enos and Perkins, 1979). In contrast, the western portions of the bay have luxuriant carpets of marine grasses (*Thalassia* spp., *Haloduli* spp.), very high carbonate production rates, and thicker sediment cover over the basins.

The mineralogy of Florida Bay sediments reflects the relative contributions of the various biogenic components. On average, the sediments are 60% aragonite, 20% high-Mg calcite (HMC), and 15% low-Mg calcite (LMC) with minor quantities of detrital quartz and opaline silica. Detrital dolomite comprises up to 5% of the sediments found in the northwestern corner of the bay and is thought to originate from exposed portions of the Hawthorn Formation (Miocene) to the north (Taft and Harbaugh, 1964; Scholl, 1966). Samples rich in LMC occur principally in the northern portion of Florida Bay and are derived from freshwater marls which form in the Everglades.

Mudbanks

Mudbanks typically consist of bioturbated peloidal wackestone, grey molluscan wackestone, and minor amounts of molluscan packstone and pelleted mudstone (Enos and Perkins, 1979; Tagett, 1988; Wanless and Tagett, 1989). The mudbanks record a history of migration, with windward erosion and leeward sedimentation. Based on the fact that the northern and eastern margins of the banks are erosional, Wanless and Tagett (1989) concluded that winter storms rather than hurricanes are responsible for the deposition and movement of the banks. In some instances, mudbanks have migrated substantially across the bay bottom and in the process obliterated the record of earlier phases of the bank's history.

Wanless and Tagett (1989) also recognized four zones of mudbank development within the bay (Fig. 6-1): (1) an inner destructional zone (where mudbanks are

shrinking); (2) a central migrational zone (where mudbanks are migrating); (3) a western constructional zone (where mudbanks are growing); and (4) an outer destructional zone. As the names imply, different processes are taking place in different portions of the bay. The controls on these processes relate mainly to sediment supply and wave energy. In eastern Florida Bay, for example, sediment supply is limited; as a result, the mudbanks are discontinuous, and there is only a thin veneer of grainstone covering the basin floor. In contrast, there is an ample supply of sediment in central Florida Bay, and so a continuous network of mudbanks has been formed (Fig. 6-4D). In the western portion of Florida Bay, there appears to be a large increase in sediment supply, for banks have coalesced and are actively expanding on all flanks (Wanless and Tagett, 1989).

MUD ISLANDS

Physiography

Islands within Florida Bay have been divided into three groups or "stages" based on their vegetation and topography (Craighead, 1964): (1) low or early stage, (2) middle stage, and (3) high islands or late stage. In their early stage, the islands are covered by mangrove swamps, algal mats, and halophytic marshes; middle-stage islands support brackish-water vegetation, mainly black mangroves (*Avicennia nitidae*) and hylophytic marshes; late-stage islands show growth of grass, palms and hardwoods. It is clear that the types and distribution of vegetation on these islands depends strongly on topography; elevation differences of mere centimeters often produce striking changes in vegetation (Davis, 1940). Extensive examination of diverse islands by Enos and Perkins (1979) led them to conclude that the "stages of development" are not related so much to island age as to the amount of storm deposition and sediment trapping. Ginsburg and Lowenstam (1958) recognized that nearly all of the supratidal sediment accumulating on the interior portions of islands is in fact brought in during storms. Hurricane Donna, which struck Florida Bay in 1960, is known to have deposited as much as 10 cm of well-sorted mud on the interior of some bay islands (Ball et al., 1967; Craighead, 1964).

Topographic features on the islands are small. Relief is generally measured in centimeters. Most islands have three principal topographic features: a high leeward side, a central depression, and a fringing levee. The high leeward side is 20–50 cm above MSL and often contains a small brackish-water lens, which supports a variety of hardwood trees and grasses. The lowest portion of a typical island includes a central area of saline mud flats and mangrove swamps, which are within 10 cm of MSL. The central mud-flat areas often contain small ridges (10–20 cm high), which are commonly colonized by black mangroves. The fringing levee is generally composed of skeletal beach sand 5–40 cm above MSL and borders much of the island shoreline. This levee is especially pronounced on low-lying islands and strongly influences the surface-water and salt balances on the islands.

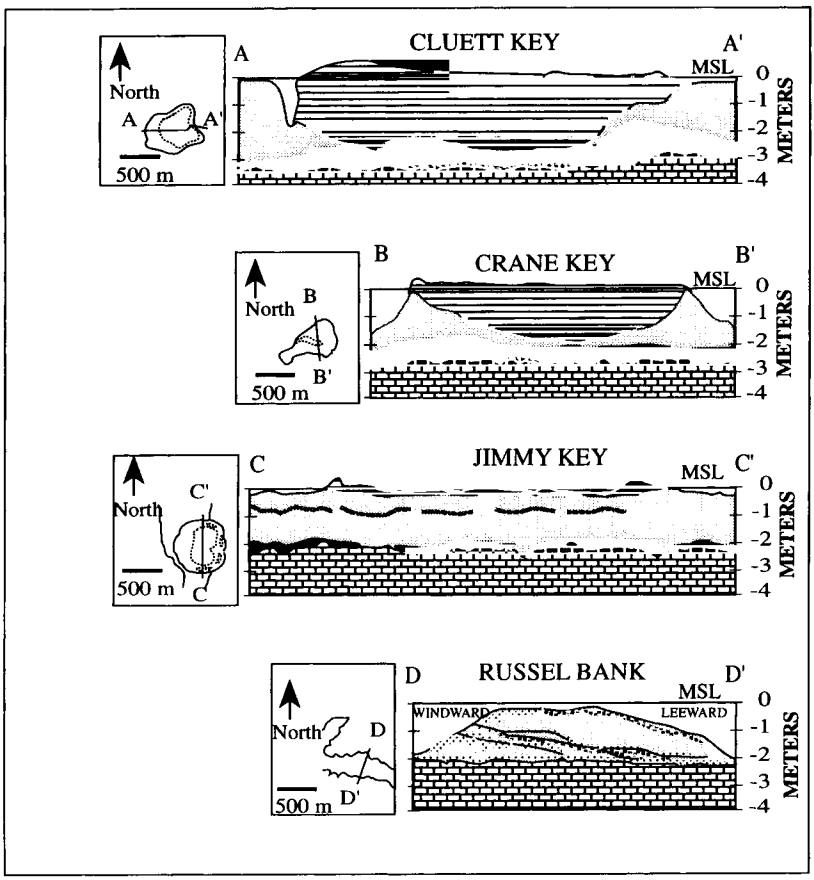


Fig. 6-4 (locations on Fig. 6-1). (A) Cross section through Cluett Key, a late-stage island, western Florida Bay. This island, which is composed primarily of supratidal sediments, nucleated during the initial transgression. (From Videlock, 1983.) (B) Cross section through Crane Key, south-central Florida Bay. In this cross section, the island is shown to have nucleated on mudbank sediments some time after initial transgression, although subsequent work has shown that, on other parts of the island, supratidal sediments sit directly atop peat layers. (From Enos and Perkins, 1979). (C) Cross section of Jimmy Key, central Florida Bay, showing that island has only recently formed on underlying mudbank. Age of island is thought to be < 400 years. (Modified from Burns and Swart, 1992.) (D) Cross section of Russel Bank, central Florida Bay, showing leeward-dipping, layered mudstone sequences capped by seagrass-influenced sediments composed primarily of bioturbated wackestones and some packstone layers. (From Wanless and Tagett, 1989.)

Geologic history

The mud islands contain the most complete sedimentological history of Florida Bay's development over the past 4,000 years. Of the hundreds of small mud islands that dot the bay, only a handful of the more sizable islands (area > 0.5 km^2) have been studied. Cores pushed through the soft mud-island sediments to the underlying

bedrock reveal a lower transgressive sequence beneath a regressive sequence (Fig. 6-4). Enos (1989) identified five distinct lithologies (Types I to V). Type I lithology, which is a supratidal mud found as the uppermost unit at most islands, is a highly oxidized, white to grey, laminated mud characterized by a crumbly texture thought to be the result of frequent drying and wetting (Enos and Perkins, 1979). Type II sediments are dark grey-brown wackestones that make up a marine mudbank succession underlying many younger islands. These sediments are characterized by numerous *Thalassia* rhizome sheaths containing successive accumulations of fining-upwards sequences broken up by occasional packstone shell layers (Wanless and Tagett, 1989). Type III sediments, which commonly overlie peat layers, consist of dark to medium grey, molluscan packstones and wackestones; often interlayered within peat layers and extensively rooted, these sediments are similar to those found forming today in the open basins of the bay. The two other lithologies are peats (IV) and freshwater calcitic mud (V), both of which are found at the base of many islands and mudbanks. Davies (1980) showed that the basal peats can be of either freshwater (*Mariscus* spp.) or brackish-water origin (*Rhizophora-Avicenna*), but all peats higher in the column are of marine origin.

Enos (1989) identified two types of island development: early colonization and late colonization, where "early" and "late" refer to the timing of colonization relative to the initial submergence of Florida Bay. Early-colonization mud islands (Fig. 6-4A, B) are characterized by a transgressive sequence consisting of calcite marls (Type V lithology) and basal peat (IV) intermixed with basin sediments (III, interpreted as representing an initial marine flooding of the bay) and an overlying regressive or progradational sequence consisting of a continuous succession of supratidal sediments (I). Enos (1989) classified the following islands as early-colonization mud islands: West Bob Allen, Calusa, Crane, Eagle, Lake, Man of War, Murray, Palm, Pigeon, Cluett, and Sid Keys.

In contrast, late-colonization mud islands, which by definition are thought to have nucleated on mudbanks some time after the initial flooding of the bay, are characterized by the occurrence of subtidal sediments (II) through a portion of the sequence, and, in some cases, a lack of basal peat. Such islands are not believed to be typical of Florida Bay; in fact, Enos (1989) suggested that the succession of sediment types on these islands may be simply the result of migration of a precursor island over an adjacent mudbank as a result of winds and currents. On the other hand, there is now good evidence that Jimmy Key (Fig. 6-4C) formed recently on a mudbank (Burns and Swart, 1992): distinctive shell layers can be traced from the islands into adjacent mudbanks, and $\delta^{13}C$ values of the organic material in the sediment change upward from an isotopically heavy marine signal (i.e., mudbank) to more depleted values characteristic of mangroves (i.e., island). In the case of Jimmy Key, the age of the veneer of island sediments is estimated to be only 200–400 years, and so this island has been emergent for only this period of time (Burns and Swart, 1992). In other regions, the mangrove colonization is known to be even more rapid; for example, Cowpens Cut through Cross Bank shows that entire area essentially has been colonized since 1949. Other islands which are suggested to have formed on mudbanks (hence late-colonization islands) include Bald Eagle, Bob

Allen (east), Bottle, Cotton, Johnson, Rabbit (north), Shell, and Stake (Enos, 1989).

Hydraulic properties

The unconsolidated carbonate muds which make up the island sediments are characterized by low hydraulic conductivity (10^{-1} to 10^{-3} m day^{-1}) and high porosity (45–85%). The majority of the sediment is micron-size aragonitic needles mixed with calcitic mollusks and HMC foraminifera. The sediments are dominantly mudstones interrupted by discontinuous wackestone and, less commonly, packstone units. In the upper 10 cm of Crane Key, the hydraulic conductivity is 10^{-3}–10^{0} m day^{-1} (Enos and Sawatsky, 1981). This large range is caused by root voids, gas bubbles, and large desiccation cracks, all of which can extend to depths of 30 cm and produce an extensive network of macroporosity (Enos and Sawatsky, 1981). In contrast, Enos and Sawatsky (1981) measured a hydraulic conductivity of 10^{-4} m day^{-1} at Ramshorn shoal, a predominantly fine-grained mudbank lacking shells. This low value may be attributable to the lack of macropores and is near the intrinsic value of pure carbonate mud, based on consolidation experiments (Juster, 1995). Hydraulic conductivity decreases towards this intrinsic value with depth on both islands and mudbanks due to compression of the pore matrix and clogging of the macropore network during burial (Juster, 1995).

Porosity in all the island sediments is very high. Enos and Sawatsky (1981) found values of 61–68% in samples from Crane Key. Videlock (1983), who used a gamma-ray attenuation method (GRAPE) for sediments from Cluett Key, found values of 53–68%, with porosity near 80% at the base due to the presence of peats. Juster (1995) measured a decrease in porosity from 69% at the surface to 65% at 2 m depth on Jimmy Key and the adjacent mudbank, but a reverse relationship was measured in Cluett Key sediments indicating that burial compression may not always be significant in reducing porosity.

Surface waters

A strong seasonality characterizes the water level and salinity of surface water bodies that form on the island interiors. During the late summer and fall months, when bay water levels are at their maximum, islands can be flooded daily with each high tide (Kramer, 1996). These months are also the wet season in south Florida, and precipitation on the islands can often exceed 20 cm during a single rain event; at such times, the pond water can be diluted to near freshwater salinities. In contrast, during the winter and spring months when rainfall is minimal and bay water levels are, on average, lower, it is not uncommon for the interior ponds of islands to dry out completely for several weeks. Evapotranspiration in the interior areas of the islands is from evaporation from free surfaces, evaporation from exposed soils, and transpiration from the low vegetation. Evapotranspiration on Florida Bay islands is not quantified. From pan-evaporation measurements, it is known (NOAA, 1989) that

evaporation in south Florida varies seasonally from 5 cm mo^{-1} to 22 cm mo^{-1}. The annual average total exceeds 200 cm y^{-1} (NOAA, 1989).

The frequency that bay waters flood onto a particular island is controlled by the location of the island within Florida Bay's tidal regime and by the elevation of the levee surrounding the island. Islands with a low levee (e.g., Jimmy Key) are wet islands that are easily overwashed by tides. Higher islands (e.g., Cluett Key) are dry islands that are flooded mainly by the spring tides and when bay water levels are at their steric maximum (summer and fall). The frequency of tidal flooding, in turn, controls the salinity of surface waters that collect on the islands; wet islands have the lower-salinity ponds. Undoubtedly, major storms and hurricanes reshape levees from time to time, thus altering the water and salt balance on each island. This periodic restructuring of the levee may explain, in part, why massive mangrove die-off can occur on the interior of some islands following major storms (Ball et al., 1967).

Groundwater

Groundwater on these islands is derived from the ponds that occupy the island interiors. Salinity of groundwater collected from the upper 100 cm of island sediment ranges from as low as 20 g kg^{-1} after a large precipitation event to more than 200 g kg^{-1} during the last stages of pond evaporation (Kramer, 1996). The presence of wind-blown salts mixed in with the upper surface sediments can mask the true origin of the waters recharging the groundwater. For example, using the δD and $\delta^{18}O$ composition of groundwater and surface waters from Cluett Key, Swart et al. (1989b) showed that isotopically light groundwater of meteoric origin can have salinities of 35 g kg^{-1} (essentially equivalent to seawater) as a result of dissolving these surface salts as the water seeps into the ground (Fig. 6-5). Although major changes occur in the upper 100 cm of groundwater associated with seasonal changes in the island's water balance, groundwater below 100 cm shows negligible salinity changes with time and probably represents a time-averaged value of the seasonal changes occurring in the overlying column. Similar processes have been documented in groundwaters of *Spartina* salt-marsh settings (Lord and Church, 1983, Casey and Lasaga, 1987).

Although it is well known that many mud islands in Florida Bay contain hypersaline waters (Davis, 1940; Halley and Steinen, 1979; Swart et al., 1989b), there has not been any extensive study of the islands to determine whether there are systematic patterns in the surface and groundwater between the various islands of different types. Our recent studies (Kramer, 1996) show that the deeper groundwater in most islands has a salinity in excess of 65 g kg^{-1}. There is a tendency for the groundwater salinity in islands in the western portion of Florida Bay to be higher than that in the more eastern islands (Fig. 6-6). This geographic zonation can be attributed to three causes. First, the levees, and the islands themselves, are higher in the western and central portions of Florida Bay and, therefore, less frequently inundated. Second, the northeastern portions of the bay receive more rainfall, which dilutes the surface water and groundwater. Finally, the water of Florida Bay itself is

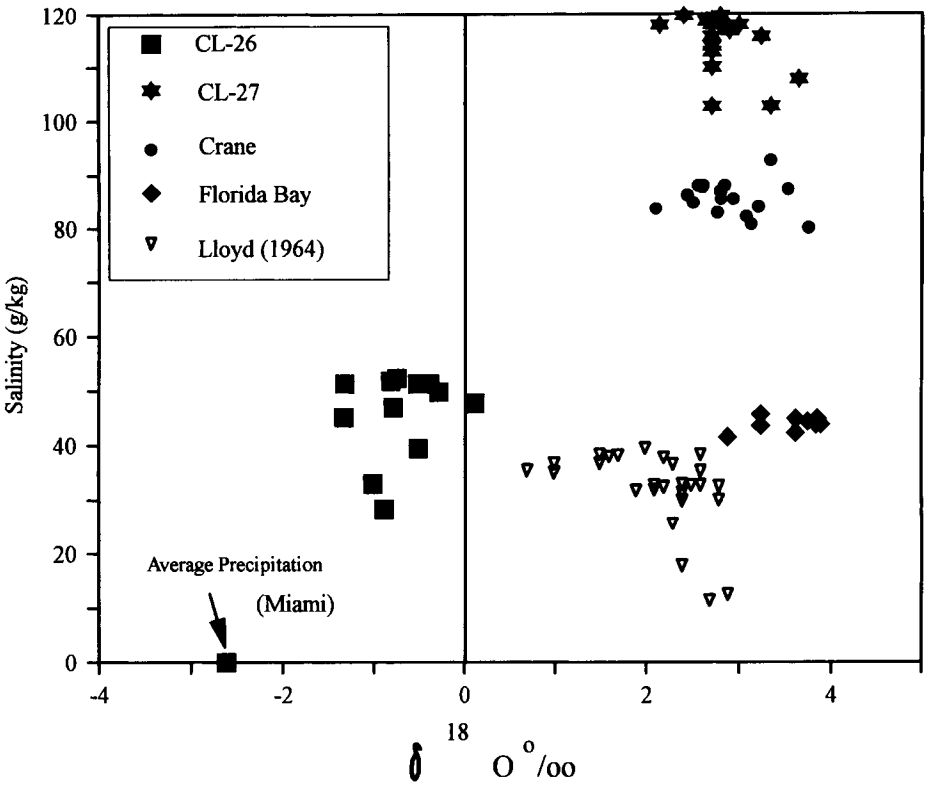


Fig. 6-5. Plot showing $\delta^{18}O$ vs. salinity for Florida Bay water, Miami rainfall, and surface and groundwaters taken from Cluett and Crane Keys. Note that as waters become progressively more evaporated (increasing salinity), they do not get any heavier than +4‰ because of exchange with atmospheric water vapor. Also note that in CL-26 the salinities of 40–50‰ are a result of dissolving surface salts from falling meteoric water. This is shown by the light ^{18}O signature of these waters (−1‰), which are clearly meteoric in origin. (From Swart et al., 1989b.)

not as saline in the northeast part of the bay because of the freshwater runoff from the Everglades.

The movement of saline groundwater in Florida Bay mud islands is becoming known. We are completing a study of the hydrology of two islands, Cluett Key and Jimmy Key as part of a long-term project aimed at quantifying the water flux through island sediments (Kramer et al., 1993; Juster, 1995; Kramer, 1996; Juster et al., 1997). Mechanisms that can drive water through the sediments are topographic head, evaporative pumping (Hsu and Sieganthaler, 1969), and density-driven reflux (Adams and Rhodes, 1960), although the importance of each remains to be fully documented and understood. Hydrological observations on Cluett Key (Juster, 1995; Juster et al., in press) indicate that the pond floor is "perched" or elevated about 10 cm above mean sea level. Thus, a large but variable hydraulic gradient (~0.1) is produced between surface waters and the underlying limestone when the

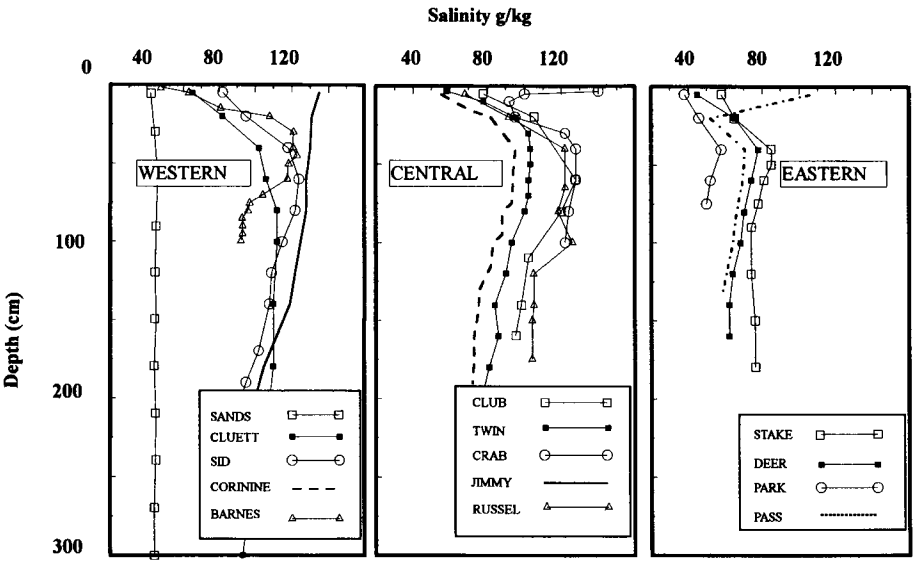


Fig. 6-6. Porewater salinity profiles from 15 islands found throughout Florida Bay showing hypersaline character of the groundwaters. Islands have been divided into western, central, and eastern regions of the Bay. Islands in the east have lower salinities probably due to lower elevation and larger amounts of rainfall.

pond is present. This gradient has the ability to move brines vertically downward and is probably the dominant hydraulic drive on the higher islands. Estimated rates of downward velocities are on the order of 10–25 cm y^{-1} (Kramer et al., 1993; Juster et al., 1997).

CASE STUDY: HYDROGEOCHEMICAL EVIDENCE OF DIAGENESIS

Diagenesis

As a result of the young age of the sediments (< 4,000 y B.P.) and the relatively slow rates of sedimentation (< 1 mm y^{-1}), the diagenetic stabilization of Florida Bay muds is in its early stages. The first study of the porewater geochemistry of the mudbanks in Florida Bay revealed little change in the concentrations of Cl^-, Ca^{2+}, Mg^{2+}, and Sr^{2+} (Berner, 1966). Subsequent studies have shown small, but nevertheless significant, changes in the concentration of SO_4^{2-} (Rosenfeld, 1979) and Ca^{2+} and alkalinity (Walter and Burton, 1990) in the upper portions of cores through the mudbanks. Walter and Burton (1990) suggested that such changes in Ca^{2+}, SO_4^{2-}, and alkalinity in porewaters from mudbanks were probably affected by some type of advection process mediated by bioturbation. These workers proposed that the rate of carbonate dissolution in the mudbanks may in fact be much larger than that indi-

cated by the porewater profiles. According to Walter and Burton (1990, p. 602), "volumetrically significant dissolution may occur" in these sediments.

In contrast to porewaters of mudbanks, groundwater squeezed from cores taken on exposed islands reveal large changes in concentrations of Ca^{2+}, Mg^{2+}, and Sr^{2+}, and SO_4^{2-} throughout the entire section (Swart et al., 1989a; Burns and Swart, 1992) (Fig. 6-7). The direction and the magnitude of these changes, however, are not always the same, and there are large differences in the nature of profiles between various islands. For example, Cluett Key shows a deficit of normalized Ca^{2+} throughout the core, whereas, in Jimmy Key, the normalized Ca^{2+} concentrations are close to that predicted from a simple evaporation model (Fig. 6-7). Differences between these and other islands relate to processes of evaporation, precipitation of minerals such as halite and gypsum, and carbonate dissolution and precipitation.

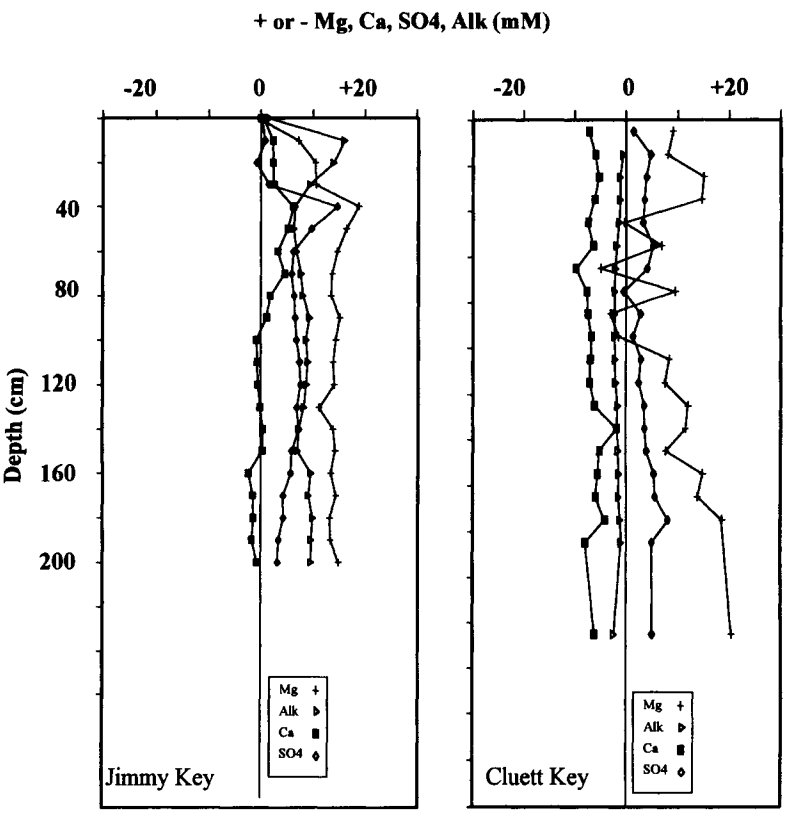


Fig. 6-7. Porewater concentration of Ca^{2+}, Mg^{2+}, SO_4^{2+}, and alkalinity taken from Jimmy and Cluett Keys. Ion concentration is given in relative mM values above or below the concentration that would be expected if Cl^- were behaving conservatively; the value is calculated by:

$$ion_{rel} = ion_{measured} - ion_{seawater} * Cl^-_{measured}/Cl^-_{seawater}.$$

(Data from Burns and Swart, 1992; R. Steinen, unpubl.)

As a result of seasonal cycles discussed previously, islands can dry out completely, which causes gypsum and halite to precipitate on the surface sediments. Although these evaporite minerals are not long-lived in that they are redissolved during subsequent flooding, they do alter the chemistry of the surface water and, consequently, the underlying groundwater. For example, precipitation of gypsum preferentially removes Ca^{2+} and SO_4^{2-} and, therefore, the ratio of these species relative to Cl^- decreases in the residual fluids (Fig. 6-8). In contrast, the ratio increases in the fluid that subsequently dissolves the minerals. The extent to which these processes alter the groundwater chemistry of an island is related to its hydrological balance; thus, a topographically lower, more frequently flooded island, such as Jimmy Key, will tend to have less precipitation of evaporate minerals than the slightly higher and relatively drier Cluett Key. Cross-plots of ion concentrations in the groundwaters reveal some of these processes. For example, the precipitation of calcite removes Ca^{2+} and causes the groundwater to plot below the line one would expect from the simple evaporation of the fluid (evaporation line) (Fig. 6-9B); groundwater in the saline portion of Cluett Key is an example. In contrast, groundwater from Jimmy Key plots near the evaporation line and thus shows relatively little evidence of precipitation.

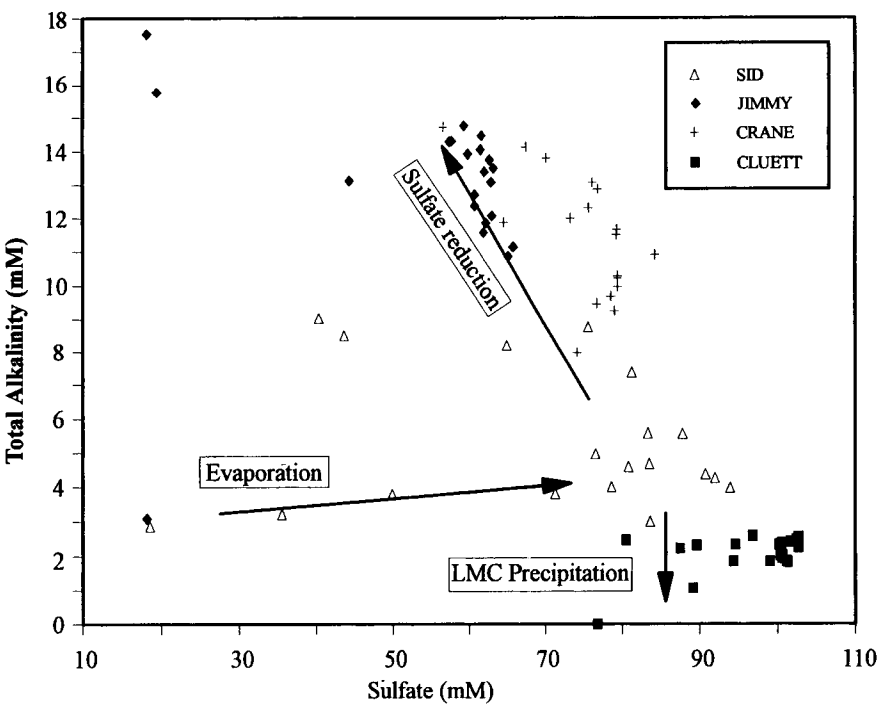


Fig. 6-8. Cross-plot of total alkalinity vs. SO_4^{2-} for four islands from Florida Bay. Evaporation of surface waters raises SO_4^{2-}. Precipitation of calcite lowers alkalinity (typical of "dry islands"). Sulfate reduction lowers sulfate and raises alkalinity (typical of "wet islands").

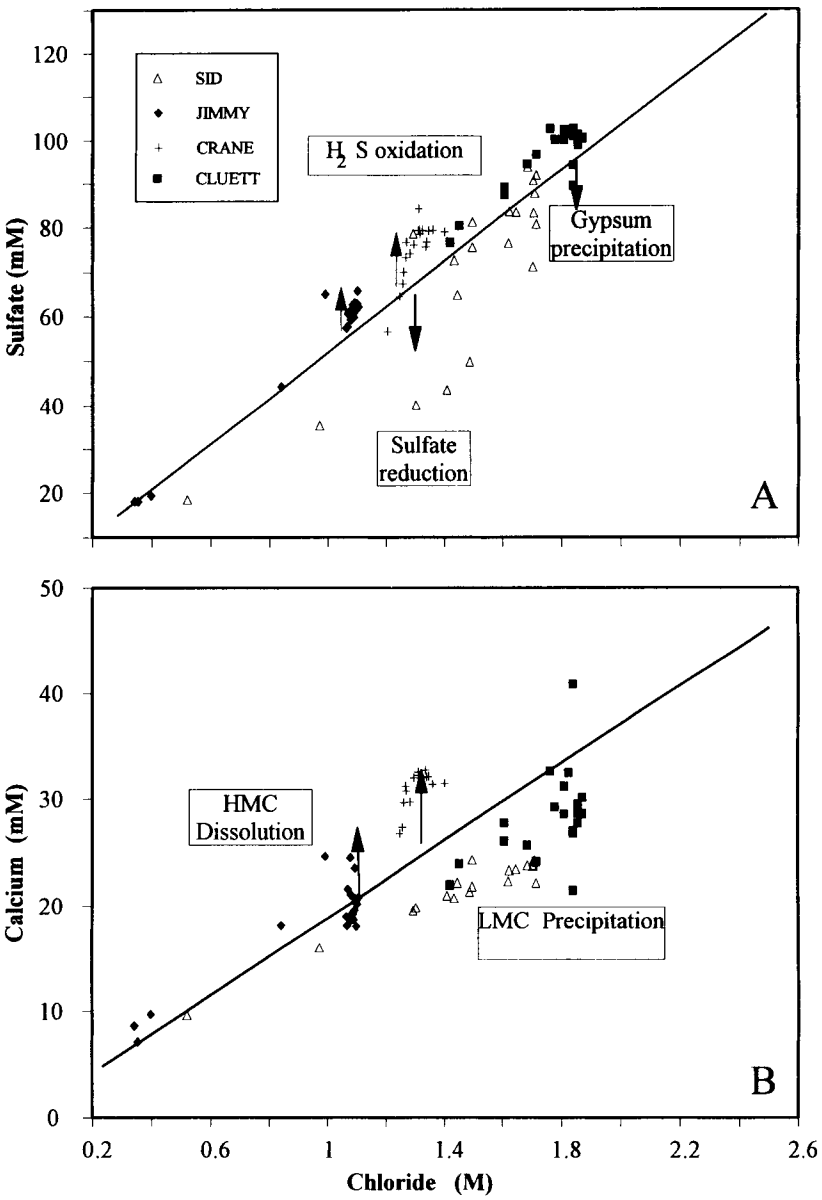


Fig. 6-9. (A) Cross-plot of sulfate vs. chloride. At low concentrations of sulfate, the process of sulfate reduction causes data to fall below the evaporation line. At high concentrations, the data fall below the line as a result of the formation of gypsum. Excess sulfate concentrations such as occur in Jimmy and Crane Keys are postulated to result from the oxidation of H_2S. (B) Cross-plot of calcium vs. chloride. Data falling below the line at high chloride concentrations are thought to reflect the precipitation of LMC. Data above the line arise from dissolution of aragonite and HMC.

The presence of sulfate reduction on most of the islands is evident from the pungent odor of H_2S emanating from the sediment. Jimmy and Crane Keys, however, are notable exceptions that exhibit a slight excess of sulfate in their groundwaters. Although this apparent excess may result from the presence of groundwater deficient in Cl^-, another explanation is that the excess results from oxidation of HS^- to SO_4^{2-} — i.e., the HS^- is produced lower in the sedimentary section by bacterial sulfate reduction and moves upwards through the pore space where it is eventually oxidized producing sulfate. Such a process may be more in evidence in low islands such as Jimmy Key which contain greater concentrations of organic material in the sediments. It should be noted that the sediments of Florida Bay islands differ fundamentally from iron-rich sediments in which the HS^- would react with iron and form iron sulfide minerals. Pyrite is virtually absent in these sediments, except for very low quantities measured in the underlying peats (Davies, 1980).

Sulfate reduction also generates alkalinity and leads to the dissolution of carbonates by the generation of additional carbonic acid. A plot of sulfate vs. alkalinity (Fig. 6-8) shows three main trends. First is the trend which reflects the evaporation of the fluids. Second, precipitation of LMC or aragonite causes a drop in alkalinity with little change in sulfate. Third, sulfate reduction causes a decrease in sulfate and an increase in alkalinity. Based on this type of plot, it appears that islands such as Sid and Cluett Keys experience evaporation followed by precipitation of carbonate and some gypsum, whereas Jimmy and Crane Keys have sulfate reduction coupled with carbonate dissolution.

Carbonate reactions

Carbonate reactions can both decrease or increase the concentration of Ca^{2+} and alkalinity and alter the ratios of Sr^{2+}/Ca^{2+} and Mg^{2+}/Ca^{2+} of the pore fluids. Dissolution of aragonite tends to increase the Ca^{2+}/Cl^- ratio but does not alter the Sr^{2+}/Ca^{2+} ratio appreciably, because aragonite has approximately the same Sr^{2+}/Ca^{2+} ratio as seawater. In contrast, HMC has a lower concentration of Sr^{2+}, and so its dissolution lowers the Sr^{2+}/Ca^{2+} ratio of the groundwater. Precipitation of LMC lowers the groundwater Ca^{2+} content but increases the Sr^{2+}/Ca^{2+} ratio, because the distribution coefficient for Sr^{2+} into calcite is significantly less than unity. Finally, precipitation of dolomite generally lowers the Mg^{2+}/Cl^- ratio and perhaps Mg^{2+}/Ca^{2+}. Depending upon the stoichiometry of the dolomitizing reaction, precipitation of dolomite may also lower the Mg^{2+}/Ca^{2+} ratio. Dolomitization of aragonite generally causes an increase in the Sr^{2+}/Ca^{2+} ratio of the fluid.

Dolomite

The occurrence of dolomite in these sediments is of particular interest, as hypersaline environments have traditionally been places in which dolomite has been thought to form (Hardie, 1987; Land, 1985). Examples of such settings are coastal sabkhas (McKenzie et al., 1980; Patterson and Kinsman, 1981; 1982), tidal flats

(Gebelein et al., 1980; Behrens and Land, 1972; Shinn, 1968), and islands (Murray, 1969). The occurrence of dolomite in the Florida Bay sediments and mud islands has been reported by numerous workers (Taft, 1961; Deffeyes and Martin, 1962; Degens and Epstein, 1964; Friedman and Sanders, 1967; Steinen et al., 1977; Videlock, 1983; Swart et al., 1989a; Andrews, 1991). The dolomite of Florida Bay islands typically consists of small (1–5 μm), euhedral rhombs, intimately intergrown with surrounding micrite and aragonite needles (Fig. 6-10). Dolomites recovered from the bay sediments are larger (> 10 μm) and generally abraded.

Although it is reasonably well established that the dolomite reported in the marine sediments of Florida Bay is of detrital origin, the dolomites within the islands are considered authigenic (Deffeyes and Martin, 1962; Degens and Epstein, 1964). This conclusion is based on the measured ^{14}C activity, petrographic observations, and the $\delta^{13}C$ and $\delta^{18}O$ composition of the dolomite (Swart et al., 1989a). For example, Fig. 6-11 shows a comparison of the $\delta^{13}C$ and $\delta^{18}O$ values of the dolomite retrieved from the marine sediments compared to the dolomite from Crane Key and other sedimentary components. The dolomite studied by Degens and Epstein (1964) has a range of $\delta^{18}O$ values (−1 to + 1‰) that is clearly isotopically too light to have formed from the hypersaline fluids presently typical of the Holocene islands. In contrast, the $\delta^{18}O$ value for Crane Key dolomites (+2‰) is in approximate equilibrium with porewaters throughout the core. $\delta^{13}C$ values (−2 to −3‰) suggest an organic influence.

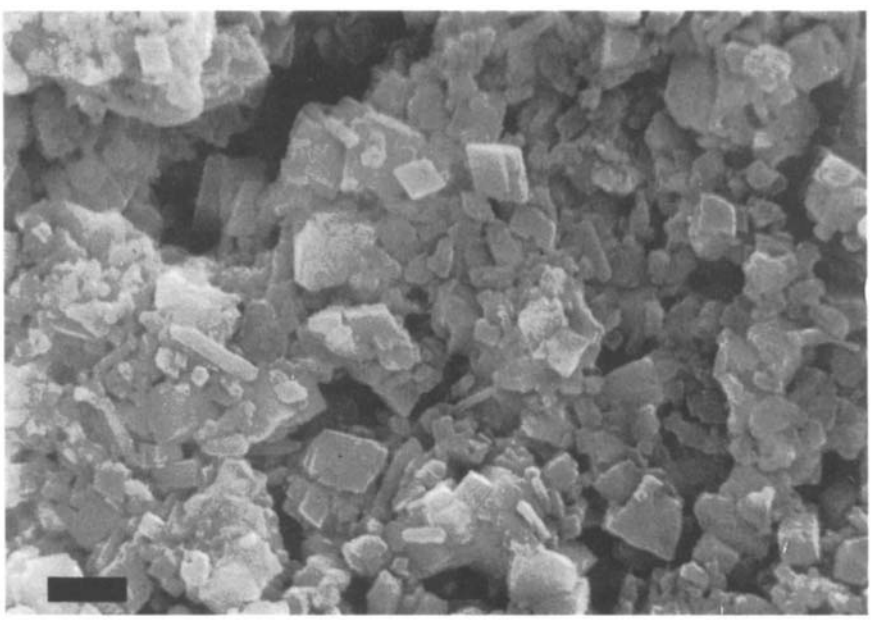


Fig. 6-10. SEM images of isolated dolomite taken from Crane Key showing small size of rhombs (scale bar = 1 μm). (From Swart et al., 1989a.)

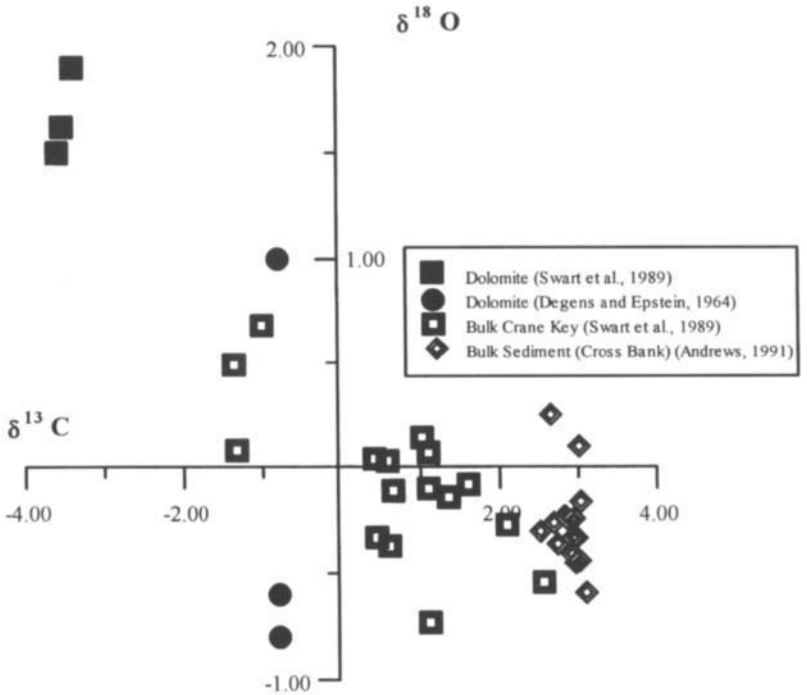


Fig. 6-11. Cross-plot of $\delta^{18}C$ vs. $\delta^{18}O$ of sediments taken from mudbanks (Cross Bank) and islands (Crane Key). Dolomite was isolated from several samples and measured separately. Cross Bank sediments are characteristically heavy in carbon, whereas island sediments become progressively lighter. The light carbon signature for isolated dolomite may indicate that its formation is influenced by microbial processes.

Although there is little doubt regarding the authigenic nature of the dolomite, it is still unknown whether dolomitization is taking place at the present time. In this regard, the most sensitive information we have is from groundwater concentrations of Ca^{2+}, Mg^{2+}, and Sr^{2+}. The behavior of these minor elements during dolomite formation was noted above and leads to revealing cross-plots of Sr^{2+}/Ca^{2+} vs. Ca^{2+}/Cl^{-} and Sr^{2+}/Ca^{2+} vs. Mg^{2+}/Cl^{-} (Figs. 6-12, 6-13). The path of dolomitization is shown on these figures, and, as can be seen, none of the data from the islands that we have studied falls into these fields. Based on these analyses of groundwater from three islands in which dolomite is present, we must conclude that there is little evidence of present-day dolomite precipitation; that is, the dolomite that is present must have formed during an earlier time.

We cannot, however, conclude that *no* dolomite is forming at the present time for there is a finite lower limit determined by the sensitivity of the geochemical analyses. For example, consider dolomitization according to the following stoichiometry:

$$2CaCO_3 + Mg^{2+} = CaMg(CO_3)_2 + Ca^{2+}$$

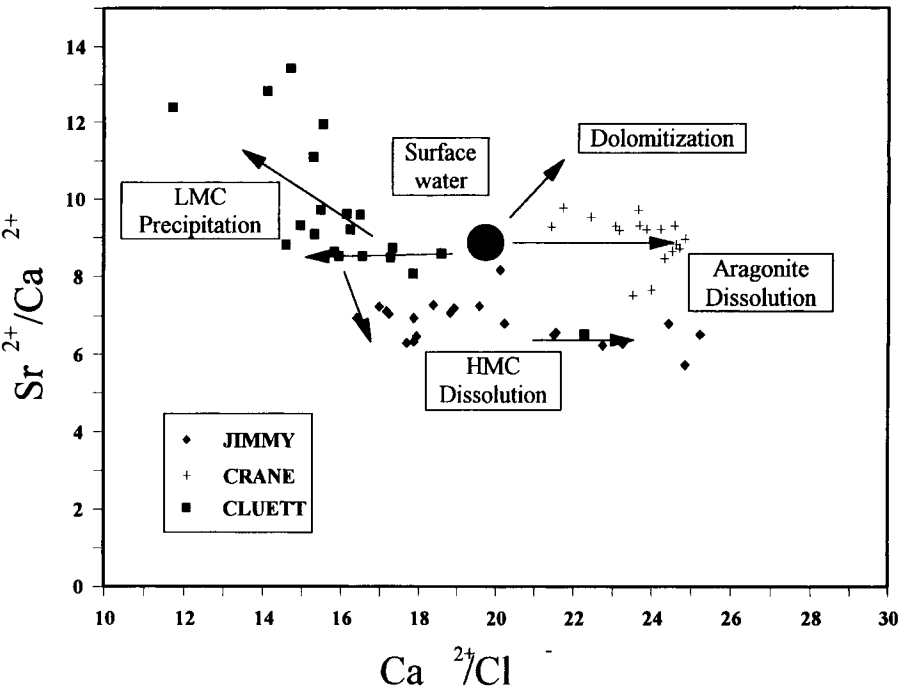


Fig. 6-12. Ratio of Ca^{2+} normalized to Cl^- vs. the Sr^{2+}/Ca^{2+} ratio from three islands, Jimmy, Crane, and Cluett Keys. Increases in the Ca^{2+}/Cl^- ratio can arise from the dissolution of HMC and aragonite, and dolomitization. The reactions may be distinguished from each other by virtue of the relationship with the Sr^{2+}/Ca^{2+} ratio. Aragonite dissolution has little effect on the Sr^{2+}/Ca^{2+} ratio, whereas HMC dissolution decreases the ratio, and dolomitization increases it. Note that none of the data from the islands studied falls in the area expected for dolomitization. Decreases in the Ca^{2+}/Cl^- ratio result from the formation of calcite and gypsum. The formation of both of these minerals increases the Sr^{2+}/Ca^{2+} ratio.

If 1 g of aragonite (density, 2.86 g cm^{-3}; porosity, 50%) is filled completely with seawater, the groundwater would contain only 1.7×10^{-5} M of Mg^{2+}. If we were able to use all the Mg^{2+} for dolomitization, we could dolomitize only 0.03% of the sediment. Assuming, therefore, that we can detect a change of 2 mM Mg^{2+} in the groundwater, then our geochemical methods should be able to detect the formation of as little as 0.002% dolomite in a closed system. This is more sensitive than X-ray diffraction methods by at least three orders of magnitude. Our results, therefore, suggest that if dolomitization is taking place at the present time, the rate must be so low that it does not produce measurable changes in the groundwater.

It is interesting to note that Jimmy Key, a young island, has very low concentrations of dolomite ($< 3\%$) compared to Crane and Cluett Keys which have been islands for much of the history of Florida Bay (Fig. 6-14). Such a correlation between age and amount of dolomite — although preliminary and needing further substantiation — would tend to suggest that the dolomitization is an ongoing

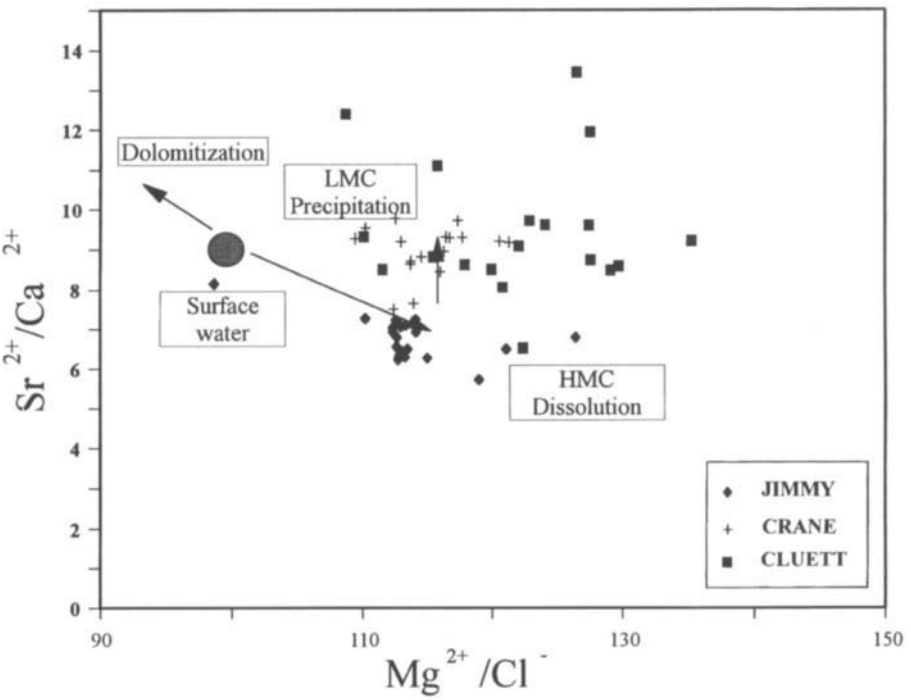


Fig. 6-13. The ratio of Mg^{2+} normalized to Cl^- vs. the Sr^{2+}/Ca^{2+} ratio from three islands, Jimmy, Crane, and Cluett Keys. Increases in the Mg^{2+}/Cl^- ratio can be expected from the dissolution of HMC and the formation of NaCl. No change can be expected in the Mg^{2+}/Cl^- ratio as a result of aragonite dissolution or calcite precipitation. Dolomitization would be manifested by a decrease in the Mg^{2+}/Cl^- and an increase in the Sr^{2+}/Ca^{2+} ratio. As in the case of the Ca^{2+}/Cl^- plot, there is little evidence of dolomitization in the samples studied.

process, perhaps related to the slow passage of the hypersaline groundwater through the sediments. On the other hand, the distribution of significant amounts of dolomite (> 3%) in these older islands is limited to deep layers; the dolomite is not disseminated throughout the column (Swart et al., 1989a; Videlock, 1983). Recent work by Andrews (1991) suggests that dolomite formation is associated with the production of HMC-rich cyanbacterial mats near the surface. Concentrations of dolomite observed at deeper levels in our cores, therefore, may simply be a result of earlier episodes of dolomite formation of the surface sediments of these islands; the dolomitization may have been similar to that occurring on the tidal flats of Andros Island (Shinn et al., 1965).

CONCLUDING REMARKS

The Holocene sediments and islands in Florida Bay have long served as a modern laboratory for the study of ancient carbonate sedimentary sequences. They represent

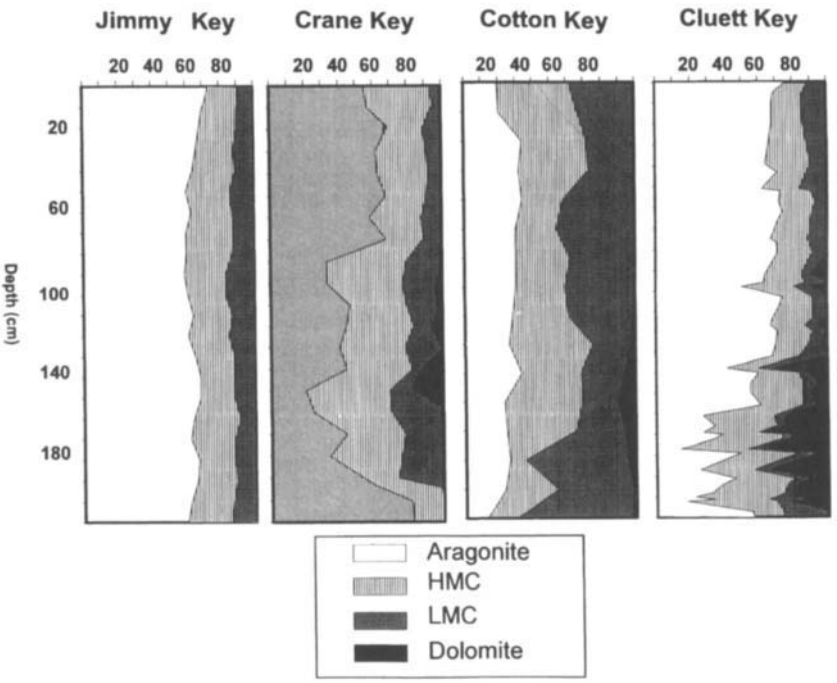


Fig. 6-14. Mineralogy of carbonate sediments taken from four islands within the Bay showing a relatively consistent composition of aragonite, HMC, and LMC, both between different islands and down-core within any given island. The amount of dolomite in any given island varies quite substantially, however, generally increasing with depth and with older islands. (Jimmy Key data from Burns and Swart, 1992; Crane Key data from Swart et al., 1989a; Cluett Key data from Videlock, 1983; Cotton Key data, this chapter.)

a record of a broad array of depositional environments and are undergoing very early stages of diagenesis.

The occurrence of dolomite on the islands has prompted speculation that these unique hydrogeochemical environments may be sites of present-day dolomitization (Friedman and Sanders, 1969; Swart et al., 1989a; Steinen et al., 1977). Others have noted that the islands may be active sites of recrystallization, and this has led to speculation that sediments in this type of island environment may to be converted to calcite and dolomite relatively rapidly. Our geochemical data — though not exhaustive — indicate that recrystallization is taking place in the subsurface of these islands but that the rate is relatively slow, and, when the relatively long residence time of the groundwater is factored in, it appears that the recrystallization may be significant only if the present hydrological conditions persist over long periods of time.

There is no evidence of measurable changes in the Mg^{2+}/Cl^{-} or Sr^{2+}/Ca^{2+} ratios that would suggest that significant dolomitization is presently taking place in the subsurface. We do not rule out the presence of specialized environments of dolomite

formation such as described by Andrews (1991), but these are not widespread. Furthermore, we do not discount the formation of very minor amounts of dolomite throughout the sediment, but in concentrations that do not appreciably alter the hydrogeochemistry. Dolomite formation by this mechanism — like the recrystallization — would be significant only if the present hydrological conditions were stable over extended periods of time. We suggest that the major concentrations of dolomite found within the islands relate to formation during a previous time, perhaps when the dolomite was close to the surface and under conditions similar to those described by Andrews (1991).

ACKNOWLEDGMENTS

We would like to thank the many people who have shared their valuable insights into the history of Florida Bay, particularly Gene Shinn, Randy Steinen, Bob Halley, Hal Wanless, and Robert Ginsburg. Some of the data used in this paper have been generated during class projects prepared by students in the Stable Isotope Laboratory at the University of Miami and by Dr. Randy Steinen at the University of Connecticut. We are indebted to these persons. Recently, we have received extensive help from the Everglades National Park, particularly Mike Robblee and Dewitt Smith and the University of South Florida Hydrogeology Group, particularly Tom Juster and Len Vacher.

REFERENCES

Adams, J.E. and Rhodes, M.L., 1960. Dolomitization by seepage refluxion. Am. Assoc. Petrol. Geol. Bull., 44: 1912–1920.

Andrews, J.E., 1991. Geochemical indicators of depositional and early diagenetic facies of Holocene carbonate muds, and their preservation potential during stabilization. Chem. Geol., 93: 267–289.

Ball, M.M., Shinn, E.A. and Stockman, K.W., 1967. The geologic effects of Hurricane Donna in South Florida. J. Geol., 75: 583–597.

Bathurst, R.G.C., 1971. Carbonate sediments and their diagenesis. Elsevier, Amsterdam, 658 pp.

Behrens, E.W. and Land, L.S., 1972. Subtidal Holocene dolomite, Baffin Bay, Texas. J. Sediment. Petrol., 42: 155–161.

Berner, R.A., 1966. Chemical diagenesis of some modern carbonate sediments. Am. J. Sci., 264: 1–36.

Bosence, D., 1989. Biogenic carbonate production in Florida Bay. Bull. Mar. Sci., 44: 419–433.

Burns, S.J. and Swart, P.K., 1992. Diagenetic processes in Holocene carbonate sediments: Florida Bay mud banks and islands. Sedimentol., 39: 285–304.

Casey, W.H. and Lasaga, A.C., 1987. Modeling solute transport and sulfate reduction in marsh sediments. Geochim. Cosmochim. Acta., 51: 1109–1120.

Craighead, F.C., 1964. Land, mangroves, and hurricanes. Fairchild Tropical Garden Bull., 19: 5–32.

Davies, T.D., 1980. Peat formation in Florida Bay and its significance in interpreting the recent vegetational and geological history of the Bay area. Ph.D. Dissertation, Pennsylvania State Univ., University Park PA, 316 pp.

Davis, J.H., Jr., 1940. The ecology and geologic role of mangroves in Florida. Carnegie Inst. Wash. Pub. 517, Papers of the Dry Tortugas Laboratory, 32: 305–412.

Deffeyes, K.S. and Martin, E.L., 1962. Absence of carbon-14 activity in dolomite from Florida Bay. Science, 136: 782.

Degens E.T. and Epstein, S., 1964. Oxygen and carbon isotope ratios in coexisting calcites and dolomites from recent and ancient sediments. Geochim. Cosmochim. Acta., 28: 23–44.

Enos, P., 1989. Islands in the Bay — A key habitat of Florida Bay. Bull. Mar. Sci., 44: 365–386.

Enos, P. and Perkins, R.D., 1979. Evolution of Florida Bay from island stratigraphy. Geol. Soc. Am. Bull., 90: 59–83.

Enos, P. and Sawatsky, L.H., 1981. Pore networks in Holocene carbonate sediments. J. Sediment. Petrol., 51: 961–985.

Friedman, G.M. and Sanders, J.E., 1967. Origin and occurrence of dolostones. In: G.V. Chiligar, H.J. Bissell and R.W. Fairbridge (Editors), Carbonate Rocks. Origin, Occurrence and Classification. Elsevier, Amsterdam, pp. 267–348.

Gebelein, C.D., Steinen, R.P., Garrett, P., Hoffman, E.J., Queen, J.M. and Plummer, L.N., 1980. Subsurface dolomitization beneath the tidal flats of central west Andros Island, Bahamas. In: D.H. Zenger, J.B. Dunham and R.L. Ethington (Editors), Concepts and Models of Dolomitization. Soc. Econ. Paleontol. Mineral. Spec. Publ., 28: 31–50.

Ginsburg, R.N., 1956. Environmental relationships of grain size and constituent particles in some south Florida carbonate sediments. Am. Assoc. Petrol. Geol. Bull., 40: 2384–2427.

Ginsburg, R.N. and James, N.P., 1974. Holocene carbonate sediments of continental shelves. In: C.A. Burk and C.L. Drake (Editors), The Geology of Continental Margins. Springer-Verlag, Berlin, pp. 137–155.

Ginsburg, R.N. and Lowenstam, H.A., 1958. The influence of marine bottom communities on the depositional environment of sediments. J. Geol., 66: 310–318.

Halley, R.B. and Steinen, R.P., 1979. Ground water observations on small carbonate islands of southern Florida. Southeast Geol. Soc. Publ. 21: 82–89.

Hardie, L.A., 1987. Dolomitization: a critical review of some current views. J. Sediment. Petrol., 57: 166–183.

Hoffmeister, J.E., Stockman, K.W. and Multer, H.G., 1967. Miami Limestone of Florida and its recent Bahamian counterpart. Geol. Soc. Am. Bull., 78: 175–190.

Hsu, K.J. and Siegenthaler, C., 1969. Preliminary experiments and hydrodynamic movement induced by evaporation and their bearing on the dolomite problem. Sedimentol., 12: 11–25.

Juster, T.C., 1995. Mechanisms and rates of seawater circulation through carbonate mud. Ph.D. Dissertation, Univ. South Florida, Tampa, 221 pp.

Juster, T., Kramer, P.A., Vacher, H.L., Swart, P.K. and Stewart, M., 1997. Groundwater flow beneath a hypersaline pond, Cluett Key, Florida Bay, Florida. J. Hydrol., 197: 339–369.

Kramer, P.A., 1996. The hydrogeology and early diagenesis of Holocene mud-islands in Florida Bay. Ph.D. Dissertation, Univ. Miami, Coral Gables FL, 247 pp.

Kramer, P.A., Swart, P.K., Vacher, H.L. and Juster, T.C., 1993. Use of tritium to estimate residence times of hyper-saline ground water from a Holocene island in Florida Bay, USA (abstr.). Geol. Soc. Am. Abstr. Programs, 25: A91.

Land, L., 1985. The origin of massive dolomite. J. Geol. Educ., 33: 112–125.

Lord, C.J. and Church, T.M., 1983. The geochemistry of salt marshes: Sedimentary ion diffusion, sulfate reduction, and pyritization. Geochim. Cosmochim. Acta., 47: 1381–1391.

McKenzie, J.A., Hsu, K.J. and Schneider, J.F., 1980. Movement of subsurface waters under the Sabkha, Abu Dhabi, UAE, and it's relationship to evaporative dolomite genesis. In: D.H. Zenger, J.B. Dunham and R.L. Ethington (Editors), Concepts and Models of Dolomitization. Soc. Econ. Paleontol. Mineral. Spec. Publ., 28: 11–30.

Murray R.C., 1969. Hydrology of south Bonaire, Netherlands Antilles — A rock selective dolomitization model. J. Sediment. Petrol., 39: 1007–1013.

Nelson, J.E. and Ginsburg, R.N., 1986. Calcium carbonate production of epibionts on Thalassia in Florida Bay. J. Sediment. Petrol., 56: 622–628.

NOAA (National Oceanographic and Atmospheric Administration), 1989. Climatological data, No. 32, Annual summary, Florida, 1989. National Climate Data Center, Asheville NC, 36 pp.

Patterson, R.J. and Kinsman, D.J.J., 1981. Hydrologic framework of a Sabkha along Arabian Gulf. Am. Assoc. Petrol. Geol. Bull., 66: 1457–1475.

Patterson, R.J. and Kinsman, D.J.J., 1982. Formation of diagenetic dolomite in coastal sabkhas along the Arabian (Persian) Gulf. Am. Assoc. Petrol. Geol. Bull., 66: 28–43.

Roberts, H.H., Rouse, L.J., Walker, N.D. and Hudson, J.H., 1982. Cold water stress in Florida Bay and northern Bahamas: A product of winter cold-air outbreaks. J. Sediment. Petrol., 52: 0145–0155.

Roberts, H.H., Whelan, T. and Smith, W.G., 1977. Holocene sedimentation at Cape Sable, South Florida. Sediment. Geol., 18: 25–60.

Rosenfeld, J.K., 1979. Interstitial water and sediment chemistry of two Florida Bay cores. J. Sediment. Petrol., 49: 989–994.

Scholl, D.W., 1966. Florida Bay: A modern site of limestone formation. In: R.W. Fairbridge (Editor), Encyclopedia of Earth Sciences. McGraw-Hill, New York, pp. 282–288.

Shinn, E.A., 1968. Selective dolomitization of recent sedimentary structures. J. Sediment. Petrol., 38: 612–616.

Shinn, E.A., Ginsburg, R.N. and Lloyd, R.M., 1965. Recent supratidal dolomitization from Andros Island, Bahamas. In: L.C. Pray and R.C. Murray (Editors), Dolomitization and Limestone Diagenesis. Soc. Econ. Paleontol. Mineral. Spec. Publ., 13: 112–123.

Steinen, R.P., Halley, R.B. and Videlock, S.L., 1977. Holocene dolomite locality in Florida Bay. Am. Assoc. Petrol. Geol. Bull., 61: 833.

Swart, P.K., Berler, D., McNeill, D., Guzikowski, M., Harrison, S.A. and Dedick, E., 1989a. Interstitial water geochemistry and carbonate diagenesis in the sub-surface of a Holocene mud island in Florida Bay. Bull. Mar. Sci., 44: 490–514.

Swart, P.K., Sternberg, L.D., Steinen, R. and Harrison, S.A., 1989b. Controls on the oxygen and hydrogen isotopic composition of waters of Florida Bay, USA. Chem. Geol., 79: 113–123.

Tabeau, C.W., 1968. Man in the Everglades: 200 years of human history in Everglades National Park. Univ. Miami Press, Coral Gables, 192 pp.

Taft, W.H., 1961. Authigenic dolomite in modern sediments along the southern coast of Florida. Science, 134: 561–562.

Taft, W.H. and Harbaugh, J.W., 1964. Modern carbonate sediments of southern Florida, Bahamas, and Espirito Santo Island, Baja California. Stanford Univ. Publ. Geol. Sci., 8(2), 133 pp.

Tagett, M.G., 1988. Stratigraphy, nucleation, and dynamic growth history of a Holocene mudbank complex, Dildo Key mudbank, western Florida Bay. M.S. Thesis, Univ. Miami, Coral Gables FL, 266 pp.

Videlock, S.L., 1983. The stratigraphy and sedimentology of Cluett Key, Florida Bay. M.S. Thesis, Univ. Conn., Storrs, 161 pp.

Walter, L.M. and Burton, E.A., 1990. Dissolution of recent platform carbonate sediments in marine pore fluids. Am. J. Sci., 290: 601–643.

Wanless, H.R. and Tagett, M.G., 1989. Origin, growth and evolution of carbonate mudbanks in Florida Bay. Bull. Mar. Sci., 44: 454–489.

Geology and Hydrogeology of Carbonate Islands. Developments in Sedimentology 54
edited by H.L. Vacher and T. Quinn
© 1997 Elsevier Science B.V. All rights reserved.

Chapter 7

GEOLOGY OF COASTAL ISLANDS, NORTHEASTERN YUCATAN PENINSULA

WILLIAM C. WARD

INTRODUCTION

The northeastern coast of the Yucatan Peninsula of Mexico was one of the first parts of North America explored by the Spanish in the early 1500s, but for the next 450 years this area remained relatively remote and undeveloped. Archaeological studies (Andrews, 1985) show that the Maya occupied the Caribbean coast and offshore islands since at least the Late Formative Period (300 B.C. to A.D. 300). Several major Maya communities were developed in the area during the Classic Period (A.D. 300–900/1100), and population along the Caribbean coast increased substantially during the Late Postclassic Period (A.D. 1200–1517). Following the Spanish conquest, population declined and many sites were abandoned. Then, after the Caste War (1847–1855), hostile Maya virtually closed eastern Yucatan to outsiders for half a century.

The first highway connecting the Caribbean coast to the more populated north-central part of the peninsula was constructed during the 1950s, and gradually the area opened to tourism. Since the 1970s, carbonate islands off the Caribbean coast of the northeastern peninsula have been the destinations for hordes of international travelers. The islands of Cancun and Cozumel (Fig. 7-1), in particular, are hubs of ever-expanding tourist facilities. These two resorts illustrate the two types of carbonate islands of the Mexican Caribbean Sea. The narrow, elongate islands of Mujeres, Cancun, Contoy, and Blanca (Fig. 7-1) are largely ridges of Quaternary eolianites. The broad, low-lying island of Cozumel is the emergent part of a horst block that is capped by Pleistocene limestones. These two types of islands will be discussed separately.

EOLIAN-RIDGE ISLANDS

Regional setting

Marine and climatic setting. Off the northeastern coast of the Yucatan Peninsula, the continental shelf narrows southward from the broad Gulf of Mexico ramp (Campeche Bank) to a Caribbean shelf only a few kilometers wide (Fig. 7-1). Northward of Puerto Morelos (Fig. 7-1), the ramp slopes seaward at about 4–15 m km^{-1} between the shoreline and the 180 m (100 fm) isobath (U.S. Navy Hydrographic Office Chart 966); this ramp probably is terraced at several levels. Just off the

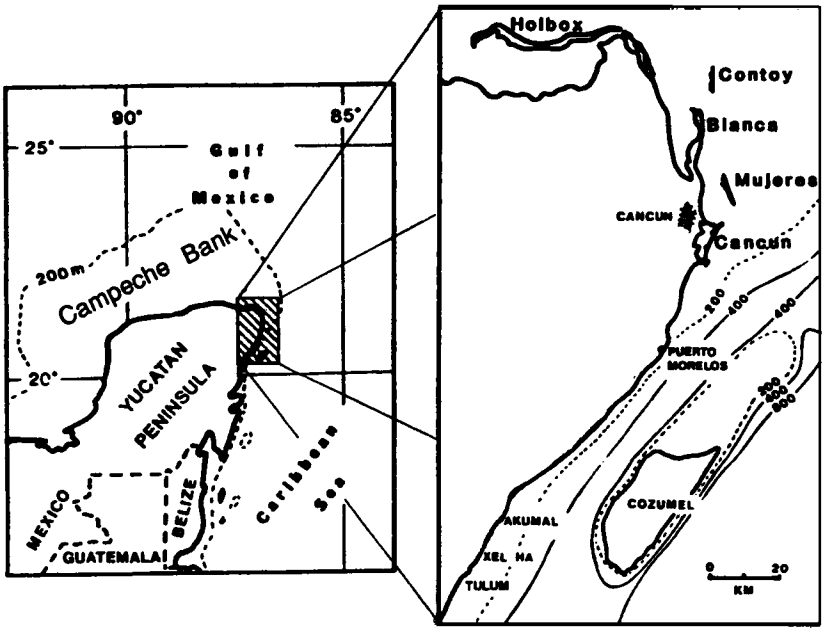


Fig. 7-1. Locations of carbonate islands of northeastern Yucatan Peninsula. Bathymetric contours in meters. (Modified after Uchupi, 1973; reprinted by permission of the American Association of Petroleum Geologists.)

coast there is a wave-cut(?) terrace at a depth of 9 m, and seaward of this level, the bottom slopes rather steeply to an apparent terrace lying at a depth of about 18 m. In addition, the submerged terraces at depths of 30–36, 51–63, and 90–135 m on the western Campeche Bank (Logan et al., 1969) probably extend into this area. At the northeastern cape of the peninsula, a terrace about 3.5 m deep underlies the coastal lagoons (Brady, 1971). Along the seaward margin of the 9-m terrace are the four eolian-ridge islands. The mainland adjacent to this area is a low-lying, jungle-covered karst platform of Quaternary and Tertiary limestones. No streams drain the northeastern peninsula; therefore, the shallow-marine sediment is purely carbonate, free of terrigenous detritus.

A portion of the strong northward-flowing Yucatan Current (Leipper, 1954; Logan et al., 1969) sweeps across the inner ramp and in some places flows at 1–2 kn. Tidal range is small, about 0.3–0.6 m. Salinities in this region are normal marine, except in many coastal areas where brackish groundwater discharges. Surface-water temperatures are about 28°C during the summer and about 24°C during the winter (Leipper, 1954). Temperature variation on the mainland is moderate, from summer highs of about 37°C to winter lows of about 15°C. Hurricanes and tropical storms occur frequently in this area. Normally rainfall in the coastal area is about 100 cm y^{-1}, with the rainy season generally from May to September. Regional rainfall provides enough recharge to the unconfined aquifer system under eastern

Yucatan that groundwater almost constantly discharges through the mainland limestones into many coastal areas (Hanshaw and Back, 1980).

Tectonic setting. The Yucatan Peninsula-Campeche Bank is a large carbonate platform, gently tilted toward the Gulf of Mexico on the north and bounded by a zone of fractures and normal faults on the east (e.g., Weidie, 1985; Muehlberger, 1992). This faulting, which apparently began during the Cretaceous and continued through much of the Cenozoic (Vedder et al., 1971), resulted in the steep eastern margin of the peninsula. The Caribbean coast south of Isla Cancun (Fig. 7-1) approximately parallels the trend of these faults.

Geologic history

During the last Pleistocene interglacial period when sea level in this area stood 5–6 m higher than present, a series of beach ridges accreted along the mainland coast of the northeastern Yucatan Peninsula (Ward and Brady, 1979) (Fig. 7-2A). Even when sea level fell several meters during the onset of the last glacial period, production of carbonate sand on the shallow ramp apparently remained high, because a series of carbonate sand ridges built up along the seaward margin of the terrace, which is now 9 m below sea level (Fig. 7-2A). The lower few meters of these elongate sand bodies may be shallow-subtidal or beach deposits, but the bulk is eolian dune sand (Ward, 1975). Different Pleistocene dune ridges in this area have different grain constituents, reflecting changes in the composition of nearshore sands during accumulation of these dunes. A greater fall in sea level left these carbonate sands exposed to subaerial diagenesis during the rest of the glacial period.

With the Holocene rise of sea level, the eolian ridges were partly eroded and inundated. The islands of Contoy, Mujeres, and Cancun are largely remnants of these Pleistocene dune ridges (Fig. 7-2B). The position and alignment of Isla Blanca suggest that it, too, is underlain by a Pleistocene dune ridge. Fig. 7-2B shows the coastal land areas that have been built up by progradation of beach and dune ridges and mangrove swamps during the Holocene highstand of sea level.

There are no reliable age dates on the Pleistocene dune rock that forms the framework of the carbonate islands of northeastern Yucatan. Depositional morphology of the eolian ridges is well preserved in many places, and there are no wave-cut notches or overlying marine deposits above the present sea level. This indicates that none of the dunes existed at the time beach ridges along the mainland were deposited. Uranium-series age dates on corals show that these Pleistocene beach ridges along the mainland were deposited at 122 ka (Szabo et al., 1978), during the oxygen isotope substage 5e (CLIMAP project members, 1984). The carbonate dunes, therefore, accumulated after substage 5e, during sea-level stands probably 5–10 m lower than present. Depth to the base of the Pleistocene dune rocks is unknown; rock cropping out 3 m below sea level on the Caribbean side of Isla Mujeres appears to be eolianite. Pebbles of mollusk wackestone among the Holocene beach gravel suggest that Pleistocene (or older?) marine limestones crop out several meters deep in front of Isla Mujeres.

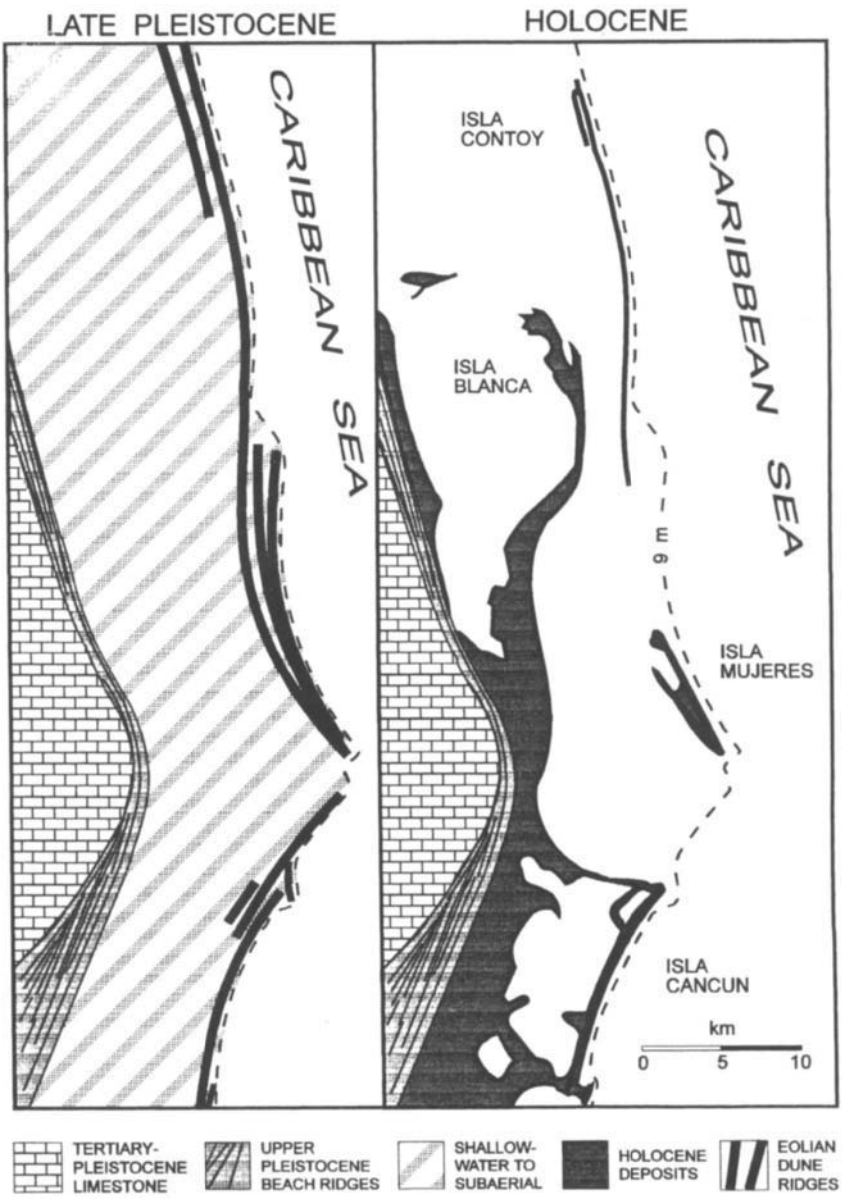


Fig. 7-2. A (left). Traces of late Pleistocene beach and dune ridges. B (right). Present configuration of coastal areas. (After Ward, 1985.)

Presumably deposition of the Pleistocene eolianites was during the regressive phase of the 122-ka highstand, before the shallow-marine source area for the carbonate grains was lowered too far below the 9-m terrace. Alternatively, there were two periods when sea level might have been high enough to supply carbonate grains

for the eolian ridges — during substages 5c at ~105 ka, and 5a at ~80 ka (Muhs, 1992). It is doubtful that any of the Pleistocene eolianites were deposited when the sea was at today's level, but some of them could have accumulated during one or perhaps both of the late stage-5 substages.

Stratigraphy

Ward (1975) separated the Quaternary dune rocks into three Pleistocene units and two Holocene units on the basis of grain composition, diagenetic characteristics, and geomorphic relationships (Fig. 7-3). These five units are treated as informal

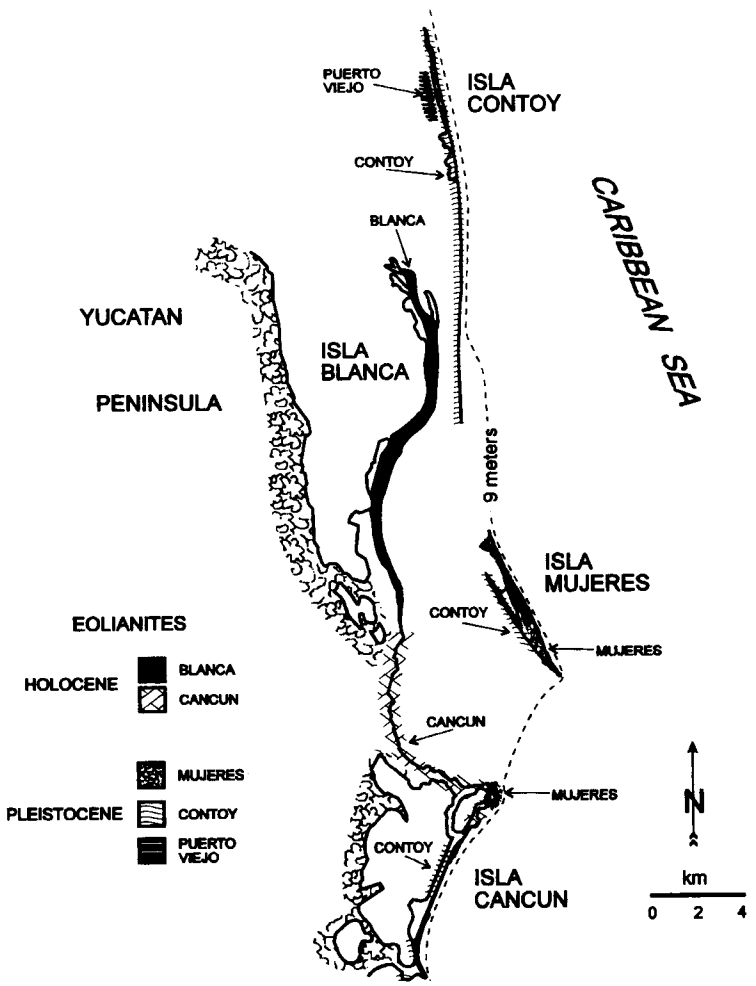


Fig. 7-3. Quaternary eolianites of northeastern Yucatan Peninsula. (Modified after Ward, 1975; reprinted by permission of the American Association of Petroleum Geologists.)

morphostratigraphic units, called eolianites. For the Pleistocene dune rocks, the most landward ridge (Puerto Viejo eolianite of Isla Contoy) is presumed to be the oldest, and the most seaward ridge (Mujeres eolianite) is the youngest. On Isla Mujeres, the Mujeres eolianite overlies the middle ridge of Contoy eolianite. The nature of the boundary between these eolianites is unknown; the contact is obscured by weathering and vegetative cover. Judging from outcrops in this vicinity, no conspicuous soil zone is developed on the Puerto Viejo eolianite. Older Holocene dunes of the Cancun eolianite are overlain by the Blanca eolianite in the central part of Isla Cancun. This contact also is poorly exposed.

Isla Contoy

The island of Contoy, about 13 km offshore (Fig. 7-1), is a major rookery for cormorants, frigate birds, pelicans, boobies, terns and other sea birds and also is a nesting ground for sea turtles. It is a national park protected from development of extensive tourist facilities.

Isla Contoy (Fig. 7-4) is about 8 km long and less than 1 km wide. The main elements of the island are remnants of Pleistocene dune ridges. These eolianite ridges are connected by Holocene sand bars on the northern and southern ends of the island. Between the ridges are shallow, muddy lagoons bordered by mangrove swamps.

On the leeward coast, a row of eolian hillocks, about 10 m high on its southern end at Puerto Viejo (Fig. 7-4), gradually decreases in elevation to below sea level on the northern end. These limestone hills are overgrown by low shrubs and cactus. The limestone is the Puerto Viejo eolianite (Fig. 7-3), which is cross-bedded, fine- to medium-grained ooid grainstone. About 90% of the grains are coated, with 40% having cortices more than 30 μm thick. Common ooid nuclei are peloids and fragments of *Halimeda*, red algae, and mollusks. Depositional morphology of the Pleistocene dunes is fairly well preserved. Steeper cross-beds (at least 15°) dip northwest to southwest, predominantly N80W to S60W. Rhizoliths are less abundant in this eolianite than in the other Pleistocene dune rocks. A discontinuous thin calcrete caps the Puerto Viejo eolianite in some places; apparently much of it was removed by recent erosion.

About half the Caribbean coast of Isla Contoy is rocky with small pocket beaches. Low sea cliffs of wave-eroded eolianite rise as high as 3 m above the intertidal zone, and these cliffs are topped by vegetated Holocene sand dunes as high as 12 m above sea level. The other half of the windward shore, especially the northern part, is edged by stretches of steep beaches. Medium- to coarse-grained beach sands on the eastern coast are composed of bioclasts of mollusks, red algae, echinoids, and coral and lithoclasts of dolostone and limestone. Dolostone grains give the Caribbean beaches of Isla Contoy a light-brown color, in contrast to the typical white beaches of other islands. Source of the dolostone lithoclasts apparently is Tertiary(?) dolostone that crops out below sea level at the northeastern cape of the peninsula. Beach sands on the northern coast of Contoy are polished and rounded, reflecting the normal high

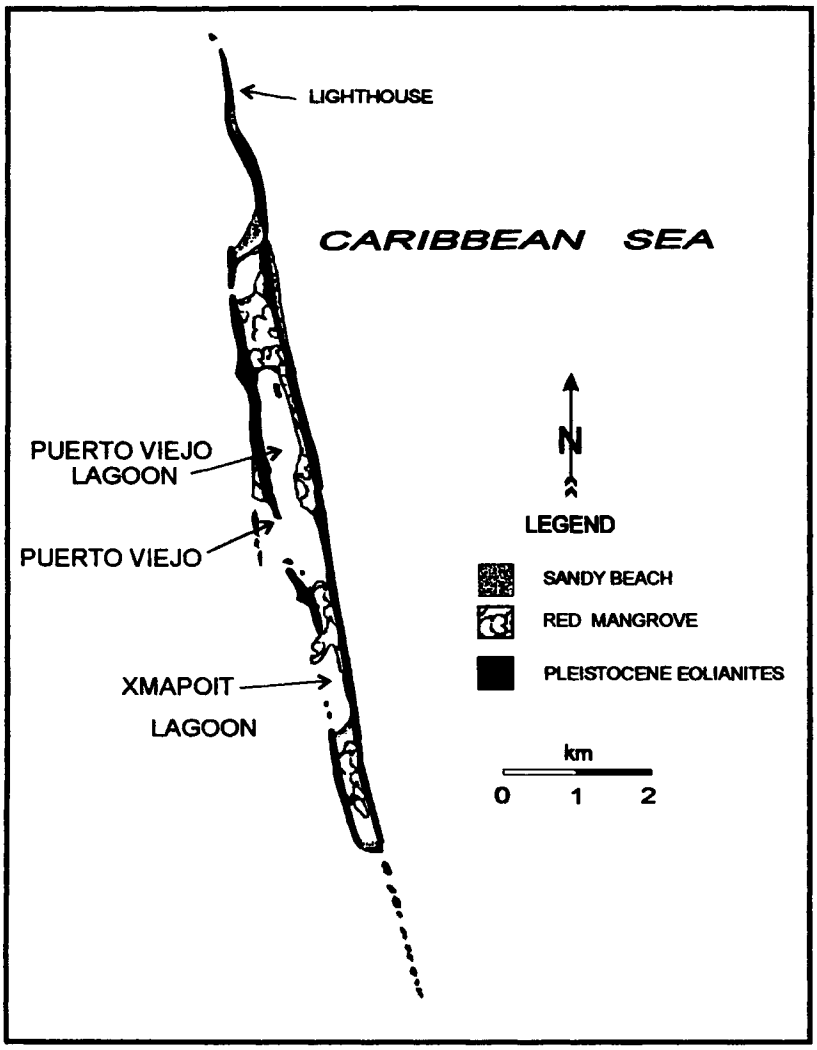


Fig. 7-4. Isla Contoy. (Modified after Ward, 1975; reprinted by permission of the American Association of Petroleum Geologists.)

wave energy in that area. Hurricane-generated waves have piled up ridges of imbricated boulders and cobbles of eolianite and dolostone 1–3 m above the high tide mark on both the northern and southern quarters of the Caribbean shore.

The eastern ridge of Isla Contoy is the Contoy eolianite (Fig. 7-3), which is cross-bedded, bimodal, fine- and medium-grained ooid grainstone. About 85% of the grains are thinly coated, with 80% of the cortices less than 10 μm thick. Ooid nuclei are predominantly *Halimeda* and peloids. This eolianite is capped by a discontinuous yellow-brown to reddish-brown subaerial crust (laminated caliche) up to several

centimeters thick, and caliche-cored rhizoliths are abundant on the northern end of the island.

For about 15 km south of Isla Contoy, waves break over a rocky, knife-edge continuation of the eastern ridge. This remnant of the eolianite ridge emerges less than one meter during low tide, and it marks the seaward edge of the 9-m terrace. The subaqueous continuation of this line of rocks can be traced into the westerly ridge of Isla Mujeres (Fig. 7-2).

Isla Mujeres

"Punta Mujeres" appeared on sixteenth century maps of the Yucatan coast, the name probably given by Grijalva in 1518 or Cortes in 1519. Tales that Amazon-type women inhabited the area, or perhaps the discovery of many "female" idols in stone temples on the southern end of this island, inspired the explorers to choose the name "Mujeres". Isla Mujeres was the major tourist center in this part of the Yucatan Peninsula ten years before the existence of the town of Cancun.

Isla Mujeres is formed by three main ridges of Pleistocene dune rock. The oldest dune ridge, forming three-fourths of the western side of the island, is less than 6 m in elevation and strikes N30W (Fig. 7-5). On the Caribbean side, two younger ridges strike N22W, intersecting the oldest dune line about 2 km northwest of the southern tip. At this intersection, where the younger eolian sands were blown atop the earlier dunes, the crest of the island is 30 m above sea level, which is the highest elevation in all of the northeastern Yucatan Peninsula. From this high elevation on the southern end of the island, the younger island ridges slope northwestward to an elevation of only a few meters at the northern point.

The northward divergence of the oldest ridge from the two younger ridges forms a protected crotch which partly encloses a bay and lagoon (Fig. 7-5). Near the middle of Isla Mujeres, three hypersaline lakes lie in swales between the limestone ridges (Ward et al., 1970). The Caribbean shore is rocky with small pocket beaches. The strait-side of the island also is rocky except for 1.5 km of beach just south of mid-island. The village is built on a large triangle of sand accreted onto the lee side of the northern end of the middle eolian ridge (Fig. 7-5).

The major limestone ridges of Isla Mujeres are remnants of the Mujeres eolianite (Fig. 7-3). In contrast to the other Pleistocene eolianites, this dune rock contains an average of only 9% coated grains. Predominant grain types in this bimodal fine- and medium-grained skeletal grainstone are noncoated *Halimeda*, mollusks, red algae, benthic foraminifers, and peloids. Spectacular cross-beds on the southern end of the island have amplitudes up to at least 15 m. Leeward cross-bed dip angles are commonly 28–32°; the maximum is 39°. Direction of steep cross-bedding is predominantly N80W to S70W.

Rhizoliths are conspicuously abundant in the 3–5 m interval below the subaerial crust which caps the Mujeres eolianite. Caliche profiles 5–20 cm thick are extensively developed on this eolianite. Typically these profiles consist of a few centimeters of micritized eolianite overlain by a few centimeters of yellow-brown to orange-brown

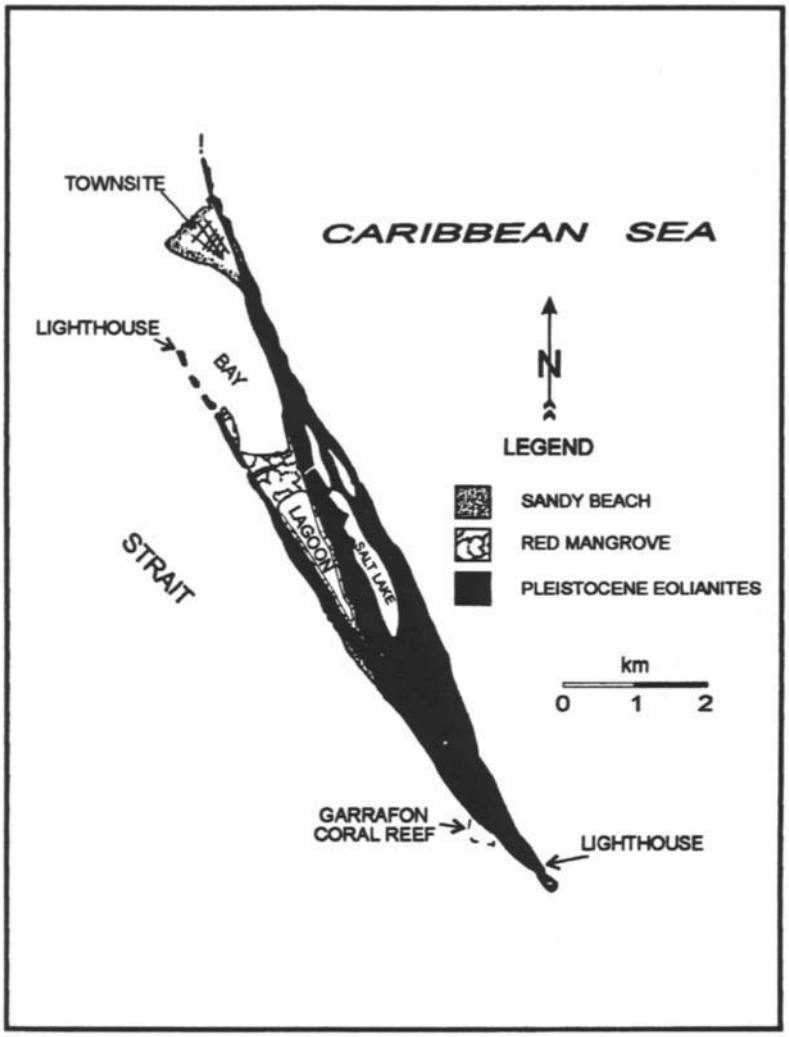


Fig. 7-5. Isla Mujeres in 1968, before cultural developments altered many of the natural features. (Modified after Ward, 1975; reprinted by permission of the American Association of Petroleum Geologists.)

laminated micritic crusts. In some places, laminated layers are overlain by several centimeters of in situ conglomerate or pisolite. A pale yellowish-brown "protosol" about 30 cm thick separates some eolianites within the younger ridge of Mujeres eolianite. This unbedded calcarenite contains abundant land snails and, in a few places, fossilized cocoons of soil insects. Karstic solution holes less than a meter in diameter pit the surface in many places, and a large cylindrical sinkhole (cenote) is developed near the center of the island.

Isla Cancun

The internationally known resort island of Cancun is an elongate complex of Pleistocene and Holocene dune ridges, almost 13 km long and less than 1 km wide (Fig. 7-6). Punta Nisuc on the south and Punta Cancun on the north are remnants of Pleistocene eolian ridges (Fig. 7-2). From these rocky points, Holocene tombolos extend toward the mainland. Complete connection is prevented by tidal

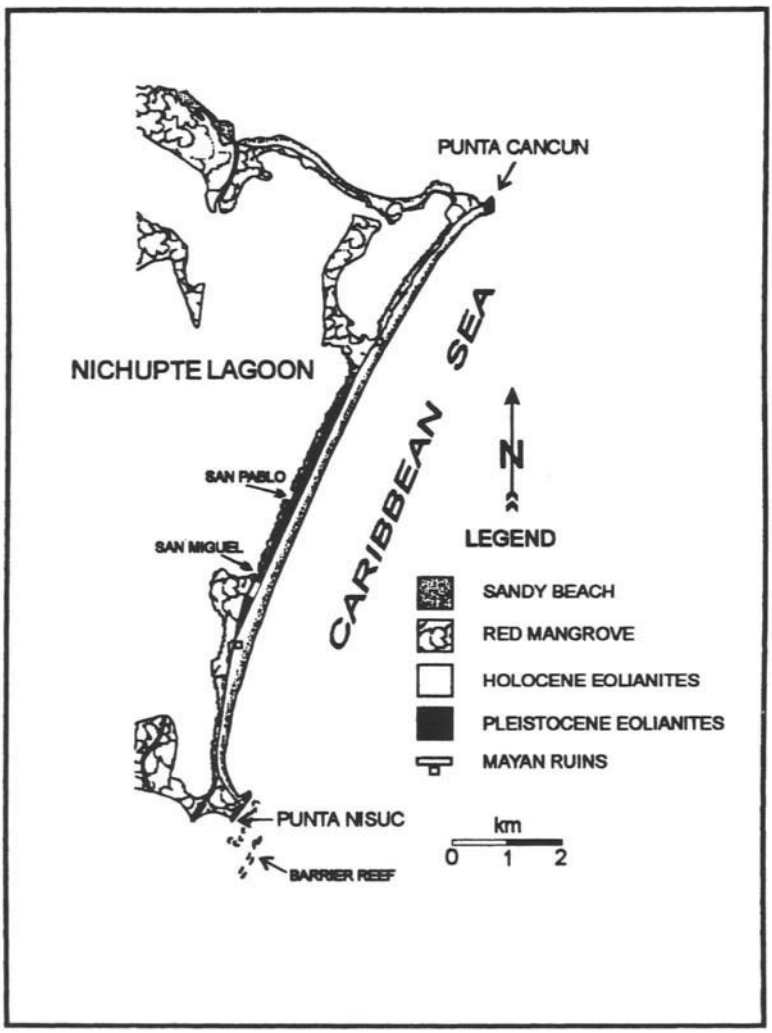


Fig. 7-6. Isla Cancun in 1968, before tourist developments altered many of the natural features. (Modified after Ward, 1975; reprinted by permission of the American Association of Petroleum Geologists.)

channels at each end of Nichupte Lagoon behind the island (Fig. 7-6). Except at the two ends, the entire Caribbean shore is a brilliantly white beach of ooid sand. Back of the beach, fine- to medium-grained thinly coated skeletal sand is blown into dunes that climb up older Holocene dunes, building up an eolian ridge as high as 17 m above sea level. The dunes here are stacked vertically because there is no room for progradation of strandline deposits in front of Isla Cancun, where the sea deepens rapidly. Rapid lithification of the dune sands has created a ridge of Holocene limestone, which now serves as the foundation for the numerous luxury hotels.

At the base of the Holocene eolianite on the northern end of the island are lenticular conglomeratic storm layers containing rounded pebbles and cobbles of corals, conchs, and pelecypods mixed with angular blocks of oolitic grainstone (Holocene beachrock and eolianite). The mollusks give radiocarbon ages which show that the older Holocene eolianite on this island is younger than 3000 y B.P.

The older Holocene dune rock, the Cancun eolianite (Fig. 7-3), is composed of about 80% coated grains with relatively thick cortices. About 70% of the ooid coatings are over 10 μm thick, and 20% are over 30 μm thick. The most abundant ooid nuclei are *Halimeda* fragments. The Cancun eolianite is highly cross-bedded with steepest leeward cross-beds dipping predominantly northwest to north. Horizontal and vertical rhizoliths are found in several zones. These rhizoliths are grainy and weakly cemented. Rhizoliths with hard cores are scarce in the Holocene eolianite; they are abundant in the Pleistocene eolianites on this island.

In the middle of the island, the Cancun eolianite is overlain by the Blanca eolianite (Fig. 7-3). This younger eolianite is composed of about 90% ooids with thin coatings. About 45% of these grains have cortices less than 10 μm thick. Main constituents are thinly coated red algae, mollusks, and lithoclasts. These grain types are being coated today in the high-energy surf and intertidal zones in front of Isla Cancun.

Two ridges of Pleistocene eolianite are exposed 2–3 m above sea level on the lagoon side of the line of Holocene eolianites. The dune rocks are similar to the Contoy eolianite, as is the eolianite at Punta Nisuc. The Pleistocene rock of Punta Cancun is like the Mujeres eolianite.

Isla Blanca

Isla Blanca is a low barrier island about 9 km long and nearly 1 km wide (Fig. 7-7). On its southern end, the island is tied to a peninsula that projects northward from the mainland in the vicinity of Puerto Juarez (Fig. 7-1). The western side of this peninsula and Isla Blanca is formed by a series of Holocene beach ridges, washover lobes, and tidal-channel deposits. This complex passes seaward into a series of dune ridges (Fig. 7-7). The third and fourth ridges landward of the modern beach contain the largest dunes, some as high as 3.5 m. These Holocene dunes are in early stages of lithification. Swales between the dunes are heavily vegetated with shrubs. Coastal erosion at mid-island has truncated the four youngest dune ridges,

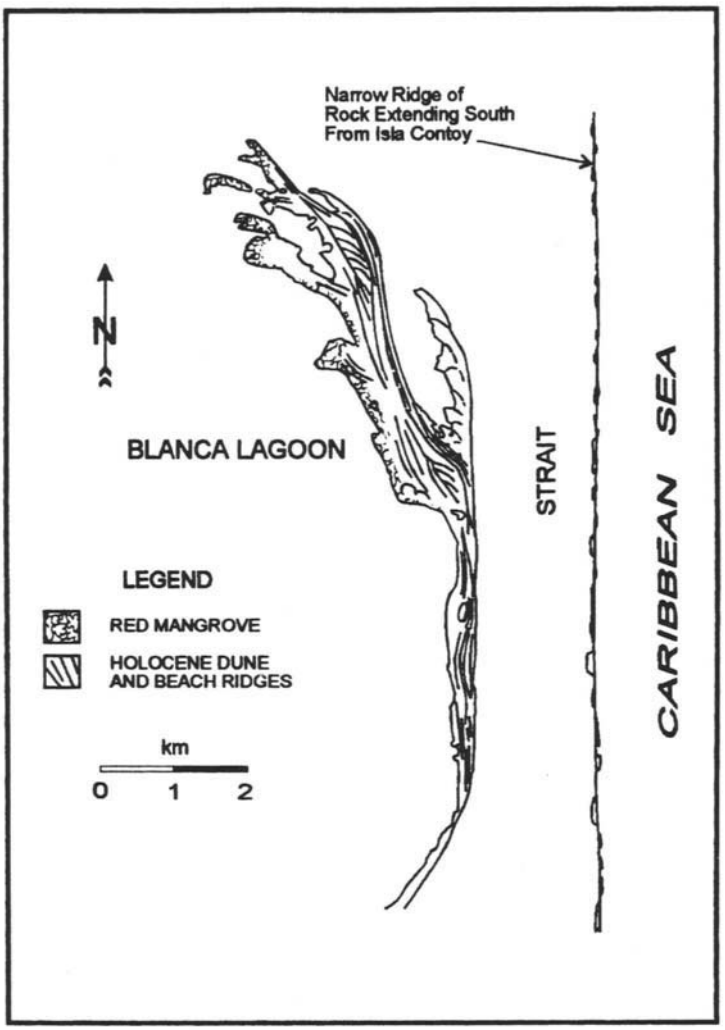


Fig. 7-7. Isla Blanca. (Modified after Ward, 1975; reprinted by permission of the American Association of Petroleum Geologists.)

and the interiors of the dunes are exposed above the beach. On the north end of Isla Blanca, finger-like recurved spits project northwestward in the downcurrent direction.

Isla Blanca dune sand is very well sorted and ranges from fine- to medium-grained. The weakly lithified dunes of this area are included in the Blanca eolianite (Fig. 3). On Isla Blanca these dune rocks are composed of over 90% thinly coated grains, about 80% of which have cortices less than 10 μm thick. Grain types are *Halimeda*, peloids, red algae, and mollusks.

FAULT-BLOCK ISLAND: ISLA COZUMEL

Regional setting

Marine and climatic setting. Cozumel island, about 20 km off the Caribbean coast of the Yucatan Peninsula (Fig. 7-8), was a prominent Mayan trading center and religious cite dating back to Late Formative times (300 B.C. to A.D. 300). The island is about 36 km long and 15 km wide, with an area of about 540 km^2. Average elevation is about 5 m, but some hills and ridges are as high as 10 m. Between the island and the mainland, water depths are as much as 400 m (Uchupi, 1973); on the seaward side of Cozumel, depths are greater (Fig. 7-8). The Yucatan Current moves northward along both the eastern and western coasts of the island. Tides are approximately 0.3–0.5 m.

Cozumel has a subtropical climate with seasonal rainfall, high humidity, and nearly constant warm temperatures. Prevailing winds are from the northeast to southeast. Tropical storms and hurricanes commonly hit the island.

Tectonic setting. Cozumel island is on a horst of a block-faulted continental margin adjacent to the 4,400-m-deep Yucatan Basin (Vedder et al., 1971; Uchupi, 1973). In this area, the fault blocks trend northeasterly, and Cozumel is on the southern end of a block that extends northward to the submerged Arrowsmith Bank (Fig. 7-8). Movement along these normal faults probably began in the Cretaceous

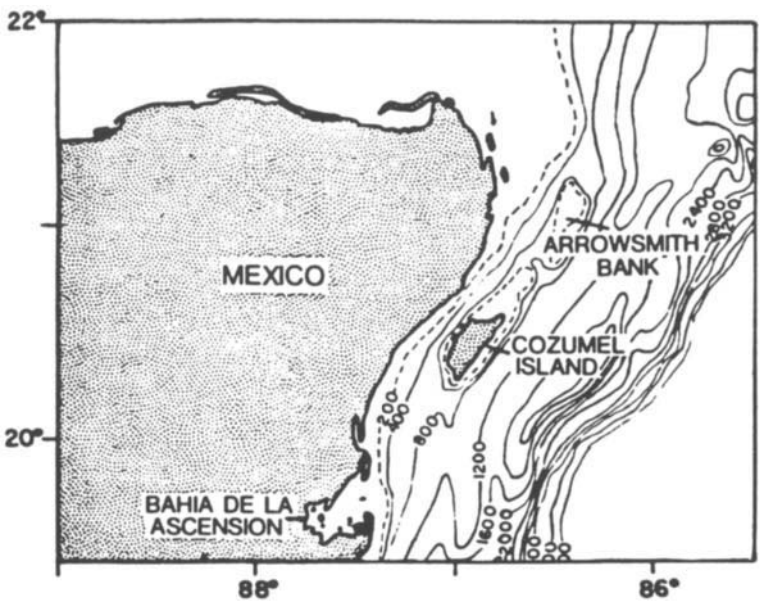


Fig. 7-8. Eastern margin of the Yucatan Peninsula showing location of Cozumel horst block. (From Spaw, 1978; after Uchupi, 1973.)

and continued throughout most of the Tertiary (Dillon and Vedder, 1973). Comparison of upper Pleistocene facies on the Yucatan Peninsula and Cozumel indicates that there has been no differential movement of these two areas during the late Quaternary (Spaw, 1978).

Geologic history

The Yucatan Peninsula has been a carbonate-evaporite platform since the Jurassic (Lopez-Ramos, 1975). During the late Mesozoic and Cenozoic, block faulting created a series of horsts and grabens along the eastern margin of the platform. The high blocks became isolated carbonate banks, at least during the Quaternary. Limestones exposed at the surface on Isla Cozumel record two periods of submergence and two periods of exposure during the late Pleistocene. Cropping out in the bottoms of some quarries is shallow-marine limestone that was deposited during an interglacial highstand of sea level (pre-substage 5e). This unit is capped by a yellow-brown laminated subaerial crust (Caliche I, Spaw, 1978), which, in turn, is overlain by a package of shallow-marine limestones with some eolianites. A coral from the reef facies of this upper unit dates at 121 ± 26 ka (Szabo et al., 1978). The eolianites are somewhat younger; they were deposited when sea level was at least a few meters lower than the present sea level, either during the close of substage 5e or during substages 5c and 5a. The upper unit, in turn, is capped by a widespread laminated calcrete (Caliche II) that developed during the last glacial period. With the Holocene sea-level rise, only the crest of the carbonate platform was left exposed. The modern shoreline is mostly rocky with short stretches of sandy beach. No study is published on the modern carbonate system around Cozumel, except for the coral-reef tracts that flourish on the southwestern leeward margin (Fenner, 1988) and the red-algal buildups on the windward side (Boyd et al., 1963).

Stratigraphy

The Pleistocene strata of Cozumel are divided into two major depositional units, bounded by the two calcretes, which serve as stratigraphic markers (Spaw, 1978). The two lithofacies recognized below the lower caliche crust are included in one unit; the nine shallow-marine lithofacies between the lower caliche and the upper caliche are included in the other unit. In addition, this upper unit includes eolianite, which is at the top of the Pleistocene section in some places.

Sub-Caliche I facies. Two facies below the lower subaerial crust are exposed in quarries in the central and eastern parts of the island (Spaw, 1978). One facies is coralline wackestone, and the other is molluscan wackestone. Both of them accumulated on a broad submerged bank with scattered patch reefs.

Super-Caliche I facies. The distribution of the super-Caliche I lithofacies is shown on Fig. 7-9. Three coral-reef facies rim the outer margins of the island. Other

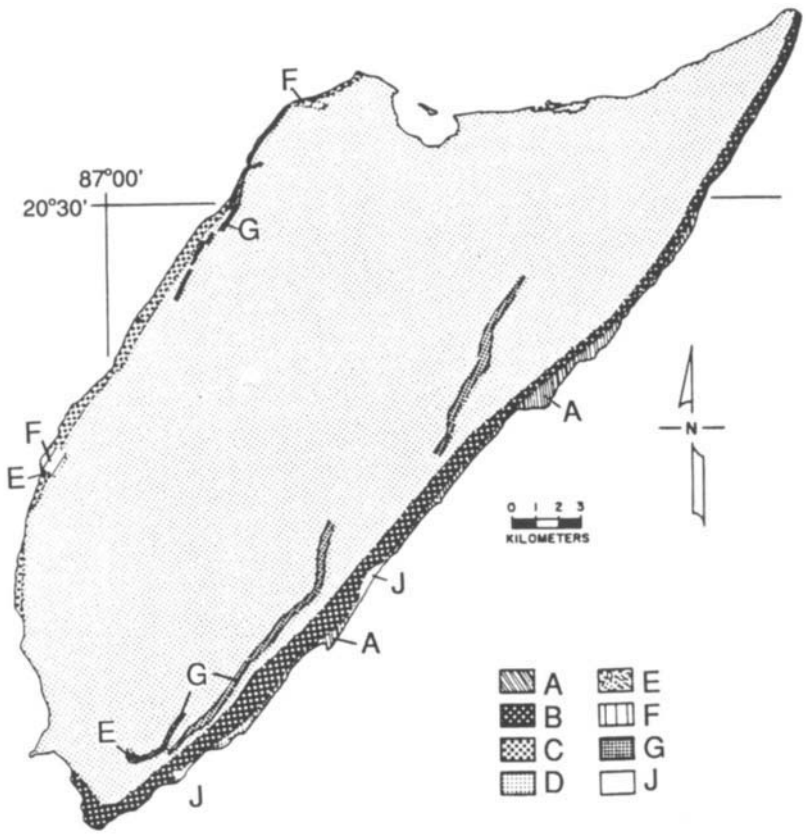


Fig. 7-9. Distribution of super-Caliche I facies in upper Pleistocene limestones of Isla Cozumel (after Spaw, 1978). Key: A, windward, outer coral facies; B, windward, inner coral facies; C, leeward coral facies; D, burrowed molluscan grainstone and packstone facies; E, bank-interior mollusk coquina; F, cross-bedded grainstone and packstone facies; G, seaward-dipping, parallel-laminated grainstone and packstone facies; J, cross-bedded eolianite facies.

contemporary facies are ridge-associated skeletal and oolitic grainstone-packstone and more widespread burrowed skeletal grainstone-packstone.

Facies A forms a 150-m-wide strip of flat-lying coral-bearing limestone interspersed with reef mounds along the eastern coast. The mounds are zoned with vertical *Agaricia* fronds dominating the top and center of the mounds and massive heads of *Diploria* and *Montastrea* and columnar *Montastrea* on the periphery. This reef tract is capped by Caliche II, except where it underlies Pleistocene eolianite.

Facies B crops out in a flat area about 150 m inland of the eastern coast. This unit contains a variety of small corals characteristic of the inner reef flat, including *Acropora cervicornis*, *Porites furcata*, *Manicina mayori*, *Montastrea annularis*, and small *Siderastrea* and *Diploria*. Grainstone-packstone layers in this facies are rich in coral, red algae, and mollusks. Caliche II covers this unit.

Facies C is exposed along most of the western coast. This unit contains abundant corals in growth position, including large *Diploria*, massive and columnar *Montastrea annularis*, and *Acropora cervicornis*. In some places this facies is capped by Caliche II, but in many places it is overlain by grainstone of Facies E.

Facies D is burrowed molluscan grainstone and packstone, probably deposited in a broad area stabilized by seagrass. Mollusks, peloids, red algae, foraminifers, *Porites*, and *Halimeda* are common constituents. Facies D is directly overlain by Caliche II, except where it underlies ridges of grainstone of Facies F.

Facies E is a bank-interior coquina that crops out at only two sites. Constituents are highly diverse and abundant mollusks, with red algae, peloids, benthic foraminifers, and *Halimeda*. At the eastern exposure, this facies rests on Caliche I; at the western exposure, it overlies the leeward reef tract.

Ridge-related facies, Facies F and G, represent bank-interior shoals. These grainstone-packstone ridges on Cozumel are of two types: linear ridges and broad high areas. Linear ridges are located on both the eastern and western sides of the island. One eastern ridge is 10 km long, 240 m wide, and rises 5–8.6 m above sea level; a western ridge is 5 km long, 50 m wide, and up to 6.8 m above sea level. The other broad high areas are 1 km by 0.5 km, 2–4.5 m high, and occur on the southwestern coast. Facies F is cross-bedded grainstone and packstone with cross-bed amplitudes of 4–26 cm. Main constituents are mollusks and peloids in the eastern ridge and ooids in the western ridge. Other grain types are *Halimeda*, coral, red algae, foraminifers, and bryozoans. Facies F overlies Facies D and in most places is overlain by beach deposits (Facies G). Facies G consists of gently seaward dipping, parallel-laminated grainstone and packstone composed of ooids, red algae, *Halimeda*, foraminifers, bryozoans, and echinoids. Caliche II overlies this ridge-crest facies.

Facies H is large-scale trough-cross-bedded grainstone-packstone found in only three west-coast localities. Amplitude of cross-beds is 32–150 cm. This lithofacies is laterally equivalent to Facies D and underlies Facies F, suggesting deposition in scour channels within the seagrass shoals. Mollusks, *Halimeda*, red algae, and ooids are common constituents.

Facies I is planar-cross-bedded grainstone cropping out on the northwest coast adjacent to the leeward coral-reef tract and underlying Facies F. Large-scale planar cross-beds strike N4E and dip 28–31°NW. These probably are accretionary foresets filling a pass through the lee-side reef. Megafauna include abundant mollusks, massive *Diploria* heads, and fragments of *Acropora cervicornis*.

Eolianite. Facies J (Fig. 7-10), cross-bedded well-sorted eolianite, is the youngest Pleistocene facies on Isla Cozumel. High-angle cross-beds dip landward. Red algae and *Halimeda* are the most common grain types, and rhizoliths are abundant in places. This rock type underlies ridges and dome-shaped hills on the southeastern coast. This unit overlies reef Facies A on the land, apparently without a well-developed weathered zone at the top of the reef (exposures of this contact are poor). The base of the dune rock passes below sea level at the coastline. This eolianite is capped by Caliche II.

	Oxygen Isotopic Stage		Eolian-Ridge Islands (Ward, 1975)		Cozumel (Spaw, 1978)	Yucatan Coast (Ward and Brady,1979; Ward,1985)
Holocene	1		Blanca Eolianite Cancun Eolianite	Lagoon Mud Beach Deposits	Coral Reef Beach Deposits	Coral Reef Lagoon Muds Beach Sediments Mangrove Swamps
Pleistocene	2		Caliche crust		Caliche II	Caliche crust
	3					
	4					
	5	A	? Mujeres Eolianite		Eolianite	Tulum Eolianite
		B				
		C	? Contoy Eolianite P. Viejo Eolianite			
		D				
		E			Super-Caliche I Facies	Strandline Grainstones: Coral Reef-Lagoon Limest.
	6				Caliche I	Caliche Crust
	7 ?				Sub-Caliche I Facies	Shallow-Marine Limestone and Dolomite

Fig. 7-10. Correlation chart showing stratigraphic relationships of Pleistocene and Holocene carbonates on islands and the mainland coast of northeastern Yucatan.

REGIONAL RELATIONS

Pleistocene reef limestones, lagoonal packstone-wackestones, strandline grainstones, and calcretes are exposed in quarries and low sea cliffs along the Caribbean coast of the Yucatan Peninsula from the northern cape to Tulum (Fig. 7-1). These shallow-marine and subaerial limestones are similar in elevation, sedimentology, stratigraphy, and age to similar limestones found on Isla Cozumel (Fig. 7-10). In addition, the single ridge of upper Pleistocene eolianite on the mainland coast near Tulum is in a similar stratigraphic position to eolianites of Isla Cozumel and those of the islands off the northeastern part of the peninsula (Fig. 7-10). Holocene eolianites (Fig. 7-10) were deposited along the northeastern shoreline that is adjacent to the narrow ramp, but these are absent south of Isla Cancun, where the margins of the peninsula and offshore platforms are steep.

The correlative upper Pleistocene limestones reflect the same history of late Quaternary sea-level fluctuation for the eastern Yucatan coast and the offshore carbonate islands. The similar elevations of these age-equivalent rocks also suggests there has been little or no differential structural movement along this portion of the Yucatan continental margin for at least the last 200 ky. Judging from the similarity of the elevations of upper Pleistocene limestone of Yucatan and those of substage-5e

limestones in stable areas of the Caribbean, there has been no appreciable subsidence or uplift of the eastern Yucatan Peninsula after mid-Pleistocene (Szabo et al., 1978).

CASE STUDY: INFLUENCE OF CLIMATE ON EARLY DIAGENESIS OF CARBONATE EOLIANITES

During the late Pleistocene and again during the Holocene, carbonate dune rocks accumulated along the same part of the northeastern coast of the Yucatan Peninsula (Fig. 7-3). The parts of the eolianites that are presently above sea level have always been above the water table; therefore, only vadose diagenesis is recorded in these grainstones. The Pleistocene eolianites were deposited and lithified after the peak of the sea-level fluctuation of the corresponding interglacial; the Holocene eolianites were deposited and lithified during or slightly before the sea-level peak of their corresponding interglacial. These sets of eolianites, therefore, record histories of early vadose diagenesis at different positions on their respective sea-level curve and different climate regimes.

Diagenetic features

Caliche. In the field, the most striking difference in the older and younger eolianites is the presence of caliche crusts and abundance of caliche-cored rhizoliths in the Pleistocene dune rocks and their rarity in the Holocene rocks.

Cements. The Pleistocene and Holocene eolianites also look dissimilar in thin section. Much of the initial intergranular cement in the Pleistocene dune rocks is more finely crystalline than that in the younger dune rocks. Furthermore, some cement types common in the Pleistocene eolianites are absent in the Holocene rocks.

Holocene cement. In the weakly indurated Blanca eolianite (younger Holocene), average crystal size of the sparry calcite cement is 10–20 μm, with a few crystals as large as 60 μm and larger overgrowths on echinoid fragments. In the more indurated Cancun eolianite (older Holocene), cement crystals average 15–30 μm, with equant crystals as large as 80 μm and columnar crystals up to 170 μm long. Meniscus and pendulous cements are well developed in many layers of the Holocene eolianites (Fig. 7-11).

Pleistocene cement. Initial intergranular cements in the Pleistocene eolianites are irregular rinds of microcrystalline calcite (less than 5 μm) and coarser blocky sparry calcite. The proportion of early sparry calcite cement is greatest in the Puerto Viejo eolianite (oldest Pleistocene eolianite) and less in the Mujeres eolianite (youngest Pleistocene eolianite). Microcrystalline cement is dominant where the interstitial pores also contain root-hair sheaths and small rhizoliths. Microcrystalline-calcite

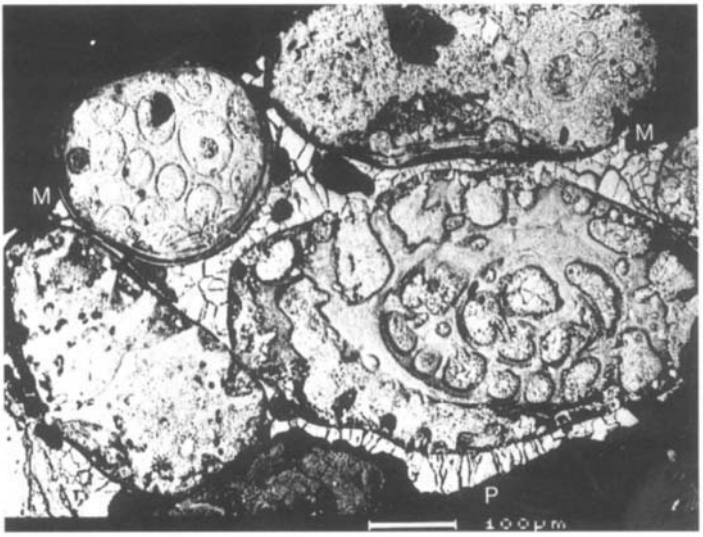


Fig. 7-11. Back-scattered-electron image of Holocene eolianite showing pendulous (P) and meniscus (M) calcite cements. Black area is pore space. Grains are coated with thin cortices, which are partly removed by dissolution.

root-hair sheaths (Fig. 7-12) are common in the Pleistocene eolianites but absent in the Holocene dune rocks. Another vadose cement type found exclusively in the Pleistocene eolianites is needle-fiber calcite (Ward, 1975; McKee and Ward, 1983). *Microcodium*, diagenetic structures composed of calcite prisms (Klappa, 1978), occur in some Pleistocene eolianites but not in the Holocene eolianites.

Metastable mineralogy. Pleistocene dune rocks of northeastern Yucatan retain a relatively high proportion of their original aragonite. The Mujeres eolianite, the youngest Pleistocene unit, also retains much of the original skeletal Mg-calcite, generally the least stable carbonate mineral in freshwater regimes. The younger Holocene eolianite is losing its metastable mineralogy at a rate which would accomplish total stabilization to calcite in roughly 20 ky (Ward, 1975). Most aragonitic coatings of ooids in the Holocene dune rocks show ample evidence of dissolution by vadose waters.

Climatic influence on diagenesis

Judging from the mineralogy of the Yucatan eolianites, the younger Holocene dune rock is progressing faster along the diagenetic route toward calcitization than are the Pleistocene eolianites. Residence time in the vadose zone, then, is not the sole controlling factor in stabilization (i.e., replacement by low-Mg calcite) of the originally aragonitic and Mg-calcitic grains. The retention of metastable mineralogy in eolianites probably depends on the climate during early subaerial diagenesis.

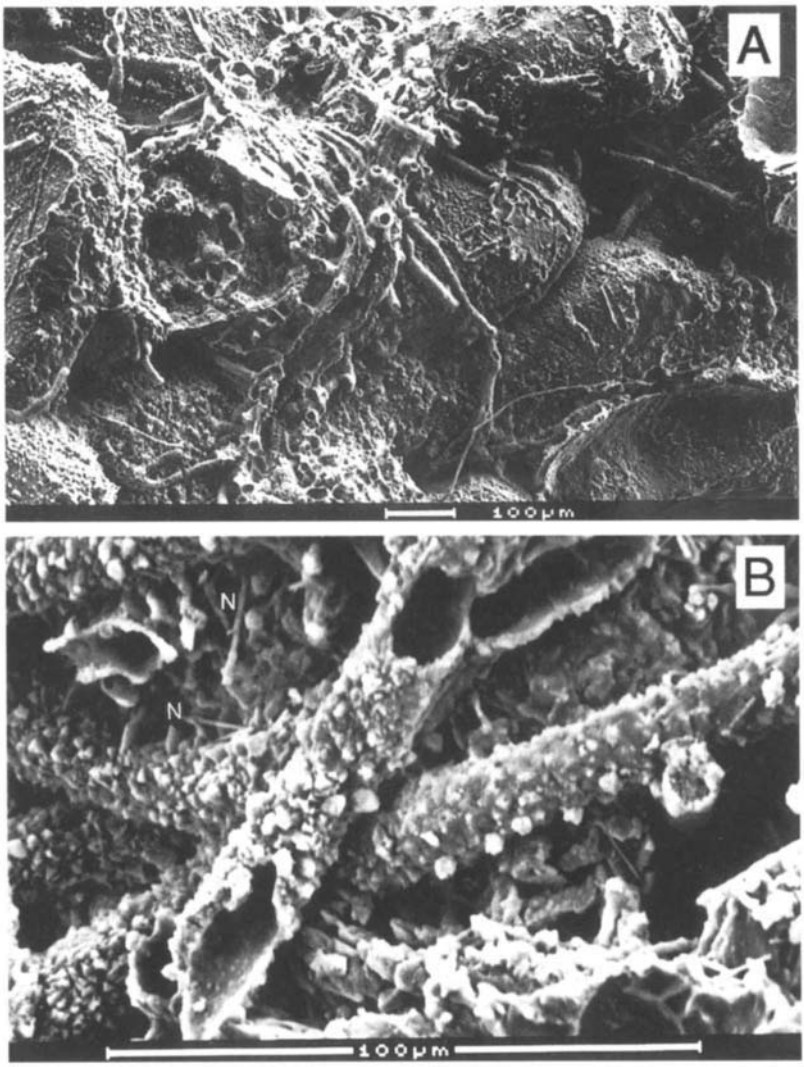


Fig. 7-12. Secondary-electron image showing microcrystalline-calcite root-hair sheaths in intergranular pores of Pleistocene eolianites. A. Near center of image is fossil rootlet with emanating root-hair sheaths. B. Root-hair sheaths composed of finely crystalline equant calcite. Small calcite needle fibers (N) are scattered between the root-hair sheaths.

Apparently, the Pleistocene dune rocks, especially the youngest ones, underwent early diagenesis in a relatively drier climate.

New excavations on the resort island of Cancun reveal that the Holocene eolianite is more or less equally indurated throughout, not merely case-hardened. This suggests that cementation of near-surface layers was an ongoing process following soon after deposition. If this is true, initial cementation takes place in the upper part of the

vadose zone, where the amount of rainfall and evapotranspiration should have a major influence on the dissolution-precipitation of $CaCO_3$. Climate, then, should be a major control over early cementation of eolianites.

Fig. 7-13 presents a summary of interstitial cement types found in the vadose zone of the Yucatan eolianites. Much of the Pleistocene dune rock, especially the Mujeres eolianite, is cemented with irregular encrustations of microcrystalline calcite, presumably the product of rapid precipitation from highly saturated vadose water. The relatively small amount of coarser calcite cement in the Mujeres eolianite could reflect the low percentage of aragonitic ooid coatings in this grainstone, but the distribution of sparry calcite cement seems unrelated to the distribution of aragonitic components in this rock. It seems reasonable, therefore, to suggest that intense evapotranspiration after soaking rains would trigger the microcrystalline-calcite cementation in carbonate eolianites. The rather poor induration of much of the Pleistocene dune rock and lack of extensive dissolution of aragonitic skeletal fragments and oolite coatings lead to the conclusion that the amount of freshwater moving through the dune was small compared to that which moves through the Holocene dunes.

Under the recent subhumid climate, the Holocene eolianite tends to be cemented with relatively large crystals of calcite precipitated at grain contacts. The coarser spar apparently is the result of relatively slower crystallization of cement crystals at fewer

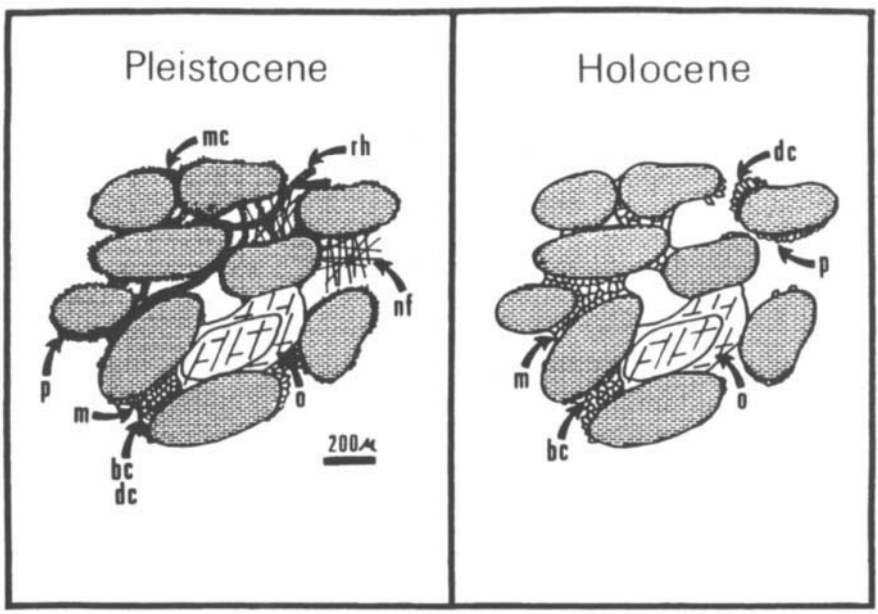


Fig. 7-13. Diagram showing differences in cementation of Pleistocene and Holocene eolianites of northeastern Yucatan. Key: bc, blocky (equant) calcite; dc, drusy (columnar) calcite; mc, microcrystalline calcite; nf, needle-fiber calcite; rh, root-hair sheaths; m, meniscus cement; p, pendulous cement; o, overgrowths on echinoid fragments. (From Ward, 1985.)

sites, under climatic conditions which favor a relatively continuous supply of $CaCO_3$-saturated vadose water. Although rainfall during the last 2–3 ky has been high enough to support growth of sparry calcite, it has been moderate enough to permit only minor removal of the dune rock by dissolution.

The limitation of the microcrystalline root-hair sheaths and needle-fiber cement to the Pleistocene provides more evidence that vadose conditions during earliest cementation of the Pleistocene dunes were different from those in Holocene dunes. The microcrystalline tubular sheaths and needle-fiber calcite are particularly abundant in proximity to rhizoliths. Root structures, root-hair sheaths, *Microcodium*, and perhaps needle-fiber cement suggest that transpiration and metabolic processes by dune plants and their mycorrhiza produced rapid precipitation of calcite in the root zones of the Pleistocene dunes. The Pleistocene dunes must have received sufficient rainfall to support some vegetation but inadequate amounts to permit extensive dissolution-precipitation of $CaCO_3$. Loose aragonitic and Mg-calcitic sand which surrounds the abundant rhizoliths in the upper layers of the Mujeres eolianite is evidence that transpiration by dune plants left very little vadose water for cementation or leaching. Although Holocene eolianites are penetrated by root systems, evapotranspiration has not been intense enough to produce hard rhizoliths, root-hair sheaths, or needle fibers. Accelerated diagenesis of the Pleistocene eolianites during the Holocene apparently is retarded by the extensive calcitic subaerial crusts that act as aquitards to infiltration of rainwater.

In summary, the mineralogy of the dune rocks, the types and abundance of initial cement, and the distribution of caliche strongly suggest that the climate of northeastern Yucatan during the late Pleistocene sea-level lowstand was more arid than during the Holocene highstand. Evidence from deep-sea sediments (e.g., Bonatti and Gartner, 1973) and other paleoclimatological studies (Crowley and North, 1991) indicate that the colder glacial-period climates in the Caribbean were more arid than the present climate.

CONCLUDING REMARKS

Carbonate rocks on the eolian-ridge islands (Mujeres, Contoy, Cancun, and Blanca) and the horst-platform island (Cozumel) record the influence of glacioeustatic sea-level fluctuations on carbonate sedimentation along the northwestern margin of the Caribbean Sea during the late Quaternary (Fig. 7-10). Most of these carbonate rocks are the highstand systems tracts of fourth-order (100 + ky) large-amplitude sea-level cycles. Lowstands are represented by laminated caliche crusts, which mark type-1 sequence boundaries. Shallow-marine Pleistocene limestones on Isla Cozumel and along the northeastern coast of the peninsula were deposited during two highstands of the fourth-order cycle (one before stage 5 and one during substage 5e).

Pleistocene eolianites on the islands and on the mainland coast near Tulum accumulated following a fall from the maximum sea-level rise of the last interglacial (stage 5). At least some of these eolianites possibly were deposited during highstands

of higher-order sea-level oscillations (substages 5a and/or 5c). Off northeastern Yucatan, where the peninsula was bordered by a ramp, several ridges of eolian sands were deposited near the margin of the terrace now 9 m below sea level. The generally higher elevation and different composition of the youngest of these eolianites (Mujeres eolianite) may suggest that this dune rock was deposited at a different sea-level highstand than the older upper Pleistocene eolianites. If so, eolianite deposition may have taken place during both substages 5a and 5c. The upper Pleistocene eolianites high on the steep margins of Isla Cozumel and the mainland coast probably were deposited when the sea was no more than a few meters below the present level. If the higher level were reached during substage 5a (Vacher and Hearty, 1989), then these eolianites may be of that age. The substantial fall in sea level that occurred shortly after the eolianites were deposited produced a drier climate, which controlled the type and rate of subaerial diagenesis of the Pleistocene limestones along northeastern Yucatan. The lowstand systems tract is represented by caliche profiles and minor karst features.

The barrier-island complexes of Isla Cancun and Isla Blanca are part of the Holocene highstand systems tract, deposited along the landward edge of the carbonate-sandy ramp. The eolian-ridge sands and lagoon sediments back of them are the thickest part of this systems tract. Under this highstand regime, diagenesis of peritidal Holocene carbonate sediments and of the underlying Pleistocene limestones is influenced by the continual flow of groundwater into coastal areas. Diagenesis of eolian carbonate sands is influenced by the humid climate of the Holocene.

ACKNOWLEDGEMENTS

The careful and constructive reviews of Jim Carew, John Mylroie, and Len Vacher greatly improved the manuscript and helped clarify some of the ideas presented here. The geology of Cozumel is taken from Richard Spaw's master's thesis done at Rice University.

REFERENCES

Andrews, A.F., 1985. The archaeology and history of northern Quintana Roo. In: W.C. Ward, A.E. Weidie and W. Back (Editors), Geology and Hydrogeology of the Yucatan and Quaternary Geology of Northeastern Yucatan Peninsula. New Orleans Geol. Soc., pp. 127–143.

Bonatti, A. and Gartner, S., 1973. Caribbean climate during Pleistocene ice ages (abstr.). Eos, Trans. Am. Geophys. Union, 54: 327–328.

Boyd, D.W., Kornicker, L.S. and Rezak, R., 1963. Coralline algal microatolls near Cozumel Island, Mexico. Wyo. Univ. Dep. Geol. Contrib. Geol., 2: 105–108.

Brady, M.J., 1971. Sedimentology and diagenesis of carbonate muds in coastal lagoons of NE Yucatan. Ph.D. Dissertation, Rice Univ., Houston TX, 288 pp.

CLIMAP Project Members, 1984. The last interglacial ocean. Quat. Res., 21: 123–224.

Crowley, T.J. and North, G.R., 1991. Paleoclimatology. Oxford, New York, 339 pp.

Dillon, W.P. and Vedder, J.G., 1973. Structure and development of the continental margin of British Honduras. Geol. Soc. Am. Bull., 84: 2713–2732.

Fenner, D.P., 1988. Some leeward reefs and corals of Cozumel, Mexico. Bull. Mar. Sci., 42: 133–148.
Hanshaw, B.B. and Back, W., 1980. Chemical mass-wasting of the northern Yucatan Peninsula by groundwater dissolution. Geology, 8: 222–224.
Klappa, C.F., 1978. Biolithogenesis of Microcodium: elucidation. Sedimentol., 25: 489–522.
Leipper, D.F., 1954. Physical oceanography of the Gulf of Mexico. In: P.S. Galstoff (Editor), Gulf of Mexico, Its Origin, Water, and Marine Life. U.S. Fish and Wildlife Serv. Fish. Bull., 89: 119–137.
Logan, B.W., Harding, J.L., Ahr, W.M., Williams, J.D. and Snead, R.G., 1969. Carbonate sediments and reefs, Yucatan shelf, Mexico. Am. Assoc. Petrol. Geol. Mem., 11: 1–198.
Lopez-Ramos, E., 1975. Geological summary of the Yucatan Peninsula. In: A.E.M. Nairn and F.G. Stehli (Editors), The Ocean Basins and Margins, v. 3, The Gulf of Mexico and Caribbean. Plenum, New York, pp. 257–282.
McKee, E.D. and Ward, W.C., 1983. Eolian environment. In: P.A. Scholle, D.G. Bebout and C.H. Moore (Editors), Carbonate Depositional Environments. Am. Assoc. Petrol. Geol. Mem., 33: 131–170.
Muehlberger, W.R. (Compiler), 1992. Tectonic Map of North America. Am. Assoc. Petrol. Geol., Tulsa, Oklahoma.
Muhs, D.R., 1992. The last interglacial-glacial transition in North America: evidence from uranium-series dating of coastal deposits. In: P.U. Clark and P.D. Lex (Editors), The Last Interglacial-Glacial Transition in North America. Geol. Soc. Am. Spec. Pap., 270: 31–51.
Spaw, R.H., 1978. Late Pleistocene stratigraphy and geologic development of Cozumel Island, Quintana Roo, Mexico. Trans. Gulf Coast Assoc. Geol. Soc., 28: 601–620.
Szabo, B.J., Ward, W.C., Weidie, A.E. and Brady, M.J., 1978. Age and magnitude of the late Pleistocene sea-level rise on the eastern Yucatan Peninsula. Geology, 6: 713–715.
Uchupi, E., 1973. Eastern Yucatan continental margin and western Caribbean tectonics. Am. Assoc. Petrol. Geol. Bull., 57: 1075–1095.
Vacher, H.L. and Hearty, P., 1989. History of stage 5 sea level in Bermuda: Review with new evidence of a brief rise to present sea level during substage 5a. Quat. Sci. Rev., 8: 159–168.
Vedder, J.G. and Scientific Staff, 1971. U.S. Geological Survey-IDOE, Leg 2. Geotimes, 16 (12): 10–12.
Ward, W.C., 1973. Influence of climate on the early diagenesis of carbonate eolianites. Geology, 1: 171–174.
Ward, W.C., 1975. Petrology and diagenesis of carbonate eolianites of the northeastern Yucatan Peninsula, Mexico. In: K.F. Wantland and W.C. Pusey (Editors), Belize Shelf-Carbonate Sediments, Clastic Sediments, Ecology. Am. Assoc. Petrol. Geol. Studies Geol., 2: 500–571.
Ward, W.C., 1985. Quaternary geology of northeastern Yucatan Peninsula. In: W.C. Ward, A.E. Weidie and W. Back (Editors), Geology and Hydrogeology of the Yucatan and Quaternary Geology of Northeastern Yucatan Peninsula. New Orleans Geol. Soc., pp. 23–95.
Ward, W.C. and Brady, M.J., 1979. Strandline sedimentation of carbonate grainstones, Yucatan Peninsula, Mexico. Am. Assoc. Petrol. Geol. Bull., 63: 362–369.
Ward, W.C., Folk, R.L. and Wilson, J.L., 1970. Blackening of eolianites and caliche adjacent to saline lakes, Isla Mujeres, Quintana Roo, Mexico. J. Sediment. Petrol., 40: 548–555.
Weidie, A.E., 1985. Geology of Yucatan platform. In: W.C. Ward, A.E. Weidie and W. Back (Editors), Geology and Hydrogeology of the Yucatan and Quaternary Geology of Northeastern Yucatan Peninsula. New Orleans Geol. Soc., pp. 1–19.

Geology and Hydrogeology of Carbonate Islands. Developments in Sedimentology 54
edited by H.L. Vacher and T. Quinn
© 1997 Elsevier Science B.V. All rights reserved.

Chapter 8

GEOLOGY AND HYDROGEOLOGY OF THE CAYMAN ISLANDS

BRIAN JONES, K.-C. NG and I.G. HUNTER

INTRODUCTION

Although the thickness of the carbonate caps on Grand Cayman, Cayman Brac and Little Cayman (Fig. 8-1) is unknown, a well drilled in the central part of Grand Cayman was still penetrating Oligocene carbonates at a depth of 401 m (Emery and Milliman, 1980). The complex stratigraphic architecture of the upper part of this succession reflects the interplay of deposition and erosion that has governed its formation over the last 30 m.y. Analysis of this succession shows that many extrinsic factors influenced the development of the depositional regimes during sea-level highstands or erosional regimes during sea-level lowstands. Evaluating the water resources on small islands such as the Cayman Islands is difficult because the hydrological and hydrogeological parameters vary with time. Nevertheless, an understanding of the modern groundwater behavior on these islands can be obtained by integrating available hydrogeological and geological information.

SETTING

Geography

Grand Cayman, with a surface area of about 196 km^2, is 35 km long, 8 km wide (average), and has elevations up to 15 m (Fig. 8-2). Elevations above 6 m are restricted to the peripheral ridge that parallels the north, south and east coasts and isolated areas such as those around "The Mountain" and Pedro Castle (Fig. 8-2). The central and western parts of Grand Cayman are generally flat, with elevations <5 m (Fig. 8-2). On the east end of the island, a transect across the peripheral ridge typically involves a rise from the coast to 6–10 m before the land drops off inland to elevations of only a few meters above sea level (Fig. 8-2). To the west, however, the ridge is more subtle because it attains heights of only 3–5 m (Section A-B in Fig. 8-2).

Little Cayman (26 km^2) and Cayman Brac (36 km^2) are considerably smaller than Grand Cayman. Little Cayman is a low-lying island like Grand Cayman. Cayman Brac, however, has elevations up to 42 m at its east end. From there it slopes gently to sea level at its western end.

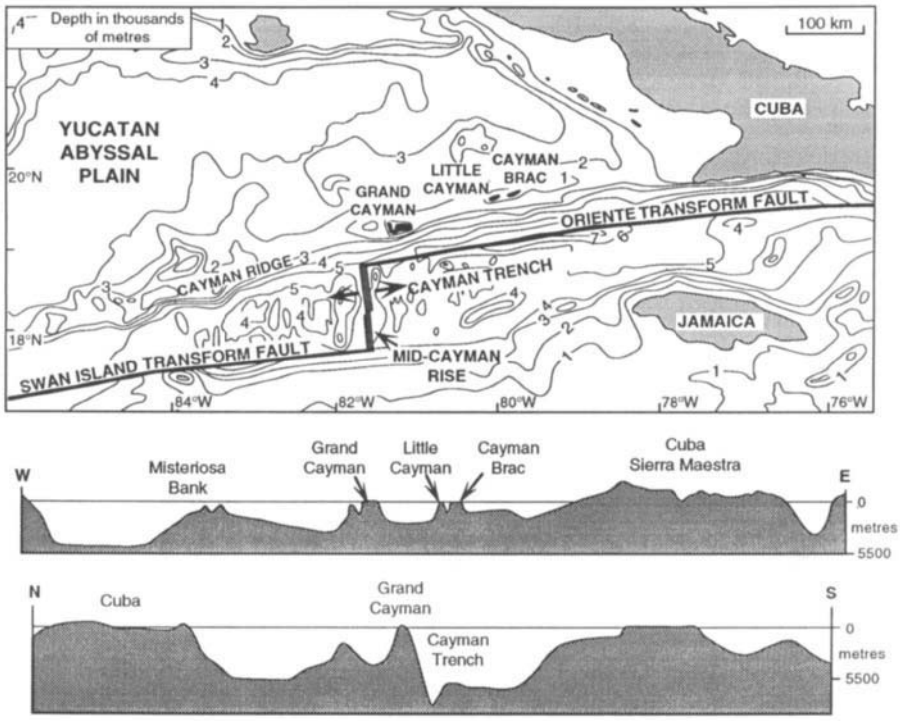


Fig. 8-1. Bathymetric map of the northern Caribbean area showing the location of Grand Cayman, Little Cayman, and Cayman Brac on the Cayman Ridge which forms the northern boundary of the Cayman Trench. Modified from Perfit and Heezen (1978, Fig. 2) and MacDonald and Holcombe (1978, Fig. 1). The cross sections show the location of Grand Cayman, Little Cayman and Cayman Brac on the Cayman Ridge, which stretches from the Sierra Maestra of Cuba to Belize and Grand Cayman, relative to the Cayman Trench. Modified from Matley (1926, Fig. 11).

Tectonic setting

The Cayman Islands are situated on the Cayman Ridge (Fig. 8-1) which forms the northern margin of the Cayman Trench (MacDonald and Holcombe, 1978). Seismic activity along the Mid-Cayman Rise and the associated transform faults indicates that the spreading center is active (MacDonald and Holcombe, 1978). Each of the Cayman Islands is probably on separate fault blocks (Horsfield, 1975) that moved independently of each other (Jones and Hunter, 1990).

Climatic regime

Rainfall is irregularly distributed over Grand Cayman with the eastern part being the driest (Fig. 8-3). This pattern is attributed to the prevailing easterly trade winds during the wet summer months (May–Oct.). Hurricanes and tropical storms may bring high-intensity rainfall in the summer (e.g., Hurricane Gilbert in 1988 delivered

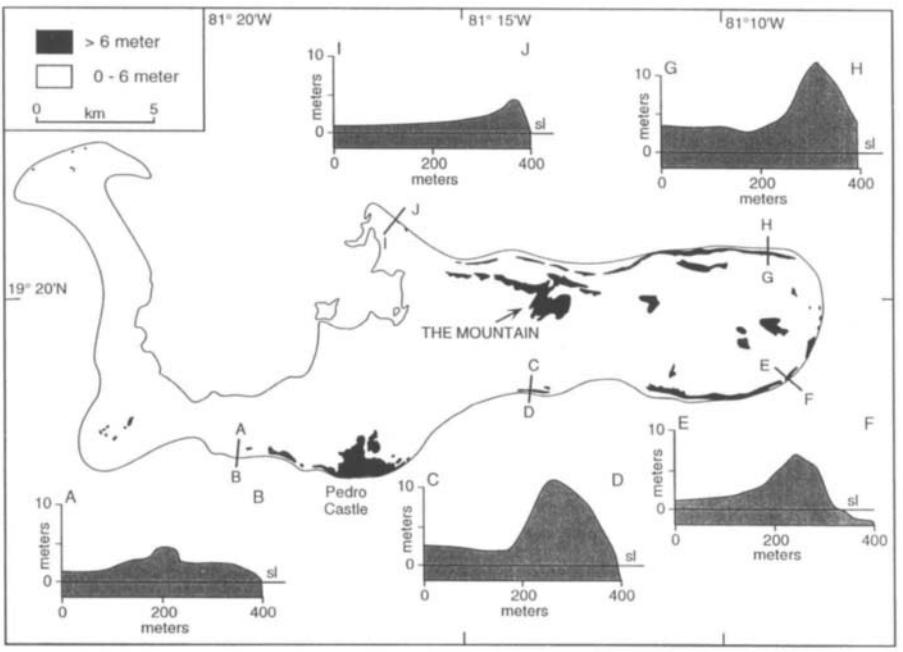


Fig. 8-2. Topography of Grand Cayman. Areas with elevations of >12 m are so small that they have been omitted from this map for the sake of simplicity. This map is based on the 1988 topographic map published by the Cayman Islands Government. The topographic transects showing the peripheral rim were constructed using spot heights obtained from the 1:2,500-scale topographic maps that give spot heights as determined by photogrammetry. (From Jones and Hunter, 1994, Fig. 4.)

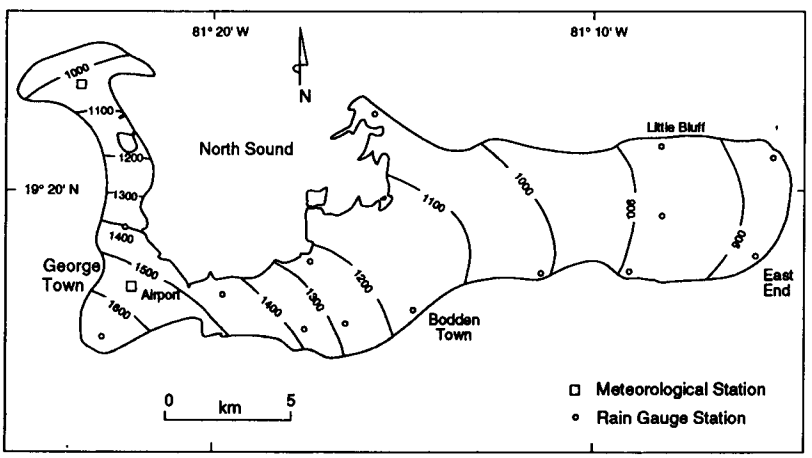


Fig. 8-3. Sketch map of Grand Cayman showing the annual rainfall distribution for 1987. Isohyets are in mm. (From Ng et al. 1992.)

120 mm of rain in 1.5 days), whereas northwesterly winds may bring rain in the winter months. Although the average annual rainfall registered at the airport was 1,476 mm between 1967–1992, there has been a gradual decline over the last 12 years. Average temperatures during the summer (May–Nov.) are ~30°C, compared to ~25°C during winter (Dec.–April). Relative humidity is above 80% throughout the year.

STRATIGRAPHIC FRAMEWORK

Each of the Cayman Islands has a core of Tertiary carbonates that is surrounded and partly overlain by the Pleistocene Ironshore Formation (Fig. 8-4). The Tertiary carbonates have traditionally been called the Bluff Limestone or Bluff Limestone Formation (Brunt et al., 1973; Woodroffe et al., 1980) following the pioneering work of Matley (1926). These terms are, however, misleading because the constituent rocks have been extensively dolomitized (Pleydell et al., 1990). Jones and Hunter (1989) used the term Bluff Formation to remove the lithological connotation attached to the original name. Jones et al. (1994a, 1994b) showed that the Bluff Formation, as defined by Matley (1926), includes three unconformity-bounded packages and therefore gave it group status. The distribution and basic characteristics of the constituent Brac, Cayman and Pedro Castle Formations are given in Figs. 8.4 and 8.5.

Brac Formation

To date, the Brac Formation has been found only on the northeast end of the Cayman Brac.

Lithofacies. On the north coast of Cayman Brac, the Brac Formation is formed of wackestones to grainstones that contain numerous large *Lepidocyclina* along with fewer red algae, echinoid plates and other foraminifera. Articulated bivalves and gastropods are present near the top of the formation. Dolomite is restricted to scattered rhombs and small pods near the upper boundary. On the south coast, the succession is formed of sucrosic, microcrystalline, or mixed sucrosic and microcrystalline dolostone with isolated limestone pods (Fig. 8-5). The sucrosic dolostone is formed of subhedral to euhedral crystals, up to 1 mm long, that have a dark core surrounded by a clear rim. The microcrystalline dolostone is fabric retentive. Limestone pods (up to 10 m long and 2 m thick), found at various levels on the south coast (Fig. 8-5), are like the limestones on the north coast. Fossil-moldic cavities after bivalves and gastropods contain internal sediment and dolomite cement.

Depositional regime. Jones and Hunter (1994) suggested that the *Lepidocyclina*-rich limestones of the Brac Formation accumulated on a bank, possibly in water <10 m deep. The paucity of corals suggests a depositional regime characterized by poor water circulation. Indirect evidence suggests that this bank may have been covered with seagrasses.

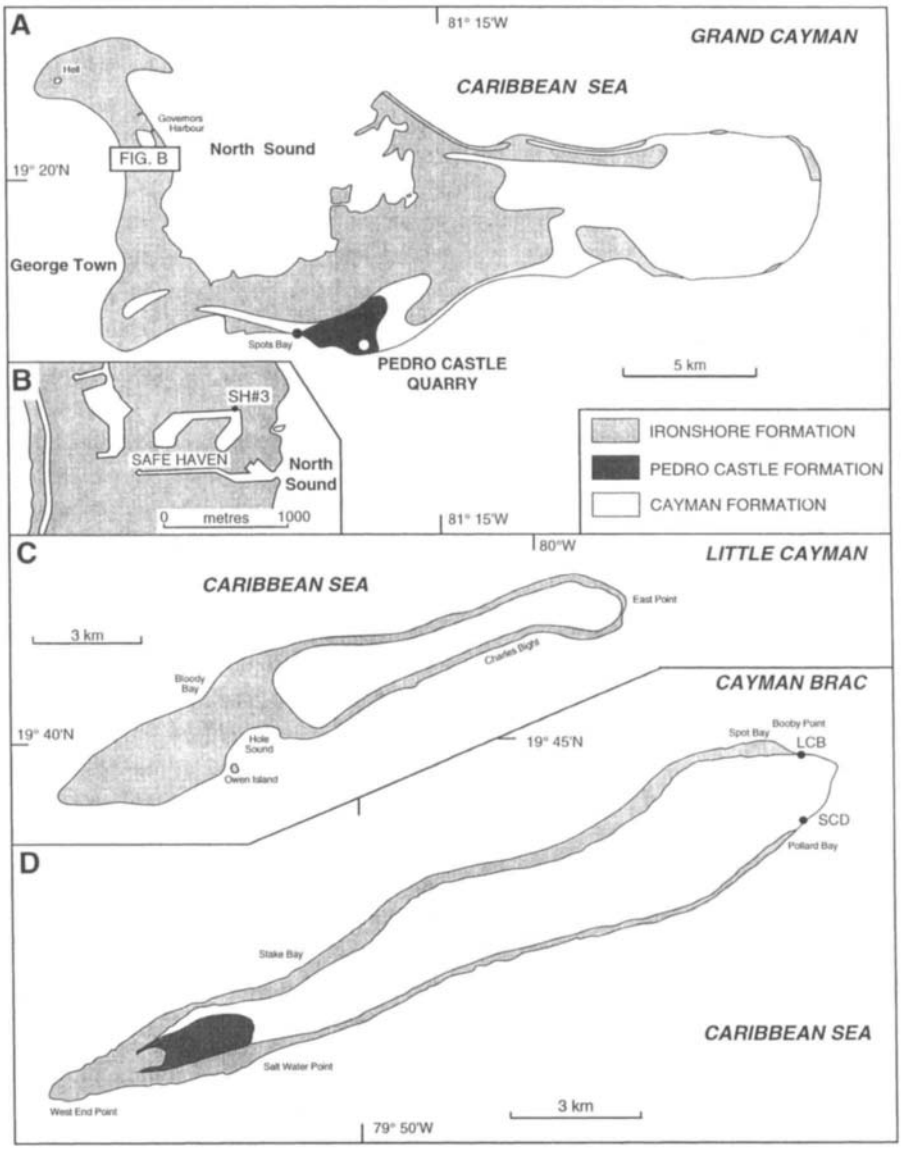
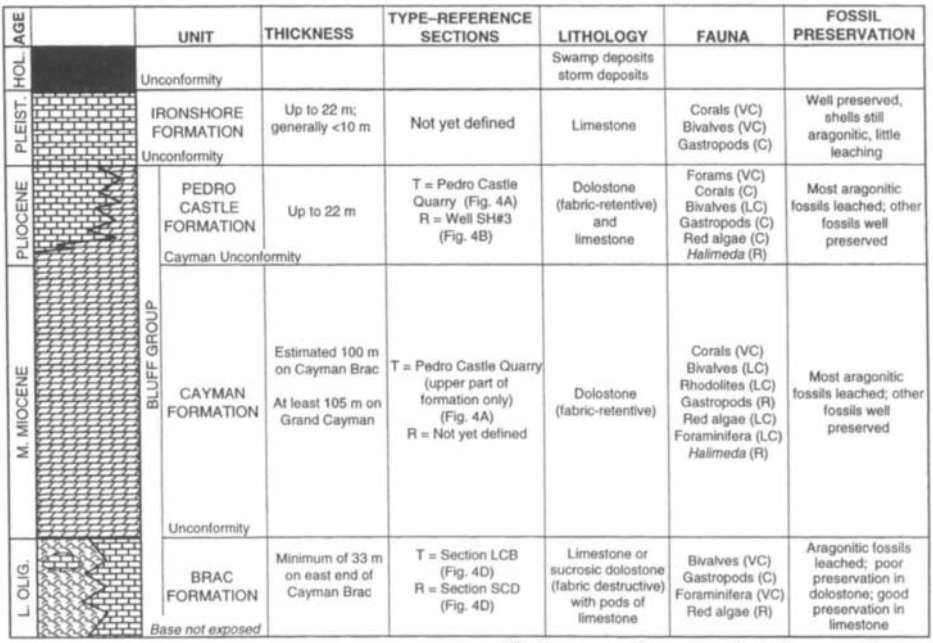


Fig. 8-4. Sketch maps showing the surface geology of the Cayman Islands. (A) Map of Grand Cayman showing location of Pedro Castle Quarry where the type section of the Cayman and Pedro Castle Formations is located. (From Jones et al., 1994b.) (B) Detailed map of the Safe Haven area showing the location of well SH#3 which is the reference section for the Pedro Castle Formation. (C) Little Cayman. (Modified from Matley 1926.) (D) Cayman Brac showing the distribution of the Cayman, Pedro Castle, and Ironshore Formations. The Brac Formation cannot be shown on the map because it is exposed only at the base of vertical cliffs at the northeast end of the island. (From Jones et al., 1994a.)



AGE	UNIT	THICKNESS	TYPE–REFERENCE SECTIONS	LITHOLOGY	FAUNA	FOSSIL PRESERVATION
HOL.	Unconformity			Swamp deposits storm deposits		
PLEIST.	IRONSHORE FORMATION Unconformity	Up to 22 m; generally <10 m	Not yet defined	Limestone	Corals (VC) Bivalves (VC) Gastropods (C)	Well preserved, shells still aragonitic, little leaching
PLIOCENE	PEDRO CASTLE FORMATION Cayman Unconformity	Up to 22 m	T = Pedro Castle Quarry (Fig. 4A) R = Well SH#3 (Fig. 4B)	Dolostone (fabric-retentive) and limestone	Forams (VC) Corals (C) Bivalves (LC) Gastropods (C) Red algae (C) *Halimeda* (R)	Most aragonitic fossils leached; other fossils well preserved
M. MIOCENE	BLUFF GROUP CAYMAN FORMATION Unconformity	Estimated 100 m on Cayman Brac At least 105 m on Grand Cayman	T = Pedro Castle Quarry (upper part of formation only) (Fig. 4A) R = Not yet defined	Dolostone (fabric-retentive)	Corals (VC) Bivalves (LC) Rhodolites (LC) Gastropods (R) Red algae (LC) Foraminifera (LC) *Halimeda* (R)	Most aragonitic fossils leached; other fossils well preserved
L. OLIG.	BRAC FORMATION *Base not exposed*	Minimum of 33 m on east end of Cayman Brac	T = Section LCB (Fig. 4D) R = Section SCD (Fig. 4D)	Limestone or sucrosic dolostone (fabric destructive) with pods of limestone	Bivalves (VC) Gastropods (C) Foraminifera (VC) Red algae (R)	Aragonitic fossils leached; poor preservation in dolostone; good preservation in limestone

VC = Very common; C = common; LC = locally common; R = rare

Fig. 8-5. Schematic stratigraphic column for the Cayman Islands showing the constituent formations, their thickness, location of type (T) and reference (R) sections, lithology, fossils, and style of fossil preservation. (Modified from Jones et al., 1994b.)

Brac-Cayman unconformity

The Brac-Cayman unconformity, between the Brac and Cayman Formations, formed over a period of 8 m.y. during the late Oligocene and part of the early Miocene (Jones et al., 1994a), when there was a major lowstand in sea level (cf., Vail and Hardenbol, 1979). Information on the Brac-Cayman unconformity is sparse because of the difficulty of examining it in the vertical seacliffs at the east end of Cayman Brac. Nevertheless, a generalized reconstruction of this unconformity suggests that it had a relief of about 25 m (Fig. 8-6).

Cayman Formation

The Cayman Formation crops out over most of Grand Cayman, Cayman Brac and Little Cayman. Matley (1926) did not designate a type section for his Bluff Limestone. Jones and Hunter (1989) designated a type section in the quarry near Pedro Castle (Fig. 8-4A); the type section incorporates the unconformity which Jones and Hunter (1989) used to divide the formation into the Cayman and Pedro Castle Members. Subsequently, Jones et al. (1994b) showed that these two members

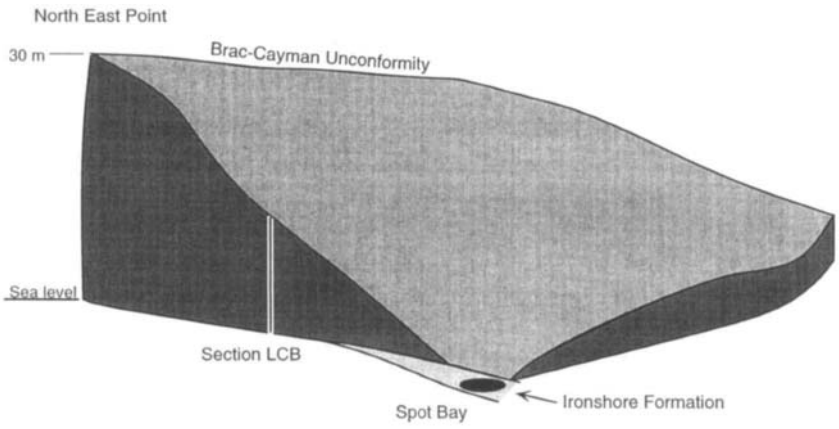


Fig. 8-6. Three-dimensional reconstruction of the Brac-Cayman unconformity on the eastern end of Cayman Brac.

are widespread on Grand Cayman and Cayman Brac and, therefore, elevated them to formational status.

Lithofacies. The formation is formed entirely of fabric-retentive microcrystalline dolostone (Jones et al., 1994b). Although mudstones and wackestones dominate, there are some grainstones and packstones (Jones and Hunter, 1994) with grains of foraminifera, red algae fragments and *Halimeda* being common. Although massive colonial (e.g., *Diploria*, *Montastrea*, *Siderastrea*, *Leptoseris*, *Porites*) and branching (*Stylophora*, *Porites*) corals are common, there is no evidence of reef development. Coral molds commonly contain casts of borings like those described by Pleydell and Jones (1988). Rhodolites, with broken branches of *Stylophora* or *Porites* as their nuclei, are commonly concentrated in beds or lenses up to 1 m thick.

Pores are lined with limpid dolomite cement and/or filled with coarsely crystalline calcite cement (Jones et al., 1984). Larger cavities contain caymanite (laminated white, red and black, microcrystalline dolostone with various sedimentary structures; Jones, 1992a), terra rossa, freshwater limestone and/or flowstone (Jones, 1992b).

Depositional regime. The diverse, coral-dominated biota throughout the formation indicates open marine conditions (Jones and Hunter, 1994). On Cayman Brac and Grand Cayman there is no evidence of reef development other than isolated thickets of *Stylophora*. The most notable feature of this formation is the lack of systematic geographic or stratigraphic variation in its constituent facies (Jones and Hunter, 1994). On Cayman Brac, the lithofacies and biofacies of the Cayman Formation are indicative of deposition on a small, open bank that had good cross-bank circulation in water <30 m deep (Jones and Hunter, 1994). Preliminary studies of the Cayman Formation on Grand Cayman suggests that it represents a similar depositional regime.

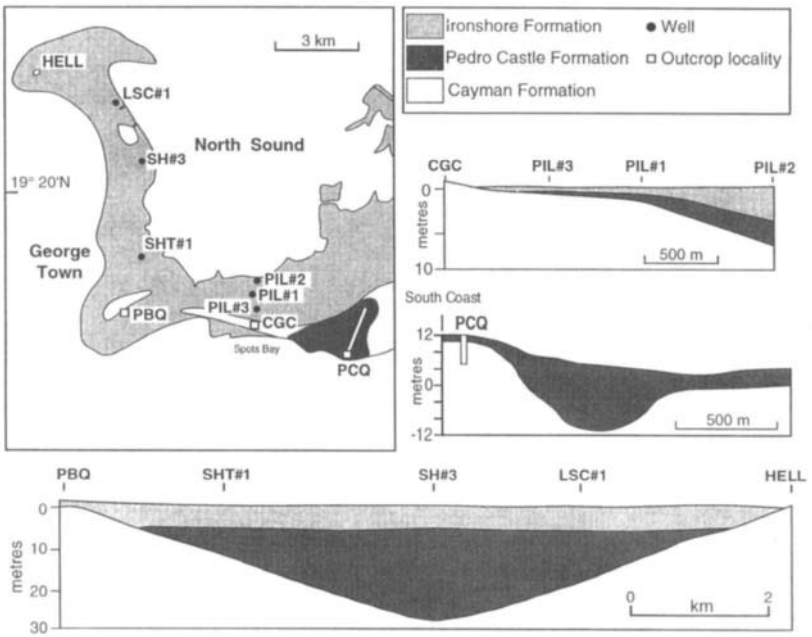


Fig. 8-7. North-south cross sections on the western part of Grand Cayman showing the spatial relationships between the Cayman, Pedro Castle, and Ironshore Formations. Information derived from surface outcrops (localities Hell, PBQ, CGC, and PCQ), continuously cored wells (localities LSC#l, SH#3, SHT#l, PIL#l, PIL#2, and PIL#3), and discontinuously cored wells (area north of locality PCQ). (Based on Jones et al., 1994b and Jones and Hunter, 1994.)

Cayman unconformity

The Cayman unconformity, between the Cayman and Pedro Castle Formation, formed during the Messinian lowstand that existed for approximately 1.5 m.y. at the end of the Miocene (Jones and Hunter, 1994). This unconformity is generally absent on the eastern half of Grand Cayman where the Cayman Formation is exposed over most of the surface (Fig. 8-4A). On the western part of the island, however, the Cayman unconformity is widespread in the subsurface despite its limited exposure at the surface. Drilling and coring in this part of the island showed that the topographically lowest parts of the unconformity lie under the modern North Sound (Figs. 8-7, 8-8). Three-dimensional modeling shows that the eastern part of the island was substantially higher than the western part of the island, where a depression with a relief of up to 40 m developed (Fig. 8-8). The peripheral rim that is readily apparent on the island today (Fig. 8-2) is a vestige of the rim that developed around the island during this period. Jones and Hunter (1994) demonstrated the karstic nature of this topography by showing that caves and sinkholes (up to 40 m deep) were genetically linked to it. Jones and Hunter (1994) suggested that maximum dissolution took place on the western part of the island because that was the site of

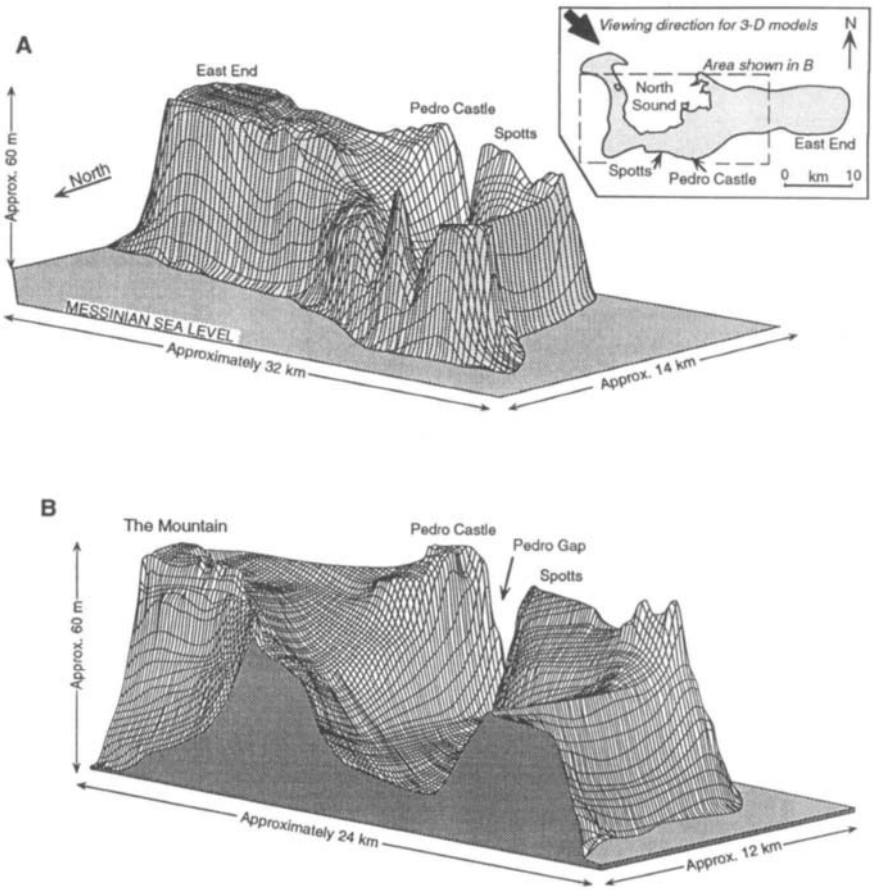


Fig. 8-8. (A) Conceptual model showing the topography on the Cayman unconformity. This represents the topography that had developed on Grand Cayman by the end of the Messinian. (B) Detailed model showing the topography on the Cayman unconformity for the western part of Grand Cayman (see inset map for area covered). The topography on the unconformity is based on a computer model that used surface outcrop data, well data, and extrapolated data. Views from northwest at viewing angle of 12° (see inset map).

maximum rainfall, as it is today. These data from Grand Cayman suggest that the Messinian sea level was at least 40 m below modern sea level.

Pedro Castle Formation

At present, the Pedro Castle Formation is exposed over small areas on Grand Cayman and the western part of Cayman Brac (Fig. 8-4). This formation, however, is extensive in the subsurface in the western part of Grand Cayman (Jones et al., 1994b).

Lithofacies. The Pedro Castle Formation is formed of white to gray dolostone, dolomitic limestone and limestone (Fig. 8-5). Skeletal wackestones and mudstones dominate. Dolomitization, which produced fabric-retentive dolostones like those in the Cayman Formation, was not pervasive. Free-living corals, foraminifera, red algae fragments, rare colonial corals, echinoids and bivalves are found throughout the succession. Rhodolites, up to 5 cm in diameter, are common at the base of the formation.

Depositional regime. The carbonates of the Pedro Castle Formation were deposited in response to the rise in sea level that signaled the end of the Messinian. In the context of Grand Cayman, that highstand must have been at least 12 m above modern sea level because that is the highest elevation of Pliocene marine carbonates found on the island.

On Cayman Brac, the Pedro Castle Formation contains more mudstone and wackestone, less packstone and grainstone, fewer rhodolites and fewer corals than the Cayman Formation (Jones and Hunter, 1994). Evidently, this succession was deposited under quieter-water conditions than those associated with the carbonates of the Cayman Formation. On Grand Cayman, the rugged topography that developed on the island during the Messinian lowstand strongly influenced lower Pliocene depositional patterns. Much of the deposition, for example, was in the atoll-like structure that dominated the western part of the island (Fig. 8-8).

Bluff-Ironshore unconformity

The Bluff-Ironshore unconformity formed over 2–3 m.y. during the Late Pliocene and most of the Quaternary (Jones et al., 1944a). On the western part of Grand Cayman, erosion removed the upper part of the Pedro Castle Formation, exhumed the peripheral rim on the Cayman unconformity and produced a depression that has its base about 8 m below modern sea level. The depression produced during this phase of erosion, however, was shallower and less rugged than the depression that developed on the Cayman unconformity during the Messinian lowstand.

Maximum relief on the Bluff-Ironshore unconformity is about 8 m. At Paul Bodden Quarry (locality PBQ, Fig. 8-7), the unconformity is about 2 m above sea level, whereas it is about 6 m below sea level in well SH#4 (Fig. 8-7).

Ironshore Formation

The Ironshore Formation, first defined by Matley (1926), was named after the hard calcrete crust that develops on its weathered surfaces (Matley 1926; Warthin, 1959; Brunt et al., 1973). Dolomite has not been found in the limestones of this formation. The Ironshore Formation underlies much of the low-lying land on the western half of Grand Cayman (Fig. 8-4A). On the eastern half of the island, the formation is restricted to small embayments around the south, east and north coasts

(Fig. 8-4A). On Cayman Brac, the Ironshore Formation forms a low-lying platform around the edge of the island (Fig. 8-4D).

Lithofacies. On Grand Cayman, the Ironshore Formation is a shallowing-upward sequence that passes vertically from subtidal lagoonal facies to foreshore-backshore facies (Jones and Hunter, 1990; Shourie, 1993). The basal subtidal facies are widely exposed, whereas the lower shoreface to backshore facies are restricted to scattered exposures (Fig. 8-6A). Oolitic grainstones exposed near Salt Creek (Jones and Goodbody, 1984) contain well-preserved trace fossils (Pemberton and Jones, 1988). Channels cut in the subtidal deposits are filled with high-angle, cross-bedded oolitic grainstone.

The basal part of the formation includes bivalve, patch-reef and reef-tract facies. Wackestones and packstones in the bivalve facies (Fig. 8-9) contain numerous bivalves (>75 species) and gastropods, a few small corals, numerous foraminifera and *Halimeda*. Reefs in the patch-reef zone (Fig. 8-9B) are separated from each other by poorly sorted bioturbated sands (Woodroffe et al., 1980; Jones and Hunter, 1990). The patch reefs, up to 300 m long, contain a diverse coral fauna (Hunter, 1994) and

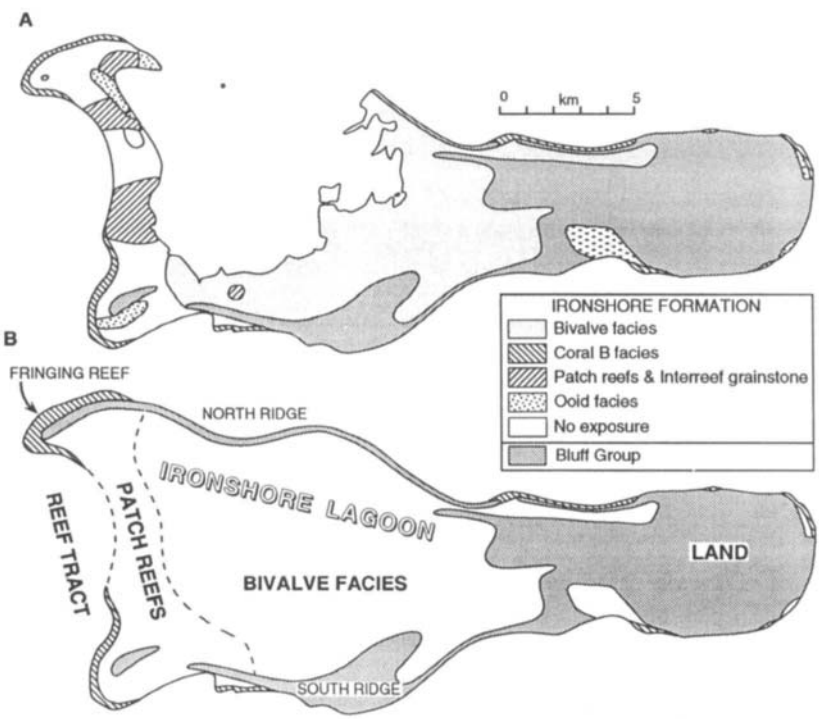


Fig. 8-9. Sketch maps of Grand Cayman showing (A) distribution of facies, and (B) paleogeographic framework in which the limestones of the Ironshore Formation were deposited. (Based on Hunter and Jones, 1988, and Jones and Hunter, 1990.)

numerous nestling and cementing bivalves (Cerridwen and Jones, 1991). Many corals were bored by *Lithophaga* (Jones and Pemberton, 1988), sponges and worms. Limestones of the reef tract and fringing-reef zone (Fig. 8-9B) contain an abundant, diverse coral fauna (Hunter and Jones, 1988; Jones and Hunter, 1990; Hunter, 1994). Bivalves and gastropods are less common than in the lagoon interior (Cerridwen and Jones, 1991), and borings of the corals are rare (Jones and Pemberton, 1988).

The Ironshore Formation is exposed in a small quarry at the northeast end of the airport on Cayman Brac. At this locality, the Ironshore Formation is capped by a calcarenite unit (Jones, 1988) and contains rhizoliths that include a diverse array of micro-organisms and cements (Jones and Ng, 1988).

Depositional regime. The carbonates of the Ironshore Formation were deposited during the +6 m sea-level highstand that occurred at 118–130 ka (Jones and Hunter, 1990). This highstand, however, did not completely inundate the island. Thus, sedimentation was restricted to the Ironshore Lagoon on the western part of Grand Cayman and small bays along the south, east and north coasts (Fig. 8-9B). The bathymetry and configuration of those depositional tracts were controlled by the topography that had developed on the island following deposition of the Pedro Castle Formation.

DOLOMITIZATION OF THE BLUFF GROUP

The Bluff Group of the Cayman Islands is formed of limestones, dolostones and limestones that have been dolomitized to varying degrees (Jones et al., 1994b). The stratigraphic distribution of the different types of dolostone places constraints on the processes that can be used to explain the widespread dolomitization of these rocks.

The Brac Formation is formed of limestone and dolostone (Fig. 8-5). On the north coast of Cayman Brac, the formation consists mostly of limestone. On the south coast, <1 km away, the same succession is formed largely of coarse sucrosic dolostone and patches of finely crystalline fabric-retentive dolostone. The geographic boundary between the limestone and dolostone has not yet been located because the vertical cliff faces on the east end of the island are difficult to access.

The Cayman Formation, which is at least 100 m thick on Cayman Brac and 105 m thick on Grand Cayman, is formed entirely of finely crystalline fabric-retentive dolostone. Thus, on the north coast of Cayman Brac the dolostones of the Cayman Formation rest directly on top of limestones of the Brac Formation (Fig. 8-5). On the south coast of Cayman Brac, the finely crystalline dolostones of the Cayman Formation overlie the sucrosic dolostones of the Brac Formation. Evidently, the unconformity between the Brac and Cayman Formations influenced the dolomitization of these successions.

The Pedro Castle Formation consists of limestone, dolostone, and limestones that have been replaced to varying degrees by dolomite. Dolostones in this formation are petrographically like those in the Cayman Formation. The Cayman unconformity, which denotes the boundary between the Cayman and Pedro Castle Formations,

does not appear to have exerted any influence on the dolomitization patterns of these formations. In this respect, the Cayman unconformity is significantly different from the Brac-Cayman unconformity.

Dolostones of the Bluff Group are geochemically homogeneous despite their great thickness (>105 m) and widespread geographic distribution. Thus, all the dolostones have $\delta^{18}O$ values between +1.0 and +3.5‰ PDB and $\delta^{13}C$ values between +1.0 and +4.0‰ PDB (Pleydell et al., 1990). Similarly, all the dolostones yield $^{87}Sr/^{86}Sr$ ratios of about 0.70905 (Pleydell et al., 1990).

The stratigraphic distribution of the dolostones coupled with their petrographic and geochemical homogeneity suggests that there was a single dolomitization event that postdated deposition of the Pedro Castle Formation or that there were numerous dolomitization events with each one overprinting the earlier phase. The $^{87}Sr/^{86}Sr$ ratios suggest that dolomitization took place during the late Pliocene. Such a suggestion is consistent with the lack of dolomite in the Ironshore Formation. Collectively, the evidence suggests that dolomitization of the Bluff Group took place over a period of ~2 m.y. Although the precise mechanism of dolomitization is not yet understood, the geographic isolation of the islands, the sedimentological evidence and the stratigraphic evidence eliminates many of the traditional dolomitization models. In the context of the Bluff Group, it seems that seawater or modified seawater is the only fluid that could have mediated such pervasive dolomitization.

POROSITY AND PERMEABILITY

The permeability and porosity characteristics of the carbonate successions on Grand Cayman are critical factors in any discussion pertaining to the transmission of water through the bedrock and its ability to store freshwater. Primary intergranular porosity is rare in the dolostones and limestones of the Bluff Group but common in the limestones of the Ironshore Formation. In addition, there is considerable intraskeletal porosity in the Ironshore Formation. Conversely, secondary porosity (locally >25%) in the form of skeletal molds, open joints, fissures and solution caverns is common in the Bluff Group, but rare in the Ironshore Formation.

Permeability in the rocks of the Bluff Group is highly variable. In the East End lens (Fig. 8-10), for example, bailing of one well volume of water from a piezometer produced a 7.5-m drop in water level that took six months to recover. Conversely, in other areas the aquifer is so transmissive that drawdowns are immeasurable. Core analysis of the Cayman Formation from well 3–84EE (Fig. 8-10C) showed that permeability ranged from <0.1 m darcy^{-1} to 34 m darcy^{-1}. Three joint sets (trending at 020°, 090° and 160°; Rigby and Roberts, 1976) in the Bluff Group of Grand Cayman are important because they allow easy passage of water through the bedrock (Fig. 8-10). Dissolution along these joints produced soft, friable dolostone that is atypical of the Cayman Formation (Jones et al., 1989).

Porosity in the dolostones and limestones of the Bluff Group is, to a large extent, controlled by the biofacies distribution because dissolution of the aragonitic skeletons of corals, bivalves and gastropods created much of it (Ng et al., 1992). The

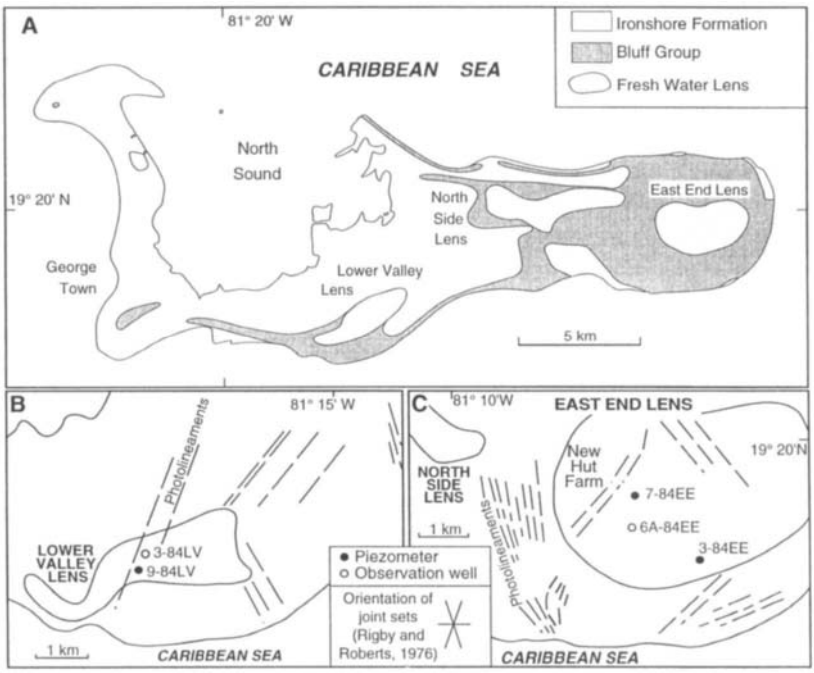


Fig. 8-10. (A) Map of Grand Cayman showing positions of the East End, North Side, and Lower Valley freshwater lenses. (B and C) Distribution of joints and photolineaments in areas surrounding the Lower Valley and East End freshwater lenses.

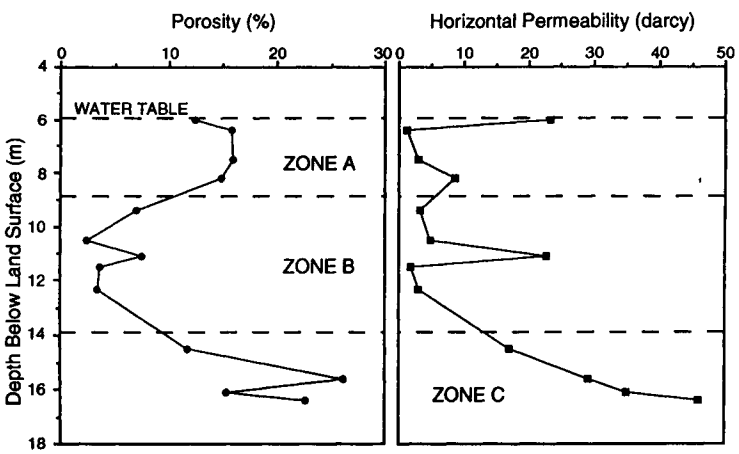


Fig. 8-11. Porosity and horizontal permeability of dolostone cores from the Cayman Formation in the East End lens. Location of well 3–84EE is shown in Fig. 8-10C.

Cayman Formation in the well 3–84EE, for example, can be divided into zones A, B and C according to porosity styles (Figs. 8-10C, 8-11). Porosity in zone A resulted from active groundwater circulation at the water table and dissolution due to mixing corrosion. The high porosity in Zone C correlates with a coral-rich biofacies whereas the low porosity in Zone B correlates with a biofacies that contains only scattered mollusks. In many parts of the Bluff Group, porosity and permeability have been substantially reduced by the precipitation of calcite and dolomite cements, flowstones, and/or deposition of internal sediments (Jones and Smith, 1988; Jones, 1992a, 1992b).

Drilling at various locations on Grand Cayman has shown that there are numerous caves in the subsurface, commonly at −20 to −30 m. These caves may be related to the submerged wave-cut notch around Grand Cayman at −18.5 m, which was probably formed during the early Holocene (P. Blanchon, pers. comm., 1993).

FRESHWATER LENSES

The Lower Valley, East End and North Side freshwater lenses (Fig. 8-10), which cover about 28.5 km^2 (~14.5% of land surface area), have safe daily abstraction rates of 310 m^3, 2,950 m^3 and 1,360 m^3, respectively. These unconfined lenses, identified by Mather (1972) and delineated by Bugg and Lloyd (1976), are located beneath topographic highs in the Bluff Group (Figs. 8-10, 8-12). The small size of the

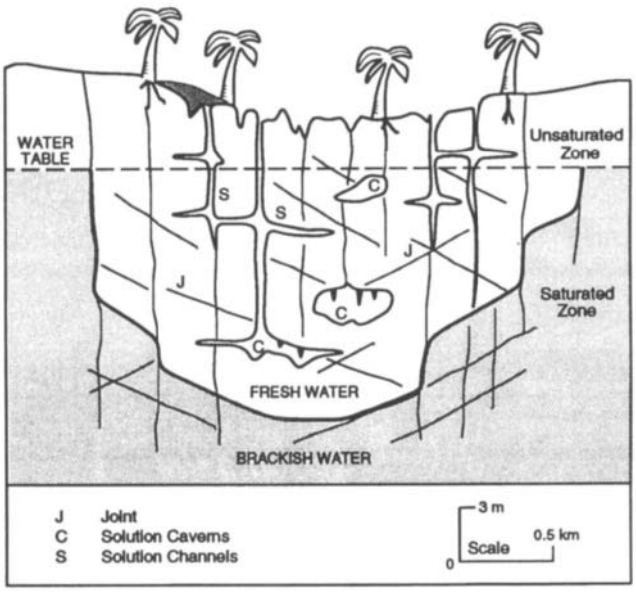


Fig. 8-12. Schematic representation of joint- and karst-controlled lens configuration for Grand Cayman.

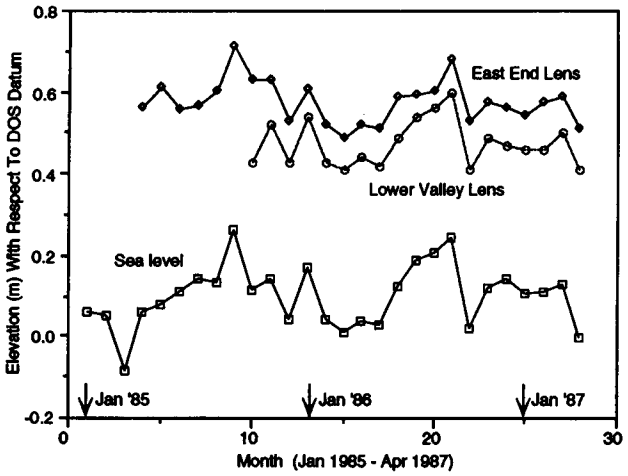


Fig. 8-13. Average monthly water-table elevation of Lower Valley and East End freshwater lens compared to sea level around Grand Cayman. DOS datum is the Directorate of Survey datum on Grand Cayman.

lenses is due to the subdued topography of the island, the abundance of brackish-water swamp and the high permeability of the aquifer. Small freshwater bodies near George Town and West Bay were damaged by excessive withdrawal and sewage contamination (Kreitler and Browning, 1983).

Water-table elevation in the freshwater zone is 0.2 and 0.7 m above mean sea level at the lens edge and center, respectively. If 500-ppm chloride is used as the limit for freshwater, the ratio of water-table elevation to thickness of the freshwater lens on Grand Cayman is 1:20 rather than 1:40 ratio of the Ghyben-Herzberg principle, which assumes no mixing zone. A thick brackish-water zone is, in fact, present between the fresh and saline water. In general, the thickness of the freshwater part of the lenses is less than 1% of its lateral dimension (Ng et al., 1992).

Around Grand Cayman the daily semidiurnal tide range is about 0.2 m with a seasonal fluctuation of about 0.4 m (Fig. 8-13). The water table fluctuates in response to the sea tides because the aquifers are hydraulically linked to the ocean. On average, the deeper wells have shorter lag time (1–2 h) and higher tidal efficiencies (70–80%) than the shallow wells (3–4 h lag time, 50–60% tidal efficiency). Similarly, the time lag and tidal efficiency decrease from the lens edge to the lens center. Tidal efficiency is higher in the Lower Valley lens than in the East End lens because it is closer to the coast (Fig. 8-10).

HYDROLOGICAL REGIME

On Grand Cayman, overland runoff is minimal because rainwater quickly dissipates into the highly permeable bedrock (Fig. 8-12). Surface ponding only takes place after prolonged heavy rain. Under normal conditions, a seaward hydraulic

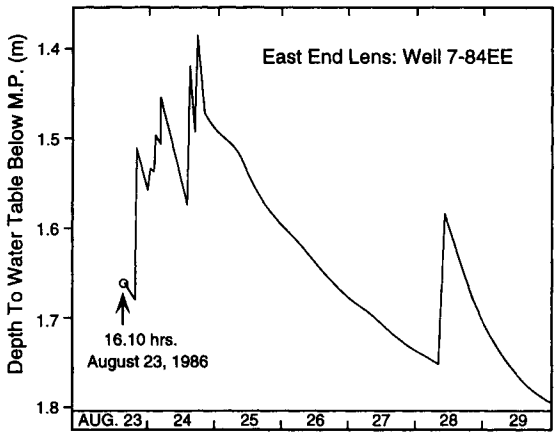


Fig. 8-14. Water-table hydrograph of well 7–84EE in the East End lens showing rapid recharge and discharge of rainwater in response to rainfall events. M.P. refers to top of the well casing. Well location is shown in Fig. 8-10C.

gradient drains groundwater into the sea. Evapotranspiration, driven by daytime temperature of 25°C (winter) to 30°C (summer), cause evaporative losses of about 80% (Ng et al., 1992). On Grand Cayman, these losses include: evaporation from sinkholes, ponds and swamps; evaporation of groundwater where the water table is

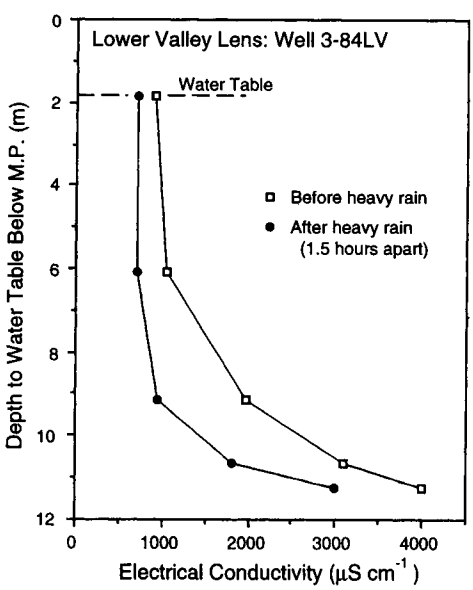


Fig. 8-15. Borehole salinity profiles of well 3–84LV in the Lower Valley lens showing improvement of water quality after a rainstorm. M.P. refers to top of the well casing. Well location is shown in Fig. 8-10B.

close to the land surface; evaporation from soil moisture; evaporation of precipitation intercepted by vegetation; transpiration from soil by plants; and direct groundwater abstraction by phreatophytes.

The fresh groundwater lenses, which have limited rainfall catchment areas because of the low-lying terrains, are recharged by infiltration of precipitation not lost to evapotranspiration or surface runoff. The variable annual rainfall means that there is a considerable fluctuation in the quantity of recharge from year to year. The aquifer on Grand Cayman is too transmissive for low-intensity rainfall to have much impact on the water table. Rises in the water table are evident only if rainfall amounts exceed 50 mm day^{-1}.

Rapid recharge, in response to each rainfall event, takes place when rainwater infiltrates through the fissures or caverns. The groundwater also dissipates quickly until a dynamic equilibrium is established (Fig. 8-14). The chemical and isotopic characteristics of the groundwater on Grand Cayman suggest that recharge of the groundwater lenses takes place during heavy rainstorms (Ng and Jones, 1990). Rapid improvement of water quality due to rapid rainwater recharge is shown by borehole salinity profiles that show significant drops in salinity throughout the water column measured after a rain storm (Fig. 8-15).

HYDROGEOCHEMISTRY

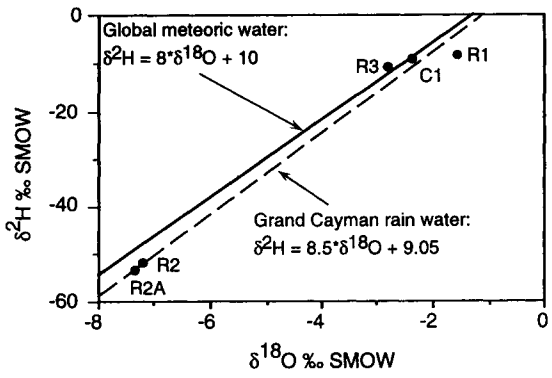
The saturated zone is divided into the fresh, brackish and saline hydrochemical zones (Ng and Jones, 1994). The freshwater zone has an upper limit of 600 mg l^{-1} Cl^-, which is the limit of potable water quality recommended by the WHO (1971). The saline-water zone has a Cl^- content ≥19,000 mg l^{-1}, which is equivalent to that in the seawater around Grand Cayman. Thus, the brackish-water zone has water with Cl^- concentrations of >600 to 19,000 mg l^{-1}.

Chemical and isotopic composition of rain water

Rainwater on Grand Cayman contains 7–13.5 mg l^{-1} of Cl^- (Ng and Jones, 1990). Its oxygen isotopic composition ranges from a low of −7.5‰ SMOW to a high of −2.0‰ SMOW (Fig. 8-16). Linear regression of the rainwater hydrogen and oxygen isotopic composition on Grand Cayman produces a trend that is similar to the global meteoric water line (Fig. 8-16). Precipitation during winter months is depleted in the heavy isotopic species relative to the summer rains. The amount effect (Dansgaard, 1964) is probably responsible for the variable isotopic contents of the rainwater that falls on Grand Cayman (Fig. 8-16).

Chemical and isotopic composition of groundwater

The major ionic species in the groundwater on Grand Cayman are Na^+, K^+, Ca^{2+}, Mg^{2+}, Cl^-, HCO_3^- and SO_4^{2-}. Fresh groundwater is of the calcium-magnesium



RAINWATER SAMPLES	
C1	George Town - April, 1987
R1	Lower Valley - September, 1987
R2	Lower Valley - October, 1987
R2A	Lower Valley - October, 1987
R3	Lower Valley - November, 1987

Fig. 8-16. Cross-plot of δ^2H versus $\delta^{18}O$ for rainwater on Grand Cayman.

bicarbonate type, whereas the underlying brackish and saline waters are of the sodium chloride type (Fig. 8-17). The low-salinity groundwater (<200 mg l^{-1} Cl^-) is typically part of the shallow, undisturbed freshwater from the groundwater lenses. Most chloride ions in the groundwater are probably derived from upward migration of the underlying saline water (Ng and Jones, 1990). The high HCO_3^- concentrations (150–400 mg l^{-1}) and pH (>7.0) are indicative of carbonate dissolution (Ng and

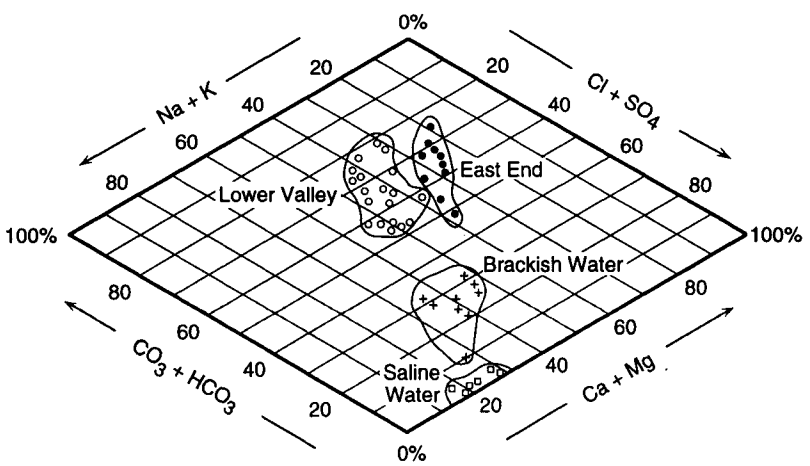


Fig. 8-17. Hydrochemical characteristics of groundwater from Grand Cayman.

Jones, 1990). The saline groundwater has a chloride ion concentration similar to that of the surrounding ocean water suggesting that it was derived from seawater.

The fresh and lightly brackish groundwaters have isotopic compositions of −3.5 to −5.3‰ for $\delta^{18}O$ and −22.0 to −35.0‰ SMOW for $\delta^{2}H$. The highly brackish to saline groundwaters have isotopic compositions of −1.82 to +1.36‰ for $\delta^{18}O$ and −8.9 to +5.7‰ SMOW for $\delta^{2}H$.

Variation in groundwater chemistry

Fresh groundwater from the Lower Valley and East End lenses on Grand Cayman have different hydrochemical characteristics (Fig. 8-18). Monitoring of piezometer 9–84LV of the Lower Valley lens (Fig. 8-10), installed in the freshwater zone, indicates that Cl^- and SO_4^{2-} concentrations increased during the dry periods, but decreased after heavy rainfall (e.g., day 260 in Fig. 8-18A). Ca^{2+}, Mg^{2+} and HCO_3^- contents gradually increased over the monitoring period (Fig. 8-18A). Data from piezometer 6A–84EE of East End lens (Fig. 8-10C), also installed in the freshwater zone, show that Cl^-, SO_4^{2-}, Ca^{2+}, Mg^{2+} and HCO_3^- concentrations were fairly constant (Fig. 8-18b)

Differences in the groundwater characteristics of the Lower Valley and East End lenses are due to variations in aquifer heterogeneity and storage capacity. The Lower Valley lens is about 3.8 km^2 in area and less than 12 m thick, whereas the East End lens is about 15.0 km^2 in area and up 20 m thick. The large volume of water in the East End lens provides a buffer against external influences such as evapotranspiration, precipitation and tides. In the Lower Valley lens, changes in salinity of the waters may be due to mixing in response to fluctuations of the water-table elevation, whereas the increase in Ca^{2+}, Mg^{2+} and HCO_3^- may be due to solution of the carbonate bedrock (Ng and Jones, 1990) caused by recharge from the relatively low pH rainwater.

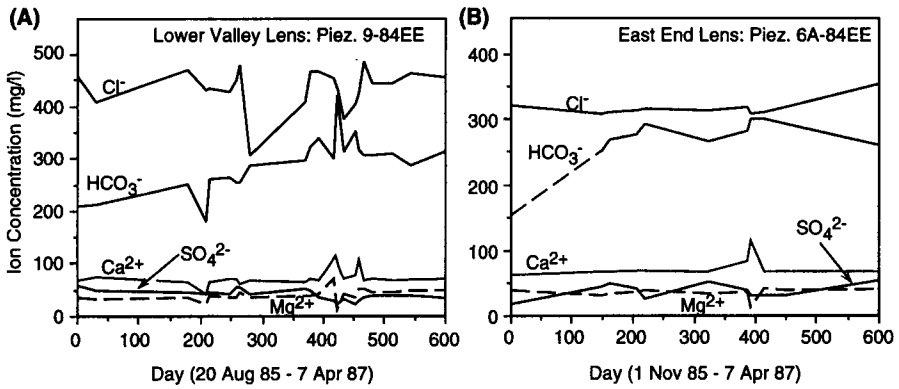


Fig. 8-18. Temporal variation of five major chemical constituents in groundwater from (A) piezometer 9–84 of Lower Valley lens and (B) piezometer 6A–84 of East End lens. Piezometer locations are shown in Figs. 8.10B and 8.10C.

Variation in groundwater isotopes

Isotopic compositions vary between lenses and between different parts of the same lens (Fig. 8-19). In the East End lens, isotopic variation between waters from the New Hut Farm (NHF) wells and the piezometers at East End Central (Fig. 8-10C) is probably caused by variable mixing with the underlying and surrounding brackish to saline water. Being near the lens edge, the groundwater at New Hut Farm is more susceptible to mixing with the isotopically enriched brackish to saline water. Like the

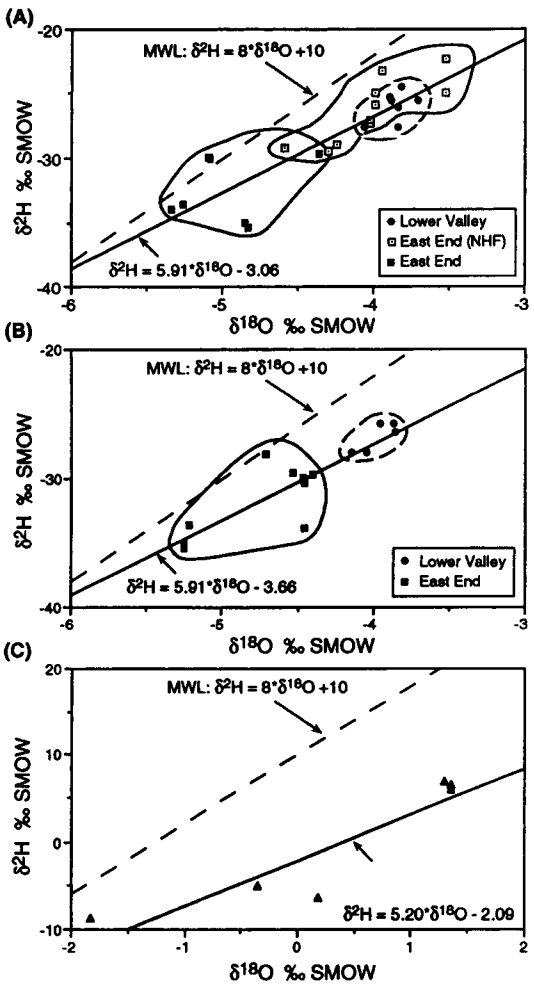


Fig. 8-19. Cross-plots of δ^2H versus $\delta^{18}O$ of the (A) fresh, (B) lightly brackish (<15% seawater salinity) and (C) highly brackish to saline groundwaters on Grand Cayman. MWL refers to meteoric water line. Samples for the latter graph were taken from various deep wells on the western part of Grand Cayman. Location of the New Hut Farm is shown in Fig. 8-10C.

freshwater zone, the lightly brackish groundwaters from the different lenses have distinct isotopic identity (Fig. 8-19B). Temporal variation of $\delta^{18}O$ is generally less than ± 0.2%.

Origin of fresh groundwater

Fresh groundwaters on Grand Cayman have $\delta^{18}O$ values of −3.50 to −5.50‰ SMOW (Fig. 8-19A). The $\delta^{18}O$ content of rainwater samples C1, R1 and R3 (Fig. 8-16) are higher than that of the fresh groundwater (Fig. 8-19A). If these rainwaters were responsible for groundwater recharge, there must have been a significant isotopic exchange between the groundwater and the host rock or mixing of rainwater and isotopically depleted groundwater. Alternatively, groundwaters may be paleo-waters that accumulated when climatic conditions were cooler than at present.

Isotopic exchange between carbonate minerals and water in low-temperature environments is slow (e.g., Welhan, 1987). On Grand Cayman, at an average temperature of ~27°C, isotopic exchange is probably insignificant. If isotopic exchange did take place, an increase in the $\delta^{18}O$ content in the groundwater would be expected because of the high ^{18}O content of the host rocks (Pleydell et al., 1990), whereas the $\delta^{2}H$ values should remain unchanged because the ^{2}H content of carbonate minerals is negligible. The stable isotopic composition of the fresh groundwater (Fig. 8-19A), however, does not show any preferential shift in $\delta^{18}O$ relative to $\delta^{2}H$. The low $\delta^{18}O$ values of the fresh groundwater cannot be attributed to mixing because the underlying brackish to saline groundwaters (Fig. 8-19C) and surface water have higher $\delta^{18}O$ values. Therefore, the groundwater probably came from recent rainfall recharge derived during periods of high-intensity rainfall when the water is isotopically more depleted than that associated with the sparse, low-intensity rainfall.

Stable isotopic signatures of the fresh groundwaters plot along a $\Delta\delta^{2}H/\Delta\delta^{18}O$ trendline (Fig. 8-19A). Departure of the groundwater line from the meteoric water line (Fig. 8-19A) shows that the groundwater underwent evaporation before the rain fell on the land surface, during infiltration through the unsaturated zone and/or by direct evaporation from the shallow water table. The intercept of the groundwater and global meteoric line gives the average $\delta^{18}O$ and $\delta^{2}H$ of the rainwater recharge as −6.25 and −40‰ SMOW, respectively.

Similarity of the $\Delta\delta^{2}H/\Delta\delta^{18}O$ values (Figs. 8.19A, 8.19B) for the fresh and lightly brackish groundwaters (<15% seawater) suggests that there is only minor mixing with the underlying saline water. The intercept of the lightly brackish groundwater line and the global meteoric water line gives average $\delta^{18}O$ and $\delta^{2}H$ values of −6.4 and −41.6‰ SMOW, respectively, for the recharge water. These values are similar to those of the freshwater zone. The better correlation between $\delta^{2}H$ and $\delta^{18}O$ relative to that of the fresh groundwater suggests that surface influences, such as direct evaporation, direct rainwater recharge and influx of surface water, are less severe.

GROUNDWATER RESOURCES DEVELOPMENT

On the Cayman Islands, potable water supply is from rain catchments and, since 1988, an expanding municipal piped distribution of desalinated water. Before the development of the Lower Valley wellfield in 1983, fresh groundwater was abstracted by truckers from privately owned trench wells to supplement domestic water supplies. Commonly, water was pumped directly from the well into the truck-mounted water tank at a high rate, with no precautions taken to ensure the integrity of the resource (Ng and Beswick, 1994). This practice was banned with the passing of the Water Authority Law in 1982.

A pragmatic methodology is practiced on Grand Cayman in managing the groundwater resources because the complicated hydrogeological conditions made it difficult to collect and measure data in sufficient detail before wellfield development. The approach encompasses groundwater legislation, abstraction control and a monitoring program (Ng et al., 1992; Ng and Beswick, 1994). The Water Authority Law vests groundwater in the Government and provides for the establishment of the Water Authority as a statutory body to protect and manage the resource. All work that could impact the resources must be assessed and approved by the Water Authority.

Comprehensive programs were established to monitor the groundwater resources of the Lower Valley lens since 1984 and the East End lens since 1985, where government wellfields are in operation (Ng et al., 1992; Ng and Beswick, 1994). In the Lower Valley wellfield, the pumping rate of each well is restricted to 0.13 l s^{-1} to prevent unacceptable drawdowns of the water table. The wells in the East End wellfield have controlled abstraction rates that range from 0.13 l s^{-1} to 0.65 l s^{-1}. Both wellfields have no piped distribution network, but rather water is delivered to reservoirs that are a source of water for the truckers. At present, the production capacity of the Lower Valley wellfield is 170 m^3 day^{-1} whereas the East End wellfield is 350 m^3 day^{-1}.

The total amount of groundwater abstracted from the Lower Valley and East End wellfields has gradually reduced from a peak production of 106,000 m^3 y^{-1} in 1989 to 66,000 m^3 y^{-1} in 1992. The decrease is due largely to the decline in demand since the Water Authority began distributing desalinated water to George Town in early 1988. Given that piped desalinated water will be available to about 90% of the island's population by the end of 1994, the pressure on groundwater extraction will be significantly reduced. The groundwater, however, remains an important resource for agricultural and other uses. Presently, there are plans to construct a piped distribution from the East End lens to the local district. To date, careful management has maintained the integrity of the lenses and ensured their use as a reliable source of potable water in the future.

CASE STUDY: THE CAYMAN ISLAND KARST

The architecture of the carbonate succession on the Cayman Islands is a reflection of multiple cycles of carbonate deposition during sea-level highstands followed by erosion during sea-level lowstands. Over the last 30 m.y. these islands have undergone at least three major phases of karst development that have significantly modified the rocks. Of critical importance is the fact that each successive phase of karst development overprinted the earlier phases of karst development.

Karst cycles

Significant drops in sea level during the late Oligocene to early Miocene and the Messinian (late Miocene) exposed the carbonate successions of these islands to subaerial weathering. Extensive bedrock dissolution during both periods produced rugged terrains and extensive subsurface dissolution. Information on the late Oligocene-early Miocene terrain is limited because the resultant unconformity is evident only in the vertical cliffs on the east end of Cayman Brac (Fig. 8-6). Reconstruction of that surface shows that it has at least 25 m of relief (Jones and Hunter, 1994). Messinian karsting on Grand Cayman produced a rugged topography with at least 40 m of relief (Fig. 8-8), deep sinkholes and numerous caves (Jones and Hunter, 1994).

Late Pliocene karsting caused erosion and removal of much of the upper part of the Pedro Castle Formation on Grand Cayman. On the western part of this island, erosion produced a depression with a relief of up to 10 m and exhumed the peripheral rim that is an integral part of the Cayman unconformity. Subsurface dissolution during this phase of exposure produced caves in the Pedro Castle and Cayman Formations.

The Cayman Islands remained exposed until the Sangamonian highstand (118–130 ka) when sea level rose to +6 m (Jones and Hunter, 1990). This rise in sea level, however, was not sufficient to completely flood Grand Cayman. Thus, much of the eastern part of the island and the peripheral rim remained in the erosional domain. Since the Sangamonian highstand, most of the island has remained above sea level. As a result, modern phytokarst is evident over much of the island (Folk et al., 1973; Jones, 1989).

Antecedent topography and sedimentation

Each cycle of karst development was terminated by a rise in sea level that led to flooding of the islands and renewed sedimentation. The topography produced during the previous phase of exposure, however, controlled sedimentation and strongly influenced the depositional patterns that developed as sea level rose. Sedimentation during the early Pliocene, for example, was strongly influenced by the rugged topography that had developed on Grand Cayman during the Messinian. Much of the sedimentation on the western part of the island took place in an atoll-like structure

with restricted water circulation. Similarly, sedimentation during the Sangamonian highstand was restricted and controlled by the topography that developed on Grand Cayman during the preceding phase of subaerial exposure (Fig. 8-9; Jones and Hunter, 1990).

Overprinting of karst features

One of the legacies of each phase of karst development was a substrate with high porosity and permeability. Thus, fossil-moldic pores, caves, solution-widened fissures and sinkholes were produced during each episode of karst development. In some cases these features were limited to the carbonate succession that was laid down during the preceding depositional episode. In other cases, these features were formed in the older successions that had been exposed at the surface. For example, the Cayman Formation contains dissolutional features that formed during the Messinian, late Pliocene, or Quaternary phases of karst development. Despite their differences in age, these features are commonly in close proximity to each other.

Cavity-filling sediments and precipitates

Cavities produced by bedrock dissolution during phases of subaerial exposure commonly become the receptacles for precipitates, exogenetic sediments and endogenetic sediments. As shown by Jones and Smith (1988), Jones (1992a, 1992b) and Jones and Kahle (1995), cavities in the Bluff Group of the Cayman Islands contain a vast array of speleothems and internal sediments. Many caves in the Brac, Cayman and Pedro Castle Formations contain spectacular arrays of stalactites, stalagmites, flowstone and various other cave precipitates (Jones and Motyka, 1987; Jones and MacDonald, 1989). Available evidence suggests that there have been many different episodes of speleothem precipitation. Internal sediments, found in cavities and caves of all size, include caymanite, terra rossa, various types of breccia, marine sediments and limestones (Jones, 1992a, 1992b). These sediments originated in the shallow lagoons around the island, in the coastal ponds and swamps (Jones, 1992b) and by various subsurface processes (Jones and Kahle, 1995). The sediment is commonly transported onshore and into the karst terrain by periodic storms and hurricanes that sweep across these islands (Jones, 1992a). As that water moves across the island it picks up sediment from the ponds, swamps and soils that are at the land surface. Eventually, this water transports the sediment into the subsurface where it deposits it in the open cavities and caves that may be far beneath the land surface. Much of the internal sediment is deposited during transgressions when there is little difference between the level of the sea and that of the land (Jones, 1992b). Under these conditions, storm waves can easily reach the interior of the islands.

There is, however, no guarantee that all of the available cavities and caves will be completely filled with sediment and/or precipitates. All of these cavities may become the sites of further precipitation and sedimentation during the next phase of sub-

aerial exposure. The upper part of the Cayman Formation in the Pedro Castle area of Grand Cayman, for example, contains internal sediments that were deposited prior to and after deposition of the Pedro Castle Formation (Jones, 1992a). In some cases, unconformities between different layers of internal sediment in the same cavity show that substantial time elapsed between different episodes of sedimentation.

The internal sediments found in the cavities and caves of a karst terrain are important because they can provide vital clues about the conditions that existed when the islands were subaerially exposed. In many cases, these sediments are the only record of the processes that were operative during these periods.

ACKNOWLEDGMENTS

This paper is based on research that has been financially supported by the Natural Sciences and Engineering Research Council of Canada (Grant No. A 6090) and logistically supported by Mr. Richard Beswick (Director, Water Authority-Cayman) and Dr. John Davies (Director, Mosquito Control and Research Unit). We are indebted to J. Bellow, P. Blanchon, S.A. Cenidwen, Q.H. Goodbody, W. Kalbfleisch, E.B. Lockhart, K. Phimester, S. Pleydell, J. Rehman, A. Shourie, C. Squair, D. Smith, and B. Tongpenyai who have assisted this research in many ways and Elsie Tsang for help in preparing the manuscript.

REFERENCES

Brunt, M.A., Giglioli, M.E., Mather, J.D., Piper, D.J.W. and Richards, H.G., 1973. The Pleistocene rocks of the Cayman Islands. Geol. Mag., 110: 209–304.

Bugg, S.F. and Lloyd, J.W., 1976. A study of freshwater lens configuration in the Cayman Islands using resistivity methods. Q. J. Eng. Geol., 9: 2911–302.

Cerridwen, S.A. and Jones, B., 1991. Distribution of bivalves and gastropods in the Pleistocene Ironshore Formation, Grand Cayman, British West Indies. Carib. Jour. Sci., 27: 97–116.

Dansgaard, W., 1964. Stable isotopes in precipitation. Tellus, 16: 436–468.

Emery, K.O. and Milliman, J.D., 1980. Shallow-water limestones from slope off Grand Cayman Island. J. Geol., 88: 483–488.

Folk, R.L., Roberts, H.H. and Moore, C.H., 1973. Black phytokarst from Hell, Cayman Islands, British West Indies. Geol. Soc. Am. Bull., 84: 2351–2360.

Horsfield, W.T., 1975. Quatemary movements in the Greater Antilles. Geol. Soc. Am. Bull., 86: 933–938.

Hunter, I.G., 1994. Modern and ancient coral associations of the Cayman Islands. Ph.D. Dissertation, University of Alberta, 345 pp.

Hunter, I.G. and Jones, B., 1988. The corals and paleogeography of the Ironstone Formation on Grand Cayman, B.W.I. Proc. Sixth Intern. Coral Reef Symp., (Townsville), 3: 431–435.

Jones, B., 1988. The influence of plants and micro-organisms on diagenetic in caliche: example from the Pleistocene Ironshore Formation on Cayman Brac, British West Indies. Bull. Can. Petrol. Geol., 36: 191–201.

Jones, B., 1989 The role of micro-organisms in phytokarst development on dolostones and limestones, Grand Cayman, British West Indies. Can. J. Earth Sci., 26: 2204–2213.

Jones, B., 1992a. Caymanite, a cavity-filling deposit in the Oligocene-Miocene Bluff Formation of the Cayman Islands. Can. J. Earth Sci., 29: 720–736.

Jones, B., 1992b. Void-filling deposits in karst terrains of isolated oceanic islands, a case study from Tertiary carbonates of the Cayman Islands. Sedimentol., 39: 857–876.

Jones, B. and Goodbody, Q.H., 1984. Biological factors in the formation of quiet-water ooids. Bull. Can. Petrol. Geol., 32: 190–200.

Jones, B. and Hunter, I.G., 1989. The Oligocene-Miocene Bluff Formation on Grand Cayman. Carib. Jour. Sci., 25: 71–85.

Jones, B. and Hunter, I.G., 1990. Pleistocene paleogeography and sea levels on the Cayman Islands, British West Indies. Coral Reefs, 9: 81–91.

Jones, B. and Hunter, I.G., 1994. Messinian (late Miocene) karst on Grand Cayman, British West Indies: an example of an erosional sequence boundary. J. Sediment. Res., B64: 531–541.

Jones, B. and Kahle, C.F., 1995. Origin of endogenetic micrite in karst terrains: a case study from the Cayman Islands. J. Sediment. Res., A65: 283–293.

Jones, B. and MacDonald, R.W., 1989. Micro-organisms and crystal fabrics in cave pisoliths from Grand Cayman, British West Indies. J. Sediment. Petrol., 58: 457–467.

Jones, B. and Motyka, A., 1987. Biogenic structures and micrite in stalactites from Grand Cayman Island, British West Indies. Can. J. Earth Sci., 24,: 1402–1411.

Jones, B. and Ng, K.-C., 1988. The structure and diagenesis of rhizoliths from Cayman Brac, British West Indies. J. Sediment. Petrol., 58: 457–467.

Jones, B. and Pemberton, S.G., 1988. Lithophaga borings and their influence on the diagenesis of corals in the Pleistocene Ironshore Formation of Grand Cayman Island, British West Indies. Palaios, 3: 3–21.

Jones, B. and Smith, D., 1988. Open and filled karst features on the Cayman Islands: implications for the recognition of paleokarst. Can. J. Earth Sci., 25: 1277–1291.

Jones, B., Lockhart, E.B. and Squair, C.A., 1984. Phreatic and vadose cements in the Tertiary Bluff Formation of Grand Cayman Island, British West Indies. Bull. Can. Petrol. Geol., 32: 382–397.

Jones, B., Pleydell, S.A., Ng, K.-C. and Longstaffe, F.J., 1989. Formation of poikilotopic calcite-dolomite fabrics in the Oligocene-Miocene Bluff Formation of Grand Cayman, British West Indies. Bull. Can. Petrol. Geol., 37: 255–265.

Jones, B., Hunter, I.G. and Kyser, T.K., 1994a. Stratigraphy of the Bluff Formation (Miocene-Pliocene) and the newly defined Brac Formation (Oligocene), Cayman Brac, British West Indies. Carib. Jour. Sci., 30: 30–51.

Jones, B., Hunter, I.G. and Kyser, T.K., 1994b. Revised stratigraphic nomenclature for the Tertiary strata of the Cayman Islands. Carib. Jour. Sci., 30: 53–68.

Kreitler, C.W. and Browning, L.A., 1983. Nitrogen-isotope analysis of groundwater nitrate in carbonate aquifers: natural sources versus human pollution. J. Hydrol., 61: 285–301.

MacDonald, K. C. and Holcombe, T.L., 1978. Inversion of magnetic anomalies and sea-floor spreading in the Cayman Trough. Earth Planet. Sci. Lett., 40: 407–414.

Mather, J.D., 1972. The geology of Grand Cayman and its control over the development of lenses of potable groundwater. Memorias-Transactions de la VI Conferencia Geologica del Caribe, Isla de Margarita, Venezuela, pp. 154–157.

Matley, C.A., 1926. The Geology of the Cayman Islands (British West Indies) and their relation to the Bartlett Trough. Q. J. Geol. Soc. London, 82: 352–387.

Ng, K.-C. and Beswick, R.G.B., 1994. Ground Water of the Cayman Islands. In: M.A. Brunt and J.E. Davies (Editors), The Cayman Islands: Natural History and Biogeography, Kluwer Academic Publishers, Dordrecht, p. 61–74.

Ng, K.-C. and Jones, B., 1990. Chemical and stable isotopic characteristics of ground water on Grand Cayman. In: J.H. Krishna, V. Quinones-Aponte, F. Gomez-Gomez and G. Morris (Editors), Proc. Intern. Symp. Tropical Hydrology, Am. Water Resour. Assoc., pp. 411–420.

Ng, K.-C. and Jones, B., 1995. Hydrogeochemistry of Grand Cayman, British West Indies: Implications for Carbonate Diagenetic Studies. J. Hydrol., 164: 193–216.

Ng, K.-C., Jones, B. and Beswick, R., 1992. Hydrogeology of Grand Cayman, British West Indies: a karstic dolostone aquifer. J. Hydrol., 134: 273–295.

Pemberton, S.G. and Jones, B., 1988. Ichnology of the Pleistocene Ironshore Formation, Grand Cayman Island, British West Indies. J. Paleont., 62: 495–505.

Perfit, M.R. and Heezen, B.C., 1978. The geology and evolution of the Cayman Trench. Bull. Geol. Soc. Am., 89: 1155–1174.

Pleydell, S.M. and Jones, B., 1988. Boring of various faunal elements in the Oligocene-Miocene Bluff Formation of Grand Cayman, British West Indies. J. Paleont., 62: 348–367.

Pleydell, S.M., Jones, B., Longstaffe, F.J. and Baadsgaard, H., 1990. Dolomitization of the Oligocene-Miocene Bluff Formation on Grand Cayman, British West Indies. Can. J. Earth Sci., 27: 1098–1110.

Rigby, J.K. and Roberts, H.H., 1976. Geology, reefs and marine communities of Grand Cayman Island, B.W.I. Brigham Young Univ. Geol. Studies, Spec. Publ., 4: 195 pp.

Shourie, A., 1993. Depositional architecture of the late Pleistocene Ironstone Formation, Grand Cayman, British West Indies. M.Sc. Thesis, University of Alberta, Edmonton, 100 pp.

Vail, P.R. and Hardenbol, J., 1979. Sea-level changes during the Tertiary. Oceanus, 22: 71–80.

Warthin, A.S., 1959. Ironshore in some West Indian Islands. Trans. N.Y. Acad. Sci., 21: 649–652.

Welhan, J.A., 1987. Stable isotope hydrology. In: T.K. Kyser (Editor), Stable Isotope Geochemistry of Low Temperature Fluids. Mineral. Assoc. Can., Short Course 13: 129–161.

Woodroffe, C.D., Stoddart, D.R. and Giglioli, M.E.C., 1980. Pleistocene patch reefs and Holocene swamp morphology, Grand Cayman Island, West Indies. J. Biogeogr., 7: 649–652.

WHO (World Health Organization), 1971. Nolmes europennes applicable a beau de boisson (European standards for potable water, 2nd edition), Geneva, 62 pp.

Geology and Hydrogeology of Carbonate Islands. Developments in Sedimentology 54
edited by H.L. Vacher and T. Quinn
© 1997 Elsevier Science B.V. All rights reserved.

Chapter 9

GEOLOGY OF ISLA DE MONA, PUERTO RICO

LUIS A. GONZALEZ, HECTOR M. RUIZ, BRUCE E. TAGGART, ANN F. BUDD, and VANESSA MONELL

INTRODUCTION

Isla de Mona (18°05'N, 67°53'W) is a carbonate island located in the south-central Mona Passage between Puerto Rico and Hispaniola in the northeastern Caribbean Sea (Fig. 9-1). It is located 72 km west of Puerto Rico and covers an area of 55 km^2 (Fig. 9-2). Isla de Mona and its small neighbor, Isla Monito, are part of the Mona Platform, a bathymetric high bounded to the north by a major northwest-trending fault zone of unknown displacement (Rodríguez et al., 1977). Isla de Mona is subject to uninterrupted easterly trade winds throughout the year (Calvesbert, 1973). The small land mass of Isla de Mona and its low elevation of <100 m result in a climate similar to that of the surrounding ocean. Specific climatic data on Isla de Mona are restricted to reports on daily rainfall. The climate of Isla de Mona is considered semi-arid with very little or no water surplus based on moisture-index calculations by Calvesbert (1973). Mean annual rainfall for the island is 809 mm with the greatest amount of rainfall occurring during October and November. Temperatures range from 24°C in January to 28°C in July and August, with a mean annual temperature of ~26°C.

Tectonic and geologic setting

The northeastern margin of the Caribbean Sea consists of a complex plate boundary dominated by strike-slip motion (Burke et al., 1978; Masson and Scanlon, 1991). The region is bounded by the Puerto Rico Trench on the north and by the Muertos Trough on the south (Fig. 9-1); both are characterized by oblique underthrusting (Schell and Tarr, 1978; Biju-Duval et al., 1983; Mason and Scanlon, 1991). Pindell and Barrett (1990) suggested that the present tectonic regime of the region reflects a change in Caribbean Plate motion from a northerly to a more easterly direction caused by the collision of the Caribbean Plate with the Bahamas Bank beginning in the Eocene. This change in plate motion in the Eocene resulted in termination of volcanism in the northeastern Caribbean. Reefs have developed in the region since the Oligocene.

Isla de Mona and Isla Monito are part of an upthrown structural block bounded by several nearly vertical faults (Rodríguez et al., 1977) (Fig. 9-3). Monito is separated from Isla de Mona by a shallow graben (Kaye, 1959; Rodríguez et al., 1977). Rodríguez et al. (1977) suggested that normal faulting in the vicinity of Isla de Mona

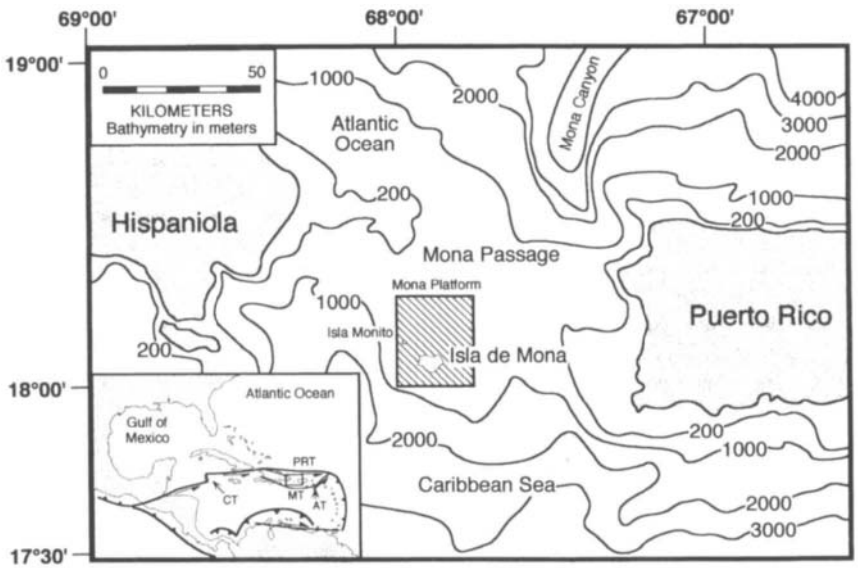


Fig. 9-1. Location map for Isla de Mona and the Mona Platform area (diagonal hatching). Inset map shows generalized tectonic features of the Caribbean region. Key: PRT, Puerto Rico Trench; MT, Muertos Trough; AT, Anegada Trough; CT, Cayman Trough.

resulted in a general tilting of both islands to the southwest. Seismic activity in the region suggests that some of the faults may still be active today (McCann, pers. comm., 1989).

The coastal plains of Isla de Mona consist of Neogene (Holocene?) carbonate-sand deposits from Playa Sardinera on the west side of the island to Punta Arenas (Fig. 9-2). Holocene beachrock (with the most recent ones containing bricks, bottles, and other artifacts from the last two centuries) is common along the sandy shore. The coastal plain on the west side of the island, North of Playa Sardinera, on the southwest part of the island south of Punta Arenas to Playa del Uvero, and along the southeast side of the island from Playa de Pajaros to Punta Este, is composed of Pleistocene coral-reef terraces covered by a thin carbonate sand layer (Kaye, 1959). The Pleistocene reef terraces are better developed on the southwest coastal plain.

The Isla de Mona plateau is composed of two Neogene lithostratigraphic units, the Lirio Limestone and the Isla de Mona Dolomite (Fig. 9-4A), originally described by Kaye (1959) and later redefined by Briggs and Seiders (1972). Kaye (1959) named the lower unit, which makes up the bulk of the carbonates of the island, the Isla de Mona Limestone; he also named what he considered a significantly thinner upper unit, the Lirio Limestone (after Lirio Cave). The lower unit (Isla de Mona Limestone) was described as thickly bedded, dense, white to light yellow, finely crystalline "exceptionally pure" limestone. Kaye (1959) noted that one sample collected from the base of Punta Este was pure dolomite, but he did not define the nature or lateral extent of dolomitization. The Lirio Limestone was described by Kaye (1959) as a thinly

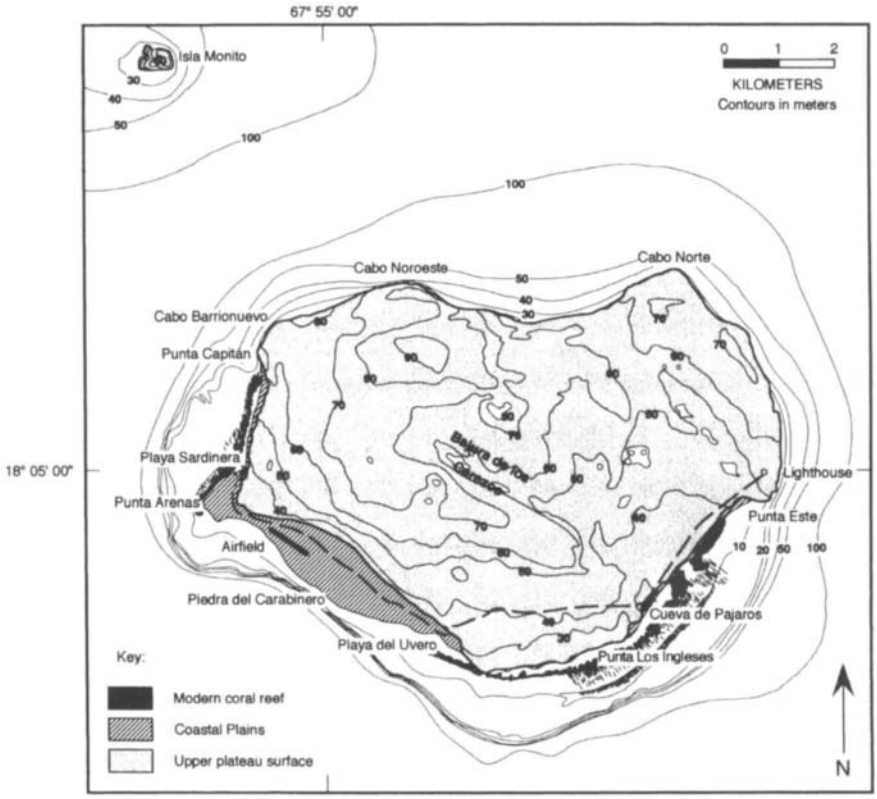


Fig. 9-2. Generalized topographic and bathymetric map of Isla de Mona. (After Briggs and Seiders, 1972, and Kaye, 1959.).

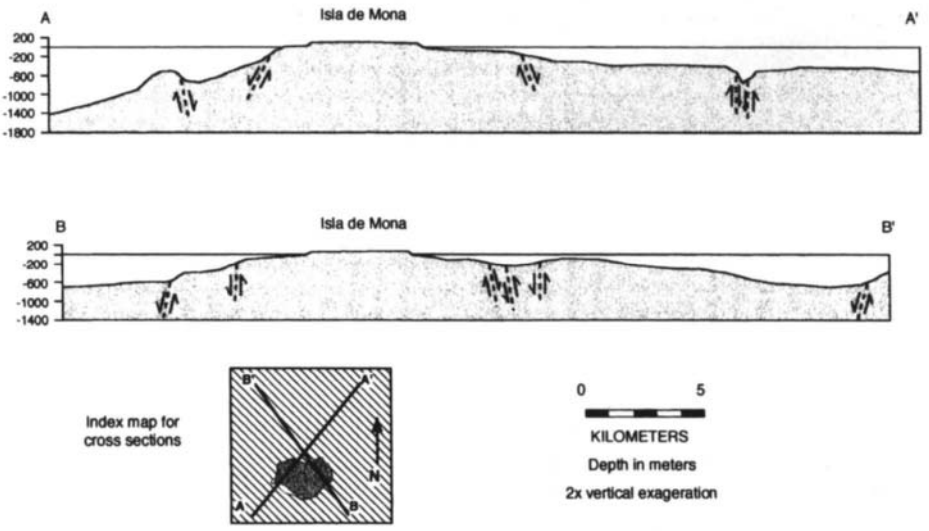


Fig. 9-3. Simplified structural and bathymetric cross sections of the Mona Platform. (Modified from Rodríguez et al., 1977.).

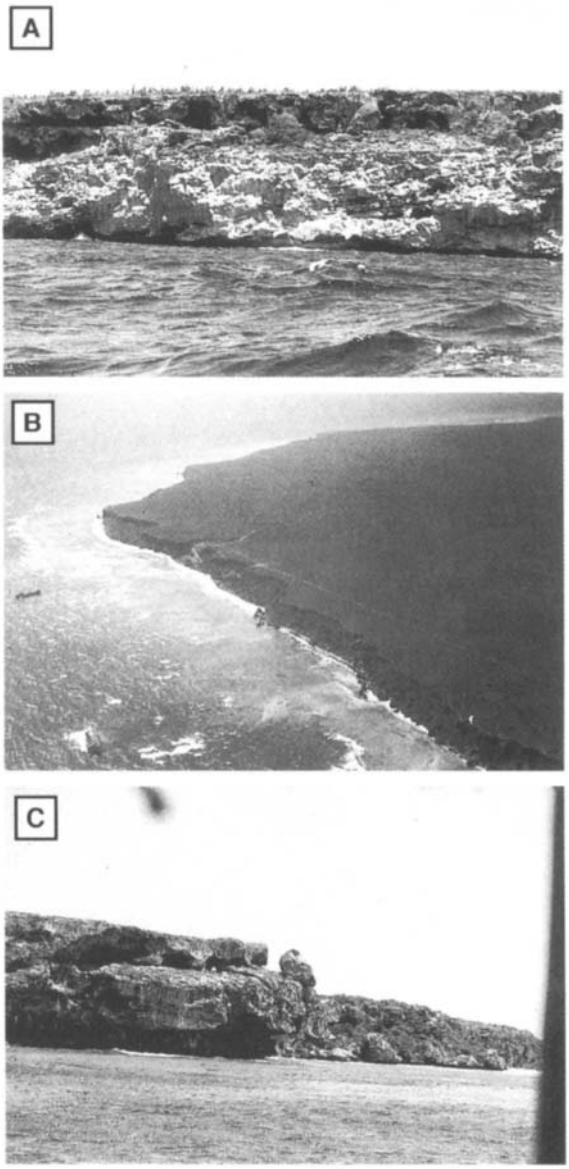


Fig. 9-4. (A) Cliff outcrops on Punta Este (Fig. 9.2). The lowermost bedded units are backreef facies of the Mona Reef Complex within the Isla de Mona Dolomite, and the uppermost cavernous layers are the reef-core facies of the Lirio Limestone. Two levels of breached flank margin caves are observed in the Lirio Limestone and produce the apparent horizontal bed. Height of the section is approximately 50 m. (B) Aerial view of the southeastern portion of Isla de Mona. Road descends to the coast at Playa Pajaros and follows east (right) to the lighthouse. Note the numerous collapse blocks on the coastal plain and the modern fringing reef delineated by the seaward surf. These cliffs are developed on the reef-core facies of the Mona Reef Complex in the Lirio Limestone. Average elevation of cliffs is approximately 35 m. (C) Cliff exposures at the southernmost tip of Isla de Mona. Note the two well-developed cave levels. These are distal forereef beds of the Mona Reef Complex (Lirio Limestone). Height of section is approximately 25 m.

bedded, dense, finely crystalline limestone. Briggs and Seiders (1972) recognized the extensive amount of dolomite present in the rocks of Isla de Mona and redefined the lower unit as a thick to very thick, locally cross-bedded, well-indurated, finely crystalline calcitic dolomite. The unit was then renamed the Isla de Mona Dolomite.

The Lirio Limestone was redescribed as a cavernous, thickly bedded, locally cross-bedded, chalky, fine-grained limestone. Kaye (1959) reported an early to middle Miocene age for the Isla de Mona Limestone and suggested a Pliocene to Pleistocene age for the Lirio Limestone, on the basis of corals collected from the southwestern corner of the island. Kaye (1959) interpreted both units as being flat-lying with local undulations of as much as 3.5° dip in the lower unit and less than 1° dip in the Lirio Limestone. The Lirio Limestone was interpreted as being deposited on an erosional surface developed on the Isla de Mona Dolomite (Kaye, 1959). Briggs and Seiders (1972) observed that the relationship between the two units was more complex than envisioned by Kaye (1959).

The Isla de Mona Dolomite is exposed in continuous exposures on the northern and eastern seacliffs, in the center of the island at Bajura de los Cerezos (Fig. 9-2), and in discontinuous exposures below the Lirio Limestone along the base of the southern seacliffs. The Isla de Mona Dolomite disappears below the Lirio Limestone along the southwestern and western coasts from Playa Uvero to the area south of Punta Capitán on the west, and in the area between Playa de Pajaros and Punta Este on the southeastern coast (Fig. 9-2). The dolomite attains a maximum exposed thickness of approximately 80 m along the northern coast. These exposures of the Isla de Mona Dolomite gradually disappear towards the southwestern and southern side of Isla de Mona and are replaced by the Lirio Limestone, which has a maximum exposed thickness of 40 m.

The plateau surface of Isla de Mona is characterized by many sinkholes, mostly in the Lirio Limestone. A vast system of NW-SE-trending fractures (Kaye, 1959; Briggs and Seiders, 1972) can be easily detected from aerial photographs. This fracture pattern appears to control major sinkhole development in the central regions of Isla de Mona. On the northern and northeastern sides of Isla de Mona, the vertical seacliffs plunge to 30 m below present sea level (Rodríguez et al., 1977). Seismic reflection studies by Rodríguez et al. (1977) indicate that the seafloor surrounding Isla de Mona (~400 km^2) is composed of similar, if not identical, lithologies as those exposed on both Isla de Mona and Isla Monito.

Geomorphic features of Isla de Mona

Isla de Mona consists of a relatively flat carbonate plateau, ranging in elevation from 20 m in the southeast to 90 m in the northwest, bounded by vertical seacliffs on its north and east sides and a low-lying discontinuous coastal plain on its south and west sides (Figs. 9-2; 9-4A, B). The surface of Isla de Mona is characterized by well-developed karst. Multiple cave systems are present along the cliffs surrounding the plateau (Fig. 9-4A, C). Sinkholes, depressions and coastal terraces are floored by soils.

The coastal cliffs of Isla de Mona, from Punta Este to Cabo Barrionuevo, are distinguished by the presence of multiple levels of caves that penetrate up to 250 m

into the plateau (Briggs and Seiders, 1972; Frank, 1993) (Fig. 9-4A, C). Caves are more common and better developed within the Lirio Limestone with cave floors extending down into the dolomite in some cases, although some caves are developed completely within the Isla de Mona Dolomite. The caves are preferentially developed with elongated mazework rooms parallel to the cliff faces (Fig. 9-5), and suggest development in flank margins (Frank, 1993; Ruiz et al., 1993; Mylroie et al., 1994) with no contemporaneous openings. Present-day openings of the caves are the result of scarp retreat after uplift of the Mona Plateau.

Dissolution features of various sizes and shapes are widely distributed across the plateau surface. Solution pits are cylindrically shaped, penetrating as much as 20 m deep into the Lirio Limestone and Isla de Mona Dolomite; they frequently become bell-shaped at the bottom (Fig. 9-6). In many areas, the bottom of the solution pits lie within the transition zone between the Isla de Mona Dolomite and the Lirio Limestone and commonly continue down several meters into the dolomite.

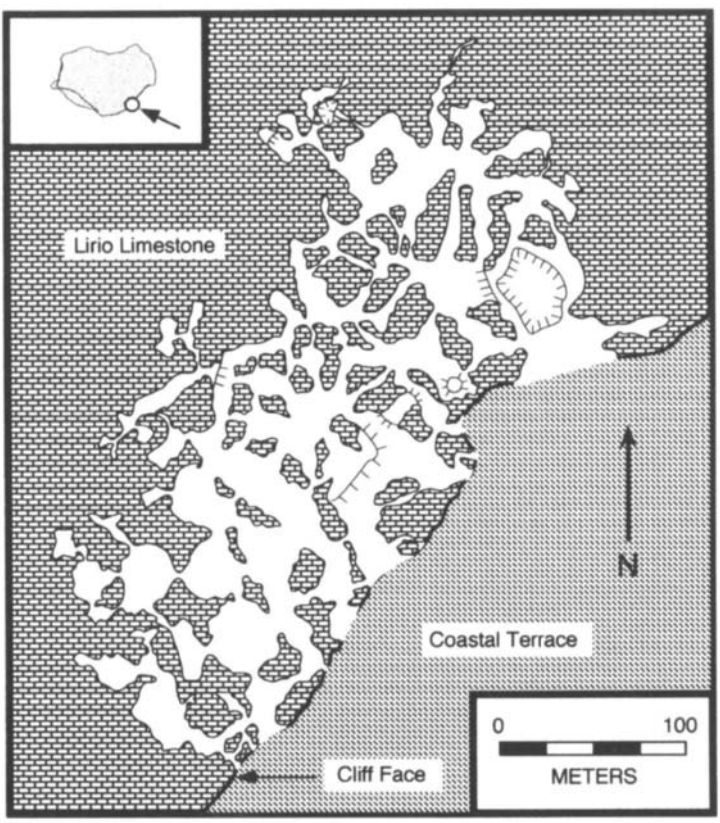


Fig. 9-5. Map of Cueva de los Pajaros (Cueva Caballo). The cave is typical of the many caves on the southeast side of the island, elongated parallel to the cliff face with a mazework formed by residual limestone pillars. (Modified from unpublished map of Ramon Carrasquillo, 1992.).

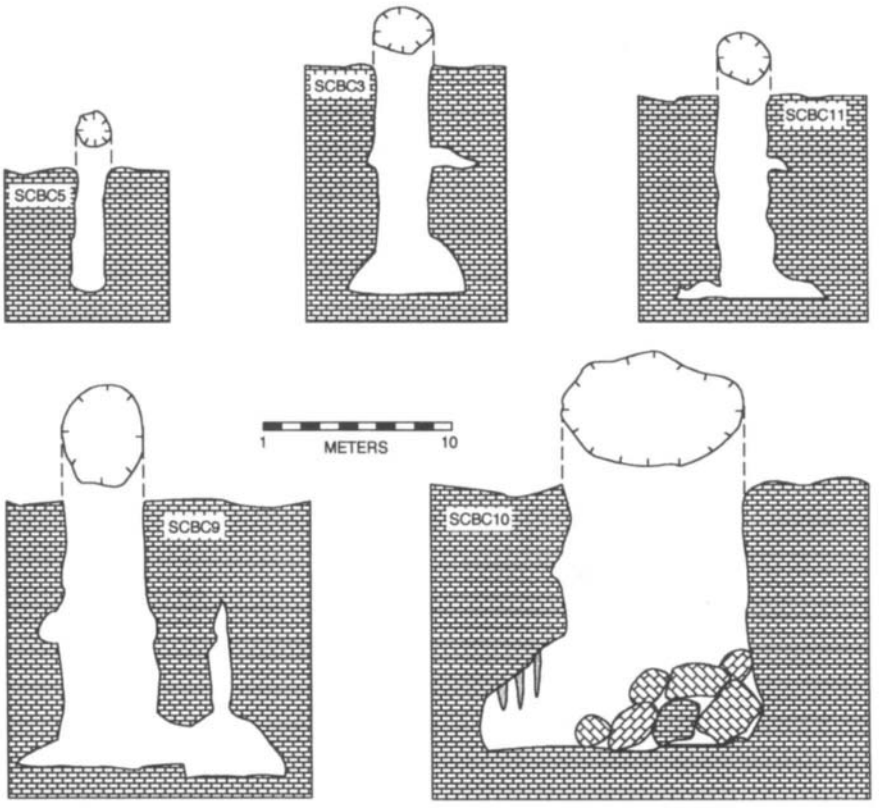


Fig. 9-6. Cross section of selected solution pits along the trail to Bajura de los Cerezos. Note that most of the pits have enlarged, bell-shaped bottoms.

Commonly, small passages, always choked with sediment, branch out from the bottom. Shallow bowl-shaped depressions, 1–5 m deep and 10–20 m wide, are also common. These shallow sinks commonly have small caves with very short lateral extension or have well-developed solution pits. Most solution pits and shallow sinkholes have bottoms filled with reddish sediments (soils). Along the coastline, collapse sinkholes related to the extensive coastal cave system are common.

A large-scale NW-SE-trending fracture system originally described by Kaye (1959) appears to control the development of sinkholes in some areas of the plateau, especially along Bajura de los Cerezos. Originally interpreted as a fault zone by Briggs and Seiders (1972), Bajura de los Cerezos consists of a zone of collapsed blocks of interbedded dolomite and limestone. This linear NW-SE-trending depression extends down into the Isla de Mona Dolomite. A thin layer of Lirio Limestone is present around the periphery of this collapse sink.

The central interior portions of Isla de Mona are characterized by the presence of residual soils (Rivera, 1973) indicating that local drainage was directed toward those

areas. The average thickness of these soils in Bajura de los Cerezos is 60 cm (Rivera, 1973). Lowlands and shallow sinkholes in other parts of the island also are covered with these red soils. The coastal terrace on the southwestern side of Isla de Mona is overlain by thin, sandy soils. The western portion of the coastal terrace at Playa Sardinera is overlain by calcareous soils and carbonate sand deposits, which are up to 1.5 m thick and are derived from the modern reef developed along this coast (Rivera, 1973).

REVISED STRATIGRAPHY AND SEDIMENTARY FRAMEWORK OF THE MIOCENE CARBONATES

In the course of diagenetic studies on Isla de Mona (Monell, 1988; Ruiz, 1989, 1993; González et al., 1990, 1992; Ruiz et al., 1991; Ruiz et al., 1993), numerous stratigraphic sections have been measured and sampled along the cliffs, sinkholes, and caves of Isla de Mona (Fig. 9-7). Data from measured sections have been supplemented by numerous observations and samples from the rock exposure on the plateau surface. The observed stratigraphic relationships, lithologic variability, and fossil faunas of the Lirio Limestone and Isla de Mona Dolomite reveal that their general lithologies and the depositional relationships are much more complex than envisioned by Kaye (1959), Briggs and Seiders (1972) and Aaron (1973).

A prominent zone of differential weathering is exposed along the cliffs bounding the northern half of Isla de Mona and is accentuated by the coincidence of numerous cave bottoms. Briggs and Seiders (1972), in mapping the contact between the Isla de Mona Dolomite and Lirio Limestone along the cliffs, identified this zone of differential weathering as an erosional surface on the Isla de Mona Dolomite. Although, from a distance (Fig. 9-4A), the cavernous Lirio Limestone does appears to be deposited over an erosional surface on the Isla de Mona Dolomite, close examination along measured sections and samples from cliff outcrops (Fig. 9-7) reveals a transitional change in lithology from almost pure dolomite at the base of the sections (e.g., Punta Este, Punta Capitán) to almost pure limestone at the top. The dolomitized units in many areas extend several meters above this apparent surface, whereas cave bottoms extend several meters below the limestone-dolomite transitional contact. In some solution pits along the trail to Bajura de Los Cerezos, the dolomite-to-limestone transition occurs within a few meters and, in one instance, within a single bed. In most places, there is no evidence of an erosional surface separating the dolomitized carbonates (Isla de Mona Dolomite) and the limestone (Lirio Limestone). For example, the contact between the Isla de Mona Dolomite and the Lirio Limestone in Punta Este (Fig. 9-4A) and along the western and northern cliffs is marked by a lithologic transition upsection from pure dolomite, calcitic dolomite, dolomitic limestone, and limestone. This lithologic transition also coincides with a gradual facies transition from backreef (packstones to wackestones) to reef flat and reef crest (packstones to boundstone). Differential weathering (Fig. 9-4A) has accentuated this transition zone which resulted from diagenetic processes leading to preferential dolomitization below and calcitization and

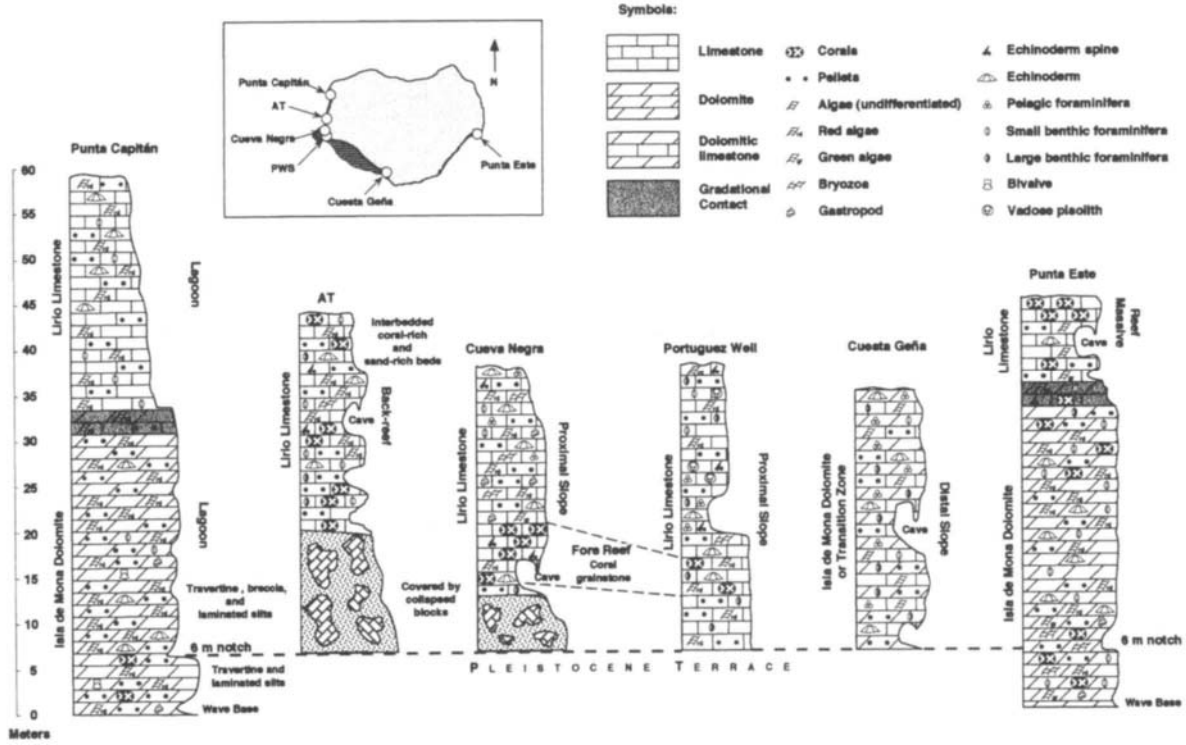


Fig. 9-7. Selected measured sections of pre-Pleistocene carbonates of Isla de Mona along the coastal cliffs. Sections are hung on the base of a 6-m wave-cut notch above the Pleistocene reef tract or beach deposits.

dissolution above this transition zone. All the observations indicate that the contact between the Isla de Mona Dolomite and the Lirio Limestone is diagenetic and not a primary depositional or erosional feature.

Although evidence for periodic subaerial exposure is present throughout the island, no islandwide erosional surface can be recognized. The only extensive exposure surfaces that can be recognized are present in the central lowland of Bajura de los Cerezos (Fig. 9-8). In Bajura de los Cerezos, three distinct paleosol horizons containing freshwater and brackish-water snails and vadose pisoliths have been identified. These paleosols are very similar in appearance to the modern red residual soils present throughout the lowlands of Isla de Mona. These paleosols are separated from each other by at least 0.5 meter of marine carbonates consisting of lagoonal and backreef sands. The carbonate beds underlying and overlying the lowermost paleosol horizon, as well as the paleosol horizon itself, are completely dolomitized. The youngest paleosol contains dolomitized grains and is overlain by nondolomitized marine carbonates. Similar paleosols can be found at scattered localities throughout the island. It is possible that a greater number of exposure surfaces are recorded by paleosols, but the highly dissected nature of the outcrops prevents the differentiation between paleosols and protosols (Carew and Mylroie, 1991).

The carbonates of Isla de Mona contain an abundant coral fauna partially obscured by extensive diagenetic alteration (González et al., 1992). Four major reef facies (distinct biofacies and lithofacies) have been recognized: forereef, reef core, backreef, and lagoon and have been referred to as the Mona Reef Complex by González et al. (1992) (Figs. 9-9, 9-10). Forereef deposits dominate the southwestern side of the island (e.g., Cuesta Geña, Cueva Negra). The reef core is exposed at Playa de Pajaros and Cueva de la Escalera along the southeastern side of the plateau and along the Los Caobos trail on the western side of the plateau. Backreef deposits are exposed in Punta Este and near Playa Sardinera. The northern and central sections of the Isla de Mona plateau consist mostly of lagoon deposits and scattered patch



Fig. 9-8. Paleosol horizons in Bajura de los Cerezos. These paleosols are the uppermost nondolomitized horizons developed on lagoon facies of the Mona Reef Complex within the Lirio Limestone.

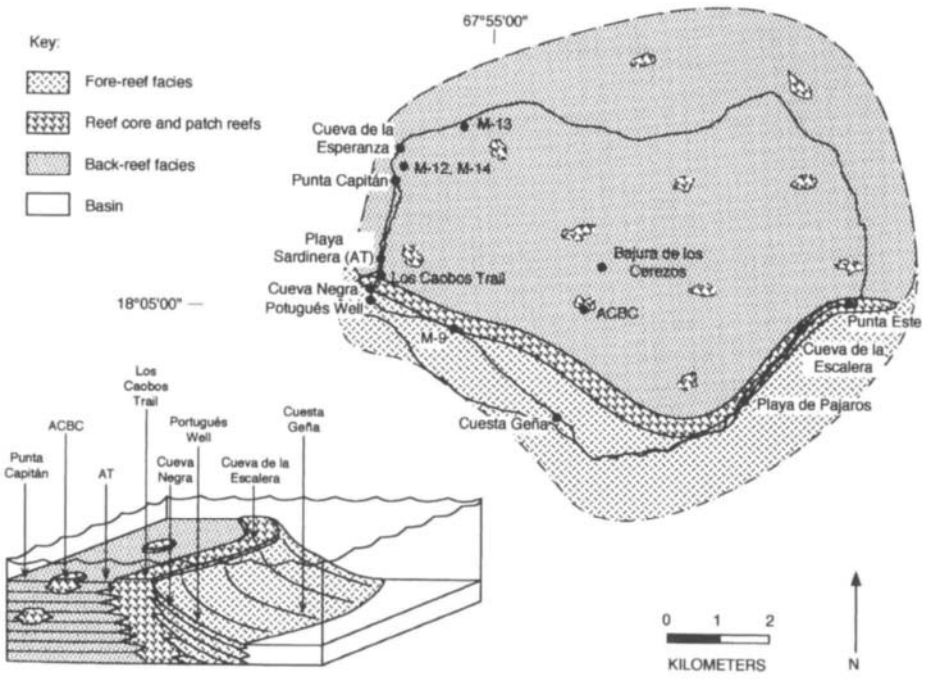


Fig. 9-9. Interpreted distribution of the Miocene Mona Reef Complex. Filled circles indicate locality of measured sections. Inset is idealized block diagram through the reef complex.

reefs. The coral fauna of the Mona Reef Complex indicate a late Miocene to earliest Pliocene age for the reef (Budd et al., 1994).

Mona reef complex

Forereef facies. The lithology on the southwestern side of Isla de Mona is predominantly fine-grained carbonates, commonly wackestones and rarely packstones and mudstones. At Cuesta Geña (Fig. 9-7), the rocks contain small amounts of encrusting red algae, benthic foraminifera and minor occurrences of small echinoid fragments, surrounded by a matrix consisting mainly of pelleted mud. Planktonic foraminifera are locally abundant, especially in the upper 5 m of this section. The absence of corals combined with the abundance of planktonic foraminifera support the interpretation that these are distal forereef deposits at Cuesta Geña. At Portugués Well near Playa Sardinera, thinly bedded deposits dipping as much as 21° to the southwest are exposed (Fig. 9-10A). At this locality, the Lirio Limestone contains abundant coral debris, minor isolated corals in growth position (commonly preserved as moldic porosity), and small amounts of planktonic foraminifera. *Stylophora granulata*, *Undaria agaricites*, and *Acropora panamensis* are recognized as the most common corals at this locality (Fig. 9-7). Higher in the section, at nearby

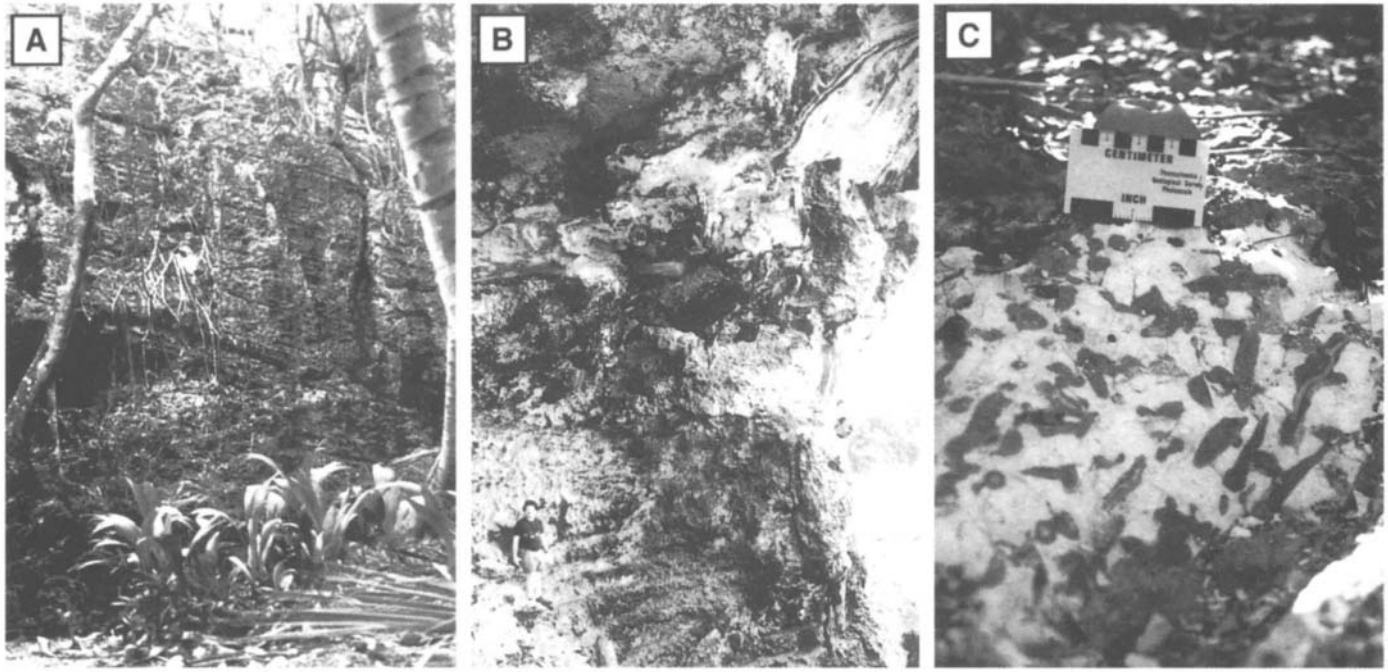


Fig. 9-10. (A) Steeply dipping forereef beds of the Mona Reef Complex at the Portugués Well. Approximate height of section is 20 m. (B) Backreef facies of the Mona Reef Complex north of Playa Sardinera (at section of Fig. 9.4). Note the thinly bedded coral-rich units at the base that grade upward into medium- to thick-bedded backreef sands. Massive-looking beds are flowstone-covered limestone. (C) Exposure of the reef-core on the cliffs at Playa Sardinera. Corals, *Stylophora*, have been preferentially dissolved and infilled by soil materials frequently containing root casts. These are the "vermicular structures" described by Kaye (1959).

Cueva Negra, the lithology consists of medium-bedded, coral-rich grainstones at the base of the cliff grading to packstones at the top of the plateau (Fig. 9-7). Both green and red algae, as well as minor amounts of benthic foraminifera and echinoderm fragments floating in a pelleted-mud matrix, are also present. To the south, these beds grade to wackestones with the relative abundance of coral debris decreasing markedly. This locality has been interpreted as a proximal forereef facies.

Reef-core facies. The cliffs along the southeastern coast of Isla de Mona (Figs. 9-4A, B; 9-7, 9-9), from Playa de Pajaros to the upper 5 m of Punta Este, expose a thick accumulation of the coral *Caulastrea portoricensis*. These corals are commonly preserved as moldic porosity. Near the surface of the plateau, coral molds are frequently filled by calcite-cemented red soil material (Fig. 9-10B). Land gastropod fragments are locally abundant within these soils. Kaye (1959) reported *Lucidella umbonata*, *Chondropoma turnerae*, *Bulimulus diaphanus*, *Cerion monaense*, *Suavitas* cf., and *Lacteoluna selenina* as the six gastropod species present in these cemented soils. A similar lithology is exposed on the plateau surface along Los Caobos Trail near Playa Sardinera. Abundant benthic foraminifera of the genus *Archaias*, as well as minor amounts of echinoid fragments and planktonic forams, (locally common at Playa de Pajaros) are also present. The grains are mostly suspended in a pelleted-mud matrix. Lithologies vary from wackestones to packstones. The abundance of corals increases toward the northeast with the thickest accumulations occurring at Cueva de la Escalera where the exposed thickness reaches approximately 20 m. The Pleistocene reef terrace fringing the cliffs includes remnants of collapsed cliff blocks of the same material, indicating that the thick accumulation of Miocene corals extended southeast at least to the edge of the Pleistocene terrace.

Backreef facies. Along the cliffs north of Playa Sardinera, the Lirio Limestone grades from medium-bedded units (up to 30 cm thick) at the base of the exposure to interbedded coral-rich and sandy units toward the top of the plateau (Figs. 9-9, 9-10C). The base of the cliff is covered by collapsed blocks of this material. The medium-bedded units exposed at the base of the cliffs are mainly wackestones and locally boundstones. The presence of thickets of *Stylophora minor*, abundant benthic foraminifera, red algae fragments and abundant echinoderm fragments and spines characterize these beds. The coral-rich layers are commonly composed of packstones with occasional boundstones and wackestones. The most common corals found in these beds include *Montastraea trinitatis*, *Mussa* cf., *M. angulosa*, *Stylophora affinis*, and *Acropora saludensis*. The sandier beds contain abundant benthic foraminifera (*Nummulites* and *Amphistegina*) as well as branching red algae. These rocks represent a transition between a reef-flat facies at the base of the section to a backreef facies closer to the top. A similar facies transition also is present at Punta Este, where the thickly bedded backreef sands in the Isla de Mona Dolomite give way to the coral-rich, reef-core facies developed in the Lirio Limestone.

Lagoon facies. The cliff face at Punta Capitán exposes both the Lirio Limestone and the Isla de Mona Dolomite. Packstones and minor amounts of wackestones

composed of abundant encrusting red algae, benthic foraminifera and echinoderm fragments as well as minor amounts of green algae, mollusks and occasional coral fragments encrusted by algae characterize both units. Allochems commonly float in a matrix of pelleted mud. In Cueva de la Esperanza, 0.5 km to the north of Punta Capitán, algal mats composed of filamentous green algae are locally abundant in the Lirio Limestone.

Patch-reef facies. A minor accumulation of corals within backreef deposits in the Lirio Limestone is exposed in shallow caves along the northern side of the island. The localized nature of this buildup indicates the presence of small patch reefs in the area. Measured sections in caves and sinkholes on the trail to Bajura de los Cerezos shows marked similarity to the backreef facies rocks of Punta Capitán. Lithologies are mainly wackestones with some sections showing varying degrees of dolomitization ranging from dolomite at the base to dolomitic limestone at the top. These rocks contain abundant red algae, corals and minor amounts of echinoid fragments. The local abundance of corals indicates that many of these sites were patch reefs that have been preferentially dissolved.

QUATERNARY REEF DEPOSITS

In addition to the Miocene Mona Reef Complex, extensive late Pleistocene fringing-reef deposits occur on the coastal terrace bounding the southern and western sides of the island. Scattered throughout the plateau surface there are smaller Pleistocene fringing reefs associated with escarpments easily recognized in aerial photographs and mapped by Kaye (1959).

Upper Pleistocene and Holocene reef deposits

Isla de Mona is bounded by a narrow and discontinuous Pleistocene reef terrace along its south and west coasts from Punta Capitán to Punta Este (Fig. 9-2). This terrace, which is up to 1 km wide, rises from an elevation of 0.5–2 m above sea level at the shoreline to a maximum of 10 m against the paleo-seacliffs. The terrace consists of Quaternary reef-tract deposits, reef-rubble deposits, reef-rubble ramparts, reef-rock boulders, and carbonate sands. Vertically continuous reef-tract deposits extend as much as 6 m above and to an unknown depth below present sea level. They are overlain by reef-rubble deposits that reach elevations of 10.2 m at the base of the paleo-seacliff at distances of several hundred meters from the present shoreline. Soil and vegetative cover progressively conceal the terrace surface landward of the shoreline exposures of boundstone and calcirudite. The upper surface of the coastal exposures of the reef terrace are commonly overlain by a dense laminated algal crust and/or caliche layer 1–6 cm thick. This crust, previously described by Kaye (1959), largely covers the upper surface of all observed inland exposures of the terrace.

Eleven corals retrieved from the reef terrace deposits north of Playa Sardinera, near Piedra del Carabinero, and southwest of Punta Este at elevations ranging from

2–6.5 m above present sea level have yielded $^{230}Th/^{234}U$ alpha-spectrometric ages between 107–128 ka. Because sea level 125 ka was approximately 6 m higher than present (e.g., Mesolella et al., 1969; Bloom et al., 1974; Ku et al., 1974; Neumann and Moore, 1975) these data indicate that Isla de Mona has been tectonically stable during the last 125 ky. Uranium-series thermal ionization mass spectrometry (TIMS) ages (Lundberg, J., unpub. data, 1993, Carleton University, Ottawa, Canada) for two samples collected from a 4-m-thick *Montastraea annularis* Pleistocene reef-tract exposure indicate that the rate of vertical reef accretion between 122–126 ka was about 0.75 m ky^{-1}. None of the colonies in this exposure are more than 20 cm in diameter (average 8–10 cm), but they are densely packed, like circular flagstones. When observed in plan view these colonies exhibit a multilobate columnar growth form, indicating a shallow-water origin (Roos, 1971; Smith, 1976; Kaplin, 1982).

An unconsolidated Holocene reef-rubble rampart has been deposited at the shoreline seaward of the northwestern tip of the airfield, about 1 km northwest of Piedra del Carabinero (Fig. 9-2). This rampart, which is located about 5 m behind the beach at an elevation of 3 m, is oriented parallel to the shoreline and is approximately 0.5 m high, 20 m long, and 5 m wide. A second more extensive unconsolidated reef-rubble rampart, located on the small Pleistocene reef terrace to the southwest of Punta Este, is approximately 30 m behind the coastline at an elevation of 7 m and is more than 50 m long. These unconsolidated deposits probably resulted from a storm event that occurred during the last 5 ky.

Many boulders of reef-rock, as much as 5 m in diameter, and a large amount of reef-rock debris, as much as 1 m in diameter, lie scattered about on the southwestern coastal plain. Several of these boulders are located within 30 m of the shoreline near Piedra del Carabinero, and many others are found as much as 600 m inland. The 100-m shelf break surrounding Isla de Mona is less than 300 m offshore along the south coast at Piedra del Carabinero. Beyond this point, depths of 1,300 m are attained within 8.5 km of the shoreline. The reef tract on the insular shelf south of Piedra del Carabinero is the only reasonable source for these boulders. A coral sample from the stratigraphic top of one of the inland boulders produced a TIMS age of 4800 y B.P.. TIMS ages of coral samples from the stratigraphic middle and top of one of the shoreline boulders are 5,376 y B.P. and 4,176 y B.P., respectively. These two samples are separated by a distance of 1.7 m, suggesting a net rate of vertical reef accretion of 1.4 m ky^{-1} during this period of time. This rate compares favorably with those determined for other Holocene reefs (Morelock et al., 1977; Shinn et al., 1977; Lighty, 1985; Macintyre et al., 1985). The size of these reef-rock boulders is such that they could have been transported to their present locations only by a seismic seawave or an extreme storm such as a hurricane. Their ages indicate that they were transported to their present locations sometime after 4,176 y B.P.

The age of the Pleistocene reef terrace places its growth at the height of the Sangamon interglacial sea-level highstand. The age of the late Holocene stranded reef-rock boulders correspond to an early stage in the growth and development of the currently active fringing reef during the present interglacial sea-level highstand. The net rates of vertical reef accretion and reef morphology of these Isla de Mona

reef tract exposures and boulders indicate that (1) the Pleistocene reef tract of 122–126 ka was able to maintain a shallow-water position relative to sea level during a period of slowing rising or stable sea level, and (2) that the Holocene reef tract was accreting at a greater rate in response to the rapid rise in sea level that took place during the Holocene (Neumann and Macintyre, 1985).

Lower Pleistocene reef deposits

Pleistocene coral assemblages on the plateau surface itself (Fig. 9-8; sites M9, M12, M13, M14) occur at elevations ranging from 20 m to as much as 70 m above present sea level. These assemblages have not been studied in detail but do include *Acropora palmata*, which is known to occur in the Caribbean only since the early Pleistocene (Budd et al., 1994). These assemblages are associated with escarpments of 1–5 m relief that can be detected from aerial photography of the plateau surface and were first described by Kaye (1959). These lower Pleistocene fringing-reef deposits were most likely the source of corals which led Kaye (1959) to assign a Pliocene-Pleistocene age to the Lirio Limestone. All sampled corals are recrystallized, with only minor aragonitic patches remaining. Attempts to radiometrically date the recrystallized corals utilizing U-series alpha spectrometry produced $^{230}Th/^{232}Th$ and $^{234}U/^{238}U$ ratios that were equilibrium values, indicating that these corals were recrystallized prior to 350 ka and possibly before 700 ka. One nearly completely recrystallized coral at 70 m yielded a recrystallization age of 192 ka. A travertine deposit developed on Pleistocene corals recovered from the plateau surface at 60 m above mean sea level has been dated at 287 ka. The presence of these early to middle Pleistocene features indicates that Isla de Mona was submerged during the early Pleistocene.

DIAGENESIS OF THE MONA REEF COMPLEX

The carbonates of Isla de Mona have been subjected to a variety of diagenetic environments. In general, diagenetic events can be divided into: (1) early submarine diagenesis manifested by the development of micritic envelopes, and marine cementation by fibrous and botryoidal cements; (2) mixed freshwater-seawater diagenesis manifested by preferential dissolution of aragonitic components followed or accompanied by extensive dolomitization in some areas and calcitization in other areas; and (3) repeated periods of meteoric diagenesis indicated by extensive calcitization and dedolomitization and cementation by equant calcite spar with karstification and travertine precipitation.

Submarine diagenesis

Micrite envelopes document a period of alteration concurrent with deposition. The micritized surfaces of grains commonly survive dissolution and provide a surface

for later precipitation of cements. In Isla de Mona, micrite envelopes are common in all sections and environments, although they are more prevalent in the lagoonal facies. Syndepositional cementation by fibrous calcite is limited to coral grainstones in forereef facies in the Lirio Limestone (Fig. 9-11A). Fibrous calcite cement consists

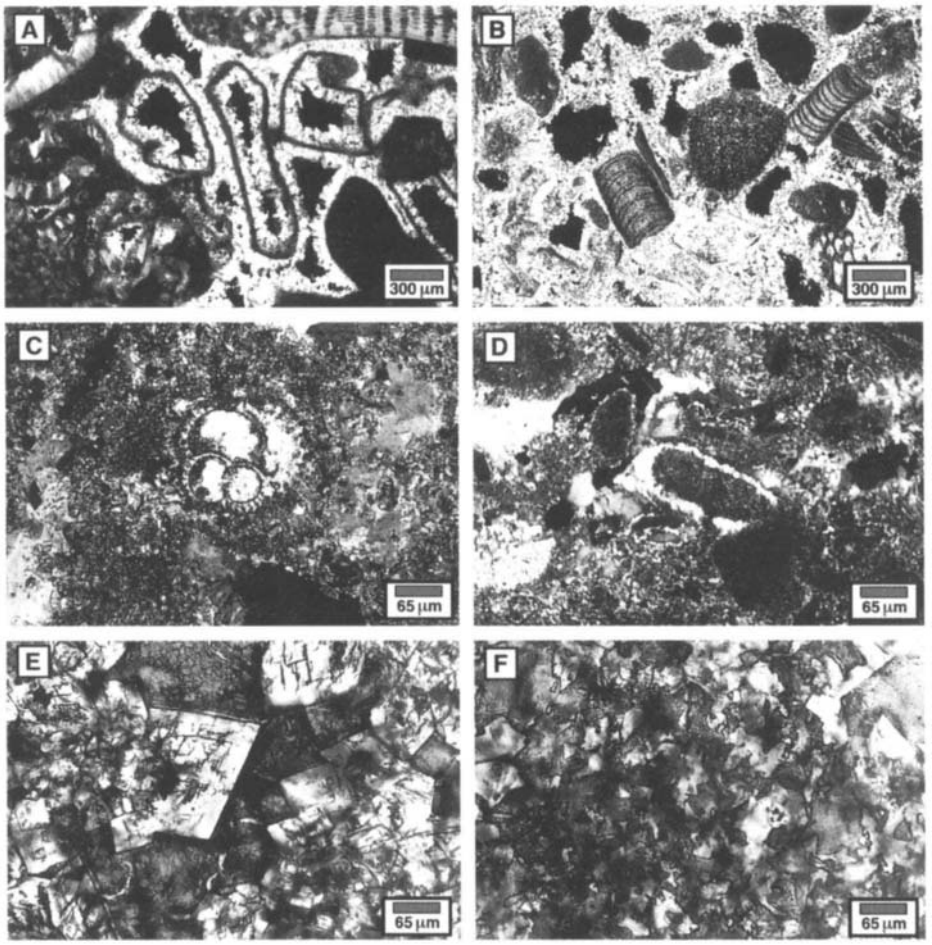


Fig. 9-11. Thin-section photomicrograph of a variety of diagenetic features found in Isla de Mona carbonates. All views are crossed polars. (A) Fibrous calcite cements, interpreted as marine, on coral grains of the Cueva Negra forereef deposits (Lirio Limestone). (B) Backreef packstone from Cueva del Esperanza. The cavities are molds of aragonitic component. The mud matrix has been replaced by microcrystalline calcite. (C) Dolomitized wackestone from Cuesta Geña. Note the fabric preservation of the dolomitized planktonic foraminifera test. A late calcite spar fills some of the early moldic porosity. (D) Dolomitized echinoderm grains and pellets. Note the clear (limpid) dolomite overgrowth followed a late calcite spar. (Slide stained with alizarin red.) (E) Cloudy-centered dolomite rhombs. (Slide stained with alizarin red.) (F) Pervasive dissolution of limpid dolomite cements in packstones from the lagoonal facies at ACBC within the limestone-dolomite transition. (Slide stained with alizarin red.)

of elongate nonluminescent fibers, 240 μm in length, forming continuous isopachous layers around skeletal fragments and thin linings inside foraminifera tests.

The occurrence of cements with botryoidal fabrics in deposits on Isla de Mona is very limited. Development of this type of cement is restricted to areas with limited primary porosity (<20% by volume) on distal forereef deposits on the southern coast of the island. In thin section, botryoidal cements consist of groups of densely packed, nonluminescent, radially oriented fibers 190 μm long showing undulatory extinction under crossed polars.

Fabric-selective dissolution

The dissolution of skeletal components in carbonates of Isla de Mona is mostly fabric-selective. Aragonitic grains such as corals and gastropods are most affected, and grains such as red algae and echinoderm fragments are least affected (Fig. 9-11B). Aragonite dissolution is widespread across the Isla de Mona plateau. Unstable skeletal components are commonly preserved as moldic porosity.

Calcitization

Microcrystalline calcite replaces most of the pelleted muds that form the matrix of the Lirio Limestone (Fig. 9-11B). Skeletal grains are also subject to alteration to microcrystalline calcite, especially in rocks that have been subjected to intense meteoric diagenesis, resulting in a rock where mostly ghosts of the original grains remain. The distribution of this type of replacement calcite is widespread across the Lirio Limestone, but is especially prominent in rocks of the reef-flat and backreef facies. Microcrystalline calcite in Isla de Mona carbonates is nonluminescent.

Bladed calcite cements are often found in the Lirio Limestone. Nonluminescent, bladed (96 μm) calcite cement is found lining interparticle and moldic porosity on coralgal packstones and grainstones of both forereef and reef-flat facies. This cement is characterized by thick and stubby blades forming an irregular layer.

Equant calcite spar is widely distributed among the rocks of the Lirio Limestone. This type of cement is composed of nonluminescent, equant crystals of 20–280 μm. Equant calcite is found associated with a variety of other cement types and fills both primary and secondary porosity (Figs. 11B, C, D, E). Near the top of the plateau, this type of cement locally fills intracoralline as well as vuggy porosity. At the dolomite-limestone transition zone, equant calcite spar postdates dolomitization and appears to be related to dolomite dissolution.

Dolomitization

Dolomite forms the bulk of the carbonates of Isla de Mona. Samples from a number of localities contain varying amounts of dolomite. A vertical transition from pure dolomite at the base of the seacliffs to pure limestone at their top is

present along the eastern and northern sides of the island from Punta Este to Punta Capitán.

Fabric-retentive microcrystalline dolomite is the most common and widely distributed type of dolomite in the island. The fine grain size of these crystals makes it difficult to distinguish them from calcite in thin section without the aid of staining (Fig. 9-11C). This type of dolomite replaces both the abundant pelleted muds as well as skeletal grains that characterize the backreef facies of Isla de Mona. The extent of replacement is variable. Rocks from the lower part of the Isla de Mona Dolomite are pervasively dolomitized including originally high-Mg calcite components such as red algae. At higher elevations, dolomitization mostly affects matrix material whereas red algae remain partially calcitic. Dull luminescence is characteristic of replacive dolomite. Nonluminescent dolomite overgrowths around dolomitized echinoderm fragments are present within the limestone-dolomite transition zone (Fig. 9-11D). The absence of overgrowths on echinoid fragments in the lower part of the measured sections of the Isla de Mona Dolomite, contrasting with their abundance in the upper Isla de Mona Dolomite and the lower Lirio Limestone, suggests that dolomitic overgrowths resulted from replacement of a calcitic precursor.

Euhedral, limpid dolomite spar commonly fills interparticle porosity in the Isla de Mona Dolomite. It commonly fills late vugs and some moldic pores. This cement nucleated around dolomitized grains as well as around areas of dolomitized matrix and increases in size toward the center of the cavities. This nonluminescent cement is commonly associated with grainstones in the Isla de Mona Dolomite.

Dolomite rhombs with cloudy centers and clear rims are also common in the Isla de Mona Dolomite. Cloudy-centered dolomite rhombs are commonly found related to the limestone-dolomite transition zone (Fig. 9-11E). Staining indicates that the center of the rhombs are calcitic. Dull luminescence is characteristic of this type of dolomite.

Zoned dolomite cements are found lining secondary porosity in the Isla de Mona Dolomite. The distribution of this cement is restricted to the lower part of the unit. Its abundance decreases upward toward the zone of transition between dolomite and limestone where it is mostly absent. This type of dolomite consists of alternating dark and light zones that are visible under both transmitted light as well as under cathodoluminescence. Commonly this dolomite cement contains an early nonluminescent inner zone followed by a single brightly luminescent outer zone. Samples from various localities, including Punta Este and Punta Capitán, contain multiple generations that are locally well developed.

Dolomite dissolution and dedolomitization

Evidence of dolomite dissolution (Fig. 9-11F) is present at several localities across Isla de Mona. Partially dissolved dolomite rhombs are locally present within the dolomite-limestone transition zone. Dissolution affects both the cloudy-centered rhombs as well as the limpid dolomite spar that are so common within this zone. Corroded crystal outlines are commonly observed in the limpid dolomite spar. Dissolution of the calcitic centers is evident in many cloudy-centered dolomite rhombs.

Karst and paleosol development

The most prominent dissolution features in Isla de Mona are the extensive caves along the coastal cliffs and the numerous sinkholes and solution pits on the plateau. Frank (1993) presented a complete and detailed description of numerous caves and some sinkholes in Isla de Mona and concluded that cave features conform to those of flank margin caves, as defined by Mylroie and Carew (1990). Several of the caves described by Frank (1993) and smaller caves we have visited along the northern cliffs show evidence of at least two episodes of phreatic dissolution as indicated by dissolution features on subaerial speleothems. In many of the deeper solution pits (>10 m), there appears to be a relict bell-shaped bottom present about 6–10 m from the pit entrance. Elliptical sinkholes, depressions and solution pits commonly are developed preferentially along fractures on the plateau surface. Many of the solution pits and depressions are developed preferentially on what are interpreted as patch reefs of the Mona Reef Complex. In caves and sinkholes, numerous paleosols and/or protosols can be identified. Paleomagnetic analysis of paleosols in Isla de Mona caves indicates that soil development was occurring prior to 780 ka (Matuyama Reversal) (Mylroie et al., 1994). Ongoing magnetostratigraphic work by Bruce Panuska and his students suggests that paleosol accumulation in the caves began no later than 1.0–1.8 Ma and possibly began in the Pliocene (USGS CDO, 1994b).

In addition to the paleosols present in Bajura de los Cerezos, karstic breccias are common throughout most caves and sinkholes. These breccias consist of limestone fragments in a matrix of reddish soil and are commonly cemented by calcite. At a few isolated sites, such as the base of the cliffs at Punta Capitán and in Punta Este, breccias consist of dolomite clasts (dolomitized prior to dolomitization of matrix) in dolomite-cemented residual soil.

Stable isotopes

Stable isotopic analyses were performed on samples of <0.2 mg, extracted with a 500-μm dental drill. Mineralogy was identified by standard staining techniques using alizarin red and potassium ferricyanide. All data presented here are for samples with >90% dolomite or calcite.

Dolomite isotopic compositions range from +4.3 to −4.4‰ for $\delta^{18}O$ and from + 3.4 to −8.3‰ for $\delta^{13}C$ (Fig. 9-12), although the bulk of the dolomite components are greater than 0.0‰ for $\delta^{18}O$ and −4.0‰ for $\delta^{13}C$. In general, dolomite from the outer fringes of the island, such as Punta Este and Punta Capitán, has relatively greater oxygen and carbon values (average $\delta^{18}O$ values of 3.6‰ and $\delta^{13}C$ values of 2.7‰) than those of the interior portions of the island. Dolomite spar and clasts have a narrower range of isotopic values than dolomitized red algae and matrix, and all are greater than −1.0‰ for $\delta^{18}O$ and −6.0‰ for $\delta^{13}C$.

Calcitic components also exhibit a broad range of values ranging from +3.6 to −5.7‰ for $\delta^{18}O$ and from +3.1 to −11.63‰ for $\delta^{13}C$ (Fig. 9-13). In contrast to the dolomite, the bulk of the calcitic components have isotopic values less than −1.0‰ for

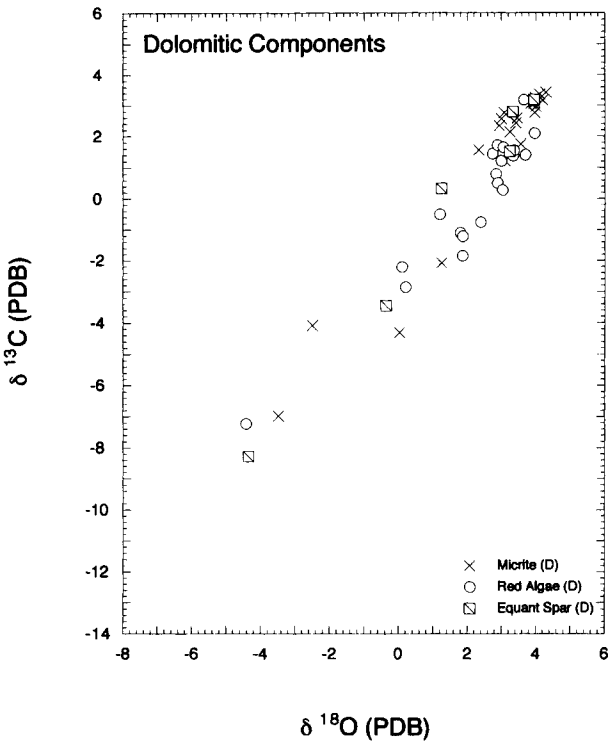


Fig. 9-12. Stable isotope composition of dolomitic (dolomite ≥ 90%) components of the Isla de Mona Dolomite.

$\delta^{18}O$ and −2.0‰ for $\delta^{13}C$. Microcrystalline calcite replacing the pelleted-mud matrix has $\delta^{18}O$ values ranging from −4.5 to −1.0‰, and $\delta^{13}C$ ranges from −6.9 to −4.3‰.

Strontium isotopes

Only two strontium isotope values have been obtained on dolomites with the heaviest $\delta^{18}O$ (Ruiz et al., 1993). Two samples from the lower section of Punta Capitán and Punta Este have $^{87}Sr/^{86}Sr$ values of 0.708915 ± 11 and 0.708829 ± 10 respectively. These data constrain dolomitization of the lower portions of the Isla de Mona Dolomite (if effected by marine fluids) to late Miocene (Tortonian to Messinian).

HYDROGEOLOGY

Modern freshwater resources of Isla de Mona

Hydrogeologic information about Isla de Mona is very limited, although a number of hydrogeologic investigations are being conducted under auspices of the

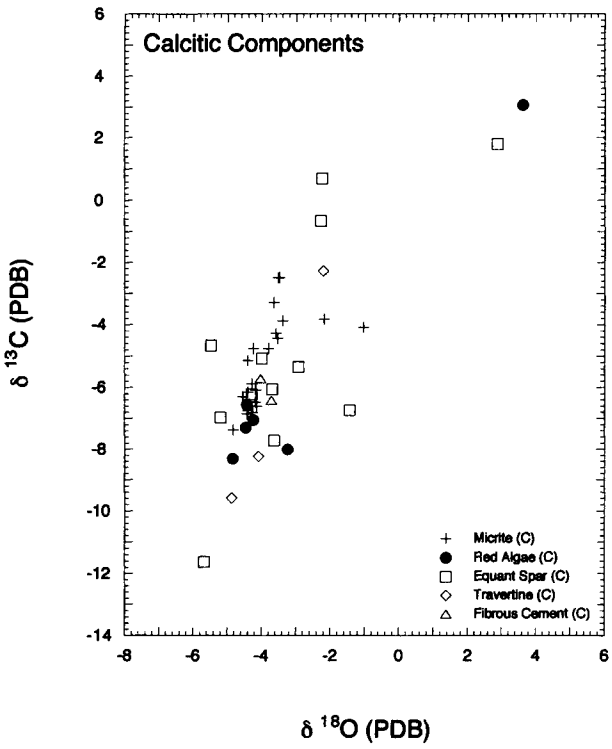


Fig. 9-13. Stable isotope composition of calcitic (calcite ≥ 90%) components of the Lirio Limestone.

U.S. Geological Survey Water Resources Division in San Juan, Puerto Rico. Historic accounts indicate that freshwater was abundant 400 years ago when the island was discovered. At that time, freshwater resources were sufficient to sustain a small population of Taino Indians living on the island. During the period of Spanish colonization in the sixteenth century, the island was denoted on nautical charts as an important watering port (Wadsworth, 1973).

Today, freshwater is in short supply in Isla de Mona. A 5-m^2 brackish-water pond (apparently of human origin) and a small mangrove swamp exist on the reef terrace at the foot of the cliff at Punta Arenas (Jordan, 1973). The evident lack of response of these two features to tidal cycles led Jordan (1973) to suggest that the pond did not have a hydraulic connection to the sea. He attributed water-level fluctuations to evapotranspiration processes and groundwater inflow (approximately 855 L d^{-1}) from the upper plateau.

Recent geophysical reconnaissance by Martínez et al. (1993) suggests that there are two separate freshwater lenses, one developed under the Pleistocene coastal plain, and one under the plateau (i.e., Exuma-type island; Vacher and Wallis, 1992). Four dug wells tapping brackish water exist on the Pleistocene reef terrace on the southwest side of the island (Jordan, 1973). Two wells near Playa Sardinera penetrate sand deposits, and both the well near the airstrip and the one near Playa del

Uvero penetrate the Pleistocene reef deposit. At present, only one of the wells near Playa Sardinera (Pozo del Portugués) is being actively used. Limited sampling by Jordan (1973) indicates that these wells tap a zone of freshwater-seawater mixing. The freshwater lens under the Pleistocene coastal plain is at least 13 m thick (Martínez et al., 1993), and it thins towards the ocean and towards the cliffs of the plateau. Data from a well at the Mona airstrip, 200 m from the shoreline, indicates that groundwater level has a daily tidal cycle with a 7-cm range as compared to the 30-cm ocean tidal cycle (USGS, CDO, 1994).

Though initial work by Martínez et al. (1993) suggested the freshwater lens under the plateau was at least 25 m thick, recent geophysical surveys (transient electromagnetic) by Martínez and others suggests that the thickness of the freshwater lens under the plateau has a maximum thickness of 10 m (USGS, CDO, 1994). These recent estimates are in marked contrast with the hypothetical freshwater lens of over 75 m calculated by Jordan (1973).

The freshwater-saltwater boundary of the freshwater lens beneath the plateau can be found in the caves along the southern side of the island near Punta Los Ingleses in Playa Brava, in a cave developed within the reef-core facies of the Lirio Limestone and infilled by Quaternary reef rubble (mostly *Acropora palmata*). A 1.5-m-diameter hole in the floor of the cave provides access to a 1.0-m-diameter pit that leads to a cave developed within the Quaternary reef rubble and Miocene reef-core facies. The cave has been surveyed by A.M. Nieves of the Puerto Rico Department of Natural Resources, and information on this cave is presented in Frank (1993). The chambers of this cave are partially to completely filled with brackish water. The cave extends at least 30 m north under the plateau, and a sloping tunnel extends south (seaward) for an undetermined distance. An increase in salinity and turbidity can be easily detected in the water in the sloping tunnel. According to statements by commercial fishermen (Tres Hermanos) who have been visiting the island since the 1940s, freshwater is available in some of the lowermost caves from Punta los Ingleses to Punta Caigo no Caigo. According to these accounts, freshwater could be obtained by carefully skimming the top of the water column in these water-filled caves.

Geologic controls on groundwater

Differences in lithology, porosity, and permeability between the Lirio Limestone and the Isla de Mona Dolomite must play a role in groundwater migration. Well-developed interconnected channel porosity contributes to the excellent permeability of the limestone as evidenced by the lack of well-developed surface drainage. Extensive dolomitization combined with equant calcite precipitation has significantly contributed to the reduction of both primary and secondary porosity in the Isla de Mona Dolomite. As a result, permeability of the Isla de Mona Dolomite is significantly lower than that of the Lirio Limestone, and so the dolomite could be an effective permeability barrier for water moving down the rock column. The many fractures present throughout the island must play a definite role in groundwater movement by providing surface runoff with direct access to the subsurface. Although

the depth of these fractures is not known, there is reason to believe that they may extend deep down into the Isla de Mona Dolomite, providing an underground channel system for water flow through the dolomite body.

The fact that no evidence of freshwater discharge can be seen along the northern and eastern cliffs, coupled with the thinness of the freshwater lens under the plateau surface, argues for structural control on groundwater distribution under the plateau. The limited thickness of the freshwater lens under the plateau surface suggests that either freshwater discharge around the periphery of Isla de Mona is much greater or infiltration rates are much smaller than those estimated by Jordan (1973). The postdepositional dip of several degrees to the southwest and the many fractures might also play an important role in groundwater distribution.

Ongoing research by the U. S. Geological Survey Caribbean District Office is aimed at providing essential data to properly evaluate groundwater distribution and its controls in Isla de Mona.

CASE STUDY: EVOLUTION OF THE MONA REEF COMPLEX

Episodic exposure

The depositional and diagenetic history of Isla de Mona is not one of simple continuous carbonate sedimentation followed by a simple sequence of diagenetic events. The Mona Reef Complex is a complex backstepping reef which was responding to episodic sea-level rise (tectono-eustatic) through the life of the complex. Portions of the Mona Reef Complex were periodically exposed allowing development of vadose and meteoric phreatic zones in the central portions of the plateau and mixed freshwater-seawater zones in the periphery of the plateau.

Although in nearby Puerto Rico the northern Oligocene-Miocene limestone belt remained exposed during late Miocene to early Pliocene (Moussa et al., 1987; Seiglie and Moussa, 1984), the events that resulted in the exposure of the limestone belt of northern Puerto Rico led to the shallowing of the Mona Platform and the initiation of reefal carbonate deposition. The repeated late Miocene to early Pliocene sea-level oscillations recorded through the Caribbean region and Florida (e.g., Pleydell et al., 1991; Mallinson et al., 1994) resulted in the frequent changes in diagenetic environments observed in the Isla de Mona Miocene carbonates.

The paleosols in the central portions of the island indicate that at least three periods of exposure of the lagoon and backreef facies took place towards the final episode of deposition of the Mona Reef Complex. Dolomitized karstic breccias and travertines in the lower portions of the Isla de Mona Dolomite indicate that a minimum of two exposure episodes occurred in the earlier stages of development of the Mona Reef Complex before dolomitization. It is likely that numerous exposure events took place through the history of deposition of the Mona Reef Complex.

The relatively large sea-level drop in the late Miocene recorded in other Caribbean localities (e.g., Lidz, 1984; Jones and Hunter, 1994) also resulted in exposure of the Mona Reef Complex. Whereas northern Puerto Rico (Moussa et al., 1987) and

Grand Cayman (Jones and Hunter, 1994; Pleydell et al., 1991) underwent Pliocene submergence, the absence of definite Pliocene fauna indicates that Isla de Mona was exposed through much of the Pliocene.

The presence of early to middle Pleistocene fringing reefs coinciding with escarpments indicate that Isla de Mona remained at or near sea level during the first half of the Pleistocene. The position of escarpments and fringing reefs on the plateau surface indicates that during the early to middle Pleistocene Isla de Mona underwent three, and possibly more, relatively rapid episodic uplift events. The lowest fringing-reef deposits of the escarpment occur at 20 m above present sea level. Several wave-cut notches and/or breached flank margin caves, the most prominent at 6, 10 and 20 m above mean sea level, are present in the cliffs. These data, in conjunction with radiometrically dated late Pleistocene reef-tract deposits, indicates that Isla de Mona underwent episodic uplift during most of the Pleistocene and has remained stable since 125 ka.

Environments of diagenesis

All of the existing data indicate that the diagenetic alteration of the Isla de Mona carbonates resulted from alteration in four distinct and frequently coeval diagenetic environments. Significant carbonate dissolution and development of paleosols and travertines took place predominantly in the meteoric vadose environments. Carbonate dissolution, particularly fabric-selective dissolution of aragonitic components and the replacement of original marine components by calcite or dolomite, took place in phreatic environments. During lowstands of sea level, the topographic highs in what is now the plateau surface were above sea level and acted as catchment areas for meteoric waters resulting in development of an extensive freshwater lens that graded downward and laterally into a marine phreatic environment. The selective dissolution of lagoon patch reefs resulting in the formation of solution pits and sinkholes suggests that these areas, because of the higher permeability relative to surrounding calcareous sands and mud, acted as conduits for aragonite and calcite-undersaturated fluids into the phreatic environment.

The presence of fabric-selective aragonite dissolution in calcitized and dolomitized rocks indicates that throughout the diagenetic history of the Miocene carbonates of Isla de Mona diagenetic fluids remained undersaturated with respect to aragonite. The preferential calcitization or dolomitization of matrix carbonate and the delicate fabric-retentive calcitization or dolomitization of skeletal components indicate that most of the observed fabrics are primary diagenetic features, although complete replacement of individual units might have required repeated exposure to the same diagenetic environment.

Zoned dolomite cements showing alternating bright and nonluminescent bands are locally abundant. Similar cements have been interpreted to form under alternating oxidizing and reducing conditions such as those found in mixed freshwater-seawater zones (e.g., Mussman et al., 1988). The presence of cloudy-centered dolomite rhombs indicates that the initial dolomitizing fluids were saturated with respect to calcite that forms the inclusion of calcitic material at the center of the dolomite

crystals. At a later stage when water became undersaturated with respect to calcite but supersaturated with respect to dolomite, continued precipitation formed inclusion-free crystals. Such evolution of porewaters is consistent with the mixed freshwater-seawater hypothesis of dolomite formation and has been suggested by Sibley (1980) to explain the cloudy-centered dolomite rhombs of Bonaire and similar features observed in Grand Cayman (Pleydell et al., 1990).

The petrographic properties are consistent with alteration in the mixed freshwater-seawater zone. The broad range of $\delta^{18}O$ and $\delta^{13}C$ isotopic values also indicate that the bulk of the replacement fabrics, dolomitic and calcitic, were formed in meteoric-marine mixed fluids. Considered together, the isotopic data can best be described by hyperbolic trends that are characteristic of mixing of fluids with different concentrations of dissolved CO_2 (Lohmann, 1988) (Fig. 9-14). The isotope data of the red algae argue against these trends being the result of mechanical mixing of components with two different isotopic compositions for two reasons: (1) mechanical mixing should result in a linear trend (Lohmann, 1988); and (2) all the data are for components with >90% calcite or dolomite, the observed range in $\delta^{13}C$ and $\delta^{18}O$ values is much greater than can be attributed to 5–10% contamination. The endmember compositions can be inferred to be meteoric and marine fluids. The relatively high isotopic values of dolomite ($\delta^{18}O \geq 0.0‰$; $\delta^{13}C \geq -4.0‰$) suggest that the bulk of the dolomitization occurred in fluids containing over 50% seawater. The lighter values for the calcitic components ($\delta^{18}O \leq -1.0‰$; $\delta^{13}C \leq -2.0‰$) indicate that calcitization took place predominantly in fluids containing over 50% meteoric water. The broader range of $\delta^{13}C$ values of the calcitic components can be attributed to: (1) different degrees of rock-water interaction; (2) a more open system leading to greater variability in PCO_2; (3) analyses including samples that have undergone surface evaporation and degassing; and (4) inclusion of modern vadose calcite indistinguishable from Miocene to Pleistocene calcite.

The dolomites from Isla de Mona show a wider range of isotopic values than those reported for other dolomites interpreted to have formed under similar mixed freshwater-seawater conditions. Microcrystalline dolomites replacing carbonate muds show greater $\delta^{18}O$ values but a similar range of $\delta^{13}C$ values compared to Pleistocene mixed freshwater-seawater dolomites from the Yucatán (Ward and Halley, 1985). Nevertheless, values are consistent with data for Neogene dolomites from the Bahamas reported by Supko (1977) and mixed freshwater-seawater dolomites reported from Mururoa Atoll in the Pacific (Aïssaoui et al., 1986) [q.v., Chap. 13]. $\delta^{18}O$ values greater than +2‰ have been considered to indicate precipitation from a fluid with a similar or greater isotopic value than seawater (Supko, 1977). The isotopic compositions of most Isla de Mona dolomites fall between 0 to +4‰ suggesting that either seawater or evaporation-concentrated freshwater could have been involved in dolomitization.

Other alternative dolomitizing fluids (e.g., pure seawater and hypersaline water) and mechanisms (e.g., burial dolomitization and thermally driven circulation of interstitial water) are judged not to be responsible for dolomitization at Isla de Mona for several reasons. Although seawater dolomitization cannot be discounted in distal portion of the mixed freshwater-seawater environment, the range of dolomite

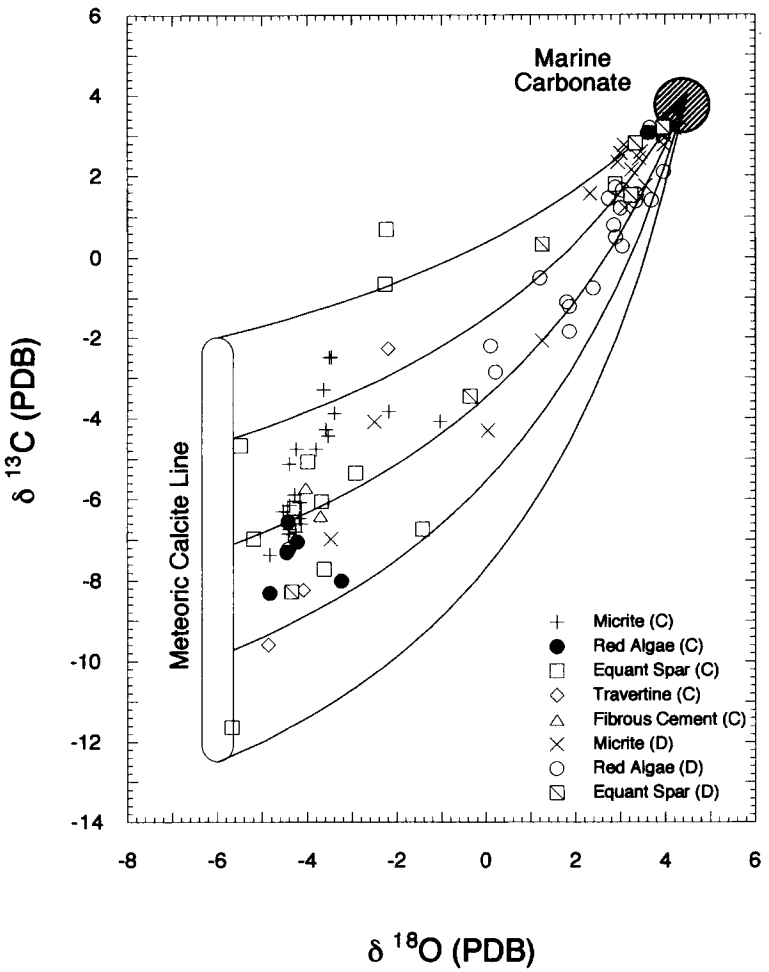


Fig. 9-14. Stable isotope composition of calcite (C) and dolomite (D) components. Hyperbolic trends generated by utilizing a marine endmember composition with a $\delta^{18}O$ of +2.2‰, $\delta^{13}C$ of +3.5‰ and a ΣCO_2 of 2.5 mmoles L^{-1} at 24°C, and the freshwater endmember with a $\delta^{18}O$ of −3.75‰, $\delta^{13}C$ ranging from −3.8 to −14.1‰ and a ΣCO_2 ranging from 5.0 to 8.0 mmoles L^{-1} at 6°C. The $\delta^{18}O$ composition of modern precipitation for this region of the Caribbean ranges from −2.0 to −5.7‰ (Rozanski et al. 1993). The $\delta^{18}O$ of coastal aquifers in southwestern Dominican Republic (with a climate similar to Isla de Mona) range from −3.2 to −4.0‰ (Febrillet et al., 1987).

isotopic composition is greater than can be accounted for by mechanical mixing of components produced by marine fluids of slightly different isotopic composition or by contamination with calcite. It is unlikely that massive dolomitization in Isla de Mona was achieved solely by circulating seawater. There is no evidence that hypersaline or evaporite depositional environments have been developed at Isla de Mona and, although the relatively heavy $\delta^{18}O$ values of the marine endmember

calcite and dolomites would suggest some evaporative enrichment of seawater, no evaporite minerals, primary or secondary, have been identified. The absence of major compaction features; the dolomitization of paleosols, karstic breccias, and travertines; the development of multiple levels of flank margin caves; and the absence of highly negative $\delta^{18}O$ values (<8‰) — all do not support diagenetic alteration in the burial environment. Finally, the absence of highly negative $\delta^{18}O$ argues against anomalous geothermal gradients to drive seawater or brine circulation. The lightest observed $\delta^{18}O$ values in Isla de Mona can be attributed to precipitation from normal freshwater, (assuming the $\delta^{18}O$ range observed for modern freshwater in the region (Rozanski et al., 1993; Febrillet et al., 1987) at temperatures ranging of 22–27°C.

The diagenetic alteration of Isla de Mona carbonates probably began shortly after the formation of reefal deposits near sea level which could be easily exposed to meteoric fluids during minor sea-level falls. Diagenetic alteration occurred in episodic fashion, and in discontinuous areas throughout the life of the Mona Reef Complex. Sustained exposure of late Miocene limestones occurred during the Pliocene and throughout the episodic uplift events that affected Isla de Mona throughout the Pleistocene. The recurrent exposure led to development of multiple cave levels in Isla de Mona where discharging groundwater reached the coast and mixed with seawater resulting in extensive dissolution of the limestone in some areas and dolomitization and calcitization in others. Analogs for the cave system of Isla de Mona are the caves of the Yucatán peninsula (Back et al., 1986) and the Bahamas (Mylroie and Carew 1990; Mylroie et al., 1991; Frank 1993). The extent of dolomitization of the Mona Reef Complex, relative to the Pleistocene analogs, is the result of repeated exposure to a mixed freshwater-seawater dolomitizing environment. The larger size of the Isla de Mona flank margin caves, surface dissolution features (kaminitzas), depth of solution pits, and solution depressions and sinkholes, when compared to Bahamian carbonates, is also a result of the repeated re-establishment of an environment of carbonate dissolution and not solely a function of the larger size of the island as suggested by Mylroie et al. (1994). The contact between the dense Isla de Mona Dolomite and the cavernous Lirio Limestone — a gradual transition from nearly pure dolomite to pure limestone — preserves the time-averaged boundary of the late Miocene mixed freshwater-seawater environment below which dolomitization took place and above which calcitization and dissolution took place.

CONCLUDING REMARKS

The carbonate buildup of Isla de Mona is the result of the development of a barrier reef of middle Miocene to earliest Pliocene age. Four reef facies have been identified in the Neogene deposits of the island. Forereef deposits characterized by muds, pelagic foraminifera, and steeply dipping strata are present on the southwestern cliffs. Reef-core deposits are exposed along the southeastern coast near Playa de Pajaros and in the western tip of the island near Playa Sardinera. A transition between reef-flat and backreef deposits is present to the north of these reef-core deposits. Lagoon deposits composed of pelleted muds, benthic foramini-

fera, and coralline algae comprise the bulk of the island's carbonates. Scattered patch reefs are locally developed in the lagoon facies. During the reef development stage, marine diagenesis caused micritization of some reefal components and the reduction of primary porosity through cementation. Recognition of the abundant coral fauna in these deposits by previous workers was obstructed by extensive diagenetic alteration.

Reef development was followed by an extended period of intermittent exposure resulting from the interaction of glacioeustasy and tectonoeustasy. Freshwater lenses developed during periods of platform exposure. Seawater and freshwater mixing resulted in the formation of flank margin caves and the dissolution of aragonitic components within the platform. Platform exposure was accompanied by multiple periods of karstification and soil formation. Calcitization of the limestone involved multiple periods of meteoric diagenesis as a product of oscillating sea levels. Extensive dolomitization followed aragonite dissolution in most of the island carbonates. The association of dolomite with aragonite dissolution combined with the abundance of cloudy-centered and zoned dolomite cements and the carbon and oxygen isotopic trends of dolomite and calcite point to a mixed freshwater-seawater origin. During the Pleistocene, carbonates of Isla de Mona were exposed to vadose diagenesis. During this period of emergence, abundant precipitation resulted in the development of cave speleothems.

Episodic uplift of the island led to development of a series of escarpments during sea-level stands along which fringing-reef deposits were formed. Isla de Mona has been relatively stable since 125 ka when an extensive fringing-reef tract developed along the cliffs of the island.

Hydrogeologically, Isla de Mona can be described as an Exuma-type island (Vacher and Wallis, 1992). Two separate freshwater lenses are developed, one under the Pleistocene coastal plain, the other under the Miocene plateau carbonates. The abundant fractures, sinkholes, and solution pits result in rapid percolation of water preventing development of surface drainage system. The thin freshwater lens under the plateaus surface suggests strong structural and lithologic control on the shape of the freshwater lens and the discharge of freshwater in periphery of the island.

ACKNOWLEDGMENTS

Research in Mona has been supported by grants to L.A. González from the Office of Research Coordination, School of Arts and Sciences, University of Puerto Rico at Mayagüez; grants to H.M. Ruiz and V. Monell from the Office of the Dean, School of Arts and Sciences, University of Puerto Rico at Mayagüez; and grants to H.M. Ruiz from the American Association of Petroleum Geologists and Chevron USA. Field work was conducted with permission from the Office of Scientific Investigations of the Puerto Rico Department of Natural Resources. Logistics and field operations were greatly assisted by the cooperation of numerous personnel of the Office of Reserves and Refuges of the Puerto Rico Department of Natural Resources, in particular Myrna Robles, José Rivera, José Rosario, José Vázquez, and

Tony Nieves, as well as numerous personnel of Cuerpo de Vigilantes of the Puerto Rico Department of Natural Resources assigned to Isla de Mona during our visits to the island. A number of individuals provided field assistance; particular thanks go to Luis F. Molina, René Fuentes, Homer Montgomery, Ivan González, Ted Wessley, and the members of SAE (Sociedad Avance Espeleológico). Thanks to H. Montgomery who assisted with preliminary facies interpretation, T.A. Stemann who provided identification of agariciid and mussid corals, to K.G. Johnson for processing microfossil samples, and to Sonia Fernández who provided assistance in many aspects of this research.

REFERENCES

Aaron, J.M., 1973. Geology and mineral resources of Isla de Mona, P.R. In: Isla de Mona-Volumen II: Junta de Calidad Ambiental, pp. B1–7.

Aïssaoui, D.M., Buigues, D. and Purser, B.H., 1986. Model of reef diagenesis: Mururoa Atoll, French Polynesia. In: J.H. Schroeder and B.H. Purser (Editors), Reef Diagenesis. Springer Verlag, New York, pp. 27–52.

Back, W., Hanshaw, B.B., Herman, J.S. and Van Driel, J.N., 1986. Differential dissolution of a Pleistocene reef in the ground-water mixing zone of coastal Yucatán, Mexico. Geology, 14: 137–140.

Biju-Duval, B., Bizon, G., Mascle, A. and Muller, C., 1983. Active margin processes; field observations in southern Hispaniola. Am. Assoc. Petrol. Geol. Mem., 34: 347–358.

Bloom, A.L., Broecker, W.S., Chappell, J.M.A., Mathews, R.K. and Mesolella, K.J., 1974. Quaternary sea level fluctuations on a tectonic coast: New 230Th/234 U dates from the Huon Peninsula, New Guinea. Quat. Res., 4: 185–205.

Briggs, R.P. and Seiders, V.M., 1972. Geologic map of Isla de Mona quadrangle, Puerto Rico. U.S. Geol. Surv. Misc. Invest., Map I-718.

Budd, A.F., Stemann, T.A. and Johnson, K.G., 1994. Stratigraphic distribution of genera and species of Neogene to Recent Caribbean Reef Corals. J. Paleont., 68: 951–977.

Burke, K., Fox, P.J. and Sengor, A.M.C., 1978. Buoyant ocean floor and the evolution of the Caribbean. J. Geophys. Res., 83: 3949–3954.

Calvesbert, R.J., 1973. The climate of Mona Island. Isla de Mona-Volumen II: Junta de Calidad Ambiental, pp. A1–10.

Carew, J.L. and Mylroie, J.E., 1991. Some pitfalls in paleosol interpretation in carbonate sequences. Carbonates and Evaporites, 6: 69–74.

Febrillet, J.F., Bueno, E., Seiler, K.P. and Stichler, W, 1987. Estudios isotópico e hidrogeológico en el suroeste de la Republica Dominicana. In: Isotope Techniques in Water Resources Development, Proc. Ser. IAEA-SM-299/31, Inter. Atom. Energy Agency, Vienna, Austria, pp. 317–333.

Frank, E.F., 1993. Aspects of karst development and speleogenesin Isla de Mona, Puerto Rico: An analogue for Pleistocene speleogenesis in the Bahamas. M.S. Thesis, Mississippi State University, 132 pp.

González, L.A., Ruiz, H. and Monell, V., 1990. Diagenesis of Isla de Mona, Puerto Rico. Am. Assoc. Petrol. Geol. Bull., 74: 663–664.

González, L.A., Ruiz, H.M., Budd, A. and Monell, V., 1992. A Late Miocene barrier reef in Isla de Mona, Puerto Rico (abstr.): Geol. Soc. Am. Abstr. Programs, 24: A350.

Hanshaw, B.B. and Back, W., 1980. Chemical mass-wasting of the northern Yucatán Peninsula by groundwater dissolution. Geology, 8: 222–224.

Jones, B. and Hunter, I.G., 1994. Messinian (Late Miocene) karst on Grand Cayman, British West Indies: An example of an erosional sequence boundary. J. Sediment. Res., B64: 531–541.

Jordan, D.G., 1973. A summary of actual and potential water resources, Isla de Mona, Puerto Rico. In: Isla de Mona-Volumen II: Junta de Calidad Ambiental, pp. D1–8.

Kaplin, E.H., 1982. A field guide to coral reefs (Caribbean and Florida). Peterson Field Guide Series, Houghton Mifflin Co., Boston, 289 pp.

Kaye, C.A., 1959. Geology of Isla de Mona, Puerto Rico and notes on the age of the Mona Passage: U.S. Geol. Surv. Prof. Pap. 317-C, 178 pp.

Ku, T.L., Kimmel, M.A., Easton, W.H. and O'Neil, T.J., 1974. Eustatic sea level 120,000 years ago on Oaju, Hawaii. Science, 183: 959–962.

Lidz, B.H., 1984. Neogene sea-level change and emergence, St. Croix, Virgin Islands: Evidence from basinal carbonate accumulations. Geol. Soc. Am. Bull., 95: 1268–1279.

Lighty, R.W., 1985. Preservation of internal reef porosity and diagenetic sealing of submerged early Holocene barrier reef, southeast Florida Shelf. In: N. Schneidermann and P.M. Harris (Editors), Carbonate Cements: Soc. Econ. Paleontol. Mineral. Spec. Publ., 36: 123–151.

Lohmann, K.C., 1988. Geochemical patterns of meteoric diagenetic systems and their application to studies of paleokarst. In: N.P. James and P.W. Choquette (Editors), Paleokarst. Springer-Verlag, New York, pp. 58–80.

Macintyre, I.G., Multer, H.G., Zankl, H.L., Hubbard, D.K., Weiss, M.P. and Stuckenrath, R., 1985. Growth and depositional facies of a windward reef complex (Nonsuch Bay, Antigua, W.I.). Proc. Fith Inter. Coral Reef Symp. (Tahiti), 6: 605–610.

Mallinson, D.J., Compton, J.S., Snyder, S.W. and Hodell, D.A., 1994. Strontium isotopes and Miocene sequence stratigraphy across the northeast Florida Platform. J. Sediment. Res., B64: 392–407.

Masson, D.G. and Scanlon, K.M., 1991. The neotectonic setting of Puerto Rico. Geol. Soc. Am. Bull., 103: 144–154.

Mesolella, K.J., Matthews, R.K., Broecker, W.S. and Thurber, D.L., 1969. The astronomical theory of climatic change: Barbados data. J. Geol., 77: 250–274.

Monell, V., 1988. Dolomitization of Isla de Mona Dolomite. B.S. Thesis, University of Puerto Rico, Mayagüez, 25 pp.

Morelock, J., Schneidermann, N. and Bryant, W.R., 1977. Shelf reefs, southwestern Puerto Rico. In: S.H. Frost, M.P. Weiss and J.B. Saunders (Editors), Reefs and Related Carbonates-Ecology and Sedimentology. Am. Assoc. Petrol. Geol., Studies Geol., 4: 17–25.

Moussa, M.T., Seiglie, G.A., Meyerhoff, A.A. and Taner, I., 1987. The Quebradillas Limestone (Miocene-Pliocene), northern Puerto Rico and tectonics of the northeastern Caribbean margin. Geol. Soc. Am. Bull., 99: 427–439.

Mussman, W.J., Montanez, I.P. and Read, J.F., 1988. Ordovician Knox paleokarst unconformity, Appalachians. In: N.P. James and P.W. Choquette (Editors), Paleokarst. Springer-Verlag, New York, pp. 211–228.

Mylroie, J.E. and Carew, J.W., 1990. The flank margin model for dissolution cave development in carbonate platforms. Earth Surf. Processes and Landf., 25: 413–424.

Mylroie, J.E., Carew, J. W. and Mylroie, J.R., 1991. Cave development of New Providence Island and Long Island, Bahamas. Cave Sci. 18(1): 139–151.

Mylroie, J.E., Carew, J.L., Frank, E.F., Panuska, B.C., Taggart, B.E., Troester, J.W. and Carrasquillo, R., 1994. Comparison of flank margin cave development: San Salvador Island, Bahamas and Isla de Mona, Puerto Rico (abstr.). Proc. Seventh Symp. Geol. Bahamas, pp. 16–17.

Neumann, A.C. and Macintyre, I., 1985. Reef response to sea level rise-keep-up, catch-up or give-up. Proc. Fifth Int. Coral Reef Symp. (Tahiti), 3: 105–110.

Neumann, A.C. and Moore, W.S., 1975. Sea level events and Pleistocene coral ages in the northern Bahamas. Quat. Res., 5: 215–224.

Pindell, J.L. and Barrett, S.F., 1990. Geological evolution of the Caribbean region: a plate tectonic perspective. In: G. Dengo and J.E. Case (Editors), The Caribbean Region. Geol. Soc. Am., The Decade of North American Geology, H: 405–432.

Pleydell, S.M., Jones, B., Longstaffe, F.J. and Baadsgaard, H., 1991. Dolomitization of the Oligocene-Miocene Bluff Formation on Grand Cayman, British West Indies. Can. J. Earth Sci., 27: 1098–1110.

Rivera, L.N., 1973. Soils of Mona Island. In: Isla de Mona-Volumen II: Junta de Calidad Ambiental, C1–4.

Rodríguez, R.W., Trumbull, J.V.A. and Dillon, W.P., 1977. Marine geologic map of Isla de Mona area, Puerto Rico. U.S. Geol. Surv. Misc. Invest., Map I-1063.

Roos, P.J., 1971. The shallow-water stony corals of the Netherlands Antilles. Studies on the Fauna of Curacao and other Caribbean Islands, 37: 108 pp.

Rozanski, K., Araguás-Araguás, L. and Gonfiantini, R., 1993. Isotopic Patterns in Modern Global Precipitation. In: P.K. Swart, J. Mackenzie and K.C Lohmann, (Editors), Climate Change in Continental Isotopic Records, Am. Geophys. Union, Monog. 78: 1–36.

Ruiz, H.M., 1989. Sedimentology and Diagenesis of the Lirio Limestone, Isla de Mona, Puerto Rico. B.S. Thesis, University of Puerto Rico, Mayagüez, 31 pp.

Ruiz, H.M., 1993. Sedimentology and Diagenesis of Isla de Mona, Puerto Rico. M.S. Thesis, University of Iowa, Iowa City, Iowa, 86 pp.

Ruiz, H.M., González, L.A. and Budd, A.F., 1991. Sedimentology and diagenesis of Miocene Lirio Limestone, Isla de Mona, Puerto Rico. Am. Assoc. Petrol. Geol. Bull., 75: 664–665.

Ruiz, H.M., González, L.A., Budd, A.F., Guoquio, G. and Monell-González, V., 1993. Late Miocene (Tortonian to Messinian) mixing-zone diagenesis of the Mona Reef Complex, Isla de Mona, Puerto Rico (abstr.). Geol. Soc. Am. Abstr. Programs, 25: A228.

Schell, B.A. and Tarr, A.C., 1978. Plate tectonics of the northeastern Caribbean Sea region. Geol. Mijnbouw, 57: 319–324.

Seiglie, G.A. and Moussa, M.T., 1984. Late Oligocene-Pliocene transgressive-regressive cycles of sedimentation in Northwestern Puerto Rico. In: J.S. Schlee (Editor), Interregional Unconformities and Hydrocarbon Accumulation. Am. Assoc. Petrol. Geol. Mem., 36: 89–95.

Shinn, E.A., Hudson, J.H., Halley, R.B. and Lidz, Barbara, 1977. Topographic control and accumulation rate of some Holocene coral reefs: South Florida and Dry Tortugas. Proc. Third Inter. Coral Reef Symp. (Miami), 2: 1–7.

Sibley, D.F., 1980. Climatic control of dolomitization, Seroe Domi Formation (Pliocene), Bonaire, N.A. In: D.H. Zenger, J.B. Dunham and R.L. Ethington (Editors), Concepts and Models of Dolomitization: Soc. Econ. Paleontol. Mineral. Spec. Publ., 23: 247–258.

Smith, F.G.W., 1976. Atlantic Reef Corals. University of Miami Press, Third Printing, Coral Gables, Florida, 164 pp.

Supko, P.R., 1977. Subsurface dolomites, San Salvador, Bahamas. J. Sediment. Petrol., 47: 1063–1077.

USGS CDO (U.S. Geol. Surv, Carib. Distr. Off.), 1994a, b, c. Isla de Mona Project: Accomplishments for expedition 1, 2, 3: 3 pp., 3 pp., 1 pp.

Vacher, H.L. and Wallis, T.N., 1992. Comparative hydrogeology of fresh-water lenses of Bermuda and Great Exuma Island, Bahamas. Groundwater, 30: 15–20.

Wadsworth, F.H., 1973. The historical resources of Mona Island. In: Isla de Mona-Volumen II: Junta de Calidad Ambiental, pp. N1–37.

Ward, W.C. and Halley, R.B., 1985. Dolomitization in a mixing zone of near-seawater composition, late Pleistocene, northeastern Yucatán Peninsula. J. Sediment. Petrol., 55: 407–420.

Geology and Hydrogeology of Carbonate Islands. Developments in Sedimentology 54
edited by H.L. Vacher and T. Quinn
© 1997 Elsevier Science B.V. All rights reserved.

Chapter 10

GEOLOGY AND HYDROGEOLOGY OF ST. CROIX, VIRGIN ISLANDS

IVAN P. GILL, DENNIS K. HUBBARD, PETER P. McLAUGHLIN and C.H. MOORE, JR.

INTRODUCTION

St. Croix, the only one of the Virgin Islands that is composed mostly of sedimentary rocks, lies about 150 km southeast of San Juan, Puerto Rico (Fig. 10-1). To the east lie the Lesser Antilles; Puerto Rico and the remainder of the Virgin Islands lie to the north. The island is 40 km long along an east-west axis and tapers to a narrow point on the eastern side (Fig. 10-1). It is the largest of the U.S. Virgin Islands, and has been a territory of the United States since its purchase from Denmark in 1917. The other two U.S. Virgin Islands are St. John and St. Thomas; portions of St. John are included in the U.S. Virgin Islands National Park. The remainder of the Virgin Islands — the British Virgin Islands — are British Territory. In both the U.S. and British Virgin Islands, the dominant language is English, which apparently was the case even prior to the purchase of the U.S. Virgin Islands from Denmark (Cederstrom, 1950).

Traditional water use in the Virgin Islands has depended on rainwater catchment and scattered, hand-dug wells. However, the dependence on agriculture in past centuries has diminished with the waning of the sugar industry, and St. Croix now looks more to industries such as oil-refining, alumina-processing and tourism. Since the 1960s, water from several desalination plants has begun to replace some of the historical dependence on rainwater, and the aquifer system of central St. Croix has been increasingly exploited in the face of development and population growth. For these reasons, a knowledge of the subsurface geologic relationships in the Tertiary basin is of greater importance now than ever before.

SETTING

History

In the last five centuries, St. Croix has witnessed a spectrum of humanity. It was the home for the farming communities of the Arawaks, and it later served as base for the warrior Caribs migrating through the Antilles arc. Columbus landed here on his second voyage and initiated European domination that was to last through the flags of seven nations. During the succeeding several centuries, St. Croix served as an agricultural locus of the slave-sugar-rum triangle that brought Africans to the sugar plantations, swelling the population and earning Danish St. Croix the nickname

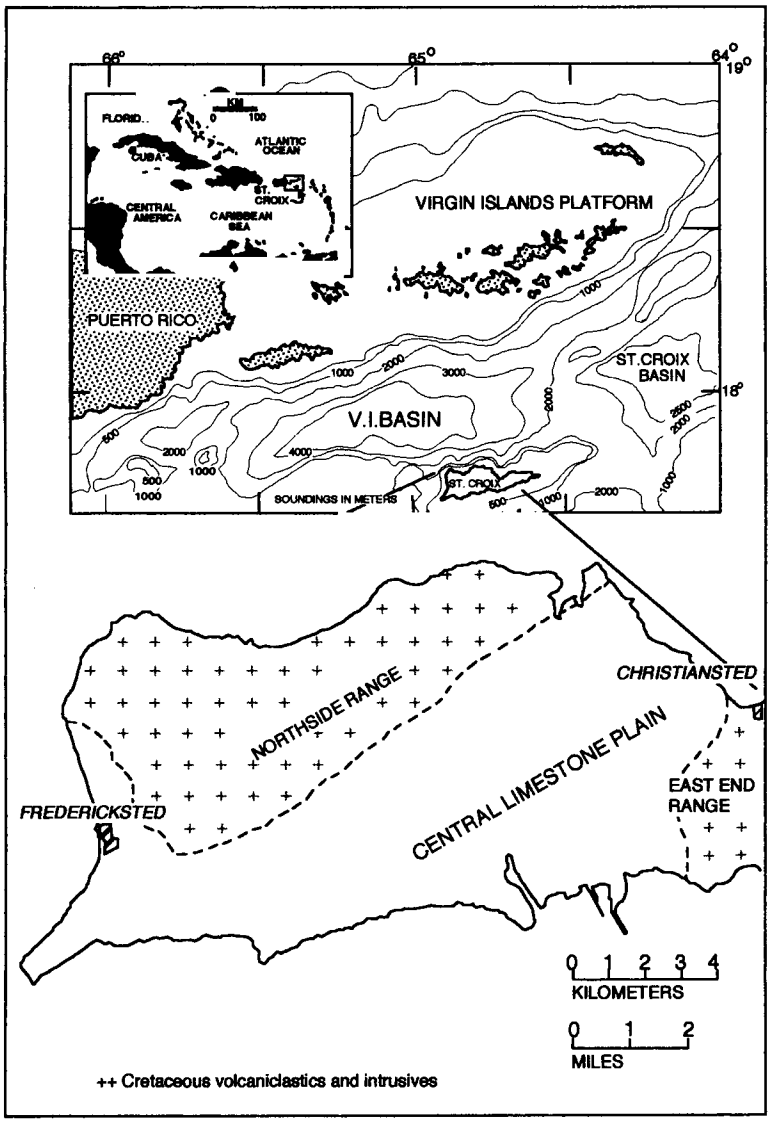


Fig. 10-1. Location map, surrounding bathymetry, and the main geomorphic provinces of St. Croix. (From Gill, 1989.)

"Emerald of the Caribbean." Organized uprisings secured emancipation two decades before the American Civil War. Now, the lime ruins of plantations and windmills decay in the fields, witnesses to the passing of an era.

At the time of Columbus' visit in 1493, St. Croix was inhabited by the Carib Indians. By the time of the first attempts at Dutch and English settlement in the early

1600s, however, the Caribs had been killed, driven out or enslaved (Evans, 1929, in Cederstrom, 1950). In the remainder of the seventeenth century, St. Croix was successively claimed by England, the Netherlands, Spain, France, the Knights of Malta, and France again. Denmark purchased St. Croix from France in 1733 and, with the exception of brief military takeovers by the British, held the island until the twentieth century. A Danish attempt at gradual emancipation led to a slave insurrection and the abolition of slavery in 1848. St. John, St. Thomas and St. Croix were bought by the United States, after two attempts, in 1917. The economic history of the island has been dominated until recently by the sugar industry, which has waxed and waned under the influence of fluctuating sugar and labor prices as well as recurrent droughts and hurricanes (Cederstrom, 1950).

Geography, climate and oceanographic setting

St. Croix lies within the belt of trade winds, with winds dominantly from the east and southeast during the summer, and from the east and northeast in the winter months. As a result, the prevailing swell is from the east, producing westerly sediment transport along the northern and southern coasts. The islands to the north and east isolate St. Croix from the Atlantic wave climate and reduce oceanic swell. Tides are mixed semidiurnal with a range of only 10–15 cm, but they can be responsible for significant tidal currents, particularly off the southwest corner of the island (Roberts et al., 1981). Coral and algal reefs rim the northern and southern shorelines with the most extensive reef development occurring generally off the eastern portion of the island.

The topography of St. Croix is strongly influenced by lithology and structure. The central part of the island is a relatively low-lying plain and is underlain by Tertiary limestones. The eastern and western portions of St. Croix rise into steep lines of hills, the East End Range and the Northside Range, respectively, that are underlain by well-indurated Cretaceous siliciclastics (Whetten, 1966). The rock of the Northside and East End Ranges weathers slowly and forms hills and low mountains with a maximum elevation approaching 335 m. These hills are dissected by gabbroic and dioritic intrusives which tend to weather rapidly, resulting in broad valleys (Cederstrom, 1950).

Rainfall on St. Croix is highly seasonal and strongly affected by topography. The greatest rainfall occurs in the hilly Northside Range in the northwestern portion of the island. Annual rainfall in the Northside Range averages 1,270 mm y^{-1}, whereas rainfall in the drier, low-altitude areas of eastern and southwestern St. Croix averages < 890 mm y^{-1}. Annual rainfall for the entire island averages around 1,170 mm y^{-1}, but drought is not uncommon and can be prolonged. Periods of above-average and below-average rainfall have alternated cyclically since rainfall has been recorded (Johnson, 1937, in Cederstrom, 1950). Vegetation patterns closely follow the areal distribution of rainfall.

Drainage from the Northside Range flows to the sea on the northern and western portions of the island. Presumably this drainage recharges the alluvial aquifers along

these coasts. Southerly drainage from the Northside Range, as well as rainfall from the East End Range to the east, flows onto the central limestone plain and feeds several ephemeral streams.

Geologic and tectonic setting

St. Croix lies within the complex, northern Caribbean plate margin (Fig. 10-1) (Lewis and Draper, 1990) that includes the four large islands of the Greater Antilles: Cuba, Jamaica, Hispaniola (Haiti and the Dominican Republic), and Puerto Rico. The Virgin Islands, which form the eastern extremity of the Greater Antilles, consist of two morphotectonic zones (Lewis and Draper, 1990, p. 117): the Northern Virgin Islands zone, an ENE extension of Puerto Rico, and the Southern Virgin Islands (or Cruzan) zone, which includes St. Croix. The Virgin Island Platform (Fig. 10-1) of the Northern Virgin Islands zone contains an archipelago of about 100 islands including the American Virgin Islands of St. John and St. Thomas at the western end of the cluster and the British Virgin Islands of Tortola and Virgin Gorda. The Northern Virgin Islands zone consists of Cretaceous crystalline rocks (Lewis and Draper, 1990). In contrast, St. Croix is composed dominantly of sedimentary rock. The exposed rocks of St. Croix consist of a Tertiary limestone graben sandwiched between uplifted blocks of Cretaceous deep-water sedimentary rocks (Fig. 10-2) (Whetten, 1966; Multer et al., 1977; Gerhard et al., 1978).

St. Croix is separated from the Virgin Islands Platform and Puerto Rico to the north by the Virgin Islands Trough, which includes the 4,500-m-deep Virgin Islands

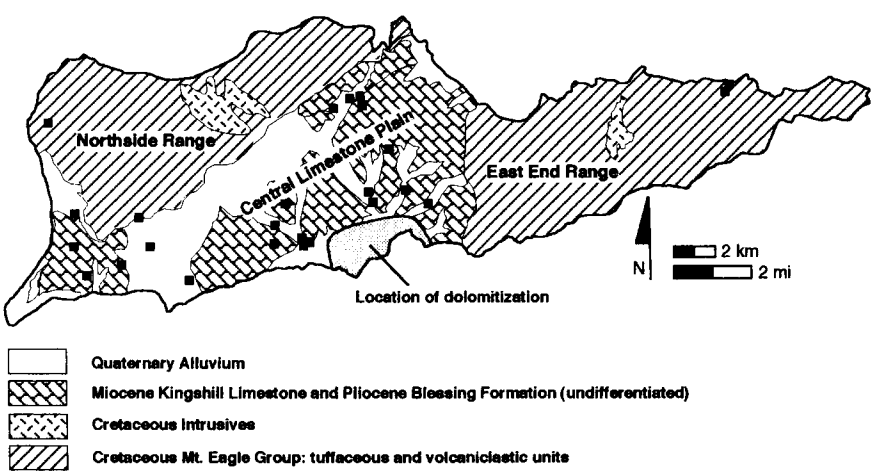


Fig. 10-2. Generalized geologic map of study area with location of water sampling stations and the location of dolomitization. Water samples were taken from existing public and private wells throughout the central plain carbonate areas, as well as from several wells in non-carbonate aquifers. Dolomite is found only within the shaded region in the southeastern portion of the central plain. (Geology modified after Whetten, 1966, and Gerhard et al., 1978. From Gill, 1989.)

Basin (Fig. 10-1). North of St. Croix, the Virgin Islands Trough extends northeastward into the Anegada Passage, a deep, narrow gap that separates the Virgin Islands Platform from the Lesser Antilles, the active island arc to the east that includes such well-known islands as Martinique, Antigua, Dominica, and Grenada (see Maury et al., 1990, for review of the geology of this arc). The St. Croix Basin (Fig. 10-1) lies between St. Croix and the Lesser Antilles. St. Croix is the exposed portion of the St. Croix Ridge, a block-faulted feature which forms the southern boundary of the Virgin Islands Trough.

The Virgin Islands Trough and the Virgin Islands Platform are seismically active today, and seismic profiling within the Virgin Islands Trough confirms that normal faulting has occurred in the past (Houlgatte, 1983). North of the Virgin Islands, the seismically active Puerto Rico Trench is part of the northern "plate boundary zone" (Pindell and Barrett, 1990) of the Caribbean plate. The opposite, southern plate boundary zone, is along the northern continental border of South America. The well-defined western and eastern boundaries of the Caribbean Plate are the Middle American subduction zone (off Central America) and the Lesser Antilles subduction zone, respectively. Pindell and Barrett (1990) review and contrast earlier mobilist models for the evolution of the complicated Caribbean Plate and present their own plate-tectonic kinematic-geologic analysis for the region since the breakup of Pangea. There is general agreement that the Caribbean Plate — in the gap between the Americas — is allochthonous (probably of Pacific provenance) and moving eastward relative to the Americas at 2–4 cm y^{-1}. However, as there are discrete terrains within the plate (Pindell and Barrett, 1990) and complicated histories of the various terrains, details such as the relative motion of a morphotectonic unit such as the southern Virgin Islands (or the island of St. Croix) are more poorly known.

STRATIGRAPHY AND GEOLOGIC HISTORY

Stratigraphy

In ascending order, the principal rock units of St. Croix include the Mt. Eagle Group, the Jealousy Formation, the Kingshill Limestone, and the Blessing Formation (Fig. 10-3). The Kingshill Limestone and Jealousy Formation constitute most of the carbonate section on St. Croix.

Mt. Eagle Group. The Cretaceous Mt. Eagle Group forms the horst blocks of the Northside and East End range and presumably floors the graben underlying the central limestone plain. The Mt. Eagle Group contains a diverse assemblage of gabbroic and dioritic intrusives, deep-water volcaniclastics, tuffaceous sandstones and pelagic sediments (Whetten, 1966). Additional information on the sedimentologic character and structure of these rocks is provided by Whetten (1966), Speed (1989), and Stanley (1989). A comprehensive compilation of the ages of these and other St. Croix rock units is given by Lidz (1988).

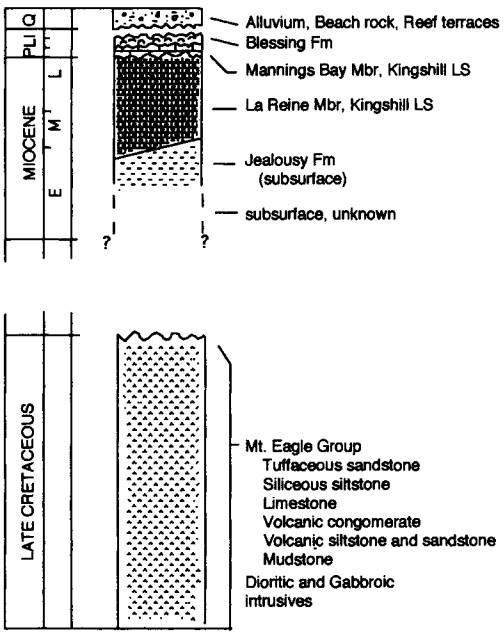


Fig. 10-3. Generalized stratigraphic column. All units listed are exposed in outcrop except the Jealousy Formation. Intrusives not shown. (Modified from Lidz, 1988; Gill, 1989.)

Jealousy Formation. A subsurface unit (Gerhard et al., 1978; Gill, 1989; Gill et al., in press; contra Cederstrom, 1950; Whetten, 1966; and Bold, 1970), the Miocene Jealousy Formation is described from test holes and consists largely of grey-blue, planktonic-foraminifera-rich calcareous muds intercalated with layers of coral-rich limestone conglomerate (Cederstrom, 1950). From gravity surveys, the maximum thickness of the Jealousy Formation and underlying sediments may be 1,800 m (Shurbet, 1956). In the center of the basin, the Jealousy Formation is thicker than 426 m, the maximum depth of penetration (Cederstrom, 1950). Known Jealousy Formation samples are Miocene in age (Gill and Hubbard, 1987; Gill, 1989; McLaughlin et al., 1995), although the thickness of the unit and the occurrence of resedimented material in the overlying Kingshill Limestone indicate the Jealousy Formation could extend into the Oligocene (Lidz, 1984a; 1988).

The boundary between the Jealousy Formation and the overlying Kingshill Limestone is diachronous and is marked by an abrupt color change from blue-grey (Jealousy) to off-white (Kingshill). There is no apparent change in bulk mineralogy, texture or fossils. Basinal sedimentation patterns and conditions apparently continued without interruption from deposition of the Jealousy Formation to deposition of the Kingshill Limestone, and the boundary between them may be strictly diagenetic or redox-controlled.

Kingshill Limestone. The Miocene Kingshill Limestone is a lithologically diverse unit dominated by planktonic foraminiferal carbonate mud and marl. Lithologic

facies that dominate the type section are included in a lower unit, the La Reine Member (Gill et al., in press). Facies in the lower member include foraminiferal packstones (chalks), quartz arenites, coral-lithic packstones and lithic-foraminiferal packstones (Gerhard et al., 1978). Tests of planktonic foraminifera, primarily *Orbulina* and *Globorotalia*, form the largest component of the chalks (Multer et al., 1977). The chalks, which are cream to white and somewhat indurated on exposure, occur in beds 10–30 cm thick that alternate with tan sandy marls and pebble- and boulder-conglomerates interpreted to be sediment-gravity flows (Multer et al., 1977; Gerhard et al., 1978; Lidz, 1982). The latter are locally graded, and many contain recrystallized Miocene coral heads and siliciclastic sand, gravel and cobbles. The siliciclastics are usually interpreted as being derived from the Cretaceous section (Multer et al., 1977; Gerhard et al., 1978; Lidz, 1982).

The upper Kingshill Limestone comprises shelf and slope skeletal-carbonate facies (Multer et al., 1977, Gerhard et al., 1978), the Mannings Bay Member (Gill, 1989; Gill et al., in press). These youngest Kingshill strata are characterized by tan foraminiferal wackestones and grainstones containing operculinoid benthic foraminifera as well as common planktonic forms. The operculinoid foraminifera are the dominant component in many beds, and are often imbricated (Multer et al., 1977; Gerhard et al., 1978). These beds grade upward into *Amphistegina* grainstones and *Amphistegina*-planktonic foraminiferal packstones, which are separated from the overlying Blessing Formation by an unconformity (Multer et al., 1977; Gerhard et al., 1978; Gill et al., 1989). In contrast to the underlying Kingshill Limestone, the Blessing Formation is poorly bedded and contains facies representative of shallow shelf, reef and lagoon deposition (Behrens, 1976; Gill et al., 1989; Gill, 1989).

Blessing Formation. Originally separated into two limestone units by Behrens (1976), these rocks are grouped here into a single formation because the units of Behrens (1976) are difficult to map and weathering has destroyed many of the features that would allow them to be differentiated. Lithologies of the lower Blessing include massive, white, well-indurated, coralline-algal and molluscan wackestones. This facies is resistant to weathering and contains scattered solitary corals and reworked operculinoid and planktonic foraminifera presumably derived from the underlying Kingshill Limestone (Behrens, 1976; Gill, 1989).

Upsection, the Blessing is characterized by porous and friable buff-colored coral, molluscan and coralline-algal wackestones separated from the previously described facies by a terra rossa (Behrens, 1976). Upsection, and again separated by an erosional surface, the Blessing becomes white, massive, and friable ("chalky"), with numerous scleractinians, mollusks and coralline algae. The Blessing is capped by high-diversity coral-reef and lagoonal facies that alternate stratigraphically and presumably spatially (Behrens, 1976; Gill et al., 1989; Gill et al., in press). The Blessing Formation is placed within the lower Pliocene on the basis of coral fauna and planktonic and benthic foraminifera (Behrens, 1976; Frost, pers. comm., 1986; Lidz 1982, 1984b, 1988; Andreieff et al., 1986).

The Blessing Formation extends around the present southern and western ends of the island, but the biostratigraphy is well constrained only in the central portion of

the southern coastline. Exposures and cores from western St. Croix are highly weathered and contain few identifiable fossils of stratigraphic importance (Lidz, 1988; Gill, 1989). The correlation between the Blessing Formation of the western coast and that of the southern coast is made on lithologic similarity and stratigraphic position (Gill et al., 1989; Gill et al., in press). Sedimentary units overlying the Blessing Formation include a raised, coral and conch-shell (*Strombus*) terrace on the western coastline (Hubbard et al., 1989), beachrock deposits (e.g., Hanor, 1978), modern coral reefs and alluvium (Lidz, 1988).

Geologic history

Deposition and uplift. During the late Cretaceous, volcanic and sedimentary rocks were deposited in a deep basin adjacent to sources of "epiclastic" (redeposited volcanic) and volcanic (tuffaceous) material (Whetten, 1966; Nagle and Hubbard, 1989). Later workers interpret much of the Cretaceous section as a complex of stacked, fault-bounded nappes (Speed, 1989; Speed and Joyce, 1989) rather than interfingering depositional facies (Whetten, 1966). Unlike most Caribbean islands, however, St. Croix's early history is dominated by deep basinal sedimentation rather than igneous emplacement and metamorphism (Whetten, 1966; Nagle and Hubbard, 1989; Stanley, 1989).

The Jealousy Formation is thought to have been deposited in estuarine environments that deepened with subsidence in the center of the basin during the Miocene and perhaps earlier (Multer et al., 1977). As the central graben — the Kingshill/Jealousy Basin — continued to subside, the Jealousy sediments became dominated by marine planktonic fauna. The basin is interpreted to have been a seaway, open to the north and south, and bounded on the east and west by the emergent East End and Northside ranges (Multer et al., 1977; Gerhard et al., 1978; Lidz, 1982).

By Kingshill time, coral reefs were established along the margins of the deepening basin. Sediment-gravity flows, perhaps channelized by submarine canyons, provided the basin floor with reefal, terrigenous and shelf-derived material (Multer et al., 1977; Gerhard et al., 1978; Lidz, 1982). Basinal water depth at the time of Kingshill deposition is thought to have been 500–750 m (Multer et al., 1977; Gerhard et al., 1979; Lidz, 1982; Gill et al., 1989; McLaughlin et al., 1995). The graben that formed the seaway could have been hinged on the northwest with the greatest subsidence occurring on the eastern fault boundary (Gerhard et al., 1978).

An alternative interpretation, from recent coring, is that graben formation occurred far later, after deposition of much of the Tertiary section. Because there is (1) no evidence of a steep-sided basin, (2) no evidence of estuarine sediments in the Jealousy Formation, (3) no significant lithological transition between the Kingshill and Jealousy rock units, (4) no evidence of in situ Jealousy and Kingshill-age reefs, and (5) evidence of fault disruption of Kingshill strata along the eastern boundary fault, it is possible that graben formation occurred during or following late Kingshill deposition (Gill and Hubbard, 1987; Gill, 1989; Gill et al., 1989). By this interpretation, the shelf-derived portions of the Kingshill and Jealousy formations must have

had a sediment source now removed from St. Croix (Gill, 1989). Puerto Rico and the Virgin Islands platform to the north are possibilities.

In either case, the Kingshill-Jealousy Basin shallowed significantly toward the end of Kingshill deposition in the late Miocene, with the increased incorporation of shelf facies such as "floods" of larger benthic foraminifera (Multer et al., 1977; Gerhard et al., 1978; Lidz, 1982, 1984b). Basinal shallowing was probably the result of both infilling and tectonic uplift (Gerhard et al., 1978; Lidz, 1984b; McLaughlin et al., 1995).

By the early Pliocene, island uplift had exposed significant portions of the Kingshill Limestone, producing soils and an unconformity surface. At this time, the southern and western coastlines of the island were the sites of extensive inner shelf and reef deposition. Reef growth appears to be limited to these coastlines because of preferential island uplift to the north. If a Pliocene reef tract existed on the northern coastline, it has been subsequently removed by uplift and erosion.

Faulting during and after the Pliocene formed a small subsidiary graben along the south coast, indicating that fault activity on St. Croix continued into at least the late Tertiary (Gill, 1989; Gill et al., 1989). The basin formed by the graben was the site of extensive Pliocene reef growth and sedimentation (the Blessing Formation) followed by dolomitization. The reef growth surfaces and bedding of the Pliocene reef tract dip southward at varying angles. These dips probably represent both differential uplift and depositional dip due to reef progradation. Pliocene eustasy and tectonic movement caused exposure, soil formation and karsting in the Blessing Formation.

Pleistocene reef growth is marked by the raised, coral and conch-shell beach terrace, which is plainly visible on the western coastline. The terrace dips to the south, suggesting that St. Croix has continued to undergo tectonic uplift at least into the late Pleistocene, and perhaps into the present (Hubbard et al., 1989).

Sea-level history. Until the late Miocene or early Pliocene, the depth of the Kingshill/Jealousy basin was probably too large to record eustatic changes. After the late Miocene, the carbonate section records several instances of exposure or erosion induced at least partly by eustatic change. The mild unconformity between the upper and lower Kingshill Limestone indicates submarine erosion (Gill et al., 1989), and may have been induced by the abrupt Messinian sea-level fall (Lidz, 1984b). However, biostratigraphic markers in this unit are not precise enough to confirm this suggestion (McLaughlin et al., 1995). In the Blessing Formation, at least three exposure surfaces indicate that cyclic exposure and inundation occurred during the Pliocene (Behrens, 1976; Lidz, 1984b; Gill et al., 1989).

AQUIFERS

Alluvial aquifers

Numerous alluvial aquifers fill the coastal and inland valleys of St. Croix. Although the composition of the alluvium makes them more permeable than under-

lying rocks, the alluvial aquifers are patchy, limited in extent, and in many cases close to the coast. Most wells in coastal alluvial aquifers are shallow wells with limited production. Wells tapping the larger inland deposits of alluvium, however, have yields of 10–50 gal min^{-1} (U.S.; 0.6–3.2 L s^{-1}), with specific capacities reaching 10 gal min^{-1} ft^{-1} (2.1 L s^{-1} m^{-1}) of drawdown (Jordan, 1975). Alluvial deposits of the River Gut area are estimated to have transmissivities of 20–450 m^2 day^{-1} (Torres-Gonzalez, in Renken, in press). All of the major public wellfields are drilled in alluvium-filled stream courses and are screened at least partially in alluvium.

Kingshill aquifer

The Kingshill aquifer comprises the Kingshill Limestone and overlying Blessing Formation. The underlying Jealousy Formation is not included in the Kingshill aquifer because it is poorly permeable and the quality of its water degrades rapidly with depth (Robison, 1972; Gill and Hubbard, 1986; Gill, 1994). Most St. Croix drillers stop upon reaching the "blue clays" of the Jealousy Formation, and it is generally considered the hydrologic basement (Gill and Hubbard, 1986).

The areal extent of the Kingshill aquifer is 78 km^2 (Gomez-Gomez, 1987). Despite its local importance, the Kingshill aquifer would not qualify as commercially viable by continental standards of water production and water quality. Its importance as a water source is derived principally from the lack of alternatives. The Kingshill Limestone is a unit of varying, but generally low, permeability. A large proportion of the water wells drilled into the Kingshill Limestone are low-volume domestic wells, and much of the northern and central portions of the Kingshill Limestone are of relatively low permeability. In areas characterized by marl, reported well yields seldom exceed a few hundred gallons per day. In areas with sand, gravel or limestone, yields may reach 5–10 gal min^{-1} (0.3–0.6 L s^{-1}), and specific capacities may reach 0.5 gal min^{-1} ft^{-1} (0.1 L s^{-1} m^{-1}) of drawdown (Jordan, 1975). Transmissivities less than 3 m^2 day^{-1} are reported in many wells producing from the Kingshill Limestone (Torres-Gonzales, in Renken, in press).

The Blessing Formation is more permeable. Jordan (1975) lists the permeability of the "reef-associated limestone and calcarenite" (presumably the Blessing Formation and uppermost Kingshill strata) as the highest of the central limestone province. Groundwater yield is 10–300 gal day^{-1} (U.S.; 0.6–19 L s^{-1}), with specific capacity about 0.5–50 gal min^{-1} ft^{-1} (0.1–10.5 L s^{-1} m^{-1}) of drawdown (Jordan, 1975). The Barren Spot public wellfield is screened at least partly in these strata. The Blessing Formation, however, is found in coastal or industrial areas potentially threatened by saltwater intrusion or industrial contamination.

From a water-supply perspective, it may be difficult to separate the contribution of Kingshill strata from that of the alluvium. Every major public wellfield on St. Croix is drilled into a stream valley and penetrates alluvium (e.g., see logs in Hendrickson, 1963). Most wells on St. Croix are screened from the water table down, and every large-yield well reportedly finished in the Kingshill aquifer is also screened in alluvium. It is possible that a significant part of the production from the Kingshill aquifer may be contributed by the alluvium.

WATER RESOURCES

Rainfall, stream flow and recharge

Rainfall on St. Croix is highly seasonal, with nearly half the yearly rainfall occurring in August and September. Rainfall is cyclic, and there have been two extended periods of drought in the 1870s and 1920s since reliable records have been kept (Jordan, 1975). As a result, stream flow on St. Croix is ephemeral and seldom reaches the sea except during heavy rainstorms. Rainstorms that produce runoff on St. Croix are generally short, high-intensity events, and individual storms often account for the majority of monthly rainfall. Runoff from these events, however, seldom exceeds 5% of the rainfall in a drainage basin (Jordan, 1975). It appears that stream flow was more abundant as recently as the 1920s and 1930s, when records show continuous flow from many of the island's major streams (Jordan, 1975).

Estimates of the hydrologic budget suggest that for an average 40 in. (100 cm) of rainfall, 36–38 in. (90–95 cm) are lost to evapotranspiration, 1 in. (2.5 cm) is discharged to the ocean by streams, and less than 1 in. (2.5 cm) is discharged to the ocean by groundwater seepage. The remaining 1–5 in. (2.5–12 cm; 3 to 12%) contributes to aquifer recharge (Robison, 1972; Jordan, 1975). Due to the intermittent nature of the rainfall and the high rates of evapotranspiration, it is possible that significant groundwater recharge occurs only during extended periods of intensive rainfall.

Present water-use and supply patterns

Traditional St. Croix water use has depended on the catchment and storage of rainwater. In pre-Columbian times, settlements were apparently located near the few areas of reliable surface-water supply. Since the late 1960s, water from several desalination plants has replaced the historical dependence on rainwater for drinking purposes, at least in areas close to the public water distribution network.

The water supply is also being augmented by increasing exploitation of groundwater resources. Early shallow wells dug during the Danish colonial period have been replaced by modern drilled wells for both household use and public supply (Jordan, 1975; Geraghty and Miller, 1983; Gomez-Gomez and others, 1985; Torres-Sierra, 1987); by far the majority of these wells are located on the central plain floored by the Tertiary carbonates and Quaternary alluvium.

While rainwater catchment is still important for domestic use, streams are presently insignificant as a water source, and the few dams on the island have not seen use for decades (Robison, 1972). Increasing industrialization as well as a population that nearly quadrupled from 1960 to 1985 have markedly changed the relative importance of water supplies. In 1985, rainfall accounted for about 0.5 Mgal day^{-1} (1.90×10^6 L day^{-1}) or approximately 0.7% of water usage. Groundwater supplied 1.3 Mgal day^{-1} (4.9×10^6 L day^{-1}) or about 1.8% of St. Croix water usage. Seawater now supplies the vast majority of the water on St. Croix: 97.5%, or a total of 70.6 Mgal day^{-1} (2.68×10^8 L day^{-1}) in 1985. The seawater use is divided almost

equally between cooling and desalination (Gomez-Gomez et al., 1987; Torres-Sierra, 1987). Because of the high TDS of the groundwater (Robison, 1972; Gill and Hubbard, 1986) and the high cost of flash-distilled seawater, public water supplies generally combine the two (Black, Crow and Eidsness, 1976; CH2 M Hill, 1983; Geraghty and Miller, 1983)

Groundwater flow model

Torres-Gonzalez (1991) constructed a two-dimensional finite-difference model of the Kingshill aquifer as part of the U.S. Geological Survey Regional-Aquifer System Assessment program. Model simulations are based on July, 1987, conditions. Modelling results suggest that increasing withdrawal rates beyond about 1.2 Mgal day^{-1} (4.55×10^6 L day^{-1}) might risk saline intrusion through lowering of the potentiometric surface (Torres-Gonzalez, 1991). The modelling results suggest that groundwater withdrawals might be increased by 10–30% with new recharge sources (Torres-Gonzalez, 1991).

GROUNDWATER GEOCHEMISTRY OF THE CARBONATE AQUIFER SYSTEM

Controls of fresh and brackish groundwater

The groundwater of the Kingshill Limestone, in general, is saline enough to exceed Federal standards for chloride (Jordan, 1975; Geraghty and Miller, 1983; Gill and Hubbard, 1986; Gill, 1994). Of 16 wells in the limestone plain area, only one had chloride below the 250 mg L^{-1} limit recommended by the U.S. Environmental Protection Agency. The rest ranged from 269 mg L^{-1} to >2,000 mg L^{-1}. The TDS of St. Croix groundwater is 856–2,970 mg L^{-1} and averages 1,730 mg L^{-1}. Despite being drawn from a carbonate aquifer, the waters are dominantly a sodium chloride type (Robison, 1972; Gill and Hubbard, 1986).

TDS and chloride increase toward the coast with two areas of particularly high salinity (Geraghty and Miller, 1983; Gill, 1994). One area is close to industrial plants on the central south coast, and the other is close to the town of Fredericksted on the western coastline. In both cases, the water is drawn from strata of the Blessing Formation and the Mannings Bay Member of the Kingshill Formation.

In addition to the general salinity increase toward coastal areas, there is a general increase in TDS with decreasing average well altitude (Robison, 1972; Gill and Hubbard, 1986). Deeper wells — wells with lower average altitudes of the screened intervals — produce higher-salinity water. However, most St. Croix wells are screened from the water table to the base of the well, making correlation between depth, altitude and salinity difficult (Geraghty and Miller, 1983). Waters with anomalously high TDS values (>20,000 mg L^{-1}), have been reported in inland regions of the central limestone plain, and attributed to contribution of formation waters from the underlying Jealousy Formation (Robison, 1972; Jordan, 1975).

However, these waters were not detected in later studies, and their origin remains conjectural (Geraghty and Miller, 1983; Gill and Hubbard, 1986).

In summary, the major controls on the salinity of St. Croix groundwater are human withdrawal rates, distance from the coast, average altitude of the screened interval, and the strata from which the groundwater is taken. In general, wells in alluvial material tend to produce water of lower overall salinity than water from the carbonates of the central plain.

Sources of solutes in St. Croix groundwater

The dissolved solids have been interpreted to be derived from seawater mixing, aerosol concentration, residual aquifer salts, contributions from formation waters, and dissolution of aquifer minerals (Robison, 1972; Jordan, 1975; Gill and Hubbard, 1986; Gomez-Gomez et al., 1985; Gill, 1994). In coastal areas of large groundwater withdrawals, seawater contamination is undoubtedly occurring.

Jordan (1975) suggested that the bulk of the dissolved solids in inland areas is the result of the concentration of aerosols. This hypothesis has been supported by mass-balance calculations on chloride along a groundwater flow path (F. Gomez-Gomez, pers. comm.,1989); the calculations assume aerosol deposition rates as obtained by Jordan (1975) on St. Thomas, and hydraulic characteristics — gradient and transmissivity — known from St. Croix. On the other hand, if oceanic aerosols are the sole source of the dissolved solids in the Kingshill Limestone, then the strontium isotopic composition of the groundwater should resemble that of modern seawater (0.70907 ± 0.00004; Burke et al., 1982). Instead, the range of $^{87}Sr/^{86}Sr$ in St. Croix groundwater is 0.7067–0.7085 (± 0.0001). Assuming the rocks have retained their original strontium chemistry, the $^{87}Sr/^{86}Sr$ ratios of the groundwater are too low to be derived from dissolution of the Kingshill Limestone as well as being too low to be derived from modern seawater.

More reasonable sources for the groundwater strontium are contributions from the soil zone and the weathering of the Cretaceous siliciclastic and mafic rocks that make up the highlands and many of the alluvial aquifers of St. Croix. Siliciclastic material forms a significant component of the Kingshill Limestone (Gerhard et al., 1978; Lidz, 1982). Rocks of this type, particularly from island-arc and near-arc settings, commonly contain $^{87}Sr/^{86}Sr$ ratios very similar to those of St. Croix groundwater (Hawkesworth, 1982).

The elemental composition of St. Croix groundwater also supports the idea that seawater mixing and the contribution of aerosols are not the sole sources of dissolved solids. Although both chloride and sodium in the groundwater decrease steadily with increasing distance from the coast, the Na^+/Cl^- changes markedly until it no longer resembles the Na^+/Cl^- ratio of seawater. In addition, rainwater-seawater mixing curves, prepared with endmembers from modern seawater and Virgin Islands rainwater, show excesses of most major and minor elements relative to chloride (Fig. 10-4).

For these reasons, St. Croix groundwater must derive a significant proportion of dissolved solutes from rock-water interaction or formation waters. The contribution

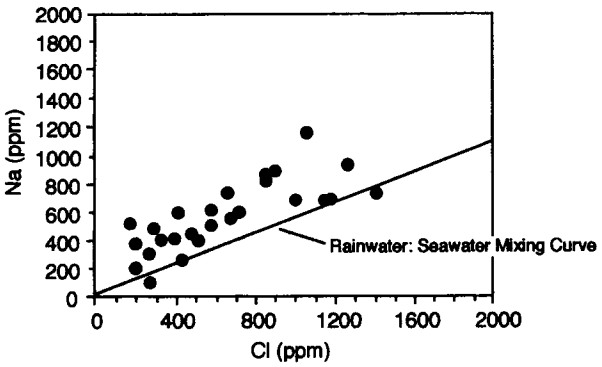


Fig. 10-4. Rainwater-seawater mixing curve for sodium. Sodium is found in excess of values that would be expected if seawater mixing were the only source of sodium in St. Croix groundwater. (After Gill, 1989.)

of water from the Jealousy Formation is a possibility in that TDS increases with well depth and there may be 2,000 m of compactable sediment beneath the Kingshill Limestone. The Jealousy Formation, however, is considered to be poorly permeable by local drillers, and the groundwaters sampled for stable isotopes all showed δ^2H:$\delta^{18}O$ signatures characteristic of meteoric waters. This chemistry is not consistent with waters buried with the marine strata of the Jealousy Formation.

In summary, the isotopic and elemental chemistry indicates that rock-water reactions contribute substantially to St. Croix groundwater. However, in spite of carbonate host rock and undersaturated groundwaters, the rock-water reactions are apparently dominated by non-carbonate components. Such conditions may not be uncommon, and may be controlled by reaction kinetics. Banner et al. (1994) have reported similar findings in Barbados.

CASE STUDY: DOLOMITIZATION ON ST. CROIX

Dolomitization is highly localized on St. Croix, and the process has not yet obliterated clues of its origin. Several sources of information have been used to determine the mechanism of dolomitization: (1) the spatial distribution of the dolomitized strata; (2) the elemental and isotopic geochemistry of the groundwater system; and 3) the elemental and isotopic geochemistry of the dolomitic and calcitic host rock (Gill et al., 1995).

Spatial distribution of dolomitic strata

The dolomitized strata on St. Croix closely outline the shoreline of Krauss Lagoon, a natural embayment modified by industrial development and dredging in the 1960s. Near-surface dolomite on St. Croix follows the distribution of reef and near-

reef strata that rimmed the lagoon in the Pliocene, whereas dolomite presently below the water table is found in the central portions of the lagoon. In cross section, the areas of dolomitization closely conform to the arcuate contact between Tertiary carbonates and Quaternary alluvium that marks the modern erosional base of the lagoon (Fig. 10-5). The spatial distribution of the dolomite suggests that the dolomitization is linked closely with processes related specifically to Krauss Lagoon.

Oxygen isotopic data

St. Croix dolomite ranges from +0.7 to +3.8‰ $\delta^{18}O$ PDB. The isotopically heaviest dolomite is found below the present water table in the center of the former Krause Lagoon (Fig. 10-6; Gill et al., 1995). This dolomite, presently below sea level, is the least likely to have been extensively altered by meteoric fluids, and is therefore used in the discussion of chemistry.

Undiluted modern or Pliocene seawater can be ruled out as the source of the most isotopically heavy dolomite using accepted isotopic fractionation relations (e.g.,

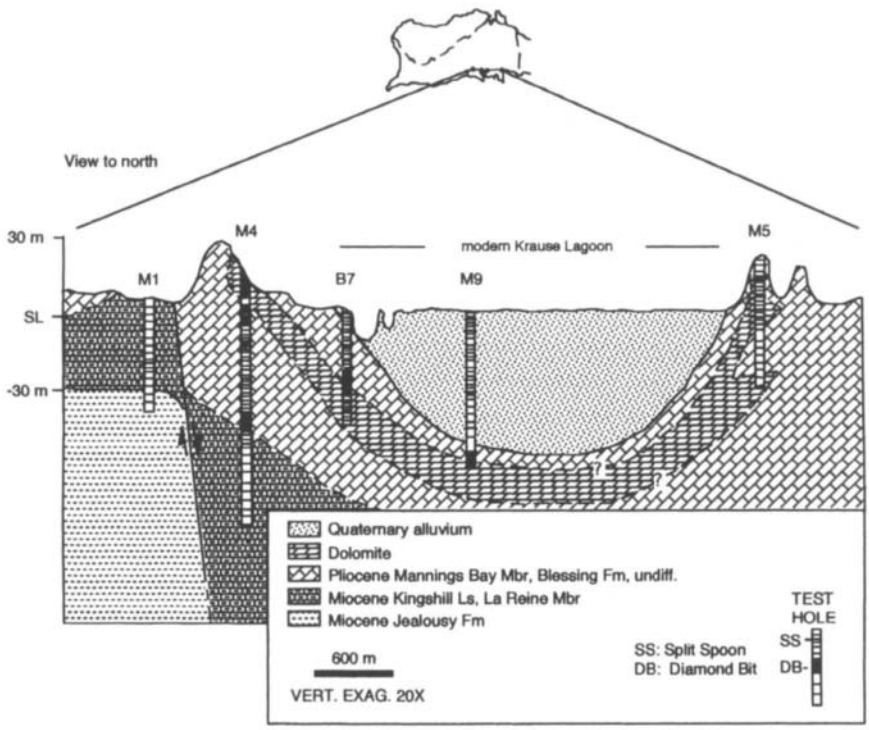


Fig. 10-5. Cross section through the southeastern central plain. Interpreted zone of dolomitization follows the base of Krause Lagoon and the upper surface of the Blessing Formation carbonates. Depth locations of split-spoon samples and cored intervals are shown for each well, with split-spoon samples taken in friable or unconsolidated material. (After Gill, 1989.)

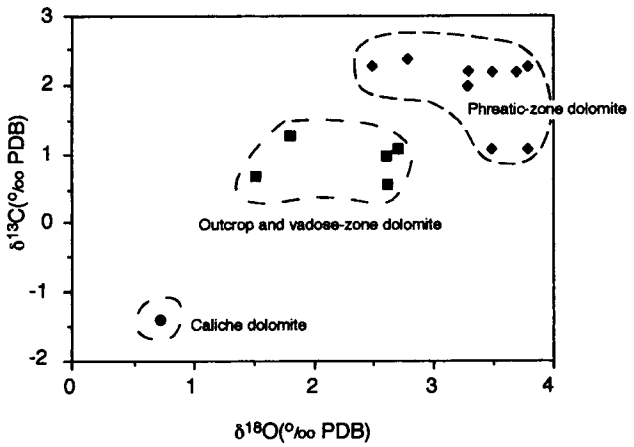


Fig. 10-6. Stable isotope compositions of St. Croix dolomites. The dolomites become depleted in both ^{18}O and ^{13}C in transects from the modern phreatic zone in the center of Krause Lagoon to the vadose zone at the margins. The trend may be controlled by chemical gradients (e.g., seaward vs. landward) during dolomitization, by meteoric recrystallization, or both. The caliche dolomite is substantially depleted even relative to samples within the same outcrop, which suggests subsequent meteoric alteration in at least this sample. (From Gill, 1989.)

Friedman and O'Neil, 1977; Land, 1980). Similarly, modern St. Croix groundwater, which ranges from −3.4 to −4.0‰ $\delta^{18}O$ SMOW, is out of equilibrium with the dolomite. The dolomitizing fluid must have had a $\delta^{18}O$ signature derived either through rock-water interactions or evaporation. Given the geologic setting, the oxygen isotopic composition of the dolomites was probably the result of fluid evaporation close to the Pliocene coastline.

Strontium isotopic data

The age of the dolomitized host rock is Pliocene, requiring the dolomitizing fluid to be Pliocene or younger. Because the strontium ratios of the dolomite are 0.70884–0.70889 (±0.00002), which corresponds to the ratios of seawater in the early to middle Miocene (Burke et al., 1982; DePaolo, 1986), it is impossible to attribute the dolomite formation to a marine fluid alone. Instead, some source of strontium with a low $^{87}Sr/^{86}Sr$ ratio must be responsible for the production of the dolomite.

The source of the low-ratio strontium could have been St. Croix groundwater. As noted above, modern St. Croix groundwater has a $^{87}Sr/^{86}Sr$ ratio of 0.7076–0.7085 (±0.0001), significantly lower than that of the dolomite. This suggests that groundwater alone could not have produced the dolomite; however, a mixture of fluids with differing strontium isotopic ratios would produce a fluid of intermediate composition. When modeled using a range of measured strontium compositions taken from St. Croix groundwater, a variety of mixtures of St. Croix groundwater

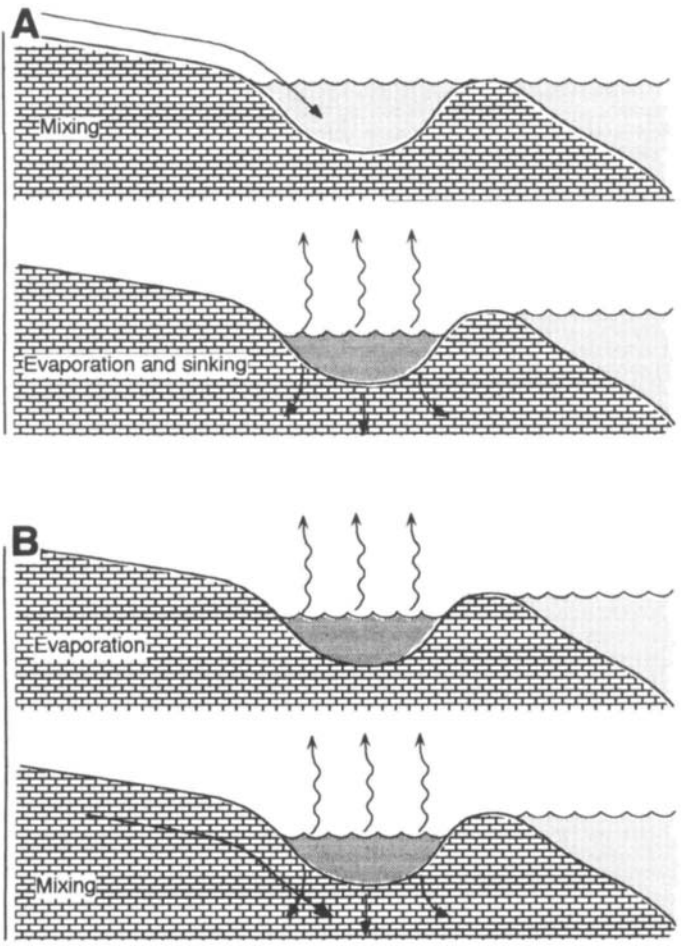


Fig. 10-7. Schematic diagrams representing the two endmembers of the evaporation and mixing sequence. (A) The mix-then-evaporate model. Meteoric water is mixed with marine water in the lagoon, and the mixture then evaporates. Such a mixture would acquire the chemical characteristics of St. Croix dolomite at approximately seawater density. (B) The evaporate-then-mix model. Lagoon waters evaporate, reflux, then mix with meteoric groundwaters. The evaporitic waters would be significantly more dense than seawater. (After Gill, 1989.)

and modern seawater could theoretically produce a diagenetic phase with the characteristics of the St. Croix dolomite (Gill et al., 1995).

Discussion

Dolomitization was probably the result of a hydrologic system that (1) allowed the mixing of groundwater and seawater to produce a fluid with a strontium isotopic

composition intermediate between modern marine water and groundwater; and (2) allowed evaporation to produce a fluid with an oxygen isotopic composition enriched in ^{18}O relative to normal seawater. Evaporation and mixing are consistent with the spatial distribution of the dolomite. The dolomitized strata occur within an embayment or lagoon that was in a freshwater discharge area and could allow extensive evaporation to take place. Similar lagoons and embayments exist on St. Croix today, and the salinity and oxygen isotopic composition of their waters shows that extensive evaporation is taking place (Gill, 1989). Calculations of the densities of these theoretical mixed fluids show that such mixtures could have the capability to displace seawater and could, therefore, have the hydrologic drive to dolomitize coastal strata (Fig. 10-7; Gill et al., 1995). Less-complicated mechanisms such as simple mixing, mineral mixing, simple evaporation and reflux, or incorporation of an enriched oxygen isotopic signature from the exposed limestone do not conform as well with the petrographic character and geochemical signature of the dolomite, the distribution of the dolomitized strata, or both.

CONCLUDING REMARKS

St. Croix contains a carbonate section that reveals a history of uplift and exposure in the late Tertiary. It is possible that St. Croix will provide clues to the tectonic and diagenetic history of the northeastern Caribbean. As a water resource, the carbonate section provides a meager supply of groundwater by most hydrologic standards. As with many islands, however, the importance of even a minor resource is made larger by the expense of the alternatives.

ACKNOWLEDGMENTS

The study was supported by a fellowship from the LSU Alumni Federation and grant support from the American Association of Petroleum Geologists, the Applied Carbonate Research Program at LSU, the Basin Research Institute, the Department of Geology, the Geological Society of America, SOHIO, Shell Oil, Chevron Oil, Union Pacific, and the V. I. Water Resources Research Center. The authors are grateful for thoughtful reviews by D. Budd, B. Jones, P. Smart and patient editor L. Vacher. Numerous thoughtful discussions came from L. Chan, T. Dickson, D. Eby, J. Hanor, E. Heydari, R. Koepnick, L. Land, S. Moshier, A. Saller, M. Simms, J. Banner, H. Cander, W. Ward and D. Thorstensen. W. LeBlanc, S. Reed, R. Snelling, A. Saller, and R. Koepnick and the Mobil Lab are thanked for laboratory assistance. B. and K. Carter, D. Eby, D. Hendrix, F. Gomez-Gomez, the Berg Brothers, T. Sedgwick, L. Schuster, and numerous well owners are thanked for field assistance. Numerous agencies on St. Croix lent valuable cooperation, including Martin Marietta Corp., Hess Oil Virgin Islands, and the Department of Public Works. Special thanks to K. Eastman and the staff of the Caribbean Drilling Service, and the staffs of the Late West Indies Lab and the Applied Carbonate Research Program.

REFERENCES

Andreieff, P., Mascle, A., Mathieu, Y. and Muller, C., 1986. Les carbonates neogenes de Sainte Croix (Iles Vierges) etude stratigraphique et petrophysique. Rev. Inst. Franc. Petrol., 41(3): 336–350.

Banner, J.L., Musgrove, M. and Capo, R.C., 1994. Tracing ground-water evolution in a limestone aquifer using Sr isotopes: Effects of multiple sources of dissolved ions and mineral-solution reactions. Geology, 22: 687–690.

Behrens, G.K., 1976. Stratigraphy, sedimentology and paleoecology of a Pliocene reef tract: St. Croix, U.S. Virgin Islands. M.S. Thesis, Northern Illinois Univ., DeKalb IL, 93 pp.

Black, Crow and Eidsness, Inc., 1976. A water management plan for St. Croix, U.S. Virgin Islands. Black, Crow and Eidsness Inc., Gainesville FL.

Bold, W. van den, 1970. Ostracoda of the lower and middle Miocene of St. Croix, St. Martin, and Anguilla. Carib. Jour. Sci., 10: 35–61.

Burke, W.H., Denison, R.E., Hetherington, E.A., Koepnick, R.B., Nelson, H.F. and Otto, J.B., 1982. Variation of seawater $^{87}Sr/^{86}Sr$ throughout Phanerozoic time. Geology, 10: 516–519.

Cederstrom, D.J., 1950. Geology and groundwater resources of St. Croix, U.S. Virgin Islands. U.S. Geol. Surv. Water-Supply Pap. 1067, 117 pp.

CH2M Hill, Inc., 1983. Water management plan for the public water system, U.S. Virgin Islands. CH2 M Hill Southeast, Gainesville FL, 290 pp.

DePaolo, D.J., 1986. Detailed record of the Neogene Sr isotopic evolution of seawater from DSDP Site 590B. Geology, 14: 103–106.

Friedman, I. and O'Neil, J.R., 1977. Chapter KK. Isotopic fractionation factors for some minerals of geologic interest. In: M. Fleischer (Technical Editor), Data in Geochemistry, Sixth Edition. U.S. Geol. Surv. Prof. Paper 440-KK.

Geraghty and Miller, Inc, 1983. Report on current groundwater conditions in the U.S. Virgin Islands. Geraghty and Miller Inc., Syosset NY, 89 pp.

Gerhard, L.C., Frost, S.H. and Curth, P.J., 1978. Stratigraphy and depositional setting, Kingshill Limestone, Miocene, St. Croix, U.S. Virgin Islands. Am. Assoc. Petrol. Geol. Bull., 62: 403–418.

Gill, I.P., 1989. The Evolution of Tertiary St. Croix. Ph.D. Dissertation, Louisiana State Univ., Baton Rouge LA, 287 pp.

Gill, I., 1994. Groundwater geochemistry of the Kingshill aquifer system, St. Croix. Environ. Geosci., 1: 40–49.

Gill, I.P. and Hubbard, D.K., 1986. Groundwater geochemistry of the St. Croix carbonate aquifer system. Tech. Rep. 27, Water Resour. Res. Cent., Coll. Virgin Islands, St. Thomas, U.S. Virgin Islands, 59 pp.

Gill, I.P. and Hubbard, D.K., 1987. Subsurface geology of the St. Croix carbonate rock system. Tech. Rep. 28, Water Resour. Res. Cent., Coll. Virgin Islands, St. Thomas, U.S. Virgin Islands, 79 pp.

Gill, I.P., Hubbard, D.K., McLaughlin, P.P. and Moore, C.H., 1989. Sedimentological and tectonic evolution of Tertiary St. Croix. In: D.K. Hubbard, (Editor), Terrestrial and Marine Geology of St. Croix, U.S. Virgin Islands. West Indies Lab. Spec. Publ., 8: 49–72.

Gill, I.P., Moore, C.H. and Aharon, P.A., 1995. Evaporitic mixed-water dolomitization on St. Croix, U.S.V.I. J. Sediment. Res., A65: 591–604.

Gill, I.P., Hubbard, D.K., McLaughlin, P.P. and Moore, C.H., in press. The geology and hydrogeology of the Kingshill Aquifer System, St. Croix. In: R.A. Renken (Editor), Geology and Hydrogeology of the Caribbean Islands Aquifer System of the Commonwealth of Puerto Rico and the U.S. Virgin Islands. U.S. Geol. Surv. Prof. Pap. 1419–A.

Gomez-Gomez, F., Quinones-Marquez, F. and Zack, A.L., 1985. U.S. Virgin Islands ground water resources. U.S. Geol. Surv. National Water Summary 1985 — U.S. Virgin Islands, pp. 409–414.

Hanor, J.S., 1978. Precipitation of beachrock cements: mixing of marine and meteoric waters vs. CO_2 degassing. J. Sediment. Petrol., 48: 489–501.

Hawkesworth, C.J., 1982. Isotope characteristics of magmas erupted along destructive plate margins. In: R.S. Thorpe (Editor), Andesites. Wiley, New York, pp. 549–571.

Hendrickson, G.E., 1963. Ground water for public supply in St. Croix, Virgin Islands. U.S. Geol. Surv. Water-Supply Pap. 1663-D: D1-D27.

Houlgatte, E., 1983. Etude d'une partie de la frontiere nord-est de la plaque Caraibe. M.S. Thesis, L'Universite de Bretagne Occidentale, 69 pp.

Hubbard, D.K., Venger, L., Parsons, K. and Stanley, D., 1989. Geologic development of the West End terrace system on St. Croix, U.S. Virgin Islands. In: D.K. Hubbard (Editor), Terrestrial and Marine Geology of St. Croix, U.S. Virgin Islands. West Indies Lab. Spec. Publ., 8: 73–84.

Jordan, D.G., 1975. A survey of the water resources of St. Croix, Virgin Islands. U.S. Geol. Surv. Open-File Rep., Caribbean District, San Juan, 51 pp.

Land, L.S., 1980. The isotopic and trace element geochemistry of dolomite: the state of the art. In: D.H. Zenger, J.B. Dunham and R.L. Ethington (Editors), Concepts and Models of Dolomitization. Soc. Econ. Paleontol. Mineral. Spec. Publ., 28: 87–110.

Lewis, J.F. and Draper, G., 1990. Geology and tectonic evolution of the northern Caribbean margin. In: G. Dengo and J.E. Chase (Editors), The Caribbean Region. Geol. Soc. Am., The Geology of North America, H: 77–140.

Lidz, B.H., 1982. Biostratigraphy and paleoenvironment of Miocene-Pliocene hemipelagic limestone, Kingshill Seaway, St. Croix, U.S. Virgin Islands. J. Foraminiferal Res., 12: 205–233.

Lidz, B.H., 1984a. Oldest (early Tertiary) subsurface carbonate rocks of St. Croix, USVI, revealed in a turbidite-mudball. J. Foraminiferal Res., 14: 213–227.

Lidz, B.H., 1984b. Neogene sea-level change and emergence, St. Croix, Virgin Islands: evidence from basinal carbonate accumulations. Geol. Soc. Am. Bull., 95: 1268–1279.

Lidz, B.H., 1988. Upper Cretaceous (Campanian) and Cenozoic stratigraphic sequence, north-east Caribbean (St. Croix, U.S. Virgin Islands). Geol. Soc. Am. Bull., 100: 282–298.

Maury, R.C., Westbrook, G.K., Baker, P.E., Bouysse, Ph. and Westercamp, D., 1990. Geology of the Lesser Antilles. In: G. Dengo and J.E. Case (Editors), The Caribbean Region. Geol. Soc. Am., The Geology of North America, H: 141–166.

McLaughlin, P.P., Gill, I.P. and Bold, W.K. van den, 1995. Biostratigraphy, paleoenvironments and stratigraphic evolution of the Neogene of St. Croix, U.S. Virgin Islands. Micropaleontol., 41: 293–320.

Multer, H.G., Frost, S.H. and Gerhard, L.C., 1977. Miocene "Kingshill Seaway" — a dynamic carbonate basin and shelf model, St. Croix, U. S. Virgin Islands. In: S.H. Frost, M.P. Weiss and J.B. Saunders (Editors), Reefs and Related Carbonates — Ecology and Sedimentology. Am. Assoc. Petrol. Geol., Studies in Geol., 4: 329–352.

Nagle, F. and Hubbard, D.K., 1989. St. Croix geology since Whetten: an introduction. In: D.K. Hubbard (Editor), Terrestrial and Marine Geology of St. Croix, U.S. Virgin Islands. West Indies Lab. Spec. Publ. 8: 1–8.

Pindell, J.L. and Barrett, S.F., 1990. Geological evolution of the Caribbean region: A plate-tectonic perspective. In: G. Dengo and J.E. Case (Editor), The Caribbean region. Geol. Soc. Am., The Geology of North America, H: 405–432.

Renken, R. (Editor), in press. Geology and hydrogeology of the Caribbean islands aquifer system of the Commonwealth of Puerto Rico and the U.S. Virgin Islands. U.S. Geol. Surv. Prof. Pap. 1419-A.

Roberts, H.H., Coleman, J.M., Murray, S.P. and Hubbard, D.K., 1981. Offshelf sediment transport on the downdrift flank of a trade wind island. Proc. Fourth Int. Coral Reef Symp. (Manila), 1: 389–397.

Robison, T.M., 1972. Ground water in central St. Croix, U.S. Virgin Islands: U. S. Geol. Surv. Open-File Report, Caribbean District, 18 pp.

Shurbet, G.L., Worzel, J.L. and Ewing, M., 1956. Gravity measurements in the Virgin Islands. Geol. Soc. Amer. Bull., 67: 1529–1536.

Speed, R.C., 1989. Tectonic Evolution of St. Croix: implications for tectonics of the northeastern Caribbean. In: D.K. Hubbard (Editor), Terrestrial and Marine Geology of St. Croix, U.S. Virgin Islands. West Indies Lab. Spec. Publ. 8: 9–22.

Speed, R.C. and Joyce, J., 1989. Depositional and structural evolution of Cretaceous Strata, St. Croix. In: D.K. Hubbard (Editor), Terrestrial and Marine Geology of St. Croix, U.S. Virgin Islands. West Indies Lab. Spec. Publ. 8: 23–35.

Stanley, D.J., 1989. Sedimentology and paleogeography of Upper Cretaceous rocks, St. Croix, U.S. Virgin Islands. In: D.K. Hubbard (Editor), Terrestrial and Marine Geology of St. Croix, U.S. Virgin Islands. West Indies Lab. Spec. Publ., 8: 37–47.

Torres-Gonzalez, S., 1991. Steady-state simulation of ground-water flow conditions in the Kingshill Aquifer, St. Croix, U.S. Virgin Islands, July, 1987. In: F. Gomez-Gomez, V. Quinones-Aponte and A.I. Johnson (Editors), Aquifers of the Caribbean Islands. Am. Water Resour. Assoc. Monogr. Ser., 15: 93–108.

Torres-Sierra, H., 1987. Estimated water use in St. Croix, U.S. Virgin Islands, October 1983–September 1985. U.S. Geol. Surv. Open-File Rep. 86–537.

Whetten, J.T., 1966. Geology of St. Croix, U.S. Virgin Islands. In: H.H. Hess (Editor), Caribbean Geological Investigations. Geol. Soc. Am. Mem. 98: 177–239.

This Page Intentionally Left Blank

Geology and Hydrogeology of Carbonate Islands. Developments in Sedimentology 54
edited by H.L. Vacher and T. Quinn
© 1997 Elsevier Science B.V. All rights reserved.

Chapter 11

GEOLOGY AND HYDROGEOLOGY OF BARBADOS

JOHN D. HUMPHREY

INTRODUCTION

Barbados is the easternmost island of the Windward Islands chain in the eastern Caribbean region. It is located at 13°10′N and 59°33′W, approximately 150 km east of the Lesser Antilles volcanic island arc. The island is 34 km long and about 23 km wide and covers an area of about 425 km^2. The highest point, Mt. Hillaby, is approximately 340 m above sea level. Nearly 85% of the island exposes reef-associated carbonate sedimentary rocks of differing Pleistocene ages. This Pleistocene limestone cover, which is known locally as the "Coral Cap" and formally as the Coral Rock Formation (Poole and Barker, 1983), averages about 70 m thick.

Barbados was originally settled by Arawak and Carib Amerindians who abandoned the island by the early 1600s. The island was charted in 1536 by the Portuguese who named it Los Barbados, or The Bearded Ones; however, the Portuguese never claimed the island. The name presumably derives from the abundance of ficus trees, which have aerial roots that look like beards. Barbados was claimed in 1625 by the British merchant Captain John Powell for King James I. Barbados' Parliament was established in 1639, making it the second oldest parliament outside the British Isles (Bermuda's was the first). On November 30, 1966, Barbados became a fully independent nation within the Commonwealth and joined the United Nations. The island supports a population of about 250,000 and has the highest literacy rate and among the highest standards of living in the Caribbean. Population density is about 590 persons km^{-2}. Although the rate of population growth is quite low (about 0.2% y^{-1}), economic and infrastructure development has been rapid. The economy is supported by tourism, sugarcane agriculture, light industry, and offshore financial services. In recent years, there has been a gradual replacement of sugarcane agriculture by other diverse cash crops, due to lower sugar prices worldwide and higher local wage costs.

Barbados lies within the belt of northeast trade winds and is characterized by a humid to subhumid tropical maritime climate. The eastern, windward side of the island experiences high-energy wave action with Atlantic rollers crashing on eroding seacliffs. The western, leeward side of the island faces the Caribbean Sea and experiences gentle waves lapping onto sandy beaches. Daily and seasonal temperatures vary little, generally ranging between 23° and 30°C. Due to orographic effects, average annual precipitation varies widely across Barbados. In the central, elevated portion of the island, annual rainfall averages over 200 cm y^{-1}; the coastal regions generally receive 110–125 cm y^{-1} (Rouse, 1962). Precipitation exceeds evapotranspiration only in the higher-elevation, inland portion of Barbados (Rouse, 1962). The rainy season occurs during the months of August to December.

GEOLOGIC AND TECTONIC SETTING

Barbados is unique in the Lesser Antilles in that, except for minor ash beds, it is not a volcanic island. Rather, the island is composed entirely of sedimentary rocks. Subduction of Atlantic oceanic crust of the North American Plate westward below the Caribbean Plate has led to the development of an elongate, arcuate accretionary complex — known as the Barbados Ridge Accretionary Prism — east of the Lesser Antilles magmatic island arc and the Tabago Trough forearc basin. Barbados is the only emergent portion of this accretionary prism.

The basement beneath the Coral Cap consists of structurally complex marine rocks that can be separated into four major geologic units (Speed, 1990) that crop out in an erosional window on the east-central portion of the island (Scotland District, Figs. 11-1, 11-2). The oldest unit, the Scotland Formation, is an accretionary complex composed primarily of terrigenous turbidite and gravity-flow deposits interbedded with hemipelagic and pelagic radiolarites of Eocene age (Larue and Speed, 1984; Speed, 1990). This basal complex extends from the surface to below the maximum well extent of 4.5 km. Prism-cover sediments were deposited on top of the basal complex through the middle Miocene in a synclinal basin known as the

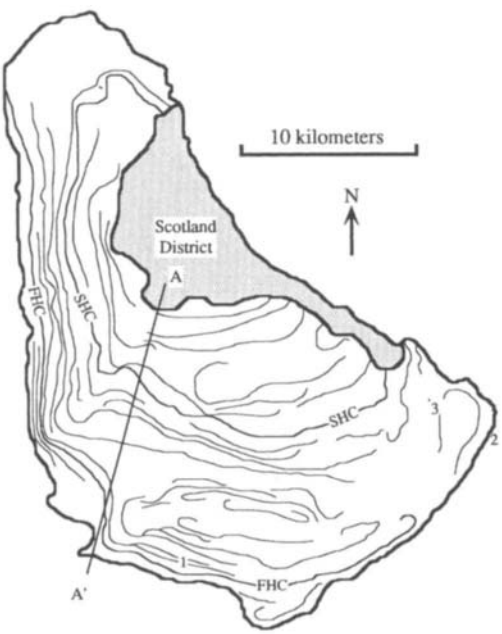


Fig. 11-1. Map of Barbados showing trends of Pleistocene reef tracts. Shaded area represents the erosional window exposing rocks of the Tertiary accretionary prism, upon which Pleistocene limestones (unshaded) unconformably lie. Reef tracts generally conform to the outline of the island and increase in age and topographic elevation toward the interior of the island. Section A-A′ shown in Fig. 11-3. Key: FHC, First High Cliff; SHC, Second High Cliff; 1, Christ Church region; 2, Bottom Bay; 3, Golden Grove. (Modified from Mesolella et al. 1969.)



Fig. 11-2. Field photograph of complexly folded and faulted Scotland Group accretionary prism rocks near Chalky Mount. Large bush at upper left is about 3 m high.

Woodbourne Trough. In thrust contact with these two underlying units are nappes of the Oceanic Formation, a Miocene forearc basin sequence composed of calcareous pelagic and hemipelagic rocks interbedded with volcanogenic ashes (Torrini et al., 1985). Finally, intruding all these units are tectonic diapirs consisting of a mélange of organic mud matrix. Emplacement of these diapirs is probably continuing today and is likely responsible for the local anomalous elevation of Barbados above the rest of the accretionary prism (Speed, 1990). Barbados has thus experienced tectonic uplift throughout most of the Neogene at rates averaging approximately 0.3 to 0.4 m ky^{-1} (Speed, 1990).

Deposition of fringing reefs occurred around the structural high during glacioeustatic highstands of the sea throughout the late Pleistocene, from more than 600 ka to the present (Broecker et al., 1968; Mesolella et al., 1969; Bender et al., 1973; Bender et al., 1979). Reef deposition during individual highstands probably occurred over a period of 10–15 ky (Mesolella et al., 1970; Humphrey and Kimbell, 1990). During intervening lowstands, tectonic uplift raised the previously deposited reef sediments and older reef limestones to higher elevations. Subsequent sea-level rises resulted in deposition of stratigraphically younger reef sediments in successively structurally lower positions. In this way, there developed a series of reef terraces whose age and elevation decrease from the higher, central portions of the island outward toward the coast (Figs. 11-1, 11-3; Table 11-1).

Actively growing (Recent) fringing coralgal reefs occur along the leeward coastline of Barbados (Lewis, 1960). Most commonly the reefs occur offshore of coastline promontories and are separated from the coast by small lagoons and sand flats. Most of the eastern coastline of Barbados is largely devoid of actively growing reefs; however, a discontinuous barrier reef with few living coral colonies occurs along the southeast coast. This reef is separated from the island by a lagoon

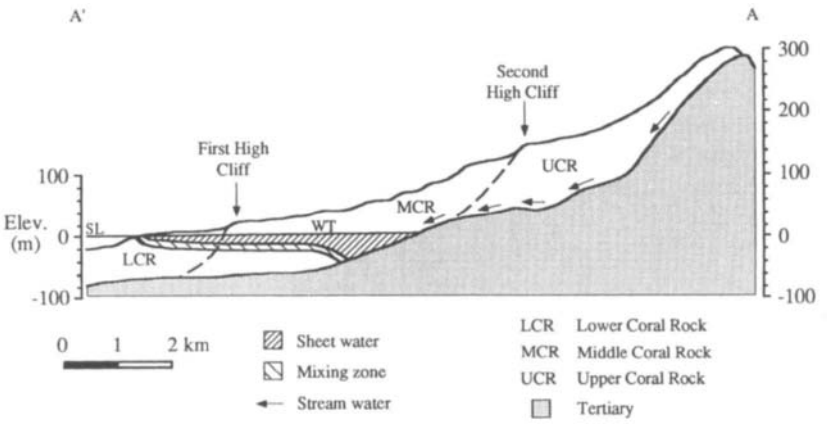


Fig. 11-3. Hydrogeologic cross section A-A′ (see Fig. 11-1). Meteoric groundwaters recharged through the Coral Rock Formation flow either as stream-water along the contact with the underlying Tertiary aquiclude, or as sheet-water that forms the coastal freshwater lens. Where the freshwater lens interfaces with marine pore fluids, a freshwater-saltwater mixing zone is formed. (Modified from Harris 1968.)

approximately 0.5 km wide. Descriptions of the west coast reefs can be found in James et al. (1977).

GENERAL GEOMORPHOLOGY

Early workers (e.g., Trechmann, 1933) explained the distinctly terraced geomorphology of the Coral Cap to be the result of intermittent tectonic uplift coupled with erosion of a shallow carbonate bank or platform. Terraces were thus thought to have been formed through active wave-cutting during periods of little or no tectonic uplift. Detailed sedimentologic and stratigraphic work by R.K. Matthews and his colleagues, however, clearly demonstrated that the terrace morphology resulted from constructional reef growth during sea-level highstands (e.g., Matthews, 1967; Mesolella et al., 1969; 1970).

Individual terraces, which are easily identified in air photographs, consist of a riser that slopes gently to steeply seaward and a flat landing that extends landward of its riser; this landing intersects the riser face of the next higher (landward) terrace (Fig. 11-4). Surface outcrops and roadcut exposures indicate that the risers are comprised of rear-zone, reef-crest, and forereef lithologies. The landings consist primarily of backreef deposits.

DEPOSITIONAL SYSTEMS

Internal facies of the raised Pleistocene reef terraces are well exposed in numerous roadcuts, quarries, and seacliffs throughout the island. In many places, the original

Table 11-1

Morphostratigraphic nomenclature, elevations, and ages for Barbados Pleistocene coral reef terraces (after Humphrey and Matthews, 1986)

Morphostratigraphic Unit	Elevation (m)	Age (ka)
Southern Christ Church		
Worthing	3	80[a]
Ventnor	6	99[a]
Rendezvous Hill	37	122[a]
Kendall Hill	49	194[a]
Kingsland	79	216[a]
Aberdare	67	238[a]
Adams Castle	91	235[b]
Kent	110	327[b]
St. David	110	283[b]
Unnamed	122	Undated
Clermont Nose		
Worthing	20	80[a]
Ventnor	30	99[a]
Rendezvous Hill	61	122[a]
Durants	67	194[a]
Cave Hill	85	216[a]
Thorpe	94	238[a]
Husbands	107	Undated
Unnamed	122	Undated
St. George's Valley		
Windsor	73	238[a]
Rowans	110	300[b]
Dayrells	92	330[b]
Bourne	125	280[b]
Walkers	137	Undated
Cottage Vale	158	490[b]
Second High Cliff	171	450[b]
Hill View	177	515[b]
Drax Hall	192	590[b]
Guinea	192	640[b]

[a] By correlation to Prell et al. (1986) deep sea oxygen isotope record.
[b] He/U dates from Bender et al. (1979).

depositional topography of the fringing reefs is preserved; in several localities, wave erosion has substantially modified the original topography. The facies patterns and biological zonations of the Pleistocene reefs are similar to those described for modern fringing reefs of Barbados (Lewis, 1960) and other reefs in the Caribbean (e.g., Goreau, 1959). From offshore to inshore, these facies consist of (1) forereef calcarenite facies, (2) reef facies, and (3) backreef facies (Fig. 11-5).

Following is a description of the facies relationships in the raised reef tracts of Barbados. The description represents a generalized model drawn from the study of numerous reef tracts. Individual reef tracts may vary, both vertically and along strike, from this generalized model.



Fig. 11-4. Field photograph showing terrace topography of Second High Cliff near Blades Hill. Sugar cane is growing on backreef deposits of next younger terrace. House at top of terrace for scale.

Forereef calcarenite facies

The best exposures of the forereef calcarenite facies occur along seacliff exposures on the southeastern coastline (Mesolella et al., 1970; Humphrey and Kimbell, 1990). These calcarenites were generally deposited seaward of the deepest zone of in situ coral growth in water depths commonly greater than 5 m (Humphrey and Kimbell, 1990). The forereef sands dip seaward and in places are more than 15 m thick (Fig. 11-6). Forereef calcarenites can be subdivided into two general categories (Mesolella et al., 1970): (1) massively bedded, poorly sorted calcarenites containing reef-derived coral rubble, and (2) medium-bedded, well-sorted cross-stratified calcarenites. A majority of the allochems making up these deposits are reef-derived (allochthonous) grains generated through mechanical erosion and transported to the forereef slope. In situ (autochthonous) allochems, primarily coralline red algae rhodoliths and benthonic foraminifers, are also common (Humphrey and Kimbell, 1990). The well-sorted calcarenites commonly occur seaward of channels or passages through the reef barrier and occur as progradational and coalescing sand aprons (Mesolella et al., 1970).

Reef facies

The reef facies is composed of resistant limestones containing abundant framework-building hermatypic corals and coralline algae. The reef facies displays a faunal zonation that is repeated over and over in successive reef terraces. This zonation can be characterized, on the basis of faunal content, into four major subfacies: (1) the mixed head coral zone, (2) the *Acropora cervicornis* zone, (3) the reef-crest *Acropora palmata* zone, and (4) the near-backreef rear zone.

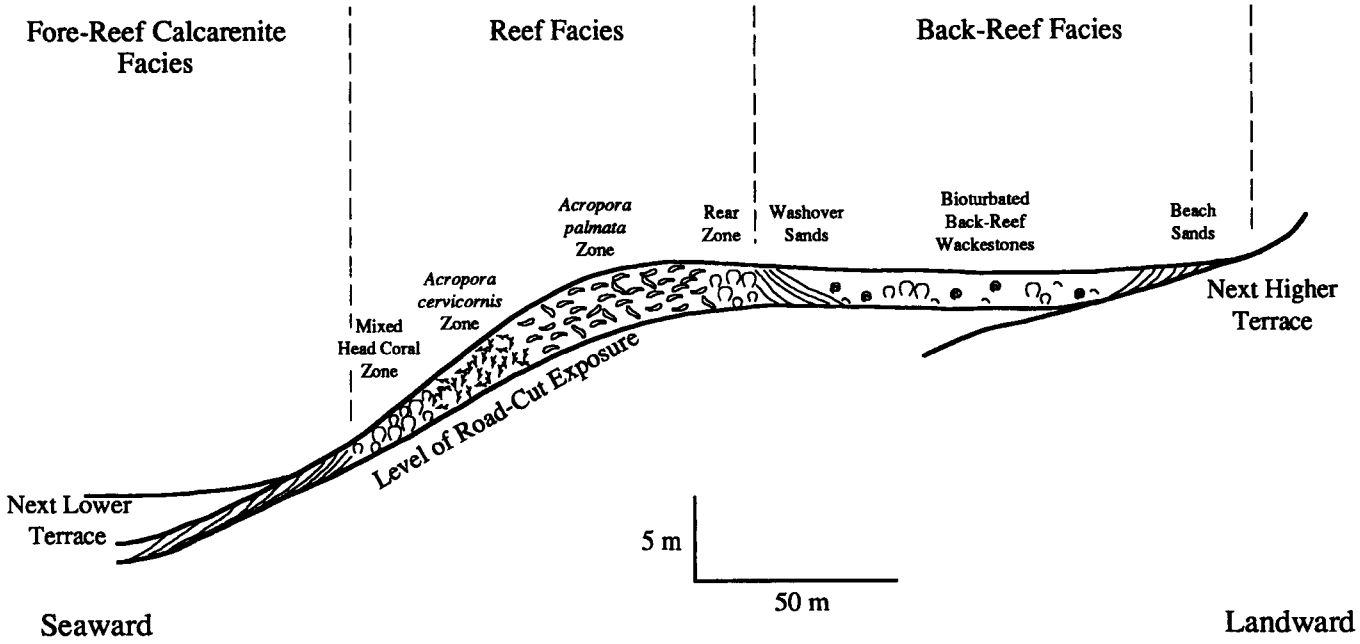


Fig. 11-5. Generalized composite facies architecture for Barbados Pleistocene reef tracts exposed in roadcuts. Refer to text for facies descriptions. (Modified from Mesolella, 1967 and James et al. 1977.)



Fig. 11-6. Field photograph showing well-bedded forereef calcarenite facies at Deebles Point. Massive upper units are progradational head-coral facies that prograded seaward (toward left of photograph). The seacliff here is approximately 25 m high.

Mixed head coral zone. Occupying the deepest zone of in situ coral growth in the Pleistocene reef terraces, the mixed head coral zone is dominated by massive hemispherical colonies of scleractinian corals. The predominant species is *Montastrea annularis*, a common denizen of Holocene reefs at depths greater than about 5 m. In places, groups of large multilobate colonies of *M. annularis* formed the seaward buttress zone of a reef spur (Humphrey and Matthews, 1986). Other common species of the mixed head coral zone include the brain corals, *Diploria strigosa* and *D. labyrinthiformis* (Fig. 11-7), along with the minor presence of *Siderastrea* spp. and *M. cavernosa*. Analogous modern fringing reefs along the west coast of Barbados contain other, more fragile species of corals that are either poorly represented or missing entirely from the Pleistocene sections. Such subordinate species in the modern reefs include: *Porites porites*, *P. astreoides*, *Favia fragum*, *Eusmilia fastigiata*, *Meandrina* spp., *Madracis* spp., and *Colpophyllia* spp. (Lewis, 1960). Roadcut sections through Pleistocene mixed head coral zones show that the large head corals commonly used previously developed, presumably deceased colonies as stable substrates for their growth. Intercoralline matrix in the Pleistocene reefs consists of reef-derived wackestones, packstones, and rudstones.

Acropora cervicornis zone. As one moves upward and landward on the forereef slope, the mixed head coral zone grades into the *Acropora cervicornis* zone. The upward transition may be gradational, with disarticulated branches of the staghorn coral, *A. cervicornis,* intermixed with *Montastrea annularis* heads, or the transition may be abrupt over a few centimeters. Because of the fragility of the staghorn coral, this facies commonly consists of broken branches of *A. cervicornis*, 5–30 cm long (Fig. 11-8). Commonly, this easily identifiable facies is composed almost entirely of broken branches in a fine-grained matrix. The upper surfaces of individual



Fig. 11-7. Outcrop photograph of Pleistocene *Diploria* sp. in growth position along the Dayrells road cut (330 ka). Note good preservation of skeletal architecture. Pencil is 14 cm.



Fig. 11-8. Outcrop photograph of *Acropora cervicornis* facies at Cole's Pasture. Note good preservation of broken *A. cervicornis* branches. Hammer is 26 cm.

A. cervicornis branches may be encrusted with coralline red algae. The *A. cervicornis* zone may not occur in every exposure of the reef facies; in such cases, the mixed head coral zone grades upward into the *A. palmata* zone.

Acropora palmata zone. Occupying the reef-crest position is a zone dominated almost entirely by the massive elkhorn coral, *Acropora palmata*, in a poorly sorted matrix of reef-derived debris. Large trunks and fronds of this massive branching coral are rarely in growth position; however, transport distances are likely small for such large pieces (Fig. 11-9). These deposits can be thought of as essentially *in situ* accumulations at the reef crest. Along the crest of individual terraces, this zone is discontinuous and may be missing entirely (Mesolella et al., 1970). Indeed, the crests of some terraces lack both the *A. cervicornis* and *A. palmata* zones, and are composed of a mixed assemblage consisting principally of head corals or coral rubble and sand (Mesolella et al., 1970). The *A. palmata* zone generally has the greatest abundance of coralline red algae, with the algae occurring as encrustations on the surfaces of the coral fronds. This occurrence is consistent with the preference of red algae for high-energy shallow-water conditions.



Fig. 11-9. Outcrop photograph showing *Acropora palmata* facies near River Bay. Largest fronds near bottom left are as large as 0.5 m. The *A. palmata* facies is overlain by rear zone floatstones containing *Porites porites* in a chalky matrix. Backreef packstones and floatstones above discontinuity have prograded over the *A. palmata* — rear zone lithologies.

Rear zone. Immediately behind, or landward, of the reef crest lies the rear zone. Here, the *Acropora palmata* rudstones of the crest gradually give way to a mixed assemblage of corals and associated sediments. The coral assemblage in the rear zone is similar to that in the mixed head coral zone; however, individual colonies are generally smaller and more sparsely distributed. Common coral species in the rear zone include *Montastrea annularis*, *Diploria* spp., and *Siderastrea radians.* Minor amounts of *A. cervicornis* and *Porites porites* are also present.

Backreef facies

A majority of the Pleistocene reef tracts of Barbados are separated from the next older, topographically higher reef tract by a broad lagoon. These shallow backreef areas may be up to 800 m wide, and the lagoonal sediments onlap the forereef deposits of the landward terraces. Two dominant lithologies occur within the backreef facies: well-sorted grainstones and packstones lying directly landward of the rear zone, and bioturbated coral-molluscan wackestones. The grainstones and wackestones behind the rear zone are commonly cross-stratified, dipping gently landward (Mesolella et al., 1970). These deposits represent washover sediments from the reef and are composed principally of coral and coralline algae debris. Rhodoliths are also a common constituent, especially on the windward, eastern side of the island. The massively bedded bioturbated wackestones represent a majority of the backreef sediments. Floating in the muddy sediments are scattered solitary corals in growth position, such as *Siderastrea siderea* and *S. radians*, and various mollusks, such as articulated bivalves and *Strombus gigas.* Locally, small patch reefs containing *Diploria* sp., *Montastrea annularis*, *Acropora cervicornis*, and *Porites porites* occur within the backreef facies. Beach deposits composed of gently seaward dipping, cross-stratified grainstones occur along the shoreward margins of several lagoons (Mesolella et al., 1970).

STRATIGRAPHY AND SEA-LEVEL HISTORY

Beginning with the studies of Broecker et al. (1968) and Mesolella et al. (1969), the geology of Barbados has been renowned for the relationship of its terrace geochronology to late Pleistocene sea-level history. Many studies have refined the stratigraphy, age relations, and sea-level history of the terraces and its strong support for the Milankovitch astronomical theory of the ice ages (e.g., Bender et al., 1973; Fairbanks and Matthews, 1978; Bender et al., 1979; Edwards et al., 1987; Ku et al., 1990; Banner et al., 1991). Results of these studies could easily comprise an entire volume and, accordingly, can only be summarized here. A majority of the geochronologic results are based on conventional Uranium-series alpha-counting techniques; however, more precise thermal ionization mass-spectrometric methods (TIMS) are currently being applied to terrace geochronology (e.g., Edwards et al., 1987; Banner et al., 1991; Gallup et al., 1994; Fairbanks, unpub. data).

The marine oxygen isotope record has not provided a direct proxy for eustatic sea level given that the record is affected by both ice-volume and temperature effects. Although discontinuous, the record of eustatic sea level may be deduced from well-dated uplifted marine terraces, such as the Pleistocene coral terraces of Barbados. Raised reef terraces provide a direct record of sea-level change and can, therefore, be used to "calibrate" indirect records of eustasy, such as deep-sea oxygen isotope and sequence-stratigraphic records. Because *Acropora palmata* is ecologically restricted to the upper few meters of the water column in the reef-crest environment, *A. palmata* provides an appropriate marker for sea-level highstands. Although other coral species are also dated (Bender et al., 1979), *A. palmata* has been the principal material used to constrain the timing and amplitude of late Pleistocene glacioeustasy.

Bender et al. (1979) reported the most complete geochronology of the Barbados terraces. Bender et al. (1979) used three regional traverses where topographic expression of the terrace succession is particularly well exposed: the southern west coast-Clermont Nose area, the southern Christ Church Parish area, and the south-central St. Georges Valley area. Ages were determined using the ^{230}Th/U and ^{4}He/U methods (Bender et al., 1979). Two prominent terraces, First High Cliff (or Rendezvous Hill) and Second High Cliff, have been dated at 125 ka and 460 ka, respectively (Figs. 11-1, 11-3). First and Second High Cliffs are used as lithostratigraphic and chronostratigraphic markers to separate the Coral Rock Formation into the Lower, Middle, and Upper Coral Rock Members (Fig. 11-3). Two terraces, the Worthing and Ventnor terraces, occur at lower elevations than First High Cliff (Lower Coral Rock) and have been dated at 82 ka and 105 ka, respectively. Thus, the Worthing, Ventnor, and Rendezvous Hill terraces may be correlated to interglacial highstands of the sea noted in the marine oxygen isotope record as isotope stages 5a, 5c, and 5e, respectively (Mesolella et al., 1969; Bender et al., 1979). This correlation is further corroborated by the relative oxygen isotopic composition of coral samples from these terraces (Fairbanks and Matthews, 1978). Correlation of these three terraces to the stacked SPECMAP marine oxygen isotope curve of Prell et al. (1986) yields ages of 80 ka, 99 ka, and 122 ka (Humphrey and Matthews, 1986). Age uncertainties increase and stratigraphic relationships become less clear for the older terraces on the island, although Bender et al. (1979) identified terraces correlating with the marine oxygen isotope record back to approximately 640 ka. With very few exceptions, the general relationship of increasing terrace age with increasing elevation of the reef terrace holds for the island of Barbados (Bender et al., 1979) (Table 11-1).

HYDROGEOLOGY OF BARBADOS

The population of Barbados, along with agriculture and industrial production, is almost entirely dependent upon groundwater resources for water supply. Increases in agricultural and industrial production, together with a growing indigenous and tourist population, place an increasing demand on the island's natural water resources.

The topography of the contact between the Coral Rock Formation and the underlying relatively impermeable Tertiary section has a profound influence on the

hydrogeology of Barbados. Meteoric groundwater is recharged in the higher portions of the island where precipitation exceeds evapotranspiration. Where the Tertiary aquiclude lies below sea level, an unconfined coastal aquifer is developed within the Pleistocene limestones. A majority of the Coral Cap today lies above the water table. Groundwater transmission occurs as concentrated conduit flow where the Tertiary aquiclude lies above sea level (Harris, 1971). The contact between the Pleistocene limestones and Tertiary marine rocks generally dips toward the west and south coasts. Groundwater flows as "stream-water" at the base of the Coral Cap in an integrated network of underground channels (Fig. 11-3). In many of these stream courses, extensive dissolution of the limestones has resulted in cavernous porosity development, with channels reaching 5 m in diameter. Groundwater divides resulting from paleotopographic variations on top of the Tertiary section separate the stream water into relatively distinct catchment areas or drainage basins (Tullstrom, 1964; Goodwin, 1980).

Stream-water channels feed into a coastal meteoric phreatic lens where they reach sea level. Locally referred to as "sheet-water" areas (Fig. 11-10), the coastal freshwater wedge floats on top of the more dense marine porewaters. Because of the high transmissivity of the Pleistocene limestones, the water table of the sheet-water zone

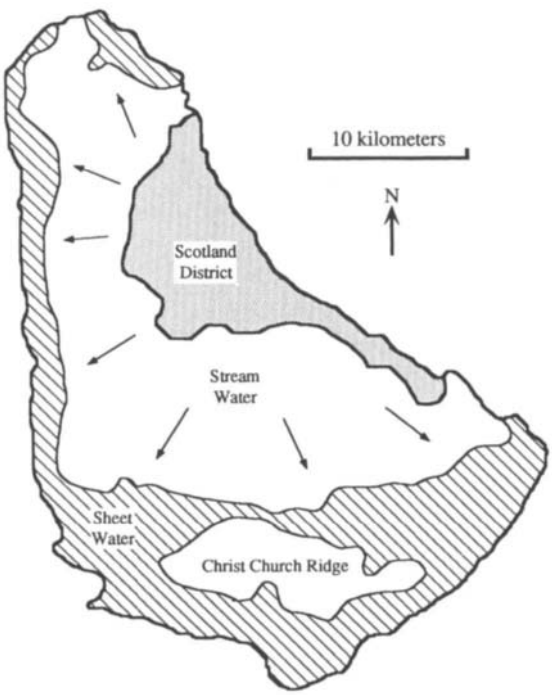


Fig. 11-10. Plan view of the distribution of stream-water and sheet-water. Stream-water occurs where the Tertiary aquiclude lies above sea level (e.g., Christ Church Ridge). (Modified from Goodwin, 1980).

rises only to a maximum of about a meter above sea level (Goodwin, 1980). A value for hydraulic conductivity of about 90 m day^{-1} was obtained from pumping tests at the Applewhaites pumping station (Chilton et al., 1990). Government water wells and pumping stations are located both within sheet-water areas and along major underground streams in the upland regions. Thickness of the freshwater wedge varies by location around the island and from rainy season to dry season (Harris, 1971; Steinen et al., 1978; Stoessell and Humphrey, unpub. data). Thickness of the wedge varied from about 4 to 15 m in a borehole drilled in the Christ Church region (RKM #16) from the dry to the rainy seasons of 1970–1971 (Steinen et al., 1978). Likewise, the freshwater wedge in borehole GD-5 at Bottom Bay (Fig. 11-1), along the southeast coast, varied in thickness from 5 m to 14 m from the end of the dry season (June, 1989) to the end of the rainy season, respectively (November, 1989) (Stoessell and Humphrey, unpub. data). At the Belle pumping station, the freshwater lens is about 20 m thick (Chilton et al., 1990).

The freshwater wedge is separated from underlying marine porewater by a freshwater-saltwater mixing zone that also varies in thickness around the island. Steinen et al. (1978) documented thickness variations in the mixing zone ranging from about 2 to 13 m seasonally in the Christ Church region. A thicker mixing zone occurs within the GD-5 borehole, located closer to the coast than the RKM #16 well. Here, the mixing zone is >20 m thick (Stoessell and Humphrey, unpub. data). Variations in the thickness of the mixing zone can be attributed to variations in freshwater recharge, tidal and storm-surge pumping, and proximity to the coast (Harris, 1971; Steinen et al., 1978; Humphrey, 1987). Approximately 20% of the freshwater outflow to the sea from the sheet-water zones mixes with seawater to form brackish water (Goodwin, 1980).

Groundwater resources

Senn (1946) made the first estimates of the water resources of Barbados. He delineated six catchment basins and calculated a water balance based on estimates of evapotranspiration, runoff, and groundwater replenishment. Evapotranspiration was calculated to be approximately 75% of precipitation, and runoff to be approximately 5% of precipitation; the remaining 20% was the calculated replenishment to the groundwater resources. Using an average rainfall of about 150 cm y^{-1}, Senn (1946) estimated the total groundwater resources to be 307 ML day^{-1} (3,600 L s^{-1}; 67.6 Mgpd Imp.). The porous nature of the Pleistocene limestones is indicated by the low percentage of runoff.

Tullstrom (1964) divided Senn's six main catchment areas into 42 subcatchments. Using infiltration tests for different soil types on Barbados, Tullstrom (1964) estimated groundwater resources of 180 ML day^{-1} (2,100 L s^{-1}; 40 Mgpd Imp.), based on an average rainfall of about 150 cm y^{-1}.

Goodwin (1980) reported the results of an assesment of Barbados groundwater resources by Stanley Associates Engineering, Ltd. These more recent data were used to separate catchment areas more accurately and resulted in the delineation of 22

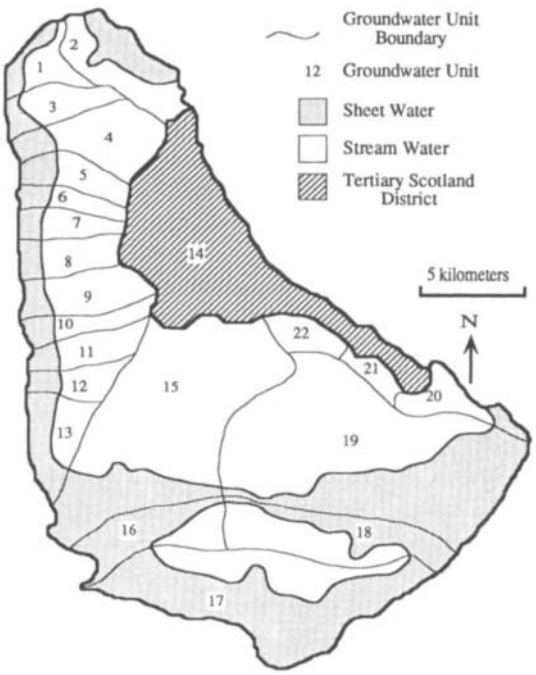


Fig. 11-11. Map showing 22 groundwater units representing sub-catchments defined by groundwater divides. These divides are delineated by structure on the Tertiary surface underlying the Coral Rock Formation. (Modified from Goodwin, 1980).

catchment regions or groundwater units (Fig. 11-11). As an example of groundwater resources, Goodwin (1980) calculated exisiting and potential groundwater abstraction for the St. Michael groundwater unit (Unit 15, Fig. 11-11). Using an average rainfall of 176 cm y^{-1}, potential abstraction was calculated to be 86.3 ML day^{-1} (1,000 L s^{-1}; 19.7 Mgpd Imp.). Calculations considered replenishment to both stream-water and sheet-water zones, outflow from stream-water to sheet-water, and freshwater-seawater mixing (Fig. 11-12). Summing potential abstraction for all 22 groundwater units resulted in an estimate of total potential abstraction for the island of 228 ML day^{-1} (2,600 L s^{-1}; 50.3 Mgpd Imp.), a figure intermediate to the estimates of Senn (1946) and Tullstrom (1964). At the time of the report of Goodwin (1980), existing abstraction for the island was 111 ML day^{-1} (1,285 L s^{-1}; 24.5 Mgpd Imp.).

Development of groundwater resources

Groundwater is exploited by means of large, hand-dug wells excavated through the Coral Rock Formation. The wells are commonly dug to 3–5 m below the water table (Fig. 11-13). Horizontal adits have been excavated at the bottom of the wells

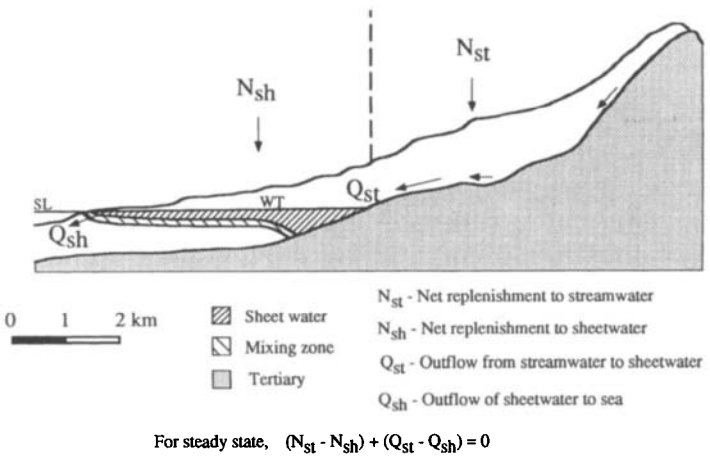


Fig. 11-12. Schematic diagram of parameters for calculation of water balance on Barbados. Steady-state conditions are assumed, such that net replenishment equals net outflow. Replenishment is a function of rainfall, catchment area, evapotranspiration, runoff, wastewater return and actual abstraction. Modified from Goodwin (1980).

such that about 1 m of adit is below the water table. Lengths of these adits vary, but they are commonly about 60 m and vary according to well design and hydraulic conductivity (Goodwin, 1980). The primary justification of adit excavation is the

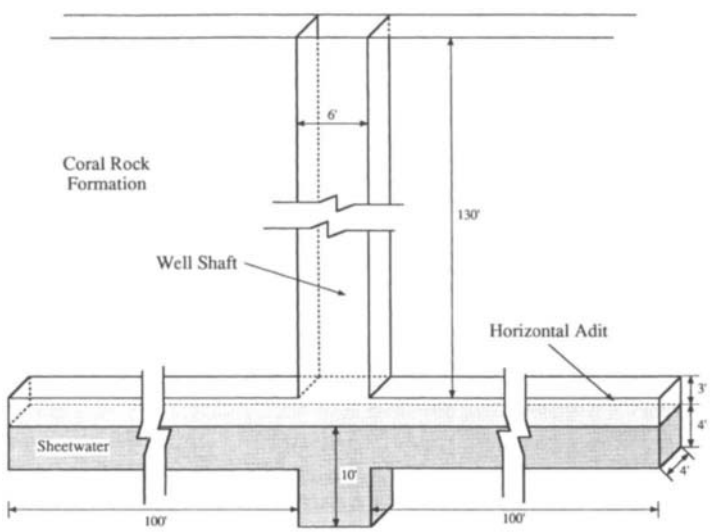


Fig. 11-13. Schematic drawing of a typical well (Whim Well, central West Coast) used for exploitation of groundwater in the sheetwater zone. Depth to water table varies with terrace elevation, and length of horizontal adits varies with hydraulic conductivity of the country rock and design yield of the well. (Modified from Goodwin, 1980).

minimization of drawdown in the wells. For purposes illustrating the importance of adits, consider two pumping tests that were conducted at the Whim pumping station, central west coast (Goodwin, 1980). The first test, with a horizontal adit of 30 m, resulted in a drawdown of over 50 cm in only 13 min of pumping at 1,800 L min^{-1} (30 L s^{-1}; 400 gpm Imp.). The second test, with the horizontal adit expanded to 60 m, resulted in only 3 cm of drawdown in over 2 h of pumping at over 2,200 L min^{-1} (37 L s^{-1}; 500 gpm Imp.). The Belle pumping station in the St. Michael groundwater unit, the principal station for the city of Bridgetown, abstracts approximately 45 ML day^{-1} (520 L s^{-1}; 10 Mgpd Imp.), with a water table drawdown of less than 1 cm. Currently there are 17 pumping stations on the island, with approximately 12 more in the planning stage.

In order that groundwater resource potential may be fully developed, wells are sited in order to maximize interception of the groundwater and minimize freshwater discharge to the sea. Furthermore, a sufficient column of freshwater is necessary so that abstraction does not result in contamination of the water supply from saltwater intrusion. A minimum freshwater thickness of about 12 m is deemed satisfactory for sheet-water areas of Barbados (Goodwin, 1980).

CASE STUDY: EARLY, NEAR-SURFACE METEORIC DIAGENESIS

Studies of the Pleistocene limestones of Barbados have provided many advances in understanding the processes of early, near-surface carbonate diagenesis. The meteoric vadose, meteoric phreatic, and mixing-zone environments have been extensively investigated since the mid-1960s, and studies are presently ongoing.

Meteoric vadose diagenesis

Pleistocene reef-associated sediments of Barbados have been uplifted into the subaerial environment. These sediments, composed primarily of aragonite and high-Mg calcite, are essentially stable in the marine fluids in which they were deposited. Upon exposure to the different chemical environment of the subaerial realm, these metastable sediments underwent both mineralogical and petrological changes. Of major importance was the presence of meteoric diagenetic fluids, in which chemical reactions dissolved aragonite and high-Mg calcite and precipitated stable low-Mg calcite.

A progressive temporal record of diagenetic change is recorded in the uplifted terraces of Barbados, inasmuch as terraces are older in sequence toward the interior of the island. One of the most easily documented effects of this equilibration of metastable marine sediments in the meteoric diagenetic environment is the pronounced decrease in the amount of aragonite and high-Mg calcite with increasing terrace age (Matthews, 1968; Harris and Matthews, 1968). Even the youngest subaerially exposed terraces on Barbados (82 and 105 ka) may contain very little, if any, high-Mg calcite (e.g., Steinen and Matthews, 1973). Subaerially exposed sections that

do contain high-Mg calcite have likely experienced only vadose diagenesis (i.e., not meteoric phreatic diagenesis) since the time of their emergence (Steinen and Matthews, 1973). Aragonite, which is slightly less soluble than high-Mg calcite, tends to persist in greater abundance in the older terraces. In terraces older than about 300 ka, nearly all aragonite has been stabilized to low-Mg calcite (Matthews, 1968); however, large scleractinian corals may remain as aragonite or may be only partially stabilized.

The stratigraphically controlled studies of diagenesis suggest that vadose diagenesis and mineralogical stabilization are primarily a function of cumulative time of subaerial exposure and climate. Obviously, the more time available for vadose diagenesis, given a particular climatic setting, the more advanced the mineralogical stabilization will be. On the other hand, given a specific time for subaerial exposure, the more meteoric water available (the more humid the climate), the more mineralogical stabilization will proceed. On Barbados, approximately 200 to 300 ky is required to produce a mineralogically stable, low-Mg calcite limestone in the vadose environment.

The petrography of vadose diagenesis in Barbados was documented by Steinen (1974), who noted only minor recrystallization of grains; however, cementation is widespread. Steinen (1974) showed that vadose cements from Barbados are principally dense micritic coatings and needle-fiber low-Mg calcite. Notably rare are the "classic" meniscus and pendant vadose cements that are common in ooid grainstones. Dissolution and the formation of moldic porosity is low in the vadose zone, and porosity averages less than 10%. Cement in the vadose section must be derived from the subaerial exposure surface through dissolution-reprecipitation. Porosity that is retained in the vadose section is primary interparticle and intraparticle, with various degrees of pore-space occlusion from the aforementioned cements.

Although diagenetic modification of the vadose zone is generally minor, an exception to this rule occurs at the subaerial exposure surface. Here, caliche profiles in various stages of development are prominently displayed over much of the island (James, 1972; Harrison, 1977). Processes occurring at the subaerial exposure surface include dissolution, precipitation, micritization, and brecciation (James, 1972); these processes are controlled mainly by duration of exposure, climate, soil cover, and characteristics of the limestone substrate. Excellent discussions of Barbados caliche profiles are given in James (1972) and Harrison (1977). Furthermore, pedogenesis on Barbados has been discussed by Muhs et al. (1987).

Meteoric phreatic diagenesis

Much of our understanding of meteoric phreatic diagenesis in young, subaerially exposed limestones has developed through studies of this diagenetic environment on Barbados (Matthews, 1971; Steinen, 1974; Steinen and Matthews, 1974; Matthews, 1974; Allan and Matthews, 1977; 1982; Wagner, 1983; Humphrey et al., 1986). Numerous boreholes drilled by R.K. Matthews and the author have provided an unparalleled look at processes, rates, and products of the freshwater phreatic environment. Of course, the most significant difference between the freshwater phreatic

and vadose environments is that the pore spaces are completely and continuously filled by water in the phreatic environment, and only intermittently filled in the vadose. This difference has profound effects on diagenetic reactions occurring in the phreatic zone. For example, mineralogical stabilization to low-Mg calcite proceeds much more rapidly in the phreatic environment, with complete stabilization occurring on the order of 5,000 years in a high-flow setting (Matthews, 1974; Wagner, 1983; Humphrey et al., 1986). Mineralogic stabilization occurs through a neomorphic dissolution-reprecipitation process with the resultant grains and matrix displaying variable degrees of textural preservation (e.g., Steinen, 1974).

Dissolution of metastable carbonate minerals and cementation by low-Mg calcite are also important processes in the meteoric phreatic environment of Barbados. Whereas allochems that were originally composed of high-Mg calcite are commonly neomorphosed, aragonitic allochems may be completely dissolved, leaving biomoldic pores. Some scleractinian corals, notably *Acropora cervicornis*, have been completely leached out of the rock, leaving a highly porous "Swiss-cheese" fabric (e.g., Canter and Humphrey, 1994) (Fig. 11-14). In regions with a large meteoric phreatic discharge, vuggy to cavernous porosity may be created (Fig. 11-15). On a microscopic scale, biomolds of presumably aragonitic grains commonly retain thin micrite envelopes that mark the former presence of the allochems.

Much of the low-Mg calcite cement precipitated in the phreatic zone in Barbados limestones occurs as equigranular microspar (e.g., Steinen, 1974). Coarser, blocky calcite spar also occurs, primarily occluding or partially occluding primary and secondary pore spaces; however, these cements are volumetrically less significant. Although present-day meteoric phreatic zones and paleo-lenses are easily identified using stable isotope and geochemical techniques (e.g., Wagner, 1983), petrographic

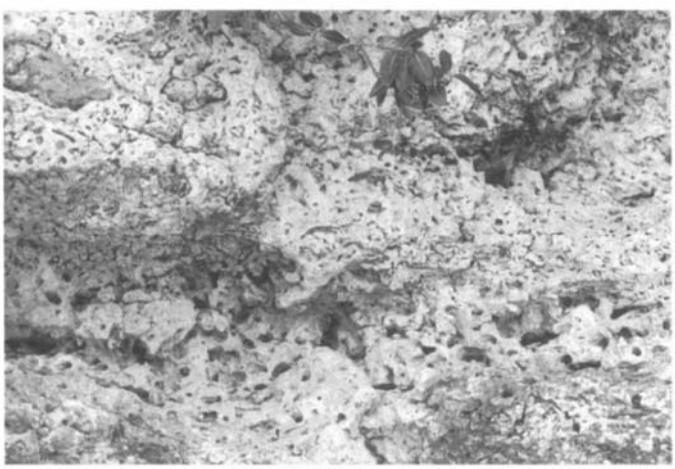


Fig. 11-14. Outcrop photograph showing dissolution of *Acropora cervicornis* facies at Foul Bay, resulting in a solution-enlarged, "swiss cheese" fabric. Matrix is stabilized to low-Mg calcite, while *A. cervicornis* sticks have been leached by meteoric fluids. Hammer at right-center is 26 cm.



Fig. 11-15. Field photograph showing development of cavernous porosity at Foul Bay. Caves here likely represent position of former water table. Note dissolution of *Acropora cervicornis* above T. Kimbell's head and facies transition upward from *A. cervicornis* to *A. palmata* facies.

recognition of these intervals is commonly equivocal. Whereas ooid grainstones that have undergone cementation in the meteoric phreatic environment typically show the "classic" well-developed equant, blocky calcite cements (e.g., Budd, 1988), phreatic lithologies from Barbados typically lack these diagnostic petrographic fabrics.

Chemostratigraphic signatures of meteoric diagenesis have been identified by stable isotopic and trace element profiling of rocks recovered in boreholes from Barbados (Allan and Matthews, 1977; 1982; Wagner, 1983). The interplay of water-rock interaction with stable isotopic fractionation and trace element partitioning behavior during diagenesis results in recognizable and repeatable geochemical patterns. The stable isotopes of carbon and oxygen can clearly discriminate the meteoric vadose and phreatic environments and can be used to identify ancient subaerial exposure surfaces (Allan and Matthews, 1977; 1982; Videtich and Matthews, 1980). The subaerial exposure surface is characterized by a pronounced depletion in carbon isotopic composition as a result of incorporation of organically derived carbon dioxide from the soil zone. Progressing downward into the vadose zone, carbon isotopic composition gradually reflects the original, more enriched marine isotopic values. Oxygen isotopic compositions throughout the meteoric diagenetic environment (vadose and phreatic) remain remarkably uniform, reflecting the overwhelming influence of the oxygen reservoir contained in the meteoric water (Allan and

Matthews, 1982). A slight enrichment in the oxygen isotopic composition may occur at the subaerial exposure surface, where fractionation due to evaporation (Rayleigh-process) enriches the remaining liquid phase. The vadose-phreatic boundary may be characterized by a carbon isotopic shift towards either more enriched or more depleted values depending on the relative isotopic compositions of the bicarbonate in vadose and phreatic waters. Along the west coast of Barbados, only about one percent of the phreatic waters are derived from waters percolating through the directly overlying vadose zone (Harris, 1971). Thus, different isotopic compositions should be expected for waters above and below the water table, resulting from differences in water-rock interaction during separate flow histories.

Minor and trace element compositions of diagenetic products likewise are useful indicators of diagenetic environment (Harris and Matthews, 1968; Wagner, 1983). Mineralogical stabilization of aragonite and high-Mg calcite to low-Mg calcite, through dissolution-reprecipitation reactions, acts to build up Sr^{2+} and Mg^{2+} in the diagenetic fluids. Using groundwater Sr^{2+} concentrations, Harris and Matthews (1968) estimated this stabilization process as being over 90% efficient, clearly indicating that metastable mineralogies were locally reprecipitated as stable low-Mg calcite (either as replacement or as cement). Wagner (1983) used Mg^{2+} and Sr^{2+} compositions to augment diagenetic interpretations for several borehole cores from Barbados. In areas of low water-rock interaction, such as the vadose zone, higher concentrations of Mg^{2+} and Sr^{2+} were retained in the diagenetic calcite. In contrast, stabilized carbonates in the high water-rock interaction environment of the freshwater phreatic zone show relatively depleted Mg and Sr concentrations.

Mixing-zone diagenesis

Investigation of the freshwater-saltwater mixing zone is typically hampered by the inaccessibility of the environment. Borehole coring projects on Barbados have enabled access to this important diagenetic environment in the modern setting. Diagenesis related to paleo-mixing zones has also been studied on Barbados (Wagner, 1983; Humphrey, 1988; Humphrey and Radjef, 1991; Radjef, 1992; Kimbell and Humphrey, 1994). The mixing zone is a dynamic hydrochemical environment where dissolution, cementation, and replacement reactions involving aragonite, calcite, and dolomite may occur.

Harris (1971) investigated the hydrochemistry of the mixing zone and its diagenetic consequences along the central west coast of Barbados. He separated the mixing zone into three hydrochemical environments (from the top downward): (1) the shallow phreatic environment, (2) the zone of maximum undersaturation with respect to aragonite, and (3) the zone of maximum carbonate alkalinity. The shallow phreatic environment and zone of maximum undersaturation with respect to aragonite are characterized principally by dissolution of calcium carbonate. The zone of maximum carbonate alkalinity represents an environment of dissolution-reprecipitation reactions (Harris, 1971), where aragonite and high-Mg calcite are replaced by low-Mg calcite.

More recently, Stoessell (1992) investigated carbonate saturation states and the effects of sulfate reduction in mixed waters of southeastern Barbados. Where sulfate reduction occurs and is followed by oxidation of the aqueous sulfide, increased undersaturation with respect to calcite occurs; therefore, the model of Stoessell (1992) predicts dissolution within the modern mixing zone. Borehole petrologic studies indicate that massive dissolution of forereef lithologies has indeed occurred, and presumably is currently occurring, within the modern mixing zone along the southeast coast (Canter and Humphrey, 1993). In addition to being undersaturated with respect to calcite and aragonite, the mixed waters of southeastern Barbados are also supersaturated with respect to dolomite (Kimbell et al., 1990; Stoessell, unpub. data). Dolomite occurs in core and outcrop along the southeastern seacliffs in quantities ranging from trace amounts up to about 25% (Kimbell et al., 1990; Kimbell, 1993). Two discrete intervals of dolomite occur in borehole GD-5 at Bottom Bay (Fig. 11-1). One of these intervals, which is several meters thick, occurs above the modern water table and clearly predates the modern mixing zone; the other interval, which is more than 10 m thick, occurs within the modern mixing zone and may be related to the present hydrochemical environment (Kimbell, 1993). Ongoing studies are addressing the relationship between dolomite occurrences in cores and the chemistry of the mixing zone within which the dolomite resides.

Dolomite of mixing-zone origin has also been recognized in a terrace corresponding to marine oxygen isotope stage 7.3, chronostratigraphically dated to be 216 ka (Humphrey, 1988). Forereef lithologies containing dolomite crop out principally at Golden Grove in the southeastern portion of the island (Fig. 11-1). The dolomite occurs as a replacement phase (mimetic and non-fabric-selective) and as limpid dolomite cement. Anomalously depleted carbon isotopic compositions, originally interpreted to be of soil-gas origin (Humphrey, 1988), have been reinterpreted in light of micro-scale isotopic variability that occurs in the dolomite cements (Radjef, 1992). Electron microprobe analyses of these dolomite cements suggest that porewaters responsible for precipitation of the cement became progressively more dilute as the mixing zone passed downward in response to glacioeustatic sea-level fall (Humphrey and Radjef, 1991). Micro-sampling of these same cements for stable-isotopic analysis indicates a similar pattern. Oxygen isotopic values become more depleted as the pore interior is approached, indicating the greater influence of meteoric water. In contrast, carbon isotopic compositions become progressively more enriched toward the interior of the pores. The anomalously light carbon derives from upward migration and oxidation of thermogenic methane produced in the underlying accretionary prism (e.g., LePichon, 1990). Oxidation occurs upon initial encounter with oxidizing waters — in this case, seawater that lies below the freshwater wedge and the mixing zone. Thus, the most-depleted carbon isotopic values in the dolomites should be those which were incorporated during the earliest stages of mixing-zone dolomitization. Petrographically, matrix-replacement dolomitization has been documented as the earliest stage in dolomite formation at Golden Grove. Matrix dolomite is also several per mil more depleted than the later dolomite cements (Radjef, 1992). Progressive enrichment of carbon isotopic compositions in the

dolomite cement toward the pore interior occurs and approaches values of the later meteoric phreatic low-Mg calcite cements (Radjef, 1992). Further discussion of these isotopic relationships will be published elsewhere.

An interesting consequence of mixing-zone diagenesis in southeastern Barbados is the occurrence of mixing-zone aragonite (Humphrey et al., 1992; Kimbell and Humphrey, 1994). Isopachous aragonite ray cement lines large secondary vuggy pores through a 4-m interval in core samples from borehole GD-5. Although these cements appear to be "typical" marine aragonite precipitates, their isotopic composition suggests that the aragonite precipitated instead from mixed meteoric-marine pore fluids. Their carbon isotope composition is depleted by several per mil in comparison with both predicted equilibrium marine aragonite precipitates and marine aragonites reported from other localities. Likewise, the oxygen isotopic composition of the Barbados aragonite cement is depleted relative to the predicted and reported compositions. In carbon-vs-oxygen space, the isotopic compositions of the aragonite cement define a mixing curve between meteoric and marine endmember compositions. Fluid mixing models, based on modern Barbados water compositions, indicate that the aragonite precipitated from mixed fluids containing 50–75% seawater.

CONCLUDING REMARKS

The island of Barbados is a relatively unique carbonate island because of its history of continual tectonic uplift. A combination of fringing-reef deposition during late Pleistocene glacioeustatic sea-level highstands and tectonic uplift has resulted in a depositional system of discrete reef tracts, the age and topographic elevation of which decrease in a stair-step fashion toward the perimeter of the island. Uplifted reef terraces provide an unparalleled look at sedimentological and facies relationships. Each terrace has a well-developed stratigraphic architecture of backreef, reef, and forereef lithologies showing faunal zonations typical of modern Caribbean reefs. Uranium-series geochronologic studies have been instrumental in deciphering late Pleistocene glacioeustasy and have been used to calibrate the marine oxygen isotope record of ice-volume change.

The porous and permeable Pleistocene Coral Cap of Barbados permits groundwater recharge where precipitation exceeds evapotranspiration. The underlying Tertiary sedimentary rocks provide an aquiclude that prevents downward water flow. Where the aquiclude lies above sea level, groundwater flows along the base of the limestones in underground streams. Towards the coast, where the aquiclude lies below sea level, a coastal phreatic freshwater wedge and associated freshwater-saltwater mixing zone are developed. Interaction of meteoric vadose, meteoric phreatic, and mixing-zone waters with the young, subaerially exposed limestones has resulted in a wide range of diagenetic modification.

Barbados has long provided a natural laboratory in which to study sedimentology, stratigraphy, hydrogeology, and diagenesis of a Pleistocene carbonate island, and ongoing studies are directed at further understanding this unique geologic setting.

ACKNOWLEDGMENTS

I wish to gratefully acknowledge the guidance and tutelage of R.K. Matthews, who introduced me and many other of his students to the island of Barbados. RKM has directed investigations of the geology of Barbados for over twenty years and has made invaluable contributions towards the understanding of the island. Without his motivation, many of the geologic secrets of the island would still be waiting to be unlocked. I have benefited greatly from discussions and collaborations regarding Barbados with T.N. Kimbell, R.G. Fairbanks, T.M. Quinn, E.M. Radjef, R.P. Major, N.P. James, J.L. Banner, R.K. Stoessell, K.L. Canter, L.H. Barker, and H.A. Sealy. Funding for my work on Barbados has come from NSF Grants EAR-7927162 (to RKM), EAR-8720376, EAR-9123842, and from the Donors of the Petroleum Research Fund of the American Chemical Society (20095-G2).

REFERENCES

Allan, J.R. and Matthews, R.K., 1977. Carbon and oxygen isotopes as diagenetic and stratigraphic tools: Data from surface and subsurface of Barbados, West Indies. Geology, 5: 16–20.

Allan, J.R. and Matthews, R.K., 1982. Isotopic signatures associated with early meteoric diagenesis. Sedimentol., 29: 797–817.

Banner, J.L., Wasserburg, G.J., Chen, J.H. and Humphrey, J.D., 1991. Uranium-series evidence on diagenesis and hydrology in Pleistocene carbonates of Barbados, West Indies. Earth Planet. Sci. Lett., 107: 129–137.

Bender, M.L., Taylor, F.T. and Matthews, R.K., 1973. Helium-uranium dating of corals from Middle Pleistocene Barbados reef tracts. Quat. Res., 3: 142–146.

Bender, M.L., Fairbanks, R.G., Taylor, F.W., Matthews, R.K. and Mesolella, K.J., 1979. Uranium-series dating of the Pleistocene reef tracts of Barbados, West Indies. Geol. Soc. Am. Bull., 90: 577–594.

Broecker, W.S., Thurber, D.L., Goddard, J., Ku, T.L., Matthews, R.K. and Mesolella, K.J., 1968. Milankovitch hypothesis supported by precise dating of coral reefs and deep sea sediments. Science, 159: 297–300.

Budd, D.A., 1988. Petrographic products of freshwater diagenesis in Holocene ooid sands, Schooner Cays, Bahamas. Carbonates and Evaporites, 3: 143–163.

Canter, K.L., and Humphrey, J.D., 1994. Carbonate dissolution within the meteoric and mixing zone diagenetic environments: Porosity development within late Pleistocene reef and reef-associated lithologies, southeastern Barbados (abstr.). Am. Assoc. Petrol. Geol. Program, 3: 115.

Chilton, P.J., Vlugman, A.A. and Foster, S.S.D., 1990. A ground-water pollution risk assessment for public water supply sources in Barbados. In: J. Hari Krishna, V. Quiñones-Aponte, F. Gómez-Gómez and G.L. Morris (Editors). Proc. Int. Symp. Tropical Hydrol. and Fourth Caribb. Islands Water Resour. Cong., Am. Water Resour. Assoc., pp. 279–289.

Edwards, R.L., Chen, J.H., Ku, T.L. and Wasserburg, G.J., 1987. Precise timing of the last interglacial period from mass spectrometric determination of thorium-230 in corals. Science, 236: 1547–1553.

Fairbanks, R.G. and Matthews, R.K., 1978. The marine oxygen isotope record in Pleistocene coral, Barbados, West Indies. Quat. Res., 10: 181–196.

Gallup, C.D., Edwards, R.L. and Johnson, R.G., 1994. The timing of high sea levels over the past 200,000 years. Science, 263: 796–800.

Goodwin, R.S., 1980. Water assessment and development in Barbados. In: P. Hadwen (Editor). Proc. Seminar on Water Resources Assessment, Development and Management in Small

Oceanic Islands of the Caribbean and West Atlantic. United Nations – Commonwealth Science Council Seminar, pp. 145–163.
Goreau, T.F., 1959. The ecology of Jamaican coral reefs. Ecology, 40: 67–90.
Harris, W.H. and Matthews, R.K., 1968. Subaerial diagenesis of carbonate sediments: Efficiency of the solution-reprecipitation process. Science, 160: 77–79.
Harris, W.H., 1971. Groundwater – carbonate rock chemical interactions, Barbados, W.I. Ph.D. Dissertation, Brown Univ., Providence, RI, 348 pp.
Harrison, R.S., 1977. Caliche profiles: Indicators of near-surface subaerial diagenesis, Barbados, West Indies. Bull. Can. Petrol. Geol., 25: 123–173.
Humphrey, J.D., 1987. Processes, rates, and products of early near-surface carbonate diagenesis: Pleistocene mixing zone dolomitization and Jurassic meteoric diagenesis. Ph.D. Dissertation, Brown University, Providence RI, 263 pp.
Humphrey, J.D., 1988. Late Pleistocene mixing zone dolomitization, southeastern Barbados, West Indies. Sedimentol., 35: 327–348.
Humphrey, J.D. and Matthews, R.K., 1986. Deposition and diagenesis of the Pleistocene Coral Cap of Barbados. Field Trip Guide, Eleventh Caribb. Geol. Conf., Bridgetown, Barbados, pp. 86–105.
Humphrey, J.D., Ransom, K.L. and Matthews, R.K., 1986. Early meteoric diagenetic control of Upper Smackover production, Oaks Field, Louisiana. Am. Assoc. Petrol. Geol. Bull., 70: 70–85.
Humphrey, J.D. and Kimbell, T.N., 1990. Sedimentology and sequence stratigraphy of Upper Pleistocene carbonates of southeastern Barbados, West Indies. Am. Assoc. Petrol. Geol. Bull., 74: 1671–1684.
Humphrey, J.D. and Radjef, E.M., 1991. Dolomite stoichiometric variability resulting from changing aquifer conditions, Barbados, West Indies. Sediment. Geol., 71: 129–136.
Humphrey, J.D., Kimbell, T.N. and Banner, J.L., 1992. Late Pleistocene aragonite cements of mixing zone origin (abstr.). Geol. Soc. Am. Abstr. Programs, 24: 105.
James, N.P., 1972. Holocene and Pleistocene calcareous crust (caliche) profiles: Criteria for subaerial exposure. J. Sediment. Petrol., 42: 817–836.
James, N.P., Stearn, C.W. and Harrison, R.S., 1977. Field Guide Book to Modern and Pleistocene Reef Carbonates, Barbados, W. I. Third Intern. Coral Reef Symp. (Miami), 30 pp.
Kimbell, T.N., 1993. Sedimentology and diagenesis of late Pleistocene fore-reef calcarenites, Barbados, West Indies: A geochemical and petrographic investigation of mixing zone diagenesis. Ph.D. Dissertation, University Texas at Dallas, Richardson TX, 322 pp.
Kimbell, T.N., Humphrey, J.D. and Stoessell, R.K., 1990. Quaternary mixing zone dolomite in a cored borehole, southeastern Barbados, West Indies (abstr.). Geol. Soc. Am. Abstr. Programs, 22: 179.
Kimbell, T.N. and Humphrey, J.D., 1994. Geochemistry and crystal morphology of aragonite cements of mixing zone origin, Barbados, West Indies. J. Sediment. Res., v. A64: 604–614.
Ku, T.L., Ivanovich, M. and Luo, S., 1990. U-Series dating of last interglacial high sea stands: Barbados revisited. Quat. Res., 33: 129–147.
Larue, D.K. and Speed, R.C., 1984. Structure of the accretionary complex of Barbados, II: Bissex Hill. Geol. Soc. Am. Bull., 95: 1360–1372.
LePichon, X., Foucher, J.-P., Boulégue, J., Henry, P., Lallemant, S., Benedetti, M., Avedik, F. and Mariotti, A., 1990. Mud volcano field seaward of the Barbados accretionary complex: A submersible survey. J. Geophys. Res., 95: 8931–8943.
Lewis, J.B., 1960. The coral reefs and coral communities of Barbados, W.I. Can. J. Zool., 33: 1133–1153.
Matthews, R.K., 1967. Diagenetic fabrics in biosparites from the Pleistocene of Barbados, West Indies. J. Sediment. Petrol., 37: 1147–1153.
Matthews, R.K., 1968. Carbonate diagenesis: Equilibration of sedimentary mineralogy to the subaerial environment: Coral Cap of Barbados, West Indies. J. Sediment. Petrol., 38: 1110–1119.
Matthews, R.K., 1971. Diagenetic environments of possible importance to the explanation of cementation fabrics in subaerially exposed carbonate sediments. In: O.P. Bricker (Editor), Carbonate Cements. Johns Hopkins Press, Baltimore, pp. 127–132.

Matthews, R.K., 1974. A process approach to diagenesis of reefs and reef-associated limestones. In: L.F. Laporte (Editor), Reefs in Time and Space. Soc. Econ. Paleontol. Mineral., Spec. Publ. 18: 234–256.

Mesolella, K.J., 1967. Zonation of uplifted Pleistocene coral reefs on Barbados, West Indies. Science, 156: 638–640.

Mesolella, K.J., Matthews, R.K., Broecker, W.S. and Thurber, D.L., 1969. The astronomical theory of climatic change: Barbados data. J. Geol., 77: 250–274.

Mesolella, K.J., Sealy, H.A. and Matthews, R.K., 1970. Facies geometries within Pleistocene reefs of Barbados, West Indies. Am. Assoc. Petrol. Geol. Bull., 54: 1899–1917.

Muhs, D.R., Crittenden, R.C., Rosholt, J.N., Bush, C.A., and Stewart, K.C., 1987. Genesis of marine terrace soils, Barbados, West Indies: Evidence from mineralogy and geochemistry. Earth Surf. Processes and Landf., 12: 605–618.

Poole, E.G. and Barker, L.H., 1983. The Geology of Barbados. Gov. Barbados, 1:50,000 geologic map, 1 sheet.

Prell, W.L., Imbrie, J., Martinson, D.G., Morley, J.J., Pisias, N.G., Shackleton, N.J. and Streeter, H.F., 1986. Graphic correlation of oxygen isotope stratigraphy: Application to the late Quaternary. Paleoceanography, 1: 137–162.

Radjef, E.M., 1992. Geochemical and stoichiometric variability of dolomite as a result of changing aquifer conditions, Barbados, West Indies. M.S. Thesis, University Texas at Dallas, Richardson TX, 82 pp.

Rouse, W.R., 1962. The moisture balance of Barbados and its influence on sugar cane yield. M.S. Thesis, McGill University, Montreal, 60 pp.

Senn, A., 1946. Geological investigations of the groundwater resources of Barbados, B.W.I. Report of the British Union Oil Co., Ltd., 110 p.

Speed, R., 1990. Volume loss and defluidization history of Barbados. J. Geophys. Res., 95: 8983–8996.

Steinen, R.P., 1974. Phreatic and vadose diagenetic modification of Pleistocene limestone: Petrographic observations from subsurface of Barbados, West Indies. Am. Assoc. Petrol. Geol. Bull., 58: 1008–1024.

Steinen, R.P. and Matthews, R.K., 1973. Phreatic vs. vadose diagenesis: Stratigraphy and mineralogy of a cored borehole on Barbados, W.I. J. Sediment. Petrol., 43: 1012–1020.

Steinen, R.P., Matthews, R.K. and Sealy, H.A., 1978. Temporal variation in geometry and chemistry of the freshwater phreatic lens: The coastal carbonate aquifer of Christ Church, Barbados, West Indies. J. Sediment. Petrol., 48: 733–742.

Stoessell, R.K., 1992. Effects of sulfate reduction on $CaCO_3$ dissolution and precipitation in mixing-zone fluids. J. Sediment. Petrol., 62: 873–880.

Torrini, R., Jr., Speed, R.C. and Mattioli, G.S., 1985. Tectonic relationships between forearc-basin strata and the accretionary complex at Bath, Barbados. Geol. Soc. Am. Bull., 96: 861–874.

Trechmann, C.T., 1933. The uplift of Barbados. Geol. Mag., 70 (823): 19–47.

Tullstrom, H., 1964. Report on the water supply of Barbados. Rep. to Gov. Barbados. UN Prog. Tech. Assist., Restricted Publ. 64–41745, 221 pp.

Videtich, P.E. and Matthews, R.K., 1980. Origin of discontinuity surfaces in limestones: Isotopic and petrographic data, Pleistocene of Barbados, West Indies. J. Sediment. Petrol., 50: 971–980.

Wagner, P.D., 1983. Geochemical characterization of meteoric diagenesis in limestone: Development and applications. Ph.D. Dissertation, Brown University, Providence RI, 384 pp.

Geology and Hydrogeology of Carbonate Islands. Developments in Sedimentology 54
edited by H.L. Vacher and T. Quinn
© 1997 Elsevier Science B.V. All rights reserved.

Chapter 12

GEOLOGY OF SELECTED ISLANDS OF THE PITCAIRN GROUP, SOUTHERN POLYNESIA

S.G. BLAKE and J.M. PANDOLFI

INTRODUCTION

Since Fletcher Christian and the *Bounty* mutineers set foot on Pitcairn Island in 1790, the Pitcairn Islands have held a special place in the history of Polynesia. Today the four islands comprising the Pitcairn Group are United Kingdom Dependent Territories. The tiny Pitcairn Island (450 ha) is the only inhabited island, still supporting around 50 of the descendants of the *Bounty*.

The Pitcairn Islands are probably the most remote and least studied group of carbonate islands in the Pacific Ocean (Fig. 12-1). The most recent scientific expeditions have been of short duration: the National Geographic Society-Oceanic Institute Expedition (1970–71), Operation Raleigh (1986) and the Smithsonian Institution's visit by RV *Rambler* (1987) all lasted only a few days. The Sir Peter Scott Commemorative Expedition, undertaken from January 1991 to March 1992, was the first year-round expedition in the Pitcairn Island Group dedicated to the study of the natural history of these islands (see also Weisler et al., 1991). We were fortunate to be a part of that expedition and we report here some preliminary findings.

REGIONAL SETTING

Geography

The Pitcairn Island Group comprises, from west to east, Oeno Atoll (23°55′S; 130°45′W), Pitcairn Island (25°04′S; 130°06′W), Henderson Island (24°22′S; 128°20′W) and Ducie Atoll (24°40′S; 124°47′W). Oeno, Henderson and Ducie are all carbonate islands and support living coral reefs. Pitcairn Island, although supporting a localized carbonate reef (corals growing on rocks) with low diversity and abundance, is not a carbonate island, but a volcanic one. Three conspicuous seamounts occur nearby: two are active, 80 km east-southeast of Pitcairn Island, lie only 59 m below modern sea level (i.e., −59 m) and are named volcano 1 and 2 (Woodhead et. al., 1990); the third is inactive, lies at 330 km east of Ducie Atoll, has a flat top supporting a dead coral community, and is called the Crough seamount (Okal and Cazenave, 1985; Woodhead pers. comm., 1995). In this chapter, we give a general overview of the Pitcairn Island Group, with special emphasis on the three carbonate islands.

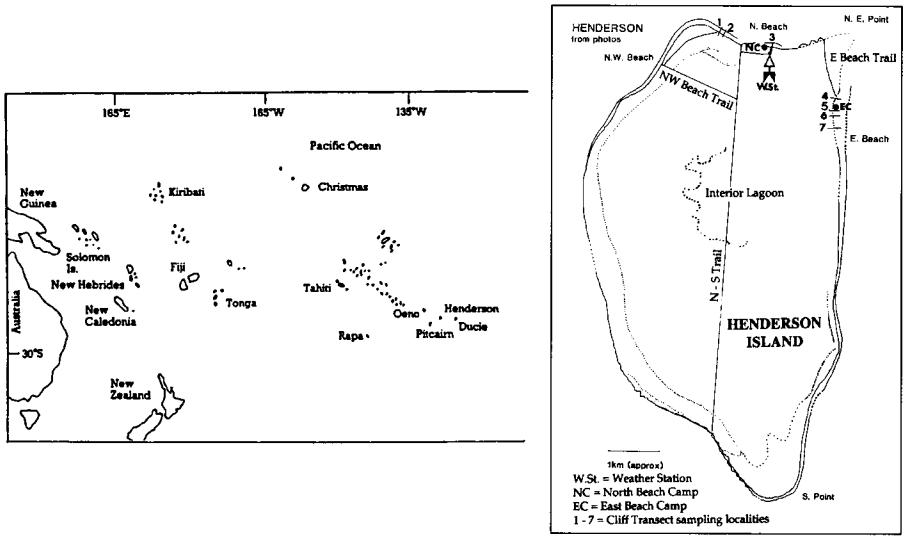


Fig. 12-1. Locality map of the Pitcairn Island Group and a detailed map of Henderson Island, an emergent limestone island with North Camp, Weather Station, beaches, paths, and cliff section sample locations marked.

The Pitcairn Island Group is a continuation of the Tuamotu-Gambier archipelago (Fig. 12-1). Oeno Atoll, Henderson Island and Ducie Atoll are part of the southern Tuamotu chain (Okal and Cazenave, 1985). The nearest land westward is Temoe Atoll (~390 km away), and eastward are Easter and Sala-y-Gomez Islands (~1,570 km away). The Pitcairn Group is the easternmost archipelago on the Pacific Plate and, together with Easter and Sala-y-Gomez Islands, forms the easternmost outposts of the Indo-West Pacific region (Paulay, 1991). The nearest continents, Australia and New Zealand to the west and South America to the east are each over 4,500 km away.

Climate

The first continuous meteorological records for Henderson Island were recorded as part of the Sir Peter Scott Commemorative Expedition to the Pitcairn Islands (hereafter called The Expedition). This recording interval (February 1991–February 1992) occurred during an El Niño Southern Oscillation (ENSO) period and more rainfall than average characterizes such El Niño periods. Total rainfall during this twelve-month period was 1,623 mm on Henderson Island compared with 2,171 mm on Pitcairn Island. The ten-year average rainfall on Pitcairn is somewhat less than the 1991–92 total (1,884 mm). Except for September, rainfall from December to May appears to be greater than that from June to November at both islands.

Henderson Island displayed similar air temperatures to Pitcairn Island. Monthly maximum temperatures during 1991–92 were 29.6–24.2°C on Henderson Island and

25.1–19.4°C on Pitcairn Island. Similarly, monthly minimum temperatures during 1991–92 were 15.7–22.2°C on Henderson Island and 16.1–20.6°C on Pitcairn. The lower minimum temperatures observed on Pitcairn Island as compared with Henderson Island probably relate to the position of the weather stations on the two islands: on Pitcairn Island the weather station was located at an elevation of 264 m and is subjected to orographic effects, whereas on Henderson Island it was at an elevation of 30 m.

Oceanography

Little oceanographic information is available for the Pitcairn region due to its isolated location. The island group lies in the northwest segment of an anti-clockwise subtropical gyre, bringing warm oligotrophic tropical surface water from a northeasterly direction. The seafloor in the region is 3–4 km deep, and pronounced forced upwelling of nutrient-rich bottom waters in response to shallow seamounts and the islands is likely. The influence of ENSO events is considered important, not only for the induced changes in rainfall, wind and storm events, but also for the strengthening of the warm eastward-flowing South Equatorial Counter Current (SECC) during such ENSO phenomena.

In most years, the weak easterly SECC has insufficient strength to be important in dispersing coral larvae, but during ENSO events the current strength increases dramatically. This may be significant in terms of larval dispersal from the southern Tuamotu Group, only 390 km away, to the easternmost outposts of the Indo-Pacific subtropical province. Coral species that become established in the Pitcairn Group would be expected to continue seeding the surrounding bare substrates. The modern reefs growing in the Pitcairn Group appear neither space-nor substrate-limited, there being a plentiful supply of both of these. Limited success of dispersal between successive intervals of sea-level fluctuations may have inhibited colonization and thus high species richness in the modern coral community (see Case Study). Paulay (1991) has also discussed the relative difficulty of successful propagules arriving in the Pitcairn Group, concluding that "their position at potentially harsh high latitudes and upstream of potential source areas yields an unstable and locally variable marine fauna."

Water temperature is another factor regulating the coral community composition, being cooler in the Pitcairn Island region (17–24°C) than nearly all other locations within the Indo-Pacific subtropical province. Whilst preferentially selecting for certain temperature-tolerant species, these cold-water temperatures and extremes of temperature might prevent many truly tropical species from surviving, even if they do manage to overcome the problem of dispersal.

We consider the reefs in the Pitcairn Group to be depauperate because: (1) successful recolonization of coral populations after Quaternary sea-level lows might have been inhibited by long oceanic distances, and (2) water temperatures are low compared to Pacific islands located to the northwest (Fig. 12-1). Low coral species richness (21 Acroporids and 48 other scleractinia species identified so far; Wallace and Veron, respectively, pers. comm., 1995) may also be due to the restricted range of modern sediments found skirting the islands in the group (Spencer, 1989).

Geology

The geologic and tectonic history of the Pitcairn Island Group has been addressed by Okal and Cazenave (1985) and summarized by Paulay and Spencer (1988) and Spencer (1989). A cruise by the F.S. *Sonne* in 1989 used Seabeam mapping, underwater video taping and grab sampling to recover more physical data than previous SEASAT missions could provide. The results of this cruise are given in Woodhead et al. (1990) and Woodhead and Devey (1993), and the geochemical characterization of the Pitcairn Island lavas is presented in Woodhead and McCulloch (1989). The following is a short summary.

The four islands of the Pitcairn Group were formed by two Pacific Plate hotspots. The Pitcairn hotspot created Mururoa [q.v. Chap. 13], the Gambier islands, Pitcairn Island and the recently discovered volcanically active seamount described by Woodhead et al. (1990, 1993).

The most recent model for the plate tectonic evolution of the Oeno-Henderson-Ducie-Crough seamount chain is based on SEASAT data describing the marine geoid (Okal and Cazenave, 1985). The chain may be the surface expression of a mid-plate southern Tuamotu hotspot (Okal and Cazenave 1985). Okal and Cazenave (1985) proposed that Oeno, Henderson, Ducie and the Crough seamount are part of the southern Tuamotu chain, and the 15° deviation of their lineament from the Pacific Plate's absolute motion is due to the interaction of this hotspot with a fossil transform fracture zone (FZ2). The speculative model of Okal and Cazenave (1985) suggests that FZ2 provides a preferential output for a hotspot in young, thin, hot lithosphere. Larger-scale fracture zones nearby might have been the result of intraplate deformation due to either differential motion between the northern and southern Pacific Plate or motion of the plate as a whole (Diament and Baudry, 1987).

The main phase of island construction at Pitcairn Island has been K-Ar dated as 0.76–0.93 Ma (Duncan et al., 1974): in contrast Okal and Cazenave (1985) proposed the following dates for island genesis: Oeno Atoll, 16 Ma; Henderson Island, 13 Ma; Ducie Atoll, 8 Ma. Confirmation of these proposed dates must await radiometric dating of their volcanic basement, which is not presently exposed on the three carbonate islands. Furthermore, the progressive timing of volcanism along FZ2 has no scientific verification to date. Indeed, FZ2 has a lateral extent mapped only between Henderson Island and Ducie; its continued extension remains tentative.

GEOMORPHOLOGY OF THE CARBONATE ISLANDS

Ducie Atoll

Ducie Atoll is composed of an island and four islets surrounding an inner lagoon with a single boat passage to the SW (Fig. 12-2; Rehder and Randall, 1975). Acadia Island is the largest islet and forms the northern and eastern sides of the atoll. Rehder and Randall (1975) described the western end of Acadia Island as "composed again of coral-rubble ridges that merge on the ocean side into the rubble

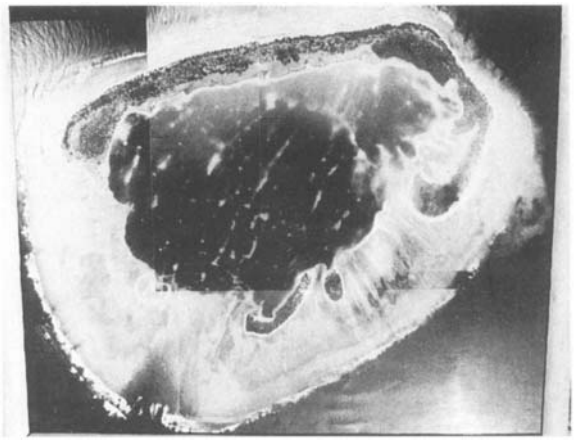


Fig. 12-2. Aerial photograph of Ducie Atoll. Acadia Island forms the northern side of the atoll. To the south are Edwards Islet (east) and Pandora Islet (west). Just northwest of the boat passage is horseshoe-shaped Westward Islet. See Rehder and Randall (1975) for discussion. (Photo courtesy of Olive Christian, Pitcairn Island.)

rampart above the shore line and that continue on the lagoon side as a steeply graded rubble beach...before terminating in the beachrock and loose coral slabs and rubble that line the remainder of the lagoon shore of the island." The island is floored by grey coral rubble, and its northern shore is characterized by ridges of beachrock.

Westward Islet is composed of coral rubble, echinoid remains and molluscan shells, in some places almost completely composed of shells from the clam *Turbo argyrostomus*. A coral-rubble ridge extends from Westward Islet about three quarters of the way northwest towards Acadia Island. Between Westward Islet and Acadia Island a very broad reef flat is developed (Fig. 12-2). Beachrock occurs near Westward Islet. Pandora Islet and Edwards Islet have either a sand, or sand and fine coral-rubble beach bordering the lagoon which merge above into the weathered coral blocks and rubble as found on Acadia Island (Rehder and Randall, 1975).

The lagoon at Ducie Atoll is striking in its preservation of a formerly prolific coral fauna. Rehder and Randall (1975) give estimates of water temperature and depth within the lagoon. Rehder and Randall (1975) noted the paucity of life over 20 years earlier in Ducie lagoon, and both the 1987 visit of the RV *Rambler* (Paulay, 1989) and our visit in 1991 showed a similar pattern. Paulay (1989) noted a low cover of mostly *Montipora* spp. In addition, the large foraminifera, *Marginopora vertebralis*, was abundant in the lagoon.

Oeno Atoll

Oeno Atoll has an island developed in the center of the lagoon with an outer reef rim surrounding the island-lagoon complex (Fig. 12-3). Devaney and Randall (1973)

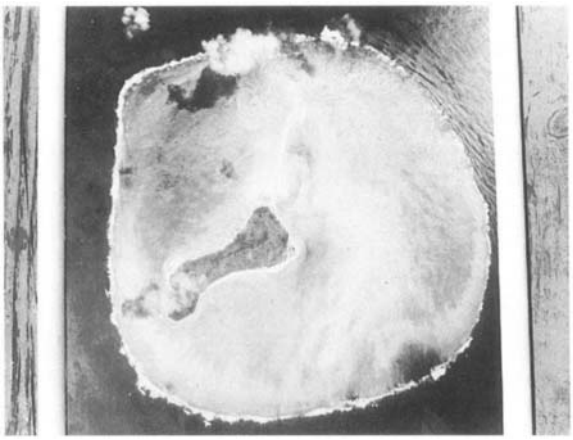


Fig. 12-3. Aerial photograph of Oeno Atoll. A single island occurs in the center of the lagoon and has a sand spit extending out from the eastern tip. The entire lagoon is less than 3 m deep. (Photo courtesy of Olive Christian, Pitcairn Island.)

and Paulay (1989) gave brief descriptions of the lagoon and forereef. The lagoon is uniformly shallow with an undulating bottom composed of coral rubble and sand, with scattered reefs (Paulay, 1989). A sand spit extends from the eastern edge of the main island, and there are spur and groove structures without a reef crest on the SE outer reef flat (Fig. 12-3). Within the lagoon the "patches of coral rock" (Devaney and Randall, 1973) show previous extensive monospecific stands of branching corals (Pandolfi, 1995). Such monospecific coral stands do not presently occur within the lagoon.

Henderson Island

Henderson Island (Fig. 12-1 and 12-4) is an *emergent limestone island* according to the definition given in Woodroffe (1992). It rises to 33.5 m above modern sea level from a seafloor depth of ~3.5 km, and conforms to the pattern of an elevated atoll, although no evidence has been found of the pre-atoll volcanic history of the island. The loading from the emplacement of Pitcairn Island has resulted in the uplift of Henderson Island through the process of lithospheric flexure first described by McNutt and Menard (1978). Emergent makatea islands in the southern Cook Islands have recently been discussed by Woodroffe et al., (1991) [see also Chap. 16]. Makatea islands have a highly eroded and degraded volcanic interior surrounded by emergent, highly karstified Cenozoic limestones (Woodroffe, 1992). The volcanic loading in the Cook Islands (dated at 1.65 Ma) took place on relatively old (> 80 Ma) ocean floor, and, as a result, differential uplift has continued over the last 1.05 m.y. In the case of Henderson Island, loading (dated at 0.93–0.60 Ma) has taken place on much younger ocean floor (30 Ma), and much of the compensatory

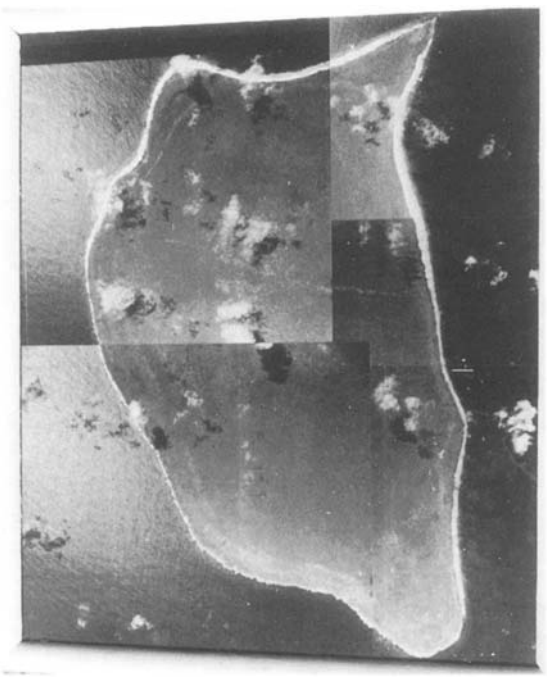


Fig. 12-4. Aerial photograph of Henderson Island, a raised fossil atoll. A raised rim characterizes the periphery of the island in the south, west and north sectors, while on the eastern side this ridge is greatly reduced. The fossil lagoon is largely a depositional feature, but severe karstification has affected the northwest and southern reef-flat areas. The lagoon is largely devoid of sandy sediments. (Photo courtesy of Olive Christian, Pitcairn Island.)

flexure is predicted to have taken place shortly afterwards (discussed further in the Case Study and in Blake, 1995).

CASE STUDY: GEOLOGICAL EVOLUTION OF HENDERSON ISLAND, AN EMERGENT LIMESTONE ISLAND

Spencer and Paulay (1989) undertook the first stratigraphic interpretation of the deposits on Henderson Island. Their fossiliferous reef unit (11–17 m above modern sea level) was interpreted to represent coral growth between 200 and 400 ka. Their low unfossiliferous limestone unit (0–10 m above modern sea level) was thought to be representative of coral growth at 100–140 ka. Field research conducted by the authors during The Expedition has led to a re-evaluation of the stratigraphy of Henderson Island.

Lithostratigraphy

The geological record preserved in the cliffs at Henderson Island varies according to location indicating that differential erosion has occurred. On North Beach and Northwest Beach, cliff height reaches a consistent level of approximately 30 m, with terraces preserved at lower altitudes composed of a friable shelly drape of loosely cemented material. Marked regional unconformities exist at elevations of 10–11 m and at 15.5 m. A highly fossiliferous well-cemented unit exists 0–6.0 m above modern sea level, and it has a similar appearance in the field to the limestones above 15 m. Cave-floor heights are interpreted to indicate the former position of sea level on both these beaches, based, in part, on their consistent altitude (25.4 m, 21.2 m, 19.7 m, 15.5 m, 10.7 m and 6.7 m above modern sea level; Table 12-1).

In contrast to North and Northwest beaches, cliff heights rise to a maximum of only 23.9 m on East Beach. This elevation difference is attributed to the enhanced subaerial erosion at East Beach due to its position relative to the prevailing storm direction. Cave-floor heights are highly variable at East Beach. This variability may indicate that these caves originated in a variety of ways including: (1) a sea-level notch (caves with gently sloping floors); (2) a product of karst erosion (caves with small jagged openings); (3) submarine caves (caves with small round openings to dome-shaped interiors); and (4) contact caves at conglomerate-massive limestone lithological contacts (caves with door-shaped openings).

As a result of the variety of proposed cave-forming processes, little former sea-level information can be gleaned from the East Beach cave data except for the notches/caves at elevations of 10.5 m and 15.5 m, which coincide with cave

Table 12-1

Elevation (m) of geomorphological features on Henderson Island[a]

Feature	North Beach (m)	Northwest Beach	East Beach
Maximum cliff height	30.2	30.5	23.9
Cave floor/notch	25.4	25.5	
Ledge	24.8	24.9	
Cave floor/notch	23.5		
Ledge	22.2		
Cave floor/notch	21.2	21.2	21.2
Ledge	20.3	20.3	20.3
Cave floor/notch	19.7	19.3	19.6
Ledge	17.9	18.2	18.2
Cave floor/notch	15.5	15.4	15.5
Ledge	13.7	13.6	
Cave floor/notch	10.7	10.7	10.5
Ledge	9.6	9.6	
Cave floor/notch	6.7	6.7	6.7
Ledge	5.8	6.0	

[a] All elevations have error terms of ± 0.05 m assuming the establishment of the correct modern sea-level datum.

elevations at North and Northwest beaches. Fossil spur-and-groove topography dominates the geology of East Beach, with two series of conglomerates and associated patchy encrusting coral growth (fining-up sequences) enshrouded by a drape of platy coral (see Table 12-2).

At the southern end of the island, steep cliffs rise vertically out of the sea and attain a height of 26 m. Present-day marine erosion is especially conspicuous, beaches are absent, and only large tumbled blocks of well-cemented limestone occur at the southern end of the island. Fossil spur-and-groove topography is especially conspicuous on the top of the southern end of the island.

Five separate geologic units have been identified from East Beach, the geological type section for Henderson Island (Table 12-1 and Figs. 12-5, 12-6, 12-7, 12-8, 12-9). In contrast to the previous stratigraphic interpretations of Spencer and Paulay (1989), we interpret the cliff sections as representing conformable carbonate overgrowths of well-preserved corals related to three distinct reef-building episodes subsequent to the main atoll-construction phase. Only our Unit 5, the loosely cemented wrap-around shelly unit, is not conformable, and this is due to island

Table 12-2

Type section from East Beach, Henderson Island[a]

Unit 4 (Elevation: 23.9–17.6)
Massive limestone with stout branching colonies, well-cemented, well-lithified, very large colony size, *Tridacna* present.

Unit 3
(Elevation: 17.6–14.8)
Large colonies of massive, cone-shaped, in situ, encrusting and branching corals (spurs).
(Elevation: 14.8–12.7)
Branching and massive, in situ corals (spurs) or branching coral rubble (grooves).
(Elevation: 12.7–12.4)
Beach sand (grooves).

Unit 2
(Elevation: 12.4–10.3)
Well-lithified, well-cemented, well-rounded conglomerate, fining upwards (grooves) or stout branching, in situ *Acropora* spp. (spurs).
(Elevation: 10.3–8.6)
Moderately well-cemented limestone, many platy forms, small colony sizes (spurs) or a finer platy conglomerate unit (grooves).
(Elevation: 8.6–8.4)
Beach sand (not always present).
(Elevation: 8.4–6.0)
Poorly lithified, coarse, blocky "infill" conglomerate (fining upwards), contains many clasts from the underlying unit.

Unit 1 (Elevation: 6.0–0.0)
Massive limestone with stout branching colonies, well-cemented, well-lithified, very large colony sizes, *Tridacna* abundant.

[a] All elevations have error terms of ±0.05 m assuming the establishment of the correct modern sea-level datum.

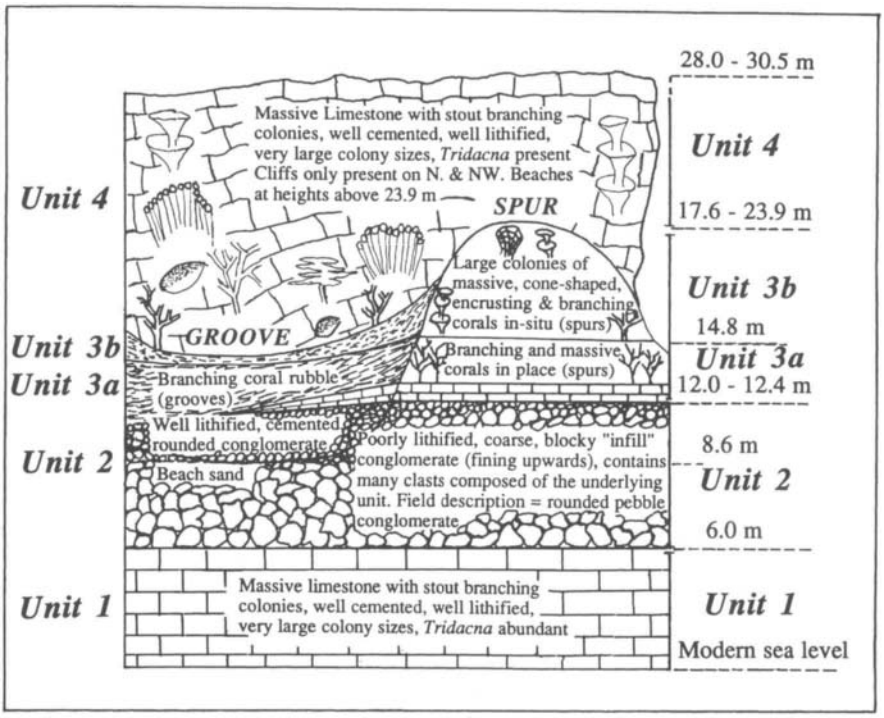


Fig. 12-5. Summary stratigraphic sketch of the depositional units of Henderson Island. These stratigraphic relations are best exposed in the spur-and-groove topography at the southern end of Henderson Island and the deeply incised cliff sections at East Beach, where this geologic type section was constructed.

emergence (uplift) as a result of crustal loading and subsequent lithospheric flexure (see below).

Stratigraphic and facies relationships on Henderson Island are preserved within: (1) the spur-and-groove structures, pinnacles and lineations found both in the cliff sections and around the perimeter of the island; and (2) the lineations and gravel patches found within the interior of the island. The top of the southern end of Henderson Island preserves the most complete stratigraphy, and stratigraphic units 2, 3 and 4 could be mapped. Stratigraphic relations are summarized in Table 12-3 and in Figures 12-5 and 12-6. More detailed descriptions of Units 2–4 are in Pandolfi (1995).

Chronostratigraphy

Fifteen conventional (alpha-counting) Uranium-series dates have been determined for Henderson Island samples (Table 12-4), and their height and stratigraphic locations are given in Fig. 12-6. It is generally considered that the conventional

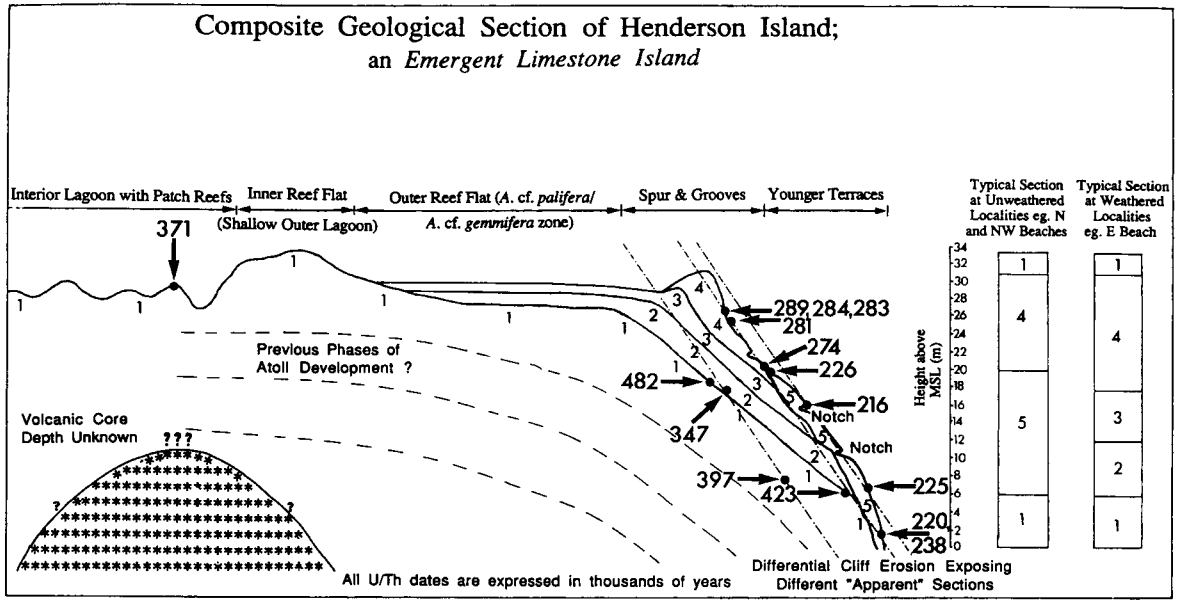


Fig. 12-6. Summary geological section of Henderson Island. Conventional U-Th dated coral samples are indicated with their corresponding elevation and age. Columns at right show two sections, at weathered and unweathered localities, with the relevant units that are expected to be exposed.



Fig. 12-7. Cliff section at central East Beach exposing fossil spur-and-groove topography. The base of the section depicted in the photograph is at an elevation of 6.7 m, and the upper cliffs are at elevations of approximately 16–18 m. Most of the units shown schematically in Fig. 12-5 are illustrated here. Note that the conglomerate and corals making up Units 2 and 3 are enveloped by later Unit 4 corals. Most conglomerates have been grown over by a later stage of coral growth. In general, the locations of spur-and-groove topographies are interpreted to have been inherited from previous phases of atoll development.

alpha-counting technique is unreliable when used on aragonitic samples older than 350 ka because the error bars on such dates become so large they could be describing a single unit. Pristine aragonite samples are ideally used in U-series dating as the presence of secondary calcite can compromise the fidelity of the age determination.

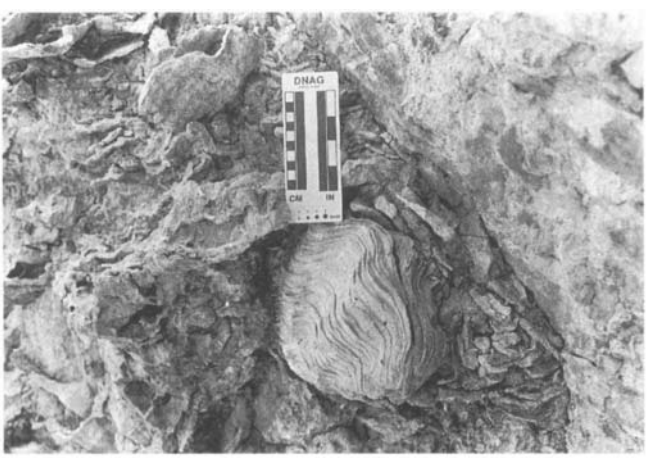


Fig. 12-8. *Tridacna maxima* in growth position in Unit 1, a massive limestone with stout branching coral colonies. The unit is characterized by being well cemented, well lithified and containing large coral colonies. Unit 1 typically is 0–6 m above modern sea level and is considered to have formed during a prolific reef-building period at 440–380 ka.



Fig. 12-9. A lower part of a central East Beach cliff section between 2.0 and 10.5 m relative to modern sea level. The pronounced unconformity (middle foreground) is located at 6.0 m and separates highly lithified Unit 1 massive corals from the overlying Unit 2 rounded-pebble conglomerate. This lithological contact between these two units is the most pronounced for all the measured, highly recessed cliff sections.

Apart from one sample, Hen 4–1 from East Beach, which comprised 97% aragonite and 3% calcite, all samples from Henderson Island had >99% aragonite in their skeletons. Cathodoluminescence analysis indicated no diagenetic cements in the samples dated by U-series, a conclusion supported by the thin-section observations. Recrystallization and contamination problems were also judged to be relatively minor in the dated samples.

East Beach mainly displays corals and conglomerates dating at 440–380 ka, 330–300 ka, and 285–275 ka (Figs. 12-5 and 12-6). The 285–275 ka corals (Unit 4) drape over earlier reefal formations (Fig. 12-7). Unit 5 deposits are characterized by a "wrap-around" phenomenon in which platy corals envelope pre-existing corals and conglomerates (i.e., Units 1, 2, 3 and 4). Deposits of Unit 5 reach an altitude of 19.6 m in several less-eroded localities (Fig. 12-7) and date at 230–215 ka. However, Unit 5 is not always well represented on East Beach due to the high erosion rates at this locality. Commonly the cliff sections are manifest by the exposure of the underlying fossil spur-and-groove topography dating from both 440–380 ka and 330–300 ka (Fig. 12-6). Superimposed on nearly all the cliff sections are erosional notches at elevations of 10.5 m and 15.5 m.

Table 12-3

Summary of stratigraphic and facies relationships on Henderson Island[a]

Unit 1. massive, well-cemented and well-lithified limestone with stout branching colonies up to 2 m in height and width (Fig. 12-5). The giant clam *Tridacna maxima* is abundant in this unit with individuals often reaching < 90 cm in length and both valves being preserved in situ.

Unit 2. composed of two litholgies: (a) a branching coral lithology with lesser amounts of platy corals. This lithology usually comprises the floor of the grooves (i.e., groove lithology is equivalent to Unit 2) and (b) a rounded pebble conglomerate in a coarse grained carbonate sand. Clasts are up to 30 cm in diameter, but are mostly smaller rounded coral bioclasts 6–8 cm in diameter. This lithology is extensive, but not continuous and may be loosely consolidated. It occurs at topographic highs (the lower portion of exposed or recessed spurs) on the southwestern side of the island, and pinches out in the grooves where it gives rise to the underlying branching coral-rubble facies. It is also present up to 500 m inland from the spur and groove structures where it underlies topographic highs adjacent to the outer margin of the fossil lagoon (Fig. 12-10). Here, the pebble conglomerate dips to the south.

Unit 3. a light grey, well-indurated, mottled, coarse-grained, skeletal limestone with abundant branching coral rubble and branching and massive corals in place (Fig. 12-5). It is the basal layer of the spurs where it is seen to drape over the underlying Unit 2. Beach sands also occur in the lower part of Unit 3 at East Beach (Blake, 1995). The contact between the pebbly conglomerate of Unit 2 and the mottled limestone of Unit 3 is characterized by loosely consolidated carbonate sand, and/or colonization of abundant massive and stout branching corals. The latter can be seen both in the lateral transition from the spur and groove structures to the outer reef flat and vertically within the pinnacles landward of the spur and groove structures (Fig. 12-10). The zone of stoutly branched acroporids found on the southern end of the island, is stratigraphically equivalent to the base of Unit 3.

Unit 4. a coral-rich unit that drapes over Unit 3 at all of the spur and groove formations, but disappears on top of the grooves and picks up again along the sides and tops of the spurs. Corals are massive and branching types, up to 2 m in height and width (Fig. 12-5). The overwhelming abundance of upright coral colonies suggests that the corals found in Unit 4 on top of the spurs are an in situ deposit. On top of the outer reef flat between the spur and groove structures and the outer lagoon margin, Unit 4 grades laterally into a coarse grained sugary lithology, that perhaps has been dolomitized.

Unit 5. a poorly lithified, friable unit that is dominated by platy corals which envelope (skirt) Units 1–4 below 19.6 m. It is absent at East Beach, South Point and the entire southern part of the island due to subaerial erosion. It is most conspicuous at the leeside embayment localities along North and Northwest Beaches.

[a] All elevations have error terms of ±0.05 m assuming the establishment of the correct modern sea-level datum.

Samples from the upper-middle cliff section and outer fossil lagoonal rim at North Beach have been dated at 285–275 ka (Unit 4). Corals with ages in the 440–380 ka and 230–215 ka periods are also present. Corals dating at 440–380 ka are exposed only in the lower 7 m of the section, where erosion has removed the younger (Unit 5) enveloping deposits. The lower cliff section beneath 19.6 m is dominated predominantly by platy corals having a 230–215 ka age (Unit 5). Occasional in situ corals and associated forereef rubble developed as two impoverished units of uncertain age

Table 12-4

Sample, elevation and U-series ages (alpha-counting) for Henderson Island[a]

Sample Number	Elevation (m AMSL)	234U/ 238U	230Th/ 234U	230Th/ 232Th	U Yield (%)	Th Yield (%)	Age (ka)
Hen 2–6	18.53 EB	1.09 ± 0.02	1.02 ± 0.03	202 ± 68	57.23	74.13	482 ± 289
Hen 1–6	6.70 NB	1.10 ± 0.02	1.01 ± 0.03	198 ± 74	51.64	57.93	423 ± 181
Hen 2–2	7.50 EB	1.09 ± 0.03	1.00 ± 0.03	232 ± 78	35.69	96.17	397 ± 187
Hen FH328	27.00 FL	1.07 ± 0.02	0.99 ± 0.03	461 ± 162	93.27	92.93	371 ± 116
Hen 2–7	17.87 EB	1.32 ± 0.03	1.04 ± 0.04	409 ± 83	26.52	75.90	347 ± 105
Hen 1–26B	26.30 NB	1.12 ± 0.01	0.96 ± 0.02	5952 ± 234	67.21	83.30	289 ± 39
Hen 1–26A	26.30 NB	1.07 ± 0.01	0.94 ± 0.02	2909 ± 204	71.43	76.03	284 ± 36
Hen 1–26C	26.30 NB	1.07 ± 0.01	0.94 ± 0.02	2908 ± 204	71.43	76.10	283 ± 35
Hen FH175	24.50 FL	1.10 ± 0.02	0.95 ± 0.03	570 ± 155	87.64	89.20	281 ± 57
Hen 1–23	19.73 NB	1.12 ± 0.03	0.95 ± 0.04	29 ± 24	40.00	83.74	274 ± 67
Hen 1–22	19.60 NB	1.11 ± 0.03	0.90 ± 0.03	119 ± 53	48.45	95.91	226 ± 39
Hen 4–1	6.85 EB	1.15 ± 0.03	0.90 ± 0.03	955 ± 174	42.58	100.00	225 ± 32
Hen 1–10A	1.75 NB	1.10 ± 0.01	0.91 ± 0.02	6170 ± 523	88.44	95.38	238 ± 27
Hen 1–10B	1.75 NB	1.16 ± 0.01	0.89 ± 0.02	5284 ± 368	92.37	84.60	220 ± 21
Hen 4–12	15.94 EB	1.14 ± 0.02	0.89 ± 0.03	9460 ± 389	93.72	92.95	216 ± 27

[a] All elevations carry error terms of +0.05 m assuming the establishment of the correct MSL datum. FL = fossil lagoon sample, NB = North Beach sample, EB = East Beach sample

are superimposed on Units 1, 2, 3 and 5. These impoverished units may represent deposition during the Last Interglacial (oxygen isotope substage 5.5, which is also referred to as substage 5e). Erosional notches exist at 10.7 m and 15.5 m with the corresponding terrace surfaces sitting below at 9.6 and 13.7 m, respectively. Evidence for this late substage-5.5 rise in sea level comes from in situ corals growing within the 10.5–10.7 m notch, encrusting corals growing around the 10.5–10.7 m notch and the field relations of these terraces. However no dateable material of substage-5.5 age has yet to be recovered. On North Beach the interval between present sea level and +6.6 m is dominated, however by corals of oxygen isotope stage 7 age underlying corals of probable substage-5.5 age. This situation also occurs on the Southern Cook Islands and Makatea Island in the South Pacific (Woodroffe et al., 1991). The North and Northwest beaches are characterized by the least amount of erosion over the entire island because of their sheltered position relative to the dominant storm direction. During ENSO periods, when the weather approaches from the northwest, however, these beaches are no longer in a sheltered position. We interpret the preferential preservation of the Unit 5 and probable substage-5.5 terraces at the North and Northwest beaches, compared to East Beach, to be the product of differential erosion. Unfortunately, the relatively poor preservation and general rarity of in situ corals comprising the substage-5.5 terraces has made it difficult to accurately date samples from these terraces. Woodroffe et al. (1991) report a similar predominance of disoriented coral boulders and a lack of in situ corals on Atiu in the southern Cook Islands.

The southern, northwestern and northeastern projections of the island are characterized by steep cliffs displaying large well-formed coral colonies of probable 440–

380 ka age, the age of the principal atoll-building phase when the oceanographic conditions were well suited for coral-reef development. Access to these locations was not possible during The Expedition. Concentrated marine erosion continues at the base of these cliffs today with little or no protection afforded by the spartan fringing reef lying offshore.

Lastly, we note that mean ages of carbonate deposition at Henderson Island — 404 ka (Unit 1); 282 ka (Unit 4) and 225 ka (Unit 5) — are similar to periods of carbonate deposition at Barbados (average U-Th TIMS dates of 402, 302, 281, 228 and 202 ka; Gallup et al., 1994) and in the southern Sinai/Red Sea region (average U-Th dates of 310 and 206 ka; Gvirtzman, 1994).

Geomorphology

Henderson Island has been interpreted as an elevated atoll with a central lagoonal depression (St. John and Philipson, 1962; Fosberg et al., 1983; Paulay and Spencer, 1988; Spencer and Paulay, 1989; Pandolfi, in press). Central depressions can represent either the erosional activity and karstification of limestone surfaces (Purdy, 1974), or the original geomorphology of the reef structure. For example, Stoddart et al. (1990) attributed the convexity of the makatea surface on cross-profile at Atiu in the southern Cook Islands to post-uplift erosion. In addition, Stoddart et al. (1985) concluded that the present topography of Mangaia was produced by karst erosion.

The top of Henderson Island, in our interpretation, preserves a fossil atoll with only limited erosional features. Evidence to support our interpretation includes: (1) the geomorphology of the top of Henderson Island, including outer rim and spur-and-groove structures; (2) stratigraphic and lateral facies relationships; and (3) the in situ occurrence and spatial variability of reef corals around the periphery and within the interior of the island.

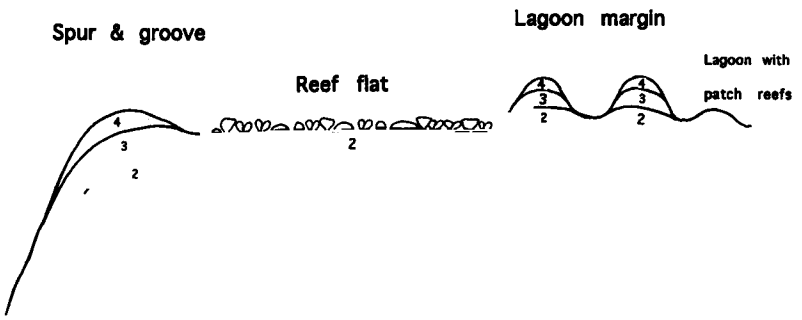


Fig. 12-10. Schematic drawing of the physiography of the ancient atoll at the southern end of Henderson Island showing: outer-rim spur-and-groove structures; the reef flat represented here as an *A. cf. palifera*/*A. cf. gemmifera* zone; the lineations of the lagoon margin; and the lagoon interior with patch reefs. Although not depicted here, the reef flat is often preserved as a karrenfeld with large pinnacles. Landward of the spurs and grooves, the lithology of Unit 4 is a grey sugary limestone. (Not to scale.)

The fossil atoll preserved on the top of Henderson Island is composed mainly of an outer rim and central lagoon, and we believe that the majority of features preserved on the top of the island represent original depositional events. On the southern windward side of the island, spur-and-groove structures give rise to an outer reef flat which itself gives rise to a zone of alternating lineations and shallow basins before descending into the lagoon proper (Fig. 12-10). On the eastern side, spur-and-groove structures also occur. Except for a limited zone at Northwest Point, there are no spur-and-groove structures on the north and northwestern sides of the atoll — although the buttress limestone of Spencer and Paulay (1989) might represent relict spur-and-groove structures — but there is a well-developed outer reef flat, and lineations separating shallow basins characterize the outer margin of the outer rim.

The fossil reef preserved at the top of Henderson Island is composed of an outer rim characterized by pinnacled limestone outcrops and an interior depression characterized by abundant corals and coral rubble in a gravel facies. The variable geomorphology of both the outer rim and the interior depression of Henderson Island is summarized in Fig. 12-11 and in the following paragraphs.

The original geomorphology of the outer rim of the fossil atoll appears to be preserved intact. On the northern, northwestern, and southern sides of the island, the outer margin of the lagoon is marked by a series of limestone lineations which probably represented very shallow basins between the outer reef flat and the deeper lagoonal basin represented in the central depression. Both the northwestern and southern sides of the island contain pinnacled limestone which preserve some evidence of the former outer reef flat.

At Northwest Point and on the southern and eastern sides of Henderson Island the seaward margin of the outer rim preserves a spur-and-groove system, which on the southern side may give rise seaward to another series of valleys and ridges. Such submarine topography is evident today on the eastern side of Henderson Island. On the north and northwestern sides of the island, excluding Northwest Point, the buttress limestone of Spencer and Paulay (1989) may also be erosional remnants of a previous spur-and-groove system. If not, then the paleo-outer reef flat there extends to the island perimeter.

A heavily vegetated central depression characterizes the interior of Henderson Island. The well-preserved coral fauna here is dominated by branching *Acropora* spp. rubble, although branching *Pavona* sp(p). and *Porites* sp(p). also occur. Massive corals are less abundant in the interior of the island, but may be locally dominant. In many places, the massive and branching coral fauna is represented by corals in growth position. The interior depression has been interpreted as a fossil lagoon (Fosberg et al., 1983; Paulay and Spencer, 1988; Spencer and Paulay, 1989; Pandolfi, 1995). Paulay and Spencer (1988) and Spencer and Paulay (1989) noted local topographic highs containing abundant coral rubble within the interior depression and interpreted these areas as large lagoonal patch reefs. We found evidence for the patch reefs throughout the interior of the central depression.

The morphological features found on Indo-Pacific atolls are presented in Scoffin (1987). The southern side of Henderson Island is represented by the most complete

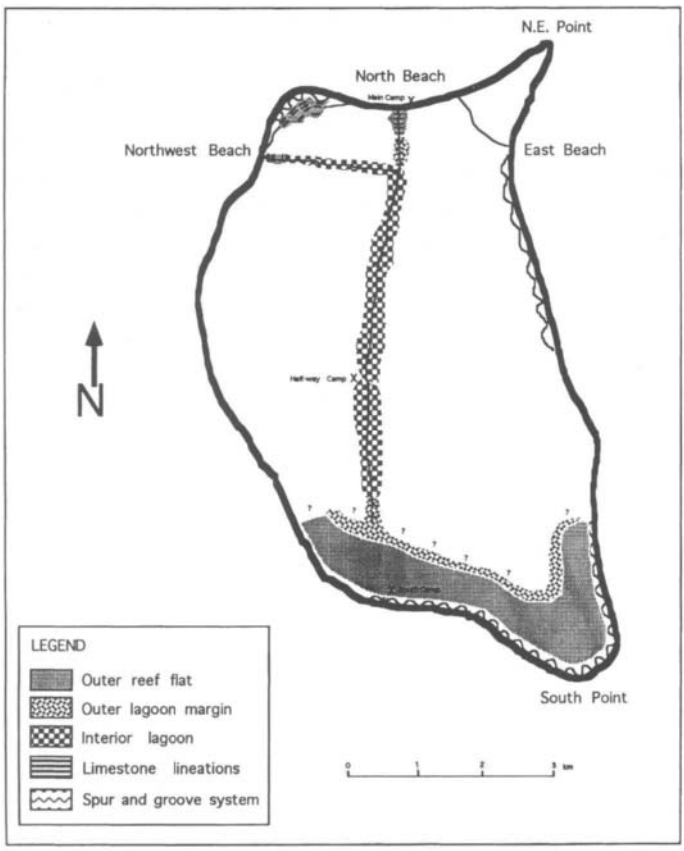


Fig. 12-11. Plan view of geomorphological structures of Henderson Island. Northwest Point and the southern and eastern sides of the island have spur-and-groove features making up the seaward margin of their outer rim. The outer rim of the northern and northwestern sides comprises a series of lineations and pinnacled limestones which occur either as the outer reef flat or the outer shallow margin of the atoll lagoon. Both the southern side and the northwestern side have a broad field of pinnacle topography (karrenfeld) between the seaward margin of the outer rim and the outer margin of the lagoon.

development of fossil spur-and-groove topography backed by the *Acropora cf. palifera/A. cf. gemmifera* outer reef flat zone (Fig. 12-10). This, coupled with the extensive zone of alternating lineations and shallow basins (outer lagoon margin/inner reef flat), which lies between the *Acropora cf. palifera/A. cf. gemmifera* outer reef flat zone and the deeper interior lagoon, indicates that the windward side of the atoll faced southeast (as it does today). North Beach and Northwest Beach represent leeward backreef recesses in the atoll's original and present-day geomorphological structure. The apparent zonation pattern and the magnitude and frequency of the spur-and-groove systems are consistent with the most pronounced reefal development having taken place on the southeast side of the original atoll. Large monospecific coral stands are present both within the more protected fossil lagoon and

backreef settings, on the top, and on the north and northwest sides of the island, respectively. Such an interpretation of the preferential weathering directions also accounts for the differential erodability of the Henderson Island cliff sections as alluded to previously.

Thus far we have stressed the depositional nature of the Henderson Island atoll. However, there is some evidence for erosional features. The pinnacle karrenfelds on the northwestern and southern sides of the island are the result of karstification, and some loss of the depositional history has occurred. The most spectacular example of this are the "dragon's teeth", 8–9 m high limestone pinnacles located in the northwest interior (fossil lagoon) of the island which stretch for a distance of up to 250 m. The stratigraphy clearly preserved within the pinnacles however, together with the facies relationships between pinnacles and areas laterally contiguous with them, suggest that the amount of information lost in the karstification process has been minimal. Perhaps this is correlated with the relatively young ages (404–225 ka) of both the lagoonal and reef crest corals.

Geologic and eustatic history

Although the deep-sea oxygen isotope record may provide an accurate proxy record of sea-level change which can be calibrated with coral terraces, no definitive sea-level curve for the south-central Pacific exists at the present time. Two widely cited sea-level curves are presented in Chappell and Shackleton (1986) and Shackleton (1987). Sea-level curves based primarily on raised coral-terrace data can be approximately related to oxygen isotope records from deep-sea foraminifera. Most previous workers (Chappell, 1974; Aharon et al., 1980; Chappell, 1983; Chappell and Shackleton, 1986; Chappell and Polach, 1991; Stein et al., 1992; Stein et al., 1993) have used uplift rates (1.9–3.4 m ky^{-1}; Ota et al., 1993) determined from the Huon Peninsula, Papua New Guinea, to reconstruct previous interglacial and interstadial periods. Other sea-level terrace data have come from Timor and Atauro Island (Chappell and Veeh, 1978); Haiti (Dodge et al., 1983); Bermuda (Harmon et al., 1981); Barbados (Bard et al., 1990); Bahamas (Chen et al., 1991) and the Southern Cook Islands (Woodroffe et al., 1991). The importance of isostatic uplift in response to ice-sheet loading has been quantified (Lambeck and Nakada, 1992a,b) and these workers concluded that Last Interglacial highstands do not necessarily imply that ocean volumes were any greater than those found today.

The oxygen isotope record indicates that at 285–275 ka the elevation of sea level was approximately equal to that of today (Shackleton and Opdyke, 1973; Shackleton, 1977; Shackleton et al., 1983; Shackleton et al., 1990; Shackleton et al., 1993). Recall that Unit 4 from Henderson Island has an average date of 282 ka. The maximum elevation of a dated sample from Unit 4 is 26.3 m, giving an uplift rate of 0.093 m ky^{-1}. If the mean maximum elevation of this unit is 30.3 m, the uplift rate of the island is 0.107 m ky^{-1}. Averaging these two estimates of uplift rate gives a mean uplift rate of 0.10 m ky^{-1}. We consider this value to represent the upper limit of rate of uplift (see below).

The oxygen isotope record indicates that sea level at 230–215 ka was several meters below modern (Chappell and Shackleton, 1986; Shackleton et al., 1990). The maximum sampled elevation of Unit 5 is 19.6 m (Hen 1–22). This indicates that island uplift is taking place at 0.086 m ky^{-1}. However, if the top of the main terrace (mean elevation of 18.1 m) is taken instead as the best sea-level indicator, then the uplift rate would be 0.080 m ky^{-1}, assuming sea level reached its present level at 226 ka. The average of these two estimates of uplift rate gives a mean uplift rate of 0.083 m ky^{-1}, a value somewhat less than the 0.10 mm/yr value described above. Taken at face value, these data indicate that sea level between 230–215 ka was below modern sea level by approximately 5–8 m. Sea level is predicted to have been only a couple of meters below modern sea level between 205–190 ka (Chappell and Shackleton, 1986; Shackleton et al., 1990; Gvirtzman, 1994); however, no corals of this age were recovered from Henderson Island.

Erosional notches at 10.7 and 15.5 m on Henderson Island are the only evidence of the higher sea levels of the Last Interglacial (oxygen isotope substage 5.5, 128–119 ka; Chappell and Shackleton, 1986). The absence of dateable material from the Last Interglacial at Henderson Island is in marked contrast to the late Pleistocene reefs in the Southern Cook Islands where reefs of substage-5.5 age skirt older carbonate complexes. If a global sea level of +6 m relative to modern for substage 5.5 (119 ka) is taken as being representative (Bloom et al., 1974; Chappell and Shackleton, 1986; Gvirtzman, 1994), and the erosional notch at 15.5 m is taken as the substage-5.5 indicator, an uplift rate of 0.08 mm/yr is established for the last 119 ka.

Recent TIMS dating of North Beach cliff samples have given ages of 292.8 ± 5.3; 306.1 ± 4.4; 317.2 ± 4.8 and 318.9 ± 4.0 ka. Another sample, taken 930m inland from North Beach on the top of the island, has a TIMS age of 637.3 ± 70.6 ka and is the subject of ongoing dating work. Such an age would indicate the oldest preserved aragonitic coral ever reported in the literature to date.

Further TIMS dating of Henderson Island samples, which is now in progress, is needed in order to more accurately fix the aforementioned depositional events in time. However, given the present data we propose the following preliminary geological evolution of Henderson Island:

(1) Sequential fringing reef, barrier reef and atoll development associated with subsidence of the original volcano (sensu, Darwin, 1842). The age of this sequence will remain unknown unless coring identifies suitable dateable material, which is unlikely.

(2) Construction of the subaerial Pitcairn volcano during two main phases of volcanism between 0.95–0.76 and 0.63–0.45 Ma with the initial period being the main shield-forming phase (Duncan et al., 1974). Loading of the oceanic crust then commenced as a result of the building of the Pitcairn volcano.

(3) Reef development beginning prior to 440 ka, the age of the oldest dateable coral samples. We think it possible, and perhaps likely, that the oldest recovered corals veneer even older corals. However, more data are needed to confirm this hypothesis.

(4) Prolific reef development between 440–380 ka (oxygen isotope stage 11; Figs. 12-8, 12-9) followed by a major glaciation (equivalent to oxygen isotope substage 10.2). Sea level during this long interglacial period has been estimated to have been at several meters above modern sea level (Shackleton et al., 1990) and would have produced a thick carbonate deposit that would have been subaerially exposed during the ensuing glacial period.

(5) Uplift of the atoll above modern sea level at 360–335 ka due to lithospheric flexure. This age of uplift is calculated assuming an uplift rate of 0.093–0.10 m ky^{-1} and a maximum elevation of the island of 33.5 m above modern sea level.

(6) Further reef development at 330–300 ka (estimated to be equivalent to oxygen isotope substages 9.1 and 9.3) followed by a minor glacial period as predicted from the deep-sea oxygen isotope record. Sea level has been estimated to be at, or slightly higher than modern sea level during the height of this interglacial period (Shackleton et al., 1990). Stratigraphic units possibly belonging to oxygen isotope stage 9 can be separated into Units 2 and 3. However, as no dateable material was recovered from these units, the age assignment for Units 2 and 3 rests solely on field relations. The majority of Unit 2 is erosional in character and is composed of conglomerates. Unit 3 represents a spur-and-groove-building period when the conglomerates were stabilized by reef-building corals. The windward side of the atoll was on the southeast side (as today), as evidenced by the conspicuous spur-and-groove topography. The highly developed *Acropora cf. palifera/A. cf. gemmifera* outer reef flat zone especially conspicuous on the southern side of the island is considered stratigraphically equivalent to the top of Unit 2. Spur-and-groove topography is especially evident at Henderson Island in the East Beach cliff sections and several hundred meters inland along the entire south and southeastern parts of the island.

(7) A shorter period of prolific reef development at 285–275 ka (Unit 4: North Beach upper cliff sections and the outer rim of the atoll). The average group of dates for Unit 4 is 282 ka. Sea level at this time has been estimated to have approximated modern sea level (Shackleton et al., 1990). Hence, these dates can be used to calculate an uplift rate (0.093–0.10 m ky^{-1}) for Henderson Island.

(8) A period of reef growth at 230–215 ka (Unit 5: North and East Beach lower cliff sections, representing oxygen isotope substage 7.3), followed by a major glaciation (stage 6) prior to the onset of the Last Interglacial (substage 5.5). The average group of U-Th dates recovered from Unit 5 is 225 ka. No dateable material from substage 7.1 (205–190 ka) was recovered from the cliff sections studied at Henderson Island.

(9) Higher sea levels of the Last Interglacial (oxygen isotope substage 5.5, 128–119 ka; Chappell and Shackleton, 1986), which is evidenced by only erosional notches at 10.7 and 15.5 m. No evidence of any stillstands subsequent to 118 ka are preserved in the cliffs of Henderson Island.

Several factors could be responsible for the paucity of well-formed reefs in the presumed oxygen isotope substage-5.5 terraces. First, fluctuations in sea level compound the difficulties of coral-larvae dispersal in such eastern outposts of the Indo-Pacific subtropical province. Second, present-day seawater temperatures in

the vicinity of Henderson Island are already near the lower limit of coral survival. A cooling of only a few degrees during substage 5.5 would place the coral communities in a very hostile environment for the dispersal, propagation and settlement of coral larvae. Third, only long-duration interglacials may result in coral-reef growth at such remote localities given the temporal lag between the onset of optimal coral growth conditions and the recolonization and subsequent coral-reef construction during an interglacial period. Fourth, well-developed reef units commonly do not form on slowly uplifting islands (e.g., < 0.1 m ky^{-1}) unless there is a long period between interglacials (e.g., the Huon Peninsula of Papua New Guinea; Chappell, 1974). Earlier reef units are therefore commonly not lifted above later ones and the resultant carbonate lithological units are directly superimposed upon one another.

Until the Pacific sea-level highstand between 6–1.6 ka (Pirazzoli and Montaggioni, 1986), all sea-level rises after 119 ka had their maximum heights below present sea level and the corresponding reefal units would not be expected to be exposed today in the cliffs of Henderson Island. Submarine terraces are preserved offshore at – 16 m, – 22 m and – 35 m (SCUBA observations by SGB). No raised micro-atolls are evident on the modern day reef flat at Henderson Island to provide evidence of a Holocene highstand, although two blocky limestone outcrops are exposed 1.0 m above modern sea level on the outer reef flat at North Beach. It is unclear whether they truly represent a 6-ka highstand or are simply storm debris resulting from nearby cliff erosion.

CONCLUDING REMARKS

Henderson Island is an emergent limestone island. It rises to 33.5 m above modern sea level from a seafloor depth of about 3,500 m and conforms to the pattern of an elevated atoll, although no field evidence was found pertaining to the pre-atoll volcanic history of the island. The emergence of this coral atoll can be explained by lithospheric flexure processes subsequent to the emplacement and loading of the Pitcairn Island volcano, built by two phases of volcanism (estimated at 855 and 540 ka by K-Ar dating). Conventional U-Th dates obtained from Henderson Island indicate that the majority of the presently visible fossil corals have an age between 404–225 ka. Henderson Island first became emergent when sea level dropped subsequent to 380 ka, as the period 440–380 ka is thought to have been characterized by sea level at least several meters above modern sea level in the Central Pacific. As a result, Henderson Island would have become subaerially exposed from 380 ka onwards. Field relations and U-Th dates indicate three main periods of reef development: (i) a prolific reef-building period (Unit 1, at 440–380 ka, and Units 2 and 3 at 330–300 ka) dominated by large, stout branching coral colonies; (ii) a shorter period of reef growth at 285–275 ka (Unit 4) dominated by well-formed large in situ coral colonies and *Tridacna maxima*; and (iii) a period of less-prolific reef growth between 230–215 ka (Unit 5) dominated by platy corals enveloping the previous lithologies below 19.6 m.

The combination of depositional ages and present mean elevation of depositional units can be used to calculate a mean uplift rate for Henderson island of 0.087 m ky^{-1}. This rate is judged to be insufficient to form well-developed reef units which are then lifted above the level of later ones to produce easily identifiable carbonate terraces. As a result, the majority of the identifiable units (Units 1–4) comprising Henderson Island are conformable. Such a model of stratigraphic evolution is at variance with the Spencer and Paulay (1989) interpretation of the geologic evolution of Henderson Island.

ACKNOWLEDGMENTS

The Expedition to the Pitcairn Islands could not have been possible without the logistic support of Alve Hendrickson, and to him we express our utmost gratitude. We thank the following field assistants: Chuck Doersch, Michelle Langer, Sean McCollum and Liz Senear. SGB wishes to thank Professor Kurt Lambeck and Mr. Trevor Blake for financial support, Audrey Chapman for help with the U-Th dating. Charlie Veron and Carden Wallace identified the modern corals collected during The Expedition. JMP acknowledges the Department of Industry, Technology and Commerce (now Department of Industry, Technology and Regional Development) of the Commonwealth Government of Australia for a grant enabling participation in the Pitcairn Islands Scientific Expedition. This paper results from the 1992-92 Sir Peter Scott Commemorative Expedition to the Pitcairn Islands and is contribution number 762 from the Australian Institute of Marine Science.

REFERENCES

Aharon, P., Chappell, J. and Compston, W., 1980. Stable isotope and sea-level data from New Guinea supports Antarctic ice-surge theory of ice ages. Nature, 283: 649–651.

Bard, E., Hamelin, B. and Fairbanks, R.G., 1990. U-Th ages obtained by mass spectrometry in corals from Barbados: sea level during the past 130,000 years. Nature, 346: 456–458.

Blake, S.G. 1995. Late Quaternary history of Henderson Island, Pitcairn Group. Biol. J. Linn. Soc., 56: 43–62

Bloom, A.L., Broecker, W.S., Chappell, J.N.A., Mathews, R.K., Mesollela, K.J., 1974. Quaternary sea-level fluctuations on a tectonic coast: New $^{230}Th/^{234}U$ dates from the Huon Peninsula, New Guinea. Quat. Res. 4: 185–205.

Chappell, J., 1974. Geology of coral terraces, Huon Peninsula, New Guinea: A study of Quaternary tectonic movements and sea-level changes. Geol. Soc. Am. Bull., 85: 553–570.

Chappell, J. and Veeh, H.H., 1978. Late Quaternary tectonic movements and sea-level changes at Timor and Atauro Island. Geol. Soc. Am. Bull., 89: 356–368.

Chappell, J., 1983. A revised sea-level record for the last 300,000 years from Papua New Guinea. Search, 14 (3–4): 99–101.

Chappell, J. and Shackleton, N.J., 1986. Oxygen isotopes and sea level. Nature, 324: 137–140.

Chappell, J. and Polach, H., 1991. Post-glacial sea-level rise from a coral record at Huon Peninsula, Papua New Guinea. Nature, 349: 147–149.

Chen, J.H., Curran, H.A., White, B. and Wasserburg, G.J., 1991. Precise chronology of the last interglacial period. ^{234}U-^{230}Th data from fossil coral reefs in the Bahamas. Geol. Soc. Am. Bull., 103: 82–97.

Darwin, C., 1842. The structure and distribution of coral reefs. Being the first part of the Geology of the voyage of the Beagle under the command of Capt. Fitzroy, RN, during the years 1832 to 1836. London, Smith Elder and Co., 214 pp.

Devaney, D.M. and Randall, J.E., 1973. Investigations of Acanthaster planci in Southeastern Polynesia during 1970–71. Atoll Res. Bull., 169: 35 pp.

Diament, M. and Baudry N., 1987. Structural trends in the Southern Cook and Austral archipelagoes (South Central Pacific) based on an analysis of SEASAT data: geodynamic implications. Earth Planet. Sci. Lett., 85: 427–438.

Dodge, R.E., Fairbanks, R.G., Benninger, L.K. and Maurrasse, F., 1983. Pleistocene sea levels from raised coral reefs of Haiti. Science, 219: 1423–1425.

Duncan, R.A., McDougall, I., Carter, R.M. and Coombs, D.S., 1974. Pitcairn Island-another Pacific hot spot? Nature, 251: 679–682.

Edwards, R.L., Chen, J.H. and Wasserburg, G.J., 1987. ^{238}U-^{234}U-^{230}Th-^{232}Th systematics and precise measurement of time over the past 500,000 years. Earth Planet. Sci. Lett., 81: 175–192.

Eisenhauer, A., Wasserburg, G.J., Chen, J.H., Bonani, G., Collins, L.B., Zhu, Z.R. and Wyrwoll, K.H., 1993. Holocene sea-level determinations relative to the Australian continent. U/Th (TIMS) and C-14 (AMS) dating of coral cores from the Abrolhos Islands. Earth Planet. Sci. Lett., 114: 529–547.

Fosberg, F.R., Sachet, M.H., and Stoddart, D.R., 1983. Henderson Island (Southeastern Polynesia): Summary of current knowledge. Atoll Res. Bull., 272: 47 pp.

Gallup, C.D., Edwards, R.L., and Johnson, R.G., 1994. The timing of high sea levels over the past 200,000 years. Science, 263: 796–800.

Gvirtzman, G. 1994. Fluctuations of sea level during the past 400,000 years: the record of Sinai, Egypt (northern Red Sea). Coral Reefs, 13: 203–214.

Harmon, R.S., Land, L.S., Mitterer, R.M., Garrett, P., Schwarcz, H.P. and Larson, G.J., 1981. Bermuda sea level during the last interglacial. Nature, 289: 481–483.

Lambeck, K. and Nakada, M., 1992a. Sea-level constraints. Nature, 350: 115–116.

Lambeck, K. and Nakada, M., 1992b. Constraints on the age and duration of the last interglacial period and on sea-level variations. Nature, 357: 125–128.

McNutt, M. and Menard H.W., 1978. Lithospheric flexure and uplifted atolls. J. Geophys. Res., 83: 1206–1212.

Okal, E.A. and Cazenave, A., 1985. A model for the plate tectonic evolution of the east-central Pacific based on SEASAT investigations. Earth Planet. Sci. Lett., 72: 99–116.

Ota, Y., Chappell, J., Kelley, R., Yonekura, N., Matsumoto, E., Nishimura, T., and Head, J., 1993. Holocene coral reef terraces and coseismic uplift of Huon Peninsula, Papua New Guinea. Quat. Res., 40: 177–188.

Pandolfi, J.M., 1995. Geomorphology of the uplifted Pleistocene atoll at Henderson Island, Pitcairn Island Group. Biol. J. Linn. Soc. 56: 63–77

Paulay, G., 1989. Marine invertebrates of the Pitcairn Islands: Species composition and biogeography of corals, molluscs, and echinoderms. Atoll Res. Bull., 326: 28 pp.

Paulay, G., 1991. Henderson Island: Biogeography and evolution at the edge of the Pacific plate. In: E.C. Dudley (Editor), The Unity of Evolutionary Biology, Proc. Fourth Intern. Congr. Syst. Evol. Biology, p. 304–313.

Paulay, G. and Spencer, T., 1988. Geomorphology, palaeoenvironments and faunal turnover, Henderson Island, S.E. Polynesia. Proc. Sixth Intern. Coral Reef Symp. (Townsville), 3: 461–466.

Pirazzoli, P.A. and Montaggioni, L.F., 1986. Late Holocene sea-level changes in the Northwest Tuamotu Islands, French Polynesia. Quat. Res., 25: 350–368.

Purdy, E.G., 1974. Reef configurations, cause and effect. In: L.F. LaPorte (Editor), Reefs in Time and Space. Soc. Econ. Paleont. Mineral. Spec. Pap. 18: 9–76.

Rehder, H. A. and Randall, J.E., 1975. Ducie Atoll: Its history, physiography, and biota. Atoll Res. Bull., 183, 40 pp.

Scoffin, T.P., 1987. An introduction to carbonate sediments and rocks: Blackie & Son Ltd: 274 pp.

Shackleton, N.J. and Opdyke N.D., 1973. Oxygen isotope and palaeomagnetic stratigraphy of equatorial Pacific core V28-238: Oxygen isotope temperatures and ice volumes on a 10^5 and 10^6 year scale. Quat. Res., 3: 39–55.

Shackleton, N.J., 1977. The oxygen isotope stratigraphic record of the Late Pleistocene. Phil. Trans. R. Soc. London Ser. B, 280: 169–182.

Shackleton, N.J., Imbrie, J., and Hall, M.A., 1983. Oxygen and carbon isotope record of East Pacific core V19–30: implications for the formation of deep water in the late Pleistocene North Atlantic. Earth Planet. Sci. Lett., 65: 233–244.

Shackleton, N.J., 1987. Oxygen isotopes, ice volume and sea level. Quat. Sci. Rev. 6: 183–190.

Shackleton, N., Berger, A. and Peltier, W., 1990. An alternative astronomical calibration of the lower Pleistocene timescale based on ODP Site 677. Trans. R. Soc. Edinburgh: Earth Sci., 81: 251–261.

Shackleton, N.J., Hall, M.A., Pate, D., Meynadier, L. and Valet, P., 1993. High-resolution stable isotope stratigraphy from bulk sediment. Paleocean., 8 (2): 141–148.

Spencer, T., 1989a. Tectonic and environmental histories in the Pitcairn Group, Palaeogene to present: Reconstructions and speculations. Atoll Res. Bull., 322: 22 pp.

Spencer, T., 1989b. Sediments and sedimentary environments of Henderson Island. Atoll Res. Bull., 324: 16 pp.

Spencer, T. and Paulay, G., 1989. Geology and geomorphology of Henderson Island. Atoll Res. Bull., 323: 50 pp.

Stein, M., Wasserburg, G.J., Chen, J.H., Aharon, P. and Chappell, J., 1992. Sea-level changes during the last interglacial event - Inferences from TIMS U-series dating of coral reefs. Twenty-Ninth Intern. Geol. Cong., Tokyo 1: 94.

Stein, M., Wasserburg, G.J., Aharon, P., Chen, J.H., Zhu, Z.R., Bloom, A. and Chappell, J., 1993. TIMS U-series dating and stable isotopes of the last interglacial event in Papua New Guinea. Geoch. Cosm. A., 57: 2541–2554.

St. John, H. and Philison, W.R., 1962. An account of the flora of Henderson Island, South Pacific Ocean. Trans. R. Soc. N.Z., Botany, 1: 175–194.

Stoddart, D.R., Scoffin, T.P., Spencer, T., Harmon, R.S., and Scott, M., 1985. Sea-level change and karst morphology, Mangaia (Cook Islands). Proc. Fifth Intern. Coral Reef Congr. (Tahiti), 3: 201.

Stoddart, D.R., Woodroffe and Spencer, T., 1990. Mauke, Mitiaro and Atiu: Geomorphology of Makatea Islands in the Southern Cooks. Atoll Res. Bull., 341, 65 pp.

Weisler, M., Benton, T.G., Brooke, M. de L., Jones, P.J., Spencer, T. and Wragg, G., 1991. The Pitcairn Islands Scientific Expedition (1991–1992): first results, future goals. Pac. Sci. Assoc. Inform. Bull., 43: 4–8.

Woodhead, J.D. and McCulloch, M.T., 1989. Ancient seafloor signals in Pitcairn Island lavas and evidence for large amplitude, small length-scale mantle heterogeneities. Earth Planet. Sci. Lett., 94: 257–273.

Woodhead, J.D. and Scientific Party, 1990. Active Pitcairn hotspot found. Mar. Geol., 95: 51–55

Woodhead, J.D. and Devey, C.W., 1993. Geochemistry of the Pitcairn seamounts, 1: source character and temporal trends. Earth Planet. Sci. Lett., 116: 81–99.

Woodroffe, C.D., Short, S.A., Stoddart, D.R., Spencer, T. and Harmon, R.S., 1991. Stratigraphy and chronology of Late Pleistocene reefs in the southern Cook Islands, South Pacific. Quat. Res., 35: 246–263.

Woodroffe, C.D., 1992. Oceanic islands, atolls, and seamounts: Encyclopedia of Earth System Science, 3: 435–443.

This Page Intentionally Left Blank

Geology and Hydrogeology of Carbonate Islands. Developments in Sedimentology 54
edited by H.L. Vacher and T. Quinn
© 1997 Elsevier Science B.V. All rights reserved.

Chapter 13

GEOLOGY AND HYDROGEOLOGY OF MURUROA AND FANGATAUFA, FRENCH POLYNESIA

DANIÈLE C. BUIGUES

INTRODUCTION TO FRENCH POLYNESIA

French Polynesia covers an area of the South Pacific extending 2,700 km from west to east and 2,300 km from north to south. The total land area of 4,000 km^2 consists exclusively of islands of both volcanic and reefal origin. The population is relatively small, numbering about 180,000 inhabitants.

The French Polynesian atolls of Mururoa and Fangataufa were selected to be France's nuclear test sites in 1966. These sites were chosen because of their isolation and great distance from any inhabited regions. Nuclear testing was carried out in the atmosphere for the first nine years, and then testing shifted to beneath the atolls, first under the rim, in 1975, and then under the lagoon, in 1981. Long-term, detailed geophysical and geological investigations of the two atolls were initiated in 1969. Since the beginning of underground nuclear testing at these two atolls, about 150 drillholes have been bored into the carbonate cap and the volcanic basement of both atolls. Systematic monitoring of the air, water, flora and fauna has been carried out throughout the entire area of Polynesia and not just at the two atolls. Such detailed investigations over a period of 30 years have led to a vast increase in the knowledge of the geologic history and subsurface structure of these atolls (Guille et al., 1993, 1996) as well as their ecosystems (Bablet et al., 1995).

The islands of French Polynesia are grouped into five archipelagoes constituting chains which are more or less parallel in a NW-SE direction. These archipelagoes comprise atolls and emergent volcanic islands, some rimmed by reefs. From north to south they are (Fig. 13-1): the Marquisas, Tuamotu, Society, Gambier and Australes Islands. Except for the Tuamotu Archipelago, the islands within the same archipelago are separated by deep oceanic basins with depths of nearly 4,000 m.

Island origin is generally related to hotspot volcanic activity (Wilson, 1963). Atolls are a result of both subsidence and plate motion, which is caused by movement of the Pacific Plate away from a fixed hotspot. Excluding the Tuamotu Islands, the volcanic ages vary between 0 and 12 Ma, compared to the 40–50 Ma for the Pacific Plate supporting them. The hotspot theory predicts a northwesterly increase in the age of the island chain. The atolls, situated principally at the northwesterly extremity of the trend, are the oldest islands. The rate of plate motion in this area is estimated to be 11 cm y^{-1} (Duncan and McDougall, 1976). Actually only four hotspot zones have been recognized: the Society hotspot, located between Mehetia and Tahiti; the Macdonald Seamount at the origin of the Australes; a hotspot at the southeastern extremity of Marquisas; and one at the southeast of Pitcairn island at

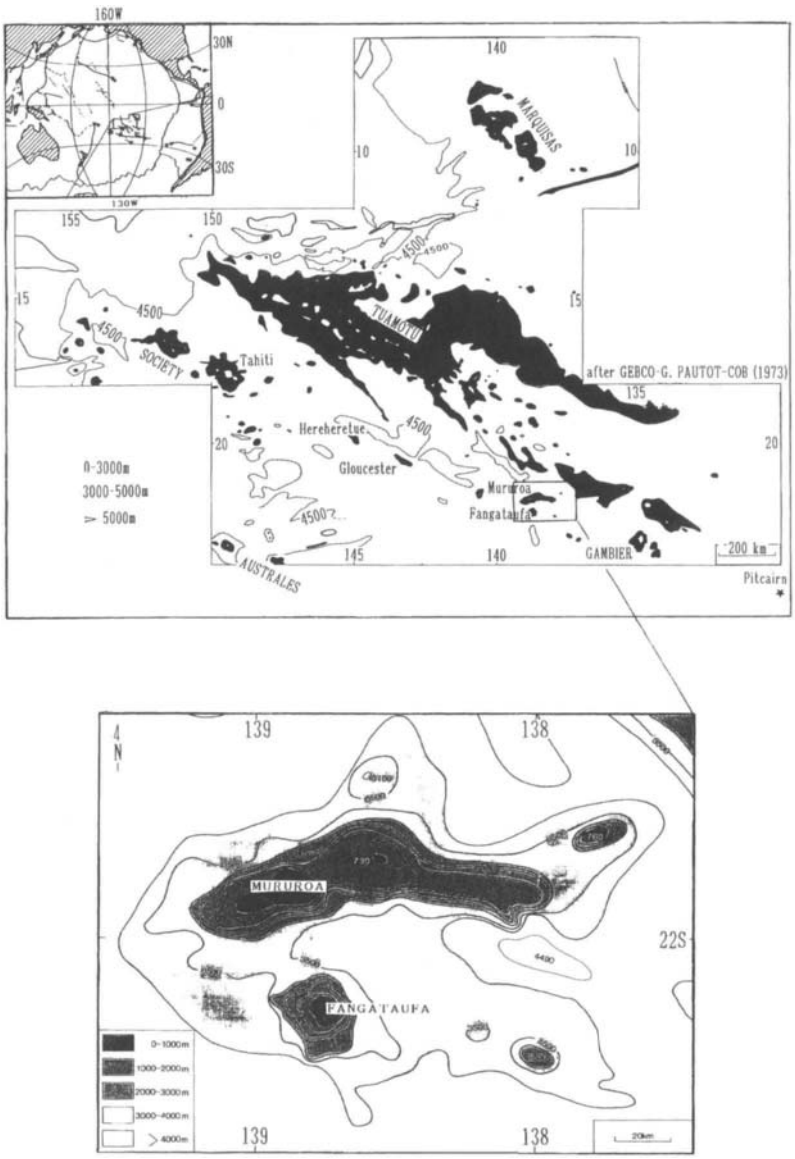


Fig. 13-1. (A) Simplified bathymetry of the islands of French Polynesia. (B) More detailed view of the bathymetry around Mururoa and Fangataufa showing an elongated plateau under Mururoa and a single seamount at Fangataufa. (After Pautot and Monti, 1974.) [See also Fig. 15-1.]

the origin of the Gambier alignment. Although these hotspots display an apparent common origin, each of the five archipelagoes has its own history, which has been influenced by local tectonic events and is reflected by the different arrangement of islands within each archipelago.

The archipelago of the Society Islands is the most like that of a classic island chain formed by hotspot activity. The younger islands (0.5–1.0 Ma) are high aerial volcanoes situated in the southeast near the hotspot zone (Mehetia and Tahiti). To the northwest, the volcanic islands have begun their submergence; all that remain are reduced central volcanic tops rimmed by fringing reefs, a lagoon, and a barrier reef (e.g., Moorea and Maupiti). In the extreme northwest, the volcanoes are completely submerged and reefs have developed, forming classical atolls (e.g., Bellinghausen).

The Australes Islands archipelago, which is extended in the northwest by the Cook Islands [q.v., Chap. 16], consists of emergent volcanic islands locally surrounded by fringing reefs and by emergent carbonates, which most likely were once fringing reefs (e.g., Rurutu). The volcanic ages are inconsistent with the classical hotspot theory; in the Australes, young ages (1–1.8 Ma) coexist with old ages (12.5 Ma). A potential explanation may be the possible existence of several hotspots along the same line (Bonatti et al., 1977; Turner and Jarrard, 1982).

The Marquisas is the only archipelago in which a modern barrier-reef ecosystem has not developed. Submerged reefs, however, have recently been recognized (Rougerie et al., 1992). The general direction of the archipelago does not coincide with the other four. Its origin is attributed to hotspot activity at the Marquisas Fracture Zone, a major WSW-ENE discontinuity of the Pacific Plate.

Tuamotu is a more diverse archipelago and comprises solely atolls supported by a volcanic plateau at −2,000 m. The volcanic pedestal of the atolls of the Tuamotu is considered to have been generated by a hotspot located at the East Pacific Rise.

The Gambier Islands extend from southeast to northwest, from Pitcairn to the atoll of Hereheretue (Fig. 13-1). The islands have been generated by a hotspot located at the southeast of Pitcairn Island. The volcanic basements of Mururoa (21°50′S, 138°53′W) and Fangataufa (22°14′S, 138°45′W), located at the southeastern extremity of the Tuamotu Archipelago (Fig. 13-1), were created when the Pacific Plate moved over the hotspot zone currently located 70 km to the southeast of Pitcairn Island. Volcanic activity ceased around 11–10.5 Ma at Mururoa (Gillot et al., 1992) and 10–9.5 Ma at Fangataufa (Guillou et al., 1990). Moreover, although they were generated by the same hotspot, their volcanic basements differ both geochemically and structurally. Thus the origin of Mururoa is related not only to a hotspot, but also to a major WSW-ENE discontinuity of the Pacific Plate (the Australes Fracture Zone). In contrast, Fangataufa was a classical seamount generated only by hotspot activity (Fig. 13-1).

MORPHOLOGY

Geological and geophysical surveys were initiated in 1969 and have provided abundant data on the deep structure, morphology and lithology of the atolls of Mururoa and Fangataufa (Buigues et al., 1992, Guille et al., 1993; 1996). Geological investigations have been carried out on samples from numerous wells, drilled both vertically and with seaward deviations of 30–45°. The subsurface of both atolls

contains a discontinuous record of sedimentation and atoll growth subsequent to the cessation of volcanic activity.

Zones of volcanic emissions or "rift-zones", which have been identified by magnetic surveys, constitute the basement of these islands. These zones are elongated and parallel to the Australes Fracture Zone at Mururoa and are nearly radial at Fangataufa. The latter pattern is more typical of a classical seamount.

Differences in size and shape of the atolls (Fig. 13-2), as seen in aerial view, reflect differences in their volcanic basements. Mururoa is wider (155 km^2) and elongated with a large natural pass. Fangataufa (45 km^2) is almost hexagonal in shape and is a naturally closed atoll. Mururoa began not far from the Australes Fracture Zone and developed into a complex volcanic edifice with rift zones parallel to the Austral Fracture Zone. Fangataufa initiated in a manner more typical of a hotspot volcano having a single volcanic edifice with radial rift zones, which produced an overall "starfish" morphology (Fig. 13-1).

The three-dimensional morphologies of the two underlying volcanic edifices are different (Fig. 13-3). Mururoa has two volcanic tops connected by an isthmus, and Fangataufa has a unique, tabular, flat cone. The different initial architectures (the rift zones), as well as the different (terminal) morphologies of the volcanic edifices, have influenced the deposition of the sedimentary sequence since the initial stages of sedimentation. Thus, at Mururoa, the elongated shape, and probably the great size,

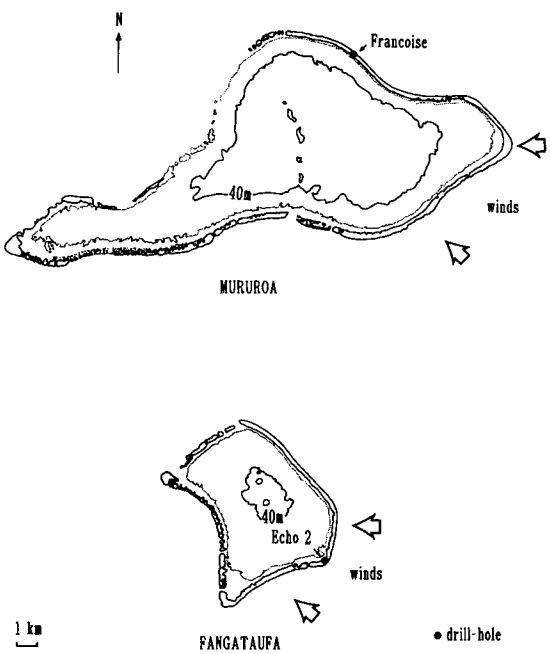


Fig. 13-2. Simplified bathymetry of the lagoons at Mururoa and Fangataufa. The solid line inside the lagoon at Mururoa denotes the 40 m isobath.

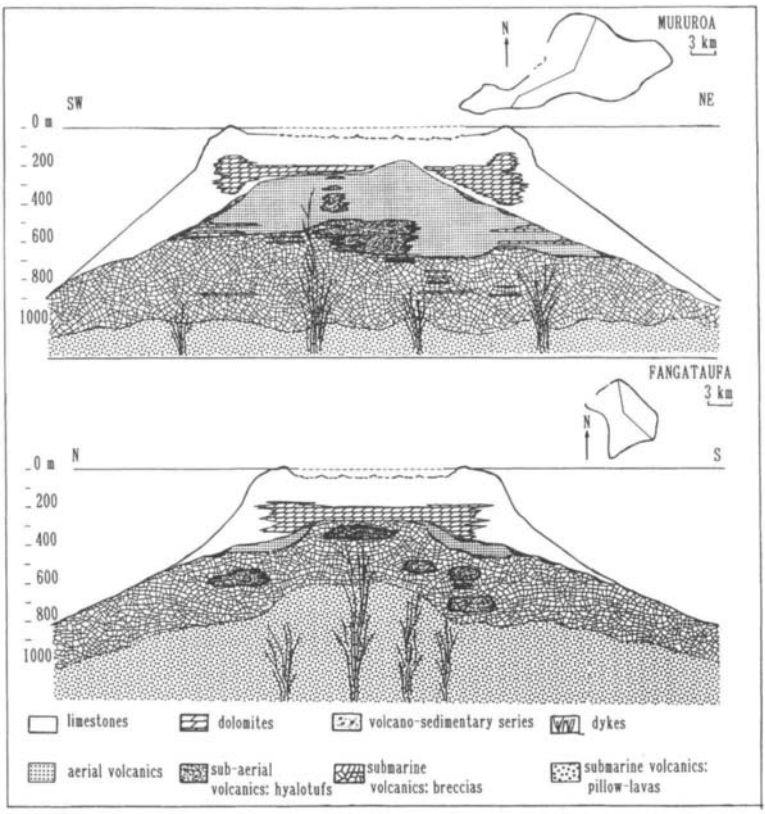


Fig. 13-3. Lithology of the two atolls Mururoa (top) and Fangataufa (bottom). Note the different shape of the volcanic basements, the divergences in the submarine volcanics under the lagoon, and the geometry of the dolomite body.

of the volcanic basement likely influenced the development of a wide (4.5 km) natural pass in the atoll above the volcanic isthmus. Coral colonization and sedimentation also differ in both lagoons. Turbid depositional conditions dominate at Mururoa in the part of the lagoon facing the pass (Buigues et al., 1993), whereas a greater number of patch reefs and pinnacles occur in the closed atoll of Fangataufa. The lagoon is also deeper at Mururoa (55 m) than at Fangataufa (42 m).

Despite the differences between the two atolls, there are obvious similarities in their depositional histories. For example, the atoll-rim morphology, which depends on oceanographic and climatological conditions, is in both cases strongly influenced by the oceanic swell from the southwest and the prevailing winds from east, northeast and southeast. On both atolls, therefore, the emergent atoll rims are continuous and well cemented on the north and east, and discontinuous on the south and west where they are characterized by islands ("motu") and numerous passages ("hoa") (Fig. 13-2).

GEOLOGICAL UNITS

Volcanic basement rocks

Evolution and growth of the volcanic basement were controlled mainly by the initial structure of the Pacific Plate. The present-day morphology of the atolls, therefore, reflects the discontinuities of the oceanic bottom which favored rift-related volcanism. The submarine volcanic basement of both atolls, penetrated by drilling to depths of 1,100 m, consists of pillow lavas and associated breccias, autoclastites and hyaloclastites. The morphology of the submarine series differs between the two atolls: there is a nearly tabular top at −500 to −550 m at Mururoa, and a culmination up to −270 m under the lagoon of Fangataufa. In some parts of the volcanic section, hyalotuffs mark the transition from the submarine to the subaerial series. The latter series consists of massive lavas and scoriaceous products and is particularly thick (300–400 m) under the lagoon of Mururoa; however, it is absent under the lagoon of Fangataufa (Fig. 13-3). Aeromagnetic studies of both atolls reveal the existence of emissive or rift zones which contain numerous dikes. At Mururoa, some massive intrusive rocks (trachytes) have been recovered from under the lagoon and from under the central southern rim, Viviane Island (Fig. 13-2), where a volcanic depression is considered to be either a caldera or a side-slump (Buigues et al., 1992).

In both atolls, the volcanic rocks are affected by early stages of hydrothermal alteration due to basalt-seawater chemical interaction. The effect is more pronounced at Fangataufa (Dudoignon et al., 1992, Dudoignon oral comm., 1994).

The entire volcanic sequence at Mururoa constitutes a typical moderated alkaline series with various products including basalts and trachytes. At Fangataufa, the geochemistry of the volcanic rocks is different: the submarine products are mainly tholeiitic, and the subaerial ones are alkalic. Moreover, the occurrence of differentiated products is rare in Fangataufa.

Intercalated transitional sequence

The discontinuous nature of the construction of the volcanic basement is indicated by disconformities in the submarine volcanic emissions, erosive surfaces with argillaceous products, or, more often, with some spectacular carbonate-rich layers, particularly at Mururoa (Gachon and Buigues, 1985; Berbey, 1986; Figs. 13-4, 13-5). These carbonate-rich layers contain corals which appear both as debris and massive boundstones. All such occurrences indicate that the volcanic basement was colonized by corals before the final cessation of volcanic activity and, therefore, that the submarine lavas were erupted not far below sea level. Above the more productive rift zones, the carbonate-rich layers occur only as coral-debris deposits enclosed in the volcanic rocks. At Mururoa, except near these zones, the carbonate-rich layers occur both under the lagoon and under the rim. At Fangataufa, the carbonate-rich layers occur only as coral-debris deposits enclosed in volcanic rocks under the rim of the atoll.

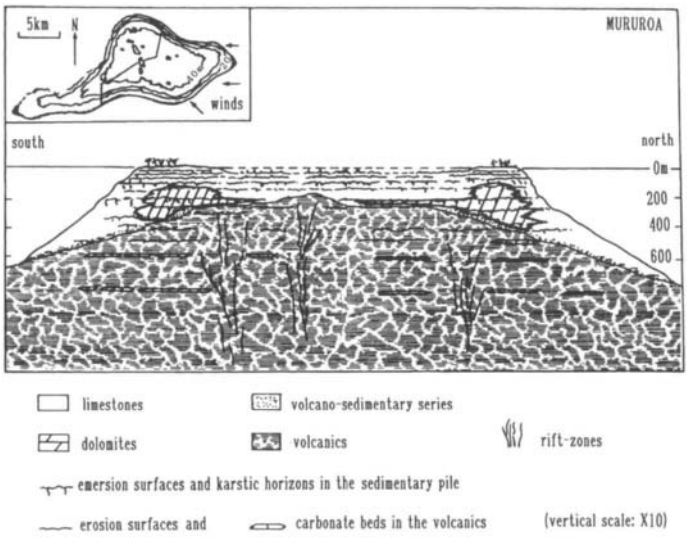


Fig. 13-4. Lithology and discontinuities at Mururoa.

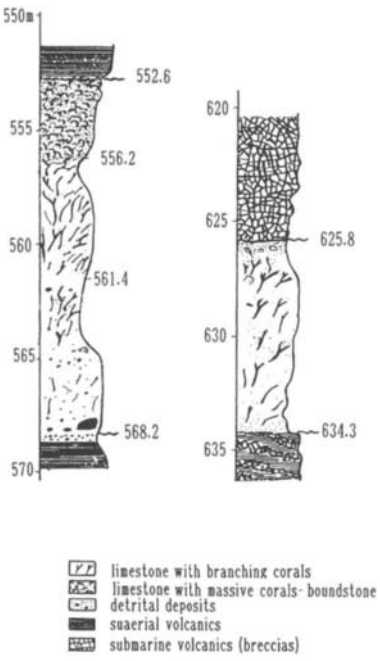


Fig. 13-5. Comparison between two upper-reef horizons intercalated with the volcanic sequence at Mururoa. (From Gachon and Buigues, 1985.)

The deepest occurrence of carbonate rocks is about −950 m (at Mururoa) in the upper 1,000–1,100 m of section that has been investigated from both atolls. The volcanic sequence is 25–100 m thick between the carbonate-rich layers. The shallowest occurrence of carbonate rocks in both atolls marks the transition between submarine and subaerial volcanism. This major transition in volcanic style occurs at about −500 to −550 m. At the northern rim of Mururoa, this depth also marks the location of a spectacular, 15-m-thick carbonate-rich layer (Fig. 13-5).

The thickest intercalated carbonate layer occurring at the periphery of Mururoa (−553 to −568 m) is initiated by a transgressive sequence similar to those found in the volcano-sedimentary series lying above the subaerial volcanics. From a basal section of intercalated volcaniclastics and carbonate-rich rocks, the sequence evolved into a pure carbonate sequence concurrently with the progressive colonization of corals, first by branched forms and then by massive corals, which formed a coral boundstone deposit at the summit. In other layers, the sequences are incomplete and interrupted by erosive surfaces with secondary marine infillings indicating periods of atoll submergence.

The carbonate mineralogy consists of low-Mg calcite and a small amount of dolomite (a few to up to 15%) occurring only in the matrix. Dissolution is common and affects both the corals and the matrix. Cementation is sparse and occurs as sparry or fibrous low-Mg calcite in the cavities of dissolved corals (Berbey, 1986). The lack of metastable carbonates and the dissolution of low-Mg calcite are consistent with the hypothesis that these carbonate rocks have undergone diagenetic alteration under the influence of meteoric water, perhaps in the meteoric phreatic zone. The change in the porewater composition from marine to freshwater may be related to variation in sea level or local tectonic activity. Similar stratigraphic elevation of these carbonate-rich layers — especially the shallowest occurrence — in these two atolls suggests that variations in sea level are responsible for the diagenesis of these layers. Where present, however, evidence of erosive episodes and marine incursions (drownings) may indicate local tectonic activity which was specific to each atoll.

The sedimentary series

Seismic studies have provided much information about the main architecture of the upper volcanic rock sequence and of the sedimentary pile under the lagoon (Ruzié and Gachon, 1985). Several seismic horizons observed in the sedimentary lagoonal sequence correspond to the tops of the different diagenetic units identified from the cores, particularly the dolomitic body near −190 to −210 m. High-resolution seismic studies have allowed the mapping of the different indurated horizons in the limestone sequence and permit this sequence to be subdivided into two main series: an upper series, (50–70 m thick), in which the indurated horizons are discontinuous, and a lower series, (50–80 m thick), where the indurated horizons are more laterally extensive. In the western part of the subsurface of Mururoa, the lower carbonate series has a westward dip that may be related to regional tectonic activity.

The distribution of the sedimentary series, as well as the distribution of the intercalated transitional sequence, is directly related to the structures present in the deep volcanic rock sequence. At Fangataufa, the regular tabular shape of the volcanic basement favored the development of a shallow-water carbonate "platform" above the whole volcano. At Mururoa, a tabular-shaped volcanic formation existed only above the volcanic isthmus; therefore, carbonate rock deposition was initiated on that isthmus before expanding to cover the rest of the volcanic basement. The overall constitution of the sedimentary pile is similar in both atolls: the thickness is 330–570 m beneath the rim and 130–230 m beneath the lagoon; the structure contains two main units, a basal volcano-sedimentary series and a pure carbonate rock sequence above. The entire sedimentary series at both atolls contain numerous discontinuities, the more spectacular ones coinciding with karstic horizons (Buigues, 1982; Buigues, 1985).

Basal volcaniclastics. The basal volcaniclastic sequence accumulated above both volcanic basements concurrently with cessation of the major volcanic activity and presumably a little later in the center than in the periphery (Berbey, 1989). The thickness of this sequence depends on the residual volcanic topography, varying progressively from 80–100 m at the periphery to zero at the center. The thickest and most argillaceous deposits are located in the volcanic valleys.

Despite differences in residual volcanic morphologies, the processes for coral colonization were similar on both atolls. Under the rim, the superposition of typically transgressive sequences indicates a discontinuous buildup in response to changes in sea level. At their base, the sequences are generally composed of volcanic conglomerates. Progressively upwards, the volcaniclastics are reduced to thin sandy layers; the various corals, which have appeared since the initial stages, become more important and form massive boundstones. In some places, argillaceous soils, formed during subaerial exposure of the platform, document periods of atoll emergence. The last detrital volcaniclastics are presently located at the same depth in both atolls, approximately at −300 m under the rim, and −270 to −280 m under the lagoon.

As in the underlying carbonate-rich layers intercalated with the volcanic rocks, aragonite and high-Mg calcite are absent in the basal volcaniclastic sequence. Carbonate rocks in this sequence are mainly low-Mg calcite and dolomite, the latter in abundance up to 25%. The products of dissolution, cementation and karstification are typical features. The cements that do occur are fibrous and are sparry low-Mg calcite containing microscopic dissolution features (Berbey, 1989). The dolomite occurs regularly in layers 0.1–1 m thick. Sometimes both calcite and dolomite coexist, an occurrence that may suggest that the "dolomitizing" fluids had met some dynamic physico-chemical front.

The sedimentary sequence contains diagenetic fabrics and products that are consistent with diagenetic alteration of limestones in the meteoric environment during intermittent periods of atoll emergence. Because the major sedimentary discontinuities occur at the same depth at both Mururoa and Fangataufa, it is probable that such periods of atoll emergence were related to changes in sea level.

The carbonate cap. The thickness of the carbonate cap varies from 300–500 m at the periphery to 120–220 m at the center. The lower two-thirds of the carbonate cap under the rim and the lagoon is completely dolomitized; however, dolomite is irregularly distributed or absent near the periphery of the atoll. The differences in the shape of the underlying volcanic edifice at the two atolls is the cause of the variation in the geometry of the dolomite body. The top of the dolomite body is located between −190 and −210 m in the subsurface of both atolls. At Mururoa, the dolomitic series disappears at the center of the atoll, above the highest volcanic top at −170 to −180 m. At Fangataufa, the dolomitic series is distributed beneath the entire lagoon and above the flat volcanic top, located close to −270 m.

Drilling at multiple sites from the center of the lagoon to the external rim has recovered material from a great diversity of sedimentary facies. Facies types identified from core material include: coralgal and boundstone facies, which are typical of the reef crest; bafflestone facies, which are typical of sheltered areas; detrital deposits from various environments (deep forereef areas, reef flats and lagoonal beaches); and muddy facies, some typical of the lagoon and some with plate-like corals typical of deep sheltered areas (deep lagoon and/or forereef areas).

At the periphery, abundant slope deposits occur, as does pelagic infilling of karst features. The latter is evidence of drowning of a once-emergent platform. These sedimentary facies document that the architecture of these atolls has undergone major morphological change during the evolution of the atolls. Indeed, the classical atoll morphology is only a relatively late development in the evolution of these atolls (Buigues, 1985).

The carbonate cap contains numerous sedimentary discontinuities, which are mostly at the same depth on the two atolls (Guyomard, 1990). Some of these discontinuities are soil horizons, but more frequently they are karstic surfaces (Guyomard, 1990). In the upper 80–100 m, karstification is more important under the rim than under the lagoon. Below that depth, the karstification is present under the whole atoll. In the upper series, the karstic surfaces under the rim are correlated to more-or-less lithified horizons under the lagoon. Under the rim, the first karstic surface, which indicates the Holocene/Pleistocene boundary, occurs between −6 m and −15 m. Under the lagoon, the thickness of the Holocene deposits is 0–20 m. The top of the Pleistocene, therefore, is a heterogeneous surface with some weak and scattered marine lithification (Buigues, 1982).

In the subsurface of each atoll, the most important dissolution and karstic features occur beginning at −90 to −100 m, with some especially spectacular karst infillings at the periphery. This karstification extends down to −150 m both under the lagoon and the rim. The most important karst surface under both lagoons affects the limestone-dolomite transition at −180 to −200 m, and the base of the dolomitic body close to −250 to −270 m. This is particularly true at Fangataufa, where the volcanic top is flat and occurs at −270 m. Generally, the whole series is karstified under the rim; however, especially prominent karstic surfaces occur between −220 m and −280 m. Such surfaces clearly document periods of atoll emergence. These surfaces are laterally correlated to discontinuities in the center of the edifices in both atolls. Probably, they mark regional events related to sea-level variations.

The most impressive karst surface under the rim is situated at the base of the series, around −310 to −350 m. This karst episode affected the massive basal dolomites, which are red colored and contain meter-sized cavities with successive deposits of marine infillings, documenting a complicated paragenesis. At the periphery of the atolls, beautiful karstic infillings document the submergence of these once-emergent carbonate islands in response to Pleistocene sea-level variations.

The mineralogy of the carbonate cap changes from coexisting metastable carbonate phases (aragonite and high-Mg calcite) near the surface to low-Mg calcite and dolomite at the base (Buigues, 1982). Typically, brown low-Mg calcite occurs in the upper karstic surfaces of the carbonate cap. The dolomite has a marine isotopic signature and imbricated dissolution fabric which suggest the presence of an extended aquifer. Dolomite likely precipitated from a fluid of mixed-water (freshwater and seawater) composition (Buigues, 1982; Aissaoui et al., 1986). At the periphery, spectacular fibrous calcite cements and some massive botryoidal aragonite, both of marine origin, massively consolidate the upper 400 m of the atoll rims. Dissolution is the predominant feature in the carbonate cap of these atolls, and even the peripheral marine cements exhibit some evidence of dissolution (Aissaoui, 1988).

CHRONOLOGY OF CARBONATE ACCUMULATION

Age determinations by classical methods (^{14}C and U/Th) and by magnetostratigraphy are available from materials collected vertically from the upper 300 m of the carbonate cap and laterally behind the reef wall from the deviated wells (Labeyrie et al., 1969; Buigues, 1982; Hoang, oral com., 1986; Aissaoui and Kirschvink, 1991 and Aissaoui intern. report, 1991). Because of the uncertainties of the duration of the numerous periods of atoll emergence and of the rate of subaerial erosion, the results obtained by magnetostratigraphy may be considered as suggestive. This method of age determination, however, provides constraints on the succession of different periods of vertical atoll growth (accretion) and deviations from this growth as related to changes in accommodation space (interaction of sea-level change and subsidence) (Fig. 13-6).

Age determinations of the carbonate rocks permit the reconstruction of the history of vertical and lateral variability that occurred in the development of these carbonate-capped atolls. Starting with the most recent, the accumulation history of these atolls includes:

(1) Holocene deposition of carbonate sediments of variable thickness ranging from some few meters to 10–20 m. The latter values occur in the lagoon.

(2) Karstification of the subaerially exposed Pleistocene carbonate island. Under the atoll rim, the Pleistocene deposits are about 50 m thick; they are interrupted by laterally discontinuous subaerial exposure surfaces, and, in some locations, karstic horizons. Under the lagoon, Pleistocene deposits have presumably the same thickness as under the rim, but they are less lithified and contain sedimentary discontinuities corresponding to the subaerial exposure surfaces and karstic horizons of the rims. In the lagoon subsurface, however, there is no evidence of the ~120-ka sea-

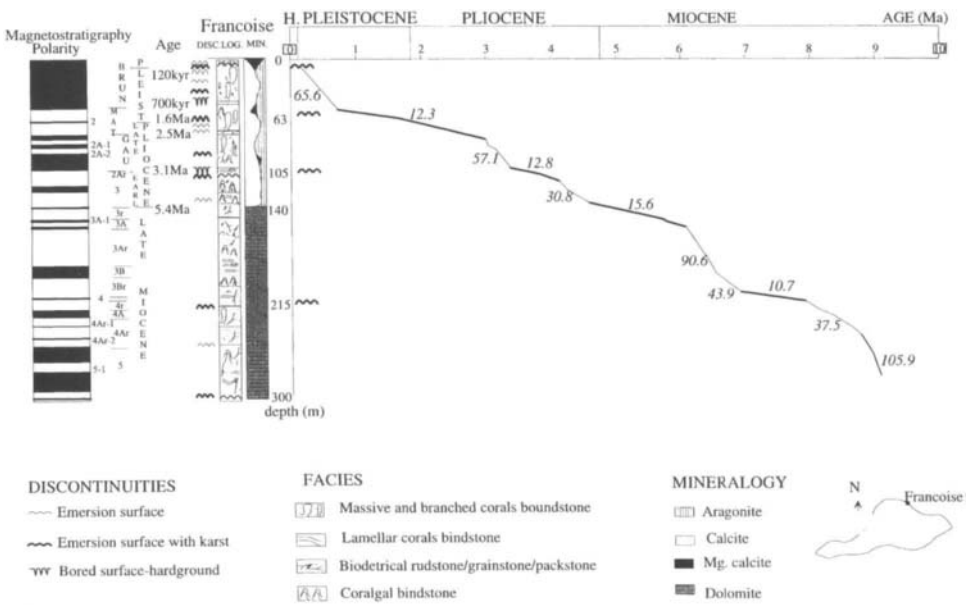


Fig. 13-6. Magnetostratigraphy from the upper 300 m of the rim at Mururoa with relative accumulation rates. (Modified from Aissaoui and Kirschvink, 1991.)

level highstand. At the periphery, behind the vertical wall, the thickness of the Pleistocene deposits is at least 150 m. These deposits, generally slope facies, consolidate the underlying series.

(3) Deposition of Pliocene deposits. Under the rim, these deposits occur between −50 to −70 m and −120 to −150 m (i.e., top of the dolomitic unit), whereas these deposits likely occur between −70 to −90 m and −190 to −210 m (i.e., top of the dolomitic unit) under the lagoon. The Pliocene sequence is better lithified than the overlying Pleistocene sequence and, like the latter, contains karstified topography, with karstification generally more important at the periphery than at other regions. Karst horizons are especially evident below −140 to −150 m. The Pliocene sequence under the rim contains large, laterally extensive, subaerial exposure surfaces and karstic horizons.

(4) Diagenetic alteration of pre-Pliocene deposits. The whole dolomitic series, possibly of Miocene age, contains the most laterally extensive karstic horizons, from the periphery (−230 to −250 m) to the center of the lagoons (−280 m) and the most spectacular karst of the whole sedimentary pile (−300 to −350 m under the rim of Mururoa, −180 to −200 m under the two lagoons).

SUBMARINE OBSERVATIONS

Submarine investigations around the flanks of Mururoa, to maximum depths of 1,200 m, by a R.O.V. (Remote Operated Vehicle) submarine have provided much

information about the history of this atolls. Submarine observations include: (1) terraces at −10, −20, −40 and −55 to −65 m; (2) a vertical wall between −110 to −120 m and −200 to −230 m; and (3) "cave"-like heterogeneities, at −80 to −90 m and −120 to −150 m. Terraces are interpreted to be the former tops of the carbonate platform developed during the Pleistocene and probably the Pliocene. The existence of a vertical wall along the flank of a carbonate island has been observed at many other sites — Enewetak (Colin et al., 1986); Bahamas (Hine and Mullins, 1983; Grammer and Ginsburg, 1992); Belize (James and Ginsburg, 1979); The Red Sea (Dullo et al., 1990); Mayotte (Thomassin, oral comm., 1992); Tahiti (Ifremer, intern. report, 1983; Salvat, 1986). Cave formation is interpreted to record former sea-level positions, with the one at 120–150 mbsl being a record of the last glacial maximum (18 ka). Combining these submarine observations with data generated through analyses of core material derived from deviated wells allow constraints to be placed on the geometry of the Pleistocene and Holocene deposits at the periphery of the atoll (Fig. 13-7).

GEOLOGIC EVOLUTION OF MURUROA AND FANGATAUFA

The earliest occurrence of sedimentary rock deposition at these atolls produced the carbonate-rich units that are intercalated with the volcanic rocks, and these carbonate-rich units may correspond to fringing reefs and, presumably, barrier reefs developed around the volcanoes. The transition from pure volcanics to carbonate sedimentation and reef growth is marked by sands and mixed-sedimentary deposits.

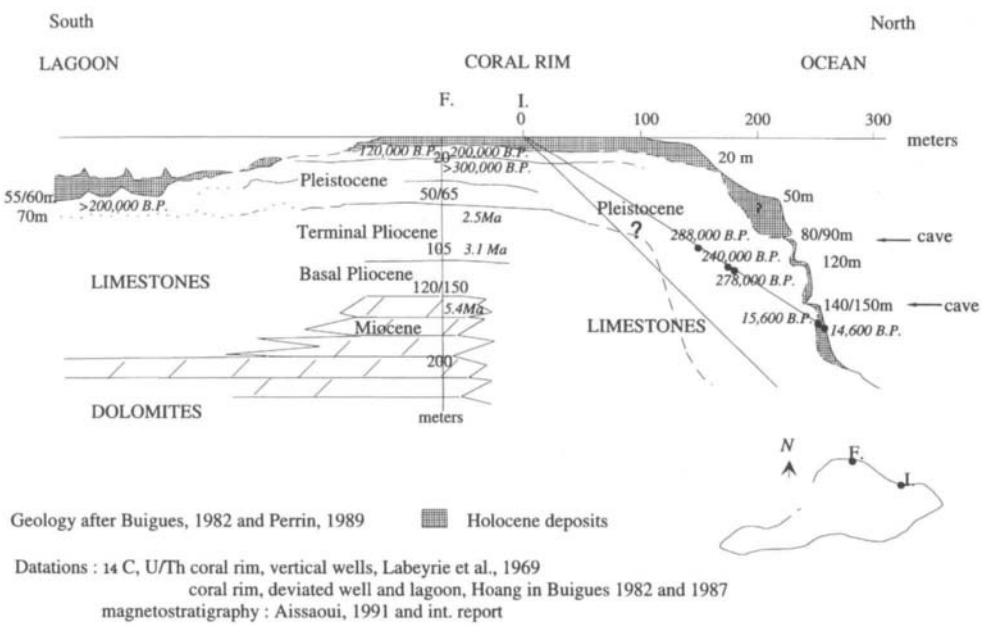


Fig. 13-7. Submarine observations (R.O.V.) and age determinations (^{14}C, U/Th) at Mururoa. Note the thickness of the Pleistocene deposits behind the reef wall is at least 150 m.

Diagenetic features in these earliest carbonate deposits attest to a period of emergence at or near their time of deposition, roughly at 12–11 Ma. With the passage of time, the volcanic discharges completely ceased and the volcanoes subsided.

Deposition of purely sedimentary rocks began shortly after the end of volcanic activity, about 10.5 Ma at Mururoa and 9.5 Ma at Fangataufa. The accumulation and buildup of the sedimentary piles at both atolls was discontinuous and controlled mainly by terminal volcanic morphology, local tectonic activity and successive sea-level variations. Fringing and barrier-reef development was certainly discontinuous, reflecting the volcanic topography; for example, there was no reef formation facing the major volcanic valleys. The "lagoons" may have been restricted in area and may have had minimal water depths.

An extensive carbonate platform covering the entire volcanic basement developed, perhaps as late as the Pliocene. Successive periods of emergence occurred during the Pliocene and during the Pleistocene, which led to intensive karstification of these two carbonate islands. The present rims of these atolls developed during the Pleistocene by lateral aggradation in response to successive sea-level variations (Perrin, 1990). Thus the present unique lagoon has been progressively created by restriction of the "platforms" and their drowning under detrital deposits (Buigues, 1985).

HYDROGEOLOGY

Thermal state of the massif

The temperatures existing within the atoll massif have been measured from numerous drillholes on both Mururoa and Fangataufa. In ocean waters, temperatures decrease rapidly from the surface (about 25°C) down to 450 m (about 10°C), and then more gradually towards greater depths (Fig. 13-8). Under the rim of the atoll, temperatures also decrease with depth within the carbonate formations; however, this negative temperature gradient is less steep than that observed in the ocean profile. At greater depths within the volcanic sequence, the thermal gradient is normal (increasing with depth) and relatively small. Under the lagoon, temperatures similarly decrease with increasing depth in the carbonates, but the gradient is less steep than under the rim. Within the volcanic sequence, the geothermal gradient becomes positive but is larger than that measured beneath the atoll rim. Hence, the proximity of cold ocean waters clearly influences the thermal gradient in the carbonate sequence beneath the rim. Near the top of the volcanic sequence, however, the thermal gradient becomes normal and within the volcanic sequence, the oceanic influence is not apparent. This thermal contrast likely is the result of the different permeabilities of the carbonate sequence relative to the volcanic sequence.

Permeability data

A special experimental protocol for the measurement of borehole permeability and extraction of the associated porewaters has been developed for exploratory

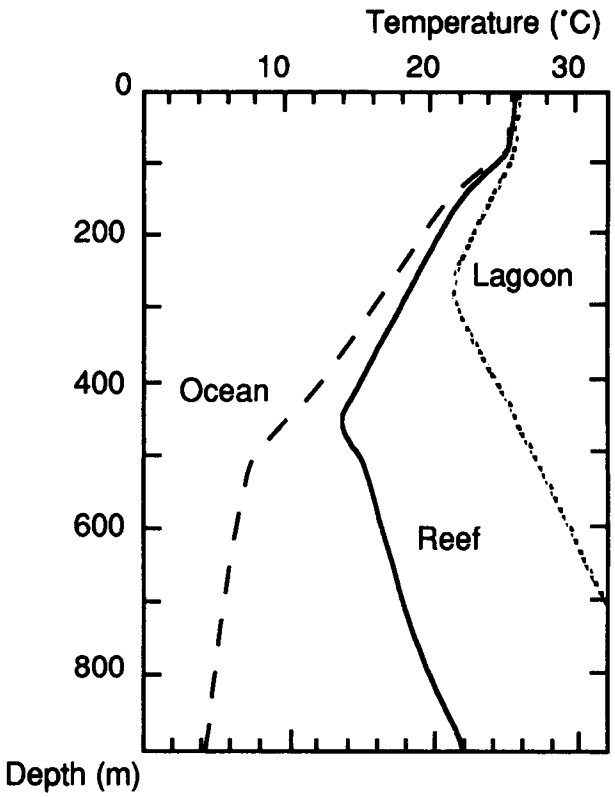


Fig. 13-8. Profiles of temperature vs. depth at Mururoa and Fangataufa. (From Guille et al., 1993, 1996.)

drillholes in both atolls. Details of this experimental protocol are discussed by Guille et al. (1993, 1996). Briefly summarized, the selected drilled intervals are isolated with packers that ensure a connection with the inside of the drill pipes, and submerged pumps draw porewaters from the rocks (Fig. 13-9). In the volcanic sequence, the permeability varies from 10^{-16} m^2 to 10^{-13} m^2 with an average of 10^{-14} m^2. Permeability variations are related to the different volcanic textures, which vary from impermeable massive lavas or argillaceous breccias to more permeable scoriaceous products.

Permeability is more variable in the carbonate sequence than in the volcanic sequence. At the sample scale, permeability can be almost nil in the hard crystalline dolomites or in certain highly cemented limestones. Permeability can also be very high, as in the sands or in porous chalky carbonates that are both calcitic and dolomitic.

At the atoll scale, permeability depends greatly on the horizontal and vertical structures present in the subsurface. Horizontal features that influence permeability include sedimentary and diagenetic discontinuities and karstic horizons; the latter are most important. Fractures, especially at the periphery of the atoll are the most

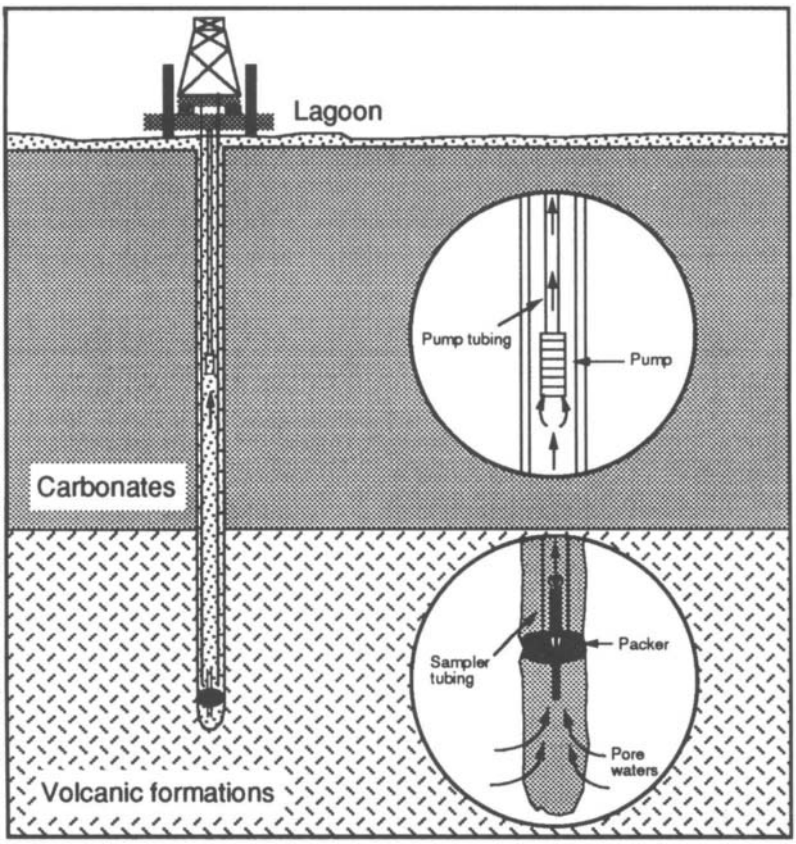


Fig. 13-9. Procedure for porewater sampling and permeability determination. The test cavity is isolated by means of a packer and drawdown is achieved by drawing off the waters in the well by means of a submerged pump. (From Guille et al., 1996.)

important vertical features that affect permeability. Total average permeability for the carbonate sequence is on the order of 10^{-11} m^2, which is a medium to high value that strongly contrasts with the low or very low values measured in the volcanic rocks (10^{-14} m^2).

Thermal exchange with oceanic waters

The large permeability of the carbonate sequence allows fluid circulation within the atoll subsurface and promotes thermal exchange between oceanic waters and subsurface fluids by convection. Geothermal heating of subsurface porewaters in the central interior of the atolls makes these waters less dense. Where the permeability is sufficiently high, these fluids are able to rise in the subsurface and are replaced laterally by the inflow of cold ocean water.

A two-dimensional model, first described for Enewetak (Samaden et al., 1985), has been developed for calculating the thermal and fluid fluxes between the massif and the ocean. This model is based on a simplified geometry of the system and uses the average properties of the different formations (i.e., permeability and thermal characteristics) as well as the boundary conditions imposed by the system (i.e., the temperature and pressure distribution of the ocean, the temperature measured at −1,100 m in the atoll subsurface, and symmetry about the center of the atoll). Calculations provide the steady-state temperature and the flow rate at all points of the model.

Fig. 13-10 shows an example of two-dimensional modeling of isotherms within the atoll and along a cross section through the center of the atoll. For this case, the permeability of the volcanics sequence was set to 10^{-14} m^2 and that of the carbonates to 10^{-11} m^2 for the lower part (dolomites) and 10^{-12} m^2 for the upper part (limestones). The calculated isotherms are in good agreement with the down-hole profiles, particularly with regard to the inversion at the top of the volcanic sequence which is very well marked at the periphery. Moreover, this modeling provides evidence of a centripetal flow in the carbonate sequence: cold oceanic waters are brought from the flanks of the atoll upwards towards the lagoon. The flow rates reach maximum values under the rim at the base of the carbonate sequence with calculations indicating a specific discharge of the order of 1 cm day^{-1} for this locality. These modeling results have been used to support the endo-upwelling concept (Rougerie and Wauthy, 1993; see Chapter 15 of this book).

The calculated flow within the volcanic sequence is very low (on the order of 1 cm y^{-1}) compared with the carbonate sequence. Thus, the transfer of heat within the volcanic sequence takes place only by conduction. If the permeability is increased, for example to 10^{-13} m^2, the calculated centripetal flow is also increased and produces a significant cooling of the atoll subsurface by convection which is in conflict with the measured temperature profiles.

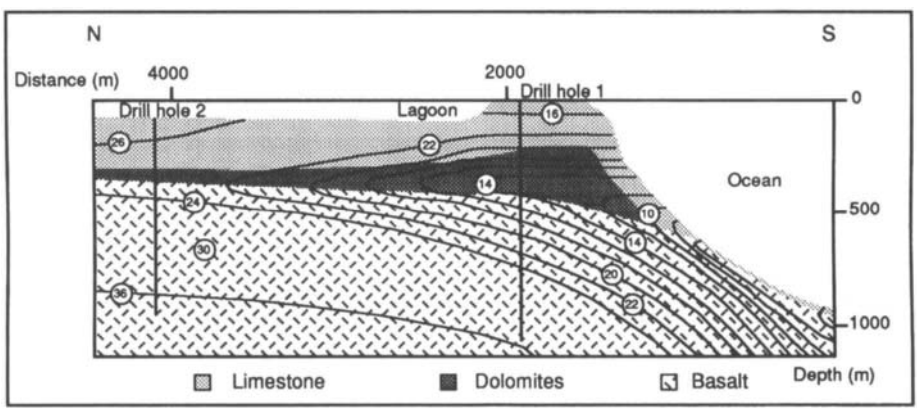


Fig. 13-10. Modeling of thermal exchange between the massif and the ocean at Mururoa. (From Guille et al., 1996.)

In conclusion, numerical modeling of the convective and conductive heat transport within Mururoa and Fangataufa provides general support for the estimates of the distribution of permeability on the scale of the atoll.

CONCLUDING REMARKS

The French Polynesian islands of Fangataufa and especially Mururoa have been intensively studied using a multitude of techniques (e.g., subsurface drilling, seismic, submarine observations) for over two decades. The geologic deposits on these islands document the transition from active hotspot volcanism, cessation of volcanism and subsidence marked by the deposition of volcaniclastic rocks intercalated with carbonate rocks, and finally the deposition of a carbonate cap. The limestones and dolomites of the carbonate cap preserve a record of the complex interaction between late Cenozoic sea-level change, carbonate deposition, diagenesis and tectonic subsidence. The integration of hydrogeologic modeling with petrologic observations at Mururoa has led to the development of a conceptual model of carbonate-island diagenesis and hence to an advancement of knowledge in both these two fields.

REFERENCES

Aissaoui, D.M., 1988. Magnesian calcite cements and their diagenesis: dissolution and dolomitization, Mururoa Atoll. Sedimentol., 35: 821–841.

Aissaoui, D.M., Buigues, D. and Purser, B.H., 1986. Model of Reef Diagenesis: Mururoa Atoll, French Polynesia. In: J.H. Schroeder and B.H. Purser (Editors), Reef Diagenesis, Springer Verlag, Berlin, 27–52.

Aissaoui, D.M. and Kirschvink, J.L., 1991. Atoll magnetostratigraphy: calibration of their eustatic records. Terra Nova, 3: 35–40.

Bablet, J.P., Gout, B. and Goutière, G., 1995. Les atolls de Mururoa et Fangataufa (Polynésie française): III, Le milieu vivant et son évolution, 306 pp.

Berbey, H., 1986. Les épisodes carbonatés miocène dans le volcanisme de Mururoa (Polynésie française). D.E.A., University of Paris XI, 35 pp.

Berbey, H., 1989. Sédimentologie et géochimie de la transition substrat volcanique-couverture sédimentaire de l'atoll de Mururoa (Polynésie française). Thèse Doc. Sci., University of Paris XI: 275 pp.

Bonatti, E., Harrison, C.G.A., Fisher, D.E., Honnorez, J., Schilling, J.G., Stipp, J.J. and Zentelli, M., 1977. Easter Volcanic Chain (Southeast Pacific): a mantle hot line. J. Geophys. Res., 82, 17: 2457–2478.

Buigues, D., 1982. Sédimentation et diagenèse des formations carbonatées de l'atoll de Mururoa (Polynésie française). Thèse Doc. 3e Cycle, University of XI: 2 vol., 309 pp.

Buigues, D., 1985. Principal facies and their distribution at Mururoa Atoll (French Polynesia). Proc. Fifth Int. Coral Reef Congr. (Tahiti), 3: 249–255.

Buigues, D., Gachon, A. and Guille, G., 1992. L'Atoll de Mururoa (Polynésie française): I) Structure et évolution géologique. Bull. Soc. Géol. France, 163, 5: 645–657.

Buigues, D., Bablet, J.P. and Gachon, A., 1993. Le lagon de Mururoa. In: ORSTOM (Editors), Altlas de Polynésie Française, Plate 33.

Colin, P.L., Devaney, D.M., Hillis-Colinvaux, L., Suchanek, T.H. and Harrison, J.T., 1986. Geology and biological zonation of the reef slopes, 50–360 m depth at Eniwetak Atoll, Marshall Islands. Bull. Mar. Sci., 38, 1: 111–128.

Dudoignon, P., Destrigneville, C., Gachon, A., Buigues, D. and Ledesert, B., 1992. Mécanismes des altérations hydrothermales associées aux formations volcaniques de l'atoll de Mururoa. Compt. Rend. Acad. Sci., 314, II: 1043–1049.

Dullo, W.C., Moussavian, E. and Brachert, T.C., 1990. The coralgal crust facies of the deeper forereefs in the Red Sea: a deep diving survey by submersible. Geobios, 23, 3: 261–281.

Duncan, R.A. and McDougall, I., 1976. Linear volcanism in French Polynesia. J. Volc. Geotherm. Res., 1: 197–227.

Gachon, A. and Buigues, D., 1985, Volcanic erosion and reef growth phases (Atoll of Mururoa, French Polynesia). Proc. Fifth Int. Coral Reef Congr. (Tahiti), 3: 185–191.

Gillot, P.Y., Cornette, Y. and Guille, G., 1992. Age (K/Ar) et conditions d'édification du soubassement volcanique de l'atoll de Mururoa (Pacifique sud). Compt. Rend. Acad. Sci., 314: 393–399.

Grammer, G.M. and Ginsburg, R.N., 1992. Highstands versus lowstand deposition on carbonate platform margins: insight from Quaternary foreslopes in the Bahamas. Mar. Geol., 103: 125–136.

Guille, G., Goutière, G., Sornein, J.F., Buigues, D., Guy, C. and Gachon, A., 1993. Les atolls de Mururoa et Fangataufa (Polynésie française): I, Géologie-Pétrologie-Hydrogéologie: Edification et évolution des édifices, 168 pp.

Guille, G., Goutière, G., Sornein, J.F., Buigues, D., Guy, C. and Gachon, A., 1996. The atolls of Mururoa and Fangataufa (French Polynesia): I, Geology-Petrology-Hydrogeology: From Volcano to Atoll, 168 pp.

Guillou, H., Guille, G., Brousse, R. and Bardintzeff, J.M., 1990. Evolution de basaltes tholeitiques vers des basaltes alcalins dans le substratum volcanique de Fangataufa (Polynésie française). Bull. Soc. Géol. France, VI, 3: 537–549.

Guyomard, T., 1990. Sédimentation et diagenèse du sondage Echo 2 de l'atoll de Fangataufa (Polynésie française). Corrélations avec Mururoa. D.E.A., University of Paris XI, 65 pp.

Hine, A.C., and Mullins, H.T., 1983. Modern carbonate shelf-slope breaks. Soc. Econ. Paleontol. Mineral., Spec. Publ. 33: 169–188.

James, N.P., and Ginsburg, R.N., 1979. The seaward margin of Belize barrier and atolls reefs. Spec. Publ. Intern. Assoc. Sediment., 3: 191 pp.

Labeyrie, J., Lalou, C. and Delebrias, G., 1969. Etude des transgressions marines sur l'Atoll de Mururoa par les datations des differents niveaux de corail. Cah. Pac., 13: 203–207.

Pautot, G., and Monti, S., 1974. Carte bathymétrique du Pacifique Sud au 1/1 000 000: feuille de Mururoa. Publication CNEXO

Perrin, C., 1990. Genèse de la morphologie des atolls: le cas de Mururoa (Polynésie française). Compt. Rend. Acad. Sci., 311, II: 671–678.

Rougerie, F. and Wauthy B., 1993. The endo-upwelling concept: from geothermal convection to reef construction. Coral Reefs, 12: 19–30.

Rougerie, F., Wauthy B. and Rancher, J., 1992. Le recif barriere ennoye des Iles Marquises et l'effet d'ile par endo-upwelling. Compt. Rend. Acad. Sci., 315, II: 677–682.

Ruzie, G. and Gachon, A., 1985. Apport des techniques géophysiques à l'étude des carbonates dans les atolls. Application à l'étude de l'atoll de Mururoa. Proc. Fifth Int. Coral Reef Congr. (Tahiti), 6: 381–388.

Salvat, B., 1989. Le littoral corallien, In C. Gleizal and Multipress (Editors), Encyclopédie de la Polynésie, 3: 9–24.

Samaden, G., Dallot, P. and Roche, R., 1985. Atoll d'Eniwetak. Système géothermique insulaire à l'état naturel. Houille blanche, 2: 143–151.

Turner, D.L. and Jarrard, R.D., 1982. K/Ar dating of the Cook-Austral island chain: a test of the hotspot hypothesis. J. Volc. Geotherm. Res., 12: 187–220.

Wilson, J.T., 1963. A possible origin of Hawaiin islands. Can. J. Phys., 41: 863–870.

This Page Intentionally Left Blank

Geology and Hydrogeology of Carbonate Islands. Developments in Sedimentology 54
edited by H.L. Vacher and T. Quinn
© 1997 Elsevier Science B.V. All rights reserved.

Chapter 14

GEOLOGY OF MAKATEA ISLAND, TUAMOTU ARCHIPELAGO, FRENCH POLYNESIA

LUCIEN F. MONTAGGIONI and GILBERT F. CAMOIN

INTRODUCTION

Makatea Island (148°15'W; 15°50'S) is located in the northwestern part of the Tuamotu archipelago (Fig. 14-1), 80 km away from the nearest atolls, Rangiroa and Tikehau, and 245 km from the closest volcanic island, Tahiti [q.v., Chap. 15]. Makatea measures 7 km by 4.5 km and displays a crescent shape.

According to bathymetric maps (Monti, 1974; Mammerickx et al., 1975), the Tuamotu atolls cap the tops of volcanic cones that rise steeply, not from the ocean floor which is 4,000–4,500 m deep in this region, but from the summit of a wide submarine plateau, at depths of 1,500–3,000 m ("Tuamotu Plateau"; Mammerickx et al., 1975; Brousse, 1985). This anomalously shallow plateau is related to the French Polynesian Superswell (in the sense of McNutt and Judge, 1990). The plateau is dated as 50–42 Ma in the northwestern part of the archipelago (Jarrard and Clague, 1977; Schlanger et al., 1984). Geomorphological and geochronological evidence indicates that the Tuamotu chain is much older than that of the adjacent islands of French Polynesia (Society, Marquesas, and Austral archipelagos). Reef development is thought to have been coeval with the cessation of volcanic activity during early Eocene time, at least in the northwestern part of the Tuamotu chain (Schlanger, 1981). Based on mean rates of subsidence of volcanic basement (Crough, 1984), the thickness of Eocene and Oligocene carbonate sequences is estimated to be 800 m and 500 m, respectively.

The Tuamotu atolls are surrounded by two active hotspot areas, Society and Hereretue-Pitcairn, dated respectively as 6.5–0 Ma (Duncan et al., 1974; Duncan and McDougall, 1976; Brousse, 1985) and 15–0.4 Ma (Duncan et al., 1974; Brousse, 1985). Some northwestern Tuamotu (NWT) atolls, situated at 15–18°S and 145–148°W (i.e., Makatea, Mataiva, Rangiroa, Tikehau, Niau, Kaukura; Fig. 14-1) have outcrops of lower Miocene (23–16 Ma) reef carbonates (Montaggioni, 1985, 1989; Montaggioni et al., 1987; Bourrouilh-Le Jan and Hottinger, 1988). These reef carbonates are partly covered by phosphates which are presumed to be Miocene-Pliocene in age. The Neogene section is overlain by Pleistocene-Holocene reef deposits.

The tectonic evolution of Makatea Island is clearly dominated by extensional processes related to normal faulting. Three main orientations of faults exist. The predominant fault trend is NE-SW and may cut the whole island. A large-scale WNW-ESE fault system (e.g., Vaiau-Tamurua fault) divides the island into two morphologically different areas: a large northern atoll-shaped block and a southern terraced block. Lastly, a minor NNE-SSW listric fault system occurs

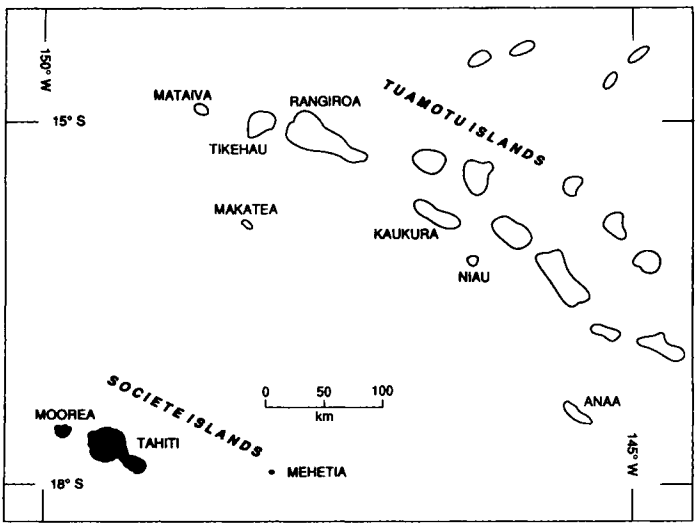


Fig. 14-1. Geographic location of Makatea Island with respect to other Tuamotu Islands and Society Islands. [See also Figs. 13-1 and 15-1 for regional location.]

principally along the west coast, where it runs parallel to the cliff and adjacent reefs.

This regional fault pattern is consistent with the large-scale lithospheric stress direction displayed in the southwestern Pacific ocean floor, especially with the fault system recorded at Moorea (Blanchard, 1978). In particular, the NE-SW fault system is comparable to the great system of SW-trending fracture zones (i.e., transform faults) described by Menard (1964) and charted by Mammerickx et al. (1975). The causes of the two other fault systems remain speculative. The WNW-ESE faults may result from uplift of the island. NNE-SSW faulting is probably linked to coastal neotectonic displacements. Vertical uplift occurred during the early Pleistocene and probably earlier, during the middle Miocene (Montaggioni, 1985; Montaggioni, 1989; see Case Study). Horizontal extensional events were initiated prior to island uplift, because magnetic lineations suggest that the regional NE-SW fracturing occurred at the beginning of the Miocene (Handschumacher, 1973). This evidence is further substantiated by the occurrence of numerous related fractures and fissures, which are entirely infilled by biogenic deposits of Miocene age and have a strong dissolution fabric.

Geomorphology and landscape

Makatea is partly surrounded by fringing reefs extending seaward some 100 m from the base of cliffs that surround almost all of the island. There are short stretches of sand beaches on the northwest, southern and northeastern sides of the islands. A plateau-like surface caps the island at an average elevation of 60–75 m. The highest elevation on Makatea is 113 m (Fig. 14-2).

The cliffs. Makatea is almost entirely flanked by abrupt cliffs that are especially prominent in the northern and northeastern parts of the island (+50 to +75 m; Fig. 14-2). On all sides, the cliffs exhibit four distinct notch and cavern lines at +1 to +1.5 m, +5 to +8 m, +20 to +25 m and at +56 m. The notches are associated inwardly with narrow open caves and galleries containing typical speleothem deposits.

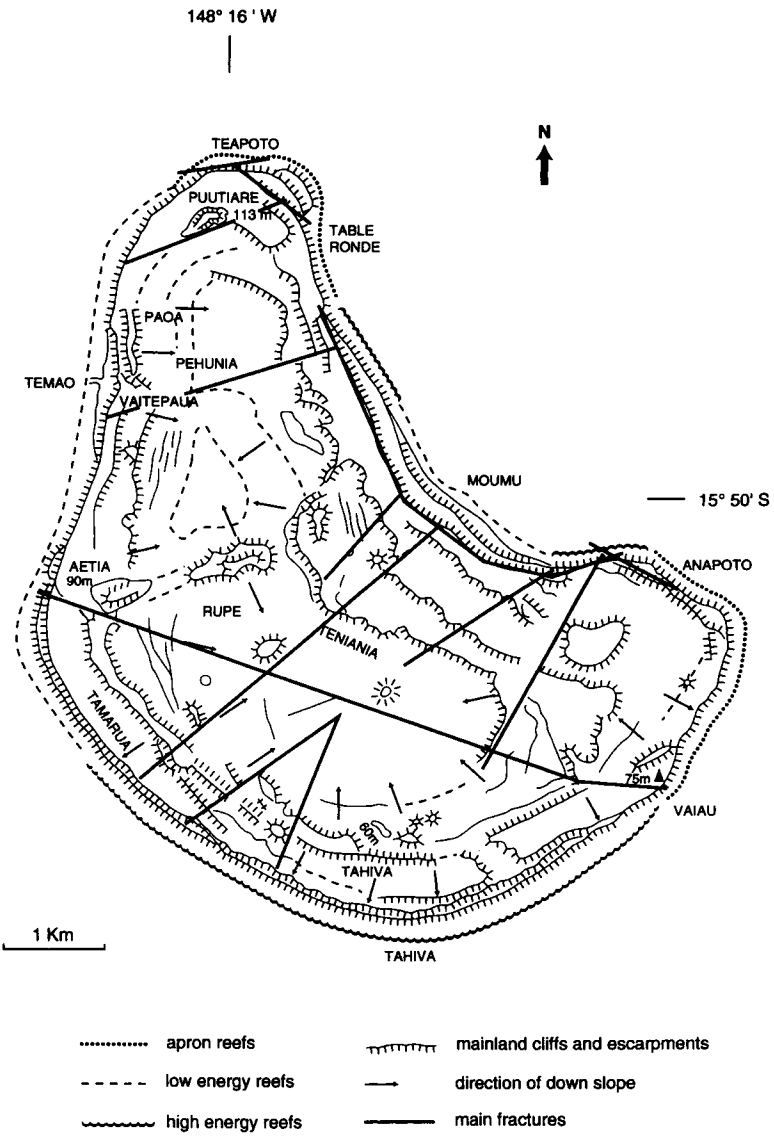


Fig. 14-2. Geomorphological and structural map of Makatea Island. (After F. Bourrouilh-Le Jan *in* L. Montaggioni, 1985.)

The west and south coasts of Makatea step down gradually towards the shoreline and display three terrace levels that form low stepped bluffs (Fig. 14-2). The present reef flat or shore platform constitutes the lowest terrace (at +0.3 to +1 m). The intermediate terrace is located between +4 and +6 m, and the uppermost one occurs at about +20 m.

The upper plateau. Ranging in elevation from 20 to 75 m, the upper plateau displays a central depression and is divided into two basins: Pehunia (north), and Rupé (south). In its northernmost part, the plateau is capped by a hill that is the highest point of the island (Puutiare Mount, 113 m). The highest point of the southern part of the island is the Aetia Mount (90 m).

The carbonate platform is deeply dissected by a karst system at different scales. At one scale in the northern and central parts of the plateau, karst features consist of cylindrical to conical close-set wells (potholes), 5–30 m in width and 1–75 m deep. These sinks are partly occluded by phosphates and probably extend below present-day sea level; residual relief occurs as peaked to planar carbonate hummocks. At Pehunia, subaerial karst features occur as narrow (0.5–3 m) pits. At another scale, numerous fissures, ranging from a few centimeters up to 2 m in width, run parallel to the cliff lines, particularly along the northern and eastern areas. These fissures give evidence of the *per descensum* circulation of meteoric waters; in many areas, such fissures have been hollowed out by dissolution and transformed into deep caves. When occluded, fissures are filled by breccias composed of skeletal elements and phosphate nodules. Lastly, the southern part of the plateau displays a strongly solution-rilled surface affected by channels oriented perpendicular to the coastline (old fractures or erosional grooves).

The fringing reefs. Apron reefs, high-energy fringing reefs and low-energy fringing reefs are three types of modern reefs that can be distinguished on the basis of their degree of evolution and exposure (Fig. 14-2). Apron reefs are located at the base of cliffs in the northernmost end and along the east coast of the island; the reef flat consists of a subhorizontal smooth surface composed mainly of coralline algae. High-energy fringing reefs are located along the southwestern and southeastern shores. They are 70–90 m in width and include two distinctive morphological units: the outer-reef front and the reef flat. Low-energy fringing reefs occur along the sheltered western coast and within the Bay of Moumu. In contrast to the exposed reef tracts, the reef front in these places corresponds to a subplanar platform, a few meters wide.

Historical overview

Phosphate ore was discovered at the end of the nineteenth century, but production did not begin until 1917; it ended in 1966. Because phosphatic deposits occur as scattered pockets within the karstic island bedrock, it was not possible to use sophisticated mining techniques. Scooping, however, was easy due to the unconsolidated nature of the ore; this process left a bare and towered landscape. Although

efficient mining techniques were hampered by the topography of the island, its profit-earning capacity was related to the high-grade (80–85% tricalcic phosphate), low iron and aluminum content (about 2%) and homogeneity of the phosphate ore, which obviated sorting and concentrating operations. The steepness of Makatea shorelines prevented the development of a sophisticated harbor. Although landing was first carried out at Moumu beach at the beginning of the mining activity, the protected Temao beach was finally selected as a harbor site.

Phosphate played an important role in the economic balance of the territory. During phosphate ore activity, Makatea was the most populated island in the Tuamotu archipelago with about 3,000 inhabitants. At that time, Makatea was a melting pot with a population composed primarily of Polynesians, French, Japanese, Annamites and Chinese. Since phosphate mining ended in 1966, the population decreased to about thirty people who are employed as copra workers.

GEOLOGY

Stratigraphy

Four major stratigraphic series, denoted I–IV, have been identified at Makatea. The Holocene, Pleistocene, and early Miocene deposits, denoted IV, III, and I_2, are shown on the generalized geologic map and cross section of Fig. 14-3.

The lower Miocene series (I). The basement of lower Miocene series, denoted I_1, is apparently restricted to the western part of Makatea Island. The series consists of a 10-m-thick section of planar-bedded dolomitized bafflestones. The occurrence of *Miogypsina* in these carbonates is indicative of Cenozoic e–f range zones (lower Miocene) according to the Indo-Pacific letter classification (Clarke and Blow, 1969).

The overlying carbonate unit (I_2), up to 60 m thick, forms the bulk of the island (Fig. 14-3). This unit unconformably overlies the basal member through a planar subaerial exposure surface. The association of benthic foraminifers, including *Miogypsina*, *Miogypsinoides*, *Austrotrillina howchini*, *A. asmariensis*, and *A. striata* indicates an Aquitanian age (i.e., Te_5 biozone according to the Tertiary Far East Letter Code of Adams (1984)). Associated molluscan fauna includes pelecypods (*Fragum* sp., *Tellina* sp., *Septifer* cf. *bilocularis*, *Codakia tigerina*) and gastropods (*Cerithium*, *Rhinoclavis*, *Cymathium*, vermetids, naticids, *Conus*, *Actaeon*). Four different facies are recognized within the overlying carbonate unit (I_2) of the lower Miocene series (Fig. 14-3).

The Mio-Pliocene series (II). The Mio-Pliocene series consists of phosphate deposits including a variety of lithofacies and structures (Fig. 14-4). Rocks are heterogeneous and many phosphate sequences display evidence of numerous episodes of precipitation, dissolution, and internal sedimentation (Montaggioni, 1985). Major microfacies include phosphate oolitic grainstone, phosphate intraclast-bearing packstone, and phosphate caliche (phoscrete) (Bourrouilh-Le Jan, 1990). These

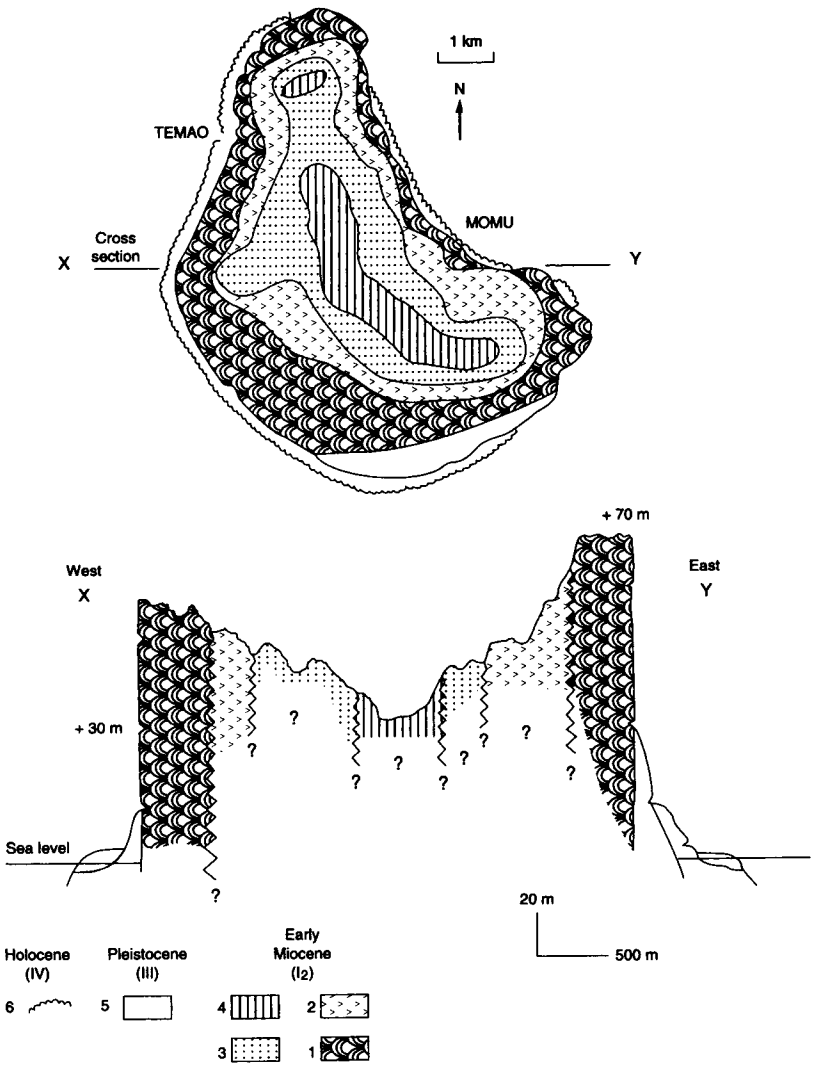


Fig. 14-3. Schematic geologic map and interpretative cross section of Makatea Island. Keys for sedimentary facies of early Miocene deposits: I_2-1, coral-algal boundstone; I_2-2, coral-molluscan grainstone, packstone and wackestone including scattered coral colonies; I_2-3, foraminiferal packstone and wackestone; I_2-4, molluscan-echinoidal-foraminiferal wackestone and mudstone. Also: III-5, Pleistocene coral-algal boundstone; IV-6, coral-algal boundstone and associated skeletal deposits related to the late Holocene fringing reef. (After Obellianne, 1963; Montaggioni, 1985 and Bourrouilh-Le Jan, 1990.)

phosphate rocks unconformably overlie the karstified surfaces of the lower Miocene carbonates. A late Miocene or Pliocene age (Tf3; Montaggioni, 1985) may be inferred from the stage of geomorphologic evolution the reef platform reached prior to deposition of the phosphorite.

The Pleistocene series (III). The Pleistocene series includes two generations of well-defined reef terraces at +7 m and +29 m that are in close proximity to the two upper notch lines at +5 to +8 m and +20 to +25 m. These two reef terraces have been dated by U-series methods at 100–140 ka and 400 ± 100 ka (Veeh, 1966). The lower of the reef terraces could be related to the 125-ka sea-level highstand corresponding to deep-sea isotope stage 5*e* (Shackleton and Opdyke, 1973). The higher terrace could be related to the 330-ka, 415-ka, or 485-ka sea-level highstands corresponding to deep-sea isotope stages 9, 11 and 13 (Shackleton and Opdyke, 1973). The present-day altitude of the terraces is partly related to a slight increase in elevation due to the ongoing uplift of the island.

The Holocene series (IV). The Holocene series corresponds to the exposed peripheral fringing-reef system, which is 0.3–1 m above mean sea level and overlies a pre-Holocene (Pleistocene?) marine erosional platform. Radiocarbon ages obtained on this reef terrace are 3730–5300 y B.P. (Montaggioni, 1985).

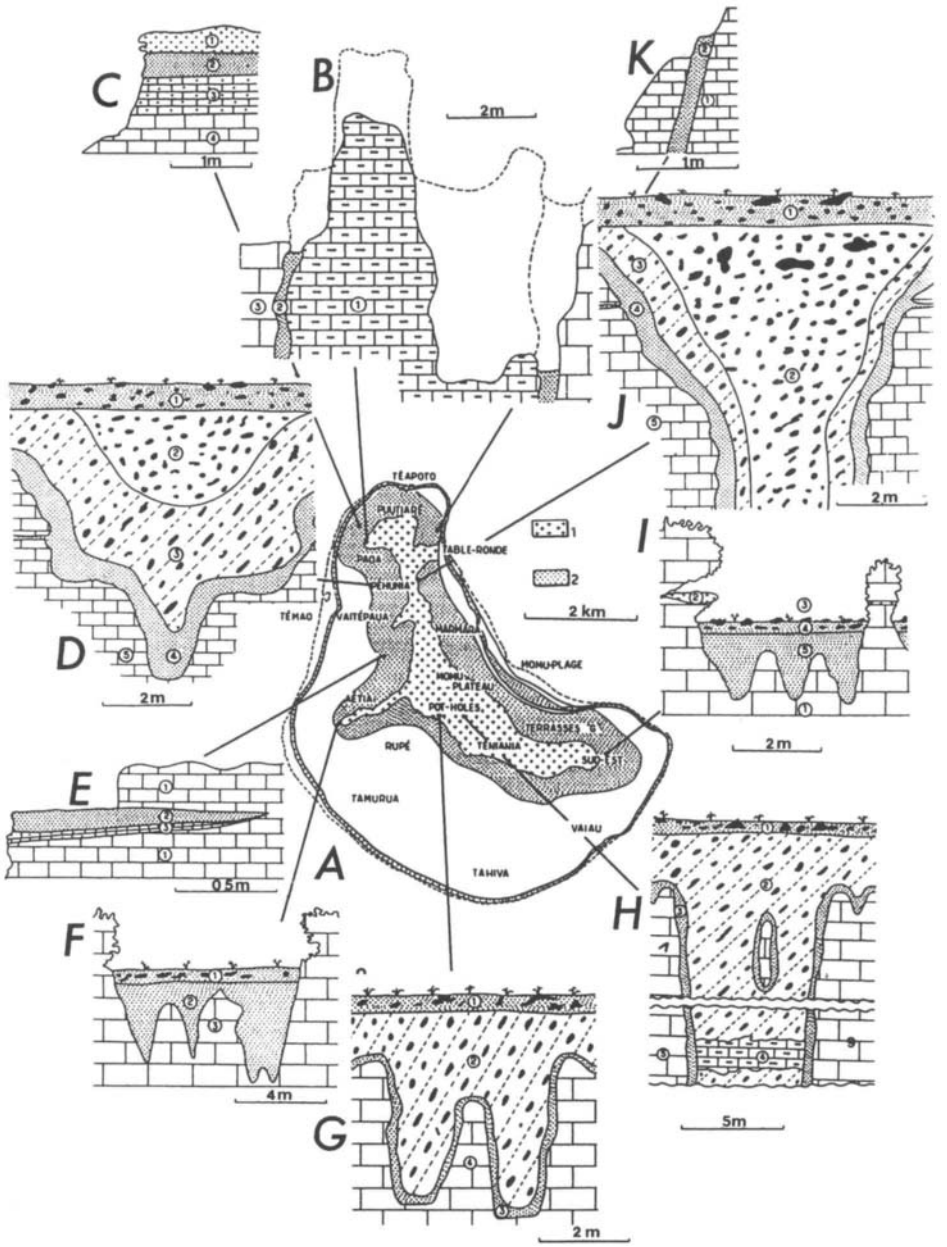
Depositional facies of the lower Miocene reef deposits

As pointed out by Obelliane (1963), major depositional facies within the Miocene reef platform of Makatea are concentrically distributed from the outer platform margin inwards (Fig. 14-3). The facies include: (1) a reef-core facies consisting of coral-algal boundstone, denoted I_2-1; and (2) a backreef association consisting successively of skeletal grainstone to wackestone with scattered coral colonies (I_2-2), foraminiferal packstone and wackestone (I_2-3), and molluscan-echinoidal-foraminiferal wackestone to mudstone (I_2-4; Fig. 14-3). All these facies are locally dolomitized. Their distribution was originally controlled by platform geometry and wave energy.

Reef-core facies. The reef-core facies crops out along and at the top of coastal cliffs where it forms a 70-m-thick unit. The lower member of this facies consists mainly of poorly bedded to massive deposits of coral bafflestone (branching *Acropora*, massive faviids and *Porites*), coarse skeletal breccia and poorly to moderately sorted skeletal grainstone to wackestone. Rocks include a wide range of skeletal fragments with the predominance of coral fragments. Encrusting coralline algae are common, and *Halimeda* plates are rare or absent. Significant concentrations of alcyonarian spicules and bryozoan fragments are present, and fragments of encrusting foraminifers (*Carpenteria*, *Gypsina*) are conspicuous contributors to the sediment. In contrast, benthic foraminifers (*Miogypsina*, rotaliids) and planktonic forms (globigerinids) are few, as are serpulids, sessile gastropods, various mollusks, and echinoids. These fossils and rock types indicate a shallow-water, moderate- to high-energy depositional environment. The breccias are interpreted to have formed at the reef front.

The upper part of this facies is 2–6 m thick and is composed of boundstone and rudstone. It also exhibits large-scale subhorizontal bedding. The rocks of this facies are interpreted as the inner parts of an outer reef rim (reef flat), cut by tidal channels that controlled the deposition of the large-scale, cross-stratified deposits in a high-energy zone. Rocks consist of in situ branching to tabular coral heads in a skeletal

grainstone matrix. Subordinate rigid framebuilders consist of lamellar to knobby coralline algae (*Porolithon*, *Lithophyllum*, *Lithothamnium*), encrusting foraminifers (homotrematids and, more rarely, *Acervulina*), and bryozoans. The reef framework consists of bafflestone and bindstone. Corals and coralline algae are the major



contributors. Larger benthic foraminifers are abundant and include *Sorites*, *Amphistegina* associated with alveolinids, textulariids, and occasional miliolids; *Halimeda* plates are also abundant. Behind the presumed reef flat, a transitional zone consists of decimeter- to meter-sized in situ coral heads scattered within algal-foraminiferal grainstone and is interpreted to have been the margin of the backreef environment. The similarities in composition between these sediments and the outer-rim deposits strongly suggest that the outer-rim deposits were transported towards inner depositional areas, possibly through tidal channels.

The original skeletal aragonite has been totally replaced by calcite. Isopachous fringes of calcitic cements occur commonly in intergranular pores. Dolomitization of reef-core facies is irregular and generally forms lens-shaped bodies, up to 100 m in

Fig. 14-4. Phosphate distribution (A) and typical cross sections (B–K) of phosphate deposits of Makatea. (After Obellianne, 1963.)

(A) Map of Makatea Island showing the distribution of tricalcic phosphate ore. Major phosphorite deposits occur in continuous outcrops containing up to 80% tricalcic phosphate (pattern 1). Minor phosphorite deposits occur in terraces and pockets (pattern 2) that surround the major deposits.

(B) Hard, brecciated phosphate deposits in the Puutiare area include light-brown, well-cemented phosphatic hummock (1) and phosphatic sands (2) enclosed in carbonates (3).

(C) Stratigraphic section in Puutiare area displaying a succession of weakly phosphatized carbonate rocks (4), partly phosphatized, shelly carbonate rocks (2, 3) and exclusively phosphatic breccia (1).

(D) Detail of the Mio-Pliocene section in Pehunia area. The cavity in the carbonate rocks (5) is filled by unconsolidated phosphate deposits including fine-grained phosphate sands (4), pisolitic-oolitic sand deposits deposited in alluvial fans (3), phosphate nodules (2), and phosphate sands containing phosphate pebbles and blocks (1).

(E) Phosphate deposits in the Aatia area horizontally fill a pre-existing notch in lower Miocene carbonate rocks (1) and contain weakly phosphatized carbonate rocks (3) overlain by phosphatic breccias (2).

(F) Phosphate deposits in the Aatia area occur in terraces and pockets in lower Miocene carbonate rocks (3) and contain phosphate sands devoid of nodules (2) and phosphate sands containing phosphate blocks (1).

(G) Detailed cross section in the "Pot-hole" area where unconsolidated phosphate deposits fill a cavity in lower Miocene carbonate rocks (4). This sedimentary sequence contains fine-grained phosphate sands (3), pisolitic-oolitic sand deposits deposited in alluvial fans (2), and phosphate sands containing phosphate pebbles and blocks (1).

(H) Detailed cross section in the "Pot-hole" area where unconsolidated phosphate deposits fill a cavity in lower Miocene carbonate rocks (5). This sedimentary sequence contains fine-grained phosphate sands (3), pisolitic-oolitic sand deposits deposited in alluvial fans (2), bedded, hard pisolitic phosphates (4) and phosphate sands containing phosphate pebbles and blocks (1).

(I) Phosphate terraces and pockets in lower Miocene carbonate rocks (1) of the Southeastern area. The sedimentary infilling is composed of fine-grained phosphate sands (5), phosphate sands (4), hard phosphate blocks (3), and in-place phosphatic breccias (2).

(J) Detail of a cavity infilling in lower Miocene carbonate rocks (5) of the Pehunia area. The phosphate deposits are unconsolidated and include fine-grained phosphate sands (4), pisolitic-oolitic sands (3), phosphate nodules (2) and phosphate sands, pebbles and blocks (1).

(K) Mixed phosphate and carbonate deposits (2) infilling a fissure in lower Miocene carbonate rocks (1) of the Table-Ronde area.

areal extent, which cross-cut stratification. Several dolomite units alternate with calcite-rich layers; the original depositional textures are more or less well preserved. The most extensively dolomitized zone is found in the northwestern and western cliffs where the upper dolomitized beds partly retain original depositional textures. In contrast, the lower units at the base of the cliff are 15 m thick and completely dolomitized.

Backreef facies. The backreef facies crops out in the central depression of Makatea Island and consists of subhorizontal, well-bedded deposits, 3–10 m thick; talus-slope deposits are lacking. These rocks display greater textural range (from grainstone to mudstone), facies variations and compositional changes than outer-reef deposits and occur in roughly concentric belts (Fig. 14-3). Rocks are composed of benthic foraminifers and branching coralline algae; coral, bryozoan, molluscan, and echinoid fragments are clearly less abundant.

In foraminifer-rich packstone and wackestone, larger foraminifers (miogypsinids, alveolinids, *Heterostegina*, *Lepidocyclina*, and soritids), or thick-shelled forms, are common and occur along with populations of small foraminifers, especially miliolids. This assemblage is very similar to modern thanatocoenoses from shallow-lagoon sediments behind the reef front. In molluscan-echinoidal-foraminiferal wackestone and mudstone, the amount of larger foraminifers clearly decreases, whereas the microfauna is more abundant and diversified; the latter includes miliolids (*Quinqueloculina*, *Triloculina*, *Pyrgo*, *Hauerina*), textulariids, bolivinitids, and cymbaloporids. This assemblage indicates a relatively closed depositional environment based on comparison with modern analogs (see Le Calvez and Salvat, 1980; Venec-Peyre and Salvat, 1981). The local abundance of preserved globigerinid tests, however, suggests an aperiodic supply of sediment from the open sea, perhaps through channels during exceptional tempest-induced swells.

In these backreef sedimentary rocks, well-preserved shelly remains are rare, except *Septifer* shells. All other bivalves have been affected by dissolution and were fossilized in the form of casts; their abundance is highly variable. The assemblage includes: *Barbatia* (*Arca*) *plicata*, *Pinna* (*Pinna*) sp., *Chlamys* sp., *Codakia* (*Codakia*) *tigerina*, *lucinids*, *Chama* (*Psilopus*?) sp., *Fragum* (*Fragum*) sp., *Tellina* (*Tellina*) cf. *chariessa*, *Tellina* (*Laciolina*?) sp., and numerous venerids (*Tapetinae*, *Marcia*, *Katelysia*). This bivalve assemblage is typical of low-energy environments. In modern reefs, all these taxa occur in backreef zones (Richard, 1982).

These rocks and fossils are indicative of a low-energy and very shallow (a few meters) depositional environment in a backreef area. As shown in modern lagoons of Takapoto and Mataiva atolls (Adjas et al., 1990), the enclosed backreef areas are self-governing depositional sites, characterized by quiet water conditions, and are not directly controlled by surrounding, emergent reef rims. The bedding observed in the units on Makatea and the lack of any talus-slope deposits suggest that this depositional area was a continuation of the adjacent reef-flat surfaces and, as a consequence, was very shallow, probably a few meters deep. No actual lagoon zone (i.e., counterpart of present-day atoll lagoon) seems to have been present during the development of the early Miocene carbonate platform.

Dolomitization of backreef deposits on the upper plateau displays great variations, both laterally and vertically. Dolomitic rocks range from sparsely to extensively dolomitized sediments with relict structures. Walls adjacent to karst cavities display a rapid decrease in the degree of dolomitization a few meters downward, indicating a close control of permeability on dolomite distribution.

The upper surface of backreef deposits usually exhibits massive, karst-produced pinnacled hummocks ("feo" in Polynesian language) composed of hard, strongly recrystallized rocks. In the central part of the upper plateau, the backreef deposits locally exhibit typical subaerial exposure features (e.g., fenestrae, caliches and root molds), suggesting that they were periodically emergent. It is likely that the emergent deposits were sandy to muddy cays that formed principally along the leeward side of the reef platform. Since the indicators of subaerial exposure lie at present at the same elevation (about 50 m) as the average height of the plateau, it may be assumed that most of the Miocene backreef deposits remained substantially intertidal to supratidal before dolomitization occurred.

Post-depositional alteration

At present, the carbonate basement of Makatea Island supports a lens of freshwater that may be observed in several areas, both on the eastern and western coasts and in the central part of the island. The water table of this freshwater lens dips from the central part of the island toward the coast and is in gravitational equilibrium with the underlying, denser seawater.

It is possible to relate fluctuations of the freshwater lens and the changing position of the freshwater-saltwater interface to variations in sea level.

Two paragenetic sequences are recorded in the carbonate units of Makatea (see also Dessay, 1990). The first one is a sequence in which marine cementation by aragonite or high-Mg calcite is followed by extensive dolomitization and then by extensive vuggy dissolution. The second paragenetic sequence is one in which marine cementation by aragonite or high-Mg calcite is followed by selective leaching of fossil allochems, meteoric cementation by low-Mg calcite, cementation by dolomite, and then the extensive vuggy dissolution.

The broadly lensoid morphology (Fig. 14-5) and distribution of the dolomite on Makatea is thought to be related to the changing position of the freshwater lens and the freshwater-saltwater interface. For these reasons, dolomite precipitation is interpreted to have occurred in a freshwater-saltwater mixing zone. On the other hand, $\delta^{18}O$ and $\delta^{13}C$ data from the dolomites, ranging respectively from $+2.2$ to $+3.0‰$ PDB, and from $+2.4$ to $+3.5‰$ PDB (Dessay, 1990), are rather indicative of dolomitization processes occurring within waters having an isotopic composition very similar to that of seawater. However, dolomite formation in the lower part of a freshwater-seawater mixing zone, with up to 40% freshwater contribution, cannot be completely ruled out as demonstrated by Hein et al., (1992) in the dolomitization of Quaternary reef limestone from the Cook Islands [q.v., Chap. 16]. The source of the carbon was predominantly seawater bicarbonate, derived directly from seawater

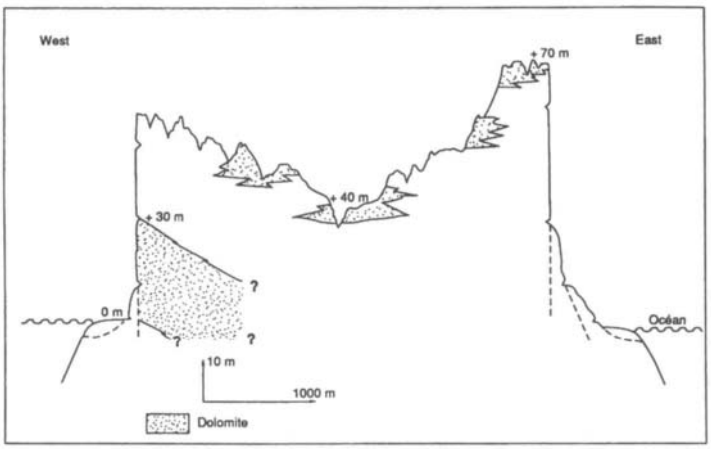


Fig. 14-5. Schematic distribution of dolomitized units on an E-W profile. (After Dessay, 1990.)

and/or indirectly from dissolution of primary carbonate (see also Hein et al., 1992). The circulation of large quantities of fluids through the Miocene reef carbonates was primarily related to tidal pumping which provided the magnesium required for dolomitization from seawater. In contrast to the dolomitization model for Niue (Aharon et al., 1987) [q.v., Chap. 17] and Aitutaki (Cook Islands), there is no evidence of thermally driven circulation on Makatea Island. In summary, geometric and isotopic data suggest formation of dolomites in seawater, just below the mixing zone, or in the lower seawater-dominated part of a freshwater-seawater mixing zone.

Several periods were favorable for the development and the stabilization of a freshwater-saltwater mixing zone throughout the evolution of Makatea, starting probably in early Miocene time. Figure 14-6 summarizes the schematic location of the interface between the mixing zone and the marine phreatic environment for four periods that were characterized both by a humid and warm climate and by a sea-level highstand: 2–1 Ma or 700 ka (N_0), 1 Ma–700 ka (N_1), 500–300 ka (N_3) and 130–110 ka (N_5). Cool and dry climatic periods, related to Quaternary glacial events, were characterized by a sharp decrease in effective rainfall, which caused a reduced discharge from the aquifer. Such conditions may have resulted in a temporary disappearance of the freshwater lens.

The present-day position of the dolomitized zones between 0 and +30 m observed on the west coast corresponds to that of the interface between the freshwater-saltwater mixing zone and the marine phreatic environment for sea levels N_1 and N_3. No additional interface (N_5, N_9, N_{10}) associated with the three other humid climatic periods reached a higher altitude. Consequently, dolomitization observed at the upper surface of the island, between +40 and +70 m, is probably more ancient, ranging in age from 2 Ma (beginning of the later uplift phase of the island; see Case Study) and 1 Ma or 700 ka for sea level N_0. Dolomitization processes related to sea levels N_5 and N_9 may have affected submerged parts of the carbonate island.

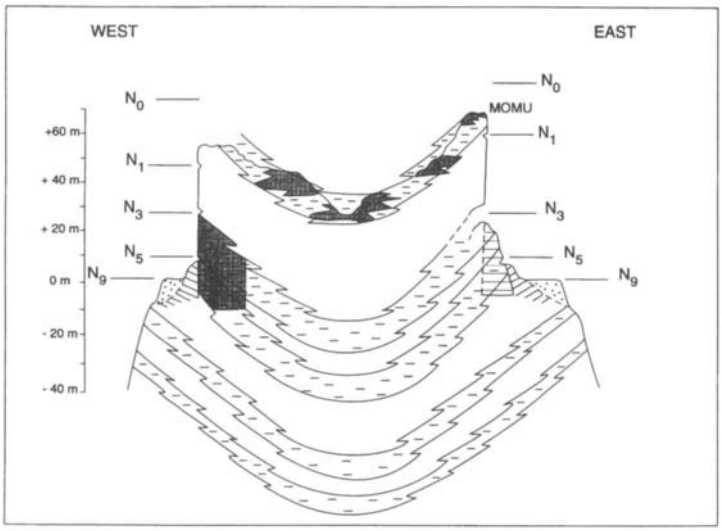


Fig. 14-6. Schematic location of the freshwater-saltwater mixing zone, denoted by dashed-line pattern, for four pre-Holocene intervals of stable sea level and warm, humid climate: N_0 (2–1 Ma or 700 ka), N_1 (1 Ma–700 ka), N_3 (500–300 ka), and N_5 (130–110 ka). N_9 is Holocene (6000–1500 y B.P.). Position of Holocene reefs denoted by light stipple pattern. Position of late Pleistocene reefs denoted by horizontally ruled pattern (250 ka) and diagonally ruled pattern (125 ka). Dolomite distribution is denoted by dark stipple pattern. (After Dessay, 1990).

Evolution of the island (Fig. 14-7)

The basement of the early Miocene reef platform on Makatea is thought to be composed of a Paleocene to Oligocene carbonate bank, up to 400 m thick, according to DSDP data from the northwestern Tuamotu area (Schlanger, 1981). The early Miocene platform exhibits a clear concentric zonation of depositional environments with a peripheral, locally emergent, outer coralgal rim enclosing a central very shallow area in which the deposition of biogenic sands and muds prevailed. Local evidence of subaerially produced features indicates that emergence due to sediment infilling occurred as the platform grew upward and, consequently, that the latter kept pace with sea-level rise during the entire growth phase. The reef rim probably grew in the form of flat-topped platforms, devoid of central depressions (i.e., table reefs; Tayama, 1935). During the early Miocene, plate motion produced tensional stresses along the regional southwest-trending transform faults and the platform was dissected by NW-SE extensional fractures.

The final stage of platform development was accompanied by complete filling-up of the backreef area producing local subaerial exposure. The position of the freshwater-saltwater interface reached various elevations in response to changes in eustatic sea level. Dolomitization was initiated within the marine phreatic realm or in the lower part of a freshwater-saltwater mixing zone, as indicated by the lenticular shape of dolomitic bodies, diagenetic sequences, and isotopic compositions, as

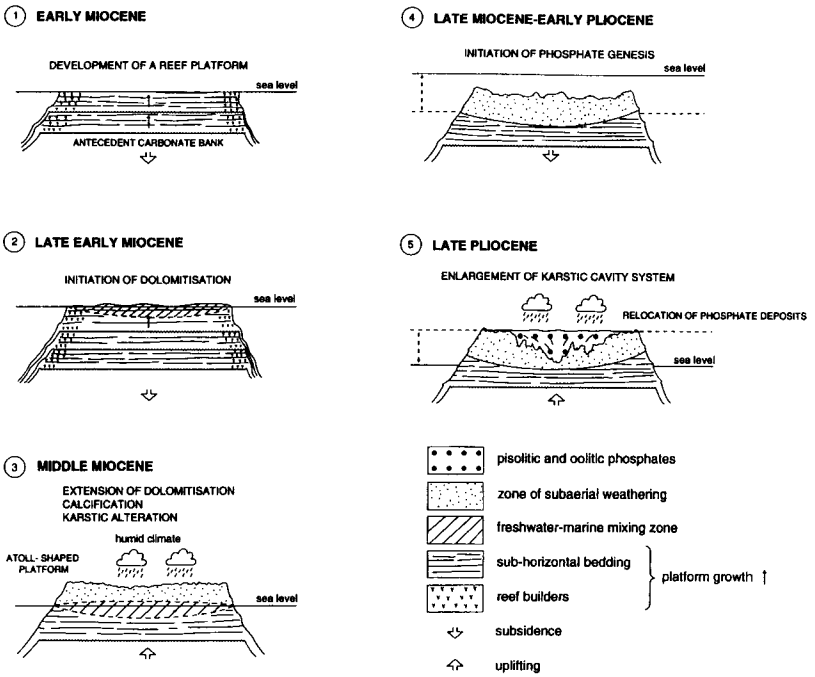


Fig. 14-7. Conceptual evolutionary scheme for the Miocene-Pliocene history of Makatea Island. (Modified from Montaggioni, 1985.)

detailed earlier. The transformation of initial metastable carbonates to low-Mg calcite is thought to have occurred coevally with dolomitization. With the fall of relative sea level of several tens of meters, the general emergence of Makatea allowed for the downward penetration of dolomitizing fluids into the limestone core. At the same time, extensive meteoric alteration affected emergent carbonate deposits, producing a large karst cavity system and the precipitation of speleothems. The typical saucer-shaped gross morphology observed on Makatea Island at present resulted from this long period of carbonate dissolution (Montaggioni et al., 1987; Bourrouilh-Le Jan, 1990). The sea-level curve of Haq et al., (1987) suggests that several periods of emergence alternating with periods of submergence may have occurred during late early to middle Miocene times.

During periods of sea-level rise, precipitation would have exceeded evaporation. Hence, a relatively humid environment may have been established and this would have promoted carbonate dissolution. Karst topography led to the development of freshwater. These pools were subsequently invaded by dense populations of ostracods producing microlaminated limestone. This limestone locally postdates not only calcite stalactitic coatings, but also detrital dolomite rhombs and sucrosic dolomite-bearing lithoclasts. This occurrence implies that dolomitization was already occurring by that time (i.e., late early to middle Miocene).

Phosphate deposits seal karstic paleotopography, thus indicating that phosphatogenesis was an active process in the late Miocene. The relevant rocks display a variety of textures: oolitic grainstone with mammilated or botryoidal cements, intraclast packstone, pelletal-oolitic wackestone. Possible phosphatization processes include alteration of seabird guano, allochthonous volcanic material, or marine organic matter on a low-oxygen submerged platform (Montaggioni, 1985). We favor the latter interpretation. Such an origin, thought to explain the formation of the major Mesozoic and Cenozoic "phosphorite giants" deposits, has also been attributed to the phosphatization processes recorded on seamount limestones and phosphatic hardgrounds in carbonate shelf sequences (Arthur and Jenkyns, 1981). Slight oxidizing conditions generally induce the greatest mobilization and redeposition of phosphate (Belayouni and Trichet, 1983). Locally, bottom-water concentrations of phosphate may reach the point at which primary precipitation of carbonate fluorapatite may occur. This process could explain the oolitic textures reported at Makatea.

From these interpretations, the following sequence of geologic events can be considered at Makatea. The original carbonate platform, previously eroded, was submerged during a marine transgression stage related to the phosphorogenic episode 3 (late Miocene) of Cook and McElhinny (1979). The source of phosphorus was presumably in nutrient-rich waters characterized by high organic productivity. Organic matter may have been trapped within oxygen-minimum zones of the submerged platform. The release of phosphorus caused primary precipitation of carbonate fluorapatite in the form of oolite phosphorites. Phosphate deposits, which mainly form conglomerates, must have been mechanically and chemically reworked and redeposited in karst cavities and pits during periods of island emergence. Phosphate-rich solutions moving downward promoted the precipitation of successive generations of crusts and cements and phosphatized former or contemporaneous carbonate deposits (e.g., caliches and pisolites).

The present-day island morphology appears to result from relative sea-level fluctuations related both to tectonic uplift and Quaternary glacioeustatic oscillations. The latest major uplift of Makatea presumably occurred coevally with a collapse of the eastern part of the island in the late Pliocene-early Pleistocene and resulted primarily from the isostatic response to the loading of the nearby Tahiti-Moorea-Meetia volcanic complex. During Pleistocene glacial stages, extensive meteoric dissolution caused enlargement of karst cavities. In addition, this meteoric dissolution remobilized subsurface phosphate deposits. At least three relative sea-level rises were recorded in island deposits during the Quaternary, probably due to the combination of positive eustatic fluctuations and tectonic uplift: (1) between 1 Ma and 700 ka (+56 m notch); (2) between 500 and 300 ka (+27 m notch and reef terrace); (3) between 130 and 120 ka (+7 m notch and reef terrace), related to the last interglacial sea-level highstand. On the basis of stratigraphic relationships, dolomitization of the cliff between 0 and +30 m is thought to have occurred during the first two sea-level highstands, whereas dolomitization of the 120-ka reef terrace probably occurred during the last highstand of sea level, by percolation of Mg-rich freshwater through the extensively dolomitized overlying Miocene rocks. Periods between these sea-level highstands (i.e., 700 to 500 ka, 300 to 130 ka) were characterized by sea-

level lowstands, related to glacial events. One of the two Wisconsinan interstades may be recorded by the break in the outer slope at a water depth of 8–11 m.

During the Holocene sea-level rise, the upper seaward margin of the island was veneered by a thin coral framework. A fringing-reef system, 5,300–3,700 years old (Montaggioni et al., 1987) and developed on an erosional bench, occurs at an elevation of 0.3–1 m due to tectonic uplift. The island is still being subjected to neotectonic events related to lithospheric flexure beneath the nearby Society Islands (see Case Study).

CASE STUDY: VOLCANIC-ISOSTATIC POLYPHASE MOTION AND UPLIFTED ATOLLS

The occurrence of exposed Miocene to Pleistocene reef carbonates on some northwestern Tuamotu (NWT) atolls implies that these islands were uplifted during the Miocene (Chevalier, 1973) and/or during the Pleistocene (Montaggioni, 1985; Pirazzoli and Montaggioni, 1988).

According to geophysical models, the uplift of NWT atolls is thought to result either from lithospheric flexure in response to loading effects induced by the nearby Tahiti volcanic complex (McNutt and Menard, 1978; Lambeck, 1981), or from a hotspot swell related to an underlying asthenospheric bump in the periphery of the Society hotspot (Detrick and Crough, 1978; Crough, 1983; 1984). However, these models are based either on an unclear set of uplift parameters (70 or 45 m of uplift has been reported for Makatea; McNutt and Menard, 1978; Lambeck, 1981), or on a calculation from the Thermal Rejuvenation Theory (about 1,100 m for NWT atolls over the past 5–3 m.y.; Detrick and Crough, 1978; Crough, 1978), neither of which are consistent with field and drilling observations from the diverse Tuamotu atolls. The newly proposed polyphase uplift model (Montaggioni, 1989) reconciles field observations and geophysical data. The model predicts that three major phases of uplift controlled the post-Oligocene evolution of the NWT atolls (Fig. 14-8).

The first phase occurred at 18–15 Ma, when sea level has been estimated to have been 150 m higher than present (Haq et al., 1987). Deposition of more than 200 m of platform carbonates occurred in the NWT islands. The transit of the NWT islands in the vicinity of the active Hereretue hotspot swell (Brousse, 1985) and its associated asthenospheric bump induced a slight uplift of a few tens of meters. At 13–14 Ma, the top of the carbonate platform was probably uplifted from +150 m to about +200 m. During the 2-m.y. time span required for deflation of the swell (Detrick and Crough, 1978; Menard and McNutt, 1982), emergent Miocene reef carbonates underwent extensive meteoric dissolution and subaerial erosion. During swell deflation, the subsequent subsidence rate of the underlying oceanic crust is assumed to be 25 m per m.y. (Detrick and Crough, 1978; Crough, 1984). This subsidence, combined with the sea-level history, may account for atoll submergence during the late Miocene-early Pliocene, thereby implying that the NWT atolls were not affected by significant subaerial erosion during this time. The surface of Miocene reef carbonates is believed to have subsided to about 100 m below present sea level by 5 Ma.

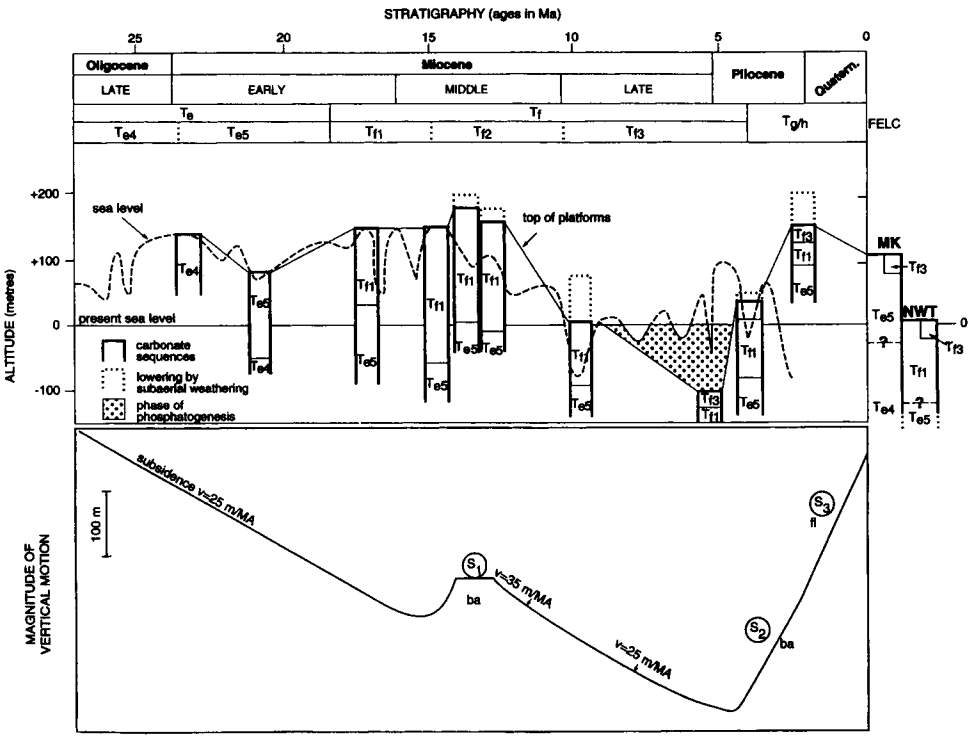


Fig. 14-8. Geologic history of the northwestern Tuamotu atolls, based mainly on the Makatea stratigraphic record. Chronostratigraphy, biozones, Tertiary Far East Letter Code from Adams (1984); sea-level curve from Haq et al. (1987). Thickness of Te_5 and Tf_1 biozones is inferred via the combination of the standard rate of atoll subsidence (25 m per m.y.; Detrick and Crough, 1976; Crough, 1984) and the rate of sea-level rise depicted in Miller et al. (1985) and Haq et al. (1987). Estimates of erosion rate (35 m per m.y.) are based on Lincoln and Schlanger (1987). S_1, S_2, and S_3 denote the first second and third phase of uplift in our polyphase uplift model (see Case Study section for detailed discussion). Other abbreviations: ba (asthenospheric bump), fl (lithospheric flexure), (MK Makatea), and NWT (other northwestern Tuamotu atolls).

At that time, sea level may have flooded the platform below the critical depth for reef formation.

The second phase of the model starts after the deposition of phosphate around the Miocene-Pliocene boundary (~6–4 Ma), when the NWT atolls began moving up the flank of the Society hotspot swell (Pirazzoli and Montaggioni, 1988). Using a mean uplift rate of 85 m per m.y., the total uplift (V) since that time is estimated to be ~350 m, where V is calculated as the sum of three terms:

$$V = a + b + c,$$

where a is the depth reached by the Miocene platform carbonates at the beginning of the Pliocene (100 m); b is the amount of stratigraphic shortening due to subaerial erosion (140 m), which is 4 m.y. of subaerial exposure times at a subaerial erosion

rate of 35 m per m.y. [Lincoln and Schlanger, 1987]; and c is the present maximum altitude at Makatea (113 m). This uplift and emergence resulted in the development of deep karst systems within early Miocene carbonate deposits and in the reworking of overlying phosphate deposits. At the end of the Pliocene, the maximum height reached by Makatea was about 100 m.

In the third phase of our model, at the beginning of the Pleistocene, Makatea moved over the arch of the lithospheric flexure generated by the loading of Tahiti and Moorea volcanoes. The combined effect of uplift due to lithospheric flexure and the asthenospheric bump resulted in an additional uplift of 170 m for Makatea. The adjacent atolls, far from the Tahiti-Moorea volcanoes, were much less affected by this uplift. This differential motion is still active as demonstrated by the altitude distribution of Holocene shorelines (Pirazzoli and Montaggioni, 1988). At Makatea, Holocene reef remnants reach a maximum height of 1 m. Anaa Atoll, located some 300 km southeastward and roughly in the same position that Makatea was at 3 Ma, is in a phase of rapid incipient uplift; exposed in situ Holocene coral colonies (2000–2600 y B.P.) occur at +1.3 m. The elevations of Holocene sea-level indicators on Mataiva, Rangiroa and Tikehau Atolls do not exceed +0.8 m suggesting that uplift due to the loading of Tahiti and Moorea volcanoes has reached its peak.

CONCLUDING REMARKS

Makatea affords the opportunity to document a complex tectono-sedimentary evolution of an uplifted carbonate island between early Miocene and Holocene time. The present-day island morphology appears to result from the combination of three major phases of tectonic uplift and Quaternary glacioeustatic sea-level fluctuations.

Lower Miocene platform carbonates exhibit a clear concentric zonation of depositional environments with a peripheral, locally emergent, flat-topped coralgal rim enclosing a central very shallow area in which the deposition of biogenic sands and muds prevailed.

The first uplift phase, in the vicinity of the Hereretue hotspot swell, occurred between 18 and 15 Ma and induced the general emergence of the lower Miocene carbonate platform. During the 2-m.y. time span required for swell deflation, emergent Miocene reef carbonates underwent extensive meteoric alteration that produced a large karst cavity system and the precipitation of speleothems. Pervasive dolomitization of reef carbonates was initiated in a marine phreatic zone or in the lower part of a mixed freshwater-saltwater mixing zone. During swell deflation, Makatea was submerged during the late Miocene-early Pliocene (6–4 Ma) and the previous karstic paleotopography was sealed by phosphate deposits.

The second uplift phase, on the flank of the Society hotspot swell, resulted in the emergence of Makatea during the Pliocene. During this emergence, deep karst systems developed within lower Miocene carbonate deposits, and phosphate deposits were mechanically and chemically reworked in karst cavities and pits.

The third uplift phase occurred at the beginning of the Pleistocene when Makatea moved over the arch of the lithospheric flexure generated by the loading of Tahiti

and Moorea volcanoes. During Pleistocene glacial stages, extensive meteoric dissolution caused enlargement of karst cavities; in addition, this meteoric dissolution remobilized phosphate deposits below present sea level. In contrast, three sea-level highstands were recorded in island deposits during Quaternary time, respectively between 1 Ma and 700 ka, 500 and 300 ka, and 130 and 120 ka. The occurrence of a Holocene fringing-reef system raised to an elevation of +0.3 to +1 m indicates neotectonic events related to the still active lithospheric flexure operating beneath the nearby Society Islands.

ACKNOWLEDGEMENTS

The authors wish to thank S. Gray, J. Hein, T.M. Quinn, H.L. Vacher and an anonymous reviewer for constructive comments which improved this paper.

REFERENCES

Adams, G.C., 1984. Neogene larger foraminifera, evolutionary and geological events in the context of datum planes. In: N. Ikebe and R. Tsuchi (Editors), Pacific Neogene Datum Planes. Univ. Tokyo Press, pp. 47–68.

Adjas, A., Masse, J.P. and Montaggioni, L.F., 1990. Fine-grained carbonates in nearly closed reef environments: Mataiva and Takapoto Atolls, Central Pacific Ocean. Sediment. Geol., 67: 115–132.

Aharon, P., Socki, R.A. and Chan, L., 1987. Dolomitization of atolls by seawater convection flow: test of a hypothesis at Niue, South Pacific. J. Geol., 95: 187–203.

Arthur, M.A. and Jenkyns, H.C., 1981. Phosphorites and paleoceanography. Oceanol. Acta: 83–96.

Belayouni, H. and Trichet, J., 1983. Preliminary data on the origin and diagenesis of the organic matter in the phosphate basin of Gafsa (Tunisia). In: Bjoroy et al. (Editors), Advances in Organic Geochemistry. John Wiley and Sons, New York, pp. 328–335.

Blanchard, F., 1978. Pétrographie et géochimie de l'île de Moorea, archipel de la Société. Ph.D. Dissertation, University of Paris XI, 156 pp.

Bourrouilh-Le Jan, F., 1990. Diagenèse des carbonates de plates-formes, récifs et mangroves, en Atlantique et Pacifique. Ph.D. Dissertation, University of Paris, 190 pp.

Bourrouilh-Le Jan, F. and Hottinger, L.C., 1988. Occurrence of rhodolites in the tropical Pacific: a consequence of Mid-Miocene palaeo-oceanographic change. Sediment. Geol., 60: 355–367.

Brousse, P., 1985. The age of the islands in the Pacific Ocean: volcanism and coral-reef buildup. Proc. Fifth Int. Coral Reef Symp. (Tahiti), 6: 389–400.

Chevalier, J.P., 1973. Geomorphology and geology of coral reefs in French Polynesia. In: O.A. Jones and R. Endean (Editors), Biology and Geology of Coral Reefs, 1. Academic Press, New York, pp. 113–141.

Clarke, W.J. and Blow, W.H., 1969. The inter-relationships of some Late Eocene, Oligocene and Miocene larger foraminifera and planktonic biostratigraphic indices. Proc. First Confer. Planktonic Microfossils, 1967, 2: 82–96.

Cook, P.J. and McIlhinny, M.W., 1979. A re-evaluation of the spatial and temporal distribution of sedimentary phosphate deposits in the light of plate tectonics. Econ. Geol., 74: 315–330.

Crough, S.T., 1978. Thermal origin of midplate hot spot swells. Geophys. J.R. Astron. Soc., 55: 4713–4729.

Crough, S.T., 1983. Hot spot swells. Annu. Rev. Earth Planet. Sci., 11: 165–193.

Crough, S.T., 1984. Seamounts as recorders of hot-spot epeirogeny. Geol. Soc. Amer. Bull., 95: 3–8.

Dessay, J., 1990. Etude paléohydrologique, pétrologique et minéralogique de la dolomitisation de l'île Makatea (Polynésie Française). Ph.D. Dissertation, University of Bordeaux, 243 pp.

Detrick, R.S. and Crough, S.T., 1978. Island subsidence, hot spots and lithospheric thinning. J. Geophys. Res., 83: 1236–1244.

Duncan, R.A. and McDougall, I., 1976. Linear volcanism in French Polynesia. J. Volc. Geotherm. Res., 1: 197–227.

Duncan, R.A., McDougall, I., Carter, R.M., and Combs, D.S., 1974. Pitcairn island. another Pacific hot spot? Nature, 251: 679–682.

Handschumacher, D., 1973. Formation of the Emperor seamount chain. Nature, 244: 150–152.

Haq, B.V., Hardenbol, J. and Vail, P.R., 1987. Chronology of fluctuating sea-levels since the Triassic. Science, 235: 1156–1167.

Hein, J.R., Gray, S., Richmond B.M. and White L.D., 1992. Dolomitization of Quaternary reef limestone, Aitutaki, Cook Islands. Sedimentol., 39: 645–661.

Jarrard, R.D. and Clague, D.A., 1977. Implication of Pacific island and seamount ages for the origin of volcanic chains. Rev. Geophys. Space Phys., 15: 57–76.

Lambeck, T., 1981. Flexure of the ocean lithosphere from island uplift, bathymetry and geoid height observations: the Society islands. Geophys. J.R. Astron. Soc., 67: 91–114.

Le Calvez, Y. and Salvat, B., 1980. Foraminifères des récifs et lagons coralliens de Mooréa, île de la Société. Cah. Micropaleontol., 4: 1–15.

Lincoln, J.M. and Schlanger, S.O., 1987. Miocene sea level falls related to the geological history of Midway Atoll. Geology, 15: 454–457.

Mammerickx, J., Anderson, R.N., Menard, H.W. and Stuart, H.W., 1975. Morphology and tectonic evolution of the East-Central Pacific. Geol. Soc. Amer. Bull., 86: 111–118.

McNutt, M.K. and Menard, H.W., 1978. Lithospheric flexure and uplifted atolls. J. Geophys. Res., 83: 1206–1212.

McNutt, M.K. and Judge, A.V., 1990. The superswell and mantle dynamics beneath the South Pacific. Science, 248: 969–975.

Menard, H.W., 1964. Marine Geology of the Pacific. McGraw-Hill, New York, 271 pp.

Menard, H.W. and McNutt, M.K., 1982. Evidence for and consequences of thermal rejuvenation. J. Geophys. Res., 87: 8570–8580.

Montaggioni, L.F., 1985. Makatea Island, Tuamotu archipelago. Proc. Fifth Int. Coral Reef Symp. (Tahiti), 1: 105–157.

Montaggioni, L.F., 1989. Le soulèvement polyphasé d'origine volcano-isostasique: clef de l'évolution post-oligocène des atolls du Nord-Ouest des Tuamotus (Pacifique Central). Compt. Rend. Acad. Sci., Paris, 309, II: 1591–1598.

Montaggioni, L.F., Gabrie, C., Naim, O., Payri, C., Richard, G. and Salvat, B., 1987. The seaward margin of Makatea, an uplifted carbonate island (Tuamotus, Central Pacific). Atoll Res. Bull., 299: 1–18.

Monti, S., 1974. Carte bathymétrique, Pacifique Sud, échelle 1/1.000.000. Centre Océanol. Bretagne, CNEXO Edit.

Obelliane, J.M., 1963. Le gisement de phosphate tricalcique de Makatea (Polynésie Française, Pacifique Sud). Sci. Terre, 9: 5–60.

Pirazzoli, P.A. and Montaggioni, L.F., 1988. The 7,000 yr sea level curve in French Polynesia: geodynamic implications for mid-plate volcanic islands. Proc. Sixth Int. Coral Reef Symp. (Townsville), 3: 467–472.

Richard, G., 1982. Mollusques lagunaires et récifaux de Polynésie Française: inventaire faunistique, bionomie, bilan quantitatif, croissance, production. Ph.D. Dissertation, University of Paris, 313 pp.

Shackleton, N.J. and Opdyke, N.D., 1973. Oxygen isotope and paleomagnetic stratigraphy of Equatorial Pacific core V28-238, oxygen isotope temperature and ice volume on a 10^5 years and 10^6 years scale. Quat. Res., 3: 39–55.

Schlanger, S.O., 1981. Shallow-water limestones in oceanic basins as tectonic and paleoceanographic indicators. In: J.E. Warme, R.G. Douglas, and E.L. Winterer (Editors), The Deep Sea Drilling Project: A Decade of Progress. Soc. Econ. Paleon. Mineral., Spec. Publ., 32: 209–226.

Schlanger, S.O., Garcia, M.O., Keating, B.H., Naughton, J.J., Sager, W.W., Haggerty, J.A. and Philpotts, J.A., 1984. Geology and geochronology of Line islands. J. Geophys. Res., 89: 11261–11272.

Tayama, R., 1935. Table reefs, a particular type of coral reefs. Proc. Imp. Acad., Tokyo, II: 268–270.

Veeh, H.H., 1966. $^{230}Th/^{238}Th$ and $^{234}U/^{238}U$ ages of Pleistocene high sea level stand. J. Geophys. Res., 71: 3379–3386.

Venec-Peyre, M.T. and Salvat, B., 1981. Les foraminifères de l'atoll de Scilly (archipel de la Société): étude comparée de la biocoenose et de la thanatocoenose. Ann. Inst. Océanogr., Paris, 57: 79–110.

This Page Intentionally Left Blank

Geology and Hydrogeology of Carbonate Islands. Developments in Sedimentology 54
edited by H.L. Vacher and T. Quinn
© 1997 Elsevier Science B.V. All rights reserved.

Chapter 15

GEOMORPHOLOGY AND HYDROGEOLOGY OF SELECTED ISLANDS OF FRENCH POLYNESIA: TIKEHAU (ATOLL) AND TAHITI (BARRIER REEF)

FRANCIS ROUGERIE, RENAUD FICHEZ and PASCALE DÉJARDIN

INTRODUCTION

Barrier reefs and atolls of French Polynesia are surrounded by warm and clear oligotrophic water of the South Pacific gyre. Atolls forming the Tuamotu Archipelago show great geomorphologic and hydrologic diversity. The diversity reflects the openness or closure of their lagoons: open, with a pass; enclosed, with or without a shallow pass (hoa); hypersaline on one extreme, or brackish on another; filled with sediment; tilted and/or uplifted. Reef-lagoon systems of other archipelagoes (Society Islands, Austral Islands) are similarly diverse. In all these cases, however, barrier reefs maintain a set of uniform morphological features and must be viewed as the first-order structure. Lagoons and pinnacles range from being second-order structures to being nonexistent.

Interstitial water samples obtained from drillings made in Tikehau Atoll (Tuamotu) and Tahiti barrier reef allow us to describe and produce a model of the behavior of the interstitial water in the reef. This model, named geothermal endoupwelling, is based on an upward circulation of interstitial water (provided by deep oceanic water), from the reef foundation to the reef rim, and is supported by measurements of nutrients and conservative markers. In the top part of reef and atoll structures, fresh and brackish groundwater are included in the interstitial circulation and govern the dissolution/precipitation balance of the carbonate matrix. Diagenetic processes (early cementation, dolomitization, phosphatogenesis, and degradation of organic matter) are affected by this upwelling of interstitial water.

REGIONAL SETTING

Geography

French Polynesia is mainly a maritime domain that extends over 5 million km^2 in the Central South Tropical Pacific (Fig. 15-1) Encompassed within this area is the Exclusive Economic Zone, which extends 200 miles outward from the islands shores, and is the domain over which the coastal state exercises sovereign rights for exploration, conservation and exploitation of resources (cf., Atlas of French Polynesia, 1993). French Polynesia consists of five archipelagoes, totaling 122 islands and 3,521 km^2. Population is 200,000 with an annual increase of 2.7%.

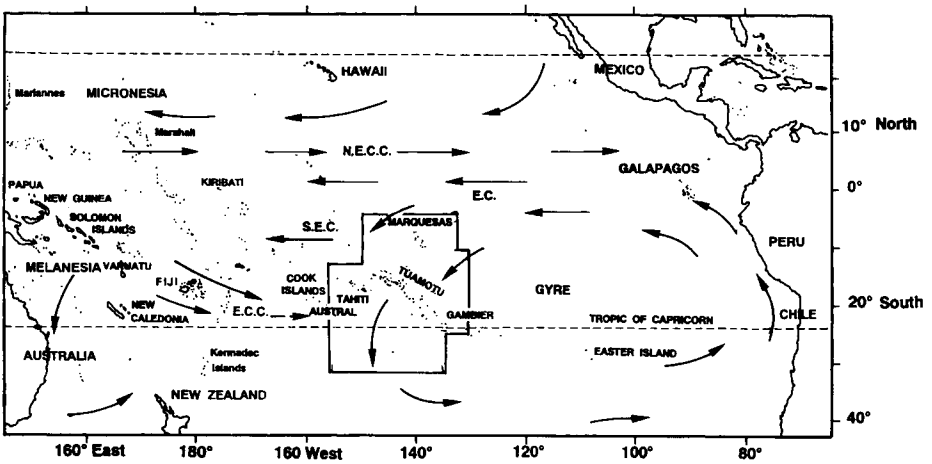


Fig. 15-1. Map of the Intertropical Pacific. French Polynesia is bathed by the oligotrophic oceanic gyre centered in the Easter island zone. Currents flow westward and counter currents flow eastward. Abbreviations: E.C., Equatorial Current; S.E.C., South Equatorial Current; N.E.C.C., North Equatorial Counter Current; E.C.C., Equatorial Counter Current.

Tahiti, the main island, is in the Society Islands archipelago. Its surface area is 1,042 km^2, and it is surrounded almost totally by a barrier reef, separated from the shoreline by a narrow lagoon (100–800 m wide). The Tuamotu Archipelago is the territory's most widely scattered group, a cluster of 77 coral islands (atolls). The most extensive island group of its kind in the tropical Pacific, the Tuamotus stretch over a distance of 1,800 km from northwest to southeast and cover an area close to 1 million km^2 of ocean. The total area of emergent land (or motu) is less than 1,000 km^2, and atolls and lagoons together barely amount to 20,000 km^2. The smallest atolls (with their lagoons) do not exceed 2 km^2, and the largest (Rangiroa) is 1,600 km^2.

Geology

In the Society Islands archipelago, islands show every stage of transition from the original hotspot of volcanism (Mehetia), to the high island with barrier reef (Tahiti), the almost-atoll (Bora-Bora), and the atoll (Tupuai). These islands are moving northwestwards by the movement of the Pacific Plate, which explains why the island groups lie parallel to each other. The linear island chains are formed by isolated volcanic structures set on a plateau lying above the ocean floor. The age of islands increases with distance from a hotspot. The height of emerged volcanoes (2,200 m in Tahiti at present) diminishes with distance from their originating hotspot. The volcanoes finally disappear at the end of the chain, subsiding into atolls and then seamounts. Between birth and atoll stage, approximately 5 m.y. elapse, but atoll

growth can keep up with subsidence for tens of millions of years (50 m.y. for atolls of the western Tuamotu).

The chemical composition of the lavas is either tholeiitic or alkaline basaltic. The volcanic flows first discharge in an underwater environment and then in an aerial one. Aerial lava flows commonly contain red layers which are interpreted to be paleosols. The rocks are frequently leached by meteoric water and contain intrusions such as dikes, sills, domes. They have moderate hydraulic conductivity of 10^{-8} to 10^{-6} m s^{-1} (Guille et al., 1993). The sediment cover comprises a transition zone containing volcaniclastic rocks, derived from the weathering of the volcano, and carbonate rocks, derived from the deposition of a chlorozoan assemblage (algae and corals) during the island subsidence and/or sea-level rise. The barrier reefs, which build up along a vertical plane from the rim of the original volcano, contain essentially porous and permeable limestones (hydraulic conductivity of 10^{-4} m s^{-1}), and, in some instances, these limestones have been dolomitized. After total subsidence of any basaltic peak below sea level, atoll morphology represents an unstable balance between chlorozoan construction processes and destruction processes such as mechanical and chemical erosion, slope slides during typhoons, and tsunami. At some localities, destructional processes exceed constructional ones, and the atoll is said to "fail"; it becomes a drowned atoll or guyot. At other localities such as Makatea [q.v., Chap. 14], lithospheric swelling related to the emergence of Tahiti and Moorea 150 km in the south has resulted in tectonic uplift. A bibliography of geology and geophysics of French Polynesia and of other islands of the intertropical Pacific is presented elsewhere (Jouannic and Thompson, 1983).

Climate

Polynesia is under the influence of the Southern Oscillation, a climatic process which involves the interaction between a high-pressure system (centered on the Tahiti Island-Easter Island area) and a low-pressure system (centered on the equatorial north Australian-Indonesian area). Pressure imbalance between these systems produces the trade winds. These winds, averaging 10–20 kn, blow mainly from the northeast sector in austral summer and from the southeast sector in winter. As the high-pressure system is broadly stretched along the subtropical Pacific, between Kermadec Island and Easter Island, it controls both types of trade winds. The northeastern and the southeastern trade winds converge, creating a zone of doldrums and high precipitation, the South Pacific Convergence Zone (SPCZ). Seasonal shifts in the location of the SPCZ are the main cause of the occurrence of a rainy season in the tropical South Pacific. In French Polynesia (Figs. 15-1, 15-5), the rainy season occurs during the austral summer and affects an area between the Tuamotu and Austral archipelagoes. In the Tahitian province (17°30′S, 150°W) mean rainfall at sea level is 150 cm y^{-1}. In central and eastern Tuamotu, rainfall is below 100 cm y^{-1}, and measured evaporation is in the range 150–250 cm y^{-1}. Precipitation minus evaporation (P-E) is hence around −50 cm y^{-1}, a value indicative of marked aridity. In the vicinity of the high islands of the Society and Austral groups, P-E is negative

during the austral winter. In the first quarter (austral summer), abundant rainfall and orographic effects on the slopes of the islands lead to positive P-E values. In the Polynesian province, air temperature is generally in the 20–33°C range.

Oceanography

In its eastern and central part, the South Pacific Ocean can be simply described as a large gyre centered on Easter Island and longitudinally limited by the equatorial zone (north of Marquesas Islands) in the north, and the Tropic of Capricorn. Circulation of surface water masses within the gyre is anticyclonic (anti-clockwise) and directly sustained by the trade wind stress (Levitus, 1982). In the surface layer, the dominant current is the Equatorial Current which is oriented westward and flows with an average speed of 20–50 cm s^{-1} (0.5–1 kn) between the latitude of 10°S and 4°N. Another current, located north of the Tropic of Capricorn and known as the South Equatorial Current, flows in the same direction with an average speed of 10 cm s^{-1}. Between these two geostrophic currents, counter currents flow eastward with generally slower, non-permanent fluxes. The Equatorial Counter Current, for example, runs along the SPCZ and brings warm, low-salinity waters originating from the Solomon Sea toward French Polynesia. This counter current is well developed in austral summer and tends to migrate during the winter towards 10°S. The Tahitian zone, located in the western branch of the tropical gyre, has sea-surface temperatures of 26–30°C and sea-surface salinities of 35.6–36.3 psu (practical salinity unit). The high value is a maximum for the entire Pacific Ocean and is typical of the Tuamotu-Pitcairn area where negative P-E differentials tend to increase surface salinity (Delcroix and Henin, 1991). Conversely, in counter currents, surface salinity may decrease to 35.5 psu during the peak of the summer rainy season. Along the Tropic of Capricorn, seawater temperature is around 21°C in winter, largely above the 18°C lower lethal limit for tropical hermatypic corals.

Vertical thermal profiles (Fig. 15-2) show the top 0–150 m of the ocean, labeled "mixed layer," as being directly influenced by air-ocean exchanges, occupied by a warm (>25°C) and saline (36 psu) water mass commonly called the Tropical Surface Water (TSW). This oceanic water is directly in contact with the barrier reefs and atolls of French Polynesia. The TSW has some specific chemical properties such as very low nutrient concentrations (inorganic dissolved phosphate and nitrate below 0.2 mM m^{-3}), saturation in dissolved oxygen (4.5–5. L m^{-3}), high pH (8.3), low chlorophyll concentration (<0.1 mg m^{-3}), low gross primary production (<30 gC m^{-2} y^{-1}) and very low turbidity resulting in the extension of the euphotic zone to a depth of 150 m (Wauthy, 1986). The very low level of net primary productivity is typical of oligotrophic ocean waters, and the South Pacific gyre is often compared to a desert (Barber, 1992).

Below the oligotrophic mixed layer, the permanent thermocline marks a significant drop in temperature between depths of 150 and 400 m. The drop is a transition from warm (>25°C) TSW to cold (5 ± 2°C) Antarctic Intermediate Water (AIW), the latter extending between depths of 500 and 1,500 m. This transition has a major hydrologic

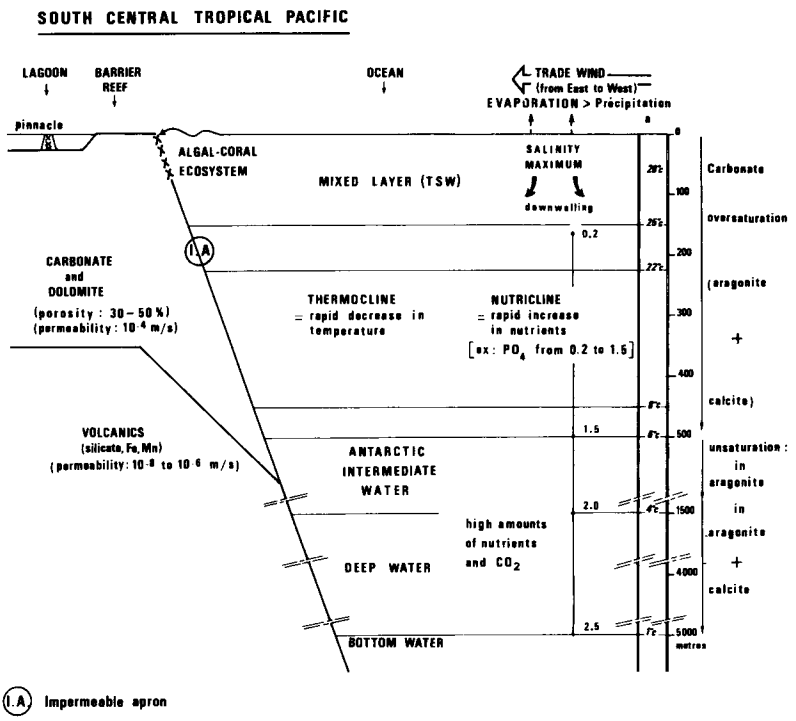


Fig. 15-2. Oceanographic, climatic and geologic setting of atolls and barrier reefs in French Polynesia. Oligotrophy of the mixed layer (0–150 m), occupied by Tropical Surface Water (TSW), is maintained by downwelling of saline surface water, thermal stratification at 150–500 m, and the great depth (> 200 m) of nutricline. High productivity of algal-coral ecosystem in such clear, low-productivity seawaters constitutes the "Darwin paradox" for which we propose a new solution – the geothermal endo-upwelling concept (Rougerie et al., 1992a). The range of the impermeable apron corresponds to the oceanic layer 0–500 m, oversaturated with respect to both calcite and aragonite.

impact because AIW is rich in nutrients (2 mM m^{-3} in phosphate, 20 mM m^{-3} in nitrate). The first kilometer of the tropical Pacific Ocean can thus be viewed as a two-layer system, separated by a permanent thermoclinic barrier: the warm and nutrient-depleted TSW (mixed layer) overlying the cold and nutrient-rich AIW. Oligotrophy is a consequence of that permanent water stratification, and there is no local or regional upwelling to push nutrient-rich water toward the surface, even in the vicinity of the islands (Rancher and Rougerie, 1993; Rougerie and Rancher, 1994). The weakness of turbulences and the thickness of the warm mixed layer prevent any dynamic turnover between the oligotrophic euphotic zone and nutrient-rich intermediate waters (Heywood et al., 1990). The tide range is only about ± 15 cm in the Tahiti-central Tuamotu zone.

Upwelling zones in the Pacific basin are located along the American coast (Peru, California) and along the equatorial band from the Galapagos (permanent upwelling) to New Guinea (non-permanent upwelling). The surface-water signature of any upwelling is well known: cool sea-surface temperature anomalies, high nutrient and chlorophyll contents, and enhanced turbidity. It is interesting to note that such

properties, which are highly favorable to planktonic development and fisheries, are not favorable to coral settlement and growth (Hallock, 1988); this is the reason why barrier reefs are absent in the coastal upwelled waters from Peru to Mexico and around the Galapagos Islands. Conversely, the oligotrophy of the South Pacific gyre is enhanced by a downwelling process (sinking of surface, highly saline water) with the apparent paradoxical result that atolls and barrier reefs thrive best in clear, nutrient-depleted waters.

GEOMORPHOLOGY

Barrier and atoll reefs

Polynesian patch, pinnacle, barrier or atoll reefs share some general patterns with other Indo-Pacific reefs (cf., Proc. Fifth Intern. Coral Reef Congress [Tahiti], 1985). The reef crest and the top of the outer slope of barrier reefs, either around high islands (Tahiti, Moorea), almost-atolls (lagoon area > emerged island area: Bora-Bora, Maupiti), or atolls, are directly impacted by oceanic high-energy swells (Guilcher, 1988). Reefs adapt to this high-energy level by (a) developing a spur- and -groove system which provides geomorphologic-hydrodynamic resistance to high-energy swells, energy absorbance, and porosity, (b) having high gross primary production and calcification rates in the algal-coral ecosystem (Hatcher, 1985), and (c) developing complex community structure as a response to highly variable environmental gradients (Fagerstrom, 1987).

Three major geomorphologic units are commonly developed in Polynesian reef systems. The first unit is a steep outer slope with continuous living algal-coral structure down to a depth of 60–80 m. The second unit is a carbonate rim dotted with fossil conglomerates upon which lie flat islands of detrital material (rubbles and sands), locally known as motu. The third unit is a lagoon of varying water depth, which varies from 0 m in a sediment-filled lagoon to 60 m in some particularly deep lagoons. Calcareous sediments line the lagoon floor, and coral pinnacles and patch reefs can also be located in the lagoon. The barrier-reef flats may be breached by passes through which lagoon waters ebb and flow. The smallest gaps in the reef flat, locally known as hoa, are shallow channels (tens of centimeters) across the reef flat through which oceanic waters can enter the lagoon.

In some reef channels, immediately below the lower limit of living corals, an impermeable apron of well-cemented carbonate sediment is found. Cementation in this environment is favored because TSW is oversaturated with respect to carbonate, especially aragonite which is five times oversaturated. This impermeable apron, which prevents horizontal exchanges between seawater and the interstitial-fluid system, is progressively dissolved below 400–500 m where seawater (AIW) becomes undersaturated with respect to aragonite; below 1 km, both aragonite and calcite are undersaturated.

Generally, the crest and reef flat of barrier and atoll reefs barely crop out at normal sea-level height. A first-order approximation based on the four archipelagoes

of French Polynesia, comprising 15 high islands with barrier reefs and 80 atolls, indicates that more than 85% of the reef system is emergent, while the remainder is slightly uplifted or drowned.

The fifth archipelago, the Marquesas, constitutes an exception having only fringing reefs. After decades of contradictory statements addressing the absence of barrier reefs, there is now evidence of a drowned reef encircling each of the ten high islands of Marquesas at −95 m (Rougerie et al., 1992c.). Other drowned reefs exist in the Tuamotu Archipelago: Portland Bank, south of Gambier (almost-atoll) is now at −50 m and continues to sink (Pirazzoli, 1985); south of Niau Atoll (152°W, 15°S), a drowned atoll or guyot has been recognized at −1,000 m (Le Suavé et al., 1986).

Northeast of Tahiti, the barrier reef remains 7–15 m below sea-level for >10 km. The deleterious effect of freshwater runoff is not thought to be responsible for keeping the barrier reef from fully developing to reach the height of sea level. Passes constitute interruptions in the reef crest for evacuation of brackish-turbid lagoonal waters opposite river mouths. In north Moorea, south Maupiti and in atolls, passes are created by movement of the excess oceanic water accumulated in their lagoons by swells and reef-crest washover. Some reefs may be tilted (Tikehau south) or uplifted (Makatea, Rurutu east), by tectonic forces or hotspot activity. These elevated reef structures surrounded by living fringing reefs may be good analogs for islands and atolls of 20 ka when sea level was −125 m. Today, the integrity of Polynesian shorelines depends on their reefs which act as barriers protecting coastlines and plains from incident wave energy.

Resistance of barrier-reef rims to oceanic high energy is promoted by coral colonies and algal encrustations, as well as by early cementation that binds dead corals blocks and rubble. Early cementation is active in high-energy zones (Aissaoui and Purser, 1986). Dolomitization is another diagenetic process that increases the strength of barrier reefs, allowing them to persist for tens of million of years as in West Tuamotu Archipelago (Humbert and Dessay, 1985). Dolomite is found deep within atolls (Mururoa [q.v., Chap. 13]), at the top of atoll reefs (Tikehau) or in uplifted atolls (Makatea [q.v., Chap. 14]) and barrier reefs (Rurutu in the Cook Islands [q.v., Chap. 16]). Some Tuamotu atolls are surprisingly small; a dozen (e.g., Tepoto, Vanavana and Pinaki) have diameters of 2–5 km, giving total emergent area <20 km^2. These atolls, rising from depths of 1–3 km from adjacent ocean floor, appear like the tips of chimneys with their dense crown of coconut trees "magically" emerging over the immense blue ocean. Severe typhoon-induced slope avalanches and normal losses of organics and sediments do not seem to alter the permanence of these islands, which provides convincing documentation of the high vitality and strength of their protective barrier reefs.

Reef gaps: hoa, passes and caverns

The various types of atolls and carbonate islands of French Polynesia can be classified according to the number and importance of interconnections (passes; shallow channels or hoa) between the lagoon and ocean (Salvat, 1985). In the

Tuamotu Archipelago, a third of the 77 atolls have passes 1–10 m deep (Rangiroa, Fakarava), a third have only hoa (Takapoto, Tetiaroa), and the last third is either totally enclosed (Taiaro), filled with sediment (Nukutavake, Aki-Aki) or uplifted (Makatea, +100 m). Some lagoons of high islands (northeast Moorea, north Huahine) can also be partly or totally filled with sediments originating from the barrier-reef rims and transported into lagoon by wave surges. These sediment-filled lagoons appear as flat plains covered with dense vegetation and coconut trees, an image somewhat different from the traditional "blue lagoon" of postcards. The oceanic water passing over the barrier-reef crest by wave surge either flows across the reef flat toward the lagoon or back to the ocean via grooves and cavities. The excess water filling the lagoon is evacuated by strong currents flowing out through the passes, sometimes forming a turbid green plume that extends far into the blue ocean. Twenty-five years of visual observations, diving and measurements have shown that oceanic water entering lagoons through hoa or passes is oligotrophic. Turbulent exchange processes, such as geostrophic pumping (Nof and Middleton, 1989) or tidal jets (Wolanski et al., 1988), do not exist significantly in the permanently stratified Polynesian ocean.

Another possible evacuation process calls for percolation of hypersaline water through the porous bottom and flanks of the lagoon. This process appears to be especially important in enclosed atolls such as Taiaro or Takapoto (Rougerie, 1983), where salt exportation can reach 3.10^{-2} g m^{-2} s^{-1}. However, these lagoons are permanently more saline (38–43 psu) than the ocean because water lost by evaporation is compensated by input of oceanic water via hoa. Hoa can carry huge volumes of water during high tides and tempests. At low tide, excess lagoon water can escape only through breaks, for a certain tide range, and the volume of escaping water is a function of lagoon area. Thus, large lagoons (600–1,600 km^2) have potential outflow 50 to 100 times greater than small lagoons (2–100 km^2) if tides are equal (Bonvallot et al., 1994). In all cases, outflow is through reef-breaks, which in large lagoons, causes them to be carved and enlarged to the stage of passes (depth >1 m). Current speeds of 5–12 kn are recorded in passes of large atolls such as Rangiroa, Fakarava and Hao, and constitute a hydrodynamic force limiting coral growth and buildup in the pass channel. Accordingly, large quantities of sediment are expelled from these lagoons in strong outflow regimes. In small atolls, modest outflows cannot erode hoa to the pass stage, and absence of sediment purge favors the infilling of the lagoon (Table 15-1).

Big caverns can puncture reef slopes as in the west of Rangiroa Atoll, at 50–80 m in a zone of apparent dissolution: coral spurs do not exist there and a large population of heterotrophs, such as filter-feeders like *Stylasterina*, have colonized the reef slope. A 60-m-deep cavern with calcite stalactites has been found in the north Raiatea lagoon. The fact that this hole is not choked by surrounding sediments suggests an active circulation and/or dissolution process by interstitial reef waters. Circulation between the bottom of the lagoon of Vanavana Atoll (−5 m) and the ocean (at unknown depth) may be the result of a suction vortex that develops during low tide and sends clear oceanic water into the lagoon during rising tidal flows. This tunnel crossing beneath a 200-m-wide emergent rim may exchange water at the rate of

Table 15-1

Summary of select geomorphologic features in atolls of Tuamotu

	Number of Atolls	Lagoon Depth (m)	Surface Area (km^2) Max.	Min.	Avg.
Atolls with several passes[1]	10	> 30	1640	152	659
Atolls with one pass	17	20 ± 10	609	50	336
Atolls with no pass	44	10 ± 5	184	2	35
Atolls with filled lagoons	5	na	29	2	9

[1] passes are defined as a passage > 1 m deep across the barrief reef.
na = not applicable.

1–5 $m^3\ s^{-1}$, a sufficient flux to explain water-level variations in this quasi-enclosed and small (5 km^2) lagoon. A similar hole is known to exist in Tepoto Atoll (Tuamotu).

Lagoon waters. Lagoon waters are generally less depleted in nutrients, chlorophyll and plankton than oceanic TSW (Table 15-2). This difference is correlated with the residence time of lagoon waters and fluctuates considerably (Delesalle and Sournia, 1992). The residence time varies from weeks to years, depending on the hydrodynamic forces of the ocean, the number and depth of passes/hoa, and the size and volume of the lagoon. Short residence times reflect free exchange with the ocean and tend to maintain lagoon-water composition close to that of the intruding oligo-

Table 15-2

Summary of the hydrogeochemistry of reef interstitial waters (RIW), lagoon waters, and seawter at Tikehau Atoll[a]

Borehole[#]	Depth (m)	Salinity (psu)	N^* (μM)	NH_4 (μM)	PO_4 (μM)	SiO_2 (μM)	pH	Redox (mV)
P_1 and P_2	1–10	25.83	2.59	2.58	1.24	4.14	7.61	8
P_1 and P_2	20–30	34.55	3.76	0.72	1.09	7.71	7.67	−60
P_3	4–17	35.87	0.23	7.15	1.08	2.24	7.61	−60
P_4 and P_5	3–11	35.86	3.48	0.59	0.49	2.80	7.79	126
P_4 and P_5	19–33	35.73	2.37	1.19	0.84	5.74	7.73	73
Lagoon	0–20	36.06	0.20	0.30	0.26	0.81	8.24	218
Ocean TSW	1–100	36.05	≤ 0.1	≤ 0.1	≤ 0.2	≤ 0.2	8.31	192
Ocean AIW	> 500	34.50	20.0	0.10	1.80	15.0	7.90	150

[a] numbers listed are average values of borehole measurements of RIW made from 1989–1992. Lagoon and seawater measurements were made from 1986–1992.
[#] P_1 and P_2 (reef crest) interstitial water is spiked by groundwater discharge from the motu phreatic lens that creates alternating oxic-anoxic conditions. P_3 (lagoon pinnacle) interstitial water is highly anoxic, except in the shallowest section facing lagoon waves. P_4 and P_5 (reef crest) have no brackish interferences and a deep oxic layer.
* $NO_3 + NO_2$

trophic TSW. Conversely, lagoons in enclosed or slightly uplifted atolls have long residence times, leading physico-chemical properties to shift away from ocean values, and can accumulate dissolved nutrients and particulate organic matter. However, it is important to note that this organic richness represents a shift towards natural eutrophication and tends to eliminate coral colonies to the benefit of plankton, benthic macro-algae and cyanobacterial mats. Steady-state reef-lagoon systems constitute organic oases in the oceanic desert and potential net exporters of organic and carbonate-rich matter. Such losses are balanced in the medium and long term by the net production/calcification of the barrier reef.

Motu interstitial waters. Motu composed of coral sediments and sandy gravels often occupy the shoreward/backward part of barrier and atoll reefs and can store rainfall as groundwater or in a meteoric lens that floats over the denser, saline interstitial water. This underground reservoir is filled during the rainy season but permanently discharges to the ocean and lagoon; after several dry months, as often observed in Tuamotu atolls, the groundwater may be partly withdrawn, with negative consequences for the vegetation and the life of Tuamotu population. As proposed by the Ghyben-Herzberg principle, the freshwater volume stored underground depends on two factors, the elevation of the motu above sea level and its size (Buddemeier and Oberdorfer, 1986; 1988). Atolls like Scilly or Toau have small motu and small storage capacity. Conversely, closed lagoons are totally surrounded by a continuous, (10–103 km) broad (0.3–1.5 km) and uplifted (+2 to +8 m) motu; their storage capacity is considerable with the result that groundwater leaks can permanently lower the salinity of lagoon waters. For example, lagoons of Mataiva and Niau have salinity from 32–25 psu, despite the fact that the Tuamotu is a region with a negative P-E value. The ecological consequences of this low-salinity lagoon water are important because these brackish lagoons are unfit for coral settlement but they are highly favorable to the development of macro-algae (e.g. Caulerpa) and thick cyanobacterial mats (Defarge and Trichet, 1985).

The maximum rainfall storage capacity is reached in completely filled atolls (Aki-Aki, Tikei) or in very large motu surrounding high islands (Bora-Bora; Maupiti) where underground freshwater is pumped through by under-lagoon pipes to villages located on the main basaltic island. In Amanu Atoll, the head gradient has generated sufficient brackish-water seepage to provoke the collapse of several square meters of the flanks of the pass. It is possible that such a process, by maintaining a permanent erosion of the flank of the pass, participates to the onset and long-term existence of these passages across the atoll rim (Fichez et al., 1992). Indeed, this hypothesis is consistent with the observation that for the 27 atolls with 1 or 2 passes (Table 15-1), 22 of these passes are through emergent motu, whereas the other 5 are through overflow over a reef-flat rim.

Groundwater of motu is rich in nutrients, the concentrations of which increase with depth. Vegetation like coconut trees grow remarkably on that nutrient pool and can produce 2–4 tons ha^{-1} y^{-1} of copra, without any addition of fertilizer. Motu can also have ponds or cavities where fresh groundwaters freely appear; these ponds may be flooded during high tides or tempests by lagoonal or oceanic waters, causing them

Table 15-3

Summary of the hydrogeochemistry of the brackish kopara ponds of the motu of Tikehau Atoll[a]

	Salinity (psu)	N^* (μM)	NH_4 (μM)	PO_4 (μM)	SiO_2 (μM)	pH (μM)	Redox (mV)	Total Alkalinity (eq m^{-3})
Free water								
Surface	8	0.3	1	0.3	2	8.5	50	1.4
Bottom$^+$	20	0.6	3	0.6	4	9.4	150	1.8
Interstitial Water								
5 cm	15	0.5	15	2.5	6	7.6	−200	3.5
50 cm	25	0.7	25	4.0	12	7.5	−300	2.5

[a] based on measurements made in 1991 and 1992
$^*NO_3 + NO_2$
$^+$ 0.5–1 m

to be brackish with salinities of 10–30 psu. These ponds are nutrient-rich both in their free water and interstitial portion (Table 15-3).

The ponds are generally colonized by algal and cyanobacterial mats named "kopara." The kopara mats, which can be >1 m thick, are highly productive and have high concentrations of chlorophyll and carotenoid pigments (Defarge and Trichet, 1985). These kopara deposits are viewed as a stromatolitic facies (MacIntyre and Marshall, 1988). In closed brackish lagoons (Niau Atoll), kopara occupy the entire area and accumulated in several distinct layers (1–6 m thick) as has been documented by subsurface drilling. Layers of fluorapatite are found inside dead kopara, in conjunction with deep anoxic conditions. In case of partial desiccation of the kopara mats, such as in the reticulated lagoon of Mataiva or the uplifted island of Makatea [q.v., Chap. 14], fluorapatite comprises thick layers, producing tens of millions of tons of ore with 30% phosphorus content. The apparent association between accumulation and degradation of dead kopara and in situ precipitation of apatite is not fortuitous, but can constitute a driving process leading to phosphogenesis (Rougerie et al., 1994). This new model of atoll phosphogenesis is important because more traditional models such as the bird-guano model, have been recently rejected for quantitative and qualitative geochemical reasons (Roe and Burnett, 1985; Bourrouilh-Le Jan, 1992; Whitehead, 1993). Indeed, the newly proposed kopara model may solve the long-standing problem of the origin of phosphate deposits at Makatea, a problem previously noted by Menard (1986).

Patch reefs and pinnacles

The abundance of corals in lagoons shows considerable variability, both in species number and in area occupied. In narrow lagoons (Tahiti, Moorea), corals are most abundant on the barrier reef and in fringing reefs. In broad lagoons of almost-atolls (Bora-Bora, Maupiti), coral settlement is mainly on the outer barrier reef and secondly as patch reefs and pinnacles, apparently scattered in a chaotic way (Guilcher,

1991). The same pattern exists in Tuamotu atolls, where some lagoons have numerous pinnacles covering up to 10% of the lagoon surface (Takapoto, Tikehau), whereas other lagoons have very few (Rangiroa, Fakarava) or none (Tetiaroa, Taenga).

These coral structures are colonized largely by varied invertebrates, especially bivalves and surrounded by a halo of fishes. Hence, lagoon biomass is correlated with the density of pinnacles. In deep lagoons, pinnacles are tall structures with steep flanks and rise from the sandy bottom to the lagoon surface. Some pinnacles may reach 50 m high, with outcropping flat tops covering 10–100 m^2, with the most productive sector facing the dominant winds and currents. In lagoonal areas lacking pinnacles or patch reefs, the bottoms are monotonous sandy plains of white sediment originating from the barrier reef: productivity of these white bottom sectors is very low, especially in shallow waters (Le Borgne et al., 1989). *Mutatis mutandis* pinnacles are to lagoons what atolls are to the ocean: highly productive stalagmitic oasis, where coral reefs develop and are surrounded by clear oligotrophic waters.

In summary, reef geomorphology can be seen to be a function of oceanic energy, water turbidity and ocean productivity (Fig. 15-3) There are four major features of the reef-atoll systems of Polynesia:

(1) The outer barrier reef is common to all of these reef systems (pure atolls, tilted atolls, uplifted or enclosed atolls, barrier reefs of high islands). This biogenic carbonate structure, which acts as a wall encircling the lagoon, is entirely built and permanently reinforced by the linked actions of primary production, calcification and early cementation that take place within the algal-coral ecosystem. Without this protective living wall, atolls and lagoons would not exist. The barrier reef is the first-order structural feature of carbonate islands, whereas lagoons range from second-order feature to being absent, as in the case of filled lagoons or uplifted atolls.

(2) Lagoonal pinnacles appear to have a chaotic distribution: abundant in some lagoons, discrete or absent in others. Much like barrier reefs, these pinnacles constitute oases for life and high productivity/calcification, compared to low productivity of lagoonal waters.

(3) Atoll enclosure and elevation control lagoon salinities, even though the Tuamotu atolls are in a zone where evaporation dominates (P-E $< -$ 50 cm y^{-1}). In closed atolls with hoa, salinity can reach 43 psu with salt excess exported by water percolation through bottom and flank sediments. In closed atolls with continuous motu, freshwater stored in the phreatic lens during the rainy season can lower the lagoon salinity to <25 psu. In uplifted atolls, rainwater input leads to erosion and karstification of the carbonate structure and formation of freshwater caverns (Fig. 15-4).

(4) The spatial distribution of Indo-Pacific reefs and atolls as well as the abundance of coral colonies within lagoons confirm that corals thrive in clear oligotrophic waters and disappear in green plankton-rich waters (Hallock and Schlager, 1986; Hallock, 1988). This apparent paradox, commonly expressed as the Darwin paradox (Atkinson, 1988), needs to be solved by a convincing heuristic model. It is for that reason that, after having proposed the concept of reef functioning by geothermal

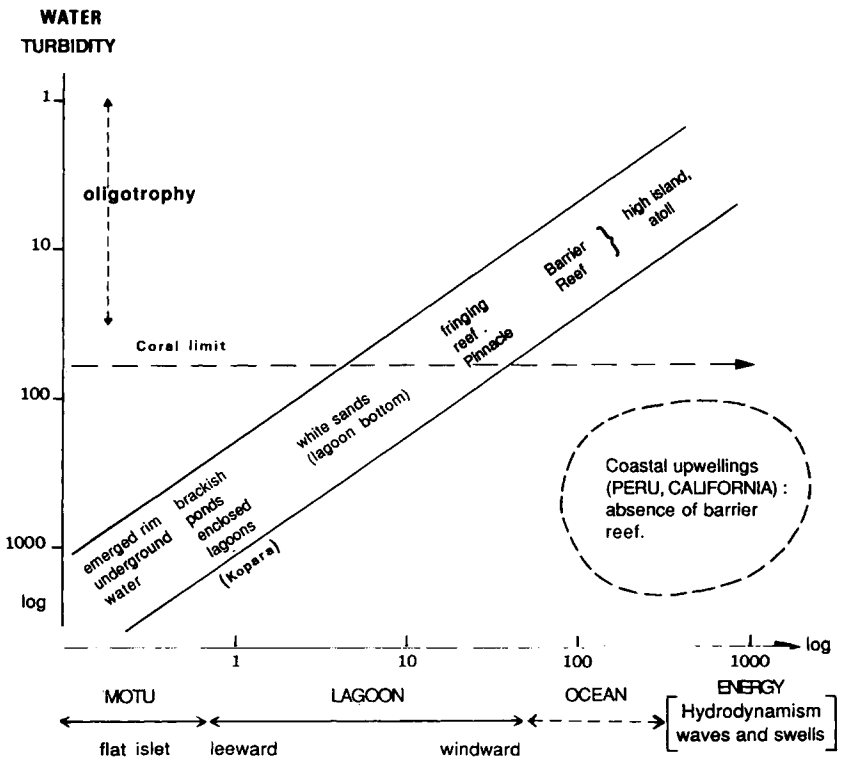


Fig. 15-3. Relation between coral-reef geomorphology and oceanographic energy regime and water turbidity (arbitrary units). Barrier and atoll reefs thrive best in coastal regions characterized by high-energy conditions and low-turbidity seawater. Barrier reefs are absent in zones of coastal upwelling. In a lagoon setting, pinnacle abundance and distribution appear chaotic. Low productivity and white sediments characterize 80–95% of the lagoon area. The water in enclosed lagoons is often hypersaline (e.g., Takapoto and Taiaro) or brackish (Niau) and coral colonies are replaced by macroalgae and/or algal mats (kopara in French Polynesia).

endo-upwelling (Rougerie and Wauthy, 1986, 1988, 1993), we have tried to maintain and support this new and controversial model by data obtained from holes drilled in atoll and barrier reefs in Polynesia.

CASE STUDY: INTERSTITIAL WATERS OF REEFS AND ENDO-UPWELLING

Previous studies of fluid flow in the subsurface of Florida and Enewetak Atoll have documented the existence of internal geothermal circulation, now often referred to as Kohout circulation, that has geologic and diagenetic consequences (Kohout, 1965; Fanning et al., 1981; Saller, 1984). The geothermal endo-upwelling concept (Rougerie and Wauthy, 1986; 1988; 1993) links thermally driven convective circu-

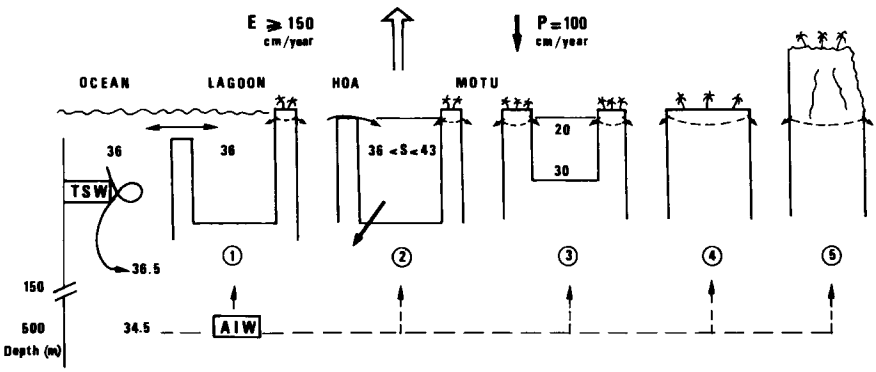


Fig. 15-4. Diversity of lagoons in Tuamotu Archipelago is a function of the amount of island enclosure and/or the elevation of motu and hence freshwater storage. Salinity values are in practical salinity units (psu). (1) Atolls with a deep oceanic pass typically have lagoon salinities that are equivalent to that of the ocean (e.g., Tikehau and Rangiroa). (2) Atolls without a deep oceanic pass, but with hoa typically have lagoon salinities that can reach 43‰ (e.g., Takapoto and Taiaro). (3) Atolls with continuous emergent motu typically have lagoon salinities that are $<25‰$ due to freshwater discharge from the motu to the lagoon (e.g., Niau). (4) Atolls in which the lagoon is completely filled with carbonate sediment typically have a maximum of freshwater storage (e.g., Aki-Aki and Nukutavake). (5) Uplifted atolls are subjected to erosion and karstification and may have caverns that are filled with freshwater (e.g., Makatea).

lation of subsurface fluids (i.e., Kohout circulation) with the biological consequences of this physical thermo-convective process on coral-reef growth.

The geothermal endo-upwelling process is particularly effective at carbonate islands because of the combination of a geothermal heat source and a porous and permeable geologic structure. Because of the cumulative buildup of heat, possible only in the absence of eddy diffusion, interstitial seawater within the reef framework loses density and a slow convective circulation is established: nutrient-rich deep ocean water penetrates the foundations of the island (basalt and/or carbonate) and ascends toward the top of the barrier or atoll reef where it escapes along the most permeable paths (i.e., mainly through the algal reef-crest spur- and -groove zone where sedimentation and porosity occlusion are prevented by ocean turbulence). Secondary circulation of endo-upwelled waters along sublagoonal faults and cracks on the lagoon bottom permits this water to escape and provide nutrients for the development of reef pinnacles within the lagoon. The nutrients supplied by endo-upwelled water promotes coral calcification via linkages to photo-autotrophic polyp growth. Thus, geothermally driven endo-upwelling can be considered as a necessary and sufficient process for the origin of hermatypic corals and continuing reef growth. The corollary is that algal-coral ecosystems of barrier and atoll reefs are biogeochemical signals marking the locations of interstitial water seepages. To test the validity of the concept for atolls and barrier reefs located in oligotrophic oceanic waters of the South Pacific Gyre, borings were drilled at two locations in French Polynesia in 1988, 1990 and 1992.

Tikehau Atoll reef

Reef features. Tikehau Atoll (150°W, 15°S) is located at the northwest end of the Tuamotu Archipelago (Fig. 15-5) Volcanoes that form the base of the atoll reef were probably formed 80–85 Ma, and their activity ceased in the Late Cretaceous to Early

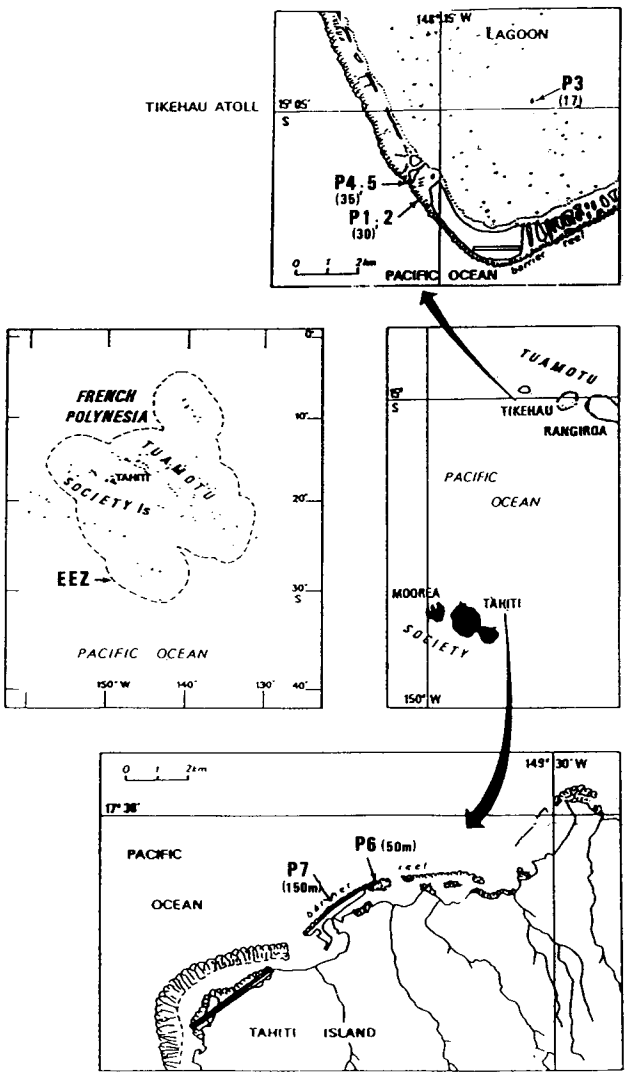


Fig. 15-5. Map of French Polynesia including the 200-miles contour outlining Exclusive Economic Zone (EEZ). Location and borehole sites for Tikehau Atoll (P_1, P_2, P_3, P_4 and P_5) and Tahiti barrier reef (P_6 and P_7). Interstitial waters are pumped at different levels via tubes that are permanently inserted inside these boreholes.

Eocene (Brousse, 1985; Montaggioni, 1993). Tikehau Atoll has a large lithified reef flat which is slightly above sea level for most of the year. High sea level due to low atmospheric pressure combined with rough seas causes waves to invade and sweep the reef-flat surface and numerous hoas. The buildup of hydraulic head in the lagoon is resisted by evaporation. Nevertheless a strong output of lagoon water occurs through the only pass, which is 4 m deep and is located on the west part of the atoll rim.

Four boreholes were drilled about 30 m from the ocean surf zone on the reef-flat and are representative of high-energy environments. The first two boreholes, denoted P_1 and P_2 (4 m apart), are also located 100 m from the emergent coral island (motu) and provided access to sampling depths of 1, 4.5, 10, 20 and 30 m. Two other boreholes, denoted P_4 and P_5 (1 m apart), were drilled on the reef flat more than 1 km away from the closest motu and provided access to sampling depths of 3, 6, 11, 19, 27 and 33 m. Another borehole, denoted P_3, was drilled through an outcropping pinnacle located in Tikehau lagoon and gave access to sampling depths of 4, 10 and 17 m. These boreholes allow comparison between interstitial waters originating from both high- and low-energy environments.

Analysis of the reef cores revealed a strongly dolomitized carbonate sequence for the whole borehole depth. Due to the hardness of dolomite, core retrieval was nearly 100% and drilling showed no large megaporosity voids. Nevertheless, cores (4 cm in diameter) had apparent porosity of 30% with mm- to cm-scale cavities. In the pinnacle, no dolomite exists, the carbonate is relatively soft, and large cavities (up to 1 m) were encountered during the drilling.

Interstitial water survey (1989–1992). Reef interstitial water (RIW) from boreholes P_4 and P_5 is oxic to a depth of 27 m and suboxic to 33 m (Table 15-2). Within boreholes P_1 and P_2, oxic conditions prevailed at the top and at the bottom of the borehole, but anoxic conditions occurred between 10 and 20 m. This anoxic layer results from the extension toward the ocean of the brackish interface between the freshwater lens (stored below the main motu) and the underlying interstitial seawater (Fig. 15-6) In borehole P_3 (pinnacle), RIW is anoxic from top to bottom. Concentrations in dissolved inorganic nutrients are significantly higher in RIW than in the surface oceanic layer. Within the boreholes, the increase in phosphate concentrations and a shift from nitrate to ammonium correlate with a shift in redox potential from positive to negative values due to biogeochemical processes and indicate a change from oxic to anoxic RIW.

The deep extension of oxic waters within the atoll reef indicates that some oxygenation processes must exist. Organic matter buried within the reef framework comes from the benthic system and undergoes mineralization with subsequent depletion in dissolved oxygen, as observed in the pinnacle borehole P_3. To compensate for this depletion, oxygen must be supplied in at least equal amount to the oxygen consumed. Our study of borehole P_3 shows that molecular diffusion of oxygen alone cannot account for this supply. Due to the observed difference between the lagoon pinnacle and the atoll RIW, it is obvious that wave surge plays a major role in providing oxygen to the interstitial system (i.e., intense wave-driven circulation in-

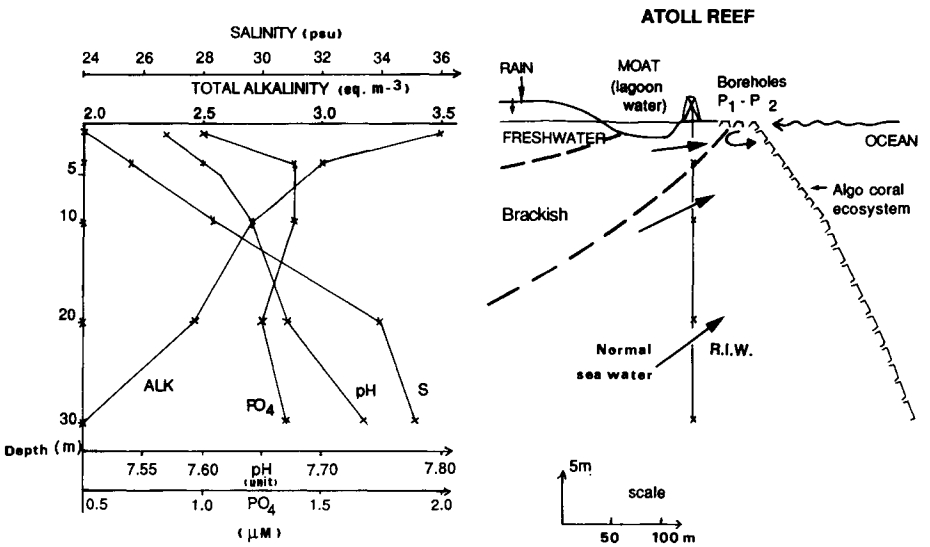


Fig. 15-6. Vertical profiles of salinity, total alkalinity, pH and inorganic dissolved phosphate in Tikehau Atoll boreholes P_1 and P_2. Groundwater discharge from the motu creates the brackish system located in the top 10 m. The low pH and high alkalinity of this brackish layer is indicative of dissolution of calcium carbonate of the reef matrix. Normal salinity (S > 35 psu) seawater (RIW) is present in the boreholes by 30 m. Main seepage zone is at the reef crest, which is characterized by high energy and high porosity and hydraulic conductivity.

jects oxygen-saturated oceanic water into the reef framework, lowering the depth of the oxic-anoxic interface).

Within the oxic interstitial environment, dissolved inorganic nutrients and CO_2 are liberated in proportion to oxygen consumption. The apparent oxygen utilization (AOU) may thus be used to assess the fraction of nutrients that come from the recycling of organic matter (D'Elia, 1988). Previous calculations estimated mineralization to contribute up to 50% to the nutrient pool with the remainder originating from exogenous deep sources (Rougerie et al., 1990). This conclusion supports the geothermal endo-upwelling circulation that considers new nutrients to come from the nutrient-rich Antarctic Intermediate Water (AIW).

Salinity is a conservative parameter and provides information on the origin and the mixing of waters within the porous carbonate framework (Table 15-2). Salinity in boreholes P_1 and P_2 is used to identify a low-salinity layer at a depth of 1–10 m related to the freshwater lens of the atoll motu. At 10–20 m, salinities are 30–34 psu, values that are significantly below ocean surface salinity (36.1 ± 0.1 psu). Thus, despite being situated on the reef flat 100 m away from the island and separated from it by a shallow channel continually flushed with ocean water, boreholes P_1 and P_2 are significantly affected by freshwater intrusion from the meteoric phreatic lens. This feature agrees with recent work demonstrating the brackish transition zone to extend oceanward even when covered with a thin layer of seawater. This layered structure is due to the combined effect of freshwater flowing toward the ocean and the under-

lying brackish and seawater flowing upward (Moore et al., 1992; Underwood et al., 1992). The motu effect becomes undetectable below 30 m, where salinity is 35.5 psu. In boreholes P_4 and P_5, where freshwater input (meteoric or groundwater) is not suspected due to the remoteness of motu, salinities range from 35.9 psu at 6-m depth to 35.7 psu at 27 and 33 m. These salinity values are significantly lower than those of oceanic TSW. The decreasing gradient with depth agrees with the input of "endo-upwelled" AIW having a salinity of 34.5 psu at depths of 600–800 m, shown in the mixing curves between AIW, TSW and RIW (Fig. 15-7).

Strong evidence of the presence of water originating from deep-sea sources within the reef interstitial network has been gained from the study of the distribution of ^3He (Rougerie et al., 1991). Distribution of δ^3He in the deep Pacific shows that primordial ^3He is being dispersed by hydrothermal venting on the East Pacific Rise at 2 ± 0.5 km depth. The δ^3He-enriched plume spreads westward into the central

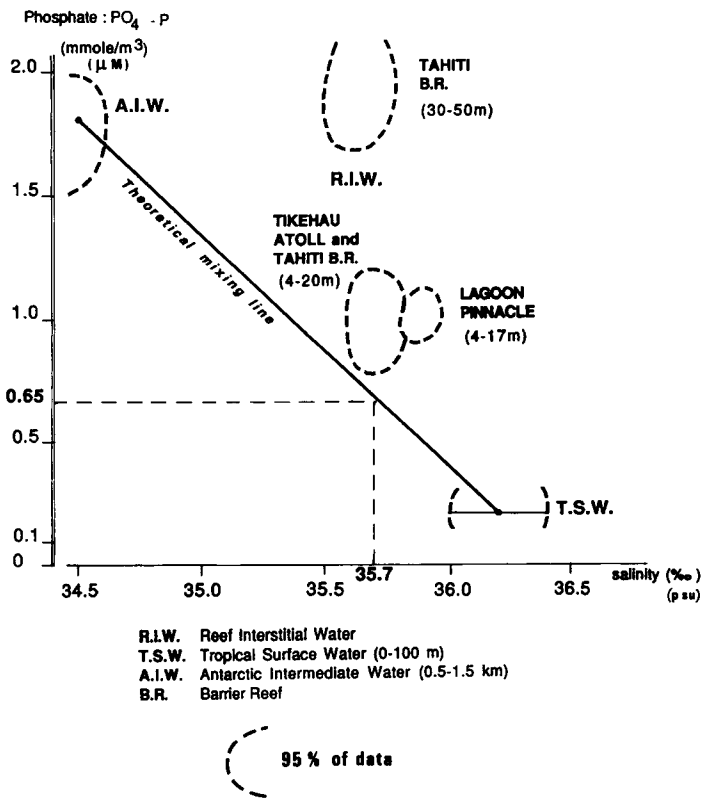


Fig. 15-7. Comparison of dissolved inorganic phosphate concentrations in oceanic (AIW and TSW) and reef interstitial waters (RIW). Phosphate concentration in RIW exceeds 0.65 mmole m^{-3}, which is the theoretical concentration of mixed AIW and TSW. This relation indicates that the chief phosphate sources are AIW plus in situ remineralization of organic matter in the reef matrix. A 0.5 psu salinity difference between RIW (35.7 ± 0.1 psu) and TSW (36.2 ± 0.2 psu) has been determined over a 3-year period (1990–1992; Rougerie et al., 1992a).

Pacific as far as the Tuamotu Archipelago where δ^3He values are up to 10% within AIW at 800-m depth. δ^3He values in Tikehau borehole waters increase with depth and are significantly higher than the values measured in the mixed layer (0–150 m) of the ocean (Fig. 15-8) Plotting δ^3He against salinity suggests that interstitial water is the result of the mixing of two endmember sources: TSW has a δ^3He of −1 to −2% and a salinity about 36.1 psu; AIW from a depth of 700–800 m has a δ^3He of 8–10% and a salinity about 34.5 psu. This result demonstrates that there is an upward flow within the reef framework driving deep oceanic water (AIW) through the carbonate pile to the top of the reef interstitial water system.

Since 1940, chlorofluorocarbon (CFC) has been anthropogenically introduced into the atmosphere through refrigerants, aerosol propellants, foams, and other products. CFCs are very useful oceanic tracers because they are conservative in seawater. The CFC (F12) concentration is homogeneous (0.8–1.0 ± 0.1 pM kg^{-1}) in the oceanic mixed layer from the surface to 200 m and sharply decreases with greater depth becoming almost undetectable in the South Pacific AIW below 400–500 m (Fig. 15-7) In Tikehau, RIW shows a F12 deficiency with concentrations around 0.2 ± 0.1 pM kg^{-1} below 10 m. Such depletion in F12 with depth can be explained either by the presence of old water trapped within the reef structure or by an input of F12-depleted ocean waters from at least 500 m. The subsurface oxygen profiles (Table 15-3; Fig. 15-6) are inconsistent with the former hypothesis. There-

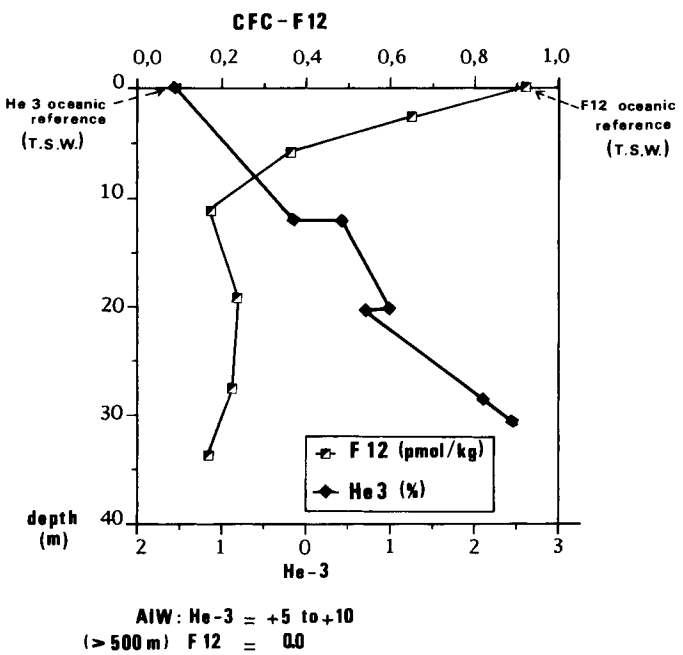


Fig. 15-8. Vertical profiles of chlorofluorocarbons (CFC-F12) and ^{3}He in RIW of Tikehau Atoll. Oceanic TSW and AIW reference values are given. Strong anomalies in the distribution of these conservative tracers into RIW can be explained by upward circulation of AIW inside reef matrix, as proposed by the geothermal endo-upwelling model (Rougerie et al., 1991).

fore, the F12 distribution strongly supports the conclusion from the study of ^3He distribution that AIW is a significant component of RIW (Fig. 15-8)

Dissolved non-aromatic hydrocarbons and fatty-acid concentrations were generally lower in the ocean than in the RIW of the Tikehau boreholes, where they increased with increasing depth (Andrié et al., 1992). Below 5 m the n-alkane profiles point to significant early diagenetic alterations due both to bacterial activity and to thermal maturation of organic matter (Bouloubassi et al., 1992). Such processes may have occurred in the deeper framework of the reef because of geothermal activity over geologic time. The presence of such mature markers in the top 30 m of the reef strongly suggests that waters follow an ascending movement from near the volcanic basement to the top. This suggests that ascending interstitial water, initially rich in dissolved organic matter from AIW and from leaching of organic matter trapped within the carbonate framework, undergoes sufficient heating in anoxic environment to produce mature alkanes.

Tahiti barrier reef (150°W, 17°30'S)

Reef features. There are a few studies dealing with the geology of carbonate reefs from high islands in French Polynesia. Boreholes have been drilled through the fringing and patch reefs surrounding Papeete harbor (Deneufbourg, 1971). However, materials from these boreholes were studied mainly from a sedimentologic perspective. Later, a 24-m-deep borehole drilled through the same reef system yielded information on sea-level variations since 7.0 ka (Pirazzoli and Montaggioni, 1986). Other drillings through a carbonate platform in Moorea Island were used to address paleohydrology issues (Faissolle, 1988).

Borehole P_6 was drilled in 1990 to a depth of 50 m through the barrier reef protecting Tahiti harbor (Fig. 15-5) Sampling tubes gave access to sampling depths of 1, 5, 20, 30 and 50 m. Unlike the reef of Tikehau Atoll, the Tahiti barrier reef lies a few tens of centimeters below sea level, is permanently flushed by waves and is emergent only in anomalous low sea levels common during peak ENSO events. The Tahiti core was studied for its petrography and mineralogy (Déjardin, 1991). Core recovery was 25–95%, with megaporosity voids (indicated by the drilling-rate logs) accounting for the low-recovery zones. Examination of the core material yielded no evidence of freshwater diagenesis, thus indicating no recent subaerial exposure events for the top 50 m of the reef. Radiocarbon dating (Bard et al., 1993) yielded ages of 3,000 and 5,500 y B.P. at depths of 2 and 3 m, respectively, corresponding to a period of relative sea-level stability. Ages regularly decreased with depth to 10,000 y B.P. at 50 m; this trend is interpreted as the consequence of a period of rapid vertical buildup of the reef in response to the Holocene eustatic sea-level rise. Today, that barrier reef is cut by two passes located in the axes of two valleys with permanent rivers (current of 0.5–2 $m^3\ s^{-1}$ with flood current $> 10\ m^3\ s^{-1}$ during typhoons). The river waters lower the salinity of the lagoon from 35 to 25 psu in the extreme case; the lagoon head, enhanced by overflow of oceanic water above the reef crest, creates current, which can reach several knots at the pass sill (10 ± 2 m) during ebb.

At the end of 1992, borehole P_7 was drilled to 150-m depth on the barrier-reef crest, 1 km west of borehole P_6. Analysis of the borehole P_7 showed the base of the reef carbonate at 110 m, followed by 30 m of mixed carbonate-volcanic detrital material (at 110–140 m) and a 10-m-thick layer of basalt (at 140–150 m). The drilling-rate log demonstrated the presence of large megaporosity voids (m^3 to tens of m^3) in agreement with observations on borehole P_6. Detailed study of the core and interstitial waters from borehole P_7 is in progress.

Interstitial water survey (1990–1992). Physico-chemical parameters (Table 15-4) for Tahiti borehole P_6 showed positive values of redox potential in the first 20 m together with the presence of free oxygen. Physico-chemical determinations confirms the turbulent penetration of aerated surface-ocean water through the outer margin of the reef, consistent with our interpretations for the reef of Tikehau Atoll. Oxic conditions sharply disappear below 20 m, demonstrating that AOU exceeds the rate of oxygen renewal. Values of pH in RIW decrease with depth, from 7.9 at the surface to 7.6 at 50 m, and are always significantly lower than those from the adjacent oceanic waters (8.3). These changes in pH values imply a correlative shift in chemical equilibrium from carbonate to bicarbonate with possible dissolution of the carbonate framework, especially within the anoxic zone.

Nitrate is the dominant inorganic nitrogenous form in the oxic zone where ammonium concentrations are low (1 μM or less). From 30-m depth, reducing conditions result in the disappearance of oxidized N species, a large increase in ammonium (up to 10 μM), an increase in phosphate (up to 2.5 μM) and a large excess in silicate (up to 80 μM). Two distinct fields of data emerge from the Tahiti borehole P_6 dataset. The first cluster contains slightly enriched values in phosphate, nitrate and

Table 15-4

Summary of the hydrogeochemistry of reef interstial waters (RIW) at Tahiti[a]

Borehole[#]	Depth (m)	Salinity (psu)	N^* (μM)	NH_4 (μM)	PO_4 (μM)	SiO_2 (μM)	pH	Redox (mV)
P_6 (reef crest)	1	35.80	2.82	1.63	0.71	17.14	7.86	211
		(0.16)	(1.48)	(0.75)	(0.20)	(6.90)	(0.17)	(26)
	5	35.71	1.63	1.67	0.91	21.27	7.78	153
		(0.13)	(1.32)	(1.02)	(0.34)	(6.64)	(0.17)	(70)
	20	35.73	1.52	0.76	1.06	21.21	7.78	111
		(0.12)	(1.22)	(0.72)	(0.60)	(5.79)	(0.16)	(88)
	30	35.78	0.16	12.00	1.56	63.62	7.65	−130
		(0.07)	(0.06)	(3.77)	(0.39)	(9.40)	(0.12)	(35)
	50	35.74	0.09	10.70	2.14	79.97	7.67	−120
		(0.11)	(0.06)	(3.97)	(0.54)	(8.11)	(0.12)	(28)

[a] numbers listed are average values of borehole measurements of RIW made from 1989–1992. Lagoon and seawater measurements were made from 1986–1992. Numbers listed in parentheses are standard deviation values.

* $NO_3 + NO_2$

silicate relative to surface-ocean values and represents oxic waters from the top 20-m layer. The second cluster contains even higher values of phosphate, ammonium and especially silicate and represents anoxic waters from the lower 30-and 50-m layers. Such a distribution clearly indicates that excess silica is provided by an exogenous source and adds to organic-matter recycling and upward transport of AIW. Leaching of the basalt, which is composed of up to 50% of soluble silica, by interstitial water flow is likely responsible for the observed excess silicate. The higher silicate concentrations in Tahiti relative to those observed in Tikehau RIW result from differences in the depth of the carbonate-basalt contact, which is located at 110–130 m at Tahiti and is estimated to be at least 1,000 m below the flanks of Tikehau Atoll.

Salinity in Tahiti borehole P_6 (35.7 ± 0.1 psu) is lower than in TSW (36.1 ± 0.1 psu). As in Tikehau, this difference may be explained by mixing between two oceanic water sources: AIW (34.5 psu) and TSW (36.1 psu). The higher salinity range in the Tahiti borehole may reflect a higher input of TSW within the reef matrix, due either to stronger wave-surge dynamics or higher carbonate porosity.

The Tahitian RIW shows a noticeable F12 deficiency with concentrations around 0.8 ± 0.1 pM kg^{-1} at depths of 1–20 m and around 0.5 ± 0.1 pM kg^{-1} below a depth of 30 m (Andrié et al., 1992). The depletion of F12 with depth can be explained by the input of F12-depleted waters from 300–400 m, a level where oceanic values correspond with RIW values and which is thought to correspond to the base of the carbonate pile overlying the volcanic basement. The higher F12 concentrations observed in Tahiti relative to those observed in Tikehau RIW can be explained similarly to the salinity differences between these boreholes: greater mixing with CFC-rich TSW (0–150 m) or by a reduced flux through the basalts. The latter perhaps is in response to the lower hydraulic conductivity of the basalt compared to that of the carbonate sequence (Guille et al., 1993). Small variability in the tracer records probably results from heterogeneity in the reef structure, producing discontinuities in RIW circulation.

Synthesis and significance

Although the initial drillings were done to test the validity of the endo-upwelling model, study of RIW allows us to address other fundamental questions regarding the functioning of the entire atoll-reef system. The following is a synthesis of our observations:

(1) High concentrations of nutrients and carbon dioxide (CO_2) within the top of the reef matrix can support huge gross productivity within the reef system, despite the oligotrophy of the surrounding ocean. Losses of organic matter and exportation of sediment from the nutrient-rich reef to the nutrient-poor ocean can be compensated for by the net productivity of the algal-coral ecosystem. Internal upward circulation from nutrient-rich oceanic AIW to the reef crest is supported by results from studies of conservative markers such as ^3He and CFC. The Darwin paradox

(i.e., oasis of barrier reef productivity in the desert of an oligotrophic tropical ocean) can then be solved in a rational way.

(2) The distribution and vertical gradients of nutrients, CO_2 and O_2 indicate that RIW can reach anoxia (i.e., it can have intermediate to high AOU values). These results are in agreement with similar approaches developed in coastal upwelling areas. The difference between upwelling and endo-upwelling lies in the driving force; upwelling is a wind-driven process whereas endo-upwelling is a geothermally driven process. Upwelling intensity and occurrence is linked to wind-current variability; endo-upwelling depends on the local heat flow and the hydraulic conductivity and porosity of the structure.

(3) Interstitial water systems of barrier and atoll reefs contain oxic water to depths of 20–30 m, a pattern evidently dependent on the oceanic hydrodynamic forcing. This feature is of paramount importance for coral growth, organic matter recycling, and diagenesis of the carbonate framework. Oxygenation of the upper interstitial water appears to result from the mixing of CO_2-rich (low pH), anoxic deep interstitial water with CO_2-poor (high pH), oxic oceanic water injected into the reef matrix by wave surge. We propose the principle of maximum (early) cementation (Aissaoui and Purser, 1986) to be a diagenetic process linked closely to the specific state of the CO_2-carbonate equilibrium of RIW. In response to rapid CO_2 degassing at the top of the reef, this equilibrium shifts toward carbonate saturation that favors early cementation.

(4) Most pinnacle interstitial waters are anoxic and nutrient-rich and are consistent with other studies in lagoon patch reefs (Sansone et al., 1988; Tribble et al., 1990). For large, emergent, lagoon pinnacles, algal-coral growth is favored in the windward side; in contrast, ecosystem development is impaired by excess sedimentation on the leeward side. Pinnacles can be viewed as localized constructions built by corals in zones of RIW seepages. Interstitial sublagoonal circulation requires that bottom sediments in the lagoon must be crossed by faults or cracks. These coral constructions are, therefore, likely related to antecedent karst topography and are the expression of an internal hydrogeologic flow pattern.

(5) Groundwater accumulated in reef-flat islets (motu) during the rainy season escapes continuously towards the lagoon and ocean. Boreholes P_1 and P_2 have been used to monitor this outflow which shifts RIW salinity to values as low as 20–30‰ psu in the top 10 m (Fig. 15-6) This brackish water has a low pH and high alkalinity which indicates that it has the potential to dissolve reef matrix and enhance porosity. The meteoric phreatic water is vital to vegetation whose outstanding productivity is forced by the interstitial nutrient reservoir present in the whole atoll-reef structure. Discharge of fresh to brackish groundwater to the reef crest, important in the rainy season, does not alter coral-reef development (e.g., coral density or spur- and -groove patterns), but can weaken motu and the atoll rim, initiating hoa and pass development. Passes constitute, for the living ecosystem, breaches that cannot be closed when the escaping volume of lagoon water is significant, as in large atolls or when it has low salinity, as in the lagoons of high islands.

(6) Some motu have brackish ponds in locations where groundwater accumulates. These ponds are colonized by cyanobacterial algal mats, kopara. In totally enclosed

atolls with a broad and continuous motu, the volume of groundwater stored may be equivalent to or greater than the lagoon water volume. Leakage of freshwater toward the lagoon transforms it to a brackish system colonized only by thick mats of kopara, as is found at Niau Atoll. Because layers of precipitated fluorapatite occur in the internal anoxic basement of dead kopara (Trichet and Fikri, 1993), we believe this stromatolitic facies (Defarge et al., 1993) is a step in atoll phosphogenesis. Previously, Rougerie and Wauthy (1989) suggested that atoll phosphogenesis is a consequence of endo-upwelling with subsequent accumulation of phosphorus in closed lagoons, massive phosphate precipitation, and deposits as observed in sediment-filled or uplifted atolls of Mataiva, Makatea, Nauru (Bernat et al., 1991). Our data on kopara ponds show that phosphorus can be sequestered in these anoxic organic mats until the final step, which is the oxidation of these mats and fluorapatite precipitation upon emergence of the atoll (Rougerie et al., 1997).

(7) Dolomite is present in numerous reefs and atolls, sometimes at great depth. Its origin is highly controversial, but several authors have clearly linked dolomitization to thermo-convection of deep oceanic water within the porous and permeable carbonate structure (Fanning et al., 1981; Saller, 1984; Aharon et al., 1987). Recent studies of the Bahamas Banks show the efficiency of the internal circulation to perform secondary dolomitization (Whitaker and Smart, 1990). Because geothermal endo-upwelling is a thermo-convective process, we believe it has good potential in dolomitization; magnesium-rich AIW, warmed by heat flow, dissolves calcite, furnishes magnesium to dolomite crystals and the exchanged calcium evacuates upward. In some atolls fluorapatite is in direct contact with massive dolomites.

CONCLUDING REMARKS

The large geomorphological diversity of Polynesian barrier and atoll reefs can be accommodated by a single heuristic model that we call geothermal endo-upwelling. The model is based on the circulation of interstitial water driven by thermal convection and modulated at the reef surface by oceanic wave surge and secondarily by the circulation of recharge-driven meteoric water. Our geothermal endo-upwelling model, which can be viewed as a form of low-energy hydrothermalism, impacts on a diversity of biogeochemical processes including (1) the productivity, calcification and cementation processes active in algal-coral reef ecosystems, (2) carbonate and phosphate diagenesis, and (3) degradation of organic matter (Fig. 15-9) A barrier reef is not only an accumulation of dead corals and carbonate sediments topped by a living veneer of algae and corals, but a complex and integrated macrocosm in which interstitial circulation is the key factor whose involvement ranges from short-term coral growth to long-term atoll evolution. We investigated the Darwinian paradox (i.e., oasis of barrier reef productivity in the desert of an oligotrophic tropical ocean) using interstitial-water studies. The results of our investigations have led us to propose a new paradigm for the development and maintenance of the entire Polynesian reef system. More studies are necessary to evaluate the robustness

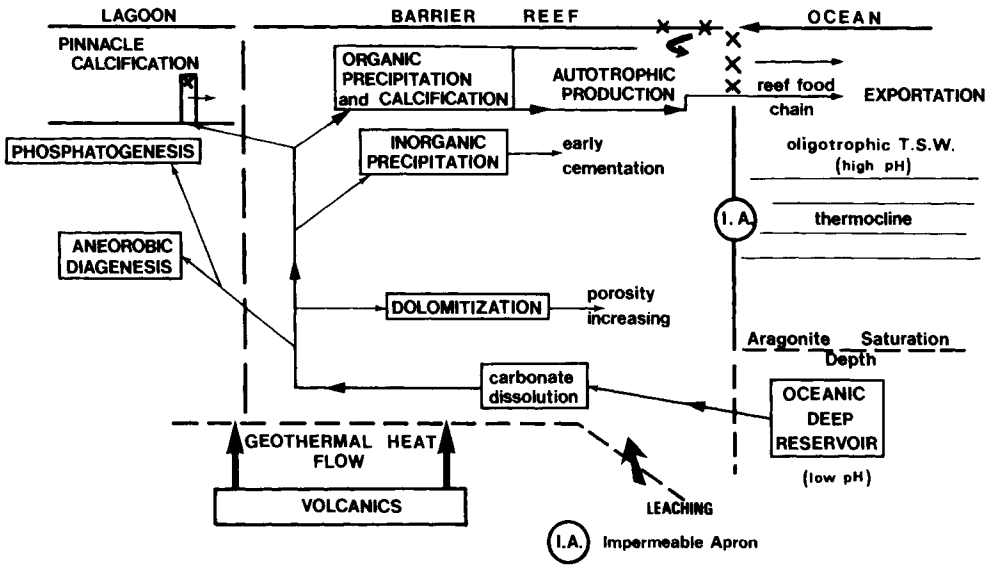


Fig. 15-9. Schematic diagram of the geothermal endo-upwelling model showing the zones of active inorganic and organic precipitation and dissolution. Flow dynamics and kinetics of the chemical exchanges are a function of heat flow, porosity, hydraulic conductivity and energy regime at the reef crest. Cementation of the impermeable apron (IA), which prevents horizontal exchange between seawater and interstitial reef water, is controlled by the carbonate saturation state of the Polynesian ocean, which is oversaturated with respect to aragonite to a depth of 400–500 m.

of our model and whether it can be applied more generally to others reef atoll provinces.

ACKNOWLEDGMENTS

We are grateful to Jean-Louis Cremoux and Joél Orempuller for technical assistance in the field, Maeva Crawley for typing and Corinne Ollier for drawings. We also thank Bob Buddemeier and 2 anonymous reviewers for comments on the manuscript. This research and drillings were supported by ORSTOM, Department TOA, by PRCO (ORSTOM-INSU) and by PROE (SPC).

REFERENCES

Aharon, P., Socki, R. and Chan L., 1987. Dolomitization of atolls by sea water convection flow: test of a hypothesis at Niue. South Pacific. J. Geol., 95: 187–203.

Aissaoui, D.M. and Purser, B.H., 1986. La cimentation dans les récifs: principe de cimentation maximale. Compt. Rend. Acad. Sci., 303, II: 301–303.

Andrews, J.C. and Pickard, G.L., 1990. The physical oceanography of coral reef systems. In: Z. Dubinsky (Editor), Ecosystems of the World, 25, Coral Reefs-II: 11–48.

Andrié, C., Bouloubassi, I., Cornu, H., Fichez, R., Pierre, C. and Rougerie, F., 1992. Chemical and tracer studies in coral reef interstitial waters (French Polynesia): implication for endo-upwelling circulation. Proc. Seventh Int. Coral Reef Symp. (Guam), 2: 1165–1173.

Atkinson, M.J., 1988. Are coral reefs nutrient limited? Proc. Sixth Int. Coral Reef Symp. (Townsville), 1: 157–166.

Barber, R.T., 1992. Geologic and climatic time scales of nutrient variability. In: P.G. Falkowski (Editor), Primary Productivity and Biogeochemical Cycles in the Sea. Plenum Press, New York, 89–106.

Bard, E., Montaggioni, L., Arnold, M. and Rougerie, F., 1993. C14 dating of a 50 m core from the Tahiti Barrier Reef. (Abstr.) Intern. Workshop on Intraplate Volcanism, Tahiti.

Bernat, M., Loubet M. and Baumer A., 1991. Sur l'origine des phosphates de l'atoll de Nauru. Oceanol. Acta, 14: 325–331.

Bonvallot, J., Laboute, P., Rougerie, F. and Vigneron, E., 1994. Les atolls des Tuamotu. Eds. ORSTOM Paris, 296 pp.

Bouloubassi, I., Saliot, A., Rougerie, F. and Trichet, J. 1992. Hydrocarbon geochemistry in coral reefs pore waters, French Polynesia, Proc. Water Rock Interaction, Balkema Rotterdam, 271–274.

Bourrouilh Le Jan, F., 1992. Evolution des karsts oceaniens (karsts, bauxites, phosphates). Karstologia, 19: 31–50.

Brousse, R., 1985. The age of the islands in the Pacific Ocean: volcanism and coral reef build up. Proc. Fifth Int. Coral Reef Symp. (Manila), 6: 389–400.

Brown, B., 1990. Coral bleaching. Coral Reefs, 8: 153–232.

Buddemeier, R.W. and Oberdorfer, J.A., 1986. Internal hydrology and geochemistry of coral reefs and atoll islands: keys to diagenetic variations. In: J.H. Schroeder and B.H. Purser (Editors), Reef Diagenesis. Springer-Verlag, Berlin, pp. 91–111.

Buddemeier, R.W. and Oberdorfer, J.A., 1988. Hydrogeology and hydrodynamics of coral reef pore waters. Proc. Sixth Int. Coral Reef Symp. (Townsville), 2: 485–490.

Defarge, C. and Trichet J., 1985. First data on the biogeochemistry of kopara deposits from Rangiroa Atoll. Proc. Fifth Int. Coral Reef Symp. (Tahiti), 3: 365–370.

Defarge, C., Trichet, J., Sansone, F., Tribble, J., Robert, M. and Jaunet, A.M., 1993. Nouvelles preuves de l'intervention de réseaux organiques hérités de procaryotes dans la micro-structuration et la carbonatation des stromatolites actuels. Compt. Rend. Acad. Sci., 316, II: 1107–1114.

Déjardin, P., 1991. Forage du récif barriére nord de Tahiti. Caractérisation petrographique et études hydrogeochimique. UFP Tahiti, 38 pp. + annexes.

Delcroix, T. and Henin, C., 1991. Seasonal and interannual variations of sea surface salinity in the tropical Pacific Ocean. J. Geophys. Res., 98: 22, 135–22, 150.

Delesalle, B. and Sournia, A., 1992. Residence time of water and phytoplankton biomass in coral reef lagoons. Cont. Shelf Res., 12: 939–949.

D'Elia, C., 1988. The cycling of essential elements in coral reefs. In: Pomeroy and Alberts (Editors), Concepts of Ecosystem Ecology. New York Ecological Studies, 67, Springer-Verlag, New York, pp. 195–204.

Deneufbourg, G., 1971. Etude géologique du Port de Papeete-Tahiti. Cah. Pac., 12 and 13.

Fagerstrom, A., 1987. The evolution of reef communities. John Wiley, New York, 600 pp.

Faissolle, F., 1988. Hydrogéologie, Paléohydrogéologie et diagénèse d'un système aquifère carbonaté récifal côtier. Thèse, Université Bordeaux III, 269 pp.

Fanning, K., Byrne, R., Breland, J., Betzer, P., Moore, W. and Elsinger, R., 1981. Geothermal springs of the west Florida Continental Shelf: evidence for dolomitization and radionuclide enrichment. Earth Planet. Sci. Lett., 52: 345–354.

Fichez, R., Buestel, D. and Quessu, D., 1992. Etude du phénomène de résurgence de Novembre 1991 dans la passe de l'atoll d'Amanu (Tuamotu). Archives d'Oceanogr., ORSTOM Tahiti, 11 pp.

Glynn, P.W., 1990. Coral mortality and disturbances to coral reefs in the tropical eastern Pacific. In: P.W. Glynn (Editor), Global Ecological Consequences of the 1982–83 El Nino Southern Oscillation. Elsevier Oceanogr., Ser. 52, Amsterdam, 55–126.

Glynn P.W., 1993. Coral reef bleaching: ecological perspectives. Coral Reefs, 12: 1–17.

Guilcher, A., 1988. Coral reef geomorphology. John Wiley, Chichester, 228 pp.

Guilcher, A., 1991. Progress and problems in knowledge of coral lagoon topography and its origin in the South Pacific by way of pinnacle study. In: R.H. Osborne (Editor), From Shoreline to Abyss: Contributions in Marine Geology in Honor of Francis Parker Shepard. Soc. Econ. Paleont. Mineral., Spec. Publ. 46: 173–188.

Guille G., Goutière G. and Sornein, J.F., 1993. Les atolls de Mururoa et de Fangataufa (Polynésie Française). Eds CEA/DIRCEN – GAP, 168 pp.

Hallock, P., 1988. The role of nutrient availability in bioerosion: consequences to carbonate build ups. Palaeogeogr. Palaeoclimat. Palaeoecol., 63, 275–291.

Hallock, P. and Schlager W., 1986. Nutrient excess and the demise of coral reefs and carbonate platforms. Palaios, 1: 389–398.

Hatcher, A.I., 1985. The relationship between coral reef structure and nitrogen dynamics. Proc. Fifth Int. Coral Reef Symp. (Tahiti), 3: 407–413.

Heywood K.J., Barton E.D. and Simpson J.H., 1990. The effects of flow disturbance by an oceanic island. J. Mar. Res., 48: 55–73.

Humbert, L. and Dessay J., 1985. Aspects de la dolomitisation de l'île de Makatea (Polynésie Française). Proc. Fifth Int. Coral Reef Symp. (Tahiti), 3: 271–276.

Jouannic, C. and Thompson, R.M., 1983. Bibliography of geology and geophysics of the South Pacific. UN-ESCAP, CCOP/SOPAC. Techn. Bull. 5, 258 pp.

Kohout, F.A., 1965. A hypothesis concerning cyclic flow of salt water related to geothermal heating in the Floridan aquifer. Trans. New York Acad. Sci., Series 2, 28: 249–271.

Laboute, P., 1985. Evaluation of damage done by the cyclones of 1982–1983 to the outer slopes of the Tikehau and Takapoto Atolls. Proc. Fifth Int. Coral Reef Symp. (Tahiti), 3: 323–329.

Le Borgne, R., Blanchot, J. and Charpy, L., 1989. Zooplankton of Tikehau Atoll (Tuamotu Archipelago) and its relationship to particulate matter. Mar. Biol. 102: 341–353.

Le Suavé, R., Pautot, G., Hoffert, M., Monti, S., Morel, Y. and Pichocki, C., 1986. Cadre géologique de concrétions poly-métalliques cobaltifères sous-marines dans l'archipel des Tuamotu. Compt. Rend. Acad. Sci., 303, II: 11, 1013–1018.

Levitus, S., 1982. Climatological atlas of the world ocean. NOAA Prof. Paper. US. Govt. Print. Off. Washington, D.C., 13, 173 pp.

MacIntyre, I. and Marshall, J., 1988. Submarine lithification in coral reefs: some facts and misconceptions. Proc. Sixth Int. Coral Reef Symp. (Townsville), 1: 263–272.

Menard, H.W., 1986. Islands. Freeman, New York, 230 pp.

Montaggioni, L., 1993. Volcano-isostatic polyphase uplift: a key to the post-oligocene evolution of the northwestern Tuamotu atolls (Central Pacific). (Abstr.) Intern. Workshop on Intraplate Volcanism, Tahiti.

Moore, P., Reddy, K. and Graetz, D., 1992. Nutrient transformations in sediments as influenced by oxygen supply. J. Environ. Qual., 21(3): 387–393.

Nof, D. and Middleton, J., 1989. Geostrophic pumping inflows and upwelling in barrier reefs. J. Phys. Oceanogr., 19: 874.

Pernetta, J.C. and Hughes, P.J., 1990. Implications of expected climate changes in the South Pacific region: an overview. UNEP, Regional Seas Rep. and Stud., 128, 279 pp.

Pirazzoli, P.A., 1985. Bathymetric mapping of coral reefs and atolls from satellite. Proc. Fifth Int. Coral Reef Symp. (Tahiti), 6: 539–544.

Rancher, J. and Rougerie, F., 1993. Hydropol. Situations océaniques du Pacifique Central Sud. Editions SMSR Montlhéry, 91 pp.

Roe, K.K. and Burnett, W.C., 1985. Uranium geochemistry and dating of Pacific island apatite. Geochim. Cosmochim. Acta, 49: 1581–1592.

Rougerie, F., 1983. Nouvelles données sur le fonctionnement interne des lagons d'atoll. Compt. Rend. Acad. Sci., 297, II: 909–912.
Rougerie, F. and Wauthy, B., 1986. Le concept d'endo-upwelling dans le fonctionnement des atolls-oasis. Oceanolog. Acta, 9: 133–148.
Rougerie, F. and Wauthy, B., 1988. The endo-upwelling concept: a new paradigm for solving an old paradox. Proc. Fifth Int. Coral Reef Symp. (Tahiti), 3: 21–26.
Rougerie, F. and Wauthy, B., 1989. Une nouvelle hypothèse sur la genèse des phosphates d'atolls: le rôle du processus d'endo-upwelling. Compt. Rend. Acad. Sci., 308, II: 1043–1047.
Rougerie, F. and Wauthy, B., 1993. The endo-upwelling concept: from geothermal convection to reef construction. Coral Reefs, 12: 19–30.
Rougerie, F and Rancher, J., 1994. The Polynesian South Ocean: features and circulation. Marine Pollution Bulletin 29 (1–3): 14–25.
Rougerie, F., Wauthy, B. and Andrié, C., 1990. Geothermal endo-upwelling model testing for atoll and high island barrier reef. Proc. Intern. Workshop, Nouméa, pp. 197–202.
Rougerie, F., Andrié, C. and Jean-Baptiste, P., 1991. Helium-3 inside atoll barrier reef interstitial water: a clue for geothermal endo-upwelling. Geophys. Res. Lett., 18: 109–112.
Rougerie, F., Fagerstrom, J., and Andrié C., 1992a. Geothermal endo-upwelling: a solution to the reef nutrient paradox. Cont. Shelf Res., 12: 785–798.
Rougerie, F., Salvat, B., Tatarata, M., 1992b. La mort blanche des coraux. La Recherche, 23: 826–834.
Rougerie, F., Wauthy, B. and Rancher, J., 1992c. Le récif barrière ennoyé des Iles Marquises et l'effet d'île par endo-upwelling. Compt. Rend. Acad. Sci., 315, II: 677–682.
Rougerie, F., Jehl, C. and Trichet, J., 1994. Phosphorus pathway in atoll. AGU-ASLO Meeting. La Jolla (poster).
Rougerie, F., Jehl, C., Trichet, J., 1997 Phosphorus pathway in atolls: endo-upwelling input, cyanobacterial accumulation and carbonate fluoro apatite (CFA) precipitation-Marine Geology.
Saller, A., 1984. Petrologic and geochemical constraints on the origin of subsurface dolomite, Enewetak Atoll: an example of dolomitization by normal sea water. Geology, 12: 217–220.
Salvat, B., 1985. An integrated (geomorphological and economical) classification of French Polynesian atolls. Proc. Fifth Int. Coral Reef Symp. (Tahiti), 2: 337.
Sansone, F.J., Andrews, C., Buddemeier, R. and Tribble, G., 1988. Well point sampling of reef interstitial water. Coral Reefs, 7: 19–22.
Smith, S.V. and Buddemeier R.W., 1992. Global change and coral reef ecosystems. Annu. Rev. Ecol. Syst., 23: 89–118.
Tribble, G., Sansone, F., Smith, S., 1990. Stoichiometric modeling of carbon diagenesis within a coral reef framework. Geochim. Cosmochim. Acta, 54: 2439–2449.
Trichet, J. and Fikri, A., 1993. Information given by organic matter on the origin of insular phosphorites. Inter. Symposium on Phosphogenesis. Interlaken (abstract).
Underwood, M.R., Peterson, F.L. and Voss, C.I., 1992. Groundwater lens dynamics of atoll islands. Wat. Resour. Res., 28 (11): 2889–2902.
Wauthy, B., 1986. Physical ocean environment in the South Pacific Commission Area. UNEP Reg. Seas Reports and Studies, 83, 90 pp.
Whitaker, F. and Smart, P., 1990. Active circulation of saline ground waters in carbonate platforms: evidence from the Geat Bahama Bank. Geology, 18: 200–203.
Whitehead, N.E., 1993. The elemental content of Niue island soils as an indicator of their origin. N.Z. J. Geol. Geophys., 36: 243–254.
Wolanski, E., Drew, E., Abel, K. and O'Brien, J., 1988. Tidal jets, nutrient upwelling and their influence on the productivity of the alga Halimeda in the ribbon reefs. G.B.R. Estuar. Coast. Shelf. Sci., 26: 169–201.

Geology and Hydrogeology of Carbonate Islands. Developments in Sedimentology 54
edited by H.L. Vacher and T. Quinn
© 1997 Elsevier Science B.V. All rights reserved.

Chapter 16

GEOLOGY AND HYDROGEOLOGY OF THE COOK ISLANDS

JAMES R. HEIN, SARAH C. GRAY, and BRUCE M. RICHMOND

INTRODUCTION

History

The Cook Islands are located in the central South Pacific between the Society Islands to the east and the Tonga and Samoa Islands to the west. The Cook Islands consist of 15 islands divided into a northern group of six islands and a southern group of nine islands. The 15 islands have a total land area of about 245 km^2 (Table 16-1), but the government of the Cook Islands claims a 370 km (200 nm) Exclusive Economic Zone that encompasses about 556,000 km^2.

The Cook Islands are part of Polynesia and the islanders are Maoris, as are the original inhabitants of New Zealand. Their language and culture are closely related to other Polynesia members, such as Tahiti and Hawaii. The Cook Islands were probably colonized between about A.D. 500 and A.D. 800 via migrations from surrounding islands, especially from the Society Islands to the east, but also from Tonga to the west. The islands were first visited by Europeans under the leadership of Alvaro de Mendaña in 1595 (Pukapuka) and Pedro Quiros in 1605 (Rakahanga). Captain James Cook visited most of the islands during his voyages of 1773 and 1777, and Fletcher Christian and the mutineers of the HMS *Bounty* visited Aitutaki and Rarotonga in 1789. In 1821, Reverend John Williams landed at Aitutaki and began the rapid conversion of the islanders to Christianity; the church maintained a tight control especially during the period 1835–1880. During that period, European diseases were introduced and island populations decreased dramatically, by about 75%. The Cook Islands became a British protectorate in 1888 and were administered by a British Resident. In 1900, Rarotonga and the other main southern islands were annexed to New Zealand, with the remainder of the Islands being annexed in 1901. In 1965, the Cook Islands became self-governing, but maintained a compact of free association with New Zealand. New Zealand provides defense and aids in foreign policy. The Cook Islands has not been accepted into the United Nations because of its close association with New Zealand.

The population of the Cook Islands has been steadily declining because of dual citizenship with New Zealand and the consequent migration of many to that country. More Cook Islanders live in New Zealand than in the Cook Islands. The population in 1976 was 18,300, and dropped to about 16,750 in 1986 (Table 16-2). Over 90% of the people live on the southern islands, which make up about 90% of the total land area.

Table 16-1

Physiographic characteristics and ages of the Cook Islands; islands listed from north to south

Island	Island Type[1]	Reef Flat Area (km^2)	Lagoon Area (km^2)	Land Area (km^2)	Percent Land	Max. Elev. (m)	Max. Elev. Makatea (m)	Crustal Age (Ma)	Edifice Age Range (Ma)	Depth to Seafloor (km)
Northern Cook Islands										
Penrhyn	Atoll	31	196	9.8	4	low	na	≈100	Unknown	5.0
Rakahanga	Atoll*	3.9	3.3	3.9	35	low	na	≈110	Unknown[a]	3.0
Manihiki	Atoll*	8.0	44	5.4	9	5	na	≈110	Unknown[a]	3.0
Pukapuka	Atoll*	18	10	3.8	12	6	na	≈110	Unknown[a]	3.0
Nassau	Reef Is.	0.5	na	1.1	66	9	na	≈110	Unknown[a]	3.0
Suwarrow	Atoll	27	99	0.4	0.3	low	na	≈110	Unknown[a]	2.8
Southern Cook Islands										
Palmerston	Atoll*	16	38	1.1	2	low	na	≈90	Unknown	4.6
Aitutaki	Almost Atoll	43	39	18	18	124	na	≈87	≥8.4 & 1.9–.7	4.5
Manuae	Atoll	15	na	5.8	28	9	na	≈85	Unknown	4.0
Mitiaro	Makatea	2.9	na	30	91	10.9	10.9	≈85	≥12.3	4.0
Takutea	Reef Is.	1.4	na	1.4	50	6	na	≈85	Unknown	4.0
Atiu	Makatea	2.5	na	29	92	70	22.1	≈87	10.3–7.4	4.0
Mauke	Makatea	2.4	na	18	88	24.4	14.7	≈85	≥6.3	4.5
Rarotonga	High volcanic	16	na	67	81	653	na	≈87	2.3–1.1	4.5
Mangaia	Makatea	4.0	na	51	93	169	73.0	≈85	19.6–17.1	4.5
Total		191.2	429.4	245.3	na	na	na	na	na	na

*(enclosed). na = not applicable.

[a] Edifice ages assumed to be close to the age of Manihiki Plateau upon which they sit, ≈110 Ma.

Physiographic data from this study, Wood and Hay (1970), Waterhouse and Petty (1986), Hein et al. (1988), Stoddart et al. (1990), and Richmond (1992); crustal ages extrapolated from magnetic anomalies for the southern group (Calmant and Cazenave, 1986) and from K-Ar age of Manihiki Plateau for the northern group (Lanphere and Dalrymple, 1976); edifice K-Ar ages from Dalrymple et al. (1975) and Turner and Jarrard (1982); depth of seafloor from Mammerickx (1992).

Table 16-2

Climate and population data for Cook Isands

Island	Island Type	Population[a]	Mean Rainfall, 1951–1980 (mm y^{-1})		Mean Temperature (°C)		Mean Wind Speed (knots)	
			Seasons Wet[b]	Dry	Seasons Wet	Dry	Seasons Wet	Dry
Northern Cook Islands								
Penrhyn	Atoll	496	1079	805	27.5	27.2	10	11
Rakahanga	Atoll	283	1121	873	27.5	27.2	7	7
Manihiki	Atoll	508	1428	867	27.7	27.2	6	7
Pukapuka	Atoll	760	1668	1066	27.8	27.4	5	6
Nassau	Reef Is.	118	–	–	–	–	7	8
Suwarrow	Atoll	0	1439	730	–	–	–	–
Southern Cook Islands								
Palmerston	Atoll	50	1337	638	–	–	–	–
Aitutaki	Almost Atoll	2307	1263	617	26.4	24.4	11	12
Manuae	Atoll	0	–	–	–	–	–	–
Mitiaro	Makatea	272	1185	641	–	–	–	–
Takutea	Reef Is.	0	–	–	–	–	–	–
Atiu	Makatea	955	1336	634	–	–	–	–
Mauke	Makatea	687	1030	578	26.0	23.4	6	7
Rarotonga	High Volcanic	9084	1292	729	25.0	22.0	9	10
Mangaia	Makatea	1235	1230	737	–	–	9	9
Total/Mean		16755	1284	743	26.8	25.5	8	9

[a] Approximate from 1986 census
[b] Wet season is November–April and dry season May–October; data from Thompson (1986a,b)
– Data not available

The economy of the Cook Islands is based primarily on tourism (southern Cook Islands) and the export of fruits and vegetables, about 85% of which go to New Zealand. The sale of stamps and coins provides additional revenues. Manihiki islanders operate a thriving pearl shell industry.

Climate and weather

The southern and northern Cook Islands are separated by over 500 km of open ocean, and their climate and oceanographic settings differ. The southern Cook Islands are within the subtropical high-pressure zone of the South Pacific, which creates a semipermanent anticyclone circulation to the east of the Cook Islands. Long-term mean rainfall is 1,608–2,027 mm y^{-1}, the mean annual temperatures are 24–26°C, and the mean wind speed is 13 kn (Table 16-2; for details about climate and weather refer to Thompson, 1986a,b). The Southern Oscillation Index (SOI) is a monitor of the pressure between the western and eastern parts of the South Pacific. When the SOI is negative (high pressures to the west), the subtropical high-pressure zone moves north of its mean position and the southern Cook Islands experience dry conditions. Major negative SOI episodes have occurred on the average of once every 4.4 years since at least 1900 with major positive excursions every 4.4 years since at least 1930.

The northern Cook Islands are within the persistent trade wind belt of the South Pacific. Rainfall is highly variable, with a long-term mean of 1,884–2,734 mm y^{-1}; the average temperature is about 28°C; the average wind speed is 11 kn (Table 16-2). When the SOI is positive, the northern Cook Islands experience a stronger Southern Pacific anticyclone, intensified easterlies, and drier conditions. Conversely, when the SOI is negative, there is generally increased precipitation, increased frequency of westerly monsoon conditions, and reduced winds. Tropical storms are born in this area when the SOI is negative.

GEOLOGY

Regional tectonic setting

The southern Cook Islands form two linear northwest-southeast chains that apparently converge to the southeast on the volcanically active Macdonald Seamount, which has been proposed to be a hotspot volcano. The eastern chain includes the islands of Aitutaki, Manuae, Takutea, Atiu, Mitiaro, and Mauke, which together form a ridge defined by the 4,500-m isobath (Fig. 16-1). The western chain includes three isolated edifices, Palmerston, Rarotonga, and Mangaia, and numerous recently discovered seamounts to the southeast (Diament and Baudry, 1987). However, the ages of the dated southern Cook Islands (Table 16-1), with the exception of Mangaia, do not fit within a single hotspot framework (Dalrymple et al., 1975). According to Turner and Jarrard (1982), a hot-line hypothesis places fewer constraints on age predictions than does the hotspot model. Renewed volcanism on Aitutaki

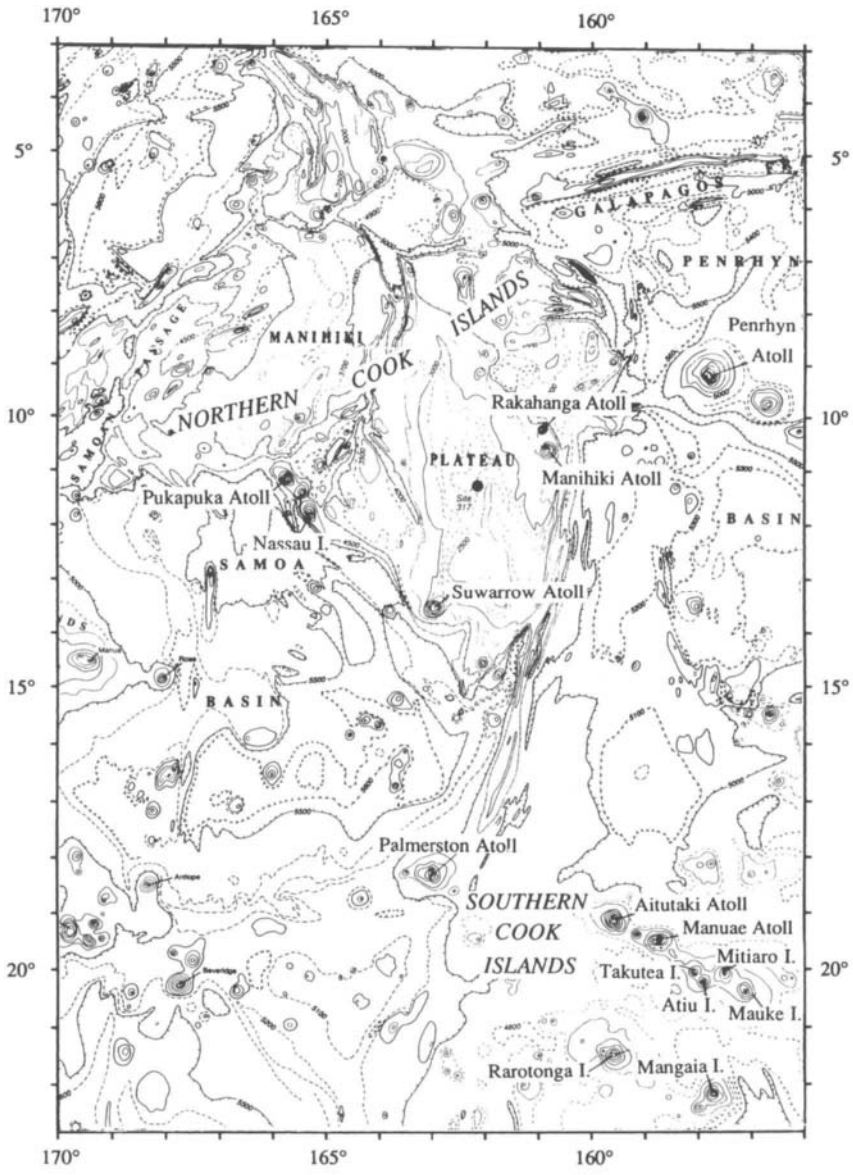


Fig. 16-1. Location of Cook Islands. Bathymetry from Mammerickx (1992). Contour interval varies from 1,000 m, to 500 m, to 100 m depending on steepness of topography. Site 317 is from DSDP Leg 33 [See also Fig. 15.1 for regional location].

during the Pleistocene after about 6 Ma of quiescence may have originated from the same hotspot that formed Rarotonga, because these two islands are within the 300-km diameter of volcanism that defines known hotspots. Alternatively, Pleistocene volcanism on Aitutaki may have been tied to crustal loading and flexure when

Rarotonga formed. Crustal loading from Rarotonga created a moat and arch; the latter uplifted the makatea islands (Mauke, Mitiaro, Atiu) to the northeast, as well as Manuae and Takutea (McNutt and Menard, 1978; Lambeck, 1981; Spencer et al., 1987). To satisfactorily resolve the southern Cook Islands hotspot controversy, it will be necessary to collect and date volcanic rocks from the submarine flanks of the islands and associated seamounts.

With one exception, Penrhyn Atoll, which is an isolated edifice built up from the abyssal seafloor, the northern Cook Islands are located at the margin of Manihiki Plateau. The Manihiki Plateau is a 5×10^5-km^2 area of anomalously shallow water and thick crust. The plateau formed at about 110 Ma, probably from an immense outpouring of lava at a triple junction between the Pacific, Antarctic, and Farallon Plates (Heezen et al., 1966; Winterer et al., 1974; Lanphere and Dalrymple, 1976; Clague, 1976). The most likely tectonic setting was a hotspot situated at or near a slow-spreading ridge (Mahoney, 1987). During the Cretaceous, the summit of the plateau was near sea level and subsequently subsided about 3 km to its present position (Winterer et al., 1974; Jenkyns, 1976). Atolls of the northern Cook Islands formed during this period of subsidence; from seismic reflection studies, the carbonate caps are estimated to be at least 500 m thick as measured on Manihiki Atoll (Hochstein, 1967). None of the volcanic edifices of the northern Cook Islands have been age dated; however, the islands are likely to be about the same age as Manihiki Plateau upon which they rest. Manihiki Plateau basement basalt has a minimum age of 106 ± 3.5 Ma (Lanphere and Dalrymple, 1976), and the plateau basement is probably as old as 112–110 Ma (Jackson and Schlanger, 1976). A seamount located just to the west of Rakahanga and Manihiki Islands was dredged, and the rocks recovered were dated as >83 Ma in age by $^{40}Ar/^{39}Ar$ fusion methods; Maastrichtian limestone was also recovered (H. Beiersdorf, BGR, personal communication, 1993; $^{40}Ar/^{39}Ar$ ages by R.A. Duncan; Beiersdorf et al., 1990). Inasmuch as the Manihiki Plateau is Early Cretaceous in age, the volcanic edifices of the northern Cook Islands are probably older than the apparent Late Cretaceous age of the seamount.

Island geomorphology

Five types of islands are represented by the nine islands that make up the southern group: Atiu, Mitiaro, Mauke, Mangaia are makatea islands; Palmerston and Manuae are atolls; Takutea is a reef island (sand cay); Aitutaki is an almost-atoll; and Rarotonga, the main island, is a high volcanic island. The northern group is made up of five atolls, Penrhyn, Rakahanga, Manihiki, Pukapuka, and Suwarrow, and a reef island, Nassau. The atolls have an annular reef rim surrounding a central lagoon. Aitutaki almost-atoll is an atoll containing remnants of the volcanic edifice. Takutea reef island is a low-lying carbonate island without a lagoon and has a single small reef top. The makatea islands consist of an uplifted karstified limestone rim encircling a central volcanic core. The high volcanic island is rugged and surrounded by a fringing reef. No reports are available on the geology of the reef islands, Nassau and Takutea, other than very brief descriptions by Wood and Hay (1970). Also, little

is known about five of the eight atolls: Penrhyn, Manihiki, Suwarrow, Palmerston, and Manuae. Most studies have focused on the makatea islands, the volcanic island of Rarotonga, and Aitutaki almost-atoll.

High volcanic islands. Rarotonga is the only high volcanic island without substantial raised reef deposits. Rarotonga has an interior of deeply incised volcanic peaks surrounded by a narrow coastal fringe of low-lying alluvium and coastal sediments. Erosion of the original volcanic cone and caldera has been extensive, resulting in knife-edged ridges separated by deep valleys. Two streams (Takuvaine and Avatiu) drain the rugged interior from presumably the former caldera, whereas all other streams originate along outer slopes. Stream valleys are typically narrow with limited alluvial deposits until they reach the coastal flat where they expand laterally. A depression that encircles most of the island separates storm-derived beach-ridge deposits from volcanic rocks and alluvium and is locally referred to as the taro swamp. Larger streams discharge directly into the sea opposite deep reef passages, whereas all other drainage is first trapped in the muck-filled coastal depression. The origin of this depression is due possibly to dissolution of former carbonate coastal deposits by freshwater (Wood and Hay, 1970), original deposition related to beach-ridge formation, or a combination of the two.

Beach-ridge deposits are important features on Rarotonga because they are the sites of most settlements and government buildings. The beach ridges are clearly storm-derived and formed under present, or slightly higher than present, sea level. The highest ridges occur along the northwest, north, and northeast coasts opposite narrow fringing reefs. Elevation of the beach ridges does not appear to be related to average wave conditions (the highest waves are typically along the south coast), but rather to wave runup during extreme events. Narrower reef flats result in higher runup, and hence deposition at the shore. Textures of the ridges are directly related to source materials on the adjacent reef flat, with coral gravel predominating along the east and northeast coasts and sand along the south and west coasts.

Makatea islands. Four islands, Mitiaro, Atiu, Mauke, and Mangaia are classified as makatea islands, and their geomorphology has been recently described in detail by Stoddart et al. (1990). The volcanic rocks and limestone are typically separated by a low-lying swampy depression formed by karst erosion (Stoddart et al., 1985). The central volcanic deposits are generally deeply weathered and mantled by well-developed soils. Along the landward edge, the dissected limestone surfaces end abruptly in steep cliffs adjacent to the swamps. Island surfaces are commonly very rugged, consisting of jagged karst pinnacles. The seaward margin of the limestone plateau is commonly marked by notches and caves. Holocene beach deposits, primarily of storm origin, cover most of the narrow coastal plains. Where beaches are absent, steep cliffs fronted by algal terraces are common. Fringing reefs encircle the islands.

Almost-atoll. An almost-atoll is a transitional phase of island development that occurs before a volcanic island with its surrounding reef develops into a true atoll.

Aitutaki is the only almost-atoll in the Cook Islands and consists of a remnant volcanic cone surrounded by fringing and barrier reefs that encircle a shallow lagoon. The relatively large (16 km^2) main volcanic island lies in the northwest part of the lagoon and two small volcanic islets are located in the southeast lagoon. Soils are well developed on the deeply eroded volcanic rocks, which are poorly exposed except along shoreline outcrops and in quarries. A coastal plain of terrigenous and carbonate sediment surrounds the main island and is the site of most settlements on the island. Carbonate sand and gravel islets dot the eastern and southwest corners of the barrier-reef rim.

Atolls. The Cook Islands include seven atolls, the most common island type in the group. They all have the general characteristics of atolls (i.e., central lagoon surrounded by a barrier-reef rim), but individually they vary considerably. Manuae has two large islets on either side of the atoll separated by a very shallow sandy lagoon. Pukapuka, Palmerston, Rakahanga, and Manihiki all have deep (mean depths >10 m) enclosed lagoons without deep passages between the open ocean and the lagoon — most water exchange occurs over the barrier reef.

Rakahanga is the smallest atoll, and its lagoon is virtually completely enclosed by islets developed on the rim. At present, water exchange with the open ocean is not sufficient for coral growth within the central lagoon. Radiocarbon dating of corals, however, indicates that conditions in the lagoon were suitable for coral growth earlier in the Holocene (Gray and Hein, 1997a). Within its small lagoon occur numerous deep (>40 m) basins separated by narrow shallow (<4 m) banks.

Manihiki has the rare feature of numerous islets developed on top of lagoon patch reefs. Pukapuka has three large islets developed at the apex of a three-arm-shaped atoll with a highly compartmentalized lagoon subdivided by sea-level sinuous reefs. Suwarrow and Penrhyn are both large atolls with deep reef passages to the open sea.

A conspicuous feature of many of these atolls is the presence of large, concave-seaward sections of the barrier rim that may indicate that large sections of the atolls and possibly the underlying volcanic rocks have been removed by large-scale submarine landslides (Summerhayes, 1967). Pukapuka would represent an endmember of this process where only a small lagoon remains bounded by arcuate reef rims.

Maximum elevation of islets is 9 m, but mean elevations are about 3–4 m. The largest islets typically develop on the convex-seaward bends of the barrier reef where wave and current activity are concentrated both on the seaward and lagoonward shores (Richmond, 1992b). Interior swamps are limited to these larger islets. Seaward beaches tend to be steep and gravel-rich with abundant coral plates, whereas lagoonside beaches tend to be flatter and sand-rich.

Reef islands. Nassau and Takutea are the only reef islands in the Cook group. They are sand and gravel cays developed on top of small reef platforms. Concentric beach ridges up to 9 m high form the bulk of the islands; a fringing reef surrounds each island. Takutea is the subaerial part of a large arcuate submarine ridge and may be a remnant of an atoll annular rim destroyed by a massive submarine slide (Wood and Hay, 1970).

Reef and lagoon morphology and sedimentation

The reef types that occur in the Cook Islands are similar to those that occur throughout the South Pacific and include: fringing reefs bordering the high and reef-platform islands; barrier reefs surrounding atoll lagoons; and patch reefs scattered within the lagoons. Although there have been only a few detailed reef studies within the Cook Islands, some generalizations can be made regarding reef development.

Fringing reefs. Shorelines of the high and reef-platform islands are bordered by narrow (50 to ~ 400 m wide) near-horizontal reef flats of the fringing reef. Reef flats are probably entirely Holocene in age although there have been some suggestions of Pleistocene reef-flat remnants, notably at Rarotonga (Schofield, 1970). Drilling results and age dating of the fringing reef of Mangaia (Yonekura et al., 1988) demonstrated the Holocene age (~5 ky to present) and upward and outward growth of the reef flat. Generally, during the Holocene transgression, the fringing reef grew mostly vertically in an effort to keep up with sea-level rise; when sea level stabilized, at about 6–5 ky, vertical growth was superseded by lateral seaward migration of the reef crest. Fossil algal ridges on the reef flats of Mangaia (Yonekura et al., 1988) are probably related to a middle Holocene highstand of sea level where they have been subsequently stranded and degraded as seaward growth of the reef continued (see Case Study).

The upper surface of the reefs typically exhibits the following seaward-to-landward zonation in the Cook Islands:

1. The submerged reef front is dominated by spur-and-groove morphology and an area of prolific coral-algal growth. Reef-front terraces separated by escarpments at various shallow water depths are common, but few data exist for correlating terrace surface elevations.
2. The reef crest, composed mostly of encrusting coralline algae, is the highest part of the living reef. Storm-derived rubble deposits are common near the reef crest and often form an algal-covered substrate.
3. Between the reef crest and the shoreline is a low-relief, nearly-horizontal reef flat that typically is a hard pavement-like surface sporadically mantled by a veneer of sediment. Sediment texture generally fines in a landward direction from coral rubble on the outer reef flat to sand-rich deposits on the inner reef flat. Broader reef flats are commonly marked by an inner shallow depression or moat.
4. Depositional shorelines are composed of mixtures of reef-derived sand and gravel that give way to bands of shore-parallel beachrock where recent erosion has taken place.
5. Larger channel systems, such as the reef passes at Avarua and Avatiu in northern Rarotonga, occasionally dissect the fringing reef. These channels are offshore extensions of onland drainage systems.

Barrier reefs and associated lagoons. In the Cook Islands, barrier reefs characterize the atolls, where they form annular rims enclosing their respective lagoons. The

upper surface and zonation of the barrier reef is commonly similar to that of the fringing reef, in part because they are both exposed, sea level-controlled features. The rim width of barrier reefs varies from a few hundred meters to more than 1,500 m, and these rims provide the basement on which coral islets develop.

Barrier reefs are Holocene in age (see Case Study). Ages of limestones in drill cores from the barrier reefs of Pukapuka, Rakahanga, and Aitutaki (Gray and Hein, 1997a) suggest that, like the fringing reefs discussed above, these barrier reefs colonized a Pleistocene reef substrate. Rapid upward reef growth predominated in the early Holocene as growth followed rising sea level. Islets developed on the barrier reefs sometime after sea level stabilized (~6–5 ky). Fossil algal ridges on the reef flats on Suwarrow (Scoffin et al., 1985) and early Holocene in situ reef above sea level on Rakahanga (Gray and Hein, 1997a) may have developed during the early Holocene (6–4 ky) when sea level may have been slightly higher than at present (see Case Study).

Lagoon water depths vary from the shallow lagoons of Manuae and Aitutaki to about 80 m deep for the lagoon of Suwarrow (Summerhayes, 1971; Irwin, 1985). Some lagoons (e.g., Aitutaki's) are relatively uniform in depth and are shallow, whereas others (e.g., Pukapuka, Rakahanga, Suwarrow) are characterized by lagoons of highly irregular topography consisting of shallow flats surrounding deep (35–60 m) basins. Rakahanga represents an extreme example of a restricted lagoon with numerous deep basins separated by shallow carbonate banks. The basins probably originated as erosional karst basins that developed when the islands were emergent during periods of low sea level. The irregular karst topography was then likely accentuated by preferential Holocene reef growth on the topographic highs.

Aitutaki lagoon is the most studied of the Cook atolls (Stoddart and Gibbs, 1975; Hein et al., 1988) and is the only volcanic island in the Cook Islands with a well-developed lagoon and barrier reef. Coral islets occur along the eastern barrier reef and at the southwest corner. The barrier reef is the primary sediment source for the islets and a significant source for lagoon deposits as indicated by a prograding wedge of barrier-reef sediment distributed along the lagoon margin (Fig. 16-2a; Summerhayes, 1971). The lagoon floor is marked by numerous coral-algal pinnacles and small patch reefs separated by areas of smooth seafloor blanketed by sediment (Fig. 16-2b). Composition of the sediment is dominantly bioclastic calcareous material with various mixtures of *Halimeda*, coral, red algae, mollusk, and foraminifer fragments. Suwarrow lagoon deposits have a similar composition with the exception of an overall higher foraminifer content and *Halimeda* meadows covering the deep (~80 m) lagoon floor (Tudhope et al., 1985). Manuae lagoon shows a lack of fine-grained sediment, which may be caused by turbulence and bottom currents in the very shallow lagoon (Summerhayes, 1971).

Patch reefs. Lagoon patch reefs are isolated, steep-sided features that rise from the lagoon floor. Patch reefs are abundant in the shallow areas, but small and sparse in deeper areas of Suwarrow lagoon (Irwin, 1985); limited sampling of surficial sediment derived from the patch reefs consists, in decreasing abundance, of mollusk, coral, coralline algae, and benthic foraminifer fragments (Tudhope et al., 1985).

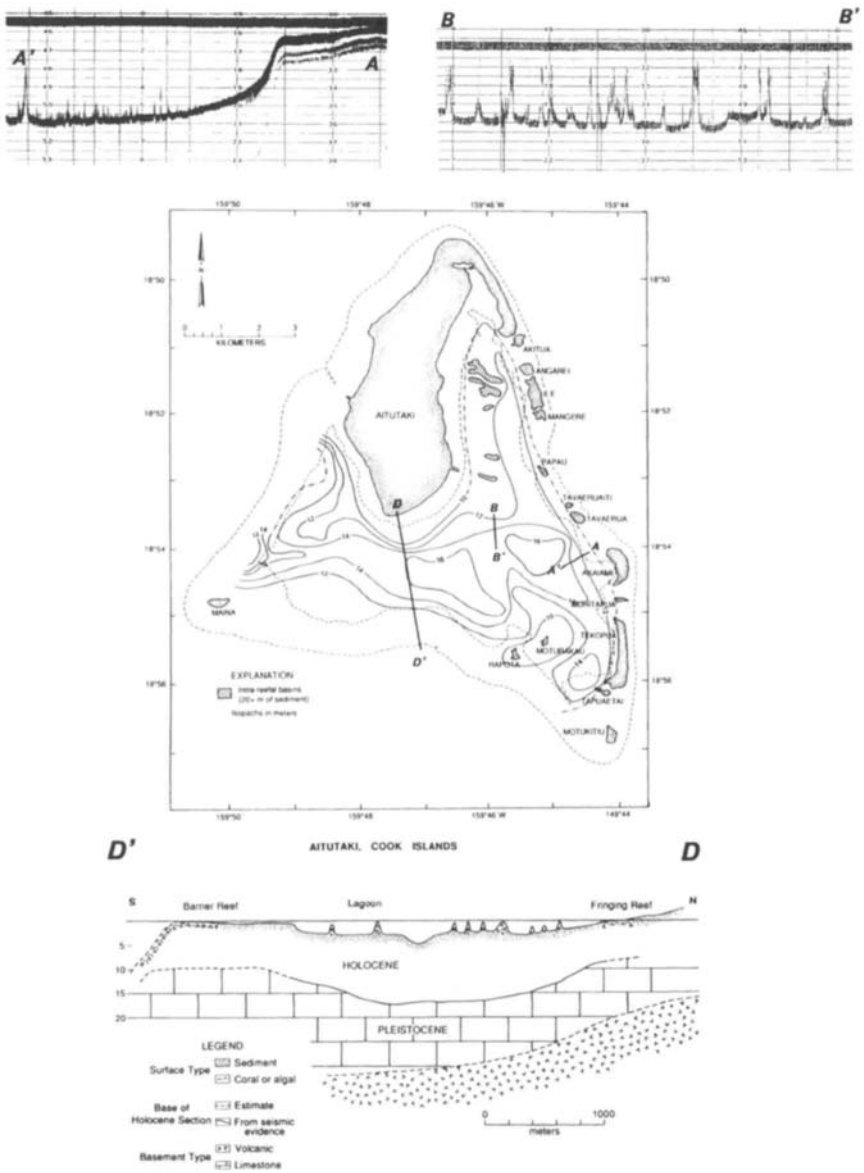


Fig. 16-2. Aitutaki: Isopach map of Holocene lagoon deposits as determined from drilling and high-resolution seismic surveys. A-A' is echosounder record from the eastern barrier rim to the lagoon floor showing the prograding sediment wedge (smooth-floored, steeply dipping surface). B-B' is echosounder profile of the lagoon floor showing numerous small patch reefs separated by sediment-floored areas. D-D' is hypothetical cross section through the southern lagoon showing the relative distribution of surficial features and subbottom deposits. Isopach map and hypothetical cross section are from Richmond (1992a).

Patch reefs in Palmerston lagoon are abundant at all water depths (to 35 m; Irwin, 1985). In contrast, the patch reefs of Manuae lagoon are nearly buried because the lagoon is in its final stages of being filled. The patch reefs of Manihiki are many and provide the substrate for many islets within the lagoon. Penrhyn is another atoll lagoon with numerous patch reefs, but only a few of them support subaerial deposits. The sea-level patch reefs of the other atolls are less numerous. In Rakahanga, small patch reefs that grew during the earlier part of the Holocene are dead and partly buried by sediment. The cause of patch reef density and occurrence is unknown.

Stratigraphy

The stratigraphy of Pukapuka, Rakahanga, and Aitutaki atolls is known from drill cores taken through the Quaternary sections. The relationship between carbonate stratigraphy and Quaternary sea-level history revealed in these cores are discussed in detail in the Case Study. The stratigraphic units comprising the Cook Islands include volcanic rocks interbedded with or underlying reef and shallow-water limestones. The carbonate units consist of primary aragonite limestones or their diagenetic products, including calcite limestone and dolostone.

The stratigraphy of Rarotonga is dominated by volcanic flows and tuff breccias that make up this 650-m-high volcanic island. Rarotonga is the youngest island in the Cook group; volcanism apparently began at about 2.3 Ma (Dalrymple et al., 1975; Turner and Jarrard, 1982). Initial basaltic eruptions were followed by caldera formation and then eruption of more differentiated, phonolite lavas, during which time partial caldera destruction occurred (Wood and Hay, 1970). The volcanic rocks have been divided into several units (Wood and Hay, 1970). At the foot of the volcanic hills occurs the weathered, volcanic Nikao Gravels that are probably of Pleistocene age. The coastal flat surrounding the island is composed of the Aroa Sands, which include cemented and unconsolidated beach sands and pebbles, breccia, beach-ridge deposits, raised reef, and beachrock. In places, the Holocene Aroa Sands are separated from the Nikao Gravels by swamp deposits, mostly of brown and gray muds (Marshall, 1930). In places, the Aroa Sands are underlain by late Pleistocene reefs (Wood and Hay, 1970). A narrow Holocene fringing reef and reef flat surrounds the entire island.

The central volcanic core of the makatea islands (Atiu, Mitiaro, Mauke, Mangaia) ranges in age from about 20–17 Ma for Mangaia, ≥12 Ma for Mitiaro, 10–7 Ma for Atiu, and ≥6 Ma for Mauke (Table 16-1; Dalrymple et al., 1975; Turner and Jarrard, 1982). The volcanic core is overlain by Tertiary reef limestone of generally poorly known age. One sample from Mangaia has been dated using foraminifers as middle early Miocene, about 17 Ma (Yonekura et al., 1988). The inner part of the reef on Atiu may be of early Pliocene age, based on foraminifers (Marshall, 1930). These ages indicate that reef growth began before or slightly after volcanism ended. Coeval reef growth and volcanism occurred on Aitutaki almost-atoll (Hein et al., 1988), Mangaia (Waterhouse and Petty, 1986), and possibly on Atiu (Campbell et al.,

1978). The central volcanic core of the makatea islands was probably exposed after erosion of the Tertiary reef following uplift of the islands during the Quaternary. The volcanic core and Tertiary reef limestone are separated in places by swamps (Fig. 16-3). The chemical composition of streams indicates that the swamps formed by solution erosion of the limestone by $CaCO_3$-undersaturated waters draining the central volcanic rocks (Stoddart et al., 1985). Tertiary limestone on Mauke is fringed by late Pleistocene reef limestone, which is distinguished from the older limestone by having abundant corals, subhorizontal stratigraphic discontinuities, and by grooves, residual pillars, and horizontal notches that record previous sea levels (Stoddart et al., 1990). There was a relatively long period of late Pleistocene reef formation on Atiu. This time period is represented by three superposed units (Stoddart et al., 1990): a lower unit consisting predominantly of massive framework corals; a middle unit consisting of bedded calcarenite that may have been a beach; and an upper unit consisting of coral rubble, which may have been forereef talus. Seaward of the Pleistocene reefs is the actively growing Holocene fringing reef.

Stratigraphic units on the almost-atoll of Aitutaki begin with volcanogenic rocks formed during the late Miocene as part of a shield-building stage. The oldest rocks consist of basaltic tuff breccia interbedded with volcanic flows. Flows alternate between alkalic basalts and nephelinites and basanites (Turner and Jarrard, 1982). As determined from drill cores taken below the lagoon floor, volcanic rocks are overlain by at least 70 m of reef limestone of mostly unknown age. In places, flows and limestone are interbedded (Fig. 16-4; Hein et al., 1988). Near the volcanic island, up to 22 m of pedogenic, volcaniclastic, and pyroclastic muds separate the volcanic rocks from the limestone. On the east side of the island, a 1-m-thick bed consisting of pyrite and organic matter occurs between the pedogenic mud and overlying reef limestone and is probably a swamp deposit. The oldest limestone located at the outer reef margin has been pervasively dolomitized over a stratigraphic interval of at least 60 m (Hein et al., 1988, 1992). The lower part of the dolostone contains thin layers of hydrothermal iron oxides. The dolostone may extend down to the basalt contact, which is estimated to be at 150 m from seismic reflection records (Hochstein, 1967). The dolostone is overlain by, and is in lateral continuity with, calcite limestone that is up to 26+ m thick (Fig. 16-4), and most likely of middle and late Pleistocene age, based on interbedding with basalt flows. The Pleistocene limestone is overlain by up to 22 m of Holocene limestone interbedded with unconsolidated bioclastic sand (Hein et al., 1988). The Pleistocene section consists of continuous coral framework typical of an outer reef crest or reef-flat environment, whereas the Holocene section represents sedimentation in a lagoon.

A distinctive aspect of the Pleistocene limestone at Aitutaki is that it is pervasively recrystallized (see section on diagenesis). Such recrystallization contrasts with the Pleistocene limestones at Pukapuka and Rakahanga (Gray and Hein, 1997b) which retain their depositional aragonite mineralogy, and with Pleistocene sections of other atolls such as Anewetak [q.v., Chap. 21], and Mururoa [q.v., Chap. 13], which contain both primary, depositional aragonite and secondary, diagenetic calcite.

Volcanic cores of the atolls are deeply buried beneath reef-carbonate deposits. Atoll limestones consist of reef and shallow-water carbonates deposited during pe-

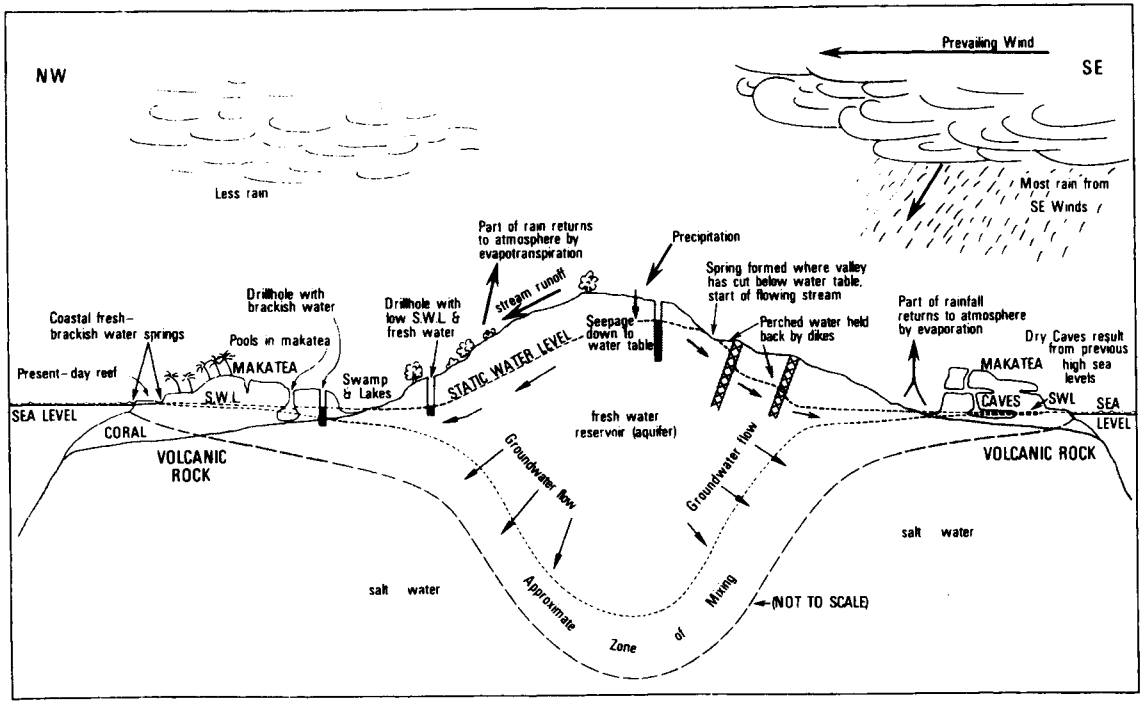


Fig. 16-3. Illustration of the hydrological cycle for the southern Cook Islands. (From Waterhouse and Petty, 1986).

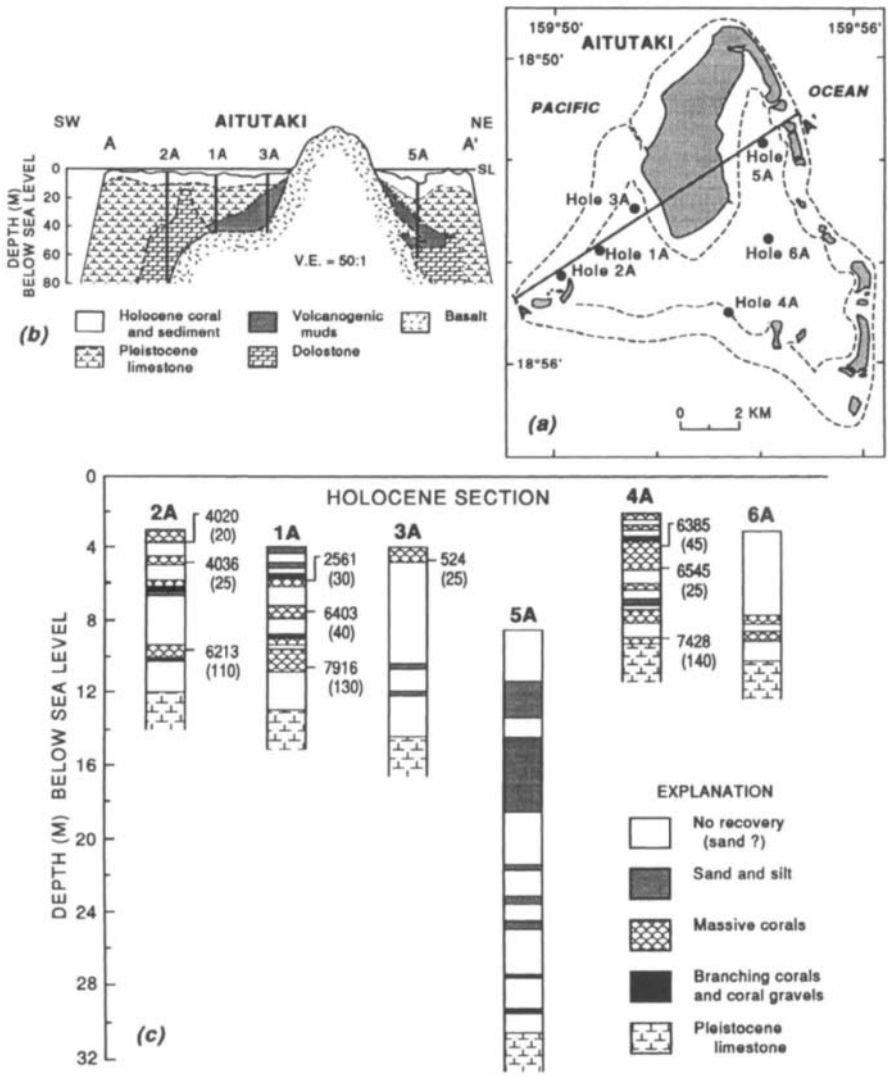


Fig. 16-4. Cores and locations of cross section for Aitutaki almost-atoll (From Hein et al., 1992 and Gray and Hein, 1997a).

riods of high sea level. Subaerial exposure during sea-level lowstands promoted diagenetic alteration and karstification. The stratigraphic sections resulting from these sea-level oscillations consist of successive reef carbonate deposits of high sea level separated by erosional unconformities. Drilling in the northern Cook atolls recovered at least five high-sea-level reefs in the upper 50 m of section (Gray et al., 1992; see Case Study).

Although guano-derived phosphate deposits are common on many equatorial Pacific islands and atolls (e.g., Mururoa, Nauru, Starbuck, Malden), they are rare in the Cook Islands and have been reported only from Manihiki (Wood and Hay, 1970).

HYDROGEOLOGY AND WATER RESOURCES

Little is known about the hydrogeology of the Cook Islands. The elevation of the water table has not been systematically determined, and the thickness of the freshwater lens and seawater-freshwater mixing zone has not been determined for any of the islands. The main sources of freshwater for agriculture, industry, and domestic use are roof catchment, streams, springs, galleries, dug wells, and drillholes. Future development should include additional drillholes and wells, perhaps pumped by wind power; desalination plants run by solar energy; and additional storage tanks and reservoirs to be filled by a variety of sources.

Southern Cook Islands

In the southern Cook Islands, the annual rainfall averages about 2,100 mm, and, although all sources of freshwater listed above are utilized, they do not always meet the demands, especially during dry periods (Waterhouse and Petty, 1986). Reliable water resources can be obtained from drillholes into water-table aquifers in volcanic and sedimentary rocks. Individual holes may yield water quantities of up to 1 L s^{-1}, but the water is likely to be brackish if pumped from levels below mean sea level.

Rarotonga is the largest island and has the largest population. It has many streams, including large permanent ones that provide a good source of freshwater. Four galleries, which consist of porous pipes buried to depths below the water table in volcanic gravel, have been constructed along several of these rivers. Collected water is distributed around the island by pipelines. Some smaller streams pass through the fringing reef in underground tunnels, while larger ones are associated with channels through the reef. The subterranean flows re-emerge at the coastline as fresh or brackish springs. Three types of aquifers exist in Rarotonga and in the volcanic cores of makatea islands: perched aquifers confined by impermeable layers; perched aquifers in compartments formed by dikes that intruded lava flows; and basal freshwater wedges floating on and displacing saltwater (Waterhouse and Petty, 1986).

Aitutaki has three galleries, as well as water from dug wells and pumped from drillholes; water is directed into reservoirs from these sources (Waterhouse and Petty, 1986). The freshwater lens is 95 cm thick on the west central coast, as determined from a drillhole located about 10 m above modern sea level. Freshwater needs for Atiu and Mitiaro are met by household and public roof catchments.

Makatea islands

Freshwater on makatea islands can be found in streams, in lakes that occur in the swamp areas between the volcanic hills and makatea, in makatea caves and pools, in springs, and in freshwater aquifers (Fig. 16-3; Waterhouse and Petty, 1986). In general, makatea islands have radial drainage patterns that enter the makatea from the surrounding volcanic hills; the streams then proceed to the coast via underground tunnels and passageways (Marshall, 1927, 1930; Wood and Hay, 1970). These subterranean passageways have formed both during growth of the limestone and by later dissolution. The subterranean flows surface at the outer reef as fresh- or brackish-water springs. During heavy rains, muddy plumes can be seen offshore from the springs.

The quality of groundwater depends on the elevation of the water table above sea level. Consequently, groundwater quality is better in the volcanic rocks, which have a thicker aquifer at higher elevations, than it is in the makatea (Fig. 16-3; Table 16-3). Makatea water may be used for agriculture or washing, but rarely for drinking, because there is commonly mixing with underlying saltwater and contamination from other uses of the water and from villages. The same problems concern water from the lakes. On Atiu, the depth to the top of the freshwater aquifer at eight locations varies from 9 to 28 m (all in volcanic rocks) at land-surface elevations of 60–70 m; two drillholes on Mauke intersected the freshwater aquifer at 4.3 m (in volcanic rocks) and 12 m (in makatea) at land-surface elevations of 22 m and 14 m, respectively; six holes in Mangaia intersected the freshwater aquifer at 17–73 m (all in volcanic rocks) at land-surface elevations of 47–87 m; and four holes on Aitutaki intersected the aquifer at 21–43 m (all in volcanic rocks) at land-surface elevations of 12–84 m (Waterhouse and Petty, 1986).

Atolls

Rainwater catchments and freshwater lenses are the only sources of freshwater for the atolls. For the atoll and reef island populations (mostly in northern Cook Islands), roof catchment is the dominant and usually the only source of freshwater. If all structures have appropriate roofs and holding tanks, this source of water is usually sufficient for island needs, as industry does not exist, except on Manihiki, where there is a pearl shell development. Agricultural needs are small. Tapping the freshwater lens could readily supply additional water resources to the atolls if needed in the future. Unpredictable dry periods can cause problems if community emergency water-storage tanks are not available and maintained. The reef island of Nassau, which is occupied intermittently by Pukapukans to harvest coconuts, has a shallow well dug at its center. This well reportedly provides a good dependable supply of freshwater (Wood and Hay, 1970).

Table 16.3

Composition of rainfall, surface water (lakes and swamps), groundwater (in volcanic rocks), and makatea pool water (surface), for the southern Cook Islands*

	Rainfall			Surface Water			Ground Water			Makatea Pools		
	M	STD	Range (No.)	M	STD	Range (No.)	M	STD	Range (No.)	M	STD	Range (No.)
Conductivity mS/m	12	0.99	11.3–12.7 (2)	113.17	149.28	9.3–444 (11)	19.6	9.34	5.1–50.6 (18)	236.26	201.93	60.6–647 (14)
pH	6.6	0.5	6.1–7.1 (3)	7.32	1.38	6.1–9.3	7.0	0.62	5.6–7.9	7.53	0.39	6.9–8.2
Total Hardness ($CaCO_3$)	29.5	2.12	28–31 (2)	179.5	264.4	39–576	59.8	25.35	12–100	340.25	168.07	52–640
HCO_3^-(g m^{-3})	36.5	6.36	32–41 (2)	50.75	16.58	35.67	58.22	35.47	6–107	192.78	70.48	135–260
Cl^- (mg/L)	10.33	2.52	8–13 (3)	333.71	510.73	17–1680	22.8	6.04	13–36	570.2	653.59	107–2460
SO_4^{2-} (mg/L)	6	2.83	4–8 (2)	53.5	87.06	6–184	12.1	10.6	2–40	72.11	77.31	20–222
Na^+ (mg/L)	5.9	2.4	4.2–7.6 (2)	222.82	411.46	12.9–840	17	6.24	9–32	209.62	227.24	62–755
K^+ (mg/L)	0.2	0.14	< 0.1–0.3 (2)	8.35	16.43	< 0.1–33	1.53	1.01	< 0.1–3.7	9.15	9.84	3.2–33
Mg^{2+} (mg/L)	0.7	0.14	0.6–0.8 (2)	29.12	48.59	3.5–101	6.34	2.73	1.5–9.2	30.84	29.91	12.2–102
Ca^{2+} (mg/L)	10.8	1.13	10–11.6 (2)	24.25	26.53	10–64	9.8	6.43	< 1–20	59.42	14.18	44.4–85
Fe^{2+} (mg/L)	0.325	0.11	0.25–0.4 (2)	0.05	0	0	1.51	3.52	0.05–12.5	0.2	0.43	< 0.05–1.4
Mn^{2+} (mg/L)	< 0.05	0	0(1)	0.05	0	0	0.09	0.08	0.02–1	0.03	0.02	0.01–0.03
Nitrate N (mg/L)	0.5	0	0 (1)	0.24	0	0	0.17	0.31	0.01–3.3	0.33	0.25	0.17–0.88

*From Waterhouse and Petty, 1986.
M = mean.
STD = standard deviation.

CASE STUDY: SUBSURFACE GEOLOGY BENEATH THE LAGOONS AS REVEALED BY DRILLING

During May—July 1986 and July—September 1987, we undertook a drilling, seismic, and bottom-sampling program in the lagoons of Aitutaki, Pukapuka, and Rakahanga. Even though the program was designed as a pilot project to explore predominantly for lagoonal phosphorite, the drill cores proved to be invaluable for deciphering Pleistocene and Holocene atoll evolution and reef diagenesis. Results of the drilling program have been published by Hein et al. (1988; 1992), Gray et al. (1992), and Gray and Hein (1997a,b). Some of the seismic and bottom sampling was discussed above in the section "Geology," and details can be found in Richmond (1992a). Here we summarize the results from this unique set of drill cores and compare the results with studies completed on outcrop samples from the southern Cook Islands.

Six holes were drilled in Aitutaki lagoon to subbottom depths of 30–69 m, three holes in Pukapuka and two holes in Rakahanga lagoons to depths between 40–50 m; water depths at drill sites are 2–8.5 m (Table 16-4; Figs. 16-4–16-6). Of the 492 m of core drilled, 134 m were recovered. Most of the missing 73% of section is vuggy to cavernous porosity in the reef, where the drillstring dropped through cavities of more than a meter high, and through unconsolidated sand in the upper parts of the holes that was commonly washed out by the drilling process. The occurrences of large

Table 16-4

Core recovery in 11 lagoonal drill cores from Aitutaki, Pukapuka, and Rakahanga, Cook Islands

Hole Number	Water Depth (m)	Drilled (m)	Recovered (m)	Recovery (%)
Aitutaki				
1A	4	38.75	16.98	44
2A	3	69.26	44.99	65
3A	3	40.10	6.29	16
4A	2	30.72	8.05	26
5A	8.5	52.86	10.23	19
6A	3	29.95	4.34	14
Total	–	261.64	90.88	35
Pukapuka				
1P	4	43.65	16.09	37
2P	4.8	48.59	9.34	19
3P	5.8	48.89	4.29	9
Total	–	141.13	29.72	21
Rakahanga				
1R	3	44.19	8.39	19
2R	3.8	44.87	4.80	11
Total	–	89.06	13.19	15
Grand Total	–	491.83	133.79	27

cavities and sand were placed in their proper stratigraphic context by monitoring the water pressure on the drilling equipment. Sand and mud was also spot sampled with a hammer corer to help define those stratigraphic intervals.

The five cores from the northern Cook Islands consist entirely of carbonate deposits (Figs. 16-5, 16-6). One of six cores from Aitutaki consists entirely of carbonate deposits; the others also include pedogenic mud, volcaniclastic deposits and basalt (Fig. 16-4; Hein et al., 1988; Gray et al., 1992). Carbonate sections from the northern and southern atolls also differ. Pleistocene carbonate deposits on Aitutaki

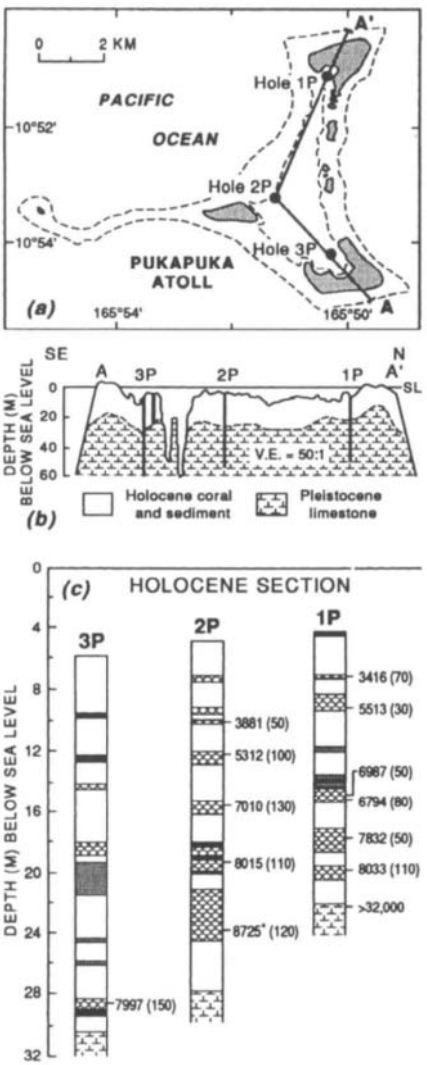


Fig. 16-5. Cores and cross section locations for Pukapuka Atoll (From Gray and Hein, 1997a).

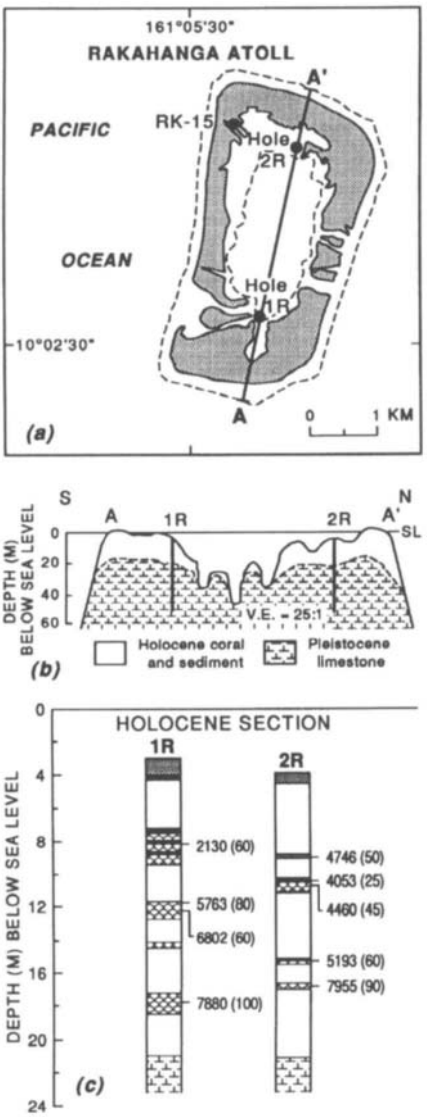


Fig. 16-6. Cores and cross section locations for Rakahanga Atoll (From Gray and Hein, 1997a).

that were originally aragonite have been replaced by calcite and then later were dolomitized in places; carbonate deposits from the northern atolls are still predominantly aragonite. Consequently, the diagenetically altered Pleistocene section from Aitutaki could not be age dated using U-series and ESR techniques; these two techniques were used to date aragonite limestones from the northern atolls. Holocene sections were dated using radiocarbon techniques (Gray and Hein, 1997a).

Pleistocene stratigraphy, reef growth and sea levels

The northern Cook Islands on Manihiki Plateau occupy a part of the Pacific that has been tectonically stable for many millions of years. The plateau formed during a short interval of extensive volcanism in the Early Cretaceous and underwent rapid subsidence due to cooling until apparently reaching near thermal stability in the Tertiary. The makatea islands (and possibly Aitutaki) to the south, however, have undergone uplift during the past 2 Ma due to lithospheric loading and flexure as the result of the formation of Rarotonga; uplift may be continuing today. Consequently, the northern group of atolls should offer a relatively stable region to determine eustatic changes in sea level. Reef corals recovered from the drillholes should record interglacial intervals when sea level has risen higher than the outer reef rim and flooded the island platform. The lagoons drilled are enclosed, without deep passages; water exchange is over the rims and presumably this was true throughout the Holocene. Once the reef rim grew to sea level, typically within a few thousand years (Davies and Montaggioni, 1985), any subsequent lowering of sea level would kill the lagoon corals. Therefore, in situ lagoon corals should date the highest sea-level stands and transgressions to those stands (Gray et al., 1992). Consequently, it is not necessary to know the water depth of coral growth within the lagoon to draw conclusions about past sea levels.

In situ aragonite corals from Pukapuka and Rakahanga yield ages of middle Pleistocene to the present-day (Gray et al., 1992). Ages fall within five reef-growth periods: 650–460, 460–300, 230–180, 180–125, and 9–0 ka (Table 16-5). These ages may correspond to oxygen isotope interglacial stages, 15 and 13, 11 and/or 9, 7, 5, and 1, although the matches are not always straightforward (Fig. 16-7). Time gaps between periods of reef growth define hiatuses that may or may not be accompanied by lithologic features characteristic of subaerial diagenesis. The Pleistocene-Holocene boundary is identified by the stratigraphically highest occurrence of secondary calcite and varies in depth from 15–22 m, with a minimum time gap of about 121 ky (130.1–9.2 ky; Gray et al., 1992).

For comparison, Woodroffe et al. (1991) determined the ages of late Pleistocene reefs on the makatea islands. They determined that the last interglacial reef corresponds to oxygen isotope substage 5e. Mean U-series ages are 126 ky for a reef that

Table 16-5

Periods of reef growth in the lagoons of Pukapuka and Rakahanga, northern Cook Islands

Reef	Age (ka)	Depth Range (m)	Thickness (m)	Oxygen Isotope Stage
1	9–0	22–0	15–22	1
2	180–125	25–15	3–10	5
3	230–180	26–22	>4	7
4	460–300	43–24	10–22	11,9
5	650–460	>36	>12	15,13

From Gray et al. (1992).

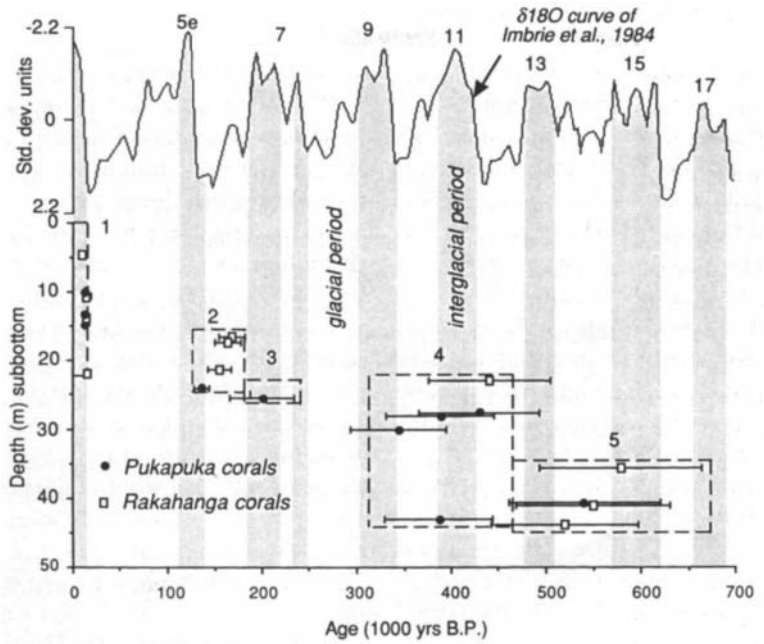


Fig. 16-7. Age versus depth of coral samples from Pukapuka (circles) and Rakahanga (squares) compared to the $\delta^{18}O$ curve from five deep-sea cores that were normalized, averaged, smoothed, and plotted against the SPECMAP time scale (Imbrie et al., 1984). Ages <300 ka are from U-series analyses (dating error is $\pm 1\sigma$) and ages >300 ka are from ESR analyses (dating error is ±15%). Stippled areas mark durations of interglacial periods suggested by negative excursion of $\delta^{18}O$ (as presented in Gray et al., 1992).

reaches elevations of 12.2 m on Atiu, 119 ky at 9.8 m for Mitiaro, 128 ky at 10.0–12.7 m on Mauke, and 115 ky at 14.5–20.0 m on Mangaia (Woodroffe et al., 1991). A lower reef on Atiu and one on Mauke are separated from the higher reefs by a sharp discontinuity and probably correlate with oxygen isotope stage 7. Mean U-series ages for these lower reefs are 196 ky for Atiu and 221 ky for Mauke. Woodroffe et al. (1991) concluded that differential uplift among the makatea islands has been continuing during the past 250 ky, and, that for the last 120 ky, uplift rates have been about 3–10 cm ky^{-1}.

Pleistocene sea-level changes are recorded in reef growth episodes sampled by drilling in the northern atolls. As discussed above, dating of the drilled sections indicates that five reef growth periods are represented. Given the depths of the five reefs and using the oxygen isotope curve to represent past sea level, then the erosion rate (ER), reef accretion rate (RAR), and subsidence rate (SR) should be related by:

$$RAR * FS = ER * FE + SR,$$

where FS and FE are the fraction of time that the reef was submerged and emerged, respectively (Gray et al., 1992).

Subsidence of the Pukapuka and Rakahanga atolls should be about the same, 4.5 ± 2.8 cm ky^{-1}, on the basis of the subsidence of oceanic crust, which is proportional to the square root of its age (Parsons and Sclater, 1977). The average Holocene accretion rate was 220 cm ky^{-1} and was used to bound the possible Pleistocene accretion rates (Gray et al., 1992). A predictive model inferred from the atoll stratigraphy indicates average subsidence and erosion rates of 3–6 cm ky^{-1} and 15–20 cm ky^{-1}, respectively, from ranges of accretion rates of 100–400 cm ky^{-1}, subsidence rates of 2–6 cm ky^{-1}, and duration of island submergence of 8–15% of the past 600 ky (Fig. 16-8; Gray et al., 1992).

Using subsidence rates of 3–6 cm ky^{-1} and a reef thickness of 500 m (as determined for Manihiki by Hochstein, 1967), reef growth would have begun sometime between 17 and 8 Ma. This result seems untenable because Manihiki Plateau subsided 3–4 km since its formation, and the volcanic islands that occur along its margin would have had to have been active long after the formation of the plateau or have been extraordinarily high volcanic islands when volcanism stopped. A problem must exist with the accuracy of the subsidence rates, reef thicknesses, or age of the volcanic

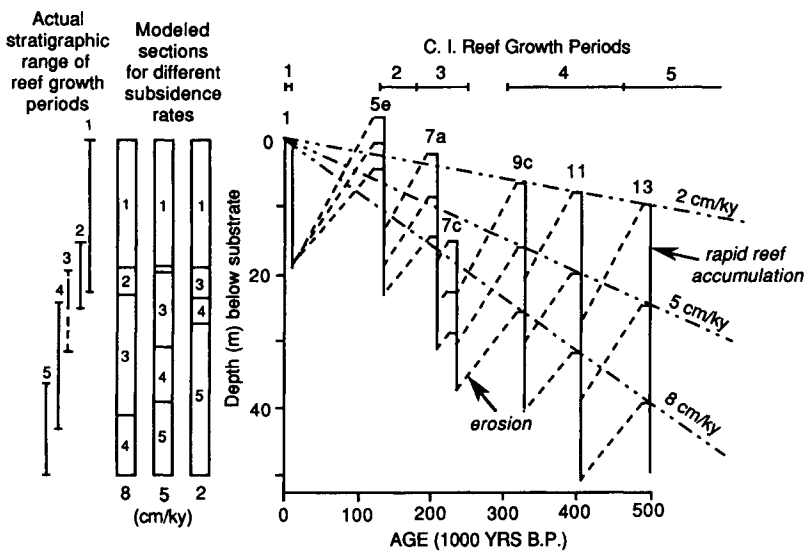


Fig. 16-8. Models of atoll reef growth and erosion for the late Quaternary showing the resulting stratigraphy from different subsidence and erosion rates. Solid vertical lines (right side of diagram) mark rapid reef accretion during major sea-level highstands indicated by the oxygen isotope curve in Fig. 16-7. Dashed diagonal lines represent erosion during periods of low sea level and subaerial exposure. Erosion rates of 14, 17 and 20 cm ky^{-1} for subsidence rates of 2, 5 and 8 cm ky^{-1}, respectively, are determined graphically. Sea-level highstands are inferred from the oxygen isotope curve and studies of Pleistocene reefs. Stratigraphic sections resulting from modeled subsidence rates of 2, 5 and 8 cm ky^{-1} are shown in the three columns on the left and compared to the observed stratigraphic positions of reef-growth periods from the Cook Islands cores (far left). According to this model, subsidence and erosion rates of 5 and 17 cm ky^{-1}, respectively, are most consistent with the observed stratigraphic sections (as presented in Gray et al., 1992.)

edifices; or, the tectonic history of Manihiki Plateau may have been more complex than that represented by a simple model of a subsiding ocean plateau.

Holocene reef growth and sea levels

Radiocarbon ages for cores from nine of the 11 drillholes in Aitutaki, Pukapuka, and Rakahanga lagoons delineate the evolution of lagoon sedimentation as Holocene sea level rose and stabilized (Fig. 16-9). On Aitutaki, the Holocene section is 7–9 m thick, except for in one hole drilled in a 10-m-deep basin, where the section is 22 m thick; on Pukapuka the section is 18–22 m thick and on Rakahanga, 17–18 m thick (Figs. 16.4–16.6; Gray and Hein, 1997a). The shallower Pleistocene basement for Aitutaki is probably the result of uplift of the atoll associated with volcanic rejuvenation during the Pleistocene. Thicknesses determined from seismic data yield a thicker mean Holocene section than that determined from drilling, because the drill sites are located chiefly on topographic highs. The Holocene section below Aitutaki lagoon is generally more than 10 m thick (Fig. 16-2). Pleistocene reef platforms,

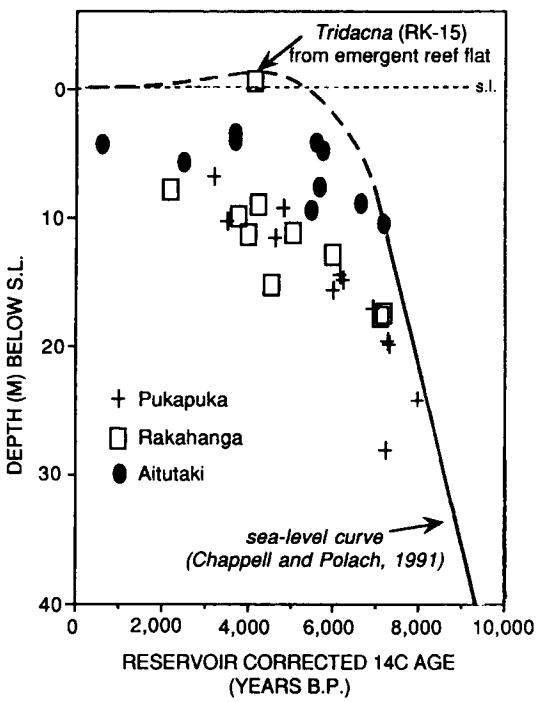


Fig. 16-9. Reservoir-corrected radiocarbon ages of corals compared to deglacial sea-level curve (solid line) (Chappell and Polach, 1991; Fairbanks, 1989) and late Holocene relative sea-level curves (dashed) from the southern Cook Islands (Yonekura et al., 1988; Woodroffe et al., 1990) and French Polynesia (Pirazzoli et al., 1985, 1988; Pirazzoli and Montaggioni, 1986, 1988). Depth and age errors are smaller than symbols.

200–130 ky in age, were colonized by Holocene reefs beginning between 8.7 and 7.8 ky (Gray and Hein, 1997a). Reef growth apparently started about 700 years later on Pukapuka than on the other atolls. The Pleistocene platforms are currently 7–22 m below the lagoon floors. Platforms were colonized within 500 years of flooding at water depths shallower than 8 m. Paleo-water depths deepened prior to about 5 ky, followed by gradual shoaling of the lagoons.

The highest mean Holocene accretion rates varied from 171–278 cm ky^{-1} for the northern atolls and 81–106 cm ky^{-1} for Aitutaki. Rates have varied greatly and generally decreased through the Holocene as lagoons shallowed and became more isolated by growth of the outer reef rim. The lower rates for Aitutaki probably reflect shallower water depths. An emergent reef at about 0.5 m above the reef flat on Rakahanga was dated as 4.6 ky, indicating that relative sea level was higher at that time then at present. The outer reef rim of Aitutaki was within a meter of modern sea level by 4.7 ky, as determined from a radiocarbon age of a sample of reef flat located 0.7 m below modern sea level (Yonekura et al., 1988).

Holocene reef development of these islands can be divided into four stages (see Fig. 16-9; Gray and Hein, 1997a). Transgression and colonization of the platform by corals at 7.8–7.0 ky marked the first stage. In the second stage, rising sea level and catch-up reef growth occured between 7.0–5.5 ky. The second stage also was characterized by rapid vertical accretion of the reef (163–436 cm ky^{-1}); however, these accretion rates were ultimately unable to keep up with rising sea level (500–1,200 cm ky^{-1}) and the lagoons deepened. The third stage was characterized by stabilization of sea-level at about 0.5–1 m above its modern level, and growth of the reef rim to sea level between 5.5 and 4.0 ky. In the final stage, from 4.0 ky to the present, sea level stabilized and the lagoon filled with sediment. In Aitutaki lagoon, large carbonate sand sheets prograde from the outer reef rim, whereas, in Rakahanga lagoon, coral growth ceased after 2.0 ky and sediments consist of muds and silts; nearly continuous islets inhibit the transport of sediment from the outer reef rim to the lagoon on Rakahanga.

A higher than modern Holocene relative sea-level stand is marked on the Cook Islands by emergent reef flats, notches, microatolls, and reef conglomerates, which have been reported to occur on Suwarrow (Scoffin et al., 1985; Woodroffe et al., 1990), Atiu, Mauke, Mitiaro (Spencer et al., 1987; Woodroffe et al., 1990), and Mangaia (Yonekura et al., 1988; Stoddart et al., 1985). An emergent Holocene reef on Aitutaki has not been conclusively found (Stoddart and Gibbs, 1975; Spencer, 1985; Hein et al., 1988). In the southern Cook Islands, it is not possible to separate relative sea-level changes caused by local vertical tectonics induced by lithospheric flexure associated with the volcanic loading of Rarotonga. In the northern group, which is far enough away from Rarotonga to be unaffected by volcanic loading and flexure, evidence for a higher than modern earlier Holocene sea level is mixed. Our results from the Rakahanga emergent reef flat are consistent with those of the previous studies, indicating that relative sea level may have fallen over the past 4.0 ky (Gray and Hein, 1997a). However, no evidence for a higher than modern Holocene sea-level reef was found on Pukapuka.

Reef diagenesis

The Holocene sections of Aitutaki, Pukapuka, and Rakahanga are composed of primary skeletal aragonite and minor high-Mg calcite. Syndepositional micrite envelopes were produced around allochems. Shallow-marine phreatic cements are composed of fibrous aragonite isopachous rims, botryoidal aragonite, rims of both blocky and fibrous high-Mg calcite, and high-Mg calcite peloids (Hein et al., 1988, 1992; Gray and Hein, 1997b). These cements occupy a minor part of the primary intergranular porosity, and, consequently, good porewater circulation has been maintained.

Pleistocene reef limestones on Aitutaki have been completely converted to calcite — no primary aragonite remains (Hein et al., 1988). Diagenetic textures and oxygen and carbon isotope values indicate that diagenesis occurred under meteoric phreatic conditions. Sparry calcite layers up to 10 cm thick, with individual calcite crystals up to 3 cm long, were also produced under meteoric phreatic conditions. Vuggy and moldic porosity are common and resulted from both fabric-selective and non-fabric-selective dissolution of allochems and cement. Large equant calcite crystals line primary and secondary pores and coarsen inward. Primary and secondary (two stages) neomorphism of grains and cements and abundant void-filling cement are common. In sections where fluid flow was restricted by interbedded impermeable basalt flows or pedogenic muds, fabric-selective neomorphism was dominant. Severe leaching of the limestone during subaerial weathering and soil formation produced muds composed of nordstrandite, goethite, lepidocrocite, and anatase that accumulated on the floor of large cavities and caves (Hein et al., 1988; 1992).

Calcite limestone at Aitutaki was replaced by dolomite at subbottom depths of >36 m under the outer reef rim and adjacent outer lagoon (Hein et al., 1992). Seismic reflection profiles indicate that the dolostone is at least 60 m thick. Stable isotopic compositions indicate that dolomitization occurred in a seawater environment, although replacement in the lower part of freshwater-seawater mixing zone may also have occurred (Hein et al., 1992). The limestones are pervasively dolomitized by fine-scale replacement, to the extent that most of the fossils are still identifiable, the textures of freshwater void-filling cements are preserved, and void space is largely unfilled. Mineralizing fluids were driven by thermal convection, probably related to rejuvenation of volcanism on Aitutaki in the middle Pleistocene. Thermal convection and hydrothermal circulation helped flush large amounts of fluids through the reef over a short time interval. The dolomitizing fluid was completely mixed with the hydrothermal component in the uppermost 33 m of dolostone section that was available for study. The hydrothermal component is characterized by enrichment of transition metals in the dolomite relative to the overlying limestone (Table 16.6). Thermal convection has also been proposed to have been involved in dolomitization of Niue Atoll (q.v., Chap. 17; Aharon et al., 1987) and the Society Islands (q.v., Chap. 15; Rougerie and Wauthy, 1993). The reef limestone was deposited during several sea-level highstands, followed by inversion to calcite. Dolomitization took place during a single sea-level stand that was several meters below modern sea level (Hein et al., 1992).

Table 16-6

Mean chemical compositions and ratios of elements in carbonate deposits from Aitutaki, Pukapuka, and Rakahanga

	Aitutaki				Pukapuka		Rakahanga	
	Primary Limestone (Holocene) (n = 1)	Secondary Limestone (Pleistocene) (n = 4)	Dolostone (n = 7)	Mottled Dolostone (n = 3)	Holocene Carbonate (n = 8)	Pleistocene Limestone (n = 16)	Holocene Carbonate (n = 5)	Pleistocene Limestone (n = 11)
Ca wt.%	37.4	40.1	24.6	21.8	38.7	38.9	38.4	38.8
Mg	1.17	0.36	11.1	10.1	0.51	0.31	0.49	0.32
Si	0.22	0.33	0.19	0.08	0.08	0.10	0.08	0.11
Al	0.15	0.12	0.08	0.17	<0.05	<0.05	<0.05	<0.05
P	0.02	0.03	0.03	0.07	<0.02	≈0.05	<0.01	≈0.09
Fe	≈0.05	≈0.06	≈0.13	6.24	<0.03	<0.03	<0.03	<0.03
Sr ppm	6100	455	250	210	6250	5018	7400	5827
Na	2500	500	≈950	≈1300	2000	≈1900	2400	2100
Co	1	2	3	9.7	1	1	2	1
Cr	6	7	17	85	2	3	2	4
Cu	2	2	5	10	7	3	3	2
Ni	3	4	6	15	<2	<2	<2	<2
V	4	<4	7	136	<2	<2	<2	<2
Mg/Ca	0.03	0.01	0.45	0.46	0.01	0.01	0.01	0.01
1000(Sr/Ca)	11.66	0.81	1.02	0.69	16.15	12.90	19.27	15.02
100(Na/Ca)	0.67	0.12	0.39	0.60	0.52	0.49	0.63	0.54
Mineralogy	Aragonite calcite	Calcite	Dolomite	Dolomite lepidocrocite hematite	Aragonite calcite	Aragonite calcite	Aragonite calcite	Aragonite calcite

Aitutaki chemistry compiled from Hein et al. (1988), where additional data are given; organic carbon in limestones from Aitutaki averages 0.26%; Pukapuka and Rakahanga chemistry from this work.

In contrast, Pleistocene reef limestones from Pukapuka and Rakahanga are composed predominantly of primary aragonite (Gray and Hein, 1997b). Apparently unaltered corals and reef gravel are interbedded with partly recrystallized corals. In Rakahanga cores, thin stratigraphic intervals are weakly cemented with amber-colored drusy spar. Minor amounts of localized calcite void-filling cement occur at some horizons in Pukapuka cores. This calcite cement is interpreted to have precipitated in the meteoric phreatic environment and to have overprinted vadose diagenetic textures (Gray and Hein, 1997b). Generally, however, diagenesis occurred in the vadose zone. During subaerial exposure, dissolution of grains and earlier-formed marine phreatic cements was extensive, producing free-standing micritic envelopes, partial dissolution of bioclasts, and secondary porosity.

The differences in diagenesis of the Pleistocene reef on Aitutaki compared to the northern atolls can be attributed to island morphology and its influence on the size of the freshwater lens (Gray and Hein, 1997b). The extent of the lens also depends on hydraulic conductivity of the rocks, climate, and sea-level changes. The northern part of the lagoon of Aitutaki almost-atoll contains a large, relatively high volcanic island, which would favor production of a large perennial freshwater lens, in contrast to the atolls to the north. Estimates of maximum lens thicknesses using the technique of Budd and Vacher (1991) yield 18–180 m for Aitutaki and 4–50 m for the northern atolls (Gray and Hein, 1997b). Such thicknesses, however, should have promoted extensive diagenesis of the northern atolls if it were not for the deep karst basins (to 60 m) that occur on the northern atolls; when sea level is lowered, these basins break up the lens into smaller units — the freshwater lens would not function as a single widely distributed lens.

A thick freshwater lens occurs on Aitutaki because of the large size, high elevation, and large rain catchment area of the island, as well as its lack of deep basins that would fragment the lens. Lower fluid transmissivity of the limestones is caused by interbedded volcanic and pedogenic deposits. All hydrologic systems on Aitutaki — the freshwater lens, mixing zone, and seawater-saturated reef pedestal — may have been influenced by convective circulation from heat sources produced during Pleistocene volcanism. This convective circulation would have increased the rate of diagenesis and may explain why the Pleistocene section at Aitutaki was completely converted to calcite.

CONCLUDING REMARKS

The fifteen Cook Islands are divided into northern and southern groups that are separated by over 500 km of open ocean and together span more than 1,400 km from north to south. The two groups have distinctively different climates and oceanographic settings, tectonic origins, geomorphologies, hydrologic resources, and geologic histories. The southern group of islands forms two linear volcanic chains; crustal loading and flexure associated with Quaternary volcanism on Rarotonga uplifted the makatea islands. In contrast, most islands of the northern group are located on the tectonically stable Manihiki Plateau, which formed from an outpouring of lava at a triple junction during the Early Cretaceous.

Drill cores from Aitutaki lagoon in the southern group consist of carbonate sediments and rocks, pedogenic mud, volcaniclastic deposits, and basalt, whereas cores from the northern atolls of Pukapuka and Rakahanga consist exclusively of carbonate deposits. Pleistocene carbonate deposits on Aitutaki were replaced by calcite and then were dolomitized in places, whereas those from the northern atolls are still predominantly aragonite. Aitutaki limestone was dolomitized in a seawater environment, although replacement in the lower part of the freshwater-seawater mixing zone may also have occurred. Mineralizing fluids were likely driven by thermal convection associated with rejuvenation of volcanism on Aitutaki. Differences in diagenesis of Pleistocene reefs on Aitutaki compared to those of the northern atolls is attributed to island morphology and its influence on the size of the freshwater lens. U-series and ESR ages of aragonite corals from northern Cook atolls define five intervals of reef growth during the Quaternary. Radiocarbon dating of drilled Holocene sections from the three islands provides a history of lagoon sedimentation in response to Holocene sea-level rise and stabilization.

ACKNOWLEDGMENTS

We thank Ann Gibbs for technical support and Terry Quinn, Len Vacher, Brian Jones, Christopher Wheeler, Harry Cook, and Ann Gibbs for helpful reviews. We thank all the Cook Islanders who helped make the field program a success and the local governments of Aitutaki, Pukapuka, and Rakahanga Islands that supported our work. We especially thank Tony Utanga and Stuart Kingan of the central government in Rarotonga who coordinated our efforts in the islands. This work would have been impossible without the cooperation of the sponsoring agencies CCOP/SOPAC, USGS, and Rijks Geologische Dienst, who provided the drilling equipment and technical staff.

REFERENCES

Aharon, P., Socki, R.A. and Chan, L., 1987. Dolomitization of atolls by sea water convection flow: Test of a hypothesis at Niue, South Pacific. J. Geol., 95: 187–203

Beiersdorf, H. and Shipboard scientific party, 1990. Mid-Cretaceous volcanism at the Manihiki Plateau (abstr.). Fifth Circum-Pacific Energy Min. Res. Conf., July 29-August 3, 1990, Honolulu, 27–28.

Budd, D.A. and Vacher, H.L., 1991. Predicting the thickness of fresh-water lenses in carbonate paleo-islands. J. Sediment. Petrol., 61: 43–53.

Calmant, S. and Cazenave, A., 1986. The effective elastic lithosphere under the Cook-Austral and Society islands. Earth Planet. Sci. Lett., 77: 187–202.

Campbell, I. B., Claridge, G.G.C. and Blakemore, L.C., 1978. Pedological study of soils from basaltic parent material on the island of Atiu, Cook Islands. N.Z. J. Sci., 21: 229–248.

Chappell, J. and Polach, H.A., 1991. Post-glacial sea-level rise from a coral record at Huon Peninsula Papua New Guinea. Nature, 349: 147–149.

Clague, D.A., 1976. Petrology of basaltic and gabbroic rocks dredged from the Danger Island troughs, Manihiki Plateau. In: S.O. Schlanger, E.D. Jackson, et al. (Editors), Initial Reports of the Deep Sea Drilling Project, 33. U.S. Gov. Printing Office, Washington D.C., pp. 891–911.

Dalrymple, G. B., Jarrard, R.D. and Clague, D.A., 1975. K-Ar ages of some volcanic rocks from the Cook and Austral islands. Geol. Soc. Am. Bull., 86: 1463–1467.

Davies, P.J. and Montaggioni, L., 1985. Reef growth and sea-level change: The environmental signature. Proc. Fifth Int. Coral Reef Symp. (Tahiti), 3: 479–503.

Diament, M. and Baudry, N., 1987. Structural trends in the Southern Cook and Austral archipelagoes (South Central Pacific) based on an analysis of SEASAT data: geodynamic implications. Earth Planet. Sci. Lett., 85: 427–438.

Fairbanks, R.G., 1989. A 17,000-year glacio-eustatic sea level record: influence of glacial melting rates on the Younger Dryas event and deep-ocean circulation. Nature, 342: 637–642.

Gray, S.C. and Hein, J.R., 1997a. Holocene reef growth and sea-level history in the Cook Islands. Coral Reefs (in press).

Gray, S.C. and Hein, J.R., 1997b. Contrasting diagenetic alteration of subsurface Pleistocene limestones in the Cook Islands. Coral Reefs (in press).

Gray, S.C., Hein, J.R., Hausmann, R. and Radtke, U., 1992. Geochronology and subsurface stratigraphy of Pukapuka and Rakahanga atolls, Cook Islands: Late Quaternary reef growth and sea-level history. Palaeogeog., Palaeoclimat., Palaeoecol., 91: 377–394.

Heezen, B.C., Glass, B. and Menard, H.W., 1966. The Manihiki Plateau. Deep Sea Res., 13: 445–458.

Hein, J.R., Richmond, B.M., Gray, S.C., Hausmann, R., Colgan, M.W., El Sabbagh, D. and Gein, L.M., 1988. Description; mineralogical, chemical and isotopic compositions; petrography; diagenesis; and uranium-series ages of drill cores from the lagoon of Aitutaki, Cook Islands. U.S. Geol. Surv. Open-File Rep. 88–419, 151 pp.

Hein, J.R., Gray, S.C., Richmond, B.M. and White, L.D., 1992. Dolomitization of Quaternary reef limestone, Aitutaki, Cook Islands. Sedimentol., 39: 645–661.

Hochstein, M.P., 1967. Seismic measurements in the Cook Islands, south-west Pacific Ocean. N.Z. J. Geol. Geophys., 10: 1499–1526.

Imbrie, J., Hays, J.D., Martinson, D.G., Mcintyre, A., Mix, A.C., Morley, J.J., Pisias, N.G., Prell, W.L. and Shackleton, N.J., 1984. The orbital theory of Pleistocene climate: Support from a revised chronology of the marine $\delta^{18}O$ record. In: A.L. Berger, J. Imbrie, J.D. Hays, G. Kukla and B. Saltzman (Editors), Milankovitch and Climate, Part I. Reidel, Boston, 269–305.

Irwin, J., 1985. The underwater morphology of Palmerston and Suwarrow Atolls. Atoll Res. Bull., 292: 109–113.

Jackson, E.D. and Schlanger, S.O., 1976. Regional syntheses, Line Islands chain, Tuamotu Island chain, and Manihiki Plateau, central Pacific Ocean. In: S.O. Schlanger, E.D. Jackson, et al. (Editors), Initial Reports of the Deep Sea Drilling Project, 33. U.S. Gov. Printing Office, Washington D.C., 915–927.

Jenkyns, H.C., 1976. Sediments and sedimentary history of the Manihiki Plateau, South Pacific Ocean. In: S.O. Schlanger, E.D. Jackson, et al. (Editors), Initial Reports of the Deep Sea Drilling Project, 33. U.S. Gov. Printing Office, Washington D.C., pp. 873–890.

Lambeck, K., 1981. Lithospheric response to volcanic loading in the Southern Cook Islands. Earth Planet. Sci. Lett., 55: 482–496.

Lanphere, M.A. and Dalrymple, G.B., 1976. K-Ar ages of basalts from DSDP Leg 33: Sites 315 (Line Islands) and 317 (Manihiki Plateau). In: S.O. Schlanger, E.D. Jackson, et al. (Editors), Initial Reports of the Deep Sea Drilling Project, 33. U.S. Gov. Printing Office, Washington D.C., pp. 649–653.

Mahoney, J.J., 1987. An isotopic survey of Pacific oceanic plateaus: Implications for their nature and origin. In: B.H. Keating, P. Fryer, R. Batiza and G.W. Boehlert (Editors), Seamounts, Islands and Atolls, Geophysical Monograph 43. Am. Geophys. Union, Washington D.C., 207–220.

Mammerickx, J., 1992. Bathymetry of the southcentral Pacific. Scripps Institution of Oceanography, La Jolla, California.

Marshall, P., 1927. Geology of Mangaia. Bernice P. Bishop Museum Bulletin 36, Honolulu, 38 pp.

Marshall, P., 1930. Geology of Rarotonga and Atiu. Bernice P. Bishop Museum Bulletin 72, Honolulu, 75 pp.

McNutt, M. and Menard, H.W., 1978. Lithospheric flexure and uplifted atolls. J. Geophys. Res., 83: 1206–1212.

Parsons, B. and Sclater, J.G., 1977. An analysis of the variation of ocean floor bathymetry and heat flow with age. J. Geophys. Res., 82: 803–827.

Pirazzoli, P.A. and Montaggioni, L.F., 1986. Late Holocene sea-level changes in the northwest Tuaislet Islands, French Polynesia. Quat. Res., 25: 350–368.

Pirazzoli, P.A. and Montaggioni, L.F., 1988. The 7000 yr sea level curve in French Polynesia geodynamic implication for mid-plate volcanic islands. Proc. Sixth Inter. Coral Reef Symp. (Townsville), Australia, 3: 467–477.

Pirazzoli, P.A., Montaggioni, L.F., Delibrias, G., Faure, G. and Salvat, B., 1985. Late Holocene sea-level changes in the Society Islands and in the northwest Tuaislet Atolls. Proc. Fifth Inter. Coral Reef Symp. (Tahiti), 3: 131–136.

Pirazzoli, P.A., Montaggioni, Salvat, B. and Faure, G., 1988. Late Holocene sea level indicators from twelve atolls in the central and eastern Tuaislets (Pacific Ocean). Coral Reefs, 7: 57–68.

Richmond, B.M., 1992a. Holocene geomorphology and reef history of islands in the South and Central Pacific. Ph.D. Dissertation, University of California, Santa Cruz, 298 pp.

Richmond, B.M., 1992b. Development of atoll islets in the central Pacific. Proc. Seventh Inter. Coral Reef Symp. (Guam), 2, 1185–1194.

Rougerie, F. and Wauthy, B., 1993. The endo-upwelling concept: from geothermal convection to reef construction. Coral Reefs, 12: 19–30.

Schofield, J.C., 1970. Notes on late Quaternary sea levels, Fiji and Rarotonga. N.Z.J. Geol. Geophys., 14: 240–241.

Scoffin, T. P., Stoddart, D.R., Tudhope, W.W. and Woodroffe, C.D., 1985. Exposed limestones of Suwarrow Atoll. Proc. Fifth Inter. Coral Reef Symp. (Tahiti), 3: 137–140.

Spencer, T., 1985. Rates of karst processes on raised reef limestones and their implications for coral reef histories. Proc. Fifth Inter. Coral Reef Symp. (Tahiti), 6: 629–634.

Spencer, T., Stoddart, D.R. and Woodroffe, C.D., 1987. Island uplift and lithospheric flexure: Observations and cautions from the South Pacific. Z. Geomorphol., Suppl.-Bd., 63: 87–102.

Stoddart, D.R. and Gibbs, P.E., 1975. Almost-atoll of Aitutaki. Atoll Res. Bull., 190: 1–158.

Stoddart, D. R., Spencer, T., Scoffin, T.P., 1985. Reef growth and karst erosion on Mangaia, Cook Islands: A reinterpretation. Z. Geomorphol., Suppl.-Bd., 57: 121–140.

Stoddart, D.R., Woodroffe, C.D. and Spencer, T., 1990. Mauke, Mitiaro and Atiu: Geomorphology of makatea islands in the southern Cooks. Atoll Res. Bull., 341: 1–65.

Summerhayes, C.P., 1967. Bathymetry and topographic lineation in the Cook Islands. N.Z. J. Geol. Geophys., 10: 1382–1399.

Summerhayes, C.P., 1971. Lagoonal sedimentation at Aitutaki and Manuae in the Cook Islands: A reconnaissance survey. N.Z. J. Geol. Geophys., 14: 351–363.

Thompson, C.S., 1986a. The climate and weather of the southern Cook Islands. N.Z. Meteorological Service Miscellaneous Publication 188 (2), 69 pp.

Thompson, C.S., 1986b. The climate and weather of the northern Cook Islands. N.Z. Meteorological Service Miscellaneous Publication 188 (3), 45 pp.

Tudhope, A.W., Scoffin, T.P., Stoddart, D.R. and Woodroffe, C.D., 1985. Sediments of Suwarrow Atoll. Proc. Fifth Inter. Coral Reef Symp. (Tahiti), 6: 611–616.

Turner, D.L. and Jarrard, R.D., 1982. K-AR dating of the Cook-Austral island chain: a test of the hot-spot hypothesis. J. Volcanol. Geotherm. Res., 12: 187–220.

Waterhouse, B.C. and Petty, D.R., 1986. Hydrogeology of the southern Cook Islands, South Pacific. N.Z. Geol. Sur. Bull. 98, Wellington, 93 pp.

Winterer, E.L., Lonsdale, P.F., Matthews, J.L. and Rosendahl, B.R., 1974. Structure and acoustic stratigraphy of the Manihiki Plateau. Deep-Sea Res., 21: 793–814.

Wood, B.L. and Hay, R.F., 1970. Geology of the Cook Islands. N.Z. Geol. Sur. Bull. 82, 103 pp.

Woodroffe, C.D., Stoddart, D.R., Spencer, T., Scoffin, T.P. and Tudhope, A.W., 1990. Holocene emergence in the Cook Islands, South Pacific. Coral Reefs, 9: 31–39.

Woodroffe, C.D., Short, S.A., Stoddart, D.R., Spencer, T. and Harmon, R.S., 1991. Stratigraphy and chronology of late Pleistocene reefs in the southern Cook Islands, South Pacific. Quat. Res., 35: 246–263.

Yonekura, N., Ishii, T., Saito, Y., Maeda, Y., Matsushima, Y., Matsumoto, E. and Kayanne, H., 1988. Holocene fringing reefs and sea-level change in Mangaia Island, southern Cook Islands. Palaeogeog., Palaeoclimat., Palaeoecol., 68: 177–188.

This Page Intentionally Left Blank

Geology and Hydrogeology of Carbonate Islands. Developments in Sedimentology 54
edited by H.L. Vacher and T. Quinn
© 1997 Elsevier Science B.V. All rights reserved.

Chapter 17

GEOLOGY AND HYDROGEOLOGY OF NIUE

CHRISTOPHER WHEELER and PAUL AHARON

INTRODUCTION

Niue is an uplifted carbonate island in the South Pacific at 19°00'S, 169°50'W (Fig. 17-1). Tonga [q.v., Chap. 18], Samoa, and the Cook Islands [q.v., Chap. 16] are its closest neighbors at distances of about 480, 560, and 670 km, respectively. The island is about 21 km along its N-S axis and 17 km along its E-W axis. The 259-km^2 land surface makes Niue one of the largest carbonate islands in the Pacific basin (Fig. 17-2A). Niue stands about 4,000 m above the surrounding ocean floor, and the highest point on the island is about 70 m above sea level. Niue's capital, Alofi, is on the west coast. In 1986, Niue had a population of 2,532; roughly another 7,500 Niueans were living in New Zealand (Douglas and Douglas, 1989).

Niue's present topography (Fig. 17-2A) has sparked curiosity ever since its European discovery in 1774 by Captain James Cook, who asked, "If these coral rocks were first formed in the sea by animals, how came they to be thrown up to such a height? Has this island been raised by an earthquake? Or has the sea receded from it?" (Cook 1777).

Among those who have visited the island, Agassiz (1903) was first to describe and document the terraces and fossils. At about the same time, members of the Funafuti expedition stopped at Niue to examine the terraces (David, 1904). More recently, Niue has been noted for the unusually high radioactivity (Marsden et al., 1958) and mercury content (Whitehead et al., 1990) of its soils. Niue is perhaps best known in carbonate sedimentology for its massive dolomite, which has been attributed to brine reflux (Schlanger, 1965; Schofield and Nelson, 1978), freshwater-saltwater mixing-zone processes (Rodgers et al., 1982), thermal convection of ocean-derived saline groundwater (Aharon et al., 1987), and tide-driven flux of saline groundwater beneath the mixing zone (Wheeler and Aharon, 1993). In this chapter, we will review past and ongoing investigations of Niue's geology, particularly its carbonate depositional system, history of sea-level fluctuations, hydrogeology, and dolomitization.

SETTING

History

Niue was settled initially by Polynesian people who first arrived more than 1,000 years ago, probably from Samoa or eastern Polynesia (Loeb, 1926). The European

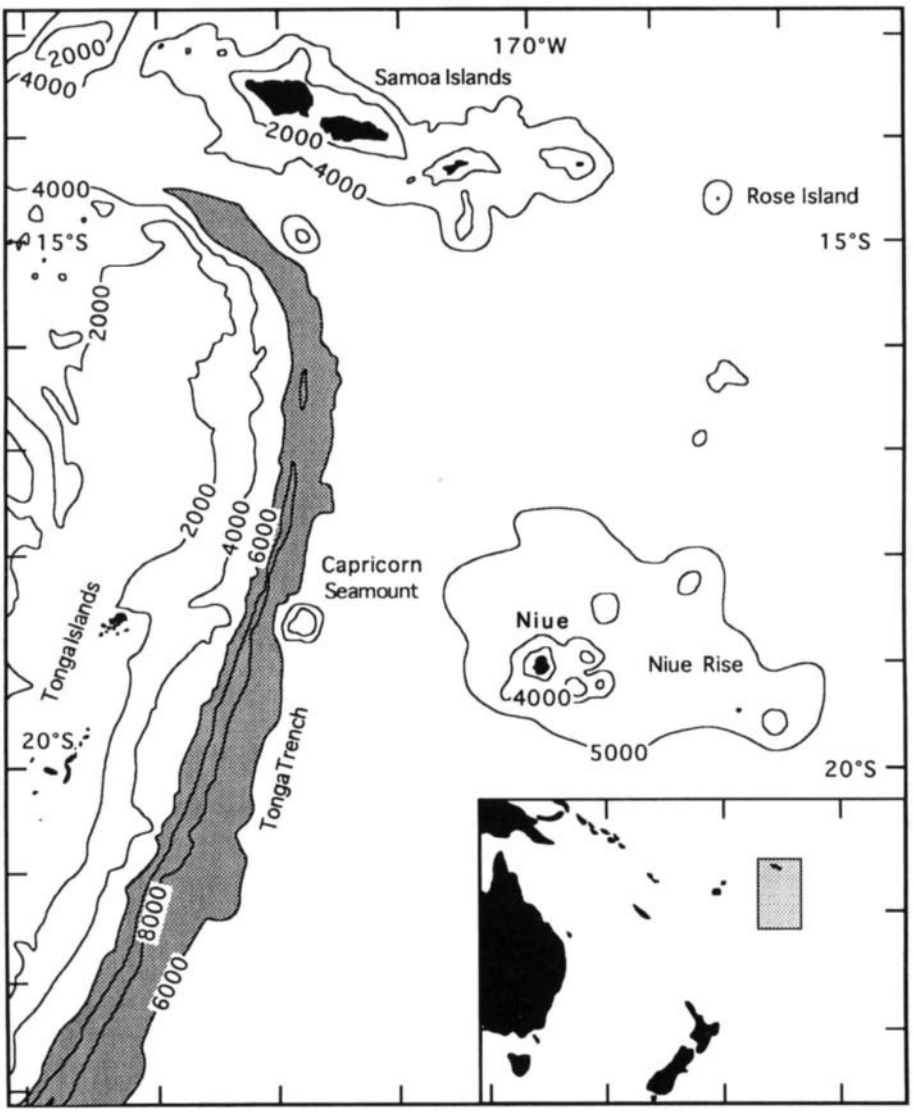


Fig. 17-1. Map showing regional setting of Niue, east of the Tonga Trench and southeast of Samoa. Bathymetric contours in meters. [See also Fig. 18.1.]

discovery of Niue was made by Captain James Cook aboard HMS *Resolution* on the afternoon of June 20, 1774, while he was heading westward from the Society and the (later named) Cook Islands. Captain Cook and his party landed on June 21 at three points on the west coast of the island, which he claimed for King George III and initially named Prince Frederic's Island in honor of the Prince of Wales. The hostile reception by the native Niueans, however, convinced Cook that his crew would be

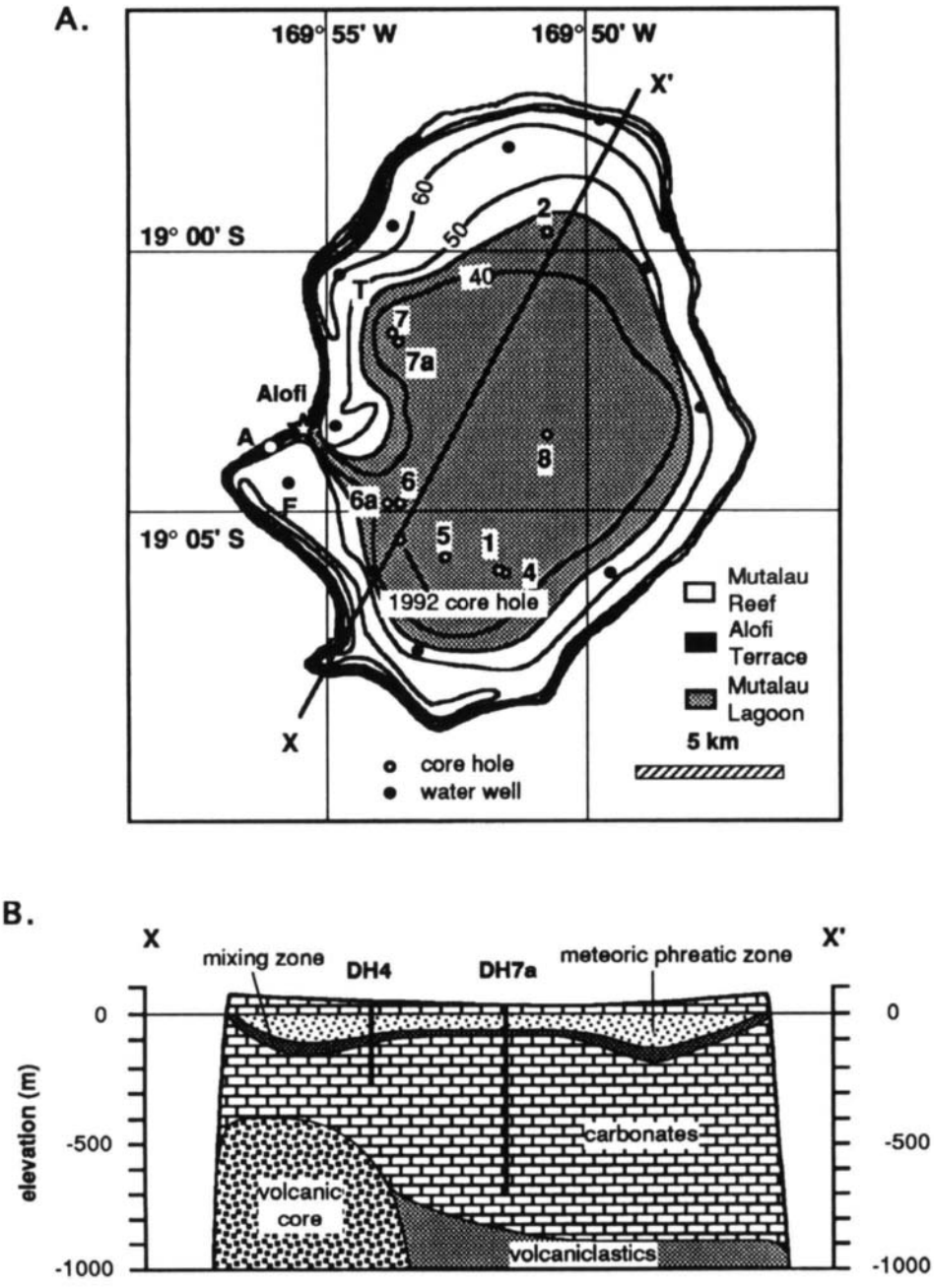


Fig. 17-2. Surface morphology and geology of Niue. A: Map showing the location of the Fonuakula dugwell (F), the Amanau coastal well (A), the Tuapa well (T) and other water wells, and stratigraphic cores (1 = PB1; 2 = PB2; 4 = DH4; 5 = DH5; 6 = DH6; 6a = DH6a; 7 = DH7; 7a = DH7a; 8 = DH8). The 1992 coring site is south of site 6. The 50-m contour encloses the former reef ridge and indicates the former ocean-lagoon channel. (Modified after Jacobson and Hill 1980b.) B: Cross section showing the carbonate platform and volcanic pedestal, the meteoric lens and mixing zone, and coring sites DH4 and DH7a. (Modified after Hill 1983.)

unable to safely re-provision at Niue and motivated him to re-name the island "Savage Island" (Cook, 1777). He and his party returned to the *Resolution* and on June 22 resumed course.

The Niueans' reputation deterred any further deliberate European contact until the missionary efforts of the mid-nineteenth century (Loeb, 1926). Niue was declared a British Protectorate in 1900 and was annexed by New Zealand in 1901 as part of the Cook Islands. In 1974, Niue was granted "self-government in free association with New Zealand," while New Zealand retained control over defense and foreign affairs.

Climate

Niue lies within the southern boundary of the southeast trade winds which blow steadily most of the year at 5–9 kn (Wright and van Westerndorp, 1965). Niue is also within the belt of typhoons, which periodically visit the island (Douglas and Douglas, 1989). The average temperatures are 26°C from December through April and 24°C from May through November. The relative humidity at 9 am is 73–95%, with an annual average of 89% (Wright and van Westerndorp, 1965).

Niue has two seasons: a wet, monsoonal season and a dry season (Jacobson and Hill, 1980a). The wet season is December-April; the maximum monthly mean rainfall (March) is 307 mm. The dry season is May-November; the minimum monthly mean rainfall (June) is 84 mm. Mean annual rainfall (1906–1978) is 2,041 mm; annual totals are 1,065–3,185 mm (Fig. 17-3). The worst drought of historical times was over a two-year period around 1890 (Wright and van Westerndorp, 1965). In the period in which records have been kept (1906-), the worst prolonged drought was 1940–1944, when average annual rainfall was 24% below the mean over a five-year period and 37% below the mean during the two worst years of the drought (Jacobson and Hill, 1980a). In the two other principal droughts (1925–1926 and 1976–1977), average annual rainfall was 32% below the mean.

As indicated in Fig. 17-3, droughts at Niue generally coincide with prolonged disturbances in the Southern Oscillation Index. Departures from "perfect" correspondence may be related to Niue's location near the fulcrum of the Darwin-Tahiti barometric pressure endmembers.

Tectonic setting

Niue lies on the Pacific Plate about 270 km east of the Tonga Trench (Fig. 17-1), into which the plate is subducting on a westerly bearing at a rate of about 9 cm y^{-1} (Dubois et al., 1975). The island is closely clustered with five seamounts, all of which are situated on the Niue Ridge, a rise enclosed by the 5,000-m isobath and whose crest lies about 120 km east of the trench axis (Lonsdale, 1986). Nearby are two other seamounts, including Capricorn Seamount, which lies on the eastern, subducting flank of the Tonga Trench and rises to a minimum depth of 395 m (Brodie, 1965). Dredge samples from the crest of Capricorn Seamount yielded shallow-water

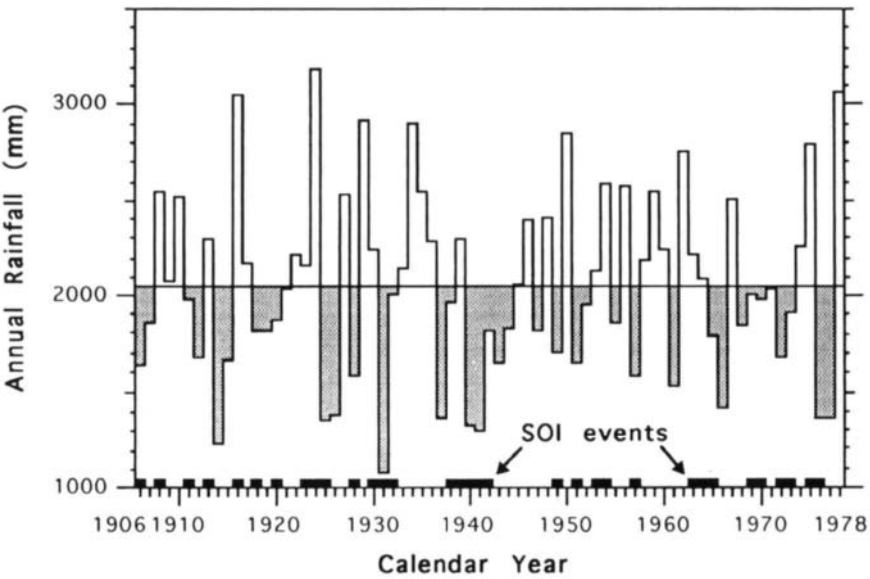


Fig. 17-3. Annual rainfall at Niue. The mean annual rainfall, shown by the horizontal line, is 2,041 mm. The heavy bars show the occurrences of Southern Oscillation Index (SOI) events (data from Cayan and Webb 1992). Droughts at Niue commonly coincide with prolonged SOI disturbances. (Rainfall data from Jacobson and Hill 1980a,b and Wright and van Westerndorp 1965.)

skeletal limestones containing fossil constituents indicative of a Miocene or younger age (Brodie, 1965). Niue, Capricorn, and the other seamounts do not display a clear linearity, but they may represent a partially subducted Cenozoic hotspot chain (Lonsdale, 1986). Niue's recent emergence in the late Plio-Pleistocene (Fieldes et al., 1960; Schofield, 1967a; Wheeler and Aharon, 1991; Whitehead et al., 1992) has been attributed to plate motion which carried it up onto a lithospheric bulge peripheral to the Tonga Trench (Dubois et al., 1975).

Niue's submarine flanks slope at 15–20°. Steeper angles occur on the southern flank where Niue's volcanic core is located (Fig. 17-2B). The west coast is marked by a series of embayments (Schofield, 1959) that continue offshore to a depth of 3,000 m, below which the slope is gentler (Summerhayes, 1967). The embayments were probably caused by slumps that deposited a debris fan on the lower western flank (Schofield, 1959; Summerhayes, 1967; Hill, 1983).

LANDSCAPE AND GEOMORPHOLOGY

The present topography of Niue, which shows a striking resemblance to a coral atoll (Fig. 17-2A), is attributable to its relatively recent emergence (Dubois et al., 1975). The topography is dominated by a shallow, centrally located, dry basin that is almost completely enclosed by a peripheral rim. The basin, formerly the lagoon and

informally called the "Mutalau Lagoon" by Schofield (1959), is broad, has a flat bottom, and lies generally about 35 m above sea level. The rim, formerly the barrier reef and informally termed the "Mutalau Reef" by Schofield (1959), lies at about 60–70 m above sea level and is generally about 1,200 m wide. A passage through the western reef rim south of Alofi formerly connected the Mutalau Lagoon to the open ocean. Now dry, the passage's floor lies at about 42 m above sea level.

Unlike the stereotypical Polynesian island which is girded by sandy beaches, the Niuean coastline is marked by seacliffs. Along the western and southern coasts, the seaward margin of the Mutalau Reef slopes steeply down to the narrow, wave-cut Alofi Terrace (Fig. 17-4), which lies at about 25 m above sea level (Schofield, 1959). The Alofi Terrace terminates in steep seacliffs on the west coast; on the south coast, it slopes seaward at 17–22°. Less well developed terraces occur 2–4 m above sea level along parts of the south and east coast. A modern coral reef about 100 m wide fringes Niue at sea level; an originally natural passage through the reef at Alofi is artificially maintained for boat traffic. Off the west coast, there are two or more submerged terraces at around −12 and −35 m (Schofield, 1959).

The surface of Niue shows clear evidence of karstification. The Mutalau Reef is in many places a well-developed karrenfeld, with some karst towers >7 m high (Schofield, 1959). The floor of the Mutalau Lagoon is flat to gently undulating, with incipient karrenfelds of pinnacles <2 m in relief. Along the coast at or just above sea level are numerous caves which have been exposed by wave erosion (Fig. 17-4) (Schofield, 1959; Jacobson and Hill, 1980a). Their rounded shapes, solutional features, and elevation indicate freshwater phreatic formation when the water table was higher. Paralleling the coast and at the border between the Alofi Terrace and the

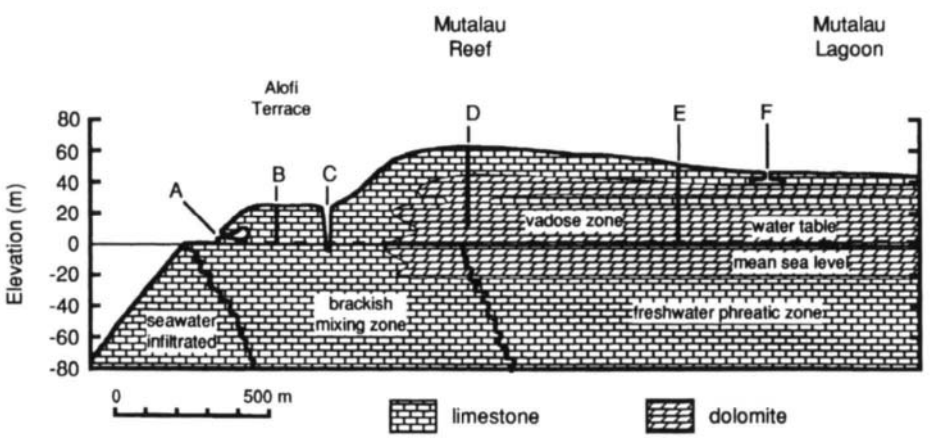


Fig. 17-4. Cross section of west coast showing geomorphologic, hydrologic, and lithologic features. Key: A, phreatic cave exposed by wave erosion; B, coastal brackish well near Alofi ("A" in Fig. 2A); C, chasm with a brackish pool; D, water well at Tuapa (T in Fig. 2a and drillhole 6 of Schofield and Nelson 1978); E, Fonuakula well; F, flat-roofed vadose cave. (Modified after Jacobson and Hill, 1980a and b; well lithologies from Schofield and Nelson, 1978.)

Mutalau Reef are linear chasms several meters wide which are linked to form systems 500 m long. These chasms typically reach to or below sea level, but where they are unbreached by coastal erosion, they are floored by brackish-water pools. In the Mutalau Lagoon, many small sinkholes lead a few meters below the surface to flat-roofed, branching caves which have been interpreted by Jacobson and Hill (1980a) as vadose caves.

On average, 84% of the surface on the Alofi Terrace and the seaward slope of the Mutalau Reef consists of rock outcrops (Wright and van Westerndorp, 1965). On the crest and lagoonward slope of the Mutalau Reef and on the Mutalau Lagoon floor, the average soil cover is about 43–47% and about 36 cm thick (Fieldes et al., 1960). About 21% of the island's surface is presently forested. The principal crops grown for export are copra, passionfruit, and limes.

Soils on the Alofi Terrace and the seaward slopes are tropical black earths, or rendzinas, which are rich in montmorillonite (Wright and van Westerndorp, 1965). Over the remainder of the island, the soils are latosols, commonly called tropical terra rossa, and are low in silica and montmorillonite and high in iron oxide and alumina. According to Whitehead et al. (1993), Niue's soils were probably derived by weathering of the carbonate platform.

The soils are notable for their high phosphate (up to 40%; Birrell et al., 1939) and high mercury content (exceeding 200 $\mu g\ kg^{-1}$; Whitehead et al., 1990) and for their unusually high radioactivity (up to 30 times that of normal soils; Marsden et al., 1958). Because the carbonate rocks are generally phosphate-poor, the source of the phosphate has been attributed to seabird guano and basaltic ash (Wright and van Westerndorp, 1965); more recent evidence suggests that the phosphate may be from weathering of the carbonates (Whitehead et al., 1993). Possible origins for the mercury are direct absorption from seawater, weathering of guano deposits, or endothermal solutions of seawater (Whitehead et al., 1990). The unusually high radioactivity of the Niuean soils is attributed to the decay of daughter nuclides of ^{238}U, the emplacement of which has been linked to marine sedimentation of the soil precursors (Fieldes et al., 1960), precipitation from volcanic hydrothermal solutions (Schofield, 1967a), and absorption of ^{238}U onto soil particles during Pleistocene marine transgressions (Whitehead et al., 1992).

GEOLOGY

Volcanic pedestal and overlying carbonates

Niue's bathymetry clearly indicates that the foundation of the carbonate island is a volcanic seamount, although no volcanic rocks are exposed at the surface. An early magnetic survey of Niue's surface (Schofield, 1967a) and a later, denser set of gravity and magnetic measurements both indicate that the crest of a dense, reversely magnetized volcanic core lies beneath the southwestern part of the island (Hill, 1983) (Fig. 17-2B). These data also suggest that the carbonate cover over the crest is about 400 m thick. Subsequent drilling to a depth of 700 m north of the crest failed to

reach the volcanic pedestal because of a probable caldera infill (Barrie, written comm., 1992). Hill (1983) hypothesized that the volcanic rocks are basic to ultrabasic intrusives and pillow lavas, and inferred that the remainder of the island is underlain by a mixture of pyroclastic and/or carbonate deposits. On the basis of the close alignment of the magnetization of the volcanic core with the modern geomagnetic field, the magnetic inclination, an inferred rate of subsidence, and biostratigraphy of the carbonates, Hill (1983) estimated that the volcanic core formed during the early to middle Miocene.

Schofield (1959) was first to describe the surface exposures of the carbonate reef platform which caps the volcano. Subsequently, Schofield and Nelson (1978) collected and described samples from seven water wells, the deepest of which (Fonuakula well) reached a subsurface depth of 56 m, or 0 m above sea level (Fig. 17-2A). More recently, seven cores drilled by Avian Mining Pty. and two cores drilled by the Australian Geological Survey Organization have tested the carbonate platform to a maximum depth of about 700 m (Fig. 17-2A). We have not yet examined the two deepest cores (DH6a and DH7a), which are reported to have remained in sedimentary carbonates throughout (Barrie, written comm., 1992). Coring in wells DH6 and DH8 was limited to a 52-m interval and a 100-m interval, respectively. Because core recovery was generally less than 20% (Barrie, written comm., 1992), we did not examine these cores. Our documentation of the carbonate cap, therefore, is derived from outcrops, the Fonuakula well, three stratigraphic cores (DH4, DH5, and DH7), and cores from two shallow water wells (PB1 and PB2). The deepest core, DH4, reached a subsurface depth of 303 m, or 269 m below sea level (Fig. 17-5).

Niue's carbonate platform consists of limestone and of dolomite that has partially to completely replaced the limestone precursor (Figs. 17-5, 17-6). In the upper 300 m, we distinguish four informal units on the basis of their mineralogical composition (Fig. 17-6): (1) upper limestone, (2) upper dolomite, (3) middle limestone, and (4) lower dolomite.

The upper limestone consists of aragonitic and calcitic limestone with little or no evidence of dolomitization. The thickness of this unit appears to be highly irregular; the maximum known thickness of about 20 m is within the Mutalau Reef at Fonuakula, but the unit is thinner elsewhere on the Mutalau Reef and apparently thins or disappears in the Mutalau Lagoon (Schofield and Nelson, 1978). This variation in thickness may be due to differential erosion and/or dolomitization, or to deposition after dolomitization of the underlying section.

The upper dolomite unit is about 55 m thick and generally has been completely dolomitized. It is present in all cores and water wells within the Mutalau Lagoon and in the Mutalau Reef, except at Alofi, where a 24.4-m-deep well located about 1 km from the coastline encountered only undolomitized limestone (Schofield and Nelson, 1978). Outcrop samples collected on the west coast from the shoreline to the crest of the Mutalau Reef are also undolomitized limestones (Schofield and Nelson, 1978). These data suggest that the upper dolomite grades laterally into undolomitized limestone within 1 km of the modern coastline. In the top of the upper dolomite unit, a roughly 10-m-thick bed of aragonitic and calcitic limestone occurs in the west (Fonuakula well) (Fig. 17-4), northeast, north (PB2), and southeast (DH4 and

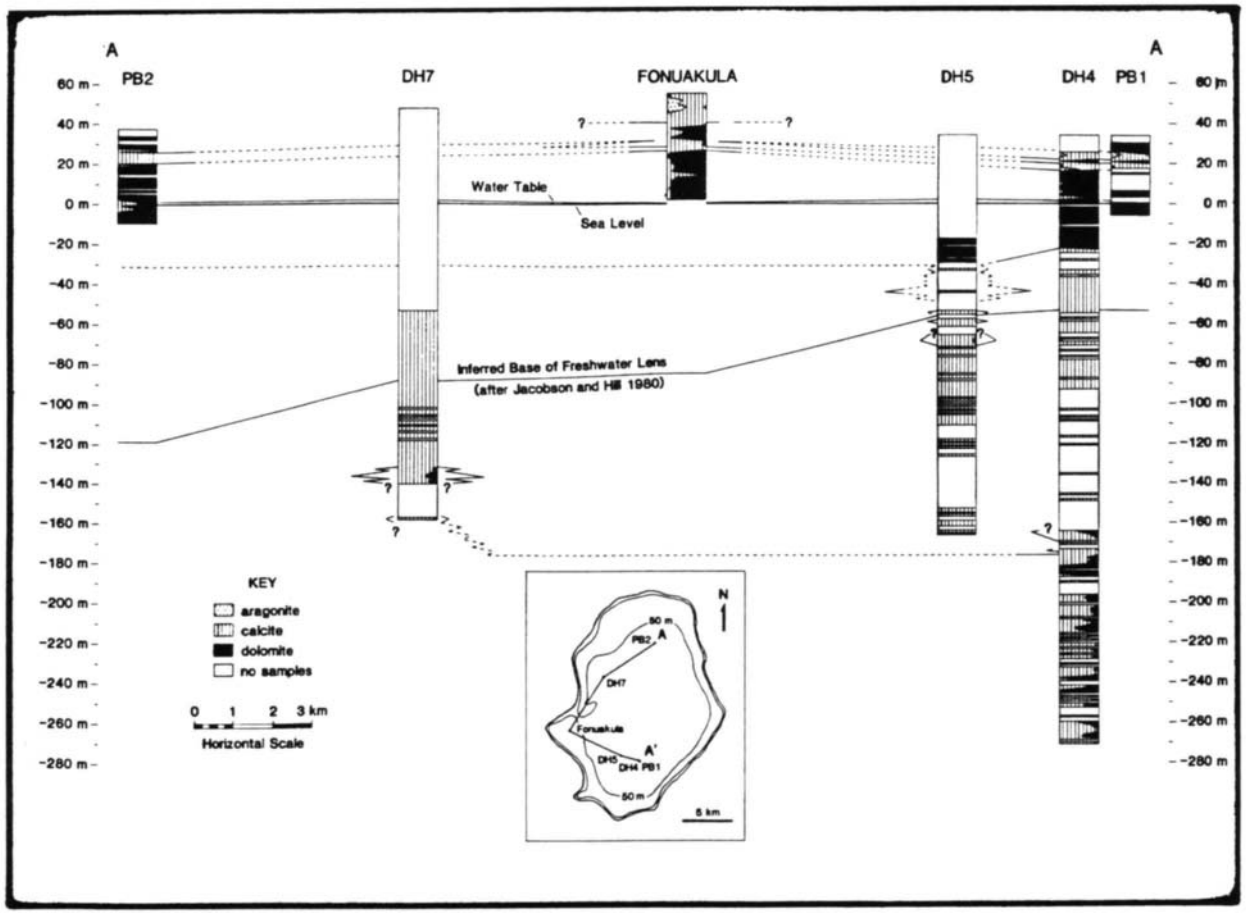


Fig. 17-5. Stratigraphic cross section based on core studies. Datum is modern sea level. The section comprises an upper undolomitized limestone interval (upper limestone), an extensively dolomitized interval (upper dolomite), a limestone interval which is virtually free of dolomite (middle limestone), and a lower, partially dolomitized interval (lower dolomite).

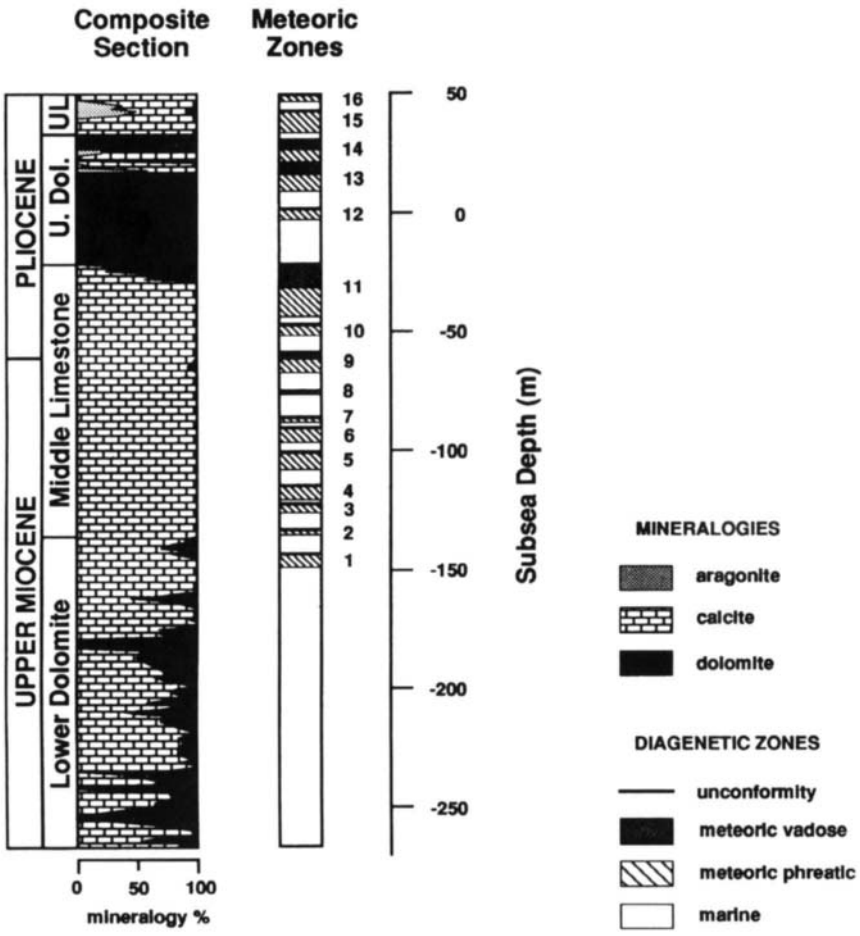


Fig. 17-6. Composite section showing unconformities and zones of meteoric diagenesis at Niue. Zones 3 through 11 correspond to zones 1 through 8 in Aharon et al. (1993).

PB1), indicating that this limestone bed probably extends over most of the island (Fig. 17-5).

The middle limestone unit is about 100–130 m thick and consists almost entirely of low-Mg calcite. In this unit, dolomite occurs only in two 5-m-thick intervals in core DH5, where it constitutes no more than 7% of the rock. The lower dolomite unit is characterized by incomplete dolomitization of low-Mg calcite limestone. Dolomite constitutes on average 30%, and ranges from 0 to 100%. The unit is at least 105 m thick in core DH4, which ended in the lower dolomite.

Age of the carbonate platform

No samples are presently available to permit dating of the lower portion of the carbonate platform, but the uppermost 300 m has been dated using biostratigraphy and strontium isotopes. Mollusks collected from outcrops in the Mutalau Lagoon (upper limestone or upper dolomite) are Plio-Pleistocene (C.A. Fleming, reported in Schofield, 1959). Larger benthic foraminifera from cores DH4, PB1, and PB2 between 34 m above sea level and 186 m below sea level (upper dolomite into the upper part of the lower dolomite) are middle to late Miocene (G.C.H. Chaproniere, reported in Jacobson and Hill, 1980a). Poor preservation of the foraminifera (Chaproniere, written comm., 1992) and the limited resolution (≥2–3 Ma) of the Letter Stage Classification dating method (Adams, 1984) have prevented a more discriminating biostratigraphic dating of the carbonates.

$^{87}Sr/^{86}Sr$ ratios in the limestone bed of the upper dolomite (range 0.709024–0.709056, relative to the NBS-987 value of 0.710230; n = 3) yield an apparent age of 2.3 Ma. Strontium isotope ratios in the middle limestone, measured primarily in DH4 samples (range 0.708936–0.709029; n = 13), yield apparent ages from 4.8 Ma at around 23 m below sea level, to 6.2 Ma at around 148 m below sea level (Aharon et al., 1993). In both intervals, strontium isotope measurements were made on whole-rock samples which were devoid of meteoric cements. These ages are derived from the seawater strontium isotope curve of Hodell et al. (1991), with a time scale based on the astrochronology of Hilgen (1991). In this time scale, the apparent ages correspond to the late Miocene (Tortonian) to late Pliocene (Piazencian) (Fig. 17-6). The strontium isotope data thus agree with the paleontologic data of Fleming and Chaproniere and provide a finer time resolution.

Carbonate facies

Our facies analysis of core material from DH4, DH5, DH7, PB1, and PB2 (Fig. 17-2A) and previous descriptions of carbonates from the Fonuakula well (Schofield and Nelson, 1978) and outcrops (Skeats, 1903; Schofield, 1959) lead to the following reconstruction of depositional history at Niue.

During the Tortonian-Piacenzian, Niue was a shallow-water carbonate platform which became progressively enclosed by a barrier reef. During the Tortonian, the platform-edge reef was sufficiently discontinuous to permit growth of patch reefs in the lagoon, as evidenced in core DH4 by coral floatstones interbedded with fine- to medium-grained skeletal packstones consisting of benthic foraminifera, echinoids, and mollusks. Throughout the Messinian and Zanclean, the platform was probably rimmed by a barrier reef along its southern margin and was open to the sea along its northwestern margin. In the south, the Messinian and Zanclean sections of cores DH4 and DH5 consist of fine- to medium-grained skeletal packstones and grainstones with little coral debris, suggesting a scarcity of lagoonal patch reefs and, therefore, a local barrier to ocean-platform water circulation. In the northwest, however, coral debris is abundant in the Messinian interval of core DH7. No information is presently available on the Zanclean section in this area.

By the Piacenzian, Niue was a full-fledged atoll. The massive and coral-rich core of the barrier reef is exposed in the seaward bluffs of the Mutalau Reef (Skeats, 1903; Schofield, 1959). In the Alofi Terrace, forereef talus deposits are preserved as seaward-dipping (20–30°) beds of limestone conglomerate (Schofield, 1959) whereas in the Fonuakula well, coralgal boundstones are interbedded with coralgal-foraminiferal grainstones and packstones, representing reef core and reef detritus, respectively (Schofield and Nelson, 1978). In cores DH4, PB1, and PB2, skeletal packstones are interbedded with skeletal grainstones. The dominant grains are benthic foraminifera, mollusks, and echinoids, whereas coral debris is scarce, thus suggesting that patch-reef development was suppressed everywhere in the lagoon by a near-continuous barrier reef.

Niue began rising above sea level during the early Pleistocene (Dubois et al., 1975). Since then, erosion of the carbonate platform has by far exceeded deposition. Surficial gravels of Plio-Pleistocene lagoonal fossils in the Mutalau Lagoon (C.A. Fleming, reported in Schofield, 1959) and the marine source of radionuclides in the lagoon soils (Whitehead et al., 1992) suggest intermittent marine flooding of Niue's interior.

Carbonate diagenesis

Petrographic examination of 88 thin sections from cores DH4, DH7, and PB1 leads to recognition of the following paragenetic sequence of carbonate diagenesis in the upper 300 m of Niue's carbonate platform: (1) cementation by high-Mg calcite or aragonite circumgranular crusts; (2) conversion of high-Mg calcite constituents to low-Mg calcite and dissolution of aragonitic components; (3) dolomitization; (4) leaching and precipitation of low-Mg calcite cements in meteoric vadose and phreatic zones; and (5) dedolomitization. Schofield and Nelson (1978) described similar diagenetic features in thin sections from the Fonuakula well. The following summarizes the evidence for this paragenetic sequence.

In the lagoonal facies, some interparticle and intraparticle pores in foraminifera and other bioclasts are lined with bladed cements whose morphologies indicate that they were formerly either high-Mg calcite or aragonite. These morphologies and distributions are indicative of synsedimentary marine cementation in sediment bodies subject to low rates of fluid flow, as in lagoons (Longman, 1980). In the reef-core and forereef facies, fibrous aragonite cement encrusts coral skeletons (Skeats, 1903). Thick high-Mg calcite cements such as observed in the reef core and forereef beds of Mururoa Atoll (Aissaoui, 1988) have not been reported at Niue, probably because Niue's platform-margin facies have not been studied in detail.

Aragonite is present in some beds of all cores within 20 m of the surface. Below this depth, however, aragonite allochems almost always occur as molds, and high-Mg calcite constituents have been converted to low-Mg calcite. The sole exception is at −185 m in DH7, where some aragonite allochems (6% of the total rock) remain. Most of the dissolution and reprecipitation was probably mediated by seawater, as the $\delta^{18}O$ and $\delta^{13}C$ values of whole-rock samples (−1.95 ± 0.95‰; −0.41 ± 0.88‰ PDB; n = 149) show no input of meteoric water or soil-gas CO_2, respectively.

Mineralogic stabilization preceded dolomitization, because dolomite cements encrust moldic pores in the upper dolomite and dolomite fills moldic pores in the lower dolomite.

Schofield (1959) presented the first chemical analyses indicating the presence of dolomite on Niue (upper dolomite in Fig. 17-6), but Schlanger (1965) was the first to recognize it as Ca-rich dolomite. A recent study of the dolomites in core material by Wheeler and Aharon (1993) indicates that the upper dolomite and the lower dolomite are petrographically and chemically distinct. The upper dolomite is characterized by near-total dolomitization via mimetic replacement of the limestone precursor and by dolomite cementation (Fig. 17-7A,B). This dolomite consists of two chemically distinct groups: (1) disordered, calcian (57–62 Ca mol%) dolomite, and (2) ordered, relatively stoichiometric (52–55 Ca mol%) dolomite. In contrast, the lower dolomite is variably dolomitized by non-fabric-selective replacement (Fig. 17-7D) and consists entirely of disordered, calcian (57 to 60 Ca mol%) dolomite.

Scattered through the section are 17 discrete zones characterized by intense leaching and/or low-Mg calcite cementation (Fig. 17-6). In the lower dolomite, the only such zone is located near the top of the section. In the upper dolomite and upper limestone units, the zones are marked by yellow, coarse, blocky and dogtooth, low-Mg calcite cements which partially to completely fill voids. Meniscus low-Mg calcite cements are also present but are less common. Whole-rock $\delta^{18}O$ and $\delta^{13}C$ values ($-5.41 \pm 2.29‰$; $-5.70 \pm 48‰$; $n = 35$; Fonuakula values from Aharon et al., 1987) of calcites from these zones are indicative of meteoric water and soil-gas input. The cements and the depleted stable isotope values indicate that these zones developed through meteoric diagenesis. In the upper dolomite, dolomite cementation alternated with meteoric diagenesis, for the dolomite crystals encrust molds, have been rounded or embayed by dissolution, and are engulfed by meteoric cements (Fig. 17-7B).

In the middle limestone, each zone of meteoric diagenesis is characterized by moderate to intense leaching of matrix and grains and by the presence of scattered, ≤1-cm-diameter patches of finely crystalline, low-Mg calcite cement (Fig. 17-7D). Some patches are syntaxial on echinoid grains, but most are not. Similar cements have been described at Enewetak, where they occur beneath subaerial exposure surfaces (Saller and Moore, 1989; Quinn, 1991) [Chap. 21]. In two zones, the interval of patchy cement is overlain by a similarly leached interval lacking cements. Whole-rock $\delta^{18}O$ and $\delta^{13}C$ compositions ($-2.47 \pm 0.77‰$; $-0.97 \pm 0.77‰$; $n = 55$) of the patchy intervals are similar to those of limestones that have not undergone meteoric diagenesis (see above). However, the whole-rock $\delta^{18}O$ and $\delta^{13}C$ compositions ($-3.55 \pm 0.53‰$; $-4.33 \pm 1.16‰$; $n = 9$) of the leached, patchy cement-free intervals show the influence of meteoric water and soil-gas CO_2. Drilled-out samples of the cement patches, which included grain substrate as well as cement, give similar $\delta^{18}O$ and $\delta^{13}C$ values ($-3.67 \pm 1.18‰$; $-2.42 \pm 0.51‰$; $n = 9$) and indicate the meteoric origin of these cements. Each zone of meteoric diagenesis is likely to represent a period of low sea level and subaerial exposure which led to the development of a freshwater lens (Quinn, 1991; Wheeler and Aharon, 1991). The cement-free leached intervals are interpreted to represent the vadose zone, which is characterized

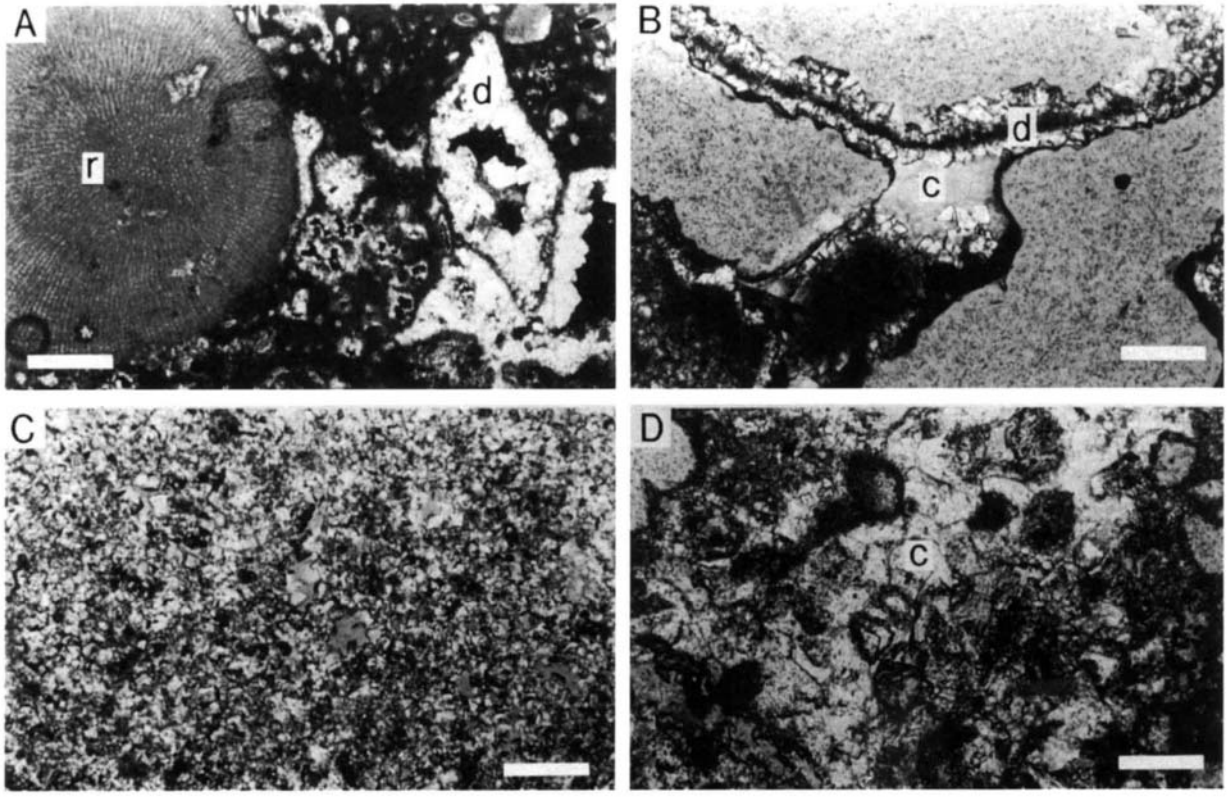


Fig. 17-7. Thin-section photomicrographs of diagenetic features. Scale bar in each photomicrograph is 0.5 mm long. A: Red algal grain mimetically replaced by dolomite (r) and limpid dolomite cement (d) lining the interior and exterior of a micrite envelope. (DH4 at 22 m; X-nicols.) B: Limpid dolomite cement (d) encrusting a micrite envelope and in turn being engulfed by calcite meniscus cement (c). (PB1 at 8 m; plane light.) C: Non-mimetic replacement in the lower dolomite. (DH4 at 219 m; plane light.) D: Calcite cement (c) patch in the end-Messinian zone of meteoric diagenesis. (DH4 at 97 m; plane light.)

by dissolution and minimal calcite precipitation (Longman, 1980). The patchy cement intervals probably record the active phreatic zone, which is characterized by calcite cementation as well as by dissolution (Longman, 1980). The contact between these intervals is at or near the paleo-water table (Wheeler and Aharon, 1991).

Dedolomite is rare in Niuean carbonates; it has been observed only in the upper dolomite unit in the Fonuakula well (23–29 m; Schofield and Nelson, 1978) and in cores PB1 (8.5 m), PB2 (36.5–38.5 m), and DH4 (32–33 m). In PB2 and DH4, dedolomite occurs mainly as white micritic calcite halos surrounding blocky-calcite cement-filled solution vugs and mollusk molds in rocks otherwise composed entirely of brown dolomite. The calcite cements encrust dolomite cements which line the molds, indicating precipitation after dolomitization. $\delta^{18}O$ and $\delta^{13}C$ compositions (-3.93 ± 0.01; $-5.85 \pm 0.75‰$ PDB; $n = 2$) of the calcites in PB2 confirm that they are meteoric in origin. In these cores, the dedolomite is limited to a zone of meteoric calcite cementation that coincides with the present water table and is likely to represent a modern, ongoing development.

Sea-level history

The eustatic record at Niue is the subject of ongoing study. Presently, the best-documented period is the Messinian-early Zanclean interval (Aharon et al., 1993). Because the discontinuous core material available to Aharon et al. (1993) contained no unconformity contacts, their positions in the cores were inferred from petrographic, strontium, and stable carbon and oxygen isotope evidence of meteoric diagenesis associated with subaerial exposure. The portion of the middle limestone unit which was deposited during Messinian-early Zanclean time contains eleven discrete meteoric zones (Fig. 17-6, zones 1 through 11; Aharon et al., 1993, focused on eight zones, 3 through 10). If the zones developed later than the host section, such as during the Pleistocene glaciations, the entire section down to the level of the lowest sea stand would have been intensely leached. Instead, the intervals between the zones are at most only mildly leached. These zones, therefore, represent eleven Messinian-early Zanclean eustatic falls, because Niue at that time was in a subsidence mode typical of a young, extinct seamount (Aharon et al., 1993).

The magnitudes of the eight eustatic falls represented by zones 3 through 10 were reconstructed Fig. 17-8 by the method of Lincoln and Schlanger (1987, 1991) in light of the following considerations. In a mid-oceanic carbonate platform, the magnitude of a eustatic fall (EF) is:

$$EF = WD + V_i$$

where WD is the depositional water depth over the sample site prior to the eustatic fall, and V_i is the initial thickness of the vadose zone at the site. This initial thickness is rarely preserved in its entirety, and, therefore, the original thickness must be reconstructed on the basis of an inferred eroded component (V_e) added to the thickness of the preserved vadose zone (V_p):

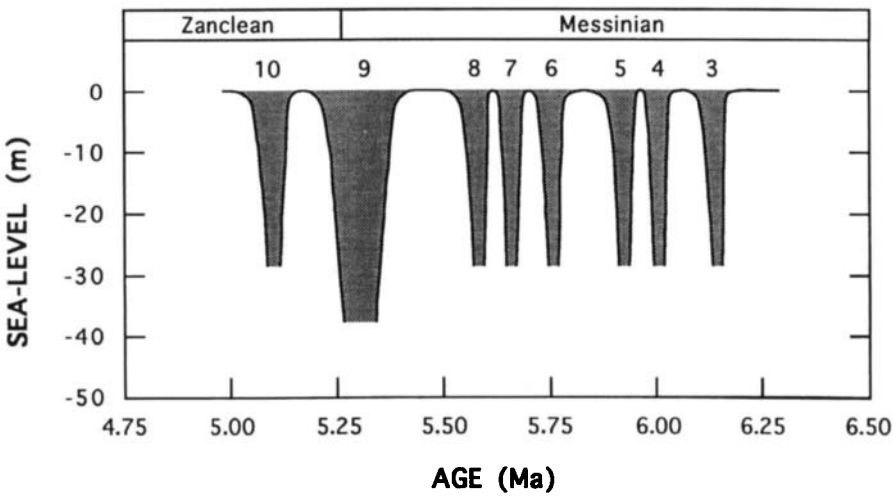


Fig. 17-8. Estimated magnitudes of Messinian and early Zanclean sea-level falls at Niue. Each magnitude was calculated from the estimated duration of the lowstand, the thickness of the remnant vadose section, an estimated rate of erosion, and the estimated depositional water depth of the Mutalau Lagoon. Datum is sea level at the onset of each fall. Ages of the lowstands are from Aharon et al. (1993).

$$V_i = V_p + V_e$$

In order to obtain the eroded component of the paleo-vadose zone, some reasonable boundary conditions must be placed on the rate of erosion (E) and the duration of the erosion event (t_e) such that:

$$V_e = E * t_e$$

It follows, therefore, that

$$EF = WD + V_p + (E * t_e)$$

Assuming that the eustatic fall and rise are brief with respect to the lowstand itself, then the duration of erosion (t_e) would closely approximate the duration of the eustatic lowstand. The latter can be obtained directly from records of eustatic fluctuations, such as from deep-sea cores, that are not subject to lowstand erosion. Where such records are unavailable, the duration of erosion may be estimated by dating the upper and lower boundaries of the erosional unconformity. Although the total time spanned by the unconformity (t_u) encompasses both the deposition of the missing section as well as its erosion, for all practical purposes t_e may be equated to t_u because the error introduced by the approximation is small and negligible compared to the large uncertainties in the erosional rate (E).

Application of the above equations to the Messinian-early Zanclean unconformities 3 through 10 at Niue (Fig. 17-6) indicates that the largest eustatic fall is represented by the end-Messinian unconformity (zone 9 in Fig. 17-6). The Messin-

ian-age facies are all subtidal at DH4; the depositional water depth (WD) is estimated to have been 28 m from the difference between the present elevations of the crest of the Mutalau Reef (70 m) and the floor (42 m) of the paleochannel at Alofi (Fig. 17-2). Beneath the end-Messinian unconformity, the erosional remnant of the meteoric vadose zone (V_p) is 4 m thick. The eroded portion of the vadose zone (V_e) is estimated to have been about 6 m on the basis of: (1) 178 ka (revised from Aharon et al., 1993) for the time ($t_u \approx t_e$) spanned by the unconformity, and (2) an average carbonate weathering rate of 0.035 m ky^{-1}, derived from tropical and temperate groundwater-budget calculations (Lincoln and Schlanger, 1987). This gives a total magnitude of 38 m (28 + 4 + 6) for the end-Messinian eustatic fall (Fig. 17-8).

The durations of the eustatic falls represented by the six other Messinian unconformities (zones 3 through 8 in Fig. 17-6) and the early Zanclean unconformity (zone 10 in Fig. 17-6) are each estimated to have been 15 ky, on the basis of correlative $\delta^{18}O$ positive excursions in DSDP core 552 (Keigwin, 1987). Here the duration of the eustatic fall provides the duration of erosion (t_e). No preserved vadose zone is discernable beneath these seven unconformities. Assuming the same depositional water depth and weathering rate, the eustatic falls were about 29 m (28 + 9 + 0.5) in magnitude (Fig. 17-8).

The Quaternary sea-level record at Niue has not yet been fully unraveled. Schofield (1959, 1967b) recognized six subaerially exposed terraces at around 70 m (the crest of the Mutalau Reef, Fig. 17-4), 55 m, 36 m, 23 m (the Alofi Terrace), 13 m, and 6 m above sea level. Some of these terraces were reported earlier by Agassiz (1903). On the southwestern slope of the Mutalau Lagoon are concentric lineaments which probably represent former coastlines (Jacobson and Hill, 1980b), but neither their elevations nor their ages have been determined. Whether there are submerged terraces is uncertain. Schofield (1959) described two submerged terraces at around 13 m and 35 m below sea level, whereas Schofield (1967b) reported only one at −6 m. Petrography and stable carbon and oxygen isotopes of core samples indicate the presence of five zones of leaching and meteoric cementation between −10 m and 50 m above sea level (Fig. 17-6) but the age and correspondence of the zones to the terraces are not yet known.

The Mutalau Reef terrace may represent barrier-reef development during an interglacial sea-level highstand sometime between 500 and 900 ka (Schofield, 1959). The presence of U-series radionuclides in soils of the Mutalau Lagoon soils suggests that it might have been completely submerged at this time (900 ka according to Schofield, 1967a; 400–750 ka according to Whitehead et al., 1992). Subsequent uplift of Niue on the Pacific Plate peripheral to the Tonga Trench (Dubois et al., 1975) permitted only partial submersion during later sea-level highstands (Whitehead et al., 1992). Other raised terraces are primarily wave-cut features and were probably formed during two later interglacials (Schofield, 1959). The last episode of partial flooding of the Mutalau Lagoon may have occurred at 100–200 ka (Whitehead et al., 1992).

HYDROGEOLOGY

Geometry and physical characteristics of the freshwater lens

Niue has no surface streams because of the porous and fissured nature of its limestone surface. Even after prolonged heavy rainfall, the ground is dry within a few minutes (Jacobson and Hill, 1980a). Consequently at least 27 water wells have been drilled since 1964 in order to provide a reliable source of potable water (Schofield, 1969; Jacobson and Hill, 1980a).

Annual rainfalls are shown in Fig. 17-3. Annual potential evapotranspiration (PET) is estimated at 1,417 mm, with a maximum PET of 153 mm in January and a minimum PET of 83 mm in July (Jacobson and Hill, 1980a). Water-balance calculations (the monthly mean rainfall minus the monthly PET) suggest that there is a net average surplus of 57 mm each month except during June, when there is a net deficit of 9 mm. The surplus available for groundwater recharge has an annual mean of 624 mm, of which 85% occurs during the December-April monsoon season. Meteoric recharge occurs mainly via vertical fissures and solution channels through the limestone and dolomite (Fig. 17-4).

Jacobson and Hill (1980a,b) mapped the thickness of the freshwater lens with resistivity soundings at 25 sites, utilizing the differences in electrical resistivity of saltwater-saturated carbonates and freshwater-saturated carbonates. Their observations led to the following interpretations concerning the geometry of the freshwater lens:

1. Niue has a single, unconfined freshwater lens that extends across the platform to within about 500 m of the coast (Fig. 17-4).
2. The water table lies at a maximum elevation of 1.83 m above sea-level in the interior and slopes downward to sea level at the margins. The vadose zone is 30–70 m thick.
3. Applying the 1:40 Ghyben-Herzberg ratio between the elevation of the water table and depth of the freshwater-saltwater interface to Niue's water-table configuration suggests the lens would be about 70 m thick beneath the Mutalau Lagoon and would taper laterally to 0 m near the coast. In fact, Jacobson and Hill (1980a,b) found that the freshwater lens is as thin as 40 m beneath the Mutalau Lagoon, increases in thickness to as much as 150 m beneath the Mutalau Reef, and then tapers out near the coast (Fig. 17-9). The freshwater-saltwater mixing zone is 40 m thick in well DH4. Jacobson and Hill (1980a,b) speculated that the variations in the thickness of the lens may be due to lower permeabilities in the reef facies and to higher permeabilities in the lagoonal facies. However, porosities and permeabilities have so far been determined only in the lagoonal facies (Table 17-1).

Due to the porous and permeable nature of Niue's carbonate platform, delayed, dampened tidal fluctuations are transmitted from the ocean to the water table in the interior. Three wells near Alofi at 0.1, 1.6, and 2.3 km from the coast and drilled only a few meters below the water table showed tidal ranges of 0.5, 0.3, and 0.1 m, respectively, compared to 0.7 m at the Alofi wharf (Jacobson and Hill,

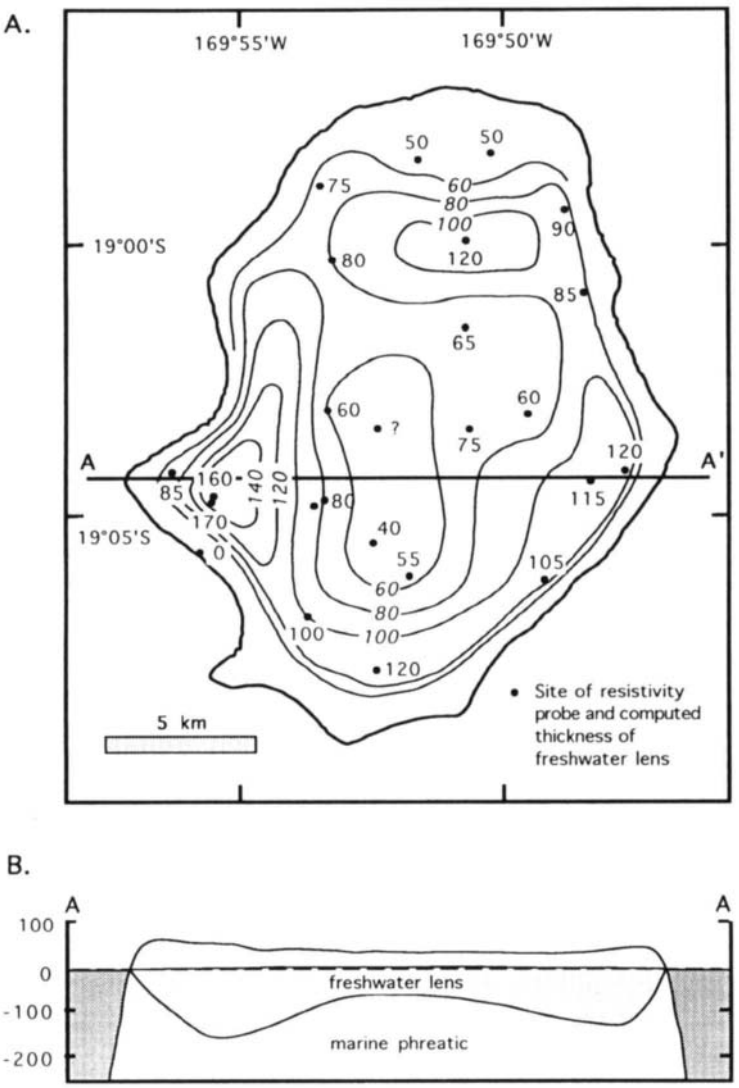


Fig. 17-9. Hydrogeology of Niue. A: Thickness of the freshwater lens. B: Cross section of the freshwater lens. (Modified from Jacobson and Hill, 1980a,b.)

1980a,b). The apparent velocity of the wave is about 900 m h^{-1}. In the PB1 and DH4 wells, which are about 3.9 km from the coast and about 8 m apart (Fig. 17-2A), the ranges are 0.03 and 0.05 m, respectively, and the time lag is about 10 min shorter in DH4 than in PB1. Because PB1 extends only into the upper dolomite unit, whereas DH4 extends into the middle limestone and lower dolomite units, these variations in the groundwater tide indicate that the deeper units are more permeable.

Table 17-1

Distribution of porosity (n) and permeability (k), lagoon facies, cores PB1, PB2, and DH4*

Hydrologic unit / Stratigraphic unit	Lithology	n (%)	k (10^{-8} cm^2) vert.	k (10^{-8} cm^2) horiz.	No. of Samples
vadose					
u. dolomite	dol	22.2	204	954	6
	ls	19.2	444	1050	3
phreatic					
u. dolomite	dol	20.4	7	167	6
m. limestone	ls	42.0	495	1600	1

*Data from Jacobson and Hill, 1980b.

Resistivity and core porosity measurements indicate that the greatest aquifer porosities (≥25%) lie in the lagoonal to backreef facies beneath the central and southeastern parts of the island (Jacobson and Hill, 1980a). The mean freshwater storage, in terms of effective water thickness, is 17.6 m and reaches a maximum of 25 m in the reef facies beneath the southeastern and southern parts of the Mutalau Reef. Given the surface area of 259 km^2, Niue's freshwater lens contains about 4.6 km^3 of water.

The small volume of Niue's freshwater lens and the periodic droughts dictate limited groundwater withdrawal in order to maintain the aquifer. Jacobson and Hill (1980a,b) calculated a safe yield of about 4,000 m^3 y^{-1} ha^{-1}, based on the method of Mather (1975) and assuming that the lens would be maintained at 25 m during a drought such as that of 1940–1944.

It should be noted that the unusual interpreted shape of the freshwater lens (Fig. 17-2) seems to imply a centripetal flow for most of the island with no indication of a groundwater sink in the interior of the island. There are two factors that reduce confidence in the original data. First, the resistivity-soundings technique used by Jacobson and Hill (1980a,b) to map the freshwater lens was in its infancy at that time (Jacobson, written comm., 1994). Second, the considerable depth to the water table may have affected the accuracy of the resistivity readings. In a more recent study of the geologically similar island of Nauru [q.v., Chap. 24], Jacobson and Hill (1988) used improved techniques for interpretation of resistivity data and direct calibration of resistivity profiles against conductivity of borehole water samples to map the freshwater lens and did not find a comparable geometry to that interpreted at Niue. It would be desirable to collect new and improved resistivity data at Niue, calibrate them against conductivity of borehole water samples, and place the geometry of the freshwater lens geometry on firmer grounds.

Groundwater chemistry

Within one kilometer of the coast, groundwaters show freshwater-saltwater mixing. In a well about 200 m inland from the coast, the water conductivity is

500 μS cm^{-1} and the total dissolved solids is 500 mg L^{-1}, compared to 321 μS cm^{-1} and 179 mg L^{-1} in the Fonuakula well about 2,200 m from the coast (Jacobson and Hill, 1980a,b). The ionic composition of this water is chloride-bicarbonate, with sodium and calcium as the dominant cations. Water samples from 14 inland wells and one cave (Jacobson and Hill, 1980a,b; Rodgers et al., 1982) indicate that, over most of the island, the groundwaters are dominated by calcium, magnesium, and bicarbonate. TDS was measured in water samples from 11 of these wells and was 136–251 mg L^{-1}, well within the WHO (1963) maximum acceptable limit for drinking water (Jacobson and Hill, 1980a). Carbonate hardness is 121–244 mg L^{-1}, and pH is 7.5–8.0.

Not unexpectedly, the distribution of calcium and magnesium within the freshwater lens reflects the mineralogy of the host rock. Between 0.5 and 1.5 km of the coast, where limited outcrop and well data suggest that the section is limestone, the Mg^{2+}/Ca^{2+} molar ratios are ≤0.1. Further inland, where well and core samples show that dolomite dominates, the Mg^{2+}/Ca^{2+} molar ratios increase rapidly to >0.25 (Fig. 17-10). Table 17-2 compares the dolomite/limestone ratios in the vadose and phreatic zones of four wells with the Mg^{2+}/Ca^{2+} molar ratios in their waters. The Mg^{2+}/Ca^{2+} molar ratios vary proportionally with the dolomite/limestone ratios

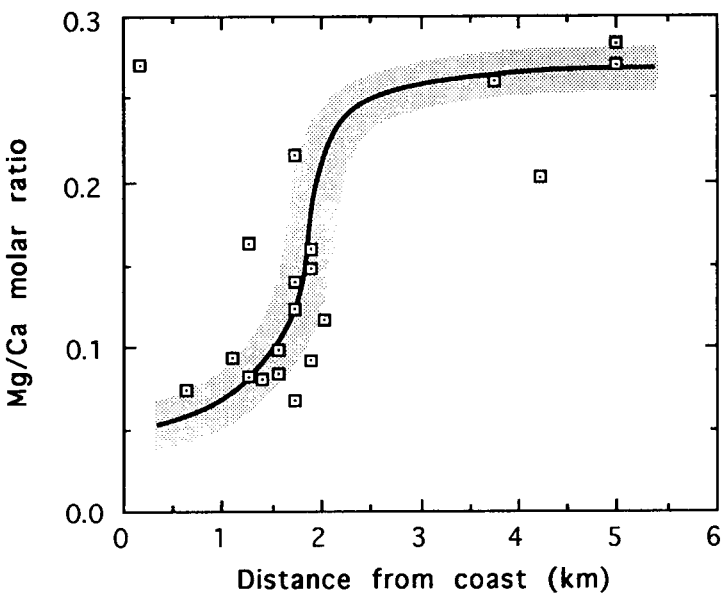


Fig. 17-10. Distribution of Mg and Ca concentrations, expressed as Mg^{2+}/Ca^{2+} molar ratio in well and cave waters in the freshwater lens as a function of distance from the coast. Within 0.5 km of the coast, seawater (Mg^{2+}/Ca^{2+} molar ratio of 5) mixes with freshwater. Increasing Mg^{2+}/Ca^{2+} molar ratios from 0.05 to 0.27 within 2 km of the coast can be attributed to increasing proportions of dolomite in the meteoric phreatic zone (Table 17-2). Further inland, dolomite/limestone proportions are relatively constant. (Hydrochemical data are from Jacobson and Hill, 1980b, and Rodgers et al., 1982.)

Table 17-2

Mg/Ca molar ratios in well waters compared to dolomite/limestone ratios in the vadose and meteoric-phreatic zones of the same wells.*

Well	Amanau[a]	Fonuakula[a]	DH4 and PB1	PB2
Distance from coast (km)	0.2	1.7	3.9	4.2
Mg/Ca molar ratio[b]	0.1	0.6	1.8	0.7
Vadose zone				
dolomite (m)	0	35	24	29
limestone (m)	27	20	9	7
dolomite/limestone similar to	0	1.8	2.7	4.1
Phreatic zone				
thickness (m)[b]	0	160	55	120
dolomite (m)[c]	0	20	20	20
limestone (m)[d]	0	140	35	100
dolomite/limestone		0.1	0.6	0.2

[a] Lithologic data from Schofield and Nelson (1978).
[b] Data from Jacobson and Hill (1980b).
[c] From DH4.
[d] Calculated by subtracting thickness of dolomite from thickness of phreatic zone. Most of the section is assumed to be limestone, on the basis of DH4.
* Note: The correspondence between the well-water Mg/Ca ratios and the dolomite/limestone ratios is stronger for the phreatic zone data than for the vadose zone data.

in the phreatic zone, which is consistent with the observation elsewhere that dissolution and diagenesis is typically more rapid in the phreatic zone than in the vadose zone (Vacher et al., 1990). On the basis of the Mg^{2+}/Ca^{2+} ratios, we conclude that within 1.5 km of Niue's coast, dolomite is scarce to absent from the section which presently lies in the phreatic zone.

CASE STUDY: DOLOMITIZATION AT NIUE

The dolomites of Niue have served as a "guinea-pig" for testing dolomitization models since the mid-1960s. The first proposed model (Schlanger, 1965) was dolomitization by seepage reflux of brines (Fig. 17-11A). Schofield (1959) collected Mg-rich carbonates from the Mutalau Lagoon, where he reported that the greatest enrichment of Mg occurs. Schlanger (1965) recognized that (1) the samples were Ca-rich dolomites, (2) the dolomites were limited to the Mutalau Lagoon, and (3) the lagoon's near-complete enclosure would restrict circulation whenever the reef was not awash. On the basis of these observations, Schlanger (1965) proposed that, following deposition of the reef, a sea-level fall isolated the lagoon from the ocean, and the resulting isolation led to partial evaporation and concentration of the lagoon waters to the point of gypsum precipitation. The hypersaline waters dolomitized as they flowed downward and laterally to the ocean through the underlying lagoonal

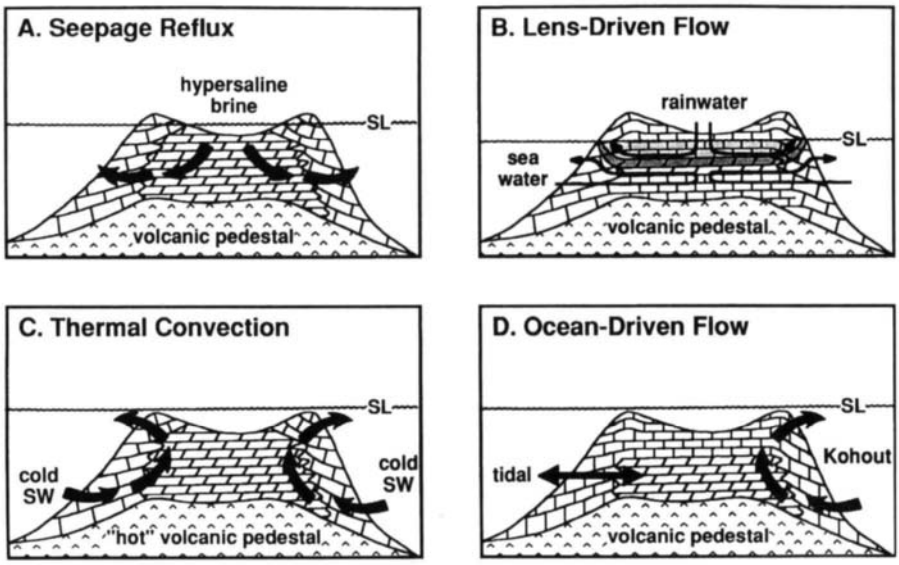


Fig. 17-11. Fluid flow models for dolomitization at Niue. A: Seepage reflux of brines. B: Freshwater-saltwater mixing and related flow of saline groundwater below the mixing zone. C: Thermal convection of saline groundwater (Kohout convection). (D) Flow of saline groundwater deep within the platform. (Modified from Aharon et al. 1987.)

and backreef sediments. Schofield and Nelson (1978) reached the same conclusion after a petrographic and elemental chemistry (i.e., Ca and Mg) study of samples from water wells, of which the Fonuakula well was the deepest (56 m).

Rodgers et al. (1982) rejected the brine-reflux model on the basis of elemental chemical analyses of the Fonuakula well dolomites and proposed that dolomitization occurred in the freshwater-saltwater mixing zone (Fig. 17-11B). Rodgers et al. (1982) used four main arguments to reject the brine-reflux model. First, a single filling of the lagoon would provide insufficient Mg to dolomitize the section observed at Niue (50 m thick and 14 km in diameter); a volume of seawater equal to the area of the lagoon and 7 km thick would be required. Second, holding lagoonal water long enough for evaporation to hypersalinity would be unlikely given the porous and permeable nature of Niue's carbonates. Third, gypsum deposits or molds have not been found in Niuean carbonates. Finally, Na concentrations of the dolomites are $< 1{,}000$ ppm, indicating precipitation from brackish rather than hypersaline waters. Rodgers et al. (1982) proposed an alternative: dolomitization occurred in the freshwater-saltwater mixing zone beneath the freshwater lens whenever Niue was subaerially exposed during a sea-level fall. They used thermodynamic calculations to show that mixtures with 3–37% seawater and 2–3 atm PCO_2 would dissolve calcite and precipitate dolomite.

Aharon et al. (1987) rejected the notion of freshwater-saltwater mixing in favor of a saltwater-circulation system from consideration of the stable carbon and oxygen

isotope composition of the Fonuakula dolomites. Given endpoints of seawater ($\delta^{18}O$ = + 0.2 to + 0.6‰ SMOW) and Fijian rainwater ($\delta^{18}O$ = −4 to −7‰ SMOW), predicted $\delta^{18}O$ values of mixing-zone dolomites would be −2 to −6‰ PDB. The $\delta^{13}C$ values of the dolomites precipitated in a mixing-zone environment should also be negative because of incorporation of soil-gas CO_2. Instead, the measured $\delta^{18}O$ and $\delta^{13}C$ values of the dolomites are + 1.9 to + 3.6‰ and + 1.1 to + 2.6‰ PDB, respectively. The measured $\delta^{18}O$ values coupled with the strontium concentrations of the dolomites (213–231 ppm) are consistent with precipitation from normal seawater at temperatures of 20–25°C, using the calcian-dolomite $\delta^{18}O$-thermometer equation of Fritz and Smith (1970). Aharon et al. (1987) proposed that the ocean-derived saline groundwater flowed upward through the platform in a thermal convection cell driven by residual heat from the extinct volcano (Fig. 17-11C). Supporting this hypothesis was the upward-decreasing gradient in Fe, Mn, Cu, and Zn concentrations, the high U content, and the elevated radioactivity reported by Rodgers et al. (1982) in the Fonuakula dolomites. The limestones have lower Fe and Mn concentrations and the cave flowstone deposits are poor in all four trace metals, suggesting that neither the limestone precursors nor the volcanic ash-derived soils are the source of the trace metals in the dolomites. The high trace-metal concentrations imply their extraction from Niue's underlying basaltic volcano by saltwater-volcanic rock reaction and some hydrothermal input. $^{87}Sr/^{86}Sr$ ratios suggested that dolomitization occurred during the Plio-Pleistocene (Aharon et al., 1987). A hydrogeologically similar thermal-convection circulation has been proposed and discussed for other carbonate islands (e.g., Enewetak by Saller, 1984 [Chap. 21]; islands of French Polynesia by Rougerie and Wauthy, 1993 [Chap. 15]) and carbonate platforms (Florida by Kohout, 1967).

With the availability of cores deeper than the dug well at Fonuakula (Fig. 17-5), it is now clear that the carbonate platform at Niue has not been dolomitized throughout (Wheeler and Aharon, 1993) as previous workers have thought. The existence of a 100-m-thick, undolomitized middle limestone sandwiched between upper and lower dolomites (Fig. 17-6) eliminates thermal convection as a flow mechanism for dolomitization of the upper unit. In the upper dolomite unit, the dolomite $\delta^{18}O$ and $\delta^{13}C$ values (+ 3.3 ± 0.4‰; + 2.6 ± 0.5‰ PDB, respectively; n = 37) and Sr concentrations (167 ± 34 ppm; n = 9) in these cores are similar to those in the Fonuakula dolomites. Under these circumstances, the dolomites seem to be consistent with precipitation from ocean-derived saline groundwater (Wheeler and Aharon, 1993), using a dolomite-calcite $\delta^{18}O$ fractionation factor of + 3.8‰ (Land, 1991) and a variable distribution factor for Sr in dolomite (Vahrenkamp and Swart 1990). The variable Ca content (52 to 62 mol%), association with meteoric diagenesis, and shallow burial imply that dolomitization in the upper dolomite occurred within tens of meters of the surface. The abrupt vertical transitions from totally dolomitized to totally undolomitized rocks suggest that the zone of active dolomitization at any one time was thin.

Two saltwater-flow mechanisms could accommodate the constraints imposed by the new data: (1) entrainment by an overlying freshwater-saltwater mixing zone (Fig. 17-11B), and (2) tidal pumping (Fig. 17-11D). Vahrenkamp et al. (1991)

noted that seaward flow in the freshwater-saltwater mixing zone of a freshwater lens entrains an opposite flow in the underlying ocean-derived groundwaters and proposed that this flow would explain the tabular distribution of dolomite in Little Bahama Bank (Fig. 17-11B). Even at the center of a 60-km-wide carbonate platform, such mixing-driven seawater exchange could be near-total in 1,000 years (Stewart and Fuller, 1993).

Herman et al. (1986) proposed, on the basis of hydrologic modeling, that tide-related variations in saltwater head may drive saltwater into and out of the carbonate platform of Enewetak Atoll via zones leached during meteoric diagenesis (Fig. 17-11D). Saltwater then could migrate vertically into adjacent less permeable layers. Initially, dolomitization would be favored in the more permeable layers, leading to tabular bodies of dolomite. Tidal ranges and lags observed in water wells at Niue (see Hydrogeology section) indicate that a similar flow pattern is present at Niue and may be a major contributor to the observed dolomitization of the upper dolomite unit.

The dolomitization in the lower dolomite unit was also likely to have proceeded from a ocean-derived saline groundwater, as indicated by $\delta^{18}O$ and $\delta^{13}C$ values ($+ 4.3 \pm 0.2‰$; $+ 2.0 \pm 0.1‰$ PDB; $n = 41$) and Sr concentrations (241 ± 27 ppm; $n = 21$) (Wheeler and Aharon, 1993). Low variability in Ca content (57–60 mol%) and the absence of any meteoric diagenesis suggest that dolomitization occurred further down from the depositional interface than it did in the upper dolomite. Observation of thermally mature kerogen in the lower dolomite unit in core DH4 (Gregory, oral comm., 1991) and evidence of hydrothermal activity (Whitehead et al., 1990, 1992) imply that reheating has occurred following sedimentary deposition of the lower dolomite interval. However, heavy $\delta^{18}O$ values suggesting dolomitization at temperatures lower than the 20–25°C projected for the upper dolomite (Aharon et al., 1987) argue that the reheating and dolomitization events were diachronous.

The exact nature of the saltwater flow into the platform during dolomitization of the lower dolomite unit is unclear. Temperature differences between the carbonate platform and the adjacent seawater column may have caused a thermal convection cell of saline groundwater (Kohout convection; Simms, 1984) similar to that which Aharon et al. (1987) proposed for the upper dolomite unit (Fig. 17-11C). An additional means of saltwater supply is tidal pumping, as discussed above (Fig. 17-11D). The concentration of dolomite in a few intervals separated by dolomite-poor intervals is consistent with the preferential dolomitization of more-permeable strata which is to be expected of tidal pumping. Studies are in progress to resolve the question of the saltwater-flow mechanism during dolomitization of the lower dolomite unit.

CONCLUDING REMARKS

Reef carbonates have accumulated at Niue since volcanism ceased in the middle to late Miocene. The uppermost 300 m consists of coral-reef and associated carbonate sediments which were deposited during the late Miocene (Tortonian) to late Pliocene

(Piacenzian) or early Pleistocene. During the Messinian-early Zanclean, Niue experienced one major sea-level fall of about 42 m and seven minor falls of about 34 m. The largest eustatic lowstand occurred at the close of the Messinian (5.3 Ma). Niue was last completely submerged during the early Pleistocene; subsequent glacial-interglacial eustatic fluctuations have cut two major and six or seven minor terraces. The post-early Pleistocene emergence is due to upward arching of the Pacific Plate as it approaches the Tonga Trench. Niue's future will be similar to that of Capricorn Seamount, now submerged on the eastern, subducting flank of the trench.

Dolomite is generally limited to two vertically distinct units which are separated by a 120-m-thick interval of undolomitized limestone. In the upper unit, dolomitization was nearly complete and was probably related to intermittent development of a meteoric lens during the Plio-Pleistocene. In contrast, dolomitization in the lower unit averages only 30% and may have occurred further below the depositional surface. All the dolomites precipitated from seawater-derived fluids.

Niue has a single, unconfined freshwater lens which floats on the underlying ocean-derived groundwaters. The water table lies at about 2 m above sea level at the island's center. The lens contains about 4.6 km^3 of a Ca-Mg-HCO_3 freshwater with TDS values within the WHO guidelines for potable water. Rainfall and recharge rates permit a sustainable extraction rate of about 4,000 $m^3\ y^{-1}\ ha^{-1}$ from the freshwater lens.

ACKNOWLEDGEMENTS

We thank J. Barrie and Avian Mining Pty. for the Niue drill cores; G. Jacobson for encouragement to delve into the hydrogeology of the island; and reviewers Len Vacher, Ivan Gill, John E. Mylroie, Mark Stewart, and John Barrie for insightful, constructive criticisms on the manuscript. The field and laboratory studies of the South Pacific carbonate platforms are supported by National Science Foundation grant EAR-9304661.

REFERENCES

Adams, C.G., 1984. Neogene larger foraminifera, evolutionary and geological events in the context of datum planes. In: N. Ikebe and R. Tsuchi (Editors), Pacific Neogene Datum Planes: Contributions to Biostratigraphy and Chronology. Univ. Tokyo Press, Tokyo, pp. 47–67.

Agassiz, A., 1903. The Coral Reefs of the Tropical Pacific. Mem. Mus. Comp. Zool., Harvard, 28, 410 pp.

Aharon, P., Socki, R.A. and Chan, L., 1987. Dolomitization of atolls by sea water convection flow: test of a hypothesis at Niue, South Pacific. J. Geol., 95: 187–203.

Aharon, P., Goldstein, S.L., Wheeler, C.W. and Jacobson, G., 1993. Sea-level events in the South Pacific linked with the Messinian salinity crisis. Geology, 21: 771–775.

Aissaoui, D.M., 1988. Magnesian calcite cements and their diagenesis: dissolution and dolomitization, Mururoa Atoll. Sedimentol., 35: 821–841.

Birrell, K.S., Seelye, F.T. and Grange, L.I., 1939. Chromium in soils of western Samoa and Niue Island. N.Z. J. Sci. Technol., 21: 91a–95a.

Brodie, J.W., 1965. Capricorn Seamount, south-west Pacific Ocean. Trans. R. Soc. N.Z., 3: 151–158.

Cayan, D.R. and Webb, R.H., 1992. El Niño/Southern Oscillation and streamflow in the western United States. In: H.F. Diaz and V. Markgraf (Editors), El Niño: Historical and Paleoclimatic Aspects of the Southern Oscillation. Cambridge University Press, Cambridge, pp. 29–68.

Cook, J., 1777. A Voyage Towards the South Pole, and Round the World. Performed in His Majesty's Ships the Resolution and Adventure, in the Years 1772, 1773, 1774, and 1775. W. Strahan and T. Cadell, London, v. 2.

David, T.W.E., 1904. Section IV. Narrative of the second and third expeditions. In: H.E. Armstrong, W.T. Blanford, T.G. Bonney, W. Crookes, F. Darwin, J. Evans, A. Geikie, G.J. Hinde, J.W. Judd, E.R. Lankester, C. Lapworth, J. Murray, W.J. Sollas, H.C. Sorby, J.J.H. Teall, W.J.L. Wharton, B. Wolfe, A.M. Field and W.W. Watts (Editors), The Atoll of Funafuti. Borings into a Coral Reef and the Results. Report of the Coral Reef Committee, The Royal Society of London, pp. 40–60.

Douglas, N. and Douglas, N., (Editors), 1989. Niue. In: Pacific Islands Yearbook. Angus and Robertson Publishers, North Ryde, Australia, pp. 377–386.

Dubois, J., Launay, J. and Recy, J., 1975. Some new evidence on lithospheric bulges close to island arcs. Tectonophys., 26: 189–196.

Fieldes, M., Bealing, G., Claridge, G.G., Wells, N. and Taylor, N.H., 1960. Mineralogy and radioactivity of Niue Island soils. N.Z. J. Sci., 3: 658–675.

Fritz, P. and Smith, D.G.W., 1970. The isotopic composition of secondary dolomites. Geochim. Cosmochim. Acta, 34: 1161–1173.

Herman, M.E., Buddemeier, R.W. and Wheatcraft, S.W., 1986. A layered aquifer model of atoll island hydrology: validation of a computer simulation. J. Hydrol., 84: 303–322.

Hilgen, F.J., 1991. Extension of the astronomically calibrated (polarity) time scale to the Miocene/Pliocene boundary. Earth Planet. Sci. Lett., 107: 349–368.

Hill, P.J., 1983. Volcanic core of Niue Island, southwest Pacific Ocean. BMR J. Aust. Geol. Geophys., 8: 323–328.

Hodell, D.A., Mueller, P.A. and Garrido, J.R., 1991. Variations in the strontium isotopic composition of seawater during the Neogene. Geology, 19: 24–27.

Jacobson, G. and Hill, P.J., 1980a. Hydrogeology of a raised coral atoll – Niue Island, South Pacific Ocean. BMR J. Aust. Geol. Geophys., 5: 271–278.

Jacobson, G. and Hill, P.J., 1980b. Groundwater resources of Niue Island. Bur. Miner. Resour. (Aust.), Geol. & Geophys., Record 1980/14, 30 pp.

Jacobson, G. and Hill, P.J., 1988. Hydrogeology and groundwater resources of Nauru Island, central Pacific Ocean. Bur. Miner. Resour. (Aust.), Geol. & Geophys., Record 1988/12, 87 pp.

Keigwin, L.D., 1987. Toward a high-resolution chronology for latest Miocene paleoceanographic events. Paleoceanography, 2: 639–660.

Kohout, F.A., 1967. Ground-water flow and the geothermal regime of the Floridian Plateau. Trans. Gulf Coast Assoc. Geol. Soc., 17: 339–354.

Land, L.S., 1991. Dolomitization of the Hope Gate Formation (north Jamaica) by seawater: Reassessment of mixing-zone dolomite. In: H.P. Taylor, Jr., J.R. O'Neil and I.R. Kaplan (Editors), Stable Isotope Geochemistry: A Tribute to Samuel Epstein. Geochem. Soc. Spec. Publ. 3: 121–133.

Lincoln, J.M. and Schlanger, S.O., 1987. Miocene sea-level falls related to the geologic history of Midway Atoll. Geology, 15: 454–457.

Lincoln, J.M. and Schlanger, S.O., 1991. Atoll stratigraphy as a record of sea level change: problems and prospects. J. Geophys. Res., 96: 6727–6752.

Loeb, E.M., 1926. History and Traditions of Niue. Bernice P. Bishop Mus. Bull. 32. Honolulu, 226 pp.

Longman, M.W., 1980. Carbonate diagenetic textures from nearsurface environments. Am. Assoc. Petrol. Geol. Bull., 64: 461–487.

Lonsdale, P., 1986. A multibeam reconnaissance of the Tonga Trench axis and its intersection with the Louisville Guyot Chain. Mar. Geophys. Res., 8: 295–327.

Marsden, E., Fergusson, G.J. and Fieldes, M., 1958. Notes on the radioactivity of soils with application to Niue Island. Proc. Second Int. Conf. on Peaceful Uses of Atomic Energy, 18: 514.

Mather, J.D., 1975. Development of the groundwater resources of small limestone islands. Q. J. Eng. Geol., 8: 141–150.
Quinn, T.M., 1991. Meteoric diagenesis of Plio-Pleistocene limestones at Enewetak Atoll. J. Sediment. Petrol., 61: 681–703.
Rodgers, K.A., Easton, A.J. and Downes, C.J., 1982. The chemistry of carbonate rocks of Niue Island, South Pacific. J. Geol., 90: 645–662.
Rougerie, F. and Wauthy, B., 1993. The endo-upwelling concept: from geothermal convection to reef construction. Coral Reefs, 12: 19–30.
Saller, A.H., 1984. Petrologic and geochemical constraints on the origin of subsurface dolomite, Enewetak Atoll: An example of dolomitization by normal seawater. Geology, 12: 217–220.
Saller, A.H. and Moore, C.H., 1989. Meteoric diagenesis, marine diagenesis, and microporosity in Pleistocene and Oligocene limestone, Enewetak Atoll, Marshall Islands. Sediment. Geol., 63: 253–272.
Schlanger, S.O., 1965. Dolomite-evaporite relations on Pacific islands. Sci. Rep. Tohoku Univ. Second Ser. (Geol.), 37: 15–29.
Schofield, J.C., 1959. The geology and hydrology of Niue Island, South Pacific. N.Z. Geol. Surv. Bull. n.s. 62, 29 pp.
Schofield, J.C., 1967a. Origin of radioactivity at Niue Island. N.Z. J. Geol. Geophys., 10: 1362–1371.
Schofield, J.C., 1967b. 1-Post glacial sea-level maxima a function of salinity? 2-Pleistocene sea-level evidence from Cook Islands. J. Geosci., 10: 115–120.
Schofield, J.C., 1969. Niue groundwater: Industrial Minerals and Rocks 1968. N.Z. Dep. Sci. Ind. Res. Inf. Ser., 63: 105–110.
Schofield, J.C. and Nelson, C.S., 1978. Dolomitization and Quaternary climate of Niue Island, Pacific Ocean. Pac. Geol., 13: 37–48.
Simms, M., 1984. Dolomitization by groundwater-flow systems in carbonate platforms. Trans. Gulf Coast Assoc. Geol. Soc., 34: 411–420.
Skeats, E.W., 1903. The chemical composition of limestones from upraised coral islands, with notes on their microscopical structures. Bull. Mus. Comp. Zool., Harvard, 42(2): 51–126.
Stewart, M. and Fuller, J., 1993. Mixing-zone-driven seawater circulation in carbonate platforms: results of numerical modeling (abstr.). Geol. Soc. Am. Abstr. Programs, 26: 183.
Summerhayes, C. P., 1967. Bathymetry and topographic lineation in the Cook Islands. N.Z. J. Geol. Geophys., 10: 1382–1399.
Vacher, H.L., Bengtsson, T.O. and Plummer, L.N., 1990. Hydrology of meteoric diagenesis: residence time of meteoric ground water in island fresh-water lenses with application to aragonite-calcite stabilization rate in Bermuda. Geol. Soc. Am. Bull., 102: 223–232.
Vahrenkamp, V.C., Swart, P.K. and Ruiz, J., 1991. Episodic dolomitization of Late Cenozoic carbonates in the Bahamas: evidence from strontium isotopes. J. Sediment. Petrol., 61: 1002–1014.
Vahrenkamp, V.C. and Swart, P.K., 1990. New distribution coefficient for the incorporation of strontium into dolomite and implications for the formation of ancient dolomites. Geology, 18: 387–391.
Wheeler, C.W. and Aharon, P., 1991. Mid-oceanic carbonate platforms as oceanic dipsticks: examples from the Pacific. Coral Reefs, 10: 101–114.
Wheeler, C.W. and Aharon, P., 1993. It isn't thermal convection after all: the dolomite record at Niue revisited (abstr.). Geol. Soc. Am. Abstr. Programs, 25: 398.
Whitehead, N.E., Barrie, J. and Rankin, P., 1990. Anomalous Hg contents in soils of Niue Island, South Pacific. Geochem. J., 24: 371–378.
Whitehead, N.E., Ditchburn, R.G., McCabe, W.J. and Rankin, P., 1992. A new model for the origin of the anomalous radioactivity in Niue Island (South Pacific) soils. Chem. Geol., 94: 247–260.
Whitehead, N.E., Hunt, J., Leslie, D. and Rankin, P., 1993. The elemental content of Niue Island soils as an indicator of their origin. N.Z. J. Geol. Geophys., 36: 243–254.
Wright, A.C.A. and van Westerndorp, F.J., 1965. Soils and agriculture of Niue Island. N.Z. Dep. Sci. Ind. Res. Soil Bur. Bull. 17, 80 pp.

Geology and Hydrogeology of Carbonate Islands. Developments in Sedimentology 54
edited by H.L. Vacher and T. Quinn
© 1997 Elsevier Science B.V. All rights reserved.

Chapter 18

HYDROGEOLOGY OF CARBONATE ISLANDS OF THE KINGDOM OF TONGA

LINDSAY J. FURNESS

INTRODUCTION AND SETTING

The Kingdom of Tonga is a Polynesian country in the southwest Pacific Ocean. It lies along the convergent boundary between the Indo-Australian and Pacific Plates about 800 km east of Fiji, 1,000 km south of Western Samoa, and 3,000 km northeast of Sydney, Australia (Fig. 18-1). On August 24, 1887, King George Tupou I, the first king of Tonga, declared the kingdom's boundaries as longitudes 177°W and 173°W and latitudes 15°S and 23°30′S (Fig. 18-2).

The NE-SW archipelago is about 800 km long and consists of two parallel belts: low, fertile limestone islands close to the trench and higher volcanic terrain along the active Tofua Arc (Fig. 18-1). There are some 176 islands, with a total land area of 440 km^2. The principal limestone islands are clustered into the Tongatapu, Ha'apai, Nomuka and Vava'u Groups (Fig. 18-2); three remote northern islands (Tafahi, Niua Toputapu and Niua Fo'ou) comprise the Niuas. By far the largest island is Tongatapu, at 257 km^2. The capital city, Nuku'alofa, is located on Tongatapu.

The Tonga Islands have been inhabited by Polynesian peoples for 3,000 years. The line of ruling dynasties can be traced back for a thousand years (Oliver, 1961). Abel Tasman visited in 1643, and Captain Cook named the islands the Friendly Islands in 1773. The kingdom was neutral until 1900, when it signed a Treaty of Friendship and Protection with Britain. Tonga became fully independent within the Commonwealth on June 4, 1970.

About 35 of the islands are inhabited. Over 98% of the population of about 100,000 are Polynesian Tongans. About two-thirds of the population live on the main island of Tongatapu, and another 15,000 live on Vava'u. The languages are Tongan, which is an Austronesian language, and English.

The main towns of Nuku'alofa on Tongatapu and Neiafu on Vava'u have undergone little development and retain a quaint "Victorian" appearance with wooden buildings up to a century old. The unique system of land tenure has divided the islands into 8.25-acre allotments for traditional subsistence cropping. The mainstay of agriculture for export this century was coconut production for copra. Beneath the canopy of coconut, farmers grew their traditional root crops of yam, tarot, casava and kumala. In recent times, there has been a shift to cash-cropping of vanilla, squash pumpkin, water melon and western vegetables.

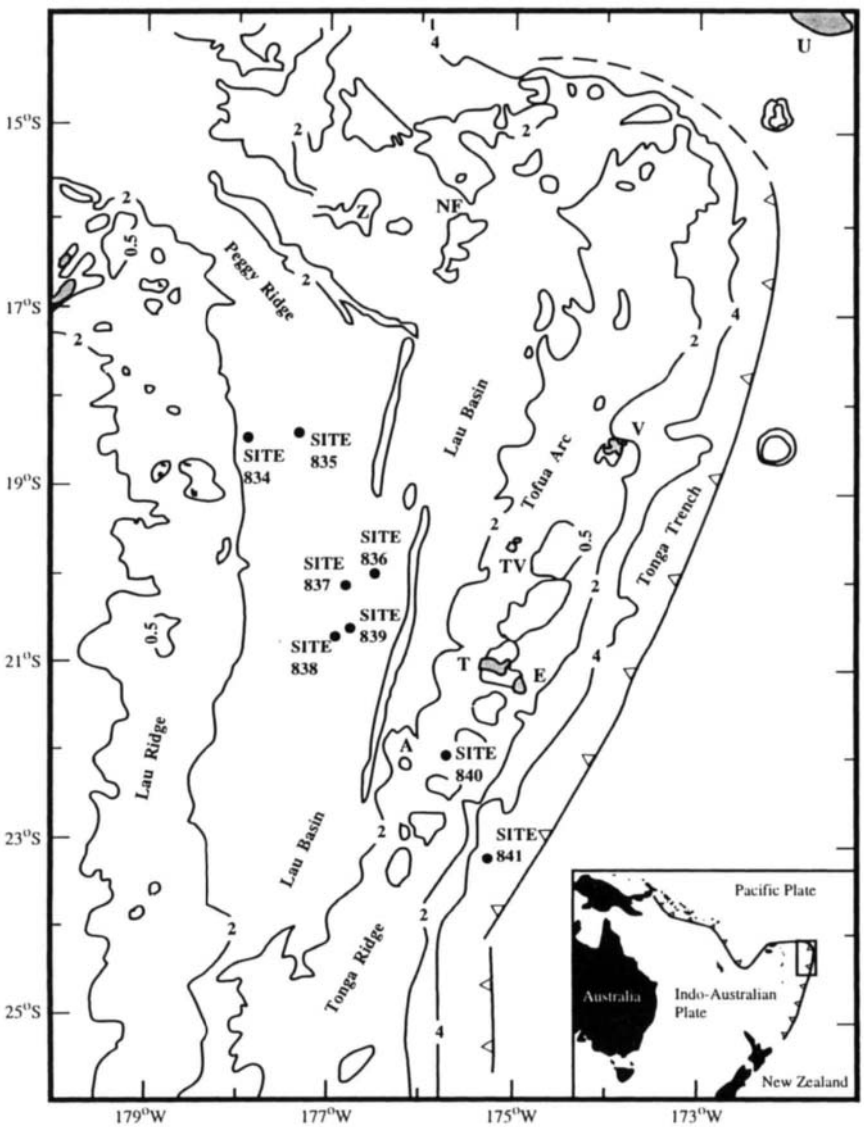


Fig. 18-1. Location of the Kingdom of Tonga in the Tonga trench-arc system. Islands are: Niua Fo'ou (NF), Vava'u (V), Tofua Volcano (TV), Tongatapu (T), 'Eua (E), 'Ata (A), and Upolu (U), Western Samoa. Contours are in km. Drill sites are from ODP Leg 135. (Adapted from Hawkins et al., 1994, Fig. 1.) [See also Fig. 26.1 for setting relative to Fiji.]

Hydrogeological studies

Before 1990, groundwater and water-supply studies were carried out on an ad hoc basis during short visits by hydrogeologists and engineers under cooperative

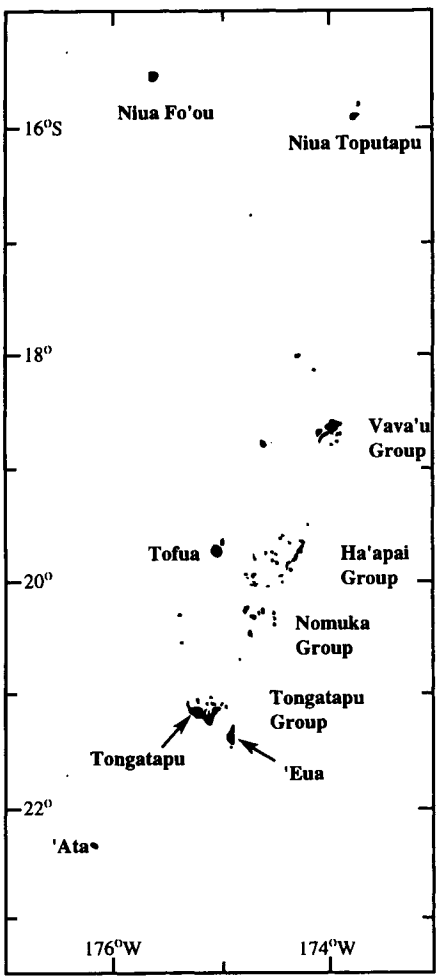


Fig. 18-2. Island groups of the Kingdom of Tonga.

agreements with the United Nations, Australia, and New Zealand. In 1990, the Tongan Ministry of Lands, Survey and Natural Resources appointed a hydrogeologist to conduct a 3-year study to evaluate the extent and quality of local water supplies in all the inhabited Tongan islands. Results of that study are in a report by Furness and Helu (1993) and form the basis of this chapter.

Climate

A belt of high pressure spans the South Pacific at about 25–30°S Thompson (1986). Within this belt is a large semipermanent anticyclone centered about 90–100°W in the eastern South Pacific, and a more migratory anticyclonic cell on the

west that moves eastward into the Pacific region from the Australian-Tasman Sea region. Between these two large high-pressure cells is the South Pacific Convergence Zone (SPCZ), an area of cyclonic circulation and a semipermanent cloud feature of the South Pacific. Middle-latitude cold fronts may enter the region of trade winds at any time of the year and become stationary. The weather of the tropical portion of these fronts is normally a broad band of showers and rain.

During the summer, the SPCZ lies midway between Western Samoa and Tonga. About 65% of the rain falls during the resulting summer wet season (Nov-Apr). During the winter, the SPCZ lies well to the north of Tonga, and easterly or southeasterly trade winds prevail.

The northernmost islands (Vava'u and the Niuas), which are most affected by the SPCZ, have the highest average rainfall (2,301 mm y^{-1} on Niua Toputapu; 2,231 mm y^{-1} at Neiafu on Vava'u). The Ha'apai Group lies in a relatively dry zone of Tonga between the region of influence of the SPCZ and the rainfall associated with the upper-air jet stream and other extra-tropical weather features (1,716 mm y^{-1} at Pangai on Ha'apai). On Tongatapu, the rainfall increases slightly to the higher southeast side of the island (1,770 mm y^{-1} at Nuku'alofa). 'Eua has a slightly higher rainfall than Tongatapu due to the orographic influence of its higher topography. There is also a north-south gradient in mean annual temperature, from 26°C at Niua Toputapu (Niuas Group) to 23°C at Nuku'alofa.

Tropical cyclones occur during the wet season. Between November 1939 and April 1985, there were 58 cyclones (on average 1.3 y^{-1}). Of these, 41 affected only northern Tonga, 38 affected southern Tonga, and 17 affected the entire archipelago.

Tectonic setting

Tonga lies at the easternmost edge of the Indo-Australian Plate (Fig. 18-1) and is part of an arc system (the Tonga Ridge, Scholl and Vallier, 1985) that has formed in response to subduction of the Pacific Plate over a period of at least 45 m.y. (Gatliff, 1990). The Tonga Ridge rises above the Tonga Trench with depths of 10 km on the east and the Lau Basin with depths of 2–3 km to the west. The Tonga Ridge comprises an active volcanic arc (the Tofua Arc) and a linear chain of uplifted platform carbonate rocks, atoll reefs, and older crystalline basement rocks (Hawkins et al., 1994). This older eastern chain is variously referred to as the "inactive Tongatapu arc" (Parson et al., 1990), the "Tonga Platform" (Clift and Dixon, 1994), and a frontal arc (Nunn, 1994). It includes the principal Tongan islands of the Vava'u, Ha'apai, Nomuka and Tongatapu Groups and is separated from the younger islands and seamounts of the Tofua Arc by the 1.8-km deep Tofua Trough.

The Lau Basin is a young backarc basin between the Tonga Ridge and the remnant Lau Ridge (Hawkins et al., 1994), which underlies most of the carbonate islands of Fiji [q.v., Chap. 26]. The Lau Basin was the focus of a recent leg of the Ocean Drilling Program (ODP), and as a result, the tectonic evolution of the Tonga area is well understood (Hawkins et al., 1994). Figure 18.3 (from Clift and Dixon, 1994) illustrates the main events, including the splitting of an older Tonga arc by the

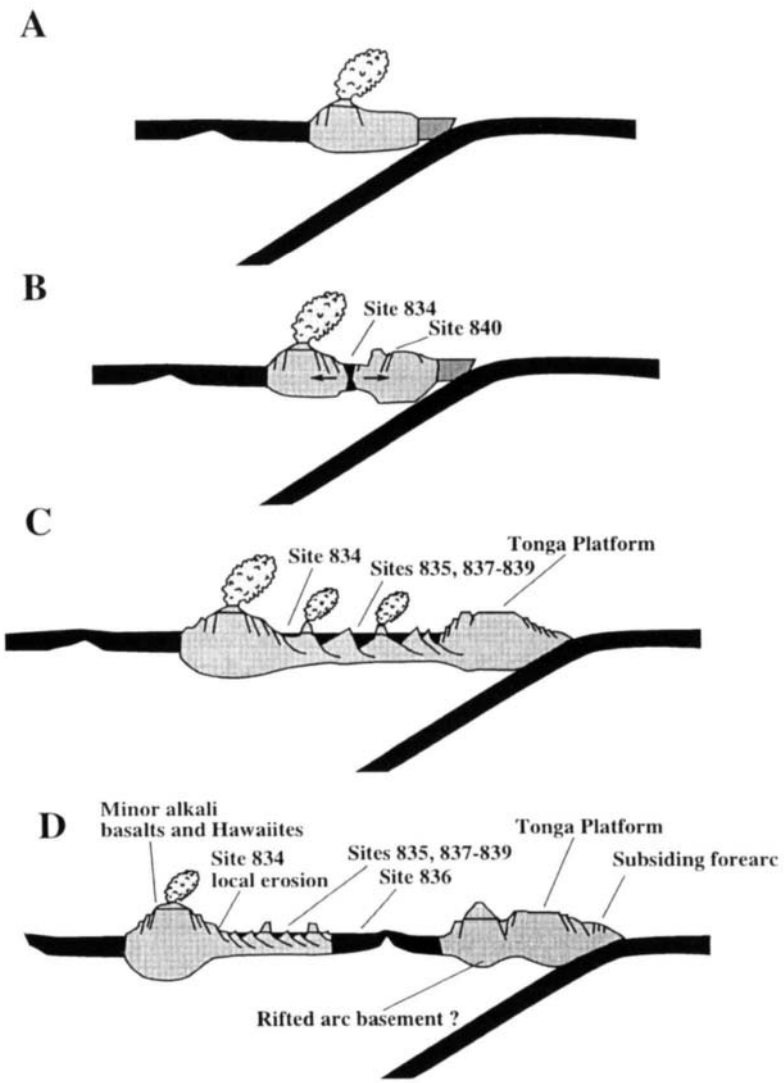


Fig. 18-3. Late Cenozoic tectonic history of the Tonga Arc according to results of ODP Leg 135. (A) Steady-state subduction during the late Miocene (7 Ma). (B) Extension of the arc during late Miocene (5.6 Ma). (C) Continued extension and seamount volcanism during the middle Pliocene (2.5 Ma). (D) Spreading at the Eastern Lau Spreading Center during the Pleistocene (0.5 Ma). See Fig. 18-1 for location of drill sites. (Adapted from Clift and Dixon, 1994, Fig. 31.)

formation of the Lau Basin; the transport of the western split, the Lau Ridge, away from the subduction zone; and the formation of the new Tofua Arc and uplift of the Tonga Platform.

Topographically and bathymetrically, the Tonga Ridge is longitudinally divided into a series of blocks 25–150 km in length. These blocks have been interpreted to be

related to bounding faults, variation in the tectonic history along the ridge, differential uplift caused by subduction of seamounts, and rotation of sectors due to oblique subduction (Gatliff, 1990).

GENERAL GEOLOGY

The Tongan limestone islands are characterized by Pliocene and Pleistocene coral-reef terraces. On Tongatapu and the Vava'u and Ha'apai Groups, older rocks are not exposed. On the Nomuka Group, the limestones unconformably overlie Miocene volcaniclastics and calcareous mudstones. On 'Eua, east of Tongatapu (Fig. 18-1), the oldest rocks occur. These are Eocene volcanics (46–17 Ma) that predate the Lau Volcanic Group (14–5 Ma) of the Lau Ridge, Fiji (Cole et al., 1990) [Chap. 26]. These volcanic rocks are unconformably overlain by a sequence of Miocene volcaniclastics with thin micritic limestones and, in turn, the terraced limestones typical of the other limestone islands of Tonga.

The limestone islands are covered with a mantle of fine volcanic ash (Orbel, 1983), which appears to have been deposited during two major periods of eruptions. The source of ash is the Tofua Arc, including the volcanoes present today and those that are now submerged. The ash is up to 5 m thick on Tongatapu, 9 m thick on Vava'u, and 13 m thick on Kotu Island (Ha'apai Group), which is closest to the Tofua volcano (Fig. 18-1). It is reported that there was an ash fall in Vava'u in 1886.

By far the greatest proportion of soils in Tonga is derived from the fine-grained, andesitic ash. Other soils, which include calcareous sandy soils derived from the weathering of the coral reefs, form an unconsolidated mantle on the leeward sides of the islands.

The topography and tilt of the limestone islands is characteristic of particular island groups. Tongatapu reaches a maximum elevation of 65 m and dips gently to the northwest. 'Eua is 310 m high and dips at angles up to 14° to the west; the eastern coast consists of spectacular cliffs, whereas the western side of the island is a series of three coral reef terraces. The Ha'apai and Nomuka Groups consist of low-lying islands, usually less than 15 m above sea level, with a slight dip to the west. The Vava'u Group consists of uplifted islands to 210 m above sea level, with a pronounced tilt to the south. The uplift rates and tilting of these blocks have been discussed by Taylor (1978) and Nunn (1994).

Extensive reefs are well developed around most of the main islands of Tonga as well as within the island groups. The largest development is in the Ha'apai Group. Reefs tend to be best developed on the leeward side of the islands in the equivalent position of a lagoon in an atoll setting. The geology of the algal ridge fringing the windward coast of Tongatapu has been studied recently by Nunn (1993).

HYDROGEOLOGY

The most important and extensively used groundwater bodies in Tonga are freshwater lenses contained within the larger uplifted coral-limestone islands. The

limestone in most cases is extremely permeable, as evidenced by the occurrence of tidal fluctuations in the center of the islands, minimal drawdown in pumped wells, and the presence of caves and submarine springs. Accordingly, there are almost no surface water bodies such as rivers and lakes. In 'Eua, caves at high elevations with perched aquifers provide the traditional source of water.

The salinity of the groundwater has been studied through a census of wells and geophysical measurements on several of the larger islands. On the larger islands of Tongatapu, 'Eua and Vava'u, the water table of the freshwater lens is less than one meter above sea level. The largest thickness of fresh groundwater is about 16 m on Tongatapu.

With few exceptions, the groundwater of Tonga is very hard and often exceeds the WHO guideline value of 500 mg L^{-1} $CaCO_3$, which is based on taste and household considerations. Water quality of the groundwater is an important issue in Tonga. On many islands, however, there is no alternative, and poorer quality water is often accepted.

Recharge

Penman estimates of evapotranspiration (Thompson, 1986) range from 1,461 mm y^{-1} in Tongatapu to 1,673 mm y^{-1} in Niua Toputapu. Comparison with the rainfall shows that there is sufficient precipitation in most months to meet the demands of evapotranspiration. A soil-water budget has been calculated from monthly data by Thompson (1986) and from daily data by Falkland (1991) [see Chap. 19 and Chap. 31 for details of similar analysis – Eds.] The available water content of the soils is 90–160 mm (Wilson and Beecroft, 1983, Wilde and Hewitt, 1983). According to Falkland (1991), recharge is 528 mm y^{-1} (30% of rainfall) on Tongatapu, 478 mm y^{-1} (28%) on Lifuka (Ha'apai Group) and 917 mm y^{-1} (41%) on Neiafu (Vava'u Group). Although recharge and soil-moisture deficits can occur any time during the year, recharge tends to be largest in the wet season, and soil-moisture deficits are largest at the end of the dry season.

Current monitoring program

Since 1990, the Ministry of Lands, Survey and Natural Resources has conducted a groundwater monitoring program. Groundwater levels in wells are measured at 3-mo intervals on Tongatapu and, when travel permits, on 'Eua, Ha'apai, Vava'u and Niua Toputapu. Automatic water-level recorders are installed on two wells on Tongatapu, one in Ha'apai, and a cave stream on 'Eua, and are accompanied by rain gauges at all four sites and a barometer in Tongatapu. Temperature, conductivity and pH are monitored at the same time as water levels. Bacterial quality is measured at infrequent intervals or when health problems occur.

Monitoring of sea level is at Nuku'alofa, at a new gauge established by the Australian National Tidal Facility at Queen Salote Wharf in 1993, superseding a tide gauge established at Vuna Wharf in 1990. The water level in Fanga'Uta lagoon on

Tongatapu has also been monitored to observe the lag in tidal response and the influence of wind on the lagoon levels.

WATER SUPPLIES

Ancient Tongan water wells (vaitupu), which can still be seen in low-lying coastal areas, consisted of a conical excavation in the soil down to the water table; such wells served as centers of water supplies for centuries. In 1909, a beginning was made on the construction of large concrete water cisterns in the villages to give people a supply of clean, disease-free rainwater. By 1946, community tanks had been established in most villages.

Towards the end of 1958, a public health engineer with WHO carried out feasibility studies on using groundwater. By 1961, a pilot project began supplying water to the villages of Houma and Vaotu'u on Tongatapu and the supply was extended to 16 more villages over the next two years (Campbell, 1992).

The supply of piped water to Nuku'alofa and Vava'u began in 1965. The first five hand-dug wells for Nuku'alofa were constructed in 1966, another in 1968 and two more in 1971. Then New Zealand aid provided a drilling rig which was used to construct village wells in Tongatapu and Vava'u. In 1985, a new rig was provided under Australian aid and has continued drilling water wells on Tongatapu, 'Eua, Ha'apai and Vava'u.

The groundwater supplies have been supplemented by rainwater tanks and public cisterns primarily for drinking-quality water. Aid programs have provided many rainwater tanks constructed of galvanised iron, concrete and fibreglass.

CASE STUDY: FRESHWATER LENS AT TONGATAPU

Tongatapu is believed to have formed initially as a reef on the southeast side of the present island and to have been progressively uplifted with new reef formation on the northwest (leeward) side. The island reaches a maximum elevation of 65 m on the southeast side and slopes down to the low-lying north coast. The Plio-Pleistocene limestones have a known thickness of up to 247 m. The surficial geology and sea-level history are discussed as a case study in the book on oceanic islands by Nunn (1994).

Hunt (1979) developed a steady-state model of the freshwater lens of Tongatapu. The model made the basic assumptions of Dupuit-Ghyben-Herzberg (DGH) analysis [Chap. 1]: that a sharp freshwater-saltwater interface is present, that the Ghyben-Herzberg ratio applies, and that equipotentials are vertical. Hunt's model was one of the first applications of DGH analysis to a carbonate island of irregular areal geometry, and he appended an analytical dispersion model from which the vertical variation of chloride could be calculated.

Figure 18.4 summarizes the result of Hunt's DGH model, which used a grid consisting of 293 nodes with a 1-km spacing. The target of the simulation was a map

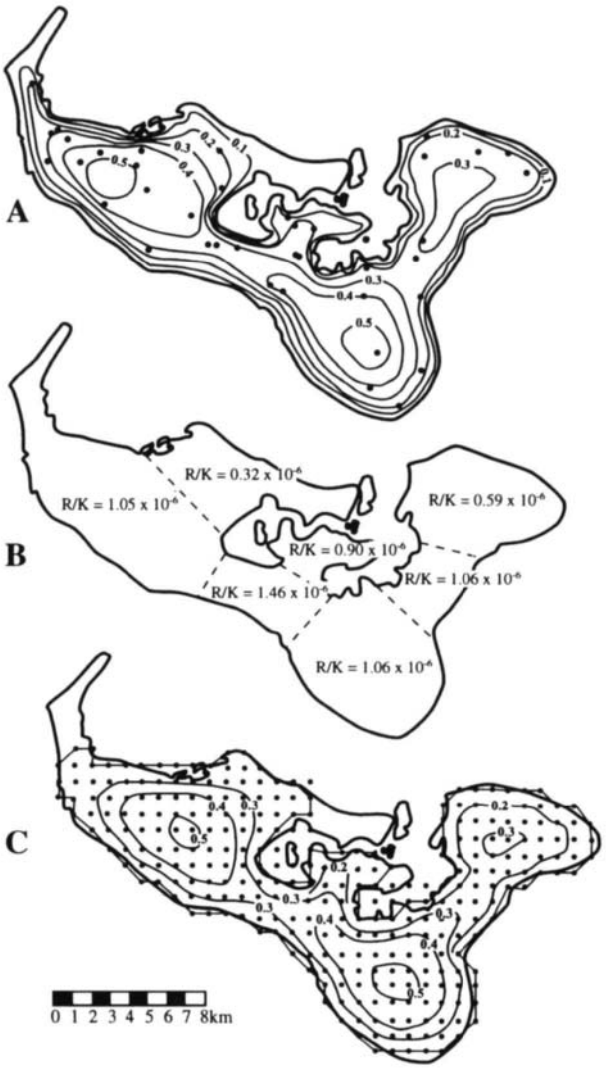


Fig. 18-4. DGH model of Tongatapu by Hunt (1979). (A) Observed water-table elevation. (B) Regions of assumed R/K. (C) Calculated water-table elevation on finite-difference grid. (Adapted from Hunt, 1979, Figs. 1, 4, and 3 respectively.)

of the water table (Fig. 18-4A) drawn from the measurements at 39 wells done in 1971 (Pfeiffer and Stach, 1972). The area was divided into different blocks with different (adjusted) ratios of recharge (R) and hydraulic conductivity (K). The distribution of R/K shown in Figure 18.4B gave the calculated water table configuration shown in Figure 18.4C. The general value of 1×10^{-6} is representative of the R/K used in this simulation.

Hunt (1979) used the R/K ratio he found from the modeling to estimate recharge. First, he calculated K from pumping test data of Waterhouse (1976): equilibrium drawdown of 0.0127 m in an observation well 3.05 m from a well pumping at 0.273 m^3 min^{-1}, where the pumping well penetrated a distance of 3.82 m into an aquifer with thickness of 16.4 m. Then, he combined the result, $K = 1.5\,cm\,s^{-1}$ (1,300 m day^{-1}), with the R/K value to obtain a recharge estimate: 25 to 30% of the rainfall. This estimate is very similar to the recharge calculated by Falkland (1991) from the soil-water balance.

Development of the freshwater lens includes wellfields at Mataki'Eua and Tongamai (Fig. 18-5) that supply water to Nuku'alofa. The wellfields include a total of 31 drilled and dug wells, most of which are pumped at about 3 L s^{-1}. The wells are in lines and are spaced at 150 m. The total production has been steadily increased to 5.1 ML day^{-1}. There is a drawdown of 0.25 m at the center of the Mataki'Eua wellfield. The wellfields supply 90 L day^{-1} $person^{-1}$ by a distribution system where the water is pumped to reinforced storage tanks on an adjacent hill and allowed to run by gravity through pipelines to Nuku'alofa.

The villages on Tongatapu are also equipped with one or more wells which pump to an overhead storage tank and then flow under gravity trough a pipe system to

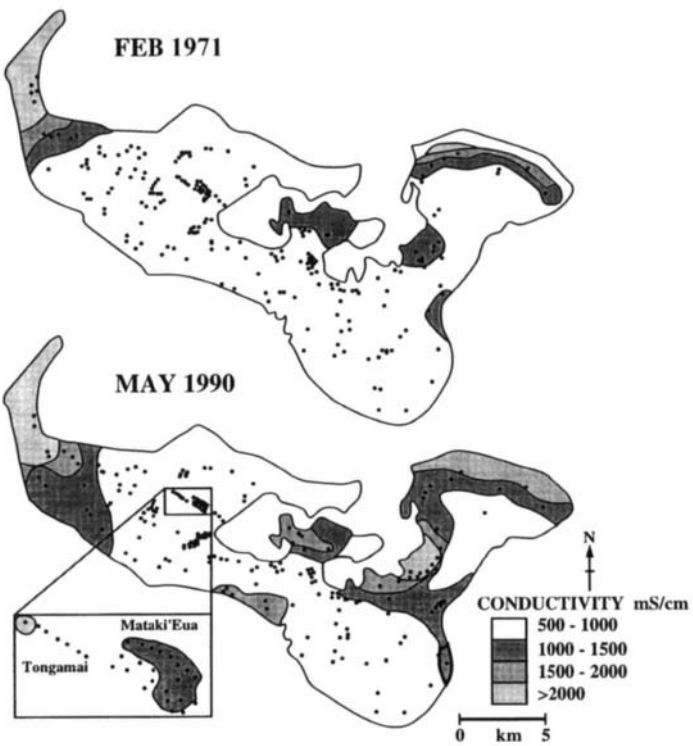


Fig. 18-5. Maps showing distribution of fluid conductivity in Tongatapu.

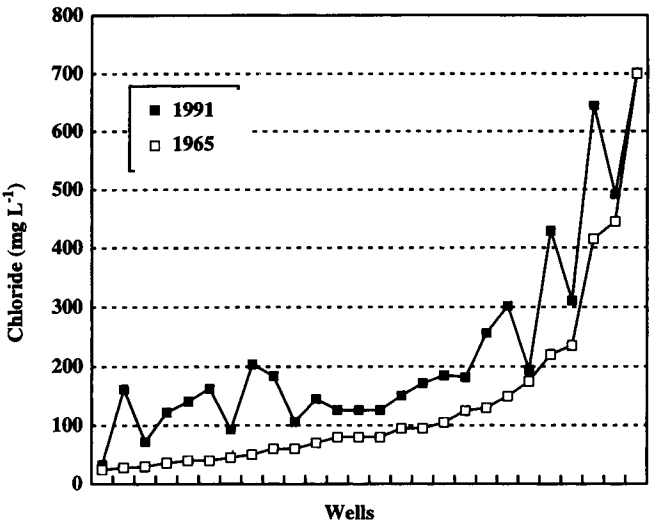


Fig. 18-6. Comparison of Cl^- data of 1965 and 1991. Cl^- increased at all wells for which data are available. Areal distribution is shown in Fig. 18-5.

individual houses. In addition, there are many private wells, most of which are hand dug and not equipped with a motorised pump.

Salinity has risen as a result of the development. Chloride values at the 27 wells for which data are available for 1965, 1971, and 1991 all show an increase (Fig. 18-6). In map view (Fig. 18-5), the rise in salinity appears as an encroachment of high-salinity water from the shoreline. Modelling suggests that the supply can be increased from the present 5.3 ML day^{-1} to about 19 ML day^{-1} by spreading abstractions and developing the area west of Nuku'alofa (Furness and Helu, 1993).

CONCLUDING REMARKS

The limestone islands of Tonga consist of uplifted and tilted Pliocene-Pleistocene limestones along a forearc ridge between the Tonga Trench and the active Tofua Arc. Annual rainfall is on the order of 2 m, and recharge is 30–40%. Freshwater lenses occur on the larger limestone islands, but the large hydraulic conductivity (e.g., ca. 1,000 m day^{-1} on Tongatapu) assures that they are thin. On the main island of Tongatapu, the hydrogeology is known through islandwide study, monitoring and resource development. On the remote, outer islands, investigations have been at a reconnaissance, village-level nature.

REFERENCES

Campbell, I.C., 1992. Island Kingdom. Tonga Ancient & Modern. Canterbury University Press, Christchurch, 257 pp.

Clift, P.D. and Dixon, J.E., 1994. Variations in arc volcanism and sedimentation related to rifting of the Lau Basin (southwest Pacific). In: J. Hawkins, L. Parson, J. Allan et al., Proc. ODP, Sci. Results, 135. Ocean Drilling Program, College Station TX, pp. 23–45.

Cole, J.W., Graham, I.J. and Gibson, I.L., 1990. Magmatic evolution of Late Cenozoic volcanic rocks of the Lau Ridge, Fiji. Contrib. Mineral. Petrol., 104: 540–554.

Furness, L.J. and Helu, S.P., 1993. The hydrogeology and water supply of the Kingdom of Tonga. Ministry of Lands, Survey and Natural Resources, Kingdom of Tonga. Government Printer, 143 pp.

Falkland, A.C., 1991. Tonga Water Supply Master Plan Study. Water Resour. Rep. for PPK Consultants Pty. Ltd.

Gatliff, R.W. 1990. The Petroleum Prospects in the Kingdom of Tonga. South Pacific Appl. Geosci. Comm., Aust. Int. Develop. Assist. Bur., 20 pp.

Hawkins, J.W., Parson, L.M., and Allan, J.F., 1994. Introduction to the scientific results of Leg 135: Lau Basin-Tonga Ridge drilling transect. In: J. Hawkins, L. Parson, J. Allan et al., Proc. ODP, Sci. Results, 135. Ocean Drilling Program, College Station TX, pp. 3–5.

Hunt, B., 1979. An analysis of the groundwater resources of Tongatapu Island, Kingdom of Tonga. J. Hydrol., 49: 185–196.

Nunn, P.D., 1993. Role of Porolithon algal-ridge growth in the development of the windward coast of Tongatapu Island, Tonga, South Pacific. Earth Surf. and Landf., 18: 427–439.

Nunn, P.D., 1994. Oceanic islands. Blackwell, Oxford, U.K., 413 pp.

Oliver, D.L., 1961. The Pacific Islands, rev. ed. Univ. Press of Hawaii, Honolulu, 456 pp.

Orbel, G.E., 1983. Soil Surveys – Vava'u and adjacent islands, Tonga Islands. R. Soc. N.Z. Bull., 8: 125–130.

Parson, L.M., Pearce, J. A., Murton, B.J., Hodkinson, R.A., Boomer, S., Huggett, Q.J., Miller, S., Johnson, L., Rodda, P. and Helu, S., 1990. Role of ridge jumps and ridge propagation in the tectonic evolution of the Lau back-arc basin, southwest Pacific. Geology, 18: 470–473.

Pfeiffer, D. and Stach, L.W., 1972. Hydrogeology of the Island of Tongatapu, Kingdom of Tonga, South Pacific. Geol. Jb. C4 Hannover.

Scholl, D.W. and Vallier, T.L. (Editors), 1985. Geology and offshore resources of Pacific Island Arcs – Tonga Region. Circum-Pacific Counc. Energy & Mineral Resour., Houston TX. Earth Sci. Ser. 2, 487 pp.

Taylor, F.W., 1978. Quaternary tectonic and sea-level history, Tonga and Fiji, southwest Pacific. Ph.D. Dissertation, Cornell Univ., Ithaca, NY.

Thompson, C.S., 1986. The Climate and Weather of Tonga. N.Z. Meteorol. Serv. Misc. Publ. 188(5).

Waterhouse, B.C., 1976. Nuku'alofa Water Supply. Tonga. N.Z. Geological Survey, Otara, Auckland.

Wilde, R.H. and Hewitt, A.E., 1983. Soils of part 'Eua Group, Kingdom of Tonga. N.Z. Soil Surv. Rep. 68.

Wilson, A.D. and Beecroft, F.G., 1983. Soils of the Ha'apai Group, Kingdom of Tonga. N.Z. Soil Survey Rep. 67.

Geology and Hydrogeology of Carbonate Islands. Developments in Sedimentology 54
edited by H.L. Vacher and T. Quinn
© 1997 Elsevier Science B.V. All rights reserved.

Chapter 19

GEOLOGY AND HYDROGEOLOGY OF TARAWA AND CHRISTMAS ISLAND, KIRIBATI

A.C. FALKLAND and C.D. WOODROFFE

REGIONAL SETTING

The Republic of Kiribati spans more than 45° of longitude in the Central Pacific. The island nation, which straddles the Equator and the International Date Line, consists of 33 small islands, mostly in three distinct archipelagoes. The Gilbert Islands, the western archipelago, consists of 16 islands and lies north of Fiji; the central archipelago, the Phoenix Islands, comprises eight islands and lies north of Samoa; and the Line Islands, in the east, comprise eight islands north of the Cook and Society Islands and south of Hawaii. With one exception, all 33 islands are low-lying atolls or reef-top islands. The exception is Banaba (formerly, Ocean Island), which is a raised atoll west of the Gilberts.

The capital of Kiribati is Tarawa (Fig. 19-1; 1°30′N, 173°00′E), an atoll in the centre of the Gilbert chain. The largest island is Christmas Island (Fig. 19-2; local name, Kiritimati) located at 2°00′N, 157°30′W in the Line Islands. Christmas Island, which is about 3,300 km east of Tarawa, is an infilled atoll. In terms of both geology and hydrogeology, these two islands are the most extensively investigated in Kiribati.

Tarawa is often classified into two parts, North Tarawa and South Tarawa. North Tarawa stretches from the island of Buota in the southeastern corner to the island of Buariki at the northern tip and consists largely of traditional village communities. South Tarawa extends from the island of Bonriki in the southeastern corner to the island of Betio at the western tip and is the "urban", political, administrative, and commercial centre. The populations of North and South Tarawa are about 3,600 and 24,000, respectively (1990 census).

In contrast, Christmas island is sparsely populated. There are about 2,500 people in 5 villages (1990 census).

Climatic and marine setting

Kiribati is influenced by the southeast trade winds for most of the year and is outside the area of cyclonic influence. The climate, particularly rainfall, is strongly influenced by El Niño Southern Oscillation (ENSO) episodes. The rainfall characteristics of the two islands (Fig. 19-3) differ because of their longitudinal position.

Tarawa is located in the humid tropical zone which extends over much of the equatorial Pacific Ocean. The mean annual rainfall (MAR) is 2,024 mm for the

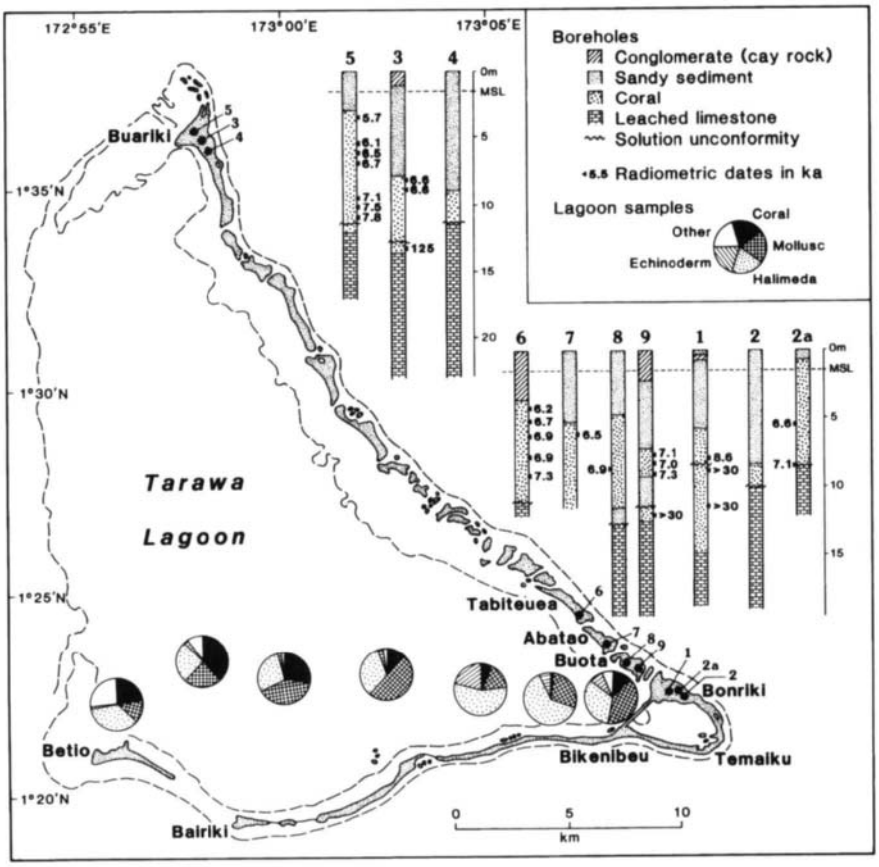


Fig. 19-1. Map of Tarawa showing stratigraphy of selected cores (after Marshall and Jacobson, 1985) and constituent-particle composition of lagoonal sediments (after Weber and Woodhead, 1972). [For location of Tarawa in the Pacific, see Fig. 23-1.]

period of record, 1947–1991; the maximum and minimum annual rainfalls are 3,843 (in 1987) and 398 mm (in 1950), respectively.

Christmas Island is in the dry equatorial zone which extends as a narrow band across the central and eastern parts of the Pacific. MAR for the same period (1947–1991) is only 869 mm. The maximum and minimum annual values are 3,374 (in 1987) and 177 mm (in 1950).

As illustrated by the large differences between maximum and minimum annual rainfalls, interannual variation of rainfall is large throughout Kiribati. The coefficients of variation of annual rainfall (0.45 and 0.7 for Tarawa and Christmas Island, respectively) are higher than many other islands in the tropical oceans (Falkland, 1991). As shown in Fig. 19-3, high rainfalls are associated with ENSO episodes, and drought periods often occur in the intervening periods. There is a strong correlation for both islands between annual rainfall and the Southern

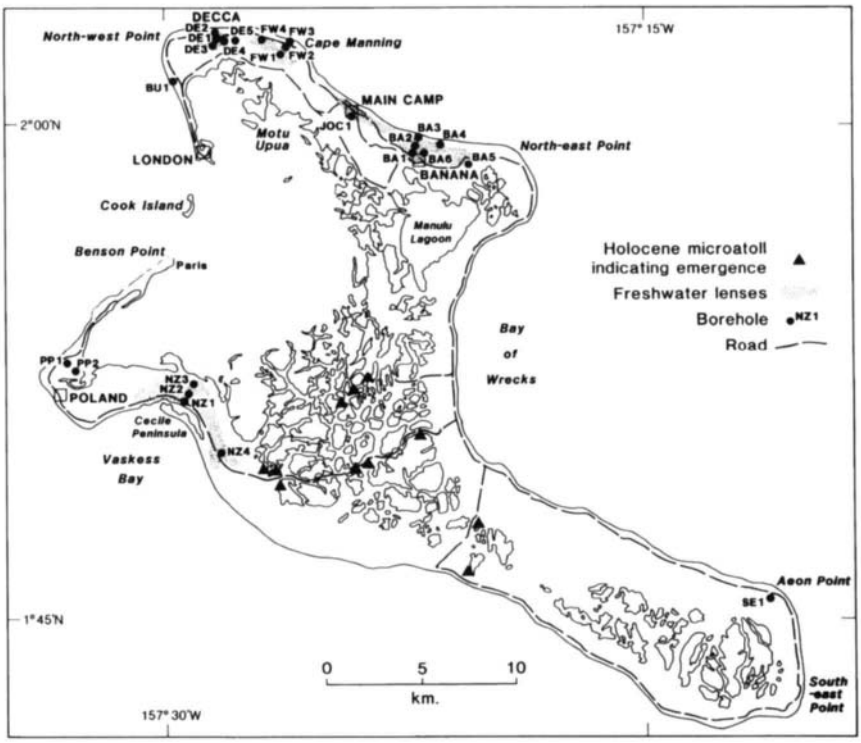


Fig. 19-2. Map of Christmas Island showing the location of fossil and live microatolls, salinity-monitoring boreholes and freshwater lenses. [For location of Christmas Island in the Pacific, see Fig. 12-1.]

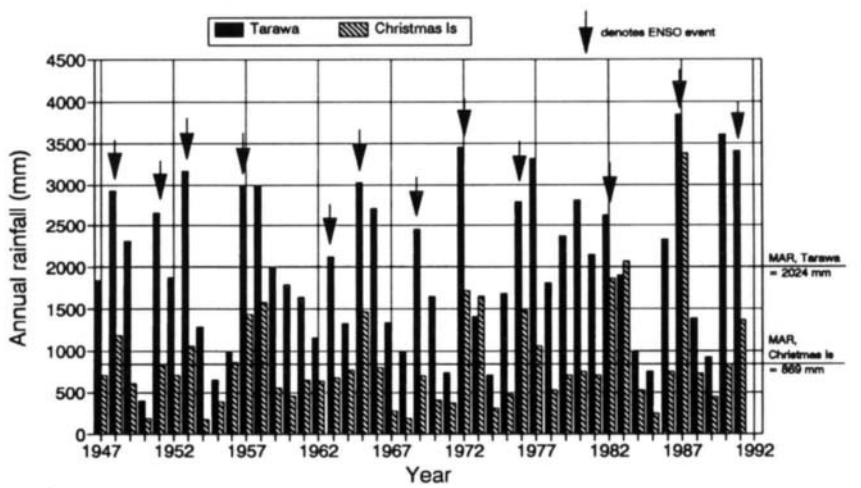


Fig. 19-3. Annual rainfall at Tarawa and Christmas Island, 1947–1991, and the influence of ENSO episodes. MAR denotes mean annual rainfall.

Oscillation Index (SOI). The correlation is particularly strong for Tarawa (Burgess, 1987; Falkland, 1993).

Long dry periods, which are significant for water supply in small islands such as these, occur often on Christmas Island and, with a lesser frequency, on Tarawa. Examples of droughts on Christmas Island are: 23 mm in 9 mo in 1949/1950, 11 mm in 5 mo (1954), 10 mm in 8 mo (1970/1971), 7 mm in 8 mo (1973/1974), 3 mm in 5 mo (1983) and 34 mm in 10 mo (1988/1989). For Tarawa, two of the longest dry periods are 57 mm in 6 mo (1973/1974) and 68 mm in 7 mo (1988/1989).

Although rainfall may vary between sites on individual atolls over short periods (daily, weekly, or even monthly) because of isolated storms, these differences average out over a longer term. Comparison of records at Betio and Bonriki, Tarawa, show generally small differences in monthly rainfall totals for periods of concurrent records (101 mo during the period 1982–1991).

Tidal records have been collected since the 1950s. Both Tarawa and Christmas Island are microtidal with spring tidal ranges <2m. There is a strong seasonal cycle in which the variation of monthly mean sea level is in the order of 0.1–0.2 m. There is also a substantial interannual variation in sea level, up to 40 cm in mean monthly sea level in 1982–1983, due to ENSO episodes (Wyrtki, 1974).

ATOLL MORPHOLOGY AND DEPOSITIONAL ENVIRONMENTS

Although Tarawa and Christmas Island are both atolls rising from an ocean floor more than 4,000 m deep, they are strikingly different in surface morphology. Tarawa (Fig. 19-1) has the typical atoll configuration of reefs (129 km^2) with small islands (totalling 31 km^2) surrounding a central lagoon (329 km^2). Christmas Island (Fig. 19-2), on the other hand, consists of a large land area (320 km^2) and a relatively small lagoon (160 km^2) at the western end, with numerous small enclosed saline lakes (Fig. 19-2). Christmas Island has the largest land area of any atoll in the world.

Tarawa

Tarawa is triangular in shape and measures about 35 km N-S and 28 km W-E. The small reef islands, which occur on the northeastern and southern rims of the atoll, are separated by shallow passages. They are joined by causeways along the southern leg. The lagoon is 6–25 m deep and contains scattered patch reefs and individual coral heads (bommies). The submerged, western rim of the atoll is shallow, 1–5 m deep, except in the main shipping channel which reaches a depth of 20 m.

The reef crest consists of a slightly elevated, intertidal algal rim or pavement. The reef flat is often broad (in places >2 km wide) and is a relatively barren, algae-veneered surface which dries in places at the lowest tides. Around the western atoll rim, this reef grades into the sandy lagoon; around the southern and eastern rims, reef flat and lagoon are separated by elongate islands.

Reef islands are composed of sands with some shingle, but rarely with extensive coral rubble deposits. The oceanward shore is dominated by steep accretionary

beaches in which coral fragments and the foraminifer *Amphistegina* are conspicuous. There are isolated outcrops of a conglomerate platform, which consists of a highly lithified breccia of coral clasts, forming a nearly horizontal upper surface slightly above mean sea level. In places, this conglomerate forms an eroded ramp thinly veneered with sand. Beachrock is a feature of some lagoon shores. The lagoon shore of reef islands merges into the lagoonal sand flats. There are stands of mangrove along the lagoon margins of the more sparsely populated islands.

The lagoonal sediments are predominantly sands, with variable seagrass and algal cover. According to Weber and Woodhead (1972), coral contributes proportionally less to lagoon sediments with distance away from the western reef crest. *Halimeda* and molluscs, on the other hand, become increasingly important and sediments become muddier eastwards across the lagoon and into the sheltered embayed area west of Temaiku (Fig. 19-1). The position and configuration of the lagoon shoreline of islands is much more dynamic than the oceanward shore (Harper, 1989; Byrne, 1991; Howorth and Radke, 1991).

Christmas Island

Shaped like a large lobster claw, Christmas Island (Fig. 19-2) is about 50 km NW-SE and 30 km NE-SW and fills a large proportion of the reef platform on which it sits. The lagoon, which is asymmetrically located, has an intricately embayed shoreline along most of its periphery and is almost closed off by two large peninsulas on the west (Keating, 1992). The peninsulas contain the settlement London, and former settlement Paris. The interior of the island is filled with numerous hypersaline lagoons or lakes with a total surface area of about 150 km^2 (Jenkin and Foale, 1968).

The fringing reef is generally narrow (30–120 m) with a spur-and-groove system on the reef front. Seaward beaches are generally steep and, around much of the island, are composed of coral shingle or platy rubble up to 50 cm in diameter (Wentworth, 1931). The modern beach is generally backed by a sequence of shingle ridges and swales rising 3–4 m above sea level with crest/swale amplitudes of around 1 m. Around the Bay of Wrecks (see Fig. 19-2), these ridge sequences are replaced by dunes which are the highest land on the island (up to about 13 m).

Jenkin and Foale (1968) have differentiated a central ridge with inland dune systems rising up to 5 m above sea level. The central ridge is pronounced along the northern part of the island, where it is separated from the present coast by a lower-lying coastal plain with elongate, land-locked hypersaline lakes (similar lakes occur on the southern coast around Cecile Peninsula). Towards the main lagoon this central ridge is bounded by a gradual scarp (about 1 m high) which is bordered by a broad lagoon flat about 1 m above sea level. The flat is dotted by many scattered hypersaline lakes. These lakes have variable water levels, both between lakes and over time, and salinities of 200–300‰ (Valencia, 1977). Fine-grained muds within the lakes commonly have an algal mat and contain gypsum and/or halite crystals. The sedimentation rate in one of these lakes is estimated to be about 1.8 cm y^{-1} (Valencia, 1977).

The interior of Christmas Island is sparsely vegetated with scrub dominated by *Scaevola*, *Tournefortia* and *Suriana* and with sickly coconut plantations. Much of the interior surface is barren and comprises a calcrete hardpan. As discussed below, Pleistocene limestone crops out locally on the surface and is widespread in the shallow subsurface. Christmas Island has experienced comparatively little, if any, subsidence since the Last Interglacial (Valencia, 1977).

STRATIGRAPHY AND SEA-LEVEL HISTORY

Tarawa

There has been no deep drilling on Tarawa, but underlying volcanic rocks are likely to be several hundreds of metres below sea level (being >300 m deep on Funafuti, Tuvalu, and >1,000 m deep at Bikini and Enewetak, Marshall Islands). The late Quaternary subsurface stratigraphy of Tarawa is known from a series of water-investigation boreholes up to 30 m deep. Marshall and Jacobson (1985) recognize four units (Fig. 19-1). In ascending order these units are: a basal, leached, reefal limestone; a coral unit; unconsolidated sand and gravel; and cemented conglomerate that Marshall and Jacobson (1985) refer to as cay rock (Fig. 19-1).

The Pleistocene limestone comprises skeletal wackestones and packstones, in which there has been some calcitization of corals by vadose and phreatic freshwater diagenesis. The unit is Pleistocene in age and beyond the reach of radiocarbon dating. A U-series date of 125 ± 9 ka (Substage 5e, Last Interglacial) has been determined on a coral at a depth of about 17 m in a borehole on Buariki. In some cores, a solutional unconformity can be recognised between the Pleistocene and the overlying Holocene coral unit. This unconformity occurs at 11–17 m below sea level. In some places, radiocarbon dates indicate that the unconformity occurs within the coral unit, not at the top of the limestone.

Radiocarbon dates of the Holocene units indicate that coral established on the Pleistocene substrate, and coral growth was prolific by 8000 y BP (Fig. 19-4). Dates from several boreholes indicate rapid vertical reef growth at up to 8 mm y^{-1}. According to Marshall and Jacobson (1985), this rapid growth rate suggests that the reefs were catching up with a rising sea level.

The cemented-sand unit (cay rock) represents a subsurface expression of the conglomerate platform that is exposed on the oceanward sides of many of the reef islands, and occurs to about 3 m below sea level. This conglomerate platform is of considerable interest because it has been variously interpreted in relation to Holocene highstands of sea level. The conglomerate at Tarawa and similar deposits at other Pacific islands were interpreted by Schofield (1977a) to have been deposited episodically in response to several second-order transgressions with a highstand of sea level 2760 y B.P. at an elevation as high as 2.3 m above present (Schofield, 1977a); on the other hand, other researchers (Guilcher, 1967) could find no evidence for emergence on Tarawa. The question of Holocene highstand vs. storm deposits is

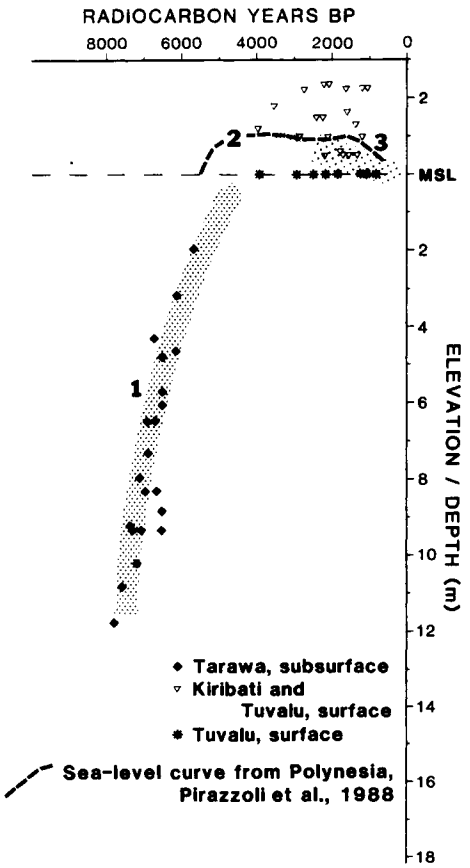


Fig. 19-4. Age-depth plot of radiocarbon dates from Tarawa and other islands of Kiribati and Tuvalu.

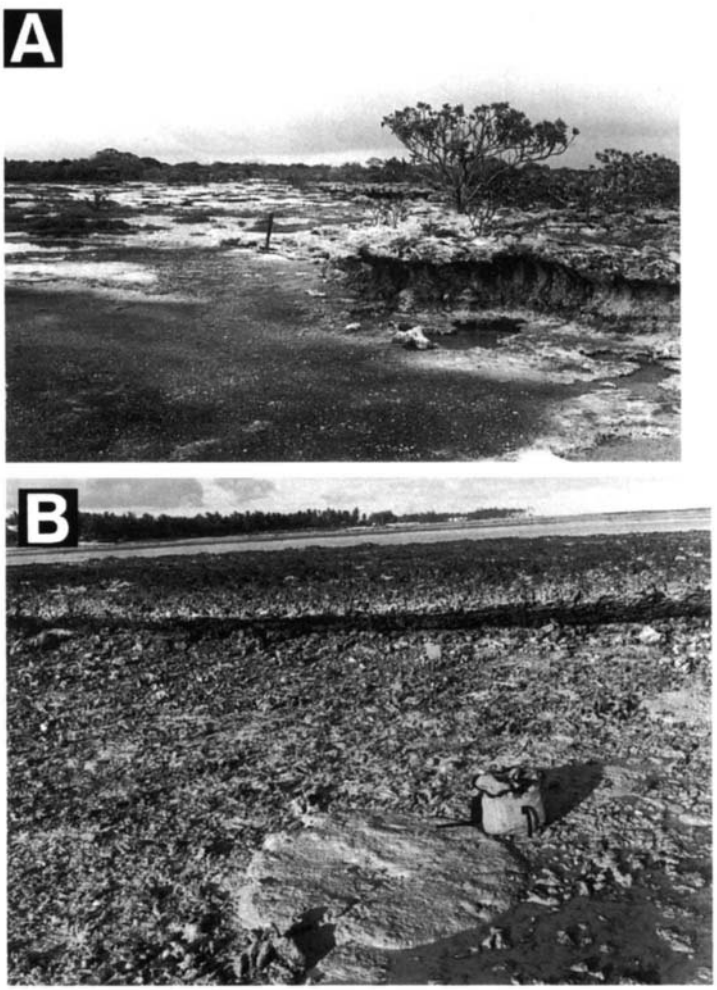
reviewed in Case Study 1 of this chapter. In Tarawa, the balance of evidence favors the interpretation of a late Holocene highstand above present sea level.

Fig. 19-4 is an age-depth plot of radiocarbon dates on subsurface and surface corals and *Tridacna* from a range of studies. Three phases of Holocene development can be identified. Phase 1, the period of rapid vertical reef growth is followed by phase 2, in which reefs caught up with sea level and reef flats formed. Phase 3, since 3500 y B.P., is when the reef islands formed.

Christmas Island

The stratigraphy and thickness of units on Christmas Island reflect a different subsidence history from that of Tarawa. Gravity and magnetic surveys suggest that the thickness of the limestones above the volcanic basement is, in general, only about 120 m thick (Valencia, 1977) and, at the western end of the island, as little as 30 m thick.

Unlike in Tarawa and many other atolls, Pleistocene limestone crops out on the surface on Christmas Island. Isolated outcrops of a heavily lithified and recrystallised limestone containing sparse coral clasts occur within an elongate, infilled lagoon along the northern coast (Fig. 19-5A). A radiocarbon date on this limestone of 26,100 ± 1,800 y B.P. has been obtained (Woodroffe, unpub. data), indicating that the deposit is pre-Holocene. Due to the possibility of contamination during recrystallization of the dated coral material, which contains some calcite, we consider it likely that the actual age of the deposit is significantly larger than indicated by the numerical date and is probably Last Interglacial. Similar Last Interglacial limestones are exposed on other islands in eastern Kiribati (Tracey, 1972; J. Tracey, pers. comm., 1992).



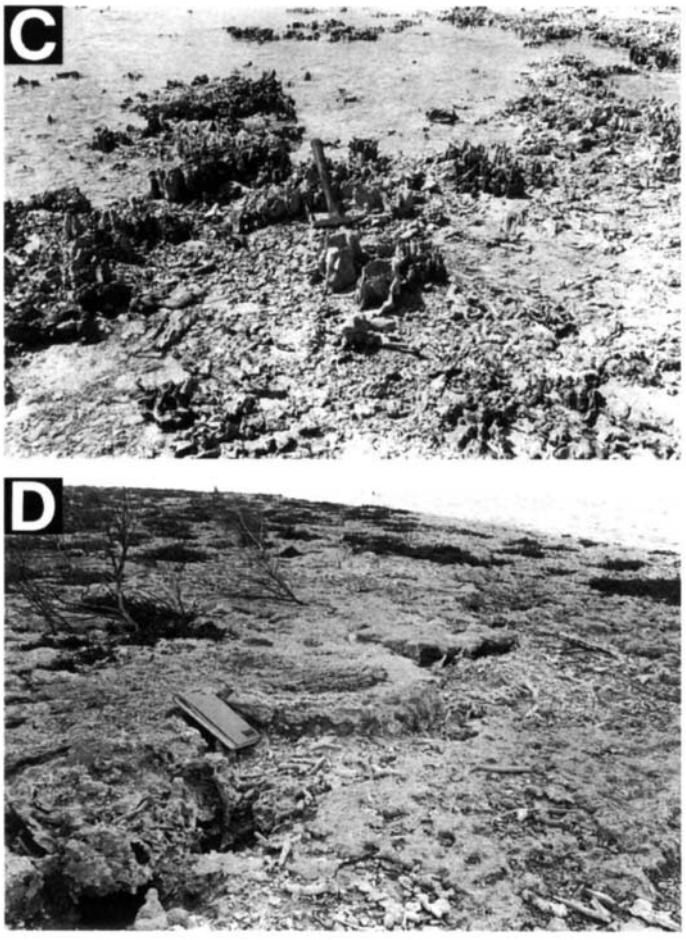


Fig. 19-5. (A) An outcrop of Pleistocene limestone on the northern coast of Christmas Island. (B) Conglomerate platform in South Tarawa. The conglomerate of coral clasts overlies an in situ reef which occurs at an elevation above the present limit of coral growth. (Photo courtesy R. McLean.) (C) In situ *Heliopora* on the reef flat at Abemama. This occurrence is above the modern upper limit of the growth of this species and is another indication of emergence. (D) In situ Holocene corals from the centre of Christmas Island. These corals are radiocarbon-dated as mid-Holocene, and indicate a sea level above present.

Drill cores indicate that the subsurface of the interior of the island is dominated by mollusc-rich calcareous marls. The top 18 m of these marls is predominantly aragonitic. Radiocarbon dating of a sample of *Tridacna* from 9 m and a coral from 13 m from borehole BA1 gave Pleistocene results. The Holocene sediments, therefore, constitute a relatively thin veneer. The drilling results indicate that the contact between unconsolidated sediments and older, harder coral limestone is at 10–20 m (Falkland, 1983), which, at least at some sites, is below the Holocene-Pleistocene

contact as indicated by radiocarbon dates. Much of the molluscan marl in the subsurface interior is probably Pleistocene in age.

The interior hypersaline lakes are fringed by Holocene in situ coral and *Tridacna* assemblages. As discussed in Case Study 1 of this chapter, the occurrence of micro-atolls indicates that the sea has fallen from a level of 50–90 cm above present during the mid and late Holocene. Prior to this fall of sea level, the centre of Christmas Island was dominated by prolific coral growth and more open water exchange.

HYDROGEOLOGY

Tarawa

History of investigations. The freshwater lenses of Tarawa have been the subject of numerous groundwater-resources investigations since the early 1960s by British and Australian consultants, the Bureau of Mineral Resources (BMR) and the Department of Housing and Construction (DHC) of the Australian Government, the Institute of Geological Sciences of the United Kingdom, and various agencies of the United Nations. Early investigations were limited to water levels and water chemistry at dug wells and focused on the resources and siting of infiltration galleries at population centres on South Tarawa. A study by Mather (1973), which included a resistivity survey and limited drilling on the outer islands of Bonriki and Buota, led to a supply of piped water to South Tarawa. Further resistivity surveys in South and North Tarawa and modeling of the known freshwater lenses at Teaoraereke, Bonriki, Buota and Buariki suggested that the potential for further groundwater development was limited and that alternative water sources, therefore, should be considered (Lloyd et al., 1980). The modeling, which made use of the Dupuit-Ghyben-Herzberg (DGH) assumptions (sharp interface, vertical equipotentials, fixed ratio of water-table elevation to depth to interface), predicted large annual variations in the freshwater zone of each lens and suggested that the freshwater lenses would not be sustainable even under very small extraction rates in a 1-in-50-year drought with a duration greater than one year.

During the 1980s, there was an extensive program by the Australian Government to assess freshwater yields (Jacobson and Taylor, 1981; Daniell, 1983). The program involved resistivity surveys, drilling, in situ permeability tests, salinity profiling and monitoring of boreholes, detailed water-balance studies, and DGH modeling. Resulting estimates of the sustainable yield of the major freshwater lenses were in the order of 30% of mean annual recharge, or 10% of MAR. Continued monitoring of the salinity-monitoring boreholes at Bonriki (Falkland, 1992) has confirmed these estimates.

The current approach to water-resources assessment and management in Tarawa and Christmas Island emphasizes tracking the actual behavior of the freshwater lenses with the data from the salinity-monitoring boreholes and comparing that behavior to the time series of recharge and pumping. These data also were used to recalibrate the DGH model from the studies of the 1980s and are intended for future use with variable-density models of the freshwater lenses.

Occurrence of freshwater lenses and distribution of hydraulic conductivity. The adopted limit of freshwater is 600 mg L^{-1} Cl^- (or its equivalent in electrical conductivity, about 2,500 μmhos cm^{-1}). This value is the maximum limit according to the former World Health Organisation guidelines for drinking water (WHO, 1972). In revised guidelines (WHO, 1984, 1993), the recommended maximum limit, based on taste considerations, is 250 mg L^{-1} Cl^{-1}.

Fresh groundwater is generally available on all the islands of Tarawa where the width is greater than about 300 m. Most islands in North Tarawa and part of South Tarawa, therefore, are underlain by freshwater lenses.

The distribution of hydraulic conductivity is like that of other dual-aquifer atoll islands [see Chap. 1]: moderately permeable Holocene deposits overlying highly permeable Pleistocene limestone. The hydraulic conductivity of the sediment cap is known from 180 individual falling-head and constant-head tests (Table 19-1;

Table 19-1

In situ falling-head and constant-head permeability tests.

General.

Tests were conducted on open zones at base of the drill casing during drilling process (see Figs. 19-6 and 19-7).

Installation.

Drill rig: JACRO 500 (Seismic Supply International) at Tarawa; JACRO 200 at Tarawa and Christmas Island. Drill rods and casing: "NW" sized: max. diam., 89 mm. Water-based polymer "mud" was used.

Drilled to desired test depth with 75-mm-diam rock-roller bit attached to drill rods. Extracted drill rods; advanced temporary casing to distance L (Figs. 19-6, 19-7) from base of hole. Re-entered with drill rods and rock-roller bit; used water as drilling fluid to clean open hole below casing. Removed drill rods.

Conducted tests. Re-entered and drilled to next depth.

Falling-head test (Fig. 19-6).

Measured h_1, from top of drill casing (about 1 m above ground) to water table (typically 2–3 m below ground).

Filled casing to overflowing with hose from pit dug 20–30 m away.

Withdrew hose, measured time for water level to drop set distances: 0.5 and 1 m; also 0.25 and 1.5 m where possible.

Equation (Cedergren, 1977, p. 75, variable head column, case e; Hvorslev, 1951):

$$K = D^2 * \ln(2 * L/D) * \ln(h_1/h_2)/[8 * L * (t_2 - t_1)]$$

Typical value: $K = 11.5\,m\,day^{-1}$ for $h_1 = 2\,m$, $h_2 = 1.5\,m$, $(t_2 - t_1) = 5\,s$, $D = 75\,mm$, $L = 1.0\,m$.

Comments: Reasonable accuracy up to about 50 m/day.

Constant-head test (Fig. 19-7).

Experimentally found Q to maintain constant water level in the casing. Hose from same pit as in falling-head test. Q measured with bucket and stopwatch.

Equation (Cedergren, 1977, p. 75, constant head column, case e; Hvorslev, 1951):

$$K = Q * \ln[L/D + (1 + L^2/D^2)^{1/2}]/(6.28 * L * h_c)$$

Typical value: $K = 15.1\,mday^{-1}$ for $Q = 0.5\,L\,s^{-1}$, $h_c = 1.5\,m$, $D = 75\,mm$, $L = 1.0\,m$.

Comments: Reasonably good estimates to about 1000 m/day. Less accurate than falling-head method for $K < 50$ m/day.

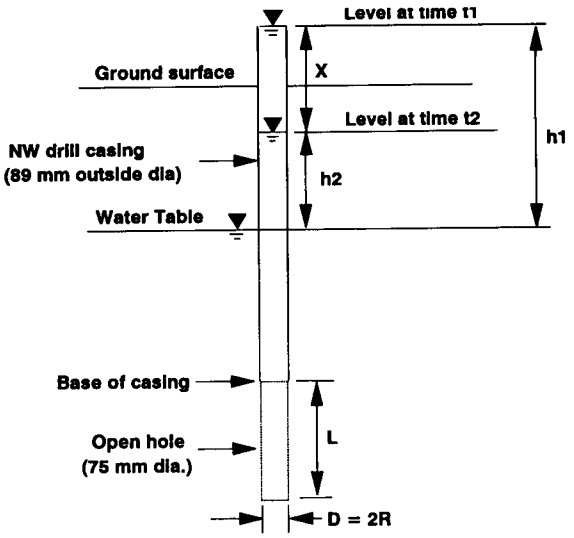


Fig. 19-6. In situ falling-head permeability test. (Adapted from Cedergren, 1977, and based on Hvorslev, 1951.)

Figs. 19-6, 19-7) conducted on 0.8-m-thick open zones at 3-m intervals during drilling of six salinity monitoring boreholes on Bonriki. The results of these tests are summarized in Table 19-2: the average value for the sediments is about 10 m day^{-1}, and there is a general increase with depth within the sediments. In detail, however, the tests reveal considerable heterogeneity, as high-permeability zones occur both above and below the unconformity (denoted by 'U' in Table 19-2). A high value (180 m day^{-1}) of hydraulic conductivity reported by Jacobson and Taylor (1981) from a larger-scale pumping test (7 L s^{-1}) over the full depth of 28 m at a borehole at Buariki (borehole 3 in Fig. 19-1), on the other hand, indicates the effect of the high-permeability limestone near the base of the hole. The reported high salinities obtained during that pumping test also illustrate the problem of inducing saline intrusion into the freshwater zone by conventional pumping tests and the desirability of using the in situ falling-head and constant-head tests in atoll islands.

As shown in Fig. 19-8 for Bonriki, the unconformity between Holocene sediments and Pleistocene limestone tends to act as an upper limit to the depth of freshwater lenses except in the middle of the largest islands. The salinity data of Fig. 19-8 illustrate the results from the DHC salinity-monitoring system, a schematic of which is shown in Fig. 31-6 in the chapter on the Cocos (Keeling) Islands. This monitoring system consists of a set of nylon tubes terminating at 3-m intervals from depths of 6 m to the base of the hole. Typically, seven or eight tubes are in each hole with the base of each tube hydraulically isolated from the others so that water samples representative of each depth can be pumped to the surface and tested. As shown by the results at Bonriki, which has the most extensive monitoring network on Tarawa

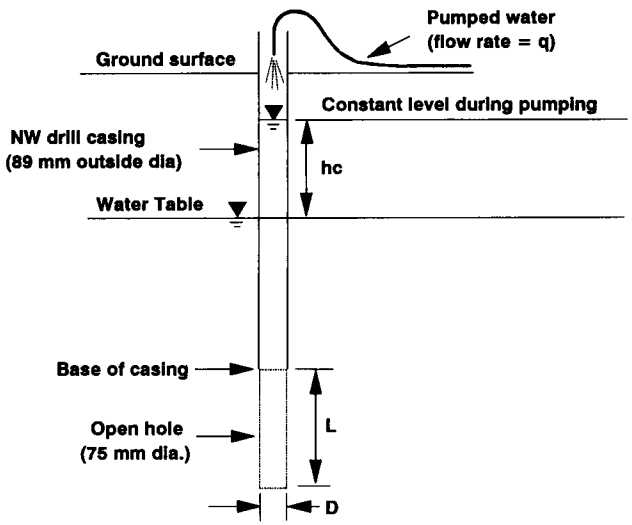


Fig. 19-7. In situ constant-head permeability test. (Adapted from Cedergren, 1977, and based on Hvorslev, 1951.)

(Fig. 19-9), the system allows good definition of the vertical and horizontal distribution of salinity in an island lens.

The thickest part of the freshwater lens at Bonriki is displaced towards the lagoon (Fig. 19-8) — as is the case on many atoll islands. This asymmetry is at least partly due to the higher recharge on the lagoon side owing to clearing of otherwise prolific coconut trees in the vicinity of the airport runway (Fig. 19-8). From the data in Table 19-2, there is no significant lateral variation in hydraulic conductivity at this

Table 19-2

Results of in situ permeability tests, Tarawa.

Borehole	Depth below ground surface (m) (base of hole)								
	6	9	12	15	18	21	24	27	30
BN1 (21 m)	9	12	*	10	*	–			
BN2 (24 m)	3	4	*	8	U*	18	6		
BN4 (30 m)	4	4	*	14	U–	18	6	*	*
BN5 (27 m)	–	10	18	14	10	U12	22	–	
BN7 (21 m)	(54)	25	(54)	*	U–	–			
BN9 (27 m)	12	8	8	*	*	25	U39		

Notes:
Values are hydraulic conductivity (m day^{-1}).
Results of constant-head tests are in brackets; all others are falling-head tests.
–indicates no test.
*indicates permeability beyond limit of test.
U indicates depth to unconformity between coral-bearing sediments and underlying limestone; not detected in BN1.

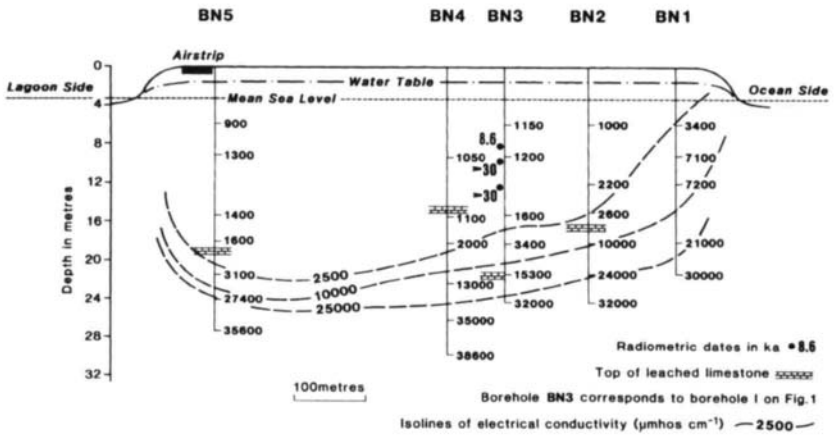


Fig. 19-8. Cross section through Bonriki, Tarawa, showing stratigraphy, radiocarbon ages (Marshall and Jacobson, 1985), and salinity distribution associated with the freshwater lens. The salinity data, shown as electrical conductivity (μmhos cm^{-1}), were obtained during routine monitoring in May, 1985, which was a relatively dry period (Figs. 19-3, 19-12).

cross section, which may mean that the shape of the lens at Bonriki is more influenced by variations in recharge than by variations in hydraulic conductivity.

Fig. 19-8 also shows the across-island variation in thickness of the transition zone at Bonriki. The midline of the transition zone is approximated by the electrical-

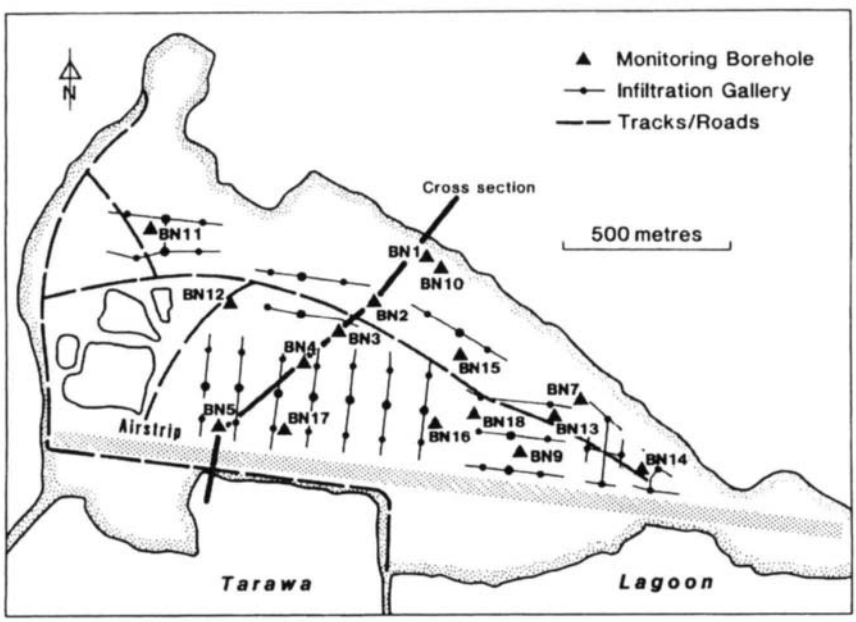


Fig. 19-9. Network of monitoring boreholes and infiltration galleries on Bonriki, Tarawa.

conductivity isoline of 25,000 μmhos cm^{-1}. The depth from the base of freshwater to the midline of the transition zone is at a minimum of 4 m where the freshwater zone is thickest near borehole BN5. As discussed below, this transition-zone thickness does not vary significantly through wet and dry periods nor does it vary much areally: over the period of monitoring from 1980 to 1992, the vertical distance between the base of the freshwater and the midline of the transition zone was 3–10 m at all salinity-monitoring boreholes on Bonriki.

The freshwater lens at Bonriki is one of the two largest lenses in Tarawa. The other is on Buariki (Fig. 19-1). The maximum freshwater thickness at Bonriki over the 12-y monitoring period was about 23 m (Falkland, 1992), and the maximum freshwater thickness at Buariki in 1980 was 29 m (Jacobson and Taylor, 1981). The maximum widths of these islands are 1,000 m and 1,200 m respectively. The pattern throughout Tarawa is that the thickness and volume of the freshwater lenses tend to increase as the width of the island increases.

Marginal groundwater is found on all of the islands of Tarawa either between the lateral extent of the freshwater lenses and the edges of the islands or on islands where no permanent freshwater lens exists. Due to the high population density along South Tarawa, the freshwater lenses there are largely polluted. Well water is, however, often used for nonpotable purposes, and chlorinated potable water is piped in from the freshwater lenses of largely unpopulated areas of Bonriki and Buota.

Recharge and temporal variability of freshwater lenses. Recharge has been calculated for Tarawa for 1948–1991 from a water-balance method using daily values of rainfall (Falkland, 1992). The rationale and assumptions of the method and some details of the calculations are presented in Case Study 2 of this chapter. The values of annual recharge for Bonriki are summarised in Fig. 19-10 together with the annual rainfall values. The recharge values assume that 80% of the island is covered by

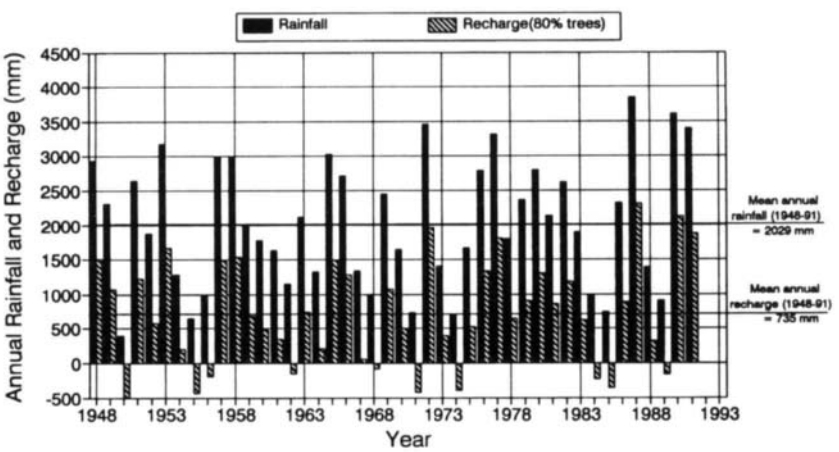


Fig. 19-10. Annual rainfall and recharge at Bonriki, Tarawa, for the period 1948–1991.

coconut trees. Over the full period of analysis, the estimated average recharge for Bonriki is 735 mm y^{-1} or 36% of the rainfall over this period (2,029 mm y^{-1}).

The assumed proportion of deep-rooted trees (mainly coconut trees) has an impact on the calculated recharge, because the water-balance model allows for extraction of the trees' transpiration requirements even when the soil-moisture zone is depleted of water. One of the effects of this extraction is that the calculated recharge can be negative in some years (e.g., 1950, 1955 and 1956; see Fig. 19-10), thus representing a net loss of water from the lens. The analysis also shows that if the coconut tree cover were reduced by half to 40%, the average recharge would be increased by about 14% to about 840 mm y^{-1}. Thus selective clearing would improve recharge. Such a land-management decision, however, would need to take into account the trade-offs between maximising freshwater resources by clearing trees and minimising the impact on the food potential and other benefits derived from maintaining coconut trees at maximum densities. In the event of total clearing, the average recharge could be increased to a maximum of about 1,020 mm y^{-1} or about 50% of average rainfall.

As shown in Fig. 19-10, years of high rainfall are generally accompanied by high recharge and vice versa. The relationship is not simple, however, because recharge depends not only on the total but on the time series of rainfall. For this reason, it is important for water-balance calculations to use actual rainfall data, preferably on a daily basis but at least on a monthly basis, rather than monthly averages. Using the information of Fig. 19-10, approximate relationships between measured annual rainfall and the corresponding estimated recharge were derived using linear regression analyses. Fig. 19-11 shows the results of these analyses for three assumed tree-cover percentages. The regression equations, correlation coefficients (r) and standard errors of estimate (SEE) are:

$$Re = 0.83Ra - 951 \text{ (80\% tree cover; } r = 0.99, SEE = 76 \text{ mm)},$$

$$Re = 0.75Ra - 684 \text{ (40\% tree cover; } r = 0.99, SEE = 92 \text{ mm)},$$

$$Re = 0.70Ra - 390 \text{ (no tree cover; } r = 0.99, SEE = 95 \text{ mm)},$$

where Re and Ra are annual recharge and rainfall, respectively, and both are in mm. These relationships, of course, are specific to Tarawa and are not transferable to other islands without further research; however, they illustrate the significance of the deep-rooted vegetation.

Fig. 19-12 compares the calculated monthly values of recharge with the depths to the base of the freshwater zone and the midline of the transition zone at a representative salinity-monitoring borehole (BN4) in the centre of the Bonriki freshwater lens. Clearly, the base of the freshwater lens rises during drought periods (1984–85, 1988–89) and deepens during periods of high recharge (1986–87). The midline of the transition zone rises and falls with the base of the freshwater lens.

Transition zone. The areal variation of the transition zone at Bonriki is shown in Fig. 19-8. Volker et al. (1985) developed an analytical model for the thickness of the transition zone and applied it to the same cross section as shown in Fig. 19-8. The

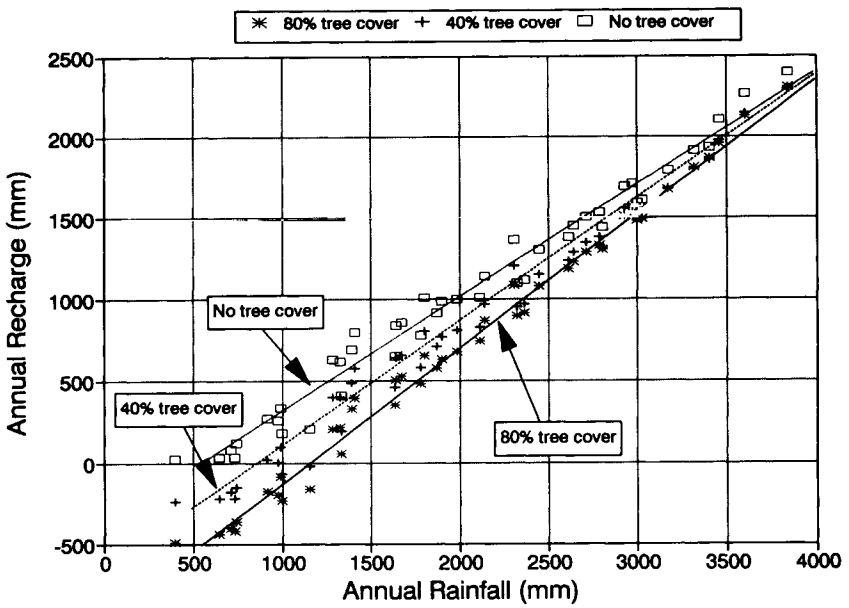


Fig. 19-11. Relationship between annual rainfall and annual recharge on Tarawa for three possible vegetation conditions (80%, 40% and zero tree cover).

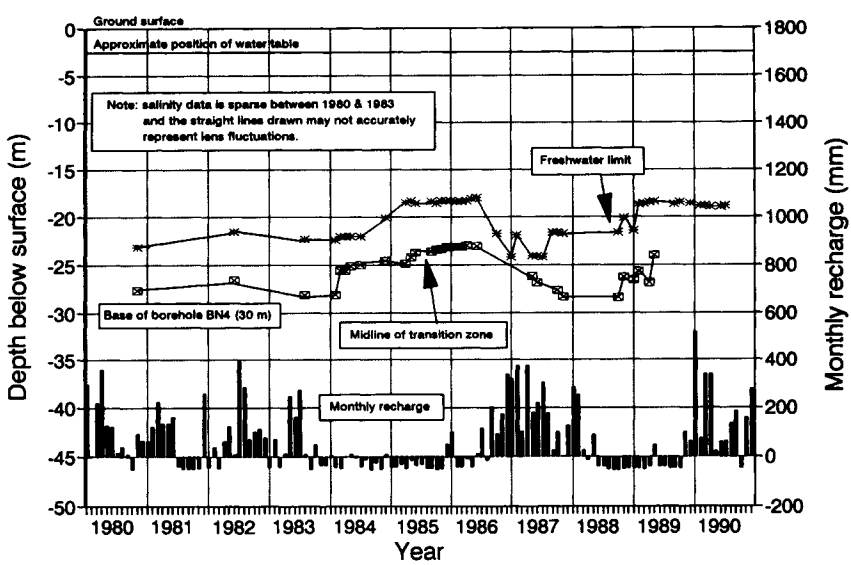


Fig. 19-12. Variations in monthly recharge, thickness of the freshwater lens, and depth to transition zone at borehole BN4, Bonriki, Tarawa, 1980–1990.

model treats the transition zone as a mixing layer between fluids moving at different velocities. The model uses steady-state estimates of recharge and sea level and, therefore, does not account for tidally induced mixing near the edges of the island. Near the centre of the island, model-generated and observed salinity-depth variations show general agreement. One of the features of the boundary-layer model, however, is that thickness varies inversely with the radius of curvature, so the predicted transition zone would be thickest in the centre of the island and thinnest near the edges. In practice, the opposite is observed to be the case (Fig. 19-8), undoubtedly because of tides (see Underwood et al., 1992).

Christmas Island

History of investigations. Following several reconnaissance-level surveys of Christmas Island by U.K. Governmental agencies for the purpose of assessing either groundwater resources or the potential of coconut plantations, the DHC of the Australian Government carried out detailed hydrological investigations in the early 1980s (Falkland, 1983; 1984a). In general, these investigations were like those of Tarawa in that they included extensive resistivity surveys, drilling and salinity monitoring of boreholes, in situ permeability tests, water-balance calculations and DGH modeling.

Occurrence of freshwater lenses. Four main freshwater lenses (Fig. 19-2) were mapped as part of the DHC study. Another lens was indicated in the southeast peninsula by a single borehole (SE1), but the extent of this lens is not known because investigations were limited in this area. Several minor lenses were indicated in other areas from resistivity surveys. Overall, the lenses were found to be discontinuous despite the relatively large width of the island.

It is thought that the discontinuous nature of the lenses is due to major lateral variations in hydraulic conductivity, which may be caused by lateral variations in the depth to the unconformity between Holocene and Pleistocene sediments. Certainly, surface features such as soils and vegetation are not a good predictor of the presence of freshwater. In particular, presence of coconut trees could not be used in many areas, because they had been purposely planted in the marginal water areas on the lagoon flats to allow young plants to obtain moisture at shallow depths. In places where the depth to fresher water was greater, like in the sand ridges between ocean and lagoon, young coconut trees often were not capable of surviving drought periods as their roots had not penetrated to the water table.

The magnitude of water-table fluctuations and the elevation of the water table itself are both poor guides to the thickness of freshwater in Christmas Island. For example, the head at DE2 and DE3, which are about 500 m apart (Figs. 19-2, 19-13), was 0.40–0.45 m above sea level in both cases at a time when the thickness of the freshwater zone, as determined from adjacent boreholes, was 1 m at DE2 and 8 m at DE3. This and other observations confirmed the need for salinity-monitoring boreholes, as opposed to simple water-table monitoring, as the main means of tracking the behaviour of the freshwater lens.

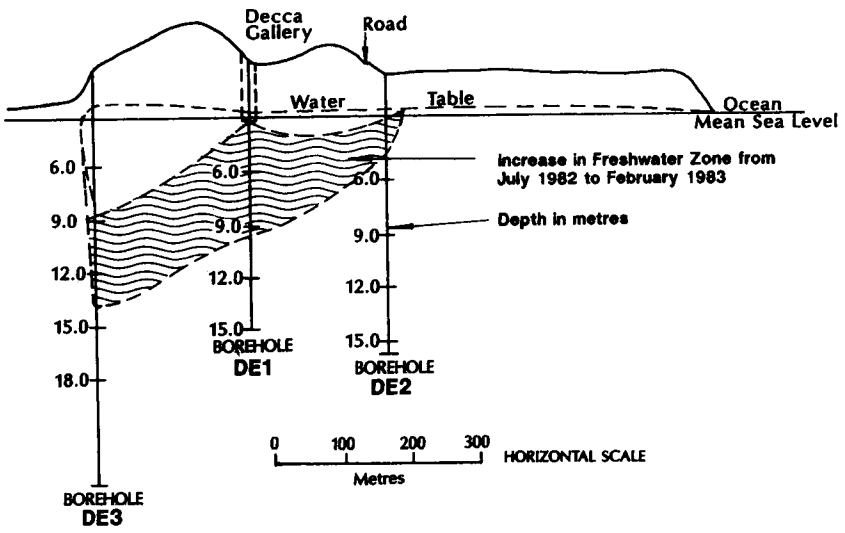


Fig. 19-13. Saline intrusion caused by high pumping and recovery of the lens due to high recharge at Decca gallery, Christmas Island, during 1982/1983 ENSO episode. Locations of the monitoring boreholes DE1, DE2 and DE3 are shown in Fig. 19-2.

Table 19-3

Results of in situ permeability tests, Christmas Island

Borehole	Depth below ground surface (m) (base of hole)						
	6	9	12	15	18	21	24
DE3 (24 m)	–	7	–	2	4	–	–
	(2)	(24)	(177)	–	–	–	–
DE5 (19 m)	11	24	14	–	–		
	(56)	(72)	(25)	–	–		
FW1 (27 m)	8	39	4	–	13		–
	(10)	(49)	(3)	(22)	(89)	–	–
BA1 (18 m)	4	13	7	3	2		
	(4)	(27)	(3)	(11)	(7)		
BA6 (27 m)	–	–	5	28	9	16	–
	(4)	(11)	(10)	(45)	(25)	(65)	–
NZ2 (22 m)	5	9	10	5	–	–	
	(17)	(17)	(16)	(18)	–	–	
NZ3 (16 m)	22	36	8	6			
	(47)	(71)	–	(26)			

Notes:
Values are hydraulic conductivity (m day^{-1}).
Results of constant-head tests are in brackets; all others are falling-head tests.
– indicates no test.

Distribution of hydraulic conductivity. Nearly 500 in situ permeability tests (Table 19-1) were conducted on Christmas Island. The results (Table 19-3) show considerable variability and a tendency for hydraulic conductivity to increase with depth, especially for the constant-head tests. For boreholes located within freshwater lenses, the mean value of permeability within the freshwater zones is about 6 m day^{-1}.

A similar value for hydraulic conductivity was obtained by applying Ferris's model (Ferris, 1951) for the dampening of the tidal signal recorded along a line of boreholes across the Banana freshwater lens (BA1, BA2, and BA3 of Fig. 19-2). Although this model, which assumes simple lateral propagation of the tidal signal, is known to be inapplicable at many atolls and reef-related islands because of the dual-aquifer structure of the island, the data at the Banana lens show an appropriate increase in the tidal lag and decrease in tidal amplitude, from the ocean to the largely land-locked lagoon. The values of hydraulic conductivity calculated from the Ferris model at Banana lens are 2–10 m day^{-1} with a mean of about 5 m day^{-1}.

Recharge and temporal variability of lenses. Water-balance accounting like that used for Tarawa (see Case Study 2) was used to calculate recharge at locations of freshwater lenses on Christmas island at various times (e.g., Falkland, 1984a). Monthly rather than daily rainfall was used because a full sequence of daily rainfall data was not available at the time.

Results of the water-balance analyses for Christmas Island show that recharge is very much lower than on Tarawa and, like Tarawa, depends on the density of coconut trees (Falkland, 1984a). For the analysis period 1949–1982, the recharge was estimated to be about 250 mm y^{-1} or only 29% of MAR (847 mm during the period) for an area completely devoid of coconut trees. For areas with 10%, 30% and 50% tree coverage, the average recharge estimates drop to, respectively, 210, 150 and 95 mm y^{-1} (or 25%, 18% and 11% of MAR).

Because monthly rather than daily rainfall was used in the analyses, these recharge values are considered underestimates. The degree of underestimation is about 5% based on comparisons of recharge estimates from daily and monthly rainfall data for the period 1980–1984.

The time series of monthly recharge from the water-balance analyses provides a clear indication of droughts and wet periods. Fig. 19-14 shows the monthly recharge for the New Zealand Airfield area, which is estimated to have a 10% tree cover.

Fig. 19-14 also shows how the base of the freshwater zone at four salinity-monitoring boreholes in the New Zealand lens responds to the calculated recharge. In periods of high recharge, which are mainly associated with ENSO episodes (e.g., 1982–83 and 1987), the freshwater zone substantially increases, and during the dry intervening periods gradually decreases. The effects on the lens at these boreholes is entirely due to natural influences as there is no pumping occurring in their vicinity.

The average residence time (or turnover time) of the New Zealand Airfield lens appears to be about 17 years, from the average recharge rate (210 mm y^{-1}), average thickness of the freshwater zone (12 m; Fig. 19-14) and a value of 0.30 for effective porosity based on laboratory core analyses (Falkland, 1984a) and observations of freshwater increase after major recharge events. This simple calculation is used only

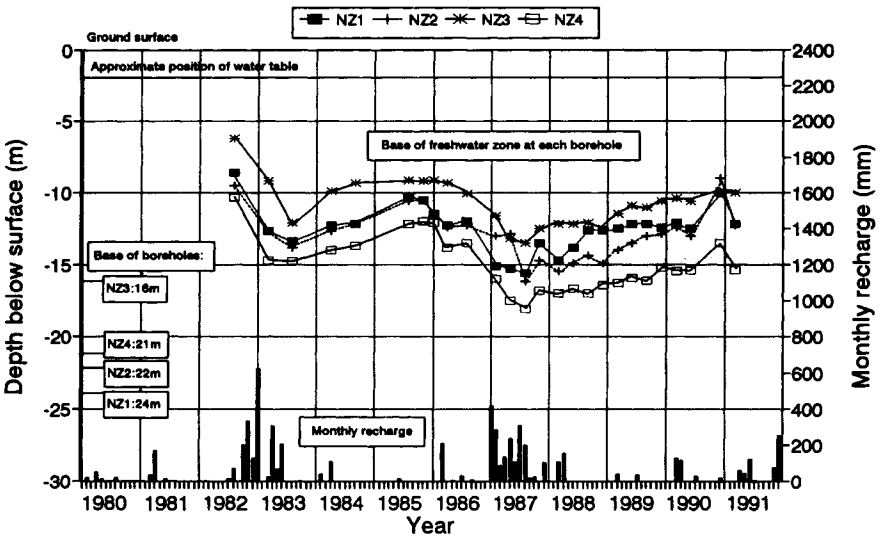


Fig. 19-14. Variation of monthly recharge and depth to the base of freshwater lens at four boreholes, New Zealand Airfield lens, Christmas Island, 1980–1991.

as a guide, as it does not take account of the dispersion process at the base of the lens [see Chap. 22]. The result is consistent, however, with the findings from radiological tests (in 1982) that there was no remaining tritium at any level within the lens from atmospheric nuclear tests conducted near the island in the 1950s and 1960s. From the 1982 tritium data, residence times in all freshwater lenses on Christmas Island are less than 20 years (Falkland, 1984a).

WATER RESOURCES

Development of groundwater in both Tarawa and Christmas Island has made extensive use of infiltration galleries [see also Chap. 31, Fig. 31-10]. In South Tarawa before the 1960s, the supply was by individual hand-dug wells and household rainwater tanks. In the 1960s, infiltration galleries were constructed first at the main centres and then on uninhabited land (Teaoraereke) with water piped back to the villages. In the mid-1970s, galleries were developed on the islands of Bonriki and Buota, and a pipeline was constructed along South Tarawa to distribute the water to consumers primarily at communal tanks. Each gallery consisted of a central well with four 15-m radial arms constructed from butt-jointed hollow concrete blocks. The total pumping rate in 1977 was about 85 m^3 day^{-1} from Bonriki, the same from Buota, and 40 m^3 day^{-1} from Teaoraereke.

The freshwater lenses at Bonriki and Buota were extensively developed in the 1980s. Seventeen infiltration galleries, each 300 m long and consisting of buried slotted PVC pipe, were constructed at Bonriki (Fig. 19-9); all but one of the old

galleries were abandoned. Six similar galleries were constructed at Buota and the old galleries abandoned. Excavation to below water table and backfilling of the PVC pipes were done by a combination of mechanical and manual methods. The total pumping rate was designed to be 750 m^3 day^{-1} from Bonriki and 250 m^3 day^{-1} from Buota. Since the commissioning of the new scheme, the total pumping rate has gradually increased to a total of about 1,300 m^3 day^{-1} from the Bonriki and Buota freshwater lenses (Falkland, 1992). The original operating strategy of resting pumps on a cyclical basis is no longer practiced. All 24 pumps currently operate continuously at an average rate of about 54 m^3 day^{-1} (0.6 L s^{-1}). The effect on the salinity of the freshwater lens is being monitored at the galleries and the monitoring boreholes. To date, the increased pumping rate has not indicated any adverse effects.

Reticulated water supplies were first constructed on Christmas Island as part of infrastructure development for the atmospheric nuclear tests conducted in the late 1950s and early 1960s by the United Kingdom and United States. The freshwater lenses at Decca, Main Camp, Banana and New Zealand Airfield were developed using open-trench infiltration galleries. Typically, a 50- to 100-m-long trench was excavated to just below the water table and stabilised with vertical side walls to above the water table. Simple gabled roofs were placed over the trenches to lower the evaporation rate, but they provide no obstacle to the entry of animals, notably crabs and birds.

Although new infiltration galleries have been recommended (Falkland, 1984b), open-trench gallery systems are still in use on Christmas Island today. Owing to large pumping rates, upconing of saltwater normally occurs, particularly at the Decca gallery (near borehole DE1 in Fig. 19-2) where the pumping rate is about 5 L s^{-1}. Fortunately, high recharge events such as that associated with the 1982/1983 ENSO episode can reverse the upconing (Fig. 19-13). The recommended galleries are similar in design to those at Tarawa but of greater length (at least 400 m) and lower pumping rate (0.3 L s^{-1}).

CASE STUDY 1: MID-HOLOCENE HIGHSTAND

Whether or not the sea has been higher than present in the central Pacific during the Holocene has been a controversial issue. David and Sweet (1904) interpreted fossil corals on Funafuti to indicate that the sea had been higher, and Cloud (1952) came to a similar conclusion on Onotoa in the southern Gilbert Islands. Guilcher (1967) could find no evidence for emergence on Tarawa. The CARMARSEL expedition to the Caroline and Marshall Islands similarly interpreted material from above sea level as storm deposits (Shepard et al., 1967) and found no unequivocal support for a Holocene sea level above present. However, other workers on Enewetak did interpret fossil corals above the modern upper limit to coral growth to indicate emergence (Tracey and Ladd, 1974; Buddemeier et al., 1975).

On the basis of radiocarbon dating, particularly of giant clams *Tridacna*, principally from Funafuti in Tuvalu, Schofield (1977a) proposed that oscillations of sea level up to 2.4 m above present at 2760 y B.P. could be identified in Kiribati and

Tuvalu (a sample at 2.3 m above sea level was dated from Bikenibeu, Tarawa). He further suggested that reef islands of atolls might have formed primarily as a result of the subsequent fall in sea level (Schofield, 1977b). His samples are plotted in Figure 19-4. However, there can be little doubt that Schofield interpreted some clasts from within the conglomerate platform as indicating higher sea level when these samples were not in situ.

Our observations indicate that on Tarawa, as on neighbouring atolls such as Maiana, Kuria and Abemama, there are fossil corals in growth position preserved beneath the conglomerate platform, but above the modern limit of coral growth (Fig. 19-5B). These are sometimes microatoll forms of *Porites* and branching heads of the blue octocoral *Heliopora*, which appear to have been constrained in terms of vertical growth by sea level (Fig. 19-5C). These fossil corals are characteristically 0.7–0.8 m above their modern living counterparts (Woodroffe and McLean, unpub. data).

There is similar evidence for a mid-Holocene sea-level highstand on Christmas Island. The interior hypersaline lagoons are fringed by Holocene in situ coral and *Tridacna* assemblages (Fig. 19-5D). Delicate subfossil branching *Acropora* corals are preserved in their position of growth, adjacent to microatolls of *Porites*. Radiocarbon dates on these indicate an age range of 4610 to 1680 y B.P. (Woodroffe and McLean, unpub. data). Surveying indicates that these fossil microatolls lie 0.5–0.9 m above their modern equivalents, and the sea appears to have fallen from around this level since the mid-Holocene. Similar emergence is indicated for a number of atolls in the Phoenix Island group of Kiribati, including Enderbury, Jarvis, Malden and Starbuck (Tracey, 1972) and for Kanton (Guinther 1978). Prior to this fall in sea level, the centre of Christmas Island was dominated by prolific coral growth, and more open water exchange.

The identification of a mid-Holocene highstand of sea level in Kiribati is consistent with its recognition widely throughout the Pacific (Hopley, 1987). Convincing evidence for such a highstand 1–2 m above present has been reported from throughout French Polynesia (Pirazzoli and Montaggioni, 1988; Pirazzoli et al., 1987, 1988). Similar evidence has also been reported from several locations in Fiji (Ash, 1987; Miyata et al., 1990), Austral Islands (Pirazzoli and Veeh, 1987), Cook Islands (Yonekura et al., 1988; Woodroffe et al., 1990), Guam (Kayanne et al., 1993) and Hawaii (Matsumoto et al., 1988; Jones, 1992). This Holocene high stand of sea level, although widespread, can still not be regarded as ubiquitous throughout the region; its occurrence in Tuvalu, for instance, still remains unproven (McLean and Hosking, 1991).

CASE STUDY 2: CALCULATING THE WATER BALANCE FOR TARAWA

A water-balance method was used to estimate recharge to the freshwater lenses on Tarawa and Christmas Island. The purpose of this Case Study is to describe the calculation for Tarawa and point out some of the findings that illuminate the hydrologic cycle on these atoll islands. The same method has been used to calculate the recharge on the Cocos (Keeling) Islands (Falkland, 1994; Chap. 31 of this book).

The time series of the calculated recharge values is compared to the time series for the size of freshwater lenses in Figures 19-12, 19-14, and 31-9.

Procedure

The water-balance method is based on a relatively simple mass-balance procedure that is given in more detail in Falkland (1991). The conceptual model is shown in Fig. 19-15. For the surface of a low-lying carbonate island, the water-balance equation can be expressed as

$$P = AET + R \pm dV$$

where P is precipitation, AET is actual evapotranspiration, R is recharge to groundwater, and dV is the change in the soil-moisture store. As these islands have thin, permeable soils and highly permeable subsurface geology, surface runoff does not need to be taken into account in the equation. AET, in turn, is broken into three primary constituents (see Fig. 19-15),

$$AET = E_I + E_S + T_L,$$

where E_I is evaporation from the interception store; E_S is evapotranspiration from the soil-moisture store; and T_L is transpiration by deep-rooted vegetation directly from groundwater. From combination of these two equations and solving for the recharge,

$$R = P - (E_I + E_S + T_L) \pm dV,$$

which is the water-balance equation used in the calculations.

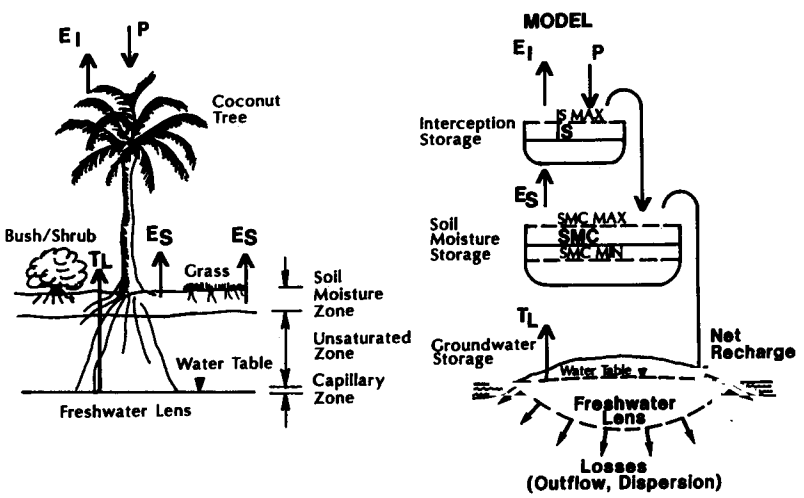


Fig. 19-15. Structure and terms for water-balance model used to calculate recharge for a typical low-lying carbonate island.

A computer program was written to simulate the water balance at the island's surface and derive a monthly time series of recharge. The principal input is daily rainfall and estimates of monthly potential evapotranspiration (PET). Computations were conducted with a daily time interval. Using monthly rather than daily rainfall tends to underestimate the recharge (Falkland, 1991).

The PET estimates are derived from mean monthly pan evaporation data for 1981–1991 using a pan coefficient of 0.8 (Falkland, 1992). Mean monthly pan data were used because Falkland (1994) found in the study at Cocos (Keeling) Islands that similar results (recharge estimates) were obtained using either actual monthly values of PET or mean monthly values of PET (Chap. 31 of this book). This finding is consistent with the generally low interannual variation of potential evaporation for particular months in humid tropical environments, including Tarawa. For simplicity, therefore, mean monthly PET estimates were used for the Tarawa study. The value for the pan coefficient is based on comparison of PET estimates from evaporation pans and the Penman method on other tropical islands including the Cocos (Keeling) Islands (Falkland, 1994). A sensitivity analysis shows that small variations of the pan coefficient either side of 0.8 makes little difference to recharge estimates for Tarawa. Earlier estimates of PET (Fleming, 1987) using the Penman method (Penman, 1956), made prior to the collection of pan evaporation data, are consistent with a pan coefficient of approximately 0.8.

In the water-balance model, it is assumed that rainfall firstly fills the interception store (to a maximum value ISMAX) with the residual (or overflow) entering the soil-moisture zone (SMZ). Typical values of ISMAX are 1 mm for predominantly grassed areas and 3 mm for areas consisting predominantly of trees (particularly coconut trees). Evaporation is assumed to occur from the interception store at the potential rate.

The SMZ is the store from which the roots of shallow-rooted vegetation (grasses, bushes) and the shallow roots of trees can obtain water (Fig. 19-15). Water requirements of plants tapping water from the SMZ are assumed to be met before any excess drains to the water table. For Tarawa, the SMZ is typically 300–500 mm thick based on observations from shallow pits and wells. A maximum soil-moisture limit (SMCMAX, which occurs at field capacity, FC) and a minimum soil-moisture limit (SMCMIN, which occurs at wilting point, WP) are set. Above FC, water is assumed to drain to the water table. Below WP, no further evaporatranspiration is assumed to occur and the shallow-rooted vegetation wilts and possibly dies. For Tarawa, FC is assumed to be 0.15 based on observations of local soil type and typical values for this type of soil, and WP is assumed to be 0.05 based on typical values (e.g., Linsley and Franzini, 1973) for sand-type soils. The operating range of soil moisture is thus assumed to be 25–75 mm.

The amount of evapotranspiration from the SMZ is assumed to vary linearly with the available soil-moisture content. Thus, evapotranspiration from the SMZ is assumed to be nil at WP, equal to PET at FC, and equal to PET/2 midway between WP and FC.

In the water-balance model, vegetation types are assigned "crop factors" (Doorenbos and Pruitt, 1977) according to their type. The crop factor is a coefficient

used to derive an adjusted, "crop"-specific value of potential evapotranspiration from that of a "reference crop". The reference-crop evapotranspiration is effectively equal to PET. As the predominant vegetation types on Tarawa are coconut trees and a variety of grasses and other shallow-rooted vegetation, only these types were considered. Based on values in Doorenbos and Pruitt (1977), a crop factor of 1.0 was assumed for grasses and shallow-rooted vegetation, and a value of 0.8 was assumed for coconut trees. Thus, the rate of potential evapotranspiration rate for coconut trees is taken to be 80% of PET, while that for grasses or other shallow-rooted vegetation is assumed to be equal to PET.

The proportions of freshwater lens areas covered by deep-rooted vegetation were estimated from ground observations. In islands with a thick coverage of coconut tree, this proportion is 100%. In islands with limited clearing for houses and possible air strips, the proportion is generally 70–90%. In urban areas with limited trees remaining, the proportion is typically <30% and may, in extreme cases, be zero.

The excess water remaining after evaporative demands E_I and E_S are met passes down to the water table. This water is assumed in the model to be "gross recharge" to the freshwater lens. A further evaporative loss (T_L) occurs due to transpiration of trees and plants whose roots penetrate to the water table. The water remaining after T_L is deducted from the gross recharge is "net recharge". Observations in pits on a number of atolls reveal that a considerable number of roots penetrate to the capillary fringe just above the water table at typical depths of about 1–2 m below ground level. It is estimated that 25–50% of the roots from mature coconut trees penetrate to the water table. Because the movement of the water table is relatively small, even during drought periods, these roots enable transpiration when the soil-moisture store has been depleted. Thus, coconut trees are able to survive prolonged drought periods on coral atolls when other shallow-rooted vegetation has wilted and possibly died.

Table 19-4 shows sample water-balance calculations using daily rainfall data for the island of Bonriki on Tarawa (Figs. 19-1, 19-9). The results are summarised in monthly segments over the two years 1989 and 1990 and are part of a 44-year water-balance simulation starting in 1948 and ending in 1991. Input data were: ISMAX, 3 mm; SMZ, 500 mm; FC, 0.15; WP, 0.05; ratio of deep-rooted vegetation to shallow-rooted vegetation, 0.8 (i.e. 80% tree cover); proportion of roots of deep-rooted vegetation reaching the water table, 0.5; proportion of roots reaching the water table, 0.5; crop factor for shallow-rooted vegetation, 1.0; and crop factor for trees (predominantly coconut trees), 0.8. Initial values (in 1948) of water in the interception store and the soil-moisture store were assumed to be 1 mm and 50 mm, respectively. These initial values make very little difference to the results, particularly for long sequences of data such as the 44-year period used in this example.

Discussion of results

The results in Table 19-4 show the effects of a dry year (1989) and a wet year (1990) on the hydrologic cycle in Tarawa. The total rainfall in 1989 (916 mm) was

Table 19-4

Water-balance calculations for 1989 and 1990, Tarawa

Month	P mm	PET mm	E_I mm	SMC1 mm	E_S mm	XCESS mm	SMC2 mm	GWR mm	T_L mm	AET mm	NETR mm	Recharge ratio
1989												
Jan	6	149	6	30	4	−4	26	0	46	55	−46	−8.34
Feb	7	143	6	26	2	−0	26	0	44	51	−44	−6.30
Mar	34	156	11	26	13	10	36	0	47	70	−47	−1.37
Apr	72	144	20	36	18	34	66	4	40	78	−36	−0.50
May	171	141	39	66	45	87	71	82	33	117	49	+0.29
June	12	134	12	71	34	−34	38	0	39	85	−39	−3.21
July	20	136	15	38	10	−5	32	0	39	64	−39	−1.98
Aug	40	156	22	32	16	2	34	0	43	81	−43	−1.07
Sept	72	166	23	34	23	26	60	0	46	91	−46	−0.64
Oct	63	171	26	60	46	−9	51	0	46	118	−46	−0.74
Nov	235	154	39	51	35	161	75	137	37	110	101	+0.43
Dec	185	144	51	75	47	87	68	94	30	127	64	+0.35
TOTAL	916	1795	269		292			318	488	1049	−171	−0.19
1990												
Jan	643	149	54	68	47	543	62	549	30	131	518	+0.81
Feb	187	143	28	62	45	114	66	110	37	110	73	+0.39
Mar	477	156	57	66	45	374	71	370	32	134	338	+0.71
Apr	468	144	61	71	42	365	71	365	27	129	339	+0.72
May	144	141	41	71	47	56	69	58	32	120	25	+0.18
June	173	134	37	69	41	96	73	92	31	109	60	+0.35
July	171	136	38	73	45	89	66	95	32	114	64	+0.37
Aug	271	156	52	66	51	168	66	168	33	136	135	+0.50
Sept	337	166	49	66	56	232	75	223	37	143	186	+0.55
Oct	19	171	10	75	42	−33	34	8	52	104	−44	−2.28
Nov	308	154	44	34	42	223	63	194	35	121	159	+0.52
Dec	407	144	54	63	40	314	71	305	29	122	276	+0.68
TOTAL	3605	1795	522		542			2537	407	1472	2130	+0.59

P: sum of daily rainfall values. PET: potential evapotranspiration. E_I: interception loss. SMC1: soil-moisture content, start of month. E_S: evaporation from soil moisture store. XCESS: $P-(E_I + E_S)$. SMC2: soil moisture content, end of month. GWR: gross recharge to freshwater lens. T_L: transpiration from deep-rooted vegetation. AET: sum $(E_I + E_S + T_L)$, NETR: net recharge $(GWR - T_L)$. RECHARGE RATIO: ratio, NETR/P.

only 45% of the long-term MAR. By comparison, the rainfall in 1990 (3,605 mm) was about 80% greater than MAR.

As shown in Table 19-4 and Fig. 19-10, the recharge in 1989 was negative reflecting a net loss from groundwater of about 170 mm. Heavy rainfall in November and December of that year prevented this loss from being even larger. For 1990, the recharge was estimated to be 2,130 mm or 59% of the total rainfall. For the period 1948–1991, the mean annual recharge was calculated to be 735 mm (36% of MAR).

The sample calculations in Table 19-4 show the relative magnitudes of evapotranspiration losses. Annual PET, obtained from the sum of monthly values, is estimated to be 1,795 mm. In 1989 (dry year) and 1,990 (wet), the AET values were calculated as 1,049 and 1,472 mm (58% and 82%, respectively, of PET), showing the general tendency for annual AET to be higher in wet years than in dry years. This tendency is clearly shown in Fig. 19-16 by the relationship between annual rainfall and AET using the results of the 44-year simulation for an assumed 80% tree cover. In wet years, interception and soil-moisture stores are filled closer to capacity for longer periods than in dry years, thus enabling evapotranspiration to occur closer to potential rates.

The amounts and relative proportions of the three evapotranspiration components also can be seen from Table 19-4. For 1989 (dry year), E_I, E_S and T_L were 26%, 28%, and 46%, respectively, of the total AET (1,049 mm for the year). For 1990 (wet year), they were 35%, 37% and 28%, respectively, of AET (1,472 mm). Thus, the evaporative losses from the interception (E_I) and soil-moisture stores (E_S)

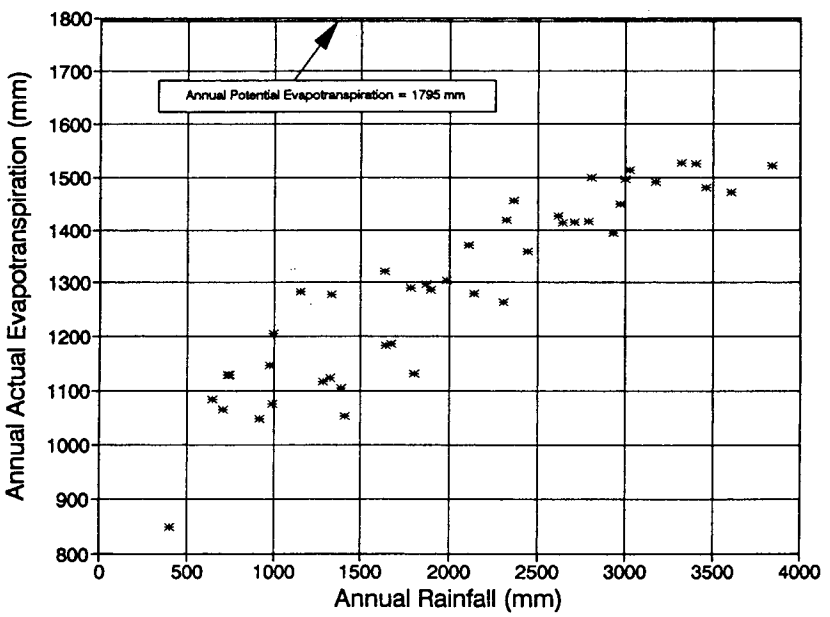


Fig. 19-16. Plot of calculated annual, actual evapotranspiration vs. annual rainfall, Bonriki, Tarawa. Calculation of AET assumes 80% tree cover.

are much greater in the wetter than the drier year. Transpiration losses directly from groundwater (T_L) by phreatophytes, primarily coconut trees, are slightly higher in absolute terms in the drier than the wetter year (488 mm in 1989 vs. 407 mm in 1990), although, as a proportion of AET, T_L is much greater in 1989 (46%) than in 1990 (28%). The reduction in T_L in the wetter year is caused primarily by the large increase in E_I and E_S which acts to meet much of the evaporative demand. Over the full period 1948–1991, the relationships between the annual values of the three evapotranspiration components and the corresponding annual rainfall values are as shown in Fig. 19-17. With increasing annual rainfall, the annual values of both E_I and E_S increase, and the annual values of T_L decrease.

Annual values of the three components of evapotranspiration and the corresponding values of recharge are shown in Fig. 19-18 for the period 1948–1991. This figure shows the time series and relative magnitudes of these four variables which sum to equal the annual rainfall. This figure, together with Fig. 19-10 (time series of rainfall) and Fig. 19-3 (time series of rainfall in relation to ENSO events) summarises the annual hydrologic cycle in Tarawa.

The water-balance calculations indicate that the effect of deep-rooted vegetation, primarily coconut trees, is very significant. If all trees were removed, the mean annual recharge would increase to about 1,020 mm or about 50% of MAR. Annual evapotranspiration losses would be restricted to the soil-moisture zone and average about 1,000 mm. If Bonriki had been totally cleared of trees, the recharge estimates for 1989 and 1990 would be 268 and 2,264 mm, respectively, or 29% and 63% of the respective annual rainfalls. The differences between rainfall and recharge in the two

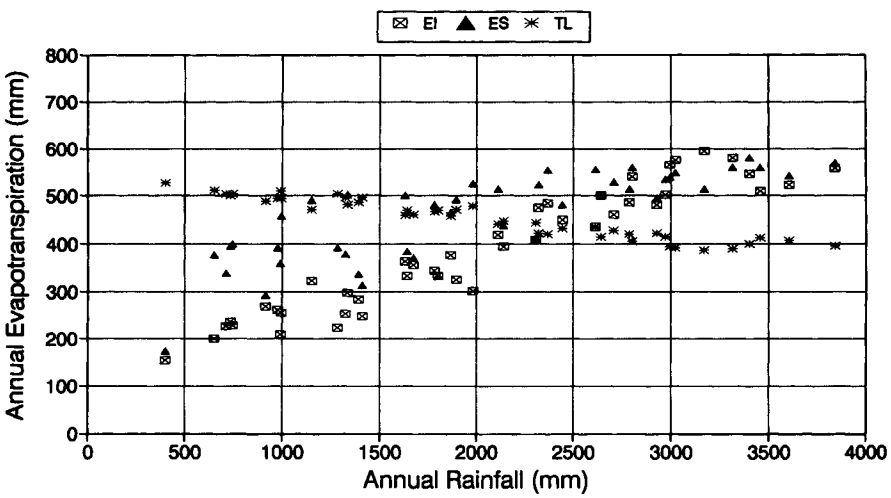


Fig. 19-17. Plot of calculated annual values for the three components of AET vs. annual rainfall, Tarawa. E_I is evaporation from interception store; E_S is evapotranspiration from soil moisture; and T_L is transpiration by deep-rooted vegetation directly from groundwater. Model assumes 80% tree cover.

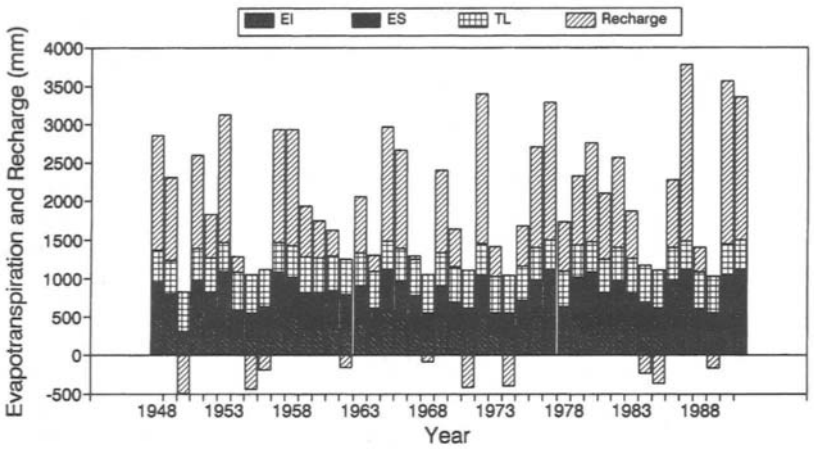


Fig. 19-18. Time series showing year-to-year variations of recharge and the components of AET (E_I, E_S and T_L), Bonriki, Tarawa, 1948–1991.

years (71% and 27%, respectively) represents evapotranspiration from the soil-moisture zone and interception losses from shallow-rooted vegetation.

CONCLUDING REMARKS

Whereas Tarawa is a triangular atoll with discontinuous reef islands on its eastern and southern margins, Christmas Island, 3,300 km to the east, is an infilled atoll with land almost completely filling the reef platform except for a small lagoon at the western end and numerous interior hypersaline lagoons. On Tarawa, there is evidence of subsidence: Pleistocene limestone, from which corals have been dated as Last Interglacial in age, occurs at depths of 11–17 m below sea level; Holocene corals re-established around 8000 y B.P., and vertical growth was rapid as the reefs strived to catch up with sea level. Christmas Island, on the other hand, does not appear to be subsiding; the underlying volcanic basement may be shallow, and limestones of probable Last Interglacial age are exposed on the northern margin of the island.

At both places, there is evidence of higher sea levels during the Holocene. At Tarawa, a mid-Holocene position of sea level 0.7–0.8 m above present is indicated by fossil microatolls in growth position within a conglomerate platform, over which the sand reef islands have accumulated during the late Holocene. On Christmas Island, even though the depth of the Holocene-Pleistocene contact appears variable, there is widespread evidence of a recent fall of sea level from a mid-Holocene level 0.5–0.9 m above present, similar to that in Tarawa.

Extensive hydrogeologic and water-resources investigations on Tarawa and Christmas Island have combined drilling and geophysics programs, in situ permeability testing, long-term monitoring of the three-dimensional distribution of salinity, and water-budget hydrological accounting. The programs provide data and

analysis both over wide areas and in considerable detail at selected locations. Networks of salinity-monitoring boreholes, albeit in a somewhat reduced form, are still being regularly monitored on both atolls. The database from some boreholes now extends over a period of 15 years. These networks may provide the most extensive detailed datasets of atoll-island freshwater lenses in the world.

From review of water-resources data and the monitoring of the freshwater lenses, it appears that the lenses on Tarawa are very robust and capable of withstanding long periods of drought. Monitoring of the pumped lenses at Bonriki and Buota have shown the installation of an extensive network of infiltration galleries to be the most effective means of water-resources development. Skimming water off the entire surface of freshwater lenses has maintained low salinity levels.

On Christmas Island, inappropriately high pumping in localised areas has caused marked increases in salinity especially during dry periods. The onset of high recharge, associated with ENSO episodes, has shown that freshwater lenses can recover even with high pumping rates. A new water-supply system based on extensive gallery systems, which has been designed for many years, is due to be installed in 1997–1998.

The studies on Tarawa and Christmas Island demonstrate the benefit of maintaining a water-resource monitoring program, however difficult it may be. The increased knowledge from direct observation of the behaviour of the freshwater lenses leads to an improved general understanding of the lenses and, more specifically, an ability to make informed decisions about pumping strategies.

ACKNOWLEDGMENTS

The authors wish to acknowledge Richard Miller of the Department of Geography, University of Wollongong for preparing many of the figures for this chapter. Much of the hydrologeological data collection and analysis of results for both Tarawa and Christmas Island was funded by the Australian International Development Assistance Bureau. The efforts of the drillers, Peter Murphy and Bryan Turner, in drilling and equipping an effective network of salinity-monitoring boreholes, most of which are still being monitored to the present date, are acknowledged. Ongoing collection of salinity-monitoring data is carried out by a number of dedicated Kiribati government personnel on Tarawa and Christmas Island and periodically analysed by personnel from ACT Electricity & Water. The efforts of Kath Hunt who has assisted in updating the database for both islands are gratefully acknowledged.

REFERENCES

Ash, J. 1987. Holocene sea levels in northern Viti Levu, Fiji. N.Z. J. Geol. Geophys., 30: 431–435.

Buddemeier, R.W., Smith, S.V. and Kinzie, R.A., 1975. Holocene windward reef-flat history, Enewetak Atoll. Geol. Soc. Am. Bull., 86: 1581–1584.

Burgess, S.M., 1987. The climate and weather of Western Kiribati. N.Z. Meteorol. Serv., Wellington, 188(7).

Byrne, G., 1991. Sediment movement on Tarawa, Kiribati. Proc. Workshop, Coastal Processes, South Pacific Nations (Lae, 1987), CCOP/SOPAC Tech. Bull. 7: 155–159.

Cedergren H.R., 1977. Seepage, Drainage and Flow Nets. 2nd ed., Wiley Interscience, New York, 534 pp.

Cloud, P.E., 1952. Preliminary report on geology and marine environments of Onotoa Atoll, Gilbert Islands. Atoll Res. Bull., 12: 1–73.

Daniell T., 1983. Investigations employed for determining yield of the groundwater resources of Tarawa atoll, Kiribati. Proc. Meeting on Water Resources Development in the South Pacific. U.N. Water Resour. Ser., 57: 108–120.

David, T.W.E. and Sweet, G., 1904. The geology of Funafuti. In: Coral Reef Committee of the Royal Society, The Atoll of Funafuti. The Royal Society, London, pp. 61–124.

Doorenbos, J. and Pruitt W.O., 1977. Guidelines for Predicting Crop Water Requirements. Irrigation and Drainage Paper 24 (revised). FAO (U.N.), Rome.

Falkland, A.C., 1983. Groundwater resource study of Christmas Island, Republic of Kiribati. Proc. Int. Conf. on Groundwater and Man (Sydney), pp. 47–56.

Falkland, A.C., 1984a. Assessment of groundwater resources on coral atolls: case studies of Tarawa and Christmas Island, Republic of Kiribati. Proc. Regional Workshop on Water Resour. Small Islands (Suva). Commonw. Sci. Counc. Tech. Publ. Ser. 154(2): 261–276.

Falkland, A.C., 1984b. Development of groundwater resources on coral atolls: experiences from Tarawa and Christmas Island, Republic of Kiribati. Proc. Regional Workshop on Water Resources of Small Islands (Suva). Commonw. Sci. Counc. Tech. Publ. Ser. 154(2): 436–452.

Falkland, A.C. (Editor), 1991. Hydrology and Water Resources of Small Islands, A Practical Guide. Studies and Reports in Hydrology 49. UNESCO, Paris, 435 pp.

Falkland, A.C., 1992. Review of Tarawa freshwater lenses, Republic of Kiribati. Hydrology and Water Resources Branch, ACT Electricity and Water, Rep. 92/682, Canberra, Australia (unpublished report).

Falkland, A.C., 1993. Hydrology and water management on small tropical islands. Proc. Symp. Hydrology of Warm Humid Regions. Int. Assoc. Hydrol. Sci. Publ., 216: 263–303.

Falkland, A.C., 1994. Climate, hydrology and water resources of the Cocos (Keeling) Islands. Atoll Res. Bull., 400: 1–52.

Ferris, J.G., 1951. Cyclic fluctuations of water level as a basis for determining aquifer transmissibility. Assem. Gen. Bruxelles, Assoc. Int. Hydrol. Sci., 2: 149–155.

Fleming P.M., 1987. The role of radiation estimation in the areal water balance in tropical regions: a review. Arch. Hydrobiol. Beih., 28: 19–27.

Guilcher, A., 1967. Les îles Gilbert comparées aux Tuamotus. J. Soc. Océanistes, 23: 101–113.

Guinther, E.B., 1978. Observations on terrestrial surface and subsurface water as related to island morphology at Canton atoll. Atoll Res. Bull., 221: 171–183.

Harper, J.R., 1989. Follow-up survey of the Betio-Bairiki causeway, Tarawa, Republic of Kiribati. CCOP/SOPAC Tech. Rep. 86.

Howorth, R. and Radke, B., 1991. Investigation of historical evidence of shoreline changes: Betio, Tarawa Atoll, Kiribati, and Fongafale, Funafuti Atoll, Tuvalu. Proc. Workshop Coastal Processes, South Pacific Nations (Lae, 1987), CCOP/SOPAC Tech. Bull. 7: 91–98.

Hopley, D., 1987. Holocene sea-level changes in Australasia and the Southern Pacific. In: R.J.N. Devoy (Editor), Sea surface studies: a global review. Croom Helm, London, pp. 375–408.

Hvorslev, M.J., 1951. Time lag and soil permeability in groundwater observations. U.S. Army Corps Engineers Waterways Expt. Sta. (Vicksburg MS), Bull. 36.

Jacobson G. and Taylor F.J., 1981. Hydrogeology of Tarawa atoll, Kiribati. Bur. Miner. Resour. (Aust.), Record 1981/31.

Jenkin, R.N. and Foale, M.A., 1968. An investigation of the coconut-growing potential of Christmas Island. Directorate of Overseas Surveys (England), Land Resour. Div., Land Resour. Study 4.

Jones, A.T., 1992. Holocene coral reef on Kauai, Hawaii: evidence for a sea-level highstand in the central Pacific. In: C.H. Fletcher III and J.F. Wehmiller (Editors), Quaternary Coasts of the United States: Marine and Lacustrine Systems. SEPM (Soc. Sediment. Geol.) Spec. Publ., 48: 267–271.

Kayanne, H., Ishii, T., Matsumoto, E. and Yonekura, N., 1993. Late Holocene sea-level change on Rota and Guam, Mariana Islands, and its constraint on geophysical predictions. Quat. Res., 40: 189–200.

Keating, B.H., 1992. Insular geology of the Line Islands. In: B.H. Keating and B.R. Bolton, (Editors), Geology and Offshore Mineral Resources of the Central Pacific Basin. Circum-Pacific Counc. Energy & Mineral Resour., Earth Sci. Ser., 14. New York, Springer-Verlag, pp. 77–99.

Linsley, R.K. and Franzini, J.B., 1972. Water Resources Engineering. 2nd ed., McGraw-Hill, New York, 690 pp.

Lloyd, J.W., Miles, J.C., Chessman, G.R. and Bugg, S.F., 1980. A ground-water resources study of a Pacific Ocean atoll — Tarawa, Gilbert Islands. Water Res. Bull., 16: 646–653.

McLean, R.F. and Hosking, P.L., 1991. Geomorphology of reef islands and atoll motu in Tuvalu. South Pac. J. Nat. Sci., 11: 167–189.

Marshall, J.F. and Jacobson, G., 1985. Holocene growth of a mid-plate atoll: Tarawa, Kiribati. Coral Reefs, 4: 11–17.

Mather J.D., 1973. The groundwater resources of Southern Tarawa, Gilbert and Ellice Islands. Hydrogeol. Dep., Inst. Geol. Sci., U.K.

Matsumoto, E., Matsushima, Y., Miyata, T. and Maeda, Y., 1988. Holocene high sea-level stand on Kauai, Hawaii. In N. Yonekura (Editor), Sea-level changes and tectonics in the middle Pacific. Rep. HIPAC Proj., Dep. Geogr., Univ. Tokyo, pp. 91–99.

Miyata, T., Maeda, Y., Matsumoto, Y., Rodda, P., Sugimura, A. and Kayanne, H., 1990. Evidence for a high sea-level stand, Vanua Levu, Fiji. Quat. Res., 33, 352–359.

Penman H.L. (1956). Estimating evapotranspiration. Trans. Am. Geophys. Union, 37: 43–46.

Pirazzoli, P.A. and Montaggioni, L.F., 1988. Holocene sea-level changes in French Polynesia. Palaeogeogr. Palaeoclimatol. Palaeoecol., 68: 153–175.

Pirazzoli, P.A. and Veeh, H.H., 1987. Age 230Th/234U d'une encoche emergee et vitesse de soulevement quaternaire a Rurutu, iles Australes. Compt. Rend. Acad. Sci., 305: 919–923.

Pirazzoli, P.A., Montaggioni, L.F., Vergnaud-Grazzini, C. and Saliege, J.F., 1987. Late Holocene sea levels and coral reef development in Vahitahi Atoll, eastern Tuamotu Islands, Pacific Ocean. Mar. Geol., 76, 105–116.

Pirazzoli, P.A., Montaggioni, L.F., Salvat, B. and Faure, G., 1988. Late Holocene sea level indicators from twelve atolls in the central and eastern Tuamotus (Pacific Ocean). Coral Reefs, 7: 57–68.

Schofield, J.C., 1977a. Late Holocene sea-level, Gilbert and Ellice Islands, west central Pacific Ocean. N.Z. J. Geol. Geophys., 20: 503–529.

Schofield, J.C., 1977b. Effect of Late Holocene sea-level fall on atoll development. N.Z. J. Geol. Geophys., 20: 531–536.

Shepard, F.P., Curray, J.R., Newman, W.A., Bloom, A.L., Newell, N.D., Tracey, J.I. and Veeh, H.H., 1967. Holocene changes in sea level: evidence in Micronesia. Science, 157: 542–544.

Tracey, J.I., 1972. Holocene emergent reefs in the central Pacific (abstr.). Am. Quat. Assoc., Second Natl. Conf. Abstr., pp. 51–52.

Tracey, J.I. and Ladd, H.S., 1974. Quaternary history of Eniwetok and Bikini atolls, Marshall Islands. Proc. Second Int. Coral Reef Symp. (Brisbane)., 2: 537–550.

Underwood, M.R., Peterson, F.L. and Voss, C.I., 1992. Groundwater lens dynamics of atoll islands. Water Resour. Res., 28: 2889–2902.

Valencia, M.J., 1977. Christmas Island (Pacific Ocean): reconnaissance geologic observations. Atoll Res. Bull., 197.

Volker R.E., Mariño M.A and Rolston D.E. (1985). Transition zone width in ground water on ocean atolls. Am. Soc. Civil Eng. J. Hyd. Eng., 111: 659–676.

Weber, J.N. and Woodhead, P.M.J., 1972. Carbonate lagoon and beach sediments of Tarawa Atoll, Gilbert Islands. Atoll Res. Bull., 157: 1–21.

Wentworth, C.K., 1931. Geology of the Pacific equatorial islands. Occasional Pap. Bernice P. Bishop Mus., Occasional Pap., 9(15). Honolulu, 25 pp.

WHO (World Health Organization), 1971. International standards for drinking-water. 3rd ed., WHO (U.N), Geneva.

WHO (World Health Organization), 1984. Guidelines for drinking-water quality. WHO (U.N.), Geneva.

WHO (World Health Organization), 1993. Guidelines for drinking-water quality, 2nd ed. WHO (U.N.), Geneva.

Woodroffe, C.D., Stoddart, D.R., Spencer, T., Scoffin, T.P. and Tudhope, A.W., 1990. Holocene emergence in the Cook Islands, South Pacific. Coral Reefs, 9: 31–39.

Wyrtki, K., 1974. Sea level and the seasonal fluctuations of the equatorial currents in the western Pacific Ocean. J. Geophys. Oceanography., 4: 91–103.

Yonekura, N., Ishii, T., Maeda, Y., Matsushima, Y., Matsumoto, E. and Kayanne, H., 1988. Holocene fringing reefs and sea-level change in Mangaia Island, southern Cook Islands. Palaeogeogr. Palaeoclimatol. Palaeoecol., 68: 177–188.

Geology and Hydrogeology of Carbonate Islands. Developments in Sedimentology 54
edited by H.L. Vacher and T. Quinn
© 1997 Elsevier Science B.V. All rights reserved.

Chapter 20

HYDROGEOLOGY OF THE MARSHALL ISLANDS

FRANK L. PETERSON

INTRODUCTION

The Republic of the Marshall Islands consists of 33 atolls containing some 1,136 separate islands in the west central Pacific (Mink, 1986). The atolls are aligned in a NW-SE direction and extend over a distance of nearly 1,100 km (Fig. 20-1). They form two roughly parallel chains, the eastern Ratak (sunrise) group and the western Ralik (sunset) group.

The indigenous people of the Marshall Islands are Micronesians. The first European contact was by Spanish explorer Alvaro Saavedra in 1529. However, the islands' general lack of wealth and resources did not encourage exploitation until 1885, when Germany declared the Marshall Islands a protectorate. In 1914, Japan took control of the Marshall Islands and after 1919 administered them under a League of Nations mandate. During World War II, U.S. forces occupied the Marshall Islands after heavy fighting on Kwajalein and Enewetak, and in 1947 the Marshall Islands became a U.S. trust territory. Finally, in 1986, under a compact of free association, the Republic of the Marshall Islands became fully self-governing and took control of all its internal and foreign affairs. Today the principal economic activities are still subsistence farming and fishing, with increasing effort being directed toward development of a tourist industry.

Although the Republic encompasses nearly 500,000 km^2 of ocean, the total exposed land area is only about 176 km^2 (Mink, 1986). Individual atoll islands are seldom larger than a few square kilometers and average only a few meters in elevation. Owing to their very small size, the lack of freshwater, and the danger of overtopping by storm waves, few of the islands are inhabited. The majority of the population lives on four major atolls: Majuro, the capital; Kwajalein, a center of U.S. defense activity; Jaluit; and Arno. The only public water systems in the Marshall Islands exist on several large islands in these atolls. Elsewhere, individual households obtain water from rainfall catchments and shallow dug wells (Mink, 1986). Most of the hydrogeologic information that serves as the basis for this chapter, therefore, comes from investigations conducted on the major atolls. In addition, a considerable body of information, especially geologic information, is from investigations conducted on Bikini and Enewetak Atolls prior to and after nuclear weapons testing during the 1940s and 1950s (Arnow, 1954; Emery et al., 1954; Ladd and Schlanger, 1960; Ristvet et al., 1978; Schlanger, 1963; Tracey and Ladd, 1974) [see also Chaps. 21, 22].

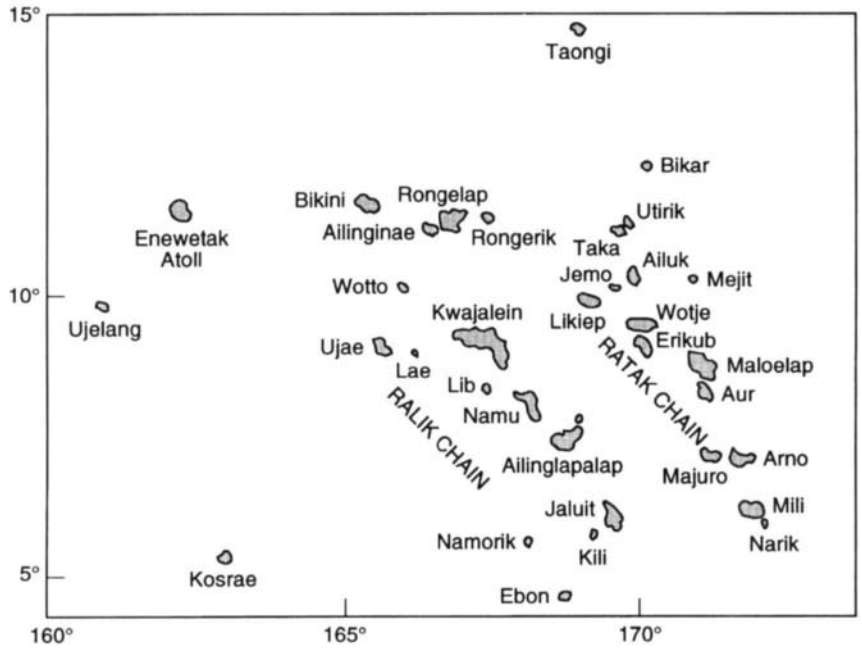


Fig. 20-1. The Republic of the Marshall Islands.

CLIMATE

The climate is hot and humid, with an average annual temperature of 27.2°C. The rainfall generally increases from northwest to southeast, with Majuro, in the far southeast, averaging approximately 356 cm y^{-1} (NOAA, 1984); Kwajalein, roughly in the middle of the Republic, averaging about 260 cm y^{-1} (Hunt and Peterson, 1980); and Enewetak, the most northwesterly of the Marshall Islands, averaging about 150 cm y^{-1} (Buddemeier and Holladay, 1977). The rainfall distribution is seasonal, with the period from June to December typically receiving about 75% of the annual rainfall. Hence, the use of groundwater generally is greatest during the dry months from January to May.

GEOLOGIC FRAMEWORK

The atolls of the Marshall Islands, like those elsewhere, consist of circular to elliptical chains of small carbonate islands associated with a coral-reef platform encircling a shallow, central, seawater lagoon. The atoll islands, which typically consist of reef debris and atoll sediments, are the exposed or emerged portion of a thick carbonate platform that has formed on top of a subsided and submerged volcanic edifice.

Geologic setting

The Marshall Islands sit atop the Pacific Plate and are thought to represent a senescent volcanic chain produced by a long-inactive hotspot (Scott and Rotondo, 1983). Unlike the nearby linear volcanic island chains in the Pacific, such as the Hawaiian Islands and the Caroline Islands, the volcanoes that underlie the present-day Marshall Islands are widely scattered and do not exhibit any apparent age linearity. Deep drilling on Bikini and Enewetak, revealed that a 1.3- to 1.4-km-thick sequence of carbonate deposits, ranging from unconsolidated lagoonal sediments to loose reef debris to well-lithified coralline limestone and reef plate, overlies the basaltic basement (Emery et al., 1954; Schlanger, 1963). The youngest age dates obtained for the uppermost basalts range are 50–59 Ma, and shallow-water fossils immediately overlying the basalts have been dated at approximately the same age (Schlanger et al., 1987).

Although the bulk of the reef formation underlying the Marshall Islands occurred in response to subsidence of the volcanic edifices since Cretaceous time, the uppermost portion of the reef sequence has been significantly affected by Quaternary glacioeustasy. Periods of emergence have resulted in solution and erosion of the reef platform, and periods of submergence have resulted in renewed limestone deposition on the eroded surface. As a result, deposits within the uppermost part of these atolls are characterized by numerous geologic (and often hydrogeologic) unconformities. For example, Goter (1979) described five unconformity surfaces separating six different stratigraphic units within the upper 76 m of deposits on the windward side of Enewetak Atoll. The unconformity of greatest significance for groundwater is the uppermost one, dated at approximately 120 ka (Thurber et al., 1965). This unconformity separates moderately permeable Holocene sediments of less than 6-ka age (Schlanger, 1963) from the underlying highly permeable Pleistocene deposits and is commonly referred to as the "Thurber Discontinuity" in this book.

Stratigraphy

Because fresh groundwater occurs only within about the upper 30 m of most atoll islands, the geology of this zone is most significant. The conceptual geological framework of atoll islands which is based largely on studies of the Marshall Island atolls of Bikini and Enewetak (Tracey and Ladd, 1974; Goter, 1979; Buddemeier and Holladay, 1977), Kwajalein (Hunt and Peterson, 1980; Gingerich, 1992), Majuro (Anthony et al., 1989), and Arno (Cox, 1951) consists of two principal units, the shallow Holocene deposits and the underlying Pleistocene deposits.

The Holocene deposits typically consist of 10–25 m of largely unconsolidated back-reef sands, gravels, and silts. These deposits often are composed of several heterogeneous sublayers, which generally grade from coarse-grained material on the ocean side of the island to finer-grained sands on the lagoon side. Such heterogeneity makes it difficult to accurately characterize aquifer parameters; however, the overall permeability of the Holocene deposits is moderate compared to that of the underlying highly permeable Pleistocene deposits. Important geologic elements often

found within the Holocene sediments are layers of indurated material. These hard layers include beachrock, reef-flat facies, and subsurface diagenetically lithified layers with greatly reduced porosity and permeability (Underwood, 1990). It is inferred that these low-permeability hard layers restrict seaward flow and hence influence the shape of the fresh groundwater body and the flow dynamics of the groundwater system within an atoll island.

Underlying the Holocene deposits is a thick sequence of Pleistocene sediments. The primary skeletal material of the Pleistocene sediments is comparable to that of the Holocene unit, but it has undergone diagenetic alteration during the numerous episodes of eustatic sea-level change. Hence, the Pleistocene deposits are characterized by weak lithification and partial dissolution, which gives them greater overall porosities and permeabilities than the relatively unaltered Holocene deposits. Estimates of hydraulic conductivity of the Pleistocene unit range from one to two orders of magnitude greater than estimates for the Holocene deposits (Hunt and Peterson, 1980; Buddemeier, 1981). The depth to the top of the Pleistocene unit for several Marshall Island atolls is given in Table 20-1 (listed as Holocene thickness). A geologic cross section of the Laura area of Majuro Atoll showing the Holocene unit, which consists of three sublayers (Upper Limestone Lithofacies and Upper and Lower Sediment Lithofacies), as well as the underlying Pleistocene deposits (Lower Stratigraphic Unit), is depicted in Fig. 20-2.

HYDROGEOLOGIC FRAMEWORK

Groundwater distribution within an atoll island generally consists of a thin lenticular-shaped body of fresh (or near-fresh) water separated from the underlying

Table 20-1

Characteristics of Holocene aquifer

Atoll Island	Source	Hydraulic cond. (m day^{-1})	Measurement type	Holocene thickness (m)
Enewetak				
Enjebi	Wheatcraft & Buddemeier (1981)	54 30–75	field pump test lab permeameter	12–15
Majuro				
Laura	Anthony (1987)	60 (US) 60–600 (LS)	grain-size analysis grain-size analysis	17–24
Kwajalein				
Kwajalein	Hunt & Peterson (1980)	56–223 60–175	field pump test lab permeameter	6–12
Roi-Namur	Gingerich (1992)	140 2–85	field pump test field slug test	7–17

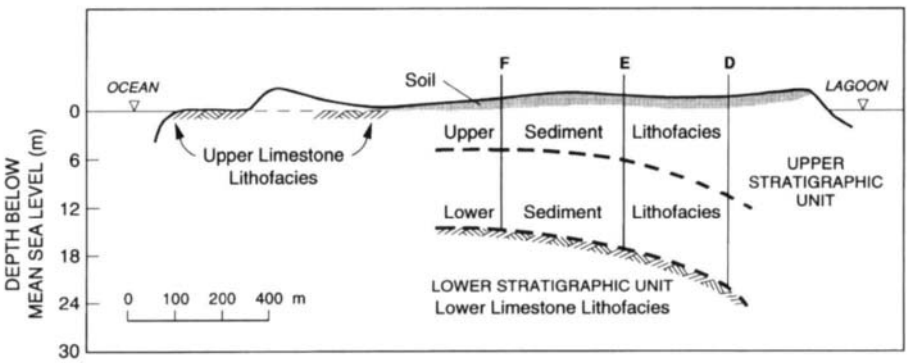


Fig. 20-2. Geologic cross section through the Laura area of Majuro Atoll. D, E, and F are borehole locations. (Adapted from Anthony, 1987.)

seawater by a zone of mixed water called the transition zone. Although atoll groundwater systems have been studied for many decades, until recently most investigators treated these systems as simple single-layer homogeneous aquifers subjected to horizontally propagated tidal signals. During roughly the past 15 years, a more realistic concept of atoll hydrogeologic systems has evolved from the detailed investigations of a number of Pacific Ocean atolls, many in the Marshall Islands (Buddemeier and Holladay, 1977; Hunt and Peterson, 1980; Wheatcraft and Buddemeier, 1981; Ayers and Vacher, 1986; Anthony et al., 1989; Oberdorfer et al., 1990; Underwood et al., 1992; Griggs and Peterson, 1993). The currently accepted conceptual hydrogeologic model is that of a dual-aquifer system consisting of about 10–25 m of moderately permeable Holocene deposits overlying the much more permeable Pleistocene aquifer (for example, see Figure 20-2 for the Laura area of Majuro Atoll). It is thought that the tidal signal is rapidly propagated laterally through the highly permeable Pleistocene aquifer and then moves more slowly upward through the less permeable Holocene aquifer.

The dual-aquifer atoll model, which is discussed in several chapters in this book [see Chap. 1, Table 1-3], generally is supported by groundwater tidal-response data collected from Holocene aquifers in the Marshall Islands (Table 20-2). As described by Underwood et al. (1992), at any given location, except very close to shore where distances are small and the tidal signal can move most easily directly inland through the Holocene aquifer, groundwater tidal efficiencies (well-to-ocean amplitude ratios) often exhibit systematic increases with increasing depth as the highly permeable Pleistocene aquifer is approached. Likewise, groundwater tidal lags (well-to-ocean time differentials) often exhibit systematic decreases with increasing depth.

Underwood (1990) used the groundwater transport model SUTRA (Voss, 1984) to simulate tidal efficiencies at different depths beneath an atoll island with (1) a dual-aquifer system in which the hydraulic conductivities of the upper and lower aquifers differed by an order of magnitude, and (2) a single-aquifer system having the hydraulic conductivity of the upper aquifer only. His results for the dual-aquifer system (Fig. 20-3) agree favorably with the field data listed in Table 20-2. The values

Table 20-2

Tidal responses beneath island centers.

Atoll Island	Source	Water-table response		Response 8m below water table	
		Efficiency	Lag (h)	Efficiency	Lag (h)
Enewetak					
Enjebi	Buddemeier &	0.09 ± 0.04	2.92 ± 0.29	0.28 ± 0.04	1.24 ± 0.30
Enewetak	Holladay (1977)	0.12 ± 0.07	3.28 ± 0.36	–	–
Japtan		0.05 ± 0.01	4.28 ± 0.10	–	–
Bikini					
Bikini	Underwood (pers.	0.06 ± 0.05	4.44 ± 0.63	0.07 ± 0.04	4.02 ± 0.75
Eneu	data, 1990)	0.10 ± 0.05	3.23 ± 0.44	0.25 ± 0.05	2.00 ± 0.50
Majuro					
Laura	Anthony (1987)	0.15 ± 0.05	2.30 ± 0.25	0.35 ± 0.10	0.80 ± 0.20
Kwajalein					
Kwajalein	Hunt & Peterson (1980)	0.18 ± 0.08	3.00 ± 1.00	0.37 ± 0.07	0.67 ± 0.20
Roi-Namur	Gingerich (1992)	0.07	2.7	0.12	1.6
		0.08	2.9	0.20	0.7

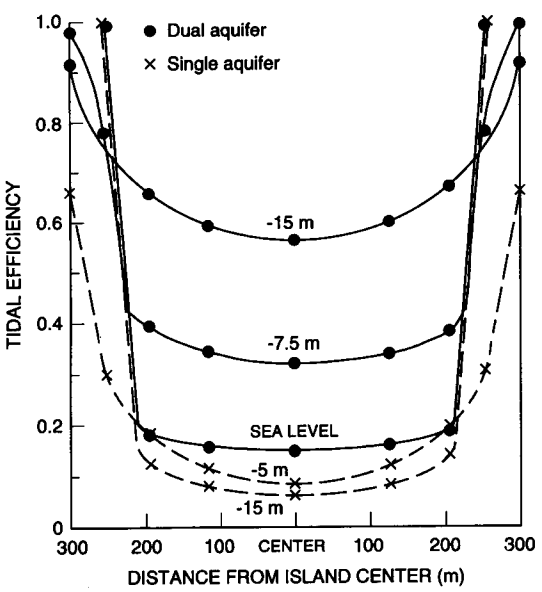


Fig. 20-3. Simulated tidal efficiency at different depths beneath an atoll island for dual-aquifer and single-aquifer cases. (Adapted from Underwood et al., 1992.)

for tidal efficiency from Figure 20-3 and Table 20-2 at given depths beneath the island centers do not exactly match because the simulated curves in Figure 20-3 assume a generic island 600 m wide with aquifer properties that are based on a compilation of all known Marshall Island aquifer data, whereas the data in Table 20-2 reflect the aquifer properties of each individual atoll island. The overall trends from the actual atoll islands listed in Table 20-2, however, are all similar to and generally agree with the simulated curves in Fig. 20-3.

Gingerich (1992), working on Roi-Namur Island, Kwajalein Atoll, conducted one of the most detailed tidal analyses ever done for the Marshall Islands. His measurements of tidal efficiency as a function of depth for numerous locations on Roi-Namur (Fig. 20-4) matches Underwood's simulated dual-aquifer results (Fig. 20-3) quite well. The magnitude of the tidal efficiency values differs because the aquifer parameters are different, but the general character of the tidal response in the real aquifer and that generated by the dual-aquifer model are remarkably similar.

GROUNDWATER OCCURRENCE AND DEVELOPMENT

The size and shape of the lens of fresh groundwater beneath an atoll island are controlled primarily by hydraulic properties of the aquifer materials and hydrodynamic processes within the freshwater-saltwater system, including recharge and tidal fluctuations. On many of the smaller and drier atoll islands, all of the recharge becomes mixed with the underlying saltwater and only brackish groundwater occurs. On some of the larger and wetter atoll islands, however, recharge is sufficient to produce sizable lenses of fresh groundwater. One example is on Kwajalein Island, where the average rainfall is about 260 cm y^{-1}. According to Hunt and Peterson (1980), hydrologic budget calculations indicate that groundwater recharge is about 50% of annual rainfall at Kwajalein Island, where the 250 mg l^{-1} isochlor extends as deep as 12 m below the water table (Fig. 20-5). Likewise, in the Laura area of Majuro Atoll, Hamlin and Anthony (1987) found that groundwater recharge is about 50% of the 356 cm of mean annual rainfall, and the 250 mg l^{-1} isochlor extends as deep as about 13–14 m (Fig. 20-6). It is interesting that on Kwajalein the thickest part of the freshwater lens occurs directly beneath an area that receives extensive recharge from the nearby runway. This is much like the situation described later for Eneu Island on Bikini Atoll.

On all atoll islands within the Marshall Island Republic for which subsurface data are available, the potable groundwater body was observed to occur entirely within the upper Holocene aquifer. This is because, first, the atoll islands are too small and the recharge too low to generate a fresh groundwater lens that would extend deeper than the Holocene deposits, and second, the high permeability within the underlying Pleistocene units provides little resistance to the rapid mixing of seawater with the overlying freshwater. In fact, on islands like Laura, the bottom portion of the freshwater lens appears to be truncated at the Holocene-Pleistocene boundary (Fig. 20-6). This is consistent with analytical and numerical simulation

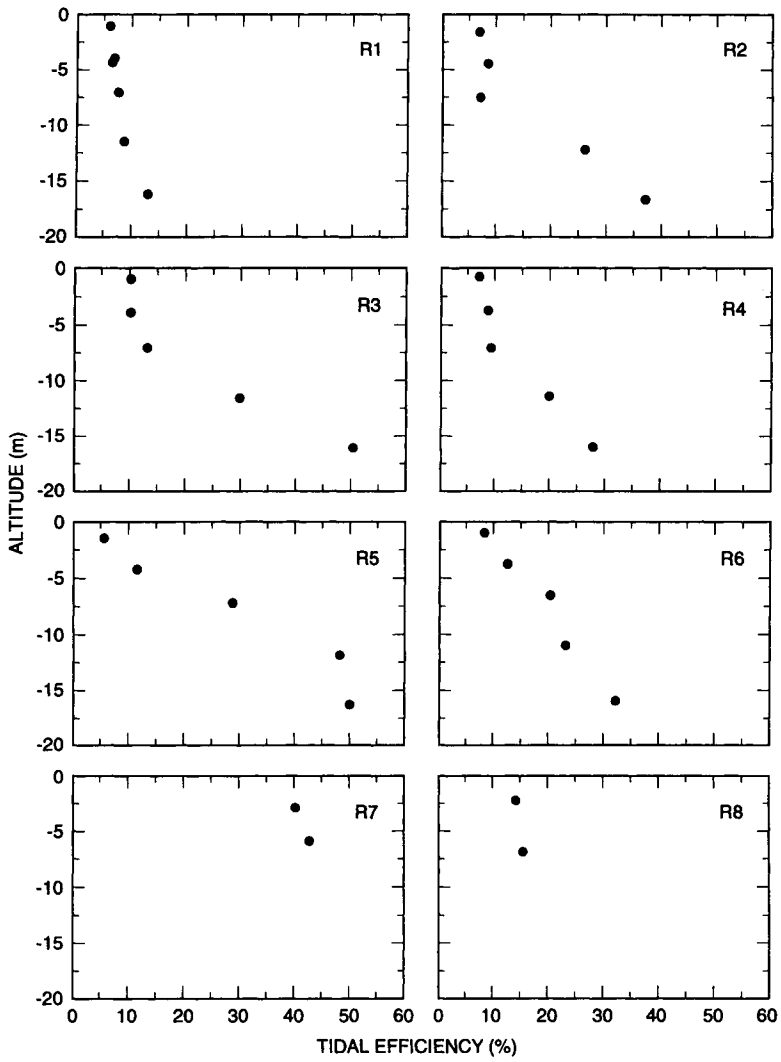


Fig. 20-4. Tidal efficiency vs. depth at monitoring wells, Roi-Namur Island, Kwajalein Atoll. See Figure 20.7A for location of wells. (After Gingerich, 1992.)

results obtained by Vacher (1988) and Griggs (1989), respectively, for a dual-aquifer system.

Fresh groundwater lenses beneath Marshall Island atolls tend to be asymmetrically distributed with respect to the lagoon side of atoll islands (Figs. 20-5–20-8). The reasons for this may be complicated and possibly are not the same for all islands. However, on the two islands for which detailed subsurface geologic data are available — Kwajalein Island in Kwajalein Atoll and the Laura area of Majuro Atoll — the freshwater lens is thicker on the lagoon side of the islands because the Ho-

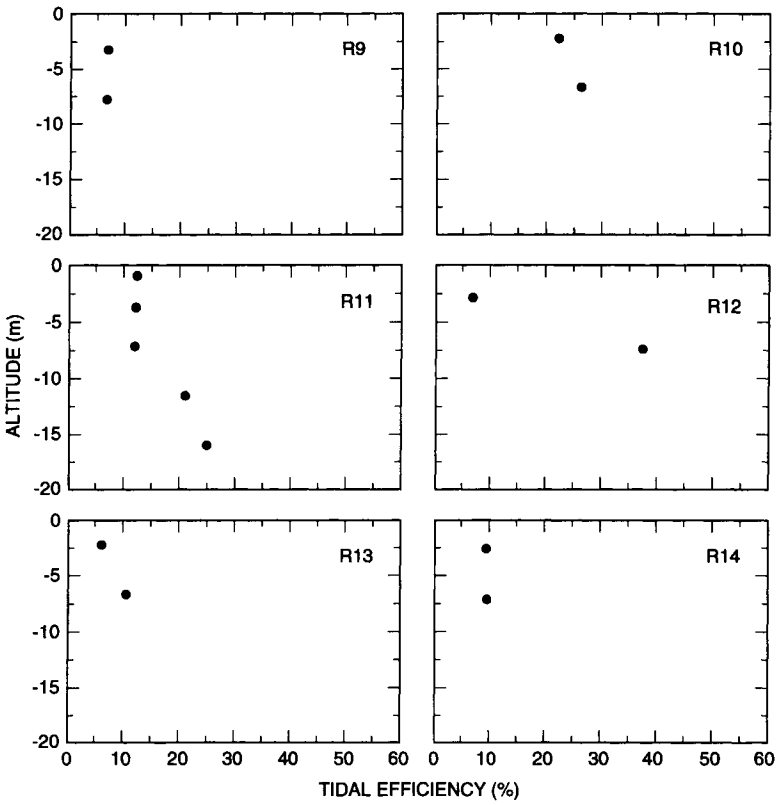


Fig. 20-4. (*Contd.*)

locene deposits there generally are fine-grained and hence less permeable than on the ocean side of the islands where coarse-grained, more permeable deposits allow easier seawater access into the aquifer. Table 20-1 lists Holocene aquifer characteristics, and Fig. 20-5–20-8 show map views and cross sections of groundwater occurrence on several of the most intensely studied islands in the Marshall Island Republic.

As stated previously, recharge is a critical factor in controlling the size and thickness of the fresh groundwater body on atoll islands. The thickness of the freshwater lens is a function of both island width (because most atoll islands tend to be elongated) and annual recharge. In order to investigate the responses of lenses to different combinations of recharge and island width, Underwood (1990) conducted a series of numerical simulations using the SUTRA model, an assumption of a dual-aquifer system, and generalized parameters representing typical Marshall Island atoll aquifers. From this modeling, Underwood (1990) generated the family of curves given in Fig. 20-9, which shows the relationship among simulated thickness of potable groundwater (2.6% salinity), island width, and recharge. Although these results apply only for a general atoll aquifer, they do agree reasonably well with actual field observations at several Marshall Island atolls (Table 20-3). Data on width of island and thickness of the freshwater lens for Bikini, Eneu, Laura, Kwajalein, and Roi-

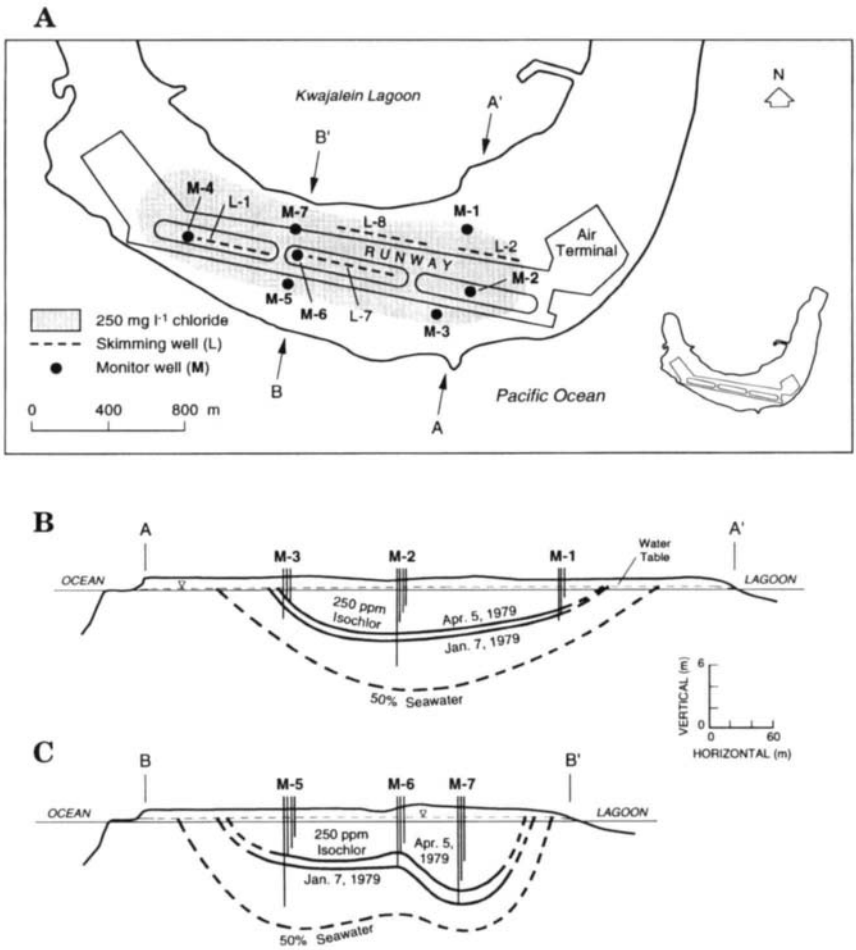


Fig. 20-5. Hydrogeology of Kwajalein Island, Kwajalein Atoll. (A) Location of production (skimming) and monitor wells and extent of fresh groundwater in 1979. (B) Groundwater cross section through AA′. (C) Groundwater cross section through BB′. (Adapted from Hunt and Peterson, 1980.)

Namur islands (Table 20-3) are shown in Fig. 20-9; with the notable exception of that for Eneu Island, these data generally fall close to or within the predicted recharge values. For example, Roi-Namur has an average width of 750 m and a freshwater lens thickness of 5–7 m; hence, its annual recharge of 0.58 m is well within the range predicted by Fig. 20-9. Likewise, Kwajalein's recharge of 1.17 m and Laura's recharge of 1.78 m are within the range predicted by the simulated curves in Fig. 20-9.

A notable exception occurs on the Bikini Atoll islands of Eneu and Bikini. Located only about 7 km apart, these islands receive approximately the same rainfall

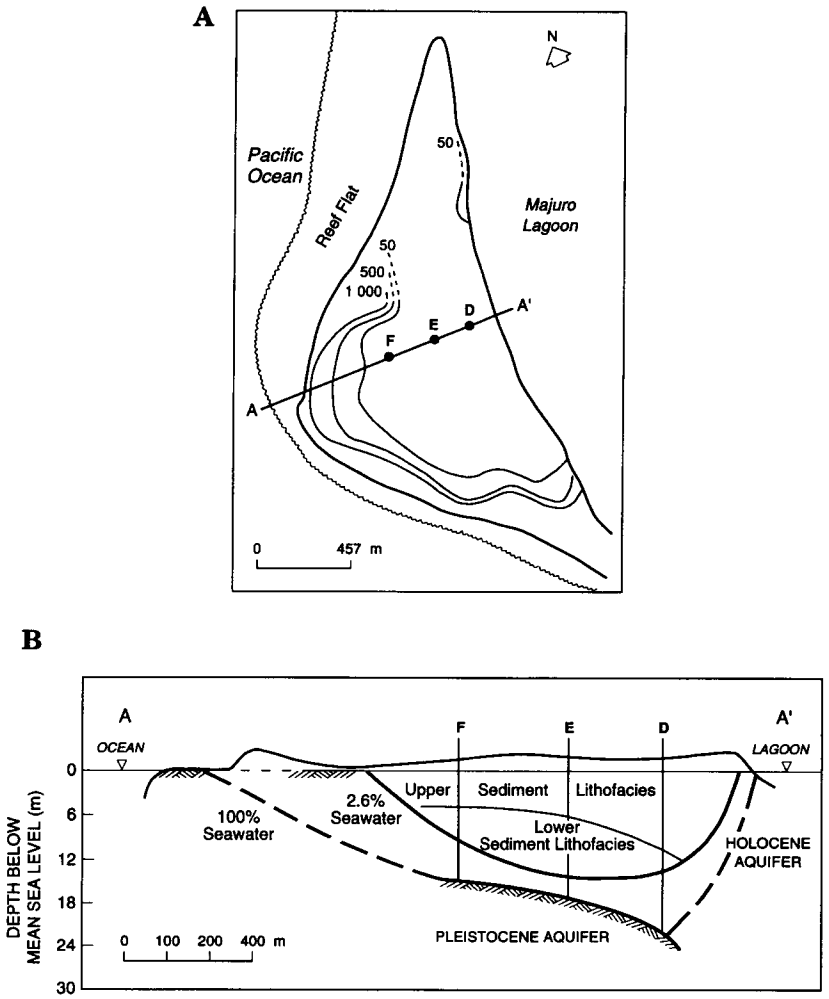


Fig. 20-6. Hydrogeology of Laura area, Majuro Atoll. (A) Map showing groundwater isochlors (mg L^{-1}), April 1985. (B) Groundwater cross section through AA'. (Adapted from Anthony, 1987.)

(145 cm y^{-1}); Bikini is about 70% wider than Eneu and has about 85% more total land area. Detailed studies by Peterson (1988) during the period from 1985 to 1987 showed that even though Bikini is wider and larger than Eneu, Bikini had virtually no fresh groundwater, whereas Eneu had a freshwater lens of nearly 100,000 m^3. There are several possible reasons for this apparently anomalous situation. Much of Eneu is covered by impervious runway material that funnels recharge into a small concentrated area directly over the freshwater lens. Conversely, most of Bikini is covered with thick vegetation that has very high evapotranspiration demands and hence diverts a significant portion of the freshwater recharge. Finally, much of the Eneu coastline is covered with poorly permeable beachrock, which probably impedes the

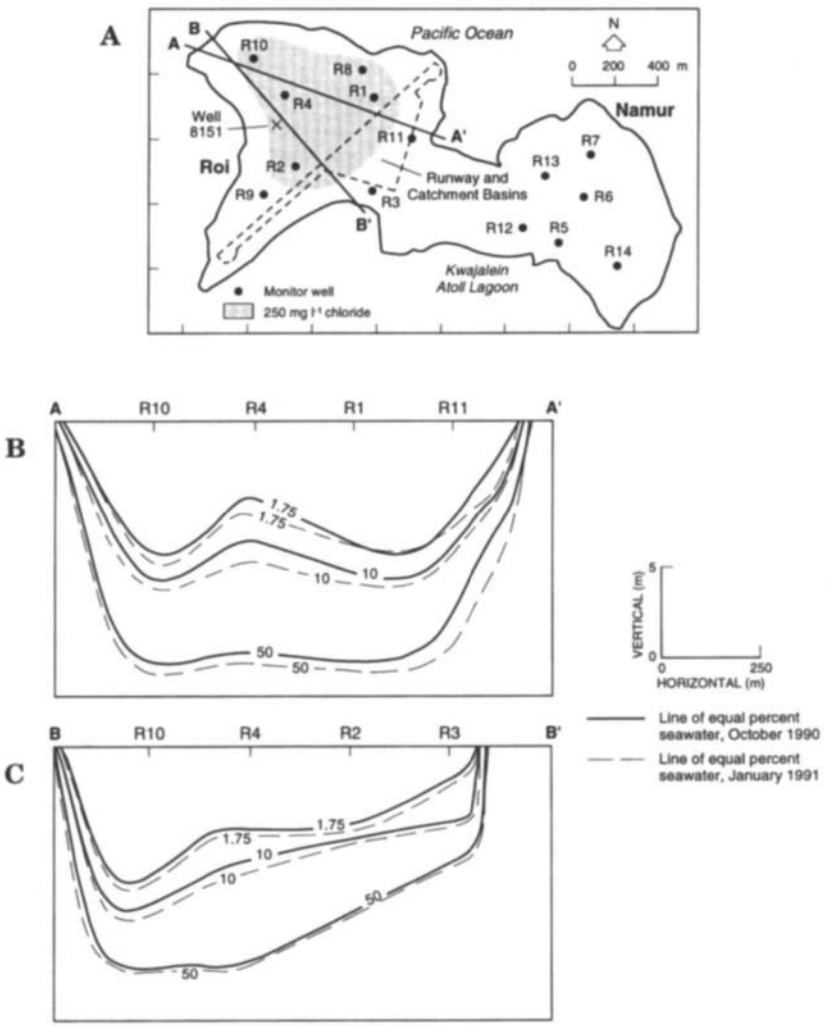


Fig. 20-7. Hydrogeology of Roi-Namur Island, Kwajalein Atoll. (A) Location of monitor wells and groundwater cross sections. (B) Groundwater cross section through AA′. (C) Groundwater cross section through BB′. (Adapted from Gingerich, 1992.)

seaward movement of fresh groundwater, thus allowing a thicker freshwater lens to develop. Hence, although the relationships shown in Fig. 20-9 may serve as a useful reconnaissance tool to evaluate freshwater potential when more detailed field data are not available (Underwood et al., 1992), care must be taken in their use because island width alone is not always a reliable indicator of groundwater recharge.

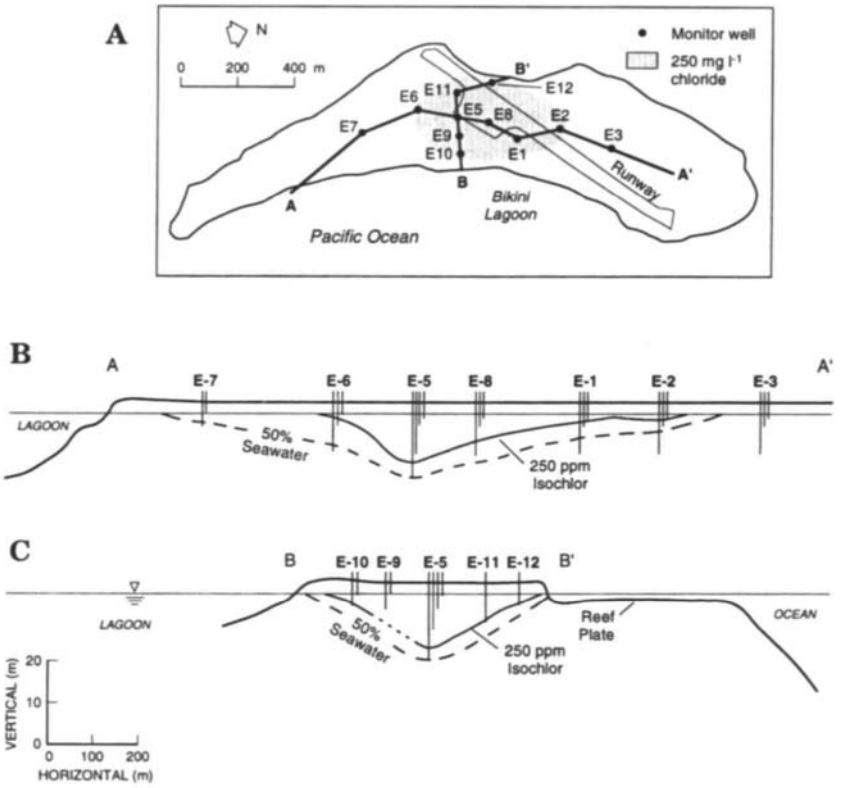


Fig. 20-8. Hydrogeology of Eneu Island, Bikini Atoll. (A) Location of monitor wells and extent of fresh groundwater. (B) Groundwater cross section through AA′. (C) Groundwater cross section through BB′. (Adapted from Peterson, 1988.)

Development and sustainable yield

Thin fresh groundwater bodies on atoll islands are very sensitive to the methods and rates of groundwater development. It has long been understood that to achieve optimum groundwater development only the freshest water should be skimmed off the top of the freshwater lens. This can most practically be achieved with extensive shallow horizontal skimming wells like those used on Kwajalein. Here, 110,000–225,000 m^3 of fresh groundwater are extracted annually from four horizontal skimming wells (Fig. 20-5) totalling about 1,200 m in length (C. Hunt, personal communication, 1993).

Two different approaches have been used to estimate sustainable yield for aquifers in the Marshall Islands. One approach is a trial-and-error method involving an empirical correlation between aquifer pumpage and key groundwater parameters such as head or salinity. Essentially this technique involves selecting a groundwater pumping rate (ideally less than sustainable yield, although this cannot be known for

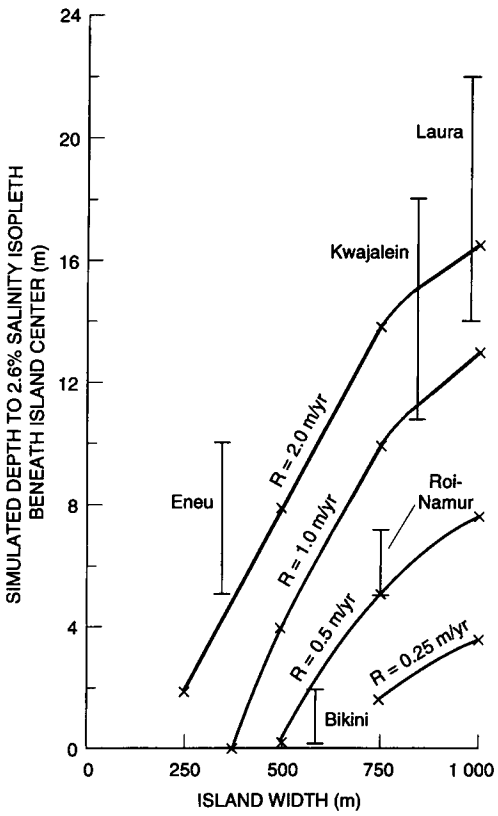


Fig. 20-9. Relationship between island width and simulated depth of potable water (2.6% salinity) at island centers for different values of annual recharge rate (R). (Adapted from Underwood et al., 1992.)

sure in advance) and then observing the effects of the pumpage on the groundwater body over time. Hunt and Peterson (1980) used this technique to estimate sustainable yield for Kwajalein Island. Alternatively, computer modeling increasingly is being used to simulate the actual mixing processes resulting from pumping stresses. Griggs (1989) and Gingerich (1992) used the SUTRA model to estimate sustainable yield for Laura and Roi-Namur, respectively. A summary of recharge, aquifer storage, and sustainable yield estimates for several islands in the Marshall Island Republic is given in Table 20-3.

CASE STUDY: MODELING DEVELOPMENT ALTERNATIVES IN DUAL-AQUIFER ATOLL ISLANDS

This Case Study describes the application of computer modeling to assess groundwater development alternatives for two different atoll island environments.

Table 20-3

Groundwater parameters, Marshall Islands

Atoll Island	Source	Estimated recharge (m y^{-1})	Width (m)	Fresh lens thickness (m)	Aquifer storage (m^3)	Sustainable yield (m^3 y^{-1})
Bikini						
Bikini	Peterson (1988)	0.50	600	< 2	–	–
Eneu		0.50	350	5–10	$9.5–10.5 \times 10^4$	24,000
Majuro						
Laura	Hamlin & Anthony (1987)	1.78	1000	14–22	$17–20.8 \times 10^5$	550,000
Kwajalein						
Kwajalein	Hunt & Peterson (1980)	1.17	870	10–18	$9.8–11.5 \times 10^5$	190,000
Roi- Namur	Gingerich (1992)	0.58	750	5–7	$3.6–4.4 \times 10^5$	13,000

The first model evaluates the impact of different spatial configurations on optimal groundwater development for the Laura area of Majuro Atoll. The second model evaluates the effect of varying extraction rates and schedules for several different recharge scenarios for Roi-Namur in Kwajalein Atoll.

Laura, Majuro Atoll

Griggs (1989) and Griggs and Peterson (1993) used computer simulations to evaluate the response of the freshwater lens beneath the Laura area of Majuro Atoll (Fig. 20-6) to several alternative development schemes. As described previously (and shown in Figs. 20-2 and 20-6), the near-surface geologic framework of Laura consists of three principal aquifer units: the Upper Sediment Lithofacies of Holocene age, the Lower Sediment Lithofacies of Holocene age, and the Lower Limestone Lithofacies of Pleistocene age. Saturated hydraulic conductivities for these units progressively increase downward and appear to differ from each other by about one order of magnitude. Based on field pump tests, grain-size analysis, and tidal-efficiency measurements, hydraulic conductivity values of 2×10^{-4}, 2×10^{-3}, and 2×10^{-2} m s^{-1}, respectively, were used for the Upper Sediment, Lower Sediment, and Lower Limestone Lithofacies in initial model simulations. After model calibration, these values were adjusted to 7×10^{-4}, 7×10^{-3}, and 7×10^{-2} m s^{-1}, respectively.

The two-dimensional, density-dependent, fluid flow and mass transport model SUTRA (Voss, 1984) was used to study the freshwater-saltwater system for Laura.

Since Laura's length is large compared to its width, it can be modeled as an infinite-strip island (Griggs and Peterson, 1993). Hence, the SUTRA model was used to simulate groundwater flow and solute transport in the vertical cross section AA′ (Fig. 20-6).

The model mesh extended laterally from the outer edge of the ocean reef plate to the center of the lagoon and vertically from the water table to the bottom of the carbonate sediments, estimated at 1,066 m. Figure 20-10 shows the portion of the mesh comprising the island and the freshwater lens. Values for input variables and constants required for the SUTRA model came from field measurements taken on Laura and other similar atoll islands and from reasonable estimates of parameters not measured. Table 20-4 lists all parameter values used in the modeling.

To determine the most efficient extraction scheme for Laura, Griggs (1989) and Griggs and Peterson (1993) modeled the effects of various extraction alternatives on the thickness of the freshwater lens (as indicated by the position of the 2.6% relative-salinity contour), including (1) number and location of pumping centers, and (2) extraction rates relative to recharge. Groundwater extraction was simulated by pumping water from cross-sectional slices of the island approximately parallel to AA′ (Fig. 20-6). Pumping rates were set by extracting a percentage of the annual average recharge (AAR) for each cross section, thus normalizing the extraction rates to the recharge volume for each cross section. In all simulations, recharge was assumed to be uniform throughout the year and water was extracted from the top 1.52 m of the saturated aquifer. It should be noted that, for pumping with this model orientation (two-dimensional vertical section through an infinite strip using cartesian

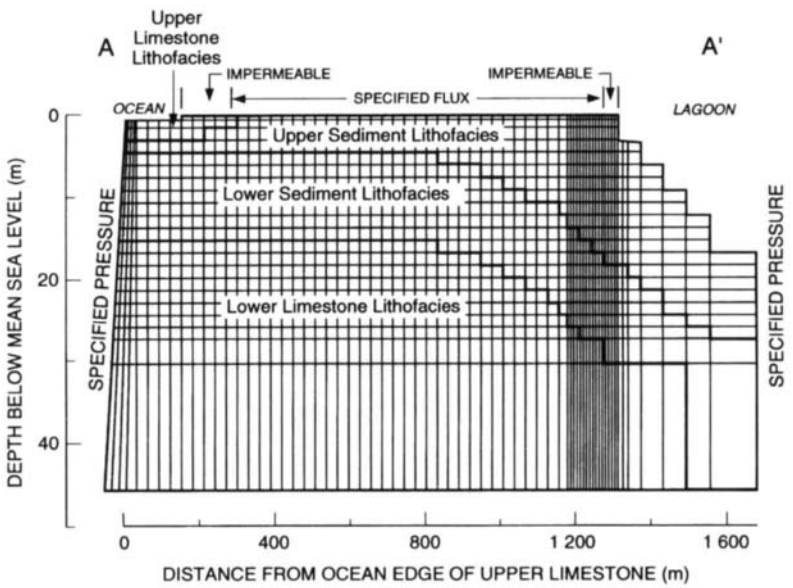


Fig. 20-10. Mesh with boundary conditions for Laura area. (Adapted from Griggs, 1989.)

Table 20-4

Parameter values, Laura Island, Majuro Atoll.*

Parameter	Value	Reference
Hydraulic conducitivity (m s^{-1})		
K_{UL}	1.16×10^{-6}	Ayers and Vacher, 1986
K_{US}	7.0×10^{-4}	This modeling
K_{LS}	7.0×10^{-3}	This modeling
K_{LL}	7.0×10^{-2}	This modeling
Dispersivity (m)		
α_{Lmax}	8.0	Voss, pers. comm.,1987
α_{Lmin}	0.4	Voss, pers. comm.,1987
α_T	0.05	
Concentration (M_s M^{-1})		
Freshwater	0	
Recharge	6.5915×10^{-6}	Anthony, 1987
Seawater	3.57×10^{-2}	Voss, 1984
Compressibility (m^{-2} N^{-1})		
Fluid	4.47×10^{-10}	Freeze and Cherry, 1979
Matrix	1.0×10^{-8}	Freeze and Cherry, 1979
Porosity (%)		
US and LS (Holocene)	20	Anthony, 1987
LL (Pleistocene)	30	Swartz, 1982
Specific yield (%)	18	
Recharge (m y^{-1})	1.78	Hamlin & Anthony,1987
ρ/C (kg m^{-3})	700	Voss, 1984
Fluid viscosity (kg m^{-1} s^{-1})	1.0×10^{-3}	CRC Handbook[a]
Molecular diffusivity (m^2 s^{-1})	1.48×10^{-9}	CRC Handbook

*After Griggs and Peterson, 1993.
Key: UL, upper limestone (reef plate); US, upper sediment; LS, lower sediment; LL, lower limestone.
[a]*CRC Handbook of Chemistry and Physics* (Weast and Astle, 1980).

coordinates), each pumping element is equivalent to an infinitely long line sink perpendicular to the section. Hence, the term "pumping center" is used to represent a single pumping element and the term "gallery" is used to represent a line of several pumping centers (Griggs and Peterson, 1993).

On most small atoll islands, groundwater can most efficiently be developed by pumping from many shallow wells or from horizontal skimming galleries. The efficiency of single-well versus multiple-well systems was evaluated by simulating

pumping from (1) a single pumping center with a pumping rate of 20% of AAR; (2) two pumping centers, each pumping at a rate of 10% of AAR; and (3) ten pumping centers (called a gallery), each pumping at a rate of 2% of AAR. Thus the total rate of pumping for each development alternative was the same, 20% of AAR (Griggs and Peterson, 1993). As can be seen in Fig. 20-11, the single pumping center is the least efficient (results in greatest upconing) and the gallery, the most efficient.

Since the previous simulations demonstrated that multiple pumping centers (galleries) are most efficient in extracting water, further simulations to estimate sustainable yield for Laura utilized galleries only. A variety of extraction rates was assumed. Figure 20-12 shows the effects on the freshwater lens of pumping from galleries at 40%, 47%, and 62% of AAR. As can be seen, the 62% pumping rate resulted in upconing that completely destroyed the freshwater lens, whereas the 40% and 47% pumping rates resulted in considerable upconing but the freshwater lens remained intact. Thus it is likely that if galleries are utilized, the sustainable yield for the Laura area may approach 40–47% of AAR.

Roi-Namur, Kwajalein Atoll

Gingerich (1992) and Peterson and Gingerich (1995) also used the SUTRA model to study groundwater development and sustainable yield under varying extraction and recharge scenarios for Roi-Namur Island. Roi-Namur, which is located at the northeastern tip of Kwajalein Atoll, is composed of two roughly circular islets (Roi

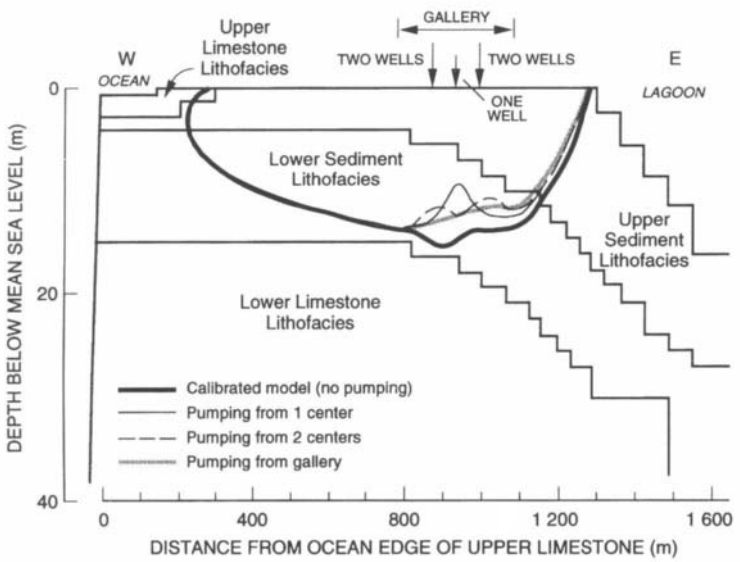


Fig. 20-11. Steady-state response of freshwater lens (2.6% salinity) to one-well, two-well, and gallery pumping situations. (Adapted from Griggs and Peterson, 1993.)

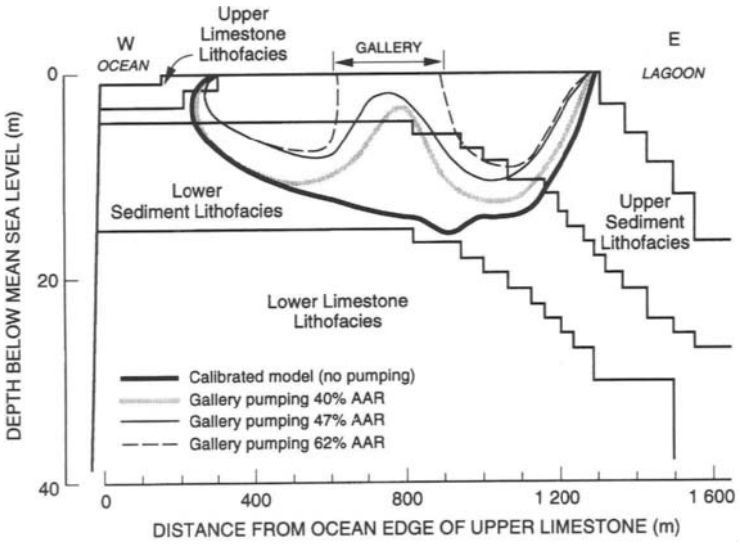


Fig. 20-12. Simulated steady-state response of freshwater lens (2.6% salinity) to galleries pumped at 40%, 47%, and 62% of the annual average recharge. (Adapted from Griggs and Peterson, 1993.)

and Namur) connected by a dredge-filled isthmus and covers an area of about 2 km^2 (Fig. 20-7).

The near-surface geology of Roi-Namur consists of a four-layer system, including three Holocene layers (two moderately permeable aquifer units separated by a low-permeability layer), with a combined thickness of 20 m overlying approximately 900 m of highly permeable Pleistocene deposits (Fig. 20-13).

For this study, the original SUTRA code used to model Laura was modified to simulate the storage of water for a water-table condition, and a fluctuating tidal boundary was added (details given in Underwood, 1990). The Roi-Namur modeling, like that for Laura, simulated variable-density saturated fluid flow and solute transport in a vertical section. However, radial symmetry, rather than an infinite-strip island, was assumed, because the freshwater lens is restricted to Roi Island, which is roughly equidimensional.

The entire model mesh extended 8,400 m laterally, from a point in the lagoon to the ocean side of the reef face, and 1,000 m vertically, from sea level to the volcanic basement. Figure 20-14 shows the portion of the mesh beneath and immediately adjacent to the island containing the freshwater lens together with the assigned boundary conditions. One node near the top of the mesh was programmed as a sink node to simulate groundwater extraction (Fig. 20-14). Extraction at this node was equivalent to pumping from an infinitely long horizontal gallery oriented perpendicular to the mesh. The extraction volume was determined by dividing the total volume of water removed from the lens by the length of the gallery (Gingerich, 1992). Input parameters for the final calibrated Roi-Namur model are given in Table 20-5.

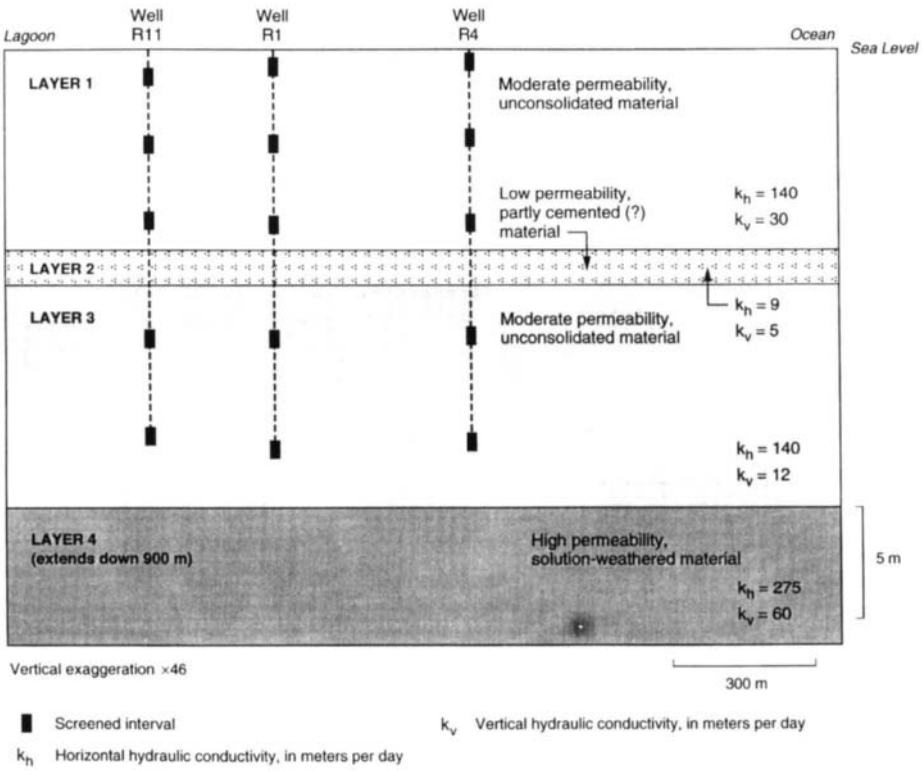


Fig. 20-13. Hydrogeologic cross section of Roi-Namur, Kwajalein Atoll. (From Gingerich, 1992.)

Five different development alternatives (summarized in Table 20-6) involving three different recharge conditions and five different pumping conditions were simulated. Development simulation 1 assumes the AAR for Roi-Namur (57.6 cm) is distributed evenly throughout the year and the current average annual pumpage (8,700 m^3), likewise, is distributed evenly throughout the year. Figure 20-15, which shows simulated recharge, pumpage, and Cl^- concentration as a function of time, illustrates that for simulation 1 the salinity of pumped groundwater increases only slightly throughout the year.

Development simulation 2 also uses the AAR and pumping rates of 57.6 cm and 8,700 m^3, respectively, but assumes, more realistically, that the recharge is spread over a 9-mo period and the pumpage is evenly distributed over the 6-mo dry period from December to May. As shown in Fig. 20-15, in this simulation the Cl^- concentration in the pumped groundwater rises and peaks in June at the end of the pumping season, but at a level well below the U.S. Environmental Protection Agency (USEPA) drinking water limit of 250 mg l^{-1}. Thus it is concluded that during normal recharge years the current pumping rate of 8,700 m^3 y^{-1} is well below the sustainable yield for the Roi-Namur groundwater system.

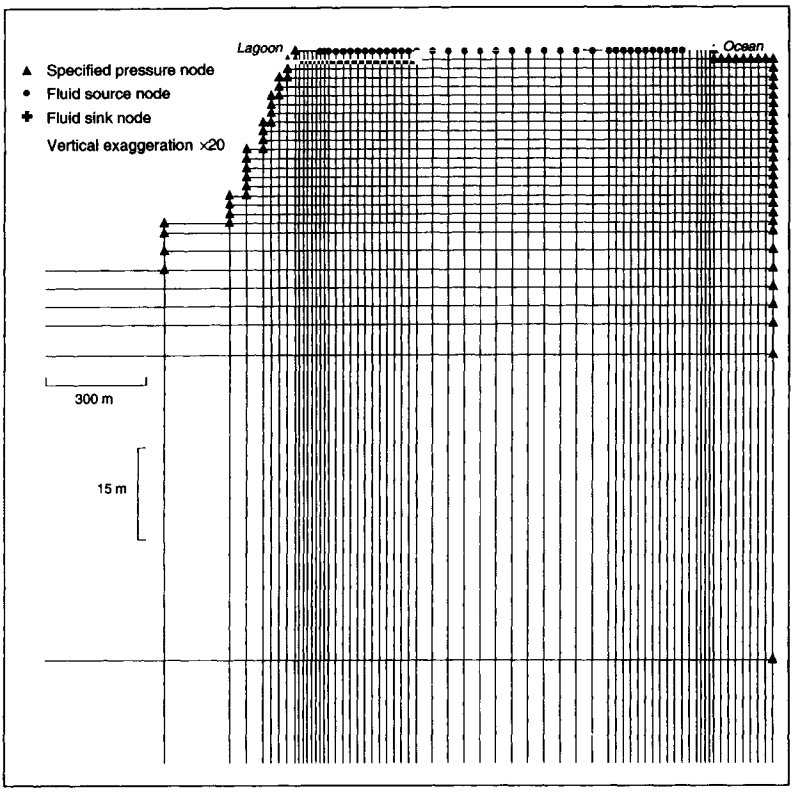


Fig. 20-14. Mesh with boundary conditions for Roi-Namur, Kwajalein Atoll. (From Gingerich, 1992.)

To better evaluate the sustainable yield for the Roi-Namur groundwater system under more stressful conditions, three additional development alternatives were simulated. Development simulation 3 assumes the AAR of 57.6 cm is distributed over the same 9-mo period as for simulation 2, but with a 50% increase in annual pumpage to 13,040 m^3 distributed over the 6-mo dry period from December to May. As shown in Fig. 20-15, under these conditions the groundwater Cl^- peaks at a level that is about double its original concentration but still slightly below the USEPA drinking water limit.

Development simulation 4 investigates the effects of a reduced recharge rate of 31.2 cm y^{-1}, which actually occurred during the drought year of 1984, applied over the 3-mo period from September to November, with pumping at the increased average annual rate of 13,050 m^3 spread over the nonrainy 9-mo period from December to August. As shown in Fig. 20-15, under these conditions the groundwater Cl^- peaks at a level that is approximately double its original concentration but still slightly below the USEPA drinking water limit.

Table 20-5

Parameter values for calibrated Roi-Namur model*

	Value	Units
Physical Constants		
Fluid compressibility (β)	4.47×10^{-10}	$m^2\ N^{-1}$
Fluid density:		
seawater (ρ_s)	1025	$kg\ m^{-3}$
freshwater (ρ_f)	1000	$kg\ m^{-3}$
Concentration, seawater (C)	0.0357	$kg\ kg^{-1}$
Fluid diffusivity (σ_w)	1.0×10^{-9}	$m^2\ s^{-1}$
Fluid viscosity (μ)	8.3×10^{-4}	$kg(m\ s)^{-1}$
Solid matrix compressibility (α)	1.0×10^{-9}	$m^2\ N^{-1}$
Density of a solid grain (ρ_{sg})	2700	$kg\ m^{-3}$
Component of gravity vector in y direction (g)	−9.81	$m\ s^{-2}$
Calibration Variables		
Horizontal permeability:		
layer 1 (k_{h1})	1.77×10^{-10}	m^2
layer 2 (k_{h2})	1.18×10^{-11}	m^2
layer 3 (k_{h3})	1.77×10^{-10}	m^2
layer 4 (k_{h4})	3.54×10^{-10}	m^2
Vertical permeability:		
layer 1 (k_{v1})	3.54×10^{-11}	m^2
layer 2 (k_{v2})	5.90×10^{-12}	m^2
layer 3 (k_{v3})	1.42×10^{-11}	m^2
layer 4 (k_{v4})	8.26×10^{-11}	m^2
Porosity (ϵ)	0.3	$m^3\ m^{-3}$
Specific storage coefficient (ST)	0.33	m^{-1}
Longitudinal dispersivity		
Maximum (α_{Lmax})	3.0	m
Minimum (α_{Lmin})	0.02	m
Transverse dispersivity (α_T)	0.001	m

* After Gingerich, 1992.

Table 20-6

Development simulation alternatives*

Development simulation	Months of recharge	Recharge ($cm\ y^{-1}$)	Months of withdrawal	Withdrawal ($m^3\ y^{-1}$)
1	12	57.6	12	8700
2	9	57.6	6	8700
3	9	57.6	6	13050
4	3	31.2	9	13050
5	3	31.2	9	19575

* Simulation period: 1 year.

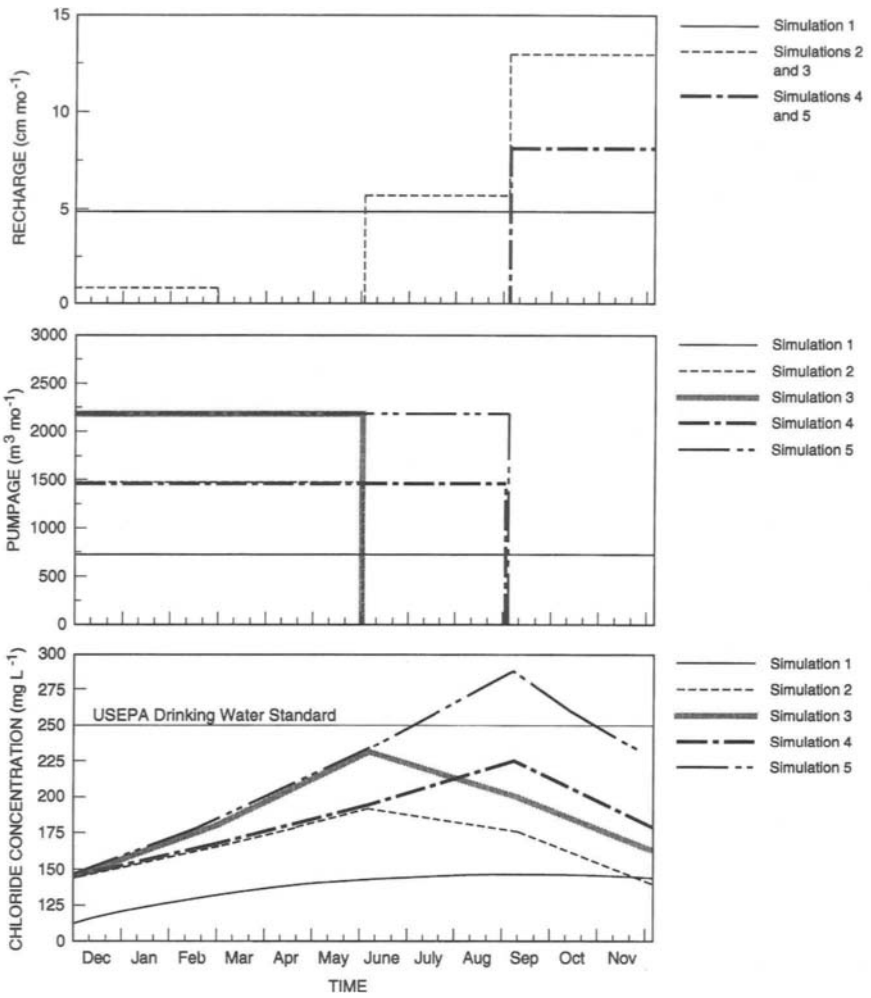


Fig. 20-15. Development simulation results for Roi-Namur, Kwajalein Atoll. (Modified from Gingerich, 1992.)

Development simulation 5 assumes the drought recharge rate of 31.2 cm y^{-1} is applied over the 3-mo period from September to November, as in simulation 4, but with an increased pumping rate of 19,575 m^3 y^{-1} distributed over the 9-mo dry period from December to August. As shown in Fig. 20-15, these conditions caused the Cl^- to rise above the USEPA drinking water limit of 250 mg l^{-1}.

Based on these development simulations, it is concluded that the sustainable yield for the Roi-Namur groundwater system is probably at least 50% greater than the current pumping rate of 8,700 m^3 y^{-1}, even during severe drought years.

CONCLUDING REMARKS

As alluded to earlier in this chapter, many of the currently accepted concepts of how atoll hydrogeologic systems function have come from pioneering work conducted in the Marshall Islands. In particular, the concept of a dual-aquifer system exerting strong control on the groundwater tidal response and salinity of the freshwater lens has originated largely from studies of Marshall Island atolls such as Enewetak, Kwajalein, Majuro, and Bikini.

In addition, computer modeling studies of these atolls have resulted in a better understanding of groundwater lens dynamics of small atoll islands, especially the factors that control the size, structure, and extent of the freshwater lens and the transition zone. Results obtained from variable-density groundwater flow and solute transport modeling (Underwood et al., 1992; Griggs and Peterson, 1993) indicate that the mixing of fresh and saline waters is controlled mainly by short-term vertical fluctuations driven by ocean tides and that mixing in directions transverse and horizontal to long-term groundwater flow paths is less important. Hence, freshwater lens thickness is controlled by the balance between recharge (controlled by recharge rate and island size) and discharge rates (controlled by upper aquifer horizontal permeability) and the dispersive mixing process, which is controlled by the combined effects of vertical longitudinal dispersivity, tidal range, and vertical permeabilities (Underwood et al., 1992).

The main purpose of much of the hydrogeologic work done in the Marshall Islands is to provide a better understanding of how most efficiently to develop fresh groundwater supplies from these small atoll islands. In this regard, the new understanding of atoll hydrogeologic framework and lens dynamics has been used to help solve problems of groundwater development and sustainable yield in the Marshall Islands. In particular, work such as that described in the Case Study of groundwater development for Majuro and Roi-Namur has provided a quantitative approach for evaluating the effectiveness of alternative development scenarios and assessing the temporal and spatial variations in sustainable yield.

ACKNOWLEDGMENTS

The work upon which this chapter is based was supported by federal and state grants for six research projects on atoll groundwater systems. The author thanks the Water Resources Research Center publications staff for their assistance in the preparation of the manuscript. This is contributed paper CP-94-02 of the Water Resources Research Center at the University of Hawaii at Manoa, Honolulu.

REFERENCES

Anthony, S.S., 1987. Hydrogeochemistry of a small limestone island: Laura, Majuro Atoll, Marshall Islands. M.S. Thesis, Univ. Hawaii, Honolulu, 114 pp.

Anthony, S.S., Peterson, F.L., Mackenzie, F.T. and Hamlin, S.N., 1989. Geohydrology of the Laura fresh-water lens, Majuro atoll: a hydrogeochemical approach. Geol. Soc. Am. Bull., 101: 1066–1075.

Arnow, T., 1954. The hydrology of the Northern Marshall Islands. Atoll Res. Bull., 30: 1–7.

Ayers, J.F. and Vacher, H.L., 1986. Hydrogeology of an atoll island: a conceptual model from detailed study of a Micronesian example. Ground Water, 24: 185–198.

Buddemeier, R.W., 1981. The geohydrology of Enewetak Atoll islands and reef. Proc. Fourth Int. Coral Reef Symp. (Manila), 1: 339–345.

Buddemeier, R.W. and Holladay, G., 1977. Atoll hydrology: island groundwater characteristics and their relationship to diagenesis. Proc. Third Int. Coral Reef Symp. (Miami), 2: 167–173.

Cox, D.C., 1951. The hydrology of Arno Atoll, Marshall Islands. Atoll Res. Bull., 3: 1–33.

Emery, K.O., Tracey, J.I. and Ladd, H.S., 1954. Geology of Bikini and nearby atolls. U.S. Geol. Surv. Prof. Pap. 260-A, 265 pp.

Freeze, R.A. and Cherry, J.A., 1979. Groundwater. Prentice Hall, Englewood Cliffs NJ, 604 pp.

Gingerich, S.B., 1992. Numerical simulation of the freshwater lens on Roi-Namur Island, Kwajalein Atoll, Republic of the Marshall Islands. M.S. Thesis, Univ. Hawaii, Honolulu, 110 pp.

Goter, E.R., 1979. Depositional and diagenetic history of the windward reef of Enewetak Atoll during the mid to late Pleistocene and Holocene. Ph.D. Dissertation, Rennselaer Polytechnic Inst., Troy NY, 239 pp.

Griggs, J.E., 1989. Numerical simulation of groundwater development schemes for the Laura area of Majuro Atoll, Marshall Islands. Ph.D. Dissertation, Univ. Hawaii, Honolulu, 203 pp.

Griggs, J.E. and Peterson, F.L., 1993. Ground-water flow dynamics and development strategies at the atoll scale. Ground Water, 31: 209–220.

Hamlin, S.N. and Anthony, S.S., 1987. Ground-water resources of the Laura area, Majuro Atoll, Marshall Islands. U.S. Geol. Surv. Water-Resour. Invest. Rep., 87-4047, 69 pp.

Hunt, C.D. and Peterson, F.L., 1980. Groundwater resources of Kwajalein Island, Marshall Islands. Univ. of Hawaii, Water Resour. Res. Cent., Tech. Rep., 126, 91 pp.

Ladd, H.S. and Schlanger, S.L., 1960. Drilling operations on Eniwetok Atoll. U.S. Geol. Surv. Prof. Pap. 260-Y: 863–903.

Mink, J.F., 1986. Trust Territory of the Pacific Islands water supply initiative, groundwater resources and development. Report submitted to U.S. Environmental Protection Agency, Region 9.

NOAA (National Oceanic and Atmospheric Administration), 1984. Climatological data, annual summary, Hawaii and Pacific Area, 80 (13), 40 pp.

Oberdorfer, J.A., Hogan, P.J. and Buddemeier, R.W., 1990. Atoll island hydrogeology: flow and fresh water occurrence in a tidally dominated system. J. Hydrol., 120: 327–340.

Peterson, F.L., 1988. Appendix B: Water. In: H.I. Kohn, A.S. Kubo, F.L. Peterson and E.L. Stone, Bikini Atoll Rehabilitation Committee Summary Report No. 6. Submitted to the U.S. Cong., House and Senate Comm., Interior Appropriations, July 22, 1988, 151 pp.

Peterson, F.L. and Gingerich, S.B., 1995. Modeling atoll groundwater systems. In: A.I. El-Kadi (Editor), Groundwater Models for Resources Analysis and Management. CRC/Lewis Publishers, Boca Raton, pp. 275–292.

Ristvet, B.L., Tremba, E.L., Couch, R.F., Fetzer, J.A., Goter, E.R., Walter, D.R. and Wendland, V.P., 1978. Geologic and geophysical investigations of Enewetak nuclear craters. U.S. Air Forces Weapons Lab. Rep., AFWL-TR-77-242, Kirtland Air Force Base, N.M., 298 pp.

Schlanger, S.O., 1963. Subsurface geology of Eniwetok Atoll. U.S. Geol. Surv. Prof. Pap. 260-BB: 991–1066.

Schlanger, S.O., Campbell, J.F. and Jackson, M.W., 1987. Post-Eocene subsidence of the Marshall Islands recorded by drowned atolls on the Harrie and Sylvania Guyots. In: B. Keating, P. Fryer,

R. Batiza and G. Boehlert (Editors), Seamounts, Islands, and Atolls. Geophys. Monog. 43, Am. Geophys. Union, Washington D.C., pp. 165–174.
Scott, G.A. and Rotondo, G.M., 1983. A model to explain the differences between Pacific plate island-atoll types. Coral Reefs, 1: 139–150.
Thurber, D.I., Broecker, W.S., Blanchard, R.L. and Potratz, A.J., 1965. Uranium-series ages of Pacific atoll coral. Science, 149: 55–58.
Tracey, J.I. and Ladd, H.S., 1974. Quaternary history of Eniwetok and Bikini atolls, Marshall Islands. Proc. Second Int. Coral Reef Symp. (Brisbane), 2: 537–550.
Underwood, M.R., 1990. Atoll island hydrogeology: conceptual and numerical models. Ph.D. Dissertation, Univ. Hawaii, Honolulu, 205 pp.
Underwood, M.R., Peterson, F.L. and Voss, C.I., 1992. Groundwater lens dynamics of atoll islands. Water Resour. Res., 28: 2889–2902.
Vacher, H.L., 1988. Dupuit-Ghyben-Herzberg analysis of strip- island lenses. Geol. Soc. Am. Bull., 100: 580–591.
Voss, C.I., 1984. A finite-element simulation model for saturated-unsaturated fluid-density-dependent ground-water flow with energy transport of chemically-reactive single-species solute transport. U.S. Geol. Surv. Water-Resour. Invest. Rep., 84-4369, 409 pp.
Weast, R.C. and Astle, M.J., 1980. CRC handbook of chemistry and physics. CRC Press, Boca Raton, FL.
Wheatcraft, S.W. and Buddemeier, R.W., 1981. Atoll island hydrology. Ground Water, 19: 311–320.

Geology and Hydrogeology of Carbonate Islands. Developments in Sedimentology 54
edited by H.L. Vacher and T. Quinn
© 1997 Elsevier Science B.V. All rights reserved.

Chapter 21

GEOLOGY OF ANEWETAK ATOLL, REPUBLIC OF THE MARSHALL ISLANDS

TERRENCE M. QUINN and ARTHUR H. SALLER

INTRODUCTION

Anewetak Atoll (formally Enewetak and Eniwetok), the northwesternmost member of the Marshall Islands [q.v., Chap. 20], is located in the western equatorial Pacific Ocean at 162°E, 11°N (Fig. 21-1). It consists of roughly 40 small, low-relief islands surrounding a lagoon, which is 40 km long by 32 km wide and has a maximum depth of ~64 m (Fig. 21-1). The islands consist of carbonate sand and gravel and have typical elevations of ~2 to 3 m above sea level (Henry et al., 1986).

The inhabitants of Anewetak are descendants of people who migrated from the Malaysian-Indonesian area several centuries ago. Anewetak was first sighted by Spanish explorers in the mid-1500s and later resighted by English explorers in the late 1700s. In 1866, Germany established a formal protectorate over the Marshall Islands and constructed a whaling base. In 1914, Japan seized German Micronesia including Anewetak and the remainder of the Marshall Islands. Japan was given a mandate to rule the former German Pacific possessions by the League of Nations at the conclusion of World War I. In subsequent years, Japan fortified Anewetak and other atolls of the Marshall Islands. Japanese rule of the Marshall Islands effectively ended early in 1944 after fierce military battles with United States. The U.S. Navy ruled Anewetak and the Marshall Islands until 1947, when the United Nations established the Trust Territory of the Pacific Islands (TTPI) and authorized the United States to govern it. After the inhabitants of Anewetak were moved to nearby atolls, forty-three nuclear devices were detonated on or in the vicinity of Anewetak Atoll between 1948–1958. In August of 1986, the TTPI was dissolved by the United Nations and the new Republic of the Marshall Islands was formed.

Geologic setting

Atolls, guyots and seamounts of the Marshall Islands are situated on three, subparallel, NW-SE-trending ridges located between the Central Pacific Basin to the east and the Mariana Basin to the west (Lincoln et al., 1993). The easternmost volcanic edifices are in the Ratik Chain, the more centrally located edifices are in the Ralik Chain, and the westernmost edifices are located in an elongated cluster centered about Anewetak Atoll (Haggerty and Premoli Silva, 1995). Research done as an outgrowth of the recent drilling of guyots in the northwest Pacific during Ocean Drilling Program Legs 143/144 has provided important refinements to the geologic

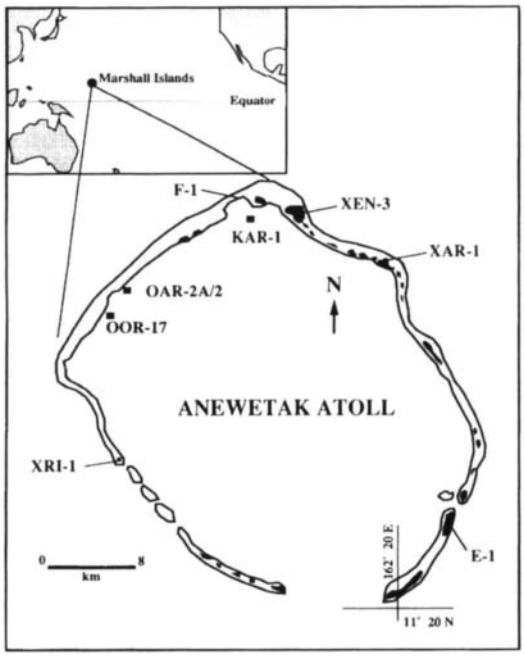


Fig. 21-1. Location maps (modified from Ladd and Schlanger, 1960). F-1 and E-1 were drilled in 1951 and 1952 (see Emery et al., 1954; Ladd and Schlanger, 1960). XAR-1, XEN-3 and XRI-1 were drilled as part of the EXPOE Program in 1973 and 1973 (see Ristvet et al., 1974; Tracey and Ladd, 1974; Couch et al., 1975). OOR-17, OAR-2/2A and KAR-1 were drilled in 1984 and 1985 as part of the PEACE Program (see Henry and Wardlaw, 1986; 1991). [See also Figs. 20-1 and 23.1 for regional location.]

history of the Marshall Islands (e.g., Bergersen, 1995; Haggerty and Premoli Silva, 1995). Multiple lines of evidence (e.g., geophysical modeling, radiometric dating) suggest that the formation of the Marshall Islands was not straightforward, but rather involved multiple episodes of volcanism, uplift, reef-building and subsidence in the Early and Late Cretaceous as the islands of this chain interacted with the Macdonald, Rurutu, and Raratonga hotspots (e.g., Lincoln et al., 1993; Bergersen, 1995; Haggerty and Premoli Silva, 1995).

Anewetak Atoll lies in the Late Jurassic magnetic quiet zone on a portion of the Pacific Plate presumed to be older than 165 Ma (Larson, 1976). The best age estimate for the basalt recovered beneath Anewetak Atoll, determined by the high-precision $^{40}Ar/^{39}Ar$ technique, is 76 Ma (Lincoln et al., 1993). This is a significant revision from the previous estimate of 61–51 Ma determined by conventional K-Ar dating (Kulp, 1963). By ~75 to ~65 Ma, the northern Marshall Islands were subsiding as they moved away from the hotspot swells. The oldest limestones recovered at Anewetak are middle to late Eocene (Cole, 1957; Todd and Low, 1960). Limestone deposition at Anewetak continued discontinuously from the middle to late Eocene to the Recent.

History of subsurface drilling

Extensive scientific and geological studies of Anewetak were conducted as part of Operation Crossroads which coincided with the nuclear program at Anewetak. Numerous shallow boreholes were drilled in 1950 and 1951, and three deep boreholes (K-1B, F-1, and E-1) were drilled on Anewetak Atoll in 1951 and 1952. Boreholes F-1 and E-1 spudded on Elugelab and Parry Islands, respectively (Fig. 21-1), and penetrated the entire limestone cap of the atoll before ending in volcanic basement at depths of ~1,405 and ~1,260 m, respectively. These penetrations of volcanic basement beneath the limestone cap confirmed the theory of atoll origin and evolution (Darwin, 1837, 1842). Extensive scientific study of materials from F-1 and E-1 boreholes led to the publication of a landmark monograph, U.S. Geological Survey Professional Paper 260, beginning in 1954 (Emery et al., 1954) and ending in 1969 (Leopold, 1969).

These initial studies revealed the general character of the limestone section: relatively thick intervals of leached, altered, cemented, calcite-rich rocks alternating with thick intervals of unleached, unaltered, uncemented, aragonite-rich sediments (Fig. 21-2; Emery et al., 1954; Schlanger, 1963). The tops of the leached and cemented zones separating less-altered zones were called "solution unconformities" by Schlanger (1963), who interpreted these features as forming during periods of atoll emergence. These solution unconformities were recognized as hiatuses and were assigned ages of top of the Eocene (Tertiary b), top of the early Miocene (Tertiary e), and Pleistocene (Tertiary g). Schlanger (1963) referred to these solution unconformities according to their depth: 20 m, 85 m, 310 m, and 825 m. Faunal analyses of materials recovered in F-1 and E-1 indicated that basal limestones of F-1 were deposited in deep water, probably on the outer slope of the atoll; in contrast, the basal limestones of E-1 were deposited in shallow reefal environments (Todd and Low, 1960; Schlanger, 1963).

Two more drilling programs were conducted in the early 1970s (PACE Program, 1970–1972; and EXPOE Program, 1973–1974). Numerous shallow boreholes were drilled on many islands of Anewetak, including Enjebi (boreholes XEN), Aranit (boreholes XAR), and Rigili (boreholes XRI), as part of these programs. Improved core and sample recovery and detailed geologic analyses permitted the identification of five major unconformities in the upper 100 m of section (Fig. 21-3; Ristvet et al., 1974; Tracey and Ladd, 1974; Couch et al., 1975). The deepest unconformity recognized in the PACE and EXPOE drilling likely corresponds to the shallowest solution unconformity recognized by Schlanger (1963) in F-1 and E-1.

The most recent drilling program on Anewetak (PEACE Program, 1986) drilled 32 boreholes. Detailed scientific studies of materials from three reference boreholes (KAR-1; OAR-2/2A and OOR-17) provided a wealth of new information which is largely summarized in Henry and Wardlaw (1986). Carbonates recovered in the upper 350 m of section at Anewetak were assigned ages of early Miocene to Holocene, and numerous disconformities and/or discontinuities were recognized (Fig. 21-4; Henry and Wardlaw, 1986).

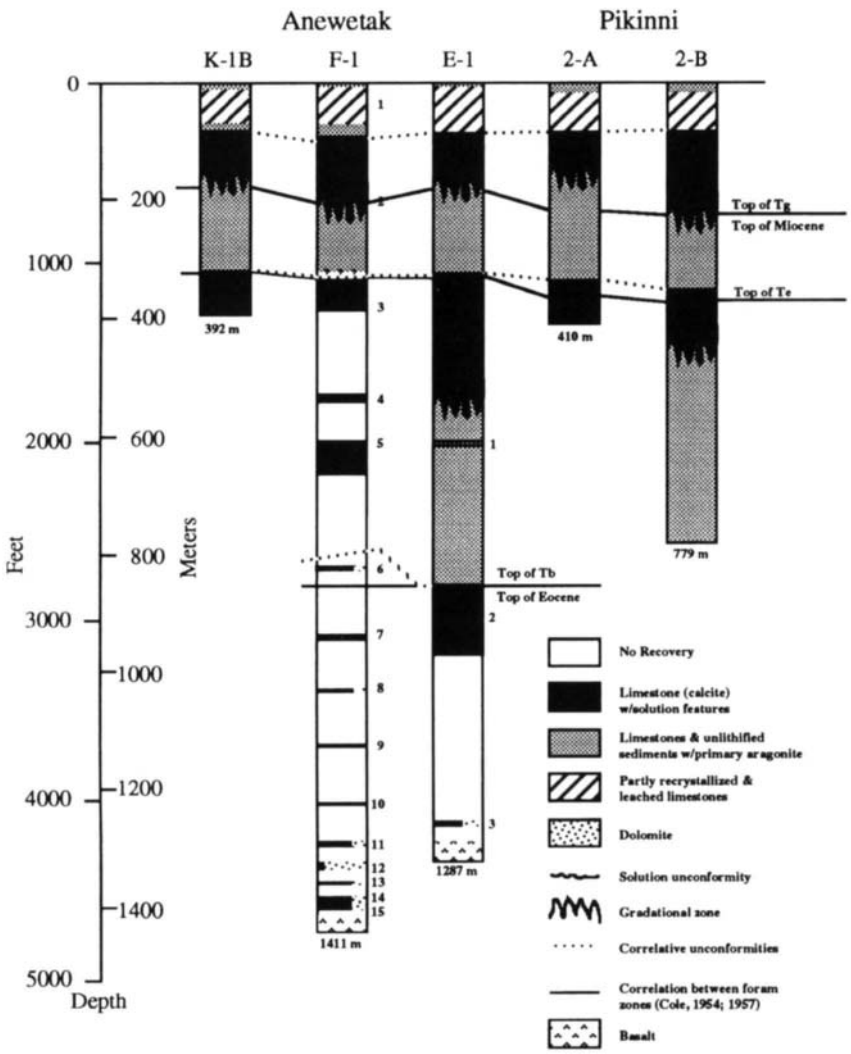


Fig. 21-2. Correlation of deep boreholes drilled on Anewetak and Pikinni (formerly Bikini) Atolls, showing general character of the limestone section (modified from Schlanger, 1963). Numbers along sides of stratigraphic columns of F-1 and E-1 indicate cored intervals. Biostratigraphy based on large benthic foraminifera assemblages (Cole 1954; 1957).

Extensive geological investigations have been associated with the drilling programs on Anewetak Atoll. The classic investigations of Anewetak material by Emery, Ladd, Tracey, Schlanger, and Gross were pioneering studies of the geology of carbonate islands and gave subsequent investigators a very solid foundation on which to build. Recent studies of the stratigraphy and geochemistry of Anewetak carbonates (e.g., Saller, 1984a; Ludwig et al., 1988; Saller and Moore, 1989; Saller

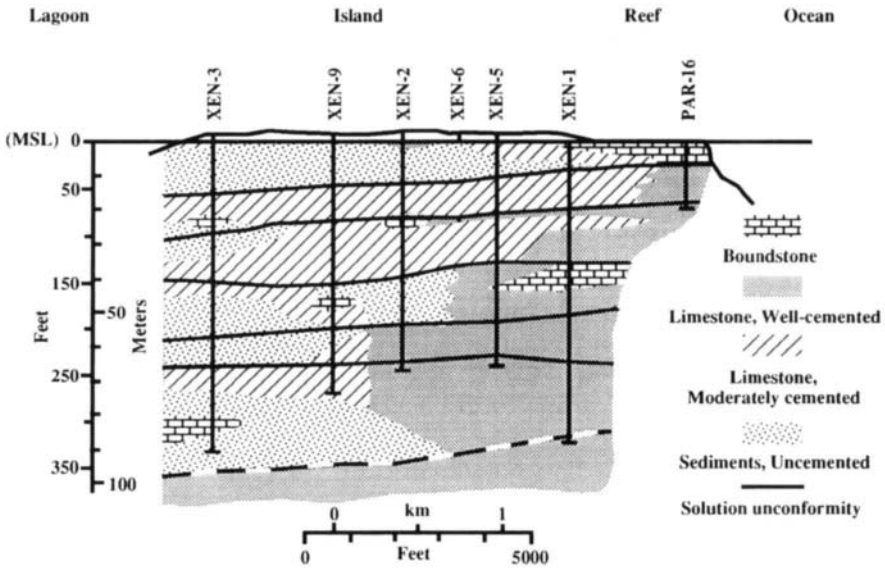


Fig. 21-3. Subsurface geologic cross section of Enjebi (JANET) Island showing five Pleistocene unconformities (from Couch et al., 1975). The deepest unconformity was identified using seismic techniques. (Modified from Ristvet et al., 1980.)

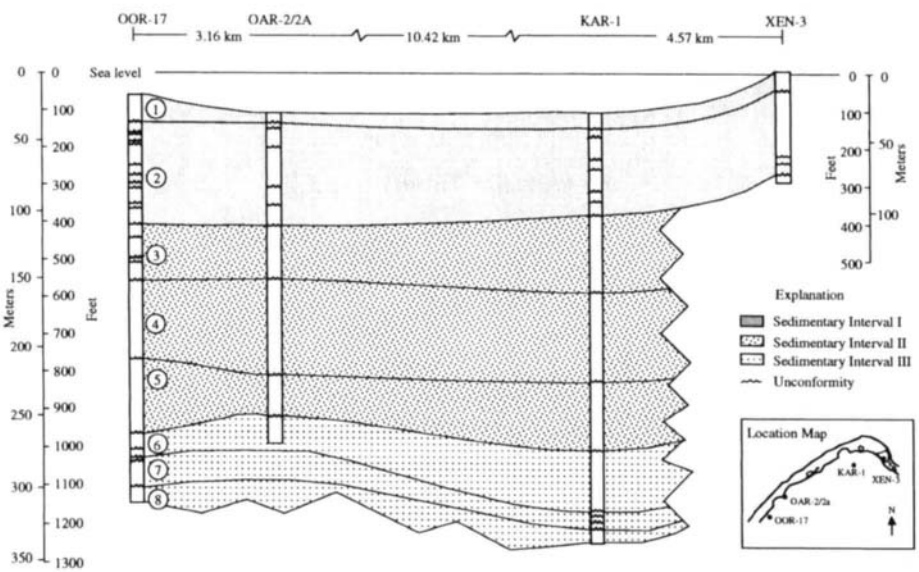


Fig. 21-4. Subsurface geologic cross section of PEACE Program reference boreholes. Stippled patterns demarcate distinctive sedimentary intervals, numbers refer to distinctive sedimentary packages, and wavy lines refer to unconformities. (Modified from Wardlaw and Henry, 1986.)

and Koepnick, 1990; Quinn, 1991a; Quinn et al., 1991) have expanded our understanding of the products and processes of carbonate deposition, diagenesis, and the role of sea-level change in the evolution of carbonate islands. The purpose of this chapter is to synthesize current knowledge of the subsurface geology of Anewetak Atoll from the more than 40 years of core study. In the next chapter, Buddemeier and Oberdorfer review the climatic and oceanographic setting, geomorphology and hydrogeology of Anewetak.

Stratigraphy

Many stratigraphic studies have been conducted on cores from Anewetak. The initial dating of Anewetak carbonates was based on larger and smaller foraminifera assemblages identified primarily from the F-1 and E-1 boreholes (Cole, 1957; Todd and Low, 1960). Biostratigraphy of larger foraminifera used the Tertiary Far East Letter Classification (TFELC). Biostratigraphic work in other areas by Adams (1970, 1983, 1984) changed the correlations of the TFELC zones to planktonic zonations and conventional stages. Revisions to the TFELC had a major impact on some of the designated ages of subsurface intervals at Anewetak (e.g., Oligocene sediments, Fig. 21-5).

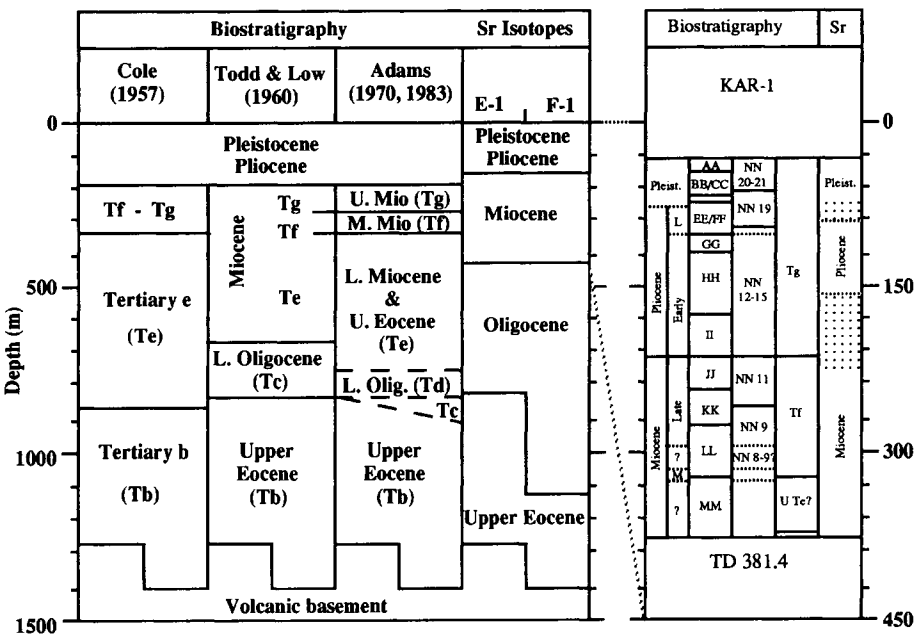


Fig. 21-5. Chronostratigraphy of Anewetak boreholes E-1, F-1 and KAR-1. Intervals denoted with double capital letters for KAR-1 refer to the local benthic microfossil biostratigraphy of Cronin et al. (1986). Nannofossil zonations from Bybell and Poore (1991). Large foraminiferal zonations (e.g., Tg) from Gibson and Margerum (1991). Sr isotope chronology from Ludwig et al. (1988). TD denotes total depth of KAR-1. (Modified from Saller and Koepnick, 1990.)

Strontium isotope chronology of the deep limestones at Anewetak (Saller and Koepnick, 1990) generally support the stratigraphic interpretations of Adams (1970; 1983; 1984) which conflict with Cole's (1957) biostratigraphy (Fig. 21-5). Cole (1957) believed TFELC zones Tc and Td represented the entire Oligocene, and hence he concluded the entire Oligocene was missing because he could not find larger foraminifera indicative of the Tc or Td in E-1 or F-1. However, recorrelation of the TFELC (Adams, 1970, 1983, 1984) indicates that the Te includes much of the Oligocene, and that a substantial Oligocene section is present on Anewetak Atoll. Strontium isotope chronostratigraphy supports a thick Oligocene section being present on Anewetak (Saller and Koepnick, 1990).

The stratigraphy of the shallow subsurface beneath the lagoon of Anewetak was recently the subject of intense investigation as part of the PEACE Program drilling initiative. Benthic microfossils, particularly ostracodes and benthic foraminifera, were used to develop a local biostratigraphy that proved useful for correlating subsurface units sampled during the PEACE Program (Cronin et al., 1986). Calcareous nannofossils and planktic foraminifera, although sporadically distributed and in low abundance in the PEACE Program cores, did provide important stratigraphic information (Bybell and Poore, 1991). A preliminary integrated biochronology of PEACE Program material was presented by Wardlaw (1989), and it has been updated in publications by Bybell and Poore (1991) and Gibson and Margerum (1991) (Fig. 21-5).

In contrast to the PEACE program, the PACE and EXPOE drilling projects focused of the stratigraphy of the shallow subsurface (< 100 m) beneath the islands of Anewetak. As a result of these projects, five correlative unconformities (Fig. 21-3), separating six stratigraphic sequences, have been recognized in the upper 90 m of boreholes from several islands of Anewetak Atoll (e.g., Tracey and Ladd, 1974; Couch et al., 1975; Goter, 1979; Szabo et al., 1985); additional other minor unconformities also have been identified (Quinn, 1991a). The ages of the unconformity-bounded intervals are still relatively poorly known. The shallowest unconformity recognized at Anewetak separates diagenetically altered Pleistocene sediments from generally unaltered Holocene sediments. This unconformity, sometimes called the Thurber discontinuity (Thurber et al., 1965), ranges in depth from ~8–12 m subsea in island boreholes to ~30–45 m subsea in lagoon boreholes. Indeed, no Pleistocene limestone shallower than ~8 m subsea has been identified at Anewetak (Szabo et al., 1985). Uranium-series dating indicates that the carbonates just below the shallowest unconformity in the island boreholes are 131 ± 3 ka (Szabo et al., 1985). The third, fifth, and sixth stratigraphic sequences are undated, but the fourth sequence is estimated at 454 ± 100 ka based on uranium-series measurements (Szabo et al., 1985). These sequences have also been "dated" via correlation and calibration with the deep-sea oxygen isotopic record of glacial-interglacial oscillations (Goter and Friedman, 1988). However, this technique does not provide unequivocal ages for these sequences. Thus, despite the large number of studies of Pleistocene Anewetak limestones, they remain relatively poorly dated.

DEPOSITIONAL SYSTEMS

Carbonate deposition at Anewetak Atoll can be divided into an early period (lower part of the Eocene section) when depositional facies rapidly aggraded, followed by a period of basinward progradation of depositional facies (upper Eocene through early Miocene), and a last period of aggradation and repeated subaerial exposure with little or no net basinward progradation of facies (early Miocene to Recent) (Saller and Koepnick, 1990).

Eocene to lower Miocene

Only E-1 and F-1 penetrated the entire Eocene and Oligocene carbonate section on Anewetak. A third borehole, OBZ-4, was drilled to 547 m subsea and encountered approximately 121 m of Oligocene strata (Gibson and Margerum, 1991). Other PEACE Program boreholes, (KBZ-4, KAR-1, OOR-17, and OBZ-4), penetrated part of the early Miocene section. All of these boreholes are near the atoll margin. Eocene, Oligocene, and lower Miocene atoll-margin carbonates can be divided into six main depositional environments (Fig. 21-6): lagoon, lagoon margin, backreef, reef, forereef, and slope. Interpretations of depositional environments are based

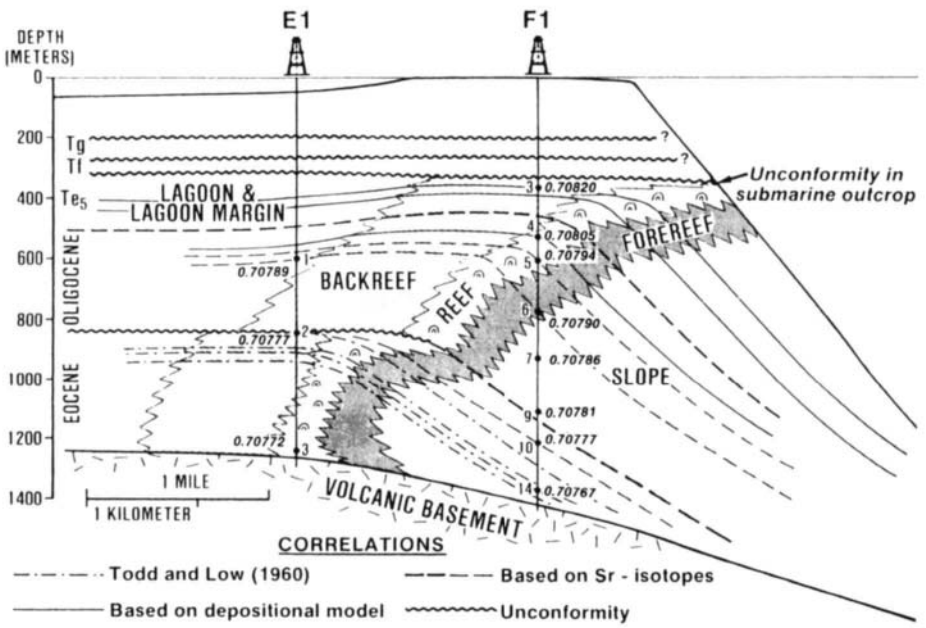


Fig. 21-6. Diagrammatic cross section depicting the stratigraphy and depositional environments of Eocene to lower Miocene strata at the margin of Anewetak Atoll E-1 and F-1 projected onto the line of section are actually on different sides of the atoll. (From Saller and Koepnick, 1990.)

Table 21-1

Summary of subsurface depositional features and environments of Anewetak

Slope Environment	
Textures:	Packstone, grainstone and wackestone.
Grain types:	Coralline algae, large foraminifera, intraclasts, echinoderms, planktonic foraminifera.
Comments:	Many aragonitic grains (coral and *Halimeda*) have been dissolved, most without a trace.
Forereef Environment	
Textures:	Boundstone, packstone and grainstone.
Grain types:	Coral, coralline algae, large foraminifera, planktonic foraminifera.
Comments:	Borings, geopetal structures, submarine cements.
Reef Environment	
Textures:	Boundstone and grainstone.
Grain types:	Coral, coralline algae, encrusting foraminifera, large foraminifera, *Halimeda*.
Comments:	Many encrusting structures, submarine cements.
Backreef Environment	
Textures:	Grainstone and boundstone.
Grain types:	Coral, coralline algae, encrusting large foraminifera, *Halimeda*.
Large	Foraminifera, miliolids.
Lagoon Margin Environment	
Textures:	Packstone and grainstone.
Grain types:	Large foraminifera, coralline algae, coral, *Halimeda*, mollusks, miliolids.
Lagoon Environment	
Textures:	Packstone and wackestone.
Grain types:	*Halimeda*, mollusks, miliolids, corals.

largely on Todd and Low (1960) and Schlanger (1963). Depositional characteristics of the six major environments are listed in Table 21-1. Large foraminifera and coralline algae are present throughout the shelf margin. Corals were also probably present throughout, though many have been dissolved without a trace in deeper slope strata (Fig. 21-7a). Planktonic foraminifera are distinct features in the slope and forereef facies. Miliolid foraminifera and substantial numbers of bivalves (pelecypods) are important for identification of lagoon and lagoon-margin deposits. Reef and forereef facies contain a substantial amount of boundstone, common sponge borings, and much submarine cement.

Depositional environments generally shifted basinward during deposition of the upper Eocene, Oligocene, and lower Miocene carbonates. E-1 is dominated by reefal boundstones in the lower Eocene which pass upward into backreef grainstones in the upper Eocene, and then into lagoon and lagoon-margin wackestones and packstones in the middle Oligocene. Slope wackestones, packstones, and grainstones dominate the Eocene of F-1. Lower Oligocene strata in F-1 contain forereef boundstones which pass upward to reefal boundstones and finally up to backreef grainstones in the lower Miocene (Fig. 21-6) (Todd and Low, 1960; Schlanger, 1963; Saller and Koepnick, 1990).

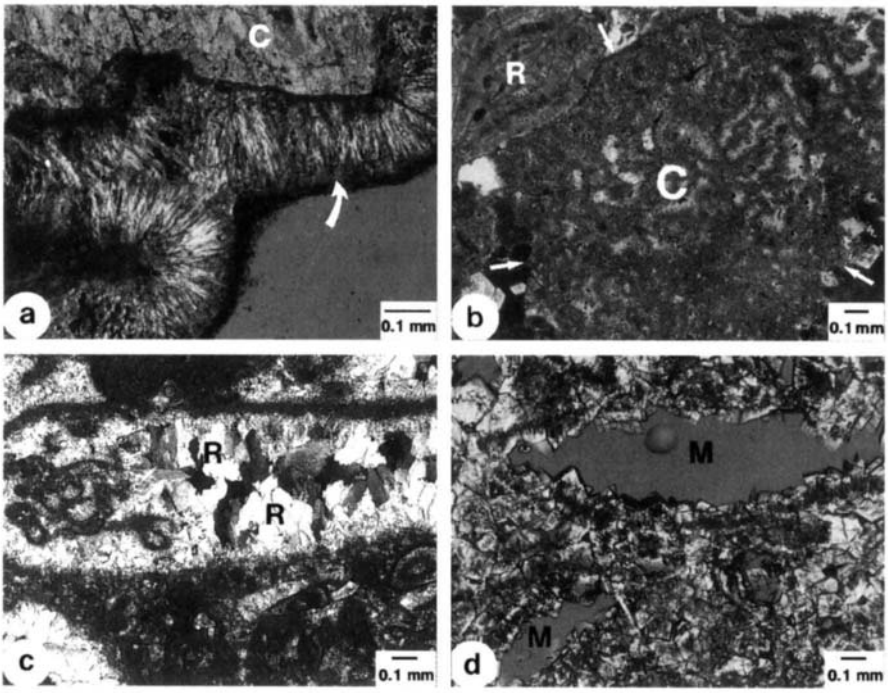


Fig. 21-7. Petrographic evidence of diagenetic alteration. (a) Photomicrograph of dissolved coral in slope deposits. (b) Photomicrograph of shallow aragonite cements (beachrock). (c) Photomicrograph of radiaxial calcite cements filling a dissolved coral/*Halimeda*. (d) Photomicrograph of deep dolomite and foraminifera mold.

Lower Miocene to Recent

Carbonate sediments of lower Miocene to Recent age can be divided into three unconformity-bounded sedimentary intervals (Fig. 21-4). Intervals I and II are separated by a major karst surface that likely correlates to the 85-m solution unconformity of Schlanger (1963). Intervals II and III are also separated by a subaerial exposure surface that likely correlates to the 310-m solution unconformity of Schlanger (1963).

Sedimentary Interval III (lower to middle Miocene) is characterized by broad, shallow-marine, backreef facies of larger foraminiferal sands and muds with subordinate amounts of coral floatstone, bafflestone and framestone in wells which were generally drilled in modern lagoon to lagoon-margin locations (Wardlaw and Henry, 1986). This interval corresponds with unit 5 of Wardlaw (1989). Mollusks and algal-coated grains are minor constituents in these deposits. Lower to middle Miocene sediments are now pervasively calcitized and well cemented. Moldic porosity is commonly well developed. At least eight unconformities have been recognized in this interval; some have well-developed laminated crusts (Wardlaw and Henry, 1986). A

pronounced unconformity at ~314 m subsea is marked by a major mineralogic transition from pervasively calcitized limestones below, to largely unaltered, aragonite-rich sediments above. This unconformity correlates with the solution unconformity (top of Tertiary e) recognized by Schlanger (1963) in F-1 and E-1.

Sedimentary Interval II contains two distinct sedimentary facies: units 3 and 4 of Wardlaw (1989). Unit 4, the lower portion of this interval, is Pliocene to late Miocene in age and is characterized by broad, shallow-water facies of coral-mollusk-rich sands and muds. These sediments are largely unaltered and rich in organic matter; this unit is sometimes referred to as the "organic interval" (Wardlaw and Henry, 1986). The organic matter increases in abundance with depth in the interval. Abundant palynomorphs, related to mangrove and other swamp pollens, are also recognized (Wardlaw and Henry, 1986). A similar distinctive sedimentary facies was recognized in F-1 and E-1 (Schlanger, 1963; Leopold, 1969). Most of unit 4 shows no evidence of subaerial exposure, except near its base.

Unit 3 is Pliocene in age and is characterized by well-cemented, generally well-lithified, pervasively leached and calcitized limestones that contain abundant karst features (e.g., vugs, fissures and caverns). Differentiation of depositional facies is difficult in unit 3 because of the pervasive alteration. At least eight unconformities are recognized in this pervasively calcitized Pliocene interval (~180–115 m subsea). The top of unit 3 is a major karst surface that occurs at ~115 m subsea in lagoon boreholes and ~85–90 m subsea in island boreholes.

Sedimentary Interval I contains Holocene (unit 1 of Wardlaw, 1989) and Pleistocene (unit 2 of Wardlaw, 1989) sediments and limestones. Carbonates from this interval have been extensively studied as part of the numerous shallow-drilling programs. Sediments of unit 2 in lagoon boreholes are generally characterized by coral floatstone, *Halimeda* and foraminiferal sands and muds with subordinate amounts of skeletal, mollusk wackestone and packstone. Sediments of unit 2 in island boreholes are dominated by fossiliferous packstones and grainstones with some wackestone and interbedded coral boundstone and coral and coralline algae clasts. Skeletal grains make up the bulk of these carbonates and include abundant coral, *Halimeda*, coralline algae and foraminifera (e.g., Couch et al., 1975; Henry and Wardlaw, 1986, Goter and Friedman, 1988; Saller, 1984b). Mollusk and echinoid fragments are a minor constituent in these sediments. In the lagoonal boreholes, Holocene sediment consists of *Halimeda*, mollusk packstone and wackestone. In the island boreholes nearest the lagoon, Holocene sediments generally consist of skeletal grainstone in the beach areas, skeletal packstone to grainstone on the islands themselves, and coarse-grained gravel and rudstone to floatstone on the oceanward margin (Henry and Wardlaw, 1986). The reef plate, a marine-cemented reef facies, is part of the armor that surrounds the atoll and is discussed in the next chapter.

No systematic change in depositional facies with depth is evident in lower Miocene to Recent carbonates on Anewetak Atoll. Seismic studies support atoll growth being aggradational not progradational during that period of time (Grow et al., 1986). Studies of submarine outcrops along the margin of the atoll report major unconformities and atoll rim facies, which support an aggradational history for early Miocene to Recent carbonates (Colin et al., 1986; Halley et al., 1986).

DIAGENETIC HISTORY

Carbonate rocks at Anewetak have provided insight into early diagenetic processes because they have been subjected to both marine and freshwater diagenesis, but have not been overprinted by deep burial diagenesis. Tertiary and Quaternary strata on Anewetak have undergone substantial diagenetic alteration including cementation, partial to complete calcitization of original high-Mg calcite and aragonite grains, and dolomitization. Identification of the environment responsible for the post-depositional alteration of carbonate rocks and sediments is facilitated by the integration of petrography (Figs. 21-7, 21-8) with stable isotope (Figs. 21-9, 21-10) and elemental (Fig. 21-11) geochemistry.

Marine diagenesis

Anewetak is a great natural laboratory for studying marine diagenesis because marine waters are currently circulating through the atoll and apparently have done so for many millions of years. The tremendous flow of seawater through the atoll margin is demonstrated by tidal fluctuations observed in deep well bores and anomalously low temperatures in deep wells. After being cased solidly to 601 m, the water level in F-1 fluctuated in phase and at the same amplitude as the adjacent open ocean indicating extremely permeable conduits between open ocean water and F-1 below 601 m (Swartz, 1958). After casing to 1,252 m, the water levels in E-1 fluctuated with a 2.5-cm amplitude at a 9.5-hour lag relative to surface tides (Swartz, 1958), indicating good permeability between E-1 and the open ocean, but not the extreme permeability associated with F-1. Temperatures within the carbonate sections of E-1 and F-1 decrease with depth supporting a substantial circulation of seawater into the atoll. Thermal convection may be the main force driving the marine circulation.

Carbonate saturation decreases with depth in modern ocean water. As a result, certain carbonate minerals become unstable in deeper seawater. Modern Pacific seawater becomes undersaturated with respect to aragonite at ~300 m, and becomes undersaturated with respect to calcite at ~1,000 m (Li et al., 1969; Scholle et al., 1983). As a result, three marine zones of diagenetic stability (Fig. 21-12) were observed with increasing depth on the Anewetak atoll margin: aragonite/high-Mg calcite (shallow), calcite (intermediate), and dolomite (deep) (Saller and Koepnick, 1990).

Aragonite/High-Mg calcite zone. The aragonite/high-Mg calcite zone occurs in shallow seawater and is dominated by precipitation of aragonite and high-Mg calcite cements (Figure 21-7a). This zone is what most geologists envisage for submarine carbonate diagenesis. These aragonite and high-Mg calcite cements include micrite, pelletal internal sediments, equant-to-prismatic, and fibrous morphologies which partially fill primary porosity in backreef, reef, forereef and beachrock environments (Fig. 21-7b). Cementation in beachrock on Anewetak was described by Schmalz (1971). Marine cementation in reef and forereef environments on Anewetak has been

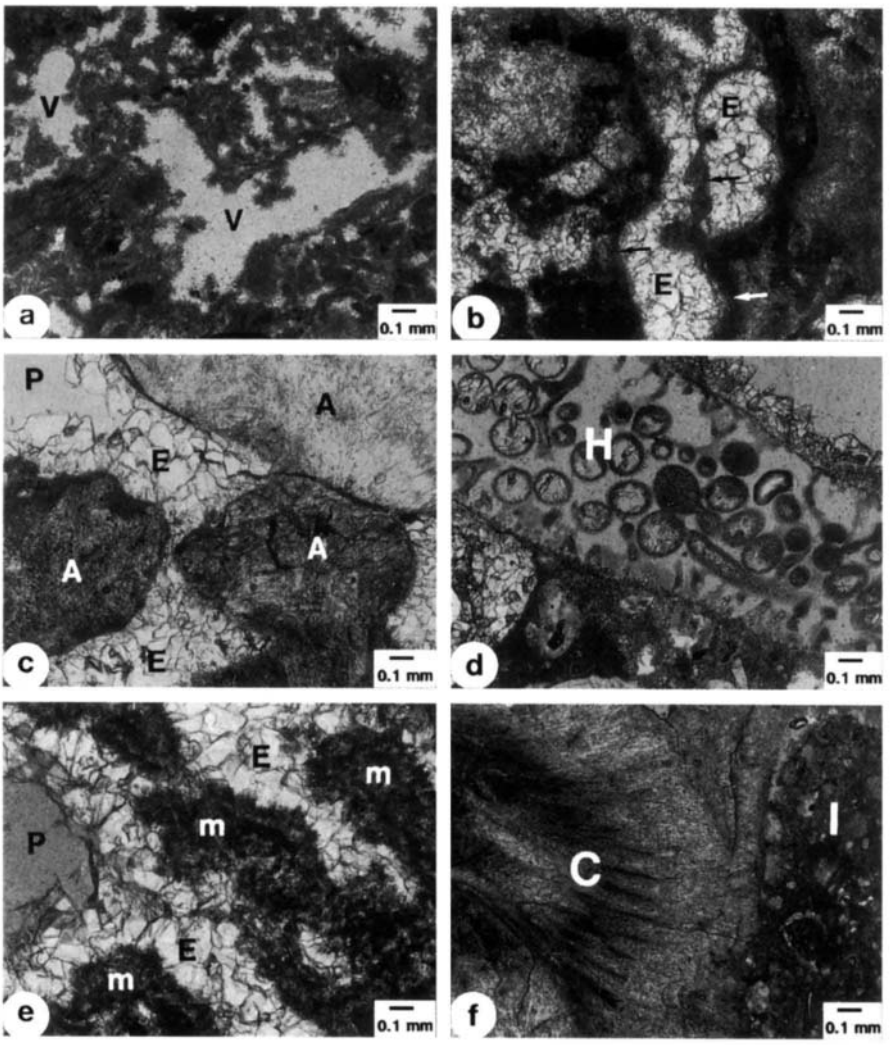


Fig. 21-8. Photomicrographs of (a) irregular soil zone dissolution, (b) soil zone micritic root sheaths, (c) capillary fringe cementation, (d) moldic dissolution of aragonite, (e) equant to prismatic crusts of cement filling aragonite molds, (f) intact aragonite deep in Pleistocene.

described by Halley and Slater (1987). No systematic dissolution of carbonate occurs in this zone, though local dissolution may occur perhaps associated with decreased carbonate saturation caused by organic reactions. Stable isotopic compositions of shallow-marine aragonite and high-Mg calcite cements were determined by Gonzalez and Lohmann (1985).

Calcite zone. Marine diagenesis in the calcite zone is characterized by dissolution of aragonite and precipitation of low-Mg calcite (Fig. 21-12). This diagenetic zone is

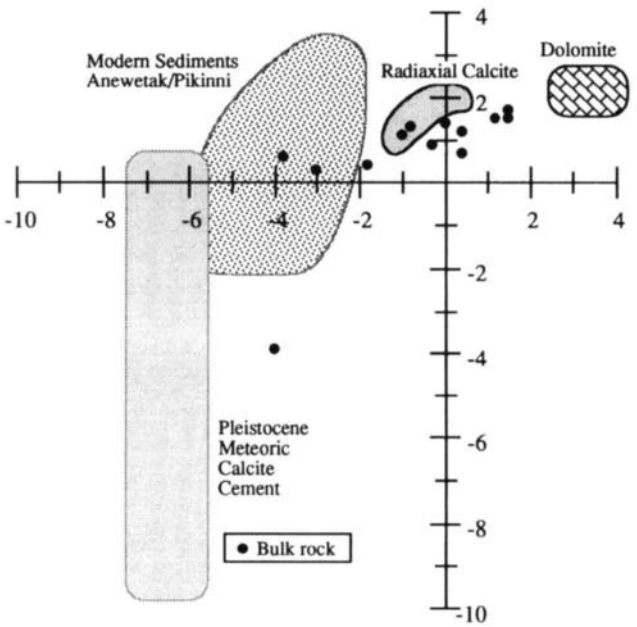


Fig. 21-9. Stable isotope cross-plot showing different compositions of modern marine sediment, radiaxial calcite cement, dolomite, and freshwater cements. (Modified from Saller and Koepnick, 1990.)

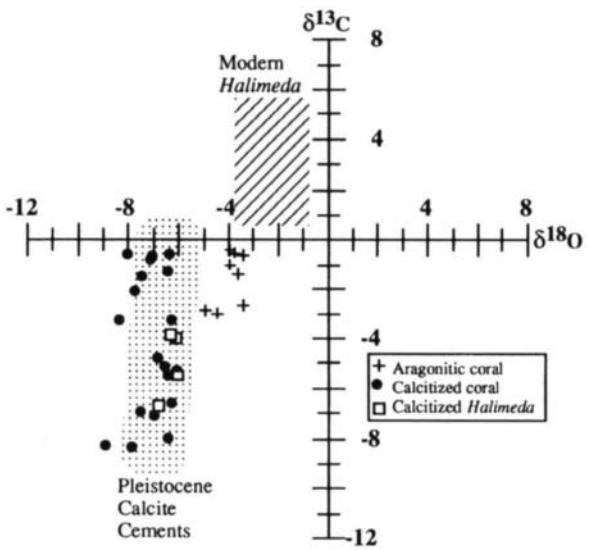


Fig. 21-10. Stable oxygen and carbon isotopic values of cements, calcitized aragonite and bulk-rock samples of Pleistocene strata.

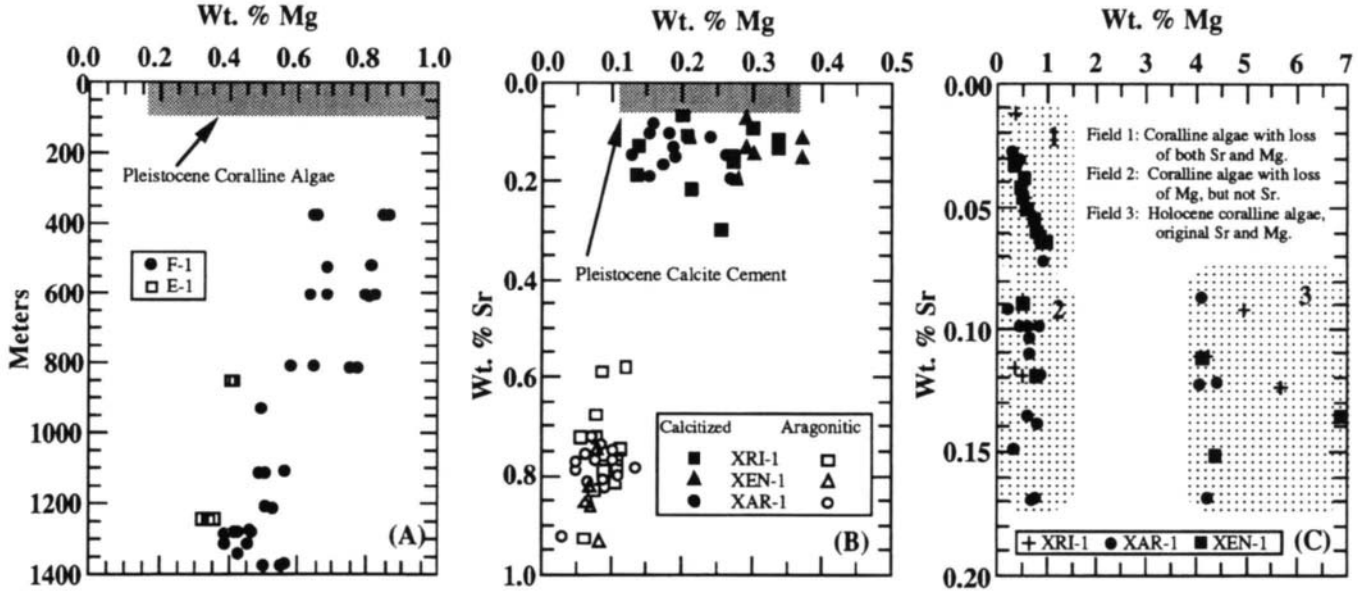


Fig. 21-11. Elemental geochemistry of selected carbonate allochems. (A) Mg content of coralline algae versus subsurface depth. (B) Cross-plot of Sr and Mg content of Pleistocene calcitized coral. (C) Cross-plot of Sr and Mg content of Pleistocene coralline algae.

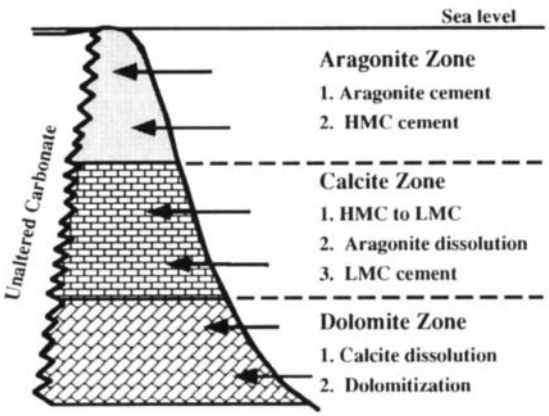


Fig. 21-12. Model for seawater diagenesis based on carbonate saturation which decreases with depth in modern oceans. In the modern Pacific Ocean, the aragonite saturation depth is at ~300 m, and the calcite saturation depth is at ~1,000 m (Scholle et al., 1983) at Anewetak Atoll. (From Saller and Koepnick, 1990.)

thought to occur in areas occupied by seawater that is (or was) undersaturated with respect to aragonite, but supersaturated with respect calcite. Seawater with these saturation levels occurs at depths of 300–1,000 m in the modern Pacific Ocean (Scholle et al., 1983). This style of diagenesis was observed in backreef, reef, and forereef strata between 300 and 1,000 m in F-1.

Diagenesis between 300 and 1,000 m in F-1 is dominated by aragonite dissolution and calcite cementation (Figure 21-7b). Those cements are mainly low-Mg calcite radiaxial calcite which have stable carbon and oxygen isotopes indicative of precipitation from seawater at temperatures of 13–26°C (Saller, 1986). Radiaxial calcite cements have strontium isotope ratios similar to depositional sediments 100–350 m higher in the section, suggesting precipitation at burial depths of 100–350 m (Saller and Koepnick, 1990). Radiaxial calcite cements commonly fill molds of aragonitic fossils (Figure 21-7c); however, calcite cements with morphologies and isotopic compositions similar to other freshwater cements were not observed in strata with radiaxial calcite cements. Therefore, aragonite dissolution is interpreted to have occurred in deep seawater, which compared to surface seawater, is more undersaturated with respect to carbonate minerals (Saller, 1986). High-Mg calcite skeletal grains have lost their magnesium and are now low-Mg calcite. Magnesium concentrations in original high-Mg calcite grains decrease with depth to the zone of dolomitization (Fig. 21-11a). This loss of magnesium with depth is thought to occur in progressively deeper seawater as carbonate saturation decreases with depth (Saller and Moore, 1989).

Dolomite zone. Marine diagenesis in the dolomite zone is characterized by dissolution of calcite and precipitation of dolomite (Fig. 21-12). The dolomite zone is present below the calcite zone and is thought to occur where deep seawater, un-

dersaturated with respect to calcite but supersaturated with respect to dolomite, circulates through the atoll margin (Saller, 1984b). Seawater undersaturated with respect to calcite occurs at depths below 1,000 m in the modern Pacific Ocean (Scholle et al., 1983).

Dolomite is present in reefal boundstones at approximately 1,250 m in E-1 and between 1,100 and 1,388 m in F-1 in wackestones, packstones, and grainstones deposited in slope environments. Dolomites are associated with partial or complete dissolution of calcite (Figure 21-7d). Most carbonate strata below 1,000 m have only scattered dolomite rhombs, but a few intervals are partially to completely dolomitized. Dolomite generally occurs as rhombs approximately 0.1 mm across. Some dolomite rhombs overgrow fractures in grains formed during burial compaction, suggesting dolomite precipitation after substantial burial (Saller, 1984b). Stable oxygen isotope values range from +2.9 to +3.9‰ (Fig. 21-9); such values are compatible with dolomite precipitation from seawater at temperatures of 10–20°C. Dolomites in Eocene strata at Anewetak have strontium isotope ratios similar to depositional carbonate in Miocene to Pleistocene strata located ~1,000 m higher in the section. This suggests dolomitization by seawater circulating through the atoll margin at depths of 1,000 m or more. Calcite dissolution is associated with dolomite precipitation suggesting that calcite dissolution and dolomitization occurred in seawater undersaturated with respect to calcite, but supersaturated with respect to dolomite.

Alternative interpretations. Other interpretations have been proposed for the origin of radiaxial calcite, aragonite dissolution, and dolomitization in Eocene and Oligocene carbonates on Anewetak. Schlanger (1963) postulated that much of the aragonite dissolution and calcite cementation in the Oligocene and lower Miocene of F-1 occurred in freshwater during subaerial exposure, although he did not recognize that radiaxial calcites were widespread. Videtich (1984) also studied radiaxial calcite cements in the Oligocene and lower Miocene of F-1, and concluded that they were formed by recrystallization of a fibrous to prismatic high-Mg calcite cement precipitated in very shallow water. Berner (1965) and Gross and Tracey (1966) thought that dolomitization in Eocene and Oligocene strata on Anewetak occurred in hypersaline water. We recommend reading the original articles for a detailed discussion of the rationale behind these alternative interpretations.

Freshwater diagenesis

Stratigraphic patterns. Due to repeated subaerial exposure, especially during the late Pliocene and Pleistocene, Anewetak is an excellent location to study meteoric diagenesis. Slightly altered aragonite-rich intervals alternate with strongly altered calcitic intervals throughout much of the upper Miocene, Pliocene, and Pleistocene section (Schlanger, 1963; Saller and Moore, 1989; Quinn, 1991a). Variations in intensity of meteoric diagenesis are probably related to length of exposure, facies type and the specific diagenetic environment that a particular rock experienced during

subaerial exposure. Intervals of intense diagenetic alteration are commonly 1–5 m thick (Saller and Moore, 1989; Quinn, 1991a). Most intervals of intense cementation and dissolution probably experienced diagenesis in a soil zone or the upper part of a freshwater lens during one or more periods of subaerial exposure (Saller and Moore, 1989; Quinn, 1991a). Intervals with dissolution, but very minor cementation, probably underwent diagenesis in a mixing zone for a significant period of time (Saller and Moore, 1989).

Stratigraphic variations in diagenetic alteration of the Pleistocene limestones on Anewetak were used to construct models for vertical and lateral patterns in meteoric diagenesis (Fig. 21-13). Pleistocene diagenetic systems were apparently characterized by thin freshwater lenses and thick mixing zones similar to hydrologic systems beneath modern Anewetak islands (Wheatcraft and Buddemeier, 1981) [see also Chap. 22]. Paleosol zones are characterized by intense diagenetic alteration including non-fabric-selective (vuggy) dissolution, fabric-selective dissolution (moldic), micritic and sparry cements, and some replacive caliches (Figure 21-8a, b). Paleo-middle vadose zones have relatively minor dissolution and cementation leaving much intact aragonite. Paleo-capillary fringe zones (just above water tables) are characterized by major amounts of equant and prismatic calcite cement, and minor

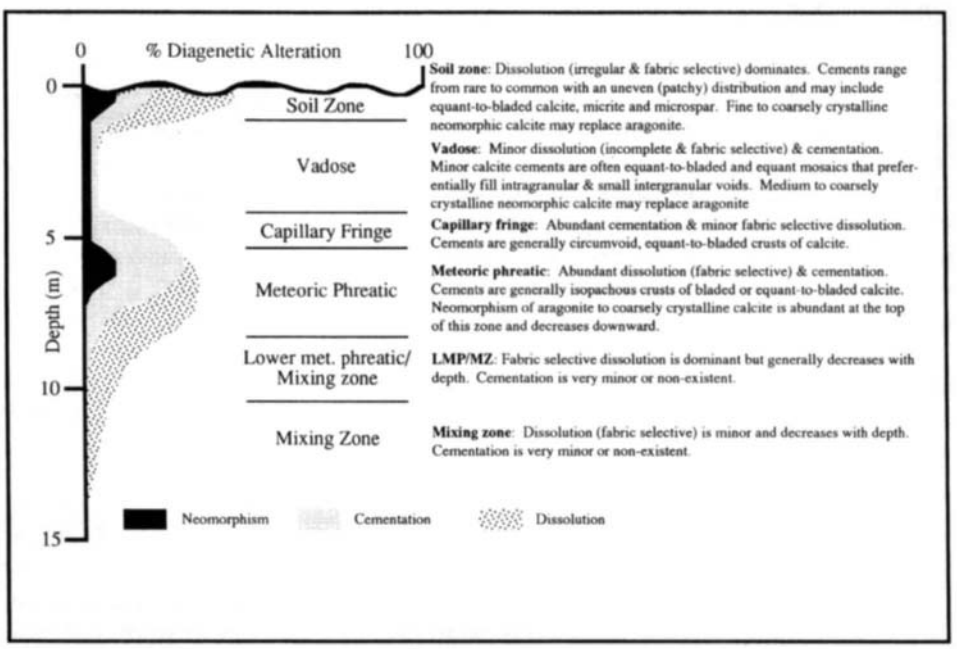


Fig. 21-13. Model for freshwater diagenesis attendant with subaerial exposure based on data on samples from the Pleistocene section of numerous EXPOE boreholes. Environment of alteration is listed along with idealized horizontal and vertical scales. The actual amounts of alteration are different below each exposure surface, but the overall trends depicted are correct. (Modified from Saller and Moore, 1989.)

amounts of fabric-selective dissolution of aragonite (Figure 21-8c). The upper 1–4 m of paleo-meteoric phreatic zones generally experienced major fabric-selective dissolution and extensive cementation by equant and prismatic calcite (Figure 21-8d, e). The lower meteoric phreatic and mixing zones were sites of moderate dissolution of aragonite with little or no calcite cementation. Lower parts of paleo-mixing zones and marine phreatic zones below islands showed little diagenetic alteration (Figure 21-8f).

At the time of deposition, the Pleistocene sediments consisted mainly of metastable high-Mg calcite and aragonite. Most high-Mg calcite in Plio-Pleistocene strata has inverted to low-Mg calcite with little or no petrographic change (Goter and Friedman, 1988; Quinn, 1991a). This loss of magnesium apparently happened very rapidly in freshwater environments. High-Mg calcite fossils were dissolved in a few locations, and a few echinoderm fragments remain as slightly Mg-rich calcite (~6 mole% $MgCO_3$). The current state of aragonitic fossils is quite variable with some completely dissolved, some chalkified, some calcitized, and some still intact. Much of the calcitized aragonite on Anewetak is thought to form by partial, intrafabric dissolution (chalkification) of aragonite followed by precipitation of sparry calcite over the chalkified aragonite (Saller, 1991). This mechanism produces calcitized aragonite which is very similar to neomorphic spar with preservation of some of the original wall structure (Bathurst, 1975).

Geochemical patterns. Calcite cements and calcitized fossils in Plio-Pleistocene strata in Anewetak boreholes have been analyzed for stable isotopes, trace elements, and strontium isotopes. Most of the Plio-Pleistocene calcite cements and calcitized fossils were the result of meteoric diagenesis.

Stable carbon and oxygen isotopes have been analyzed in bulk-rock samples, calcite cements, calcitized aragonite, and coralline algae. Meteoric calcite cements are characterized by a narrow range of stable oxygen isotope values and a broad range of stable carbon isotope values (Saller and Moore, 1991; Quinn, 1991a). The stable oxygen isotopic values of these cements range from −8 to −5‰ (PDB) and are similar to values expected for calcite precipitated from modern freshwater ($\delta^{18}O$ of −5.8 to −3.8‰ SMOW) at 28°C in the vicinity of Anewetak (Saller and Moore, 1991). The broad range of stable carbon isotope values (i.e., −9.6 to +0.4‰ PDB; Saller and Moore, 1991; Quinn, 1991a) reflects variable mixtures of organic soil-derived carbon ($\delta^{13}C$ of −25‰; Quinn, 1991a) and depositional carbon (−2 to + 4‰; Gross and Tracey, 1966; Gonzalez and Lohmann, 1985). Calcitized aragonite has stable isotopic values similar to the meteoric cement values (Saller, 1992). Bulk-rock isotope profiles in many boreholes indicate lower $\delta^{13}C$ and $\delta^{18}O$ values in paleosol zones, paleofreshwater lenses, and other calcitized intervals (Quinn, 1991a).

As with stable carbon and oxygen isotopes, trace element concentrations have been determined for bulk-rock samples and a variety of components in Plio-Pleistocene carbonates affected by freshwater diagenesis. Strontium and magnesium concentrations were determined for bulk-rock samples in Plio-Pleistocene strata by Quinn (1991a), in Pleistocene calcite cements by Saller and Moore (1991), in calcitized aragonitic fossils in Pleistocene strata by Saller (1992), and in Pleistocene

coralline algae and echinoderm fragments (originally high-Mg calcite) by Saller (1984a). Bulk reefal rocks and calcitized coral and *Halimeda* have strontium concentrations well below those present in aragonitic coral and *Halimeda*, but distinctly higher than co-existing calcite cements (Figure 21-11b). Lagoonal carbonates (mollusk-rich) have substantially lower strontium concentrations apparently reflecting lower original strontium concentration than observed in coral and *Halimeda*-rich sediments (Quinn, 1991a). Calcitized coral and *Halimeda* have magnesium concentrations similar to co-existing calcite cements. Strontium and magnesium concentrations of Pleistocene coralline algae and echinoderm fragments fall into two fields — one with strontium concentrations similar to high-Mg calcite precursor and one with lower strontium concentration (Figure 21-11c). This suggests that two different processes were involved in the conversions of high-Mg calcite to low-Mg calcite, though that was never demonstrated.

CASE STUDY: USE OF SR ISOTOPES TO DETERMINE ACCOMMODATION, SUBSIDENCE, AND SEA-LEVEL CHANGE

Strontium isotope data from Anewetak have been used by several workers to derive a more accurate record of accommodation, subsidence, and Cenozoic sea-level change (Halley and Ludwig, 1987, 1989; Ludwig et al., 1988; Saller and Koepnick, 1990; Quinn et al., 1991). Two different approaches have been used to constrain the record of sea-level change at Anewetak. The first approach uses strontium isotope ratios of samples and curves of strontium isotope variations in seawater through time to determine depositional ages (e.g., Ludwig et al., 1988; Saller and Koepnick, 1990; Quinn et al., 1991). Strontium isotope ratios give substantially greater resolution than biostratigraphy in dating most shallow-marine limestones deposited between the Oligocene and the present. Appropriate measures must be taken to avoid the incorporation of allochthonous strontium to ensure accurate results. More accurate dating of shallow-marine carbonates allows better estimations of rate of carbonate accumulation and accommodation (subsidence plus sea-level change). The second approach compares the strontium isotope ratios of depositional and diagenetic components to estimate the timing and depth of the diagenetic event. Strontium isotope ratios of marine cements and dolomite provided constraints on the timing and depth of burial at the time of cementation and dolomitization (Saller, 1984b; Saller and Koepnick, 1990). Alternatively, strontium isotope ratios determined from freshwater cements can be used to relate site of dissolution with site of precipitation (Quinn et al., 1991). The stratigraphic redistribution of strontium during subaerial exposure can be used to estimate the timing and magnitude of sea-level change.

Depositional age

Strontium isotope data from Cenozoic carbonates of Anewetak have been used to better constrain rates of accommodation, subsidence, and relative sea-level change.

Saller and Koepnick (1990) determined the strontium isotopic ratios of carbonate samples in E-1 and F-1 between depths of 370 m and the volcanic basement at 1,255 and 1,400 m subsea, respectively. Meters in core have been converted to subsea meters in these two boreholes (Lincoln and Schlanger, 1991). Age determinations based on strontium isotope ratios indicated that the section deeper than 370 m subsea spans the late Eocene to early Miocene (~23 Ma). The only distinct break in sedimentation (subaerial exposure) during this interval was observed at ~845 m subsea in E-1 in rocks that were deposited in a backreef environment. No correlative unconformity was found in F-1, probably because time-equivalent rocks in that well were deposited in a slope environment and hence were not subaerially exposed.

Strontium isotope stratigraphy was also determined on two PEACE Program boreholes (KAR-1; Ludwig et al., 1988, and OOR-17; Quinn et al., 1991). Ludwig et al. (1988) identified subsurface intervals of little or no change in strontium isotopic ratio, punctuated by sharp transitions to lower values with increasing subsurface depth. These intervals of invariant strontium isotopic ratio were termed strontium isotope plateaus by Ludwig et al. (1988). Age determinations based on strontium isotope ratios indicate that the upper 380 m subsea spans the early Miocene (~21 Ma) to Recent. Ludwig et al. (1988) identified major hiatuses at ~314 m subsea (rocks of 12.3–18.2 Ma missing) and at ~153 m subsea (rocks of 3.0–5.3 Ma missing). Quinn et al. (1991) used strontium isotopic data on carbonate samples from OOR-17 and KAR-1. These authors concluded that correlative stratigraphic intervals of similar strontium isotopic values did exist between the two boreholes, especially at depths less than 140 m subsea. However, temporal discrepancies between the two boreholes were also identified (e.g., a ~5-m.y. hiatus identified in OOR-17 was not identified in KAR-1).

The strontium isotope age-depth trend for Anewetak samples has three characteristic patterns, as first determined by Ludwig et al. (1988). The first pattern, intervals where strontium isotope ratios show no resolvable change with depth, documents periods of rapid accumulation of carbonate sediments during highstands of sea level. These periods occur at 0.6, 1.4, 3.0, 5.3 and 5.6 Ma in KAR-1 (Ludwig et al., 1988). The second pattern, intervals where strontium isotope ratios decrease continuously with depth, documents periods of slow accumulation of sediments during highstands of sea level. These periods occur at ~18.2–21 Ma and ~9–12.3 Ma in KAR-1 (Ludwig et al., 1988) and at ~22–30 Ma and 31–45 Ma in F-1 and E-1, respectively (Saller and Koepnick, 1990). The third pattern, intervals where strontium isotope ratios change abruptly with depth, are indicative of periods of subaerial exposure during lowstands of sea level when no carbonate was being accumulated and/or carbonate was being eroded. Abrupt shifts in apparent age occur in KAR-1 at 3.0–5.3 Ma and at ~12.3–18.2 Ma.

An age-depth profile of the limestone section at Anewetak (Fig. 21-14) was constructed using strontium isotope ages (e.g., Halley and Ludwig, 1987; Saller and Koepnick, 1990; Lincoln and Schlanger, 1991). Such a profile permits the calculation of average rates of accumulation and accommodation. Rates of accommodation can be calculated in an atoll setting if deposition is near sea level, carbonate sedimentation roughly keeps pace with sea-level rise, and post-depositional compaction is

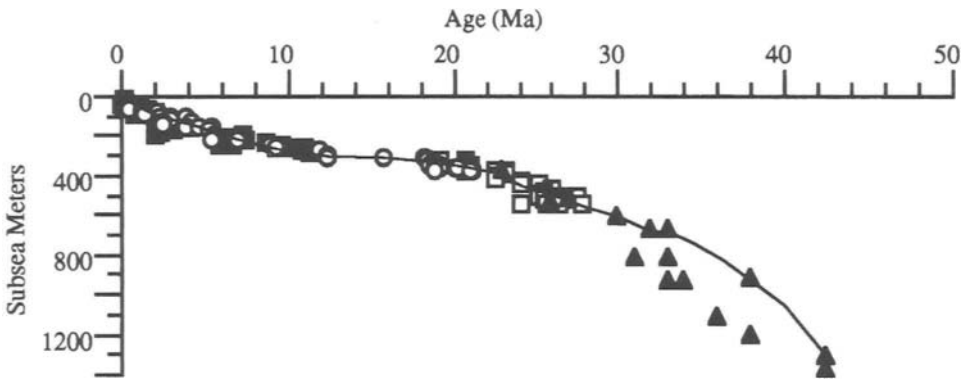


Fig. 21-14. Depth-age profile based on Sr isotope ages. Data are from KAR-1 (open circles; Ludwig et al., 1988), OOR-17 (closed squares; Quinn et al., 1991), OBZ-4 (open squares; Quinn, unpublished data), and F-1 (closed triangles; Saller and Koepnick, 1990). Solid line through the data is an approximate accommodation curve which may also be a first approximation of a subsidence curve for Anewetak. (Modified from Saller and Moore, 1989.)

negligible. Rates of accommodation are 50–130 m per m.y. for Eocene carbonates, 48 m per m.y. for early Oligocene carbonates, 26 m per m.y. for late early Oligocene to early Miocene carbonates (Saller and Koepnick, 1990), and 23 m per m.y. for early Miocene to Recent carbonates (Halley and Ludwig, 1987). It is also possible to use the age-depth profile as an approximate subsidence curve for the atoll assuming no systematic long-term variations in eustatic sea level (Figure 21-14; Halley and Ludwig, 1987; Saller and Koepnick, 1990); however, to support these assumptions, one should use a complete subsidence model including such variables as thermal subsidence of the volcanic basement, lithospheric flexure due to sediment load and paleodepths as presented in Lincoln and Schlanger (1991).

Diagenetic ages and constraints on sea level

Diagenesis can redistribute and hence alter the strontium isotopic composition of carbonate rocks. While redistribution of strontium isotopes will complicate their use for chronostratigraphy (Quinn et al., 1991), it can help to monitor diagenetic fluids and determine the timing of diagenetic alteration (e.g., Swart et al., 1987; Muller et al. 1990). Ludwig et al. (1988) found that freshwater calcite cements had strontium isotope ratios similar to surrounding depositional strata and proposed that strontium had limited mobility in freshwater systems. In contrast, Quinn et al. (1991) found that strontium isotope ratios in some freshwater calcite cements were substantially different than depositional strontium in the host rock. Strontium in those meteoric calcites was apparently dissolved from higher (younger, more radiogenic) carbonate strata and moved down tens of meters through the vadose zone during lowstands of sea level and precipitated as phreatic cements in older carbonate strata. Theoretical calculations and empirical measurements indicate that the position of the

top of the phreatic lens and mean sea level are closely associated on mid-ocean atolls (e.g., Wheatcraft and Buddemeier, 1981; Ayers and Vacher, 1986). The position of the phreatic lens changes with time and space in response to changes in sea level (e.g., Steinen and Matthews, 1973; Matthews and Frohlich, 1987). Given the intimate association of the meteoric phreatic lens and mean sea level, the position of sea level during subaerial exposure (generally lowstands) can be constructed from diagenetic calcite cements that have precipitated in a freshwater phreatic lens.

Strontium isotope data from those phreatic calcite cements can be used to determine the magnitude of sea-level change and the location of sea level during specific lowstands. For example, calcite cements with distinctly Pleistocene strontium isotopic values occur at ~119.0 and 128.1 m within Pliocene strata of KAR-1 (Fig. 21-15). Those cements have stable isotope and minor element values and petrographic features characteristic of precipitation in the meteoric phreatic environment (Quinn, 1991a). Strontium isotopic ratios of the cements are identical to the strontium isotopic values of the overlying strontium isotope plateau (II) (Fig. 21-15), and support calcite cementation at 1.20 Ma with limits of 1.12 and 1.47 Ma. Four

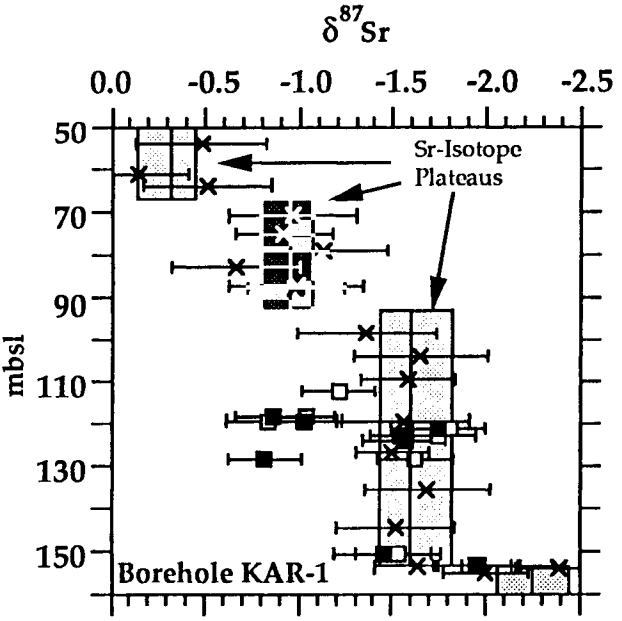


Fig. 21-15. Sr isotope plateaus and cements at Anewetak Atoll. Comparison of Sr isotope data from KAR-1 (Quinn et al., 1991; open and solid squares) with Sr isotope plateaus and data of Ludwig et al. (1988) (x's). Open squares indicate low-Mg calcite whole-rock matrix samples, and solid squares indicate low-Mg calcite cement samples. Calcitization and cement precipitation occurred in the meteoric phreatic environment (Quinn, 1991). These data confirm previously established Sr isotope plateaus and identify intervals of anomalously high $\delta^{87}Sr$ values compared to adjacent samples. These intervals of anomalous $\delta^{87}Sr$ values document the stratigraphic redistribution of Sr from overlying younger rocks to underlying older rocks. (From Quinn et al., 1991.)

ancient soil zones (i.e., subaerial exposure surfaces) have been identified within strontium isotope plateau II (Fig. 21-16). The stratigraphic relation between the site of carbonate dissolution (i.e., ancient soil zone), diagenetic calcite precipitation (i.e., paleo-phreatic lens), and the apparent age of the calcite cement, place minimum and maximum constraints on the magnitude of the sea-level fall. A minimum sea-level fall of 34 m is required from the shallowest occurrence of calcite cement (119 m) and the deepest occurrence of a ancient soil zone within plateau II (85 m) (Fig. 21-16). In contrast, a maximum sea-level fall of 64 m is based on the deepest occurrence of calcite cement (128 m) and the shallowest occurrence of a plateau II soil zone (64 m) (Fig. 21-16). The present position and inferred age of the calcite cement can also be used to place constraints on the elevation of ancient sea level during lowstands of sea level. The apparent age of calcite cementation and its age limits suggest that early Pleistocene sea-level lowstand elevation was between 72 and 81 m (range of 60 to 100 m) below modern sea level (Fig. 21-17) given subsidence rates ranging from 25 to 40 m per m.y. (typical of atolls like Anewetak, e.g., Detrick and Crough, 1978; Menard and McNutt, 1982; Schlanger et al., 1987).

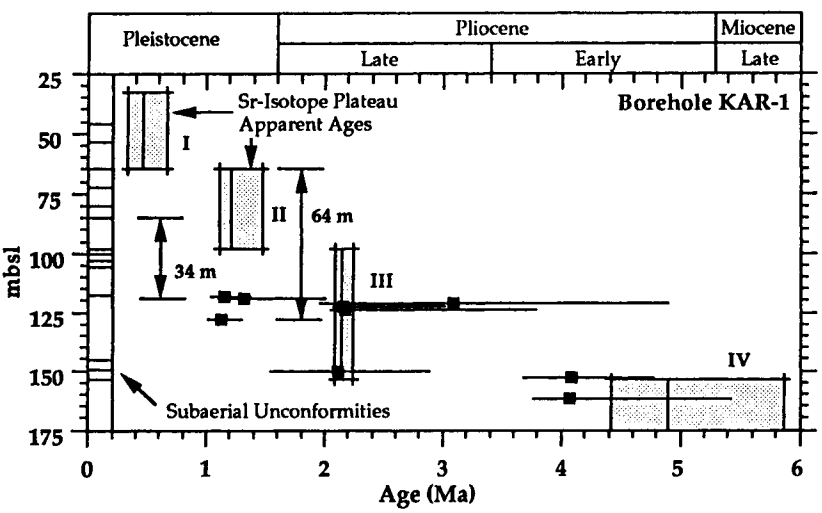


Fig. 21-16. Sea-level falls and Sr isotopes at Anewetak Atoll. Stratigraphic column on the left inset denotes stratigraphic distribution of subaerial unconformities. Light stippled rectangles denote apparent age and its uncertainty of Sr isotope plateaus. Roman numerals within the inset panel identify apparent Sr isotope plateaus. Solid black squares are apparent ages of calcite cements that were precipitated in the meteoric phreatic environment, an environment whose position is intimately related to mean sea-level. A minimum sea-level fall of 34 m at 1.2 Ma is estimated from the difference between the deepest subaerial unconformity within plateau II (i.e., site of carbonate dissolution and source of Sr) and the shallowest, anomalously young, meteoric calcite cement within plateau III (i.e., site of carbonate precipitation). A maximum sea-level fall of 64 m at 1.2 Ma is estimated from the difference between the shallowest subaerial unconformity within plateau II and the deepest, anomalously young, meteoric calcite cement within plateau III. (From Quinn et al., 1991.)

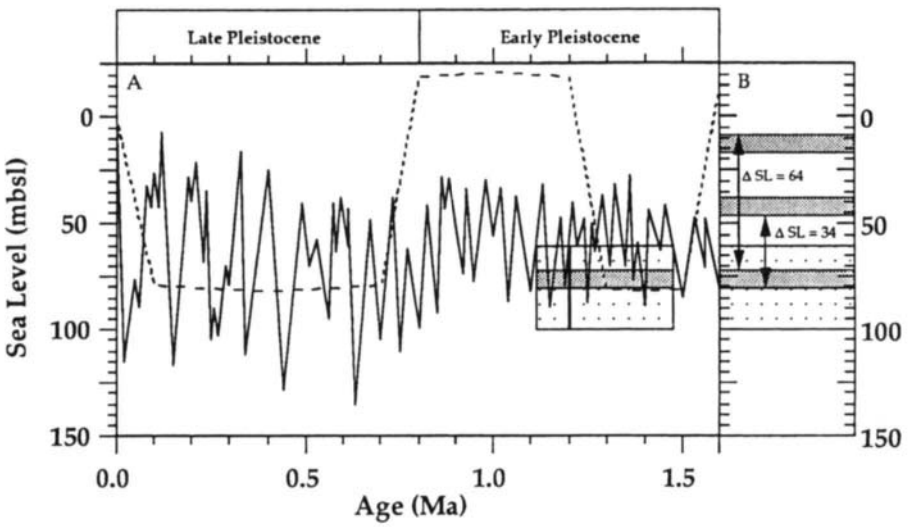


Fig. 21-17. (A) Sea-level elevations at Anewetak Atoll compared to the proxy sea-level records based on sequence stratigraphy (dashed line; Haq et al., 1987) and foraminiferal $\delta^{18}O$ data (solid line; Prentice and Matthews, 1989). The present-day stratigraphic position of the anomalously young, meteoric calcite cements within plateau III are backtracked for subsidence, using subsidence rates of 25–40 m per m.y. to estimate an ancient sea-level elevation. The width of the light stippled rectangle denotes the range of possible ages given the apparent age (solid vertical line) and its uncertainty of the calcite cements. The height of the light stippled rectangle denotes the range of possible sea-level elevations given the range of subsidence rates. The position of the dark stippled rectangle is calculated using a subsidence rate of 39 m per m.y., a rate that previously has been estimated for Anewetak (Quinn and Matthews, 1990). (B) Estimate of the elevation of sea level immediately prior to the early Pleistocene sea-level lowstand that resulted in the precipitation of early Pleistocene calcite cements within the Pliocene sequence at Anewetak. A change in sea level of between 34 to 64 m (Fig. 21.16) suggests that early Pleistocene sea-level highstand elevation was between 8 and 47 mbsl. (From Quinn et al., 1991.)

Comparisons with published sea-level curves

Truly eustatic sea-level curves should represent sea-level changes on a worldwide basis. To construct a eustatic sea-level curve, relative sea levels should be compared in many different basins around the world. Anewetak is an excellent place to test eustatic sea-level curves because it has been accumulating shallow-marine carbonate sediment since the Eocene and is away from basins commonly used to construct other sea-level curves. Any rapid sea-level drop of more than 10–20 m should result in a hiatus and distinct subaerial exposure surface in these shallow-marine carbonates. In contrast, thick intervals of carbonate sediment should be deposited during periods of rapid sea-level rise, unless the atoll was drowned.

The Haq et al. (1988) sea-level curve depicts sea-level fluctuations for the Mesozoic and Cenozoic, including the time represented by carbonate sediments on Anewetak. Patterns of deposition and subaerial exposure on Anewetak do not

support some parts of the Haq et al. (1988) sea-level curve. Subaerial exposure of shallow-marine carbonates should have been associated with the large 30 Ma sea-level drop if the drop had the amplitude and rate of change depicted in Haq et al. (1988). No such subaerial exposure surface was observed in Oligocene strata on Anewetak (Saller and Koepnick, 1990). Anewetak cores show a subaerial hiatus at 3.0–5.3 Ma and another one at 12–18 Ma — times of long-term highstands of sea level according to Haq et al. (1988). Patterns of Pleistocene sedimentation also do not agree with parts of the Pleistocene curve in Haq et al. (1988), although clearly the Pleistocene part of the Haq et al. (1988) curve is generalized and higher-frequency sea-level fluctuations are present (Quinn, 1991b). In summary, several "eustatic" trends and events shown on the Haq et al. (1988) sea-level curve were not observed in Anewetak carbonates as dated by strontium isotope ratios. This finding suggests that relative sea-level fluctuations on Anewetak were controlled primarily by local subsidence and/or that the Haq et al. (1988) curve is not correct in several time periods during the Cenozoic.

Stratigraphic modeling indicates that Plio/Pleistocene deposition and subaerial exposure on Anewetak are generally compatible with the deep-sea oxygen isotope sea-level proxy of Prentice and Matthews (1989), although tectonic subsidence probably controls long-term depositional patterns (Quinn, 1991b; Wardlaw and Quinn, 1991).

CONCLUDING REMARKS

Carbonate rocks at Anewetak Atoll have been studied for many decades, and the results of these studies have led to a better understanding of the dynamic processes and products associated with carbonate-island geology. Landmark biostratigraphic studies based on Anewetak material range from the early classic work of Cole (1957) and Todd and Low (1960) to the recent pioneering studies of Cronin et al. (1986) and Wardlaw (1989). Schlanger (1963) contains pioneering work in atoll depositional systems and carbonate diagenesis. Geochemical studies of Anewetak material range from some of the earliest applications of isotope geochemistry (e.g., Kulp, 1963; Berner, 1965; Gross and Tracey, 1966) to applications of some of recent advances in isotope geochemistry (e.g., Ludwig et al., 1988; Saller and Koepnick, 1990; Lincoln et al., 1993). Studies at Anewetak have also provided strong evidence for the direct linkages between hydrogeologic processes and diagenetic products. For example, Saller (1984b) provided some of the best evidence to date that subsurface dolomitization can result from thermally driven subsurface seawater flow. Lastly, stratigraphic studies have provided the temporal framework required to evaluate the record of sea-level change at Anewetak. Sea-level history from the perspective of a mid-ocean atoll like Anewetak provides independent constraints on the records of sea-level change inferred from continental-margin stratigraphies and from deep-sea foraminiferal oxygen isotope stratigraphies.

ACKNOLWEDGMENTS

The present authors are only just the latest in a long line of geologists who "cut their geologic teeth" by studying the carbonate rocks at Anewetak. We both are indebted to the all of our predecessors who contributed to our knowledge about the geology of Anewetak. Quinn would like to personally thank Rob Matthews, Bruce Wardlaw, Bob Halley, Woody Henry, Dick Poore, Tom Cronin, John Humphrey, David Budd, and Rick Major for all of their help over the years.

REFERENCES

Adams, C.G., 1970. A reconsideration of the East Indian letter classification of the Tertiary. Bull. Br. Mus. (Nat. Hist.) Geol., 19, (3): 85–137.

Adams, C.G., 1983. Speciation, phylogenesis, tectonism, climate and eustasy: Factors in the evolution of Cenozoic larger foraminiferal bioprovinces. In: R.W. Sims, J.H. Price and P.E.S. Whalley (Editors), Evolution, Time and Space: The Emergence of the Biosphere. Academic Press, New York, pp. 255–289.

Adams, C.G., 1984. Neogene larger Foraminifera, evolutionary and geological events in the context of datum planes. In: N. Ikebe and R. Tsuchi (Editors), Pacific Neogene Datum Planes: Contributions to Biostratigraphy and Chronology. Univ. Tokyo Press, Tokyo, pp. 47–67.

Ayers, J.F. and Vacher, H.L., 1986. Hydrogeology of an atoll island: a conceptual model from detailed study of a Micronesian example. Groundwater, 24: 185–198.

Bathurst, R.G.C., 1975. Carbonate Sediments and Their Diagenesis, 2nd ed. Elsevier, Amsterdam, 658 pp.

Berggren, D.D., 1995. Creataceous hotspot tracks through the Marshall Islands. In: J.A. Haggerty, I. Premoli Silva, F. Rack and M.K. McNutt (Editors), Proc. ODP, Sci. Results, 144: Ocean Drilling Program, College Station TX, pp. 605–613.

Berner, R.A., 1965. Dolomitization of mid-Pacific atolls. Science, 147: 1297–1299.

Bybell, L.M., and Poore, R.Z., 1991. Calcareous nannofossils and planktic foraminifers from Enewetak Atoll, western Pacific Ocean, Geological and Geophysical Investigations of Enewetak Atoll, Republic of the Marshall Islands. U.S. Geol. Surv. Prof. Pap., 1513-C, 21 pp.

Cole, W.S., 1954. Larger foraminifera and smaller diagnostic foraminifera from Bikini drill holes. U.S. Geol. Surv. Prof. Pap., 260-O: 569–608.

Cole, W.S., 1957. Larger foraminifera from Eniwetok drill holes. U.S. Geol. Surv. Prof. Pap., 260-V: 742–784.

Colin, P.L., Devaney, D.M., Hillis-Colinvaux, L., Suchanek, T.H. and Harrison, J. T., III, 1986. Geology and biological zonation of the reef slope, 50–360 m depth at Enewetak Atoll, Marshall Islands. Bull. Mar. Sci., 38: 111–128.

Couch, R.F., Fetzer, JA., Goter, E.R., Ristvet, B.L., Tremba, E.L., Walter, D.R. and Wendland, V.P., 1975. Drilling operations on Eniwetok Atoll during Project EXPOE. Tech. Rep. TR-75-216, Air Force Weapons Lab., Kirtland Air Force Base, N.M., 278 pp.

Cronin, T.M., Brouwers, E., Bybell, L., Edwards, L., Gibson, T., Margerum, R. and Poore, R.Z., 1986. Pacific Enewetak Crater Exploration (PEACE) Program, Enewetak Atoll, Republic of the Marshall Islands, Part 2: Paleontology and Biostratigraphy of Enewetak Atoll, Marshall Islands: Application to OAK and KOA Craters. U.S. Geol. Surv. Open File Rep. 86–159, 39 pp.

Darwin, C.R., 1837. On certain areas of elevation and subsidence in the Pacific and Indian oceans as deduced from the study of coral formations. Proc. Geol. Soc. London: 2, 51, 552–554.

Darwin, C.R., 1842. On the structure and distribution of coral reefs. Smith, Elder, and Co., London, 278 pp. (reprinted by Cambridge University Press, London and New York, 1962, and by the University of Arizona Press, Tucson, 1984)

Detrick, R.S. and Crough, S.T., 1978. Island subsidence, hot spots, and lithospheric thinning. J. Geophys. Res., 83: 1236–1244.

Emery, K.D., Tracey, J.I., Jr. and Ladd, H.S., 1954. Geology of Bikini and nearby atolls. U.S. Geol. Surv. Prof. Pap., 260-A, 265 pp.

Gibson, T.G. and Margerum, R., 1991. Larger foraminifer biostratigraphy of PEACE boreholes, Enewetak Atoll, Western Pacific Ocean, Geological and Geophysical Investigations of Enewetak Atoll, Republic of the Marshall Islands. U.S. Geol. Surv. Prof. Pap., 1513-D, 14 pp.

Gonzalez, L.A. and Lohmann, K.C., 1985. Carbon and oxygen isotopic composition of Holocene reefal carbonates. Geology, 13: 811–814.

Goter, E.R., 1979. Depositional and diagenetic history of the windward reef of Anewetak atoll during the mid to late Pleistocene and Holocene. Ph.D. Dissertation, Rensselaer Polytechnic Institute, Troy NY, 240 pp.

Goter, E.R. and Friedman, G.M., 1988. Deposition and diagenesis of the windward reef of Anewetak Atoll. Carbonates and Evaporites, 2: 157–180.

Gross, M.G. and Tracey, J.I., Jr., 1966. Oxygen and carbon isotope composition of limestones and dolomites, Bikini and Enewetak Atolls. Science, 151: 1082–1084.

Haggerty, J.A. and Premoli Silva, I., 1995. Comparison of the origin and evolution of northwest Pacific guyots drilled during Leg 144. In: J.A. Haggerty, I. Premoli Silva, F. Rack and M.K. McNutt (Editors), Proc. ODP, Sci. Results, 144. Ocean Drilling Program, College Station TX, pp. 935–949.

Halley, R.B. and Ludwig, K.R., 1987. Disconformities and Sr-isotope stratigraphy reveal a Neogene sea-level history from Enewetak Atoll, Marshall Islands, Central Pacific (abstr.). Geol. Soc. Am. Abstr. Programs, 19: 1370.

Halley, R.B. and Ludwig, K.R., 1989. Ancient sea levels from atoll stratigraphy: the Enewetak model (abstr.). EOS, Trans. Am. Geophys. Union, 70: 1370.

Halley, R.B. and Slater, R.A., 1987. Geologic reconnaissance of natural fore-reef slope and a large submarine rockfall exposure, Enewetak Atoll (abstr.). Am. Assoc. Petrol. Geol. Bull., 71 (5): 563–564.

Haq, B.U., Hardenbol, J. and Vail, P.R., 1987. Chronology of fluctuating sea levels since the Triassic. Science, 235: 1156–1167.

Henry, T.W., Wardlaw, B.R., Skipp, B., Major, R.P. and Tracey, J.I., Jr., 1986. Pacific Enewetak Crater Exploration (PEACE) Program, Enewetak Atoll, Republic of the Marshall Islands, Part 1: Drilling operations and descriptions of bore holes in vicinity of KOA and OAK craters. U.S. Geol. Surv. Open File Rep. 86–419, 583 pp.

Henry, T.W. and Wardlaw, B.R., 1991. Introduction: Enewetak Atoll and the PEACE Program, Geological and Geophysical Investigations of Enewetak Atoll, Republic of the Marshall Islands. U.S. Geol. Surv. Prof. Pap., 1513-A, 29 pp.

Kulp, L.J., 1963. Potassium-Argon dating of volcanic rocks. Bull. Volcanol. 26: 247–258.

Ladd, H.S. and Schlanger, S.O., 1960. Drilling operations on Enewetak Atoll. U.S. Geol. Surv. Prof. Pap. 260-Y, 863–905.

Larson, R.L., 1976. Late Jurassic and Early Cretaceous evolution of the western central Pacific Ocean. J. Geomag. Geoelect., 28: 219–236.

Leopold, E.B., 1969. Miocene pollen and spore flora of Enewetak Atoll, Marshall Islands. U.S. Geol. Surv. Prof. Pap. 260-II, 1133–1184.

Li, Y.H., Takahashi, T. and Broecker, W.S., 1969. Degree of saturation of $CaCO_3$ in the ocean. J. Geophys. Res., 74: 5507–5525.

Lincoln, J.M. and Schlanger, S.O., 1991. Atoll stratigraphy as a record of sea level change: Problems and prospects. J. Geophys. Res., 96: 6727–6752.

Lincoln, J.M., Pringle, M.S. and I. Premoli Silva., 1993. Early and Late Cretaceous volcanism and reef-building in the Marshall Islands. In: M.S. Pringle, W.W. Sager, W.V. Sliter, and S. Stein, (Editors), The Mesozoic Pacific: Geology, Tectonics, and Volcanism. Geophys. Monogr., Am. Geophys. Union, 77: 279–305.

Ludwig, K.R., Halley, R.B., Simmons, K.R. and Peterman, Z.E., 1988. Sr isotope stratigraphy of Enewetak Atoll. Geology, 16: 173–177.

Major, R.P. and Matthews, R.K., 1983. Isotopic composition of bank-margin carbonates on Midway Atoll: Amplitude constraint on post-early Miocene eustasy. Geology, 11: 335–338.

Matthews, R.K. and Frohlich, C., 1987. Forward modeling of bank-margin carbonate diagenesis. Geology, 15: 673–676.

Menard, H.W. and McNutt, M.K., 1982. Evidence for and consequences of thermal rejuvenation. J. Geophys. Res., 87: 8570–8580.

Miller, K.G., 1987. Tertiary oxygen isotope synthesis, sea level history, and continental margin erosion. Paleoceanography, 2: 1–19.

Miller, K.G., Fairbanks, R.G. and Mountain, G.S., 1987. Tertiary oxygen isotope synthesis, sea level history, and continental margin erosion. Paleoceanography, 2: 1–19.

Muller, D.W., McKenzie, J.A. and Mueller, P.A., 1990. Abu Dhabi Sabkha, Persian Gulf, revisited: Application of strontium isotopes to test an early dolomitization model. Geology, 18: 618–621.

Prentice, M.L. and Matthews, R.K., 1989. Cenozoic ice volume history: Development of a composite oxygen isotope record. Geology, 16: 963–966.

Quinn, T.M., 1989. The post-Miocene meteoric diagenetic and glacioeustatic history of Enewetak Atoll: Core study and forward modeling results. Ph.D. Dissertation, Brown University, Providence RI, 484 pp.

Quinn, T.M., 1991a. Meteoric diagenesis of post-Miocene limestones on Enewetak Atoll. J. Sediment. Petrol., 61: 681–703.

Quinn, T.M., 1991b., The history of post-Miocene sea level change: inferences from stratigraphic modeling of Enewetak Atoll: J. Geophys. Res., 96 (B4), 6713–6725.

Quinn, T.M., Lohmann, K.C. and Halliday, A.N., 1991. Sr isotopic variation in shallow water carbonate sequences: Stratigraphic, chronostratigraphic, and eustatic implicatons of the record at Anewetak Atoll. Paleoceanography, 6: 371–385.

Quinn, T.M. and Matthews, R.K., 1990. Post-Miocene diagenetic and eustatic history of Enewetak Atoll: model and data comparison. Geology, 18: 942–945.

Ristvet, B.L., Couch, R.F., Jr., Fetzer, J.D., Goter, E.R., Tremba, E.L., Walter, D.R. and Wendland, V.P., 1974. A Quaternary diagenetic history of Enewetak Atoll (abstr.). Geol. Soc. Am. Abstr. Programs, 928–929.

Ristvet, B.L., Couch, R.F., Jr., and Tremba, E.L., 1980. Late Cenozoic solution unconformities at Enewetak Atoll (abstr.). Geol. Soc. Am. Abstr. Programs, 12: 510.

Saller, A.H., 1984a. Diagenesis of Cenozoic Limestone on Enewetak Atoll. Ph.D. Dissertation, Louisiana State University, Baton Rouge LA, 362 pp.

Saller, A.H., 1984b. Petrologic and geochemical constraints on the origin of subsurface dolomite, Enewetak atoll: an example of dolomitization by normal seawater. Geology, 12: 217–220.

Saller, A.H., 1986. Radiaxial calcite in lower Miocene strata, subsurface Enewetak Atoll. J. Sediment. Petrol., 56: 743–762.

Saller, A.H., 1992. Calcitization of aragonite in Pleistocene limestones of Enewetak atoll, Bahamas, and Yucatan — an alternative to thin-film neomorphism. Carbonates and Evaporites, 7: 56–73.

Saller, A.H. and Koepnick, R. B., 1990. Eocene to early Miocene growth of Enewetak Atoll: Insight from strontium isotope data. Geol. Soc. Am. Bull., 102: 381–390.

Saller, A.H. and Moore, C.H., 1989. Meteoric diagenesis, marine diagenesis, and microporosity in Pleistocene and Oligocene limestones, Enewetak Atoll, Marshall Islands. Sediment. Geol., 63: 253–272.

Schlanger, S.O., 1963. Subsurface geology of Eniwetok atoll. U.S. Geol. Surv. Prof. Pap. 260-BB: 991–1066.

Schlanger, S.O. and Premoli Silva, I., 1986. Oligocene sea level falls recorded in mid-Pacific atoll and archipelagic apron settings. Geology, 14: 392–395.

Schlanger, S.O., Campbell, J.F. and Jackson, M.W., 1987. Post-Eocene subsidence of the Marshall Islands recorded by drowned atolls on Harrie and Sylvania guyots. In B.H. Keating, P. Fryer, R. Batiza and G.W. Boehlert (Editors), Seamounts, Islands, and Atolls. Geophys. Monogr., Am. Geophys. Union, 43: 165–174.

Schmalz, R.F., 1971. Formation of beachrock at Enewetak Atoll, In O.P. Bricker (Editor) Carbonate Cements, Johns Hopkins Univ. Studies Geol., 19: 17–24.

Scholle, P.A., Arthur, M.A. and Ekdale, A.A., 1983. Pelagic environment, In P.A. Scholle, D.G. Bebout and C.H. Moore (Editors), Carbonate Depositional Environments, Am. Assoc. Petrol. Geol. Mem., 27: 620–691.

Steinen, R.P. and Matthews, R.K., 1973. Phreatic versus vadose diagenesis: Stratigraphy and mineralogy of a cored borehole on Barbados, West Indies. J. Sediment. Petrol., 43: 1012–1020.

Swart, P.K., Ruiz, J. and Holmes, C.W., 1987. Use of strontium isotopes to constrain the timing and mode of dolomitization of upper Cenozoic sediments in a core from San Salvador, Bahamas. Geology, 15: 262–265.

Swartz, J.H., 1958. Geothermal measurements on Eniwetok and Bikini Atolls, Bikini and nearby atolls. U.S. Geol. Surv. Prof. Pap. 260-U: 711–739.

Szabo, B.J., Tracey, J.I., Jr. and Goter, E.R., 1985. Ages of subsurface stratigraphic intervals in the Quaternary of Enewetak Atoll, Marshall Islands. Quat. Res., 23: 54–61.

Thurber, D.I., Broecker, W.S. Blanchard, R.L. and Potratz, A.J., 1965. Uranium-series ages of Pacific atoll coral. Science 149: 55–58.

Todd, R. and Low, D., 1960. Smaller foraminifera from Eniwetok drill holes. U.S. Geol. Surv. Prof. Pap. 260-X: 790–857.

Tracey, J.I., Jr. and Ladd, H.S., 1974. Quaternary history of Eniwetok and Bikini atolls, Marshall Islands. Proc. Second Int. Coral Reef Symp. (Brisbane), 2, 537–550.

Wardlaw, B.R., 1989. Comment and reply on "Strontium-isotope stratigraphy of Enewetak Atoll" -- Comment. Geology, 17, 190–191.

Wardlaw, B.R. and Henry, T.H., 1986. Physical stratigraphic framework, Pacific Enewetak Crater Exploration (PEACE) Program, Enewetak Atoll, Republic of the Marshall Islands. In: T.W. Henry and B.R. Wardlaw (Editors), Part 3, Stratigraphic analysis and other geologic and geophysical studies in vicinity of KOA and OAK craters. U.S. Geol. Surv. Open File Rep. 86–555: 2.1–2.36.

Geology and Hydrogeology of Carbonate Islands. Developments in Sedimentology 54
edited by H.L. Vacher and T. Quinn
© 1997 Elsevier Science B.V. All rights reserved.

Chapter 22

HYDROGEOLOGY OF ENEWETAK ATOLL

ROBERT W. BUDDEMEIER and JUNE A. OBERDORFER

INTRODUCTION

Groundwater investigations at Enewetak Atoll (Fig. 22-1) have been the source of some unique and important conceptual contributions to the science of small-island hydrology. Studies conducted at Enewetak — confirmed and extended elsewhere — have demonstrated the importance of aquifer heterogeneity and marine hydraulic forcing functions as factors controlling carbonate-island groundwater quantity and quality. These factors are commonly ignored or inadequately considered in models of island groundwater systems, particularly Dupuit-Ghyben-Herzberg analysis (DGH; Vacher, 1988) in which it is assumed that there is a sharp freshwater/saltwater interface, a Ghyben-Herzberg (GH) ratio of 40, constant hydraulic conductivity, vertical equipotentials, and static and uniform saltwater heads. In particular, the hydrostratigraphy of Enewetak includes a highly permeable Pleistocene foundation overlain by less-permeable Holocene islands, and such an arrangement is a feature common to many atolls and coral-reef systems. Thus one outcome of the Enewetak investigations that has found wide application is the "dual aquifer" conceptual model of reef-island hydrology [see Chap. 1].

The comprehensive nature of geologic and hydrologic investigations at Enewetak can be traced to the atoll's unusual history. Enewetak was a Japanese outpost invaded by U.S. forces in 1944, and after World War II it was incorporated into the Pacific Proving Grounds, the U.S. nuclear testing site in the Pacific. Enewetak was the site of numerous nuclear detonations between 1948 and 1958, after which it was used for limited non-nuclear experiments and as a backup to Kwajelein Missile Range. As a result of negotiations with the original owners of the atoll, the 1970s saw intensive survey and cleanup efforts in preparation for the return of the indigenous inhabitants. Because of the geopolitical importance of these varied activities, a wealth of scientific data has been collected. Geology, geophysics, hydrology, and oceanography of the atoll were investigated at scales that would not be feasible on inhabited atolls with more ordinary economic and logistic constraints. Fig. 22-2 gives some impression of the density of observations on Enjebi Island — and this figure omits the locations of 16 early boreholes and a seismic transect along the lagoon shore (Ristvet et al., 1978)!

The scale of these studies and the nature of their outcomes provide some lessons in research strategy by suggesting that intensive, comprehensive, multidisciplinary studies of a type locality may advance basic understanding more rapidly than numerous small or partial investigations at a variety of localities. The lessons learned at Enewetak about scale, variability, and controlling factors for atoll-island

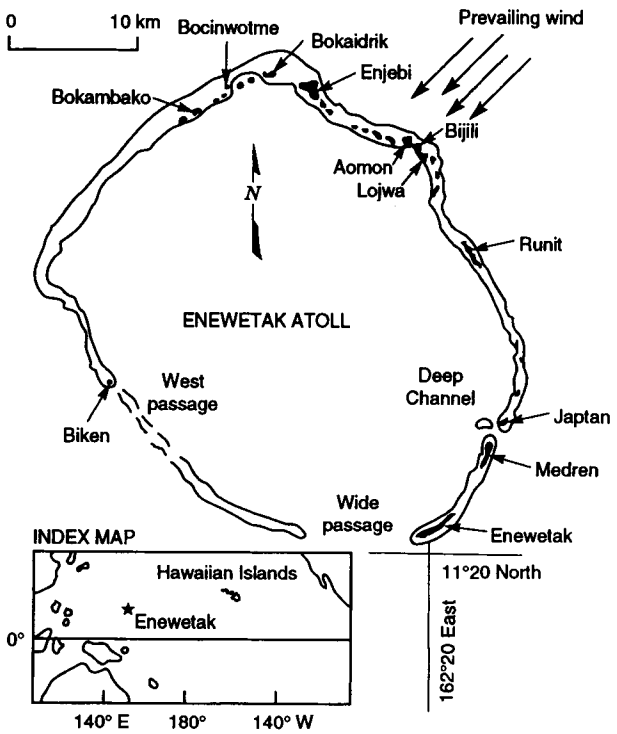


Fig. 22-1. Map of Enewetak Atoll. Named islands are locations of groundwater observations or measurements. See Figure 23-1 for location of Enewetak relative to several other Pacific islands discussed in this book.

groundwater resources increasingly are being applied to predict and interpret hydrogeologic data from other coral-reef and reef-island environments.

The hydrologic data on which this chapter is primarily based were obtained during a period of intensive study from 1974 to 1979. The conditions described refer to that period of observation and do not necessarily reflect present conditions on the atoll. Similarly, the place names and spellings used are those that were generally accepted at the time of the study.

SETTING

Geographic and climatic setting

Enewetak is the most northwestern atoll of the Marshall Island group. It is a relatively large deep-sea atoll, with a roughly elliptical reef structure 40 km by 32 km (Fig. 22-1). Compared to most other Pacific atolls, the lagoon is relatively deep, but there is an unusually large number of pinnacle or patch reefs rising from the lagoon floor; Ladd (1973) indicated that there are over 2,000 "coral knolls" in the lagoon.

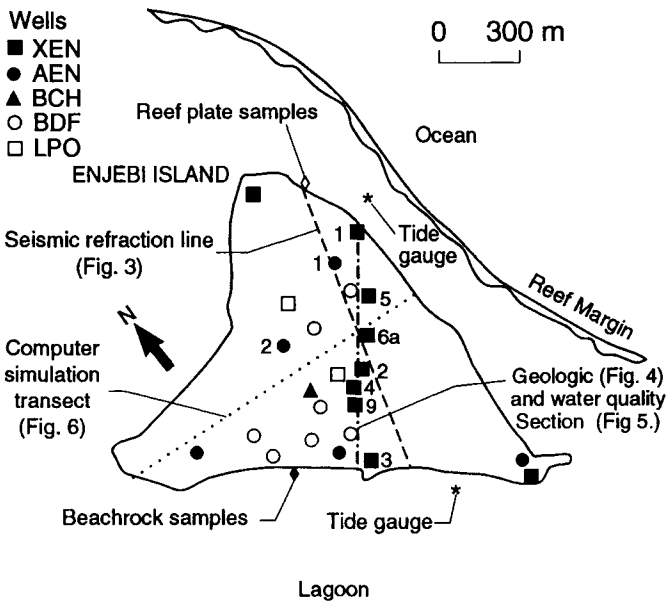


Fig. 22-2. Map of Enjebi Island, showing location of sections and wells referenced in this chapter. The BDF and LPO wells were shallow, penetrating no more than a meter below the water table; the others ranged in depth from 8 to 88 m, and were continuously screened.

Two major passes breach the reef structure in the south, but elsewhere the lagoon is enclosed by a continuous reef system that is emergent or within a very few meters below the surface at extreme low tides (the West Passage shown in Fig. 22-1 is negotiable only by small boats). The reef supports over 30 small, low-relief islands and bars composed of carbonate sand and gravel. Total dry land area is approximately 6.7 km^2; the largest islands are about 1 km^2 in area (USAEC, 1973).

Its location at 11°20′N and 162°20′E places Enewetak generally within the zone of the northeast trade winds, but the seasonal movement of the Intertropical Convergence Zone (Falkland, 1991, p. 14) imposes a pronounced but highly variable seasonality on the weather patterns. Annual rainfall during and prior to the period of investigation averaged 1,470 mm, with an observed range of 605–2,422 mm.

Most of the rain and, therefore, most of the groundwater recharge typically occur during the August-December period, which may also have lighter winds with a more easterly or southeasterly component. The northeast trades are strongest during January–June, which is also commonly a period of low precipitation (commonly 10–20% of the annual total). The atoll experiences major tropical storms or cyclones only infrequently; when these occur they tend to arrive from the south or southwest. Air and water temperatures exhibit some seasonal variation, but not at levels likely to have major effects on island hydrology.

Potential annual evapotranspiration (PET) is about 1,700 mm (Falkland, 1991, p. 71). A. Falkland (pers. comm., 1993) estimated monthly ET values for the years

Table 22-1

Estimates of recharge-related parameters, Enewetak Atoll
A. Recharge vs rainfall and tree cover.[a]

Year	Rain (mm)	0% trees	40% trees	80% trees
1970	1040	18%	11%	04%
1971	1878	46%	27%	25%
1972	2423	55%	46%	43%

B. Average annual recharge and groundwater equivalents.

	Rain (mm)	0% trees	40% trees	80% trees
	1470	(35%)	(25%)	(17%)
Recharge		0.515 m	0.368 m	0.250 m
Groundwater equiv.[b]		2.58 m	1.84 m	1.25 m
Head above MSL[c]		0.065 m	0.046 m	0.031 m

[a] Calculated by A. Falkland.
[b] Assuming an average annual recharge and 20% porosity.
[c] Head equivalent to annual recharge, estimated as 1/40 of the idealized freshwater depth below MSL.

1970–72, and used these results and precipitation records to calculate the annual percentage of rainfall that would recharge the groundwater under various conditions of vegetation cover. These results are given in Table 22-1, along with an estimate of the corresponding values for an average rainfall year and their equivalent values in terms of groundwater measurements.

During the period of investigations at Enewetak Atoll, Enjebi, Enewetak and Runit Islands had virtually no tree cover (although shrubs were widespread on Enjebi), the leeward and small southern islands had approximately 80% tree cover, and the rest were intermediate.

Sea-level variations can be an important hydrologic forcing function in the small-island environment, and tidal fluctuations are usually the dominant sea-level signal. Tides at Enewetak are mixed semidiurnal, with a mean range of 0.8 m, a mean spring tide range of 1.2 m, and maximum spring tide range of approximately 1.5–1.6 m (NOAA, 1983); the maximum observed amplitude of sea-level variation (which includes atmospheric pressure and sea-state effects as well as tidal variation) is approximately 1.85 m (K. Wyrtki, pers. comm., 1993). Wave energy and direction are important factors in controlling geomorphology and lagoon circulation; waves are strongest and most consistent during the period of consistent northeast trades and low rainfall, but, as discussed below, the entire eastern side of the atoll exhibits "windward" characteristics. The trade-wind seas breaking on the windward reefs create wave set-up and cross-reef transport that leads to lagoon ponding (Atkinson et al., 1981; Buddemeier, 1981). These local alterations of sea level generate marine

head gradients that may be important influences on island groundwater flow (see discussion below).

In addition to the natural features, man-made alterations to the island environments must be noted as important to the hydrologic observations. During the period of most intensive study, all of the larger islands had been wholly or partially cleared of trees and other large plants, and substantial amounts of paving and construction had been completed (most notably the large airfield on Enewetak Island). These alterations almost certainly had the effect of enhancing the inventories of freshwater above what would have been present under more nearly natural conditions, as demonstrated by the effect of tree cover on recharge shown in Table 22-1.

Geologic and tectonic setting

The general geology of Enewetak is described in detail in Chapter 21 of this book. The atoll consists of over 1,200 m of Tertiary and Quaternary carbonates atop a basalt foundation. Aseismic subsidence is occurring, but the long-term rates (ca. 0.03 m ky^{-1}) are small compared to the sea-level fluctuations of the late Quaternary and correspond to negligible changes over the late Holocene history of the atoll islands. The present form of the atoll is Pleistocene in origin, modified slightly by a relatively thin veneer of Holocene sediments. Although hydrologic activity of geochemical significance may occur to great depths within the carbonates (Buddemeier and Oberdorfer, 1986, 1988), only the late Quaternary sediments are significant in terms of the hydrology of fresh and brackish groundwater, and so the discussion that follows is generally limited to these units.

GEOLOGIC FRAMEWORK

General features of geology and geomorphology

The geomorphology of Enewetak Atoll is intimately related to the oceanographic features of the atoll and its lagoon, and these in turn are closely coupled to the characteristics of the island groundwater bodies. The description that follows therefore includes discussion of morphologic controls on the marine dynamics of the atoll system.

The present reefs and islands have developed on a late Pleistocene substructure. Evidence for this includes solution unconformities observed in drillholes as well as seismic-reflection data (Ristvet et al., 1978; see Fig. 22-3), and large-scale geomorphic features such as the 20-m terrace encountered both inside and outside the lagoon. This terrace appears to be an extension of the "Thurber Discontinuity," between carbonates dating from about 8 ka and material deposited during the last interglacial (ca. 125 ka). This discontinuity was encountered beneath the islands at depths as shallow as 8–10 m (Tracey and Ladd, 1974). It probably coincides with the first solution unconformity described by Ristvet et al. (1978) and corresponds to the first seismic boundary shown by them and indicated in Fig. 22-3 as occurring at a

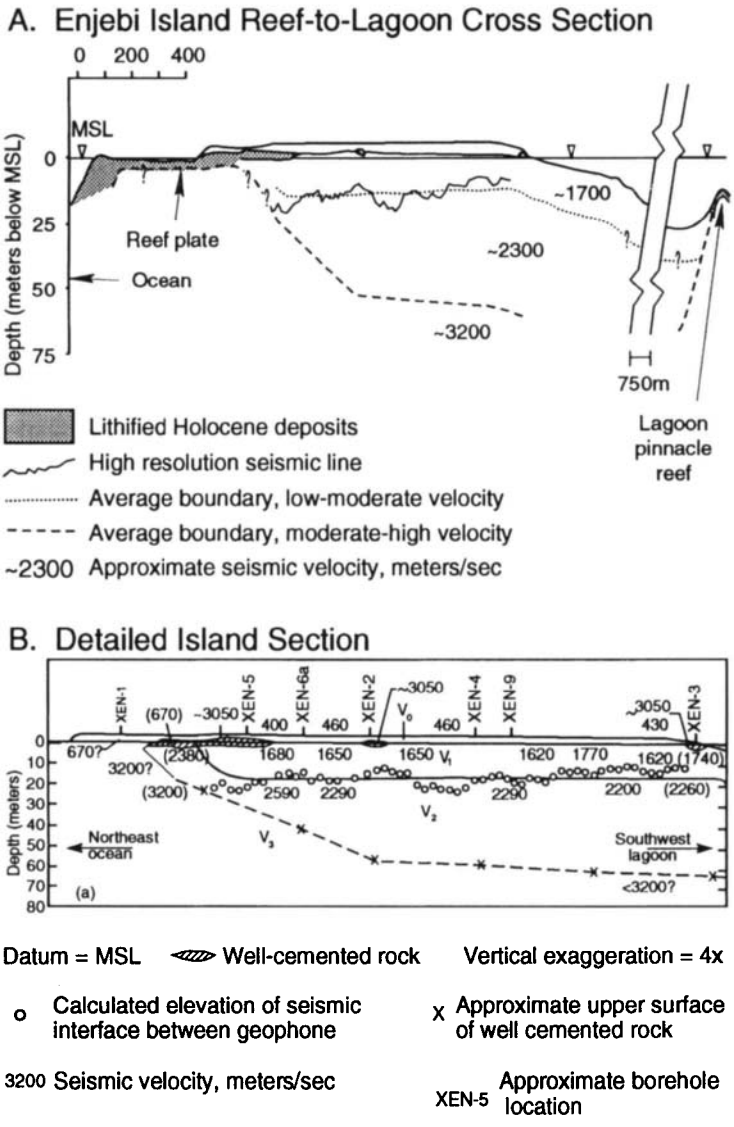


Fig. 22-3. Sections across Enjebi Island (see Fig. 22-2 for location of seismic transect and drillholes). A. Generalized shallow cross section from forereef to lagoon pinnacle reef. B. Detailed island cross section showing seismic results and location of drillholes (from Ristvet et al., 1978). Elevations of seismic reflector (V_1-V_2 boundary) suggest the irregularity and scale of variation of the Pleistocene surface.

mean depth of about 15 m. The lagoon pinnacles and patch reefs have also been shown to have a Pleistocene core (Shinn, pers. commun., 1993).

There are numerous lines of evidence indicating that the upper Pleistocene deposits have a very high hydraulic conductivity, probably of solution origin.

Drilling records showed frequent bit drop and loss of circulation below the unconformity (Ladd and Schlanger, 1960). Although Ristvet et al. (1978) cautioned that the results have considerable uncertainty, high-resolution seismic records suggest elevation variations in the unconformity much greater than any observed on modern reef and island surfaces — as much as 10 m over distances of less than 100 m (Fig. 22-2). The lagoon pinnacles are also suggestive of a karstic landscape substructure. Both vertical and horizontal distributions of tidal responses in observation wells (Wheatcraft and Buddemeier, 1981) and hydrologic modeling (discussed below) evidence high hydraulic conductivity in the Pleistocene material.

Holocene reefal sediments are generally less than 8 ka and are distributed according to their biogenic origin and the habitat and energy regimes of the atoll. Biolithification is pronounced on the windward (eastern) reefs. These windward reefs have: a distinct algal ridge rising into the low intertidal zone; algal cementation of the forereef slope; and a lithified reef plate that may extend as much as hundreds of meters lagoonward from the reef crest across the seaward portion of the reef flat and beneath the seaward side of the islands (Fig. 22-3). These cemented sediments may be vertically continuous beneath and for some distance behind the algal ridge; Couch et al. (1975) reported that drillholes along the ocean shore of Enewetak Island (where the island edge is much closer to the algal ridge than at Enjebi Island) indicated continuous well-cemented layers to depths exceeding 50 m. However, at their lagoonward edge, the plate formations typically thin to a few tens of centimeters and overlie unconsolidated sediments. At some windward locations (e.g., seaward of Runit Island), the algal ridge and reef plate are dissected by fissures and narrow channels oriented perpendicular to the trend of the reef edge; in some cases, these openings appear to connect with substantial void spaces beneath the reef plate. Behind the reef plate, the reef flats are sandy with discontinuous areas of consolidation and patch reefs or coral heads. Holocene sediments beneath the reef plate and above the first unconformity are much less consolidated (Couch et al., 1975; Ladd and Schlanger, 1960; Schlanger, 1963) than the reef plate.

The leeward (southwestern) reefs generally lack a pronounced algal ridge, are less well consolidated, and are somewhat narrower. The outer slope is steeper, and a natural pruning process results in blocks of poorly supported extensions of the oceanward reef breaking loose and slumping down the outer reef face. The northwestern reef is very broad, but, because it supports no islands, its only hydrologic relevance is that it is an effective barrier to outflow from the lagoon.

The lagoon is large and open. This, in combination with the trade-wind environment and the large tidal range, means that there are few if any calm and protected depositional environments in the upper few tens of meters. This is consistent with observations that there are virtually no extensive shallow-water deposits of fine unconsolidated sediments such as lime muds. The fine-grained sedimentary materials that do occur are found either in relatively deep lagoon environments or as a component of poorly sorted shallow-water sediment assemblages.

The combination of a relatively consistent wind-driven NE swell and the barrier erected by the reef crest results in wave set-up and cross-reef transport of water into the lagoon, with outflow impeded by the encircling reefs. Atkinson et al. (1981)

studied the circulation and water budget of the Enewetak lagoon, and concluded that net transport through the passes was small; most of the cross-reef inflow exited the lagoon across the leeward reef, but the impediment to flow necessarily resulted in ponding and head buildup, especially in the northern part of the lagoon. This effect was independently observed by Buddemeier (1981), who analyzed tide patterns and concluded that net lagoon-ocean head differentials of several centimeters to tens of centimeters were likely to occur in various parts of the atoll.

The reef islands appear to be rather young features, which may have been formed at the end of an erosional episode caused by a drop in sea level from a Holocene highstand that locally peaked earlier than 4000 y B.P. (Buddemeier et al., 1975). Tracey and Ladd (1974) dated in situ coral from slightly above present MSL beneath Runit Island at <2000 y B.P., and similarly situated colonies were uncovered during trenching on Enjebi Island (Buddemeier, unpub.). Most of the surficial island sediments are medium to coarse sand, grading into gravel and rubble at the seaward margins (especially on the windward islands). Some minor cementation is present in the vicinity of the modern water table (Buddemeier and Holladay, 1977; Goff, 1979), but the lightly cemented sands are not competent and appear hydrogeologically indistinguishable from the uncemented sands in which they occur. The islands sit mostly atop Holocene backreef sediments, which generally consist of sands similar to the elevated part of the islands. However, coral heads, consolidated areas, and constructional reef channel features have been observed or inferred in the reef structures underlying some islands.

On the windward reefs, the islands overlap the lagoonward edge of the reef plate (e.g., Fig. 22-3), a continuous cemented feature that has been identified at about MSL at least 100 m inland from the oceanward edge of Enjebi, and several tens of meters in from the ocean margin of Enewetak Island. "Hard layers" encountered near the water table in central regions of Lojwa, Bijili, and Aomon are probably also reef plate. Approximately half of the over 40 boreholes drilled by Project EXPOE (Couch et al., 1975) encountered well-cemented or moderately cemented boundstone or grainstone in the general depth range of sea level. The windward islands also have a beach berm or rubble ridge which is typically cemented into the upper intertidal. This cementation, which is essentially continuous with the reef-plate structure, effectively seals and stabilizes the seaward edge of the island. Cemented beach berms are generally not observed on lower-energy beaches, such as channel and lagoon beaches and on the oceanward sides of leeward islands.

Beachrock is common but not ubiquitous on lagoon beaches. Although extensive in places, beachrock layers are commonly fractured and discontinuous, so it is questionable whether they have much hydrologic significance. Aerial photos (USAEC, 1973, vols. 2 and 3) indicate the presence of relict beachrock and reef-rock ridges beyond existing island margins, suggesting that, in spite of their recent origins, the present islands may be erosional remnants of larger or more continuous structures.

Hydrostratigraphy

From the foregoing, the modern reef and island structures can be seen as built from three basic components: (1) the underlying Pleistocene formation, which is

consolidated macroporous material with an irregular surface and variable but very large solution-derived hydraulic conductivity; (2) the backreef and island sediments, which, although quite variable in detail, can be reasonably generalized as coarse to medium sand; and (3) "reef rock" — the consolidated algal ridge, reef plate and windward intertidal conglomerate (i.e., lagoonward beachrock, which, although differing in origin and environment, can be treated hydrologically as a variant of the reef rock).

The characteristics of the first two categories of materials — loosely referred to as the Pleistocene and Holocene "aquifers" — dominate the large-scale hydrologic responses of the islands. Where consolidated reef rock is present, it will be locally important to the hydrologic responses of the seaward edges of some islands and will affect the shallow hydrology of the underlying reef and island by retarding both recharge and outflow of freshwater and the lateral intrusion of seawater into the intertidal margin of the island. The major features of island hydrology on Enewetak Atoll, however, are controlled by the hydraulic connection between the high-permeability Pleistocene aquifer and the overlying moderate-permeability unconsolidated Holocene material.

HYDROGEOLOGY

Distribution of hydraulic conductivity

The hydraulic conductivity of the hydrostratigraphic units was originally assessed on the basis of the propagation of the tidal signal (Buddemeier and Holladay, 1977; Wheatcraft and Buddemeier, 1981). Hydraulic conductivity was further tested by field, laboratory, and computer simulation techniques; the results are summarized in Table 22-2. It should be noted that experimental determinations were all carried out at ambient temperatures using fresh or low-salinity water, and that any variations in

Table 22-2

Summary of hydraulic conductivities, Engebi Island[a]

Material	K (m day^{-1})		n	Method
	Mean	Range		
Holocene sands	54	49–61	4	pump tests
	77	24–200	5	permeameter
	60			model calibration[b]
	10			model optimization[c]
Pleistocene	600			model calibration[b]
	1000			model optimization[c]
Reef/beach rock	7.8	1.2–17	4	permeameter

[a] from Wheatcraft and Buddemeier 1981 unless otherwise noted.
[b] Herman et al. (1986).
[c] Oberdorfer et al. (1990); optimized to reproduce observed tidal efficiencies and salinity profiles.

results due to variations in fluid characteristics are insignificant compared to those due to the observed variations in the geologic media. The results are all from Enjebi Island, but all of the major islands have comparable groundwater tidal responses, heads, salinity distributions, and geologic structures. Given these similarities, the order-of-magnitude nature of the results, and agreement with other studies (Buddemeier and Oberdorfer, 1988), we believe that these values apply to similar materials on other islands at Enewetak Atoll, and can with caution be adapted for use on other reefs and reef islands.

As an example of the range of variations and the uncertainties involved in moving between islandwide and local observational scales, Herman et al. (1986) produced a very satisfactory fit to the field data using 60 and 600 m day^{-1} for the Holocene and Pleistocene aquifers respectively, while Oberdorfer et al. (1990) subsequently used sensitivity and optimization analyses in a density-dependent mixing model to arrive at values of 10 and 1,000 m day^{-1} . Similar model tests have not yet been done in the case of beachrock and reef-rock characteristics, and a cautionary statement is appropriate relative to the values in Table 22-2. The determinations were on hand samples from surface formations near the island; these samples were clearly more heterogeneous and less competent than samples from within the algal crest. From visual observations (Buddemeier et al., 1975, plus core examination), we suspect that limestone of the seaward reef plate and algal ridge might typically have hydraulic conductivities one to two orders of magnitude lower than the values for reef rock reported here.

Distribution of fresh and brackish groundwater

Definitions. The Enewetak experience has taught us to be careful with resolving issues of definition and scale. A particularly vexing issue is the potential for confusion between the total freshwater inventory in a groundwater body (i.e., the fraction of the total water that is of meteoric rather than oceanic origin, as determined by comparing salt and water inventories in a specified volume of porous medium), and the inventory of water that is fresh (e.g., potable) as opposed to brackish or saline. It is the total recharge-derived freshwater inventory that is relevant to such hydrologic parameters as head, recharge, and (in most cases) residence time, and it is in this sense that we use the term *meteoric water* unless otherwise qualified. We use the term *freshwater* when we refer to water that is fresh from the perspective of human use or ecosystem requirements (e.g., with a salinity or total dissolved solids concentration of less than about one part per thousand, although more-saline water can be used for many purposes if necessary). Brackish water — by far the largest category at Enewetak — is simply water that is not potable, but that has a salinity significantly less than oceanic.

Spatial distribution. Groundwater occurrence and characteristics were investigated on ten of the atoll islands, including all of the larger ones (see Fig. 22-1). At the interisland scale of comparison, meteoric-water inventories based on head and

recharge relationships were estimated for a number of islands in the form of residence times of the meteoric water (Buddemeier, 1981). These estimates of residence time were: Enjebi, 5.4 y; Aomon, 4.2 y; Japtan, 6.0 y; and Enewetak, 5.6 y. The estimate for Enewetak Island was for the wide, paved, west end only, and may significantly overestimate the residence time because the recharge is probably substantially enhanced by the pavement and effective runoff collection in the low central area. Rough estimates on Runit Island suggested a residence time on the order of 2 years; Runit is the narrowest of the islands studied and is close to an unusually dissected, low-relief portion of the windward reef. The smaller islands had extremely brackish or saline groundwater, and quantitative inventory estimates were not attempted.

Only Enewetak Island consistently had a freshwater body that was sufficiently persistent and extensive to be considered a potentially reliable resource. Japtan, Aomon, and possibly Medren were found to have small, variable freshwater lenses of marginal resource significance. On all other islands, and on significant portions of the islands named, the groundwater was either brackish or only seasonally fresh; this includes Enjebi, which, as one of the largest islands, might be expected to support a superior lens. In all cases where data were available, the freshwater lenses were thin (extending only a few meters below the water table), were associated with a much more extensive brackish transition zone, and appeared to be associated with anthropogenic features that would act to enhance localized recharge by concentrating runoff and/or reducing evapotranspiration (clearings on Japtan and Aomon, an airstrip on Enewetak). Enewetak had the combined advantage of minimal vegetation, a recharge-enhancing airstrip, and proximity to major passes that minimizes lagoon-to-ocean hydraulic gradients (Buddemeier, 1981). In other locations, however, similar features were not necessarily associated with significant freshwater lenses.

An important feature of the spatial distribution is the apparently random variation in groundwater characteristics on spatial scales much smaller than island dimensions. On Enjebi Island, an array of 23 shallow pits and wells (Fig. 22-2) showed substantial variations in head, tidal response and water quality over distances of tens of meters (Wheatcraft and Buddemeier, 1981). Considering only the nine water-table wells on Enjebi, the observed ranges of variation were: head, 0.20–0.34 m; tidal efficiency (i.e., the well-to-ocean amplitude ratio), 0.04–0.16; and tidal lag, 2.47–3.37 h. A similar comparison of seven shallow pit wells on Enewetak Island gave: head, 0.20–0.44 m; tidal efficiency, 0.05–0.33, and lag, 1.7–3.77 h. The fact that these variations exhibited no coherent geographic pattern or trends was one of the major factors that originally forced consideration of alternatives to the conceptual models of island groundwater that permit consideration only of lateral propagation of the tidal signal (Buddemeier and Holladay, 1977; Wheatcraft and Buddemeier, 1981). The lack of geographic trends led to formulation of the dual-aquifer concept, which in turn led to reconsideration of other assumptions commonly applied to island hydrology (e.g., the DGH assumptions of a steady-state unmixed freshwater lens that loses water only at the shoreline). We attribute the range of variation in the hydrologic characteristics primarily to short-range variations in the elevation and hydraulic conductivity of the presumed karst-like Pleistocene aquifer (see Fig. 22-2), and possibly to lagoon-to-ocean trends in subsurface sediment consolidation noted

by Ristvet et al. (1978). We conclude that, where vertical coupling with a shallow, high-permeability aquifer may control the groundwater dynamics, it is impossible or imprudent to infer the extent and dynamics of a groundwater lens from one or a few observation points.

Geologic controls on the vertical distribution of meteoric water may be seen in Fig. 22-4, which compares selected temperature and salinity profiles observed in four of the deeper boreholes on Enjebi Island with the lithology in cores from those holes (Ristvet et al., 1978). The correspondence of inflection points and transition zones with stratigraphic horizons and units is striking. The depth of the first solution unconformity in these four boreholes occurs at 8–15 m.

Numerous salinity profiles were measured in the deeper boreholes on Enjebi Island over the period 1974–1976. Because the wells were continuously screened across units of different head and hydraulic conductivity, borehole-induced interactions at certain tide stages produced large artificial variations in the profiles (Buddemeier and Holladay, 1977). However, consistent patterns of vertical structure occurred in many of the profiles so that, by eliminating the records most obviously distorted by borehole effects, a noisy but consistent picture of distribution and variation of groundwater salinity was obtained. Fig. 22-5 shows the average depth and variability of isochlors corresponding to 20, 40, 60 and 80% seawater in the form of a composite section. It appears that the meteoric-water inventory (as indicated, for example, by the estimated depth of the 50% isochlor) is greatest in the middle of the island, but that the transition zone is thickest on the lagoon side and the inventory of low-salinity water increases from lagoon to ocean.

Two important estimates can be derived from Fig. 22-5. First, the physical principles relating average water density and relative elevation (head) that were elucidated by Ghyben and Herzberg are independent of mixing and flow pathways, and can be used to compare independent estimates of meteoric-water inventory. Over the central 90% of the section (that portion between the outermost wells), the average depth of the estimated 50% isochlor is approximately 9.5 m. If this is taken as equivalent to the depth of the saltwater interface in an idealized GH lens, it would correspond to a head of 0.24 m if the standard 40:1 ratio is applied. This is well within the observed range of water-table heads cited above (0.20–0.34 m). Second, if we take an average depth of 15 m for the first solution unconformity and do a simple area summation of the contour intervals under the central 90% of the island section, we estimate that approximately 37% of the total meteoric-water inventory is within the Pleistocene formation; if a depth of 12 m is used, the corresponding inventory figure is 42%. This is significant to the issue of inventory controls discussed below.

The distributions of fresh and meteoric water do not appear to be strongly correlated with depth of well or tidal lag, and they are counter to the conventional wisdom that lenses are thicker or fresher (or both) on the lagoon side of reef islands because the sediments are finer there. The patterns may relate to the marine head or consolidation gradients discussed above. In particular, the combination of a low meteoric-water inventory but a relatively higher inventory of water fresher than 20% seawater near the seaward shore may point to the important role of the relatively impermeable reef plate and cemented shoreline in reducing fluxes of both water and

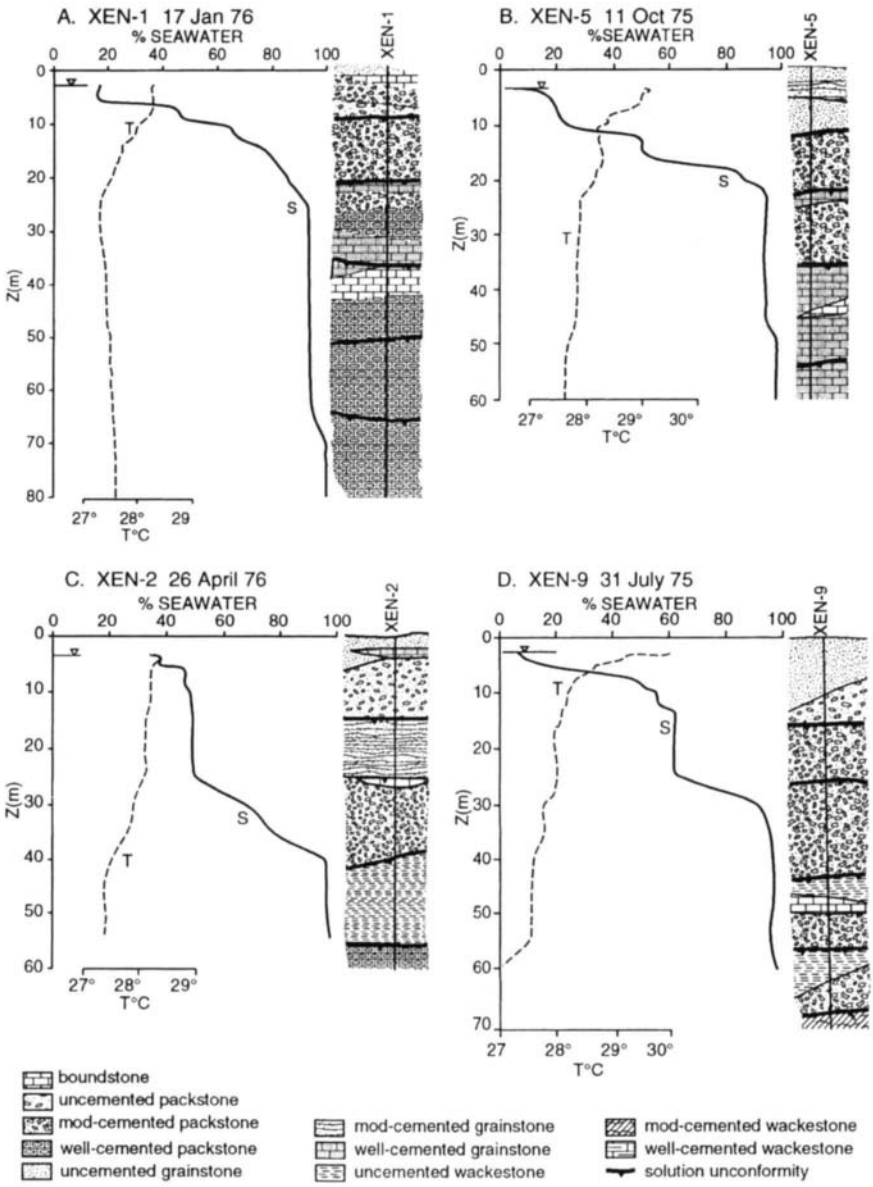


Fig. 22-4. Comparison of selected profiles of salinity vs depth and temperature vs depth with lithostratigraphy derived from core descriptions (from Ristvet et al., 1978) in four of the deeper drillholes on Enjebi Island (see Fig. 22-2 for approximate locations). Note the strong correlation between inflection points in the profiles and unconformities or lithologic boundaries (especially changes in degree of cementation).

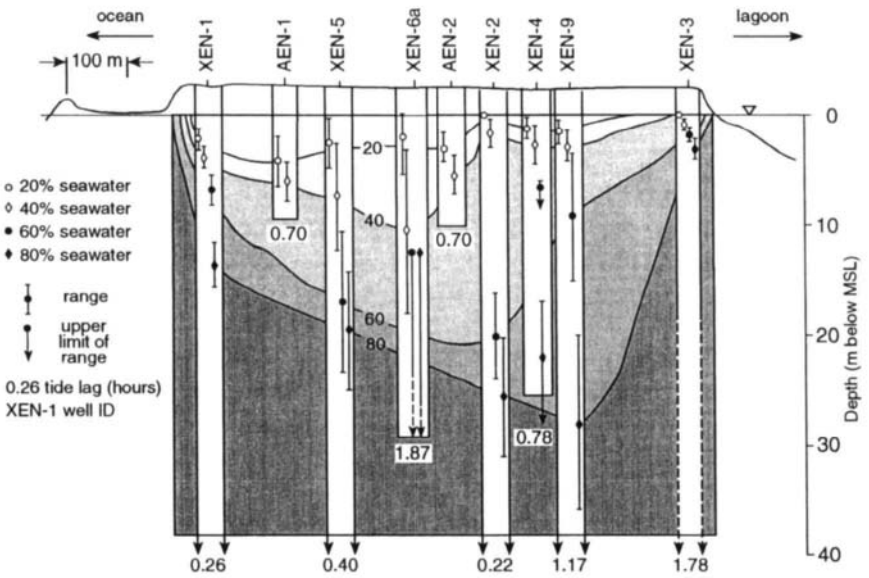


Fig. 22-5. Average locations of groundwater isochlors in the Enjebi cross section, based on multiple well profiles (see Fig. 22-2 for locations and Fig. 22-11 for comparison with simulated isochlors). Bars represent standard deviations of the average estimate; downward pointing arrows indicate upper limits; the true average is probably below the point plotted. Numbers beneath each well are the average tide lag in hours; small numbers indicate good hydraulic connection with the ocean tide signal.

salt. An additional effect might be the areal redistribution of recharge from the seaward side to the center of the island due to perching and subsurface runoff on the lagoonward-sloping reef plate (e.g., compare cemented zones in Fig. 22-3 with salinity distributions in Fig. 22-5).

Temporal variability. As would be expected in a setting where rainfall is seasonally and interannually variable and similar in magnitude to the average evapotranspiration, the seasonal and interannual variations in meteoric and freshwater inventories are substantial. This appears to be due in large measure to variations in recharge (see Table 22-1 for interannual variations; seasonal variations are even more extreme). The variable input of freshwater is superimposed on an approximately constant rate of tidal mixing within the island groundwater body. The standard deviations plotted in Fig. 22-5, although exaggerated by borehole effects, give a qualitative idea of the rapidity and extent of the mixing forces that act to alter vertical salinity distributions.

Salinities in shallow wells and pits on Enjebi, Aomon, and Enewetak were observed to vary by several parts per thousand on a time scale of months, and by a significant fraction of that range over periods of weeks. Recharge tends to flush the system and renew the surficial layer of freshwater, which is then degraded by the

spatially heterogeneous patterns of vertical mixing. Heavy vegetation cover (such as on Biken and parts of Japtan) adds a surface sink for freshwater in the form of evapotranspiration. This can combine with the deeper mixing sink to produce a thoroughly brackish water column even where meteoric-water inventories remain relatively high, as on the forested part of Japtan Island.

Inventory controls. If mixing is the primary means of loss of freshwater (by transformation into brackish water), controls on the limited inventory of meteoric water need to be considered. Buddemeier (1981) suggested that the lagoon-to-ocean head gradient (discussed previously) drives a net under-island flow that entrains the brackish water mixed downward into the Pleistocene aquifer, replaces it with saline lagoon water, and results in a net loss of meteoric water from Pleistocene exposures at depth (in this case on the ocean side; Fig. 22-6). This process would introduce an important distinction into water-budget calculations; if outflow occurs only at the shoreline of the island as in conventional DGH conceptualizations, then vertical mixing under the center of the island would represent a loss of freshwater but not a loss in the overall inventory of meteoric water. However, if vertical mixing entrains the water into a different flow path, the mixing could result in a net loss of meteoric water beyond that calculated from DGH principles. There has been no unequivocal confirmation of subsurface discharge of meteoric water, but during submarine surveys of Johnston Atoll, "shimmering water" (presumably resulting from density contrast) was observed flowing out of caves at 200 m depth on the east side of the atoll (Keating, 1987)

Although outflow at the island margin as modeled in DGH formulations undoubtedly occurs to some extent, shallow outflow at the seaward side must be

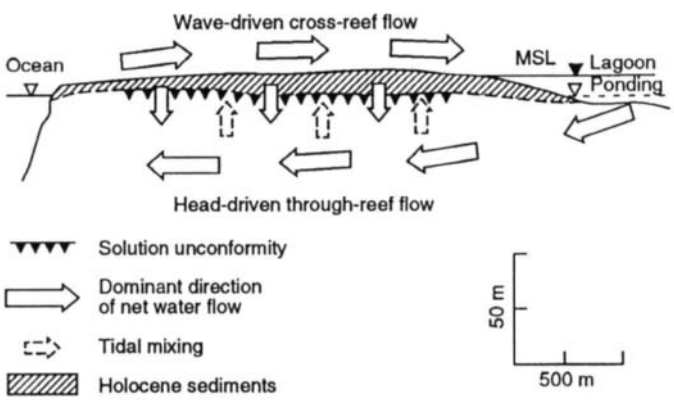


Fig. 22-6. Conceptual drawing of potential marine influences on both the freshwater and meteoric-water inventories. Based on observations at Enjebi Island, freshwater is mixed with saltwater, and part of the meteoric-water inventory is thus drawn into the Pleistocene aquifer by tidal processes. Observed wave set-up and lagoon ponding provide a mechanism by which brackish water (including some fraction of the meteoric-water inventory) may be flushed out of the reef-island system by underflow through the high-permeability Pleistocene aquifer.

inhibited by the low-permeability reef plate and cemented intertidal zone. Subsurface outflow might provide a substitute for that flow path and thus maintain an overall water budget similar to that estimated from DGH calculations, albeit with very different flow paths and salinity distributions. When we consider that (1) the lagoon-to-ocean head difference (Buddemeier, 1981) may be of the same magnitude as the average difference between the water table and mean sea level (Wheatcraft and Buddemeier, 1981), (2) permeability of the Pleistocene formation may exceed that of the Holocene material by two orders of magnitude, and (3) over a third of the meteoric-water inventory may reside in the Pleistocene aquifer (see discussion above and Fig. 22-5), it is reasonable to consider the additional effect of mixing combined with underflow as a potentially significant component of the total outflow. Residence times and flow rates based on aquifer and head characteristics (Buddemeier and Oberdorfer, 1988) are of the same order of magnitude for both the marine-dominated and island-groundwater components of the system (Buddemeier, 1981), implying that they should not be treated independently.

Stress response and recovery. The rapid mixing loss of freshwater, the extended transition zone, and the spatial and temporal variability of island freshwater inventories — all of these distinguish the island groundwater hydrology at Enewetak from the steady, recharge-driven island groundwater lenses generally envisaged in discussions of "Ghyben-Herzberg lenses." Although the dynamic nature of the lens means that freshwater resources are both limited and vulnerable to natural variation (Oberdorfer and Buddemeier, 1988; Buddemeier and Oberdorfer, 1990), it also has a positive aspect in that contamination may prove at least as ephemeral as the potable water. For example, Enewetak Atoll was struck by a typhoon in early January, 1979, and the storm surge washed a substantial amount of seawater onto Enewetak Island. Fortuitously, some wells and pits in the vicinity of the potable lens around the airstrip made it possible to monitor the effects on the lens in that area and to obtain some measurements of the rate of recovery. These are shown in Fig. 22-7 (Oberdorfer and Buddemeier, 1984, unpub. data). Seawater ponded in a low area in the center of the unpaved strips between the runway and taxiway; this low area was one of enhanced recharge because of the runoff generated by the pavement. A few weeks after the event, the well nearest the center of the affected zone still had salinity about two-thirds that of seawater, but surface salinities dropped off rapidly, and much of the original area of the freshwater appeared to have substantially recovered in a period of 6 months. This recovery occurred in the absence of substantial recharge. In less than a year, surface salinities approached pre-storm values. Presumably conservative contaminants will exhibit residence times and movement paths similar to the potable and/or freshwater inventories. In this case, the density of the saltwater is believed to have promoted loss by causing it to sink into the brackish transition zone and thus add to vertical mixing; the salinity contours show little evidence of lateral flow at the surface (Fig. 22-8). This self-cleansing feature of small dynamic lenses may somewhat make up for their limited resources and vulnerability to drought.

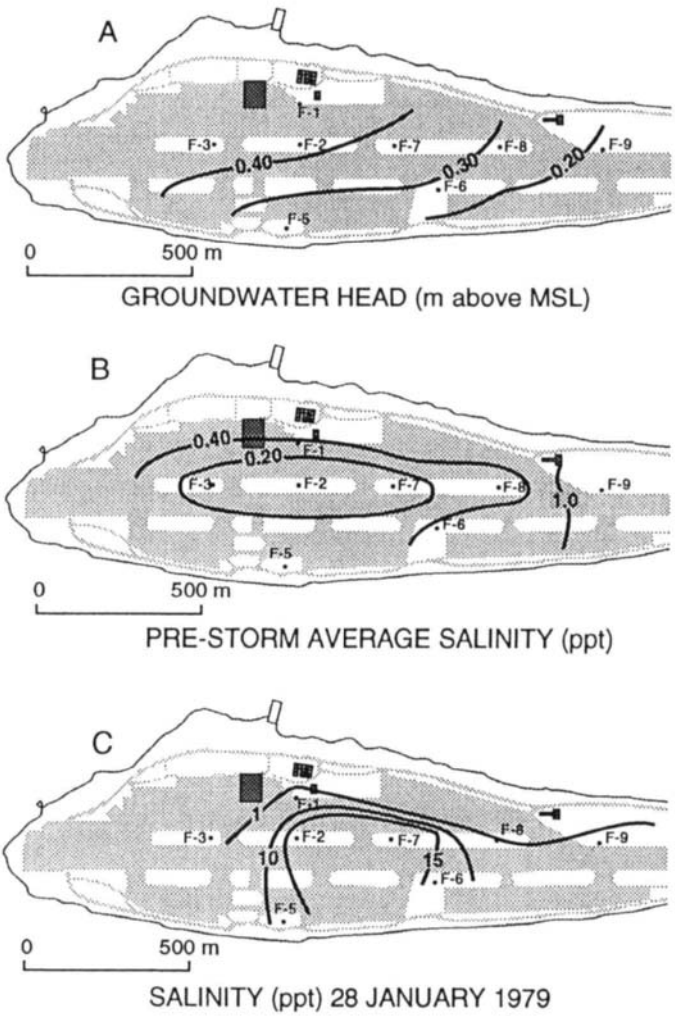


Fig. 22-7. Storm-surge contamination and recovery of the water table at the southwest end of Enewetak Island. Maps of typical head (A) and salinity at the water table (B) are from measurements over 1976–1978 in the shallow wells, F-1 to F-9. In early January 1979, the low-lying central portion of the runway received substantial input of seawater from a storm surge. Well salinities were measured and contoured after 3 wk (C), 2.5 mo (D), 6.5 mo (E), and 11.5 mo (F). Shaded areas indicate paving or buildings.

CASE STUDY: NUMERICAL MODELING OF ENJEBI ISLAND GROUNDWATER

Model characteristics

Enjebi Island (Fig. 22-2) was chosen as the basis for a numerical model of the hydrogeology and solute transport of an atoll island because of a good set of field

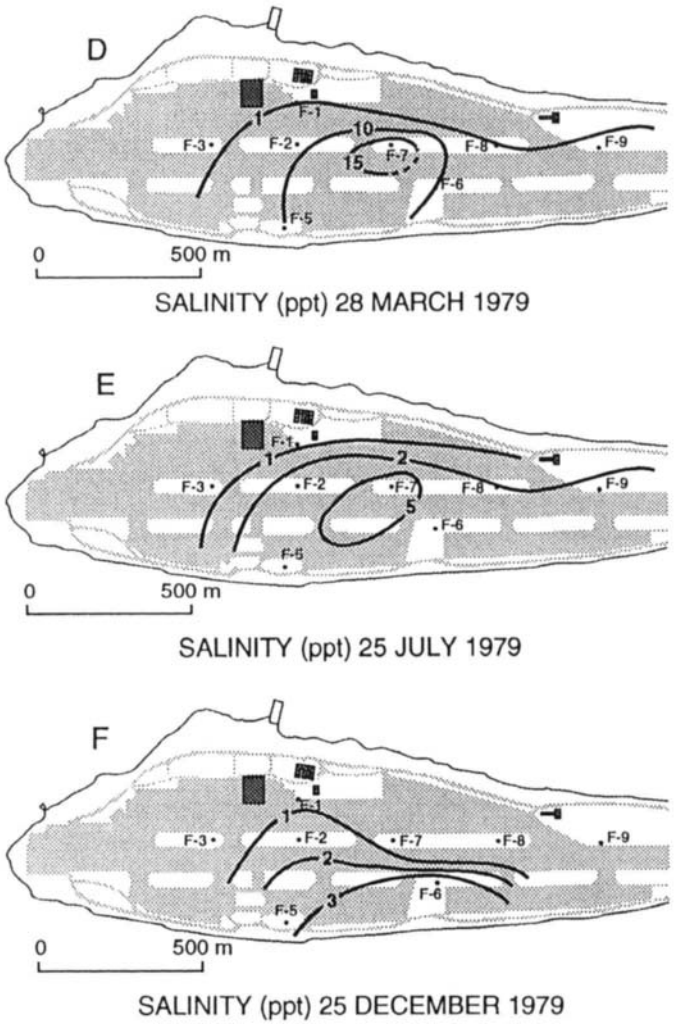


Fig. 22-7D,E,F.

data and a previous modeling effort (Herman et al., 1986) that successfully simulated the tidal control of the flow patterns. Details of the model and results can be found in Oberdorfer et al. (1990) and Hogan (1988).

The U.S. Geological Survey computer model SUTRA (Voss, 1984) was used because it solves equations for both fluid and solute transport, including density-dependent flow. The numerical methods used to approximate these two interdependent processes are a two-dimensional, hybrid, finite-element method and an integrated, finite-difference method. Fluid pressure (p) is the primary variable in the flow equation whereas the primary variable for the solute transport equation is solute concentration (C). Fluid density varies with concentration.

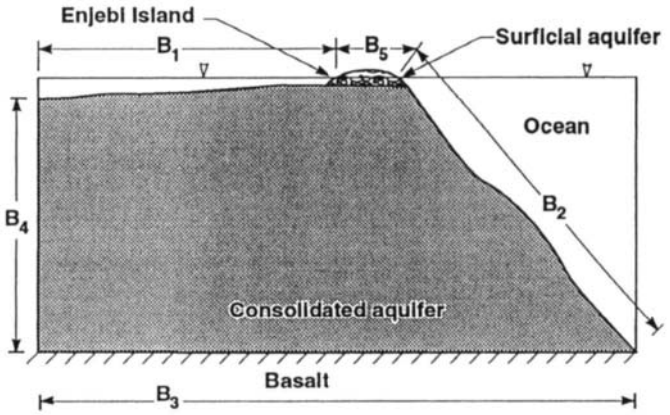


Fig. 22-8. Conceptual model of a layered-aquifer system. B_1 and B_2 are time-dependent pressure boundaries, where fluid pressure varies with a tidal cycle represented by a sine wave with 1.8-m amplitude and 12-h period. B_3 and B_4 are no-flow boundaries. B_5 is a recharge boundary.

The model was configured (Fig. 22-8) to represent the conceptual model of a two-layer, permeability-contrast system in order to test hypotheses on geological control of the flow patterns in the island. The model island consisted of a moderate-permeability Holocene aquifer to a depth of 12 m below sea level overlying a high-permeability Pleistocene aquifer to a total depth of 1,277 m, with both aquifers treated as homogeneous and isotropic. The maximum elevation of the island was taken as 3 m. The finite-element grid consisting of 672 nodes and 605 elements, with greater element density in the Holocene aquifer, was set up to represent a cross section through the island from ocean front to lagoon. A detailed description of the model configuration is given in Hogan (1988).

The salinity distribution within the island varies with time because of seasonal and interannual variations in recharge. The computational demands of oscillating tidal boundaries are so great that in order to keep computational times within manageable limits, average annual salinity budgets and recharge estimates were used. The average configuration of the lens (Fig. 22-9) was determined from salinity profiles measured from surface to full-seawater salinity in nine deep wells at various seasons over a period of two years. The corresponding average annual recharge (inflow at Boundary B_5) was estimated to be 0.5 m y^{-1}, about one-third the annual precipitation of 1.5 m y^{-1} at Enewetak, distributed equally over the year.

Initial conditions for the simulation were a completely saltwater system with the pressures everywhere reflecting mean sea level. Tidal variations in sea level were represented by a sine wave with an amplitude of 1.8 m and a period of 12 h. With a time step of 0.25 h, it required two simulated days for the pressures to reach a stable pattern of hydraulic response; three years of simulated time at a time step of 1 h were required for the salinity distribution to reach a stable configuration.

Some input parameters for the model were taken from standard values in the literature; others were estimated from field data and then refined through sensitivity

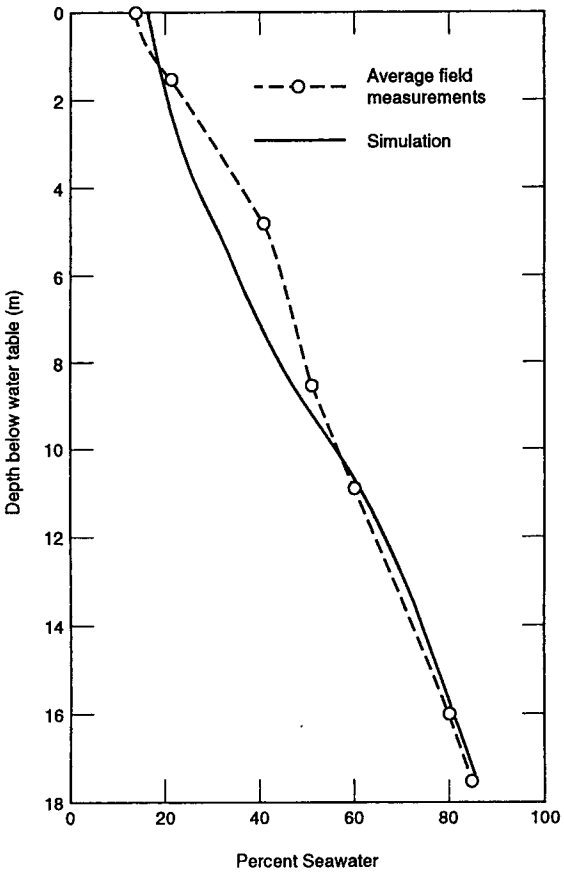


Fig. 22-9. Averaged salinity profiles of Enjebi groundwater from field data and from SUTRA simulation (Oberdorfer et al., 1990).

analysis. The input parameters determined from literature values are given in Table 22-3.

Parameters determined through sensitivity analysis (Table 22-4) were calibrated to the tidal response observed in wells at Enjebi (Wheatcraft and Buddemeier, 1981) and to the observed average salinity distribution (Fig. 22-9). The mean tidal efficiency in nine shallow-pit wells was 0.09 ± 0.29 h, and the average water-table elevation was 0.26 ± 0.05 m. Field data showed that tidal efficiency increased and tidal lag decreased with depth; efficiencies near the Holocene-Pleistocene contact were in excess of 0.40, and lags were as low as 0.25 h.

Tests of the surficial aquifer indicate a hydraulic conductivity range of 1–100 m day^{-1} (corresponding to an intrinsic permeability of 1.2×10^{-12} to 1.2×10^{-10} m^2), and Pleistocene aquifer values are thought to exceed those of the Holocene by one to two orders of magnitude. A range of 5–50 m day^{-1} was tested in the sensitivity analysis, with both 10:1 and 100:1 ratios of Pleistocene to Holocene hydraulic

Table 22-3

Input parameters determined from literature values

Parameter	Value
Compressibility of water, β	4.4×10^{-10} m^2 N^{-1}
Porosity, ϵ	0.30
Fluid viscosity, μ	1.0×10^{-3} kg m^{-1} s^{-1}
Solute mass fraction, seawater, C_S	0.0357 kg salt kg^{-1} seawater
Density, seawater, ρ_S	1025 kg m^{-3}
Density, fresh water, ρ_f	1000 kg m^{-3}

Table 22-4

Input parameters determined from sensitivity analysis

Parameter	Value
Upper aquifer permeability, k_u	1.2×10^{-11} m^2
Lower aquifer permeability, k_l	1.2×10^{-9} m^2
Compressibility of porous media, α	1.0×10^{-9} m^{2}N^{-1}
Longitudinal dispersivity, α_L	0.02 m
Transverse dispersivity, α_T	0.0

conductivity. The sensitivity analysis indicated that the closest match to the observed or inferred tidal responses was obtained with values of 10 m day^{-1} (intrinsic permeability of 1.2×10^{-11} m^2) for the Holocene sediments and 1,000 m day^{-1} (intrinsic permeability of 1.2×10^{-9} m^2) for the Pleistocene. These values gave tidal efficiencies of 0.14 at the water table and 0.70 at the Holocene-Pleistocene contact, tidal lags of 2.75 h at the water table and 0.25 h at the Holocene-Pleistocene contact, and water-table elevations in agreement with observed averages. These results are considered to be in excellent agreement with the field data.

The dispersion coefficient is the product of the dispersivity of the porous medium and the fluid velocity. The longitudinal dispersivity value is a fitted parameter that best reproduced the observed mixing of freshwater and saltwater beneath the island. The value obtained (0.02 m) is certainly within the range of reasonable values, and was used for both aquifers. The transverse dispersivity was not used for this simulation because the large variations in flow directions and magnitudes at a given point would cause the longitudinal dispersivity to mask the effects of the smaller transverse dispersivity.

Results

SUTRA calculates flow velocities (v) as part of its output; examples from the results presented by Oberdorfer et al. (1990) and Hogan (1988) are shown in Fig. 22-10. The very strong effects of the tidal variations on the flow field can be seen

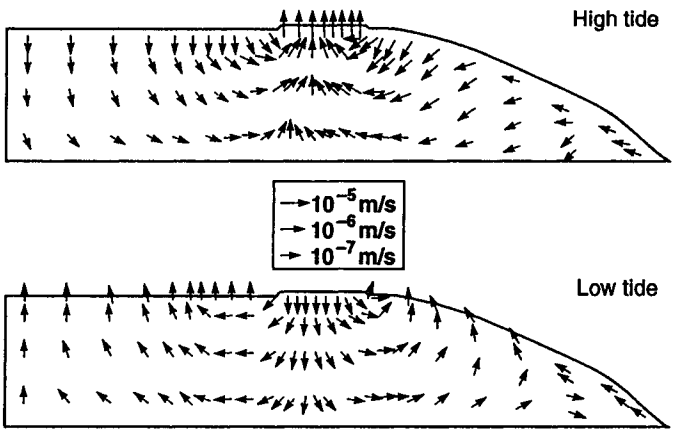


Fig. 22-10. Velocity vectors in the simulated region at high tide (upper panel) and low tide (lower panel). Arrow lengths indicate velocity (log scale).

in this figure. These instantaneous flow estimates were selected to illustrate the complete reversal in flow direction occurring between high and low tide and the conditions of maximum vertical flow, where the vertical component of flow dominates the horizontal component. The flow field is nearly uniform across the width of the island, with only small edge effects showing in the immediate vicinity of the island's margin. On average there is a net horizontal flow component that preserves the steady-state inventory of meteoric water, but this figure demonstrates the relative importance of oscillatory vertical flow in controlling the inventory of freshwater by mixing, and the substantial depth range over which this mixing can occur.

Fig. 22-9 compares simulation results for the average vertical salinity profile with the average of measured salinity profiles. This agreement is considered very good in view of the patchy nature of the measurements and the strong seasonal and annual variations in the upper portions of the field curve (averages had standard deviations approaching 100%).

The computer-generated salinity distribution within the island's groundwater is given in Fig. 22-11, which predicts that the isochlors are relatively flat beneath the center of the island where mixing by vertical transport is dominant (see Fig. 22-10). The 50% isochlor occurs at a depth of about 9 m, which is in excellent agreement with the value of 9.5 m estimated from field data (see Fig. 22-5 and accompanying discussion) and is consistent with water-table elevations. The isochlors estimated from measured profiles (Fig. 22-5) show the importance of heterogeneity in the island structure, but, at the very large scale, patterns of form and depth are reasonably consistent with the isochlors modeled for the homogeneous island case. When contour intervals below a depth of 12 m are integrated over the central 90% of the section, we obtain an estimate of meteoric-water inventory in the Pleistocene unit that is about 30% of the total. This is somewhat lower than, but of the same magnitude as, the estimates similarly obtained from the field data summarized in Fig. 22-5.

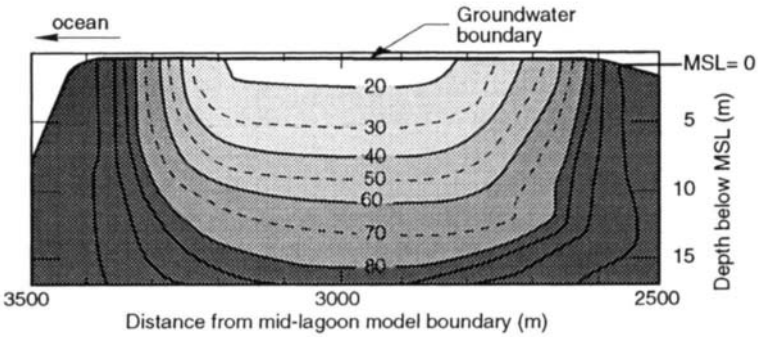


Fig. 22-11. Annual average isochlors for Enjebi simulated by Oberdorfer et al. (1990) using density-dependent flow and tidal mixing in a two-layer analog of Enjebi Island. See Fig. 22-2 for location of simulation section. The figure is scaled and shaded similarly to Fig. 22-5 to facilitate comparison.

Discussion

The ability of numerical simulations based on a simple version of the layered-aquifer model to reproduce quantitatively the hydraulic responses in wells, the elevation of the water table, and the average vertical distributions of salinity, attests to the accuracy of the conceptual model in describing atoll island hydrogeology. It must be remembered that the two-layer model used here is still only an approximation for a much more complex reality, but for Enjebi and similar atoll islands it appears to be a much more realistic model than the simple Ghyben-Herzberg lens with Dupuit assumptions.

The traditional DGH analysis (Fetter, 1972; Vacher, 1988) treats horizontal flow of freshwater as driven by recharge-generated head gradients. Although this mechanism undoubtedly occurs in layered-aquifer systems, there are also other possible driving forces for horizontal flow. Dispersion and horizontal mixing as a result of tidal pumping can result in enhanced loss of meteoric (originally fresh) water by the discharge of brackish water to the surrounding ocean over an extensive area of the submerged island surface, and the asymmetry of the reefs and island structure may interact with the tidal oscillations to generate net gradients (e.g., compare the relative changes in velocity vectors on the lagoon and ocean sides of Fig. 22-10). Although these and other alternative mechanisms were not specifically investigated in the present study, various observations tend to suggest that recharge-generated head gradients may not completely control the horizontal flow of fresh groundwater, and that flow in the lens is not separate from flow in the underlying saltwater (see Fig. 22-6 and discussion of inventory controls above). To the extent that the saltwater flows in response to oceanic forces rather than the freshwater recharge (Buddemeier, 1981; Buddemeier and Oberdorfer, 1988), the Dupuit assumptions as conventionally applied to the GH lenses may not be valid for the extensive transition zone that contains most of the meteoric-water inventory.

The broad transition zone that exists beneath the island is produced by the oscillating vertical flow that causes mixing between the freshwater and saltwater on

each tidal cycle. Ignoring tide-driven flow would mean ignoring this mixing mechanism and could lead to gross overestimation of the amount of potable water (<3% seawater) that might be available. Solute-transport models of atoll islands that do not include tide-driven flow would have to use unreasonably large dispersivities to reproduce the observed broad transition zone. This could lead to unrealistic responses when the model is later used in a predictive mode.

CONCLUDING REMARKS

In the introduction to this chapter we commented on the conceptual contributions that the work on Enewetak has made to reef-island groundwater studies. Although the atoll is not unique or atypical in any individual respect, its geomorphology and hydrodynamic features probably combine to make its islands closer to an endmember rather than a typical case along the continuum from the homogeneous, stable DGH groundwater lens to multilayered, highly variable island groundwater systems.

At Enewetak, the effect of the Pleistocene-Holocene aquifer coupling on the tidal response and salinity of the freshwater lens is pronounced because the Pleistocene surface is relatively shallow, probably has high relief, and the Pleistocene limestone apparently has karst permeability. These characteristics are common, though not universal, among reef island structures; in settings where the saturated thickness of the Holocene material is larger, the effects of the underlying aquifer will be damped. For locations that were relatively dry during the last interglacial, solution permeability in the upper Pleistocene formation may be substantially less than at Enewetak.

Furthermore, the coupling between the Pleistocene aquifer and the marine environment at Enewetak may be particularly strong because of the deep, open lagoon and the large number of lagoon patch and pinnacle reefs that can act to transmit marine hydraulic signals to the Pleistocene aquifer. In lagoons with a relatively thick and continuous layer of fine sediment, the effects of hydraulic coupling between the lagoon and the island groundwater may be reduced by the low-permeability layer interposed between the tide signal or the lagoon-ocean head difference and the Pleistocene aquifer.

The physical environment at Enewetak also contributes to its "endmember" classification. It has a relatively large tidal amplitude for an oceanic island, its position in the trade-wind zone means a steady supply of wave-driven set-up to create head differences, and rainfall is small and variable compared to more equatorial locations.

This combination of features has forced recognition that the conventional approaches to application of the DGH model could not adequately describe this environment. Once the determinants and forcing functions of the island hydrology were recognized at Enewetak and at similar atolls in the northern Marshall Islands, similar effects were more easily recognized in other environments. The dual-aquifer concept has been relatively readily accepted, as the phenomenon is very common

among reef islands [see Chap. 1]; comparable situations arise in terrestrial environments. Even more basic, however (and somewhat more difficult for terrestrially trained hydrologists to appreciate), has been the importance of coupling between the terrestrial island groundwater environment and features normally associated with oceanography and marine geology. Many of the other contributions in this book make use of dual-aquifer and tidal-mixing concepts, and some address the issues of larger oceanic controls on island hydrogeology and related diagenesis. The findings at Enewetak and their wider applicability underscore the importance of viewing small-island hydrologic problems in terms of integrated systems requiring truly interdisciplinary study.

ACKNOWLEDGMENTS

We are grateful to A. Falkland for assistance with the water-balance estimates, to H.L. Vacher for both scientific and editorial review, to M. Schoneweis for preparation of the figures, and to the many colleagues who have contributed to field work and the refinement of concepts. Most of the data collection and experimental work described here was funded by the U.S. Department of Energy and its predecessor agencies, the U.S. Energy Research and Development Administration and the U.S. Atomic Energy Commission.

REFERENCES

Atkinson, M., Smith, S.V. and Stroup, E.D., 1981. Circulation of Enewetak atoll lagoon. Limnol. Oceanogr., 26: 1074–1083.

Buddemeier, R.W., 1981. The geohydrology of Enewetak atoll islands and reefs. Proc. Fourth Int. Coral Reef Symp. (Manila), 1: 339–345.

Buddemeier, R.W. and Holladay, G.L., 1977. Atoll hydrology: island groundwater characteristics and their relationship to diagenesis. Proc. Third Int. Coral Reef Symp. (Miami), 2: 167–174.

Buddemeier, R.W. and Oberdorfer, J.A., 1986. Internal hydrology and geochemistry of coral reefs and atoll islands: key to diagenetic variations. In: J.H. Schroeder and B.H. Purser (Editors), Reef Diagenesis. Springer-Verlag, Heidelberg, pp. 91–111.

Buddemeier, R.W. and Oberdorfer, J.A., 1988. Hydrogeology and hydrodynamics of coral reef pore waters. Proc. Sixth Int. Coral Reef Symp. (Townsville), 2: 485–490.

Buddemeier, R.W. and Oberdorfer, J.A., 1990. Climate change and island groundwater resources. In: J.C. Pernetta and P.J. Hughes (Editors), Implications of Expected Climate Changes in the South Pacific Region: An Overview. UNEP Regional Seas Reports and Studies, 128: 16–27.

Buddemeier, R.W., Smith, S.V. and Kinzie, R.A. III, 1975. Holocene windward reef-flat history, Enewetak atoll. Geol. Soc. Am. Bull., 86: 1581–1584.

Couch, R.F., Fetzer, J.A., Goter, E.R., Ristvet, B.L., Tremba, E.L., Walter, D.R. and Wendland, V.P., 1975. Drilling Operations at Enewetak Atoll during Project EXPOE. U.S. Air Force Weapons Lab. Rep., AFWL-TR-75-216, Kirtland Air Force Base, NM, 269 pp.

Falkland, A.C. (Editor), 1991. Hydrology and Water Resources of Small Islands: A Practical Guide. Studies and Reports in Hydrology 49, UNESCO, Paris, 435 pp.

Fetter, C.W., Jr., 1972. Position of the saline water interface beneath oceanic islands. Water Resour. Res., 8:1307–1314.

Goff, S.K., 1979. Early carbonate cementation and diagenesis as related to the present surficial water regime, Engebi Island, Enewetak Atoll. Appl. Carb. Res. Prog. Tech. Ser. Contrib. 1, Louisiana State Univ., Baton Rouge, 83 pp.

Herman, M.E., Buddemeier, R.W. and Wheatcraft, S.W., 1986. A layered aquifer model of atoll island hydrology: validation of a computer simulation, J. Hydrol., 84: 303–322.

Hogan, P., 1988. Modeling of freshwater-seawater interaction on Enjebi Island, Enewetak Atoll. M.S. Thesis, San Jose State Univ., 141 pp.

Keating, B.H., 1987. Structural failure and drowning of Johnston Atoll, Central Pacific Basin. In: B.H. Keating, P. Fryer, R. Batiza and G.H. Boehlert (Editors), Seamounts, Islands, and Atolls. Geophys. Monog. 43, Am. Geophys. Union, Washington D.C., pp. 49–59.

Ladd, H.S., 1973. Bikini and Enewetak atolls, Marshall Islands. In: O.A. Jones and R. Edean (Editors), Biology and Geology of Coral Reefs, 1, Geology 1. Academic Press, New York, pp. 93–112.

Ladd, H.S. and Schlanger, S.O., 1960. Drilling Operations on Enewetak Atoll. U.S. Geol. Surv. Prof. Pap. 260-Y: 863–905.

NOAA (National Oceanic and Atmospheric Administration), 1983. Tide Tables 1984: Central and Western Pacific Ocean and Indian Ocean. U.S. Dep. Commer., Washington, D.C., 379 pp.

Oberdorfer, J.A. and Buddemeier, R.W., 1984. Atoll island groundwater contamination: rapid recovery from saltwater intrusion (abstr.). Assoc. Eng. Geol. 27th Annu. Meet. Program Abstr. pp. 71–72.

Oberdorfer, J.A. and Buddemeier, R.W., 1988. Climate change: effects on reef island resources. Proc. Sixth Int. Coral Reef Symp. (Townsville), 3: 523–528.

Oberdorfer, J.A., Hogan, P.J. and Buddemeier, R.W., 1990. Atoll island hydrogeology: flow and freshwater occurrence in a tidally dominated system. J. Hydrol., 120: 327–340.

Ristvet, B.L., Tremba, E.L., Couch, R.F., Fetzer, J.A., Goter, E.R., Walter, D.R. and Wendland, V.P., 1978. Geologic and Geophysical Investigations of the Enewetak Nuclear Craters. U.S. Air Force Weapons Lab. Rep., AFWL-TR-77-242, Kirtland Air Force Base, NM, 298 pp.

Schlanger, S.O., 1963. Subsurface Geology of Enewetak Atoll. U.S. Geol. Surv. Prof. Pap., 260-BB: 991–1066.

Tracey, J.I., Jr. and Ladd, H.S., 1974. Quaternary history of Enewetak and Bikini atolls, Marshall Islands. Proc. Second Int. Coral Reef Symp. (Brisbane), 2: 537–550.

USAEC (U.S. Atomic Energy Commission), 1973. Enewetak Radiological Survey. Nevada Operations Office Rep., NVO-140, Las Vegas, NV, v. 1, 736 pp.

Vacher, H.L., 1988. Dupuit-Ghyben-Herzberg analysis of strip-island lenses. Geol. Soc. Am. Bull., 100: 580–591.

Voss, C.I., 1984. SUTRA, Saturated-Unsaturated Transport: A finite-element simulation model for saturated-unsaturated, fluid-density-dependent groundwater flow with energy transport or chemically-reactive single-species solute transport. U.S. Geol. Surv. Water-Resour. Invest. Rep., 84–4369, 409 pp.

Wheatcraft, S.W. and Buddemeier, R.W., 1981. Atoll island hydrology. Ground Water, 19: 311–320.

Geology and Hydrogeology of Carbonate Islands. Developments in Sedimentology 54
edited by H.L. Vacher and T. Quinn
© 1997 Elsevier Science B.V. All rights reserved.

Chapter 23

HYDROGEOLOGY OF SELECTED ISLANDS OF THE FEDERATED STATES OF MICRONESIA

STEPHEN S. ANTHONY

INTRODUCTION

The Federated States of Micronesia (FSM) is one of the newest nations in the Pacific. It consists of 607 islands spread across more than 2 million km^2 of the western Pacific Ocean (Fig. 23-1) within an east-west chain of islands known collectively as the Carolinian archipelago. The modern history of the Carolinian people stems from their contact with whalers, traders, and missionaries. Before 1986, the western Pacific area occupied by the FSM was controlled and influenced by foreign nations: Spain from 1886 to 1899, Germany from 1899 to 1914, Japan from 1914 to 1945, and the United States from 1945 to 1986. The FSM was carved from the former Trust Territory of the Pacific Islands, administered by the United States under a U.N. mandate after World War II. The nation comprises four states (Fig. 23-1): Chuuk (formerly Truk), Pohnpei (Ponape), Yap, and Kosrae (Kusaie).

The Carolinian archipelago is made up of 31 atolls, 12 single coral islands, and five complex assemblages of predominantly volcanic islands (Kosrae, Pohnpei, Chuuk, Yap, and Palau). In general, volcanic islands are found in the east and atolls in the west. K-Ar ages on lavas from volcanic islands in the eastern Caroline Islands (Chuuk 9–14 Ma; Pohnpei 3.0–7.6 Ma; Kosrae 1.2–2.6 Ma) indicate that these islands are products of hotspot activity (Keating et al., 1984). Spengler (1990) estimates the rate of east-to-west migration of volcanism in the Caroline Islands to be 107 mm y^{-1}.

The Caroline Islands have characteristic climatic features of high temperature, cloudiness, and high humidity. Precipitation is heavy, averaging 3–4 m y^{-1} on the low coral atolls; however, droughts of 6-mo duration are common. In general, wind direction and strength rather than rainfall or temperature distinguish one season from the other. Northeasterly trade winds dominate from about November to June. By about April, the trades begin to diminish in strength; by July, the trades have given way to the lighter, more variable winds of the Intertropical Convergence Zone (ITCZ). Between July and November, the climate of the islands is frequently under the influence of the ITCZ, which has moved northward. This is the season when moist southerly winds and tropical disturbances are most frequent. Occasionally, typhoons cause extensive damage to crops and homes.

Communities on the low coral atolls rely almost entirely on rainwater catchment for a water supply. Water rationing is often necessary during periods of normal rainfall, and droughts can cause severe water-supply problems. To help alleviate the chronic water-supply shortage, the U.S. Geological Survey made a groundwater

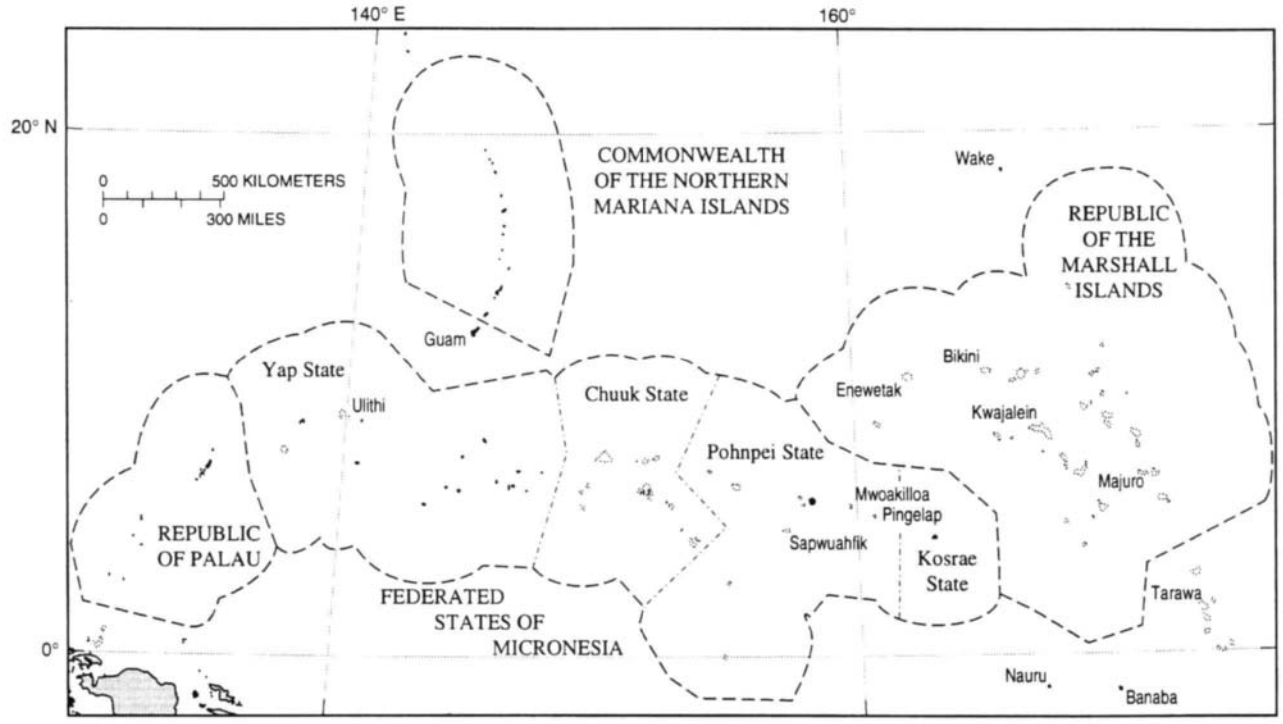


Fig. 23-1. Location of the Federated States of Micronesia and the individual states of Yap, Chuuk, Pohnpei and Kosrae. Also shown are several other Pacific islands and island groups that are discussed in this book: Tarawa, in Kiribati (Chap. 19), the Marshall Islands (Chap. 20), Enewetak (Chaps. 21 and 22), Nauru (Chap. 24) and Guam (Chap. 25).

resource appraisal of the most populated islands at Mwoakilloa (formerly Mokil), Pingelap, and Sapwuahfik (formerly Ngatik) Atolls in the State of Pohnpei, and Ulithi Atoll in the State of Yap (Anthony, 1996a,b,c; Anthony, unpub. data).

Mwoakilloa Atoll lies at 6°41′N and 159°47′E (Fig. 23-2) 140 km southeast of Pohnpei. Mwoakilloa is small compared with other atolls: 4 km long N-S, and about 1.6 km wide E-W. Three islets are scattered along a reef that encloses a lagoon

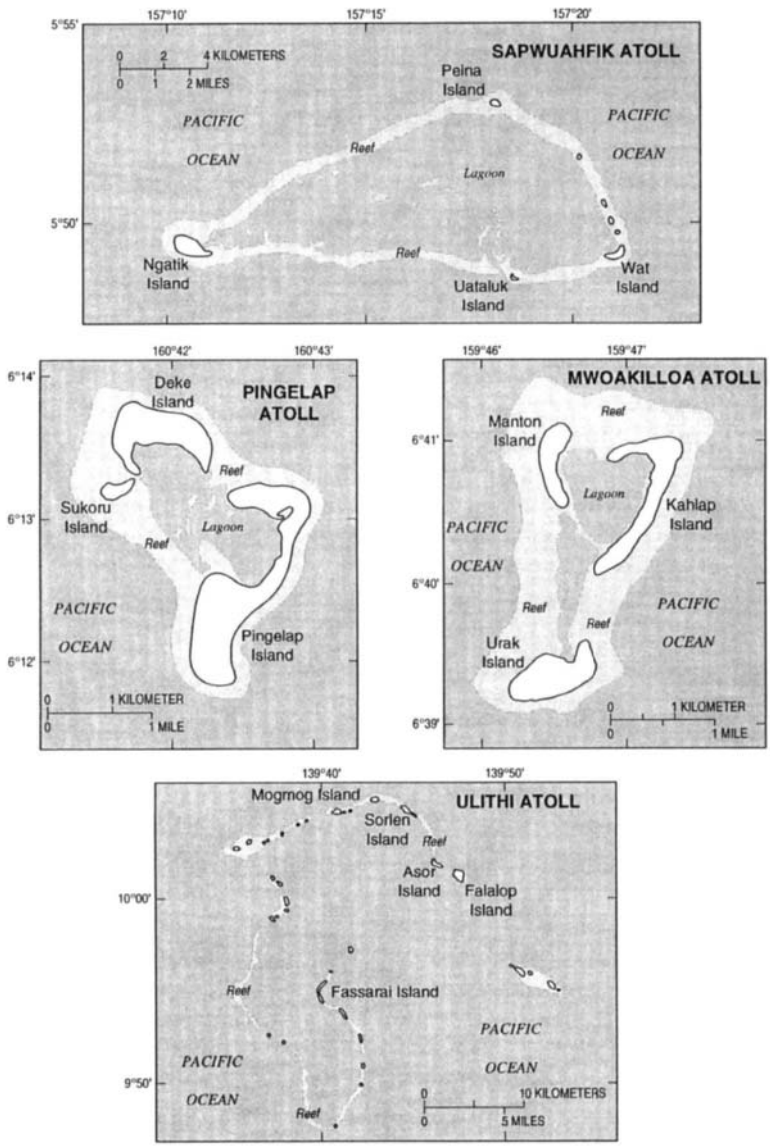


Fig. 23-2. The four atolls, Sapwuahfik, Pingelap, Mwoakilloa, and Ulithi, and their major islands.

having a surface area of 6.7 km^2. Kahlap, located on the northeast and windward side of the atoll, is the only inhabited island at Mwoakilloa and has a total land area of 0.6 km^2. A population of about 270 people live in a village strung along the lagoon side of the island.

Pingelap Atoll, at 6°12′N and 160°42′E (Fig. 23-2), is 300 km southeast of Pohnpei. This atoll also is small compared with other atolls: 4 km long N-S, and 3.2 km wide E-W. Three islets are scattered along a reef that encloses a lagoon with a surface area of 1.2 km^2. The total land area of the atoll islets is 1.8 km^2 with a maximum altitude of less than 7 m. Pingelap Island, on the southern and leeward side of the atoll, is the only inhabited island at Pingelap Atoll and has a total land area of 1.2 km^2. About 870 people live in a village along the western shore of the island. The island of Deke, on the northern and windward side of the atoll, was the site of a hydrogeologic study by Ayers and Vacher (1986) that is discussed below.

Sapwuahfik Atoll is at 5°48′N and 157°15′E (Fig. 23-2), about 145 km southwest of Pohnpei. Sapwuahfik extends 23 km E-W and 9 km N-S between the islets of Peina and Uataluk. Nine islets are scattered along a reef that encloses a lagoon of 78 km^2. The island of Ngatik, on the southwest and leeward side of the atoll, is the only inhabited island at Sapwuahfik and has a total land area of 0.83 km^2. About 600 people live along the perimeter of the island.

Ulithi Atoll, at 10°05′N and 139°43′E (Fig. 23-2), is 170 km northeast of Yap. The atoll is 26 km long N-S, 19 km wide E-W at its northern end, and 6 km wide E-W at its southern end. Forty-nine islets are scattered along a reef that partially encloses a lagoon of 474 km^2. Only four of these islands are inhabited: Falalop, Asor, Mogmog, and Fassarai. Falalop, the largest (0.4 km^2) and most populated island, is situated on a submarine promontory off the northeast and windward sides of the atoll. About 600 people live on Falalop.

GEOLOGIC FRAMEWORK

Mwoakilloa, Pingelap, Sapwuahfik, and Ulithi are remote atolls and, therefore, are logistically difficult for geologic and hydrogeologic study. As a result, knowledge of the geologic framework of these atolls is limited to direct observation in shallow (<3 m) pits and results of the Deke field study (Ayers and Vacher, 1986), which included seismic-refraction surveys and limited core drilling to depths of 5–20 m. From this work, Ayers and Vacher (1986) developed a conceptual model for the hydrogeology, including the geologic framework of the shallow subsurface. The geologic framework of that model is similar to that documented in earlier geologic investigations of Bikini [in the Marshall Islands, q.v., Chap. 20], Enewetak [q.v., Chaps. 21, 22], and Tarawa [in Kiribati, q.v., Chap. 19] by Tracey and Ladd (1974), Goter (1979), and Marshall and Jacobson (1985), respectively. In addition, a detailed study including core drilling at Laura (Anthony et al., 1989) on Majuro Atoll in the Marshall Islands [q.v.], revealed a similar geologic framework. It is likely, therefore, that a comparable distribution of geologic units occurs in the shallow subsurface of the study islands at Mwoakilloa, Pingelap, Sapwuahfik, and Ulithi because of the

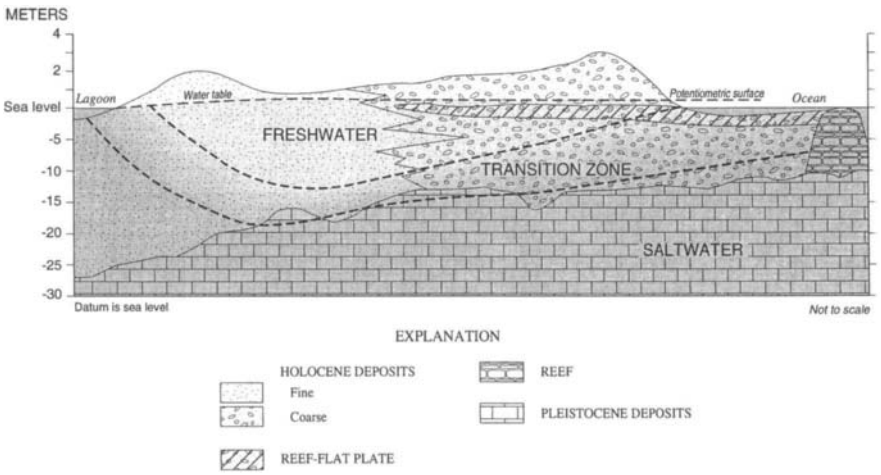


Fig. 23-3. Generalized schematic section of an atoll island illustrating the stratigraphy and distribution of freshwater. The occurrence of low-permeability (fine-grained) sediments adjacent to the lagoon results in an asymmetric distribution of freshwater. The reef-flat plate, which extends beneath much of the windward islands, acts as a confining layer. Elsewhere the freshwater lens is unconfined. (Modified from Ayers and Vacher, 1986.)

similar tectonic, eustatic, and sedimentologic histories. This distribution of geologic units consists of four principal elements (Fig. 23-3): surficial sediments, reef-flat plate, Holocene deposits, and Pleistocene deposits.

Surficial sediments of the study islands at Mwoakilloa, Pingelap, Sapwuahfik, and Ulithi exhibit an asymmetrical cross section defined by a relatively high and steep ocean side underlain by coarse-grained sediments and a lower and more level lagoon side underlain by finer-grained sediment. Between the ocean- and lagoon-side beach ridges, there is an elongated interior or central depression. Central depressions have been deepened by the islanders for cultivating wetland taro. Beachrock and cemented storm deposits are also common features. Surficial sediments are derived from the surrounding reefs. The dominant wind direction in the FSM is from the northeast; however, many of the larger storms generate southerly winds. In general, the surficial sediments of the windward islands of Kahlap (Mwoakilloa Atoll) and Falalop (Ulithi Atoll) are coarser than those of the leeward islands of Pingelap (Pingelap Atoll) and Ngatik (Sapwuahfik Atoll).

The reef-flat plate, which is overlain by surficial sediments, is composed of poorly sorted algal boundstones (reef flat) and grainstones (beachrock and water-table cementation), and forms a stable foundation on which the island sediments accumulate. The reef-flat plate lies near sea level behind the reef crest and extends lagoonward beneath the islands. On Deke, the reef-flat plate is no more than 2 m thick and extends beneath the ocean side of the island (Ayers and Vacher, 1986). The reef-flat plate at the windward islands of Kahlap and Falalop is nearly ubiquitous beneath the surficial sediments on these islands. On the leeward islands of Pingelap and Ngatik, the reef-flat plate thins from the reef crest lagoonward and pinches out

beneath the island, usually within 100–200 m of the ocean-side shoreline. Elsewhere on these leeward islands, surficial sediments are underlain by unconsolidated Holocene deposits.

Holocene deposits underlie the reef-flat plate and the surficial sediments that are not underlain by the reef-flat plate. The Holocene deposits at Deke are composed of a heterogeneous mixture of unconsolidated sand and gravel-sized reef-derived detritus, and generally exhibit a coarse-to-fine grain-size gradation from the ocean to lagoon (Ayers and Vacher, 1986). At elevations of −15 to −17 m, plates of *Halimeda* become abundant (Ayers and Vacher, 1986). Although core drilling has not been done at the study islands, results from a shallow seismic-refraction survey (Ayers, 1990) made on the island of Nukuoro (on Nukuoro Atoll, also in the FSM) indicate a similar assemblage of sediments.

Pleistocene deposits, which were exposed to subaerial weathering and erosion during glacial periods, underlie the Holocene deposits. On Enewetak and Tarawa, the primary skeletal material of the Pleistocene deposits is similar to that of the Holocene deposits but has been modified by diagenetic processes. Although the depth of the contact between the Holocene and Pleistocene deposits is not known on the study islands, the contact is at −15 to −25 m on Bikini, Enewetak, Majuro, and Tarawa (Tracey and Ladd, 1974; Goter, 1979; Anthony et al, 1989; Marshall and Jacobson, 1985). Seismic-refraction survey results (Ayers, 1990) indicate that the contact is at −15 m on Nukuoro.

HYDROGEOLOGY

Freshwater lenses

The distribution of fresh and brackish groundwater is known mainly through reconnaissance surveying using driven wells to define the thickness of freshwater, and electromagnetic (EM) surveying techniques to interpolate lens thickness data between driven wells. These techniques are described in the Case Study section of this chapter. In general, the freshwater lenses on the study islands are centered on the lagoon side of each island. This asymmetric distribution of freshwater is influenced by two factors: (1) a gradation from coarse- to fine-grained sediment (high to low permeability) between the ocean and lagoon, and (2) a greater accumulation of fine-grained (low-permeability) sediment on the lagoon side of each island (Fig. 23-3).

Results from the Deke study (Ayers and Vacher, 1986) indicate that the reef-flat plate acts as a confining layer along the ocean side of the island; elsewhere, the lens is unconfined, receives recharge directly, and forms a thicker freshwater lens. Because of the confining layer, it is not appropriate to assume that the discharge boundary is located at the ocean shoreline of Deke (Fig. 23-3). In fact, groundwater probably flows beyond the ocean shoreline and discharges either through fractures in the reef-flat plate or along the reef margin itself (Ayers and Vacher, 1986). Results from the EM survey on Ngatik indicate that more than 5 m of freshwater occurs beneath the ocean-side shoreline of that island (see Case Study).

Ayers and Vacher (1986) conclude that taro cultivation in the central depression on Deke has a hydrologically significant effect on groundwater flow patterns. Accordingly, their hydrogeologic model of Deke includes two flow patterns: a wet-season pattern in which groundwater radiates outward from the unconfined, lagoon side of the island, and a dry-season pattern in which there is also a superimposed centripetal flow in the vicinity of the central depression (Ayers and Vacher, 1986). Although this change in groundwater flow patterns between the wet and dry seasons seems likely, a dry-season thinning of the freshwater lens beneath the central depressions on the study islands could not be confirmed because islanders resisted having wells driven within the central depression.

Distribution of hydraulic conductivity

Tidal fluctuation of water levels in the study islands reflect the presence of a dual-aquifer system [see Chap. 1] consisting of Holocene deposits overlying more permeable Pleistocene deposits. On Ngatik, tidal efficiency (well-to-ocean amplitude ratio) shows a systematic increase with depth regardless of the distance from shore (Fig. 23-4). Tidal efficiencies of 0.8 m and tidal lags on the order of 15–30 min at 28 m below land surface (Fig. 23-4) illustrate that these tidal signals have undergone very little attenuation. According to the dual-aquifer model, the tidal signal is

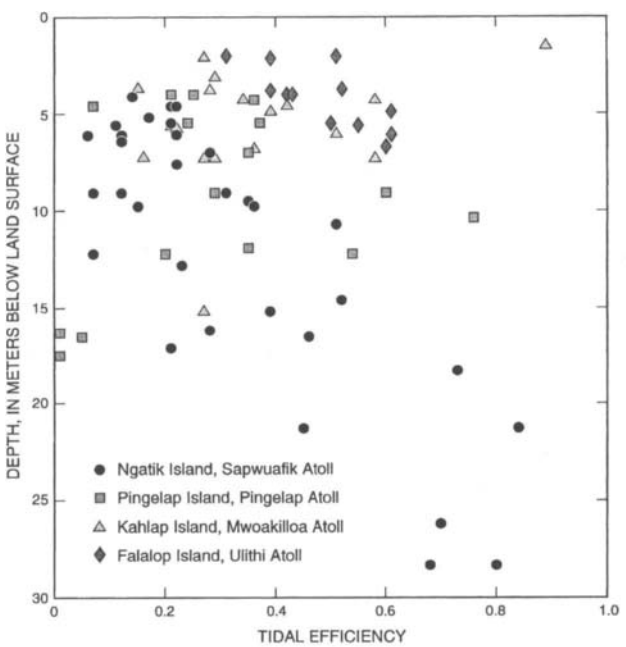


Fig. 23-4. Variation in tidal efficiency with depth from Ngatik (Sapwuahfik), Pingelap (Pingelap), Kahlap (Mwoakilloa), and Falalap (Ulithi).

propagated vertically in the Holocene deposits after little attenuation in its travel at depth through highly permeable Pleistocene deposits.

On Pingelap Island, tidal efficiency increases with depth from a median of 0.24 at 4–8 m below land surface to a median of 0.44 at 9–12 m below land surface. At 16–18 m below land surface, however, tidal efficiency is less than 0.1 (Fig. 23-4). Without subsurface geologic information and relying on the dual-aquifer model, it can only be speculated that a lens of low-permeability sediment, perhaps lagoonal muds, retards the vertical propagation of the tidal signal in the vicinity of these wells.

Wells on the windward islands of Kahlap and Falalop are not deep enough to observe variations in tidal efficiency with depth. Tidal efficiencies in wells that penetrate <8 m below land surface are generally larger on Kahlap (median = 0.34) and Falalop (median = 0.51) than they are on the leeward islands of Pingelap (median = 0.25) and Ngatik (median = 0.17) (Table 23-1 and Fig. 23-4).

Slug (bail) tests, which provide quick and inexpensive measurement of hydraulic conductivity for sediment near the wells, were made at each of the study islands. The tests were made by lowering the water level in driven wells by short-duration pumping with a hand pump and attached suction hose that was rapidly removed from the well after the water level had been lowered 3–6 m. The recovery of the water level was timed by stopwatch and measured with a hand-held electric measuring tape. Recovery times ranged from too fast to measure to more than 4 h. The salinity of water in the wells ranged from freshwater to saltwater. The tests were analyzed using the methods of Hvorslev (1951) and Freeze and Cherry (1970). The method assumes a homogeneous, isotropic, infinite medium and single-density fluid.

The median values of hydraulic conductivity determined by the slug tests are 0.16 and 0.31 m day^{-1} for the Holocene deposits on the leeward islands of Pingelap and

Table 23-1

Hydrogeologic parameters

	Island, Atoll			
	Kahlap Mwoakilloa	Falalop Ulithi	Pingelap Pingelap	Ngatik Sapwuahfik
Island setting	Windward	Windward	Leeward	Leeward
Land area (km^2)	0.6	0.4	1.2	0.8
Hydraulic conductivity[a] (m/day)	2.7	–	0.16	0.31
Tidal efficiency[a]	0.34	0.51	0.25	0.17
Rainfall[b] (m/yr)	3.0 (4)	2.8 (16)	4.0 (3)	4.0 (1)
Recharge[c] (m/yr)	1.5	1.4	2.0	2.0
Freshwater lens				
Max. thickness (m)	6	5	16	20
Volume (1000 m^3)	80	96	1454	1927

[a] Median value for the Holocene deposits.
[b] Duration of rainfall record in years shown in parentheses.
[c] Recharge is assumed to equal 50% of rainfall (Anthony, 1996, a,b,c).

Ngatik, respectively. On the windward island of Kahlap, the median hydraulic conductivity of the Holocene deposits is 2.7 m day^{-1}. By both the tidal efficiencies and slug tests, therefore, the Holocene deposits on windward islands were found to be more permeable than those on leeward islands.

CASE STUDY: HYDROGEOLOGIC RECONNAISSANCE ON REMOTE ATOLL ISLANDS BY ELECTROMAGNETIC SURVEYING

The methods available to map freshwater lenses on islands at Mwoakilloa, Pingelap, Sapwuahfik, and Ulithi are constrained by available transportation to and from each atoll, as well as on each atoll itself. To reach these remote atolls, equipment and supplies must be shipped by an interisland shipping service that calls on the atolls only once in four to six weeks. In addition, all equipment and supplies must be portable enough to be hand-carried because no docking facilities or vehicles are available on the atolls. In our reconnaissance study of these atolls, we drove well points as a means to define the thickness of freshwater because of the ease with which well points can be driven into unconsolidated sediments, and we used EM surveying methods on Mwoakilloa, Pingelap, and Sapwuahfik Atolls to interpolate lens thickness data between driven wells and to areally map the thickness of freshwater.

To determine the salinity distribution with depth, five or more clusters of driven wells were installed on each study island. Each cluster contains three or more wells driven to various depths that bracket the potable part of the freshwater lens. The wells, which consist of 5-cm-diameter steel pipe in 2-m lengths and well points with 0.6-m-long screens, were installed with a tripod, 45-kg drop hammer, and motorized cathead. Driven wells with well points allowed water-quality data to be collected at specific depths without disrupting the natural salinity distribution. The fine-grained sediments on the leeward island of Ngatik allowed wells to be driven 28 m below land surface. The nearly ubiquitous reef-flat plate at or near the water table on the windward islands of Falalop and Kahlap limited the location of driven wells to within existing shallow dug wells or excavations dug during each study that penetrate the reef-flat plate.

Nature of the electromagnetic data

The application and limitation of EM surveying methods to the mapping of freshwater lenses on small carbonate islands has been described by Kauahikaua (1987), Stewart (1988), and Anthony (1992). In this study, apparent conductivity readings were collected with the Geonics EM34-3XL terrain conductivity meter; a dual-loop, frequency-domain, EM surveying system (use of brand or firm names in this chapter is for identification purposes only and does not constitute endorsement by the U.S. Geological Survey).

In the operation of the EM34-3XL, the transmitter coil is energized with an alternating current at an audio frequency of 0.4 kHz, 1.6 kHz, and 6.4 kHz for the three coil spacings of 10 m, 20 m, and 40 m, respectively. The resulting time-varying

magnetic field induces small currents in the ground that generate secondary magnetic fields. The primary and secondary magnetic field is sensed at the receiver coil. The secondary magnetic field is a function of the intercoil spacing, operating frequency, and ground conductivity. Under certain constraints, defined as the low-induction-number principle, apparent conductivity is proportional to the ratio of the secondary to the primary magnetic field (McNeill, 1980). The EM34-3XL records terrain or apparent conductivity in units of mmhos m^{-1}.

Conductivity profiles consisting of at least 20 stations were run along footpaths that cross the width of the study islands at Mwoakilloa (10 profiles; Fig. 23-5), Pingelap (4 profiles), and Sapwauhfik (4 profiles) Atolls. Six apparent-conductivity readings consisting of three coil spacings (10, 20, and 40 m) and two coil orientations (horizontal and vertical coplanar) were made at each station. These readings were used to interpret layer conductivities and/or thicknesses. Control stations for calibrating layer conductivities were established near sites of driven wells where the salinity distribution with depth is known. The maximum exploration depth of the EM34-3XL on the study islands was estimated to be 40 m (Anthony, 1992).

Interpretation

EMIX 34, a forward and inverse modeling program, was used to obtain a quantitative interpretation of apparent-conductivity data measured in the field in

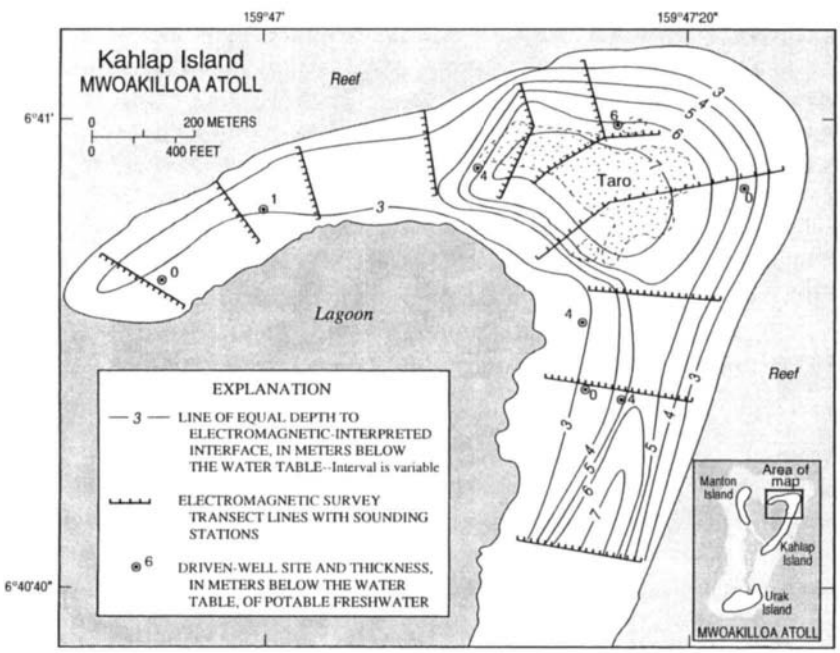


Fig. 23-5. EM-survey transect lines and the estimated depth to the EM-interpreted interface, Kahlap (Mwoakilloa). (Modified from Anthony, 1996a.)

terms of a three-layer solution that includes an unsaturated, a freshwater, and a saltwater zone. A ridge-regression-based inversion option was used to determine the thickness of the freshwater layer and the conductivity of the freshwater and saltwater layers that best fit the measured data. The synthetic data were fit to the measured data with a least-squares procedure. The modeling and inversion program has an option where the user can set one or more of the model parameters to a fixed value.

The sensitivity of the inversion routine to unknown variables was examined by comparing the fitting errors between the measured and synthetic data for four cases in which successive layers were allowed to vary. The unknown variables are the thickness of the freshwater layer and the conductivity of the freshwater and saltwater layers. The thickness of the unsaturated zone was assumed to be the elevation of land surface above sea level. Because the contrast between the conductivity of the unsaturated layer and the freshwater layer is not large enough to be resolved (Kauahikaua, 1987), the conductivity of the unsaturated layer was assumed to be 1.0 mmhos m^{-1}. Results from the sensitivity analysis show that the conductivity of the saltwater layer has the greatest effect on reducing the fitting error between the measured and synthetic data.

Interpreted results were compared with Cl^- concentration data from driven wells and indicate that the contact between freshwater and saltwater layers, defined from EM data, is located in the upper part of the transition zone, where the Cl^- profile shows a rapid increase with depth (Fig. 23-6). The section through the freshwater lens on Ngatik (Fig. 23-7) shows that the EM-interpreted interface is located in the upper part of the transition zone, but there is considerable variability at the island margins. Because no groundwater is pumped on the island, the thinning of the

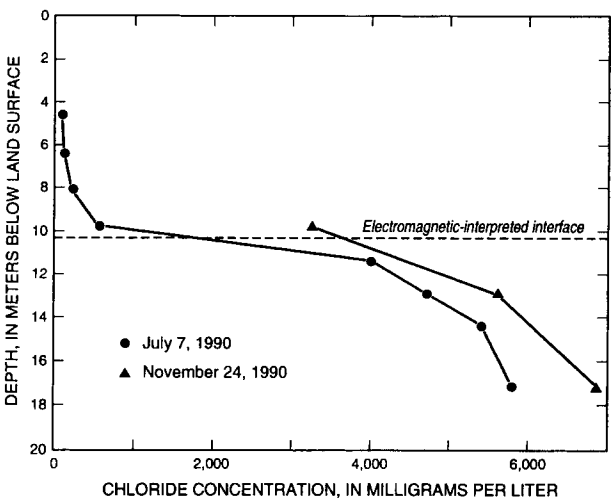


Fig. 23-6. Comparison of the location of the EM-interpreted interface with the downhole variation in Cl^-, at the E-site, Ngatik (Sapwuahfik). The EM survey was done November, 1990. The Cl^- data collected during well construction (7 July, 1990) more completely define the variation of Cl^- with depth. (Modified from Anthony, 1992.)

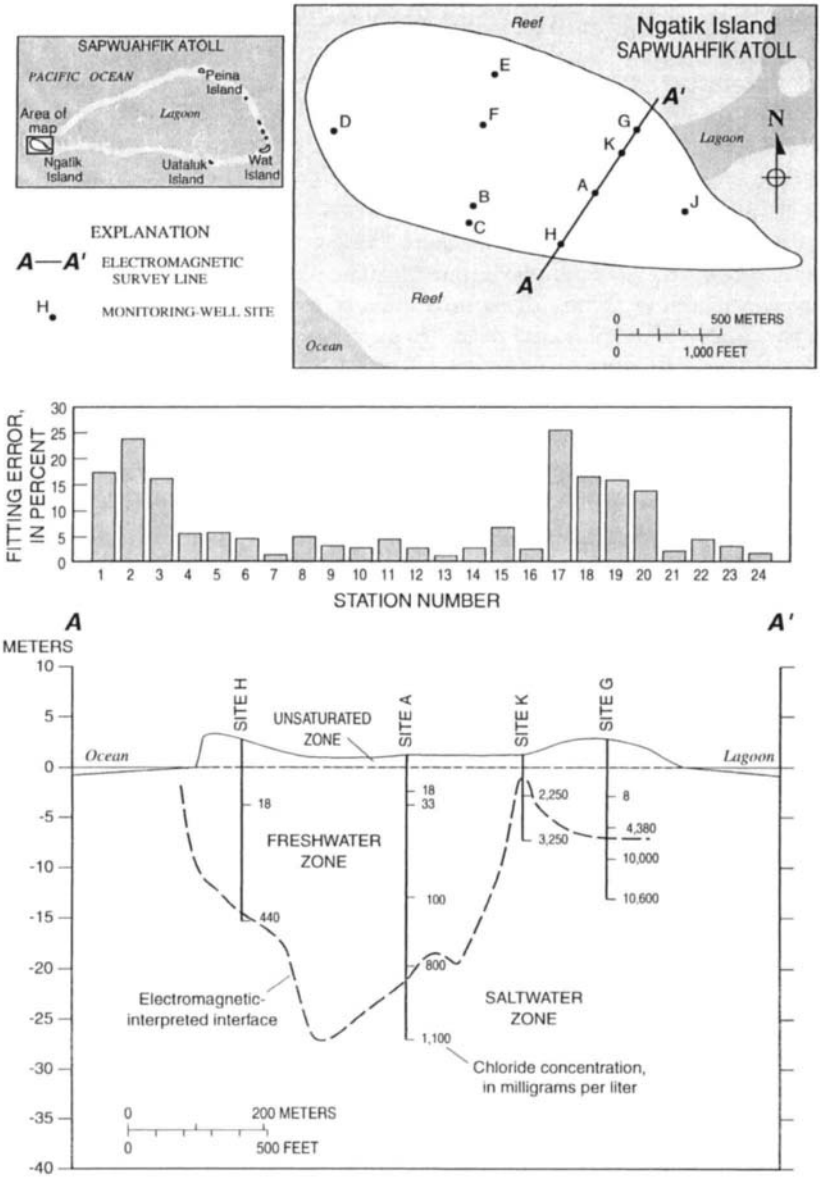


Fig. 23-7. Hydrologic and geophysical section through the freshwater lens at Ngatik (Sapwuahfik). The location of the EM survey line and clusters of driven wells are shown in the map of Ngatik Island. The bar graph shows the percent fitting error between measured and synthetic data for stations along the section. Note that this section runs from one ocean-side shoreline to another. (Modified from Anthony, 1992.)

freshwater lens at the K-site (Fig. 23-7) is probably the result of differences in permeability.

A comparison between the potable freshwater thickness at sites of driven wells and the line of equal depth to the EM-interpreted interface on Kahlap (Fig. 23-5) illustrates the poor correlation obtained at the island margins where brackish water rather than freshwater occurs. A fitting error between the measured and synthetic data of more than 20% is commonly obtained for stations that are underlain by brackish water rather than freshwater, because a large contrast in layer conductivities, which is assumed in the layered-earth model, may not be present in the absence of freshwater. On the other hand, a fitting error of less than 10–15% does not mean that a station is underlain by freshwater. For example, a low fitting error will result when modeling a salinity distribution with depth that increases abruptly from brackish water to saltwater, because the assumption that a large contrast in layer conductivities is present has been satisfied.

Results

The volume of potable groundwater in the freshwater lens on each of the study islands was approximated by combining Cl^- profiles from driven wells with results from the EM surveys. To provide a conservative estimate of the storage of groundwater, the volume was adjusted to account for a porosity of 20%. Potable groundwater in the freshwater lens on the windward island of Kahlap was estimated to be 80×10^3 m^3 (Anthony, 1996a). On the leeward islands of Pingelap and Ngatik, the volume of potable groundwater was estimated to be $1{,}450 \times 10^3$ m^3 (Anthony, 1996b) and $1{,}930 \times 10^3$ m^3 (Anthony, 1996c), respectively. In general, freshwater lenses on leeward islands are larger than those on windward islands because leeward islands have more surface area and are composed of less-permeable sediments (Table 23-1). Differences in rainfall between islands of different atolls are assumed to be negligible considering the abundance of rainfall and the short duration of rainfall records (Table 23-1). Interisland differences in land area at Ulithi Atoll were ignored owing to Falalop's location on a submarine promontory off the northeast side of the atoll (Fig. 23-2).

CONCLUDING REMARKS

Hydrogeologic reconnaissance studies at Mwoakilloa, Pingelap, Sapwuahfik, and Ulithi Atolls indicate that freshwater lenses are centered on the lagoon side of islands. The asymmetric distribution of freshwater is influenced by two factors: (1) a gradation from coarse- to fine-grained sediment (high to low permeability) between the ocean and lagoon, and (2) a greater accumulation of fine-grained (low-permeability) sediments on the lagoon side of each island. Freshwater lenses of islands on the leeward side of atoll reef complexes are thicker and larger than those of islands on the windward sides. Compared with windward islands, leeward islands have more

surface area and are composed of less-permeable sediments. This combination of attributes results in larger freshwater lenses.

REFERENCES

Anthony, S.S., 1992. Electromagnetic methods for mapping freshwater lenses on Micronesian atoll islands. J. Hydrol., 137: 99–111.

Anthony, S.S., 1996a. Hydrogeology and ground-water resources of Kahlap island, Mwoakilloa atoll, Pohnpei State, Federated States of Micronesia. U.S. Geol. Surv. Water-Resour. Invest. Rep., 91–4184, 44 pp.

Anthony, S.S., 1996b. Hydrogeology and ground-water resources of Pingelap island, Pingelap atoll, Pohnpei State, Federated States of Micronesia. U.S. Geol. Surv. Water-Resour. Invest. Rep., 92–4005, 40 pp.

Anthony, S.S., 1996c. Hydrogeology and ground-water resources of Ngatik island, Sapwuahfik atoll, Pohnpei State, Federated States of Micronesia. U.S. Geol. Surv. Water-Resour. Invest. Rep., 93–4117, 44 pp.

Anthony, S.S., Peterson, F.L., Mackenzie, F.T. and Hamlin, S.N., 1989. Geohydrology of the Laura fresh-water lens, Majuro atoll: A hydrogeochemical approach. Geol. Soc. Am. Bull., 101: 1066–1075.

Ayers, J.F., 1990. Shallow seismic refraction used to map the hydrostratigraphy of Nukuoro atoll, Micronesia. J. Hydrol., 113: 123–133.

Ayers, J.F. and Vacher, H.L., 1986. Hydrogeology of an atoll island: A conceptual model from detailed study of a Micronesian example. Ground Water, 24: 185–198.

Freeze, R.A. and Cherry, J.A., 1979. Groundwater. Prentice Hall, Englewood Cliffs NJ, 604 pp.

Goter, E.R., 1979. Depositional and diagenetic history of the windward reef of Enewetak atoll during the mid to late Pleistocene and Holocene. Ph.D. Dissertation, Rennselaer Polytechnic Inst., Troy NY, 239 pp.

Hvorslev, M.J., 1951. Time lag and soil permeability in ground-water observations. U.S. Army Corps Engineers Waterways Expt. Sta. (Vicksburg MS), Bull. 36.

Kauahikaua, J., 1987. Description of a freshwater lens at Laura island, Majuro atoll, Republic of the Marshall Islands, using electromagnetic profiling. U.S. Geol. Surv. Open-File Rep. 87–582, 32 pp.

Keating, B.H., Mattey, D.P., Helsley, C.E., Naughton, J.J., Lazarewicz, A., Schwank, D. and Epp, D., 1984. Evidence for a hot spot origin of the Caroline Islands. J. Geophys. Res., 89: 9937–9948.

Marshall, J.F. and Jacobson, G., 1985. Holocene growth of a Mid-Pacific atoll, Tarawa, Kiribati. Coral Reefs, 4: 11–17.

McNeill, J.D., 1980. Electromagnetic terrain conductivity measurement at low induction numbers. Geonics Ltd., Mississauga, Ont., Tech. Note TN-6, 15 pp.

Spengler, S.R., 1990. Geology and hydrogeology of the island of Pohnpei, Federated States of Micronesia. Ph.D. Dissertation, Univ. of Hawaii, Honolulu, 265 pp.

Stewart, M.T., 1988. Electromagnetic mapping of fresh-water lenses on small oceanic islands. Ground Water, 26: 187–191.

Tracey, J.I. and Ladd, H.S., 1974. Quaternary history of Eniwetok and Bikini atolls, Marshall Islands. Proc. Second Int. Coral Reef Symp. (Brisbane), 2: 537–550.

Geology and Hydrogeology of Carbonate Islands. Developments in Sedimentology 54
edited by H.L. Vacher and T. Quinn
© 1997 Elsevier Science B.V. All rights reserved.

Chapter 24

GEOLOGY AND HYDROGEOLOGY OF NAURU ISLAND

GERRY JACOBSON, PETER J. HILL and FEREIDOUN GHASSEMI

> "*...rugged contours/of dug-out land/exposing pinnacles/stark and sturdy/dark and light/blinding/the naked eye/capturing/the strength and might/the true essence/of forces/leading to/total destruction.*"
> From the title poem, "Pinnacles" in *Pinnacles* by Makerita Va'ai, Mana Publications, Suva 1993.

INTRODUCTION

Nauru Island occupies a land area of 22 km^2 in the central Pacific Ocean at 0°32'S, 166°56'E (Fig. 24-1). Nauru is an independent country, with a population of 10,000 who live around the coastline. The interior of the island has been mined for its surficial phosphate deposits for about 90 years. The current phosphate reserves indicate that the mine has only a few years life left at present production rates. About 80% of the land area has been denuded of its vegetation and soil cover by mining. Strip mining has left an exposed limestone pinnacle surface, or karrenfeld, with relief of up to 15 m (Fig. 24-2). This surface is untrafficable, and this formerly beautiful tropical island is now largely a desert of karst pinnacles. Nauru Island, with its alternative name Pleasant Island, ranks among the world's great environmental disasters.

Rehabilitation works are proposed by the Nauru government, and the financing of these works has been the subject of international litigation. In August 1993, the Australian government agreed to fund the rehabilitation works program and a joint Nauru/Australia team is now planning this program. It is expected that the mined-out lands will be restored progressively by demolishing the pinnacles and filling in the gaps between them. A layer of crushed rock will form the base of a new land surface which will be revegetated.

The proposed rehabilitation of the mined-out land is expected to increase the demand for water especially as reforestation will require irrigation of young trees in drought periods. Nauru's present water supply is derived from rainwater tanks (20%), dug wells (20%) and desalination of seawater (60%). Formerly, water was also imported as ballast on the ships that loaded phosphate.

Concern about the adequacy of the island's water resources led to an investigation of the hydrogeology and groundwater resources which we undertook on behalf of the Nauru Government's Commission of Inquiry into Rehabilitation of the Worked-out Phosphate Lands in 1987. The field investigation, documented by Jacobson and Hill (1988, 1993), included inspections and sampling of springs and wells; gravity and magnetic surveys to determine the depth and configuration of the island's basement;

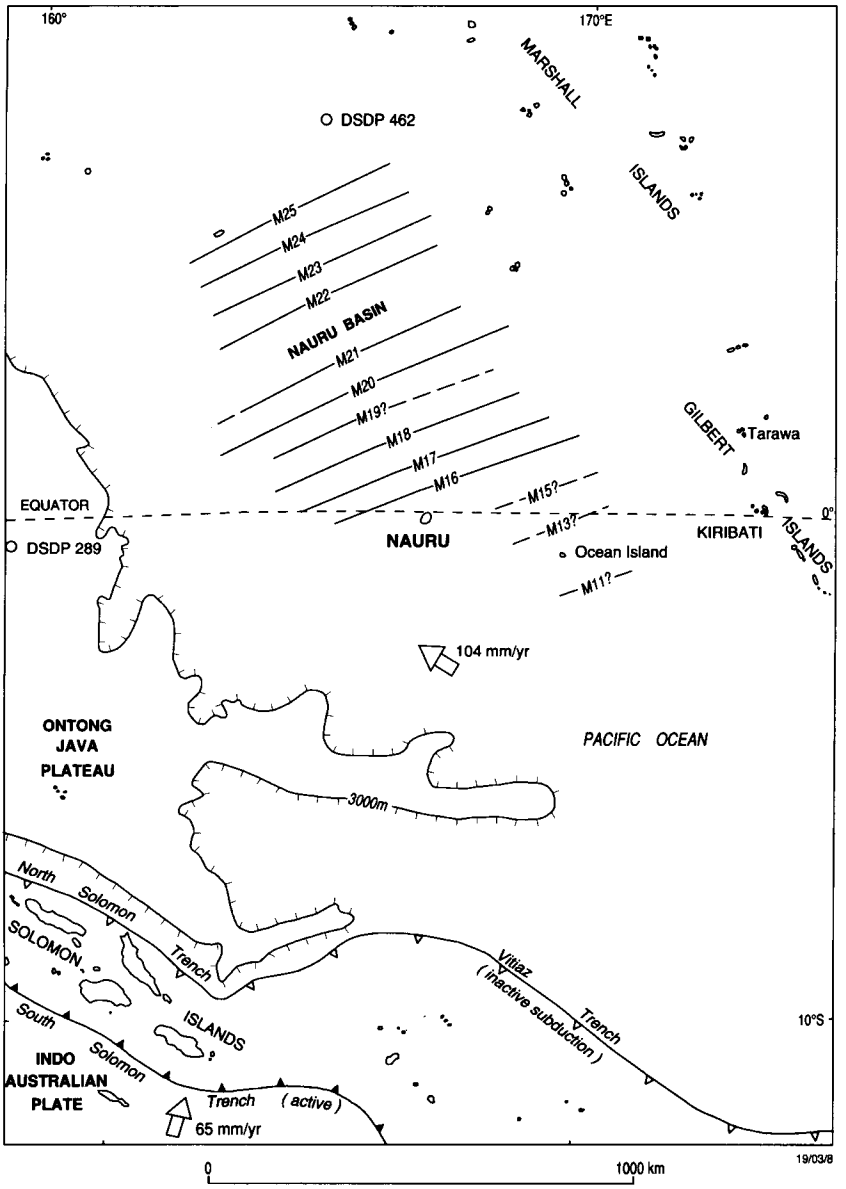


Fig. 24-1. Map showing location and tectonic setting of Nauru Island. Magnetic lineations after Larson (1976); absolute plate movement (broad arrows) after Minster and Jordan (1978). (Adapted from Hill and Jacobson, 1989.) [See Fig. 23-1 for regional location of Nauru relative to some other islands discussed in this book.]

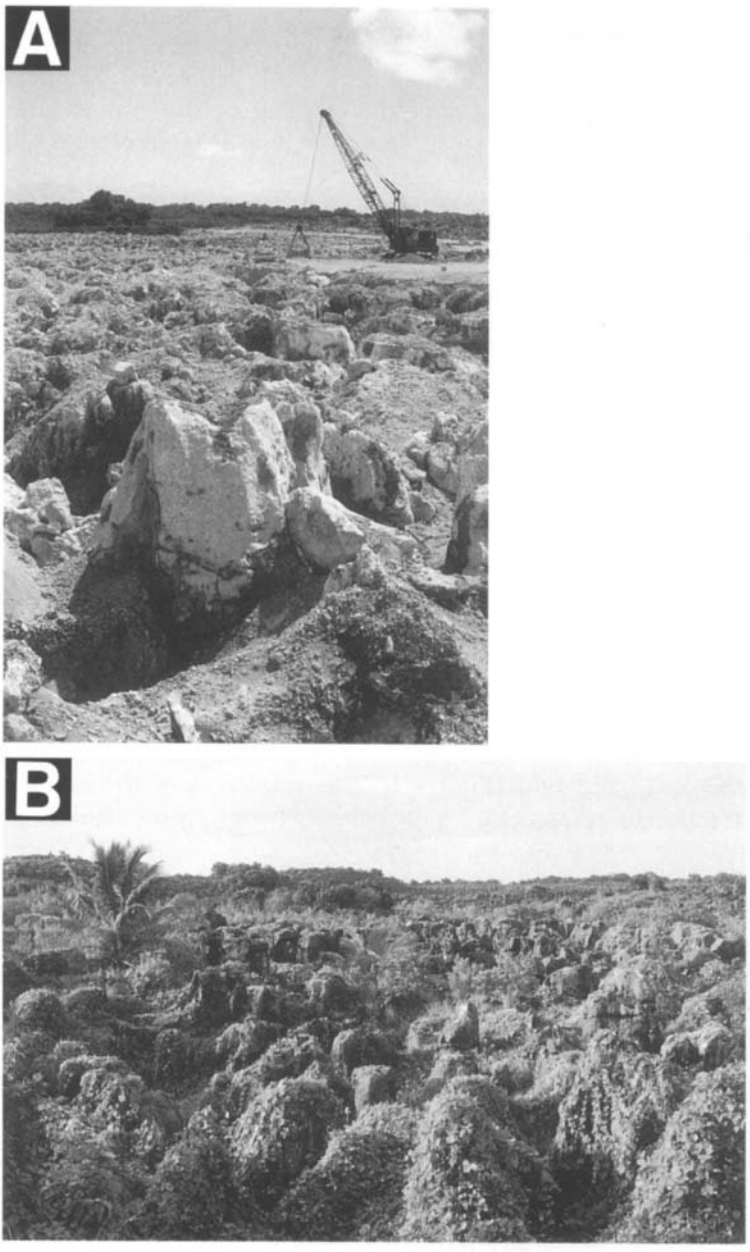


Fig. 24-2. Phosphate mining and the underlying karrenfeld. Note the remnants of the initial level surface in the upper photograph. The lower photograph shows the extent of revegetation about two decades after strip mining.

electrical resistivity surveys and drilling to determine the thickness of the freshwater layer; a gamma-ray spectrometer survey to establish radioactivity and radio-element concentrations in soil; and measurements of tidal response in boreholes. The field work has since been supplemented by numerical modelling of the groundwater system using two- and three-dimensional solute-transport models (Ghassemi et al., 1993, 1996), and by additional water quality sampling undertaken in 1994.

SETTING

Climatic setting

Nauru is hot and humid throughout the year. The mean daily maximum temperature for each month is 29–31°C, and the mean daily minimum temperature for each month is 24–26°C.

Rainfall records are available for Nauru for 67 years, although there are significant gaps with no information. The data for annual rainfall for 1916–1993 (Fig. 24-3) indicate a mean annual rainfall of 2,085 mm, with a high degree of variability. The maximum recorded annual rainfall was 4,590 mm in 1930 and the minimum was 280 mm in 1950. Monthly records indicate that mean monthly rainfall ranges from 118 mm in May to 279 mm in January (Fig. 24-4). During the wet season, December to March, the monthly average exceeds 200 mm.

High annual rainfall commonly occurs in the years corresponding to, or immediately following, major El Niño-Southern Oscillation Events (Philander, 1983), such as those of 1957, 1964, 1972 and 1982 (Fig. 24-3). The occurrence of the El Niño phenomenon every few years is responsible for the bimodal frequency distribution of Nauru annual rainfall.

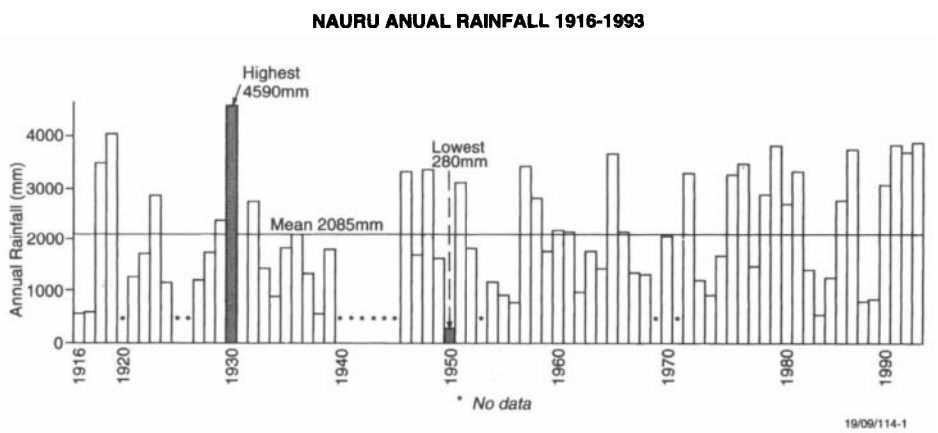


Fig. 24-3. Annual rainfall, 1916–1993. Data from Australian Bureau of Meteorology and Nauru Phosphate Corporation. (Adapted from Jacobson and Hill, 1993.)

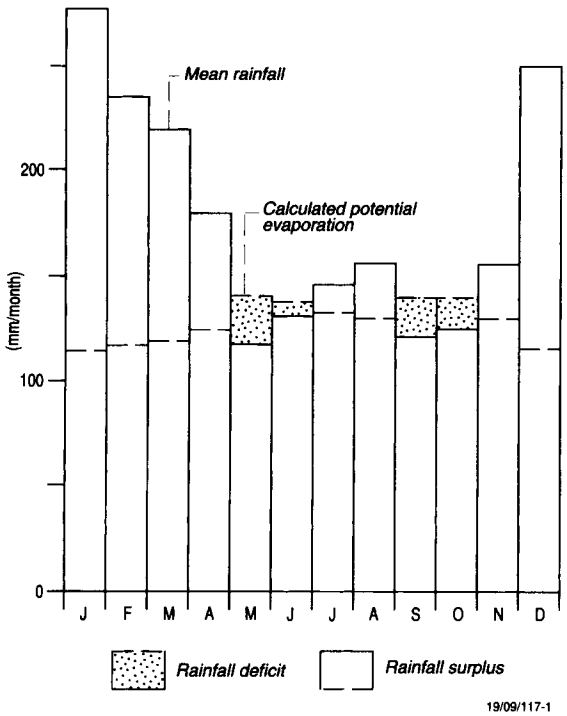


Fig. 24-4. Mean monthly rainfall (solid bar) and potential evaporation (dashed), 1916–1986. PE calculated from Fleming (1987) formula. (Adapted from Jacobson and Hill, 1993.)

During 12 of the 67 years for which records are available, less than 1,000 mm of rain fell on Nauru. Drought periods (<100 mm in ≥3 mo) occurred in 36 of the 67 years. The most severe historical droughts occurred in 1916–17 (95 mm of rain recorded in 8 mo), 1938 (97 mm in 8 mo), 1950 (83 mm in 6 mo), and 1988–89 (only 23 mm in 6 mo). Frequent drought is thus a significant factor in water resources planning for this ostensibly wet-tropical island.

Bathymetric setting

A nearshore bathymetric survey for port facilities in 1980 showed that, beyond the fringing reef, the submarine slope descends at about 34° (Jacobson and Hill, 1988). No other bathymetric data are available within the 3,000-m isobath surrounding Nauru. Beyond the 3,000-m isobath, data from various sources have been used to compile a bathymetric contour map (Fig. 24-5). The submarine slopes descend steeply to water depths of ~3,000 m and then level off to the surrounding abyssal plain at a depth of ~4,300 m.

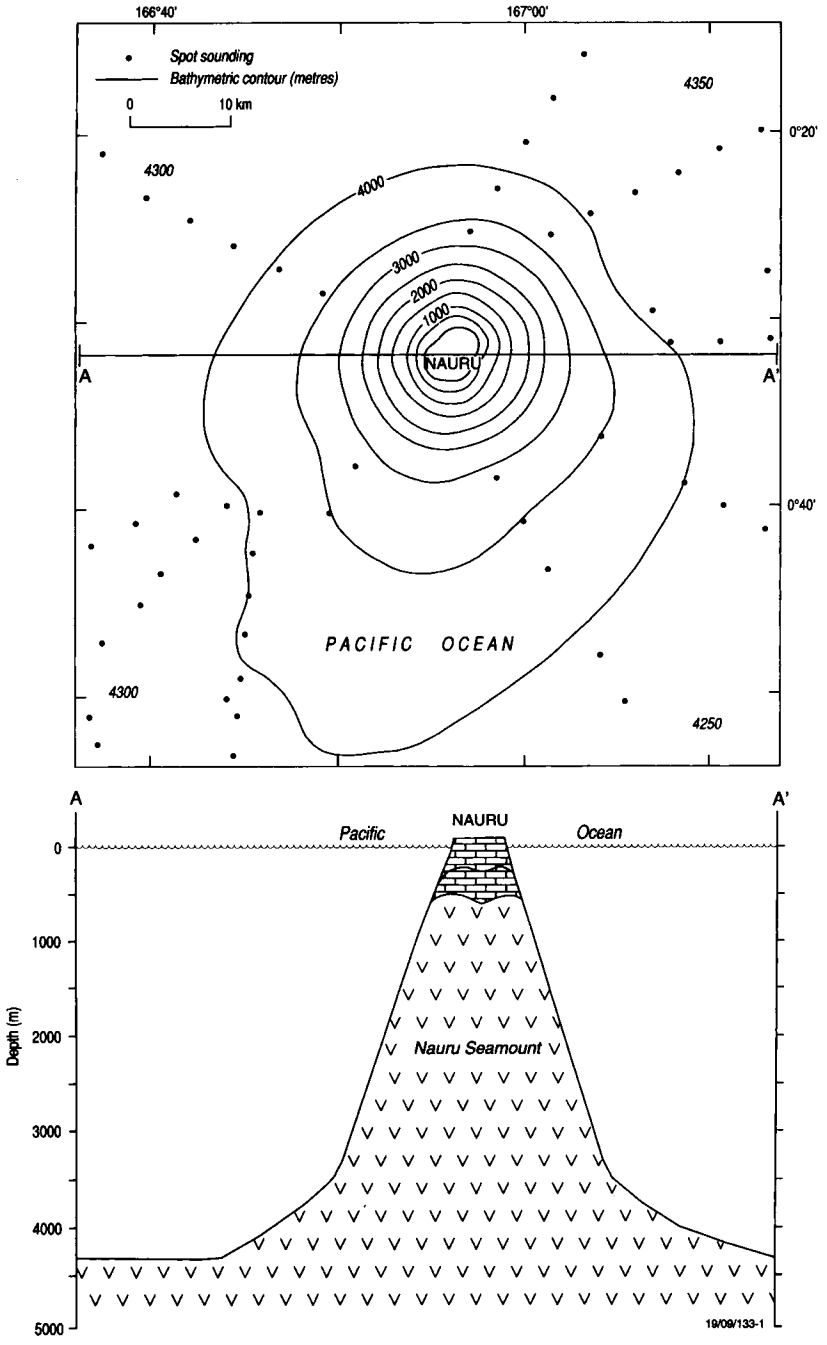


Fig. 24-5. Bathymetry of the Nauru seamount. (Adapted from Hill and Jacobson, 1989.)

Tides, mean sea level and island survey datum

Tidal information for Nauru is available for 13 years. The relationships between local mean sea level, adopted for survey purposes on Nauru, tidal extremes, and the island survey datum are shown in Figure 24-6. The mean monthly sea level is

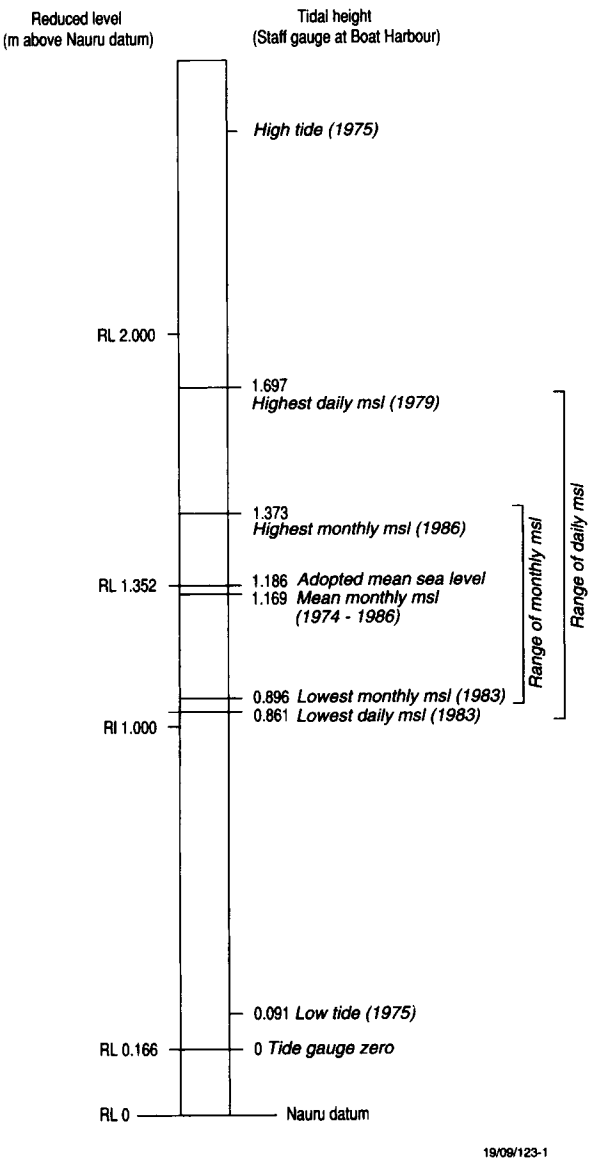


Fig. 24-6. Mean sea level and relationship of Reduced Level to tidal height. (Adapted from Jacobson and Hill, 1993.)

1.169 m above tide gauge zero. This compares with the adopted mean sea level for survey purposes of 1.186 m above tide gauge zero (Fig. 24-6). Reduced Levels (RL) are used for survey purposes. The Nauru survey datum, RL = 0, is 1.352 m below the adopted mean sea level.

The tidal range at Nauru is from 0.86 m above tide gauge zero, the lowest mean daily tide, to 1.70 m above tide gauge zero, the highest mean daily tide, over the 13-year record. The range of monthly mean sea level is between 0.896 m and 1.373 m above tide gauge zero (Fig. 24-6).

Tectonic setting

Nauru is located at the southern end of the Nauru Basin, an ocean basin, 4–5 km deep, that extends from the Marshall and Gilbert Islands in the northeast to the Ontong Java Plateau in the southwest (Fig. 24-1). The Nauru Basin contains a lineated sequence of Jurassic-Early Cretaceous magnetic anomalies (Larsen, 1976; Cande et al., 1978). This magnetic lineation pattern implies that Nauru was constructed on oceanic crust formed at about the time of magnetic anomaly M15, or at 132 Ma during Early Cretaceous time. This age represents the maximum possible age for the basalts underlying Nauru Island.

Drilling at DSDP Site 462 in the northern Nauru Basin intersected over 500 m of Early and mid-Cretaceous basalt (Larson and Schlanger, 1981). Mapping of an acoustically reverberant sub-bottom layer over most of the Nauru Basin by Houtz and Ludwig (1979) suggests that this volcanic complex is more than 600 m thick both at DSDP Site 462 and in the vicinity of Nauru.

Drilling at DSDP Site 289 on the Ontong Java Plateau (Fig. 24-1) intersected basalt of Early Cretaceous age beneath 1,200 m of calcareous sediments (Andrews et al., 1975). This oceanic basalt may be coeval with that in the Nauru Basin, and suggests an extensive volcanic and seafloor-spreading episode in the Early Cretaceous. This episode was the forerunner of even more widespread mid-plate volcanic activity during the Late Cretaceous.

Two magnetic models have led to two possible reconstructions of the latitude and orientation of the Nauru seamount at the time of its construction (Hill and Jacobson, 1989). For the two alternative models, the calculated palaeomagnetic poles are 76°N, 321°E and 80°N, 297°E, respectively, and the palaeolatitudes for the island are 12.8°S and 7.1°S, respectively. The palaeomagnetic poles for Nauru are just west of the apparent polar wander curve for the Pacific Plate (Suarez and Molnar, 1980). The degree of misfit implies a clockwise rotation of the Nauru region by ~8° relative to the rest of the Pacific Plate. The palaeolatitude positions indicate that, since its evolution, the seamount has drifted northwards on the Pacific Plate by 12.3° (model 1) or 6.6° (model 2). The northwards movement of the Pacific Plate in the Nauru region is estimated as 25 mm y^{-1} since 43 Ma, and 72 mm y^{-1} from 43 to 64 Ma, based on absolute Cainozoic angular velocities of the plate determined by Gordon and Jurdy (1986). The age of the Nauru seamount would therefore be

47 Ma according to model 1, or 29 Ma according to model 2. It is likely, therefore, that Nauru evolved in mid-Eocene to Oligocene time.

Within this period there was a major change in the motion of the Pacific Plate at 43 Ma, which is marked by the bend in the Hawaiian-Emperor chain (Dalrymple et al., 1980). Plate re-organisation was associated with this event and possibly triggered the volcanism that created the Nauru seamount. The Samoa hotspot passed within a few hundred kilometres of Nauru's present position at about 38 Ma according to reconstructions of Pacific Plate hotspot traces by Duncan and Clague (1985). A bend in the hotspot trace corresponds to change in plate motion at 42–43 Ma, and this also plots close to Nauru. The evidence suggests that the Nauru seamount was constructed by hotspot volcanism coinciding with major plate re-organisation.

The emergence of the island was probably due to uplift of the Pacific seafloor as the Pacific Plate rode over a thermal anomaly in the mantle. The Pacific Plate at Nauru is presently moving northwest at about 104 mm y^{-1} (Minster and Jordan, 1978).

GEOLOGY AND GEOMORPHOLOGY

Nauru Island is a raised coral atoll. Its topography is shown in Figure 24-7, the areal geology in Figure 24-8, and a cross section in Figure 24-9. The geologic history of the island is summarised in Table 24-1.

Table 24-1

Geological evolution of Nauru

Holocene	Coastal terrace formed during high sea level (+3m). Continued karstification.
Pleistocene	Nauru uplifted and carbonate platform exposed as Pacific plate passed over thermal anomaly in upper mantle. Exposure increased by sea-level lowstands during glacial periods. Phosphatic guano deposited from 0.3 Ma. Karstification while island emergent.
?Oligocene to Pleistocene	Subaerial erosional truncation of volcano and growth of carbonate platform as volcano subsided. Isostatic adjustment to crustal load and lithospheric cooling.
Mid-Eocene to Oligocene	Sea-floor eruption of basalts produced by rupture of Pacific plate and/or transit of Samoan hot spot, constructing volcanic pedestal of Nauru. Possibly associated minor thermal uplift.
Latest Cretaceous (70 Ma)	End of volcano-thermal episode and onset of regional subsidence due to cooling of lithosphere.
Mid-Late Cretaceous	Thermally induced regional uplift (elevation of Darwin rise) and emplacement of extensive mid-plate volcanic complex.
Early Cretaceous (132 Ma)	Oceanic lithosphere formed by sea-floor spreading.

The maximum elevation on Nauru is 71 m above sea level. Raised atoll topography is discernible (Fig. 24-7) with Command Ridge on the west side and patches of high ground on the south marking the former atoll rim. Traces of high ground (over 50 m above sea level) across the centre of Nauru may mark the line of a former reef. The interior plateau rises abruptly from the coastal terrace. A major karstic subsidence feature forms the catchment of Buada Lagoon and may be the locus of the former atoll lagoon. Buada Lagoon is a shallow lake with a mud bottom. There are two other substantial areas of doline subsidence below 25 m, in the northern half of Nauru.

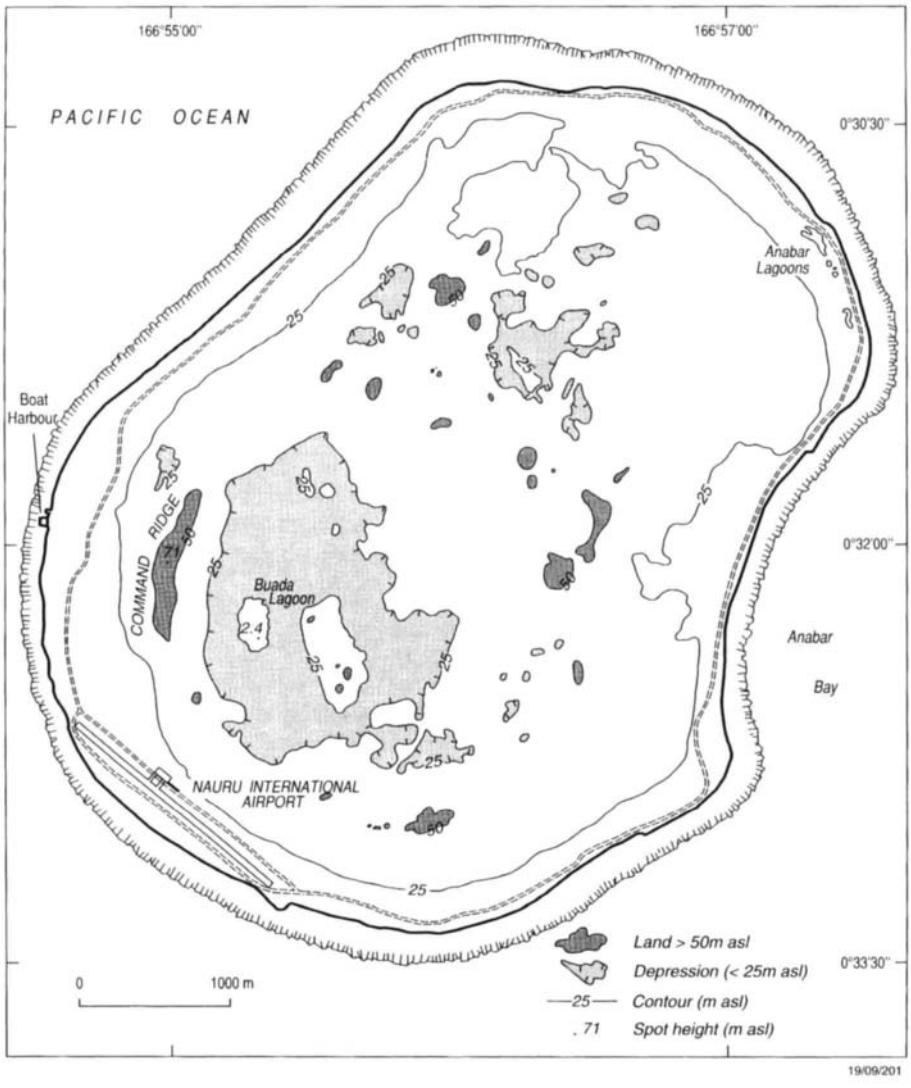


Fig. 24-7. Map showing generalised topography (metres above sea level).

The inland plateau (Figs. 24-8–10) is known locally as "Topside" and comprises dolomitic limestone with a phosphate capping that is now largely mined out. The mined-out land exposes a karrenfeld of karst pinnacles (Fig. 24-2). A scarp (Fig. 24-10) connects the inland plateau with the coastal terrace, which is known locally as "Bottomside". The inland margin of the coastal terrace is marked with depressions and brackish lagoons such as the Anabar Lagoons. The island is surrounded by a fringing reef which is up to 300 m wide.

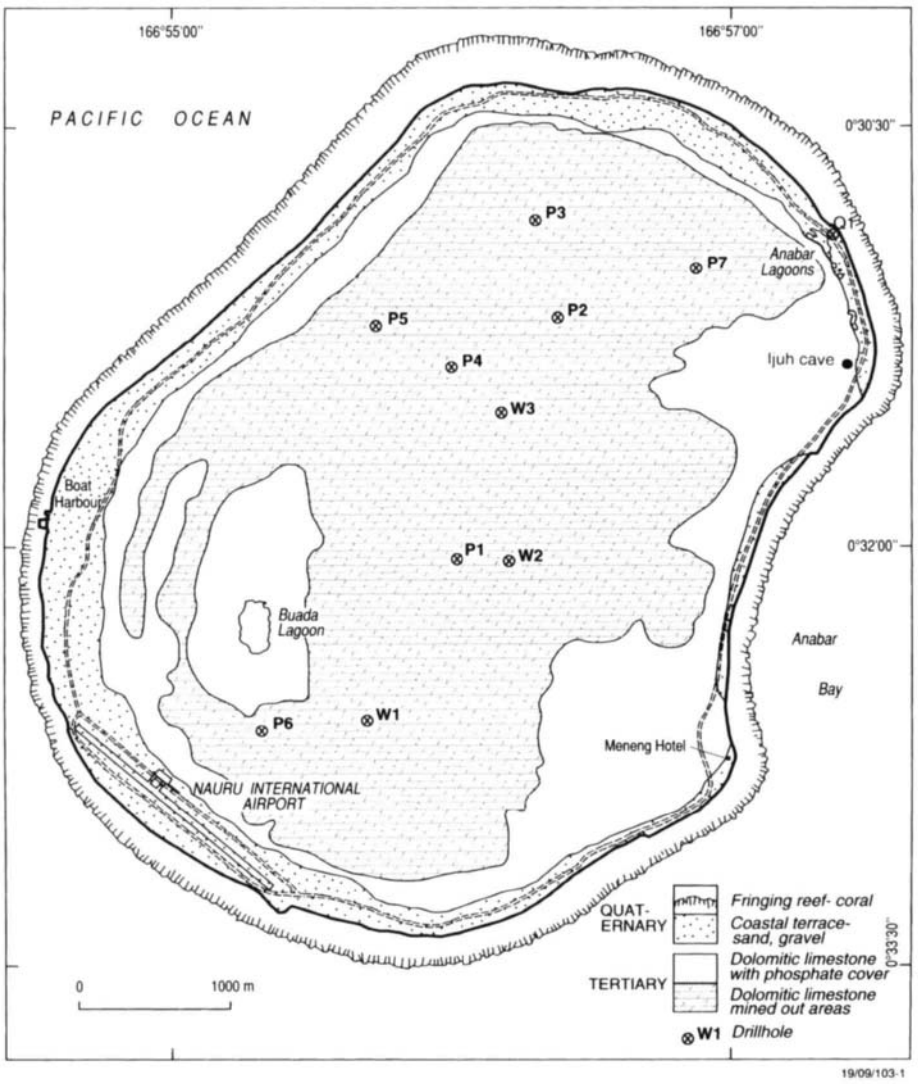


Fig. 24-8. Geologic map and location of boreholes. (Adapted from Jacobson and Hill, 1988.)

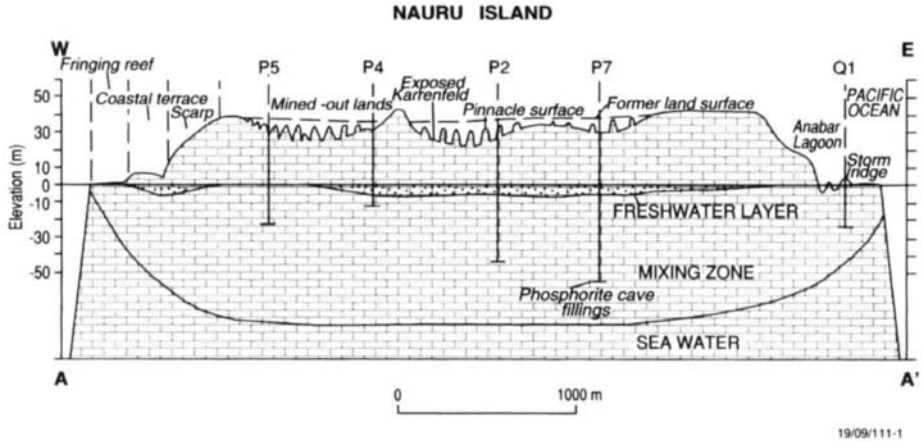


Fig. 24-9. Cross section showing geomorphological features. Location of cross section is shown on Figure. 24-13

Inland plateau

The original topography of the inland plateau has now been substantially modified by phosphate mining, but even prior to mining, the topography showed the effects of karstic erosion. An early map reproduced by Hutchinson (1950) shows an

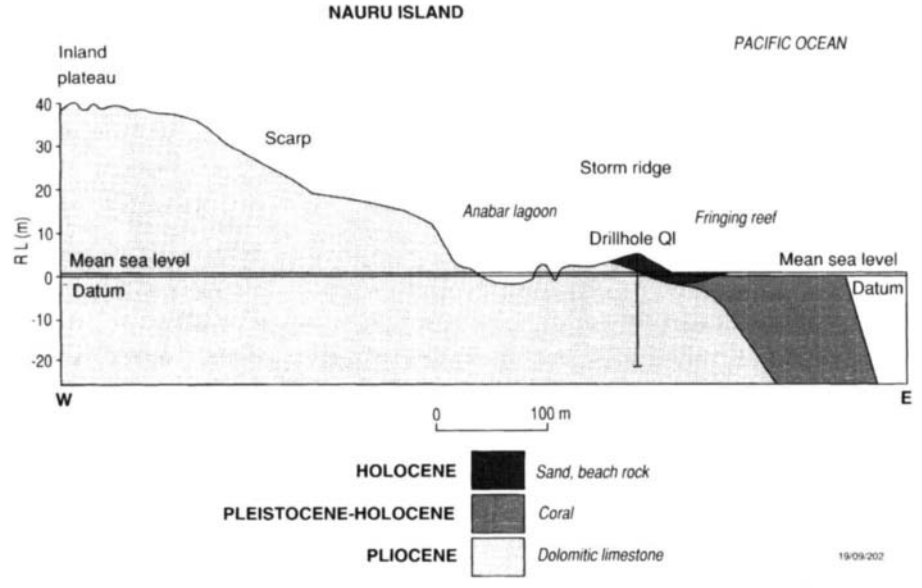


Fig. 24-10. Geological cross section through the Anabar lagoons, northeast Nauru. (Adapted from Jacobson and Hill, 1988.)

irregular island rim, 30–60 m above sea level surrounding four interior depressions. Three of the depressions had a base level of about 20 m, and the fourth, which contains Buada Lagoon, is just above sea level.

Phosphate mining has revealed the underlying karrenfeld that now forms the surface of much of the island. Dissolution of the limestone to form the karrenfeld was probably facilitated by acidity generated by the oxidation of the guano (Piper et al., 1990).

Coastal terrace

The coastal terrace surrounding the island is up to 400 m wide (Figs. 24-8–10) and lies a few metres above sea level. Between the coastal terrace and the inland plateau is a narrow chain of depressions including brackish lagoons at Anabar in the northeast of the island. Peripheral to the coastal terrace is a fringing reef which extends up to 300 m offshore with an outer slope dipping 34° into deep water. Around the southeast coast, the top of the reef is a platform eroded into Pliocene rocks.

Radiocarbon dates of 2730 and 2820 y B.P. have been obtained for aragonitic coral on the storm ridge separating the Anabar lagoons from the sea (Jacobson and Hill, 1988). Equivalent ESR dates of ~10 ka were obtained for these samples (Chen et al., 1991). These dates suggest that the storm ridge is a relatively youthful feature, related to a high stage of Holocene sea level, and built up on a Pleistocene terrace.

The arcuate eastern coastline of Nauru, facing Anabar Bay, probably represents the headward scarp of a submarine slump. Arcuate fractures subparallel to the coastline in the southwest and northwest of the island may be observed on air photos (Barrett, 1988). There is also a series of NW-SE linear fractures across the island (Fig. 24-11). Some of these fractures have exposed vertical displacements of several metres.

Substructure

Nauru is underlain by a volcanic seamount that rises 4,300 m from the floor of the Pacific Ocean (Fig. 24-5). The results of gravity and magnetic surveys in the present investigation indicate that about 500 m of partially dolomitised limestone caps the seamount. Figure 24-12 shows logs of boreholes that were drilled in the present investigation. It is known that the limestone is intensely karstified to a depth of at least 55 m below sea level, with phosphate cavity fillings that suggest that Nauru has been above sea level for much of its recent history.

Micropalaeontological examination of drill-core samples by G.C.H. Chapronière (in Jacobson and Hill, 1988) indicates that the limestone is of late Miocene to Quaternary age to the depth tested by drilling, i.e., 55 m below sea level. Chapronière describes the sequence intersected in boreholes P2 and W3 as bioclastic packstone and grainstone deposited in a lagoonal setting, i.e., "backreef" sediments. The microfaunal assemblage suggests deposition in hypersaline conditions with a restricted lagoonal circulation. Quaternary mollusks have been identified in a limestone sample from one of the island's highest points (Ludbrook, 1964).

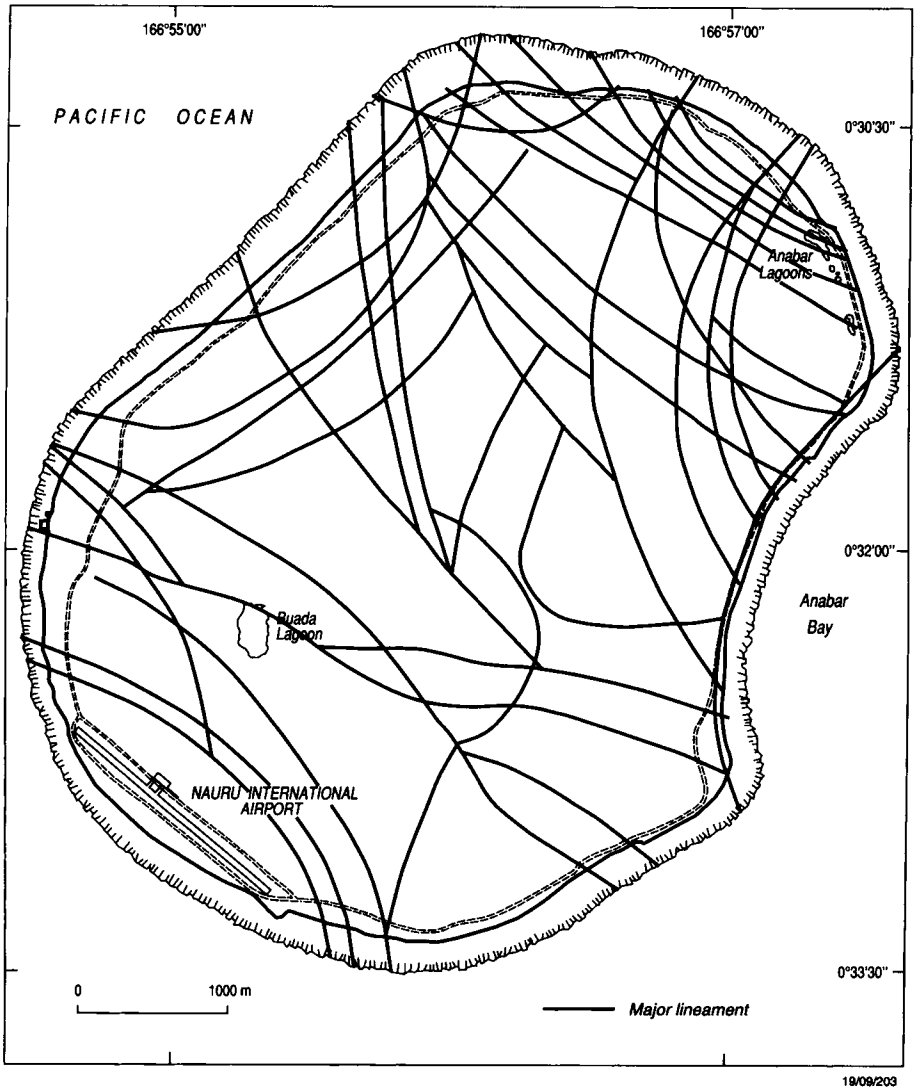


Fig. 24-11. Major lineaments from photointerpretation. (After Barrett, 1988.)

ESR dating of limestone drill-core samples has been undertaken by Chen et al. (1991). The results are: 0.50–0.60 Ma for the uppermost limestone on the inland plateau; 1.00–2.00 Ma for limestone at a depth of about 15 m beneath the inland plateau; and 3.00–5.00 Ma for limestone under the modern reef flat, which possibly extends inland at this elevation. A Plio-Pleistocene age for the uppermost part of the limestone sequence is most likely.

Gravity and magnetic surveys indicate that the substructure of Nauru is approximately radially symmetrical (Hill and Jacobson, 1989). Bouguer anomaly in-

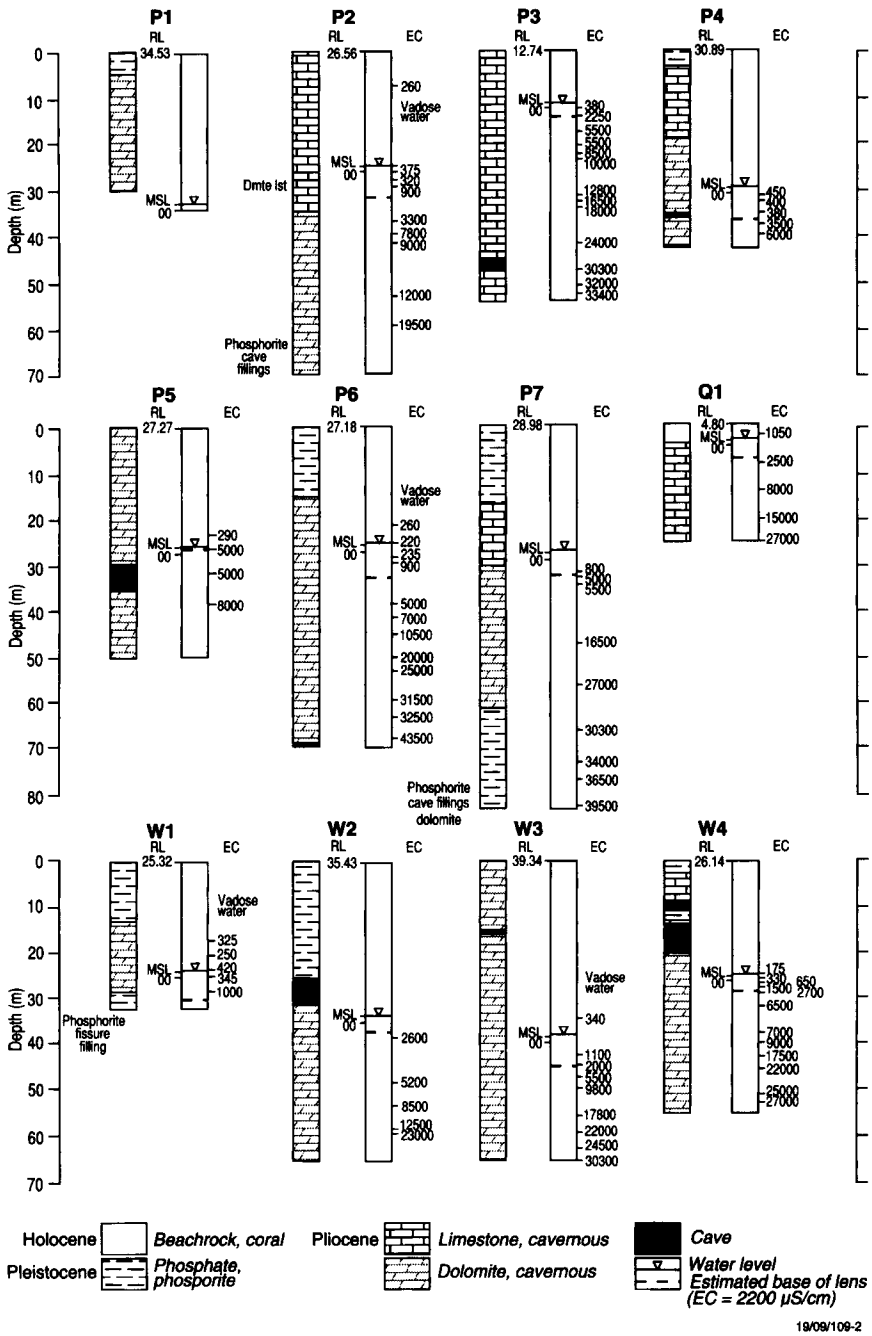


Fig. 24-12. Logs of boreholes drilled in the 1987 investigation. E.C. is electrical conductivity in µS cm^{-1}. RL (Reduced Level) is the elevation in metres relative to the Nauru survey datum (Fig. 24-6). Location of boreholes is shown on Figure 24-8. (Adapted from Jacobson and Hill, 1993.)

creases by 18 mgal from the coast to the centre of the island. The magnetic field has a range of 830 nT with a negative anomaly located over the north-northwest coastline and a large east-west positive anomaly over the southern sector of Nauru. Modelling of the magnetic field suggests that the island is underlain by a reversely magnetised core with magnetisation of 1.5–1.9 A m^{-1}, and at a depth of about 500 m. The orientation of the magnetisation vector gives the palaeomagnetic age of the core as mid-Eocene to Oligocene. This age range for the evolution of Nauru is confirmed by an estimate based on possible rates of island subsidence (Hill and Jacobson, 1989). Gravity modelling indicates a density of 2,500 kg m^{-3} for the island pedestal. The calculated values for density and magnetisation are typical for Pacific seamounts, implying that basement beneath Nauru's carbonate platform is composed mainly of basaltic lavas.

PHOSPHATE DEPOSITS

Nauru contained one of the largest island phosphate deposits in the world, and this deposit has been economically important since mining started in 1906. The original reserves were probably around 90 million tonnes (Hutchinson, 1950), but the mine now has only a few years of life left. The possibility of mining residues of phosphate between the pinnacles is being considered.

The phosphate capping of Nauru is, or was, several metres thick, and overlies the intensely dissected karrenfeld. The phosphate deposits also occupy the space between the pinnacles and infill caves and joints in the limestone.

Nauru's phosphate deposits have formed from avian guano (Power, 1910; Hutchinson, 1950). The guano has altered to carbonate fluorapatite, which is generally pelletal and forms earthy to massive deposits. The chemistry of the formation of the deposit (Piper et al., 1990) is broadly similar to that of other sedimentary phosphate deposits. Thus, during diagenesis, organic matter such as guano was oxidised, releasing phosphate and carbon dioxide into solution. Under oxygenated conditions, either on the coral island or on the seafloor, the phosphate-charged solution was acidified by carbon dioxide. Reaction with solid calcium carbonate led to supersaturation with, and precipitation of, carbonate fluorapatite. On Nauru, the carbon and oxygen isotopic values of the apatite suggest that the guano reacted with rainwater to produce the acidic phosphate solution (Piper et al., 1990) and that this solution reacted with the carbonate rocks to precipitate apatite in the freshwater zone.

Hutchinson (1950) observed strandlines on some of the pinnacles, and also commented on the absence of terra rossa, the usual limestone weathering residue. He suggested that Nauru has undergone submergence since the formation of the karrenfeld. He also suggested that the guano was deposited under conditions of lower rainfall and greater biological productivity than today, probably in glacial periods. Aharon and Veeh (1984) considered the carbon and oxygen isotopic composition of the carbonate fluorapatite which is the main component of the phosphate deposit. From this they suggested that the phosphate deposits of Nauru and other islands are related to drier climates associated with equatorial upwelling in the Pacific.

The age of the phosphate deposits has been the subject of some investigation. Hutchinson (1950) cited an early description of a well dug in the coastal terrace that exposed alluvial phosphate, probably a cave filling, at least 3 m below mean sea level. This indicates that processes of leaching and redeposition in karst fissures predate the formation of the coastal terrace. Uranium-series dates of Nauru phosphate were reported by Roe and Burnett (1985): one banded phosphorite sample was dated at 0.14 Ma, and several other samples were dated as older than 0.30 Ma. The island's phosphate cap may date from about 0.22 Ma according to ESR dating of phosphate samples by Chen et al. (1991). The suggested ESR time framework for the diagenesis and recrystallisation of the deposits is: 0.08–0.10 Ma for the superficial phosphate deposits; and 0.18–0.22 Ma for massive phosphorite with nodules and replaced coral.

HYDROGEOLOGY

The locations of investigation boreholes are shown on Figure 24-8. In the 1987 investigation, fragmented core was obtained with a reverse-circulation drilling rig. Water samples were obtained at intervals during drilling for electrical-conductivity measurement. Some difficulty was experienced in differentiating groundwater from drilling water which was used in the section of the borehole above the aquifer. Twelve boreholes were completed to depths of 26–83 m below surface (Table 24-2). Three of the holes were completed as open-hole piezometers with 40-mm-diameter plastic casing to enable the measurement of standing water level. Cavernous ground prevented the installation of casing in the other boreholes. Geological logs of the

Table 24-2

Investigation drill holes, Nauru, October 1987

Drillhole	Reduced Level (m)	Total depth (m)	Standing water level (m)	Estimated freshwater level thickness (m)	Bottom hole salinity ($\mu S\ cm^{-1}$)
P1	34.53	30	–	–	–
P2	26.56	70	–	7	19500
P3	12.74	54	11.23	3	33400
P4	30.89	43	–	7	6000
P5	27.27	50	–	0.5	22100
P6	27.18	70	–	7	43500
P7	28.98	83	–	4.5	39500
Q1	4.80	26	–	3.5	27000
W1	25.32	32	–	6.5	1000
W2	35.43	65	–	3.5	22000
W3	39.34	65	37.85	6.5	30300
W4	26.14	55	24.56	3.5	27000

boreholes and electrical-conductivity measurements of groundwater samples are given on Figure 24-12.

Locations and results of the geoelectrical soundings are shown on Figure 24-13. A total of 10 soundings were made in three hydrogeological environments: on the interior plateau of Nauru, at elevations of 12–27 m (depth probes 1, 2, 6 and 8); adjacent to Buada Lagoon, at elevations of 2–3 m (depth probes 3, 4, 5 and 7); and on the coastal terrace, at elevations of 3–4 m (depth probes 9 and 10).

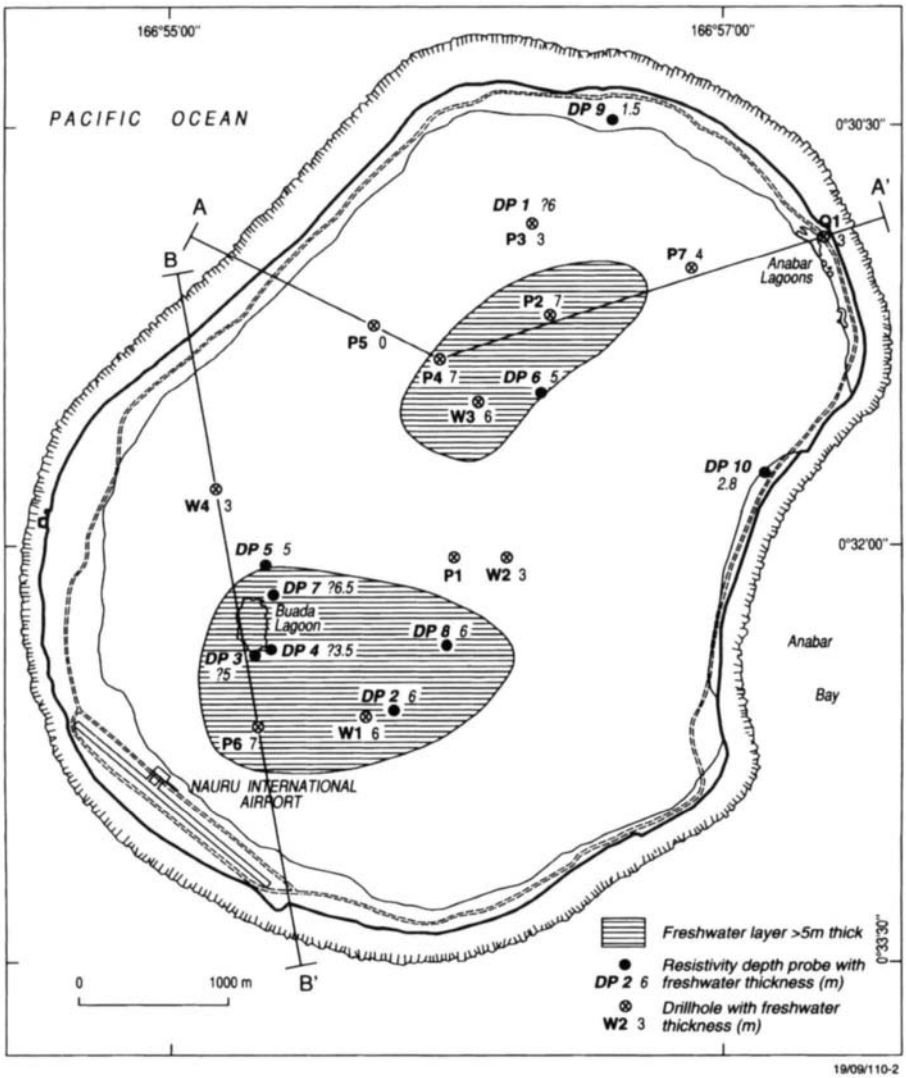


Fig. 24-13. Thickness of freshwater layer, and location of geoelectrical soundings (Fig. 24-15). (Adapted from Jacobson and Hill, 1993.)

The method used was the 4-electrode Schlumberger sounding method and the instrument used was an ABEM Terrameter SAS 300B with Booster SAS 2000. A typical field curve of apparent resistivity and its interpretation are shown on Figure 24-14. The other field curves and their interpretation are documented in Jacobson and Hill (1988). Interpretation was done by iterative modelling, during which the apparent-resistivity model curves were computed by the linear filter method of O'Neill (1975). The resistivity models were constrained to comply with the observation, from drilling, that the water table invariably lies just above mean sea level. The depth of resistivity reduction associated with the top of the aquifer was set at a RL = 1.00 m above the local Nauru survey datum (Fig. 24-6).

Routine interpretation of subsurface resistivity structure is practical only for horizontal layering. Complex mathematical analysis and modified field techniques are required for more complicated configurations. In selecting electrical sounding sites on Nauru, therefore, the requirement for at least approximate horizontal resistivity stratification was an important consideration. Two of the deeper soundings, DP6 and DP8, were completed in the interior of Nauru (Fig. 24-13) where long electrical arrays are possible only along linear sections of mine roads. In these cases, some departure from horizontal stratification is evident from distortion of the field curves. This distortion is caused by the channelling of electrical current through the

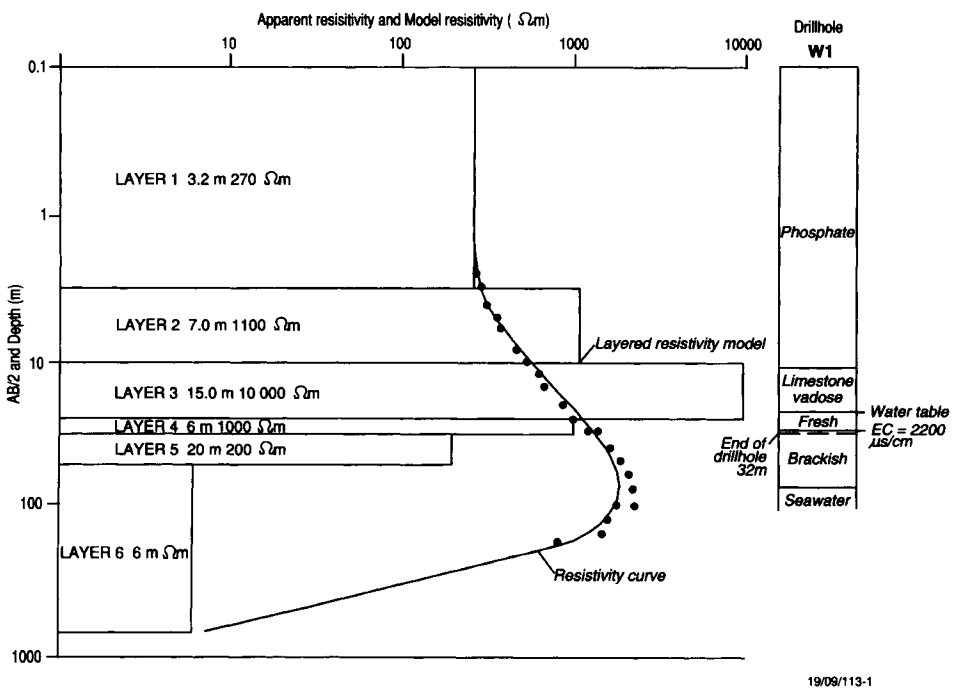


Fig. 24-14. Comparison of layered-model interpretation of resistivity (depth probe 2) and drill log (W1). AB is the distance between the current electrodes. (Adapted from Jacobson and Hill, 1993.)

relatively low-resistivity soil and phosphate forming the road foundation. In contrast, the mined-out, pinnacle areas adjacent to the roads are significantly more resistive.

Configuration of freshwater layer and mixing zone

The drilling results and the geoelectrical soundings show that Nauru Island is underlain by a discontinuous layer of freshwater up to 7 m thick (Fig. 24-13). There are two main lenses of freshwater, underlying about 1.3 km^2 in the north-central part of Nauru, and about 2.4 km^2 in the south-central part. The freshwater layer overlies a mixing zone of brackish water up to 60 m thick, which in turn overlies seawater. The groundwater salinity increases gradationally downwards through the mixing zone as shown in the cross sections of Figure 24-15.

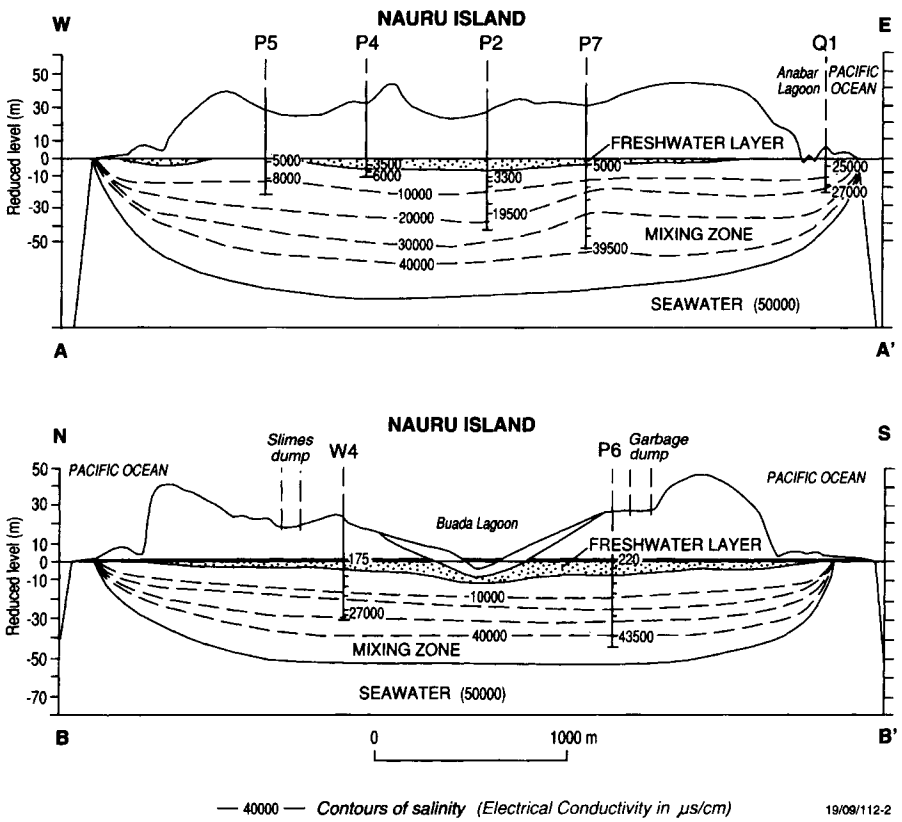


Fig. 24-15. Cross sections showing groundwater salinity (electrical conductivity in μS cm^{-1}). Location of cross sections is shown on Figure 24-13. Vertical axis is RL (Reduced level), the elevation in metres relative to the Nauru survey datum (Fig. 24-6). (After Jacobson and Hill, 1988.)

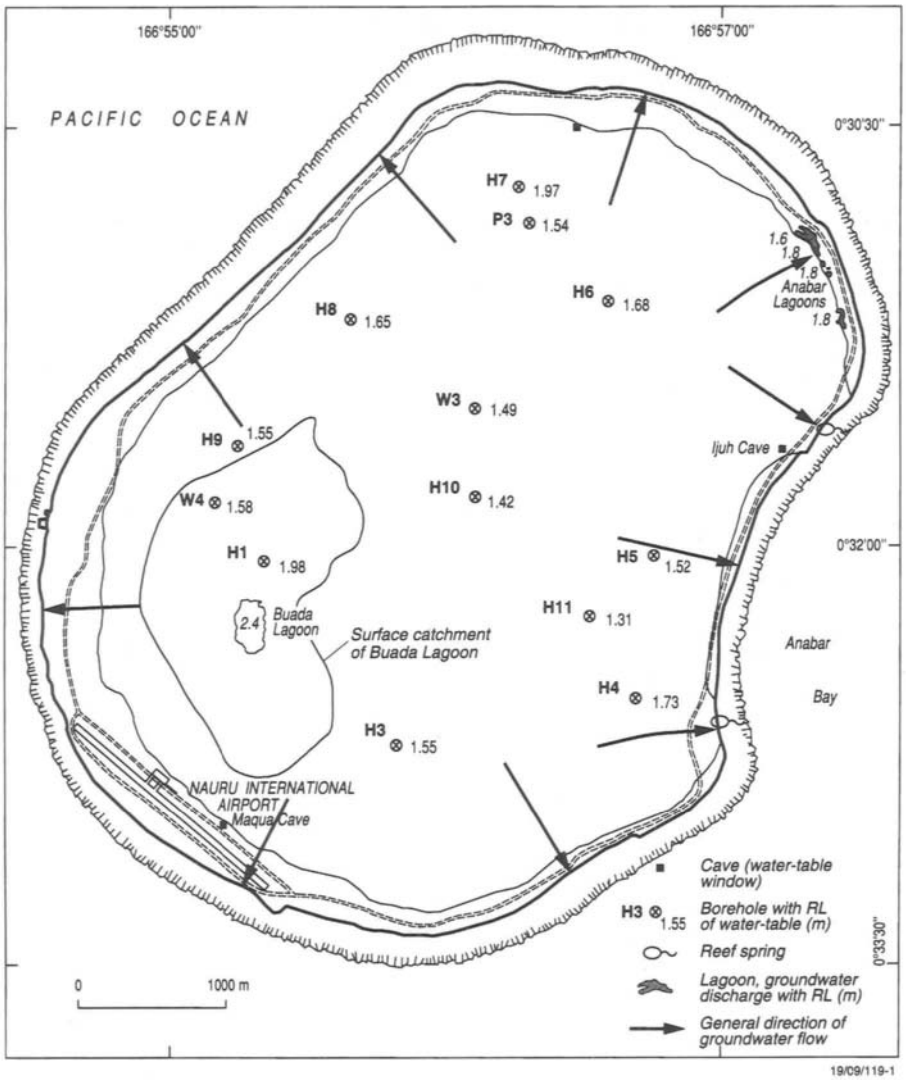


Fig. 24-16. The Nauru Island groundwater flow system, and water-table elevations relative to the Nauru survey datum (Fig. 24.6). (After Jacobson and Hill, 1988.)

Most of the island has a continuous water table forming the upper boundary of the freshwater layer at an average elevation of RL = 1.50 m (about 0.20 m above mean sea level). The catchment of Buada Lagoon is an exception: it appears to be a different hydrological system (Fig. 24-16). Buada Lagoon is at an elevation of RL = 2.40 m, and is perched above the regional water table, presumably on impermeable phosphatic alluvium. Observations of Buada Lagoon water levels show a

lack of tidal response, but there is anecdotal evidence for a lowering of water level by evaporation in drought periods.

The average thickness of the freshwater layer is 4.7 m as determined by intersections in eleven boreholes (Fig. 24-12). The lower boundary of the freshwater layer is defined at a salinity level of 1,500 mg L^{-1} total dissolved solids (TDS), which is equivalent to electrical conductivity (EC) of 2,200 μS cm^{-1} and is used as the upper limit for drinking water. The unusually thick mixing zone of brackish water is due to high permeability in the limestone. Open karst fissures allow intrusion of seawater throughout the island's substructure, and diffusion by tidal mixing forms the zone of brackish water. Quantitative estimates of hydraulic conductivity have not been undertaken on Nauru. However, investigations of groundwater systems on some other raised limestone islands have indicated values of hydraulic conductivity of 1,000–3,000 m day^{-1}; this includes Tongatapu (Hunt, 1979) [Chap. 18], Barbados (Goodwin, 1980) [Chap. 11], and northern Guam (Goodrich and Mink, 1983) [Chap. 25].

Groundwater recharge

Potential evapotranspiration (PE) has been calculated for Nauru on the basis of Fleming's (1987) formula. This empirical formula was derived for Tarawa [q.v., Chap. 19], which has a similar climate and is 700 km to the east. The relationship is:

$$PE = 115 + (300 - R)^2/1286$$

where PE and R are monthly values in mm. From this relationship, and monthly data, the PE estimated for Nauru ranges from 115 mm in January to 141 mm in May (Table 24-3). The mean annual total is 1547 mm.

There is no direct surface runoff to the sea in Nauru. Therefore, disregarding some groundwater discharge to and surface water evaporation from lagoons, the approximate water balance for Nauru can be considered as

$$R = AET + GWR,$$

where AET is actual evapotranspiration (<PET), and GWR is groundwater recharge. Estimating AET requires information on soil moisture and vegetation characteristics, and this information is not available for Nauru Island. However, an estimate for Nauru can be made from studies at nearby atolls.

A detailed estimate of AET for Kiritimati [Christmas Island, q.v., Chap. 19] showed that recharge is 29% of rainfall for a freshwater lens where the land is not vegetated (Falkland, 1984). Kiritimati is appreciably drier than Nauru.

Tarawa is the closest atoll with comparable annual rainfall and available information. Recharge for Tarawa has been estimated at 36% of rainfall for the case of 80% coconut tree cover and 20% grass [see Case Study 2, Chap. 19]. This result suggests that for Nauru — with its extensive bare karrenfeld surface — a value for recharge of about 40% of rainfall is appropriate. Adopting this value, the approximate annual water balance for Nauru is

Table 24-3

Monthly rainfall and potential evaporation

	Mean rainfall (mm)	Potential evaporation* (mm)
January	279	115
February	236	118
March	220	120
April	179	126
May	118	141
June	130	137
July	146	133
August	156	131
September	123	139
October	126	139
November	155	131
December	252	117

* Estimated from Fleming's (1987) formula.

$$R(2,000\ \text{mm}) = AET(1,200\ \text{mm}) + GWR(800\ \text{mm}).$$

Groundwater flow and discharge

The amount of recharge indicates that a substantial amount of groundwater flows through the Nauru groundwater system. Water-table measurements in present and previous investigation boreholes indicate that the groundwater head throughout most of the interior of Nauru is about RL = 1.50 m, which is about 0.20 m above mean sea level. There are some difficulties in establishing this, as tidal oscillations of groundwater level are significant, and mean sea level is also not static (Fig. 24-6).

Averaged elevations of the water table are shown on Figure 24-16. Groundwater flow is probably radially outwards to the sea, and is generated by the 0.20-m head differential between the water table and mean sea level. There is a potentiometric high in the north of the island and a low in the east central part (vicinity of H11, Fig. 24-16). It is not clear whether this is an artifact of limited measurements or whether there are areal permeability differences, possibly due to major fractures allowing ingress of seawater into the island's substructure (Fig. 24-11). It is possible that the inferred submarine landslide forming Anabar Bay has removed fringing reef deposits and allowed better access to the permeable interior.

Groundwater discharges around the circumference of the island. Known discharge features include the chain of lagoons at Anabar in the northeast. Several springs have also been observed to discharge on the fringing reef at low tide (Fig. 24-16). Several caves at the inland edge of the coastal terrace provide a window on the water table close to the discharge end of the flow system. The largest of these is Maqua Cave in the southwest of Nauru.

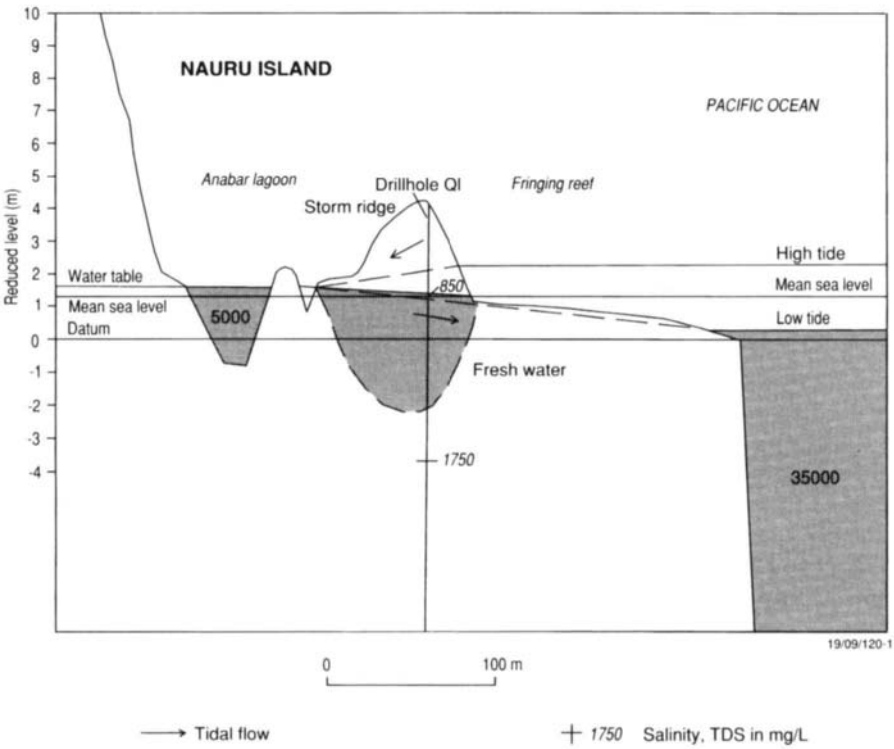


Fig. 24-17. Schematic cross section through the coastline showing the reversal of hydraulic gradient with tidal fluctuation. Vertical axis is RL (Fig. 24-6). (Adapted from Jacobson and Hill, 1993.)

Tidal fluctuations

The effect of daily and longer-term fluctuations in ocean tide level is shown on Figure 24-17. There is a reversal of hydraulic gradient at the shoreline with drainage outwards at low tide, and seawater flow inwards at high tide.

Tidal effects in observation borehole P3, which is 800 m inland, were measured during the present investigation (Jacobson and Hill, 1988), and additional information on this phenomenon is available from an unpublished report of the Nauru Phosphate Corporation (R. Gormley, unpublished memo, 1987). Tidal effects on groundwater levels are substantial, being close to half the amplitude of the ocean tidal stage throughout the island. The tidal movement of the water table is commonly of the order of 0.5 m and the lag of the tidal peak in inland water boreholes is generally 1.5–3 h.

NUMERICAL MODELLING OF THE GROUNDWATER SYSTEM

Two numerical models have been used to simulate the Nauru groundwater system: SUTRA (Voss, 1984) and HST3D (Kipp, 1987). Both are solute-transport

models. SUTRA employs a two-dimensional finite-element approximation of the governing equations in space, and an implicit finite-difference approximation in time. HST3D employs three-dimensional finite-difference approximations of the governing equations.

Two-dimensional model

In order to simulate the Nauru Island aquifer using the SUTRA model, a vertical cross section of the aquifer was considered (Ghassemi et al., 1990). The cross section was 6,400 m long and 120 m deep with an arbitrary thickness of 1 m. The cross section was discretised to 832 rectangular elements and 891 nodes. The horizontal spacing was constant at 200 m, and the vertical spacing was variable from 2 m to 10 m from the top of the aquifer to a depth of 120 m. Boundary conditions for the model were specified as: a no-flow boundary along the bottom of the mesh; a recharge boundary due to rainfall at the top of the aquifer; and hydrostatic boundaries along the right and left boundaries of the model. Boundary conditions for the solute-transport simulation are dependent on the flow boundary conditions.

Calibration of the model was undertaken with the objective of reproducing measured salinity in the observation wells and the inferred distribution of salinity along the cross section. In the absence of detailed information for Nauru, the hydraulic parameters were estimated by trial and error and by analogy with similar cases elsewhere. A wide range of values for each parameter was tested to estimate the most appropriate value. Satisfactory calibration was obtained with the following parameters: hydraulic conductivity, 900 m day^{-1}; anisotropy ratio (K_h/K_v), 50; recharge, 540 mm y^{-1}; porosity, 30%; longitudinal and transverse dispersivity, 65 m and 0.15 m respectively; and molecular diffusivity 10^{-10} m^2 s^{-1}. A comparison of measured and computed salinity concentrations at depth in the boreholes showed that the calibrated model reproduced the steady-state behaviour of the aquifer quite well and could be used to simulate management options.

The calibrated model was then used to simulate groundwater-management options in terms of different pumping rates, depths and locations. Five possible water boreholes were selected at distances of about one kilometre apart along the cross section. Results of the simulations showed that pumping one or two boreholes at a rate of 2.5 L s^{-1} and 2–4 m in depth would increase the salinity concentration significantly at the pumping sites (Fig. 24-18). Pumping at a rate of 1.25 L s^{-1} would have less effect on groundwater salinity.

One of the simulated options indicated that simultaneous pumping in all five boreholes would lead to the reciprocal effects of intersecting drawdown cones. These effects would appear after 3.5 years of continuous pumping at a rate of 2.5 L s^{-1} per borehole and would increase the salinity above the level computed for the operation of individual boreholes. Figure 24-19 shows the predicted increase in salinity with time at two outer boreholes, 1 and 5, and two central boreholes, 2 and 4, which would occur as a result of pumping all five boreholes simultaneously.

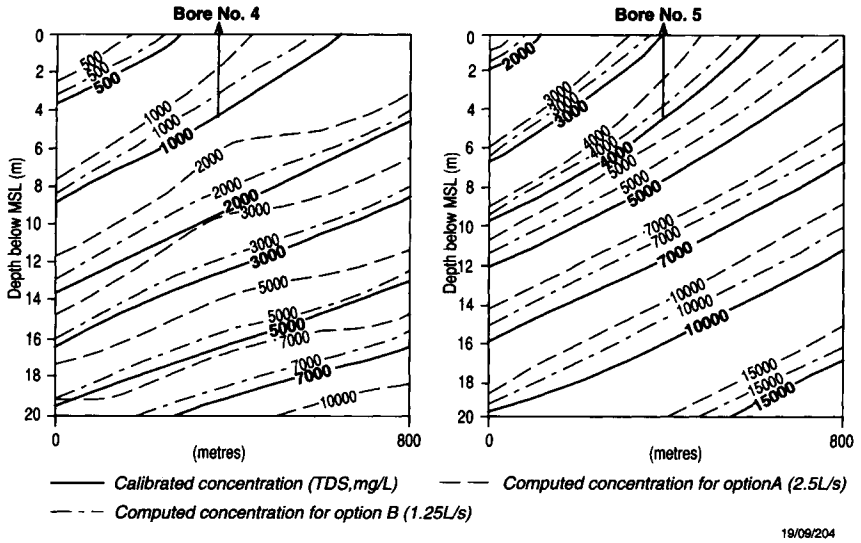


Fig. 24-18. Calibrated and computed salinity (TDS in mg L^{-1}) at two simulated bores (wells) numbered 4 and 5, on Nauru, derived from the SUTRA model. Bore 4 is about 2 km inland and bore 5 is 1 km inland. Pumping option A represents pumping of a single bore at a depth of 2–4 m and a rate of 2.5 L s^{-1}. Pumping option B represents pumping of a single bore at a depth of 2 m and a rate of 1.25 L s^{-1}. (Adapted from Ghassemi et al., 1990.)

Three-dimensional model

The limitations of using a 2-D model to simulate a 3-D problem include the inability to consider the real boundary conditions of the problem, and the difficulty that the influence of the pumping is partly outside the simulated slice of the aquifer.

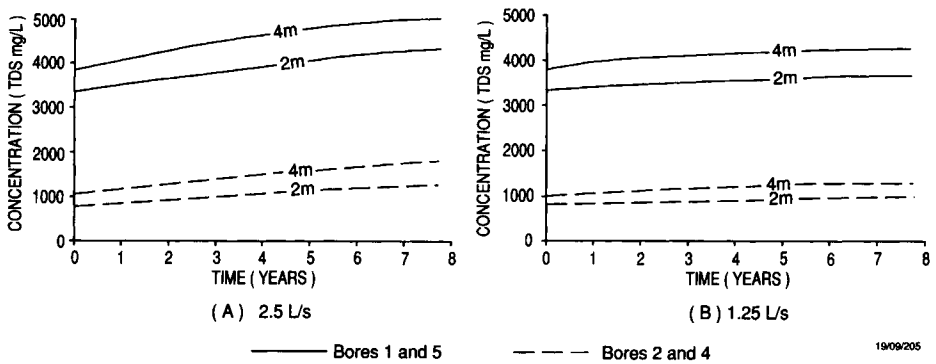


Fig. 24-19. SUTRA model simulation of the Nauru aquifer. The rise in groundwater salinity (TDS in mg L^{-1}) with time is due to simulated pumping of five wells simultaneously. Option A represents pumping of selected bores at a depth of 2–4 m and a rate of 2.5 L s^{-1}. Option B represents pumping of selected bores at a depth of 2–4 m and a rate of 1.25 L s^{-1}. (Adapted from Ghassemi et al., 1990.)

Simulation of the aquifer with the 3-D model HST3D was then undertaken (Ghassemi et al., 1993, 1996). This model has the advantage of enabling the specification of natural boundary conditions as well as the stresses on the aquifer, but the disadvantage that it requires access to supercomputer facilities. After testing the model in 2-D mode against the SUTRA discretisation, it was applied in 3-D mode to the Nauru Island aquifer using supercomputer facilities at the Australian National University. The aquifer was discretised with about 10,000 nodes, with a uniform grid of 200 m in the X-Y directions and a variable grid in the vertical direction, ranging from 2 m at the top of the aquifer to 9 m at a depth of 40 m.

The 3-D model was calibrated for steady-state conditions with a hydraulic conductivity of 700 m day^{-1}, a spatially variable recharge rate of 750–850 mm y^{-1}, and other parameters similar to those of the calibration for the SUTRA model. Computed salinities for observation wells from this calibration for steady-state did not match the values measured during drilling closely, probably because of the lack of data regarding the spatial distribution of the hydraulic conductivity and other parameters. The sensitivity of computed salinity profiles to major hydraulic parameters was analysed; it was found that the modelled aquifer is particularly sensitive to variations in hydraulic conductivity, recharge rate, and dispersivity.

The calibrated model was then used to simulate the effects of pumping at four boreholes in the interior plateau of Nauru. The simulated pumping was at a depth of 2 m with pumping rates of 1, 2 and 4 L s^{-1}. The simulation indicated progressive increases in salinity due to upconing of saltwater at the higher pumping rates (Fig. 24-20). However pumping at a rate of 1 L s^{-1} at these sites would have little effect on the salinity even after several years. It was concluded that, with certain safeguards, a borefield could be developed in the centre of the island to supply some of the water required for reforestation.

HYDROCHEMISTRY

Samples were obtained at specified depths during drilling, and several of the production wells on the island were also sampled. Typical chemical analyses of Nauru waters are shown in Table 24-4. Measurements for about 50 samples indicate that, with a high correlation, the TDS content of Nauru waters in mg L^{-1} is $0.69 \times$ EC where EC is the electrical conductivity in $\mu S\ cm^{-1}$.

Nauru rainwater contains about 10 mg L^{-1} TDS, and is slightly acid and bicarbonate-rich. Buada Lagoon was fresh when sampled in October 1987, with about 200 mg L^{-1} TDS; it is believed to become brackish with evaporation in long dry periods. The Anabar Lagoons (Fig. 24-17) are brackish with about 5,000 mg L^{-1} TDS. Accessible cave waters at Ijuh and Anatan are potable and used for small-scale water supplies. The largest cave supply, at Maqua Cave, is brackish, containing about 1,750 mg L^{-1} TDS when sampled in October 1967.

Samples from the freshwater layer taken during drilling (e.g., W1, Table 24-4) are in the range 85–295 mg L^{-1} TDS. The freshwater is bicarbonate-rich and is moderately hard (55–108 mg L^{-1}). The pH is 6.90–7.80, and the temperature is 25–26°C.

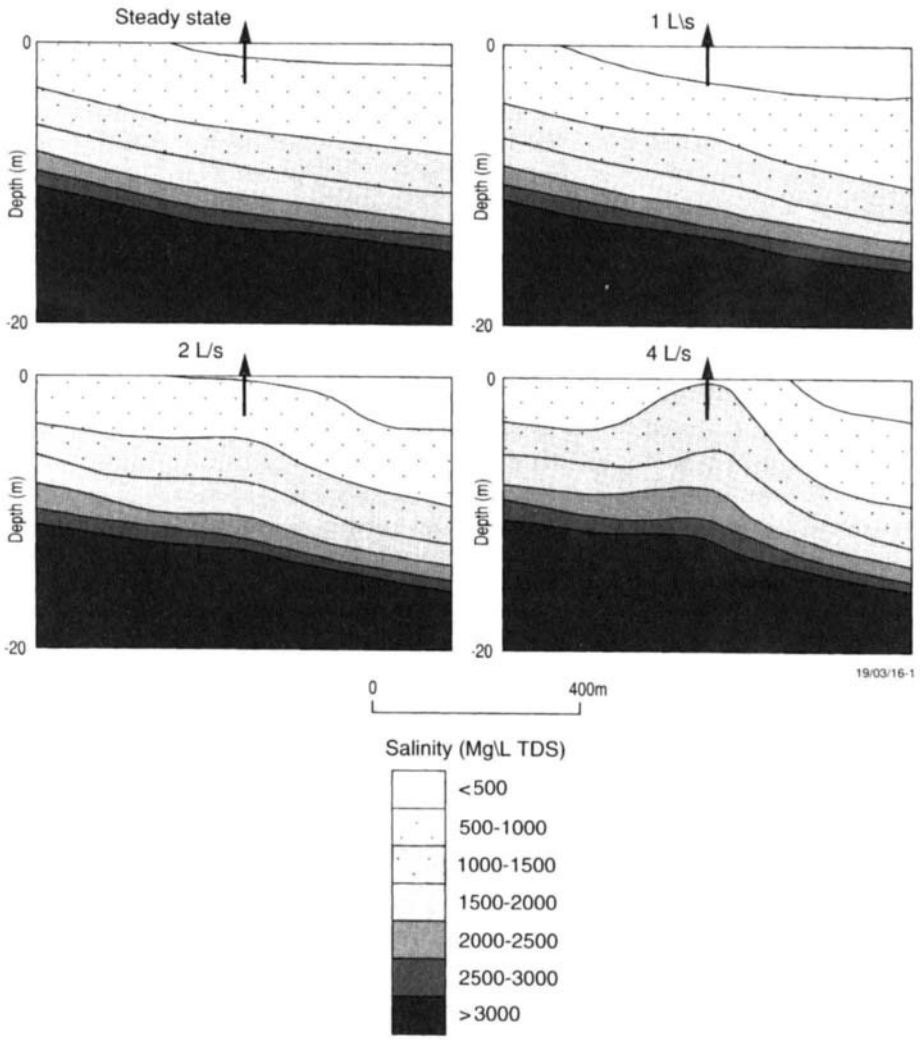


Fig. 24-20. HST3D model simulation: Computed steady-state distribution of groundwater salinity at a well in central Nauru and the simulated effects of pumping at three different rates. (Ghassemi et al., 1996.)

Concentrations of nitrate, fluoride and iron are all below the standard limits for drinking water.

Samples from the brackish-water zone (e.g., borehole P4, Table 24-4) are increasingly saline with depth, and the water is very hard with more than 400 mg L^{-1} total hardness. These waters are alkaline with pH of 7.4–8.9. With increasing salinity, the groundwater approaches seawater composition and becomes a chloride water, with sodium the dominant cation. The nitrate content of brackish-water zone

Table 24-4

Selected chemical analyses of Nauru groundwaters

	Site and depth (m)			
	P6	W1	Ijuh	P4
	25.5	25.5	cave	39.5
Ca	14	22	32	40
Mg	5	13	37	84
Na	16	36	182	555
K	0.5	0.5	5	20
HCO_3	71	121	211	168
SO_4	5	10	66	114
Cl	23	55	272	1018
NO_3	0.1	—	13	0.2
pH	7.9	7.8	7.6	8.3
E.C.	200	380	1370	3600
TDS	85	295	730	2000

Elemental analyses in mg L^{-1}.
Electrical conductivity (E.C.) in μS cm^{-1}.
Locations on Figure 24-8.

samples is generally low, less than 13 mg L^{-1} NO_3, with the exception of samples from borehole H10, in the centre of the island, where concentrations of 150 mg L^{-1} NO_3 suggest pollution from septic tanks.

Chemical analyses of 22 shallow dug wells sampled in the coastal terrace are 290–3,245 mg L^{-1} TDS. Of these wells, 17 are within the limit for drinking water of 1,500 mg L^{-1} TDS, and five contain more-saline water. The variation in salinity is due to factors such as the depth of the well and its pumping rate; it is likely that nearly everywhere in the coastal terrace a thin layer of freshwater overlies a mixing zone of brackish water. Composition ranges from bicarbonate-dominant in the fresher waters to chloride-dominant in the saltier waters. Nearly all the coastal-terrace groundwaters are hard or very hard, with total hardness of 172–776 mg L^{-1}. Most of these waters are slightly acid or neutral (pH, 6.70–7.16). The temperature of the coastal-terrace groundwater is constant at 28°C. Nitrate concentrations are generally low, up to 35 mg L^{-1}, and fluoride and iron concentrations are also below recommended limits for drinking water.

The chemical evolution of groundwaters in the brackish-water zone has been studied by Jankowski and Jacobson (1991). The fresh HCO_3-Ca-Mg groundwaters evolve to seawater by a combination of mixing, dissolution and precipitation reactions, and the ingassing or outgassing of CO_2. As the groundwater salinity increases with depth in the mixing zone, the saturation indices for particular carbonate minerals also increase. Supersaturation is achieved with respect to dolomite at 300 mg L^{-1} TDS; with respect to calcite at 5,000 mg L^{-1} TDS; and with respect to aragonite at 6,000 mg L^{-1} TDS. As the groundwaters throughout the mixing zone are saturated with respect to dolomite, there is potential for dolomitisation to occur.

Hydrochemical processes in the mixing zone follow either an open- or a closed-system trend, depending on the P_{CO_2}. The open system, with lower P_{CO_2}, includes the vadose-zone waters and cave waters, which are in contact with the atmosphere. It also includes the more-saline, mixing-zone waters in which chemical evolution is controlled mainly by mixing with seawater. The closed system comprises the freshwater and part of the brackish-water layer, and its chemistry is controlled by ingassing of CO_2, and by dissolution and precipitation reactions. Thus the dominant chemical processes change with the degree of mixing with seawater.

WATER SUPPLY OPTIONS

Nauru's present freshwater consumption is estimated at about 1,300 m^3 day^{-1}. There is a reticulated water supply to the Nauru Phosphate Corporation facilities on the west coast (Fig. 24-21), and this area also has a saltwater sewerage system. Elsewhere on the island, individual buildings have their own water supply, generally rainwater tanks supplemented by dug wells and tankered desalinated water. Most individual houses have cesspits. There is presently a shortfall in water supply in dry periods, and it is likely that population growth, the aspirations of the people, and reforestation will lead to increased demand for water. Additional sources of freshwater will be needed shortly.

Rainwater

Rainwater is particularly important in the island context as it is the best-quality water available for domestic use and some industrial purposes. A tank sample taken July 1994 had 52 mg L^{-1} TDS concentration. Rainwater supply systems are likely to fail in severe droughts, and further study is needed on Nauru to assess total catchment area and storage capacity installation in relation to water demand and probability of failure. Rainwater catchments could be extended by construction of special purpose catchments and storage tanks in the interior of the island for reticulation to the coastal terrace.

Groundwater of the coastal terrace

The coastal-terrace groundwater is presently abstracted from several hundred shallow dug wells; it is regarded as a second-class water source, being used for sewage and other secondary domestic purposes and as a backup domestic supply in drought years. Improvement to the present extraction of coastal-terrace groundwater could be made by the introduction of skimming well/infiltration gallery technology. However, treatment would be necessary for the coastal-terrace groundwater to be widely used for drinking water, owing to the variations in salinity and the incidence of bacteriological pollution. The coastal-terrace groundwater would be suitable as brackish-water feedstock for desalination.

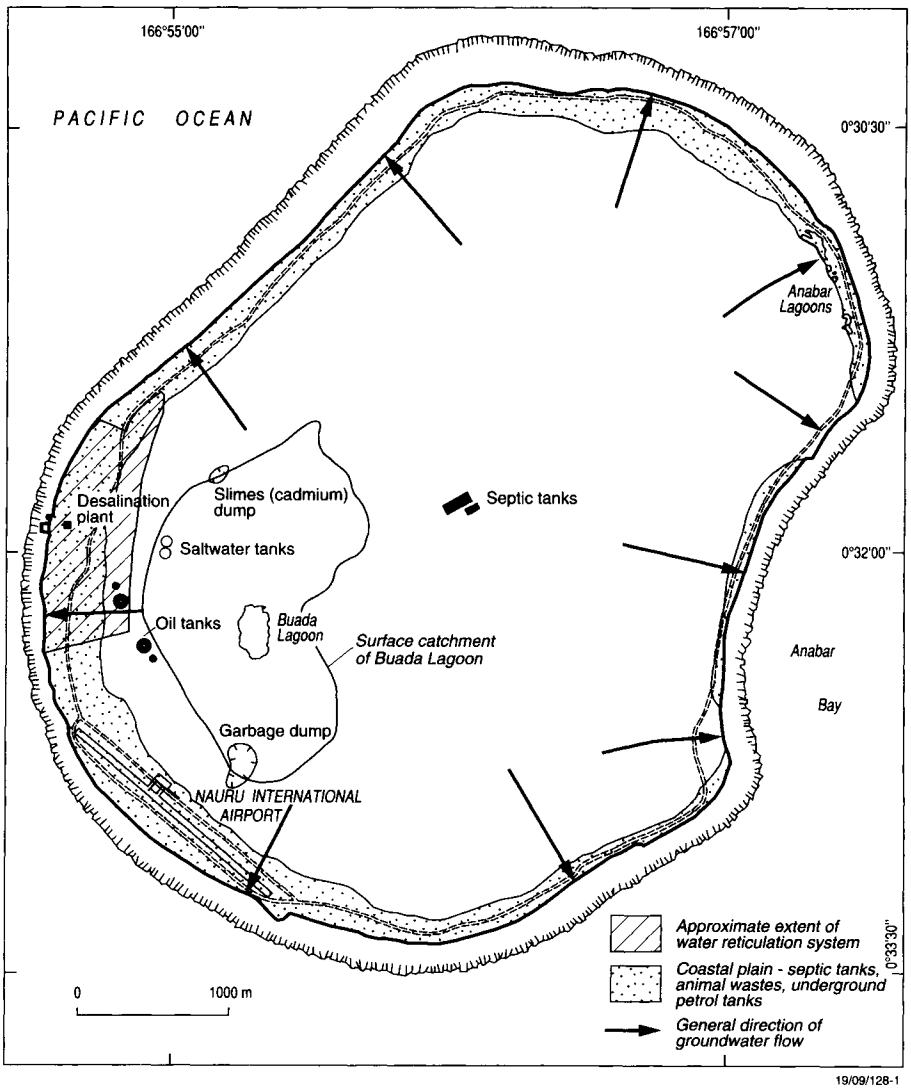


Fig. 24-21. Approximate extent of the water reticulation system and potential sources of groundwater pollution.

Groundwater of the inland plateau

A large amount of groundwater is available beneath the inland plateau of Nauru. The vulnerability of the freshwater layer, which is only a few metres thick, precludes the pumping of deep boreholes because of the likelihood of upconing saltwater. However, modelling studies indicate that eight low-yielding (1 L s^{-1}) water boreholes

spaced at about one kilometre apart, and drawing from the top 2 m of the freshwater layer could pump about 400 m^3 day^{-1} of water for irrigation. It may also be possible to use shafts and infiltration galleries or tunnels to skim the freshwater layer. This technology is used in some islands to abstract water beneath thick limestone cover and has previously been proposed for Nauru (R. Gormley, Nauru Phosphate Corporation, unpublished memo, 1987).

Desalination

Desalination of seawater is presently undertaken using an evaporation technique that uses excess heat from the power station as an energy source. The capacity of the desalination plant is 1,200 m^3 day^{-1} and about 700 m^3 day^{-1} of freshwater is presently produced. To fully develop the capacity of the plant, some additional storage tanks need to be constructed. A sample of desalinated water taken in July 1994 had a concentration of 34 mg L^{-1} TDS.

WATER QUALITY CONSIDERATIONS

Future groundwater development on Nauru requires consideration of the possibility of saltwater intrusion, and of pollution from sewage and other wastes and natural radioactive elements. The main threat to future groundwater development would be saltwater intrusion through overpumping, and for this reason careful management of groundwater extraction will be necessary. At the present time, some saltwater intrusion is evident in the deeper and more heavily pumped coastal wells. There is also some possible contamination from overflowing saltwater storage tanks.

In order to assess the effects of pollution from sewage and animal wastes, 23 wells and three cave-water supplies on the coastal terrace were sampled. The wells were selected at 1-km intervals around the island. Of the 26 groundwater sources sampled, 12 had bacterial counts below the MPN index (Most Probable Number of *E. coli*) of 23, indicating the suitability of the water for human consumption, untreated. The 14 samples with bacterial counts greater than the MPN index of 23 indicated that these water supplies would require chlorination. One of these samples had a count of 1,100. The wells with high bacterial counts are located at intervals around the coastal plain and the contamination is probably of local origin, i.e., sewage and animal wastes. Approximately half the wells in the coastal-plain aquifer, therefore, are bacteriologically polluted by sewage and animal wastes. Nitrate levels in the fresh groundwater remain generally low at the present time.

Natural soils on Nauru contain 6–173 ppm of cadmium with a mean content of 70 ppm at 16 sampling points. Formerly, a calcination process was undertaken, and raw phosphate was roasted at 1050° to remove cadmium and organic carbon. Sludge from the calcination plant contained about 200 ppm cadmium and about 2,000 ppm zinc. For many years, the sludge was dumped in mined-out areas where leaching to the water table could occur (Fig. 24-21). Municipal garbage is also dumped in mined-out areas (Fig. 24-21).

Groundwater samples collected in 1987 showed low concentrations of zinc and less than 0.01 mg L^{-1} cadmium. The upper limits in drinking water are generally taken as 5 mg L^{-1} zinc and 0.01 mg L^{-1} cadmium; the upper limit for cadmium in irrigation water is also 0.01 mg L^{-1} (Hem, 1985). Although groundwater is not polluted from this source at present, the freshwater layer is vulnerable. Waste disposal policy must be considered in conjunction with proposals for future water supply development.

Some phosphatic soils are known to contain radioactive elements deleterious to health. For this reason we carried out a gamma-ray spectrometer survey of Nauru soils and mapped the distribution of radiometric properties. The total-count contours (Jacobson and Hill, 1988) showed a very low level of radioactivity along the coastal strip, increasing greatly across the coastal escarpment and forming a broad high over the island's interior. The area of highest radioactivity was located to the northeast of Buada Lagoon (920 counts s^{-1}), and a subsidiary high occurred in the north-central part of the island (720 counts s^{-1}). The patterns for K, U and Th concentrations differ in detail, but show similar distribution. Maximum recorded concentrations are: K, 4.8%; U, 84 ppm; and Th, 67 ppm. As a comparison, the average abundances of these elements in the earth's crust are: K, 2.1%; U, 2.7 ppm; and Th 9.6 ppm.

The uranium concentration in the soil is relatively high, about 31 times the average in the earth's crust. However, uranium is likely to be fixed in the soil profile by the absorbing action of the phosphate and organic carbon, and it is unlikely that sufficient uranium leaches down to the aquifer to cause a groundwater pollution problem.

In July 1994, samples were taken from two dug wells in the coastal plain, and from Buada Lagoon and Maqua Cave in order to assess the leaching of radioactive elements to the groundwater system. Analytical results are shown in Table 24-5. Considering the alpha radiation emitters, ^{238}U, ^{234}U, ^{232}Th, ^{230}Th, ^{226}Ra and ^{210}Po, it is evident that the total alpha activity exceeds 100 mBq L^{-1}in the Buada Lagoon

Table 24-5

Radioactive constituents in Nauru groundwaters, July 1994*

	Daniel's Well	Heine's Well	Buada Lagoon	Maqua Cave
U-238	12.30	5.0	31.6	5.0
U-234	11.4	7.2	32.9	5.4
Th-232	0.3	0.2	0.0	0.0
Th-230	0.1	0.4	2.0	0.3
Ra-226	19.4	3.1	46.2	9.3
Ra-228	0	0	0	0.5
Po-210	3.8	0.9	6.5	1.2
Pb-210	4.1	0.9	6.2	1.8
TDS (mg L^{-1})	334	1130	284	2640

* Concentrations in mBq L^{-1}.

water. This is the international standard for drinking water (WHO, 1984) based on consumption of 2 L day^{-1}. Total alpha activity in the other three samples is within recommended limits. Beta radiation appears to be much less than the international standard of 1 Bq L^{-1}. These results indicate a need for careful monitoring should the lagoon water be considered as a source of drinking water. It also has implications for the assessment of water quality on other phosphatic islands.

CONCLUSIONS

(1) Drilling and geophysical investigations have shown that the Nauru seamount is capped by at least 100 m of late Miocene to Quaternary limestone, and that the total thickness of the limestone capping is about 500 m. The limestone is karstified to at least 55 m below sea level.

(2) Gravity and magnetic properties of the island's volcanic core indicate that it is composed of basaltic lavas and is of mid-Eocene to Oligocene age.

(3) The island's formerly valuable phosphate deposits are late Quaternary in age and formed from avian guano.

(4) The combined use of reverse-circulation drilling, groundwater sampling and geophysical techniques has enabled the first estimate of Nauru's groundwater resources to be made. Drilling and geoelectrical soundings indicate that the freshwater layer on Nauru is discontinuous and averages 4–5 m in thickness with a maximum of 7 m. The brackish-water zone beneath the freshwater layer is about 60 m thick, and salinity increases progressively downwards in the brackish-water zone. The thickness of the mixing zone is due to the intrusion of seawater through major fractures in the limestone.

(5) Simulation of Nauru's groundwater system with the SUTRA and HST3D numerical models has led to the evaluation of pumping options, and to an appreciation of the likelihood of upconing of saltwater if the aquifer is pumped beyond the rate of recharge.

(6) The conjunctive use of desalination, rainwater catchments and dug wells in the coastal terrace will form the basis of Nauru's water supply for the foreseeable future, and some improvements to these systems are desirable.

(7) Additional groundwater development is desirable to make up the shortfall in water supply for reforestation of the inland plateau. Skimming from shafts and infiltration galleries may be possible.

(8) The coastal-terrace aquifer is polluted in part from sewage and animal wastes, as evidenced by bacterial counts in a number of wells. Waste disposal in mined-out areas is a potential hazard, and a waste disposal policy is needed to protect future groundwater resources from pollution.

(9) Significant concentrations of radioactive elements are present in the Buada Lagoon water, and this is a health concern for future water supply development.

ACKNOWLEDGMENTS

The investigation was originally undertaken on behalf of a Nauru government agency, the Commission of Inquiry into Rehabilitation of the Worked-out Phosphate Lands in Nauru. Field work in 1987 was facilitated by the Nauru Phosphate Corporation. We thank John Barrie (consulting geologist) and Peter J. Barrett (consulting geologist) for facilitating the field investigation; Prof. K. Wyrtki (University of Hawaii) for tidal data; and George Chaproniere (Australian Geological Survey Organisation) for palaeontological determinations. Radioactive elements in Nauru waters were determined by Gary Hancock of CSIRO Water Resources, Canberra. The chapter was reviewed by Tony Falkland, June Ann Oberdorfer, John E. Mylroie, Christopher Wheeler, and Ivan Gill, and we thank them for their perceptive and helpful comments. The chapter is published by permission of the Executive Director of the Australian Geological Survey Organisation.

REFERENCES

Aharon, P. and Veeh, H.H., 1984. Isotope studies of insular phosphates explain atoll phosphatization. Nature, 309: 614–616.

Andrews, J.E., Packham, G., et al., 1975. Initial Reports of the Deep Sea Drilling Project, 30. U.S. Gov. Printing Office, Washington D.C., 753 pp.

Barrett, P.J., 1988. Report on phosphate, other minerals and groundwater resources, and on aspects of rehabilitation planning and methodology, Nauru, Pacific Ocean. Report. Commission of Inquiry into the Rehabilitation of the Worked-out Phosphate Lands of Nauru, 9: D946–D999.

Cande, S.C., Larson, R.L. and LaBrecque, J.L., 1978. Magnetic lineations in the Pacific Jurassic quiet zone. Earth Planet. Sci. Lett., 41: 434–440.

Chen, Y., Brumby, S., Jacobson, G., Beckwith, A.L J. and Polach, H.A., 1991. A novel application of the ESR method: dating of insular phosphorites and reef limestone. Quat. Sci. Rev., 11: 209–217.

Dalrymple, G.B., Lanpher, M.A. and Clague, D.A., 1980. Conventional and ^{40}Ar-^{39}Ar and K-Ar ages of volcanic rocks from Ojin (site 430), Nintoku (site 432), and Suiko (site 433) seamounts and the chronology of volcanic propagation along the Hawaiian-Emporer chain. In: E.D. Jackson, I.Koisumi, et al., Initial Reports of the Deep Sea Drilling Project, 55. U.S. Gov. Printing Office, Washington D.C., pp. 659–676.

Duncan, R.A. and Clague, D.A., 1985. Pacific plate motion recorded by linear volcanic chains. In: A.E.M. Nairn, F.G. Stehli and S. Uyeda (Editors), The Ocean Basins and Margins, Vol. 7A, The Pacific Ocean. Plenum, New York, pp. 89–121.

Falkland, A.C., 1984. Assessment of groundwater resources on coral atolls: case studies of Tarawa and Christmas Island, Republic of Kiribati. Proc. Regional Workshop Water Resour. Small Islands (Suva). Commonw. Sci. Counc. Tech. Publ. Ser. 154(2): 261–276.

Fleming, P.M., 1987. The role of radiation estimation in the areal water balance in tropical regions: a review. Arch. Hydrobiol. Beih., 28: 19–27.

Ghassemi, F., Jakeman, A.J. and Jacobson, G., 1990. Mathematical modelling of sea water intrusion, Nauru Island. Hydrol. Processes, 4: 269–281.

Ghassemi, F., Chen, T.H., Jakeman, A.J. and Jacobson, G., 1993. Two and three-dimensional simulation of seawater intrusion: performances of the "SUTRA" and "HST3D" models. AGSO J. Aust. Geol. Geophys., 14: 219–226.

Ghassemi, F., Jakeman, A.J., Jacobson, G. and Howard, K.W.F., 1996. Simulation of seawater intrusion with 2D and 3D models: Nauru Island case study. Hydrogeol. J., 4(3): 4–22.

Goodrich, J.A. and Mink, J.F., 1983. Groundwater management in the Guam Island aquifer system. Papers, Int. Conf. Groundwater and Man. Aust. Water Resour. Counc., Conf. Ser. 8, 3, pp. 73–82.

Goodwin, R.S., 1980. Water assessment and development in Barbados. Proc. Sem. Small Island Water Problems, Barbados. U.N. and Commonw. Sci. Counc., SOWRADAM Rep., pp. 145–163.

Gordon, R.G. and Jurdy, D.M., 1986. Cenozoic global plate motions. J. Geophys. Res., 91: 12389–12406.

Hem, J.D., 1985. Study and interpretation of the chemical characteristics of natural water. U.S. Geol. Surv. Water-Supply Pap. 2254, 263 pp.

Hill, P.J. and Jacobson, G., 1989. Structure and evolution of Nauru Island, central Pacific Ocean. Aust. J. Earth Sci., 36: 365–381.

Houtz, R.E. and Ludwig, W.J., 1979. Distribution of reverberant sub-bottom layers in the southwest Pacific basin. J. Geophys. Res., 84: 3497–3504.

Hunt, B., 1979. An analysis of the groundwater resources of Tongatapu Island, Kingdom of Tonga. J. Hydrol., 40: 185–196.

Hutchinson, G.E., 1950. Survey of contemporary knowledge of biogeochemistry. 3. The biogeochemistry of vertebrate excretion. Am. Mus. Nat. History Bull. 96, 554 pp.

Jacobson, G. and Hill, P.J., 1988. Hydrogeology and groundwater resources of Nauru Island, central Pacific Ocean. Bur. Miner. Resour. (Aust.), Geol & Geophys., Record 1988/12, 85 pp.

Jacobson, G. and Hill, P.J., 1993. Groundwater and the rehabilitation of Nauru. In: G. McNally, M.J. Knight and R. Smith (Editors), Collected Case Studies in Engineering geology, Hydrogeology & Environmental geology. Geol. Soc. Aust. Butterfly Books, Sydney, pp. 103–119.

Jankowski, J. and Jacobson, G., 1991. Hydrochemistry of a groundwater-seawater mixing zone, Nauru Island, central Pacific Ocean. BMR J. Aust. Geol. Geophys., 12: 51–64.

Kipp, K.L., 1987. HST3D: a computer code for simulation of heat and solute transport in three-dimensional ground-water flow systems. U.S. Geol. Surv. Water-Resour. Invest. Rep., 86–4095: 517 pp.

Larson, R.L., 1976. Late Jurassic and Early Cretaceous evolution of the western central Pacific Ocean. J. Geomagn. Geoelec., 28: 219–236.

Larson, R.L. and Schlanger, S.O., 1981. Geological evolution of the Nauru Basin, and regional implications. In: R.L. Larson, S.O. Schlanger, et al., Initial Reports of the Deep Sea Drilling Project, 61. U.S. Gov. Printing Office, Washington D.C., pp. 841–862.

Ludbrook, N.H., 1964. Fossiliferous limestone of Quaternary age from Nauru. Appendix 1. In: W.C. White and O.N. Warin, A Survey of Phosphate Deposits in the Southwest Pacific and Australian Waters. Bur. Miner. Resour. (Aust.), Bull. 69: 171–173.

Minster, J.B. and Jordan, T.H., 1978. Present-day plate motions. J. Geophys. Res., 83: 5331–5354.

O'Neill, D.J, 1975. Improved linear filter coefficients for application in apparent resistivity computations. Bull. Aust. Soc. Explor. Geophys., 6: 104–109.

Philander, S.G.H., 1983. El Nino Southern Oscillation phenomena. Nature, 302: 295–301.

Piper, D.Z., Loebner, B. and Aharon, P., 1990. Physical and chemical properties of the phosphate deposit on Nauru, western equatorial Pacific Ocean. In: W.C. Burnett and S.R. Riggs (Editors), Phosphate Deposits of the World; Neogene to Modern Phosphorites. Cambridge Univ. Press, New York, pp. 176–194.

Power, D.F., 1910. Phosphate deposits of Ocean and Pleasant Islands. Aust. Inst. Min. Eng., Trans., 10: 213–232.

Roe, K.K. and Burnett, W.C., 1985. Uranium geochemistry and dating of Pacific island apatite. Geochim. Cosmochim. Acta, 49: 1581–1592.

Suarez, G. and Molnar, P., 1980. Paleomagnetic data and pelagic sediment facies and the motion of the Pacific plate relative to the spin axis since the late Cretaceous. J. Geophys. Res., 85: 5257–5280.

Voss, C.I., 1984. SUTRA, Saturated-Unsaturated Transport: a finite-element simulation model for saturated-unsaturated fluid-density-dependent groundwater flow with energy transport or chemically reactive single-species solute transport. U.S. Geol. Surv. Water-Resour. Invest. Rep., 84–4369: 409 pp.

WHO (World Health Organization), 1984. Guidelines for drinking water quality. WHO (U.N.), Geneva.

Geology and Hydrogeology of Carbonate Islands. Developments in Sedimentology 54
edited by H.L. Vacher and T. Quinn
© 1997 Elsevier Science B.V. All rights reserved.

Chapter 25

HYDROGEOLOGY OF NORTHERN GUAM

JOHN F. MINK and H.L. VACHER

INTRODUCTION

The Mariana Islands (Fig. 25-1) overlie the westward-dipping subduction zone that includes the deep Mariana Trench and bounds the Pacific and Philippine Plates. Guam (13°28′N, 144°45′E) is the southernmost, the largest, and most populated of the Mariana Islands. It lies about 1,200 nautical miles (2,200 km) east of the Philippine Islands and approximately halfway between Japan and New Guinea.

The first truly informative hydrogeological study of Guam was made in 1937 by Harold T. Stearns at the request of the U.S. Navy. Stearns identified the fundamental elements of the island geology and recommended means of groundwater development. His report did not enter the open literature until after World War II because it was "classified."

The site of major battles during World War II, Guam was the subject of intensive geologic mapping in a post-War program by the U.S. Army Corps of Engineers and the U.S. Geological Survey. One of the outcomes of that effort was a monumental report on the geology of Guam by Tracey et al. (1964). Similar reports are available for Saipan (Cloud et al., 1956) and Tinian (Doan et al., 1960), other largely limestone islands in the Mariana arc.

Guam, which is 212 mi^2 (550 km^2) in area, is 30 mi (48 km) long and 4–11.5 mi (6–19 km) wide. The smallest width forms a narrow waist that divides the island into two nearly equal physiographic provinces (Fig. 25-2). Southern Guam is composed predominantly of a dissected volcanic upland. Northern Guam is mostly a limestone plateau. In terms of geology and hydrogeology, the two parts of Guam are like two separate islands.

Before western Europeans arrived in Guam, the native Chamorro society lived in equilibrium with its environment in an early stage of material development. The people lived in huts resting on pillars of stone called "latte" in hamlets now called "latte sites" by archeologists. Subsistence was by wetland farming of taro, gathering of wild plants, and fishing. No common meat animals are native to the island.

Magellan made landfall in the Marianas in 1521, and, about 150 years later, the arc was named after Queen Maria Ana of Spain. Spain maintained sovereignty for more than three centuries. The Chamorro were nearly exterminated by disease and famine, by punitive expeditions, and by forced migrations from one island to another. The United States seized the island in 1898 in a far-flung extension of the Spanish-American War and purchased it in 1898. Japan captured the island on Dec. 9, 1941, and the United States recaptured it in July, 1944. In 1951, the U.S. Congress voted Guam an unincorporated territory of the United States. The Guamanians

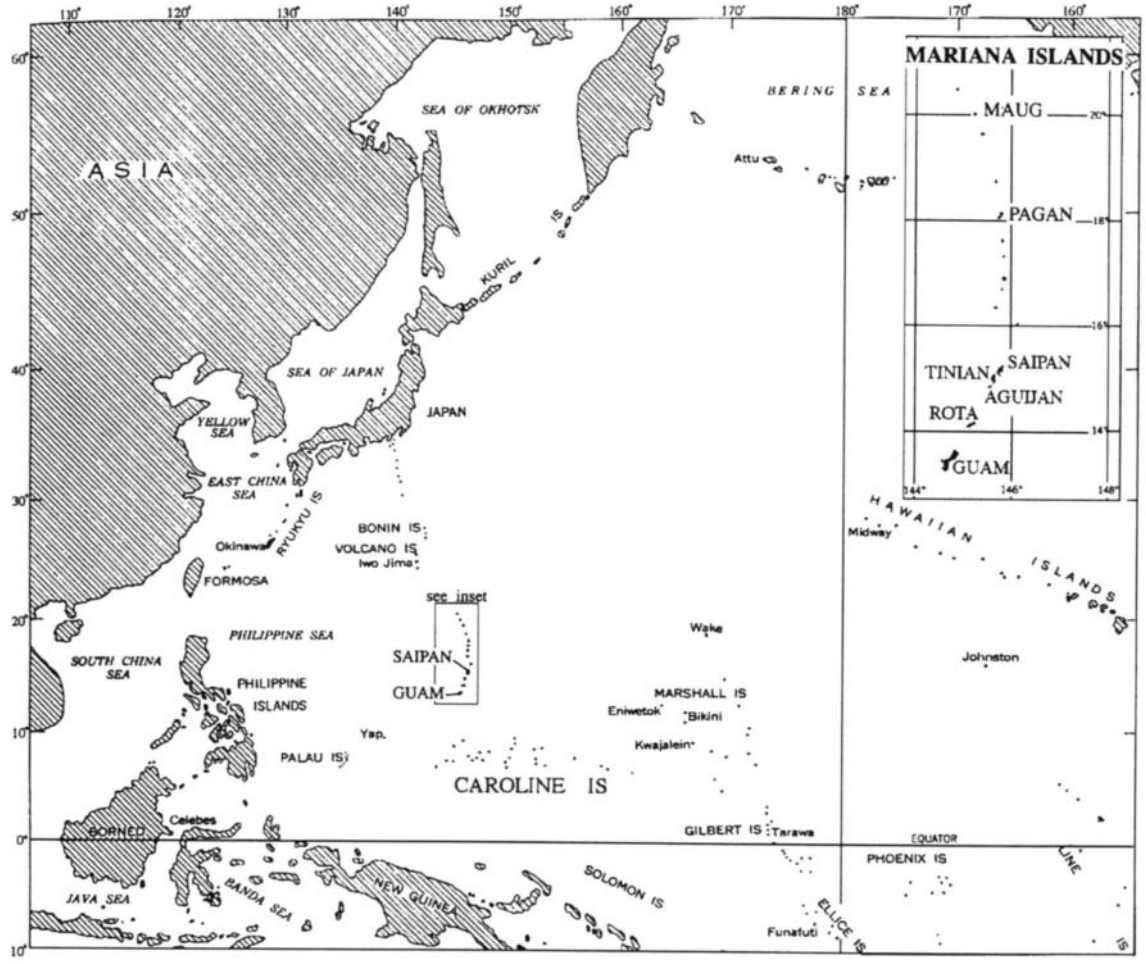


Fig. 25-1. Map showing location of the Mariana Islands in the western Pacific, and the location of Guam in the Marianas. (Adapted from Tracey et

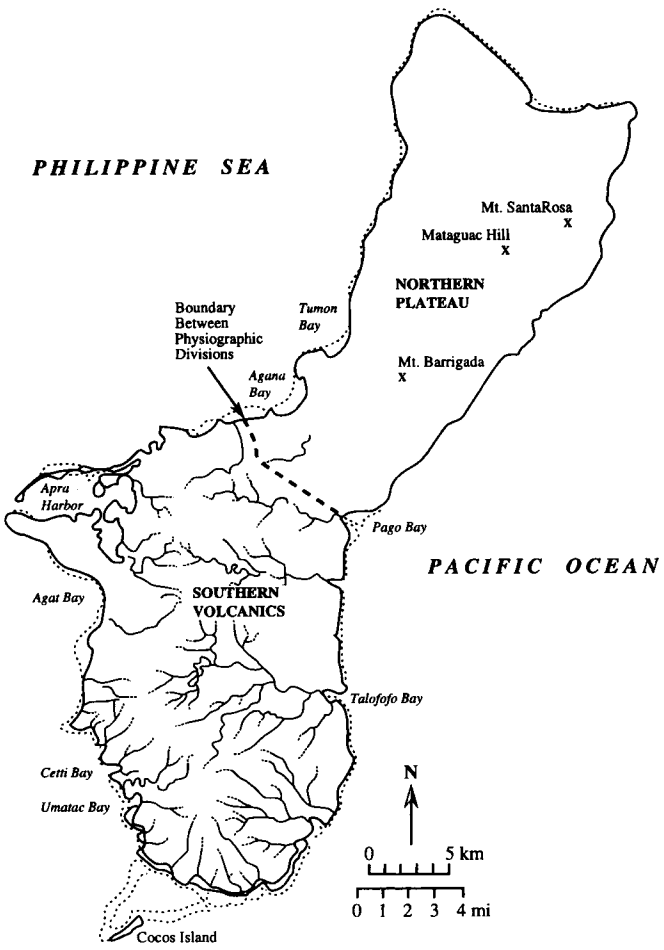


Fig. 25-2. Map showing the two physiographic regions of Guam and localities mentioned in text. (Simplified from CDM, 1982.)

have U.S. citizenship; they are governed by an elected governor and legislature, and they have a Delegate in the U.S. House of Representatives.

The population of Guam in the 1990 census was 133,150, and the estimated population in 1994 is 146,700. The average growth rate is high at 2.3%, but it was even higher before 1990. The civilian population water demand is about 25 Mgpd (25×10^6 U.S. gal day^{-1}; 1,100 L s^{-1}), virtually all of which is supplied with groundwater extracted from the limestone aquifers of northern Guam. The military demand is about 10 Mgpd (440 L s^{-1}), a large fraction of which is derived from groundwater issuing from limestone springs before becoming surface water.

CLIMATE

Although Guam is warm and humid throughout the year, there are two distinct seasons, one wet and the other dry. The mean annual temperature is 81°F (27°C), about which daily maximums and minimums vary no more than 10°F (6°C). The relative humidity typically ranges from values of 65–80% during the day to 85–100% at night.

A subtropical high-pressure area lying north of the island throughout much of the year results in a dominant air-flow pattern characterized by trade winds. Frequent storms in the summer and fall disrupt this pattern. These storms sometimes intensify to typhoons which cause serious damage to the island.

From January through May the constant trade winds result in a well-defined dry season broken only by occasional showers. July through November is the wet season, when the trades are frequently interrupted by tropical storms with heavy rainfall. The months of June and December are transitional. About two-thirds of the annual precipitation falls in the 5-month wet season.

The mean annual rainfall in the northern limestone plateau is 85–100 in. (2,200–2,500 mm). Although severe droughts in the dry season are common, the wet season is highly reliable. The wet-season average is 63 in. (1,600 mm); the lowest on record (1973) is 45 in. (1,140 mm).

Although the southern, volcanic terrain has many streams, the limestone plateau of the north has none. A large depression in the limestone near Agana receives a minor quantity of surface runoff, but the marsh in the depression is sustained by groundwater.

GENERAL GEOLOGY

Geological studies of Guam first concerned the reefs (Agassiz, 1903). Stearns conducted islandwide reconnaissance mapping for the U.S. Navy before the War (Stearns, 1937, 1940) and called attention to Guam's striking erosional notches in important papers giving a Pacific Ocean perspective on Quaternary eustasy (Stearns, 1937, 1941). The post-War report by Tracey et al. (1964) is still the premier reference. The limestones have been described in a companion report by Schlanger (1964) and most recently by Siegrist and Randall (1992), who include a field trip itinerary.

As shown in Fig. 25-2, the first-order geological feature in Guam is its division into a southern half throughout which volcanic and volcaniclastic rocks are exposed and a northern half consisting of a limestone plateau. The contact is a normal fault having a displacement of about 400 ft (120 m) (Tracey et al., 1964).

The northern plateau slopes along the long axis of the island from a maximum elevation of about 600 ft (180 m) in the north to 100 ft (30 m) near the southern boundary. Along much of the northern coastline, the plateau ends in abrupt, nearly vertical cliffs. The uniformity of the plateau is broken by several small protuberances of volcanic rocks at Mt. Santa Rosa and Mataguac Hill (Fig. 25-2). Volcanic rocks also form the basement on which the thick succession of limestone was deposited. In

general, the volcanic surface was shaped by submarine processes before the major epochs of limestone deposition occurred, and a major unconformity separates the limestones from the volcanic rocks. The limestones, which include the entire spectrum of reef facies from argillaceous lagoonal sediments to massive and compact forereef assemblages, are so permeable that a normal stream drainage pattern has not been able to form. Instead, a gentle karst topography has evolved, and drainage takes place directly into the ground or through shallow sinkholes. Thick, nearly impenetrable shrubby growth covers uncleared portions of the plateau.

The extrusive and pyroclastic rocks of the southern, dissected uplands were deposited under submarine conditions. A narrow cap of limestone covers the highest mountain range, which lies several miles inland and parallel to the western coast of the island. The highest peak, which is also the highest point on the island, is 1,334 ft (407 m) above sea level. The coastline in many places is characterized by a narrow fringe of Holocene reef limestone. The alluviated stream valleys, coastal fringes and limestone caps carry a heavy foliage that contrasts with the coarse sword grass that characterizes the volcanic rocks. The contact between limestone and volcanics is commonly clearly marked by the vegetation change.

Geologic history

The Mariana arc has split longitudinally twice to form two remnant arcs (Palau-Kyushu Ridge and West Mariana Ridge) and two extensional basins (Parece Vela Rift and Mariana Trough; see Fig. 25-3) (Karig, 1971; Scott et al., 1980; Hussong and Uyeda, 1981). As summarized by Reagan and Meijer (1983), the tectonic history has the following highlights. The West Philippine Basin (Fig. 25-3) is the oldest back-arc basin of the Philippine Sea and represents either a back-arc basin from an early phase of Mariana subduction or a piece of trapped ocean floor. Due to a change in the motion of the Pacific Plate, subduction began parallel to the present Palau-Kyushu Ridge at about 43 Ma, and the ridge was built by arc volcanism between 43 Ma and 32 Ma. Beginning around 32 Ma, the ridge rifted apart to form the Parece Vela inter-arc basin; Guam was located at the southwestern end of the West Mariana Ridge, which was volcanically active from 32–20 Ma to 9–5 Ma. At the latter date, the West Mariana Ridge split again to form the Mariana Trough, where spreading continues, and the Mariana Ridge. Volcanism in the present Mariana Ridge began before 1.3 Ma. Guam is in the forearc region of this ridge.

The main volcanic basement of Guam was constructed during the 43–32 Ma interval, according to Reagan and Meijer (1984) who studied the igneous geology and geochemistry of southern Guam. There are two major units: the Facpi Formation (late middle Eocene), consisting of pillow lavas, pillow breccias, and dikes; and the Alutom Formation (late Eocene to early Oligocene), consisting of breccias, tuffaceous sandstones, flows and sills. In addition, there is an early Miocene unit, the Umatac Formation, that unconformably overlies the older volcanics and contains a limestone member (the Maemong Member). Reagan and Meijer (1984) found a succession of compositions: boninites in the Facpi; a mixture of boninites, arc tholeiites and low-K calcalkaline lavas in the Alutom; and high-K rocks in the Umatac.

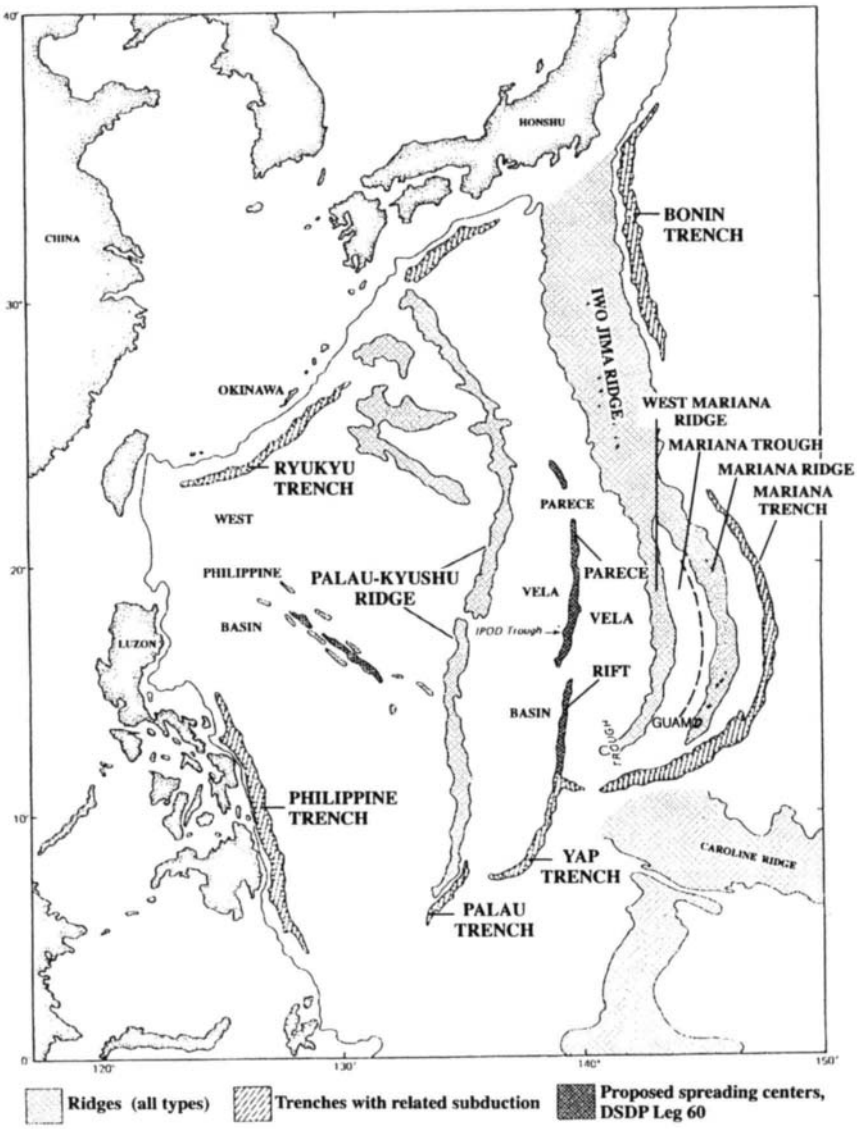


Fig. 25-3. Map showing tectonic features of the Mariana arc and related basins. (After Hussong and Uyeda, 1981.)

The volcanic stratigraphy of southern Guam records the shoaling of the volcanic edifice (Reagan and Meijer, 1984; Siegrist and Randall, 1992). Within the Facpi, which consists predominantly of pillow lavas, interpillow calcite is nearly absent low in the section and abundant high in the section, suggesting buildup to above the carbonate compensation depth (Reagan and Meijer, 1984). Early in the history of

the Alutom, the edifice was near sea level (Reagan and Meijer, 1984), as indicated by the occurrence of clasts of shallow-water limestones (Tracey et al, 1964; Schlanger, 1964; Garrison et al., 1975). Schlanger described silicified, coral-rich fossil debris from the Alutom Formation, and Siegrist and Randall (1992) have reported the occurrence in that formation of a large body of tightly packed silicified reef fossils that may be either an in situ bioherm or an allochthonous block.

Limestones formed around three main volcanic highs during the Miocene (Siegrist and Randall, 1992) (Fig. 25-4). There are a number of Miocene units mapped and described by Tracey et al. (1964), and their stratigraphy and facies relationships are currently being studied (Siegrist and Randall, 1992). Hydrogeologically, the most important of these limestones is the Barrigada Limestone. According to Cole (1963), the Barrigada is late Miocene in age and correlative with a major unit in the famous Bikini drill core; according to Siegrist and Randall (1992, p. 1199), it "may be termed more accurately MioPliocene". In outcrop, the limestone wraps around the Mt. Santa Rosa-Mataguac high. Siegrist and Randall (1992) believe that the Barrigada Limestone is the up-dip, shallow-water, time-equivalent facies of at least one of the other named formations.

Overall, the general pattern is a shallowing upward of the limestone succession in Guam. Siegrist and Randall (1992, p. 1199), referring to the Miocene (including their MioPliocene) limestones state, "None of the units contains reef-margin buildups, but all show unequivocal field evidence of reef coral growth nearby." The major reef-

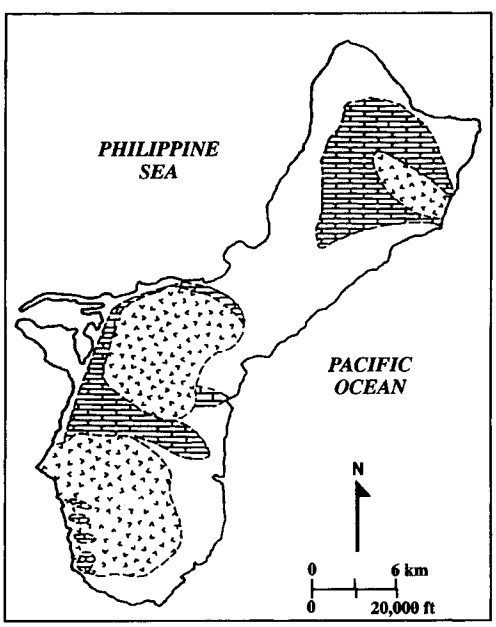


Fig. 25-4. Map showing early Miocene volcanic highs and present outcrop and subcrop pattern of Miocene limestones. (Simplified from Siegrist and Randall, 1992.)

forming interval in Guam was that of the Plio-Pleistocene Mariana Limestone, which was mapped and subdivided into facies on Guam by Tracey et al. (1964). The Mariana Limestone, which was named by Risaburo Tayama in 1936 from exposures in Tinian (Tracey et al., 1964), is the predominant carbonate unit throughout the forearc islands of Guam, Rota, Aguijan, Tinian, and Saipan. It may reach an aggregate thickness of 174 m on Guam (Siegrist and Randall, 1992).

The youngest limestone on Guam is an exquisite, beautifully exposed, mid-Holocene reef that occurs at many places along the shoreline (Tracey et al., 1964; Easton et al., 1978; Siegrist and Randall, 1992). This unit, the Merizo Limestone, usually extends up to an elevation of 1.5–2.0 m, and locally up to 4–5 m elevation (Easton et al., 1978; Siegrist and Randall, 1992). According to Siegrist and Randall (1992, p. 1206), the reef formation "accumulated at rates of 1 to 2 meters/thousand years reaching its apex of development somewhere between 5000 and 3000 years ago." Its emergence is attributed to tectonics by Siegrist and Randall (1992) because of the nonuniformity of its elevation. The petrography of the unit is described by H.G. Siegrist et al. (1984), and the paleoecology by A.W. Siegrist et al. (1984) and Randall et al. (1984).

In summary, the geologic history of Guam reflects the buildup, shoaling, and uplift on the arc side of the Mariana Trench. The limestone surface has risen to more than 600 ft (180 m) above present sea level in the far northern sector of the island and to 1,334 ft (407 m) on the highest mountains in the south.

HYDROGEOLOGY

Since 1964, the policy of the Government of Guam has been to rely on the water resources of northern Guam the Northern Guam Lens to fill long-term water-supply needs. The Northern Guam Lens occurs hundreds of feet below the surface of the limestone plateau. Additionally, fresh and/or brackish groundwater occurs in the limestone fringe which occurs along parts of the shoreline of southern Guam (Ward et al., 1965; Mink, 1976); perched on volcanic rocks and feeding springs at the base of limestone successions in northern and southern Guam (Ward et al., 1965; Mink, 1976); and in thin valley-fill aquifers close to the coast in southern Guam (Ayers and Clayshulte, 1983a).

The comprehensive reference concerning the hydrogeology of northern Guam is a series of reports resulting from the Northern Guam Lens Study (NGLS) initiated and administrated by the Guam Environmental Protection Agency and carried out by John Mink (project director); Camp, Dresser and McKee, Inc. (CDM); Barrett, Harris & Associates, Inc. (BHA); the Water and Energy Research Institute of the Western Pacific (WERI) at the University of Guam; and the U.S. Geological Survey (USGS). In 1991, ten years later, the NGLS investigation was revisited in a report for the Public Utility Agency of Guam by Mink (1991) in association with the Barrett Consulting Group.

Geologic framework

Because the position of the volcanic basement relative to the overlying limestone determines the mode of occurrence of groundwater in northern Guam (Mink, 1976), seismic refraction surveys have been used to locate the contact of the limestone with the basement (CDM, 1982). Velocities in the limestones are 3,000–7,000 ft s^{-1} (900–2,100 m s^{-1}), whereas that of the basement normally exceeds 9,000 ft s^{-1} (2,700 m s^{-1}). This sharp contrast is highly definitive and, with well control, enabled the underlying basement to be mapped across the plateau (Fig. 25-5). The partially buried volcanic rocks of Mt. Santa Rosa and Mataguac Hill extend as a completely buried ridge beneath Mt. Barrigada.

Both the Barrigada Limestone (Miocene) and the Mariana Limestone (Plio-Pleistocene) are important to the hydrogeology of northern Guam (Fig. 25-6). According to Tracey et al. (1964), the contact between the two is gradational in places and unconformable in others. The Barrigada may underlie the Mariana throughout northern Guam except where the surface elevation is 200 ft (60 m) and less in the area close to the dividing line between the northern and southern provinces.

Tracey et al. (1964) described the Barrigada Limestone as an intensely white, medium- to coarse-grained detrital limestone in which larger foraminifera are generally so abundant as to be characteristic of the formation. According to the types of benthonic foraminifera present, much of the limestone was deposited in open water, as much as 100 fm deep (Cole, in Tracey et al., 1964), in a setting that Tracey et al. (1964) picture as an areally extensive bank around a volcanic highland.

By contrast to the Barrigada Limestone, the Mariana Limestone grew as reef and associated lagoonal facies in an atoll-like environment. The Mariana covers most of northern Guam and constitutes many of the principal aquifers. It consists of two members: one is nearly pure limestone, free of clay and volcanic detritus, and the

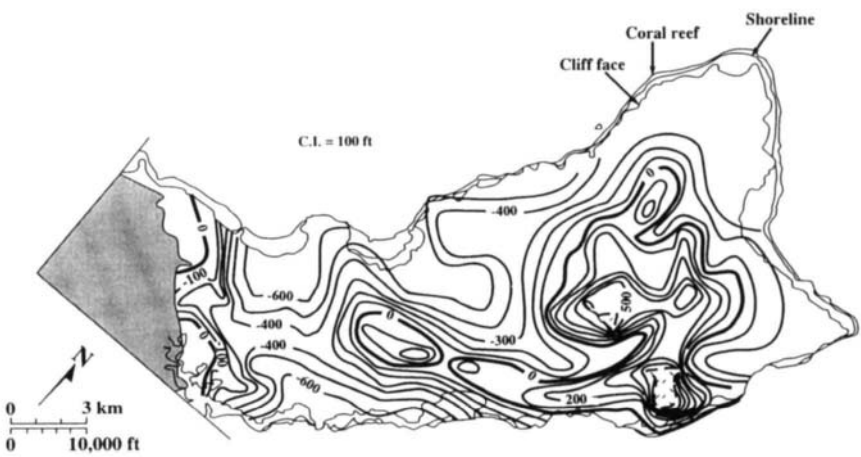


Fig. 25-5. Configuration of the volcanic basement beneath the limestones of northern Guam. Contours show elevation of contact relative to sea level. (Redrawn from CDM, 1982.)

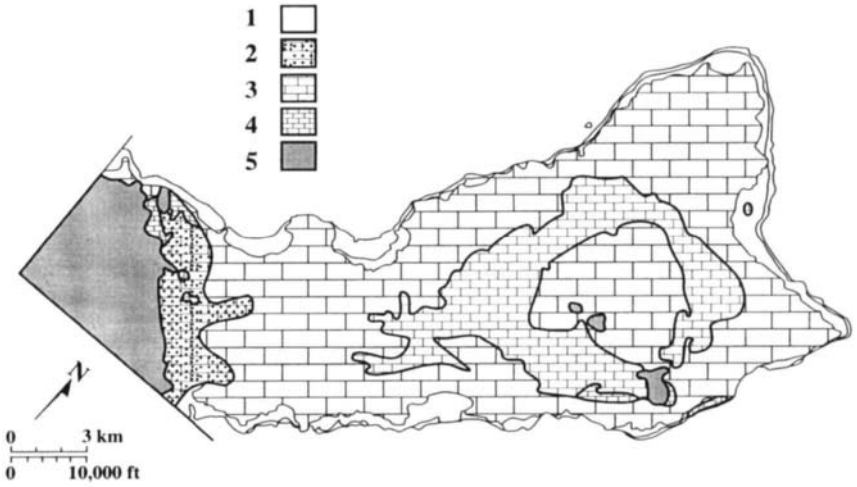


Fig. 25-6. Generalized geologic map of northern Guam. Key: (1) Slopes, cliffs, and embayments; (2) Argillaceous member of the Mariana Limestone; (3) Mariana Limestone; (4) Barrigada Limestone; (5) Alutom Formation. (Redrawn from CDM, 1982, after Tracey et al., 1964.)

other is argillaceous as a result of clastic sediments eroded from volcanic highlands. The "clean" member is dominant north of the 200-ft (60-m) topographic contour, and the argillaceous member covers approximately 15 mi^2 between that contour and the boundary of the two geologic provinces.

Except at and near the coast where the massive reef facies occurs, the Mariana Limestone comprises lagoonal facies dominated by accumulations of carbonate detritus. This facies is extremely heterogeneous and includes, in addition to typical shell and fragmental coral debris, beach sands and marls. The lagoonal facies constitutes the major aquifers of Northern Guam.

Hydraulic properties

Because of the large vertical and horizontal heterogeneity of the limestones in northern Guam, it has been found useful to consider scale regional vs. local when adopting numerical values. The total flow of groundwater, for example, is described on a regional scale, and so aquifer parameters relating to this phenomenon would represent an average between impermeable rock and open caverns. On the other hand, groundwater flow to a line or point sink, such as a gallery or well, involves local aquifer characteristics in the immediate vicinity of the sink. Regional parameters are skewed toward favorable conditions for flow; local parameters, especially hydraulic conductivity, are skewed toward the lower range of values. Regional hydraulic conductivity in the "clean" lagoonal facies of the Mariana Limestone averages about 2,000 ft day^{-1} (600 m day^{-1}) and an order of magnitude less in the argillaceous facies. Local hydraulic conductivities are typically a tenth of corre-

sponding regional values. Values of hydraulic conductivity found by calibrating regional flow models span an even great range (Contractor and Srivastava, 1990)

Porosity varies over short distances but on both regional and local scales averages about 10–25%. In primary carbonates before diagenesis, porosity is 40–70% (Bathurst, 1971); this reduces to 36–57% when primary aragonite recrystallizes to calcite, as it has in the limestones of Guam (Schlanger, 1964). The interpretation of a gravity survey in northern Guam used a value of 13% for the limestone porosity (Mink, 1982), and calibration of flow models used a value of 25% (Contractor and Srivastava, 1990).

The geologic evolution of porosity of the Mariana Limestone has been analyzed by Ayers and Clayshulte (1983b) and Harbour (1983) from a set of cores made available from site evaluation for an ammunition wharf at the tip of the peninsula south of Apra Harbor (Fig. 25-2). According to site investigations at Andersen Air Force Base (northeasternmost Guam) in connection with landfills and waste piles (Barner, 1995), geophysical and video logging of boreholes suggest that caverns and dissolution porosity are concentrated at the vadose-phreatic and freshwater-saltwater interfaces, and at horizons that correspond to emerged caves of coastal terraces and former sea levels.

Groundwater occurrence

The freshwater lens in the limestones of northern Guam is intersected in places by the impermeable volcanic basement. "Basal" groundwater (Fig. 25-7) is the part of the lens that is underlain by seawater; "parabasal" groundwater is hydraulically continuous with basal groundwater but is underlain by the basement (Mink, 1976). The basal groundwater can be divided into three parts: a freshwater core at the top; the upper limb of the transition zone in an intermediate position; and the lower limb of the transition zone at the bottom. The freshwater core carries fresh or somewhat

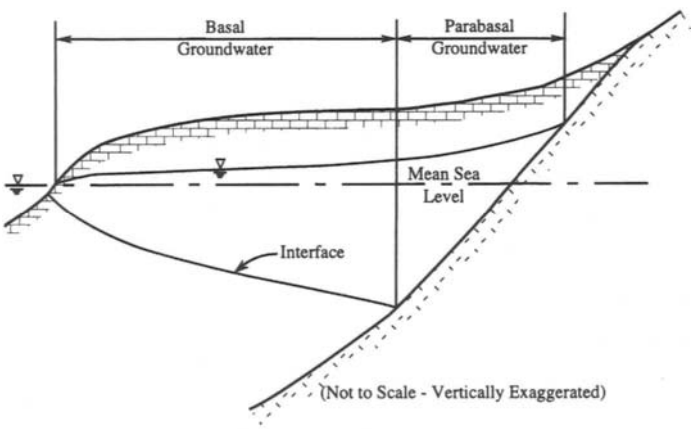


Fig. 25-7. Definition of basal and parabasal groundwater (Mink, 1976). (After CDM, 1982.)

brackish water and is the most dynamic part of the lens. The less dynamic upper limb of the transition zone ranges in salinity to half that of seawater, and the lower limb varies in salinity from half that of seawater to seawater. The Ghyben-Herzberg 40:1 ratio applies to the middle of the transition zone.

Throughout Northern Guam a continuum of basal and parabasal groundwaters occurs, but basal water occurs in most of the area (Fig. 25-8). Parabasal water is normally found where the basement is shallower than 150 ft (46 m) below sea level at the boundary between the two provinces and around the partially buried to buried volcanic highlands farther north. Although restricted to small areas, parabasal groundwater is the premier resource in northern Guam because it is immune from upconing and distant from seawater intrusion.

The elevation of the water table in the Northern Guam Lens is shown in Fig. 25-9. The very low gradient reflects the large regional-scale hydraulic conductivity of the clean limestones in the core of the plateau. The larger gradient near the southern border of the plateau reflects the lower hydraulic conductivity in the argillaceous facies of the Mariana Limestone (Mink, 1982).

The NGLS report (CDM, 1982) includes conductivity profiles from six wells that are open through the freshwater-saltwater transition zone. Two examples (of later profiles) are shown in Fig. 25-10. In general, the thickness of freshwater is about 100 ft (30 m) and locally ranges up to about 150 ft (46 m) (CDM, 1982; Contractor and Srivastava, 1990); the thickness of the transition zone is mostly 30–80 ft (9–24 m) and locally ranges up to about 100 ft (30 m) (CDM, 1982). There is an inverse correlation between the thickness of the transition zone and hydraulic conductivity (CDM, 1982); the thickest transition zone, for example, occurs in the argillaceous facies of the Mariana Limestone.

Cl^- concentration correlates with hydrogeology (Mink, 1982). In parabasal water, Cl^- is less than 30 mg L^{-1}, whereas it generally exceeds 70 mg L^{-1} in basal water, although it may resemble parabasal water in the complete absence of seawater mixing. In areas of seawater intrusion, Cl^- exceeds 150 mg L^{-1}.

Dye-trace experiments at Andersen Air Force Base (Barner, 1995) indicated diffuse flow in the saturated zone at rates of 20–36 ft day^{-1} (6–11 m day^{-1}) along the hydraulic gradient. The tests indicated flow rates several times as large with more unpredictable paths in the vadose zone because of the presence of the cavernous porosity that occurs there.

Recharge

A variety of methods has been used to estimate recharge in the limestone plateau of northern Guam (CDM, 1982). A method developed by Mink (1976) makes use of the hydrological distinction between northern and southern Guam. Surface runoff from the volcanic lands of southern Guam includes both direct runoff and groundwater seepage, and, assuming no escape of groundwater to the sea because of the extremely low permeability of the volcanics, the actual evapotranspiration can be calculated as the difference between rainfall and average stream flow. Because climatic conditions in the north and south are about the same, the calculated evapo-

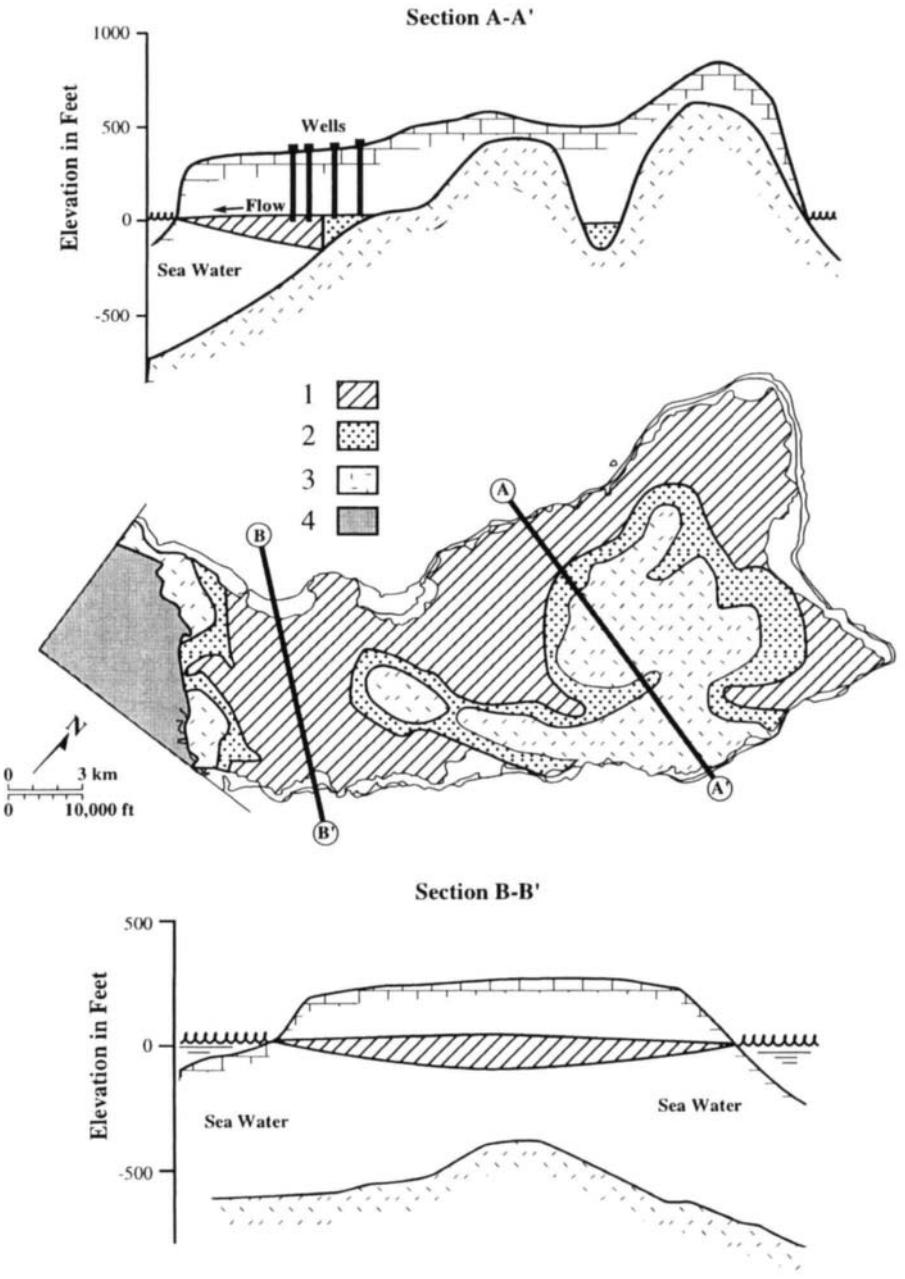


Fig. 25-8. Distribution of basal and parabasal groundwater in northern Guam. Key: (1) Basal groundwater. (2) Parabasal groundwater. (3) Where base of carbonate is above the water table. (4) Outcrop of basement rocks. (After CDM, 1982.)

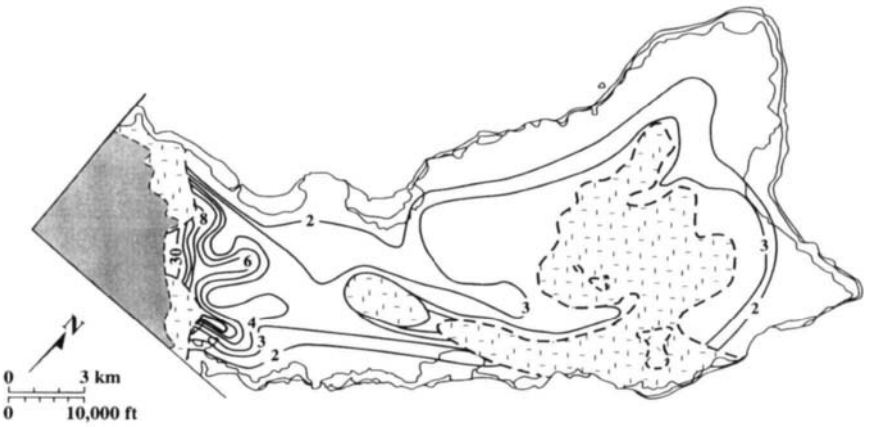


Fig. 25-9. Configuration of the water table in northern Guam. Water level contours in feet relative to sea level; basal and parabasal groundwater. (Redrawn from CDM, 1982.)

transpiration for the south can be applied directly to the north where no appreciable runoff occurs. The recharge is calculated as the difference between rainfall and this evapotranspiration.

For the NGLS, CDM (1982) used a variation of this method together with alternative ways of estimating evapotranspiration and calculating the water budget

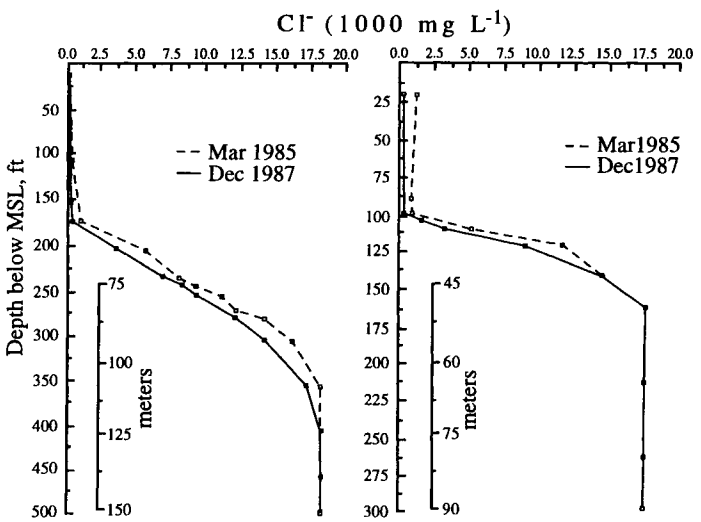


Fig. 25-10. Downward variation in Cl^- through the freshwater-saltwater transition zone at two observation wells. Measured by downhole conductivity probe. The curve on the left is exceptional in the relative proportions of the thickness of the freshwater zone vs. the transition zone; the well (Ex-1) is located in the lower-permeability argillaceous facies (Region I of Fig. 25-11). (Adapted from Contractor and Srivastava, 1990.)

(e.g., Thornthwaite-type budget; Blaney-Criddle method; pan evaporation). In addition, Ayers (1981) estimated the recharge-to-rainfall ratio from the ratio of Cl^- concentration in rainfall to the Cl^- concentration in parabasal groundwater. Ayers (1981) and CDM (1982) noted that the results of the chloride ratio and Blaney-Criddle methods were in general agreement, with both grouping into a range of 30–38 in. y^{-1} (0.9–1.2 m y^{-1}), or about 35–40% of the rainfall. Mink (1991), however, reassessed the hydrologic budget and concluded that the chloride ratio and Blaney-Criddle methods overestimated evapotranspiration for Guam, noting, for example, that the chloride ratio method does not take into account the effect of seaspray on infiltration. Mink (1991) concluded that recharge for northern Guam is nearer 60% of rainfall than 40%.

Numerical modeling

As part of the NGLS, WERI developed a two-dimensional, finite-element model of the Northern Guam Lens (Contractor, 1981; Contractor et al., 1981; Contractor, 1983). More recently, the model has been modified so that it can be run on a microcomputer (Contractor and Srivastava, 1990).

Contractor's model is a derivative of the two-fluid model developed by Sa da Costa and Wilson (1979) that simultaneously treats flow in both the freshwater and saltwater. The computations assume horizontal flow, a sharp interface between the two single-density fluids, and isotropic hydraulic conductivities. To simulate the Northern Guam Lens, Contractor used a network of 295 triangular elements with 189 nodes (Fig. 25-11) and a time step of 1 month for the verification and calibration simulations.

The most recent attempt to model the northern Guam aquifers was made by Mink (1991) employing an iterative analytical model. The seasonal distribution of recharge was taken into account, and resulting cyclic change in head was simulated. Sample results for the largest basal aquifer sector (Yigo-Tumon) are plotted in Fig. 25-12. The simulation is a good representation of actual groundwater behavior.

WATER RESOURCES

For the purpose of evaluating Guam's water resources, sustainable yield has been defined as the rate of pumpage of groundwater that can be continuously sustained without affecting either the quality or quantity of the water withdrawn (Mink, 1976, 1982, 1991; CDM, 1982). It is a global rather than a well or wellfield field concept. Mink (1976) applied the concept to Guam, estimated that the value for the Northern Guam Lens is at least 50 Mgpd (2,000 L s^{-1}) from limited data, and recommended that a detailed hydrogeologic study be conducted in order to make a better determination. Thus, estimation of sustainable yield was one of the principal goals of the NGLS.

For the NGLS, the area of the Northern Guam Lens was divided into six groundwater subbasins, which were further subdivided into 47 management zones

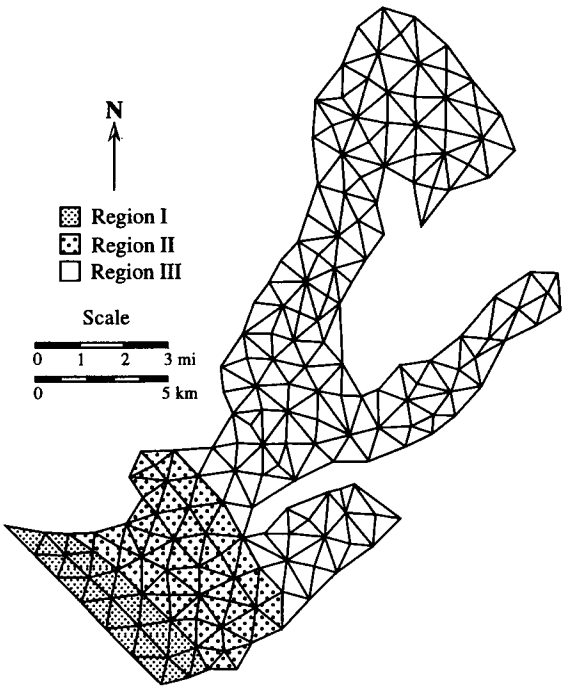


Fig. 25-11. Finite-element mesh used in Contractor's model of the Northern Guam Lens. From calibration of the model, results for the hydraulic conductivity of the three regions were: I, 80 ft day^{-1} (25 m day^{-1}); II, 5,000 ft day^{-1} (1,500 m day^{-1}); III, 2×10^4 ft day^{-1} (6,100 m day^{-1}).

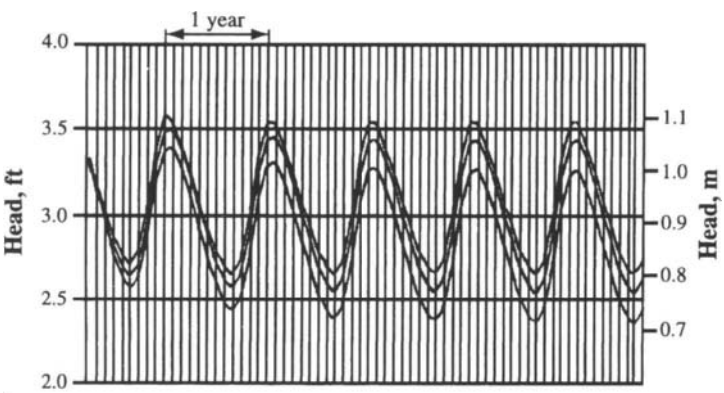


Fig. 25-12. Simulation of seasonal variation in water level, Yigo-Tumon aquifer sector, for three development options. Sustainable yield of the sector is 20 Mgpd (880 L s^{-1}), or 30% of the average annual recharge. When draft is 10 Mgpd (440 L s^{-1}) or less, full recovery from a seasonal low of 2.7 ft (82 cm) takes place every year, assuming an initial head of 3.5 ft (107 cm). At 15 Mgpd (660 L s^{-1}), the low head approaches 2.5 ft (76 cm) and recovery peaks at 3.4 ft (104 cm), and at 20 Mgpd (880 L s^{-1}), the dry-season minimum is at 2.4 ft (73 cm) and the wet-season recovery is at 3.2 ft (98 cm). (Adapted from Mink, 1991.)

(Fig. 25-13). The subbasins were defined from the basement topography. The management zones were of two types: basal zones (18) and parabasal zones (29). Water entering each management zone as recharge was calculated for each zone independently from contoured rainfall data and estimated evapotranspiration. Sustainable yield was calculated zone by zone, by taking 60% of the recharge in parabasal zones and 40% of the recharge in basal zones and not counting a 4,000-ft (1,200-m) buffer zone along the shoreline. From this calculation, the total recharge to the Northern Guam Lens was about 112 Mgpd (4,900 L s^{-1}) and the sustainable yield about 59 Mgpd (2,600 L s^{-1}) (Mink, 1982; CDM, 1982). These values have been revised upward (Mink, 1991). The estimated sustainable yield is 70–80 Mgpd (3,100–3,500 L s^{-1}) under proper operational practices.

Groundwater production in Northern Guam from wells and galleries averages 25 Mgpd (1,100 L s^{-1}), less than half the sustainable yield. Poor production practices, however, have resulted in the loss of wells to salinity. Contamination from above is also a threat because of the open structure of the limestone mass. With respect to salinity, experience has shown that wells pumping at 200 gpm (200 U.S. gal min^{-1}; 13 L s^{-1}) have few failures due to upconing with present well design practices in basal zones (CDM, 1982). Wells in parabasal zones avoid upconing and, if more than 500 ft (150 m) from the nearest basal water, should avoid saltwater intrusion, too, for pumping rates up to 500–750 gpm (31–47 L s^{-1}) (CDM, 1982).

Contractor (1983) used his model to explore water-development options after calibration with 1978 estimated recharge and extractions. He found that doubling the pumping had only a minor effect on the water table and freshwater volumes. The water table responded quickly and then declined at a slower rate to approach a steady-state value. The interface, on the other hand, moved much more gradually over a much longer period of time.

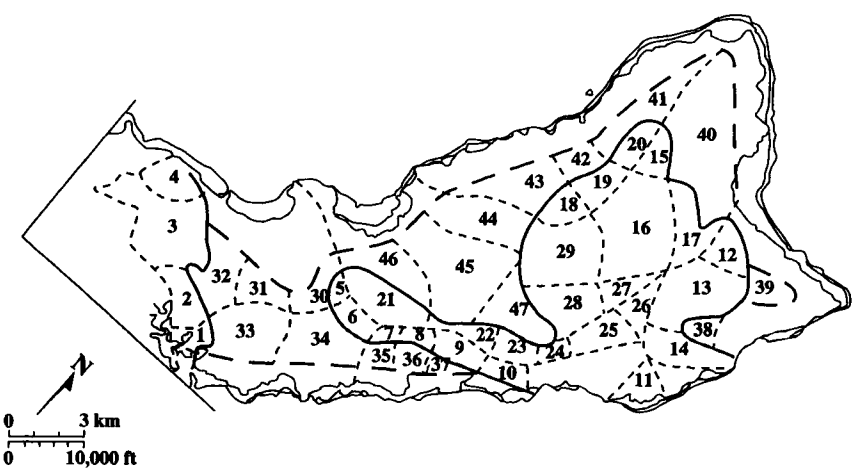


Fig. 25-13. Groundwater subbasins and management zones in northern Guam. The heavy dashed line delimits a 4,000-foot (1.2-km) coastal buffer zone. (Redrawn from CDM, 1982).

CONCLUDING REMARKS

In the limestones of northern Guam are aquifers which contain the most voluminous and reliable resources of freshwater in the island. Without this resource, Guam would not be able to sustain its growing population and dynamic economy.

The Guam experience in groundwater development is a fine example of evolution in understanding the relationships among hydrogeological variables in an island limestone terrain. The geological investigation by Stearns (1937) provided the reconnaissance framework for the hydrogeology; then the exhaustive geological investigations of Tracey et al. (1964) established the framework to a level which has become the standard for all subsequent work. The application of geophysics, especially seismic refraction and resistivity, has refined the framework, and well-drilling and operational experience has yielded local subsurface information that is necessary for successful development practices.

ACKNOWLEDGMENTS

JFM thanks James Branch, former Director of the Guam Environmental Protection Agency, for his limitless cooperation in supporting the Northern Guam Lens Study. We both benefitted from our work and discussions with Jerry Ayers, Steve Winter, and Dinshaw Contractor of WERI of the University of Guam.

REFERENCES

Agassiz, Alexander, 1903. The coral reefs of the tropical Pacific. Mem. Mus. Comp. Zool., Harvard, 28: 1–410.

Ayers, J.F., 1981. Estimate of recharge to the freshwater lens of northern Guam. Univ. Guam, WERI Tech. Rep. 21., 20 pp.

Ayers, J.F. and Clayshulte, R.N., 1983a. Feasibility study of developing valley-fill aquifers for village water supplies in southern Guam. Univ. Guam, WERI Tech. Rep. 41., 91 pp.

Ayers, J.F. and Clayshulte, R.N., 1983b. Diagenesis and pore-space evolution within recent and Pleistocene carbonate units of Orote Peninsula, Guam. Univ. Guam, WERI Tech. Rep. 47, 113 pp.

Barner, W.L., 1995. Ground water flow in a young karst terrane developed along a coastal setting, northern Guam, Mariana Islands. Int. Res. Appl. Cen. Karst Water Res., Karst Water Inst. Sem. Field Course, Beldibi/Antalya, Turkey, Sept. 10–20, 1995, 12 pp.

Bathurst, R.G.C., 1971, Carbonate Sediments and Their Diagenesis. Elsevier, Amsterdam, 658 pp.

CDM (Camp, Dresser and McKee Inc.), 1982. Final Report, Northern Guam Lens Study, Groundwater Management Program, Aquifer Yield Report. (Prepared by CDM in association with Barrett, Harris & Associates for Guam Environmental Protection Agency.)

Cloud, P.E., Jr., Schmidt, R.G., and Burke, H.W., 1956. Geology of Guam, Mariana Islands, Part 1. General Geology. U.S. Geol. Surv. Prof. Pap 280-A, 126 pp.

Cole, W.S., 1963. Tertiary larger Foraminifera from Guam. U.S. Geol. Surv., Prof. Pap. 403-E, 28 pp.

Contractor, D.N., 1981. A two-dimensional, finite element model of salt water intrusion in groundwater systems. Univ. Guam, WERI Tech. Rep. 26.

Contractor, D.N., 1983. Numerical modeling of saltwater intrusion in the Northern Guam Lens. Water Resour. Bull., 19: 745–751.

Contractor, D.N., Ayers, J.F. and Winter, S.J., 1981. Numerical modeling of salt-water intrusion in the Northern Guam Lens. Univ. Guam, WERI Tech Rep. 27., 48 pp.

Contractor, D.N. and Srivastava, R., 1990. Simulation of saltwater intrusion in the Northern Guam Lens using a microcomputer. J. Hydrol., 118: 87–106.

Doan, D.B., Burke, H.W., May, H.G. and Stensland, C.H., 1960. Military geology of Tinian, Mariana Islands. U.S. Geol. Surv. Rep. to U.S. Army Corps Engineers.

Easton, W.H., Ku, T.L. and Randall, R.H., 1978. Recent reefs and shore lines of Guam. Micronesica 14(1): 1–11.

Garrison, R.E., Schlanger, S.O. and Wachs, D., 1975. Petrology and paleogeographic significance of Tertiary nannoplankton-foraminiferal limestones, Guam. Palaeogeogr. Palaeoclimatol. Palaeoecol., 17: 49–64.

Harbour, J.L., 1983. Porosity evolution of the Pleistocene Mariana Limestone, Orote Peninsula, Guam. In: P.M. Harris (Editor), Carbonate Buildups: a core workshop. Soc. Econ. Paleontol. Mineral. Core Workshop, 4: 540–557.

Hussong, D.M. and Uyeda, S., 1981. Tectonic processes and the history of the Marianas Arc: A synthesis of the results of Deep Sea Drilling Project Leg 60. In: D.M. Hussong and S. Uyeda et al., Initial Reports of the Deep Sea Drilling Project, 60. U.S. Gov. Printing Office, Washington D.C., pp. 803–815.

Karig, D.E., 1971. Structural history of the Mariana island arc system. Geol. Soc. Am. Bull., 82: 323–344.

Mink, J.F., 1976. Groundwater Resources of Guam: Occurrence and Development. Univ. Guam, WERI Tech. Rep. 1.

Mink, J.F., 1982. Summary Report, Northern Guam lens Study. Guam Environmental Protection Agency, 52 pp.

Mink, J.F., 1991. Groundwater in Northern Guam. Sustainable yield and groundwater development. Barrett Consulting Group, Honolulu HI, Report to Public Utility Agency of Guam.

Randall, R.H., Siegrist, H.G., Jr. and Siegrist, A.W., 1984. Community structure of reef-building corals on a recently raised Holocene reef on Guam, Mariana Islands. Palaeontogr. Am., 54: 394–398.

Reagan, M. and Meijer, A. (1983). Geology and geochemistry of early arc-volcanic rocks from Guam. Geol. Soc. Am. Bull., 95: 701–713.

Schlanger, S.O., 1964, Petrology of the Limestones of Guam: U.S. Geological Survey Prof. Paper 403-D: D1-D52.

Scott, R.B., Kroenke, L., Zakariadzde, G., and Sharaskin, A., 1980. Evolution of the South Philippine Sea: Deep Sea Drilling Project Leg 59 results. In: L. Kroenke, R. Scott et al., Initial Reports of the Deep Sea Drilling Project, 59. U.S. Gov. Printing Office, Washington D.C., pp. 803–815.

Siegrist, A.W., Randall, R.H. and Siegrist, H.G., Jr., 1984. Functional morphological group variation within an emergent Holocene reef, Ylig Point, Guam. Palaeontogr. Am., 54: 390–393.

Siegrist, H.G., Jr., and Randall, R.H., 1992. Carbonate geology of Guam. Proc. Seventh Int. Coral Reef Symp. (Guam), 2: 1195–1216.

Siegrist, H.G., Jr., Randall, R.H. and Siegrist, A.W., 1984. Petrography of the Merizo Limestone, an emergent Holocene reef, Ylig Point, Guam. Palaeontogr. Am., 54: 399–405.

Sa da Costa, A.A.G. and Wilson, J.L., 1979. Numerical model of seawater intrusion in aquifers. Massachusetts Inst. Tech. Rep. 247.

Stearns, H.T., 1937. Geology and water resources of the island of Guam, Mariana Islands. U.S. Navy Manuscript Report.

Stearns, H.T., 1940. Geologic history of Guam (abstr.). Geol. Soc. Am. Bull., 52: 1948.

Stearns, H.T., 1941. Shore benches on north Pacific islands. Geol. Soc. Am. Bull., 52: 773–780.

Tracey, J.I., Jr., Schlanger, S.O., Stark, J.T., Doan, D.B. and May, H.G., 1964. General Geology of Guam. U.S. Geol. Surv. Prof. Pap. 403-A, 104 pp.

Ward, P.E., Hoffard, S.H. and Davis, D.A., 1965. Hydrology of Guam. U.S. Geol. Surv. Prof. Pap. 403-H, 28 pp.

This Page Intentionally Left Blank

Geology and Hydrogeology of Carbonate Islands. Developments in Sedimentology 54
edited by H.L. Vacher and T. Quinn
© 1997 Elsevier Science B.V. All rights reserved.

Chapter 26

HYDROGEOLOGY OF CARBONATE ISLANDS OF FIJI

J. FERRY, P.B. KUMAR, J. BRONDERS and J. LEWIS

INTRODUCTION AND SETTING

Fiji lies in the southwest Pacific Ocean along the convergent boundary between the Indo-Australian and Pacific Plates (Fig. 26-1). About 3,000 km due east of the Great Barrier Reef and 2,100 km north of Auckland N.Z., the island nation consists of more than 300 islands, the vast majority of which are between longitudes 176°50′E and 178°W, and latitudes 16°S and 20°S (Fig. 26-2). The total land area is 18,272 km^2; the territorial waters cover 141,800 km^2. About a hundred of the islands are permanently inhabited. More than 80% of the country's population of 715,000 (1986 census) resides on the two main islands, Viti Levu and Vanua Levu (Fig. 26-2). The capital, Suva, is on Viti Levu.

Austronesian-speaking peoples settled Fiji in the second millennium, B.C. The Dutch explorer Abel Tasman visited the area in 1643 and encountered a Melanesian-Polynesian population. The first European settlers were sandalwood traders, missionaries, and shipwrecked sailors. In 1874, Fiji was ceded to Britain. After 96 years as a British crown colony, Fiji became a dominion in the British Commonwealth in 1970, and a republic in 1987. The 1990 Constitution provides for a parliamentary form of government with a President. Indigenous Fijians comprise the majority of the population. The rest of the population consists largely of Indians, descendants of laborers of the sugar estates in the late nineteenth century. Although Fijian and Hindi are the principal languages, English is widely spoken and is one of the three official languages.

Viti Levu and Vanua Levu are volcanic islands that rise abruptly from densely populated coasts to generally uninhabited, rugged mountains. The highest mountain, Tomaniivi on Viti Levu, reaches an elevation of 1,323 m. Volcanic islands also predominate in the outer islands, which make up the various named island groups shown in Figure 26-2.

Overall, there are only 32 limestone islands in Fiji with an area exceeding 1 km^2 (Table 26-1; Fig. 26-2). They total 391 km^2 in area, or 2% of the total land area of Fiji. About half of them have an exposed volcanic core. Most of the limestone islands occur in the Lau Group.

In addition to the limestone islands, there are many low carbonate sand cays of present-day barrier-reef systems throughout Fiji. There are also recent carbonate beach deposits of in situ beachrock and calcareous sand and gravel on most of the islands.

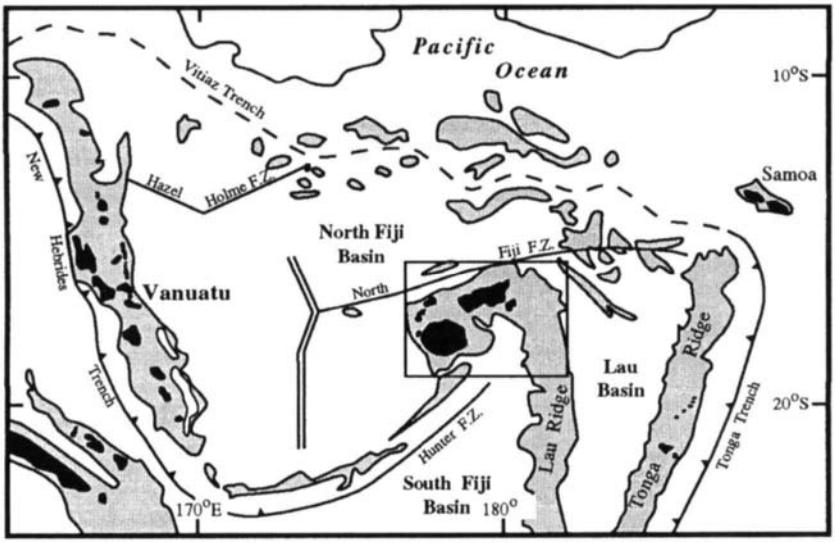


Fig. 26-1. Location of Fiji along a complicated sector of the boundary between the Indo-Australian and Pacific Plates in the Southwest Pacific. (Adapted from Charvis and Pelletier, 1989.)

Infrastructure

Populations of the inhabited carbonate islands are generally small and total approximately 10,000 (Table 26-1). The people reside in villages or settlements located on recent coastal deposits. There is no water legislation in force, customary law prevails, and community ownership of water sources is the norm. Activities on the smaller islands are essentially subsistence, although there is a small cash economy from coconuts, fishing, tourism and handicrafts. There are no roads nor motor vehicles except on several of the larger islands. There are few jetties, and equipment has to be landed by small craft or landing barge. In some cases, there is no large boat access through the reef. There are airstrips on some of the more remote or populous islands.

Hydrogeologic studies

Hydrogeologic studies have been undertaken in Fiji since the late 1960s. These studies have ranged from government geologists attempting to resolve water-shortage problems in villages, to international agencies such as the U.N. Development Programme and British Aid, carrying out detailed resource investigations for urban, rural, agricultural, or tourist-development requirements. Most of these projects were carried out by or in cooperation with the Hydrogeology Section of the Mineral Resources Department (MRD). All projects contributed to compiling of hydrogeologic maps; identifying and assessing major groundwater resources for domestic supply, tourism and agricultural development; identifying and assessing minor

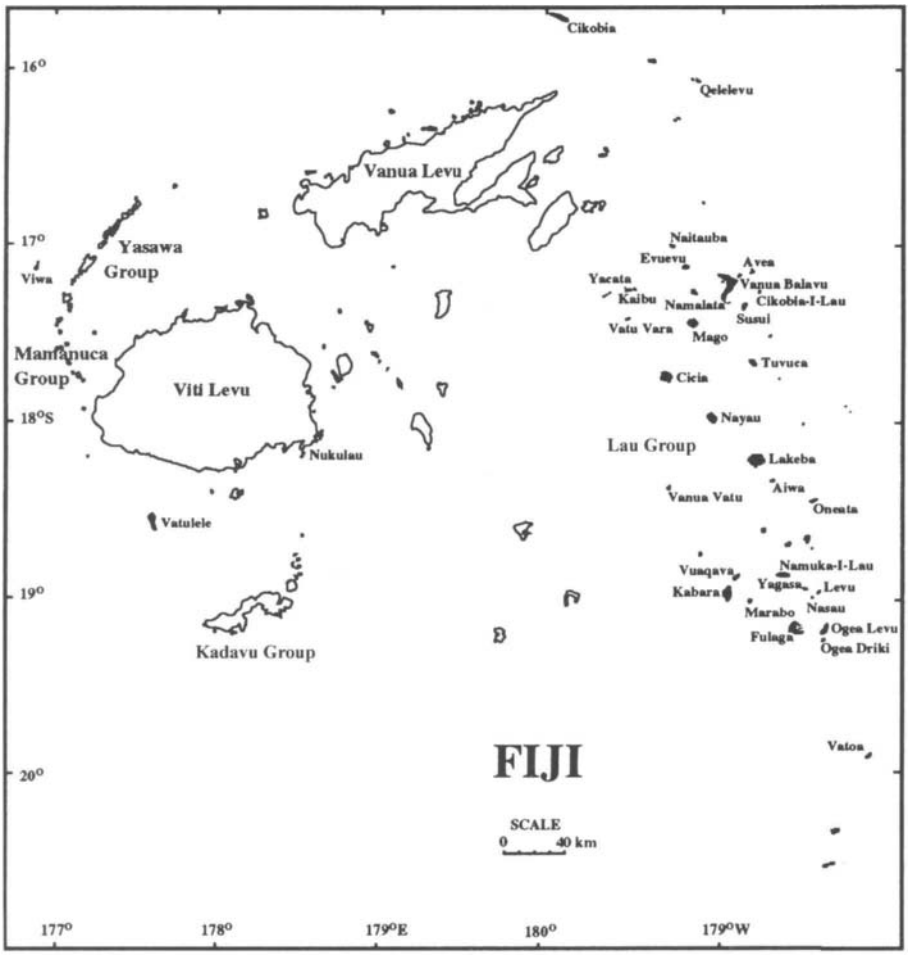


Fig. 26-2. Map of Fiji showing the major island groups. The 32 carbonate islands (Table 26-1), shown in black, account for 2% of Fiji's land area.

resources for rural villages and small islands; and establishing a system for continued collection of groundwater data and monitoring.

This chapter draws heavily on the comprehensive report of Gale and Booth (1993), geologic maps (Woodhall, 1984, 1985a) and a forthcoming MRD Bulletin on the Lau Group by Woodhall (in prep.), unpublished technical MRD reports, and our own investigations.

Climate

Temperatures are 16–32°C. May to October is dominated by the southeast trade winds and is relatively cool and dry. November to April is the warm and wet season,

Table 26-1

Carbonate islands in Fiji with an area greater than one square kilometer

Island	Location	Area (km^2)	Max. Elev. (m)	Carbonate Unit[a]	Geology (%)[b]	Population[c]
LIMESTONE ISLANDS						
Aiwa	C Lau	1.2	60.0	Ko	100	0
Evuevu	N Lau	1.3	155.4	Ko	100	0
Fulaga	S Lau	18.5	79.2	Ko	100	376
Marabo	C Lau	1.3	48.8	Ko	100	0
Namuka-I-Lau	S Lau	12.8	79.2	Ko	100	377
Nasau	S Lau	1.0	64.0	Ko	100	0
Ogea Driki	S Lau	5.2	91.4	Ko	100	0
Ogea Levu	S Lau	13.3	82.3	Ko	100	79
Qelelevu	NE Fiji	1.5	18.0	Uc	100	10
Vanua Vatu	C Lau	4.1	101.8	Ko, Uc	100	197
Vatoa	S Lau	4.5	45.0	Ko	100	283
Vatu Vara	N Lau	3.8	313.9	Ko, Uc	100	0
Viwa	Yasawa	4.6	18.0	Uc	100	237
Vuaqava	S Lau	8.1	106.7	Ko	100	0
Yagasa Levu	S Lau	2.6	118.9	Ko	100	0
MIXED GEOLOGY ISLANDS						
Avea	N Lau	2.2	182.9	Ko	85	168
Cicia	N Lau	34.6	164.6	Da, Ko	10	1062
Cikobia	NE Fiji	15.0	186.0	Na, Uc	85	211
Cikobia-I-Lau	N Lau	3.0	167.7	Da, Ko	40	78
Kabara	S Lau	31.2	143.3	Ko	95	563
Kaibu	N Lau	1.5	45.7	Uc	60	3
Lakeba	C Lau	55.9	219.5	Ta, Ko	10	2444
Mago	N Lau	21.9	204.2	Ko, Da, Uc	50	79
Naitauba	N Lau	8.8	185.9	Da, Ko	70	87
Namalata	N Lau	2.1	128.0	Ko	80	55
Nayau	C Lau	18.4	178.0	Ko, Da, Uc	80	432
Oneata	C Lau	4.0	48.8	Da,Wa, Ko	95	194
Susui	N Lau	3.3	131.1	Ko	40	119
Tuvuca	N Lau	12.5	243.8	Da, Ko	95	178
Vanua Balavu	N Lau	53.2	283.4	Fu, Da, Ko	35	2239
Vatulete	SW Fiji	31.6	38.0	Wt	90	660
Yacata	N Lau	8.3	256.0	Ko, Uc	80	140

[a] Da: Daliconi Limestone; Fu: Futuna Limestone; Ko: Koroqara Limestone; Na: Naibalebale Sandstone; Ta: Tabusue; Uc: Ucuna Limestone; Wa: Waiqori Sandstone; Wt: Waituka Limestone.
[b] percent of island composed of carbonate rock.
[c] 1986 cenus.

during which tropical depressions, often with winds of hurricane force, are the major influence on weather.

Average annual rainfall in Fiji ranges from 1,500 mm on the smaller islands to over 7,000 mm on the larger islands. The latter value is large because of orographic effects.

The carbonate islands generally have elevations below 200 m and virtually no orographic effect on precipitation. A few of the smaller islands (Viwa, Ono-i-Lau and Lakeba) have meteorological stations that record daily rainfall and maximum and minimum temperatures. These data indicate that 70% of all rainfall occurs during the wet season and that mean annual rainfall for these islands varies from 1,500 to 1,800 mm.

Tectonic setting

Outer Melanesia (Colley and Hindle, 1984) includes the island chains of Vanuatu (formerly the New Hebrides), Fiji and Tonga (Fig. 26-1). These chains are part of a geodynamically complex convergent boundary between the Indo-Australian and Pacific Plates. This boundary is marked by a complex of ridges and basins that extend from New Guinea through Fiji to New Zealand (Gill, 1976).

The islands of Fiji are the emergent parts of a remnant arc (Gill, 1976), which includes the Fiji Platform and the Lau-Colville Ridge. The main islands Viti Levu and Vanua Levu are on the Fiji Platform, and the outer islands of the Lau Group are on the northern part of the Lau-Colville Ridge. The remnant arc system is surrounded by three marginal basins: the recently (5.5 Ma) formed Lau Basin behind the Tonga Ridge; the North Fiji Basin (or Fiji Plateau), which is bounded on the north by the Vitiaz Trench, a fossil subduction zone (Auzende et al., 1988; Charvis and Pelletier, 1989); and the South Fiji Basin (or Minerva Plain), the oldest of the basins. The geologic history of Fiji "is apparently restricted to the Cenozoic Era" (Colley and Hindle, 1984, p. 153) and reflects the history and extension of these marginal basins (Colley and Hindle, 1984; Gill et al., 1984).

There is general consensus (Rodda and Kroenke, 1984; Colley and Hindle, 1984; Gill et al., 1984; Auzende et al., 1988) that before about 8 Ma, there was a single arc including Vanuatu, Fiji, and Tonga. This Vitiaz Arc was associated with the Vitiaz Trench along which the Pacific Plate was subducted beneath the Indo-Australian Plate. At about 8 Ma, a collision of the trench with the Ontong-Java Plateau (Auzende et al., 1988; Clift, 1994) brought about a reversal of subduction polarity (New Hebrides Trench; Fig 26-2) and reorganization of the western part of the Vitiaz subduction zone. The New Hebrides Arc rotated clockwise away from the Vitiaz Trench and the Fiji Plateau rotated counterclockwise as the North Fiji Basin opened. The opening of the Lau Basin beginning at 5–6 Ma (Hawkins et al., 1994; Parson et al., 1994) separated the Lau Ridge from the site of subduction along the Tonga Trench and made the ridge a remnant arc (Karig, 1970; Gill, 1976; Nunn, 1987).

GENERAL GEOLOGY OF THE CARBONATE ISLANDS

Geologically and hydrogeologically, the carbonate islands of Fiji can be classified into three main types. The first is limestone islands in which the volcanic core is completely buried. The second is a mixed-geology island, where the underlying volcanic core is partially exposed and/or igneous activity has occurred subsequent to

the main carbonate deposition. The third is the low, sandy cays associated with fringing and barrier reefs. The general stratigraphy and character of the limestones of the first two types of islands are similar.

Stratigraphy and geologic history

In the islands of the Lau Group, all the limestones are collected together as the Tokalau Limestone Group (Woodhall, 1985b), which includes the Futuna Limestone (middle Miocene), Koroqara Limestone (late Miocene and early Pliocene), and Ucuna Limestone (Quaternary). The succession of limestone formations is related to the volcanic history of the Lau Ridge, which is also represented by three main groups of lavas (Woodhall, 1985b; Cole et al., 1990): the Lau Volcanic Group (LVG, 14.0–5.4 Ma), Korobasaga Volcanic Group (KVG, 4.4–2.4 Ma), and the Mago Volcanic Group (MVG, 2.0–0.3 Ma). According to Cole et al. (1990), LVG is predominantly subaerial andesite that was erupted in a primary island arc (Vitiaz Arc); KVG is predominantly submarine basalt that was erupted immediately prior to or during the initial stages of rifting of the Lau Basin; and MVG consists of basalt-hawaiite typical of intra-plate ocean-island settings unrelated to present-day subduction. LVG is widely distributed, cropping out on 16 islands in the Lau Group and "probably forming the basement to many reefs and atolls" (Cole et al., 1990, p. 542). In contrast, KVG is exposed on only six islands, and MVG on four, the principal one of which is Mago where there are three scoria cones and associated short flows (Cole et al., 1990).

According to Gale and Booth (1993), the Koroqara Limestone formed around the active volcanoes of the younger part of the LVG. During early Pliocene times (5–3 Ma), the volcanic cones were submerged, and most of them were covered by thick deposits and varied facies of the Koroqara Limestone. The Daliconi Limestone, a conglomeratic unit consisting of corals and igneous clasts in a calcarenite matrix, formed as a subsidiary unit (Gale and Booth, 1993) and is everywhere overlain by the Korogara Limestone (Woodhall, 1985b).

Gale and Booth (1993, p. 85–86) give the following description of the Koroqara and Ucuna Limestones, the most widespread units:

> "The Koroqara Limestone is a massive, highly recrystallised, non-terrigenous limestone that is usually poor in coral and represents lagoonal facies. More coral is sometimes found nearer the coast, but in the majority of cases the reef coral has been eroded. The islands are now relatively elevated and typically terraced in erosional surfaces, testifying to previous sea levels. The number of terraces varies from seven in northern Lau to three or four further south. The maximum heights of the islands also decrease to the south, from 310 m on Vatu Vara to 118 m on Yagasa Levu [and 45 m on Vatoa].
>
> These elevated limestones have been subjected to karstic weathering forming rugged terraces, ridges and pinnacles and shallow holes in the central "lagoon" which in some cases is now close to sea level. The formation of the terraces is considered to have occurred mostly during the late Pliocene in conjunction with a worldwide fall in sea level (Woodhall, in prep). The number and elevations of terraces can be correlated to some extent throughout the group (Nunn, 1988), but uneven tectonism may have occurred, probably associated with block faulting.
>
> A further stage of coral growth occurred during the Quaternary, forming the youngest limestone in Lau, the Ucuna Limestone. This is mostly reef limestone and coral-rich

calcareous sediments and deposits which are found sporadically throughout the Lau Group, and similar limestones elsewhere have been correlated with it."

Geochemically, the Koroqara Limestone ranges from high-calcium limestone to dolomite with calcitic dolomite being predominant. The Ucuna Limestone ranges from high-calcium limestone to dolomitic limestone, but most of it is magnesian limestone and dolomitic limestone.

On Vatulele (Fig. 26-2), which is known to contain a freshwater lens, the limestone is the Waituka Limestone (late Miocene). It is massive and has a low coral content.

In addition to the carbonate units, there are calcareous sandstones that also affect the hydrogeology. On Oneata (Fig. 26-1), the foraminiferal Waiqori Sandstone (late Miocene, early Pliocene) consists of up to 30 m of volcaniclastic sand and gravel intermixed with a coarse bioclastic fraction including echinoid debris and molluscan shells. Freshwater lenses and perched aquifers are known to occur within the sandstone aquifer of Oneata.

Two other calcareous sandstones are found in the carbonate islands of Fiji (Table 26-1). The Naibalebale Sandstone (early Pliocene) which occurs on Cikobia (Fig. 26-1) is a calcareous sandstone with a noncalcareous component of volcanic detritus. The Tabusue Sandstone (late Miocene, early Pliocene) on Lakeba consists of calcareous and/or noncalcareous sandstone. The noncalcareous sandstone components are entirely volcanic debris, whereas the calcareous facies contains abundant carbonate material as well volcanic detritus. Hydrogeologically, these two deposits have not been studied in detail but it is presumed that their groundwater potential is poor.

Geomorphology

The carbonate islands are normally surrounded by barrier and/or fringing reefs. Patch and transverse reefs occur within many of the lagoons. The transverse reefs frequently link an island to its surrounding reefs.

The geomorphology of the limestone islands is dominated by karst topography which developed on multiple wave-cut terraces of the Koroqara Limestone. The dominating features are ramparts, solution rims and ridges, solution basins and pinnacles (Hoffmeister and Ladd, 1945). These erosional features cut across many of the facies variations that are evident in the limestone. Submerged terraces are also evident around some of the Lau islands. The terrace elevations on Lau Islands were systematically analyzed by Nunn (1987); these analyses were updated slightly in his 1995 monograph. A few of the terrace scarps and ridges were formed from or influenced by faulting as were the configurations of some of the barrier and atoll reefs. The solution basins form low-lying depressions within high solution rims. Depending on elevation, these basins are dry or contain brackish-water swamps, marine lakes or lagoons.

Many of the islands have small associated satellite islets which were originally part of the main islands but are now separated by subsidence and/or erosion (e.g., Viwa, Fulaga). A wide variety of island shapes can be found. Figure 26-3 presents three

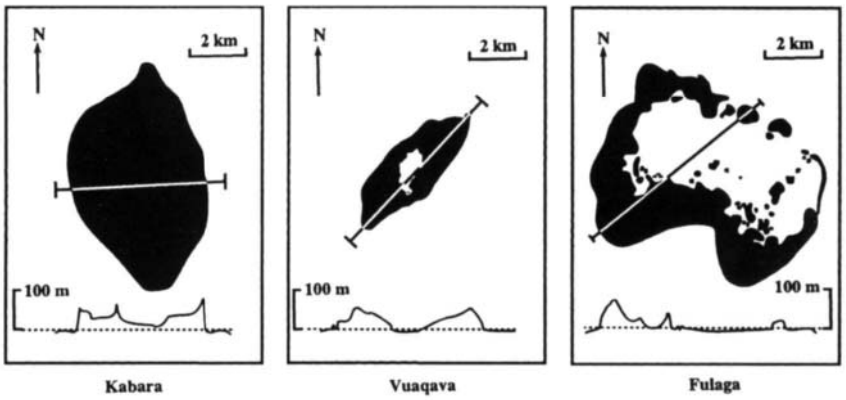


Fig 26-3. Shape and topographic profile of three islands in the Lau Group.

basic shapes of Lau islands (Kabara, Vuaqava, Fulaga). Kabara is a high-standing island with a dry solution basin which is completely surrounded by a solution rim with elevation of 40–100 m. Vuaqava is also completely ringed by a solution rim (30–105 m) but its solution basin is partially flooded by seawater. On Fulaga, the ocean has breached the solution rim, and so the island has an atoll shape. These three islands taken as a series tend to support the idea developed by Purdy (1974) that the submergence of this type of karstic eroded island can lead to atoll-shaped islands and reefs. The absence of in situ corals in the rims of many high-level basins in Lau also supports Purdy's view (Nunn, 1994, 1995). The topography developed on the carbonate sandstone differs from that on the limestone in that the ridges are rounded in profile and have gentle slopes.

Depositional landforms are common on most islands in the form of coastal plains rarely more than 3 m above sea level. Topographic features on these landforms are restricted to low-lying beach berms.

In spite of thin and patchy soil distribution, which is the general rule on the carbonate islands, many islands are densely vegetated. The type of vegetation varies from island to island and shows strong human influence where areas of better soil development has been utilized for agriculture.

SURFACE WATERS

There are few permanent surface-water flows on the carbonate islands of Fiji because of the high permeability of the carbonate rocks. Sheet runoff is common.

On two islands of mixed geology, Lakeba and Mago in the Lau Group, permanent streams fed by high-level springs in the volcanic terrain flow as far as the limestones, disappear underground via swallow holes, and emerge at the sea as coastal submarine springs. In Mago, the swallow holes are prevented from clogging with debris by iron grilles to ensure free drainage of flood water. Drainage channels

in the limestone are small, shallow, and ephemeral; they provide no storage. Drainage on mixed-geology islands is restricted to occasional very small seasonal creeks which are absent on all limestone islands.

COMPARATIVE HYDROGEOLOGY AND OCCURRENCE OF GROUNDWATER

Limestone islands

Of the islands consisting only of limestone (Table 26-1), only Vatulele is known by direct observation to have a freshwater lens. Freshwater lenses are strongly suspected on Vatoa (see Case Study), Kabara and Fulaga. Freshwater lenses are also considered likely on some other limestone islands, but to date no detailed groundwater studies have been carried out on them. For some islands, it is known that there is no freshwater lens, or one that is so thin that it is difficult to identify (e.g., Viwa). Brackish-water lenses are common in some of the highly karstic limestones.

There are no known perched aquifers or high-level springs on the limestone islands. Submarine and intertidal coastal-flat springs are quite common.

Groundwater discharges into inland solution basins as well as to the shoreline. Such discharge forms inland freshwater lakes on clayey soils on Nayau and freshwater marshes on Kabara and Oneata.

The distribution of facies exerts a major control on the development of lenses. Groundwater lenses develop preferentially in backreef biocalcarenites rather than in the coarser reef limestone and coralline calcarenite on which the solution rims develop. Accordingly, the maximum development of the lens occurs in wide parts of the island, toward the lagoon side and away from the solution rims, where these exist. On Fulaga, the development of the lens occurs under lobes of land, away from the cliff terraces. On Vatulele, the lens that occurs at the widest part of the island is fresh and potable near the low-lying side of the island and brackish in the center of the island; groundwater is saline under the high cliff terraces. On Nukulau, a well-studied sand cay of about 10 ha located on the barrier reef near Suva, beachrock is the main control on maximum lens development. The brackish lens is well developed under the beachrock to one side of the island and poorly developed in the center of the island because the distribution of beachrock is asymmetric.

Changes in depositional facies are probably accompanied by changes in permeability. In the finer backreef facies, permeability is less developed and, therefore, allows better buildup of the lenses. In the coarser facies, on the other hand, the solutionally developed permeability allows seawater intrusion further inland and leads to groundwater heads that are only marginally above sea level; consequently, there are thin fresh and/or brackish-water lenses in these rocks. Viwa is a good example of a reef-facies limestone island with little or no development of a freshwater lens, even though the island measures 3 km by 1.5 km.

Faults also exert a control on the development of the lenses, either directly by providing conduits for seawater intrusion far inland (e.g., Viwa and Vatulele) or indirectly by their effect on lateral facies distribution. Development of solution

basins, often with significant clay accumulations, can also influence development of the lens.

Freshwater lenses range up to 20 m thick (e.g., Vatoa; see Case Study) but with water levels only up to 1 m above sea level. The true saline base of the lenses has only rarely been proven by drilling (Nukulau and Vatulele) and is known mostly from geophysical work. The thickness of the transition zone depends very much on the presence of underlying low-permeability rock and secondary permeability. On the edges of lenses, the groundwater is brackish, and the transition zone is much thicker than the freshwater zone.

There is hardly any long-term monitoring of water levels in these outlying limestone islands, and seasonal fluctuations are only poorly known. Groundwater heads are known to fluctuate up to 60% (e.g., on Nukulau). Water levels in the calcareous sand and beachrock of the coastal plain fluctuate with tide, with lag times of 0.5–2 hours, and measured tidal ranges 10–40% of those of the ocean.

Calcareous sandstone

In the only known extensive occurrence of calcareous sandstone, the Waiqori Sandstone on Oneata, a series of lenses has developed under the ridges. A high-level perched aquifer occurs on the largest of the sandstone ridge possibly associated with fault controls. Storage is significant in this aquifer.

Carbonate aquifers on islands of mixed geology

Springs often issue from the base of the limestone in contact with underlying volcanics. The contact is commonly a seepage zone. Freshwater ponds can occur along the contact (e.g., Vanua Balavu, Nayau, Yacata).

Freshwater wedges occur in wedge aquifers on several islands. The freshwater is bounded by saline water on the coastal side and the volcanic core at the base. Production boreholes at Lomaloma on Vanua Balavu penetrate an aquifer of this type composed of reefal deposits of coarse coral debris. Where the underlying volcanic rocks are permeable, the limestone can form a composite aquifer with the volcanics.

Groundwater discharge on mixed-geology islands, as with the wholly carbonate islands, can be towards the coast, inland, or both, depending on the geomorphology of the island and the existence of central depressions and solution basins. An example of inland discharge of carbonate aquifers on an island of mixed geology is on Nayau, where a high-permeability fault zone leads fresh groundwater from limestone down to an inland freshwater lake. This lake lies in broken limestone country at the base of volcanic outcrops. On Mago, karstic stream discharge can be traced through limestone tunnels to discharge into a semi-enclosed lagoon which, although connected to the sea, is only 30% seawater.

Hot springs occur at or near the coast on two islands of mixed geology, Vanua Balavu and Lakeba. One of those on Lakeba reaches 80°C. The water is salty. The

carbonate rocks only influence the hot springs at or close to the points of emergence, not origin which is generally very much deeper than the carbonate systems.

Carbonate aquifers of coastal flats

Permeability in the young carbonate sands of the coastal flats is often primary, and significant quantities of water can be stored. Saline intrusion is common, but the primary porosity leads to less extensive spread of intrusion than in the karstic limestones. Both freshwater lenses and freshwater wedges occur. Fresh groundwater is often found under beachrock. The carbonate aquifers of the coastal flats are usually recharged by both direct precipitation and lateral flow from the volcanics or limestones that form higher ground inland.

RECHARGE

Recharge values have been estimated from a number of water balances using Penman-type methods. On Nukulau, recharge has been estimated at 1,200–1,400 mm y^{-1} or 40–45% of rainfall; on Vatoa, recharge has been estimated at 600 mm y^{-1} or 30% of rainfall; and on Fulaga, it has been estimated at 95 mm y^{-1} or 5% of rainfall. The wide variation in these values indicates that the methodology used does not yield reliable results for carbonate islands in Fiji. This variation is most likely due to the lack of field data on processes such as interception by vegetation, sheet flow, and recharge by fissure flow.

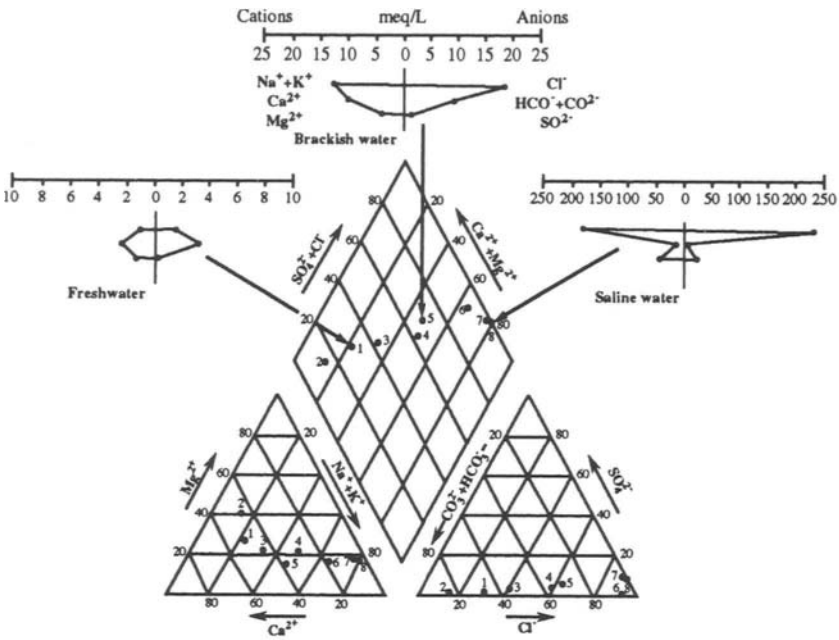
WATER QUALITY

For the purposes of this summary, freshwater is defined as TDS <1,000 mg L^{-1}, brackish water as TDS of 1,000–10,000 mg L^{-1}, and saline as TDS > 10,000 mg L^{-1}.

Major-ion composition

Fig. 26-4 illustrates the major-ion concentrations in waters from several carbonate aquifers. All waters plot along a mixing band on the Piper diagram. The endmembers are fresh, calcium-bicarbonate groundwater and seawater. The lowest TDS is 340 mg L^{-1} for the groundwater-fed lake on Nayau. Groundwaters which plot close to the seawater endmember are saline cave waters, brackish sinkhole wells and brackish and saline hand-dug wells (e.g., the TDS 14,500 mg L^{-1} on Viwa). Groundwaters that plot close to the freshwater endmember are freshwater discharge points (springs, ponds, freshwater lakes) and boreholes. The Stiff diagrams of Fig. 26-4 show the changing proportions of ions along the mixing line.

Although it is not shown on Fig. 26-4, it is important to mention that the major-ion composition is useful for distinguishing groundwaters of carbonate origin from



Sample Number	TDS (mg/L)	Sample Site
1	347	Nayau Lake
2	369	Vanua Balavu Well
3	642	Nayau Spring
4	829	Fulaga Well
5	1873	Oneata Pond
6	3435	Vatoa Sinkhole
7	14694	Viwa Well
8	37445	Viwa Lagoon

Fig. 26-4. Piper and Stiff diagrams for selected carbonate water samples.

those of volcanic origin on the mixed-geology islands. The primary indicator is the Ca^{2+}/Na^{+} ratio.

Salinity

Direct seawater intrusion along faults, macro-fissures and open solution channels (up to several meters wide) is common in the karstic terrain. There seems to be little dispersion around high-permeability zones. Highly saline water (up to 35,000 $\mu S\ cm^{-1}$) can penetrate to the center of an island, yet freshwater lenses can still occur nearby. On Vatulele, for example, two sinkhole wells less than 100 m apart contain water of 34,000 $\mu S\ cm^{-1}$ and 640 $\mu S\ cm^{-1}$, respectively.

Seawater intrusion through the primary porosity is important within less-karstic limestone in coastal carbonate aquifers and carbonate-sand and coral-debris aquifers. However, the distribution of permeabilities and beachrock can still lead to variable salinity distributions even in these nonkarstic aquifers.

Minor salt-spray aerosol contamination of both low-lying and high-elevation carbonate aquifers is common. Cl^- from this route is thought to reach up to 60 mg L^{-1} in fresh groundwater (e.g., at Nayau).

Surge events associated with cyclones and other storms can also cause saline contamination. For example, a storm surge that inundated part of Viwa during Cyclone Nigel in 1985 left residual salinity traces identifiable by electrical-resistivity survey some two years later. Such contamination is of major importance on low-lying sand cays and coastal-flat aquifers.

In all aquifer types, drought periods lead to increased saline intrusion.

Microbiology

Microbiological analyses show that most wells, springs and sinkholes are grossly contaminated with faecal coliform, often in excess of 200 *E. coli* per 100 mL, and greatly exceed WHO Guideline recommendations for water for human consumption in unpiped supply. These results indicate that sanitary borehole and well construction, and source location away from human and animal activities, are essential to ensure good quality potable water.

WATER SUPPLY

As the carbonate islands do not have surface-water resources, islanders rely on rainwater and groundwater for water supply. Commonly, less than 50% of available roof space is used for harvesting rainwater. In tourist resorts, the desire to replicate traditional methods of roofing for resort ambience denies the use of rainwater harvesting as a source of water.

Aquifers in coastal flats located close to population centers are exploited through hand-dug wells. Freshwater and slightly brackish seepage ponds and sinkholes in karstic limestone, and springs at the contact between limestone and volcanic rocks on mixed-geology islands, are also used for water supply. Natural groundwater drained to freshwater lakes is used in the few islands on which these occur. Some highly karstic islands rely entirely on rainwater for potable supply.

Islanders have developed a partial capability to alleviate effects of droughts by such practices as: using brackish ponds, wells and sinkholes for purposes not requiring potable water; rationing water; and drinking green coconut milk. Nonetheless, expensive barging of emergency water supplies from the main islands is common.

Abstraction is commonly by bucket, although several diesel and solar pumps are in operation. There is some evidence that even with the low-volume bucket method of abstraction, the quality of water deteriorates with use.

Although many rapid reconnaissance hydrogeological surveys have been carried out, development by drilling has been restricted because of difficult access and the large expense for small populations. However, investigation and production boreholes have been drilled into carbonate rocks on some of the limestone and mixed-geology islands (e.g., Vanua Balavu, Lakeba, Vatulele, and Viwa), and borehole locations have been identified and marked on the ground in other islands (Ogea,

Fulaga, Kabara, Oneata and Vatoa). Yields of up to 7 L s^{-1} have been obtained for 10-m drawdown, and transmissivity values of 200 m^2 day^{-1} have been derived on Vanua Balavu in coral sand and debris and in limestone arenite aquifers. Saline-guard boreholes have been drilled in association with the Vanua Balavu well fields.

CASE STUDY: RECONNAISSANCE INVESTIGATIONS OF GROUNDWATER LENSES IN LIMESTONE ON VATOA AND ONEATA

In 1992, the Hydrogeology Section of MRD conducted reconnaissance investigations on two carbonate islands with severe water shortages: Vatoa (Fig. 26-5) and Oneata (Fig. 26-6). Both islands are in the Lau Group.

Vatoa has a total land area of 4.45 km^2 and maximum elevation of about 50 m. It is composed entirely of Koroqara Limestone occurring in a series of limestone

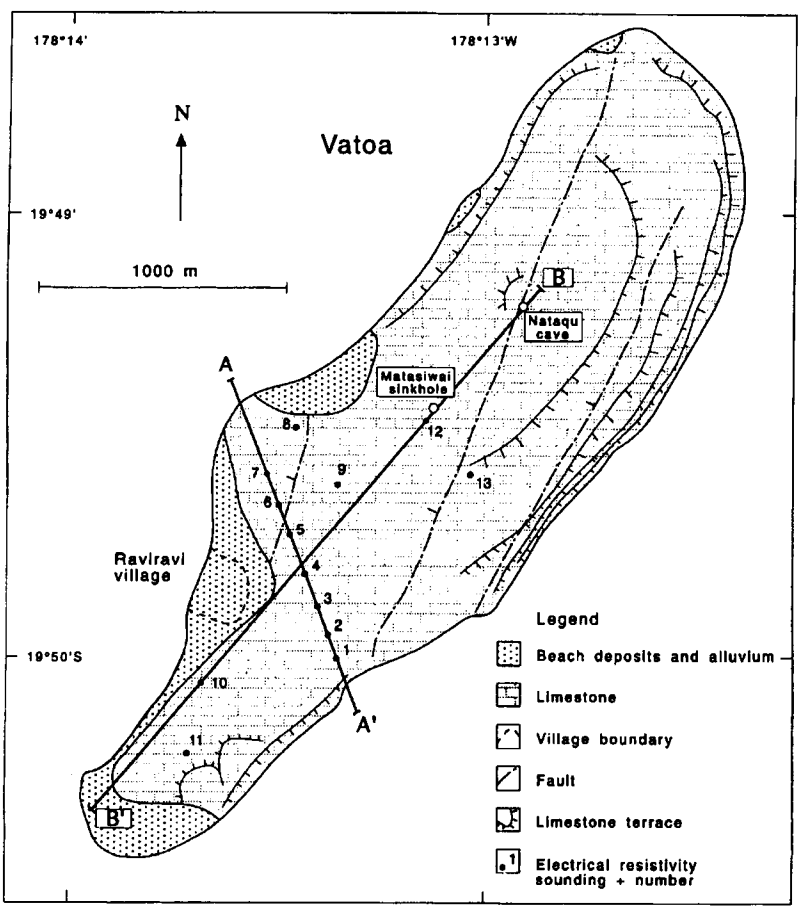


Fig. 26-5. Geological map of Vatoa (Woodhall, 1985a). Hydrogeologic cross sections from DC-resistivity soundings are shown in Fig. 26-7.

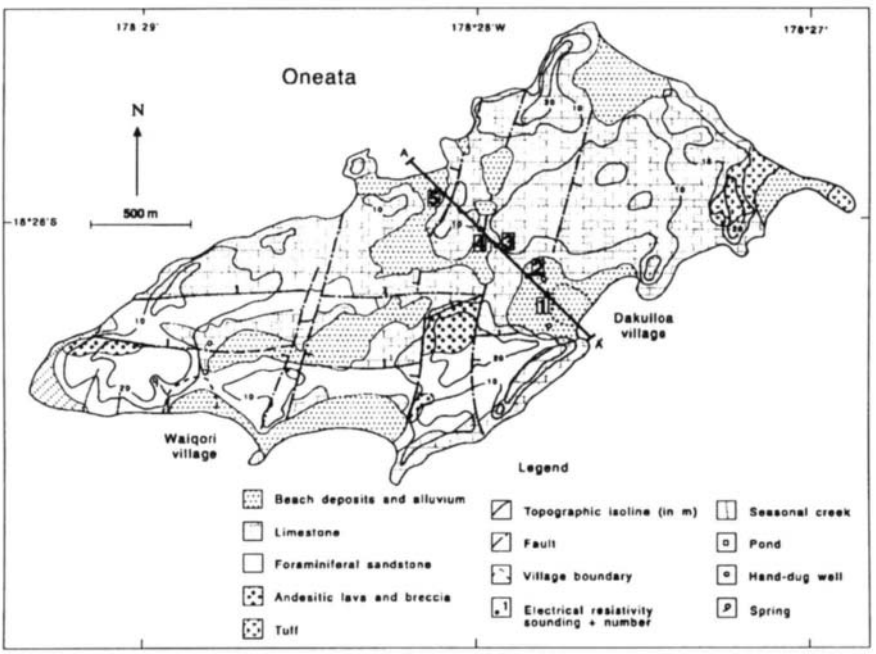


Fig. 26-6. Geological map of Oneata (Woodhall, 1984). Hydrogeological cross section from DC-resistivity soundings is shown in Fig. 26-8.

terraces with solution rims and ridges. Oneata, on the other hand, is a mixed-geology island. The land area is 4 km^2, and the maximum elevation is 49 m. The northern and eastern parts of Oneata consist of karstic Koroqara Limestone in low terraces with higher limestone solution rims along the northern coast. The foraminiferal Waiqori Sandstone is found on the west side of the island. There are coastal plains of carbonate sands on both islands.

All the 283 people of Vatoa (1986 census) live in one village, Raviravi, located on a coastal plain on the southwest side of the island. The two villages Dakuiloa and Waiqori on Oneata, with 86 and 108 people respectively (1986 census), are also situated on coastal plains. Dakuiloa is located adjacent to the limestone on the southeast side of the island.

Groundwater investigations comprising photogeological interpretations, hydrochemical sampling and DC-resistivity soundings were concentrated on areas close to Raviravi on Vatoa and near Dakuiloa on Oneata. The geoelectrical soundings were carried out using the Schlumberger electrode configuration with an ABEM Terrameter SAS 300 transmitter/receiver system. A simple curve-matching program written by MRD staff using the methods of linear filtering described by Ghosh (1972) was used to interpret the data.

There are no creeks or surface-water features on the limestones, and both villages rely almost exclusively on rainwater catchment systems for potable water. In Vatoa, there is a limestone sinkhole, Matasiwai, located 1.5 km from the village. Dakuiloa,

on Oneata, has a nearby well on the coastal plain and a pond on inland alluvium overlying the limestone. All three sources contain brackish water and are used for non-drinking purposes.

Tidal groundwater, 95% seawater, was noted in a cave bottom at a depth of approximately 35 m, at a location 450 m inland, in the center of Vatoa. The seawater probably intruded along a fault.

DC-resistivity survey

MRD has found DC resistivity to be the best geophysical method for mapping fresh- and brackish-water lenses. The method of electromagnetic profiling [e.g.,

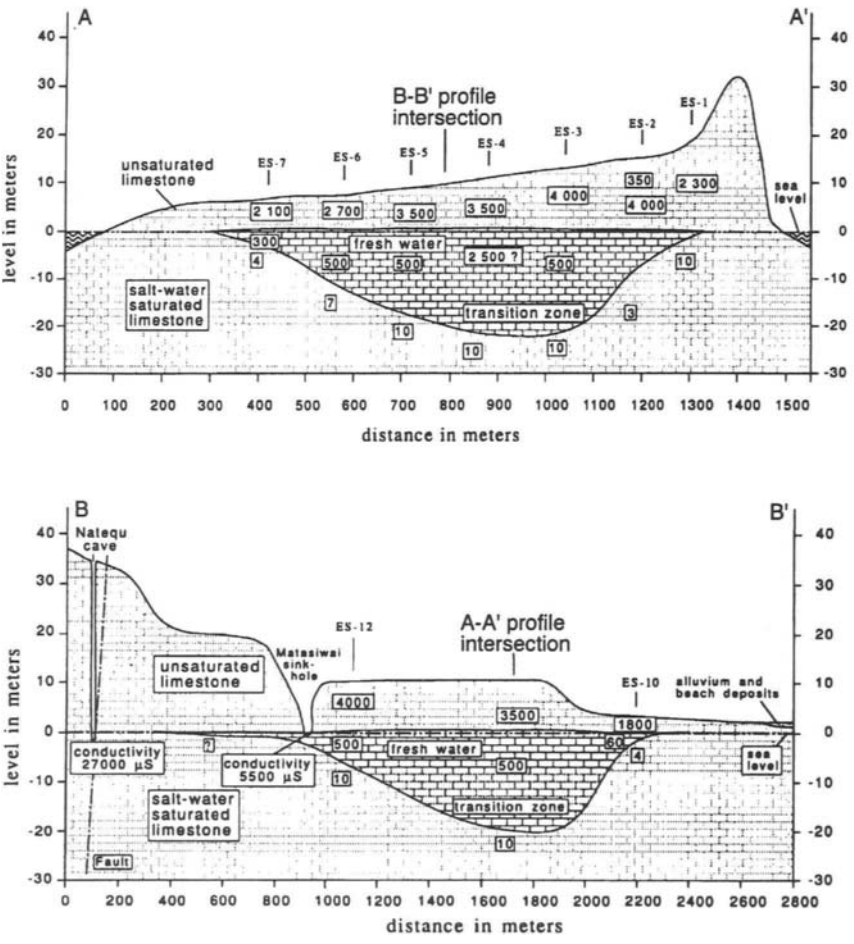


Fig. 26-7. Hydrogeologic cross sections of Vatoa, showing the resistivity of the various layers (in Ω-m) and the interpreted freshwater lens. Locations of the sections and the electrical-sounding sites (ES) are shown in Fig. 26-5.

Chap. 23] cannot be used because the height and relief of the limestone surface produces a variation in the depth to water that overwhelms the signal from the variation in conductivity (Stewart, 1988).

Interpretive DC-resistivity profiles for the two islands are shown in Fig. 26-7 and 26-8. The profiles identify lenticular bodies of presumably fresh to brackish groundwater. On both islands, the lenses occur away from the solution rims. Although the geology is insufficiently known for verification, it is suspected that a finer-grained backreef facies is responsible for the significant groundwater storage. Heads above sea level are less than one meter. Lens thicknesses vary from 18 m beneath the higher elevations of Vatoa to 5 m on lower-lying Oneata.

The sinkhole on the edge of the Vatoa lens and the dug well within the Oneata lens provide water samples for comparison. TDS contents are 4,000 and 3,400 mg L^{-1} respectively. Resistivity soundings close to the sinkhole at Vatoa gave a resistivity of 500 Ω-m, and a sounding in Oneata gave a resistivity of 30 Ω-m close to the well.

The identification of the lenses on Vatoa and Oneata is made on the basis of resistivity readings and comparison with other known resistivities across lenses on limestone islands of Fiji. On Vatoa, it is thought that the lens is fresh and underlain by a brackish transition zone, and on Oneata, that the lens is brackish. Table 26-2 shows the correspondence between observed field values of resistivity of limestone aquifers and equivalent TDS values for the water found in these aquifers. Unsaturated limestone has a very high inherent resistivity compared to other rocks. For the saturated limestone, the TDS is calculated from the resistivity by means of a formula in Jorgensen (1989).

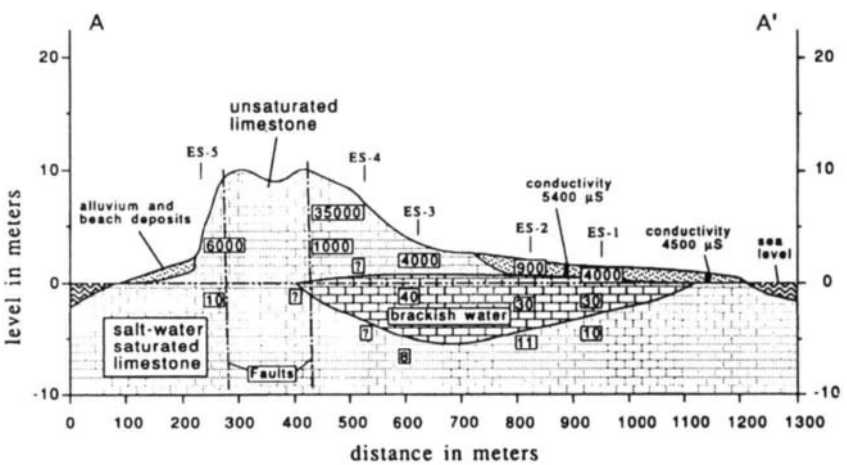


Fig. 26-8. Hydrogeologic cross section of Oneata, showing the resistivity of the various layers (in Ω-m) and the interpreted brackish-water lens. Locations of the section and the electrical-sounding sites (ES) are shown in Fig. 26-6.

Table 26-2

Observed resistivities and related dissolved-solids concentrations for limestone aquifers in Fiji

	Resistivity Ω-m	TDS* (mg L^{-1})
Limestone-unsaturated (dry)	3000–15,000	–
Freshwater-saturated limestone	50–500	130–13
Brackish transition zone	3–30	2200–220
Saltwater-saturated limestone	<3	>2200

*Calculated from 6700/R where R is resistivity in Ω-m at 25°C (Jorgensen, 1989).

Full interpretation of the hydrogeology is limited by the lack of control boreholes to allow sampling of the lenses and accurate definition of the water table. The DC-resistivity survey does establish that a meteoric lens is present.

CONCLUDING REMARKS

The carbonate islands of Fiji are small, remote, scattered, and sparsely inhabited. Drilling has been limited and must be carefully planned. The Hydrogeology Section of the MRD has found the relatively fast and inexpensive groundwater-resources investigations emphasizing DC-resistivity surveys to be very useful. Several boreholes have been drilled with success on small volcanic islands, and borehole sites have been located on several other volcanic and carbonate islands. Drilling is expected to be undertaken in the near future.

ACKNOWLEDGMENTS

This paper is presented with the kind permission of the Director of Mineral Development, Ministry of Lands and Mineral Resources, Fiji. The authors are grateful to Mr. Peter Rodda, Senior Geologist of MRD, for his assistance during the preparation of this paper.

REFERENCES

Auzende, J.-M., Lafoy, Y. and Marsset, B., 1988. Recent geodynamic evolution of the north Fiji basin (southwestern Pacific). Geology, 16: 925–929.

Charvis, P. and Pelletier, B., 1989. The northern New Hebrides back-arc troughs: history and relation with the North Fiji basin. Tectonophys., 170: 259–277.

Clift, P.D., 1994. Controls on the sedimentary and subsidence history of an active plate margin: an example from the Tonga Arc (southwest Pacific). In: J. Hawkins, L. Parson, J. Allan et al., Proc. ODP, Sci. Results, 135. Ocean Drilling Program, College Station TX, pp. 173–188.

Cole, J.W., Graham, I.J. and Gibson, I.L., 1990. Magmatic evolution of Late Cenozoic volcanic rocks of the Lau Ridge, Fiji. Contrib. Mineral. Petrol., 104: 540–554.

Colley, H. and Hindle, W. J., 1984. Volcano-tectonic evolution of Fiji and adjoining marginal basins. In: B.P. Kokelaar and M.F. Howells (Editors), Marginal Basin Geology. Geol. Soc. London, pp. 151–162.

Gale, I.N. and Booth, S.K., 1993. Hydrogeology of Fiji. Fiji Min. Res. Dep. Hydrogeol. Rep. 2, 179 pp +2 multicolored hydrogeological maps scale 1:250,000.

Ghosh, H.S., 1972. Inverse filter coefficients for the computation of apparent resistivity standard curves for a horizontally stratified earth. Geophys. Prospecting, 19, 769–775.

Gill, J.B., 1976. Composition and age of Lau Basin and Ridge volcanic rocks: Implications for evolution of an interac basin and remnant arc. Geol. Soc. Am. Bull., 87: 1384–1395.

Gill, J.B., Stork, A.L., and Whelan, P. M., 1984. Volcanism accompanying back-arc basin development in the southwest Pacific. Tectonophys., 102: 207–224.

Green, D. and Cullen D.J., 1973. The tectonic evolution of the Fiji region. In: P.J. Coleman (Editor), The Western Pacific: Island Arcs, Marginal Seas, Geochemistry. Univ. Western Australia Press, Nedlands, pp. 127–145.

Hawkins, J.W., Parson, L.M., and Allan, J.F., 1994. Introduction to the scientific results of Leg 135: Lau Basin-Tonga Ridge drilling transect. In: J. Hawkins, L. Parson, J. Allan et al., Proc. ODP, Sci. Results, 135. Ocean Drilling Program, College Station, pp. 3–5.

Hoffmeister, J.E. and Ladd, H.S., 1945. Solution effects on elevated limestone terraces. Geol. Soc. Am. Bull., 56: 809–818.

Jorgensen, D.G., 1989. Using geophysical logs to estimate porosity, water resistivity, and intrinsic permeability. U.S. Geol. Surv. Water-Supply Pap. 2321, 24 pp.

Karig, D.E., 1970. Ridges and basins of the Tonga-Kermadec island arc system. J. Geophys. Res., 75: 239–254.

Nunn, P.D., 1987. Late Cenozoic tectonic history of Lau Ridge, southwest Pacific, and associated shoreline displacements: review and analysis. N.Z. J. Geol. Geophys., 30: 241–260.

Nunn, P.D., 1988. Vatulele: A study in the geomorphological development of a Fiji island. Fiji Min. Resour. Dep. Mem. 2, 99 pp.

Nunn, P.D., 1994. Oceanic Islands. Blackwell, Oxford, U.K., 413 pp.

Nunn, P.D., 1995. Emerged shorelines of the Lau Islands. Fiji Min. Resour. Dep. Mem. (in press)

Parson, L.M., Rothwell, R.G., and MacLeod, C.J., 1994. Tectonics and sedimentation in the Lau Basin (southwest Pacific). In: J. Hawkins, L. Parson, J. Allan et al., Proc. ODP, Sci. Results, 135. Ocean Drilling Program, College Station TX, pp. 9–21.

Purdy, E.G., 1974, Reef configurations: Cause and effect. In: L.F. Laporte (Editor), Reefs in Time and Space. Soc. Econ. Paleontol. and Mineral. Spec. Publ. 18, p. 9–76.

Rodda, P. and Kroenke, L.W., 1984. Fiji: a fragmented arc. In: L.W. Kroenke (Editor), Cenozoic Tectonic Development of the Southwest Pacific: CCOP/SOPAX Tech. Bull., 6: 86–108.

Stewart, M., 1988. Electromagnetic mapping of fresh-water Lenses on small oceanic islands. Ground Water, 26: 187–191.

Woodhall, D., 1984. Geology of Vanau Vatu, Nayau, Lakeba, Reid Reef, Moce and Karoni, Aiwa, Oneata, Komo, Olorua and Bukatatanoa Reef. [Multicoloured map, scale 1:25,000] Fiji Min. Resour. Dep., Suva.

Woodhall, D., 1985a. Geology of Namuka, Yagasa, Fulaga, Kabara, Tavu-nasici, Marabo, Vuaqava, Vatoa, Naievo, Tuvana-i-colo, Tuvana-i-ra, Ono-i-Lau and Ogea. [Multicoloured map, scale 1:25,000] Fiji Min. Resour. Dep., Suva.

Woodhall, D., 1985b. Geology of the Lau Ridge. In: D.W. Scholl and T.L. Vallier (Editors), Geology and Offshore Resources of Pacific Island Arcs-Tonga region. Circum-Pacific Counc. Energy & Mineral Resour., Houston TX. Earth Sci. Ser. 2, pp. 351–378.

Woodhall, D. in prep. Geology of the Lau Group, Fiji Min. Resour. Dep. Bull. 9.

This Page Intentionally Left Blank

Geology and Hydrogeology of Carbonate Islands. Developments in Sedimentology 54
edited by H.L. Vacher and T. Quinn
© 1997 Elsevier Science B.V. All rights reserved.

Chapter 27

GEOLOGY AND HYDROGEOLOGY OF ROTTNEST ISLAND, WESTERN AUSTRALIA

PHILLIP E. PLAYFORD

INTRODUCTION

Rottnest is the largest island in a chain of limestone islands and shoals, including Garden, Carnac, and Penguin Islands, and Five Fathom Bank, on the shallow continental shelf opposite Perth in Western Australia (Fig. 27-1). The island is about 10.5 km long and up to 4.5 km wide, covers about 1900 ha, and is situated some 18 km from the mainland coast. The highest point, Wadjemup Hill, is 45 m above sea level. About 10% of the interior of the island is occupied by a chain of salt lakes (Fig. 27-2).

Rottnest Island was originally given the name *Eÿlandt Rottenest*, meaning "Rats' Nest Island", by the Dutch navigator Willem de Vlamingh in 1696 (Schilder, 1985). It was so named because of the abundance of a rat-like marsupial, the quokka, which still abounds there. Rottnest was known to the Aborigines of the Perth area as *Wadjemup*, although they no longer visited there after the island separated from the mainland some 6,500 years ago.

In 1839, ten years after the British established the colony of Western Australia, Rottnest became a prison for Aboriginal convicts, and it was used for this purpose for some 70 years. When the prison closed, Rottnest became a holiday resort, and as such it has become legendary among Western Australians. The island is also of considerable scientific interest to biologists and geologists (Bradshaw, 1983). A research station is available for the use of scientists working on the island and its surrounding marine environment.

The first detailed work on the geology of Rottnest, focusing especially on evidence of Quaternary sea-level changes, was carried out by staff and students of the University of Western Australia (Teichert, 1950; Fairbridge, 1953; Glenister et al., 1959; Hassell and Kneebone, 1960). My own research on the island began during holiday visits, and continued on behalf of the Geological Survey of Western Australia from 1976, initially as part of an investigation into the island's groundwater potential (Playford, 1976, 1983; Playford and Leech, 1977). Further research results were published in a guidebook (Playford, 1988), which was produced primarily for local use and distribution. Data from that guidebook are used freely in this chapter and are supplemented by the results of subsequent research.

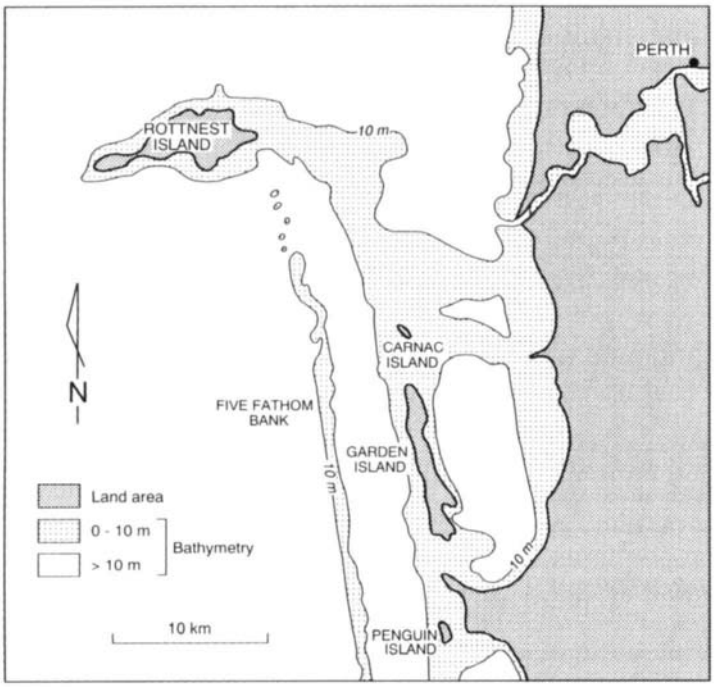


Fig. 27-1. Locality map showing the offshore bathymetry and relationship of Rottnest Island to the chain of islands and reefs opposite Perth, Western Australia. (This and other figures are selected from the guidebook by Playford, 1988.)

GEOGRAPHIC SETTING AND MARINE ENVIRONMENT

The climate of Rottnest is mediterranean, characterised by wet winters and very dry summers. Of the annual rainfall (average 720 mm), nearly 75% falls in the winter months (May–August), and only 5% falls in the summer (November–February). Annual evaporation is about 1,500 mm. The island has no significant watercourses, and much of the rainfall is absorbed through the surface sand.

Native forest of tea tree, Rottnest Island pine, and wattle once covered some 65% of the island. By 1941 this coverage had been reduced to 23%, and today it is down to about 5%, with an additional 6% of reforested areas (Pen and Green, 1983; Playford, 1988). The rest of the island is covered by low grassy heath. The forest decline resulted from human activities, primarily a combination of uncontrolled bush fires and widespread wood-cutting for fuel. An active program of reforestation is now in progress, associated with other measures designed to ensure adequate environmental management of the island.

There were once eight brackish-water swamps on the island. All except three of these were excavated for road-building marl prior to the mid-1970s, thereby converting them into hypersaline pools and largely eliminating the swamp biotas

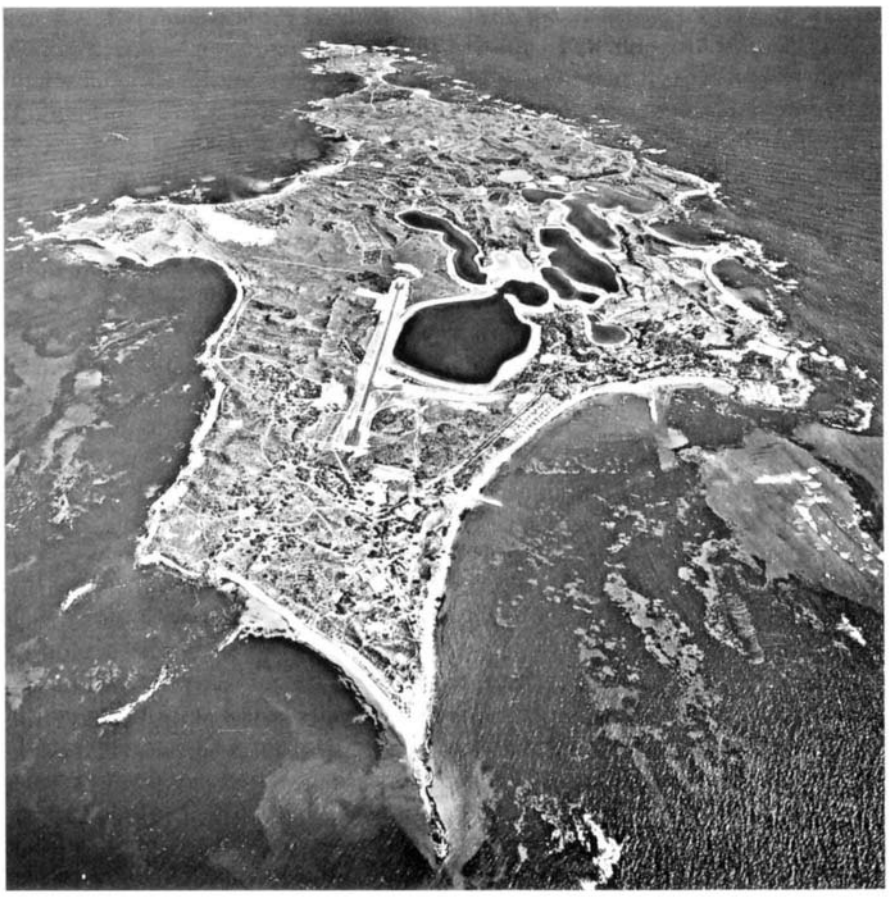


Fig. 27-2. Aerial view looking west over Rottnest Island. Note the prominent salt lakes in the centre of the island.

(Edward, 1983). In this chapter, water with salinity up to about 2,000 mg L^{-1}, which is suitable for drinking by most animals, is referred to as "brackish water"; "potable water" refers to water suitable for human consumption and has a salinity less than 1,000 mg L^{-1}

The tide level along this part of the Western Australian coast is strongly influenced by air pressure, water temperature, and the prevailing winds (Hodgkin and Di Lollo, 1958; Playford, 1990). Highest tides are associated with low-pressure systems, and vice versa. The daily tidal range at Rottnest normally does not exceed 1 m, and the extreme range is about 1.5 m.

The prevailing wave swell is from the southwest, and waves are strongly refracted around the island (Gozzard, 1990). Water temperatures are increased significantly in autumn and winter by the southward-flowing Leeuwin Current, which brings warm tropical water from the north over the continental slope and outer shelf. As a result,

the waters around Rottnest are significantly warmer (up to 3°C) than those beside the mainland coast during autumn and winter (Pearce and Cresswell, 1983; Pearce and Walker, 1991).

GEOMORPHOLOGY

General

The coastline of Rottnest Island is characterised by alternating rocky headlands and bays, with sandy beaches backed by dunes (Figs. 27-2–27-4). Much of the coast is fringed by shallow shoreline platforms (colloquially termed "reefs") cut in Pleistocene to early Holocene dune limestone (eolianite) of the Tamala Limestone (Fig. 27-4). This limestone underlies most of the island. It is prominently exposed on the headlands and is largely covered in the interior by a veneer of residual or wind-blown sand. The topography of the island interior is undulating, reflecting the original dune morphology of the Tamala Limestone, subdued by Holocene erosion.

Salt lakes

The salt lakes have elongate-ovoid to subcircular shapes (Hodgkin, 1959) (Fig. 27-2), and the deepest, Government House Lake (Fig. 27-3), is up to 8.5 m deep. The lakes are believed to be partly filled remnants of "blue holes", controlled by karst topography of the type developed in reefal platforms throughout the world during Pleistocene sea-level lowstands (Purdy, 1974). The lakes closely resemble the shapes and dimensions of the extensive networks of blue holes that characterise the Houtman Abrolhos reefs, 450 km to the north (Playford et al., 1976; Playford 1988; Collins et al., 1991, Collins et al., 1993) [see also Chap. 28].

Water levels in the lakes rise to about mean sea level in winter as a result of rainfall intake, and fall more than a metre in summer through evaporation. Impervious algal-cyanobacterial mats and muddy sediments act as seals on the floors of the lakes and prevent the inflow of groundwater from below. The larger lakes commonly have late-summer salinities exceeding 150,000 mg L^{-1} (Playford, 1977). Some of the smaller lakes dry out completely by the end of summer, leaving a halite crust, which was once exploited commercially as a source of common salt (Playford, 1988).

Very high salinities are maintained in the lakes, even though some are separated from the ocean by only narrow strips of limestone or sand, as little as 100 m wide. During summer, small seepages of seawater can be observed entering the lakes beside the narrow coastal strips, and brackish-water springs are fed by adjoining groundwater mounds. Clearly, the extreme evaporation during summer far exceeds the influx of water from these sources.

The three deeper lakes (Serpentine, Government House, and Herschell) (Fig. 27-3) become meromictic ("hot lakes") during winter and spring. Water below

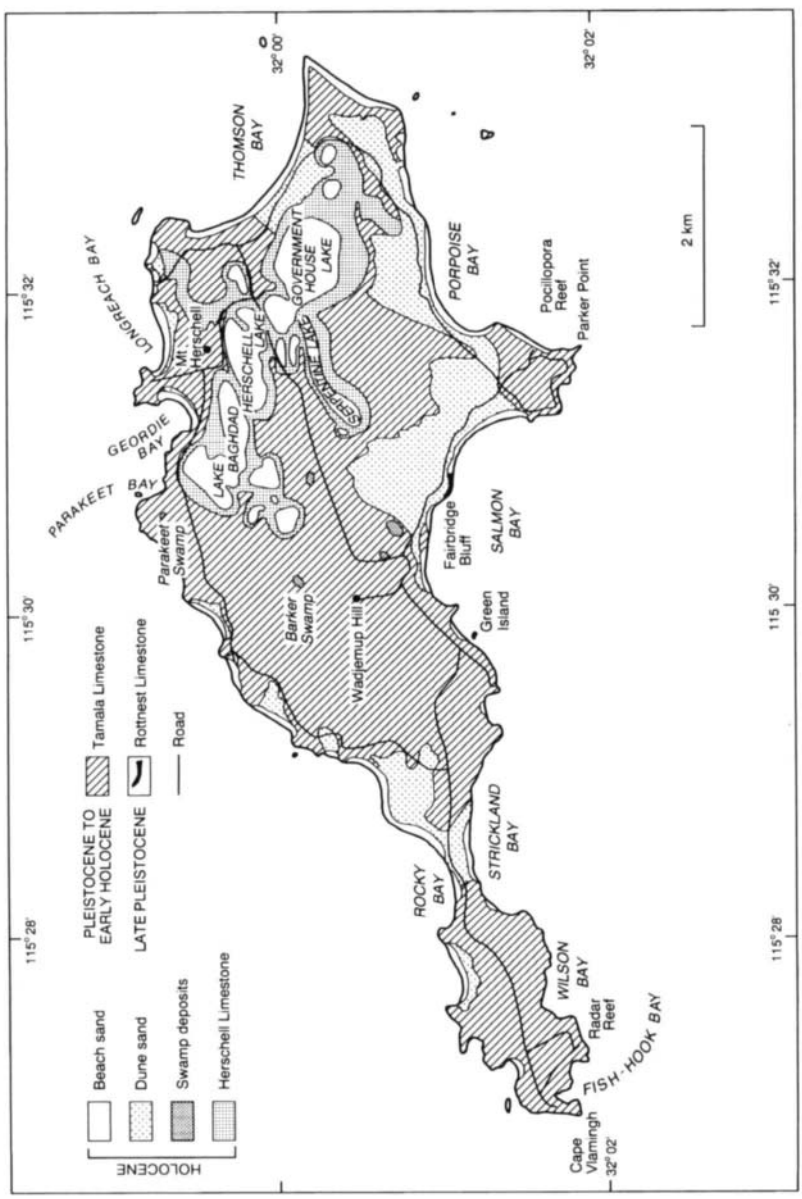


Fig. 27-3. Simplified geological map of Rottnest Island.



Fig. 27-4. View looking east over The Basin, a popular swimming place, during very low tide. Note the well-developed shoreline platform, rocky headlands, beaches, and sand dunes.

the thermocline is up to 10°C warmer than that at the surface (Bunn and Edward, 1984). The stratification responsible for meromixis is caused by a layer of less-saline water originating from rainfall and springs spreading over the heavier hypersaline water. This stratification is destroyed by evaporation and wind action during early summer, and is not re-established until the following winter.

Shoreline features

Shoreline platforms which fringe most of the island range from a few metres to about 200 m in width (Figs. 27-4–27-6). They are cut almost horizontally into dune limestone of the Tamala Limestone and Last Interglacial reef limestone of the Rottnest Limestone, and at measured localities range from 0.18 to 0.56 m below mean sea level (Playford, 1988). The highest platforms occur where wave action is strongest. The mean elevation is −0.41 m, which is about 0.2 m below mean low-water level. A platform at this elevation would be exposed for about 3% of the time each year (Playford, 1988).

The platforms normally meet limestone headlands and cliffs at shoreline notches, 1–2.5 m high and 1–2 m deep, below overhanging visors. Where a platform meets a cliff there is commonly a narrow storm bench immediately above the shoreline notch and visor, about 2–4 m above mean sea level (Figs. 27-5, 27-6).

A thin zone of the limestone below each shoreline platform is strongly indurated, apparently because of marine cementation (Fig. 27-6). Each shoreline notch and visor is also well cemented, although generally to a lesser extent than the platforms. This cementation apparently results from alternate wetting and drying of the



Fig. 27-5. View of the western side of Fish-hook Bay, showing the shoreline platform, notch, and visor, and a well-developed storm bench above the visor.

limestone through tide action and wave splash. The dune limestone above the reach of normal wave splash is much less indurated. Storm waves preferentially erode this softer limestone, forming storm benches above the indurated zone. Because waves splash higher on the headlands than in the bays, the storm benches are not horizontal; they slope conspicuously away from the headlands and become progressively lower in elevation as they pass back into the bays (Playford, 1988).

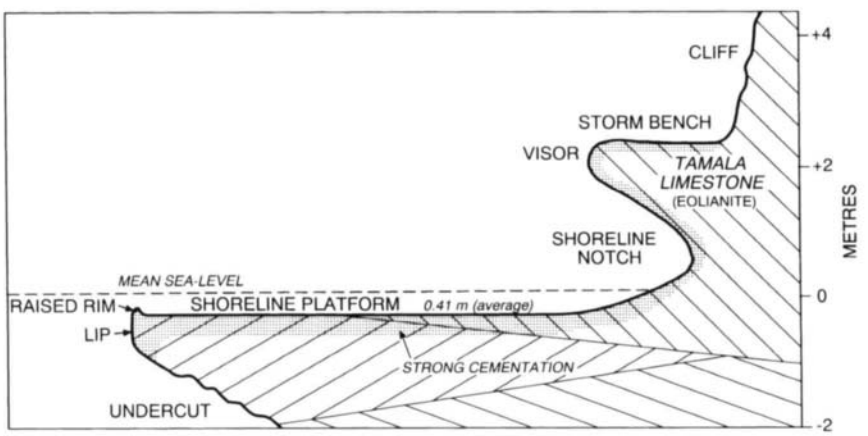


Fig. 27-6. Diagrammatic cross section illustrating shoreline platforms and associated features developed around the coastline of Rottnest Island.

Similarly, the limestone underneath the indurated surface layer of the shoreline platforms is less strongly cemented. As a result, the platforms are commonly undercut where this softer limestone is eroded by wave action and boring organisms. The undercutting results in the collapse of parts of platforms in some areas.

The outer edge of each platform commonly has a raised rim of limestone, several centimetres high and as much as 10–15 cm wide. These raised rims are erosional in origin, as they are composed of the same eolianite as the rest of the platforms, although some are coated with a thin crust of the coralline alga *Lithothamnion*. They may form because the rim is the most strongly cemented part of the platform, and is, therefore, more resistant to erosion, "lagging behind" as the rest of the platform is progressively lowered.

Spectacular stepped terraces, termed "paddy-field terraces", are conspicuous features of the outer platforms in a few places (Fig. 27-7). They extend through a vertical range of as much as 70 cm above the general platform level. The terraces are cut into eolianite like the rest of the platforms, and they are clearly erosional rather than constructional features (Playford, 1988). Each terrace has its own raised rim, and water from breaking waves cascades down from one terrace to another, leaving a thin layer of water dammed behind each rim. The terraces represent progressive stages in the downward erosion of platforms, but the origin of their remarkable morphology has yet to be explained.

Algal polygons, defined by "hedgerows" of brown macroalgae (*Sargassum*), are conspicuous features of many platforms during spring (Fig. 27-8). They are submerged other than during exceptionally low tides, and extend to maximum water



Fig. 27-7. Paddy-field terraces on the shoreline platform at Wilson Bay, cut in dune limestone of the Tamala Limestone. Each terrace has a raised rim, and water cascades from one to another, over a total vertical height of about 0.7 m.

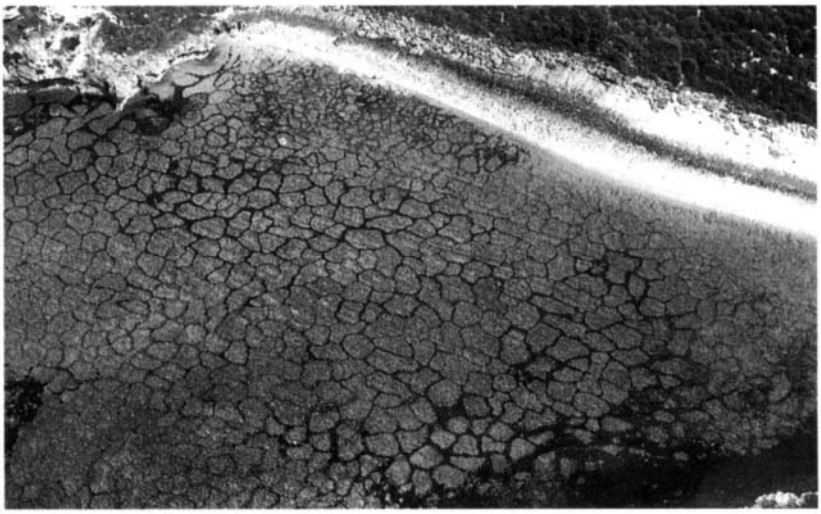


Fig. 27-8. Aerial view of the Radar Reef shoreline platform, taken from an elevation of about 200 m in November 1991, showing algal polygons defined by "hedgerows" of brown macroalgae, in water depths of about 0.4 m below mean sea level. Each polygon defines the territory of a Western Buffalo Bream (a kyphosid fish) and covers an area of about 12 m^2.

depths of 1.5 m. The average area covered by each polygon is about 12 m^2 and the width of the brown algal "hedgerow" borders is 10–35 cm. The polygons fade or disappear in summer. They reappear in spring, with their shapes almost unchanged.

Until recently, biologists studying the platforms had noted but not documented these polygons in the expectation that they were controlled by the underlying geology. However, my observations showed that the polygons are not linked with any jointing or other geological features of the limestone, despite their superficial resemblance to shrinkage cracks (Playford, 1988). It has now been shown that each polygon defines the territory of an individual kyphosid fish, the Western Buffalo Bream (*Kyphosus cornelii*) (Berry and Playford, 1992). Each fish grazes on algae within its territory, up to the polygonal "hedgerow" that the fish maintains to separate its territory from that of its neighbours. The grazing activities of these fish are believed to be very important in maintaining the ecological balance between various algae on shoreline platforms in many areas of southwestern Australia, as far north as the Houtman Abrolhos. The Western Buffalo Bream is not sought after for human consumption so that its role in maintaining the ecological balance has not been affected by fishing activities.

Limestone crusts precipitated by the coralline alga *Lithothamnion* coat the shoreline platforms in some areas, while rhodoliths of *Neogoniolithon*? *darwinii* are very abundant near Green Island, filling small depressions on the platform surface. The sub-spherical rhodoliths can be seen to whirl around rapidly with each passing wave (Playford, 1988).

Hermatypic corals grow on the platforms in many places, although generally only as scattered colonies. A well-developed coral reef occurs at one locality, Pocillopora Reef, near Parker Point. The coral fauna of this reef comprises some 22 hermatypic species, dominated by *Pocillopora damicornis* (L.M. Marsh, in Playford, 1988). It is notable that *Acropora* is very rare in the waters around Rottnest Island today, in contrast to its abundance in the Last Interglacial coral reef exposed on the island, and in the modern coral reefs of the Houtman Abrolhos, 350 km to the north (Playford, 1988). The reason for the paucity of *Acropora* around the island today has yet to be fully explained. Water temperatures around the island are only slightly below those of the Houtman Abrolhos, where *Acropora* is abundant (Hatcher, 1991).

The processes of erosion that form the shoreline platforms and their associated notches and paddy-field terraces are not yet well understood. It is thought that they result from a combination of chemical corrosion by seawater, bioerosion by marine organisms, and mechanical erosion by wave action. Such mechanisms have been discussed by Fairbridge (1952), Revelle and Fairbridge (1957), Hodgkin (1964, 1970), Black and Johnson (1983), and Semeniuk and Johnson (1985).

It is clear that molluscs play an important role in eroding the shoreline platforms and notches. Limpets, other gastropods, and chitons actively abrade the limestone with their radulae while scraping away the algae on which they feed. Other boring organisms that erode limestone on the platforms include regular echinoids, bivalves, and clionid sponges (Playford, 1988).

Measurements on the rate of bioerosion by molluscs were carried out nearby by Hodgkin (1964). He showed that the notch adjoining the shoreline platform at Point Peron, 40 km south of Perth, was retreating at about 1 mm y^{-1}, and he suggested that this rate applied generally to similar notches elsewhere. However, if bioerosion at such a rate were the only agent involved in platform development, about 200 ky would be needed to form the widest platform at Rottnest (which is nearly 200 m wide), yet sea level has been at or near its present level at the island for only about 6 ky. Clearly, some other agent of erosion must be even more important in platform development, and I believe that dissolution of calcium carbonate under intertidal conditions, resulting from changes in the pH, CO_2 content, and temperature of thin films of seawater, is a possible explanation.

As previously noted, the highest platforms are at localities where there is strong wave action, and vice versa. When the tide level is low, a platform in an area that is not subject to strong wave action will be covered by a thin layer of static water, dammed behind the raised rim, whereas under the same tide conditions, another platform in a more exposed location may be repeatedly covered by wave swash. It seems likely that a thin static layer of water under low-tide conditions facilitates the dissolution of limestone and lowering of platforms. Such a layer may absorb higher levels of CO_2 from the atmosphere, with consequent reduction in pH.

However, it is also necessary to explain the strong induration that occurs due to cement precipitation below the platform surfaces. Clearly, there is a need for detailed research to unravel the processes involved in carbonate/bicarbonate solution and precipitation on these limestone platforms.

A conspicuous feature of the rocky surface of most headlands on the island is the occurrence of masses of weathered operculae and nacreous shell fragments of the gastropod *Turbo intercostalis* and a few other shells. It is clear that these weathered shell accumulations formed long ago; operculae from two localities (Salmon Point and Kitson Point) have been radiocarbon dated (by Peter Thorpe of the Geological Survey of Western Australia) as 1100 ± 250 and 1800 ± 150 y B.P. Elsewhere in coastal areas of Western Australia (north of Rottnest) the Pacific Gull has been observed picking up living shells from shoreline platforms and dropping them from considerable heights on to the rocks, in order to break them open and extract the contained flesh (Teichert and Serventy, 1947). This gull no longer frequents Rottnest, and it seems probable that it was responsible for forming the shell accumulations many hundreds of years ago, long before European settlement in southwestern Australia.

STRATIGRAPHY

Rottnest Island is situated over the Vlamingh Sub-basin of the Perth Basin, a deep downwarp containing up to 15,000 m of Cenozoic, Mesozoic, and Palaeozoic deposits, including a very thick (up to 11,000 m) Cretaceous section (Playford et al., 1976). The structure of the sub-basin is characterised by normal faulting, most of which ceased during the Early Cretaceous following the continental breakup of Gondwanaland in this area. Some faults, however, were active to a small extent after the Early Cretaceous, and possibly as late as the Tertiary. Conceivably, some moved during the Quaternary, although there is no definitive evidence of this, and the area has been seismically quiescent in historic times.

Holocene sedimentation on the Rottnest Shelf, the continental shelf adjoining the island, is described by Collins (1988). He reported only a thin (< 1 m) blanket of Holocene skeletal lime sands overlying Pleistocene limestones over most of this shelf.

Rocks exposed on Rottnest Island are entirely of late Quaternary age. The most widespread unit is a late Pleistocene to early Holocene eolianite (Tamala Limestone), with a thin intercalation of a Last Interglacial coral reef (Rottnest Limestone). The youngest units are middle to late Holocene shell beds (Herschell Limestone), dune sands, swamp deposits, and lake deposits (Fig. 27-3).

Tamala Limestone

The Tamala Limestone is a unit of eolianite composed of abraded shell fragments (mainly molluscan) with variable amounts of quartz sand (up to a maximum of about 50% in some areas, but generally less than 20%). The Tamala Limestone is characterised by large-scale eolian cross-bedding (Fig. 27-9). The formation is widespread in the coastal belt and adjoining islands of the southwestern part of Western Australia, from Shark Bay to the south coast. It was originally known as the "Coastal Limestone" (e.g., Fairbridge, 1953, Fairbridge and Teichert, 1953) and was renamed as the "Tamala Eolianite" (Logan et al., 1970) and Tamala Limestone



Fig. 27-9. Tamala Limestone on the north shore of Salmon Bay, showing well-developed eolian cross-bedding.

(Playford et al., 1976). No detailed studies have yet been carried out to identify and date dune-building and calcrete-forming episodes in the Tamala Limestone, either at Rottnest Island or elsewhere.

The Tamala Limestone accumulated as coastal sand dunes, mostly during periods of lowered sea level during the Pleistocene and early Holocene, when wide areas of the continental shelf were exposed, and carbonate productivity was high. This is shown by the fact that the dune limestones extend well below modern sea level along the coast from Shark Bay to the south coast of Western Australia, and the dunes themselves were much higher than those forming today. It is clear that the prevailing southerly to southwesterly winds were considerably stronger during the glacial periods, so that Pleistocene dunes in the Shark Bay area were up to 300 m high (Playford et al., 1976, Playford, 1990).

In the subsurface, the Tamala Limestone consists largely of weakly cemented lime sand with lesser amounts of quartz sand and constitutes the main aquifer on the island. Over most of the interior of the island, the formation weathers to quartz-rich sandy soil. Hard calcrete horizons, which are prominent in some coastal exposures, are normally underlain by softer limestones with abundant rhizoliths and may be overlain by grey to brown fossil soils. These fossil soils and calcretes, which mark periods of local interruption in dune building, are thought to have formed during humid periods of the Pleistocene (Semeniuk, 1986).

The rhizolith horizons commonly include conspicuous vertical cylindrical bodies known colloquially as "solution pipes", but better termed "root pipes", as they can be shown to have formed around the tap roots of large trees, presumably eucalypts. Commonly 10–50 cm in diameter, they each consist of an outer casing of strongly

cemented dune limestone around a softer core that was once occupied by a tree root. The core is commonly now filled with calcareous soil or breccia that entered after the original root decayed. However, some pipes still contain calcified fossil roots (Playford, 1988, Figs. 34, 35).

In the Rottnest area, the Tamala Limestone is probably up to 150 m thick and includes a section at least 70 m below sea level that overlies older Pleistocene and Tertiary sands. Most of the exposed formation is believed to be younger than the Rottnest Limestone coral reef, which formed at about 130 ka (Szabo, 1979). Part of the Tamala Limestone near Fairbridge Bluff, however, underlies the reef, and must have formed a little earlier, perhaps at about 135–140 ka. The youngest part of the formation accumulated during the early Holocene transgression. Its contact with overlying modern dune sands is transitional, as gradual cementation of those sands is progressing below the surface.

Rottnest Limestone

The Rottnest Limestone (Fairbridge, 1953) is a late Pleistocene unit of coral-reef limestone and associated shelly limestone that is exposed for about 150 m along the coast at Fairbridge Bluff. I named this important locality Fairbridge Bluff in honour of Rhodes W. Fairbridge, in recognition of his major contributions to knowledge of the Quaternary geology of Western Australia.

The Rottnest Limestone at the type locality is overlain and underlain by Tamala Limestone, and regionally it represents a marine tongue intercalated in that formation. The exposed thickness of the Rottnest Limestone is 3.2 m, but its full thickness must be more than this, as the lowest part disappears below sea level on the erosional contact with the underlying Tamala Limestone. The Rottnest Limestone has been dated by uranium/thorium methods at 132 ± 5 ka (Szabo, 1979). Sea level at that time must have been at least 3.2 m higher relative to Rottnest than at present.

Branching (staghorn) and platy species of *Acropora* predominate in the reef (Fig. 27-10), and there are also colonies of several other genera, of which *Goniastrea* is the most conspicuous (L.M. Marsh, in Playford, 1988). Shelly (gastropod-rich) calcarenites are associated with the reef. Most corals and shells are strongly encrusted by coralline algae, which constitute an important binding element of the reef.

Herschell Limestone

The Herschell Limestone (Playford, 1977) is exposed around margins of the salt lakes. It is a unit of middle to late Holocene marine shell beds with interbedded lime sand that varies from friable to strongly cemented. The formation overlies and abuts the Tamala Limestone and, in various areas, interfingers with dune sand or is overlain by salt-lake or swamp deposits. The unit is at least 2.5 m thick. It is believed to have been deposited in subtidal to intertidal environments, when the present salt lakes were lagoonal arms of the sea and relative sea level was as much as 2.4 m higher than today.

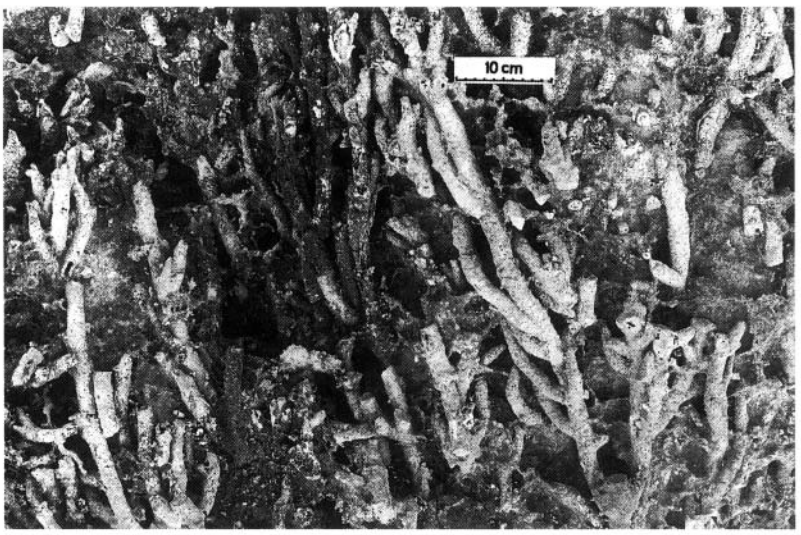


Fig. 27-10. Staghorn coral (*Acropora* sp.) coated by coralline algae, in the Last Interglacial coral reef (Rottnest Limestone) at Fairbridge Bluff.

The formation contains a very rich molluscan fauna (Fig. 27-11). G.W. Kendrick (in Playford, 1988) has recorded 223 species in the formation. The fauna is mostly gastropods and bivalves, but there are also numbers of chitons, scaphopods, arthropods, echinoderms, fish, foraminifers, corals, and polychaetes.None of the



Fig. 27-11. Shelly limestone of the Vincent Member of the Herschell Limestone, showing undisturbed paired valves (mainly *Katelysia rhytiphora)* and randomly oriented single valves, indicating subtidal deposition below effective wave base.

species are extinct, but Kendrick records that 12 are not known in the waters around Rottnest today. The affinities of half of these are northern-tropical, while the others are southern-temperate.

The Herschell Limestone is divided into two members: the lower Vincent Member and upper Baghdad Member. The Vincent Member consists of unbedded or crudely bedded bivalve-gastropod coquina and coquinite, with lesser amounts of fossiliferous calcarenite, and is at least 1.2 m thick. Radiocarbon dating indicates that the unit was deposited between 5900 and 4800 y B.P. (Playford, 1988). In the type section of the member, exposed in a quarry near Mt. Herschell, the diverse fauna is dominated by bivalves. Many of them occur as closed pairs (Fig. 27-11), and single valves show no sign of current orientation. Thus, the member at this locality was deposited in quiet-water conditions, below effective wave base.

The Baghdad Member is the upper unit of the Herschell Limestone. It consists of bedded bivalve-gastropod coquina and coquinite, with interbedded shelly calcarenites, and has been radiocarbon dated as 3100 to 2200 y B.P. (Playford, 1988). The fauna is less diverse than that of the Vincent Member. Bivalves are abundant and are usually present as single valves, laid down convex upward (Fig. 27-12). Much of the member was deposited above wave base, probably as a beach deposit in the upper intertidal zone.

Other Holocene deposits

Beach and dune sand. Late Holocene to modern beach and dune sands occur in various parts of the island. The sands are composed of rounded shell fragments with



Fig. 27-12. Shelly limestone of the Baghdad Member of the Herschell Limestone, showing very abundant single valves of *Katelysia scalarina*, oriented convex upwards (as a result of wave action), and believed to have been laid down as a beach deposit.

variable amounts of quartz sand. Modern dunes are up to 35 m high, but they generally form only a thin veneer over Tamala Limestone.

Swamp deposits. Holocene swamp deposits on the island consist of thin layers of limestone, lime sand, marl, peat, and algal sediments. They are described by Hassell and Kneebone (1960) and Backhouse (1993). The maximum thickness of swamp sediments ranges from 2.6 m in Salmon and Parakeet Swamps to 4.4 m in Barker Swamp.

Backhouse (1993) studied the palynology of a core taken below Barker Swamp. This study showed that just prior to separation of Rottnest as an island, between 7500 and 6600 y B.P., peat was deposited at this site in an open lake surrounded by sedges and low forest of Rottnest Island pine, with nearby eucalypt woodland. Thin charcoal-rich layers above the peat record fires that largely destroyed the pine forest, and caused other elements of the flora to decline. There is evidence of increased aridity and sparser vegetation at the Barker Swamp site at about 5300 y B.P., when Rottnest consisted of several islands. A large increase in charcoal in the near-surface sediments indicates man-induced bushfires and the beginning of European settlement.

Salt-lake deposits. Modern salt-lake deposits consist of algal, cyanobacterial, and evaporitic (gypsiferous) sediments. These sediments form veneers on the floors of the salt lakes and around their margins, and overlie the Herschell and Tamala Limestones.

Edward (1983) recorded benthic microbial mats on the floors of the lakes. The mats are formed by green algae, cyanobacteria, and diatoms. At some localities these mats form undulous to columnar stromatolites, up to 20 cm high, notably on the north side of Government House Lake in summer water depths of about 0.2 m to 3 m. Playford (1988) estimated that these stromatolites grow at rates of up to 1.5 mm y^{-1}.

Tepee structures are well developed around the margins of the salt lakes and form conspicuous polygonal and rectilinear shapes or simple linear ridges in indurated algal-cyanobacterial limestones. The tepee structures have apparently formed as a result of expansion associated with precipitation of evaporite minerals. Research is required on these structures to document their origin and diagenesis.

SEA-LEVEL HISTORY

The most striking feature of the geology of Rottnest Island is the clear evidence of Quaternary sea-level changes (Teichert, 1950; Churchill, 1959; Fairbridge, 1958, 1961; Hassell and Kneebone, 1960; Playford, 1977, 1983, 1988). This evidence is in the form of elevated marine deposits, elevated shoreline platforms and notches, and subaerially formed features that now extend below sea level. Curves illustrating Quaternary sea-level changes that have affected Rottnest Island are shown in Figures 27-13 and 27-14.

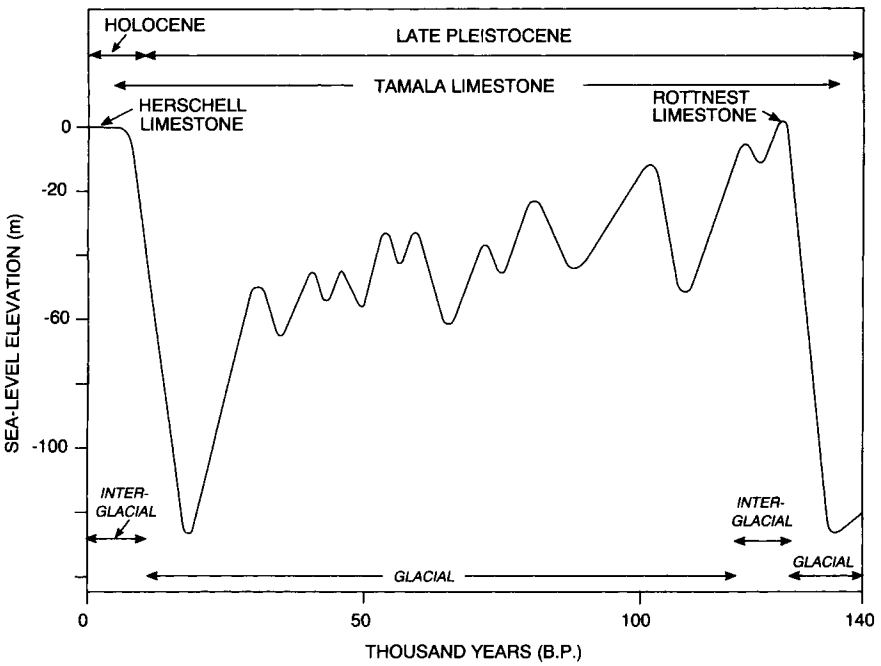


Fig. 27-13. Global eustatic sea-level curve for the past 140 ky, modified after Chappell and Shackleton (1986), shown in relation to deposition of the Rottnest, Tamala, and Herschell Limestones.

Elevated marine deposits

The fossil coral reef of the Rottnest Limestone extends to 3.02 m above the adjoining shoreline platform. Consequently it seems that sea level relative to the island during the Last Interglacial was at least this amount higher than it is today. However, the sea may have reached higher than this, as the upper surface of the reef is eroded, and the thickness lost by erosion is unknown. Moreover, the reef as now exposed may have grown in water up to 2 or 3 m deep. Consequently, it is possible that relative sea level during the Last Interglacial could have extended more than 5 m higher than it is today.

As noted earlier, the Rottnest Limestone coral reef was built mainly by *Acropora*, which today does not form coral reefs south of the Houtman Abrolhos, 350 km to the north. The reef-building role of *Acropora* in the Rottnest Limestone suggests that water temperatures in this area during the Last Interglacial were a little warmer (perhaps 1–3°C) than they are today, which would be consistent with a higher sea level and/or stronger Leeuwin Current at that time.

Subtidal shell beds of the Vincent Member (5900–4800 y B.P.) extend to at least 1.29 m above mean sea level. It seems clear, however, that these shell beds were deposited when relative sea level was at the elevation of the upper shoreline platform (discussed below), or about 2.4 m above present mean sea level.

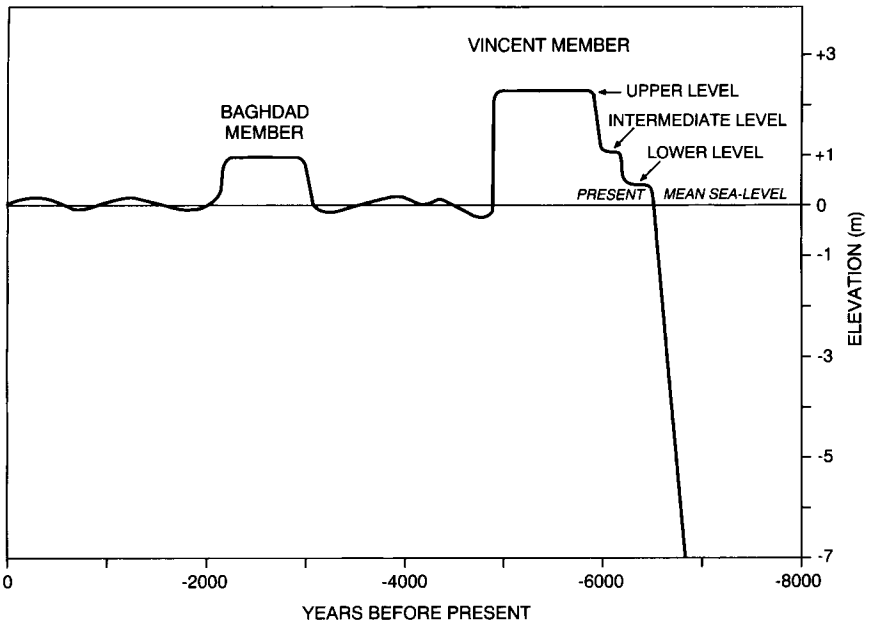


Fig. 27-14. Relative sea-level curve for the Rottnest area over the past 8000 years, shown in relation to the Vincent and Baghdad Members of the Herschell Limestone and the lower-, intermediate-, and upper-level shoreline notches and platforms.

The parts of the Baghdad Member (3100–2200 y B.P.) that are believed to represent beach deposits extend to 1.5 m above mean sea level. It seems likely that they were laid down when relative sea level was about 1 m higher than it is today.

Elevated shoreline platforms and notches

Three levels of elevated shoreline platforms and notches are cut in Tamala Limestone alongside the salt lakes on Rottnest: an upper level at about 2.4 m, an intermediate level at about 1.1 m, and a lower level at about 0.5 m above the modern shoreline platforms (Figs. 27-14–27-16). These features are believed to have developed at the end of the Holocene transgression, during brief stillstands in sea level. The highest level was followed by an abrupt regression, and then the sea settled at or about its present level some hundreds of years ago (Figs. 27-14, 27-15). The two notches and the upper platform are well preserved around the salt lakes where they are protected from modern marine erosion. Such features cannot be recognised with any confidence around the coast of the island because of the strong marine erosion that occurs in those areas today.

The upper level is represented by remnants of very narrow shoreline platforms and weakly developed notches formed when relative sea level was about 2.4 m higher than today (Figs. 27-15, 27-16). This highest sea level relative to Rottnest is thought

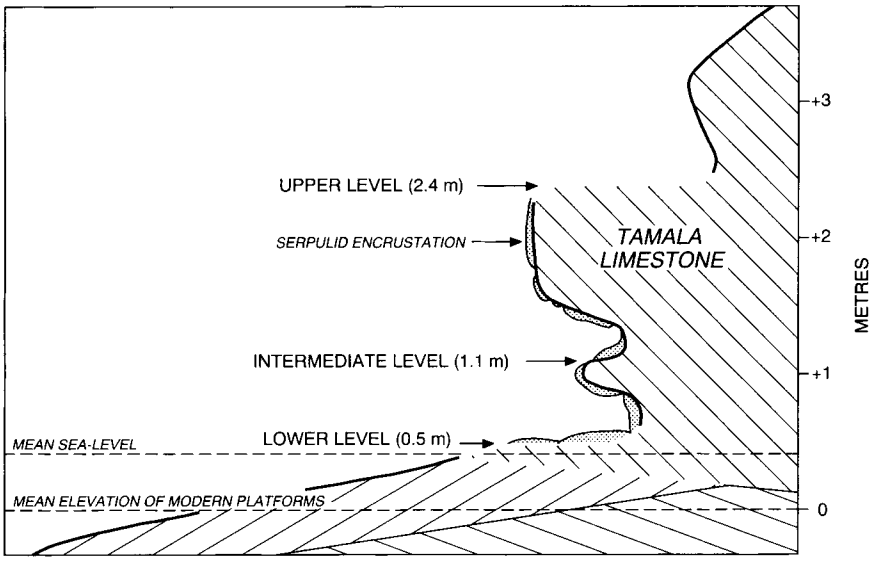


Fig. 27-15. Diagrammatic cross section illustrating elevated shoreline platforms and notches in Tamala Limestone around the margins of the salt lakes.



Fig. 27-16. North side of Government House Lake, adjoining Herschell Lake, showing the upper-level (2.4 m) platform and the intermediate- and lower-level notches. The platform and notches are cut in Tamala Limestone showing prominent foreset bedding.

to have been reached some 5900 to 4800 y B.P. during deposition of the Vincent Member. The intermediate and lower levels are represented around the lakes by conspicuous "double notches" with associated weakly developed narrow platforms.

The two notches are apparently older than the upper-level platform. The evidence for this interpretation consists of a discontinuous layer of entwined serpulid worm tubes up to 5 cm thick that encrusts the lower two notches and extends to the level of the upper platform (Fig. 27-15), showing that the notches were already in existence when the sea reached its highest level. The limestone on which the serpulids grew was commonly strongly bored by clionid sponges and bivalves (probably mainly *Lithophaga*). Small pockets of bivalves and gastropods, equivalent to parts of the Vincent Member, are associated with the serpulid layer, as are some encrustations of small solitary corals and bryozoans. A sample of serpulids encrusting the intermediate-level notch has been dated as 5040 ± 290 y B.P. (Playford, 1988). This date ties in well with the age of the Vincent Member and the deduced age of the upper-level platform.

The two lower notches formed over only a short time (probably less than 200 or 300 years) before the sea reached the upper level (2.4 m). These notches testify to brief stillstands in the rise in sea level at the close of the Holocene transgression in this area. The relative fall in sea level that occurred after development of the upper-level platform seems to have been quite abrupt; if the fall in sea level had been gradual, it would be expected to have resulted in more extensive removal of the fragile serpulid crust.

Subaerial features extending below sea level

Dune limestone of the Tamala Limestone extends below sea level around the coast of Rottnest Island and probably reaches water depths of more than 100 m. Most of the formation is believed to have accumulated during the Last Glacial Period and the following Holocene transgression; however, a small part of the exposed unit pre-dates the Last Interglacial. Root pipes in the Tamala Limestone extend below sea level at many localities around the coast (e.g., at Fairbridge Bluff), and the trees from which they originated must have grown when sea level was significantly lower than today.

As discussed earlier, the salt lakes are believed to mark the sites of former blue holes that were controlled by karst developed during sea-level lowstands of the Pleistocene glacial periods.

Origin of sea-level changes

The major Pleistocene changes of sea level that affected the mainland and the adjoining part of the continental shelf around Rottnest clearly resulted from global eustatism associated with waxing and waning of the continental ice sheets. However, the Holocene highstands of sea level recognised on Rottnest Island are of particular international importance. These highstands were attributed to global eustatic

changes by Teichert (1950) and Fairbridge (1961). Playford (1977, 1983, 1988), however, cast doubt on this interpretation, as the highstands evident at Rottnest have no generally accepted eustatic correlatives elsewhere in Australia or the world (Thom and Chappell, 1975; Mörner, 1976). He suggested that the alternative of a tectonic origin also needed to be considered.

It is still not clear whether the Holocene high sea levels evidenced at Rottnest were of local or regional extent. If they were regional (e.g., over the whole of the southwest of Western Australia), did they result from epeirogenic movements, changes in the shape of the geoid, abrupt changes in water circulation and temperature in this part of the Indian Ocean, or some other cause? If the relative sea-level changes were of local extent (i.e., confined to Rottnest and adjoining areas), did they result (1) from fault movements on or adjoining the continental shelf (possibly triggered by rapid loading of water on the continental shelf [hydro-isostasy] during the Holocene transgression, in the manner postulated by Pirazzoli, 1976); or (2) from movements on a major fault, such as the Darling Fault along the eastern margin of the Perth Basin; or (3) from local response of the crust to remote glacial unloading and local water loading of the continental shelf (glacio-hydro-isostasy), as postulated by Nakada and Lambeck (1987). Other papers bearing on Holocene tectonism and sea-level changes in the southwest of Western Australia have included those by Cope (1975), Kendrick (1977), Gordon and Lewis (1980), Searle and Woods (1986), Semeniuk and Searle (1986), Semeniuk and Semeniuk (1991), Nakada and Lambeck (1987), Lambeck and Nakada (1992), Lambeck (1987), Lambeck (1990), and Playford (1988). It is clear from this work that a lot more research is required on the evidence for Quaternary sea-level fluctuations in southwestern Australia, in order to resolve the basic question of whether the changes in relative sea level evidenced at Rottnest and elsewhere were local or regional in extent, and to deduce the origin of those changes.

QUATERNARY EVOLUTION OF ROTTNEST ISLAND

A late Tertiary or early Pleistocene sand shoal may have formed the foundation for Rottnest Island by localizing the calcareous coastal dunes that accumulated to form the Tamala Limestone. The dune ridge is in turn known to have localised a coral-reef platform when sea level approached its highest level at about 120–130 ka. Sea level fell during the ensuing glacial period, reaching its lowest level of about −130 m at about 18 ka. The mainland coastline was then some 12 km west of Rottnest (Fig. 27-17), and the old dune and reef platform formed a conspicuous hill, high above the surrounding coastal plain. Nomadic Aboriginal people roamed this plain and "Rottnest Hill". The ancestral Swan River flowed north of the hill, to meet the coast where a submarine canyon, the Perth Canyon, is incised into the continental slope. Karst dissolution magnified older blue holes in the coral-reef platform, and these were later to localise the Rottnest salt lakes.

Sea level rose rapidly during the latest Pleistocene and Holocene transgression, while dune sands of the younger Tamala Limestone accumulated on the Rottnest

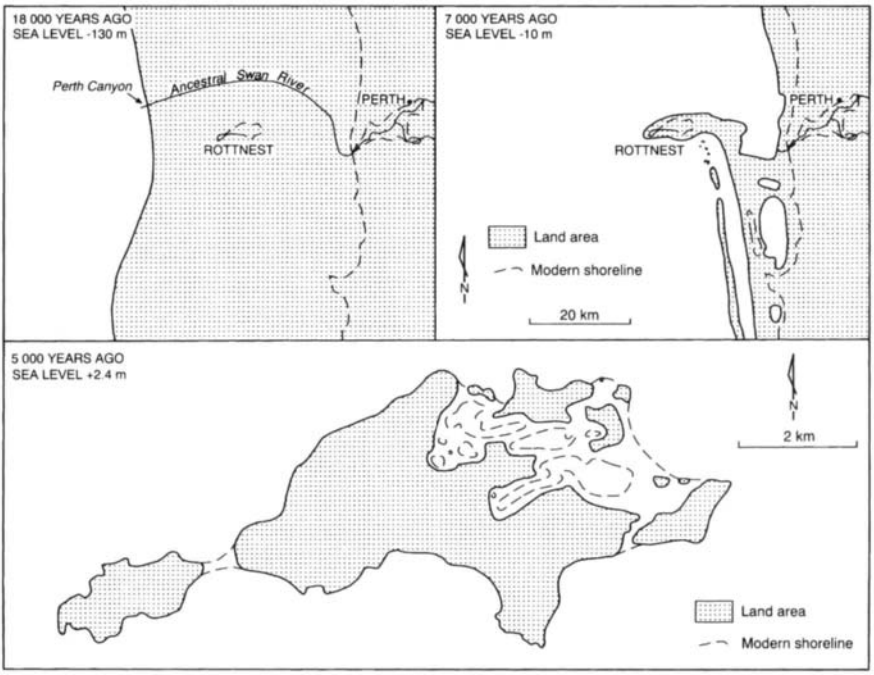


Fig. 27-17. Palaeogeographic maps showing shorelines of the Perth-Rottnest area at 18,000 y B.P. (when the sea was at its lowest level during the Last Glacial Period) and 7000 y B.P. (just before separation of the island from the mainland), and the Rottnest Island area at 5000 y B.P. (when the sea was at its highest level relative to the island).

platform. As the sea continued rising, Rottnest remained in connection with the mainland until about 6500 y B.P., when separation finally occurred. Major changes in the fauna and flora resulted from this separation; only a few of the original plants and animals survived. All eucalypts disappeared, and only one marsupial, the quokka, remained.

The peak transgression relative to the island was reached about 2.4 m above present sea level, at some 5900 to 4800 y B.P. At that time, the area of the modern salt lakes was occupied by lagoonal arms of the sea between more than ten separate islands (Fig. 27-17).

Abrupt uplift or a sudden fall in sea level occurred at about 4800 y B.P., and the sea then probably reached about its present level in relation to the island. A subsequent rise in relative sea level, to about 1 m above its present level, occurred from 3100 to 2200 y B.P., followed by another regression to about the present level.

The area of the modern salt lakes probably remained in communication with the sea for some time after the sea reached its present level, but the lakes were eventually cut off by the accumulation of beach ridges and sand dunes. There have probably been no major changes in the configuration of the island over the past few hundred years.

HYDROGEOLOGY

Introduction

Water for the Aboriginal prison on Rottnest Island was supplied from roof catchments, supplemented by brackish water from shallow wells. When a decision was made in 1903 to close the prison and develop the island as a holiday resort, it was concluded that a larger reliable source of potable water would be needed. Consequently, an exploratory deep borehole was proposed, with the objective of intersecting extensions of the artesian aquifers that were then being utilised on the mainland.

This borehole was drilled in 1911–1913 to a depth of 788 m, penetrating the Cretaceous confined aquifers, but it yielded only small flows of salt water and was abandoned (Playford, 1976). No deep boreholes have since been drilled on the island because of the likelihood that they will encounter only saline or brackish water. The results of oil exploration suggest that faulting between Rottnest and the mainland may have formed a partial hydraulic barrier, impeding the movement of water through the confined aquifers beneath the island.

Hydrogeologically, the Thomson Bay settlement is situated in one of the worst parts of the island to obtain shallow potable groundwater, in a low-lying area between the coast and salt lakes. Early wells put down in the area intersected a thin layer of potable water, but supplies quickly turned brackish to saline on pumping. This experience led to a long-held belief that significant supplies of potable unconfined groundwater could not be obtained on the island. Consequently, until 1976, the potable water needs of the Thomson Bay settlement were provided by rainwater collected from a bituminised catchment beside Mt. Herschell, supplemented in later years by water brought by barge from the mainland. Shallow brackish to saline groundwater from wells near the settlement was used in a second-class water system serving ablution and sanitary requirements.

The water-supply problem was brought to a head in 1976 when it was decided to construct a new holiday settlement at Longreach and Geordie Bays, as this would require a major increase in potable water supplies. The Geological Survey was consequently asked to re-evaluate the groundwater potential of the island. I undertook the task because of my familiarity with the geology of the island through earlier "holiday" research. Investigation soon showed that the most prospective areas on the island for shallow groundwater had never been tested. These were two broad areas, west of Wadjemup Hill and south of the salt lakes, where there should be maximum intake of rainwater to shallow unconfined aquifers. Exploratory drilling of these areas was therefore recommended (Playford, 1976, 1977).

This drilling was undertaken in 1976, shortly after the recommendation was made. It demonstrated the presence of two groundwater lenses, as had been predicted. The largest of these, west of Wadjemup Hill, was suitable for immediate development to supply the settlements (Figs. 27-18, 27-19). Production began in the same year and has continued since without major problems.

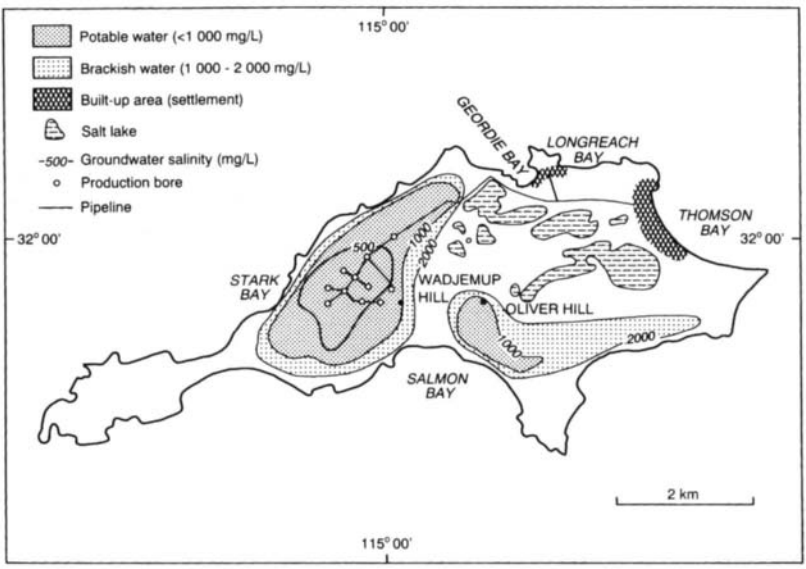


Fig. 27-18. Hydrogeological map of Rottnest Island, showing the locations of the two principal groundwater lenses. Isohalines are based on the average salinity of the upper 5 m of groundwater.

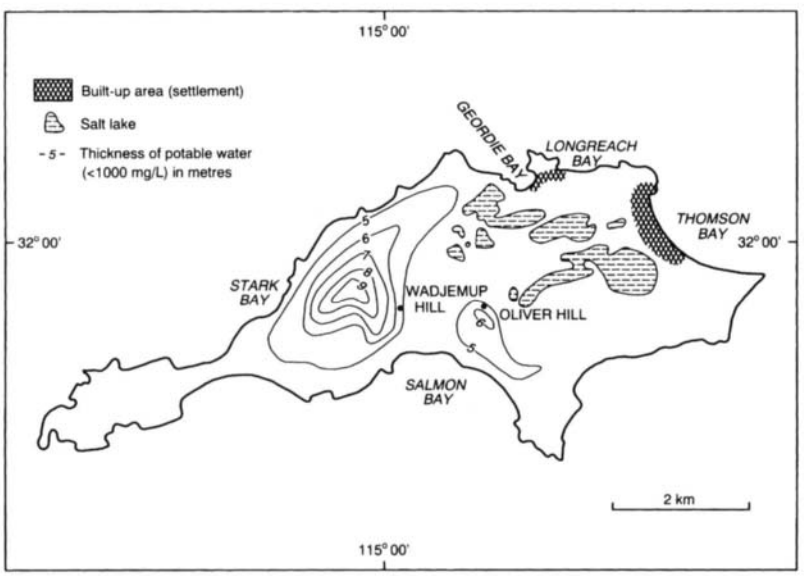


Fig. 27-19. Isopachs of potable water on Rottnest Island.

Aquifer characteristics

The hydrology of the shallow groundwater on Rottnest Island is described by Leech (1977) in Playford and Leech (1977). A more recent appraisal is by Hirschberg and Smith (1990).

The producing aquifer consists of weakly cemented limestone and lime sand of the Tamala Limestone, which is highly porous and permeable. The potable-water lens west of Wadjemup Hill is up to 11 m thick and is underlain by a mixing zone up to 15 m thick before passing into water of oceanic salinity. There is no indication of mixing-zone dolomitization in the Tamala Limestone below the potable water.

Recharge of the unconfined aquifer at Rottnest is totally dependent on rainfall. By comparing the groundwater Cl^- with that of rainwater, Leech (1977) estimated that the recharge is about 20% of the annual rainfall (average 720 mm), the remainder being lost by evaporation and plant transpiration. This recharge estimate was based on the ratio of the Cl^- of rainwater collected in the Thomson Bay settlement area in June 1976 (39 mg L^{-1}), to the average Cl^- of the main groundwater mound (194 mg L^{-1}). Hirschberg and Smith (1990) also applied this figure in estimating that the total recharge to the part of the potable-water lens that is usable (thicker than 5 m) amounts to about 380,000 kL y^{-1}. They considered that approximately 50% of this amount would be available for exploitation without inducing overproduction problems or significantly diminishing the flow of springs adjoining the salt lakes.

Groundwater production

Boreholes are pumped at constant low rates, with an average daily production of 17 kL per well during the summer months. The salinity of each is regularly monitored to ensure that overpumping, which would result in upconing of brackish water from below, does not occur. These procedures are in accord with recommendations made by Leech (1977) to ensure efficient usage of the groundwater mound. Current production from the borefield is about 45,000 kL y^{-1}. This supply meets about 65% of the island's requirements for potable water, the balance being provided by rainwater from the Mt. Herschell catchment.

Until very recently, the island's settlements operated with two classes of water supply, potable and non-potable. The non-potable supply, for sanitary and ablution purposes, was provided from brackish and salty wells situated near the settlements. However, a decision was made in 1993 to change to a one-class (potable) system, as freshwater is preferable for both sewage treatment and equipment maintenance. Available resources of potable groundwater from the shallow aquifer and bituminised catchments were insufficient to fully meet the needs of the new system, and consequently it was decided to supplement supplies by using a reverse-osmosis plant to desalinate salty water from two shallow wells. The new one-class system came into operation in October 1995.

CONCLUDING REMARKS

Rottnest Island is of particular importance in relation to the geology of limestone islands in that it exhibits: (1) exceptionally well-preserved evidence of mid-Holocene highstands in sea level, extending to almost 2.5 m above present sea level, in an area that is now seismically quiescent; (2) good evidence that major eolianite accumulation occurred during the Last Glacial Period; (3) excellent examples of shoreline notches and wide shoreline platforms cut a little below mean low-water level by marine erosion of both eolianite and a Last Interglacial coral reef; (4) extensive deposition of evaporites in salt lakes localized by Pleistocene "blue holes;" (5) a detailed palynological record in swamp deposits of vegetation changes on the island during the mid- to late Holocene; (6) a classic freshwater lens beneath the widest part of the island; and (7) no evidence of dolomitization of limestone in the mixing zone below the freshwater lens.

Future geoscientific research on Rottnest is expected to concentrate on: (1) evidence that has recently come to light of a brief late Holocene highstand in sea level (previously unrecognized, and not described in this chapter); (2) the stratigraphic record preserved in the salt-lake sediments; and (3) the mechanical and chemical processes involved in development of the shoreline platforms. A lot of interesting research remains to be done!

ACKNOWLEDGMENTS

I would like to acknowledge the assistance that I have received in my research from the following persons: Drs. John Backhouse and Peter Thorpe of the Geological Survey of Western Australia, Dr. Patrick Berry and Mr. George Kendrick of the Western Australian Museum, and Dr. Joseph McKee of the New Zealand Institute of Geological and Nuclear Sciences. I would also like to thank Mr. Joe Lord, Dr. Alec Trendall, and Dr. Peitro Gij, Directors of the Geological Survey of Western Australia, for their support. My wife, Cynthia, and daughters Julia and Katherine, deserve special thanks for their tolerance of my use of holidays on Rottnest to undertake "hobby" research on this delightful island. Published by permission of the Director, Geological Survey of Western Australia.

REFERENCES

Backhouse, J., 1993. Holocene vegetation and climate record from Barker Swamp, Rottnest Island, Western Australia. J.R. Soc. West. Aust., 76: 53–61.

Berry, P.F. and Playford, P.E., 1992. Territoriality in a subtropical kyphosid fish associated with macroalgal polygons on reef platforms at Rottnest Island, Western Australia. J.R. Soc. West. Aust., 75: 67–73.

Black, R. and Johnson, M.S., 1983. Marine biological studies on Rottnest Island. J.R. Soc. West. Aust., 66: 24–28.

Bradshaw, S.D. (Editor), 1983. Research on Rottnest Island. J. R. Soc. West. Aust., 66, 61 pp.

Bunn, S.E. and Edward, D.H.D., 1984. Seasonal meromixis in three hypersaline lakes on Rottnest Island, Western Australia. Aust. J. Mar. Freshwater Res., 35: 261–265.

Chappell J. and Shackleton, N.J., 1986. Oxygen isotopes and sea level. Nature, 324: 137–140.
Churchill, D.M., 1959. Late Quaternary eustatic changes in the Swan River district. J. R. Soc. West. Aust., 42: 53–55.
Collins, L.B., 1988. Sediments and history of the Rottnest Shelf, southwest Australia: a swell-dominated, non-tropical carbonate margin. Sediment. Geol., 60: 15–49.
Collins, L.B., Wyrwoll, K.H. and France, R.E., 1991. The Abrolhos carbonate platforms: geological evolution and Leeuwin Current activity. J. R. Soc. West. Aust., 74: 47–57.
Collins, L.B., Zhu, Z.R., Wyrwoll, K.H., Hatcher, B.G., Playford, P.E., Chen, J.H., Eisenhauer, A. and Wasserburg, G.J., 1993. Late Quaternary evolution of coral reefs on a cool-water carbonate margin: the Abrolhos carbonate platforms, southwest Australia. Mar. Geol., 110: 203–212.
Cope, R.N., 1975. Tertiary epeirogeny in the southern part of Western Australia. West. Aust. Geol. Surv. Ann. Rep., 1974: 40–46.
Edward, D.H.D., 1983. Inland waters of Rottnest Island. J. R. Soc. West. Aust., 66: 41–47.
Fairbridge, R.W., 1952. Marine erosion. Seventh Pacific Sci. Cong. (Wellington), III: 1–11.
Fairbridge, R.W., 1953. Australian stratigraphy. Univ. Western Australia, Text Books Board, Nedlands.
Fairbridge, R.W., 1958. Dating the latest movements of the Quaternary sea level. N.Y. Acad. Sci. Trans., Ser. 2: 471–482.
Fairbridge, R.W., 1961. Eustatic changes in sea level. Phys. Chem. Earth, 4: 99–185.
Fairbridge, R.W. and Teichert, C., 1953. Soil horizons and marine bands in the Coastal Limestones of Western Australia, between Cape Naturaliste and Cape Leeuwin. J. Proc. R. Soc. N.S.W., 86: 68–87.
Glenister, B.F., Hassell, C.W. and Kneebone, E.W.S., 1959. Geology of Rottnest Island. J.R. Soc. West. Aust., 42: 69–70.
Gordon, F.R. and Lewis, J.D., 1980. The Meckering and Calingiri Earthquakes, October 1968 and March 1970. West. Aust. Geol. Surv. Bull. 126, 229 pp.
Gozzard, J.R., 1990. Rottnest Island Environmental Geology. Geol. Surv. West. Aust. Environ. Geol., 1: 250 000 map series.
Hassell, C.W. and Kneebone, E.W.S., 1960. The geology of Rottnest Island. B.Sc. Hons. Thesis, Univ. Western Australia.
Hatcher, B.G., 1991. Coral reefs in the Leeuwin Current – an ecological perspective. J.R. Soc. West. Aust., 74: 101–114.
Hirschberg, K.J. and Smith, R.A., 1990. A reassessment of the shallow groundwater resources of Rottnest Island. Geol. Surv. West. Aust. Hydrogeol. Rep., 1990/61, 6 pp.
Hodgkin, E.P., 1959. The salt lakes of Rottnest Island. J.R. Soc. West Aust., 42: 84–85.
Hodgkin, E.P., 1964. Rate of erosion of intertidal limestone. Z. Geomorph., N.F., 8: 385–392.
Hodgkin, E.P., 1970. Geomorphology and biological erosion of limestone coasts in Malaysia. Geol. Soc. Malays. Bull., 3: 27–51.
Hodgkin, E.P. and Di Lollo, V., 1958. The tides of south-western Australia. J.R. Soc. West. Aust., 41: 42–54.
Kendrick, G.W., 1977. Middle Holocene marine molluscs from near Guildford, Western Australia, and evidence for climatic change. J.R. Soc. West Aust., 59: 97–104.
Lambeck, K., 1987. The Perth Basin: a possible framework for its formation and evolution. Explor. Geophys., 18: 124–128.
Lambeck, K., 1990. Late Pleistocene, Holocene, and present sea-levels: constraints on future change. Palaeogeogr. Palaeoclimatol. Palaeoecol., 89: 205–217.
Lambeck, K. and Nakada, M., 1992. Constraints on the age and duration of the last interglacial period and on sea-level variations. Nature, 357: 125–128.
Leech, R.E.J., 1977. Hydrology. In: P.E. Playford and R.E.J. Leech, Geology and Hydrology of Rottnest Island. West. Aust. Geol. Surv. Rep., 6: 54–98.
Logan, B.W., Read, J.F. and Davies, G.R., 1970. History of carbonate sedimentation, Quaternary Epoch, Shark Bay, Western Australia. Carbonate sedimentation and Environments, Shark Bay, Western Australia. Am. Assoc. Petrol. Mem., 13: 38–84.

Mörner, N.A., 1976. Eustatic changes during the last 8,000 years in view of radiocarbon calibration and new information from the Kattegart region and other northwestern European coastal areas. Palaeogeogr. Palaeoclimatol. Palaeoecol., 19: 63–85.

Nakada, M. and Lambeck, K., 1987. Glacial rebound and relative sea-level variations: a new appraisal. J. Geophys., 90: 171–224.

Pearce, A.F. and Cresswell, G., 1985. Ocean circulation off Western Australia and the Leeuwin Current. CSIRO Div. Oceanog., Inf. Service Sheet 16–3.

Pearce, A.F. and Walker, D.I. (Editors), 1991. The Leeuwin Current: An Influence on the Coastal Climate and Marine Life of Western Australia. J. R. Soc. West. Aust., 74: 1–140.

Penn, L.J. and Green, J.W., 1983. Botanical exploration and vegetational changes on Rottnest Island. J.R. Soc. West. Aust., 66: 20–24.

Pirazzoli, P., 1976. Les variations du Niveau marin depuis 2,000 ans. Mem. Lab. de Géomorph. L'école Pratique Hautes Etudes Dinard, 30: 1–421.

Playford, P.E., 1976. Rottnest Island: geology and groundwater potential. West. Aust. Geol. Surv. Rec., 1976/7.

Playford, P.E., 1977. Geology and groundwater potential. In: P.E. Playford and R.E.J. Leech, Geology and Hydrology of Rottnest Island. West. Aust. Geol. Surv., Rep., 6: 1–53.

Playford, P.E., 1983. Geological research on Rottnest Island. J.R. Soc. West. Aust., 66: 10–15.

Playford, P.E., 1988. Guidebook to the geology of Rottnest Island. Geol. Soc. Aust. West. Aust. Div. and Geol. Surv. West. Aust., Guidebook 2., 67 pp.

Playford, P.E., 1990. Geology of the Shark Bay area, Western Australia. In: P.F. Berry, S.D. Bradshaw and B.R. Wilson (Editors), Research in Shark Bay. West Aust. Mus., Perth, pp. 13–31.

Playford, P.E. and Leech, R.E.J., 1977. Geology and hydrology of Rottnest Island. West. Aust. Geol. Surv., Rep. 6, 98 pp.

Playford, P.E., Cockbain, A.E. and Low, G.H., 1976. Geology of the Perth Basin, Western Australia. West. Aust. Geol. Surv. Bull. 124, 311 pp.

Purdy, E.G., 1974. Reef configurations: cause and effect. In: L.F. Laporte (Editor), Reefs in Time and Space. Soc. Econ. Paleontol. Mineral. Spec. Publ., 18: 9–76.

Revelle, R. and Fairbridge, R.W., 1957. Carbonates and carbon dioxide. In: J.W. Hedgpeth (Editor), Treatise on Marine Ecology and Paleoecology. Geol. Soc. Am. Mem., 67: 239–296.

Schilder, G., 1985. Voyage to the Great South Land. R. Aust. Hist. Soc., Sydney, 259 pp.

Searle, D.J. and Woods, P.J., 1986. Detailed documentation of a Holocene sea-level record in the Perth region, southern Western Australia. Quat. Res., 26: 299–308.

Semeniuk, V., 1986. Holocene climate history of coastal South-western Australia using calcrete as an indicator. Palaeogeogr. Palaeoclimatol. Palaeoecol., 53: 289–308.

Semeniuk, V. and Johnson, D.P., 1985. Modern and Pleistocene rocky shore sequences along carbonate coastlines, Western Australia. Sediment. Geol., 44: 225–261.

Semeniuk, V. and Searle, D.J., 1986. Variability of Holocene sealevel history along the southwestern coast of Australia - evidence for the effect of significant local tectonism. Mar. Geol., 72: 47–58.

Semeniuk, V. and Semeniuk, C.A., 1991. Radiocarbon ages of some coastal landforms in the Peel-Harvey estuary, south-western Australia. J. R. Soc. West. Aust., 73: 61–71.

Szabo, B.J., 1979. Uranium-series age of coral reef growth on Rottnest Island, Western Australia. Mar. Geol., 29: M11–M15.

Teichert, C., 1950. Late Quaternary changes of sea level at Rottnest Island, Western Australia. Proc. R. Soc. Victoria, 59: 63–79.

Teichert, C. and Serventy, D.L., 1947. Deposits of shells transported by birds. Am. J. Sci., 245: 322–328.

Thom, B.G. and Chappell, J., 1975. Holocene sea levels relative to Australia. Search, 6: 90–93.

Geology and Hydrogeology of Carbonate Islands. Developments in Sedimentology 54
edited by H.L. Vacher and T. Quinn
© 1997 Elsevier Science B.V. All rights reserved.

Chapter 28

GEOLOGY OF THE HOUTMAN ABROLHOS ISLANDS

LINDSAY B. COLLINS, ZHONG RONG ZHU, and KARL-HEINZ WYRWOLL

INTRODUCTION

The Houtman Abrolhos islands are small rocky islands of Holocene and Pleistocene coral-reef limestone along the shelf margin 70 km from the coast of Western Australia. The exposed parts of this coral-reef complex consist of over 100 islands which exist in three groups (the Wallabi, Easter and Pelsaert Groups: see Fig. 28-1). The islands, which generally have an elevation of only a few meters, are mainly rocky, sparsely vegetated, and uninhabited except during the 3-month-long, rock lobster fishing season.

The Houtman Abrolhos Islands were named by Frederick de Houtman in 1619, after the Portuguese expression "Abri vossos olhos!" ("look out" or "be careful"), and have been the site of several disastrous shipwrecks. The wreck of the Dutch ship *Batavia* in 1629 was followed by a mutiny and the murder of 125 of the survivors by the mutineers while on the islands (Edwards, 1989). Aside from the archaeological record from the *Batavia*, these early inhabitants constructed Australia's first European "buildings", the stone walls of which are still standing. They also provided the first description of Australian marsupials and the "peculiar mating behavior of these cats" on the islands. In 1727, the Dutch ship *Zeewyk* was wrecked on Half Moon Reef, the western reef of the Pelsaert Group (Fig. 28-1). Using salvaged timbers, survivors were able to construct a small ocean-going vessel on nearby Gun Island and continue their voyage.

Almost a century of guano mining occurred on the islands until the late 1940s, when the rock lobster industry commenced. In 1992–1993 this export industry, of which the Abrolhos yield 15% of the total catch from 3% of the fishing ground in Western Australia, generated an income of $250-million (Australian). The Abrolhos have both commercial fishery significance and conservation value as coral reefs.

Early descriptions of the islands were provided by Wickham (1841) and Stokes (1846). Darwin did not visit the islands, but relying heavily on the descriptions of Wickham, he commented that from the "extreme irregularity" and "position on a bank" of the reefs, he had "not ventured to class them with atolls" (Darwin, 1842, p. 130). Teichert (1947) and Fairbridge (1948) provided important introductions to the geology and geomorphology. More recently, France (1985) studied the Holocene geology of the Pelsaert Group. Geological mapping and subsurface investigations have been in progress during the 1990s (Eisenhauer et al., 1993; Collins et al., 1993a, 1993b; Zhu et al., 1993; Wyrwoll et al., in press).

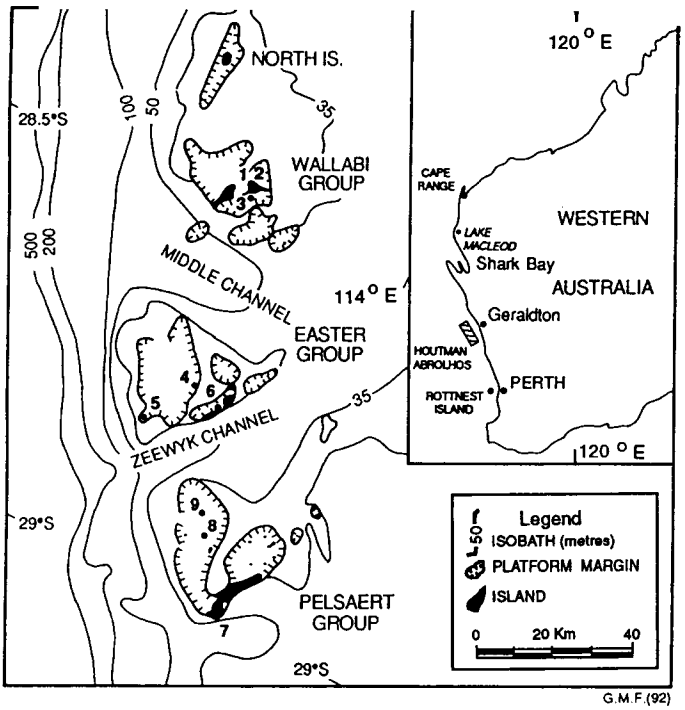


Fig. 28-1. Location of the Houtman Abrolhos Islands. Numbers indicate the location of dated samples: 1, East Wallabi Island; 2, Turtle Bay reef; 3, Mangrove Island; 4, Rat Island; 5, Disappearing Island; 6, Morley Island; 7, Jon Jim Island; 8, Murray Island; 9, "4" Island.

ISLAND GEOMORPHOLOGY

The Houtman Abrolhos, at latitude 28.3° to 29°S, are the southernmost coral reefs in the Indian Ocean (Fig. 28-1). The islands of the Houtman Abrolhos are on three carbonate platforms that are separated by deep (~40 m) channels (Fig. 28-1). The islands are the emergent parts of shallow reef platforms. Each island group differs significantly in its overall geomorphologic expression, with a general organizational plan which decreases in regularity from south to north (Fig. 28-1). Each platform consists of a windward (western) reef, a leeward (eastern) reef, and a lagoon with a central platform. The central platforms are Last Interglacial in age (Zhu et al., 1993), and Holocene reef facies occur within the windward and leeward reefs (Collins et al., 1993b). Islands are absent from the windward reefs (with the exception of one ephemeral sand cay), but present in the central platforms and leeward reefs. The islands are generally little more than small tabular platforms, rising some 3–5 m above present sea level (i.e., +3 to +5 m). The exception is provided by a few islands where late Quaternary dune units result in elevations of up to 15 m. Extensive "blue-hole" terrains occur at the eastern parts of the island groups, but are absent from the western and central parts.

Island types

Five types of islands have been identified according to their morphological and stratigraphic features (France, 1985; Collins et al., 1991). These are eolianite islands, "high" rock islands, composite islands, low coral-shingle/sand cays, and cemented coral-shingle cays (Fig. 28-2).

The eolianite islands consist of a core of reef limestone which has a tabular surface at +2 to +3 m that is overlain by eolianites and unconsolidated dune sands. They are

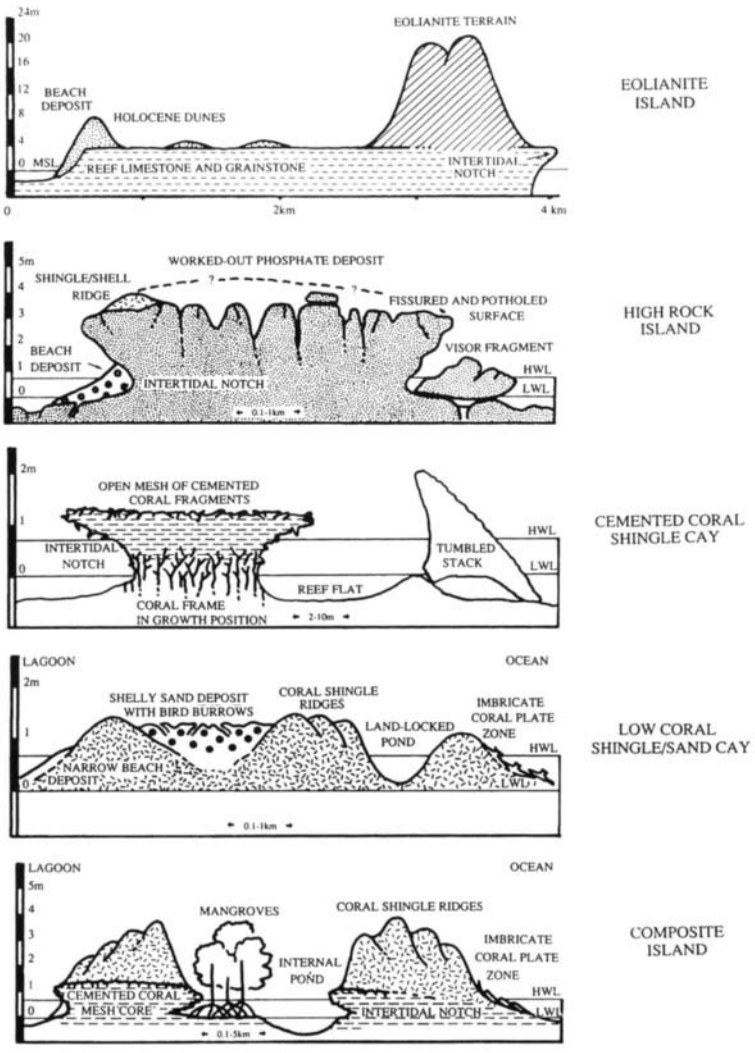


Fig. 28-2. Morphostratigraphic characteristics of islands in the Houtman Abrolhos. (Modified after France, 1985, and Collins et al., 1991.)

the largest islands in the Houtman Abrolhos and are normally a few kilometers across and up to 15 m in elevation.

"High" rock islands are usually about 1 km across and are flat-topped, rocky islands a few meters in elevation, whose coastal morphology is dominated by a well-developed intertidal notch (Fig. 28-2). The rocky island surfaces are barren or sparsely vegetated depending on the extent to which they have been subjected to phosphate mining, in which unconsolidated materials were stripped from their surfaces.

Composite islands are long (up to several kilometers) and narrow (~0.5 km). They consist of a core of emergent coral reef and cemented, imbricated coral rubble, overlain by elongate coral-shingle ridges which are +1 to +4 m.

Cemented coral-shingle cays are composed of coral shingles, bound and cemented by coralline algae and marine cements. They mimic composite islands in shape, but are small (up to a few tens of meters long) and lack unconsolidated coral-shingle ridges. Low coral-shingle/sand cays are ovoid to elongate islands of 1–2 m elevation, consisting of coral-shingle ridges and associated carbonate sands (Fig. 28-2).

Eolianite and "high" rock islands form the emergent part of the central platforms which rise from lagoons. These central platform islands are composed of well-lithified and dense, calcretized reef limestones which are Last Interglacial in age. The Wallabi Group is dominated by three eolianite islands (East and West Wallabi, and North Island; Fig. 28-1), whereas the central platforms of the Easter and Pelsaert Groups each consist of several "high" rock islands. These central platform islands are significantly higher in elevation than the composite islands, low coral-shingle/sand cays, and cemented coral-shingle cays, all of which form the emergent parts of the leeward reefs. These leeward islands are composed of poorly lithified reef limestones and unconsolidated coral rubble and sand. They lack calcrete and are Holocene in age, in contrast to the denser limestones of the central platform islands. The leeward islands also overlie an extensive network of "blue holes."

"Blue-hole" terrains

"Blue-hole" terrains are a conspicuous element of the leeward (eastern) parts of the island groups. The "blue holes" are ovoid to irregular depressions in the reef flats. These depressions are 100–1500 m across, up to 20 m deep, and are cylindrical to conical in shape. Most of the "blue holes" contain <3 m of carbonate sediment within them. "Blue holes" in reef terrains have frequently been interpreted as having a solutional karst-doline origin (see the summary discussion by Purdy, 1974). Although the shape of the pre-Holocene surface is still unknown, the occurrence of the "blue holes" exclusively in areas of well-developed leeward Holocene reefs, the absence of "blue holes" from western reefs and central platforms, the very high Holocene reef accretion rates shown by the core data, relatively low rainfall in the region, and a lack of karst features within the "blue holes" themselves, all indicate that these Abrolhos "blue holes" have resulted from Holocene reef construction, rather than being karst dolines (see Wyrwoll et al., in press).

REGIONAL SETTING

The Abrolhos region has a mediterranean-type climate, with hot, dry summers and cool, wet winters. Rainfall is about 500 mm y^{-1}. The region is in a microtidal environment. Dominant winds are from the southwest to southeast. Storms are significant and summer tropical cyclones have an average recurrence interval of 3 years (Steedman et al., 1977). Up to 90% of the cyclones approach from the northwest. Persistent swell waves with a mean height of 1.2 m impinge on the Abrolhos throughout the year; these swells approach from the south and west 78% of the time (Steedman et al., 1977). Wave impact energy is strongest on the southwest reef margins, whereas significant refracted swell waves and wind waves impinge on southeastern reefs. Mean annual sea-surface temperatures normally range from 26°C in summer to 18°C in winter (Wilson and Marsh, 1979). They fall below 20°C for up to 30% of the time (France, 1985) and may fall below 17–18°C for several days at a time in areas of restricted circulation (Wilson and Marsh, 1978; Hatcher et al., 1987). Conditions are thus often near the limits for the growth of reef-building coral (Crossland, 1984). A southward-flowing, warm-water current, the Leeuwin Current, flows along the continental margin to seaward of the reef complex (Cresswell and Golding, 1980; Pearce, 1991). The current is relatively narrow (50–200 km) and shallow (50–200 m). It flows more strongly during the autumn, winter and early spring months than in summer. Peak current speeds can exceed 1.5 m s^{-1} (Pearce, 1991).

Biogeographically, the Abrolhos region is located in the West Coast Overlap Zone between the Northern Australian Tropical and Southern Australian Warm Temperate Provinces, where a tropical fauna in the north is gradually replaced by a predominantly temperate fauna in the south (Morgan and Wells, 1991). Ecological research in the Abrolhos has described these reefs as "high-latitude reefs" (Hatcher, 1985; Crossland, 1988) and has demonstrated significant differences in community structure and function compared to tropical reefs, with competition between temperate macroalgal and tropical coral communities (Wilson and Marsh, 1979; Hatcher, 1991). Marine life is rich and diverse with more than 230 species of fish, 220 species of mollusks and over 100 species of algae. Coral communities are highly diverse; 184 species and 42 genera of corals are recorded (Veron and Marsh, 1988). *Acropora* spp. and *Monipora* spp. are the dominant taxa (Wilson and Marsh, 1979).

The windward section of the reef platforms generally lacks well-developed coral communities and is dominated by an assemblage of macroalgae of temperate and tropical affinities (Wilson and Marsh, 1979; Hatcher et al., 1990). The leeward section of the reefs and the lagoons support rich coral communities with high community production and calcification rates (Wilson and Marsh, 1979; Smith, 1981). The most dense living cover occurs on leeward reef-front slopes, around the upper edges of "blue holes", and on lagoon patch reefs. In all of these areas, the diversity of corals is relatively low and dominated by tabular, staghorn and corymbose *Acropora* (Wilson and Marsh, 1979). A high diversity of corals occurs at the bottom of leeward reef fronts, and along channel slopes at depths of >20 m, where massive, encrusting, foliose and branching corals exist (Wilson and Marsh, 1979). Submerged reef plat-

forms and intertidal reef flats generally have very sparse coral growth, although diversity can be relatively high.

GEOLOGY

The Abrolhos reef complex is at the northern end of the Perth Basin, which lies along the quiescent rifted margin of southwest Australia (Veevers, 1974; Collins, 1988). As a consequence, the Abrolhos area is tectonically relatively stable. During the Tertiary, the region developed a suite of cool-water carbonate sediments, dominated by bryozoan-mollusk-echinoid calcarenites and calcilutites, and lacking reef-building corals (Hawkins, 1969). The deepest position where coral has been found in cuttings of a well in the Pelsaert Group is at 67 m below sea level (i.e., −67 m) (Hawkins, 1969), which may indicate the approximate thickness of the Abrolhos coral reefs. The age of this coral material is unknown.

Little is known of the early to middle Pleistocene evolutionary history of the Abrolhos reefs. Geological mapping and coring of the reefs and radiometric dating of corals have shown that the reefs formed largely during the Last Interglacial. Remnants of these reefs constitute the contemporary central platforms. Drilling in the Easter Group has penetrated 15 m of the Last Interglacial reef facies without reaching an older unit (Fig. 28-3). The Holocene reefs in the Pelsaert and Easter Groups consist of a crescent-shaped windward reef backed by a lagoon sand sheet, and a leeward reef complex of reticulate reefs and lagoon patch reefs. In the Wallabi Group, the windward reef and associated lagoon are less well developed. Sediments on the shelf to the south of and surrounding the Abrolhos platforms consist of a suite of cool-water carbonates in which bryozoans and calcareous red algae are the most important elements, and mollusks, foraminifers and echinoids are minor constituents (France, 1985; Collins, 1988).

Pleistocene reef limestones

Reef limestones of Last Interglacial age are dense and calcretized, in marked contrast with the more porous Holocene lithofacies. Coral-framestone facies of the Last Interglacial consist mainly of branching and head corals, with minor encrusting coralline algae and white lime mud. In islands of the central platforms, the exposed uppermost part of the Last Interglacial reefs normally consists of an upward-shallowing sequence (Fig. 28-4a), commonly 2–3 m thick (Fig. 28-5a) and locally up to 5 m thick (as in the Turtle Bay Reef in the Wallabi Group; Fig. 28-5c). The upward-shallowing sequence consists of coral framestone and/or coralline algal bindstone, in which coral framestone is thinly overlain by coralline algal bindstone (Fig. 28-5b). This lithofacies is gradationally overlain by up to 50 cm of medium- to coarse-grained, shelly, skeletal grainstone to rudstone, in which molluscan debris and whole shells of bivalves and gastropods are common (Fig. 28-4a). In some outcrops, this sequence is overlain by horizontally bedded, shelly, skeletal grainstone to rudstone,

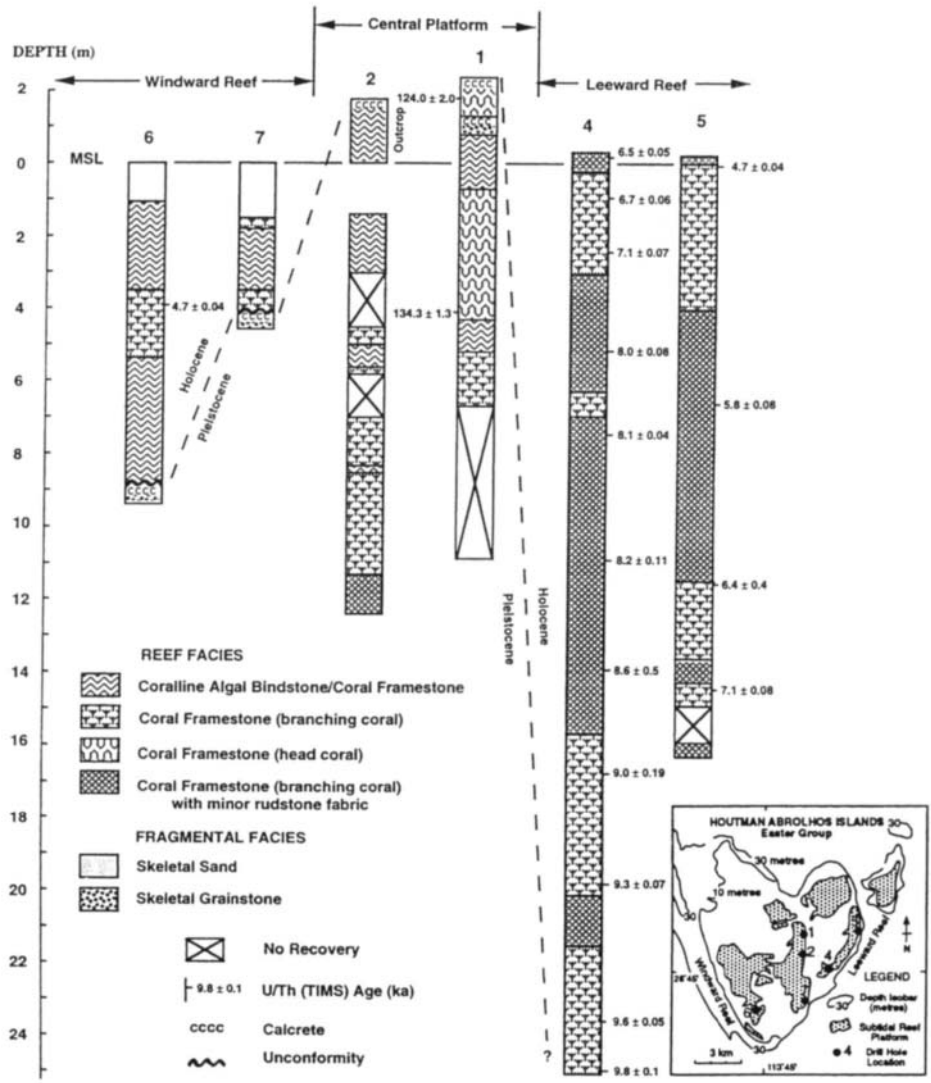


Fig. 28-3. Stratigraphy of the Easter Group. Windward and leeward reefs are Holocene; central platform consists of Last Interglacial reefs. Cores (see inset) were taken in the Windward Reef (6, Disappearing Island; 7, Sandy Island); Central Platform (1, Rat Island; 2, Roma Island) and Leeward Reef (4, Morley Island; 5, Suomi Island). (After Collins et al., 1993b.)

about 50 cm thick and locally up to 3 m thick. This unit is overlain in the eolianite islands of the Wallabi Group by 2–6 m of well-sorted, fine- to medium-grained skeletal grainstone which is eolian cross-bedded and has well-developed calcrete horizons (Fig. 28-5d).

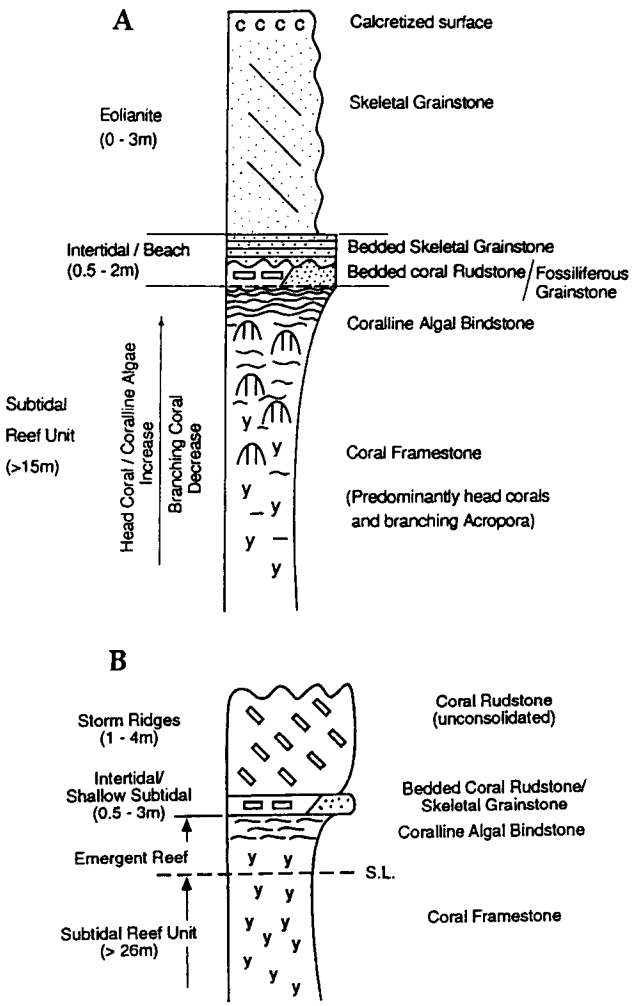


Fig. 28-4. Generalized stratigraphy of Last Interglacial and Holocene islands, based on outcrop and cores. (A) Widespread reef platforms of Last Interglacial age consist of an upward-shallowing sequence of coral framestone, coralline-algal bindstone, and skeletal grainstone to rudstone. This sequence is overlain by eolian skeletal grainstone on East and West Wallabi Islands. (B) Holocene reefs consist of an upward-shallowing sequence of coral framestone, coralline-algal bindstone, and bedded coral rudstone. This sequence is overlain in the leeward islands by storm ridges composed of unconsolidated coral rudstone. Windward Holocene reefs are subtidal and are overlain by sand sheets composed of skeletal grainstone.

Holocene reef limestones and sediments

In contrast to the central platform limestones, the Holocene facies are relatively poorly lithified and lack calcrete (Fig. 28-6). The Holocene sequence consists of five types of sedimentary facies (Fig. 28-4b): coral-framestone facies; algal-bindstone

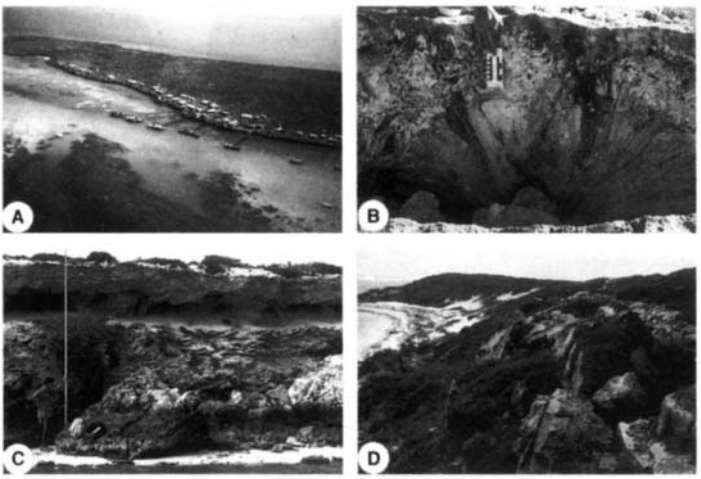


Fig. 28-5. Morphology and geology of Last Interglacial islands. (A) Rat Island in the Easter Group is typical of many central platform "high" rock islands, and is a reef platform only +2 to +3 m. (B) Coastal exposure of emergent reef unit, eastern margin of Rat Island. Head coral is about 1 m across and is thinly overlain by calcretized skeletal grainstone. (C) Outcrop of the Turtle Bay reef at East Wallabi Island shows coral framestone (mainly platy *Acropora*) overlain by bedded skeletal grainstone to rudstone. The top of the reef unit is up to +4 m. (D) View of west coast of West Wallabi Island, an eolianite island, showing well-developed eolianite. The arched upper surface (right) beneath the vegetation commonly consists of 0.5 m of calcretized skeletal grainstone.

facies; well-bedded coral-rudstone facies; unlithified coral-rudstone facies; and skeletal grainstone facies. The first four of these facies are found within islands and comprise an upward-shallowing sequence, while the fifth comprises lagoonal sand sheets.

Coral-framestone facies. This facies, which is over 26 m thick, is formed predominantly by in situ staghorn branching corals (*Acropora* spp) (Fig. 28-3). The framework is normally very porous, and the pores are partially filled by skeletal matrix and marine carbonate cements (Fig. 28-6e). Tabular *Acropora* species and encrustation of corals by coralline algae and foraminifers increase in the upper parts of the facies. Some parts of the framestones have rudstone fabric, expressed by preferentially oriented fragments of branching corals, but these coral fragments lack well-defined stratification and have relatively well-preserved surface textures, indicating little transportation or abrasion (Fig. 28-6f). This fabric is believed to be an integral portion of the growing reef and probably results from small-scale collapse and compaction of porous reef. Framestone facies forms a major part of the leeward reefs and the patch reefs in lagoons. In the windward reef, the framestone facies occurs as thin units within bindstones and is normally modified by extensive boring and encrustation by mollusks, serpulids and coralline algae. The coral-framestone facies normally crops out on the lagoon shores of the leeward islands from +0.2 to +0.5 m (Fig. 28-6b). The framestones occur about 0.5 m above the uppermost

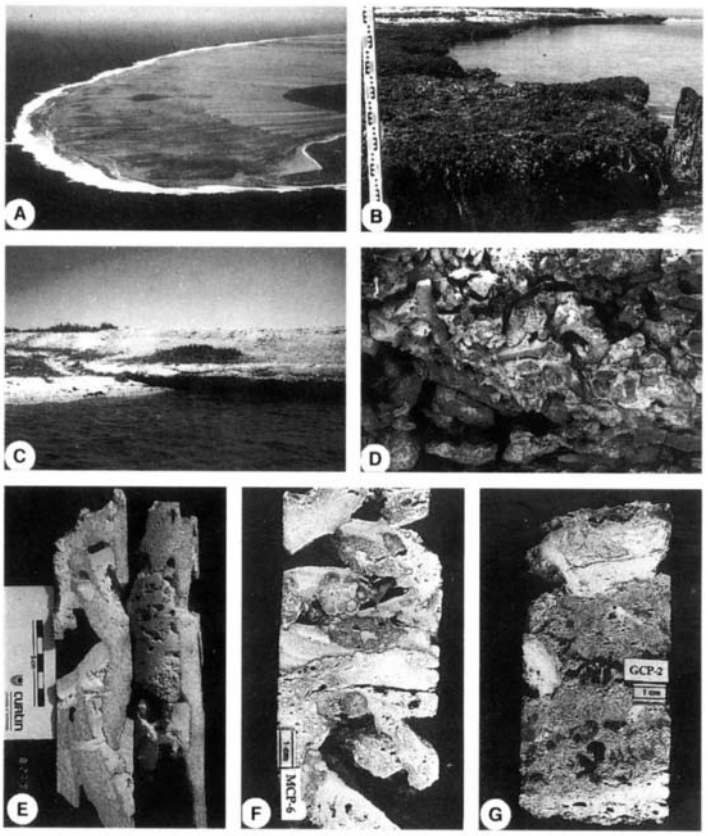


Fig. 28-6. Morphology and lithofacies of Holocene reefs and islands. (A) Oblique aerial view of Half Moon Reef in the southern Pelsaert Group shows (left to right) windward reef, reef flat (dark), sand sheet (light) and lagoon. The southernmost part of Pelsaert Island (right foreground) is Last Interglacial in age. (Photo: Dr. P.E. Playford). (B) Emergent coral framestone (commonly up to +0.5 m) fringing the lagoon shores of Pelsaert Island and other leeward islands is late Holocene in age. (C) View (looking west) of northern part of Serventy Island, a leeward island in the Easter Group, showing bedded coral rudstone (right foreground) overlain by storm ridges of unconsolidated coral rudstone. Note that elevation of storm ridges falls with decreasing age (towards observer). (D) Close-up of bedded coral rudstone, Serventy Island (height of field is 30 cm). Oriented, branching *Acropora* fragments are bound by encrusting coralline algae (white). (E) Core photograph of coral-framestone facies from leeward Holocene reefs. Branching *Acropora* is partly bound by marine cements consisting of high-Mg calcite micrite and aragonite. (F) Rudstone fabric within coral framestone from the leeward Holocene reef. (G) Algal bindstone from the windward Holocene reef consists of coralline algae and serpulids (dark) with interbedded coral framestone (light).

growth of their modern analogs, indicating sea levels at the time when the framestones formed were at least 0.5 m higher than the present position.

Algal-bindstone facies. Coralline algae, foraminifers and serpulids are the primary constituents of the algal-bindstone facies (Fig. 28-6g), which predominates in

windward reefs. The encrusting assemblage of coralline algae, foraminifers and serpulids is interbedded with thin intervals of coral framestone in which corals are heavily bored by mollusks and encrusted by serpulids, algae and foraminifers. Compared with coral framestones in the leeward reefs, bindstones in the windward reefs have relatively fewer voids, and less skeletal sediment infills and lime muds. The bindstones unconformably overlie pre-Holocene calcretized limestones at depths of 4.5–9 m in the windward reefs. The bindstones are rare in cores in the leeward reefs, but frequently form a thin (<20cm) veneer overlying emergent coral framestone in the leeward islands.

Well-bedded, coral-rudstone facies. Branching and platy coral fragments and forms dominate the coral rudstone facies. This facies is 0.5–2 m thick and occurs in the intertidal zone of the leeward islands (Fig. 28-6d). The fragments of corals vary are 1–20 cm long and frequently subhorizontally oriented. The rudstones are widely distributed in the leeward reefs, forming reef platforms and islands. They contain less matrix than the underlying framestones. They are porous but relatively well lithified, bound by encrusting coralline algae and marine cement. The rudstones differ from the underlying framestones in their distinct subhorizontal bedding and orientation of coral debris. This facies has not been observed in the windward reefs.

Unlithified coral-rudstone facies. Branching and platy coral fragments, commonly 5–20 cm in length, are the dominant constituents of the coral rudstone facies. The facies is normally 1–2 m thick and comprises most of the exposures of the emergent Holocene islands in the leeward reefs (Fig. 28-6c). It is rarely lithified, and the voids lack sand-sized sediment and cement. The facies forms linear rubble ridges, usually overlying the well-lithified, bedded coral rudstone. A few to more than ten such ridges are often present. Overturned, fan-shaped coral skeletons up to 50 cm across are sometimes found in swales between coral rubble ridges. These subaerial ridges are believed to be formed in the supratidal zone by the transportation and deposition of coral fragments during severe storms.

Skeletal grainstone facies. Corals and coralline algae are volumetrically most important, and minor mollusks, foraminifers, bryozoans and echinoids are also present in the skeletal grainstone facies. The size of skeletal grains is mainly medium to coarse sand, and may vary from fine sand to silt in deep lagoonal areas. The skeletal-grainstone facies comprises the sediments of sand cays in the windward reefs and laterally extensive sandsheets in lagoons (Fig. 28-6a). Thickness ranges from a few centimeters to up to 3 m. Whereas the sediments on the shelf surrounding the platforms are coralline algal-bryozoan-dominated typical of a cool-water carbonate environment, the skeletal-grainstone facies consists of corals and coralline algae and is more tropical in character.

The Holocene windward and leeward reefs differ in their thickness and lithofacies. The windward reef grew on the wave-exposed margin of the Last Interglacial platform and is less than 9 m thick; in contrast, the thickness of the leeward reefs exceeds 26 m. Whereas the windward reef is composed of an assemblage of coralline algae,

serpulids and corals, the leeward reef consists predominantly of platy and branching corals. The facies sequence in the leeward reefs indicates that, when the reef grew to sea level, it was progressively overlain by peritidal and subaerial facies that now comprise the emergent islands.

DIAGENESIS

Petrologic investigations have shown that the Abrolhos coral reefs have experienced both marine and meteoric diagenesis. The most important diagenesis in the marine environment is cementation by aragonite and high-Mg calcite cements. These cements include micritic, peloidal, and bladed high-Mg calcite, and fibrous and botryoidal aragonite. While the aragonite cements occur mostly in intragranular cavities of organic skeletons, high-Mg calcite cements are present in both intergranular and intragranular cavities. Marine cementation plays a significant role in the formation of rigid reef framework, particularly in the leeward reefs where the porous branching coral framework has been partially filled by a matrix of skeletal fragments that are cemented by high-Mg calcite cements.

The most pronounced effects of meteoric diagenesis occur in the upper part of the Last Interglacial reefs, which are extensively calcretized. In the calcretization zone, dissolution of carbonate skeletons and reprecipitation of calcite cements are common, and neomorphic transformation of coral skeletons to calcite is frequently observed. The overall meteoric diagenesis of the Abrolhos reefs is not as strong as that of most tropical Pleistocene reefs (e.g., Matthews 1968; Dullo, 1986; Zhu et al., 1989; Quinn, 1991). Corals beneath the calcretized zone normally retain their original aragonite mineralogy. Some coralline algae have lost Mg and have been transformed to low-Mg calcite. Sparry calcite cements are not as common as observed in other tropical Pleistocene reefs. The relatively slight diagenetic alteration of the Abrolhos reefs may be related to climatic features, such as the comparatively low rainfall and low temperature of the area.

GROWTH HISTORY

Lithostratigraphic analysis and radiometric dating of corals from cores and outcrops reveal the growth history of coral reefs during the late Quaternary (Fig. 28-7). Late Pleistocene reefs started to grow before 135 ka, with the rapid transgression of the Last Interglacial seas. The reefs were active during the Last Interglacial highstand (132–117 ka), when extensive reef platforms were formed in the area. The Pleistocene reefs provided a suitable substrate for colonization by the Holocene reefs, except in the central parts of platforms, where Pleistocene substrates are usually +2–3 m.

Holocene reefs grew on Pleistocene substrates of a variety of lithologies, such as eolianite and coralline algal bindstone. The depths of the contacts between the Holocene and Pleistocene reefs vary significantly, from >26 m under the leeward

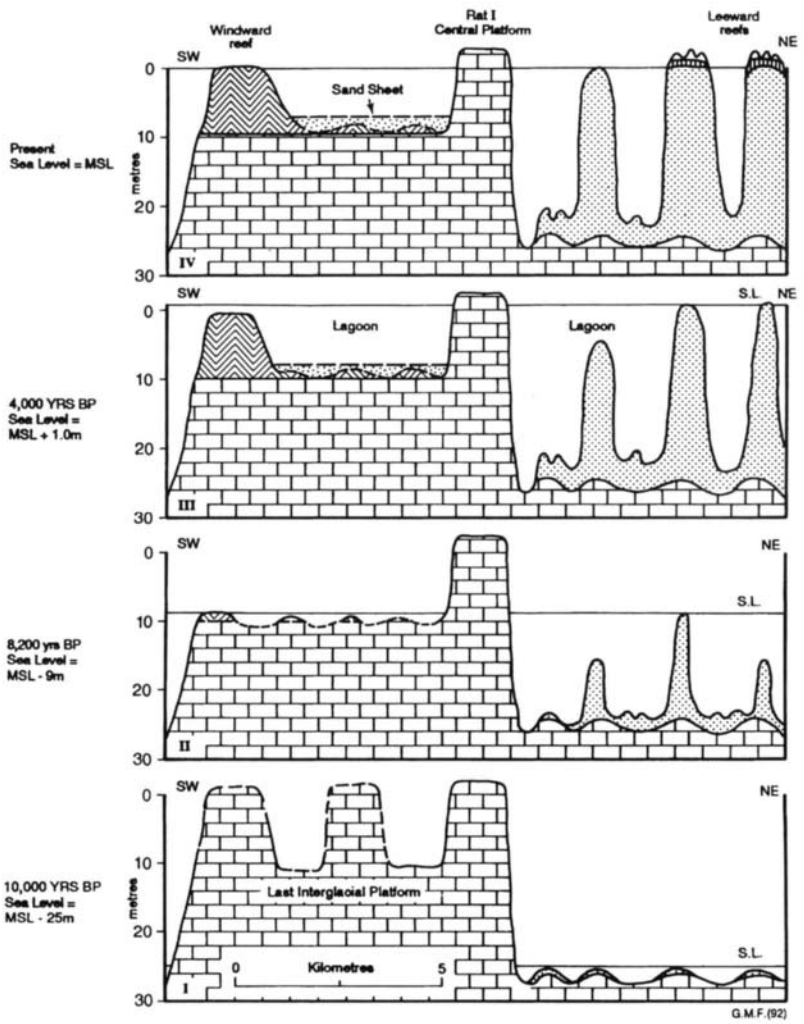


Fig. 28-7. Schematic cross section of the Easter Group depicting Holocene evolution. (I) Holocene reef colonization took place on Last Interglacial substrate of unknown lithology in the lee of the Last Interglacial platform. (Note that the morphology of the platform surface is schematic.) (II) Rising seas of the postglacial transgression beveled the western and central part of the Last Interglacial platform, allowing colonization by the windward reefs (chevron pattern). Leeward reefs (stippled) continued to grow as both "keep-up" and "catch-up" reefs. (III) Sea level rose to transgressive peak by 4 ka, allowing continued growth of windward and leeward reefs, and development of a lagoon sand sheet derived from sediment transported leewards from the windward reef crest. (IV) Late Holocene sea-level fall to present mean sea level produced emergent islands with upward-shallowing sequences capped by storm ridges in the leeward reefs. "Blue-hole" terrains were generated by lateral expansion and coalescence of patch reefs in the leeward reefs.

reefs, to 5 m under the windward reefs. Coral reefs in areas with different substrates and energy regimes have different growth histories. Corals started to colonize Pleistocene substrates at depths >26 m earlier than 9.8 ka (U/Th y B.P.) in the leeward reefs. Colonization of windward reef substrates did not take place until after 8.2 ka (U/Th y B.P.) because of the relatively higher elevation (−10 m) of Pleistocene substrates.

The growth of some leeward patch reefs (represented by the Morley core; see Fig. 28-3) apparently kept pace with the Holocene transgression. The reefs consist predominantly of fast-growing branching *Acropora* and grew at an average accretion rate of 7.7 m ky^{-1}. These reefs recorded a high sea-level event which was ca. +0.5 m by 6.4 ka (U/Th y B.P.; 5500 ^{14}C y B.P.). However, the leeward reef crest (represented by the Suomi core; see Fig. 28-3) has a slightly lower accretion rate (6 m ky^{-1}) and lagged behind sea-level rise. The lag of the reef crest behind the transgression may be due to frequent interruptions to coral growth there by destructive storms.

The colonization of windward coral reefs took place when sea level reached about −9 m. Coral growth was not as extensive as in the leeward reefs. Rather, the coralline algal bindstone, which is interbedded with coral framestone, developed slowly in the windward coral reefs. Windward coral reefs lagged far behind sea-level rise. At about 4.8 ka (U/Th y B.P.), the windward reef at Disappearing Island (Fig. 28-3) was still −4 m. No data are available yet to show when the windward Holocene reef reached present sea level.

After sea level reached its peak at about 6400 y (U/Th y B.P.; 5500 ^{14}C y B.P.), the rate of sea-level change was very slow. Windward and some leeward reefs gradually grew to sea level (by about 4.5 ka in the case of the leeward reefs), eventually forming reef platforms. Leeward coral reefs prograded toward the east. Progradation rates of up to 60 m ky^{-1} have been calculated for leeward-prograding storm ridges on the platforms. Isolated patch reefs in the lagoon gradually anastomosed, forming extensive, reticulated reef flats having a circular "blue-hole" topography.

CONTROLS ON REEF GROWTH

The persistence of reef growth at the Abrolhos is believed to be related to the presence of the warm, southward-flowing Leeuwin Current (Cresswell and Golding, 1980; Pearce 1991). The Leeuwin Current influences many of the factors essential for coral-reef accretion, such as temperature, larval delivery and nutrient concentration, and it favors the maintenance of the coral communities at such a high latitude (Hatcher, 1991). Although little is known about the behavior of the Leeuwin Current during the late Quaternary (Kendrick et al., 1991), it appears to have favored coral growth during the Last Interglacial and in the Holocene.

Whereas sea-level transgression controlled the timing and rate of reef growth, substrates affected the onset and distribution of the reefs. Holocene reef growth was asymmetrical about the Last Interglacial platforms. The shallow, and relatively high, windward margins of platforms were colonized by relatively thin reefs dominated by coralline algae (<9 m thick). In the leeward reefs, on the other hand, where eleva-

tions of pre-Holocene substrates were relatively low, Holocene reefs are well developed, reaching thicknesses >26 m.

The most likely control on the lithostratigraphic features of the windward and leeward reefs seems to be different wave-energy regimes in these areas. The effects of energy regimes on growth characteristics of coral-reef margins are well documented (Adey, 1978; Davies and Marshall, 1980; Macintyre, 1988, Macintyre et al., 1977). The emergent and barely submerged central platforms of Last Interglacial reefs in the Abrolhos form barriers and refract waves, producing two distinct environments on their southwest (windward) and northeast (leeward) sides in terms of wave energy, nutrient concentrations, and habitats for coral growth. High wave energy and the abundance of large, canopy-forming algae have resulted in the dominance of coralline algae and slow growth rates of the windward reefs, compared to the rapidly growing, coral-dominated leeward reefs.

Because of their location at latitudes where conditions for reef development are not as favorable as those in tropical environments, the Abrolhos reefs have distinctive geological and sedimentary features in comparison to tropical coral reefs. Although the lagoon sand sheets are similar to tropical/subtropical chlorozoan-type skeletal carbonates (Lees and Buller, 1975) and are mainly composed of corals, coralline algae and mollusks, they almost totally lack green (*Halimeda*-type) algae which are significant sediment producers in tropical reefs (Goreau and Goreau, 1973; Scoffin and Tudhope, 1985; Liddell, et al., 1989), and they also lack nonskeletal grains such as ooids. The reef corals (e.g. *Acropora*) are relatively poorly calcified (Crossland, 1984). Also, although the accumulation rates of reefs at the Abrolhos are comparable with those of tropical reefs, the Abrolhos reef facies generally lack sandy infill sediment and have high porosities. These characteristics reflect a combination of the fast growth of branching *Acropora*, the relatively slow destruction of framework by biological and physical processes, and the low production rates of sand-sized carbonate sediments.

CASE STUDY: CHRONOLOGY AND SEA-LEVEL HISTORY OF THE ABROLHOS REEFS IN THE LATE QUATERNARY

In using coral-reef growth history as an indicator of sea-level change, there are always uncertainties relating to the ability of reef growth to keep pace with rising sea level because most corals grow in a wide range of water depth (Hopley, 1983; Davies and Hopley, 1983; Davies and Montaggioni, 1985). More accurate records, however, can be obtained by using key indicator species or facies associations. For instance, the Caribbean reef-crest coral *Acropora palmata* is believed to be restricted to water depths of less than 5 m and, therefore, has been used as a reliable sea-level indicator (Lighty et al., 1982; Fairbanks 1989). Microatolls on reef flats in the Great Barrier Reef have been similarly used (Hopley, 1982; Chappell, 1983; Chappell et al., 1983). In the absence of corals restricted to shallow water, the lag between sea level and reef elevation is more difficult to estimate, but the elevation and age of corals in growth position may still provide a reliable indication of minimum sea-level elevations.

Another concern is the reliability of U-series dates determined by high-precision mass spectrometry, which depends on the suitability of the samples dated. Corals are frequently altered by marine and meteoric diagenesis. It is imperative, therefore, to develop criteria which allow assessment of closed-system behavior of samples to be dated. It has been shown that no single criterion is absolutely reliable (Chen et al., 1991; Zhu et al., 1993). Consequently, we use a set of mineralogic, petrologic and isotopic criteria (150 ± 10‰ of $\delta^{234}U(T)$ and low ^{232}Th concentration; see Zhu et al., 1993) and check the consistency of the ages obtained in terms of the details of the stratigraphy before accepting the reliability of age determinations.

Last interglacial

Using stratigraphic evidence and dates from only those samples that have met our criteria for being diagenetically "pristine", we have determined a curve giving the position of minimum sea level during the Last Interglacial at the Abrolhos (Fig. 28-8; Zhu et al., 1993). Dating of corals from the Rat Island core reveals that the Last Interglacial sea level was about −4 m by 134 ka. This finding is in accord with other records, such as the mass-spectrometric dating of submerged speleothem deposits in a cave in the Grand Bahamas Islands (Li et al., 1989) and corals from reef VIIb of the Huon Peninsula (Stein et al., 1993). Collectively, these data indicate that during Termination II most of the glacial-interglacial sea-level increase of 100 m or so (Shackleton, 1987) occurred before 134 ka.

From stratigraphic evidence, the peak of the Last Interglacial sea level at the Abrolhos reached about +6 m. The exact timing of the Last Interglacial peak, however, cannot yet be determined because the only dated sample of the reef of highest elevation, at Turtle Bay, lies outside the criteria established for dating reli-



Fig. 28-8. A plot showing the elevations and ages of coral samples and the consequent interpretation of sea-level history of the Last Interglacial at the Abrolhos. Open circles denote samples whose dates are reliable; closed circles denote samples whose dates have been used as a reference; closed squares denote samples whose dates are not reliable. The maximum sea-level height of the Last Interglacial is based on the elevation of the Turtle Bay reef (From Zhu et al., 1993.)

ability (see Zhu et al., 1993). Nevertheless, sea level at the Abrolhos probably reached at least + 1–2 m by ca. 132 ka. The high sea level of the Last Interglacial persisted until ca. 116 ka. The detailed character of the sea-level curve of the high-stand is not clear. Based on the difference of some 2 m between the elevation of coral-framestone facies of the unique Turtle Bay reef and the widespread 2–3 m reef platform elsewhere in the Abrolhos, we have suggested that there was a 2 m fall of sea level early in the Last Interglacial (Zhu et al., 1993). For most of the time during the Last Interglacial sea level was about +4 m. A similar elevation has been recorded from other sites on the Western Australian coast, such as at Rottnest Island [q.v., Chap. 27].

The timing of the Last Interglacial highstand at the Abrolhos is comparable with other mass-spectrometrically dated records from the coral reefs of Barbados [q.v., Chap. 11] and the New Hebrides (Edwards et al., 1987; Bard et al., 1990), the Bahamas (Chen et al., 1991), and the Huon Peninsula (Stein et al., 1993). Corals from the Last Interglacial reefs at Barbados range from 130 to 122 ka (Edwards et al., 1987; Bard et al., 1990). Corals of the Last Interglacial reefs on Efate Island in the New Hebrides Arc have ages around 130 ka (Edwards et al., 1987). Extensive chronological work on two coral reefs at the Bahamas shows that the highstand of sea level began possibly by 132 ka and certainly by 129 ka. The highstand was sustained until 120 ka, followed by a rapid fall in sea level. Sea-level changes during the Last Interglacial at the Bahamas [q.v., Chaps. 3A, 3B] are believed to have been either a series of short-lived maxima, fine oscillations of one broad maximum, or one well-developed maximum of a prolonged "stillstand" (Chen et al., 1991). The chronology of reef VII of the Huon Peninsula indicates the Last Interglacial sea level was at about −40 m at around 135 ka and the sea-level highstand continued until around 118 ka (Stein et al., 1993).

The possibility of a highstand of sea level during the early part of oxygen isotope stage 5e has been recognized for some time (see summaries in Moore, 1982, and Johnson, 1991). The existence of such an early sea-level highstand has, in part, been used to question the validity of Milankovitch-insolation changes as the forcing function of deglaciation (e.g., Winograd et al., 1992). A significantly longer duration of the Last Interglacial is usually obtained from coral reefs than from the oxygen isotope records of deep-sea cores (Johnson, 1991). This discrepancy has been attributed to the lack of resolution of conventional U-series (alpha-counting) dates. But the Abrolhos record of high-precision mass-spectrometric dates still reveals the wide span in age of the Last Interglacial highstand. This finding, in conjunction with data from other coral reefs, shows the great complexities inherent in global glacial-interglacial transitions and provokes questions as to the details of the mechanisms driving deglaciation.

Holocene

The trend of the Morley reef growth, as shown by the growth curve, has been used as a Holocene sea-level record (Eisenhauer et al., 1993). Because the cored lithofacies

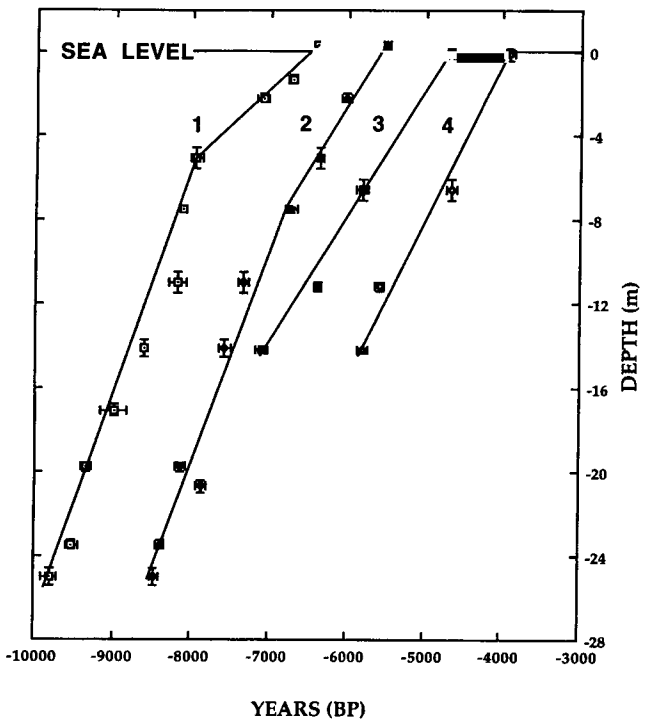


Fig. 28-9. Growth history of Morley and Suomi reefs in the Holocene, based on dated core material. Note the two-stage growth history of Morley core (1, U/Th TIMS data; 2, AMS ^{14}C data) and uniform growth rate of Suomi core (3, U/Th TIMS data; 4, AMS ^{14}C data). For discussion see text. (From Collins et al., 1993b.)

represent continuous reef growth, sea level at any time could not have been below this reef-growth curve, which represents a minimum sea-level curve in the Abrolhos region (Fig. 28-9). This curve, in conjunction with data from outcrops, thus approximates the sea-level history from ~10 ka (U/Th y B.P.) to present in the region.

The Morley core data show that Holocene sea level had reached −25 m at ~9.8 ka (U/Th y B.P.). From 9.8 to 8.0 ka (U/Th y B.P.), there was a generally rapid rise, with a rate of about 10 m ky^{-1}. When sea level had reached −5 m at ~8.0 ka (U/Th y B.P.), the rate of rise decreased to about 3.4 m ky^{-1}. Sea level at the Abrolhos reached a high of +0.5 m by 6.4 ka (U/Th y B.P.). From dated reef outcrops, we know that sea level in the region remained at a height of about +1 m until at least 4000 ^{14}C y B.P.. After that, relative sea level gradually fell to its present elevation.

Comparison of the empirical data with the theoretical modeling of the Holocene sea-level history from isostatic considerations (Lambeck and Nakada, 1990) shows a general correspondence between the two (Eisenhauer et al., 1993). This correspondence indicates that the sea-level highstand of the middle Holocene at the Abrolhos can be explained by hydro-isostatic readjustment, and no significant interpreted overprint of local tectonism needs to be invoked.

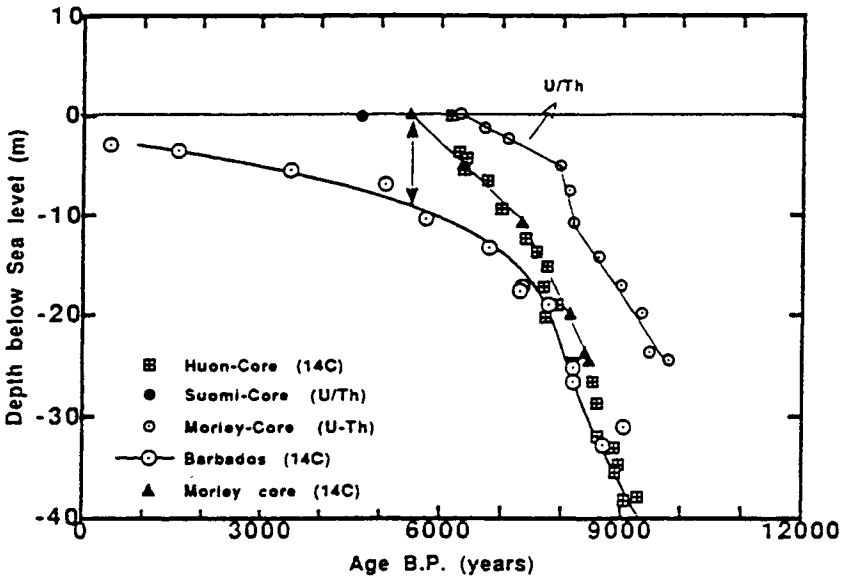


Fig. 28-10. Plot of the U/Th-based and the ^{14}C-based sea-level curve for the Morley and Suomi data, together with observations from Barbados (data after Fairbanks, 1989) and Papua New Guinea, Huon peninsula (data after Chappell and Polach, 1991). There is a good agreement between the Morley core curve and the observations from the Huon peninsula (based on the ^{14}C scale). However, major discrepancies can be observed between these two curves and the results from Barbados. The arrow indicates a difference in apparent sea-level depth of ~10 m at 6.3 ka (U/Th y B.P.; 5500 ^{14}C y B.P.). (After Eisenhauer et al. 1993.)

The sea-level records obtained from the Abrolhos provide the first complete dataset on sea-level history for the Holocene of the coast of Western Australia. Comparison of the Abrolhos sea-level data has been made with those of coral reefs in Barbados (Fairbanks, 1989) and the Huon Peninsula (Chappell and Polach, 1991), which are the two relatively long and rather complete records of Holocene sea-level events (Fig. 28-10; Eisenhauer et al., 1993). All these records show rapid sea-level transgression before 8 ka. Significant differences exist between these datasets after 8 ka. The Abrolhos and Huon data show that sea level rose rapidly and reached the present position between 5.5 and 6.0 ka, whereas the Barbados data indicate that sea level was still rising after 5.5 ka and that it reached the present height after 2.0 ka. The differences are anticipated from global isostatic considerations (Eisenhauer et al., 1993). The Abrolhos coral reefs record the sea-level history in the Holocene at the stable "far field" shelf-margin of the Indian Ocean, which provides a useful database for modeling of the rheology of the earth.

It is imperative that further Holocene sea-level curves are obtained from other tectonically stable areas. Once wider coverage is available, it will be possible to resolve the details of sea-level changes following the Last Glacial Maximum and the issue of global variations in Holocene sea-level history. This, in turn, will lead to a more complete understanding of earth rheology and global climate change.

CONCLUDING REMARKS

The islands of the Houtman Abrolhos are the outcropping portions of three shelf-edge carbonate platforms. Consequently they provide windows into platform geology, which includes coral-reef development in the late Quaternary. The Pleistocene reefs and islands provided a nucleus about which the Holocene reefs developed, so a unique record of reef growth and sea-level history for both the Holocene and Last Interglacial is available. The combination of careful stratigraphic work and high-precision radiometric dating has made these paleoenvironmental records accessible.

One of the important findings of our studies to date is that under certain conditions, coral reefs at relatively high latitude have grown as vigorously as their tropical counterparts during the Holocene. The Houtman Abrolhos should prove to be sensitive indicators of environmental change as they have developed near the temperature limits for coral growth. Indeed, a more detailed record of paleoceanographic and paleoclimatic change than presently determined for the Quaternary is still available through a longer cored record from these islands. It is hoped that with more detailed research such a long-term record can also be coupled to an understanding of such short-term processes of environmental change as variations in sea-surface temperature related to fluctuations of the Leeuwin Current.

REFERENCES

Adey, W.H., 1978. Coral reef morphogenesis: a multidimensional model. Science, 202: 831–837.

Bard, E., Hamelin, B., Fairbanks, R.G. and Zindler, A., 1990. Calibration of ^{14}C timescale over the past 30,000 years using mass spectrometric U-Th ages from Barbados corals. Nature, 345: 405–410.

Chappell, J., 1983. Evidence for smoothly falling sea-level relative to north Queensland, Australia, during the past 6000 years. Nature, 302: 406–408.

Chappell, J. and Polach, H.A., 1991. Post-glacial sea-level rise from a coral record at Huon Peninsula, Papua New Guinea. Nature, 349: 147–149.

Chappell, J., Chivas, A., Wallensky, E., Polach, H.A. and Aharon, P., 1983. Holocene palaeoenvironmental changes, central to north Great Barrier Reef inner zone. BMR J. Aust. Geol. Geophys., 8: 223–235.

Chen, J.H., Curran, H.A., White, B. and Wasserburg, G.J., 1991. Precise chronology of the last interglacial period: ^{234}U-^{230}Th data from fossil coral reefs in the Bahamas. Geol. Soc. Amer. Bull., 103: 82–97.

Collins, L.B., 1988. Sediments and history of the Rottnest Shelf, Southwest Australia: a swell-dominated, non-tropical carbonate margin. Sediment. Geol., 60: 15–49.

Collins, L.B., Zhu, Z.R., Wyrwoll, K-H, Hatcher, B.G., Playford, P.E., Chen J.H., Eisenhauer, A. and Wasserburg, G.J, 1993a. Late Quaternary facies characteristics and growth history of a high latitude reef complex: the Abrolhos carbonate platforms, eastern Indian Ocean. Mar. Geol., 111: 203–212.

Collins, L., Zhu, Z.R., Wyrwoll, K-H, Hatcher, B.G., Playford, P., Eisenhauer, A., Chen, J., Wasserburg, G.J. and Bonani, G., 1993b. Holocene growth history of a reef complex on a cool-water carbonate margin: Easter group of the Abrolhos, Eastern Indian Ocean. Mar. Geol., 115: 29–46.

Cresswell, G.R. and Golding, T.J., 1980. Observations of a southward flowing current in the southeast Indian Ocean. Deep-Sea Res., 27: 449–466.

Crossland, C.J., 1984. Seasonal variations in the rates of calcification and productivity in the coral *Acropora formosa* on a high-latitude reef. Mar. Biol. Prog. Ser., 15: 135–140.

Crossland, C.J., 1988. Latitudinal comparisons of coral reef structure and function. Proc. Sixth Int. Coral Reef Symp. (Townsville), 1: 221–226.

Darwin, C., 1842. The Structure and Distribution of Coral Reefs. London, 1st ed., 214 pp.

Davies, P.J. and Hopley, D., 1983. Growth fabrics and growth rates of Holocene reefs in the Great Barrier Reef. BMR J. Aust. Geol. Geophys., 8: 237–251.

Davies, P.J. and Marshall, J.F., 1980. A model of epicontinental reef growth. Nature, 287: 37–38.

Davies, P.J. and Montaggioni, L., 1985. Reef growth and sea-level change: the environment signature. Proc. Fifth Int. Coral Reef Symp. (Tahiti), 3: 477–515.

Dullo, W.C., 1986. Variation in diagenetic sequences: an example from Pleistocene coral reefs, Red Sea, Saudi Arabia. In: J.H. Schroeder and B.H. Purser (Editors), Reef Diagenesis, Springer-Verlag, Berlin, pp. 77–90.

Edwards, H., 1989. Islands of angry ghosts. Angus and Roberson, 207 pp.

Edwards, R.L., Chen, J.H., Ku, T-L and Wasserburg, G.J., 1987. ^{238}U-^{234}U-^{230}Th-^{232}Th systematics and the precise measurement of time over the past 500,000 years. Earth Planet. Sci. Lett., 81: 175–192.

Edwards, R.L., Beck, J.W., Burr, G.S., Donahue, D.J., Chappell, J.M.A., Bloom., A.L., Druffel, E.R.M. and Taylor, F.W., 1993. A large drop in atmospheric $^{14}C/^{12}C$ and reduced melting in the Younger Dryas, documented with ^{230}Th ages of corals. Science, 260: 962–967.

Eisenhauer, A., Wasserburg, G.J., Chen, J., Bonani, G.J., Collins, L., Zhu, Z.R. and Wyrwoll, K.-H., 1993. Holocene sea-level determination relative to the Australia continent — U/Th (TIMS) and ^{14}C (AMS) dating of coral cores from the Abrolhos Islands. Earth Planet. Sci. Lett., 114: 529–547.

Fairbanks, R.G., 1989. A 17,000-year glacio-eustatic sea-level record: influence of glacial melting rates on the Younger Dryas event and deep-ocean circulation. Nature, 342: 637–642.

Fairbridge, R.W., 1948. Notes on the geomorphology of the Pelsaert Group of the Houtman's Abrolhos Islands. J. R. Soc. West. Aust., 33: 1–43.

France, R.E., 1985. The Holocene geology of the Pelsaert reef complex, southern Houtman Abrolhos, Western Australia. Ph.D. Dissertation, University of Western Australia.

Goreau, T.F. and Goreau, N.I., 1973. The ecology of Jamaican coral reefs. II. Geomorphology, zonation and sedimentary phases. Bull. Mar. Sci., 23: 399–464.

Hatcher, B.G., 1985. Ecological research at the Houtman Abrolhos: high latitude reefs of Western Australia. Proc. Fifth Int. Coral Reef Symp. (Townsville), 6: 291–297.

Hatcher, B.G., 1991. Coral reefs in the Leeuwin Current — an ecological perspective. J. R. Soc. W. Aust., 74: 115–127.

Hatcher, B.G., Kirkman, H. and Wood, W.F., 1987. The growth of the kelp *Ecklonia* near the northern limit of its range in Western Australia. Mar. Biol., 95: 63–73.

Hawkins, R.D., 1969. Gun Island No. 1 completion report. Bur. Min. Resour. (Aust.) Record 1968/205.

Hopley, D., 1982. The Geomorphology of the Great Barrier Reef: Quaternary development of coral reefs. John Wiley-Interscience, New York, 453 pp.

Hopley, D., 1983. Deformation of the north Queensland continental shelf in the Late Quaternary. In: D.E. Smith and A.G. Dawson (Editors), Shorelines and Isostacy. Academic Press, London, pp. 347–366.

Johnson, R.G., 1991. Major Northern Hemisphere deglaciation caused by a moisture deficit 140 ka. Geology, 19: 686–689.

Kendrick, G.W., Wyrwoll, K-H. and Szabo, B.J., 1991. Pliocene-Pleistocene coastal events and history along the western margin of Australia. Quat. Sci. Rev., 10: 419–439.

Lambeck, K. and Nakada, M., 1990. Late Pleistocene and Holocene sea-level change along the Australian coast. Palaeogeogr. Palaeoclimatol. Palaeoecol., 89: 143–176.

Lees, A. and Buller, A.T., 1975. Modern temperate-water and warm water shelf carbonate sediments contrasted. Mar. Geol., 13: M67–M73.

Li, W-X., Lundberg, J., Dickin, A.P., Ford, D.C., Schwarcz, H.P., McNutt, R. and Williams, D., 1989. High-precision mass-spectrometric dating of cave deposits and implications for palaeoclimatic studies. Nature, 339: 534–536.

Liddell, W.D., Ohlhorst, S.L. and Boss, S.K., 1989. The significance of *Halimeda* as a space-occupier and sediment-producer, 1–750 m, North Jamaica. Proc. Sixth Int. Coral Reef Symp. (Townsville), 3: 127–132.

Lighty, R.G., Macintyre, I.G. and Stuckenrath, R., 1982. *Acropora palmata* framework: a reliable indicator of sea-level in the western Atlantic for the past 10,000 years. Coral Reefs, 1: 125–130.

Macintyre, I.G., 1988. Modern coral reefs of western Atlantic: new geological perspective. Am. Assoc. Petrol. Geol. Bull., 72: 1360–1369.

Macintyre, I.G., Burke, R.B. and Stuckenrath, R., 1977. Thickest recorded Holocene reef section, Isla Perez core hole, Alacran Reef, Mexico. Geology, 5: 749–754.

Matthews, R.K., 1968. Carbonate diagenesis: equilibration of sedimentary mineralogy to the subaerial environment, coral cap of Barbados, West Indies. J. Sediment. Petrol., 38: 1110–1119.

Moore, W.S., 1982. Late Pleistocene sea-level history. In: M. Ivanovich and R.S. Harmon (Editors), Uranium Series Disequilibrium: Applications to Environmental Problems. Oxford, England, 481–495.

Morgan, G.J. and Wells, F.E., 1991. Zoogeographic provinces of the Humboldt, Benguela and Leeuwin Current systems. J. Roy. Soc. West. Aust., 74: 59–69.

Pearce, A.F., 1991. Eastern boundary currents of the southern hemisphere. J. R. Soc. West. Aust., 74: 35–45.

Quinn, T.M. 1991. Meteoric diagenesis of Plio-Pleistocene limestones at Enewetak Atoll. J. Sediment. Petrol., 61: 681–703.

Purdy, E.G., 1974. Reef configurations: cause and effect. In: L.F. Laporte (Editor), Reefs in Time and Space. Soc. Econ. Palaeont. Mineral., Spec. Publ., 18: 9–76.

Scoffin, T.P. and Tudhope, A.W., 1985. Sedimentary environments of the central region of the Great Barrier Reef of Australia. Coral Reefs, 4: 81–93.

Shackleton, N.J., 1987. Oxygen isotopes, ice volume and sea-level. Quat. Sci. Rev., 6: 783–790.

Smith, S.V., 1981. The Houtman Abrolhos Islands: carbon metabolism of coral reefs at high latitude. Limnol. Oceanogr., 26: 612–621.

Steedman, R.K., 1977. Preliminary study of oceanographic and meteorological conditions as affecting offshore exploration drilling on WA-59-P, Abrolhos Islands area, Western Australia (unpublished company report, Job. No. 053).

Stein, M., Wasserburg, J., Aharon, P., Chen, J., Zhu, Z.R., Bloom, A. and Chappell, J., 1993. TIMS U-series dating and stable isotopes of the last interglacial event in Papua New Guinea. Geochim. Cosmochim. Acta, 57: 2541–2554.

Stokes, J.L., 1846. Discoveries in Australia 1837–1843, Volume II. T. and W. Boone, London.

Teichert, C., 1947. Contributions to the geology of the Houtman's Abrolhos, Western Australia. Proc. Linnean Soc. NSW, 71 (3, 4): 145–196.

Veevers, J.J., 1974. Western continental margin of Australia. In: C.A. Burke and C.L. Drake (Editors), The Geology of Continental Margins. Springer-Verlag, New York, pp. 605–615.

Veron, J.E.N. and Marsh, L.M., 1988. Hermatypic corals of Western Australia. Rec. West. Aust. Mus., Suppl. 29.

Wickham, 1841. Houtman's Abrolhos. The Nautical Magazine and Navigation Chronicle for 1841: 507–512.

Wilson, B.R. and Marsh, L.M., 1979. Coral reef communities at the Houtman Abrolhos Western Australia in a zone of biogeographic overlap. Proc. Int. Symp. Mar. Biogeog. Evol. Southern Hemisphere, Auckland, 137: 259–278.

Winograd, I.J., Coplen, T.B., Landwehr, J.M., Riggs, A.C., Ludwig, K.R., Szabo, B.J., Kolesar, P.T. and Revesz, K.M., 1992. Continuous 500,000-year climate record from vein calcite in Devils Hole, Nevada, Science, 258: 284–287.

Wyrwoll, K.-H., Zhu, Z.R., Collins, L.B., Eisenhauer, A., Hatcher, B.G., Chen, J. and Wasserburg, G.J., in press. The origin of blue-hole terrain in the Houtman Abrolhos reef complex: western margin of Australia. Geomorphology.

Zhu, Z.R., Marshall, J. and Chappell, J., 1989. Diagenetic sequences of reef-corals in the late Quaternary raised coral reefs of the Huon Peninsula, New Guinea, Proc. Sixth Int. Coral Reef Symp. (Townsville), 3: 565–573.

Zhu, Z.R., Wyrwoll, K.-H., Collins, L.B., Chen, J. Wasserburg, G.J. and Eisenhauer, A. 1993. High-precision U-series dating of Last Interglacial events by mass spectrometry: Houtman Abrolhos Islands, Western Australia. Earth Planet. Sci. Lett., 118: 281–293.

This Page Intentionally Left Blank

Geology and Hydrogeology of Carbonate Islands. Developments in Sedimentology 54
edited by H.L. Vacher and T. Quinn
© 1997 Elsevier Science B.V. All rights reserved.

Chapter 29

GEOLOGY OF REEF ISLANDS OF THE GREAT BARRIER REEF, AUSTRALIA

DAVID HOPLEY

INTRODUCTION

Australia's Great Barrier Reef (GBR) extends over 15° of latitude. Clearly visible from space, the GBR is probably the largest structure on earth built by plants and animals. Its intricate reefal structures were mapped fully only when satellite imagery first became available after 1972. Many areas of submerged shoals have yet to be charted.

The GBR has always been a major navigational hazard. Captain James Cook in the *Endeavour* spent three months in 1770 "barricaded with shoals". The great navigator Matthew Flinders wrote in 1802 that any captain who wished to sail these waters

> "... must not, however, be one who throws his ships head round in a hurry, as soon as breakers are announced from aloft; if he do not feel his nerves strong enough to thread the needle, as it is called, amongst the reefs, whilst he directs the steerage from the mast head, I would strongly recommend him not to approach the coast in this part of New South Wales (Flinders, 1814)."

Cook damaged the *Endeavour* on the reef now named after the vessel and after laborious repairs and an anxious voyage through to the open Coral Sea, was within a few days just as relieved to re-enter the Reef further north after light winds left him with little control of his vessel in waters much too deep in which to anchor (depths of more than 1,000 m are found just outside the outer reef). Such problems not only hindered the charting of the GBR over the next 200 years but also slowed down scientific research, which until 30 years ago remained on an expeditionary basis.

In the 1960s and early 1970s, Australia's growing environmental concern for the GBR was precipitated by specific issues such as limestone mining, oil drilling and damage caused by Crown of Thorns starfish plagues. In 1975, the Great Barrier Reef Marine Park Act was passed and the Great Barrier Reef Marine Park Authority established, the primary role of which was "the protection, wise use, appreciation and management of the GBR in perpetuity".

The 344,000 km^2 of the Great Barrier Reef Marine Park (GBRMP) make it the world's largest managed marine reserve. In 1981, it was inscribed on the World Heritage List. The Park extends to the tip of Cape York, and many of the data given in this chapter relate to the Park area. The Park does not include the many reefs and islands that extend into Torres Strait (Fig. 29-1).

Recently, the bulk of the GBR has been shown to be less than half a million years old (Davies and McKenzie, 1993), far younger than even the majority of open ocean atolls. Minor reef facies may have first appeared in the Eocene when Australia,

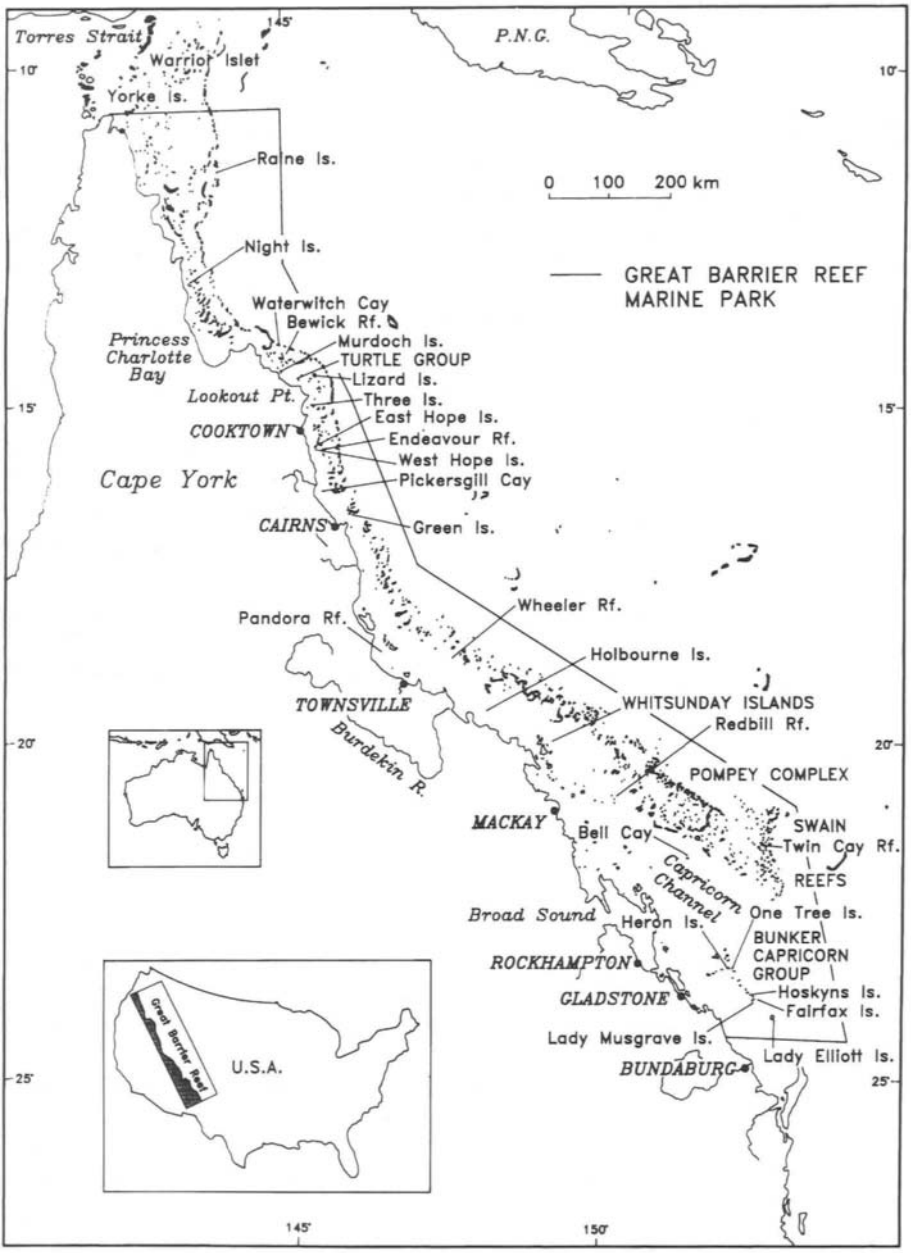


Fig. 29-1. Map of the Great Barrier Reef, Australia, showing locations mentioned in text and the boundary of the Great Barrier Reef Marine Park. Inset shows length of the Marine Park in comparison to the western United States. P.N.G. is Papua New Guinea.

breaking from Gondwanaland, had migrated sufficiently far northward to have its northern waters within the tropics. The GBR, however, was established as an extensive, apparently shelf-dominating facies, only during the high sea levels of the middle and late Pleistocene (Symonds et al., 1983). The reefs of the GBR occur as discrete carbonate slabs rarely more than 250 m in thickness and are developed largely on the outer one-third of the continental shelf. The reefs have apparently experienced continuous subsidence since their early evolution.

The GBR formed during a period of glacially controlled, rapidly fluctuating sea levels. Short periods of reef growth were limited to interglacial highstands; long periods of subaerial exposure occurred during lowstands when at least some karstic landforms were produced (e.g., see Backshall et al., 1979). Typically, the thickness of reef added during each highstand has been about 10–20 m. Distinctive solution unconformities occur between each highstand layer and delimit contrasts in porosity and permeability that play an important role in reef hydrological processes (Buddemeier and Oberdorfer, 1986).

The final veneer on the GBR has been added only in the last 8 ky or so (Davies et al., 1985). Accordingly, the carbonate islands of the GBR are all Holocene in age. They have accumulated since the stabilisation of sea level off the north Queensland coast at ~6500 y B.P. The islands are entirely sedimentary, but they have been stabilised by extensive Holocene cementation. Although numerous, most of the islands are small and have only ephemeral fresh or brackish-water lenses. Nonetheless, these islands have been a major focus of study and their distributions and wide range of morphologies have provided insight into the formation and dynamics of young reef islands worldwide.

SETTING: THE GREAT BARRIER REEF

Atmospheric and oceanic environment (Hopley, 1982, Chap. 2)

Coral reefs require warm water (18°C) with a salinity optimally close to that of the open ocean. Other requirements include low turbidity and minimal sediment settlement. These conditions are found throughout the outer GBR where, even in the south, winter ocean temperatures rarely fall below 20°C, and the climate is everywhere tropical to subtropical (Pickard, 1977). The paucity of mainland fringing reefs south of Cairns is in part the result of mainland runoff; salinities may fall from an optimum 35–36‰ to < 20‰ after heavy summer rainfall. Runoff from the mainland also introduces enormous amounts of sediment into the coastal zone. This sediment reduces the necessary amount of light reaching the corals and other marine life and has the potential to physically smother the reefs. The present annual sediment input from north Queensland rivers is estimated at 28-million tonnes, including 4-million tonnes from the Burdekin River alone (Pringle, 1986). Close to river mouths, therefore, coral growth is very restricted.

Rainfall and runoff are very seasonal along the entire GBR. Winters are generally dry with southeast trade winds blowing frequently at 31–40 km h^{-1}. Even within the

partially protected waters within the Reef this can result in uncomfortable seas of up to 3 m. The winds are generally parallel to the coast, and only where the coastline is oriented more N-S do the coastal ranges intercept them and give some reliability to winter rainfall. This is particularly true between Townsville and Cooktown and to a lesser extent just north of Mackay. Summer monsoonal rains are more intense but may be very irregular even in the wettest areas, and high variability south of Townsville can result in the non-materialisation of several consecutive "wet seasons". Nevertheless, average annual rainfall totals along the entire coastline opposite the GBR are above 1,000 mm, and on the wet coast south of Cairns exceed 4,000 mm. Even here there is still a distinctive summer maximum. Although wind speeds at this time of the year are usually lower (11–20 km h^{-1}), short bursts of higher wind speeds from the southeast and from the northwest can occur.

Even more significant in summer are tropical cyclones. Two or three of these intense tropical storms may be experienced on average in the Coral Sea each year; in some seasons, there have been 15 or more. Not only do cyclones bring destructive winds (200 km h^{-1} or more), but rainfall intensities may be extreme and result in severe flooding. For example, 2,159 mm fell in 120 h at Kuranda near Cairns in 1911; 878 mm in 24 h at Finch Hatton near Mackay in 1958; and 305 mm in 2 h near Townsville in 1946. Storm surges are also produced by cyclones; the combined low pressure and high wind speeds are capable of raising ocean levels by up to 6 m, allowing very large waves to break well inland.

Outside the GBR, the oceanic current is essentially southwards (the East Australian current). In contrast, water movement within the Reef is a product of wind (essentially from the south) and a superimposed tidal regime which produces a northward-flowing ebb-tide current and a southward-flowing flood-tide stream over all except the southernmost Reef. Tides are semidiurnal and generally high, with a range of over 3 m throughout the region. On the mainland near Broad Sound, tides exceed 10 m and on reefs of the region can exceed 6 m, some of the highest tides in the world for coral reefs. An important product of the high tidal range is the very good exchange of water which takes place within and between reefs and around the high continental islands of the Great Barrier Reef.

Size and extent of the GBR (Fig. 29-1)

The "Great Barrier Reef" is made up of over 2,900 individual reefs and about 750 fringing reefs attached to the mainland or the numerous islands of the Queensland coastline (Hopley et al., 1989). The GBR forms a true near-continuous barrier only in its most northern third. The outer perimeter of the Reef is about 2,300 km long. Its southernmost tip is just south of Gladstone at Lady Elliott Island (24°07′S), and it extends northwards into the Gulf of Papua to about 9°15′S. The GBRMP for which the most accurate data are available, ends at 10°41′S opposite the tip of Cape York.

Reefs vary in size from small isolated pinnacles to massive structures over 25 km in length and 125 km^2 in area. In some parts of the region the reefs are closely spaced but elsewhere there may be several kilometres of open water between them. The total

reef area is just over 20,000 km^2, which represents about 9% of the total area of the continental shelf of the GBRMP.

In the north, to just south of Cooktown, the outer barrier is formed by ribbon reefs, which are long reefs (up to 27 km) about 500 m wide and with narrow restricted passages between them. Behind this barrier is an area of apparently open water which actually contains many submerged *Halimeda*-dominated shoals and banks (e.g., Drew and Abel, 1985, 1988; Marshall and Davies, 1988). Further shorewards are numerous closely spaced reefs with large areas of reef flat exposed at low tide; many small sandbanks and vegetated coral islands (cays) occur on these reefs. The innermost reefs, often no more than 8 km from the mainland, sometimes have not only vegetated coral cays but also large areas of mangrove on the intertidal reef flat and are referred to as "low wooded islands". Even the outer reefs of this northern region may be only 30 km from the mainland because the continental shelf is narrow. High islands, made up of the continental rocks of the mainland, are not numerous, although those that occur have extensive fringing reefs. Much of the mainland coastline, particularly where it is steep and rocky or close to headlands, also has narrow fringes of reef (e.g., Partain and Hopley, 1989).

Southwards of 18°S, from about Cairns, the GBR changes. The continental shelf gradually widens to over 125 km opposite the Whitsunday Islands, and even the innermost reefs are 40 to 50 km from shore. There is no outer barrier of ribbon reefs, and, although the main reef tract contains large and numerous reefs, they are often in the form of crescentic outer rims and large sheltered backreef lagoons with coral patches. Fringing reefs are very rare along the mainland but there are great numbers of continental islands, most of which have fringing reefs. Coral cays with vegetation are completely lacking in this part of the GBR.

South of the Whitsunday Islands, there are further changes. Many continental islands are present, but the fringing reefs are smaller and more patchy. In this area, the GBR is at least 90 km from the mainland; the outermost reefs may be as much as 290 km from land. However, here are some of the most closely spaced reefs of the entire GBR. The northern section, known as the Pompey Complex, has narrow tidal channels between very large reefs with intricate closed lagoons. By contrast the southern section, the Swain Reefs, has much smaller but even more closely spaced reefs (599 reefs occur between 21° and 22°S). Many have small coral cays.

The southern tip of the Swain Reefs is 200 km from the mainland and separated from it by the Capricorn Channel. To the south, the continental shelf region narrows and the southernmost reefs, the Bunker and Capricorn Groups, are little more than 50 km from the mainland. Many have large vegetated sand cays and distinctive sheltered lagoons.

SEDIMENTARY AND GEOMORPHOLOGICAL PROCESSES OF REEF ISLANDS

Sediments of reef islands

Sediments of the GBR have been a major focus for study (e.g., Maxwell, 1968, 1973), though reef islands have not figured prominently in this research. The

tendency for shingle and rubble to next break down into sand sizes of approximately 2 ϕ (Orme, 1977) means that there is a distinctly bimodal distribution of sediment sizes that result from the ambient wave-energy conditions and a clear division of depositional environments. Nonetheless, it would be an oversimplification to subdivide reef islands into only windward shingle cays and leeward sand cays.

Studies of sediments of GBR cays (Maxwell et al., 1961, 1964; McLean and Stoddart, 1978) suggest that, in sand and shingle cays, there is a remarkable uniformity in the sediments over the entire province. The most comprehensive study is that of McLean and Stoddart (1978) on the northern GBR. According to their study, shingle, which is relatively homogeneous in composition (mainly fragmented *Acropora*), shows a great range of size and shape. In contrast, sediments of sand cays are much more uniform, mainly in the range of medium to coarse well-sorted sands.

The most common size range in the sand cays is 0–1.5 ϕ, and sorting is generally less than 1 ϕ. Constituents are similar to those of the reef-flat sediments. Compared to the reef flat, however, the cay sediments are generally better sorted, though of a similar mean size. The beaches of the sand cays are the coarsest sediments, particularly on the windward side. Winnowing by the wind moves finer sand to the cay interior or berm. McLean and Stoddart (1978) found the finest sediments to be associated with present and buried soils and suggested that this was due in part to the incorporation of fine organic matter.

Studies of cay sediments elsewhere on the GBR indicate that the findings on cays north of Cairns are more generally applicable. Although sediments of sand cays occur within a narrow range, local differences can be noted. McLean and Stoddart (1978) suggest that small but distinct differences between cays are due to various causes: proportions of constituent components, which may be related to the nature of the reef flat; differences in distances, modes, and rates of transport from source area to cay, all of which are dependent on the size of the reef and the location of the cay; and variations in residence time since deposition. On Redbill Reef, for example, cay sediments of Bushy Island are coarser and more strongly negatively skewed than those of the northern sand cays and have a higher proportion of coralline algae. These features result from the proximity of the cay to the massive algal ridges of the reef margin. Sediments are also coarsest on the windward southern and eastern beaches of this cay (Hopley, 1981).

Shingle deposits are more heterogeneous. Recently formed shingle ridges are brilliant white in colour; they remain this colour only when occasionally moved by waves. Shingle deposits of the island ridges, however, rapidly acquire a dull, grey appearance as they are colonised by boring algae. As noted by McLean and Stoddart (1978), old surfaces may be extremely pitted and irregular; clam valves are similarly weathered in the subaerial environment. Although the fresh shingle undergoes some abrasion, McLean and Stoddart (1978) showed that older blackened shingle sticks were only 51–67% of their original size. Also, calcite is present in the clasts, indicating early diagenesis. The proportion commonly is in the range of 3–10% but values up to 52% were recorded by McLean and Stoddart (1978). Internal boring also increases primary porosity by up to 20% in the clasts, though much of this is achieved on the reef flat rather than in island deposits.

Some noncarbonate sediments are incorporated in coral cays. The most common are pumice fragments that are floated in from their source area in the Solomon Sea-Vanuatu area. Individual fragments up to 0.5 m in diameter have been found, but more commonly the fragments are about 1–5 cm long. Pumice fragments form distinctive strata in cay sediments; thickness of the strata ranges up to 30 cm. Occasionally continental rocks reach the GBR cays in the roots of floating trees.

Depositional processes and landforms

The only pre-existing condition required for the formation of a coral island is a sufficient area of reef flat, and this need not be large. The outermost reef flat is normally fringed by a living coral zone which, if it has 100% coral cover, will be producing calcium carbonate at a rate of about 10 kg m^{-2} y^{-1}. It is from here that the material for reef-island development mostly comes. The reef-front zone of living coral gives way to algal pavement. On outer reefs this may be formed of encrusting calcareous algae, but on mid-shelf and more sheltered inner-shelf areas, it is covered by a turf of green and brown algae. Yet further from the reef front is a rubble zone, the first depositional area on the reef flat from which initial islands may form. On the GBR, the general level of the reef flat is about mean low water springs (MLWS). The spring tidal range over much of the reef is approximately 3 m and the highest points of the islands which accumulate over the reef flat can be as high as 6 m above reef-flat level or 3 m above mean high water springs (MHWS).

As noted above, the sediments on the reef tops are essentially bimodal. Coarser sediments including reef blocks several metres in diameter are located close to the reef front. These, and much of the rubble and shingle of the reef top, are deposited during high-energy cyclonic storms. During such storms, the water levels may be higher due to storm surge, and wave energy is considerably greater than under normal weather conditions. Nonetheless, the competency of wave-generated currents to carry material from the reef front is rapidly reduced by frictional forces, and so material is deposited in a zone 50–100 m from the reef front. Initially this is a heterogeneous rubble zone, but at a later stage, with more sorting of material, the deposit becomes a shingle rampart (Fig. 29-2). Shingle ramparts consisting of gravel-sized coral debris, usually well sorted, are single or multiple ridges 1–2 m above the level of the reef flat and form the first stage of a shingle island. The features are described by Stoddart et al. (1978a, p. 49):

> "Ramparts are asymmetric ridges of coral shingle with a steep inward face locally reaching 80° and a gentle seaward slope of less than 10°. Their outer margin is a feather edge of shingle on the reef flat and is often too indistinct to map; in the plan it roughly parallels the edge of the reef. The inner edges are arcuate with occasional shingle tongues which on the windward side are at right angles to the reef edges, but elsewhere are at an angle to it."

These shingle tongues often take the form of hammerhead spits. Although modified in normal weather conditions, each rampart may represent a single storm and several rampart systems may be separated by moated pools in which microatolls grow.

The competency of wave-generated currents to transport biogenic carbonate sediments is related not only to size but also to the shape and bulk density of the



Fig. 29-2. Rampart of coarse rubble consisting mainly of branching coral shingle on the windward margin of a low wooded island reef.

particles. However, the finer sand of reef flats can be transported during most normal weather conditions. Because of the height of reef flats, movement may be episodic, dependent on the state of the tide. Sand-sized material may result from the breakdown of coarser deposits thrown up during storms, but can also be directly generated by plants and animals, such as foraminifera and *Halimeda*. The characteristic centripetal action of refracted waves which pass over the reef front, breaking and reforming, has the tendency to concentrate sand-sized sediments towards the lee side of the reef. At least initially, the product of this movement is a highly mobile sandbank but, with increasing size and increasing maturity of the reef flat, mobility decreases and the bank becomes the focus for additional material in the form of concentric sand ridges. Whilst these can develop from a normal high tide berm, the occurrence of coarse beach materials several metres above normal tidal levels suggests that major modification to the ridges takes place during storms, possibly with associated storm surge. Nonetheless, the heights of ridges at any particular location, especially on larger islands, show a surprising degree of uniformity. As intervening swales become infilled, ridges are modified into sand terraces displaying only minimal surface relief.

Although stability in any reef-top island is relative, once an island has grown to a particular size, a most important process in the evolution of island morphology is cementation. The processes of carbonate cementation have been the focus of a considerable discussion that is beyond the scope of this chapter (see Hopley, 1982, Chap. 5). Suffice it to say, however, the product in the sand cays is beachrock: firmly cemented beach materials dipping seaward within the intertidal zone. The absolute level of cementation appears to be MHWS, but is more commonly a near-horizontal

cemented surface produced internally within the beach at a level between mean sea level (MSL) and MHWS. However, cemented levels can be considerably higher than this in coral islands as the result of downward leaching of bird droppings in the form of guano. The internal water table of the island plays a part in this cementation process, and the uppermost level of cementation may be considerably higher than that of beachrock. The fabric tends to be more massive and homogeneous and the cement is phosphatic, sometimes of high enough content to be mined for the phosphate.

Cementation also takes place in the coarser shingle and boulder materials of windward ramparts. Here the cemented material is a coarse conglomerate, the upper level of which is very horizontal. The original depositional structures are retained within these rampart rocks, but, in contrast to beachrock, the dip, which reflects deposition of materials thrown over the rampart and down the steeper face that faces the centre of the reef, is steep and away from the sea. Around the margins of cemented conglomerate, the steeply dipping beds form sharp serrated ridges to which the term "basset edges" has been given (Fig. 29-3). The upper level of cementation in these coarser deposits is almost exactly MHWS in contemporary deposits. However, on the GBR, conglomerate platforms can be more than 1 m higher than this and apparently relate to a higher sea level in the past (see below).

Cementation clearly gives greater permanence to both shingle and sand islands of reef tops. In addition, as the rampart rocks tend to follow the line of the ramparts within which they formed (i.e., tend to be found around the perimeter of the reef at



Fig. 29-3. Landward-dipping basset edges and conglomerate platforms, Three Isles Reef (northern GBR).

least on the windward margins), their height and distribution tend to provide considerable protection from wave action to the central reef flat. Under these conditions, it is possible for mangroves to colonise the reef top. Accordingly, extensive areas of mangroves and associated organic deposits that accumulate around the roots form a distinctive element in some islands of the GBR.

CLASSIFICATION AND GEOMORPHOLOGY OF REEF ISLANDS AND CARBONATE DEPOSITS OF CONTINENTAL ISLANDS

Due to the quiescent tectonic setting of the GBR, there are no emerged carbonate islands anywhere along the Queensland coast. In a review of the literature of reef islands worldwide, however, Stoddart and Steers (1977) suggested that the cays and low wooded islands of the GBR display greater variety and more complex morphology than reef islands of any other region of coral reefs. Because of the variety of shapes and sizes of reefs of the GBR, their latitudinal spread across several climatic zones, and variations in age (see below), reef islands of the GBR vary from small ephemeral sand patches that emerge only at low water, to complex, low, wooded islands that consist of a leeward sand cay, a windward shingle island with cemented rampart rocks and a central mangrove swamp. Some continental islands, with extensive reef flat, also have areas of carbonate deposits which are very similar lithologically and morphologically to the more complex cays of the GBR.

Hopley (1982) has reviewed the extensive literature on these islands and their classification. Criteria used in classification have included four main elements:

1. Sediment type — sand or shingle. Sand cays are formed more frequently on leeward margins; shingle cays occur towards the windward side. There are also examples of mixed sand and shingle islands.
2. Island location — windward or leeward.
3. Island shape — linear or compact. This characteristic is the result of reef shape and patterns of wave refraction. Compact islands result from more efficient centripetal movement of sediment towards a single focal point. In general, compact islands are more stable; greater linearity indicates instability.
4. Stage of vegetation cover — a reflection, at least in part, of age, size and stability.

There is a continuum from the sanded reef flat with low sandbanks to the most complex morphology of the multiple low, wooded islands. The following classification is a synthesis of that described more fully in Chapter 12 of Hopley (1982).

Unvegetated solitary islands

Unvegetated cays are unstable and may migrate over several hundreds of metres of reef flat during periods of several years, changing shape and height as they move (Taylor, 1924; Stoddart et al., 1978a; Hopley, 1982). Their small size and instability are obvious reasons for the lack of vegetation, although some larger cays have been stable enough for beachrock to form (Fig. 29-4). Probably, windward shingle cays,

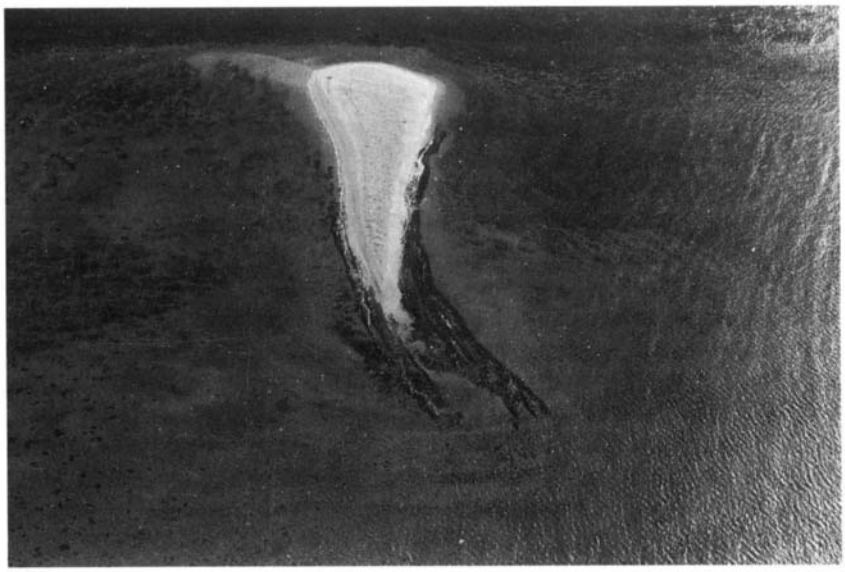


Fig. 29-4. Waterwitch Cay (northern GBR), an unvegetated cay which has been stable enough for massive beachrock to have formed.

which owe much of their development to cyclonic storms, may be more stable or move more slowly than sand cays. Greater stability of the unvegetated shingle cays is suggested by the common occurrence of cemented deposits such as basset edges or conglomerate with the coarser materials. However, examination of a number of unvegetated shingle cays suggests that they acquire a plant cover more slowly than sand cays. The slow colonisation is probably due to the exposed location of the islands and the open framework of coarse shingle that will not retain freshwater.

Vegetated solitary islands

Occasionally even unstable cays may acquire an ephemeral vegetation from drift seeds or seeds brought in by birds. Only if there is a core area of the cay that does not alter over a period of several years, however, can a permanent vegetation develop. Even then, a single storm or a period of prolonged erosion can revert the cay to its original unvegetated condition.

Solitary vegetated islands are divided by Hopley (1982) into four main types: vegetated sand cays, vegetated mixed sand and shingle cays, vegetated shingle cays and mangrove islands.

Vegetated sand cays. Vegetated sand cays of the GBR range in size from less than 1 ha to over 1 km^2 in area (Fig. 29-5). Similarly, the heights of cays vary from only a little above MHWS, making them liable to overtopping on the highest spring tides, to several metres above MHWS on older cays with dunes.



Fig. 29-5. Bushy Island, a vegetated sand cay on Redbill Reef (south central GBR). The climax forest is *Pisonia grandis*. The tidal range here is about 5 m, and the reef flat is dammed behind a series of algal ridges, which can be seen in the left foreground.

Beachrock on the sand cays forms an integral part of the morphology of these islands and plays a major role in their stabilisation. The occurrence of beachrock outlining the location of islands that are now completely disappeared, however, indicates that major storms can remove the uncemented deposits from within the defences provided by beachrock.

The internal morphology of vegetated sand cays is quite variable. Some apparently older islands have a central area that rises up to 4.5 m above MHWS and consists of a series of low sand ridges with probable dune capping, even though the material is medium to coarse sand and may contain drift pumice (McLean et al., 1978). McLean et al. (1978) recognised two distinct levels of sand ridges which they termed "high terrace" and "low terrace". The high terraces, which generally have deeper soils, have surveyed heights of 2.2–4.5 m above MHWS. A dense broadleaf forest occupies the interior of high terraces. On some cays, where erosion has cut into the high terrace, horizontal beachrock is found in the area of erosion up to a metre above the level of what is considered as contemporary beachrock (McLean et al., 1978). In contrast, low terraces have incipient soil development and a more open scrub or herbaceous vegetation. Heights are 0.9–2.2 m above MHWS. Beachrock adjacent to low terraces is consistently lower and inclined towards the sea. Clearly at least two periods of cay sediment accumulation, possibly associated with different sea levels, are recorded in these older vegetated islands and their high and low terraces.

Vegetated mixed sand and shingle cays. Mixed sand and shingle islands can form in various ways. Most commonly, the shingle originates from specific storm events and sand is added during more normal weather. In some cases, the shingle is supplied from the windward margin of the reef, and sand is derived from the lee-side reef flat. Such cases are most likely in areas where there is a marked seasonal change in direction of dominant winds, and the sparse data available suggest that some cays of the Torres Strait area may be of this type. In other cases, a decline in productivity and supply of sediment from the reef flat may also cause a change in calibre of the material supplied to a cay. Such a decline may result from changes in storminess, sea-level variations, or changes in geometry of the reef top with time. Solitary mixed sand and shingle islands are not common, but some of the low wooded islands of the northern reef contain admixtures of these sediments, and some may have evolved initially from this type of cay.

Vegetated shingle cays (Fig. 29-6). The vegetated shingle cays are located either on the windward margins of larger reefs, or centrally on the reef flat of exposed small reefs. The majority are of a compact morphology, as linear shingle cays are sufficiently mobile to prevent the establishment of permanent vegetation. Nonetheless, some vegetated shingle cays appear to have developed from the more stable areas of older rampart systems. The windward shingle components of the low wooded islands are most certainly developed from old linear ramparts.



Fig. 29-6. One Tree Island (southernmost GBR), a vegetated shingle cay, is composed of overlapping shingle ridges and has formed just back from the windward margin of the reef.

Shingle cays most frequently develop from the coalescence of several coral shingle ridges. The initial focus for developing a shingle island may be a hammerhead spit or tongue of shingle in the rubble zone of the outer reef flat.

Mangrove islands. Stoddart and Steers (1977) described islands formed by the mangrove colonisation of shoal areas that lack the shingle ramparts and rampart rocks of the low wooded islands. Without windward protection, such islands can form only on high reef tops, in low energy conditions, and in areas of relatively low tidal range. The few examples on the GBR occupy a high proportion of the reef top and, in places, approach to within 100 m of the reef edge.

Multiple islands (Fig. 29-7)

There are a small number of examples of two vegetated islands on a single reef. Invariably in such cases, a shingle cay occurs on the windward side of the reef flat and a sand cay occurs on the leeward side.

Complex low wooded islands

On the inner reefs north of Cairns, there is a group of reef islands with a complexity unique to the GBR (Stoddart et al., 1978a). Described by many explorers and



Fig. 29-7. Fairfax Reef (Bunker Group), with windward shingle and leeward sand cays and a partially infilled lagoon. The shingle cay in the foreground has had its vegetation greatly disturbed by human activities.

expeditions, these islands were termed "low wooded islands" by Steers (1929). At their simplest, they consist of a windward shingle island and leeward sand cay, with intervening mangroves typically occupying 25–50% of the reef top in the lee of the shingle (Fig. 29-8). However, these islands display a complex range of features not associated with discrete sand or shingle cays and the presence of mangroves provides both an immediately recognisable unique feature and a unifying reef-top unit.

The shingle island (or, sometimes, islands) are formed of ramparts which may extend around almost the entire reef perimeter, with long shingle tongues extending more than 100 m onto the reef flat (Fig. 29-9). Where older rampart systems are eroded, basset edges indicate the former extent of the ridges. Most low wooded islands have several shingle ramparts making up the outer part of the shingle island. The ramparts are occupied by a low mangrove scrub and swards of succulents (*Sesuvium*, *Salicornia*, *Suaeda*) particularly on the older cemented areas. Between the ramparts and the platforms are moats that retain their water at low tide and form the location for extensive microatoll growth.

The most stable part of the windward shingle islands is provided by conglomerate platforms of rampart rock. These platforms are usually cliffed on the seaward margins where, on some islands, they can be seen to overlie older microatolls. Some microatolls are probably related to sea levels about 1 m higher than present. Elsewhere, the lowest platforms may disappear seawards beneath the reef-flat rubble without a sharp break of slope, or they may degenerate into basset edges. Most researchers have recognised two distinct levels of platforms on low wooded islands, although on some islands the distinction is not clear and the upper platform is not always present. The mean level of the lower platform is almost exactly MHWS, whereas the upper platform has a mean level 0.6–1.2 m higher. At specific locations, the two platforms are usually separated vertically by about 1 m. Both upper and lower platforms vary in width from < 10 m to mean widths of 30 m and a maximum width of almost 70 m. The majority of platforms are surmounted by a series of old shingle ridges that form the highest part of the shingle cay. Maximum elevation is 3.5–4.9 m.

In the lee of the shingle island and peripheral ramparts are mangrove swamps, the areas of which range to over 125 ha on Bewick Island, where they occupy up to 68% of the reef top (Stoddart et al., 1978a). *Rhizophora stylosa* is the predominant mangrove, but Stoddart (1980) recorded 15 species from the low wooded islands. Although extending onto reef-flat sands on some islands, the mangroves, where well established, have accumulated thick, black, organic mud deposits up to 2 m deep.

The leeward sand cays display a great range of size and morphology from ephemeral unvegetated sand patches to massive vegetated cays approaching the dimensions of the Capricorn Group of islands. Two terrace levels are well displayed by the majority of the larger cays, with difference in soils, vegetation, and elevation as noted above. Beachrock is also widely distributed around the sand cays of low wooded islands, with exceptionally high levels up to 0.4–0.7 m above MHWS where the older terrace has been eroded to expose the outcrop.

Although the cays of the Turtle Group just north of Lookout Point have all the features of low wooded islands, they lack a central reef-flat area and appear to be a separate island type (Fig. 29-10). Ramparts and associated rampart rocks are closely

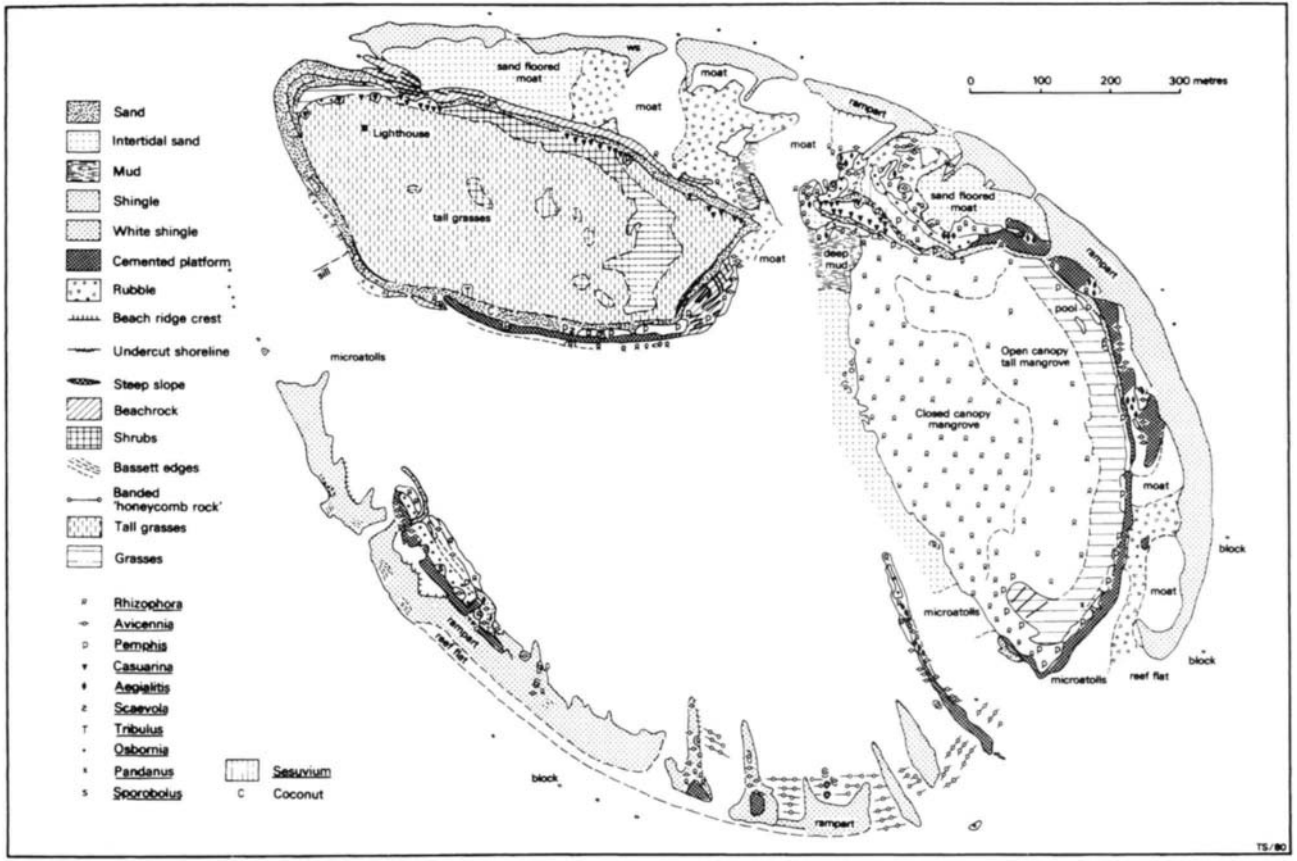


Fig. 29-8. Geomorphological map of Three Isles (northern GBR), a classic low wooded island. The southeastern edge is the windward margin where ramparts and rampart rocks give shelter to a small area of closed-canopy mangrove. A large sand cay is on the leeward side of the reef. (After Stoddart et al., 1978c.)



Fig. 29-9. Aerial view of Three Isles (northern GBR).

linked with the leeward cay, which is constructed largely of shingle ridges rather than sand, and mangroves are limited to the linear depressions between shingle ridges or between the platforms and main cay. All these islands are on very small reefs (generally < 60 ha) and occupy a large proportion of the reef top. Larger ones have shown central lagoons lined with mangroves.

Carbonate deposits of the high islands

Some 617 high islands with fringing reefs have been identified within the GBRMP. Many of these high islands have extensive areas of carbonate deposits and cemented materials of Holocene age (Fig. 29-11). Although some older terrigenous deposits around which the carbonate materials have accumulated may be Pleistocene in age (e.g., Hopley and Barnes, 1985), all carbonate deposits have accumulated entirely during the Holocene (Fig. 29-12). Considerable work has been carried out on them (Hopley, 1968, 1971, 1975, 1982; Chappell et al., 1983). Typically they have formed as bayhead beaches and associated deposits, or as lee-side spits attached to high islands. Although terrigenous boulders of Pleistocene age may be found, the younger carbonate deposits contain most of the morphological components of the low wooded islands including terraces of carbonate sands and beach ridges, extensive areas of emerged beachrock, platform rocks and phosphatic cay sandstone, and occasionally small areas of emerged reef (Fig. 29-12).

Available dates indicate that development of fringing reef flat commenced before 6000 y B.P. (e.g., Hopley et al., 1983; Hopley and Barnes, 1985; Partain and Hopley, 1989, Kleypas, 1992). These carbonate deposits fringing the high islands, therefore,

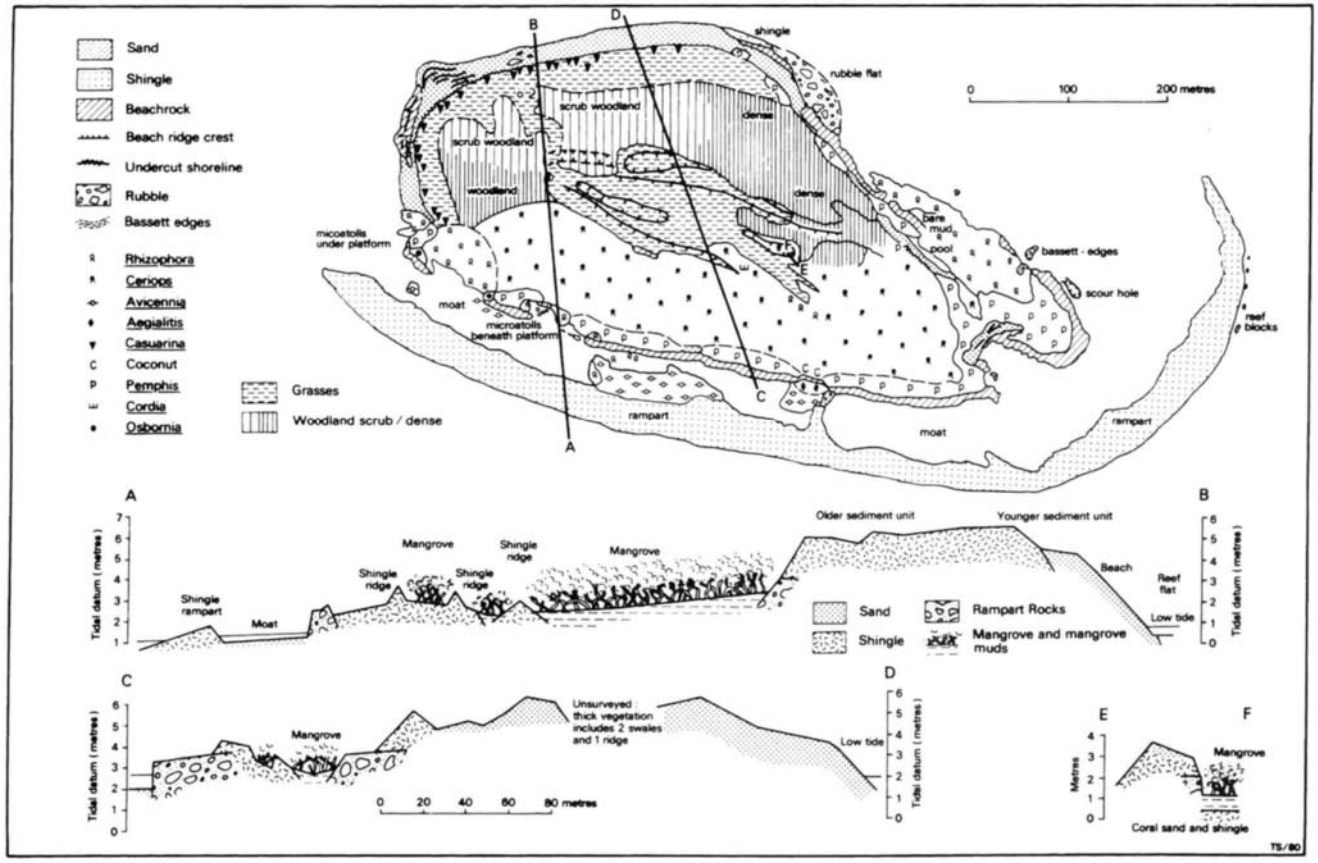


Fig. 29-10. Geomorphology of Turtle I Island from a survey in 1973 by D.R. Stoddart with profiles added by the author. Turtle I Island is a special type of low wooded island in which the shingle cay and sand cay have been pushed together and are separated only by a relatively narrow strip of mangroves.



Fig. 29-11. Holbourne Island (central GBR). This continental island has a fringing reef and an extensive area of Holocene deposits (in foreground) in which many of the elements of low wooded islands are found including beach ridges, beachrock, platform rock, and phosphatic sandstone. The latter has been mined commercially in the past.

appear to be older than the similar features found on the low wooded islands of the outer reefs (see below).

NUMBERS AND DISTRIBUTION OF ISLANDS

The distribution of reef islands is a product of the Holocene history of the reef top and current conditions of exposure to both everyday weather and cyclonic storms. Thus reef islands are far from evenly distributed in the GBR. They are most numerous at the northern and southern extremities of the Reef. A large part of the central area lacks even unvegetated cays. Distribution of major island types is seen in Fig. 29-13. Within the GBRMP, 10.3% of the reefs have islands.

Unvegetated cays are the most numerous. Many are small, <50 m in length, and very few have beachrock. Particular concentrations occur in the Swain Reefs, between 18° and 19°S, and from Cairns northward where they become most numerous in the approaches to the Torres Strait. Unvegetated cays occur on all types of reefs including those in relatively exposed locations such as the southern Swains and on the outer ribbon reefs north of Lizard Island. There are no unvegetated cays between the northern Pompey Reefs and Wheeler Reef off Townsville, a distance of 315 km.

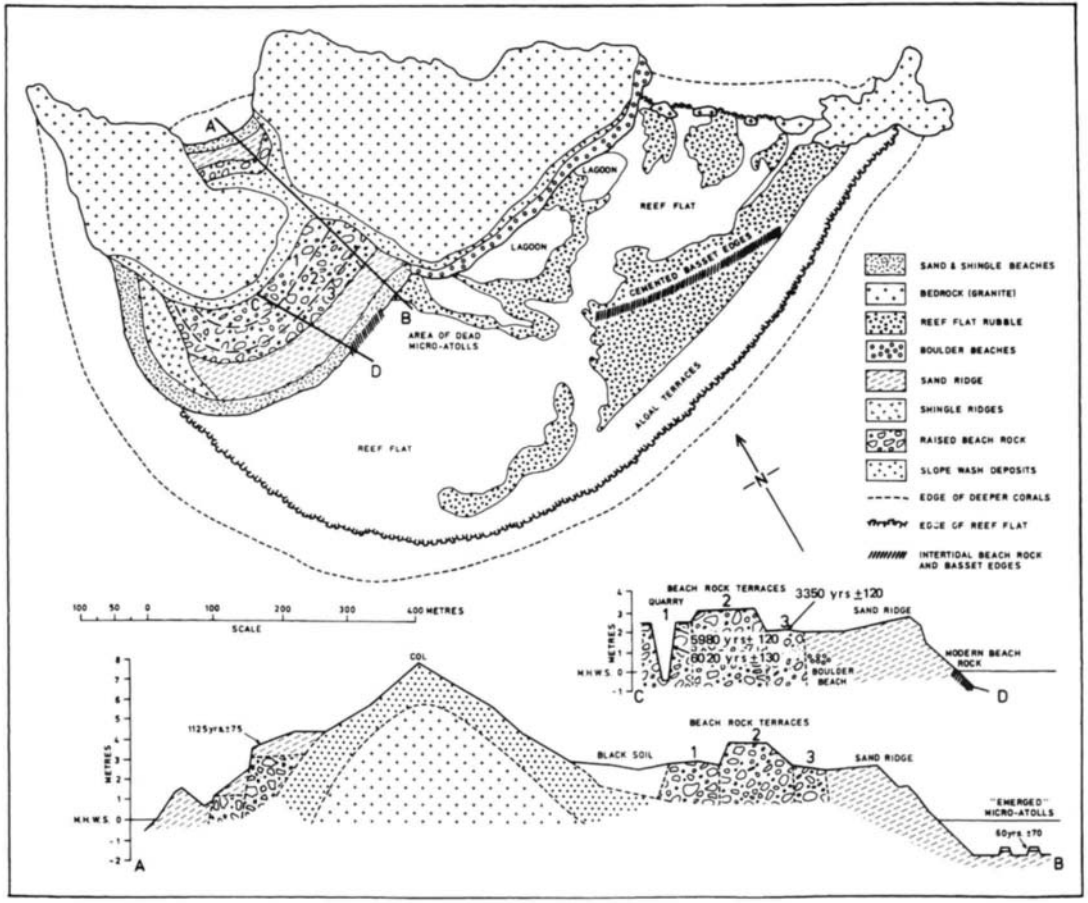


Fig. 29-12. Geomorphological map of Holbourne Island and surveyed transects indicating the carbonate elements which are common with low wooded islands. Radiocarbon ages in the rearmost beachrock terraces indicate a mid-Holocene age; i.e., these features formed shortly after the mid-Holocene sea level stabilised close to its present position.

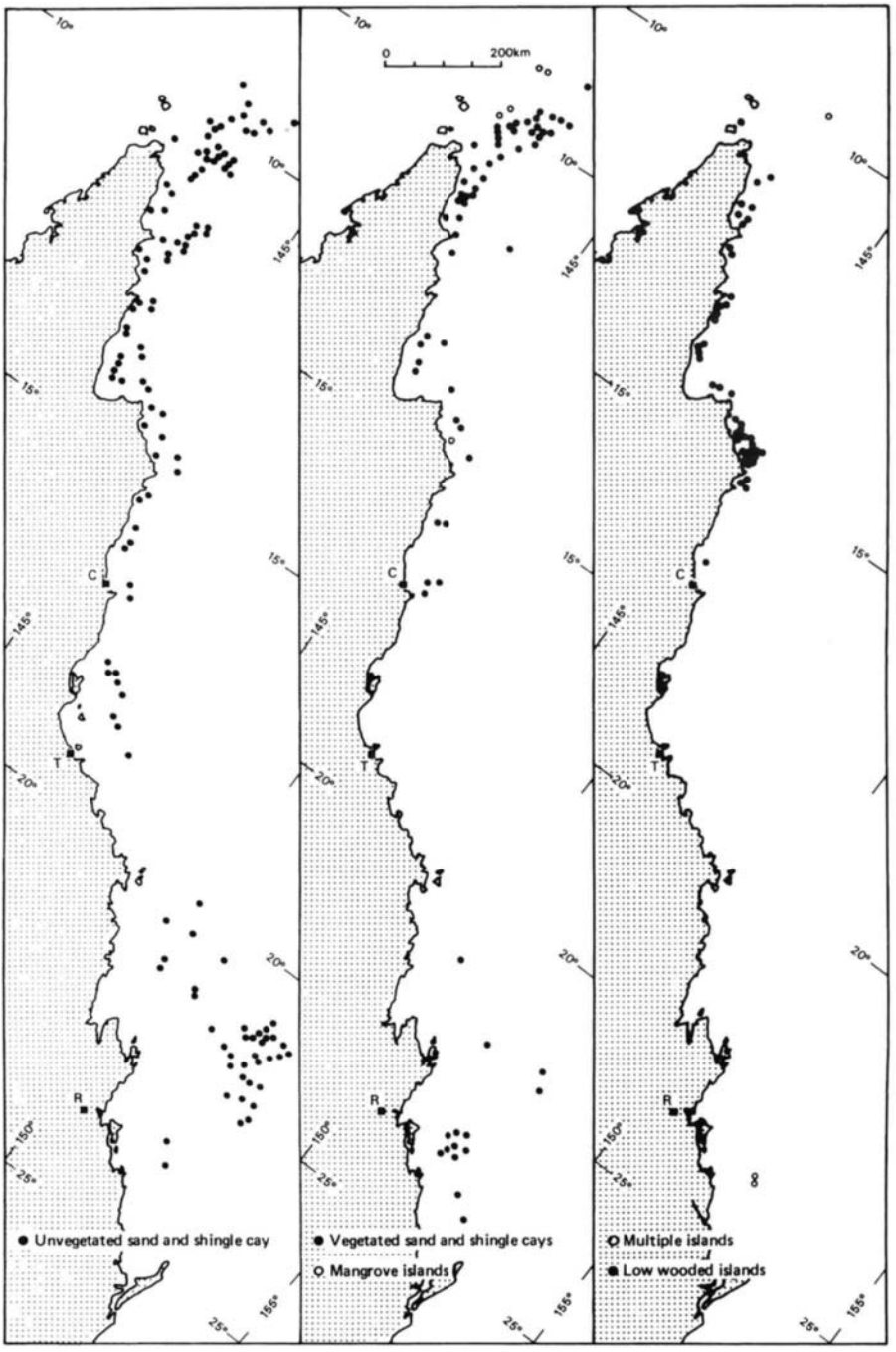


Fig. 29-13. Distribution of major reef island types on the GBR. (After Hopley, 1982.)

Vegetated islands are also most numerous in the Torres Strait region; some of them are inhabited. Vegetated islands are common on inner reefs and the western ends of large midshelf reefs on the northern GBR north of Cairns. On the southern GBR, the Bunker-Capricorn Group forms a distinctive set of well-vegetated islands. Some lightly vegetated cays are located in the Swain Reefs, and there are two well-vegetated cays on inner reefs — Bell Cay and Bushy Island. Between Bushy Island (20°57′S) and Green Island (16°46′S) near Cairns, a distance of 640 km, there are no vegetated cays on the GBR.

All but one of the five mangrove islands of the GBR occur in the Torres Strait area. The exception is Murdoch Island (14°37′S). All the mangrove islands occur in sheltered areas with only low to moderate tidal ranges. Also, they are located where they may receive terrigenous sediments, as is especially the case for the mangrove islands that are close to the New Guinea coastline.

Multiple islands are even more sparse. Apart from the two in the Bunker Group (Hoskyns and Fairfax), the only other example mapped is the Yorke Islands in Torres Strait (9°45′S).

Low wooded islands have a very clustered distribution as previously noted by Steers (1929, 1937, 1938) and Fairbridge (1950, 1967). Forty-three have been mapped in Fig. 29-13. All except Warrior Islet in Torres Strait (9°48′S) are between 11°10′S and 16°23′S and occupy small high reefs of the inner shelf. In this area, some of the islands mapped as solitary vegetated cays, such as East and West Hope, have characteristics of low wooded islands and have been classified as such elsewhere.

Spender (1930) considered that the distribution of the low wooded islands was the result of a difference in height of reef surfaces caused by tilting normal to the mainland coastline, whilst Steers (1929, 1937) and Stoddart (1965) attributed the distribution to variation in wave energy. As discussed by Hopley (1982, 1989), however, there is a difference in height of the reefs across the shelf. In the central reef area from Cairns southward, where the main reef tract diverges from the coastline, there is evidence suggesting widespread submergence, deeper Pleistocene foundations, and younger reef tops (see Fig. 6-11 of Hopley, 1982). Younger, lower, more submerged reef flats have a greater cover of living coral and, therefore, the reef top has a much more irregular surface. This surface more effectively dampens the wave energy and creates conditions that are unsuited for sediment movement, decreasing the likelihood of island formation.

Not surprisingly, the distribution of islands shows some correlation with reef type (Hopley et al., 1989). As indicated in Table 29-1, a large majority of reef islands are found on the planar reefs, not only the reefs with oldest reef flat but also those with highest sediment cover. However, all types of reef may incorporate an island; even fringing reefs occasionally have small unvegetated cays. Table 29-1 also shows that low wooded islands can be found on fringing reef, but this is somewhat misleading as the two examples are planar reefs which incorporate very small outcrops of continental rock. A significant number of vegetated cays are also associated with the reef patches. Planar reefs and occasional reef patches have the required morphology to produce centripetal wave refraction that concentrates sediment in a particular part of the reef, something which is not normally found on lagoon,

Table 29-1

Reef islands of the Great Barrier Reef Marine Park

Reef type	Island type					
	Unvegetated cay	Vegetated sand cay	Vegetated shingle cay	Low wooded island	Total	%
Fringing	7	0	0	2	9	3.0
Patches	42	0	0	0	42	14.0
Crescentic	14	2	0	0	16	5.3
Lagoonal	11	0	0	0	11	3.7
Planar	135	38	3	42	218	72.7
Ribbon	4	0	0	0	4	1.3
TOTAL	213	40	3	44	300	
%	71.0	13.3	1.0	14.7		

crescentic, or ribbon reefs. Cays are least associated with large reefs. This is also because the wave refraction tends to spread sediment more evenly over the reef top instead of producing the necessary centripetal action.

Other factors contribute to the lack of islands on the central GBR. Stoddart and Steers (1977) noted that lack of island development coincides with greater tidal range, greater submergence at high tide, and greater effective exposure of the reef top. The cayless area of the GBR corresponds in general terms with the area of highest tides (range >4 m). The few islands in this area, such as Bushy Island and Bell Cay, are situated on high reefs with large algal terraces, which allow the main reef flats to be raised to almost mean sea level. This effectively negates the effect of the high tidal range.

The cayless area of the GBR also corresponds to the zone of maximum cyclone occurrence. Although these storms undoubtedly play a part in the formation of some island features, particularly shingle islands and ramparts, sand cays can be severely eroded, if not removed, during a major cyclonic event. Cyclone frequency, especially in conjunction with high surges, may be a factor extending the cayless area northward from the zone of high tidal range. In contrast, all but one of the mangrove islands occur in Torres Strait where there is a great increase in the density of cays. At these lower latitudes, cyclones are rarer and generally less intense. Similarly at the southern end of the GBR, tropical cyclones usually, though not always, are weakening and islands are again more numerous.

HOLOCENE SEA LEVEL HISTORY AND THE AGE OF THE REEF ISLANDS

Although Pleistocene reef may be exposed or very close to the modern reef-flat surface in the fringing reefs of the Northumberland Islands (Kleypas 1992) and also in Torres Strait (Hopley 1982, p. 268), the Holocene age of almost all reef flats on the GBR provides a minimum age for the islands which rest on them. The considerable

work that has been undertaken on the Holocene growth of reefs of the GBR (for summaries see Davies and Hopley, 1983, and Davies et al., 1985) indicates that the majority of reefs commenced growth from Pleistocene foundations generally varying in depth between 10 and 20 m below present sea level. Between 8000 and approximately 7300 y B.P., many reefs, particularly those growing off shallower foundations in the far south and northern GBR tracked upwards with sea level. Some reef flat was formed shortly after the stabilisation of sea level at ~6500 y B.P. Many other reefs, particularly in the central GBR, however, adopted a "katchup" (*sic*) mode (Davies et al., 1985). These reefs reached sea level and developed reef flat up to 4,000 years after modern sea level was first attained.

The relationship between reef-flat development and sea level is complicated by distinctive shelf warping along the Queensland coast as a result of hydroisostatic response to the transgression (Chappell et al., 1982; Hopley, 1983; Chappell, 1987; Nakada and Lambeck, 1989). Close to the mainland, there is evidence for up to 1.5 m of emergence ~5500 y B.P., after which sea level fell relatively smoothly to its present position (Chappell, 1982). As most of this emergence is on the inner shelf, only a few of the reefs of the main reef tract were affected. These are mainly the inner shelf reefs of the northern GBR and include particularly those on which low wooded islands have developed and possibly one or two of the innermost reefs in the south central section of the GBR where the shelf is more than 200 km wide (Kleypas and Hopley, 1993). Some compensatory subsidence may have taken place on the outer shelf, especially in the central GBR. This subsidence has delayed the time of attainment of modern sea level and, as a result, the development of reef flat on which islands could form.

Although extensive reef flat may not be necessary for carbonate island development, the requirement of some foundation on which the island can form gives a finite date of approximately 6500 y B.P. for the oldest islands on the GBR. A major advance made by the 1972 Great Barrier Reef Expedition was to provide an age framework for the construction of the low wooded islands. According to the reports of the Expedition (Polach et al., 1978; McLean et al., 1978; Stoddart et al., 1978a,b,c) the reef tops on which the low wooded islands are situated were developing at modern sea level prior to 5000 y B.P. and in some examples prior to 5800 y B.P. Emerged reef in the form of excessively high microatolls is associated with many low wooded islands. McLean et al. (1978) suggest that high cay terraces, high beachrock, and upper platforms with associated shingle ridges may all have been formed during a sea-level highstand about 1 m above present lasting until 3000 y B.P. Although each island type shows individual features, Turtle I Island (Fig. 29-10) gives a good example of the dated evolution. Radiocarbon ages (Polach et al., 1978) show that a reef flat existed about 5,000 years ago, as a date 4910 ± 90 y B.P. was obtained for coral shingle beneath mangrove deposits in the small depression enclosed by two shingle ridges. Overlying organic mud was dated as 1100 ± 80 y B.P. and 2210 ± 170 y B.P. A *Tridacna* shell from the upper platform gave an age of 4420 ± 90 y B.P., and similar material from the lower platform was dated at 1430 ± 70 y B.P. Shingle samples from the island ridges were dated between 3320 ± 80 and 2480 ± 70 y B.P. (see Polach et al., 1978, for details). On all the low wooded islands, most of the low-

terrace sediment, ramparts, younger shingle ridges, and lower platforms have developed over the last 2,500 years, and especially over the last 1,500 years.

Vegetated sand cays appear to have a very wide range of ages. High-terrace samples ranged from 3020 ± 70 to 4380 ± 80 y B.P., and low-terrace samples were from 2190 ± 70 to 3280 ± 80 y B.P. (McLean et al., 1978). Although the ages overlap, two periods of accumulation are confirmed. What is surprising is the relatively old and consistent set of dates for the younger terrace deposits. Although no dates are published for other vegetated sand cays of the GBR, descriptions of the islands of the Capricorn Group (Steers, 1937, 1938; Domm, 1971; Flood, 1977) are very similar.

Age information is available for only two vegetated shingle cays on the GBR, and it generally indicates a long period of formation. The stability of One Tree Island (Fig. 29-6) is indicated by an age of ~4000 y B.P. for material from the cemented foundations (Davies and Marshall, 1979). Very similar dates come from Lady Elliot Island, the southernmost island of the GBR (Flood et al., 1979). This shingle cay occupies about 30% of the reef-top area and consists of a concentric arrangement of lithified beach ridges composed of coral shingle and *Tridacna* clam shells lithified in a phosphate cement. The lithified beach ridges are more than 4 m high. Beachrock occurs around the eastern side of the island and eroded cay rock is exposed within the beach zone, suggesting at least some migration of the island. Radiocarbon dates from *Tridacna* valves range from 3635 ± 85 to 3195 ± 85 y B.P. Although closely spaced, the dates and concentric arrangement of the shingle ridges indicate the rapid growth of the island about 3000 y B.P. from a cay lying across the dominant southeasterlies.

Unvegetated cays are generally the youngest islands, although surprisingly old dates have been obtained from the still-mobile deposits of these islands. A radiocarbon date of 2330 ± 70 y B.P. was obtained for a bulk sample from the top of unvegetated Pickersgill Cay (Polach et al., 1978; McLean and Stoddart, 1978). On Twin Cay Reef in the Swains Group, two small cays exist on separate reef patches each with coarse beachrock from which dates of 630 ± 90 y B.P. for the southern and 1110 ± 80 y B.P. for the northern cay were obtained by Maxwell (1969, 1973). These dates, like that for Pickersgill Reef, suggest a degree of permanence for non-vegetated cay deposits and even for the shingle cays themselves.

CASE STUDY: STATUS OF CORAL CAYS OF THE GBR DURING A PERIOD OF GLOBAL CLIMATIC CHANGE (Hopley, 1993)

The confirmation of increases in CO_2 and other greenhouse gases in the Earth's atmosphere in recent times has focussed a great deal of environmental concern on the effects of global climatic change. One result of the global warming predicted for the next 100–200 years is a sea-level rise, resulting from both the thermal expansion of ocean surface waters due to warming and probably, at a later stage, partial melting of the Earth's ice caps. Predictions for sea-level rise have become more conservative over the last ten years and the envelope of predicted sea-level rise for the

mid-twenty-first Century is now 30–50 cm (IPCC, 1990). Such a rise has been demonstrated to have an effect on many of the world's coastal lowlands (e.g., Hopley, 1992), and considerable concern has been expressed for coral-reef islands worldwide (e.g., Falk and Brownlow, 1989; Roy and Connell, 1989). Opinions have been expressed that most reef islands will disappear completely in the next 50–100 years, including those of the GBR.

Much of the concern has been raised by authors whose experience with reef islands, and particularly reef-flat processes, is extremely limited. More informed opinion has suggested that the impact on coral reefs generally, and reef islands specifically, may be less dramatic and that there may be positive feedbacks which will, at the very least, maintain reef islands (Buddemeier and Smith, 1988; Gourlay and Hacker, 1991; Hopley, 1993; Hopley and Kinsey, 1988; Kinsey and Hopley, 1991; McLean, 1989, Parnell, 1989). As Buddemeier and Smith (1988) have noted, reef response to the rising sea level will be on a time scale of years to decades with the potential for reefs to keep up with the rise in at least the next 50 years. With reference to reef islands, it has been suggested that the present limitation to their growth is not a shortage of sediment on reef flats, but the inability of wave currents to transport that material to the island. It is predicted that a rise in sea level will result in more efficient sediment transport over the reef flat. However, that same rise is also predicted to increase the carbonate productivity of reef flats. The result of both processes is an increase, rather than decrease, in island size.

Hopley and Kinsey (1988) suggested that at the present time there was an overabundance of sediments on reef flats of the GBR (and elsewhere in the world), a result of the reef flats' being at sea level for a period of 5,000 years or more during which time the reef flats have grown to their maximum height with respect to present sea level. In some instances, a slight fall in sea level since 5000 y B.P. has reinforced the high level of some inner reef flats. The major constraint to sediment transport and to cay growth has been the limited time available when there is sufficient wave power passing across the reef flat to transport the sediment. Sediment movement is normally restricted to less than 50% of the time, when water levels are sufficiently deep over the reef flat to allow waves of significant size, and therefore transportational ability, to pass over the reef. This limitation is particularly prominent in areas of significant tidal range, such as the GBR. A rise in sea level of up to 0.5 m may unlock reef-flat sediments for longer periods and allow them to be moved towards coral islands. The end result is an increase in the size of the sand store which under normal weather conditions has the potential for further island construction.

Hopley and Kinsey (1988) further suggested that a small rise in sea level would also lead to greater productivity of reef-flat areas. It was suggested that with an increase from the present yield of about 0.5 kg m^{-2} y^{-1} to as much as 4 kg m^{-2} y^{-1} during the early rise in sea level, the reef flat would have the potential to supply even more sediment towards the nodal point of wave refraction.

Although most beach models and empirical formulae suggest that, given an adequate sediment supply, a higher water level will produce a higher beach, there have been few applications to coral islands (for exceptions see Gourlay, 1988, 1990). Sediment supply does not appear to be a problem on most reef tops of the GBR.

Observations and application of empirical formulae to Raine Island on the northern GBR by Gourlay and Hacker (1991) have indicated the relationships between wave action, height of reef flat and beach morphology. These relationships indicate that the height of the upper beach berm is determined by the run-up height of the dominant wave action which occurs on the highest spring tides. They also suggest that the present beach berm, with an elevation of about 2.0 m above MHWS, could be built either by small flat waves of 0.5-m height breaking directly onto the beach with a water level over the reef flat of about 2.0 m, or by maximum breaking waves of 1.6 m height at an extreme water depth of 2.7 m over the reef flat. Gourlay and Hacker (1991) indicate that a small rise in sea level without any responding build-up of reef-flat level would result in the attainment of greater berm heights under most weather conditions. They calculate that the buildup of berm height would exceed the amount of increase in water level. For example, in the case of Raine Island they suggest that with a 0.6-m rise in sea level, the larger 1.6-m waves would increase berm height by a further 0.8 m, whilst the flatter 0.5-m waves would increase berm height by 1.2 m. Thus, island height would increase by 0.2 m or 0.6 m relative to the new sea level.

In addition to a rise in sea level, an increase in the incidence and intensity of tropical cyclones (hurricanes and typhoons) is also quoted as a major threat to the existence of tropical coral islands as a result of climatic warming. Although such storms can already cause catastrophic damage to reef islands, there is ample evidence to suggest that most higher elevations on cays (as well as on atoll islands) are the result of deposition during these high-energy events (e.g., Bayliss-Smith, 1988). The highest elevations on GBR islands appear to be produced not by windblown sand, but largely wave-deposited materials. Even the highest reef islands may be overtopped by exceptional storm waves causing major ecological disturbance and occasionally loss of life. Because of the sedimentological response of reef flats, a small increase in sea level forecast into the next century is unlikely to greatly increase this risk. The response to global change, particularly in the GBR, is thus predicted to be a growth in island size. However, as this may be accompanied by small changes in weather patterns which will alter the centripetal effect of wave refraction, there is a possibility of reorientation of some reef islands (Flood, 1986). This could see a decline in the proportion, and even overall area, of the older terrace areas in which more mature soils and vegetation are present.

CONCLUDING REMARKS

The great variety and complexity of form of GBR cays results from the range of factors that affect island-building. The range of controlling variables cannot be matched in any other single reef province. Variations in reef-top ages, reef shape and sea-level history combined with the differences in energy conditions and tidal ranges produce the diverse morphology of reef islands. Some authors suggest that variations in reef-island morphology are indicative of an evolutionary sequence (e.g., Umbgrove, 1928). However, as Stoddart and Steers (1977) have pointed out, most of the

changes observed in historical time are ecological rather than geomorphic. Even the catastrophic damage carried out during major storms (e.g., Stoddart 1971, Stoddart and Walsh, 1992) may be part of the environment to which the morphology of reef islands is adapted. It is possible that all the island types distinguished are equilibrium forms continually adjusting to the controlling processes (Stoddart and Steers, 1977).

Nonetheless, reef islands are dynamic and respond to changes in controlling factors such as climate, sea level, and reef-top morphology (e.g., Verstappen, 1954; Flood, 1986). The accumulation of sediments on the cays of the GBR has been episodic; radiometric dates suggest that cays formed rapidly in leeward situations once the level of reef tops and sea level coincided at about 5000 y B.P. (McLean and Stoddart, 1978; Stoddart et al., 1978a). The existence of a high-energy "window", as suggested by Neumann (1972), when outer reefs not quite at sea level may have given less protection to the inner shelf reefs on which the oldest islands are located, may have been an important factor at this early stage, (see Hopley, 1984, for discussion of this concept applied to the GBR). On inner-shelf reefs subjected to hydroisostatic adjustment, indications are that subsequent to this initial period of cay development, sediment supply diminished until a fall in sea level of about 1 m led to a new wave of sand and shingle being added to the cays as low terraces. The importance of negative movements of sea level in the formation of reef islands has been a major controversy in reef literature (Stoddart 1969, p., 472). Evidence from the GBR suggests that, while not mandatory for the accumulation of sediment masses, it is certainly a very helpful factor.

Changes in the reef-top geometry are also important factors in long-term changes to reef islands. Widening of windward reef zones and heightening of rubble zones and algal ridges can greatly decrease the wave energy transmitted to the leeward reef flat. Of equal importance is the loss of wave energy due to friction over a rough coral bottom as shown by Dexter (1973), which suggests that the episodic nature of sediment accumulation in cays could be the result of changes in reef-top morphology. After the first phase of sediment accrual, there may be a paucity of sediments, resulting not only from the form of the windward margins, but also from the great loss of wave energy over a reef flat with aligned or scattered coral heads. Only as the reef flat becomes smoother with infilling of the irregular reef-flat surface is there a decrease in the frictional loss of energy, and this together with the adequate supply of sediment now available on the sanded reef flat may lead to a second period of cay growth.

If an evolutionary sequence does exist for reef islands, a degenerative phase of cay erosion may be the last stage of development. In the long term, reef islands are merely a temporary store of sediments in the total reef system, a store that may increase or decrease in size according to internal storage characteristics (cementation and vegetation), internal reef factors (changing morphology and reef-top smoothness), or completely external factors over which the reef itself has no control (sea-level and climatic changes).

REFERENCES

Backshall, D.G., Barnett, J., Davies, P.J., Duncan, D.C., Harvey, N., Hopley, D., Isdale, P., Jennings, J.N. and Moss, R., 1979. Drowned dolines — the blue holes of the Pompey Reefs, Great Barrier Reef. BMR J. Aust. Geol Geophys. 4: 99–109.

Bayliss-Smith, T.P., 1988. The role of hurricanes in the development of reef islands, Ontong Java Atoll, Solomon Islands. Geogr. J., 154: 377–391.

Buddemeier, R.W. and Oberdorfer, J.A., 1986. Internal hydrology and geochemistry of coral reefs and atoll islands: key to diagenetic variations. In: J.H. Schroeder and B.H. Purser (Editors), Reef Diagenesis. Springer Verlag, Heidelberg, 91–111.

Buddemeier, R.W. and Smith, S.V., 1988. Coral reef research in an era of rapidly rising sea level; predictions and suggestions for long term research. Coral Reefs, 7: 51–56.

Chappell, J., 1982. Evidence for smoothly falling sea level relative to North Queensland, Australia during the past 6000 years. Nature, 302: 406–8.

Chappell, J., 1987. Late Quaternary sea level changes in the Australian region. In: M.J. Tooley and I. Shennan (Editors), Sea Level Changes. Inst. Br. Geogr. Spec. Publ., 20: 296–331.

Chappell, J., Rhodes, E.G., Thom. H.G. and Wallensky, E., 1982. Hydroisostasy and the sea level isobase of 5500 BP in North Queensland, Australia. Mar. Geol., 49: 81–90.

Chappell, J., Chivas, A., Wallensky, E., Polach, H.A. and Aharon, P., 1983. Holocene palaeoenvironmental changes, central to north Great Barrier Reef, inner zone. BMR J. Aust. Geol. Geophys., 8: 223–236.

Davies, P.J. and Hopley, D., 1983. Growth facies and growth rates of Holocene reefs in the Great Barrier Reef. BMR J. Aust. Geol. Geophys., 8: 237–251.

Davies, P.J. and Marshall, J.F., 1979. Aspects of Holocene reef growth — substrate age and accretion rate. Search, 10: 276–279.

Davies, P.J. and McKenzie, J.A., 1993. Controls on the Plio-Pleistocene evolution of the northeastern Australian continental margin. In: J.A. McKenzie, P.J. Davies, A. Palmer-Julson et al., Proc. ODP, Sci. Results, 133. Ocean Drilling Project, College Station TX, 755–762.

Davies, P.J., Marshall, J.F. and Hopley, D., 1985. Relationships between reef growth and sea level in the Great Barrier Reef. Proc. Fifth Int. Coral Reef Cong. (Tahiti), 3: 95–103.

Dexter, P.E., 1973. A shallow water design wave procedure applicable to small cays and submerged reefs. Engin. Dynam. Coastal Zone, First Aust. Conf. on Coastal Eng., 1973, 74–81.

Domm, S.B., 1971. The uninhabited cays of the Capricorn Group, Great Barrier Reef, Australia. Atoll Res. Bull., 142: 1–27.

Drew, E.A. and Abel, K.M., 1985. Biology, sedimentology and geography of the vast inter reefal *Halimeda* meadows within the Great Barrier Reef province. Proc. Fifth Int. Coral Reef Cong. (Tahiti), 5: 15–20.

Drew, E.A. and Abel, K.M., 1988. Studies of *Halimeda* I. The distribution and species composition of *Halimeda* meadows throughout the Great Barrier Reef province. Coral Reefs, 6: 195–205.

Fairbridge, R.W., 1950. Recent and Pleistocene coral reefs of Australia. J. Geol., 58: 330–401.

Fairbridge, R.W., 1967. Coral reefs of the Australian region. In: J.N. Jennings and J.A. Mabbutt, (Editors), Landform Studies from Australia and New Guinea. A.N.U. Press, Canberra, 386–451.

Falk, J. and Brownlow, A., 1989. The Greenhouse Challenge — What's To Be Done? Penguin Books Australia, Ringwood, 841 pp.

Flinders, M., 1814. A Voyage to Terra Australis. G. & W. Nicol, London, 2 vols.

Flood, P.G., 1977. Coral cays of the Capricorn and Bunker Groups, Great Barrier Reef province, Australia. Atoll Res. Bull., 195: 1–7.

Flood, P.G., 1986. Sensitivity of coral cays to climate variations, southern Great Barrier Reef, Australia. Coral Reefs, 5: 13–18.

Flood, P.G., Harjanto, S. and Orme, G.R., 1979. Carbon-14 dates, Lady Elliott Reef, Great Barrier Reef. Qld. Gov. Min. J., Sept 1979, 444–447.

Gourlay, M.R., 1988. Coral cays: products of wave action and geological processes in a biogenic environment. Proc. Sixth Int Coral Reef Symp. (Townsville), 2: 491–496.

Gourlay, M.R., 1990. Waves, setup and currents on reefs. Cay formation and stability. In: Engineering in Coral Reef Regions Conf. Reports of papers GBRMPA, 163–178.
Gourlay, M.R. and Hacker, J.L.F., 1991. Raine Island: Coastal Processes and Sedimentology. Dep. Civ. Eng., Univ. Queensland, Ch. 40/91, 68 pp.
Hopley, D., 1968. Morphology of Curacoa Island spit, North Queensland. Aust. J. Sci., 31: 122–123.
Hopley, D., 1971. The origin and significance of North Queensland island spits. Z. Geomorph., 15: 371–389.
Hopley, D., 1975. Contrasting evidence for Holocene sea levels with special reference to the Bowen-Whitsunday area of Queensland. In: J. Douglas, J.E. Hobbs and J.J. Pigram (Editors), Geographical Essays in Honour of Gilbert J. Butland. Univ. New England, Armidale, 51–84.
Hopley, D., 1981. Sediment movement around a coral cay, Great Barrier Reef, Australia. Pac. Geol., 15: 17–37.
Hopley, D., 1982. Geomorphology of the Great Barrier Reef: Quaternary Development of Coral Reefs. Wiley Interscience, New York, 453 pp.
Hopley, D., 1983. Deformation of the North Queensland continental shelf in the late Quaternary. In: D.E. Smith and A.G. Dawson (Editors), Shorelines and Isostasy. Inst. Br. Geogr. Spec. Publ., 16: 347–366.
Hopley, D., 1984. The Holocene high energy window in the central Great Barrier Reef. In: B.G. Thom, (Editor), Coastal Geomorphology in Australia. Academic Press, North Ryde, Australia, 135–150.
Hopley, D., 1989. Coral reefs: zonation, zonality and gradients. Essen. Geogr. Arbeit., 18: 79–123.
Hopley, D., 1992. Global change and the coastline: assessment and mitigation planning. J. S.E. Asian Earth Sci., 7: 5–15.
Hopley, D., 1993. Coral reef islands in a period of global sea level rise. In: N. Saxena, (Editor), Recent Advances in Marine Science and Technology 92. PACON International, Honolulu, 453–462.
Hopley, D. and Barnes, R.G., 1985. Structure and development of a windward fringing reef, Orpheus Island, Palm Group, Great Barrier Reef. Proc. Fifth Int. Coral Reef Cong. (Tahiti), 3: 141–146.
Hopley, D. and Kinsey, D.W., 1988. The effects of rapid short term sea level rise on the Great Barrier Reef. In: G.I. Pearman (Editor), Greenhouse: Planning for Climatic Change. CSIRO, Melbourne, 189–201.
Hopley, D., Slocombe, A.M., Muir, F. and Grant, C., 1983. Nearshore fringing reefs in North Queensland. Coral Reefs, 1: 151–160.
Hopley, D., Parnell, K.E. and Isdale, P.J., 1989. The Great Barrier Reef Marine Park: dimensions and regional patterns. Aust. Geogr. Studies, 27: 47–66.
IPCC, 1990. Climatic Change: The IPCC Response Strategies. Report of the Response Strategies Working Group of the IPCC, Geneva and Nairobi, WMO and UNEP.
Kinsey, D.W. and Hopley, D., 1991. The significance of coral reefs as global carbon sinks – response to Greenhouse. Palaeogeogr. Palaeoclimatol. Palaeoecol., 89: 1–15.
Kleypas, J.A., 1992. Geological Development of Fringing Reefs of the Southern Great Barrier Reef, Australia. Ph.D. Dissertation, James Cook Univ., North Queensland, 199 pp.
Kleypas, J.A. and Hopley, D., 1993. Reef development across a broad continental shelf, southern Great Barrier Reef, Australia. Proc. Seventh Int. Coral Reef Symp. (Guam), 1129–1141.
Marshall, J.F. and Davies, P.J., 1988. *Halimeda* bioherms of the northern Great Barrier Reef. Coral Reefs, 3/4: 139–148.
Maxwell, W.G.H., 1968. Atlas of the Great Barrier Reef. Elsevier, Amsterdam, 258 pp.
Maxwell, W.G.H., 1969. Radiocarbon ages of sediment: Great Barrier Reef. Sediment. Geol., 3: 331–333.
Maxwell, W.G.H., 1973. Sediments of the Great Barrier Reef province. In: O.A. Jones and R. Endean (Editors), Biology and Geology of Coral Reefs, 1: Geology 1. Academic Press, New York, 299–345.
Maxwell, W.G.H., Day, R.W. and Fleming, P.J.G., 1961. Carbonate sedimentation on the Heron Island reef, Great Barrier Reef. J. Sediment. Petrol., 31: 215–230.

Maxwell, W.G.H., Jell, J.S. and McKellar, R.G., 1964. Differentiation of carbonate sediments on the Heron Island reef. J. Sediment. Petrol., 34: 294–308.

McLean, R.F., 1989. Kiribati and sea level rise. Report to Commonwealth Secretariat, Expert Group on Climatic Change and Sea Level Rise. Dept. Geogr. Ocean., Univ. New South Wales, Aust. Defence Force Academy, Canberra, 87 pp.

McLean, R.F. and Stoddart, D.R., 1978. Reef island sediments of the northern Great Barrier Reef. Philos. Trans. R. Soc. London Ser. A, 291: 101–117.

McLean, R.F., Stoddart, D.R., Hopley D. and Polach, H.A., 1978. Sea level change in the Holocene on the northern Great Barrier Reef. Philos. Trans. R. Soc. London Ser. A, 291: 167–186.

Nakada, K. and Lambeck, K., 1989. Late Pleistocene and Holocene sea level change in the Australian region and mantle rheology. Geophys. J., 96: 497–517.

Neumann, A.C., 1972. Quaternary sea level history of Bermuda and the Bahamas (abstr.). Am. Quat. Assoc., Second Natl. Conf. Abstr., 41–44.

Orme, G.R., 1977. Aspects of sedimentation in the coral reef environment. In: O.A. Jones and R. Endean (Editors), Biology and Geology of Coral Reefs, 4: Geology, 2. Academic Press, New York, 129–182.

Parnell, K.E., 1989. Reefs in the greenhouse: a review. Paper presented to the 15th Conf., N.Z. Geogr. Soc., 17 pp.

Partain, B.R. and Hopley, D., 1989. Morphology and Development of the Cape Tribulation Fringing Reefs, Great Barrier Reef, Australia. GBRMPA Tech. Mem., TM 21, 45 pp.

Pickard, G.L., 1977. The Great Barrier Reef. In: G.L. Pickard, J.R. Donguy, C. Henin and F. Rougert (Editors), A Review of the Physical Oceanography of the Great Barrier Reef and Western Coral Sea. Aust. Inst. Mar. Sci. Monogr. Ser., 2: 1–59.

Polach, H.A., McLean, L.F., Caldwell, J.R. and Thom B.G., 1978. Radiocarbon ages from the northern Great Barrier Reef. Philos. Trans. R. Soc. London Ser. A, 291: 139–158.

Pringle, A.W., 1986. Causes and effects of changes in fluvial sediment yield to the northeast Queensland coast, Australia. Dept. Geogr., James Cook Univ., Monogr. Ser. Occ. Pap. 4., 232 pp.

Roy, P. and Connell, J., 1989. 'Greenhouse': the impact of sea level rise on low coral islands in the South Pacific. Research Institute for Asia and the Pacific, Univ. Sydney, Occasional Paper 6, 55 pp.

Spender, M., 1930. Island reefs of the Queensland coast. Geogr. J., 76: 194–214, 273–297.

Steers, J.A., 1929. The Queensland coast and the Great Barrier Reef. Geogr. J., 74: 232–257, 341–370.

Steers, J.A., 1937. The coral islands and associated features of the Great Barrier Reef. Geogr. J., 89: 1–28, 119–146.

Steers, J.A., 1938. Detailed notes on the islands surveyed and examined by the Geographical Expedition to the Great Barrier Reef in 1936. Rep. Great Barrier Reef Comm., 4: 51–94.

Stoddart, D.R.,1965. British Honduras cays and the low wooded island problem. Inst. Br. Geogr. Trans., 36: 131–147.

Stoddart, D.R., 1969. Ecology and morphology of recent coral reefs. Biol. Rev., 44: 433–498.

Stoddart, D.R., 1971. Coral reefs and islands and catastrophic storms. In: J.A. Steers (Editor), Applied Coastal Geomorphology. Macmillan, London, 155–197.

Stoddart, D.R., 1980. Mangroves as successional stages, inner reefs of the northern Great Barrier Reef. J. Biogeogr., 7: 269–284.

Stoddart, D.R. and Steers, J.A., 1977. The nature and origin of coral reef islands. In: O.A. Jones and R. Endean (Editors), Biology and Geology of Coral Reefs, 4: Geology 2. Academic Press, New York, 59–105.

Stoddart, D.R. and Walsh, P.P.D 1992. Environmental variability and environmental extremes as factors in island ecosystems. Atoll Res. Bull., 356, 71 pp.

Stoddart, D.R., McLean, R.F. and Hopley, D., 1978a. Geomorphology of reef islands, northern Great Barrier Reef. Philos. Trans. R. Soc. London Ser. B, 284: 39–61.

Stoddart, D.R., McLean, R.F., Scoffin, T.P., Thom, B.G. and Hopley, D., 1978b. Evolution of reefs and islands, northern Great Barrier Reef: synthesis and interpretation. Philos. Trans. R. Soc. London Ser. B, 284: 149–159.

Stoddart, D.R., McLean, R.F., Scoffin, T.P. and Gibbs, P.E., 1978c. Forty-five years of change on low wooded islands, Great Barrier Reef. Philos. Trans. R. Soc. London Ser. B, 284: 63–80.

Symonds, P.A., Davies, P.J. and Parisi, A., 1983. Structure and stratigraphy of the central Great Barrier Reef. BMR J. Aust. Geol. Geophys., 8: 277–291.

Taylor, T., 1924. Movement of sand cays. Qld. Geogr. J., 39: 38–39.

Umbgrove, J.H.F., 1928. De Kioralriffen in de Baai van Batavia. Wet. Med. Dienst. v.d. Mijn. in Ned.-Indic. 7, 68 pp.

Verstappen H. Th., 1954. The influence of climatic changes on the formation of coral islands. Am. J. Sci., 252: 428–435.

Geology and Hydrogeology of Carbonate Islands. Developments in Sedimentology 54
edited by H.L. Vacher and T. Quinn
© 1997 Elsevier Science B.V. All rights reserved.

Chapter 30

HYDROGEOLOGY OF HERON ISLAND, GREAT BARRIER REEF, AUSTRALIA

DELTON CHEN and ANDRÉ KROL

INTRODUCTION

Geographical setting

There are some 40 vegetated sand cays among the ~300 reef islands in the huge expanse of the Great Barrier Reef Marine Park (GBRMP) [Chap. 29, Table 29-1]. One of these is Heron Island, at 23°26′S and 15°57′E. Approximately 19 ha in area, Heron Island is perched on the leeward margin of an elongated platform reef known as Heron Reef (Fig. 30-1). Heron Reef and 21 other major reefs in the vicinity including Lady Elliott Reef, a number of smaller shoals, and fifteen well-established sand and shingle cays of various sizes, constitute the Capricorn-Bunker Group of islands and reefs. The Capricorn-Bunker Group is situated within the Mackay/ Capricorn Section of the GBRMP [Fig. 29-1].

Heron Island (Fig. 30-2) supports one of the ten largest nesting colonies of green sea turtles (*Chelonia mydas*) in eastern Australia, and the third largest surviving stand in Australia of a now uncommon tree, the *Pisonia grandis* (Walker, 1991a). During the summer breeding season of 1991–92, Staunton Smith (1992) observed that the island provided a habitat for as many as 34,000 wedgetail shearwaters

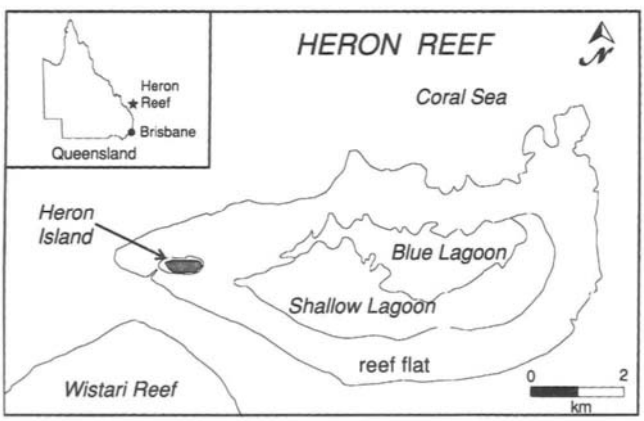


Fig. 30-1. Map showing physiographic zonation of Heron Reef and location of Heron Island. (Adapted from Flood, 1977.)

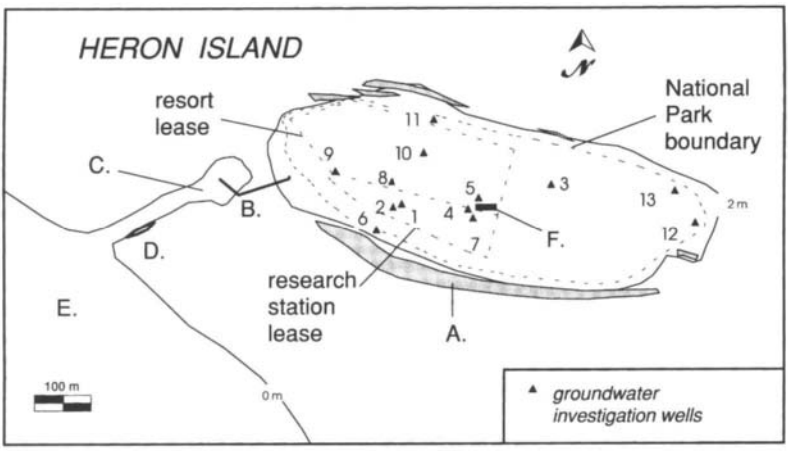


Fig. 30-2. Map of Heron Island. Key: A, beachrock; B, jetty; C, harbor; D, shipwreck; E, channel; F, sewage and soakage trench.

(*Puffinus pacificus*) and 130,000 white-capped noddies (*Anous minutus*). Published estimates of seabird populations for Heron Island indicate that there has been a dramatic increase in arrivals of wedgetail shearwaters and white-capped noddies since the 1930's. The reason for this increase is uncertain, although it has been suggested by Walker (1991a) that previous mass mortalities of white-capped noddies may have occurred as a consequence of cyclonic activity, epidemics, or predation by introduced species.

Human occupation over the last seven decades has resulted in substantial degradation of the island's flora and fauna (Walker, 1991a). The island was first occupied in 1925 when a turtle soup factory was established. The closure of the factory in 1928 was followed by the founding of a resort in 1932 and a research station in 1951. Heron Island is a popular tourist destination being one of only three coral cay resort islands on the Great Barrier Reef (GBR). Since the 1960's, visitation to the island has tripled, reaching nearly 100,000 user nights per year in 1991.

The land surface of the island has been subdivided to provide a national park, a tourist resort lease, and a research station lease (Fig. 30-2). The Capricorn-Bunker Group of reefs are renowned for their natural beauty. Heron Reef, in particular, has received considerable scientific attention.

Climatic setting

Heron Island is situated on the Tropic of Capricorn and has a subtropical maritime climate with a seasonal pattern of hot wet summers and warm and moderately dry winters. Most of the average annual rainfall of 1,069 mm falls during the months of December to June. Although annual rainfall off the Queensland coastline is greatest in the northern areas, the most variable rainfall occurs between latitudes 18°S and 25°S. This variability is due to irregular cyclonic activity which brings

extreme rain and wind events. On average, 14 cyclones per decade occur within the area within 150–155°E and 20–25°S (Lourensz, 1977). ESE to SE winds dominate at Heron Island with more variable N to NW winds also occurring between September and January (Flood, 1986). The tidal oscillations at Heron Reef are semidiurnal, with an average range of 2.28 m for spring tides and 1.09 m for neap tides.

GEOLOGIC FRAMEWORK

Geologic setting

The geologic structure of eastern Queensland has been a critical factor in the distribution of coral reefs in the GBR (Hopley, 1982; Chapter 29 of this book). In the proximity of Heron Island, the Queensland shelf is relatively narrow (about 60 km wide), unrimmed and forms the Bunker High which is 20–40 m below sea level. Just to the east of the Capricorn-Bunker Group, and roughly parallel with the coastline, the Bunker High abruptly slopes down some 300 m into the Capricorn Basin.

In 1926, drilling operations were carried out to a depth of 183 m in the northern region of the GBR at Michaelmas Cay (Richards and Hill, 1942). In 1937, similar drilling was undertaken to a depth of 223 m at Heron Island (Richards, 1938). The material retrieved from these drill holes was similar, despite their separation by some 1,000 km. The drill logs show coralline material to a depth of 120 m at Michaelmas Cay, and to a depth of 150 m at Heron Island. In both instances, this coralline material was shown to be underlain by a foundation of loosely coherent terrigenous sands. Both cores were poorly lithified and lacked dolomite.

General features of geology

The 1937 drill hole at Heron Island (Richards and Hill, 1942) started at a height of approximately 5 m above low water datum (LWD) and revealed a sequence consisting of calcareous sands, in situ reef rock, foraminiferal and quartz sands, and lime muds. Maxwell (1962) generalised the geologic succession into three zones: shallow reef rock (0–30 m), intermediate reef rock (30–150 m), and subreef sands (150–223 m).

The top 15–20 m of Heron Reef constitutes a veneer of Holocene reef growth above a Pleistocene limestone basement (Jell and Flood, 1977). The pre-Holocene reef rock has experienced a series of eustatic sea-level changes; mineralogic alteration, marked cementation, and brown staining delineate at least four zones, with solution unconformities at 20 m, 35 m, and possibly at 75 m, 95 m, and 140 m (Davies, 1974). Since 1978, at least 24 other reefs throughout the GBR have been shallow-drilled, including One Tree, Fairfax and Fitzroy Islands in the Capricorn-Bunker Group (Davies and Hopley, 1983). Solution unconformities in these reefs of the southern GBR were encountered at depths of 7.4–14.3 m, and were easily delineated on the basis of the appearance of *Halimeda*-rich limestone, which is often found in the cavities of the coral framework (Marshall, 1983).

General features of geomorphology

It is convenient to describe Heron Reef as having six major physiographic zones (Fig. 30-1): reef slope, reef flat, reef rim, Shallow Lagoon, Blue Lagoon and Heron Island itself (Fig. 30-2). The following descriptions of these zones are adapted from Jell and Flood (1977):

The reef slope, which marks the transition between the channel floor and the reef rim, is steep with gradients between 1:20 and 1:4. These slopes exhibit spur-and-groove structures due to the erosional effects of wave scour and tidal runoff in conjunction with coral growth.

The reef flat is the portion of the reef top which may be exposed during low tides. The surface of the reef flat around Heron Island consists mainly of bioclastic sands and living corals with encrustations of coralline algae.

The reef rim marks the highest part of the intertidal portion of the reef and is generally continuous with only a few channels to the open sea. During low tides, the flow of seawater off the reef is impeded by the topography and surface impermeability of the reef rim and reef flat. Dredging of a man-made harbour through the reef and close to the cay has altered the hydrodynamics of the waters around the cay (Gourlay, pers. comm., 1993).

Shallow Lagoon has a low-tide water depth of 0.3–1 m. Corals are sparser and smaller than on either the reef flat or the reef rim.

Blue Lagoon, which makes up the central physiographic unit of Heron Reef, is defined by an abrupt increase in water depth to an average of 3.5 m. This lagoon is characterised by numerous small patch reefs and a floor of fine sediment.

Heron Island has a maximum elevation of about 8 m. It was formed from the gradual accretion of bioclastic sediments at a focal zone where wind-induced waves dissipated sufficiently for suspended sediments to be deposited. Gourlay (1988) explained that the position of this focal zone is governed primarily by reef size, shape, and orientation with respect to the direction of prevailing winds and wind-induced waves. Tides modulate these processes, and vegetative cover and beachrock formations play a role in further trapping and stabilising sediments. At Heron Island, exposed beachrock formations outline an earlier shoreline. The changing shoreline of Heron Island is the result of decadal-scale oscillations of annual wind-energy vectors (Flood, 1986).

HYDROGEOLOGY

Thirteen groundwater wells were installed at Heron Island in 1991. The wells, which were installed in approximately N-S and E-W transects and concentrated in the area of wastewater soakage trenches (Fig. 30-2), have provided subsurface information and have been used to sample groundwater and monitor piezometric levels. Each well included up to four nested 3-cm-diameter PVC piezometers which were hydraulically isolated from each other and located at different depths (Fig. 30-3).

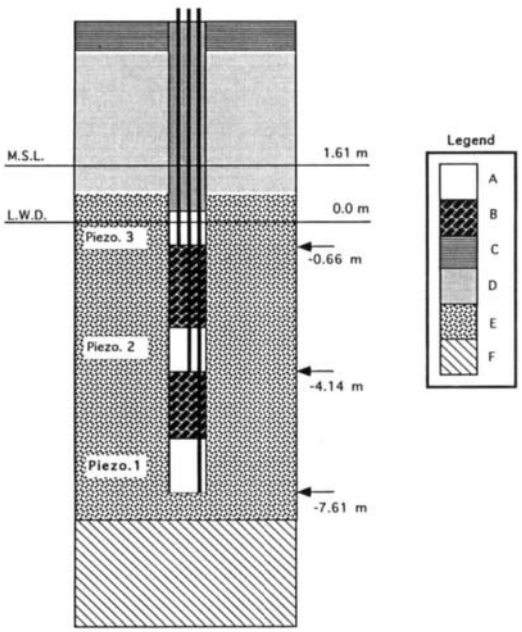


Fig. 30-3. Details of Well No. 8: stratigraphy and location of piezometers. Key: A, river sand; B, clay layer; C, sand with organic material; D, coral sand with shingle; E, hard bands, fragments, coarse sand and fines; F, reef rock with cavities.

Hydrostratigraphy

The hydrostratigraphy of Heron Island and its accompanying reef is shown as a conceptual model in Figure 30-4. There are three main units: an unconsolidated surficial aquifer beneath the island; a lower aquifer consisting of Holocene and Pleistocene reef rock; and the reef plate which acts as an offshore confining layer above the lower aquifer. The conceptual model is much like those of other low islands on atoll reefs (e.g., Lam, 1974; Buddemeier and Oberdorfer, 1988; Oberdorfer et al., 1990; Underwood et al., 1992) and, as will be seen, a GBR version of the type of dual-aquifer system that characterizes the hydrogeology of atoll islands [Chap. 1].

Surficial aquifer. The surficial aquifer consists of cay sands. Within the unsaturated zone, the sands are mostly cream-colored and medium- to coarse-grained bioclastic grainstone with no quartz. A soft, dark brown organic layer occurs beneath the forested areas and is underlain, at about 1.3-m depth, by clean, well-sorted aeolian sand. The chemical composition by weight of this unconsolidated sand is 91–93% $CaCO_3$, 1–5% $MgCO_3$ and 2–3% organic matter (Richards and Hill, 1942). At about 2.5–3 m below ground level, a transition occurs to slightly coarser, moderately sorted sands of beach origin. Below the level of mean high water neaps

(MHWN, 2.15 m above LWD) this sediment is well rounded, whiter than above and either partially or fully saturated. At this level, pebble-sized fragments are common and include shells, coral fragments, and some nodules. Between MHWN and the level of the reef flat (approximately 0.8 m above LWD), limited hardening occurs, and beachrock is encountered in some areas near the shoreline. Fragments of corals, shells, coralline algae and some pumice are common. In the region immediately above LWD, the sediment is characterised by a layering of hard, consolidated bands and intervening layers of loose nodules in a matrix of medium- to coarse-grained sands, shells and coral fragments.

Lower aquifer. The Holocene reef rock beneath the surficial sands was drilled and cored at the 13 sites shown in Figure 30-2. Due to the techniques employed, megapores in the reef rock limited the subsurface investigation to depths above about -7 ± 3 m LWD. The reef material consists of variously consolidated layers, typically 0.25–2.5 m thick. Loose, infilling material includes nodules, fine gravels, medium- to coarse-grained sand, shells, and mud.

The drilling logs describe a general transition from hard layers to what appears to be a series of interconnected or large cavities. Although this transition was not always clear, the general trend was the same; "banded layering with porous vents" and "interconnected cavities and preferential pathways" overtopped cavities. Richards and Hill (1942) encountered a 2-m-thick cavity beneath the cay at −2.9 m LWD. Cavities up to 1 m thick were also found in the open framework of branching-coral facies at One Tree Reef (23°30′S, 152°05′E) (Marshall and Davies, 1982), which is nearby. The branching-coral facies of the Holocene at One Tree Reef is a low-energy facies characteristic of that reef's leeward internal structure. Heron Island, too, is in the leeward margin of its reef, and the predominant corals in the Heron Island borehole are, similarly, the branching *Acropora* spp. (Richards and Hill, 1942). A high but variable permeability for the Holocene aquifer is expected due to the presence of megapores and irregular layering.

Richards and Hill (1942) described the Pleistocene material as being mostly a soft, porous reef rock, often containing chalky muds and large fragments, and showing some evidence of cementation and cavities. It is believed that the Pleistocene component of the lower aquifer is highly permeable because of solution features formed during sea-level lowstands (Hopley, 1982).

Reef plate. Buddemeier and Oberdorfer (1986) described a 0.5– to 1.5-m-thick reef plate on Davies Reef, GBR, as a cemented framework of corals, encrustations of coralline algae, and sediments. According to Buddemeier and Oberdorfer (1986), this reef plate at Davies Reef acts as a leaky confining layer. The ability of Heron Reef to support stranded seawater during low tide (see below) supports the notion that Heron Reef is capped by a similar type of confining layer.

Hydraulic conductivity. Constant-head permeability tests were used to determine the saturated hydraulic conductivities of disturbed sand samples taken from the

surficial aquifer. We found that hydraulic conductivity increases considerably from the organic zone (4–45 m day^{-1}) to the clean coral sand zone (170–260 m day^{-1}). The lower hydraulic conductivity of the surface organic layer would slow moisture movement and promote uptake by plants; *Pisonia grandis*, for example, has a very shallow root system that facilitates near-surface water removal and avoids the saline water table (Walker, 1991b).

The values of hydraulic conductivity of the lower aquifer are thought to be similar to those estimated by Oberdorfer and Buddemeier (1986) for the reef aquifer at Davies Reef. In that study, hydraulic conductivity was estimated at ≥2,000 m day^{-1} for "major interconnected voids", 10–2,000 m day^{-1} for "unconsolidated deposits, fine sand to coarse gravel" and 0.1–2 m day^{-1} for "consolidated deposits as cemented bands or fragments".

Water levels

Charley et al. (1990) found that the water table at Heron Island oscillates in response to the tide cycle and that the amplitude and timing of these oscillations vary according to location on the island. Detailed data obtained in our study has led us to conclude that the lower aquifer (Fig. 30-4) is the main pathway for the transmission of the tidal signal to the surficial aquifer and that the reef plate acts as a confining layer. Although the beach provides a hydraulic connection between the cay's aquifer and the waters of the reef flat, the presence of such a connection fails to explain the tidal signals observed near the cay's centre. This is because tidal signals moving laterally through beach sands tend to decay exponentially with distance (Nielsen, 1990). Further, as Wheatcraft and Buddemeier (1981) have shown, horizontal

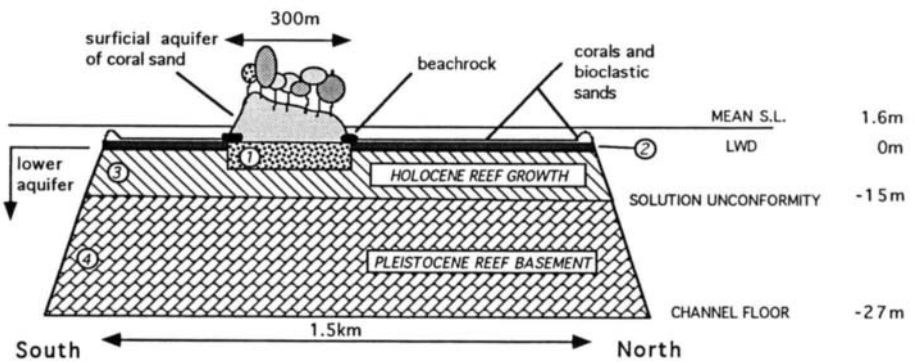


Fig. 30-4. Conceptual hydrogeologic model of Heron Island. Key: 1, cemented layers with interconnected cavities and infilling by loose fragments, sand and fines; 2, reef plate of cemented corals, fragments, and sediments; 3, porous reef rock with growth cavities; 4, porous reef rock with solution cavities.

propagation of tidal signals in a dual-aquifer atoll island may be neglected as a good first approximation.

Our data on island groundwater tides are from recordings at 21 piezometers from eight wells at various times during 1994. Piezometric levels and the tide were measured with pressure transducers calibrated to LWD. Readings were taken electronically at 10-min intervals and recorded by computer. Although the duration of the observations varied (54–117 tide half-cycles), most features of a lunar cycle were included in each case. The simultaneous record of the harbour tide was used for determination of efficiencies (amplitude ratio) and lags (timing differential) of the groundwater tides.

Figure 30-5 shows a representative comparison of the harbour tide and the variation in head at a three-piezometer nest, well 8. It is clear from Figure 30-5 that there is a shallow-to-deep increase in efficiency and decrease in lag; such variation is typical of the tidal dynamics of dual-aquifer systems of atoll islands (Wheatcraft and Buddemeier, 1981) [Chap.1, Table 1-3]. Figure 30-5 also shows that there is one time between each high and low tide that the levels in all the piezometers are equal; this occurs when the vertical gradient in head is zero, the vertical flow direction is reversing, and the water table is at a maximum or minimum. Finally, it can be noted that the minimum seawater levels on the reef flat can exceed groundwater heads within the lower aquifer, indicating that this aquifer is hydraulically insensitive to the seawater stranded on the reef flat. The water-level data, therefore, support the hypothesis that the lower aquifer is capped by a confining layer, namely the reef plate.

Tidal efficiency and lag vary with time and position. Variation with time is illustrated in Figures 30-6 and 30-7; we found a positive correlation between the diurnal inequality of the tide (Fig 30-5) and the tidal efficiencies in most of the piezometers (correlation coefficients were 0.50–0.92). The variation with depth is

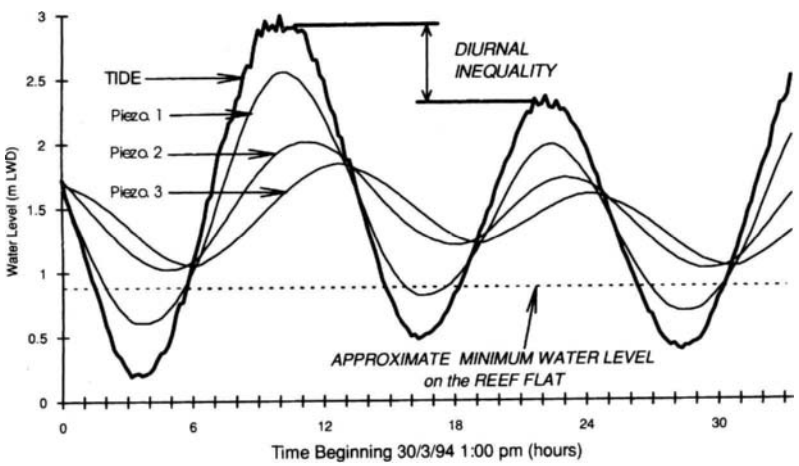


Fig. 30-5. Tide and groundwater heads at Well No. 8. See Figure 30.3 for details of well.

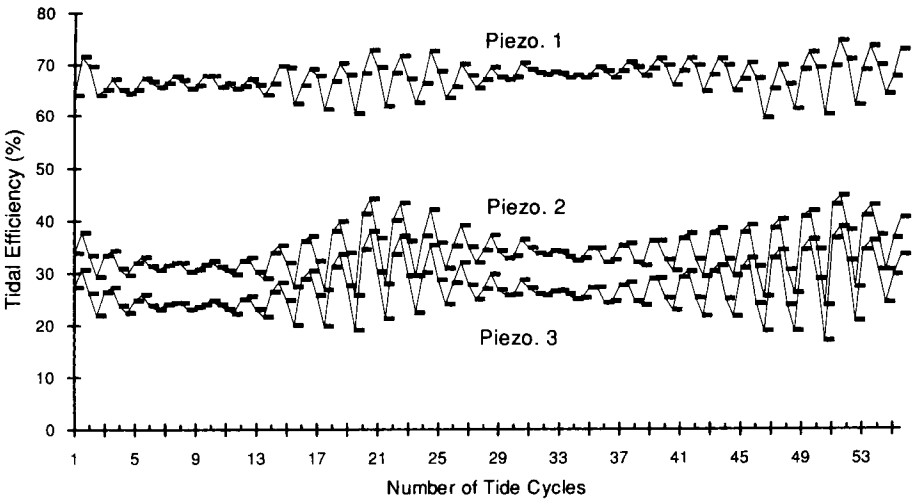


Fig. 30-6. Tidal efficiencies at Well No. 8 for the period 24/3/94 to 21/4/94.

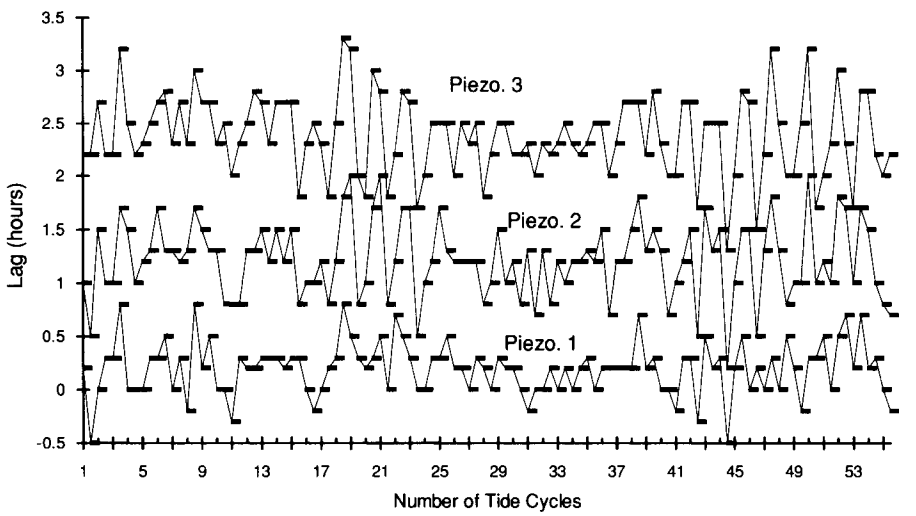


Fig. 30-7. Tidal lags at Well No. 8 for the period 24/3/94 to 21/4/94.

shown in Figures 30-8 and 30-9: in nearly every case, efficiency increases with depth, and, in every case, lag decreases with depth. Also, extrapolation of the efficiency- and lag-vs.-depth plots for wells 1, 6, 8, 10, 12 and 13 (Figs. 30-8, 30-9) down to the Holocene-Pleistocene contact (Fig. 30-4) shows such large efficiencies (> 90%) and small lags (effectively 0 h) at that level, that the tidal signal in the Holocene unit can be thought of as having originated in the very permeable Pleistocene unit. Finally, the areal variation is shown in Figures 30-10 and 30-11: the tidal fluctuation close to

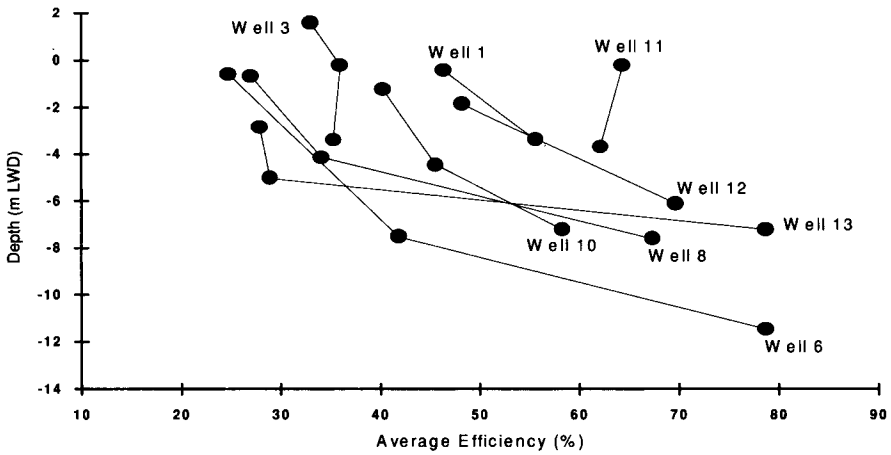


Fig. 30-8. Variation of tidal efficiency with depth at eight piezometer nests in the Holocene aquifer.

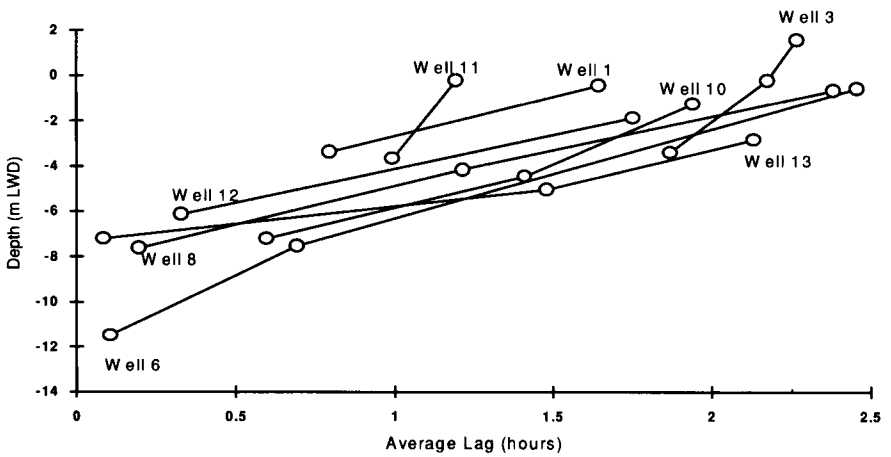


Fig. 30-9. Variation of tidal lag with depth at eight piezometer nests in the Holocene aquifer.

the shoreline is more like that of the offshore signal, but, further inland, neither efficiency nor lag varies with distance from the shoreline.

Distribution of brackish groundwater

Groundwater salinity was determined at 42 piezometers at the 13 wells (Fig. 30-2). The groundwater, which was sampled to a maximum depth of −11.5 m LWD, is of

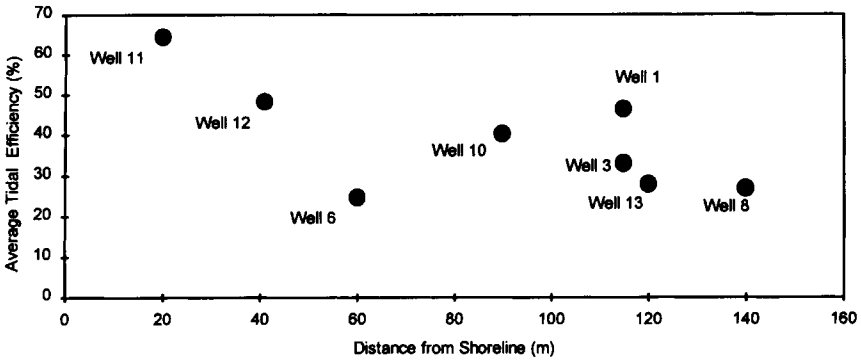


Fig. 30-10. Tidal efficiency in shallow piezometer as function of distance from the nearest shoreline.

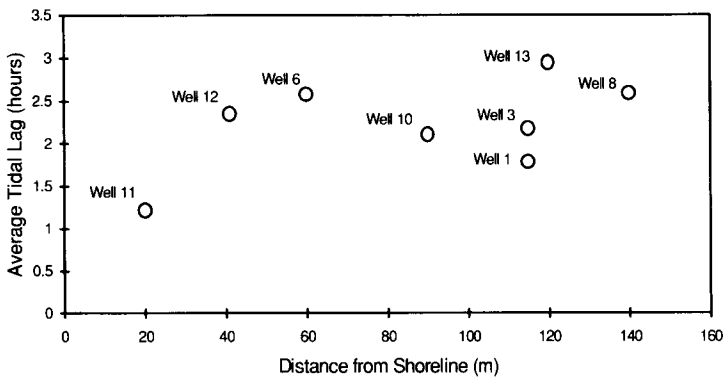


Fig. 30-11. Tidal lag in shallow piezometer as a function of distance from the nearest shoreline.

brackish to seawater salinity (Table 30-1). Values at 0 m LWD are presented in Table 30-2. In the six months before the February 1992 sampling, 259 mm of rainfall was recorded. Between the February 1992 and the December 1992 sampling, 1,273 mm of rain fell, and between the December 1992 and the April 1993 sampling, 362 mm of rain fell. Rainwater recharge is indicated by the generally lower groundwater salinities recorded in December 1992 (Table 30-2). Underwood et al. (1992) estimated that for a potable groundwater resource to form in a tidally coupled island aquifer with a width of 250 m, a recharge rate of at least 2 m y^{-1} is needed [see Fig. 20-9]. Given this estimate, it is not surprising that a significant freshwater lens is not present at Heron Island.

Throughout the sampling period, sewage effluent, which consisted of about 75% "freshwater" and 25% seawater, was released at a rate of 60–140 m^3 day^{-1}. This effluent, which was discharged below ground level in the centre of the cay, results in lower values of groundwater salinity at well 5 (Table 30-2).

Table 30-1

Summary of groundwater quality

	>60 m from shoreline			<60 m from shoreline		
	mean	stand. dev.	n	mean	stand. dev.	n
DO, mg/L	3.6	2.1	110	4.8	1.9	24
pH	7.23	0.22	116	7.53	0.19	22
Redox, mV	321	160	117	327	147	24
Salinity, ppt	24.9	6.0	118	33.3	3.4	24
TOC, ppm	25	34	31	1.7	1.0	7
$NH3^*$	0.49	2.88	103	0.013	0.010	21
Organic N^*	<0.27	0.29	18	<0.10	0.00	7
$N\text{-}NO_2^*$	<0.024	0.061	36	<0.002	<0.001	9
$N\text{-}NO_3^*$	28.0	17.5	36	4.73	4.75	9
Total P^{**}	0.097	0.048	21	0.060	0.026	7
$P\text{-}PO_4^{**}$	0.098	0.100	103	0.039	0.011	21

Notes: Sampling periods were Feb., April and Dec. 1992 and April 1993.
Key: n, number of observations; DO, Dissolved Oxygen; <, some values below detectable limits; TOC, total organic carbon (unfiltered).
*mg/L as N;** mg/L as P.

Table 30-2

Groundwater salinity at low-water datum

Well	1	2	3	4	5	6	7	8	9	10	11	12	13
2/92	32	33	29	24	14	36	27	26	26	29	36	35	21
12/92	30	11	14	16	16	32	25	24	11	22	32	23	27
4/93	30	34	28	24	18	35	26	26	26	29	36	34	31

CASE STUDY: NUTRIENT DYNAMICS IN A VULNERABLE ECOSYSTEM

Introduction

Urban and agricultural runoff has been linked to anthropogenic nutrient buildup in the coastal waters of the GBR (Bell, 1991). Ecological risk to the GBR from eutrophication on a regional scale, however, is not adequately understood (Walker, 1991c; Kinsey, 1991). Despite some uncertainty in the matter, it has been suggested that the levels of dissolved orthophosphate ($P\text{-}PO_4$) and dissolved inorganic nitrogen (DIN) associated with the eutrophication of coral reefs are very low: 3–6 $\mu g\ L^{-1}$ as phosphorus (P) and 14 $\mu g\ L^{-1}$ as nitrogen (N) (Bell, 1992). Consequently, coral reefs are potentially vulnerable to eutrophication from concentrated forms of pollution that are not adequately dispersed. Surface-water and waste-water discharges into the GBR must now meet stringent water-quality standards (Kinsey, 1991). Sewage at Heron Island is treated and then discharged into the groundwater system.

The high nutrient capital associated with guano accessions has prompted recent interest in the nutrient dynamics of coral cays in the GBR (e.g., Charley et al., 1990). In our study of Heron Island's groundwater system, we have evaluated the relative importance of waste-water discharges and guano deposition to the groundwater nutrient budget. We have also shown that average $P\text{-}PO_4$ and DIN concentrations in the groundwater of Heron Island (Table 30-1) are very high compared with ambient seawater levels. $P\text{-}PO_4$ in the groundwater is one order of magnitude, and DIN three orders of magnitude greater than the eutrophication levels previously mentioned.

Bird Guano. Guano deposition at Heron Island varies seasonally. During the peak of the 1992 summer breeding period, 164,000 shearwaters (*Puffinus pacificus*) and white-capped noddies (*Anous minutus*) deposited nearly 5,000 kg of guano wk^{-1} over the 19-ha cay (Staunton Smith, 1992). This guano contains 7.3% N and 1.5% P by weight, and delivers to the cay surface a nutrient load of approximately 9,800 kg of N and 2,000 kg of P annually (Staunton Smith, 1992).

In fresh guano at Heron Island, the ammonium ion (NH_4^+) content accounts for 15% of the total N, with the balance being present in organic form (Staunton Smith, 1992). The moisture from rainfall, which increases bacterial activity in the guano, was shown under experimental conditions to cause a 58% decrease in the total N of fresh guano within four days, and 87% within 28 days (Staunton Smith, 1992). This loss of total N is due to the ammonification of organic N to NH_4^+ by bacteria

$$\text{Organic N} \longrightarrow NH_4^+ + OH^-$$

and the subsequent volatilization of ammonia (NH_3)

$$NH_4^+ + OH^- \longrightarrow NH_3 + H_2O.$$

When moisture, temperature and oxygen conditions are favourable, the nitrification of NH_4^+ by bacteria to nitrite ($N\text{-}NO_2$) and finally nitrate ($N\text{-}NO_3$) takes place according to

$$2NH_4^+ + 3O_2 \longrightarrow 2NO_2^- + 4H^+ + 2H_2O$$

$$2NO_2^- + O_2 \longrightarrow 2NO_3^-.$$

$N\text{-}NO_3$ is not volatile and is readily leached and mobile, giving credence to the hypothesis that the periodic leaching of guano by rain is responsible for the high N capital of the groundwater. However, it is currently not known what proportions of N and P in the guano actually reach the water table.

Coral sands have a great capacity to assimilate phosphate. For example, concentrations of 14 wt% (as P) were recorded by Fosberg (1957). Guano accumulations on the carbonate islands of the GBR have resulted in only a few commercially viable phosphatic rock deposits – e.g., Holbourne Island (19°44′S, 148°22′E) and Lady Elliott Islet (24°08′S, 152°46′E), (Hutchinson, 1950). The guano at Heron Island, however, is found mostly on the soil surface as a thin layer, and phosphate

rock has not formed. In the coral-cay environment, dissolved inorganic P is sorbed by aragonite and calcite, a process which is well recognised by soil scientists and has been shown experimentally to be represented by the Elovichian chemisorption model (DeKanel and Morse, 1978). At Heron Island, rainfall events during our study have not resulted in significant perturbations in groundwater concentrations of $P\text{-}PO_4$. If most of the leached guano P is sorbed by coral sediments in the unsaturated zone, then the observed groundwater concentrations of $P\text{-}PO_4$ may be the result of a chemical equilibrium with the aquifer matrix (Froelich, 1988).

Anthropogenic contaminants. Because of the high nutrient contents often found in sewage discharges, these discharges are considered to be potentially damaging to nearby coral-reef communities (Bell, 1992). The Great Barrier Reef Marine Park Authority (GBRMPA) now requires that resort islands in the GBR treat their sewage effluent to a tertiary level, prior to discharge to the sea via ocean outfalls. At Heron Island, the disposal of treated sewage effluent relies on groundwater recharge. It may be argued that further removal of P from sewage (i.e., tertiary treatment) is unnecessary if natural processes sufficiently attenuate P concentrations in the effluent following discharge. The total nutrient loading to the cay's vadose zone from treated sewage effluent is approximately 290 kg of N and 320 kg of P annually (Staunton Smith, 1992). By comparison, this nutrient load represents only a small fraction (3% of N and 15% of P) of the nutrient load delivered to the cay surface as guano. Unlike guano, however, the sewage effluent is discharged continuously and at fixed positions.

Most of the DIN in treated sewage was accounted for by $N\text{-}NO_3$. During the study period, the secondary treated sewage with a $N\text{-}NO_3$ level of < 10 mg L^{-1} in fact diluted the groundwater $N\text{-}NO_3$, which was typically present at 20–60 mg L^{-1} (as N) below the forested areas of the cay. The discharges of treated sewage influenced the local groundwater quality in other ways, most notably in terms of severe oxygen depletion, and elevated ammonia (NH_3) and total organic carbon (TOC) concentrations. Faecal coliform levels of 50 organisms per 100 mL have also been recorded in well 5 at a time when the treated effluent contained about 7,000 organisms per 100 mL. On the other hand, the very high $P\text{-}PO_4$ levels of 12–20 mg L^{-1} (as P) in the treated sewage had no significant impact on the groundwater, and groundwater from well 5 contained only 0.043–0.18 mg L^{-1} (as P) of $P\text{-}PO_4$.

During sampling at well 9, which was located beside a fuel storage/supply area (Fig. 30-2), we smelled hydrogen sulphide (H_2S) gas on occasions. The groundwater redox potential recorded from this well varied between −50 and 216 mV, indicating that sulphate reduction was occurring. At all other locations the groundwater was aerobic.

Groundwater N and P. Groundwater N and P concentrations are dominated by $N\text{-}NO_3$ and $P\text{-}PO_4$ (Table 30-1). The very high $N\text{-}NO_3$ levels are particularly conspicuous and far exceed (often by three orders of magnitude) the $N\text{-}NO_3$ levels in ambient seawater in the GBR (Walker, 1991c), porewaters of reef sediment at

Checker Reef in Hawaii (Tribble et al., 1988; Sansone et al., 1988a; Sansone et al., 1988b; Sansone, 1985), porewater in coral heads (Risk and Müller, 1983), and the internally circulating water of a patch reef in the GBR (Andrews and Müller, 1983). By contrast, $P\text{-}PO_4$ levels in groundwater at Heron Island are comparable to the levels in reef-sediment porewater (Tribble et al., 1988; Sansone et al, 1988a; Sansone et al., 1988b; Sansone, 1985) and to the interstitial porewater from live coral heads (Risk and Müller, 1983).

Another feature of the groundwater chemistry is that lower nutrient concentrations occur near the shoreline (i.e., < 60 m from the beach; Table 30-1). A likely explanation is the combined effect of smaller guano loading on the beaches and dilution of groundwater by seawater as a consequence of lateral flow through the beachface. This feature is more pronounced for N than for P, which is consistent with N being more mobile than P and the previously discussed buffering of P concentrations in the groundwater system. The average N/P ratio of the groundwater sampled more than 60 m from the shoreline (N/P = 300) is much higher than for the flux of both guano and treated sewage combined (N/P = 4.3). If the source of these nutrients is principally guano and treated sewage, then these ratios are also consistent with higher N mobility and P sorption.

Discussion

Disposal of secondary treated sewage at Heron Island is via a soakage trench located in the unsaturated zone. This disposal has some impact on local groundwater quality. It appears, however, that the groundwater nutrient chemistry is governed primarily by natural processes, such as the leaching of guano and the sorption of $P\text{-}PO_4$ by calcium carbonate. From the high natural levels of $N\text{-}NO_3$ in the groundwater and the sorption of $P\text{-}PO_4$, therefore, our data suggest that current sewage treatment and disposal practices are acceptable.

CONCLUDING REMARKS

Tidal phenomena dominate the groundwater hydrodynamics of the 19-ha cay, Heron Island. Other hydrodynamic processes, such as wave set-up, ponding and currents are likely to have insignificant effect on the surficial aquifer. Our data indicate that the lower aquifer is highly permeable, and there is circumstantial evidence to suggest that the top of this aquifer is capped by a confining layer (i.e. the reef plate). The spatial variability of the average tidal signals recorded in the Holocene aquifer reflects large-scale heterogeneities in permeability and porosity. Overall, the cay is hydrogeologically like other dual-aquifer islands of atoll and reef environments.

Because of its nutrient-rich groundwater, Heron Island has the potential to influence ambient N and P levels in its reef environment. This potential depends on a number of factors, including nutrient transport through the beachface, tidal flushing, and the capacity of the reef to assimilate additional nutrients. In addition, a com-

pletely separate process that can elevate seawater nutrient levels around coral cays is the deposition of guano over the intertidal zone by seabirds (Charley et al., 1990). If the gross N and P concentrations in the groundwater are insensitive to anthropogenic inputs, which they appear to be, then any concentrated nutrient transport to the reef ecosystem from the groundwater would constitute natural "pollution". Could natural "pollution", if present, be used to study the long-term effects of nutrients on reef ecosystems?

Although we have identified some fundamental properties of N and P dynamics in the coral-cay system, the quantitative effect on gross groundwater quality will require a fully mechanistic model explaining the N and P content of the groundwater and its fate in terms of physical, chemical and biological processes documented in the field. Such ongoing research will add to our current understanding of coral-cay hydrogeology and provide better understanding of the environmental implications of human activities at Heron Island.

ACKNOWLEDGMENTS

The authors wish to acknowledge the assistance provided Micheal Noordink (Enschede Technical College, Holland), Eva Biosca (Madrid University, Spain), Aino Jensen (The Engineering Academy of Denmark) and Jonathon Staunton Smith. Funding for this project was provided mainly by The University of Queensland. Other funding and assistance has been provided by the GBRMPA, P&O Resorts Ltd., and the Queensland National Parks and Wildlife Service. The access provided by Jim Charley and M. Wrighton and Associates to unpublished data is gratefully acknowledged.

REFERENCES

Andrews, J.C. and Müller, H., 1983. Space-time variability of nutrients in a lagoonal patch reef. Limnol. Oceanogr., 28: 215–227.

Bell, P.R.F., 1991. Must GBR pollution become chronic before management reacts? Search, 22: 117–119.

Bell, P.R.F., 1992. Eutrophication and coral reefs - some examples in the Great Barrier Reef Lagoon. Water Res., 26: 553–568.

Buddemeier, R.W. and Oberdorfer, J.A., 1986. Internal hydrology and geochemistry of coral reefs and atoll islands: key to diagenetic variations. In: J.H. Schroeder and B.H. Purser (Editors), Reef Diagenesis. Springer-Verlag, Heidelberg, pp. 91–111.

Buddemeier, R.W. and Oberdorfer, J.A., 1988. Hydrogeology and hydrodynamics of coral reef pore waters. Proc. Sixth Int. Coral Reef Symp. (Townsville), 2: 485–490.

Charley, J., Heatwole, H. and Brock, M., 1990. Nutrient dynamics on coral cays. Final report to the Aust. Res. Counc. (unpublished), Proj. No. A18615988, 206 pp.

Davies, P. J., 1974. Subsurface solution unconformities at Heron Island, Great Barrier Reef. Proc. Second Int. Coral Reef Symp. (Brisbane), 2: 573–578.

Davies, P. J. and Hopley, D., 1983. Growth fabrics and growth rates of Holocene reefs in the Great Barrier Reef. BMR J. Aust. Geol. Geophys., 8: 237–251.

DeKanel, J. and Morse, J.W., 1978. The chemistry of orthophosphate uptake from seawater on to calcite and aragonite. Geochim. Cosmochim. Acta, 42: 1335–1340.
Flood, P.G., 1977. Coral cays of the Capricorn and Bunker groups, Great Barrier Reef Province, Australia. Atoll Res. Bull., 195: 1–7.
Flood, P.G., 1986. Sensitivity of coral cays to climatic variations, southern Great Barrier Reef, Australia. Coral Reefs, 5: 13–18.
Fosberg, F.R., 1957. Description and occurrence of atoll phosphate rock in Micronesia. Am. J. Sci., 255: 584–592.
Froelich, P.N., 1988. Kinetic control of dissolved phosphate in natural rivers and estuaries: a primer on the phosphate buffer mechanism. Limnol. Oceanogr., 33: 649–668.
Gourlay, M.R., 1988. Coral cays: products of wave action and geological processes in a biogenic environment. Proc. Sixth Int. Coral Reefs Symp. (Townsville), 2: 491–496.
Hopley, D., 1982. Geomorphology of the Great Barrier Reef: Quaternary development of coral reefs. Wiley Interscience, New York, 453 pp.
Hutchinson, G.E., 1950. Survey of existing knowledge of biogeochemistry. 3. The biogeochemistry of vertebrate excretion. Am. Mus. Nat. History Bull. 96, 554 pp.
Jell, J.S. and Flood, P.G., 1977. Guide to the geology of reefs of the Capricorn and Bunker Groups, Great Barrier Reef Province, with special attention to Heron Reef. In: Papers Dep. Geol., Univ. Queensland, Aust. Sedimentol. Group, 8(3): 1–85.
Kinsey, D.W., 1991. Can we resolve the nutrient issue for the Reef? Search, 22: 119–121.
Lam, R.K., 1974. Atoll permeability calculated from tidal diffusion. J. Geophys. Res., 79: 3073–3081.
Lourensz, R.S., 1977. Tropical cyclones in the Australian region July 1909 to June 1975. Aust. Gov. Publ. Serv., Canberra, 110 pp.
Marshall, J.F., 1983. Lithology and diagenesis of the carbonate foundations of modern reefs in the Southern Great Barrier Reef. BMR J. Aust. Geol. Geophys., 8: 253–265.
Marshall, J.F. and Davies, P.J., 1982. Internal structure and Holocene evolution of One Tree Reef, Southern Great Barrier Reef. Coral Reefs, 1: 21–28.
Maxwell, W.G.H., 1962. Lithification of carbonate sediments, in the Heron Island Reef, Great Barrier Reef. J. Geol. Soc. Aust., 8: 217–238.
Nielsen, P., 1990. Tidal dynamics of the water table in beaches. Water Resour. Res., 26: 2127–2134.
Oberdorfer, J.A. and Buddemeier, R.W., 1986. Coral-reef hydrology: field studies of water movement within a barrier reef. Coral Reefs, 5: 7–12.
Oberdorfer, J.A., Hogan, P.J. and Buddemeier, R.W., 1990. Atoll island hydrogeology: flow and freshwater occurrence in a tidally dominated system. J. Hydrol., 120: 327–340.
Richards, H.C., 1938. Boring operations at Heron Island, Great Barrier Reef (17 May to 13 August 1937). Rep. of the Great Barrier Reef Comm., 4(3): 135–142.
Richards, H.C. and Hill, D., 1942. Great Barrier Reef bores, 1926 and 1937: descriptions, analyses and interpretations. Rep. of the Great Barrier Reef Comm., 5: 1–111.
Risk, M.J. and Müller, H.R., 1983. Porewater in coral heads: Evidence for nutrient regeneration. Limnol. Oceanogr., 28: 1004–1008.
Sansone, F.J., 1985. Methane in the reef flat porewaters of Davies Reef, Great Barrier Reef (Australia). Proc. Fifth Int. Coral Reef Cong. (Tahiti), 3: 415–419.
Sansone, F.J., Tribble, G.W., Buddemeier, R.W. and Andrews, C.C., 1988a. Time and space scales of anaerobic diagenesis within a coral reef framework. Proc. Sixth Int. Coral Reef Symp. (Townsville), 3: 367–372.
Sansone, F.J., Andrews, C.C., Buddemeier, R.B. and Tribble, G.W., 1988b. Well-point sampling of reef interstitial water. Coral Reefs, 7: 19–22.
Staunton Smith, J., 1992. Bird guano and local eutrophication at Heron Island. B.Sc. (Hons.) Thesis, Univ. of Queensland, Australia, 79 pp.
Tribble, G.W., Sansone, F.J., Li, Y.H., Smith, S.V. and Buddemeier, R.W., 1988. Material fluxes from a reef framework. Proc. Sixth Int. Coral Reef Symp. (Townsville), 2: 577–582.

Underwood, M.R., Peterson, F.L. and Voss, C.I., 1992. Groundwater lens dynamics of atoll islands. Water Resour. Res., 28: 2889–2902.
Walker, T.A., 1991a. Tourism development and environmental limitations at Heron Island, Great Barrier Reef. J. Environ. Manage., 33: 117–122.
Walker, T.A., 1991b. The distribution, abundance and dispersal by seabirds of *Pisonia grandis*. In: Pisonia islands of the Great Barrier Reef. Atoll Res. Bull., 350: 1–23.
Walker, T.A., 1991c. Is the Reef really suffering from chronic pollution? Search, 22: 115–117.
Wheatcraft, S.W. and Buddemeier, R.W., 1981. Atoll island hydrology. Ground Water, 19(3): 311–320.

Geology and Hydrogeology of Carbonate Islands. Developments in Sedimentology 54
edited by H.L. Vacher and T. Quinn
© 1997 Elsevier Science B.V. All rights reserved.

Chapter 31

GEOLOGY AND HYDROGEOLOGY OF THE COCOS (KEELING) ISLANDS

C.D. WOODROFFE and A.C. FALKLAND

INTRODUCTION

The Cocos (Keeling) Islands lie in the eastern Indian Ocean about halfway between Australia and Sri Lanka, or approximately 1,000 km southwest of Java Head, Indonesia (Fig. 31-1). They were discovered in 1609 by Captain William Keeling of the East India Company. An Australian territory since 1955, this small group of islands is officially named Cocos (Keeling) to distinguish it from the several other islands in the Pacific and Indian Oceans that are similarly named after the coconut palm (*Cocos nucifera*).

Surrounded by ocean floor with a depth of 5,000 m or more deep and age of 60–90 Ma (Jongsma, 1976), the Cocos (Keeling) Islands consist of an atoll, South Keeling (12°12′S, 96°54′E), and a single horseshoe-shaped island (or atollon; Guppy, 1889), North Keeling (11°50′S, 96°49′E). North and South Keeling are 27 km apart and connected by a submarine ridge around 1,000 m deep. The islands form part of the Cocos Rise, within a discontinuous chain of seamounts, the Vening Meinesz seamounts, which can be traced towards Christmas Island near the Java Trench (Fig. 31-1).

South Keeling (henceforth referred to as Cocos in this chapter) has a land area of 14 km^2 and currently supports a population of about 600. As shown in Fig. 31-2, Cocos includes five main islands, three of which support at least one freshwater lens. North Keeling has a land area of 1.2 km^2 and is unpopulated.

Cocos (Keeling) and the origin of atolls

The Cocos (Keeling) Islands hold a special place in the history of geologic concepts regarding carbonate islands. Cocos is the only atoll on which Charles Darwin landed (on the HMS *Beagle* in April, 1836). It, therefore, became central to his subsidence theory for the development of coral reefs (Darwin, 1842). John Clunies Ross, who owned the island and was temporarily absent at the time of Darwin's visit, strongly challenged Darwin's ideas (Ross, 1855). Ross and other early naturalists (Fitzroy, 1839; Forbes, 1885; Guppy, 1889) considered the geological evolution of the islands in detail and often drew contradictory inferences. One particular item of confusion has been the conglomerate platform which is discussed in some detail in this chapter.

Through deep drilling in islands such as Funafuti, Enewetak, and Midway after World War II (Ladd et al., 1948, 1953), the subsidence theory has long been sub-

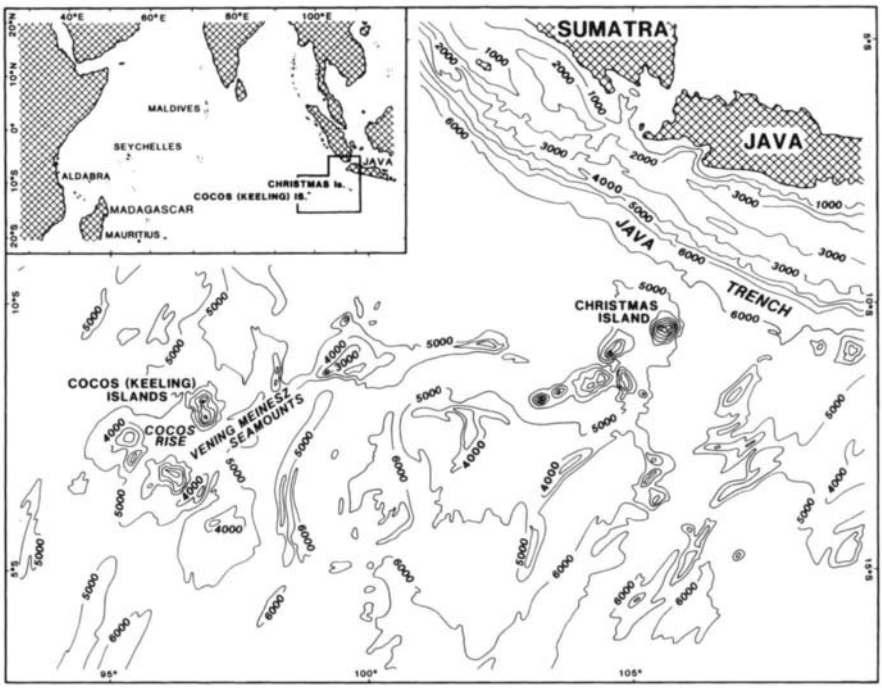


Fig. 31-1. Location of the Cocos (Keeling) Islands in the northeastern Indian Ocean. Bathymetry is in metres.

stantiated. As Stoddart (1973) has pointed out, however, Darwin's subsidence theory relates to the *structure* of the atoll; the actual *surface morphology* of the atoll is related more to other phenomena such as sea-level history and karst processes. Shallow drilling on the Cocos (Keeling) Islands — first for water-resources investigations (Falkland, 1994a) and more recently for geomorphologic studies (Woodroffe et al., 1990a, 1990b, 1991) — allows assessment of the morphological development of Cocos. This subject is taken up in the Case Study at the end of this chapter.

Climatic and marine setting

The Cocos (Keeling) Islands are situated in the humid tropical zone and are influenced by the southeast trade winds for most of the year. The islands are exposed to tropical cyclones, which have affected the islands on a number of occasions. The climate of the Cocos (Keeling) Islands, particularly the rainfall pattern, is also influenced to some extent by El Niño Southern Oscillation (ENSO) episodes. A reasonable correlation exists between the Southern Oscillation Index (SOI), an index of the strength of ENSO episodes, and the annual rainfall, expressed as a proportion of mean annual rainfall (Falkland, 1994a). Thus, in years when ENSO episodes occur, and the SOI is negative, the annual rainfall tends to be lower than normal and vice versa.

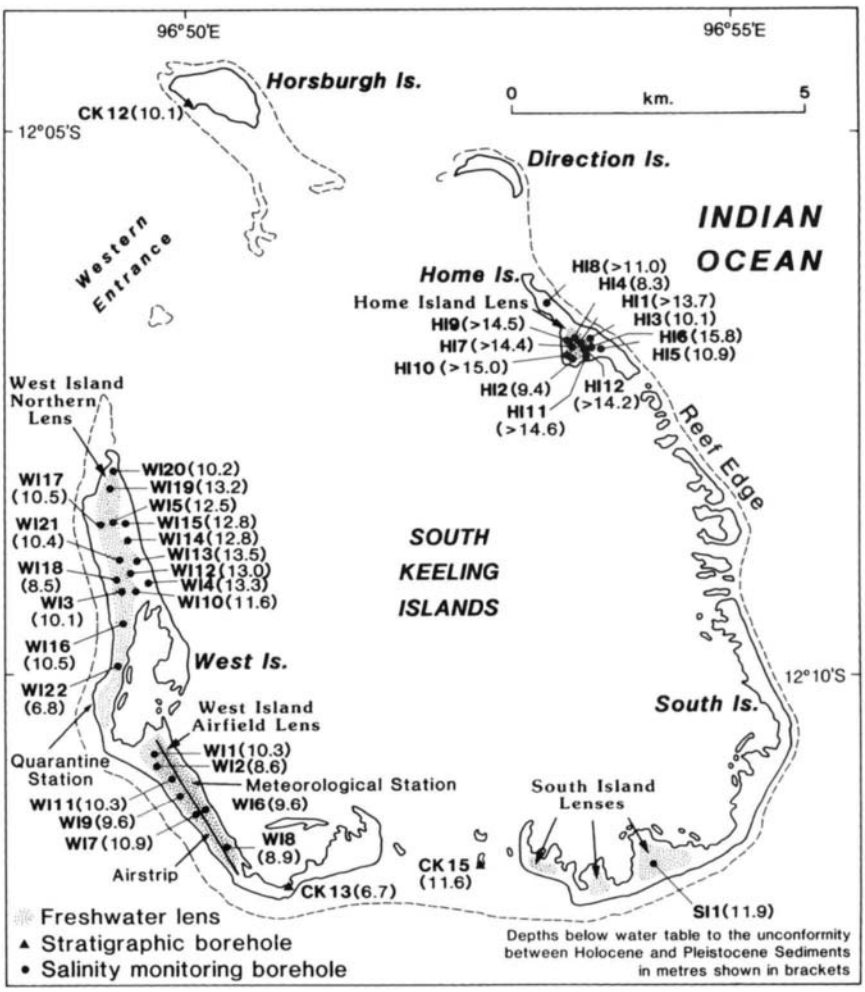


Fig. 31-2. Map of Cocos showing boreholes with depth below mean sea level to the Holocene/Pleistocene unconformity and the distribution of freshwater lenses.

Weather data. Annual rainfall is 850–3,300 mm with a mean of about 1,950 mm. Annual evaporation from a U.S. Class A pan is 2,370–2,600 mm with a mean of about 2,490 mm. Potential evapotranspiration (PET) is estimated to be, on average, about 2,000 mm. Temperatures are relatively uniform, 18–32°C. Relative humidity is 65–85%, and mean daily wind speeds are 17–29 km h^{-1}. The maximum wind gust, recorded while cyclone Doreen passed over Cocos in January 1968, was 176 km h^{-1}.

A meteorological station is located on the eastern side of the airstrip on West Island (Fig. 31-2) and has been operated continuously since February 1952. This station has been an invaluable resource for data used in water-balance calculations. Available data include air temperature (wet and dry bulb; dew point), atmospheric

pressure, cloud cover, wind speed and direction at 3-hour intervals, and rainfall and pan evaporation on a daily basis. Rainfall data for all but 17 months are available from 1901 onwards. Prior to 1952, most of the data were collected on Direction Island.

Daily rainfall has also been measured and recorded on Home Island since May 1986, and at the Quarantine Station on West Island (Fig. 31-2) since December 1991. Over the long term, there is little variation between the three sites; during the 4-year period, 1989 to 1992, total rainfall at Home Island and the Quarantine Station were 3.4% less and 5.3% greater, respectively, than at the meteorological station. In the short term (e.g. daily records), there is considerable variation. This variation is consistent with the general observation that individual storms can affect only small areas of the atoll, while others are left quite dry.

Long dry periods are particularly relevant to utilization of water resources. The longest period of no rainfall at the meteorological station was 28 days in November 1985. The longest period with a total less than 10 mm was 69 days (6.2 mm between November 1985 and January 1986).

Marine environment. Swell is dominantly from the southeast, associated with the trade winds. There is usually a westward-flowing equatorial current of about 1 kn, although in November-December when the Intertropical Convergence Zone moves south of the equator, the eastward-flowing equatorial counter current may develop. Tides are mixed, mainly semidiurnal, with large inequalities of range and timing between consecutive tides. The maximum tidal range is 1.2 m.

ATOLL MORPHOLOGY

The reef which encircles Cocos is horseshoe-shaped (Fig. 31-2). The reef is continuous along the eastern, southern and western margins and, on the northwest, is separated from an outlier reef (and Horsburgh Island) by two passages 12–14 m deep (Fig. 31-2). Reef islands around the main atoll rim are either elongate islands, such as West Island and South Island, or small generally crescentic islands separated by shallow interisland passages which shoal at low-water spring tides.

The reef front shelves gradually to a terrace in water depths of around 18 m. It is surprisingly barren of hard coral growth, but contains an erosional spur-and-groove system (Colin, 1977). The reef crest is generally emergent at low water and consists, on the eastern atoll rim, of a thin algal veneer over dead *Millepora*. At the southern end of the atoll, the rim is less pronounced, and the reef crest consists of a broad algal pavement strewn with coral boulders up to 1 m in diameter. The reef flat is of variable width and depth. In the broad southern passage (Fig. 31-2), the reef flat dries at lowest tides to a shallowly exposed irregular flat veneered with fragmented colonies of massive *Porites* interspersed with branching *Acropora* and *Montipora*. Along the eastern margin of the atoll, there are deeper pockets of water over the reef flat; these are similar to, but less continuous than, the "boat passage" found in atolls of the Marshall Islands (Emery et al., 1954).

Reef islands are located for much of their extent on a platform of cemented coral conglomerate. This conglomerate platform is exposed along the ocean margin of many of the islands; it rises to about 0.5 m above mean sea level and is, therefore, inundated by wave action at the highest tides (Woodroffe et al., 1990a, 1990b). The islands are composed either of coral rubble or, more generally, of sand and shingle. They are highest on their ocean shore, reaching a maximum elevation of over 11 m where there is a distinct wind-blown dune formed on the southern shore of South Island. Dunes, though unusual on coral atolls, are also found on the ocean shores of Home and West Islands.

In planform, the smaller reef islands are crescentic or horseshoe-shaped with accretionary sandy spits formed at the lagoonward ends of the interisland channels. The form of these spits led Guppy to suggest that islands represented stages in the formation of atoll-rim atollons, similar to the annular faroes which are characteristic of atolls in the Maldives (Guppy, 1889).

The elongate reef islands, West and South Islands, contain several large embayments on the lagoon side of the islands. These embayments, locally termed "teloks", are shallow, muddy areas which dry or almost dry at low tide. They are separated from the ocean side of the islands by low, often shingle-dominated ridges, which resemble the "barachois" described from Diego Garcia (Stoddart, 1971). These narrow corridors of land give the impression that they may occupy the site of former interisland channels, a view propounded by Darwin. These shingle-dominated ridges are poorly consolidated, are underlain only rarely by an extensive conglomerate platform, and are covered with only immature soils. The coconut growth is sparse and stunted on these ridges, which are dominated instead by thickets of *Scaevola*. Although radiocarbon dates do not support the suggestion that they were recently open as passages, these areas do not favor the development of freshwater lenses (Jacobson, 1976a, 1976b). Instead, the freshwater lenses are most extensive in the broader parts of the elongate reef islands, and on Home Island which is wider than the islands adjacent to it (Fig. 31-2).

The lagoon covers an area of about 190 km^2 and can be divided into a shallow southern half and a deeper northern half. The southern part includes a broad island border that dries out at low tide. This intertidal zone is 1–2 km wide in places and grades into a subtidal, sandy seagrass-covered plain (Williams, 1994; Smithers et al., 1994). Within the interior of the southern lagoon, there is a reticulate pattern of blue holes. In the lower intertidal zone, the blue holes have a sparse covering of coral on their rims, and their interiors are muddy with predominantly a dead veneer of branching corals on the walls down to depths of 10–15 m. The deepest blue hole, just southwest of Direction Island, is up to 30 m deep. The northern section of the lagoon is composed of sand with sparse, often dead, coral heads scattered throughout.

The unconsolidated sediments that comprise the reef islands and infill the lagoon are composed of skeletal biogenic mud, sand and shingle. Sediments within the lagoon have been examined in detail and are dominated by coral fragments — more so than in other Pacific atolls at which sediment components have been analysed (Smithers, 1994; Smithers et al., 1994). *Halimeda* blades are far less important than in most Pacific atolls. Foraminifera, especially *Amphistegina*, and coralline algae

fragments, particularly ones derived from rhodoliths of *Spongites* which occur in the interisland channels, are significant contributors to lagoonal sediments and are carried in from more oceanward environments. Teloks are dominated by gravelly muds in which molluscan debris is significant (Smithers et al., 1994).

PLEISTOCENE LIMESTONES

Pleistocene limestones are nowhere exposed on Cocos. However, drilling around the atoll has encountered a well-lithified, porous limestone underlying the generally poorly consolidated Holocene coral shingle and sands at typical depths of 8–13 m below mean sea level (Fig. 31-2). Although boreholes are concentrated on West Island and Home Island where the only permanent settlements are, drilling on Horsburgh, South Island, and a small island in the southern passage indicates that the limestone is found at similar depths throughout the atoll.

The first U-series disequilibrium date from this limestone was on a sample of coral at the top of the unit at a depth of 12.6 m (10.5 m below mean sea level) in borehole WI1. The result was 118 ± 7 ka on a bulk sample. A subsequent date on a subsample from which secondary calcite was removed gave a date of 123 ± 7 ka (Woodroffe et al., 1991). These results indicate that the unconformity encountered with such consistency in boreholes corresponds to the "Thurber Discontinuity", which separates Pleistocene limestone deposited during the Last Interglacial from Holocene sediments deposited during the post-glacial marine transgression and subsequent stillstand (Thurber et al., 1965).

The Thurber Discontinuity appears to be at a relatively uniform depth beneath the reef islands. The shallowest depths at which it has been encountered are 6.7 and 6.8 m on West Island. Continuous seismic-reflection profiling across the lagoon, however, indicates greater depths. A reflector intersects the known unconformity surface on the atoll rim and reaches depths of 22–24 m below sea level within the center of the lagoon (Searle, 1994). This reflector, the Pleistocene surface, reaches depths of around 20 m even beneath the blue holes, the rims of which appear to be located over slight topographic highs in the Pleistocene surface. The occurrence of the Pleistocene limestone at depths of 8–14 m below present sea level, when it is likely that reefs grew at least up to present sea level, and probably up to 5–6 m above present (Lambeck and Nakada, 1992), indicates gradual subsidence of the atoll at a rate on the order of 0.02–0.2 mm y^{-1} (Woodroffe et al., 1991, 1994; Searle, 1994). The topography, on the other hand, points to the significance of karstification during phases of subaerial exposure since the Last Interglacial, with blue holes representing collapsed dolines and the modern morphology of the reefs reflecting an antecedent karst topography as proposed for reef systems in general by Purdy (1974a, 1974b).

HOLOCENE SEDIMENTS

The Pleistocene limestone surface on Cocos is overlain by largely unconsolidated Holocene sands and shingle. Drilling, even where drilling muds have been employed,

rarely recovered continuous core, but does indicate that much of the thickness of the Holocene reefal sediment is composed of shingle fragments of branching acroporid corals in a matrix of sand. The best-cemented units occur within the surface conglomerate platform where coral clasts, including plates and blocks of *Porites* up to about 1 m in diameter, are cemented, most conspicuously by coralline algae. Cementation is usually most pronounced in cores taken at the ocean side of this conglomerate platform.

Fig. 31-3 shows the location at which transects of boreholes, additional to those used for salinity monitoring (see below), have been drilled, and also shows radiocarbon dates on coral clasts from within the conglomerate platform (Woodroffe et al., 1994). Fig. 31-4 illustrates the stratigraphy at three of the transects together

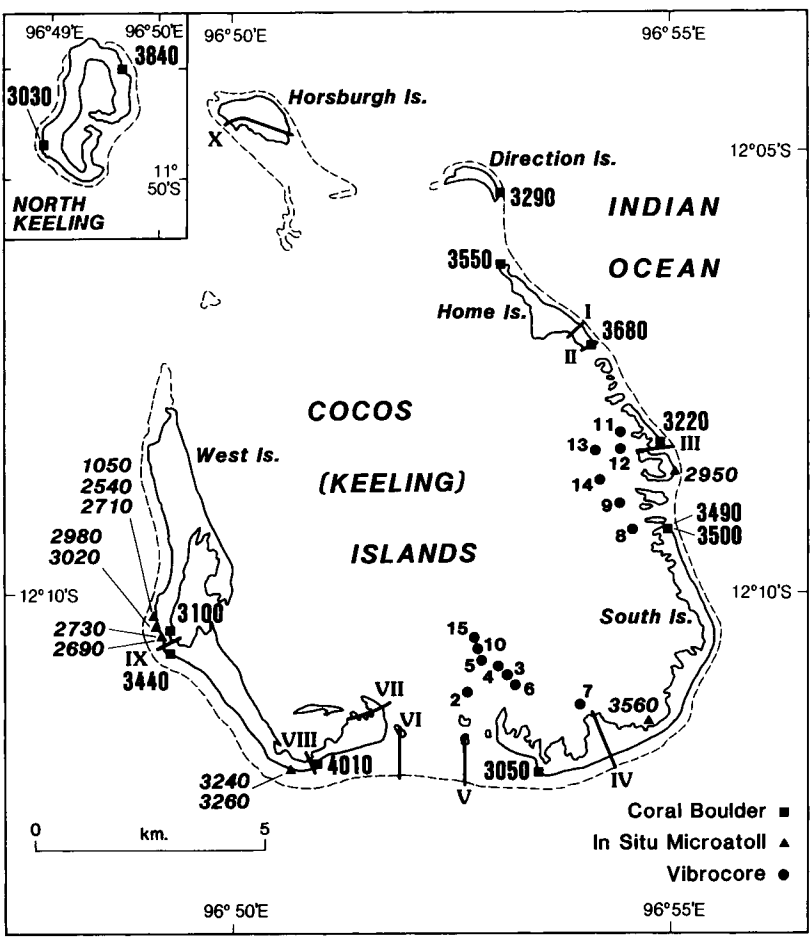


Fig. 31-3. Map of Cocos showing locations of stratigraphic transects I-X, vibrocores, and radiocarbon ages on coral from conglomerate platform and fossil microatolls. (From Woodroffe et al., 1994.)

with radiocarbon dates on coral clasts or pieces of *Tridacna*. The oldest radiocarbon dates are around 7000 y B.P. at 14 m below sea level in borehole HI12 on Home Island, and 6800 y B.P. at 9 m below sea level in borehole CK15 in the southern passage. These dates record reef establishment over the Pleistocene surface after flooding by the rapidly rising sea level. Vertical reef growth appears to have been rapid with dates of 6200 y B.P. at 6 m in borehole CK3, and a series of dates around 6000 y B.P. at 2–3 m below present sea level from around the atoll rim. The pattern of reef growth recorded by the radiocarbon dates is shown in Fig. 31-5 in relation to inferred sea-level history. The dates suggest that the reef at Cocos lagged behind sea level, which appears to have been at present level by this time in most of the region (i.e., Sri Lanka, Katupotha, 1988; Malacca, Geyh et al., 1979; Australia, Thom and Chappell, 1975; McLean et al., 1978; Thom and Roy, 1985).

The conglomerate platform is exposed along the ocean shores of islands, particularly those on the eastern rim. The conglomerate is composed of clasts of coral shingle or rubble cemented into a nearly horizontal surface. This surface was referred to as "brecciated coral-rock" by Darwin (1842), "reef conglomerate" by Guppy (1889) and "breccia platform" by Wood-Jones (1912). Similar conglomerate platforms on Pacific atolls have been interpreted either as lithified storm deposits that formed incrementally under sea-level conditions like those at present (Shepard et al., 1967), or as emergent reef flat indicating a sea level higher than present (Tracey and Ladd, 1974; Buddemeier et al., 1975; Montaggioni and Pirazzoli, 1984; see also

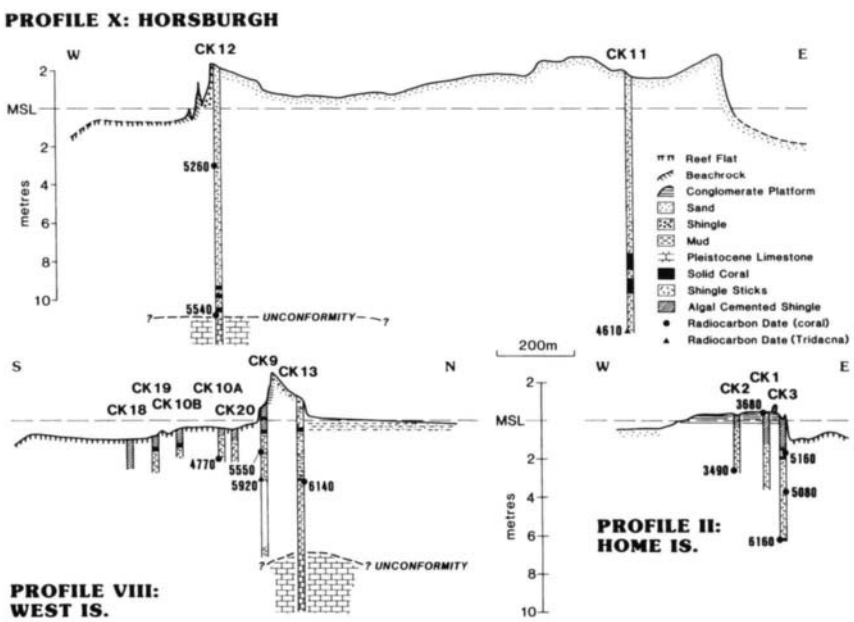


Fig. 31-4. Selected stratigraphic profiles from Cocos showing boreholes, sediments recovered and radiocarbon dates. See Fig. 31-3 for location of profiles. (From McLean and Woodroffe, 1994.)

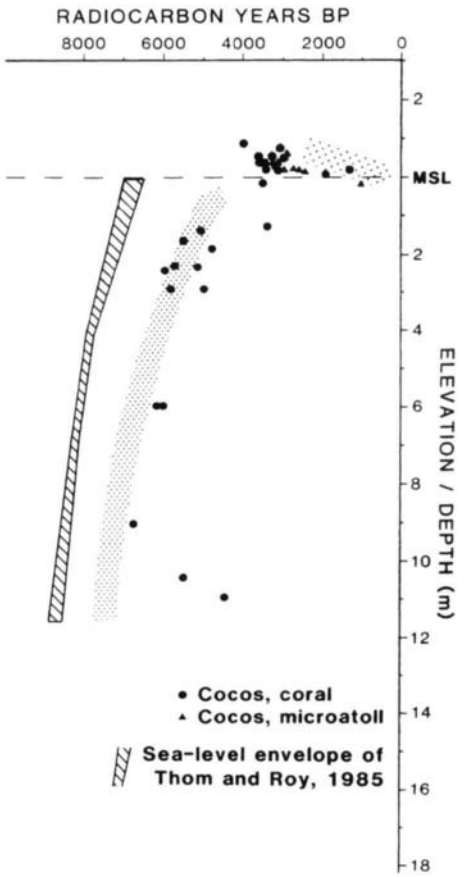


Fig. 31-5. Age-depth plot of samples (mainly coral, some *Tridacna*) from drilling and surface exposures. Three phases of Holocene development are shown: a rapid rise of sea level; a Holocene submergence; and a subsequent fall in sea level to its present position. These three phases of the Holocene history of Cocos are discussed in detail in the Case Study.

Chapter 19 of this book). As discussed in the Case Study of this chapter, the latter interpretation is favored in Cocos (Woodroffe et al., 1990a, 1990b).

Reef islands have formed since the conglomerate platform developed, and their planform morphology is partly controlled by outcrops of the platform. The islands appear to have developed continuously over the last 3,000 years, with abundant accretion on the oceanward shores (Woodroffe and McLean, 1994).

HYDROGEOLOGY

Following initial evaluation of the groundwater resources of Home Island in the mid-1970s (Jacobson, 1976a, 1976b), a detailed water-resources and groundwater-

exploration program for the main islands of Cocos was carried out by a number of Australian Government agencies from 1987 to 1992 (Falkland, 1994a). Some of the results of that program are reviewed in this section.

The groundwater-exploration program included drilling of 35 boreholes (Fig. 31-2) on West, Home, and South Islands. These boreholes, some of which were cored, were used for in situ permeability tests during drilling, were outfitted as permanent salinity-monitoring systems, and were used for calibration of electrical-resistivity surveys. The salinity-monitoring systems (Fig. 31-6) consist of several hydraulically isolated tubes that terminate at different depths. The lower end of the tubes are separated from each other by bentonite layers. The tubes allow water samples to be pumped to the surface and tested. Monitoring is being continued with sampling at 3-mo intervals.

Distribution of hydraulic conductivity

Hydraulic conductivity was mapped from the same type of in situ falling-head and constant-head permeability tests like those at Tarawa and Christmas Island, Kiribati

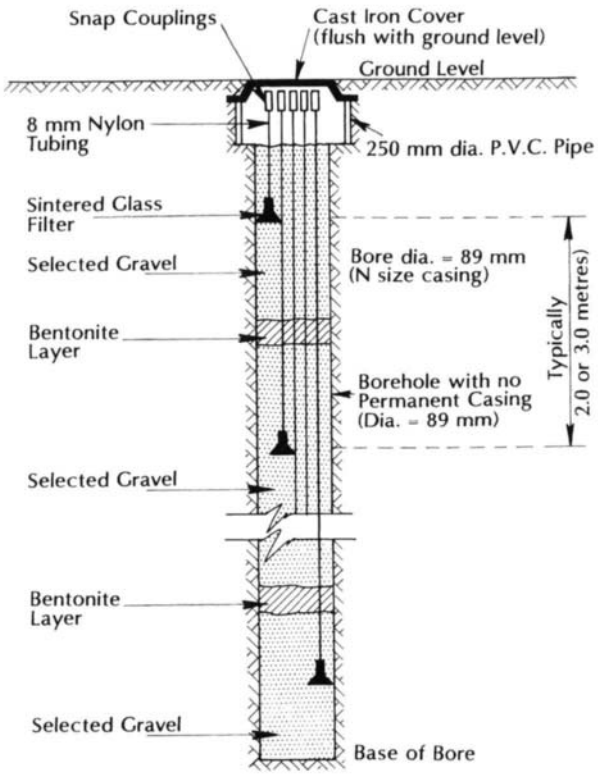


Fig. 31-6. Borehole salinity-monitoring system.

(Table 19.1; Figs. 19.6, 19.7). In all, about 550 tests were done on Cocos. These were at 1.5- to 3-m intervals at ten sites on West Island and eight sites on Home Island. Generally, eight falling-head tests and one constant-head test were conducted at each test zone, which was 0.8 m in length. Hydraulic conductivities were calculated using methods outlined in Cedergren (1977).

The results from the in situ tests, which were generally consistent with each other, indicate a hydraulic conductivity for the Holocene sediments of 3–12 m day^{-1} and a sharp increase in permeability below the unconformity. Typical results for the Pleistocene limestone are 30–500 m day^{-1} with some values as high as 1,000 m day^{-1}. The largest values occur at depths of 15 and 18 m.

The results indicate that these islands are dual-aquifer systems like those at many other atolls (Buddemeier and Holladay, 1977; Underwood et al., 1992) [Chap. 1]. The results also underscore the importance of the unconformity to the occurrence of fresh groundwater. The less-permeable sediments above the Thurber Discontinuity are favourable to the occurrence of freshwater lenses, in contrast to the lower, more-permeable Pleistocene sediments where mixing of freshwater and seawater is readily facilitated.

Distribution of fresh and brackish groundwater

A Cl^- concentration of 600 mg L^{-1} has been adopted as the upper limit, in terms of salinity, for potable water on Cocos (WHO, 1971). The equivalent electrical conductivity value (at 25°C) is approximately 2,500 μmhos cm^{-1} (Falkland, 1994b). Although more stringent guidelines (250 and 400 mg L^{-1}, based on taste considerations) are now recommended (WHO, 1984, 1993; NHMRC/ARMCANZ, 1994), the value of 600 mg L^{-1} was used to delineate the freshwater lenses because the available groundwater resource that could be developed at reasonable cost is limited and because rainwater catchments are available as a supplementary source of low-salinity, potable water. In ten years of monitoring of the Cocos water supplies pumped from the freshwater lenses, the 600-mg L^{-1} limit for Cl^- has not been reached; only rarely has 400 mg L^{-1} been exceeded.

The results of the exploration program indicate that significant permanent freshwater lenses are located on West, Home and South Islands (Fig. 31-2; Table 31-1). Approximate areas, maximum freshwater thicknesses, and the range of volumes during the period of record are included in Table 31-1. The areas and volumes vary with time according to antecedent recharge conditions. In addition, a small but largely unexplored lens is known to exist on Horsburgh Island (Jacobson, 1976a; Falkland, 1994a), and a very thin freshwater lens is present on North Keeling (Falkland, 1994a). Brackish groundwater is found on most of the islands between the lateral extent of freshwater lenses and the edges of the islands.

The cross-sectional shape of the major freshwater lenses on Cocos varies between locations. On Home Island, the freshwater occurs preferentially closer to the lagoon. At the West Island Airfield Lens (Fig. 31-2), there is no apparent asymmetry from the ocean side to the lagoon side, while in the Northern Lens, the freshwater is deepest towards the ocean side. According to the in situ permeability tests, however,

Table 31-1

Selected characteristics of freshwater lenses

Lens	Area (ha)	Maximum thickness (m)	Volume ($m^3 \times 1000$)	Turnover time (yrs)	Sustainable yield ($m^3\ day^{-1}$)
West Is Airfield	100	15	3000–3500	3	520
West Is Northern	115	14	1500–2700	4.5	300
Home Is	23	8	70–350	1	115
South Is (3)	72	11	1500	2–4	220

hydraulic conductivity is fairly uniform across the island at given depths. Across-island variation in hydraulic conductivity, therefore, does not appear to explain the asymmetry of the freshwater lenses in Cocos.

The freshwater lenses on Cocos generally become thicker as the island width increases. Because of the buried, more-permeable Pleistocene limestone, however, there tends to be an upper limit of about 15 m for the thickness of the freshwater zone. In areas where island width and antecedent recharge would appear to favour a thicker freshwater lens, the base of the freshwater zone has been found to occur at or near the unconformity.

The smallest known island width where a freshwater column is present on Cocos is 270 m at WI22 on West Island (Fig. 31-2). Since monitoring began at this borehole in August 1992, the freshwater zone has remained about 7 m thick, with its base just above the unconformity. The thickness from the water table to the midline of the transition zone has varied between 10 and 12 m during the same period. This thickness is considerably larger than the value of 5 m that is calculated for this location from an approximate empirical relationship between lens thickness, annual rainfall and island width that Oberdorfer and Buddemeier (1988) derived from a number of coral islands. The discrepancy indicates that under very favourable conditions, a freshwater lens may be supported on atoll islands where the island width is less than 300 m.

Recharge

Recharge to the freshwater lenses on Cocos was computed using a water balance like that discussed in more detail in Falkland (1991) and illustrated for Tarawa in Case Study 2 of Chapter 19 of this book.

Potential evapotranspiration (PET). Estimates of PET were made from measured pan evaporation data using a pan coefficient of 0.8. These estimates were compared with estimates using the Penman equation and relevant available meteorological data (dry and wet bulb temperature, dew point temperature, cloud cover and wind speed). The two estimation methods, using data for the period 1982–1986, gave similar results: the mean annual PET estimates for the 5-year period are 1,983 mm and 2,048 mm for pan and Penman methods, respectively. The monthly distribution

of PET is also very similar. Because PET in tropical regions does not vary much on a daily basis, it was found (Falkland, 1993a) that mean daily PET estimates derived from monthly estimates could be used instead of actual daily PET estimates for daily water-balance analyses without loss of accuracy.

Water-balance calculation. Recharge was calculated for a 41-year period, 1953–1993, for West, Home and South Islands (Falkland, 1994b) using the water-balance procedure. The calculations used a daily balance with measured daily rainfall for this period and daily PET estimated from monthly average pan-evaporation data for a 10-year period, 1982–1991. The soil-moisture-zone thickness (SMZ), field capacity (FC), and wilting point (WP) were estimated at 500 mm, 0.15, and 0.05, respectively. A linear relationship between evaporative losses and soil moisture was assumed between FC and WP. Crop factors (Doorenbos and Pruitt, 1977) were estimated to be 1.0 for grasses and other shallow-rooted vegetation, and 0.8 for deep-rooted vegetation, predominantly coconut trees. The percentage of the areas of freshwater lenses that are covered by deep-rooted vegetation were estimated from colored aerial photographs and ground inspection to be 0.15 for the Home Island Lens, zero for the West Island Airfield Lens, and 0.8 for the West Island Northern Lens and for the lenses on South Island (Falkland, 1994b).

The results of the water balance are that rates of mean annual recharge over the 41-year period of record are: 950 mm y^{-1} (49% of rainfall) for the West Island Airfield Lens; 850 mm y^{-1} (44% of rainfall) for the Home Island Lens; and 560 mm y^{-1} (29% of rainfall) for the West Island Northern Lens and the South Island lenses. The time series of monthly values is illustrated by the example (Northern Lens) shown in Fig. 31-7. There is significant year-to-year variation. In some years (1953, 1962, 1977 and 1991), recharge is negative, indicating there is a net loss of water from

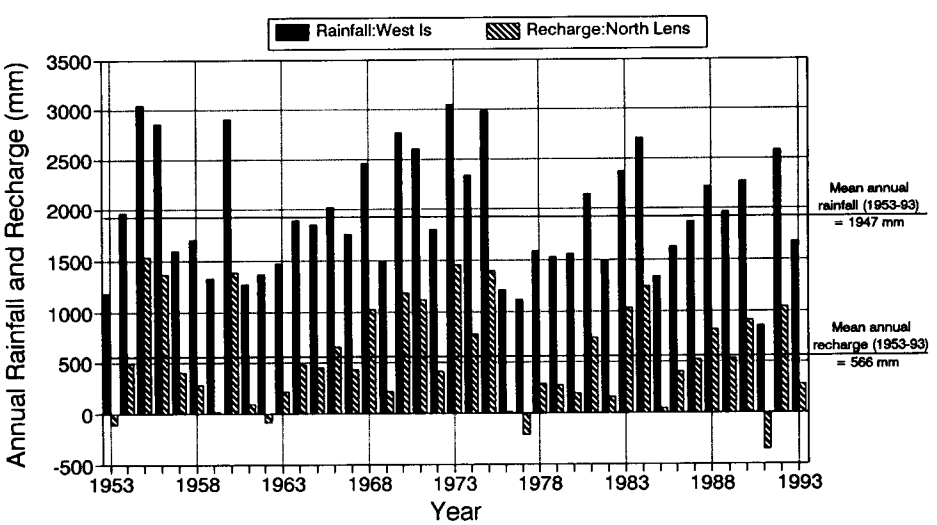


Fig. 31-7. Annual rainfall and recharge, Northern Lens, 1953–1993.

the freshwater lens because of the deep-rooted coconut trees. The largest negative recharge was in 1991, when there was the lowest annual rainfall. In general, years of high annual rainfall correspond to years of high annual recharge and vice versa. There is no simple relationship, however, between the two parameters, because annual recharge reflects the pattern of daily rainfall, not simply the annual total.

Effect of coconut trees. Cocos nucifera, which is prolific on most atolls including Cocos, can cause significant transpiration loss from freshwater lenses. Over a one-week period in 1987, transpiration from coconut trees on Cocos was measured with a heat-pulse velocity meter. The results, while considered preliminary owing to a number of simplifying assumptions and the short period of observations, suggest transpiration rates per tree of 70–130 L day^{-1} (Falkland, 1993a, 1993b). Higher transpiration rates are considered quite possible. Assuming 150 coconut trees per hectare (i.e., tree spacing of about 8 m), the measured transpiration rates are equivalent to about 400–700 mm y^{-1}. This estimate compares favourably with results for average transpiration losses from the water-balance calculations: 560 mm y^{-1} and 510 mm y^{-1} for a tree cover of 80% and 100%, respectively, over the 41-year calculation period.

The water-balance calculation indicates nearly a two-fold between-lens variation for mean annual recharge. This large difference reflects differences in the density of coconut trees (Fig. 31-8). As shown in Fig. 31-8, recharge is nearly doubled by reducing the tree cover from 80% (as for the West Island Northern Lens and South Island lenses) to zero (as for the West Island Airfield Lens). In areas where freshwater lenses need to be used for groundwater development, it may be prudent to selectively clear coconut trees to maximise the supply of water.

Dynamics of the lenses

Data obtained from salinity-monitoring boreholes enable variations in the thickness of the freshwater column to be compared with variations in recharge as

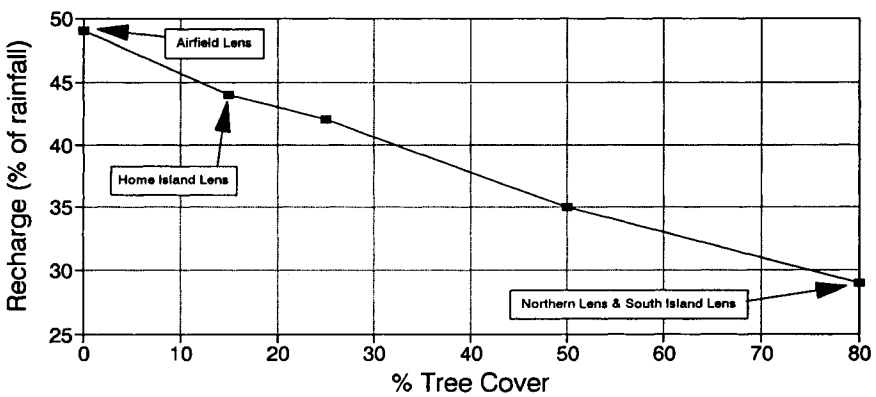


Fig. 31-8. Effect of tree vegetation on mean annual recharge.

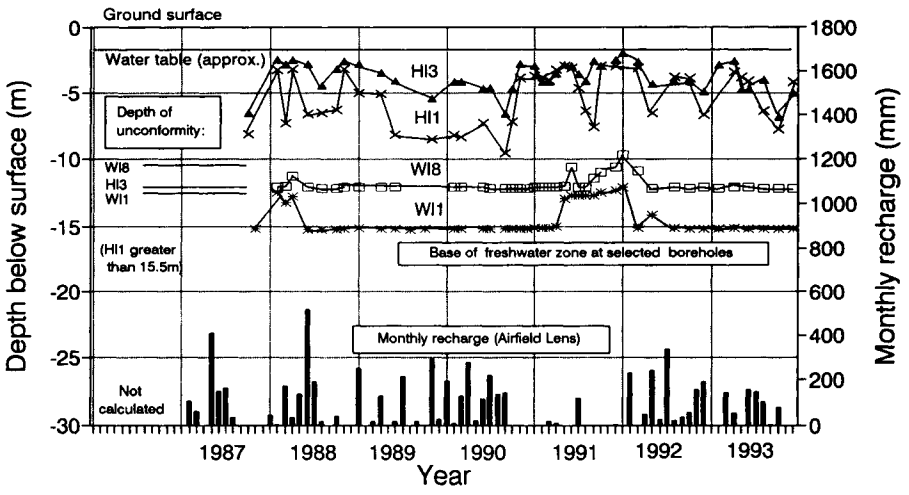


Fig. 31-9. Recharge and the response of the freshwater lens at the West Island Airfield Lens (boreholes WI1, WI8) and Home Island Lens (boreholes HI1 and HI3) for the period 1987–1993.

calculated by the water-balance procedure. Fig. 31-9 shows the comparison for 1987–1993. There are large changes in response to recharge variations for the two Home Island boreholes but much smaller fluctuations for the two boreholes in the West Island Airfield Lens. At the two West Island boreholes, the unconformity tends to act as a lower boundary to the formation of the freshwater zone. On Home Island, the freshwater zone is well within the Holocene sediments at all monitoring boreholes including the two shown in Fig. 31-9. The effect of the dry periods on the thickness of the freshwater zone can be seen at all boreholes in late 1987, late 1990, and for most of 1991.

Turnover times are a measure of the average residence time of water within the freshwater zone and are calculated by dividing the average thickness of the freshwater zone by the mean annual recharge. For the four main lenses in Cocos, turnover times are in the range of 1–5 years (Table 31-1).

The sustainable yields of the freshwater lenses are also related to recharge. On Cocos (Table 31-1), the assumption is made that, in general, 20% of the mean annual recharge can be extracted without thinning the lens to the extent that there are long-term, adverse effects. Home Island lens is considered to be "fragile", and a lesser value (17%) equivalent to the current average pumping rate of 115 m^3 day^{-1} is adopted at least until more extensive salinity-monitoring records are obtained and analysed. From detailed modeling studies of other atoll islands (Griggs and Peterson, 1993 [see also Chap. 20 of this book], it appears that these percentages are likely conservative. Future monitoring results, and possibly modeling studies, may indicate that larger pumping rates, indeed, are sustainable.

GROUNDWATER DEVELOPMENT

Infiltration galleries (or "skimming wells") have been used for groundwater development on Cocos. They are considered preferable to dug wells or boreholes because they skim water from the surface of the lens and minimize drawdown. These types of systems have recently been installed on Home Island and in the West Island Northern Lens. In some cases, they have replaced earlier dug well systems with short radial pipes extending from the base of the wells.

Infiltration galleries consist of a system of horizontal permeable conduits that are laid below the water table at or close to mean sea level and enable water to be easily drawn towards a central pump pit. Fig. 31-10 shows the type of infiltration gallery used on Home Island (Falkland, 1993a, 1994b), where there are six 300-m galleries each pumping continuously at an average of slightly less than 20 m^3 day^{-1}. Salinity data collected from the pumped wells before and after gallery installation show a reduction in the salinity of the pumped water. As part of regular monitoring, salinity is tested in the pumped wells and at special monitoring points along the gallery pipes.

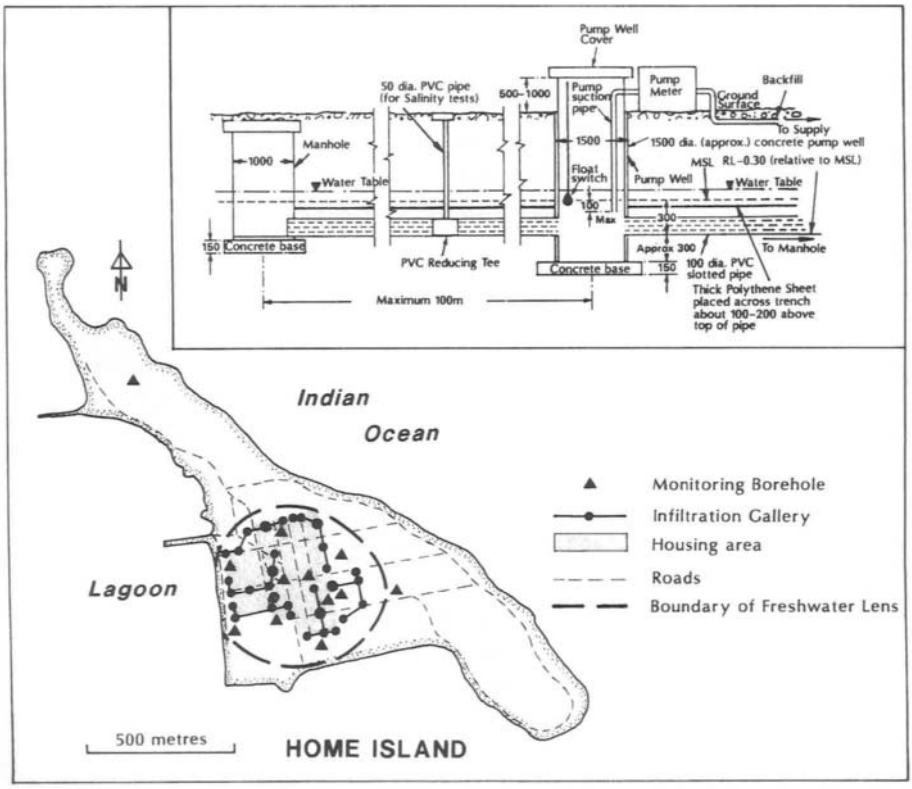


Fig. 31-10. Layout of Home Island infiltration galleries and cross section through a typical infiltration gallery.

The current water usage is approximately 100% of estimated sustainable yield at the Home Island Lens, 27% at the West Island Airfield Lens, and zero at the South Island lenses. At the West Island Northern Lens, the usage is 50% of estimated sustainable yield under current vegetated conditions but only 30% if the vegetation is extensively cleared (Falkland, 1994b). There is ample capacity, therefore, for expansion of current water usage at the Airfield Lens, but no or very limited spare capacity on Home Island. The Northern Lens can accommodate some additional use, particularly if some of the thick vegetation were cleared. South Island remains at present an untapped resource.

CASE STUDY: DEVELOPMENT OF SURFACE MORPHOLOGY OF COCOS ATOLL

The concept that the long-term development of mid-ocean coral atolls is driven by gradual subsidence of a volcanic basement occurred to Darwin while he was in South America and before he had seen a coral atoll. He refined his ideas after visiting the Society Islands, where he passed close to atolls but did not land on them. He had written the first draft of his theory before reaching New Zealand (see Stoddart, 1962), and, when he reached Cocos, he was especially keen to find evidence in support of his theory. He left considering that erosion of the shoreline on West Island was "moderately conclusive evidence" of his theory, and in his book on coral reefs (Darwin, 1842), he illustrated his argument with examples from Cocos (see Armstrong, 1991). Subsequently, the gradual subsidence of atoll foundations was shown by deep drilling in the Pacific, initially on Funafuti where drilling revealed over 300 m of shallow-water carbonates without encountering basement, and subsequently in Enewetak, Bikini, Midway and Mururoa where basalts were encountered beneath Tertiary carbonates (Braithwaite, 1982). But it is also becoming clear that the factors which control atoll structure, and those which determine the surface morphology of atolls are different (Stoddart, 1973). In this Case Study, the role of sea-level history on the shaping of the surface of Cocos is discussed.

Three distinct phases of development during the Holocene can be identified (Fig. 31-5). The first is a phase of vertical reef growth as reefs accreted in an effort to catch up with a rapidly rising sea level. The second phase (approximately 5000–3500 y B.P.) is one of reef-flat development, represented by the conglomerate platform, which appears to have formed at a sea level slightly higher than present (Fig. 31-11A). The third phase is one of reef-island formation and lagoon infilling.

Radiocarbon dates on individual clasts within the conglomerate platform are shown in Fig. 31-3 and indicate that the boulders composing the platform generally fall into a narrow age range of 3000–4000 y B.P. The platform resembles modern reef flats in terms of constituent materials, gross fabric and surface morphology (Woodroffe et al., 1990a, 1990b). In particular, fossil microatolls of both massive and branching species of *Porites* (Fig. 31-11B) occur above the modern upper limit of coral growth. These microatolls corroborate the interpretation that the platform was deposited as reef flat (Woodroffe et al., 1994), which has probably been lithified as sea level has fallen 50–80 cm relative to Cocos.

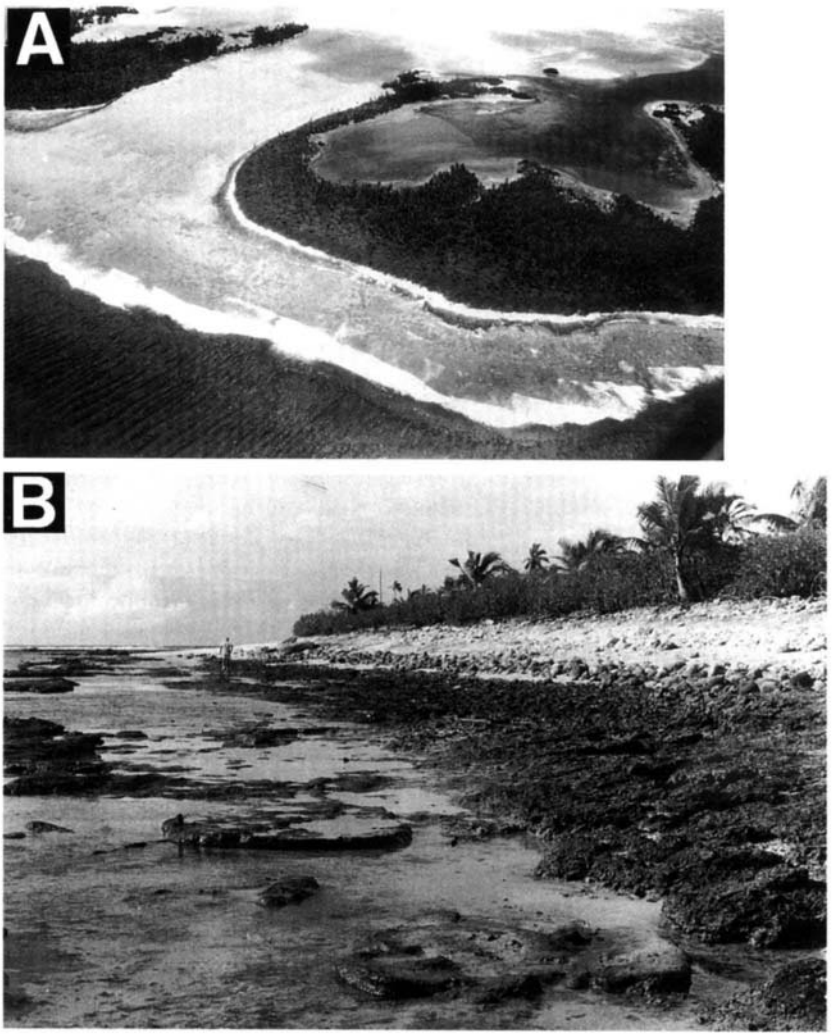


Fig. 31-11. (A) Reef islands on eastern rim of Cocos (Pulu Pandan in foreground). The conglomerate platform can be seen underlying each of the reef islands and cropping out on the oceanward side. (B) Evidence for Holocene highstand of sea level. The large corals in the foreground are microatolls, and they are presently found above their modern counterparts. They are overlain by conglomerate platform. There is also beachrock which appears elevated in the background.

Sedimentation in the lagoon has also been rapid during mid- and late Holocene times and appears to have been rapid also in historical times. Guppy (1889) estimated an input of sediment into the lagoon of 5,000 tons y^{-1}; the estimate was calculated from the area of live coral cover and preliminary filtering of sand carried in suspension toward the lagoon through the interisland channels. Wood-Jones (1912) considered that the accumulation of sediment in the lagoon acted to decrease

coral growth in the lagoon and was fundamental to generating and maintaining the overall atoll morphology. A series of vibrocores in the sand sheets at the southern and eastern margins of the lagoon (Fig. 31-3) indicates significant textural changes with depth and suggest that the sand has prograded into the lagoon and infilled blue holes. Cores contain numerous layers of coral shingle. Radiocarbon dating indicates that much of the sand in the upper 4 m has accumulated in the last 4,000 years (Smithers et al., 1994). It is inferred that, prior to that time, coral growth was more abundant in a more open lagoonal environment. The formation of reef islands in the last 3,000 years appears to have restricted flows and formed quieter-water environments in their lee. Vertical accumulation rates appear higher in sand aprons associated with interisland channels where they are 0.5–1.0 mm y^{-1} based on radiocarbon dating, compared with 0.25–0.5 mm y^{-1} over the last 2,000 years in the lee of reef islands (Smithers et al., 1994).

The surface morphology of atolls reflects the overall structure but is a response to controls on sediment production and deposition over the last few millennia. Thus on Cocos it appears that the overall structure is a result of gradual subsidence of a volcanic basement, but that the surface morphology of the atoll is determined by the pattern of sea-level change over the last few thousand years and resulting pathways of sediment movement. Although the atoll foundations may be subsiding — and the depth to Last Interglacial limestones suggests subsidence (Woodroffe et al., 1991, 1994; Searle, 1994) — the conglomerate platform results from a slight recent emergence of the atoll. This emergence probably resulted from subtle hydro-isostatic adjustments of the ocean floor to postglacial ice melt (Clark et al., 1978; Nakada, 1986; Peltier, 1988).

Significant late Quaternary changes in the atoll's environment can be inferred from the stratigraphic and geochronologic studies. The history is summarised in Fig. 31-12. During the Last Interglacial, around 120 ka (1 in Fig. 31-12), the sea appears to have been at the present level, or perhaps up to 6 m higher than present (Lambeck and Nakada, 1992); at that time, an atoll much like the present one is likely to have existed at Cocos. The sea remained high for around 12,000 y; therefore, it seems likely that much of the lagoon would have filled as has occurred in the Holocene. When the sea fell through a series of progressively lower oscillations, the reef and lagoon sediments deposited during the Last Interglacial highstand would have been cemented and subjected to dissolution by karst processes. Solutional unconformities within the limestones of atolls indicate repeated subaerial exposure as a result of sea level fluctuations (Schlanger, 1963). Also, at the peak of the glaciation around 18,000 y B.P. (2 in Fig. 31-12), the island would have been exposed as a karstified plateau. Since then, the sea has risen rapidly and the atoll morphology has evolved in three distinct phases during the Holocene (Fig. 31-5). First, 7000–5000 y B.P. (3 in Fig. 31-12), there was a phase of rapid vertical reef growth as reefs tried to catch up with sea level. This was followed by a phase of reef-flat development, 5000–3500 y B.P. (4 in Fig. 31-12). Reefs caught up with sea level during this phase and reef flats were formed; presently they are exposed as a conglomerate platform through a subsequent fall in sea level. The final phase, since 3500 y B.P. (5 in Fig. 31-12), has seen the formation of reef islands on the atoll rim and the infill of

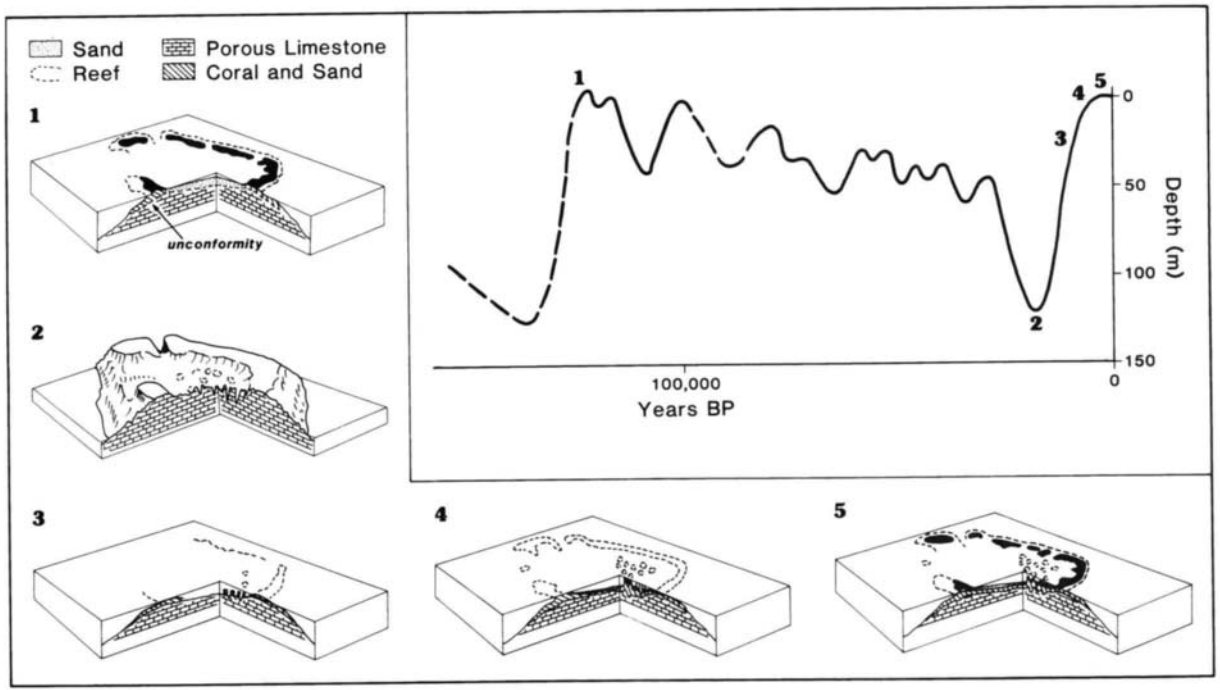


Fig. 31-12. Five phases of reef development over an interglacial-glacial-interglacial cycle (McLean and Woodroffe, 1994) keyed to the sea-level curve for the last 150,000 years (Chappell and Shackleton, 1986): 1, Last Interglacial, when an atoll much like the present one existed. 2, Glacial maximum, when sea level was some 120 m below present and the island was undergoing rapid subaerial karst erosion. 3, Postglacial sea-level rise, drowning the interglacial limestone plateau, which had continued to subside; corals were re-established, and reefs built upward. 4, Mid-Holocene highstand, when reefs caught up with sea level. 5, Development of the modern atoll during the Late Holocene when there was a slight sea-level fall, development of reef islands, and sedimentation in the lagoon. (After McLean and Woodroffe, 1994.)

the southern lagoon with sand being deposited over earlier reefal areas. The islands appear to have accreted incrementally over the last 3000 years. This pattern of surface morphology development is presumed to have recurred, with minor modifications, over previous interglacial-glacial-interglacial cycles, forming a sequence which is punctuated by solutional unconformities in deep boreholes on other atolls.

CONCLUDING REMARKS

Drilling on several of the reef islands of the Cocos (Keeling) Islands has revealed that Holocene reefal limestones are underlain by Pleistocene limestones at depths of 8–13 m below sea level. Uranium-series dating indicates that the upper part of the Pleistocene limestone was deposited during the Last Interglacial. The solutional unconformity between Pleistocene and Holocene limestones can be traced on continuous seismic-reflection profiles dipping into the lagoon to depths of up to 24 m below sea level — topography which may reflect karstification during the last glaciation.

The Cocos (Keeling) Islands were central to Darwin's theory of coral-reef development in which he hypothesised that atolls developed through gradual subsidence combined with vertical reef growth. The depth to the unconformity, as on other atolls in the Pacific, supports the notion that atoll structure results from gradual subsidence. The surface morphology of the atoll, on the other hand, is a response to Holocene patterns of reef growth and sediment redistribution, and indicates recent emergence of the atoll. The first phase of the Holocene development of the atoll began with reef establishment on the Pleistocene surface around 7000 y B.P. and consisted of rapid vertical reef growth lagging slightly behind sea level. Reefs appear to have been 2–3 m below sea level at 6000 y B.P. when the sea reached a level close to the present. The second phase, approximately 5000–3500 y B.P. was one of reef-flat development at a sea level 0.5–0.8 m above present, and is recorded by a conglomerate platform, widespread on reef islands, comprising coral clasts and in situ microatolls. The third phase of Holocene development since 3500 y B.P. was one of gradual reef-island formation and lagoonal infilling.

The study of the hydrogeology of the Cocos (Keeling) Islands has been well served by a network of strategically placed multi-level salinity-monitoring boreholes. These have enabled a detailed study of the dynamics of the freshwater lenses on West Island, where the lenses are relatively thick and "robust", and on Home Island where the lens is very thin and relatively "fragile". The data obtained over an 8-year period since the first holes were drilled has become a useful water-resources monitoring tool. Combined with an ongoing monitoring program of salinity in the infiltration galleries, the vertical salinity-profile data, obtained at 3-mo intervals has enabled decisions about pumping rates to made in the light of real data.

On Home Island, the network of infiltration galleries installed in recent years, has shown itself to be a most appropriate method of extracting groundwater from thin freshwater lenses (maximum of about 6 m thick and often less than 3 m thick). The galleries, each consisting of 300-m-long slotted-pipe systems laid horizontally below

the water table, enable water to be skimmed from the surface of a large part of the freshwater lens. Prior to the galleries, the salinity of the water in the original pumping wells, which had only very short lateral pipes, was considerably greater than that now obtained from the infiltration galleries. Fine-tuning of the gallery system is now being conducted where galleries close to the edge of the lens are being downrated (pumping rates are decreased) and additional galleries are being considered in those parts of the lens known to be more robust.

Water-balance studies on the island using measured rainfall and estimates of evapotranspiration are most useful at estimating recharge to the groundwater. Estimates of recharge are consistent with observed data from direct measurements of coconut-tree transpiration and freshwater-lens dynamics. Such water-balance studies are an effective method of highlighting critical periods for the management of groundwater resources.

ACKNOWLEDGMENTS

Hydrological data collection and analysis of results has been funded by the Australian Government. Drilling of the salinity-monitoring boreholes was conducted by Peter Murphy and Bryan Turner. The field collection of data is being regularly undertaken by personnel from Asset Services, Department of Administrative Services. Ongoing processing and analysis of data are conducted by staff of the Hydrology Branch, particularly Helen Jobson and Kath Hunt, of ACT Electricity and Water. Their inputs and efforts are gratefully acknowledged.

REFERENCES

Armstrong, P., 1991. Under the blue vault of heaven: a study of Charles Darwin's sojourn in the Cocos (Keeling) Islands. Indian Ocean Centre for Peace Studies, Univ. Western Australia, Perth, 120 pp.

Braithwaite, C.J.R., 1982. Progress in understanding reef structure. Prog. Phys. Geogr., 6, 505–523.

Buddemeier, R.W. and Holladay, G., 1977. Atoll hydrology: island groundwater characteristics and their relationship to diagenesis. Proc. Third Int. Coral Reef Symp. (Miami), 2: 167–173.

Buddemeier, R.W., Smith, S.V. and Kinzie, R.A., 1975. Holocene windward reef-flat history, Enewetak Atoll. Geol. Soc. Am. Bull., 86: 1581–1584.

Cedergren H.R., 1977. Seepage, Drainage and Flow Nets. 2nd. ed., Wiley Interscience, New York, 534 pp.

Chappell, J. and Shackleton, N.J., 1986. Oxygen isotopes and sea level. Nature, 324: 137–140.

Clark, J.A., Farrell, W.E. and Peltier, W.R., 1978. Global change in postglacial sea level: a numerical calculation. Quat. Res., 9: 265–287.

Colin, P., 1977. Reefs of the Cocos-Keeling atoll, eastern Indian Ocean. Proc. Third Int. Coral Reef Symp. (Miami), 1: 63–68.

Darwin, C., 1842. The Structure and Distribution of Coral Reefs. Smith, Elder and Co., London.

Doorenbos, J. and Pruitt, W.O., 1977. Crop water requirements. FAO Irrigation and Drainage Paper 24 (revised). FAO (U.N.), Rome, 144 pp.

Emery, K.O., Tracey, J.I. and Ladd, H.S., 1954. Geology of Bikini and nearby atolls. U.S. Geol. Surv. Prof. Pap. 260-A, 265 pp.

Falkland, A.C. (Editor), 1991. Hydrology and Water Resources of Small Islands: A Practical Guide. Studies and Reports in Hydrology 49, UNESCO, Paris, 435 pp.

Falkland, A.C., 1993a. Water resources assessment, development and management of small coral islands. Proc. Regional Workshop on Small Island Hydrology, Batam Is, Indonesia, UNESCO-ROSTSEA.

Falkland, A.C., 1993b. Review of hydrology and water resources of humid tropical islands. In: M. Bonell, M.M. Hufschmidt and J.S. Gladwell (Editors), Hydrology and Water Management in the Humid Tropics., Cambridge University Press and UNESCO.

Falkland, A.C., 1994a. Climate, hydrology and water resources of the Cocos (Keeling) Islands. Atoll Res. Bull., 400: 1–52.

Falkland, A.C., 1994b. Management of freshwater lenses on small coral islands. Proc. Water Down Under '94 Conf. (Adelaide), 1: 417–422.

Fitzroy, R., 1839. Narrative of the Surveying Voyages of His Majesty's Ships Adventure and Beagle, Between the Years 1826 and 1836, Describing their Examination of the Southern Shores of South America, and the Beagle's Circumnavigation of the Globe. Henry Colburn, London.

Forbes, H.O., 1885. A Naturalist's Wanderings in the Eastern Archipelago. A Narrative of Travel and Exploration from 1878 to 1883. Sampson Row, London.

Geyh, M.A., Kudrass, H.R. and Streif, H., 1979. Sea-level changes during the late Pleistocene and Holocene in the Strait of Malacca. Nature, 278: 441–443.

Griggs, J.E. and Peterson, F.L., 1993. Ground-water flow dynamics and development strategies at the atoll scale. Ground Water, 31(2): 209–220.

Guppy, H.B., 1889. The Cocos-Keeling Islands. Scott. Geogr. Mag., 5: 281–297, 457–474, 569–588.

Jacobson, G., 1976a. The freshwater lens on Home Island in the Cocos (Keeling) Islands. BMR J. Aust. Geol. Geophys., 1/4: 335–343.

Jacobson, G., 1976b. Preliminary investigation of groundwater resources, Cocos (Keeling) Islands, Indian Ocean, 1975. Bur. Miner. Resour. (Aust.), Record 1976/64, 23 pp.

Jongsma, D., 1976. A review of the geology and geophysics of the Cocos Islands and Cocos Rise. Bur. Miner. Resour. (Aust.), Record 1976/38.

Katupotha, J., 1988. Evidence of high sea level during the mid-Holocene on the southwest coast of Sri Lanka. Boreas, 17: 209–213.

Ladd, H.S., Tracey, J.I. Jr. and Lill, G.G., 1948. Drilling on Bikini Atoll, Marshall Islands. Science, 107: 51–55.

Ladd, H.S., Ingerson, E., Tonsend, R.G., Russell, M. and Stephenson, H.K., 1953. Drilling on Eniwetok Atoll, Marshall Islands. Am. Assoc. Petrol. Geol. Bull., 37: 2257–2280.

Lambeck, K. and Nakada, M., 1992. Constraints on the age and duration of the last interglacial period and on sea-level variations. Nature, 357, 125–128.

McLean, R.F. and Woodroffe, C.D., 1994. Coral atolls. In: R.W.G. Carter and C.D. Woodroffe (Editors), Coastal Evolution: Late Quaternary Shoreline Morphodynamics. Cambridge Univ. Press, Cambridge, pp. 267–302.

McLean, R.F., Stoddart, D.R., Hopley, D. and Polach, H. A., 1978. Sea level change in the Holocene on the northern Great Barrier Reef. Philos. Trans. R. Soc. London Ser. A, 291: 167–186.

Montaggioni, L.F. and Pirazzoli, P.A., 1984. The significance of exposed coral conglomerates from French Polynesia (Pacific Ocean) as indications of recent sea-level changes. Coral Reefs, 3: 29–42.

Nakada, M., 1986. Holocene sea levels in oceanic islands: implications for the rheological structure of the Earth's mantle. Tectonophys., 121, 263–276.

NHMRC/ARMCANZ, (National Health and Medical Research Council, and the Agriculture and Resource Management Council of Australia and New Zealand), 1994. Australian Drinking Water Guidelines. Draft.

Oberdorfer, J.A. and Buddemeier, R.W., 1988. Climate change, effects on reef island resources. Proc. Sixth Int. Coral Reef Symp. (Townsville), 3: 523–527.

Peltier, W.R., 1988. Lithospheric thickness, Antarctic deglaciation history, and ocean basin discretization effects in a global model of postglacial sea level change: a summary of some sources of nonuniqueness. Quat. Res., 29, 93–112.

Purdy, E.G., 1974a. Reef configurations, cause and effect. In: L.F. Laporte (Editor), Reefs in Time and Space. Soc. Econ. Paleontol. Mineral. Spec. Publ. 18: 9–76.

Purdy, E.G., 1974b. Karst-determined facies patterns in British Honduras: Holocene carbonate sedimentation model. Am. Assoc. Petrol. Geol. Bull., 58: 925–855.

Ross, J.C., 1855. Review of the theory of coral formations set forth by Ch. Darwin in his book entitled: Researches in Geology and Natural History. Natuurkd. Tijdschr. Ned. Indie, 8: 1–43.

Searle, D.E., 1994. Late Quaternary morphology of the Cocos (Keeling) Islands. Atoll Res. Bull., 401: 1–13.

Shepard, F.P., Curray, J.R., Newman, W.A., Bloom, A.L., Newell, N.D., Tracey, J.I. and Veeh, H.H., 1967. Holocene changes in sea level: evidence in Micronesia. Science, 157: 542–544.

Smithers, S.G., 1994. Sediment facies of the Cocos (Keeling) Islands. Atoll Res. Bull., 407: 1–34.

Smithers, S.G., Woodroffe, C.D., McLean, R.F. and Wallensky, E.P., 1994. Lagoonal sedimentation in the Cocos (Keeling) Islands, Indian Ocean. Proc. Seventh Int. Coral Reef Symp. (Guam), 1: 273–288.

Stoddart, D.R., 1962. Coral islands by Charles Darwin. Atoll Res. Bull., 88: 1–20.

Stoddart, D.R., 1971. Geomorphology of Diego Garcia Atoll. Atoll Res. Bull., 149: 7–26.

Stoddart, D.R., 1973. Coral reefs: the last two million years. Geography, 58: 313–323.

Thom, B.G. and Chappell, J., 1975. Holocene sea levels relative to Australia. Search, 6: 90–93.

Thom, B.G. and Roy, P., 1985. Relative sea levels and coastal sedimentation in southeast Australia in the Holocene. J. Sediment. Petrol., 55: 257–264.

Thurber, D.L., Broecker, W.S., Blanchard, R.L. and Potratz, H.A., 1965. Uranium–series ages of Pacific atoll coral. Science, 149, 55–58.

Tracey, J.I. and Ladd, H.S., 1974. Quaternary history of Eniwetok and Bikini atolls, Marshall Islands. Proc. Second Int. Coral Reef Symp. (Brisbane), 2: 537–550.

Underwood, M.R., Peterson, F.L. and Voss, C.I., 1992. Groundwater lens dynamics of atoll islands. Water Resour. Res., 28: 2889–2902.

WHO (World Health Organization), 1971. International standards for drinking-water, WHO (U.N.)., Geneva.

WHO (World Health Organization), 1984. Guidelines for drinking-water quality, WHO (U.N.), Geneva.

WHO (World Health Organization), 1993. Guidelines for drinking-water quality, WHO (U.N.), Geneva.

Williams, D.G., 1994. Marine habitats of the Cocos (Keeling) Islands. Atoll Res. Bull., 406.

Wood-Jones, F., 1912. Coral and Atolls: A history and Description of the Keeling-Cocos Islands, with an Account of Their Fauna and Flora, and a Discussion of the Method of Development and Transformation of Coral Structures in General. Lovell Reeve and Co., London, 392 pp.

Woodroffe, C.D. and McLean, R.F., 1994. Reef islands of the Cocos (Keeling) Islands. Atoll Res. Bull., 403: 1–36.

Woodroffe, C.D., McLean, R.F. and Wallensky, E., 1990. Darwin's coral atoll: geomorphology and recent development of the Cocos (Keeling) Islands, Indian Ocean. Natl. Geogr. Res., 6: 262–275.

Woodroffe, C.D., McLean, R.F., Polach, H.A. and Wallensky, E., 1990. Sea level and coral atolls: Late Holocene emergence in the Indian Ocean. Geology, 18: 62–66.

Woodroffe, C.D., Veeh, H.H., Falkland, A., McLean, R.F. and Wallensky, E., 1991. Last interglacial reef and subsidence of the Cocos (Keeling) Islands, Indian Ocean. Mar. Geol., 96: 137–143.

Woodroffe, C.D., McLean, R.F. and Wallensky, E., 1994. Geomorphology of the Cocos (Keeling) Islands. Atoll Res. Bull., 402: 1–33.

Geology and Hydrogeology of Carbonate Islands. Developments in Sedimentology 54
edited by H.L. Vacher and T. Quinn
© 1997 Elsevier Science B.V. All rights reserved.

Chapter 32

HYDROGEOLOGY OF DIEGO GARCIA

CHARLES D. HUNT

INTRODUCTION

Although Diego Garcia is one of the world's most remote sites, its strategic role as a British-U.S. naval facility has prompted intensive groundwater development and hydrogeologic study. Diego Garcia is particularly relevant to the study of island hydrology for several reasons: (1) effects of aquifer layering on groundwater salinity and tidal response can be described in detail; (2) groundwater withdrawal is unusually large for an atoll (3,300 m^3 day^{-1} of freshwater are pumped from more than 100 shallow wells); (3) the water supply has a 17-year operating history that shows distinct dry-season increases in salinity; and (4) the 44-year rainfall record contains interannual and even decadal periods of persistently wet and dry climate. Given that salinity has risen during brief (seasonal) rainfall deficits, the past occurrence of much more prolonged and severe deficits underscores the potential for droughts to disrupt water supplies on Diego Garcia and other small islands.

Geographic setting

Diego Garcia Atoll (7°20′S., 72°25′E.) is the southernmost and largest island of the Chagos Archipelago in the central Indian Ocean. The Chagos are part of a chain of atolls that extend northward through the Maldive and Laccadive Islands to India. Great Chagos Bank, a 13,500-km^2 plateau of mostly submerged reefs and shallows, lies 55 km to the north. The emergent land rim extends around the southern 90% of the atoll, with reef passes only at the north end (Fig. 32-1). Land width ranges from about 50 m to 2.2 km. Stoddart (1971a) listed areas of 170 km^2 for the entire atoll, 124 km^2 for the central lagoon, 47 km^2 for the peripheral reef and dryland rim, and 30 km^2 for the land itself. An additional 3 km^2 of land was added in 1983 by dredge-filling former lagoonal sand flats near the airstrip. Tides are semidiurnal, with a 0.7-m neap-tide range and a 1.6-m spring-tide range. Stoddart (1971b) discerned no lag or difference in tidal amplitude between a tide station just inside the lagoon entrance and a station 15 km inside the lagoon.

History of settlement and development

A history of early development has been given by Stoddart (1971c). The Chagos Archipelago was probably discovered by the Portuguese soon after their initial voyage through the area in 1498. Diego Garcia was uninhabited until 1786, when the

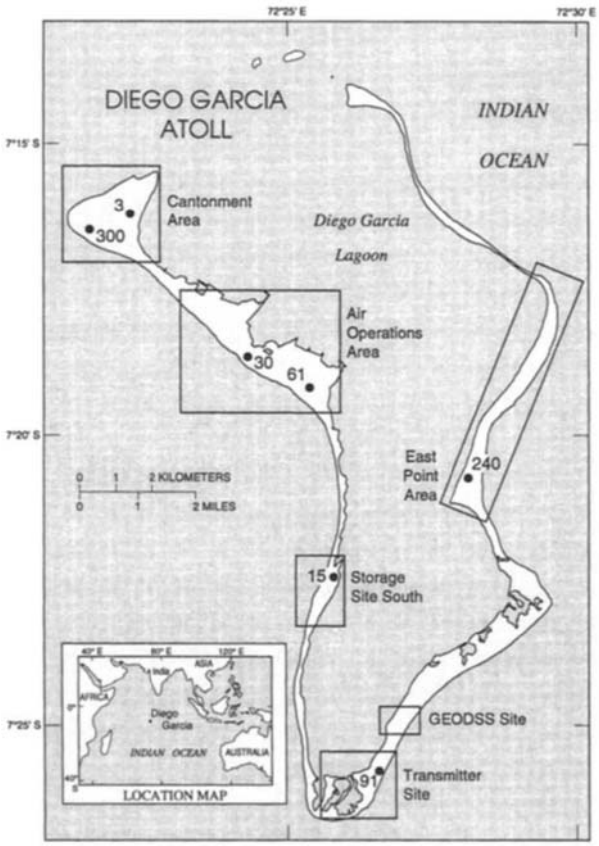


Fig. 32-1. Diego Garcia Atoll. Boxes enclose areas of present or potential groundwater development. Numeric values are estimates of hydraulic conductivity (in m day^{-1}) from pumping tests by PRC Toups (1983).

British attempted an initial settlement that lasted about 6 months. It was then settled by the French, who started the first of several coconut plantations in the late 1780s. The island was used for whaling in the mid-nineteenth century and as a coaling station for steamships in the latter part of that century. Diego Garcia has been under British control since 1810 and became part of the newly formed British Indian Ocean Territory in 1965. A year later, the United Kingdom and the United States agreed to make joint use of the Territory for defense. In 1971 the coconut plantations were closed, civilian residents were resettled in their countries of origin, and construction was begun on a naval support facility (Surface and Lau, 1988).

Facilities are concentrated on the western side of the atoll and include an airstrip, wharves, warehouses, and residential areas. Much of the east side of the island is maintained as a nature preserve. About 3,000 military personnel and civilians reside under westernized living conditions. Groundwater is developed in five areas

(Fig. 32-1): (1) Cantonment, (2) Air Operations, (3) Storage Site South (a former construction support site also known as Industrial Site South), (4) Transmitter Site, and (5) GEODSS Site (Ground-based Electro-Optical Deep Space Surveillance). Most of the island's water is supplied by wells at Cantonment and Air Operations (Figs. 32-2, 32-3).

Climatic setting

Climate is influenced by the equatorial, mid-ocean location of the island and by the monsoon circulations of southern Asia and Africa. Air temperature averages 27°C and its diurnal variation is slight (USNWSD, 1978). Southeast trade winds prevail from June through September, and calm or west winds occur from January through March; remaining months are transitional between the two regimes. Rainfall averages 2,700 mm y^{-1} (1951–94) and can be viewed as defining semiannual seasons: a wet season from September through February, when the intertropical convergence zone (ITCZ) is overhead or nearby; and a dry season from March through August, when the ITCZ is drawn northward by the summer monsoon of the Indian subcontinent. Rainfall is mainly from localized deep convection, with occasional contributions from passing tropical cyclones.

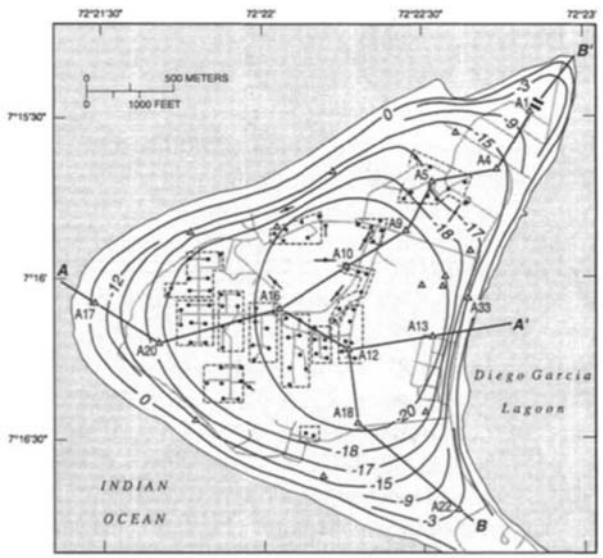


Fig. 32-2. Freshwater lens and wells at Cantonment. Contours show the base of freshwater in 1982, in m below sea level (modified from PRC Toups, 1983). Well symbols: •, vertical withdrawal well; —•—, horizontal withdrawal well; Δ, site of multi-depth monitoring wells, numbered if on line of section. Dashed lines outline wellfields (groups of several wells that are pumped simultaneously). A–A′ and B–B′ are lines of cross sections shown in Figures 32-4 and 32-6.

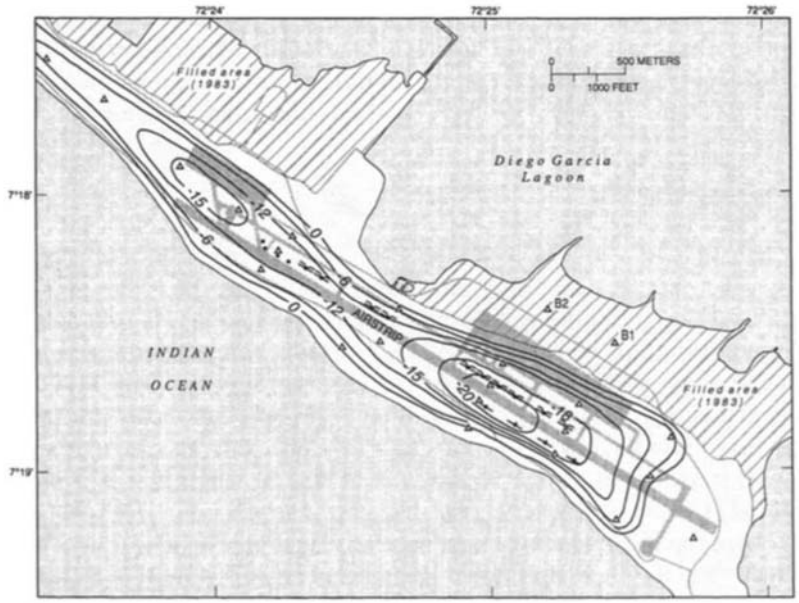


Fig. 32-3. Freshwater lens and wells at Air Operations. Contours show the base of freshwater in 1982, in m below sea level (modified from PRC Toups, 1983). Well symbols as in Fig. 32-2. Dotted line marks former shoreline and area filled by dredging in 1983; data from sites B1 and B2 indicate subsequent expansion of the freshwater lens beneath the former lagoon flats (see Fig. 32-5).

Geologic and tectonic setting

Diego Garcia is at the southern terminus of the Chagos-Maldive-Laccadive Ridge, a chain of submarine mountains that extends south from India on the Indo-Australian tectonic plate. As discussed in detail by Duncan (1990), results of the Ocean Drilling Program (ODP) have confirmed that the ridge was built by the mantle hotspot that is presently active at Reunion Island. According to Duncan (1990), the hotspot originated at about 66 Ma (the Cretaceous-Tertiary boundary) with rapid effusion of the voluminous Deccan flood basalts that cover much of western India. Geologic age decreases progressively to the south along the volcanic ridge, marking the apparent track of the Reunion hotspot given northward plate motion. The hotspot track continues on the African plate some 1,000 km southwest of Diego Garcia, through the eastern Mascarene Plateau, Mauritius, and Reunion. This ridge has been offset from the Chagos-Maldive-Laccadive Ridge by plate divergence at the Central Indian Ridge, a mid-ocean spreading ridge (Duncan, 1990).

All but the youngest volcanic products of the Reunion hotspot have subsided and are covered with thick caps of carbonate sediment. Basaltic basement rocks have been sampled at several sites along the hotspot track, and radiometric ages of the samples are in close agreement with age estimates derived from models of plate motion (Duncan, 1990). Basement has not been sampled at Diego Garcia, but the

modeled age for nearby southern Great Chagos Bank is 34 Ma (early Oligocene). Depth to basement also is unknown, but Simmons (1990) estimated 2.4 km of post-volcanic subsidence for a site on northern Great Chagos Bank, and seismic surveys near the Bank indicated basement beneath 1 km of water and 0.6–1.7 km of sediments (Francis and Shor, 1966). Away from the Chagos Ridge, the sea floor is about 4.5 km deep.

GEOLOGIC FRAMEWORK

Surficial geology, geomorphology, and ecology have long been studied at Diego Garcia (Stoddart and Taylor, 1971, contains early references). In contrast, the subsurface has been explored only recently, for foundation-engineering and water-resources investigations. A formal stratigraphy has yet to be established, but the geologic framework is known in fairly good detail as it relates to occurrence and flow of groundwater.

General geology and geomorphology

Depositional facies and surficial features at Diego Garcia are those common to most atolls: a seaward reef flat of coral-algal boundstone; lagoonal sediments and coral knolls; beach and washover sediments ranging in size from sand to boulders; and cemented sediments such as beachrock and cay sandstone (grainstone). Conglomerate and sandstone extend up to 3 m above sea level but contain no corals in growth position that would unequivocally confirm a Holocene relative highstand of the sea (Stoddart, 1971a). Some wide parts of the land rim have central depressions or swamps between higher ocean-side and lagoon-side beach ridges. Maximum lagoon depth is 31 m, and bathymetry defines three subbasins: a large northern basin with a general floor at 25–30 m, a central basin floored at 16–20 m, and a small southern basin with shallow, irregular topography (Stoddart, 1971a). Stoddart noted that the lagoon is unusually shallow compared with other atolls in the Chagos and Maldives, and that it lacks mangroves.

Lithologic units

A tentative stratigraphic framework for the Cantonment area is proposed here (Table 32-1, Fig. 32-4). It is based on drilling logs from the water-resources study of PRC Toups (1983), who presented a similar but slightly less detailed classification of units. Units 1–3 are mostly unconsolidated, are distinguished by grain size and composition, and likely are true depositional lithofacies. Units 4–6 are partly to wholly indurated, are distinguished more by diagenetic textures than by grain textures, and likely correspond to former diagenetic zones or to depositional facies with diagenetic overprint.

Age and facies relations are a matter of speculation given that there are no radiometric dates, mineralogic analyses, or petrographic analyses of diagenetic

Table 32-1

Lithologic units at Cantonment, in order of increasing depth

Unit[a]	Description[b] and Key Distinguishing Characteristics[c]
Holocene (?) Units:	
1	SAND, SAND WITH SILT–With minor gravel, a few coral fragments. • Key characteristics: sand as primary descriptor; paucity of coral fragments or gravel.
2	GRAVEL AND SAND, SAND AND CORAL FRAGMENTS– • Key characteristic: gravel or sand as primary descriptor.
3	CORAL FRAGMENTS–Branching and blocky fragments, with sand, gravel, shells (including whole *Turritella*), "platy shell fragments" (*Halimeda*?), "chips of cement" (*Halimeda*?). • Key characteristic: coral fragments as primary descriptor.
PLEISTOCENE-HOLOCENE UNCONFORMITY?	
Pleistocene (?) Units:	
4	CEMENTED SAND, CEMENTED CORAL FRAGMENTS–Locally or weakly cemented sandstone and conglomerate; hard drilling. • Key characteristics: shallowest occurrence of: recrystallization or near-pervasive cementation, shell molds, loss of drilling mud.
5	HARD OR SOLID CORAL, POROUS LIMESTONE–With shell molds and solution voids; typically recovered as sand- to gravel-size angular fragments (drill cuttings?); hard drilling. • Key characteristics: shallowest occurrence of hard coral or limestone descriptor.
6	HARD OR SOLID CORAL, POROUS LIMESTONE–Like Unit 5 but harder; very hard, rock-like, fine-grained; inertial oscillation of well water at 2 of 4 sites during bailer tests. • Key characteristics: very hard; inertial oscillations.

[a] The units are shown in cross section in Figures 32-4 and 32-6

[b] Descriptions are summarized from drilling logs at 8 sites by PRC Toups (1983). Drilling method was cable-tool percussion with the exception of one site (A12) where the method was mud-rotary.

[c] Key characteristics, unit assignments, ages, unconformity, and queries (*Halimeda*? drill cuttings?) are by the author. Units 1–3 are distinguished by grain size and composition (e.g., sand, gravel, coral fragments), whereas units 4–6 are distinguished mainly by diagenetic textures (e.g., cementation, moldic porosity) and hydraulic responses (inertial oscillation).

fabrics. I tentatively place the Pleistocene-Holocene unconformity at the top of unit 4 (average depth, −16.6 m), because moldic porosity and recrystallization were observed below this horizon but not above it. These textures are characteristic of meteoric diagenesis (Bathurst, 1975) and their absence suggests that units 1–3 have not undergone lengthy emergence — such as during a Pleistocene glacial lowstand of sea level — and, therefore, constitute a Holocene transgressive sequence. Unit 3 is a probable lagoonal facies (markers: mollusks, *Halimeda*?) deposited early in the transgression when the carbonate platform was inundated rapidly. Units 1 and 2 are probable beach or shoal-water overwash facies (marker: predominance of sand or gravel) that reflect shoaling and emergence of sandy islands as sediment accretion

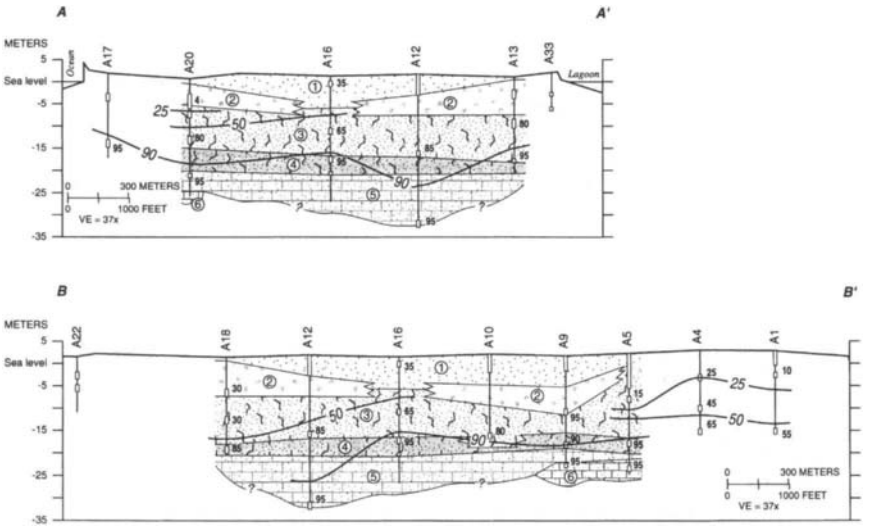


Fig. 32-4. Hydrogeologic sections A–A′ and B–B′, and aquifer tidal efficiency at Cantonment (based on data from PRC Toups, 1983). Lithologic units are identified by shading patterns and circled numbers: 1, sand and silt; 2, gravel and sand; 3, coral fragments and sand; 4, cemented sand and coral fragments; 5, hard limestone; 6, hard limestone. See Fig. 32-2 for locations of the cross sections and Table 32-1 for fuller descriptions of the units. Monitoring-well sites are labelled at land surface ("A5", etc.); vertical lines show maximum depths of exploratory drilling and slim rectangles show depth intervals of perforated wellscreens. Aquifer tidal efficiency (in percent) is shown by contours and by numeric values posted next to wellscreens. Note the strong dependence of tidal efficiency on depth, with maximum values (95%) in lithologic units 4–6.

outpaced the slowing rate of sea-level rise in the waning phase of the transgression. Only after islands emerged in the late Holocene could meteoric circulation have begun in units 1–3, thus explaining their minimal diagenesis. Similar facies and/or age relations have been described at other atoll islands (Emery et al., 1954; Goter, 1979; Marshall and Jacobson, 1984; Ayers and Vacher, 1986; Anthony et al., 1989) [see also Chapters 19, 20, 23 and 31].

Units 4–6 are depositional units or diagenetic zones of an unknown number of Pleistocene interglacial highstands. There may be unconformities and large age differences between the units, which could explain the pronounced contrast in induration between units 4 and 5. An alternative interpretation is that the units are a transgressive sequence of the last Pleistocene interglacial highstand — in essence late Pleistocene analogues of units 1–3. If true, then units 4–6 would differ little in age, and contrasts in their physical properties would reflect differences in composition of the parent sediments or in past diagenetic processes or rates. Modern cementation may serve as a plausible model in this regard. In the modern back-reef environment, cementation is greatest in the marine intertidal zone and near the water table within islands, forming shallow marine hardgrounds, beachrock, and cay sandstone mainly near sea level (Hanor, 1978; Wheeler and Aharon, 1991). By analogy, the contact between units 4 and 5 could mark an upward transition from marine hardground to

less-indurated supratidal sediments. Or, because diagenesis is more rapid in the phreatic zone than in the vadose zone (Land, 1970), the contact between units 4 and 5 could mark the paleo-water table of a former reef island, in which units 5 and 6 underwent pervasive phreatic recrystallization and unit 4 was weakly cemented in the coeval vadose zone. Regardless of their earlier history, if units 4–6 are Pleistocene then they were exposed to at least 100,000 years of vadose meteoric diagenesis during lowstands of the last Pleistocene glacial stage. This late diagenesis would have altered preexisting textures, but it does not readily explain the contrast in induration between units 4 and 5, the widespread extent and near-horizontal attitude of which imply a phreatic or depositional control. Alternative interpretations are certainly possible. Additional drilling and analysis of core samples are required if a definitive stratigraphy and geologic history are to be established at Diego Garcia.

HYDROGEOLOGY

Groundwater flow and salinity are influenced strongly by the depositional and diagenetic layering described above. Hydraulic conductivity of the aquifer has been estimated from pumping tests at only a few locations, but additional insight into aquifer properties can be gained from measurements of aquifer tidal response and salinity.

Distribution of hydraulic conductivity

Hydraulic properties of the unconsolidated sediments depend on grain size and sorting; those of the consolidated rocks depend on primary pore structure, cementation, dissolution, and fracturing. High permeability is to be expected in coarse-grained gravel and rubble, in cavernous reef limestone, and where dissolution has imparted extensive secondary porosity. Low permeability is to be expected in fine-grained or poorly sorted sediments, and where cementation has reduced porosity.

Hydraulic conductivity has been estimated from pumping tests at seven sites (PRC Toups, 1983). The estimates span two orders of magnitude, from 3 to 300 m day^{-1} (Fig. 32-1), and have a median value of 61 m day^{-1}. The minimum and maximum values are both at Cantonment and appear to reflect expected cross-island gradations in grain size and depositional energy: the high (seaward) value probably corresponds to coarse-grained rubble, and the low (lagoonward) value corresponds to finer-grained sand and silt. The estimates characterize unconsolidated units 1–3 because test wells extended no deeper than −8 m and were screened in these units. No direct tests of units 4–6 have been made.

Aquifer tidal response

Water levels in coastal wells commonly fluctuate with the ocean tide. The well response can be characterized by a tidal efficiency (well-to-ocean amplitude ratio)

and a tidal lag (delay of the tidal peak in the well from that in the ocean). On Diego Garcia, tidal response depends strongly on depth. At Cantonment, tidal efficiency is 4–35% near the water table and 95% at a depth of −20 m (Fig. 32-4). Tidal lag (not shown in Fig. 32-4) varies inversely with efficiency, decreasing with depth from about 3 hours to near zero. Several aspects of the tidal response are notable: (1) the tidal pressure signal is transmitted nearly 1 km inland in units 4–6 with almost no damping or lag; (2) damping is much greater over a vertical distance of only 15 m or so within units 1–3; and (3) the very high efficiency (95%) is itself unusual — values this high are not common in the literature, at least not at mid-island locations.

Similar depth-dependence of tidal response on other atolls has led to wide acceptance of a dual-aquifer model (Buddemeier and Holladay, 1977 [see Chap. 1]), in which high efficiency and short lag at depth are attributed to high hydraulic conductivity in Pleistocene sediments. Dissolution textures in cores provide some support for this view, but values of hydraulic conductivity from direct measurements range widely and lack conclusive depth trends (e.g., Oberdorfer and Buddemeier, 1986, although they point out that coring and testing methods may not detect large voids). Several numerical modeling studies have reproduced the depth-dependence of tidal response in atolls by assigning hydraulic conductivity to be 1–2 orders of magnitude greater in a deeper aquifer than in the surficial aquifer (Hogan, 1988; Oberdorfer, et al., 1990; Underwood, et al., 1992).

Although high hydraulic conductivity may indeed be a main cause of high tidal efficiency at Cantonment, the strong induration of units 5 and 6 offers a clue that poroelastic aquifer storage (Green and Wang, 1990) may also play a contributing role. Aquifer tides are governed, not solely by hydraulic *conductivity*, but by hydraulic *diffusivity*: the ratio of hydraulic conductivity to specific storage — or of transmissivity to storage coefficient as in the well-known, one-dimensional Ferris model (Ferris, 1951, 1963) that treats horizontally propagated signals in a single, horizontal layer. Although atoll aquifers are heterogeneous and more complex geometrically than the simple case treated by Ferris's analytical solution, the fundamental diffusive nature of aquifer tides requires at least some dependence on poroelastic storage. Because aquifer diffusivity is the ratio of a conductivity parameter to a storage parameter, a large value for the storage parameter is like a small value for the conductivity parameter — either one favors dampening of the tidal signal.

In the case of an atoll island, not only is the aquifer layered in terms of aquifer properties (including aquifer compressibility, which contributes to specific storage), but there is the added complication that the uppermost layer is unconfined, and so storage changes are also affected by the phenomenon of draining and refilling of pores at the water table. This phenomenon is represented by the specific yield, which is typically at least 1–2 orders of magnitude larger than the storage coefficient (specific storage times aquifer thickness) of the same material under confined conditions. Therefore, the storage changes affecting the transient behavior at a particular depth below the water table would be a combination of: (1) the effects of the local specific storage, and (2) a contribution from the specific yield of the water table, via vertical flow. The magnitude of the water-table contribution at depth would depend largely on the vertical hydraulic conductivity of the intervening material

between that point and the water table. For the case of the tidal phenomenon, a large vertical hydraulic conductivity would allow easy flow and a large water-table contribution, causing greater damping at depth than would be the case if the storage-related response there were solely elastic. In contrast, low vertical hydraulic conductivity will impede the water-table contribution, bringing the response at depth more in line with that from the specific storage alone.

Some of the results of the numerical modeling by Underwood (1990), I believe, illustrate the interplay of drained and poroelastic storage in an atoll setting. The modeled two-layer aquifer system was 1,000 m thick, with a 15-m-thick Holocene aquifer lying atop older limestones ("Pleistocene aquifer"). Porosity and aquifer compressibility were the same in both layers: 0.25 and 10^{-9} m^2 N^{-1}, respectively. Specific yield was set at 0.25 along the top row of grid cells corresponding to the water table. After using isotropic hydraulic conductivities of 50 and 500 m day^{-1} in the Holocene and Pleistocene aquifers, respectively, Underwood then introduced anisotropy into the Holocene aquifer by decreasing its vertical conductivity from 50 to 10 m day^{-1} (his simulations KHV4 and KPH3). The result was that tidal efficiency at the top of the Pleistocene aquifer (at −15 m) increased from 0.39 to 0.55, and the tidal efficiency at the water table decreased from 0.32 to 0.19; there was a steeper gradient of tidal efficiency with respect to depth in the second case, reflecting the greater dampening due to the lower vertical conductivity. The noteworthy point is that lower vertical hydraulic conductivity of the Holocene aquifer in the second case produced a higher efficiency in the Pleistocene aquifer; there were no changes made to the hydraulic parameters of the Pleistocene aquifer nor to the storage parameters of either aquifer. By decreasing vertical conductivity in the Holocene aquifer, Underwood (1990) attenuated the influence of specific yield at depth and confined the Pleistocene aquifer more strongly; this increased the tidal efficiency of the confined layer and, with respect to the tidal phenomenon, increased the apparent aquifer diffusivity (decreasing the apparent storage parameter).

In the case of Diego Garcia, there is an added effect: there is a contrast in specific storage between the two layers, not necessarily (or perhaps not) a contrast in hydraulic conductivity between the two layers. This differs from the conventional view of the dual-aquifer framework, which is modeled by Underwood (1990): a contrast in hydraulic conductivity and no contrast in specific storage. Regarding hydraulic conductivity of the Pleistocene(?) sediments at Cantonment, drilling logs are ambiguous: although dissolution textures are present in units 4–6, it is difficult to judge whether porosity and hydraulic conductivity are generally higher than in unaltered parent sediments (due to dissolution) or lower (due to cementation). But there is no question that units 5 and 6 are well consolidated and less compressible than their parent sediments. Published values of compressibility for consolidated limestone are more than two orders of magnitude lower than for unconsolidated dense, sandy gravel: $1.2–3.4 \times 10^{-11}$ vs. $5.2–10 \times 10^{-9}$ m^2 N^{-1} (Johnson, 1970; Domenico and Mifflin, 1965). This range in compressibility equates to possible contrasts in specific storage of 30:1 to 65:1 between the unconsolidated and consolidated units at Cantonment, assuming a porosity of 0.3 (Oberdorfer et al., 1990). It is plausible, then, that such contrasts in specific storage impart contrasts in hydraulic diffusivity that

affect tidal response, independent of contrasts in hydraulic conductivity that may or may not also be present.

Modeling is required to evaluate the relative importance of these various factors. For now, the preceding discussion suggests that the prevailing dual-aquifer hypothesis of atoll tidal response could be reasonably expanded to consider two possible storage-related effects: (1) the diminishing influence of water-table storage with depth and distance from the water table; and (2) lower compressibility and specific storage in the Pleistocene aquifer, if it is highly indurated as at Cantonment.

Distribution of fresh and brackish groundwater

Wide parts of the island are underlain by freshwater lenses as thick as 20 m, whereas narrow parts are underlain by thinner lenses or by brackish water. The thickness of freshwater was mapped in 1982 by PRC Toups (1983), who conducted geoelectrical surveys and sampled water at various depths in monitoring wells and during drilling. Freshwater was defined as having an upper limit of 1,400 μS cm^{-1} specific conductance or 250 mg L^{-1} Cl^- concentration (the latter is a secondary drinking-water standard; EPA, 1990). These values equate to about 1.3% seawater, in which Cl^- is about 19,600 mg L^{-1} at Diego Garcia.

At Cantonment (Fig. 32-2), the base of freshwater was deeper than −20 m over a broad central area and was surprisingly deep near the shore (−15 m just 150 m inland). At Air Operations (Fig. 32-3), the freshwater lens had two lobes that extended to maximum depths of −15 and −20 m. The Air Operations area was widened by dredging in 1983, and Cl^- trends in monitoring wells near the lagoon (at sites B1 and B2; see also Fig. 32-5) indicate subsequent invasion and thickening of freshwater beneath the filled areas, which were former intertidal lagoon sand flats. From the contours of freshwater thickness in Figs. 32-2 and 32-3, and assuming a porosity of

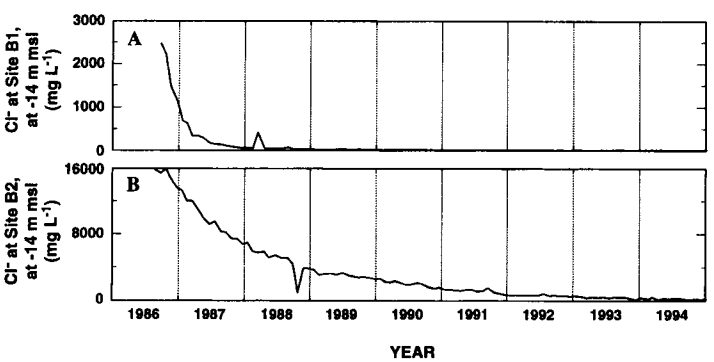


Fig. 32-5. Cl^- in deep monitoring wells at sites B1 and B2, Air Operations (see Fig. 32-3 for locations). Declining concentrations reflect expansion of the freshwater lens beneath former lagoon flats filled by dredging in 1983.

0.3 (Oberdorfer et al., 1990), I have computed the volumes of freshwater stored in the lenses in 1982 to be 19×10^6 m^3 at Cantonment and 9×10^6 m^3 at Air Operations.

The freshwater lens and freshwater-saltwater mixing zone at Cantonment are shown in Fig. 32-6. A strong lithologic control is evident. Where freshwater is thin near the shores, the base of the lens dips steeply and the mixing zone is thick. But inland, where freshwater extends below unit 3, the transition zone is thin and the base of freshwater conforms roughly to the top of unit 5. In a uniform aquifer, one would expect a more rounded curvature in the base of the lens; instead, the lens base is flat, as if truncated by the lithologic layering. This configuration is consistent with an inference of high hydraulic conductivity at depth. Vacher (1988) modeled a sharp-interface lens in a two-layer aquifer with Dupuit horizontal flow and showed that higher hydraulic conductivity in the deeper layer flattens the base of the lens. In essence, the high conductivity lessens frictional resistance to flow, and so there is less buildup of hydraulic head and the lens does not extend as deep as it would in a homogeneous aquifer having the hydraulic conductivity of the shallow layer. Similarly, a numerical flow and solute-transport model produced a compressed and flattened mixing zone when high conductivity was specified at depth (Underwood et al., 1992).

Fig. 32-6 also shows pronounced upconing of the mixing zone at sites A1 and A5. The upconing resulted from prior dry weather and excessive withdrawal from too small an area. Each of theses sites is surrounded by a wellfield that was pumped heavily in 1982 and earlier, before additional wellfields were spread throughout the rest of Cantonment. Well depth also may have contributed to upconing at site A5

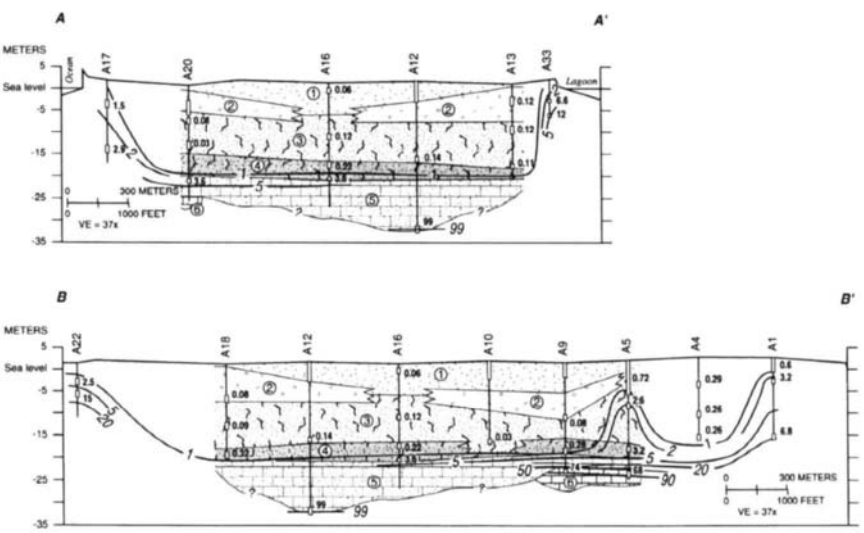


Fig. 32-6. Freshwater lens and freshwater-saltwater mixing zone at Cantonment in 1982 (based on data from PRC Toups, 1983). Lithologic units and monitoring wells are the same as in Fig. 32-4. See Fig. 32-2 for locations of the cross sections. Relative salinity of groundwater (in percent seawater) is shown by contours and by numeric values posted next to wellscreens. Note apparent truncation of the freshwater lens near the top of unit 5, and upconing of the mixing zone at sites A1 and A5.

(the long-screened well in Fig. 32-6 is the nearest withdrawal well, projected onto the section). The map of Fig. 32-2 shows evidence of upconing also: note the inland displacement of the −17 m contour (and possibly the −9 m contour) in the northeast part of Cantonment.

Recharge

Groundwater recharge was estimated by PRC Toups (1983) to be the difference between mean annual rainfall (1951–81) and mean annual pan evaporation (1964–71); runoff was assumed to be negligible. The resulting rate was 1020 mm y^{-1}, or 40% of rainfall. This simple approach tends to underestimate recharge in one sense, because rainfall is episodic and moisture is not continuously available for evapotranspiration; and tends to overestimate it in another sense, in that parts of the island have been graded with drainage swales and so there is some runoff. Volumetric recharge rates were estimated by PRC Toups (1983) for five areas of existing or potential groundwater development (Table 32-2, Fig. 32-1). Using these recharge rates and the freshwater lens volumes computed earlier, I estimate average groundwater residence time in the freshwater lens to be 5 years at Cantonment and 4 years at Air Operations (by computing the lens-volume:recharge ratio).

GROUNDWATER DEVELOPMENT

The water supply at Diego Garcia is derived entirely from groundwater. As on other islands, rainwater infiltrates into the aquifer, and fresh groundwater flows seaward and discharges at the coast. Some fraction of the natural discharge can be captured by wells, with the amount and salinity of pumped water depending on (1) thickness of the freshwater lens; (2) number, locations, and depths of wells; and (3) rates of withdrawal, at each well and in aggregate. Withdrawal causes regional depletion of the lens and raises the brackish mixing zone closer to wells generally. At an individual well, too great a well depth or pumping rate will cause localized saltwater upconing.

Sustainable yield

PRC Toups (1983) presented estimates of sustainable yield, which they defined as the "maximum quantity of fresh groundwater which can be consistently extracted over a long period of time under steady state conditions without jeopardizing the utility of the fresh water lens through overdraft and subsequent development of seawater intrusion." The estimates (Table 32-2) ranged from 10% of recharge for thin (< 10 m) freshwater lenses to 35% for thick (20–25 m) lenses, and were derived in a two-step method. The first step was an equation by Mink (1980) for one-dimensional, transient, horizontal flow and storage in a freshwater lens, with pumping approximated by an equivalent reduction in recharge. This equation was

Table 32-2

Estimates of recharge and sustainable yield (PRC Toups, 1983), and average groundwater withdrawal during the years 1985–94 for comparison [–, not applicable (estimates of area, recharge, and sustainable yield have not been made for area 6)]

Area of Present or Potential Groundwater Development[a] No.	Name of Area	Area[b] (km^2)	Recharge[b] (10^3 m^3 day^{-1})	Sustainable yield[b] (10^3 m^3 day^{-1})	Sustainable yield, as percent of recharge	Average Withdrawal,[a] 1985–94 (10^3 m^3 day^{-1})	Withdrawal, as percent of recharge	Withdrawal, as percent of sustainable yield
1	Cantonment	3.72	10.37	3.63	35	2.49	24	69
2	Air Operations	2.21	6.13	2.16	35	0.72	12	33
3	Storage Site South[d]	0.24	0.68	0.15	20	0.06	9	40
4	Transmitter Site	0.92	2.57	0.26	10	0.004	0.2	2
5	East Point	2.81	7.80	2.35	30	0	0	0
6	GEODSS[e] Site	–	–	–	–	0.002[e]	–	–
	Total, areas 1–2	5.93	16.50	5.79	35	3.21	19	55
	Total, areas 1–4	7.09	19.75	6.20	31	3.27	17	53
	Total, areas 1–5	9.90	27.55	8.55	31	3.27	12	38
	Total, areas 1–4, 6	–	–	–	–	3.28	–	–

[a] Locations of the groundwater development areas are shown in Figure 32.1.
[b] Area, recharge, and sustainable yield for areas 1–5 are from PRC Toups (1983). They estimated mean annual recharge to be 1020 mm, about 40% of rainfall.
[c] Withdrawal data are from the U.S. Navy and are maintained in files of the U.S. Geological Survey, Honolulu, Hawaii.
[d] Storage Site South is a former construction-support site previously referred to as Industrial Site South.
[e] Abbreviation: GEODSS, Ground-based Electro-Optical Deep Space Surveillance. This area was not pumped until 1987 and was not included in the earlier estimates of recharge and sustainable yield.

used to estimate steady-state lens thickness for hypothetical rates of areal withdrawal. The second step used the upconing approximation of Schmorak and Mercado (1969) to estimate saltwater upconing at an individual well, given: (1) values of lens thickness predicted by step 1, (2) pumping rate and depth of a typical well, and (3) thickness of the mixing zone from salinity profiles measured in deep monitoring wells or during drilling. Steps 1 and 2 were applied iteratively, and the sustainable yield of an area was chosen to be the largest value of areal withdrawal that maintained an acceptable level of upconing.

Distribution of groundwater withdrawal

The freshwater lenses are areally extensive but thin, and so a large number of scattered wells are used to minimize saltwater intrusion and upconing. There presently are 130 production wells, of which about 100 are in use on any given day. The wells are shallow and are pumped at low rates, effectively spreading withdrawal over wide areas and "skimming" freshwater from the lenses. Wells are of two basic designs: (1) vertical wells, which extend about 3 m below sea level and are pumped at rates of 15–30 $m^3\ day^{-1}$; and (2) horizontal wells, which typically are 120 m long, are emplaced just beneath the water table, and are pumped at 110–190 $m^3\ day^{-1}$. Cantonment and Air Operations account for 98% of islandwide withdrawal, and much of the Air Operations water is exported to Cantonment via pipeline. Salinity varies from well to well (lower inland, higher near the shore) but most pumped water is blended in the main distribution tank at Cantonment and the composite salinity typically remains low. Although it may seem counterintuitive, nearshore wells are kept in operation even if salinities in them exceed drinking-water standards. If these wells were to be shut down, the brackish water they capture would be lost to the sea and inland wells would have to be pumped at higher rates, causing greater storage depletion and risk of upconing inland. As long as the composite blend is sufficiently fresh, the nearshore brackish water augments the overall capacity of the production system.

Ten-year averages of groundwater withdrawal are listed by area in Table 32-2, and these can be compared with prior estimates of recharge and sustainable yield. For the period 1985–94, withdrawal averaged 69% of estimated sustainable yield at Cantonment, 33% at Air Operations, and 55% for the two areas combined. Thus, the two principal areas of withdrawal have been developed to about half their estimated joint capacity. On average, 19% of estimated recharge to the two combined areas has been captured by pumping. In addition, there is untapped water-supply potential at the East Point area (Table 32-2, Fig. 32-1). This area has not been developed, but its sustainable yield has been estimated to be roughly equal to that of the Air Operations area.

CASE STUDY: EFFECTS OF CLIMATIC VARIATIONS ON GROUNDWATER SUPPLY

The ultimate limitation on freshwater availability is salinity. The amount of fresh groundwater stored in the aquifer is small, and recharge is episodic. As a result, the

freshwater lenses expand and contract naturally at short time scales: seasonal and even monthly changes in salinity have been observed (Hunt, 1991).

The 17-year operating history of the water-production system illustrates two issues of relevance to small-island water supplies. First, there is the style of development: the production system has very successfully exploited the fundamental concept of widespread, low-rate pumping to minimize salinity. The second issue is the sensitivity of groundwater storage and salinity to variations in climate, specifically rainfall. The linkage to climatic variations is demonstrated by the salinity history of the production system (Fig. 32-7). The greater significance of this linkage can be seen

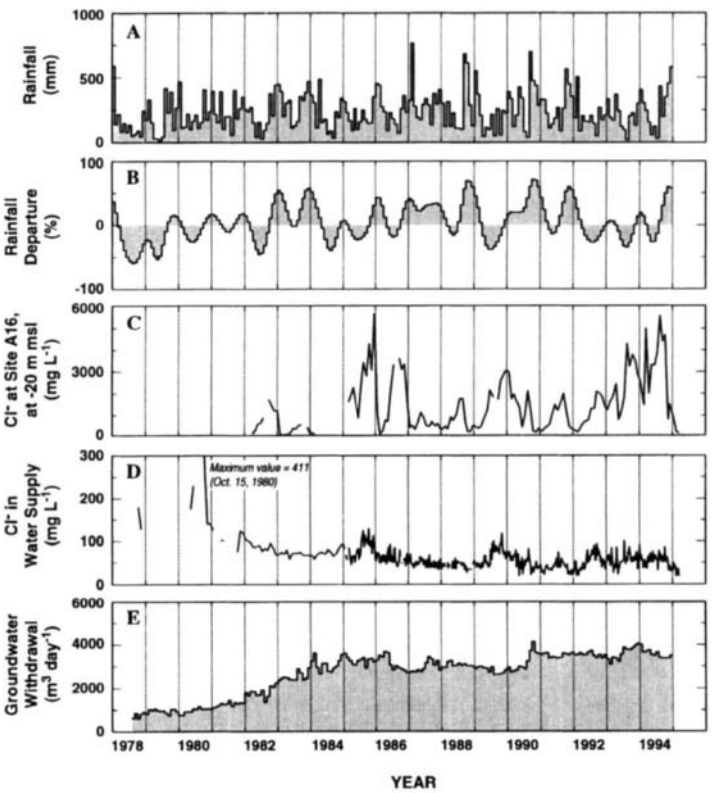


Fig. 32-7. Performance of the water-production system under varying climatic conditions, 1978–94. Data are monthly except in Panel D, which is weekly since 1985. (A) Rainfall. (B) Departure from mean rainfall (filtered; see text). (C) Cl^- in deep monitoring well at site A16, Cantonment (see Fig. 32-2 for location), which provides an index of thickness of freshwater lens; increases imply saltwater intrusion and depletion of the freshwater lens and may foreshadow increases in Cl^- of the composite water supply; decreases imply lens replenishment by recharge. (D) Cl^- in the composite water supply. (E) Island-wide groundwater withdrawal. Note the general decline in Cl^- of the composite water supply despite the three-fold increase in withdrawal afforded by the construction of 100+ wells since 1976, and the correspondence of distinct dry periods (Panel B: 1978–79, 1984–85, 1989, 1992–94) with brief increases in Cl^- at the indicator well and in the composite water supply.

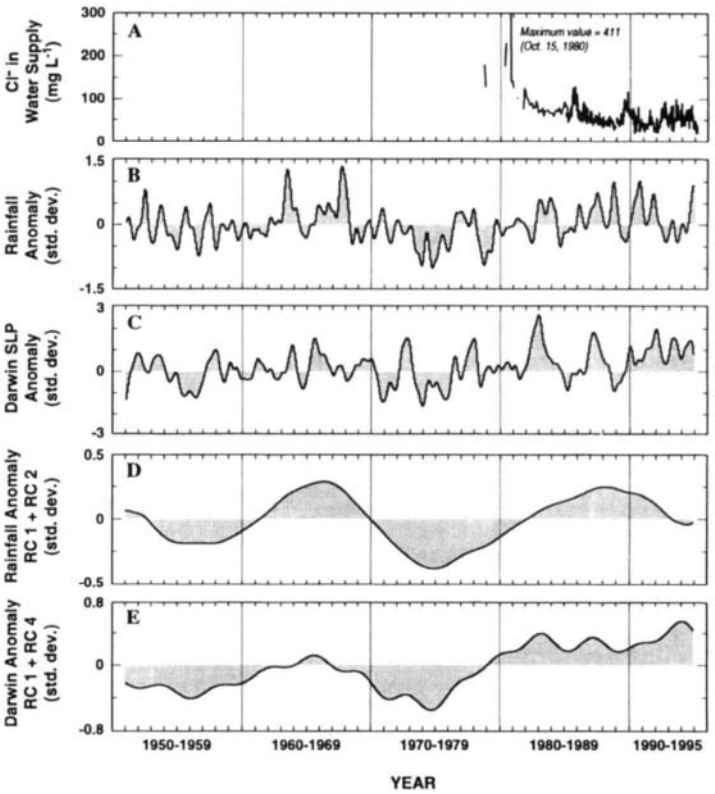


Fig. 32-8. Salinity history of the water-production system, viewed in the context of long-term climatic records, 1951–94. Data are monthly except in Panel A, which is weekly since 1985. (A) Cl^- in the composite water supply. (B) Rainfall anomaly (standardized and filtered; see text). (C) Sea level pressure (SLP) anomaly at Darwin, Australia (standardized and filtered). (D) Sum of reconstructed components (RC's) 1 + 2 from singular-spectrum analysis (SSA) of the rainfall anomaly. (E) Sum of RC's 1 + 4 from SSA of the SLP anomaly. Note the occurrence of interannual and even decadal periods of persistently wet or dry climate. The dry decade 1970–79 contrasts with subsequent wet conditions under which the modern water-production system has operated. The extreme dryness of the 1970s was a main cause of high Cl^- in the composite water supply near the end of that decade, although a contributing factor was concentration of pumpage at only a few wells.

by examining long-term climatic records that extend back through several earlier decades (Fig. 32-8).

Evolution and performance of the water-production system

The U.S. Navy constructed several wells as early as 1971, but groundwater development began in earnest in 1976 when 24 wells were built at Cantonment, Air Operations, Storage Site South, and Transmitter Site. Another 100 or so wells were added in the 1980s to accommodate increases in population and activities. The

expanded production system afforded a three-fold increase in groundwater withdrawal from 1980 to 1984 (Fig. 32-7E), yet salinity in the water supply declined gradually throughout this period (Fig. 32-7D) because the new wells spread withdrawal much more widely than before. In addition, newer wells were shallower than the wells drilled in 1976, which extended to about −7 m. During the earlier period 1978–80, Cl^- concentration in the water supply ranged from 120 to 411 mg L^{-1}, exceeding the drinking water standard several times. The high salinity was due partly to concentration of withdrawal at deep, closely spaced wells in four small areas. Another factor was that the freshwater lenses had been depleted by severe droughts in the 1970s (Fig. 32-8 and next section). Groundwater withdrawal remained fairly steady after the period of wellfield expansion in the early 1980s and has averaged 3,280 m^3 day^{-1} since 1985.

Rainfall at Diego Garcia is influenced by several modes of atmospheric circulation specific to the tropics. Seasonal migration of the ITCZ imparts a strong annual cycle in rainfall, and the strength of convection within the ITCZ itself is perturbed by oscillations on the order of 40–50 days (Madden and Julian, 1971). There is interannual variation as well, perhaps related to factors such as the quasi-biennial and quasi-quadrennial components of El Niño/Southern Oscillation (ENSO) variability (Rasmusson et al., 1990).

The relation between rainfall and salinity is examined in Fig. 32-7. Month-to-month variations in the monthly rainfall record (Fig. 32-7A) tend to obscure the seasonal and interannual components that are also present. The longer components are shown in Fig. 32-7B, which was derived from Fig. 32-7A by converting the monthly rainfall to a departure index, calculated as the percentage deviation from the mean of all months, and then screening the resultant time series with a low-pass filter. The filter used here (and elsewhere in this Case Study) is an 11-mo, centered, Gaussian-weighted moving average. The filtered time series shows key events such as the annual dry season that occurs mid-year, as well as several multi-year periods of above- or below-average rainfall.

Several dry periods are conspicuous — in 1978–79, 1984–85, 1989, and 1992–94. Some are single, severe dry seasons and others comprise two or more dry seasons and intervening, subnormal wet seasons that coalesce into sustained dry periods that last 18 mo or longer. The dry periods correspond to distinct increases in Cl^- in deep monitoring wells (Fig. 32-7C) and in the composite water supply (Fig. 32-7D). In the water supply, Cl^- has fluctuated mostly between 30–70 mg L^{-1} since 1981, with notable increases to near 130 mg L^{-1} in 1985 and 1989, and near 100 mg L^{-1} in 1992, 1993, and 1994. In the deep monitoring well, increases in Cl^- are more extreme than in the water supply and signify depletion of the freshwater lens and accompanying saltwater intrusion. Particularly noteworthy are, first, the rapid onset of high-salinity episodes (within a single dry season) and, second, their even quicker amelioration (typically within 1–2 mo when heavy rains resume).

The performance history of the production system can be summarized as follows. From 1985 to 1994, groundwater withdrawal was roughly half the estimated sustainable yield of the areas presently developed. Cl^- rose during dry periods, but only to about half the drinking-water standard. Dry periods since 1980 have lasted less

than 3 years and have been much milder than a drought in 1978–80 during which the drinking-water standard for Cl^- was exceeded. If withdrawal were to be raised nearer the estimated sustainable yield, salinity would rise also; however, the magnitude of increase cannot be predicted without further study.

Climatic persistence and implications for water supply

The rapid onset of high-salinity episodes defines the fundamental character of the resource: it is a small-storage hydrologic system subject to rapid depletion if recharge is deficient. Although the production system performed very successfully during the 1980s and 1990s, a longer climatic view (Fig. 32-8) raises a justifiable concern: What is the possibility of dry periods that are much more severe and persistent than those of recent experience?

The salinity history of the water supply (Fig. 32-7E) is reproduced in Fig. 32-8A and juxtaposed with the time series of a filtered, standardized, monthly rainfall anomaly (Fig. 32-8B). The rainfall anomaly here is the deviation of the monthly rainfall from the historical mean for each respective month (in contrast to the mean of all months, which was used in Fig. 32-7B where the intent was to preserve the seasonal variation). The anomaly is shown on a standardized z-scale (number of standard deviations from the mean), to facilitate comparison with an atmospheric index (Fig. 32-8C) that is calculated the same way, and the low-pass filter is, again, an 11-mo, Gaussian-weighted, moving average.

The long rainfall-anomaly time series shows the full sequence of events leading up to the high-salinity episode of 1978–80. The 1970s were a persistently dry decade. A severe 3-y drought in 1973–75 was followed shortly by a severe 2-y drought in1978–79. In contrast, the 1980s and 1990s were much wetter, as were the 1960s. If the droughts of the 1970s were to recur, the result would be saltwater intrusion of a magnitude that is unprecedented in the post-1984 period in which the expanded production system has operated. The probable composite Cl^- concentration under such conditions cannot be predicted without extensive further studies, including modeling. But simply judging from the water-system history, I speculate that Cl^- would likely rise above the drinking-water standard of 250 mg L^{-1}, requiring temporary relaxation of the standard or desalination if the standard is maintained. Of course, water conservation and proper management of the pumping distribution would help postpone these actions or alleviate the severity of the salinity crisis.

What are the possible causes of the pattern of persistence in rainfall at Diego Garcia? The answer may lie in linkages to regional elements of the ocean-atmosphere circulation. Although the topic merits more exhaustive study, I can report one apparent linkage which is illustrated in Fig. 32-8. Fig. 32-8C shows the standardized Darwin sea-level pressure (SLP) anomaly after low-pass filtering. This barometric anomaly makes up half of the well-known Tahiti-minus-Darwin Southern Oscillation Index (SOI), which tracks the most influential and widespread mode of tropical atmospheric variability. I have elected to show the Darwin SLP anomaly rather than the SOI because Darwin, Australia, is much closer to Diego Garcia than is Tahiti;

therefore, the Darwin anomaly should be more closely related to Diego Garcia rainfall than is the SOI.

Visually there is a striking positive correspondence between the filtered, standardized anomalies of Figs. 32-8B and C. Cross-correlation bears this out, giving a maximum correlation coefficient r = 0.37 with rainfall lagging by 3 mo. The rainfall anomaly also correlates with the SOI, though the correlation is inverse and slightly smaller (r = −0.29, with rainfall lagging by 4 mo).

Both the rainfall and Darwin SLP anomalies appear to have a high degree of embedded, decadal-scale persistence. I have examined this frequency range by using the singular-spectrum analysis (SSA) program of Dettinger et al. (1995). SSA is a form of principal components analysis that uses data-adaptive filters to decompose time series into oscillatory, trending, and noise components (Dettinger et al. 1995). Using a window length of 132 mo, both series produced leading reconstructed components (RC's) of strong interdecadal variation (Fig. 32-8D,E). Correlation between these low-frequency time series is r = 0.72 with rainfall lagging by 18 mo. Additional components of variation were isolated from the rainfall anomaly by SSA, some with periods of 2–5 y that may correspond to components of ENSO variability.

The exact meaning and origin of the interdecadal variations are topics for future consideration. Decadal-scale variability in the coupled ocean-atmosphere system is increasingly recognized (e.g., Miller et al., 1994), and Wunsch (1992) argues persuasively that it should be expected rather than cause for surprise. The positive correlation between rainfall at Diego Garcia and barometric pressure at Darwin implies a negative correlation between rainfall at the two stations, because high pressure at Darwin corresponds to low rainfall there; by implication, there is a tendency for dipolar oscillation in rainfall between Diego Garcia and Darwin, an interesting finding in itself. Of more immediate practical interest is the promise shown by correlation of Diego Garcia rainfall with other climatic indexes that may lead to a meaningful degree of prediction for Diego Garcia. For example, the SOI is presently predicted by climatologists at lead times of several seasons. For now, it is noteworthy that the low-frequency oscillation in rainfall-anomaly RC's 1+2 (Fig. 32-8D) appears to be in transition from positive phase (wet) to negative (dry); this transition may be signaling a tendency for prolonged dryness in the near future.

CONCLUDING REMARKS

Diego Garcia will likely retain its strategic importance to the British and U.S. governments, and this is fortunate for hydrogeologists in that monitoring studies will continue to provide new information. Early exploratory studies provided interesting views of aquifer tidal response and a freshwater lens "truncated" by aquifer layering. The present water-production system is unparalleled for such a small island, and the low salinity of pumped water has validated the development strategy of numerous, widely spaced wells and low pumping rates. Much of the knowledge gained at Diego Garcia is readily transferrable to other small islands.

A long-standing program of hydrologic monitoring has revealed fundamental characteristics of the groundwater resource such as small storage and a rapid saltwater intrusion response to short-term rainfall deficit. These characteristics are unsettling in view of a tendency for long-term persistence in the rainfall record, the most notable examples being the severe multi-year droughts of the 1970s. Droughts of this magnitude would pose severe challenges to water management on any small island that depends on natural resources. Recurrence of such severe droughts on Diego Garcia would require knowledgeable, adaptive management of the complex production system to minimize salinity while conserving groundwater storage. Success in this approach could lessen or eliminate the need for desalination, which is a costly option. Ongoing hydrologic monitoring provides a solid conceptual foundation for developing successful drought-management strategies for Diego Garcia and for other islands as well.

ACKNOWLEDGMENTS

Funding, hydrologic records, and logistical support have been provided by the U.S. Navy Public Works Department, Diego Garcia, under the "Long-Term Groundwater Management Program." Logistical assistance has also been provided by the Pacific Division Naval Facilities Engineering Command, Pearl Harbor, Hawaii; by the British Representative and Command, Diego Garcia; and by the civilian staff of the water plant (special thanks to Mr. Rick Weber, plant supervisor). The U.S. Naval Oceanography Command Detachment has provided climatic data. Technical reviews by Stephen Anthony, Robert Buddemeier, June Oberdorfer, and Len Vacher improved the manuscript considerably.

I am especially indebted to the late Dan Davis (1913–1995), a valued collaborator and mentor. Mr. Davis initiated USGS studies at Diego Garcia in 1978 and conceived the system of shallow, low-yield wells in collaboration with Navy engineers. He later selected well sites, supervised well construction by Navy Seabees and contractors, and conducted various pumping tests and field investigations. The "Long-Term Ground-Water Management Program" is in large measure a product of his vision; it continues to furnish hydrologic data that contribute to the management of Diego Garcia's well fields and to the larger scientific study of atoll islands.

REFERENCES

Anthony, S.S., Peterson, F.L., Mackenzie, F.T. and Hamlin, S.N., 1989. Geohydrology of the Laura fresh-water lens, Majuro atoll: a hydrogeochemical approach. Geol. Soc. Am. Bull., 101: 1066–1075.

Ayers, J.F. and Vacher, H.L., 1986. Hydrogeology of an atoll island: a conceptual model from detailed study of a Micronesian example. Ground Water, 24: 185–198.

Bathurst, G.C., 1975. Carbonate Sediments And Their Diagenesis. Elsevier, Amsterdam, 658 pp.

Buddemeier, R.W. and Holladay, G., 1977. Atoll hydrology: island groundwater characteristics and their relationship to diagenesis. Proc. Third Int. Coral Reef Symp. (Miami), 2: 167–173.

Dettinger, M.D., Ghil, M., Strong, C.M., Weibel, W. and Yiou, P., 1995. Software expedites singular-spectrum analysis of noisy time series. Eos, Trans. Am. Geophys. Union, 76(2): 12–21.
Domenico, P.A. and Mifflin, M.D., 1965. Water from low-permeability sediments and land subsidence. Water Resour. Res., 1: 563–576.
Duncan, R.A., 1990. The volcanic record of the Reunion hotspot. In: R.A. Duncan, J. Backman, L.C. Peterson et al., Proc. ODP, Sci. Results, 115. Ocean Drilling Program, College Station TX, pp. 3–10.
Emery, K.O., Tracey, J.I. Jr. and Ladd, H.S., 1954. Geology of Bikini and nearby atolls. U.S. Geol. Surv., Prof. Pap. 260-A, 265 pp.
EPA (U.S. Environmental Protection Agency), 1990. Fact sheet – drinking water regulations under the Safe Drinking Water Act. Washington, D.C., May 1990, 43 pp.
Ferris, J.G., 1951. Cyclic fluctuations of water level as a basis for determining aquifer transmissibility. Assem. Gen. Bruxelles, Assoc. Int. Hydrol. Sci., 2: 149–155.
Ferris, J.G., 1963. Cyclic water-level fluctuations as a basis for determining aquifer transmissibility. In: R. Bentall (Compiler), Methods of determining permeability, transmissibility, and drawdown. U.S. Geol. Surv. Water-Supply Pap. 1536-I: 305–318.
Francis, T.J.G. and Shor, G.G. Jr., 1966. Seismic refraction measurements in the northwest Indian Ocean. J. Geophys. Res., 71: 427–449.
Goter, E.R. Jr., 1979. Depositional and diagenetic history of the windward reef of Enewetak Atoll during the mid to late Pleistocene and Holocene. Ph.D. Dissertation, Rensselaer Polytechnic Inst., Troy NY, 239 pp.
Green, D.H. and Wang, H.F., 1990. Specific storage as a poroelastic coefficient. Water Resour. Res., 26: 1631–1637.
Hanor, J.S., 1978. Precipitation of beachrock cements: mixing of marine and meteoric waters vs. CO_2 degassing. J. Sediment. Petrol., 48: 489–501.
Hogan, P., 1988. Modeling of freshwater-seawater interaction on Enjebi Island, Enewetak Atoll. M.S. Thesis, San Jose State Univ., San Jose CA, 75 pp.
Hunt, C.D. Jr., 1991. Climate-driven saltwater intrusion in atolls. In: H.J. Peters (Editor), Ground Water in the Pacific Rim Countries. Am. Soc. Civil Eng., Symp. Irrig. and Drainage Div., pp. 43–49.
Johnson, A.M., 1970. Physical Processes in Geology. Freeman, Cooper & Co., San Francisco, 577 pp.
Land, L.S., 1970. Phreatic versus vadose meteoric diagenesis of limestones. Sedimentol., 14: 175–185.
Madden, R.A. and Julian, P.R., 1971. Detection of a 40–50 day oscillation in the zonal wind in the tropical Pacific. J. Atmos. Sci., 28: 702–708.
Marshall, J.F. and Jacobson, G., 1985. Holocene growth of a mid-Pacific atoll: Tarawa, Kiribati. Coral Reefs, 4: 11–17.
Miller, A.J., Cayan, D.R., Barnett, T.P., Graham, N.E. and Oberhuber, J.M., 1994. The 1976-77 climate shift of the Pacific Ocean. Oceanography, 7: 21–26.
Mink, J.F., 1980. State of the groundwater resources of Southern Oahu. Unpublished report to Board of Water Supply, City and County of Honolulu, 630 South Beretania Street, Honolulu, HI, 96813, USA, 83 pp.
Oberdorfer, J.A. and Buddemeier, R.W., 1986. Coral-reef hydrology: field studies of water movement within a barrier reef. Coral Reefs, 5: 7–12.
Oberdorfer, J.A., Hogan, P.J. and Buddemeier, R.W., 1990. Atoll island hydrogeology: flow and freshwater occurrence in a tidally dominated system. J. Hydrol., 120: 327–340.
PRC Toups, 1983. Engineering study to evaluate potable water supply alternatives and groundwater yield at Diego Garcia, BIOT. Unpublished report to the U.S. Navy: PRC Toups, 972 Town and Country Road, P.O. Box 5367, Orange, CA, 92668, USA.
Rasmusson, E.M., Wang, X. and Ropelewski, C.F., 1990. The biennial component of ENSO variability. J. Marine Sys., 1: 71–96.

Schmorak, S. and Mercado, A., 1969. Upconing of freshwater-seawater interface below pumping wells, field study. Water Resour. Res., 5: 1290–1311.

Simmons, G.R., 1990. Subsidence history of basement sites and sites along a carbonate dissolution profile, Leg 115. In: R.A. Duncan, J. Backman, L.C. Peterson et al., Proc. ODP, Sci. Results, 115. Ocean Drilling Program, College Station, pp. 123–126.

Stoddart, D.R., 1971a. Geomorphology of Diego Garcia Atoll. In: D.R. Stoddart and J.D. Taylor (Editors), Geography and Ecology of Diego Garcia Atoll, Chagos Archipelago. Atoll Res. Bull., 149: 7–26.

Stoddart, D.R., 1971b. Diego Garcia climate and marine environment. In: D.R. Stoddart and J.D. Taylor (Editors), Geography and Ecology of Diego Garcia Atoll, Chagos Archipelago. Atoll Res. Bull., 149: 27–30.

Stoddart, D.R., 1971c. Settlement and development of Diego Garcia. In: D.R. Stoddart and J.D. Taylor (Editors), Geography and Ecology of Diego Garcia Atoll, Chagos Archipelago. Atoll Res. Bull., 149: 209–218.

Stoddart, D.R. and Taylor, J.D. (Editors), 1971. Geography and ecology of Diego Garcia Atoll, Chagos Archipelago. Atoll Res. Bull. 149, 234 pp.

Surface, S.W. and Lau, E.F.C., 1988. Development and management of groundwater resources on Diego Garcia. J. Am. Water Works Assoc., 80: 67–72.

Underwood, M.R., 1990. Atoll island hydrogeology: conceptual and numerical models. Ph.D. Dissertation, Univ. Hawaii, Honolulu, 204 pp.

Underwood, M.R., Peterson, F.L. and Voss, C.I., 1992. Groundwater lens dynamics of atoll islands. Water Resour. Res., 28: 2889–2902.

USNWSD (U.S. Naval Weather Service Detachment), 1978. Station climatic summary, Diego Garcia. Federal Building, Asheville, NC, 4 pp.

Vacher, H.L., 1988. Dupuit-Ghyben-Herzberg analysis of strip-island lenses. Geol. Soc. Am. Bull., 100: 580–591.

Wheeler, C.W. and Aharon, P., 1991. Mid-oceanic carbonate platforms as oceanic dipsticks: examples from the Pacific. Coral Reefs, 10: 101–114.

Wunsch, C., 1992. Decade-to-century changes in the ocean circulation. Oceanography, 5: 99–106.

This Page Intentionally Left Blank

SUBJECT INDEX

AAR data and geochronology
  Bahamas, 120, 124, 142–143
  Bermuda, 55–56, 74
  Florida keys, 231
Abaco (Bahamas), 146, 148, 151–152
Abemama Atoll (Repub. Kiribati), 585, 599
Abrolhos Islands. *See* Houtman Abrolhos Islands
Accommodation, 656–658
Acklins Island, 146,148
Acropora, 224, 226, 342, 349, 599, 792, 815, 872
Agassiz, Alexander, 3, 7–9, 12–13, 28, 219, 746
Aitutaki (Cook Islands), 2, 18, 32, 472, 503, 506–508, 510, 512–515, 521, 524, 527–534
Aki-Aki (Tuamotu Archipelago), 484, 488
Algal bindstone
  Houtman Abrolhos, 818–821
Algal pavement (*see also* reef plate)
  Cocos (Keeling) Islands, 888
  Great Barrier Reef, 841
Algal ridges
  Enewetak Atoll, 673
  Great Barrier Reef, 840–856
  Suwarrow Atoll, 512
Alluvial aquifers (*see also* valley-fill aquifers)
  St Croix, 367–368
Almost atoll, 2, 12, 16, 18, 476, 508–510 (*see also* Aitutaki, Bora-Bora)
Amino acid racemization. *See* AAR data and geochronology
Andros Island (Bahamas), 92, 96, 101–102, 113, 126–127, 131, 138, 146, 151, 162, 170
Anewetak Atoll (Marshall Islands; *see also* Enewetak Atoll; Marshall Islands), 637–666
Antarctic surges, 70, 72–73, 81, 154–156
Antigua (Leeward Islands), 20, 363
Arno Atoll (Marshall Islands), 611
Aruba (Netherlands Antilles), 20
Atiu Island (Cook Islands), 2, 5, 12, 16, 32, 431, 504–509, 514–515, 519, 525, 528, 532–534
Atoll (*see also* Darwin theory of coral reefs; dual aquifer atoll hydrogeology; endo-upwelling), 2, 4, 7–19, 22–24, 94, 200, 835
  ancient (uplifted)
    Henderson I., 413, 423–428
    Makatea, 462, 498
    Mataiva, 498
    Nauru, 178, 498, 715–716
    Niue, 178, 548
  modern
    Caroline Islands, 693–706
    Cocos (Keeling) Islands, 885–906
    Cook Islands, 504–512, 514–515, 517–519, 522, 533
    Diego Garcia, 909–929
    Fr. Polynesia, 433–450, 453, 462, 468–470, 475–494, 496–499, 548
    Kiribati (Tarawa and Christmas I.), 577–607, 728
    Marshall Islands (*including* Enewetak [Anewetak] Atoll), 611–691
    Pitcairn Islands, 407–408, 410–412
Australes Fracture Zone, 435–436
Australia, 4–6, 8, 17, 20, 42, 83, 544, 571–572, 707, 710, 733, 783–810, 811–833, 835–866, 867–884, 885, 892, 894, 906, 927–928
Austral Islands (Australes, Fr. Polynesia), 19, 32, 433–435, 453, 475–477, 599

Backreef
  ancient (*see also* lagoon facies)
    Anewetak Atoll, 644–645
    Barbados, 386–387, 391
    Isla de Mona, 336, 339
    Makatea, 459, 462–463
  modern (*see* lagoon)
Bahamas, 2, 7, 16, 17, 20, 23–25, 27, 29, 52, 58–59, 73, 83, 91–216, 219, 222, 445, 498
Bahamas Drilling Project (*see also* Clino; Unda), 96, 161
Bahamian Field Station, 133–139, 152
Banaba (Repub. Kiribati; *see also* Ocean Island), 577, 694
Banana holes, 100–101, 135, 192
Barbados, 2, 9, 11–13, 16, 18, 20, 22, 71, 82–83, 230, 381–406, 829

Barbuda (Leeward Islands), 20
Barrier reef (*see also* Great Barrier Reef), 12–13, 16, 18, 113
  ancient
    Mururoa and Fangataufa, 446
    Niue, 547
  modern
    Cook Islands, 510–513
    Fiji, 763, 769
    Fr. Polynesia, 435, 475–482, 485–488, 494496, 541
Basal groundwater, 21–22, 753–756, 759
Basalt. *See* volcanics
Beachrock
  Anewetak Atoll, 646, 648, 674–675
  Caroline Islands, 697
  Diego Garcia, 915
  Ducie Atoll, 411
  Fiji, 763, 771
  Great Barrier Reef, 842–846, 849–854, 858–859, 870
  Marshall Islands, 614, 621
  Rarotonga, 514
  St. Croix, 366
  Tarawa, 581
Beagle, HMS, 3, 4, 17, 30, 86, 907
Belize, 445
Bellinghausen Atoll (Society Islands), 435
Bermuda, 2, 7, 11, 15–18, 23, 27, 35–90, 94, 157, 219, 231
Bermuda Biological Station (BBSR), 37, 85
Bermuda Rise, 36, 38
Berry Islands (Bahamas), 146, 148
Big Pine Key (Florida), 27, 217, 224, 237–239, 241, 244–245, 248
Bikini Atoll (Marshall Islands), 2, 4, 24, 582, 611—613, 616–617, 619–621, 623, 625, 634, 640, 694, 698, 901
Bimini (Bahamas), 146, 148
Blue holes
  Bahamas, 101, 137, 177, 201, 207–211
  Cocos (Keeling) Islands, 889
  Houtman Abrolhos Islands, 812, 814
  Rottnest I., 786, 806
Bonaire (Netherlands Antilles), 20
Bora-Bora (Society Islands), 12, 19, 476, 480, 484
Bounty, H.M.S., 5, 503
Brackish (*see also* freshwater-saltwater mixing zone), 25, 69, 484, 491–492, 497–498, 676–684, 728, 733–735, 769, 771, 773, 784, 805–807, 919
Caicos Islands. *See* Turks and Caicos Islands
Calcrete (*see also* caliche)
  Bahamas, 129–130, 142, 208
  Florida Keys, 229
  Houtman Abrolhos Islands, 818
  Rottnest I., 794
  Yucatan Islands, 288, 291
Caliche (*see also* calcrete)
  Barbados, 398
  Isla de Mona, 340
  Makatea, 463, 467
  Yucatan Islands, 281–282, 288–292
Capricorn-Bunker Group (GBR), 849, 856, 869
Carbon isotope. *See* stable isotopes, diagenesis
Caroline Islands, 8, 12, 598, 613, 693–694
Caroline Islands atolls, 693–706
Cat Island (Bahamas), 17, 91, 143, 146
Cavernous porosity (*see also* cavities; porosity), 170, 172, 393, 521
Caves and caverns (*see also* banana holes, cavities, cenotes, flank margin caves, fracture caves, solution pits)
  Bahamas, 100–101, 111, 171, 207–212
  Cayman Islands, 322–324
  Cook Islands, 509, 519
  Fr. Polynesia, 445, 456, 482
  Guam, 752–753
  Henderson I., 414–415
  Isla de Mona, 346, 349, 351, 354
  Johnston Atoll, 681
  Makatea, 455, 488
  Tonga, 571
Cavities, 305, 467, 470–471
  in drilling, 171, 521–522, 872
  of organic skeletons, 440, 822
  sediment and infillings of, 305, 323–324, 443, 529, 723
Cay (*see also* islands, types of; motu), 20, 99–100, 145–146, 510, 582, 763, 768, 813–814, 913
  Great Barrier Reef, 840–841, 844–853, 855–857, 859–862, 867
Cayman Brac (Cayman Islands), 299–300, 302–310, 322
Cayman Islands, 299–326
Cement and cementation (*see also* beachrock; conglomerate platform; diagenesis; rampart rock; reef plate)
  Anewetak Atoll, 645–656, 658–661; 656, 674, 679
  Bahama Banks, 172, 174–176

Cement and cementation (*continued*)
Bahamas, 99, 111, 114–115, 118–119, 126, 131, 142–143, 157
Barbados, 399–400
Bermuda, 55
Caroline Islands, 697
Cayman Islands, 310, 313
Cocos (Keeling) Islands, 891
Cook Islands, 529, 531
Diego Garcia, 914–918
Great Barrier Reef, 837, 842–843, 859
Houtman Abrolhos Islands, 813–814, 819–822
Makatea, 461, 467
Mururoa and Fangataufa, 443
Niue, 547–551
Rottnest I., 788–790, 795
Yucatan Islands, 285, 292–296
Cenotes (*see also* solution pits), 201, 207–209, 283
Cerion, 149, 151, 153
Chagos Archipelago, 2, 909
Challenger, H.M.S., 4, 8
Chlorozoan carbonates, 477, 825
Christian, Fletcher, 5, 503
Christmas Island (Indian Ocean), 4, 8
Christmas Island [Kirimati] (Repub. Kiribati), 2, 5, 15, 25, 26, 577–586, 594–598, 599, 894
Clino, 163–164, 170, 172–173, 176, 178
Coastal terrace
Fiji, 773
Isla de Mona, 24, 328, 330–331, 334, 348–349
Nauru, 24, 716–719, 735–736
St. Croix, 366
Coconut palm (*Cocos nucifera*), 24, 482, 592, 594, 602, 605, 885, 889, 897–898, 910
Cocos (Keeling) Islands, 2, 8, 14, 15, 885–908
Conglomerate platform (*see also* rampart rocks)
Cocos (Keeling) Islands, 885, 889, 891–892, 901–905
Great Barrier Reef, 843
Tarawa, 581–582, 584
Convection. (*See* endo-upwelling; geothermal gradient; Kohout convection)
Cook, Captain James, 3–5, 503, 537–538, 540, 563, 835
Cook Islands, 2, 8, 16, 19, 22, 83, 435, 476, 503–535, 537, 538, 540, 599
Cozumel (Yucatan), 2, 20, 287–288, 290, 298
Cretaceous, 19, 95, 164–167, 170, 363, 366, 508, 524, 638, 714–715, 793
Crooked Island (Bahamas), 146, 148
Crown of Thorns, 835
Cuba, 7, 20, 95, 164, 167, 217, 362
Cyanobacterial mats (*see also* stromatolite), 270, 484–485, 497–498, 798

Darwin, Charles, 3, 16, 889
Darwin paradox, 480, 486, 496–497
Darwin theory of coral reefs, 4, 7–9, 12–13, 19, 28, 885–886, 901, 905
Dedolomitization
Isla de Mona, 345
Niue, 548, 551
Deep-sea oxygen isotope record. (*See* oxygen isotope chronology)
Depositional facies (*see also* eolianite; lagoon facies; reef facies)
Bahamas, 97–98, 109–118, 143
Cayman Islands, 302, 305, 308–310
Florida Bay mud islands, 254–257
Florida Keys, 224–228
St. Croix, 365–367
DGH models, 27–28, 667, 681, 689–690
Bermuda, 64, 68
Florida Keys, 238–240
Kiribati (Tarawa and Christmas I.), 586, 594,
Tongatapu, 572–574
Diagenesis (*see also* cement and cementation; dedolomitization; dolomite and dolomitization; endo-upwelling; marine diagenesis; meteoric diagenesis; mixing-zone diagenesis; phosphate deposits; stable isotopes), 9
Anewetak Atoll, 646, 648–656, 658–660
Bahama Banks, 171–177
Bahamas, 142
Barbados, 397–403
Bermuda, 56
Cook islands, 529–531
Diego Garcia, 913, 916
Florida Bay, 262–272
Florida Keys, 228–230, 233
Great Barrier Reef, 840
Isla de Mona, 342–347, 351–354
Makatea, 463–465
Mururoa and Fangataufa, 440–443
Niue, 548–551
Yucatan Islands, 292–296
Diego Garcia, 2, 23, 889, 909–931
Dikes, 438, 477, 747
Dike water, 21
Dolomite and dolomitization, 9, 15, 28, 475, 498
Anewetak Atoll, 640, 648, 650, 652–653, 656, 662

Dolomite and dolomitization (*continued*)
Bahama Banks, 96, 163, 172, 174–177, 202–204
Barbados, 402
Cayman Islands, 305, 308, 310–311
Cook Islands, 515, 517, 529–532
Fiji, 769
Florida Bay, 249, 266–272
Florida Keys, 233
Isla Contoy, 280
Isla de Mona, 330–331, 335–336, 344–345
Makatea, 457, 463–465
Mururoa and Fangataufa, 440–443
Nauru, 721, 735
Niue, 537, 544–551, 557–562
St. Croix, 372–376
Tikehau, 490
Drought
Caroline Islands, 693
Diego Garcia, 909, 926–927, 929
Fiji, 775
Guam, 746
Kiribati (Tarawa and Christmas I.), 578–580, 596, 607
Nauru, 707, 711, 736
Niue, 540, 556
St. Croix, 361
Dual-aquifer atoll hydrogeology (*see also* Thurber Discontinuity), 22, 23
Caroline Islands atolls, 699–700
Cocos (Keeling) Islands, 895, 901
Diego Garcia, 913–921
Enewetak Atoll, 667, 671–691
Marshall Islands, 615–634
Tarawa, 587
Dual-aquifer hydrogeology (*see also* dual-aquifer atoll hydrogeology), 22–23
Bahamas, 199
Florida Keys, 238
Heron I. (GBR), 871–878, 881
Ducie Atoll (Pitcairn Island Group), 407–408, 410–411, 430
Dupuit-Ghyben-Herzberg analysis. *See* DGH models

Electrical resistivity surveying
Cocos (Keeling) Islands, 894
Fiji, 776–780
Nauru, 710, 724
Niue, 554–556
Electromagnetic (EM) surveying
Caroline Islands atolls, 701–705
Fiji, 778–780
Florida Keys, 235–239, 241
Isla de Mona, 349
Electron spin resonance. *See* ESR data and geochronology
Eleuthera (Bahamas), 92, 135, 142–144, 146–148, 152–153, 155, 157
Ellice Islands [Tuvalu]. *See* Funafuti
El Niño Southern Oscillation. *See* ENSO
Elugelab (Anewetak Atoll), 639
Enderbury Atoll (Repub. Kiribati), 599
Endo-upwelling (*see also* geothermal gradient; Kohout convection), 446–450, 475, 487–499, 502
Eneu Island. *See* Bikini Atoll
Enewetak Atoll (Marshall Islands; *see also* Anewetak Atoll), 2, 4, 9, 18, 23, 26, 27, 445, 449, 487, 549, 582, 611–613, 634, 694, 696, 698
Enewetak Island (Enewetak Atoll), 670, 677, 680, 682–685
Enjebi Island (Enewetak Atoll), 639, 669–670, 672–681, 684–690, 692, 930
ENSO (*see also* Southern Oscillation), 408–409, 494, 577–580, 595–596, 605, 710, 886, 926
Eocene, 38, 570, 638, 639, 644–645, 657, 715
Eolianite, 1, 13, 17
Bahamas, 96, 98–99, 101, 107–119, 123–127, 141–153, 155–157
Bermuda, 41–60, 70–71, 75–80, 85
Florida Keys, 223
Houtman Abrolhos Islands, 819
Rottnest I., 793–795
Yucatan Islands, 275, 277–286, 288, 290–298
Eolianite Islands (*see also* eolian ridge islands), 2, 13, 16–18, 20, 813–814, 819
Eolian ridge islands, 275–286
ESR data and geochronology
Cook Islands, 523–525
Nauru, 719–720
'Eua (Tonga), 566–568, 570–572
Eustasy (*see also* glacioeustasy; sea-level history), 82–83, 84, 392
Evaporation, 259–260. 315–316, 320, 374, 466, 490, 600–601, 729, 757, 786, 921
Evapotranspiration (*see also* Penman method; recharge; water balance), 57, 65, 191–192, 259, 315, 318, 369, 394, 396, 554, 571, 592, 600–606, 669–670, 677, 681, 728–729, 754, 756–757, 807, 896–898, 921
Everglades (Florida), 250

EXPOE Program (Anewetak), 639, 643, 663, 692
Exuma Islands (Bahamas), 25, 27, 33, 92, 138, 148, 151–152, 155
Exuma Sound (Bahamas), 146, 148, 150

Facies. *See* depositional facies; seismic facies
Fangataufa (Tuamotu Archipelago), 2, 433–438, 440–443, 445–447, 450
Federated States of Micronesia (*see also* Caroline Islands; Caroline Islands atolls), 2, 15, 693–694
Fiji, 2, 7, 14, 19, 22, 83, 565, 763–781
Fissuration index, 188–189
Flank margin caves
  Bahamas, 86, 100–101, 134, 137, 158, 209
  Isla de Mona, 332, 346
Flinders, Matthew, 835
Florida Bay, 2, 17, 20, 217, 249–274
Florida Keys, 2, 4, 7, 17, 20, 157, 217–248, 249, 251, 253–254
Florida Straits, 95, 148, 182
Forereef and slope (*see also* reef front and slope; spur and groove)
  ancient
    Anewetak Atoll, 644–645
    Bahama Platform, 164
    Barbados, 386–387
    Isla de Mona, 336–339
  modern
    Heron I., 870
    Oeno Atoll, 412,
    Rangiroa, 482
Fracture caves, 209, 211
French Polynesia, 2, 12, 19, 433–502, 527
Freshwater diagenesis. *See* meteoric diagenesis
Freshwater lens (*see also* inventories, freshwater and meteoric-water), 23–26
  Bahamas, 100–101, 194–200
  Bermuda, 57, 60–65
  Caroline Islands atolls, 697–699
  Christmas I., 594–598, 599–600
  Cocos (Keeling) Islands, 885, 889, 895–899, 905–906
  Cook Islands, 518–519, 531–532
  Diego Garcia, 919–921, 923–924, 926, 928
  Enewetak Atoll, 677, 689
  Fiji, 769, 771–774, 776, 778–780
  Florida Keys, 233–238
  Grand Cayman Islands, 312–320
  Guam, 750, 754–757
  Isla de Mona, 348–349
  Marshall Islands, 614, 617–623, 625–628
  Nauru, 178, 723–728
  Niue, 178, 554–557, 561
  Rottnest I., 806–808
  Tarawa, 586–593, 597–598, 599–600, 607
  Tikehau, 491
  Tonga, 570–574
Freshwater-saltwater interface (*see also* DGH models; electrical resistivity surveying; electromagnetic surveying; freshwater-saltwater transition zone; Ghyben-Herzberg ratio), 22, 25–27, 349, 463, 667, 702–704
Freshwater-saltwater transition zone [hydrogeology] (*see also* mixing-zone diagenesis), 21, 25–28
  Bahamas, 200–202, 211
  Bermuda, 62–64
  Caroline Islands atolls, 697, 701, 703
  Cayman Islands, 314–315
  Cocos (Keeling) Islands, 894–896
  Diego Garcia, 920–923
  Enewetak Atoll, 677–681, 684, 686, 689–690
  Florida Keys, 236, 238
  Guam, 753–754, 756
  Isla de Mona, 349
  Marshall Islands, 615, 634
  Nauru, 725–726, 728, 734–736
  Niue, 539, 554, 556–557
  Rottnest I., 807
  Tarawa, 590–591, 592–594
  Tikehau, 491
Freshwater wedge, 21, 384, 393–394, 518, 772
Fringing reef, 4, 12, 16
  ancient
    Barbados, 13, 383, 385
    Isla de Mona, 342
    Mururoa and Fangataufa, 446
  modern
    Cook Islands, 508–512, 514
    Fiji, 768, 769
    Fr. Polynesia, 435, 454–456, 458, 481, 485
    Grand Cayman Islands, 310
    Great Barrier Reef, 837–839, 851, 856–857
    Isla de Mona, 342
    Nauru, 711
Funafuti Atoll (Tuvalu), 4, 8–10, 28, 537, 582, 598, 901

Galleries (*see also* water resources), 518, 590, 597–598, 627, 900, 905–906
Gambier Islands (Fr. Polynesia), 19, 433–435, 476

Geochronology. *See* AAR data and geochronology; ESR data and geochronology; oxygen isotope stages; radiocarbon ages and geochronology; sea-level history; strontium isotope geochronology; U-series ages and geochronology
Geophysical exploration. *See* electrical resistivity surveying; electromagnetic surveying; gravity surveys; magnetic surveys; seismic surveys
Geothermal gradient (*see also* endo-upwelling Kohout convection), 188, 446–447, 449
Ghyben-Herzberg lens (*see also* freshwater lens), 25–26, 684, 689
Ghyben-Herzberg ratio (*see also* DGH models), 25–26, 64–65, 68, 554, 572, 754
Gilbert Islands (Repub. Kiribati), 8, 577, 708
Glacioeustasy (*see also* eustasy; New Guinea sea-level chronology; sea-level highstands; sea-level history; sea-level lowstands), 13, 17, 52, 82, 85, 223, 613
Gotland, 1, 31
Grand Bahama I., 92, 96, 146, 151–152
Grand Cayman I. (Cayman Islands), 2, 11, 299, 303–324
Gravity surveys, 96, 720, 722, 753
Great Bahama Bank, 91, 92, 96–98, 146, 161–179
Great Barrier Reef [GBR], 2, 4, 7, 13, 14, 20, 219, 835–866, 867–869, 878–879, 907
Groundwater chemistry. *See* hydrogeochemistry
Groundwater development. *See* water resources
Groundwater, occurrence of. *See* alluvial aquifer; basal groundwater; dike water; dual-aquifer atoll hydrogeology; freshwater lens; freshwater-saltwater transition zone; freshwater wedge; parabasal groundwater; perched aquifer; sheet water; "stream water"; valley-fill aquifer
Guam, 2, 9, 10, 11, 21–22, 26–27, 31, 599, 694, 743–761
Guano (*see also* phosphate deposits), 467, 543, 715, 843, 879, 882
Guyot, 477, 637

Ha'apai Island Group (Tonga), 565, 567–568, 570–572
Hawaii, 5, 21, 39, 503, 577, 599, 715, 881, 929
Henderson Island (Pitcairn Island Group), 2, 14, 407–410, 412–428
Hereheretue Atoll (Tuamotu Archipelago), 434–435
Hereheretue hotspot, 453, 468, 470
Heron Island (GBR), 2, 22, 836, 867–884
Highstands (*see also* Holocene highstand; interglacial highstands)
  Anewetak Atoll, 657–662
  Cayman Islands, 299, 322
  Isla de Mona, 355
Holocene. *See* Holocene highstand; radiocarbon ages and geochronology; sea-level history; stratigraphy
Holocene highstand
  Cocos (Keeling) Islands, 892–893, 901
  Cook Islands, 528
  Enewetak Atoll, 598, 674
  Funafuti, 9–10, 598
  Guam, 599, 750
  Great Barrier Reef, 843, 858–859
  Houtman Abrolhos Islands, 828
  Kiribati, 599
  Rottnest I., 799–803, 808
Holocene-Pleistocene unconformity. *See* Thurber Discontinuity
Hotspot
  Bermuda, 39
  Pacific Ocean, 433–436, 468–469, 476, 506–508, 541, 638, 715 (*see also* Macdonald Seamount; Hereheretue hotspot)
  Reunion, 912
Houtman Abrolhos Islands, 2, 4, 14, 20, 83, 786, 791–792, 811–833
HST3D, 27, 742
Hydraulic conductivity [K] (*see also* intrinsic permeability [k]; permeability; permeability tests)
  Bahamas 184–191, 212
  Barbados, 394,
  Bermuda, 62–64
  Caroline Islands atolls, 700–701
  Christmas I., 596
  Cocos (Keeling) Islands, 894–896
  Cook Islands, 531
  Diego Garcia, 910, 916–917
  Enewetak Atoll, 667, 672, 675–676, 678, 686–687
  Florida Bay Islands, 259
  Florida Keys, 238–239
  Grand Cayman Islands, 311
  Guam, 752–753
  Heron I., 872
  Majuro Atoll, 625, 627
  Nauru, 728, 731, 733

Hydraulic conductivity [K] (*continued*)
Tarawa, 587–590
Tikehau, 491
Tongatapu, 573–575
Hydrogeochemistry (*see also* freshwater-saltwater transition zone; stable isotopes, diagenesis)
Bermuda, 68
Cook Islands, 520
Fiji, 773–775
Florida Bay islands, 253–254, 261–272
Grand Cayman Islands, 316–320
Heron I., 877–882
Nauru, 733–736
Niue, 556–558
St. Croix, 370–372
Tahiti barrier reef, 495–496
Tikehau, 483, 485, 490–496

Inagua Island (Bahamas), 91, 96, 115, 139, 146, 152
Interglacial highstands (*see also* sea-level history; U-series dates and geochronology), 17
Aitutaki, 529
Bahamas, 98, 101, 106–113, 117–119, 123–130, 132, 153–157, 176–177
Barbados, 384
Bermuda, 51, 57, 71–72, 75, 77–84
Diego Garcia, 915
Florida Keys, 223, 228, 230
Grand Cayman Islands, 310, 322–323
Great Barrier Reef, 837
Henderson I., 426–428
Houtman Abrolhos Islands, 826–827
Isla de Mona, 341, 355
Makatea, 459, 464, 467–468, 471
Mururoa, 443
Niue, 553
Rottnest I., 799
Yucatan Islands, 278, 288, 296–297
Intrinsic permeability [k] (*see also* hydraulic conductivity [K], permeability)
Bahama Banks, 172
Enewetak Atoll, 686–687
Grand Cayman Islands, 312
Kwajalein Atoll, 630, 632
Mururoa and Fangataufa, 446–450
Niue, 556
Inventories, freshwater and meteoric-water, 26, 676, 678, 680–681, 684
Isla Blanca (Yucatan), 285–286
Isla Cancun (Yucatan), 2, 20, 275, 280, 284–285, 291, 296
Isla Contoy (Yucatan), 280–282
Isla de Mona, 2, 14, 24, 327–358
Isla Mujeres (Yucatan), 280, 282, 298
Islands, types of, 10–25
Bahamas, 141, 145–153
Caroline Islands, 693
Cook Islands, 504–510
Fiji, 763, 766–770
Fr. Polynesia, 433–435, 475–477
Great Barrier Reef, 844–857
Houtman Abrolhos Islands, 813–814
Kiribati, 577
Marshall Islands, 611–612

Jaluit Atoll (Marshall Islands), 611
Jamaica, 9, 11, 20, 362
Jarvis Atoll (Repub. Kiribati), 599
Joulters Cays (Bahamas), 153

Kankura (Tuamotu Archipelago), 453–454
Kanton Atoll (Repub. Kiribati), 599
Karren and karrenfeld (*see also* pinnacles)
Bahamas, 100
Henderson I., 424–425
Nauru, 707, 709, 722
Niue, 542
Karst and karstification (*see also* blue holes; caves and caverns; karren and karrenfeld; pinnacles), 13–14, 16, 21
Anewetak Atoll, 646–647
Bahamas, 100–101, 118
Bermuda, 42, 57–59
Cayman Islands, 322–324, 414, 422
Cocos (Keeling) Islands, 886, 890, 903
Cook Islands, 512, 517, 531
Enewetak Atoll, 673
Fiji, 769–770
Florida Keys, 228
Great Barrier Reef, 837
Guam, 747
Makatea, 456, 466–467, 470–471
Mururoa and Fangataufa, 441–444, 447
Nauru, 709, 715, 718–719
Niue, 542–543
Key Largo (Florida), 14, 218, 224, 228–229
Key West (Florida), 18, 173, 217–218, 233–234, 236–237
Kiribati (*see also* Christmas I.; Tarawa), 2, 577–578, 607, 696
Kirimati *See* Christmas Island (Repub. Kiribati)

Kohout convection (*see also* endo-upwelling; geothermal gradient), 176, 203, 487–488, 559–561
Kuria Atoll (Repub. Kiribati), 599
Kwajalein Atoll (Marshall Islands), 2, 27, 611–614, 616–620, 622–626, 628–634, 694
Kwajalein Island (Kwajalein Atoll), 617, 620, 624, 635

Lagoon (including lagoon sediments), 12, 14–16
  Bahamas, 109, 113
  Bermuda, 36
  Caroline Islands atolls, 698, 705
  Cayman Islands, 323
  Cocos (Keeling) Islands, 889–890, 895, 902–904
  Cook Islands, 504, 508–514
  Diego Garcia, 909
  Enewetak Atoll, 637, 668, 670–674, 690–691
  Fiji, 769–770
  Great Barrier Reef, 839, 848, 851, 856, 879
  Houtman Abrolhos Islands, 814–815, 819–821
  Marshall Islands, 612, 618–619
  Mururoa and Fangataufa, 436–437
  Nauru, 717–719, 728–729
  St. Croix, 372–376
  Tarawa and Christmas Island, 578–581
  Tikehau and Tahiti, 479–487; 497–500
  Yucatan Islands, 276, 280, 297
Lagoon facies (*see also* backreef)
  Anewetak Atoll, 644–645
  Fiji, 768
  Henderson I., 417, 423
  Isla de Mona, 336, 339–340
  Mururoa and Fangataufa, 442
  Nauru, 716
  Niue, 547–548
Lagoon pinnacles (*see also* patch reefs, pinnacles [karst])
  Cook Islands, 512
  Enewetak Atoll, 672–673
  Fr. Polynesia, 475, 479–480; 483, 485–486, 488, 490, 492, 497
Lagoon, rocks below the modern
  Cook Islands (Aitutaki, Pukapuka and Rakahanga), 521–532
  Mururoa and Fangataufa, 437–443
Lakes, 24–25
  Bahamas, 98, 103, 199
  Cook Islands, 519–520
  Isla Mujeres, 282
  Rottnest I., 785–788, 798
  Tonga, 771–775
Last Interglacial, 788, 793, 802, 816–819, 822–827, 890, 903–905
Lau Basin, 566, 569
Lau Island Group (Fiji), 2, 19, 763, 767–770, 781
Lau Ridge, 566, 569–570, 576, 767–768, 780–781
Laura Island. *See* Majuro Atoll
Lee Stocking Island (Bahamas), 139, 143, 146, 150–151
Leeuwin Current, 785, 810, 815, 824
Lesser Antilles, 2, 20, 359, 363
Limestone Caribbes (Lesser Antilles), 20
Line Islands (Repub. Kiribati), 577
Lithospheric flexure, 19, 412, 416, 421, 468–470, 477, 508
Little Bahama Bank, 91, 146, 148, 152, 174, 180, 182
Little Cayman Island (Cayman Islands), 299–300, 303–304
Little Inagua Island (Bahamas), 146
Long Island (Bahamas), 101, 104, 146, 162
Long Island (New York), 1
Lord Howe Island, 17, 18, 33

Macdonald Seamount, 19, 433, 638
Magnetic surveys, 96, 438, 720, 722
Magnetostratigraphy, 443–444
Maiana Atoll (Repub. Kiribati), 599
Majuro Atoll (Marshall Islands), 2, 23, 611–619, 621, 624–628, 629, 634, 694
Makatea, 16
Makatea Island (Tuamotu Archipelago), 2, 4, 14, 16, 18–19, 453–473, 477, 481, 482, 485, 488, 498
Makatea island, 16, 18–19, 22, 32, 412, 508–509, 514–515, 518, 519, 524–525, 531, 534
Malden Atoll (Repub. Kiribati), 518, 599
Maldives, 8, 889, 913
Mangaia Island (Cook Islands), 2, 5, 504–509, 511, 514, 525, 528, 533–534
Mangrove (*see also* swamp, mangrove)
  Florida Keys and Bay, 221, 256, 358
  Great Barrier Reef, 839, 844, 848–852, 855–856, 858
  Tarawa, 581
  Yucatan Islands, 280–281, 283–384, 286
Manihiki Atoll (Cook Islands), 504–506, 508–510, 514, 519, 526
Manihiki Plateau, 508, 524, 526–527, 531–534

Manuae (Cook Islands), 504–506, 508–510, 512, 514
Marine diagenesis (*see also* cements and cementation; diagenesis)
  Anewetak Atoll, 648–653, 655, 666
  Bahama Platform, 172–174
  Houtman Abrolhos Islands, 822
  Isla de Mona, 342
Marquesas Islands (I. Marquisas, Fr. Polynesia), 5, 7–8, 19, 433–435, 453, 476, 478, 481
Marshall Islands (*see also* Anewetak Atoll; Enewetak Atoll), 2, 4, 8, 24, 582, 598, 611–635, 638, 668, 696, 708
Mataiva (Tuamotu Archipelago), 453–454, 462, 470, 485, 498
Mauke Island (Cook Islands), 2, 12, 16, 19, 32, 431, 514, 525, 528, 534
Mayaguana (Bahamas), 146, 152
Megabank, 95, 222
Mehetia (Society Islands), 454, 467
Messinian, 306–307, 323, 547, 551–553, 562
Meteoric diagenesis (*see also* cements and cementation; diagenesis)
  Anewetak Atoll, 650, 653–660
  Bahamas Platform, 171–174, 176–179
  Barbados, 397–398
  Bermuda, 55
  Cook Islands, 515, 517, 529, 531
  Florida Keys, 228–230
  Houtman Abrolhos Islands, 822, 826
  Isla de Mona, 342
  Mururoa and Fangataufa, 440, 442
  Niue, 546, 548–550, 560
  Tarawa, 582
  Yucatan Islands, 292–296
Microatoll, 825
  Christmas I., 586, 599
  Cocos (Keeling) Islands, 891, 901–902, 905
  Cook Islands, 528
  Cozumel, 288, 297
  Tarawa, 599
Midway, 4, 901
Miocene (*see also* sea-level history; Messinian; stratigraphy)
  Anewetak Atoll, 639, 642, 644–646, 653, 657–658, 660
  Bahama Banks, 170, 174–176, 178
  Cayman Islands, 304, 306, 322–323
  Cook Islands, 514–515
  Guam, 749
  Isla de Mona, 331, 350–352, 354
  Makatea, 453, 457–463, 465–470
  Mururoa and Fangataufa, 444
  Niue, 546–548, 551–553, 561–562
  St. Croix, 364–365
Mitiaro Island (Cook Islands), 2, 12, 504–509, 514, 525, 528
Mixing-zone diagenesis (*see also* flank margin caves; freshwater-saltwater transition zone), 9
  Aitutaki, 529, 531–532
  Anewetak Atoll, 654–655
  Bahama Banks, 174
  Bahamas, 211
  Barbados, 397, 401–403
  Bermuda, 58
  Isla de Mona, 342, 352–354
  Makatea, 463–466, 470
  Mururoa, 443
  Niue, 559–560
  Rottnest I., 807
Mixing-zone dolomitization. *See* mixing-zone diagenesis
Mona. *See* Isla de Mona
Moorea (Society Islands), 19, 435, 454, 467, 470–471, 480–482
Moore's Island (Bahamas), 146, 152
Motu (*see also* cay; reef island)
  Fr. Polynesia, 437, 480, 484–485, 488, 490–492, 497–498
Mururoa (Tuamotu Archipelago), 2, 9, 433–451, 518
Mwoakilloa Atoll. *See* Caroline Islands atolls

Nassau (Bahamas), 150, 155
Nassau Island (Cook Islands), 504, 505, 507, 508, 510, 519
Nauru Island, 2, 4, 11, 14, 23, 27, 178, 498, 518, 694, 707–742
New Guinea sea-level chronology (*see also* eustasy; glacioeustasy; oxygen isotope chronology; sea-level history), 4, 71, 80, 105, 425, 829
New Providence Island (Bahamas), 91, 123, 128, 133–135, 141–142, 148, 150, 153–155, 157–160
New Zealand, 5, 503, 506, 537, 567, 907
Niau Atoll (Tuamotu Archipelago), 453–454, 484–485, 488, 498
Nitrogen species. *See* nutrient ions
Niuas, the (Tonga), 565, 567, 568, 571
Niue, 2, 5, 8, 11, 14, 83, 529, 537–564

Nomuka Island Group (Tonga), 565, 567–568, 570
Northern Guam Lens, 26, 29, 750, 753–760
Notch (*see also* highstands; terrace)
  Bahamas, 101–102, 104, 156
  Bermuda, 47
  Cook Islands, 528
  Guam, 746
  Henderson I., 414, 420–421, 426
  Makatea, 455, 467
  Rottnest I., 788–789, 792, 798, 800–802
Numerical modeling (groundwater), 27
  Enewetak Atoll, 449, 675, 684–690
  Guam, 757–759
  Marshall Islands, 615–617, 619–622, 624–634
  Mururoa, 449–450
  Nauru, 710, 730–734
  St. Croix, 370
Nutrient ions
  Heron I., 878–882
  Tikehau and Tahiti, 475, 479, 483–485, 490–492, 495–497

Ocean Island (*see also* Banaba), 4, 577, 708
Oeno Atoll (Pitcairn Island Group), 407–408, 410, 411–412
Oligocene, 38, 304, 322–323, 327, 331, 350, 364, 642, 645, 653, 657, 715
Oolite
  Bahamas, 96–97, 100, 109–110, 122, 124–127, 131, 135, 141, 143, 147, 149, 151, 153–157, 169, 178
  Florida Keys, 17, 222–225, 227, 230
  Yucatan Islands, 280–281, 285–286, 289–290
Operation Crossroads (Anewetak), 639
Oxygen isotopes. *See* oxygen isotope chronology; stable isotopes, diagenesis
Oxygen isotope chronology (*see also* New Guinea sea-evel chronology)
  Anewetak Atoll, 643, 662
  Bahamas, 105–107, 125–130, 132, 142–145, 147–158
  Bermuda, 55–56, 71, 73, 78–82, 84
  Cocos (Keeling) Islands, 904
  Cook Islands, 524–425
  Florida Keys, 230–232
  Henderson I., 420–422
  Houtman Abrolhos Islands, 827
  Makatea, 459
  Rottnest I., 799
  Tarawa, 582
  Yucatan Islands, 277–279
Oxygen isotope ice-volume curves. *See* oxygen isotope chronology
Oxygen isotope stages. *See* oxygen isotope chronology

PACE Program (Anewetak), 639, 643
Paddy field terraces
  Rottnest I., 790
Palau-Kyushu Ridge, 747–748
Paleosol (*see also* calcrete, caliche, rhizoliths, root pipes, soil pipes, vegemorphs), 17
  Anewetak Atoll, 654–655
  Bahamas, 99, 106, 108–109, 113, 115–119, 125–127, 129–130, 132, 142–145, 149, 153–157
  Bermuda, 42–45, 47–49, 52, 54, 56–57, 73–79
  Cayman Islands, 305–323
  Great Barrier Reef, 840
  Isla de Mona, 333, 336, 350–351
  Mururoa and Fangataufa, 441–443
  Nauru, 722
  Niue, 543
  Rottnest I., 794
  Society Islands, 477
  Yucatan Islands, 282–283
Palmerston Atoll (Cook Islands), 5, 504–506, 508–510, 514
Parabasal groundwater, 21–22, 753, 755–756, 759
Parry Islands (Anewetak), 639
Patch reef (*see also* lagoon pinnacles)
  ancient
    Florida Keys, 226
    Grand Cayman Islands, 309
    Henderson I., 422–423
    Isla de Mona, 336–337, 340
  modern
    Cook Islands, 510–514
    Enewetak Atoll, 668, 672, 690
    Fiji, 769
    Florida Keys, 220
    Fr. Polynesia, 437, 480, 485–487, 497, 499
    Great Barrier Reef, 838–839
    Houtman Abrolhos Islands, 815–816
PEACE Program (Anewetak Atoll), 639, 643, 664
Penman method (*see also* evapotranspiration; water balance), 191, 571, 601, 773, 896
Penryn Atoll (Cook Islands), 504–505, 598–510, 514

Perched aquifer, 518, 769, 771
Permeability (*see also* hydraulic conductivity [K]; intrinsic permeability [k]; permeability tests)
  Bahama Banks, 174
  Caroline Islands atolls, 698, 705
  Enewetak Atoll, 675, 690
  Grand Cayman Islands, 311–314, 323
  Isla de Mona, 349
  St. Croix, 367–368
Permeability tests
  constant-head and falling head, 587–589, 595–596, 894–895
  packer, 184, 447
  pumping, 184–185, 188, 394, 397, 588, 614, 910, 916, 929
  slug and bail, 184, 614, 700–701
Perth Basin, 793, 803, 809–810, 816
Perth Canyon, 803
Phoenix Islands (Repub. Kiribati), 577, 599
Phosphate deposits (*see also* guano; nutrient ions), 4, 8, 485, 498
  Great Barrier Reef, 843, 851, 853, 859
  Houtman Abrolhos Islands, 814
  Makatea, 453, 456–457, 460–461, 467
  Nauru, 178, 707, 709, 717, 719, 722–723
  Niue, 543
Phosphate ion. *See* nutrient ions
Phosphogenesis. *See* phosphate deposits
Pingelap Atoll. *See* Caroline Islands atolls
Pinnacle reef. *See* lagoon pinnacles; patch reef
Pinnacles (karst)
  Cook Islands, 509
  Enewetak Atoll, 673
  Henderson I., 420, 422–425
  Makatea, 463
  Nauru, 707, 717, 722
  Niue, 542
Pitcairn I. (*see also* Hereheretue hotspot), 2, 5, 14, 19, 407–410, 434–435
Pitcairn Island Group (*see also* Ducie Atoll, Henderson I., Oeno Atoll, Pitcairn Island), 407–410, 429
Pleistocene. *See* interglacial highstands sea-level history sea-level lowstands stratigraphy U-series ages and geochronology
Pliocene
  Anewetak Atoll, 642, 653, 660
  Bahama Banks, 123, 168–170, 175–176, 178
  Cayman Islands, 304, 308, 311, 322
  Cook Islands, 514
  Isla de Mona, 350–351, 354
  Makatea, 453, 457–458, 466, 469–471
  Mururoa and Fangataufa, 444–446
  Niue, 541, 546–548, 551–553, 561–562
  St. Croix, 367, 373–374
Poecilozonites, 47, 74
Polyphase uplift model, 468–470
Ponape [Pohnpei] (Caroline Islands), 12, 693–694
Poroelastic storage, 917–918
Porosity (*see also* cavernous porosity)
  Bahamas, 142–143, 184, 187–188
  Bermuda, 62
  Cook Islands, 529, 531
  Diego Garcia, 916, 919
  Fiji, 773–774
  Florida Bay islands, 259
  Florida Keys, 229–230
  Grand Cayman Islands, 311–313, 322–323
  Guam, 753
  Isla de Mona, 349
  Nauru, 731
  Niue, 556
  Tonga, 570, 572–575
Protosol. *See* paleosol
Puerto Rico, 11, 20, 327, 360, 362
Pukapuka Atoll (Cook Islands), 2, 503–505, 508, 510, 512, 514, 521–522, 524–532

Quaternary eolianite. *See* eolianite

Radiocarbon ages and geochronology
  Bahamas, 131, 142
  Cocos (Keeling) Islands, 892–893, 901
  Cook Islands, 510, 527–528
  Florida Keys, 232
  Great Barrier Reef, 858–859
  Houtman Abrolhos Islands, 822–824
  Nauru, 719
  Rottnest, I. 793, 797–800
  Tahiti, 494
  Tarawa, 582–584
  Yucatan Islands, 285
Rainwater catchment (*see also* water resources), 40, 68–69, 205, 321, 369, 518–519, 572, 597, 611, 693, 736, 740, 775, 805, 807
Rakahanga (Cook Islands), 2, 503–505, 508, 510, 512, 514, 521, 523–531
Ralik Chain (Marshall Islands), 611–612, 637
Rampart rocks
  Great Barrier Reef, 841–844, 848–850, 857, 859

Rangiroa (Tuamotu Archipelago), 453, 470, 476, 482, 486, 488
Rarotonga (Cook Islands), 14, 19, 503–509, 511, 514, 524, 528, 534
Ratik Chain (Marshall Islands), 611–612, 637
Recharge (*see also* water balance), 20, 23, 24
  Bahamas, 192–195
  Barbados, 393–394
  Bermuda, 65, 68–69
  Caroline Islands atolls, 698
  Christmas I., 586, 596–597, 599–603
  Cocos (Keeling) Islands, 895–899
  Diego Garcia, 921–924
  Enewetak Atoll, 669–671, 676–677, 680, 684
  Florida Keys, 237, 239
  Grand Cayman Islands, 316, 320
  Guam, 754, 756–757
  Marshall Islands, 617, 619–622, 624–625, 628–631, 633–634
  Nauru, 728–729, 733
  Niue, 554
  Rottnest I., 807
  St. Croix, 361, 369
  Tarawa, 586, 591–593, 599
  Tongatapu, 573–574
Reef crest (*see also* reef flat)
  ancient
    Barbados, 390
    Cook Islands, 515
    Fr. Polynesia, 442
  modern
    Cocos, 888
    Cook Islands, 511
    Houtman Abrolhos Islands, 824
    Fr. Polynesia, 491, 494, 497, 499
    Tarawa, 581
Reef facies
  Anewetak Atoll, 644–647
  Bahama Platform, 164, 172
  Barbados, 385–391
  Cozumel, 288–290
  Great Barrier Reef, 837–839
  Guam, 750
  Henderson I., 416–420
  Houtman Abrolhos Islands, 812, 818–822
  Isla de Mona, 335–340
  Makatea, 459–463
  Mururoa and Fangataufa, 442
  Niue, 547–548, 556
  Rottnest I., 795
Reef flat (*see also* reef crest)
  ancient
    Cook Islands, 515
    Cozumel, 289
    Henderson I., 417, 422–423
    Makatea, 456, 459, 462
    Mururoa and Fangataufa, 442
  modern (*see also* conglomerate platform, microatoll, reef plate)
    Cocos (Keeling) Islands, 888, 901–903
    Cook Islands, 511–512, 528
    Enewetak Atoll, 673
    Fr. Polynesia, 480, 497
    Great Barrier Reef, 840–842, 844, 847, 856–857, 860–862, 870, 873–874
    Houtman Abrolhos Islands, 816, 824–825
    Makatea, 456
    Nauru, 720
    Tarawa, 583
Reef front and slope (*see also* forereef and slope; spur and groove)
  ancient
    Makatea, 462
  modern
    Christmas Island, 581
    Cook Islands, 511
    Great Barrier Reef, 841–842
    Houtman-Abrolhos Islands, 815
Reef growth, 15, 164, 488, 905
  Anewetak (*see* accommodation)
  Cook Islands, 511–512, 524–528
  Florida Keys, 242, 243
  Great Barrier Reef, 835, 837
  Houtman Abrolhos Islands, 822–825, 828
  Mururoa and Fangataufa, 445–446
Reef island (*see also* atoll, ancient; cay; dual-aquifer atoll hydrogeology; motu), 2, 11, 13–14, 17, 18, 22–23
  Cocos (Keeling) Islands, 888–890, 893, 901–905
  Cook Islands, 508, 510
  Diego Garcia, 916
  Enewetak Atoll, 674, 676
  Great Barrier Reef, 839–862, 867–882
  Tarawa, 580
Reef plate (*see also* algal pavement), 24
  Caroline Islands atolls, 697–698
  Enewetak Atoll, 647, 672–675
  Heron I., 871–874, 881
  Marshall Islands, 613–614
Reef rim (*see also* algal ridges), 462, 475, 510, 528, 870

Residence time, island lenses
Bermuda, 90
Big Pine Key, 239–240
Christmas I., 596–597
Cocos (Keeling) Islands, 899
Diego Garcia, 921
Enewetak Atoll, 676–677, 684
Residence time, French Polynesian lagoons, 483–484
Resistivity surveying. *See* electrical resistivity surveying
Rhizolith (*see also* paleosol, vegemorph)
Grand Cayman Islands, 310
Rottnest I., 794
Yucatan Islands, 282
Ribbon reef, 839, 857
Rigili (Anewetak), 639
Rocky Dundas (Bahamas), 152
Roi-Namur I. (Kwajalein Atoll), 617–618, 622, 628, 630–631, 633, 635
Root pipes (*see also* soil pipes), 794
Rottnest I., 2, 4, 11, 17, 20, 25, 42, 783–810
Rurutu (Australes), 5, 435, 481, 609, 638

Safe yield. *See* yield
St. Croix (Virgin Islands), 2, 13, 18, 20, 359–379
Samana Cay (Bahamas), 146, 152
San Salvador I. (Bahamas), 94, 96, 102, 104–105, 110–113, 115–118, 124, 127, 129–130, 133–139, 141, 142, 152, 157–160, 175, 666
Sapwuahfik Atoll. *See* Caroline Islands atolls
Schooner Cays (Bahamas), 131, 133–134, 153
Sea-level curves (*see also* oxygen isotope chronology; sea-level history), 9, 59, 69, 73, 154, 232–233, 425, 461, 469, 525, 583, 661, 799, 800, 826–829, 893
Sea-level highstands. *See* highstands; Holocene highstand; interglacial highstands; U-series dates and geochronology
Sea-level history (*see also* eustasy; oxygen isotope chronology; sea-level highstands; sea-level lowstands; stratigraphy), 29
Anewetak Atoll, 656–662
Bahamas, 105–118, 153–157
Barbados, 391–392
Bermuda, 59–60, 69–84
Cayman Islands, 310
Christmas I., 583–586, 599
Cocos (Keeling) Islands, 901–905
Cook Islands, 524–528
Florida Keys, 232–233
Great Barrier Reef, 857–859
Houtman Abrolhos Islands, 825–829
Isla de Mona, 340–342; 350–351
Makatea, 459, 465–468
Niue, 551–553
Rottnest I, 798–803
St. Croix, 367
Tarawa, 582–583, 599
Yucatan Islands, 277–279, 288
Sea-level lowstands, 17
Anewetak Atoll, 657, 659–660
Bahama Platform, 171, 173–174, 176, 178
Bahamas, 106, 108–109, 112, 118, 123
Bermuda, 52, 58, 70
Cayman Islands, 299, 322
Cook Islands, 517
Diego Garcia, 916
Great Barrier Reef, 837
Makatea, 459, 464, 467–468
Mururoa, 444–445
Niue, 551–553
Rottnest I., 796, 794, 802
Yucatan Islands, 296
Seamount, 407, 409, 435–436, 476, 506, 508, 540–541, 543, 568, 570, 637, 712, 714–715, 719, 722, 885
Seismic facies
Bahama Platform, 168–171
Seismic surveys
Aitutaki, 513
Bahama Platform, 96, 163, 168–170
Cocos (Keeling) Islands, 890
Enewetak Atoll, 641, 647, 671–672
Guam, 751
Sheet water, 22, 384, 393–397
Silba, 1, 29
Skimming wells. *See* water resources
Society Islands (Fr. Polynesia), 8, 19, 433–435, 467, 469–471, 475–477, 489, 529, 577, 901
Soil pipes (*see also* root pipes), 47–48
Solution pits (*see also* cenotes), 332–333
Solution unconformity (*see also* exposure surface, Thurber Discontinuity), 9, 905
Anewetak Atoll, 639–641, 646–647, 657, 671
Cocos (Keeling) Islands, 905
Great Barrier Reef, 837, 869
Tarawa, 582
Southern Oscillation (*see also* ENSO), 477, 506, 540–541, 579–580, 886, 927–928
Springs, 22, 516, 519, 571, 745, 770–772, 775

Spur and groove, 414, 417–418, 422–424, 480, 511, 581, 870, 888
Stable isotopes (carbon and oxygen), diagenesis
Aitutaki, 529
Anewetak Atoll, 648–650, 652–653, 655, 659
Bahama Banks, 172–174
Barbados, 400–403
Bermuda, 56
Florida Bay, 253–254, 261, 267–268
Grand Cayman Islands, 317–320
Isla de Mona, 346–348, 352–354
Mururoa and Fangataufa, 440–441, 443
Niue, 548–549, 551, 553
St. Croix, 372–374, 376
Starbuck Atoll (Repub. Kiribati), 599
Stratigraphy (*see also* sea-level history)
Anewetak Atoll (Cenoz.), 640–643, 671–675
Bahama Banks (Tert.), 96, 168–171
Bahamas (Quat.), 118–132, 142–143
Barbados (Pleist.), 391–392
Bermuda (Pleist.), 44–56
Cayman Islands (Cenoz.), 302–310
Christmas I. (Quat.), 583–586
Cocos (Keeling) Islands(Quat.), 890–893
Cook Islands (Cenoz.), 514–518, 524–528
Diego Garcia (Quat.), 913–916
Fiji (Cenoz.), 768–769
Florida Keys (Pleist.) 227–228
Great Barrier Reef (Quat.), 837
Guam (Cenoz.), 748–750
Henderson I. (Pleist.), 413–422
Houtman Abrolhos Islands (Quat.), 816–822
Isla de Mona (Tert.), 334–340
Makatea (Cenoz.), 457–459
Marshall Islands (Quat.), 613–614
Mururoa and Fangataufa (Cenoz.) 440–444
Nauru (Cenoz.), 715–721
Niue (Cenoz.), 544–546
Rottnest I. (Quat.), 793–798
St. Croix (Tert.), 364–366
Tarawa (Quat.), 582–583
Tonga (Cenoz.), 570
Yucatan Islands (Quat.), 279–280, 288–291
"Stream water", 22, 384, 393, 395
Stromatolite (*see also* cyanobacterial mats), 98, 485, 495, 798
Strontium isotope geochronology
Anewetak Atoll, 642–643, 653, 656–662
Bahama Banks, 176
Isla de Mona, 347
Niue, 547, 560
St. Croix, 374–375
Subaerial exposure surface (*see also* karst, paleosol, solution unconformity
Anewetak Atoll, 654, 660–662
Bahama Banks, 169, 172–173
Florida Keys, 228
Makatea, 457
Mururoa and Fangataufa, 442–444
Niue, 549
St. Croix, 367
Subsidence
Anewetak Atoll, 638, 656–658, 661–662, 671
Bahamas, 95, 105–106, 109, 125
Bermuda, 39, 59
Christmas I., 582–583
Cook Islands, 508, 534–527
Diego Garcia, 912–913
Fiji, 769
Florida Keys, 222
Fr. Polynesia, 433, 443, 450, 468–469, 476
Niue, 544
Sulfate reduction, 211, 264–266
Sustainable yield. *See* yield
SUTRA, 27, 615, 625, 628, 684
Suwarrow Atoll (Cook Islands), 504–510, 512, 528
Swamp, 16, 315, 323, 769, 913
Cook Islands, 16, 509–510, 514–515, 519–520
Mangrove, 183, 221, 256, 277, 280, 844, 849
Rottnest Island, 784, 793, 795, 798, 808

Tahiti (Society Islands), 5, 14, 19, 433, 434, 445, 454, 467–471, 475–477, 479–481, 494–496, 540, 927
Takutea (Cook Islands), 504–506, 508, 510
Tarawa (Repub. Kiribati), 2, 9, 24, 577–584, 586–594, 597–607, 694, 696, 698, 708, 894
Tepee structures, 798
Terraces (*see also* coastal terrace; notch; paddy field terraces)
Barbados, 16, 382, 384–387, 392
Enewetak Atoll, 671
Fiji, 769
Great Barrier Reef, 846, 857–858, 862
Guam, 753
Henderson I., 414, 420–421, 428
Isla de Mona, 328
Makatea, 456, 467
Nauru, 24, 716–719, 736, 740
Niue, 537, 542–543, 562
Tonga, 570
Yucatan Islands, 276

Terra rossa. *See* paleosol
Thurber Discontinuity (*see also* dual-aquifer atoll hydrogeology)
  Cocos (Keeling) Islands, 890, 895–896, 905
  Diego Garcia, 914
  Marshall Islands, 613, 643, 671
  Mururoa and Fangataufa, 442
  Tarawa, 582
Tidal efficiency. *See* tides, groundwater
Tidal lag. *See* tides, groundwater
Tides, depositional environment
  Enewetak Atoll, 669–670, 673–674
  Florida Bay, 249–250, 253, 260
  Great Barrier Reef, 842, 845, 848, 856–857, 860–861, 869–870
  Rottnest I., 788–790
  Tuamotu Archipelago, 482, 484
Tides, groundwater, 21–23
  Bahamas, 184–186, 193, 210
  Bermuda, 63–67
  Caroline Islands atolls, 699–701
  Diego Garcia, 916–917, 919
  Enewetak Atoll, 648, 670, 677, 686–690
  Fiji, 772
  Florida Keys, 236
  Grand Cayman Islands, 314
  Heron I., 873–877
  Marshall Islands, 615–619, 634
  Nauru, 730
  Niue, 554–555, 561
Tides, ocean
  Bermuda, 40–41
  Cocos (Keeling) Islands, 888
  Enewetak Atoll, 670
  Grand Cayman Islands, 314
  Great Barrier Reef, 838, 869
  Kiribati (Tarawa and Christmas I,), 580
  Nauru, 713–714
  Niue, 554
  Rottnest I., 785
Tikehau Atoll (Tuamotu Archipelago), 2, 454, 470, 475, 481, 483, 486, 488, 489–494
Tofua Arc, 568–570, 575
Tofua Volcano (Tonga), 566–567
Tonga, 2, 8, 537, 538, 565–576, 742, 767
Tonga Ridge, 566, 568–569, 764, 767
Tongatapu (Kingdom of Tonga), 2, 11, 14, 565–568, 570–575
Tonga Trench, 19–20, 562, 566, 575
Tongue of the Ocean (Bahamas), 170, 203, 211, 222
Tritium, 597
Tuamotu Archipelago, 5, 19, 433–435, 453, 476–477, 481–483, 486, 488, 489, 493
Tupuai Atoll (Society Islands), 476
Turks and Caicos Islands, 91, 148, 183, 205
Tuvalu. *See* Funafuti

Ulithi Atoll. *See* Caroline Islands atolls
Unconformity (*see also* paleosol; sea-level lowstand; solution unconformity; subaerial exposure surface; Thurber Discontinuity)
  Bahamas, 124
  Bermuda, 49
  Cayman Islands, 304–308, 310, 322
  Niue, 551–553
Uplift (*see also* lithospheric flexure), 12–14, 19
  Barbados, 384
  Cook Islands, 508, 524–525, 527
  Fiji, 570
  Guam, 750
  Henderson I., 412, 416, 422, 425–428
  Makatea, 454, 467–470, 477
  Marshall Islands, 638
  Nauru, 715
  Niue, 537, 541
U-series ages and geochronology (*see also* sea-level history), 4
  Anewetak Atoll, 643
  Bahamas, 99, 120, 128, 149–150
  Barbados, 385, 391–392
  Bermuda, 56, 71, 74
  Cocos (Keeling) Islands, 890
  Cook Islands, 523–525
  Florida Keys, 230–232
  Henderson Island, 416–422
  Houtman Abrolhos Islands, 822–824, 826–830
  Isla de Mona, 340–342
  Makatea, 459
  Mururoa, 443–445
  Rottnest I., 795
  Tarawa, 582
U.S. Geological Survey, 21, 219, 684, 701, 750, 922

Valley-fill aquifers (*see also* alluvial aquifers)
  Guam, 750
Vanua Levu (Fiji), 763, 765
Variable-density flow and solute transport modeling. *See* numerical modeling (groundwater)

Vava'u Island Group (Tonga), 565–568, 570–572
Vegemorph (*see also* rhizolith)
  Bahamas, 112, 115–118, 129
Viti Levu (Fiji), 607, 763, 865
Volcanic basement. *See* volcanics
Volcanic rocks. *See* volcanics.
Volcanics (*see also* seamount, hotspot), 9, 12–13, 15–17, 19–22
  Bermuda, 36–39
  Christmas I., 583
  Caroline Islands, 693
  Cook Islands, 506, 508–510, 514–515, 517, 519–520, 522, 526–527, 529, 531–532
  Diego Garcia, 912
  Fiji, 763, 767–768, 770, 772–773
  Guam, 743, 745–751
  Marshall Islands, 9, 613, 629, 637–638, 642, 658, 671
  Mururoa and fangataufa, 9, 433–442, 446–450
  Nauru, 707, 714–715
  Niue, 539, 541, 543–544, 559–560
  Society Islands, 470–471, 476, 496
  Tonga, 566, 568–570
  Tuamotu plateau, 453
Volcanism. *See* volcanics

Water balance (*see also* evapotranspiration, recharge), 394, 396, 554, 586, 591–593, 596–597, 599–606, 773, 896–898, 906
Water quality. *See* hydrogeochemistry
Water resources (*see also* rainwater catchment)
  Bahamas, 205–207
  Barbados, 392, 394–397
  Bermuda, 68–69
  Caroline Islands atolls, 693, 695
  Cayman Islands, 321
  Christmas I., 597–598
  Cocos (Keeling) Islands, 900–901
  Cook Islands, 518
  Diego Garcia, 909, 911, 921–929
  Fiji, 764–765, 775–776
  Florida Keys, 236, 239, 241–242
  Guam, 743, 745, 750, 757, 759
  Isla de Mona, 348
  Marshall Islands, 623–633
  Nauru, 733, 736–738
  Rottnest I., 805–807
  St. Croix, 369–370
  Tarawa, 586, 597–598
  Tonga, 572, 574–575
Water supply. *See* water resources

Yield (*see also* water resources)
  Bermuda, 69
  Cocos (Keeling) Islands, 899
  Diego Garcia, 921–923, 927
  Guam, 757, 759
  Marshall Islands, 623–633
  Tarawa, 586
Yucatan Islands, 2, 42, 275–298
Yucatan peninsula, 7, 20, 222, 275–277, 291–292, 297